UCLA School of Engineering and Applied Science

AD-A266 367

DTIC
ELECTE
JUN 2 8 1993
S D

Attachment No. 1

to

EXPERIMENTAL STUDY OF NONASSOCIATED FLOW AND INSTABILITY OF FRICTIONAL MATERIALS

Poul V. Lade and Jerry A. Yamamuro

AFOSR Grant No. 91-0117

UCLA-ENG-93-26
APRIL 1993

INSTABILITY AND BEHAVIOR OF GRANULAR MATERIALS AT HIGH PRESSURES

Approved for public release
Distribution Unlimited

JERRY A. YAMAMURO
POUL V. LADE

Reproduced From
Best Available Copy

UCLA-ENG-93-26
APRIL 1993

INSTABILITY AND BEHAVIOR of GRANULAR MATERIALS at HIGH PRESSURES

DTIC QUALITY INSPECTED 2

by

Jerry A. Yamamuro

and

Poul V. Lade

Accession For
NTIS CRA&I
DTIC TAB
Unannounced
Justification
By
Distribution /
Availability Codes
Dist | Avail and/or Special
A-1

Report to the

Air Force Office of Scientific Research

AFOSR Contract No. 91-0117

DTIC

Principal Investigator: Poul V. Lade

Civil Engineering Department
School of Engineering and Applied Science
University of California
Los Angeles, California

93-14658

FOREWORD AND ACKNOWLEDGEMENT

The research described in this report is part of continuing efforts at University of California, Los Angeles towards investigating the general behavior of frictional materials. This particular report formed the basis of the Ph.D. dissertation of the first named author, who worked on his research studies under the direction of the second named author. Also serving on the advisory committee for this Ph.D. dissertation were Professors S.B. Dong, M.E. Fourney, J.M. Christie, and R.V. Ingersoll. Grateful appreciation is expressed for their valuable advice and review of this manuscript.

This report was prepared as part of an "Experimental Study of Nonassociated Flow and Instability of Frictional Materials," sponsored by the Air Force Office of Scientific Research under Contract No. AFOSR 91-0117. Grateful appreciation is expressed for this support.

TABLE OF CONTENTS

Page

1. INTRODUCTION TO INSTABILITY 1

1.1 Significance of Instability in Soils 1

1.2 Instability of Granular Materials 2

1.3 Stability Postulates 2

1.4 Consequences of Nonassociated Flow 4

1.5 Nonassociated Flow in Granular Materials 8

1.6 Instability in Drained Triaxial Compression Under Low Confining Pressures 12

1.7 Instability in Undrained Triaxial Compression Under Low Confining Pressures 14

1.8 Conditions of Instability 16

1.9 Location of the Region of Instability 17

1.10 Needs for High Pressure Testing 19

1.11 Evolved Research Goals 21

2. LITERATURE REVIEW 24

2.1 Review of Prior Investigations at High Pressures and Particle Breakage 24

2.2 Review of Prior Investigations Involving Extension Testing on Granular Materials 37

3. EXPERIMENTAL PROCEDURES 46

3.1 UCLA High Pressure Testing Facility 46

3.2 Modifications to Existing Testing Equipment and Software . . 49

3.3 Granular Materials Used for Testing and Test Specimen Preparation 50

3.4 Membranes and O-Rings 52

3.5 Lubricated Ends 53

3.6 Saturation 57

3.7 Membrane Penetration 58

3.8 Detailed Testing Procedures for Triaxial Compression Tests . 60

3.9 Detailed Testing Procedures for Triaxial Extension Tests . . . 67

4. STRAIN LOCALIZATION AND NONUNIFORM STRAINS 73

4.1 Introduction 73

4.2 Desirability of Maintaining Uniform Strains in Soil Testing . . 73

4.3 Review of Strain Localization in Low Pressure Triaxial Compression 74

4.4 Observations in High Pressure Triaxial Compression Tests 76

4.5 Review of Strain Localization in Low Pressure Triaxial Extension 78

4.6 Observations in Conventional High Pressure Triaxial Extension Tests 81

4.6.1 Observations from Conventional Drained Extension Tests 82

4.6.2 Observations from Undrained Strain Localized Extension Tests 91

4.7 Progression of Strain Localization at High Pressures 97

4.8 Enforcing Uniform Strains in Triaxial Extension 105

4.9 Comparison of Uniform Strain and Conventional Extension Tests 111

4.10 Discussion 130

5. STRESS-STRAIN BEHAVIOR IN TRIAXIAL COMPRESSION AND EXTENSION AT HIGH PRESSURES 134

5.1 Triaxial Compression Tests 134

5.2 Results from Drained Triaxial Compression Tests 135

5.3 Results from Undrained Triaxial Compression Tests 151

5.4 Discussion of Triaxial Compression Tests 158

5.5 Triaxial Extension Tests 167

5.6 Results from Drained Uniform Strain Extension Tests 172

5.7 Results from Undrained Uniform Strain Extension Tests 180

5.8 Comparisons Between Extension and Compression Tests . . . 185

5.9 Repeatability and Experimental Scatter 200

6. SOIL INSTABILITY IN TRIAXIAL COMPRESSION AND EXTENSION AT HIGH PRESSURES 206

6.1 Instability of Soils at High Pressures 206

6.2 Location of Instability Region at High Pressures 206

6.3 Instability Test Procedures 214

6.4 Results of Triaxial Compression Instability Tests 217

6.5 Results of Triaxial Extension Instability Tests 229

6.6 Discussion 240

7. THE B-VALUE, THE EFFECTIVE STRESS PRINCIPLE, AND STRAIN RATE EFFECTS AT HIGH CONFINING PRESSURE 243

7.1 Introduction 243

7.2 Soil and Testing Procedures 245

7.3 Tests to Determined B-Values at High Confining Pressure . . . 246

7.4 B-Value Predictions 254

7.5 The Effective Stress Principle at High Pressures 255

7.6 Previous Studies of Strain Rate Effects in Cohesionless Soils 259

7.7 Strain Rate Effects in Undrained Triaxial Compression Tests 261

7.8 Strain Rate Effects in Drained Triaxial Compression Tests 268

7.9 Grain Size Analysis 282

7.10 Conclusions 284

8. PARTICLE BREAKAGE AT HIGH PRESSURES 287

8.1 Introduction 287

8.2 Measures of Particle Breakage 287

8.3 Factors Affecting Particle Breakage 290

8.4 Reasons to Quantify Crushing 291

8.5 Observations at High Pressures 293

8.6 Discussion of Different Crushing Parameters 305

8.7 Effects of Particle Crushing on Stress-Strain Behavior 312

8.8 Particle Breakage Factors Correlated with Energy 314

8.9 Evaluation of Particle Breakage on a Grain Level 316

8.10 Using the B_{10} Particle Breakage Factor to Obtain Permeability 324

8.11 Effect of Strain Localization on Particle Breakage 329

8.12 Conclusions 336

9. ONE-DIMENSIONAL COMPRESSION TESTING AND ELASTIC PARAMETERS 338

9.1 Introduction 338

9.2 One-Dimensional Testing Equipment and Control Software . 338

9.3 One-Dimensional Testing Procedures 343

9.4 Sands Tested and Corrections to Data 345

9.5 Results from One-Dimensional Compression Tests 349

9.6 Appearance of Sheared Specimens 358

9.7 K_o at High Pressures 358

9.8 Elastic Parameters for Cambria Sand 381

9.9 Conclusions 388

10. GENERAL SOIL BEHAVIOR AT HIGH PRESSURES 390

10.1 Introduction 390

10.2 Stress Dilatancy 390

10.3 Observations at High Pressures Regarding Stress-Dilatancy . 393

10.4 Critical State Soil Mechanics 399

10.5 Observations at High Pressures Regarding Critical State . . . 402

10.6 Experimental Results and Correlations with Energy 422

10.7 Discussion 433

11. CONCLUSIONS 437

11.1 Introduction 437

11.2 Strain Localization (Chapter 4) 437

11.3 Stress-Strain Behavior at High Pressure (Chapter 5) 439

11.4 Instability of Soils at High Pressures (Chapter 6) 440

11.5 B-Values, The Effective Stress Principle, and Strain Rate Effects (Chapter 7) 441

11.6 Particle Breakage at High Pressures (Chapter 8) 443

11.7 One-Dimensional Compression Tests and Elastic Parameters (Chapter 9) 445

11.8 General Soil Behavior at High Pressures (Chapter 10) 446

REFERENCES 450

Table of Contents of Appendices 460

Appendix A Equations used in data analysis 462

Appendix B Summary of testing data 467

Appendix C Drained triaxial compression tests 534

Appendix D Undrained triaxial compression tests 564

Appendix E Drained/undrained stability tests in triaxial compression . . 587

Appendix F Successful drained uniform strain triaxial extension tests . . 593

Appendix G Drained conventional triaxial extension tests 620

Appendix H Drained uniform strain triaxial extension tests with strain localization 644

Appendix I Successful undrained uniform strain triaxial extension tests 659

Appendix J Undrained uniform strain triaxial extension tests with strain localization 665

Appendix K Successful drained/undrained uniform strain stability tests in triaxial extension 674

Appendix L Isotropic compression/B-value tests 679

Appendix M One-dimensional compression tests on three sands 698

Appendix N Drained triaxial compression loading/unloading test 712

LIST OF FIGURES

Page

Figure 1-1 Pattern of yield surfaces for isotropic soils. Stress path for conventional triaxial compression test.(BC) 5

Figure 1-2 Wedge-shaped region of stress paths with decreasing stresses in which soils with nonassociated flow may be unstable during hardening inside the failure surface 7

Figure 1-3 (a) Stress-strain and volume change curves, and (b) stress path and plastic strain increment vectors for test on fine silica sand. 9

Figure 1-4 Evaluation of relative inclinations of yield (f) and plastic potential (g) surfaces along undrained stress path 11

Figure 1-5 Effective stress paths for stress-controlled triaxial compression tests on loose Sacramento River sand 13

Figure 1-6 Stress-strain, volume change, and pore pressure relations in stress-controlled triaxial compression test on loose Sacramento River sand. 15

Figure 1-7 Location of instability line for loose sand 18

Figure 3-1 High pressure testing loading system 47

Figure 3-2 High pressure testing system-process control flow 48

Figure 3-3 Diagram demonstrating effects of cap separation in ext. test 55

Figure 3-4 Extension test experiencing cap separation, deviator stress and volumetric strain, dense Cambria sand 56

Figure 3-5 Membrane penetration effects, isotropic compression test, dense Cambria sand 59

Figure 3-6 Triaxial extension test setup 68

Figure 4-1 Photographs exhibiting test specimens showing uniform strain conditions after 52.0 MPa drained triaxial compression tests. (Top) Inside membranes. (Bottom) Removed from membranes. 79

Figure 4-2 Photographs exhibiting two test specimens showing uniform strain conditions after undrained triaxial compression tests 80

Figure 4-3 Photograph exhibiting test specimen showing strain localization in a drained triaxial extension test 83

Figure 4-4 Stress ratio, 0.25 to 8.0 MPa, conventional drained triaxial extension, dense Cambria sand 84

Figure 4-5 Stress ratio, 17.5 to 68.0 MPa, coventional drained triaxial extension, dense Cambria sand 85

Figure 4-6 Deviator stress, 0.25 to 8.0 MPa, conventional drained triaxial extension, dense Cambria sand 86

Figure 4-7 Deviator stress, 17.5 to 68.0 MPa, conventional drained triaxial extension, dense Cambria sand 87

Figure 4-8 Volumetric strain, 0.25 to 8.0 MPa, conventional drained triaxial extension, dense Cambria sand 89

Figure 4-9 Volumetric strain, 17.5 to 68.0 MPa, conventional drained triaxial extension, dense Cambria sand 90

Figure 4-10 Effective stress ratio, strain localized undrained triaxial extension, dense Cambria sand 92

Figure 4-11 Deviator stress, strain localized undrained triaxial extension, dense Cambria sand 93

Figure 4-12 Effective stress path, Cambridge p'-q, strain localized undrained triaxial extension, dense Cambria sand 95

Figure 4-13 Pore pressure, strain localized undrained triaxial extension, dense Cambria sand 96

Figure 4-14 Area ratio: strain localization, conventional drained triaxial extension, dense Cambria sand 98

Figure 4-15 Stress ratio at 17.5 MPa, several different drained extension tests, dense Cambria sand 100

Figure 4-16 Diagram showing compression tests is a stable test 102

Figure 4-17 Diagram showing tension tests is an unstable test 103

Figure 4-18 Method using plates for enforcing uniform strains in extension 108

Figure 4-19 Photographs showing specimen assembly process with plates to enforce uniform strains in extension. (Top) First layer of plates. (Bottom) Final specimen before testing 109

Figure 4-20 Deviator stress and volumetric strain, comparison of conventional & uniform strain extension test at 8.0 MPa . . 112

Figure 4-21 Deviator stress and volumetric strain, comparison of conventional, uniform strain, & uniform strain tests with plate friction at 12.0 MPa 113

Figure 4-22 Deviator stress and volumetric strain, comparison of conventional, uniform strain, & uniform strain tests with plate friction at 17.5 MPa 114

Figure 4-23 Deviator stress and volumetric strain, comparison of conventional, uniform strain, & uniform strain tests with plate friction at 26.0 MPa 115

Figure 4-24 Deviator stress and volumetric strain, comparison of conventional, uniform strain, & uniform strain tests with plate friction at 35.0 MPa 116

Figure 4-25 Deviator stress and volumetric strain, comparison of conventional & uniform strain extension test at 52.0 MPa . 117

Figure 4-26 Deviator stress and pore pressure, comparison of strain localized & uniform strain undrained extension tests at 12.0 MPa 120

Figure 4-27 Effective stress path, Cambridge p'-q, comparison of strain localized & uniform strain undrained extension tests at 12.0 MPa 121

Figure 4-28 Deviator stress and pore pressure, comparison of strain localized & uniform strain undrained extension tests at 17.6 MPa 122

Figure 4-29 Effective stress path, Cambridge p'-q, comparison of strain localized & uniform strain undrained extension tests at 17.6 MPa 123

Figure 4-30 Deviator stress and pore pressure, comparison of strain localized & uniform strain undrained extension tests at 26.0 MPa 124

Figure 4-31 Effective stress path, Cambridge p'-q, comparison of strain localized & uniform strain undrained extension tests at 26.0 MPa 125

Figure 4-32 Deviator stress and pore pressure, comparison of strain localized & uniform strain undrained extension tests at 52.0 MPa 126

Figure 4-33 Effective stress path, Cambridge p'-q, comparison of strain localized & uniform strain undrained extension tests at 52.0 MPa 127

Figure 4-34 Mohr-Coulomb secant friction angles, drained and undrained extension tests with and without strain localization on dense Cambria sand 129

Figure 4-35 Comparison of volumetric strain at failure, conventional and uniform strain extension tests, dense Cambria sand . . 131

Figure 4-36 Comparison of principal strain at failure, all conventional and uniform strain extension tests, dense Cambria sand . . 132

Figure 5-1 Effective stress ratio, 2.1 to 11.5 MPa, drained triaxial compression, dense Cambria sand 136

Figure 5-2 Effective stress ratio, 15.0 to 52.0 MPa, drained triaxial compression, dense Cambria sand 137

Figure 5-3 Effective stress ratio, 12.0 to 52.0 MPa, drained triaxial compression, dense quartz sand 138

Figure 5-4 Deviator stresses, 2.1 to 11.5 MPa, drained triaxial compression, dense Cambria sand 139

Figure 5-5 Deviator stresses, 15.0 to 52.0 MPa, drained

triaxial compression, dense Cambria sand 140

Figure 5-6 Deviator stresses, 12.0 to 52.0 MPa, drained triaxial compression, dense quartz sand 141

Figure 5-7 Volumetric strain, 2.1 to 11.5 MPa, drained triaxial compression, dense Cambria sand 142

Figure 5-8 Volumetric strain, 15.0 to 52.0 MPa, drained triaxial compression, dense Cambria sand 143

Figure 5-9 Volumetric strain, 12.0 to 52.0 MPa, drained triaxial compression, dense quartz sand 144

Figure 5-10 Effective stress ratio and volumetric strain, buckling, slippage, and effect of height-to-diameter ratio, 52.0 MPa drained triaxial compression tests 150

Figure 5-11 Effective stress ratio, 6.4 to 68.9 MPa, undrained triaxial compression, dense Cambria sand 152

Figure 5-12 Deviator stress, 6.4 to 68.9 MPa, undrained triaxial compression, dense Cambria sand 153

Figure 5-13 Pore pressure, 6.4 to 68.9 MPa, undrained triaxial compression, dense Cambria sand 155

Figure 5-14 Effective stress path, Cambridge p'-q, 6.4 to 68.9 MPa, undrained triaxial compression, dense Cambria sand 157

Figure 5-15 Rate of dilation at failure, drained triaxial compression, dense Cambria sand 159

Figure 5-16 Volumetric strain at failure, drained triaxial compression, dense Cambria sand and quartz sand 161

Figure 5-17 Major principal strain at failure, drained and undrained triaxial compression, dense Cambria sand and quartz sand 163

Figure 5-18 Mohr-Coulomb secant friction angles, drained and undrained compression, dense Cambria sand and quartz sand 165

Figure 5-19 Void ratio at failure, drained and undrained triaxial

compression tests, dense Cambria sand 168

Figure 5-20 Extension Connector 170

Figure 5-21 Extension Test 171

Figure 5-22 Effective stress ratio, 0.25 to 12.0 MPa, drained triaxial extension, dense Cambria sand 173

Figure 5-23 Effective stress ratio, 14.5 to 52.0 MPa, drained triaxial extension, dense Cambria sand 174

Figure 5-24 Deviator stress, 0.25 to 12.0 MPa, drained triaxial extension, dense Cambria sand 176

Figure 5-25 Deviator stress, 14.5 to 52.0 MPa, drained triaxial extension, dense Cambria sand 177

Figure 5-26 Volumetric strain, 0.25 to 12.0 MPa, drained triaxial extension, dense Cambria sand 178

Figure 5-27 Volumetric strain, 14.5 to 52.0 MPa, drained triaxial extension, dense Cambria sand 179

Figure 5-28 Effective stress ratio, 12.0 to 52.0 MPa, Undrained triaxial extension, dense Cambria sand 181

Figure 5-29 Deviator stress, 12.0 to 52.0 MPa, Undrained triaxial extension, dense Cambria sand 183

Figure 5-30 Pore pressure, 12.0 to 52.0 MPa, Undrained triaxial extension, dense Cambria sand 184

Figure 5-31 Effective stress paths, Cambridge p'-q, 12.0 to 52.0 MPa, Undrained triaxial extension, dense Cambria sand 186

Figure 5-32 Major principal strain at failure, drained and undrained compression and extension, dense Cambria and quartz sand 187

Figure 5-33 Hardin's relative crushing, drained triaxial compression and extension, dense Cambria sand 189

Figure 5-34 Volumetric strain at failure, drained and undrained compression and extension, dense Cambria and quartz sand 191

Figure 5-35 Rate of dilation at failure, drained triaxial compression and extension, dense Cambria sand 193

Figure 5-36 Mohr-Coulomb secant friction angles, drained triaxial compression and extension, dense Cambria sand 195

Figure 5-37 Mohr-Coulomb secant friction angles, undrained triaxial compression and extension, dense Cambria sand 197

Figure 5-38 Void ratio at failure, drained and undrained compression and extension, dense Cambria sand 199

Figure 5-39 5.85 and 17.23 MPa drained tests, repeatability in drained triaxial compression, dense Cambria sand 201

Figure 5-40 16.7 and 34.0 MPa undrained tests, repeatability in undrained triaxial compression, dense Cambria sand 202

Figure 6-1 Instability lines and failure lines, Cambridge p'-q, undrained triaxial compression and extension, dense Cambria sand 208

Figure 6-2 Instability lines from maximum deviator stresses from undrained compression and extension tests, dense Cambria sand 209

Figure 6-3 Temporary instability zone, low pressure undrained compression tests, dense Cambria sand 210

Figure 6-4 Temporary instability zone, low pressure undrained extension tests, dense Cambria sand 213

Figure 6-5 Instability and temporary instability region, Cambridge p'-q, undrained triaxial compression, dense Cambria sand 215

Figure 6-6 Instability and temporary instability region, Cambridge p'-q, undrained triaxial extension, dense Cambria sand 216

Figure 6-7 Instability tests inside instability region, Cambridge p'-q,

drained-undrained stability compression tests
dense Cambria sand 219

Figure 6-8 Pore pressure, drained-undrained compression stability
test, dense Cambria sand 220

Figure 6-9 Deviator stress, drained-undrained compression stability
test, dense Cambria sand 221

Figure 6-10 Effective stress ratio, drained-undrained
compression stability test, dense Cambria sand 223

Figure 6-11 Volumetric strains, drained-undrained
compression stability test, dense Cambria sand 224

Figure 6-12 Instability tests creeping into instability region,
Cambridge p'-q, drained-undrained stability
compression tests, dense Cambria sand 225

Figure 6-13 Point of instability, drained-undrained compression
stability test, dense Cambria sand 227

Figure 6-14 Point of instability, drained-undrained compression
stability test, dense Cambria sand 228

Figure 6-15 Instability tests within instability region,
Cambridge p'-q, drained-undrained
stability extension tests, dense Cambria sand 231

Figure 6-16 Deviator stress, drained-undrained extension
stability tests, dense Cambria sand 232

Figure 6-17 Pore pressure, drained-undrained extension
stability tests, dense Cambria sand 233

Figure 6-18 Effective stress ratio, drained-undrained extension
stability tests, dense Cambria sand 234

Figure 6-19 Volumetric strains, drained-undrained extension
stability tests, dense Cambria sand 235

Figure 6-20 Instability tests creeping into instability region,
Cambridge p'-q, drained-undrained stability

extension tests, dense Cambria sand 237

Figure 6-21 Point of instability, drained-undrained extension stability test, dense Cambria sand 238

Figure 6-22 Point of instability, drained-undrained extension stability test, dense Cambria sand 239

Figure 7-1 Isotropic compression and unloading with enlarged individual test locations of B-value tests, dense Cambria sand 247

Figure 7-2 Variation in B-values during individual B-value test at 12.0 MPa effective confining pressure, dense Cambria sand 249

Figure 7-3 Variation of Measured and Projected B-values over different confining pressure, dense Cambria sand 250

Figure 7-4 Experimental and predicted B-values for reloading and unloading conditions, dense Cambria sand 252

Figure 7-5 Volumetric compressibilities of virgin isotropic compression, reloading and unloading conditions for dense Cambria sand 253

Figure 7-6 Effective stress paths, Cambridge p'-q, for different total stress paths, and different expected directions at 34.0 MPa confining pressure, dense Cambria sand 256

Figure 7-7 Deviator stress, undrained triaxial compression tests at different strain rates, initial effective confining pressure 34.0 MPa 263

Figure 7-8 Pore pressure, undrained triaxial compression tests at different strain rates, initial effective confining pressure 34.0 MPa 264

Figure 7-9 Effective stress path, Cambridge p'-q, undrained triaxial compression tests at different strain rates, initial effective confining pressure 34.0 MPa 265

Figure 7-10 Deviator stress, undrained triaxial compression tests at different strain rates, initial effective confining pressure 34.0 MPa 267

Figure 7-11 Effective stress ratio, undrained triaxial compression tests at different strain rates, initial effective confining pressure 34.0 MPa 269

Figure 7-12 Effective stress ratio, undrained triaxial compression tests at different strain rates, initial effective confining pressure 34.0 MPa 270

Figure 7-13 Axial strain to stress ratio, undrained triaxial compression tests at different strain rates, initial effective confining pressure 34.0 MPa 271

Figure 7-14 Effective confining pressure, undrained triaxial compression tests at different strain rates, initial effective confining pressure 34.0 MPa 272

Figure 7-15 Deviator stress, drained triaxial compression tests at different strain rates, 17.2 MPa initial effective confining pressure 275

Figure 7-16 Volumetric strain, drained triaxial compression tests at different strain rates, 17.2 MPa initial effective confining pressure 276

Figure 7-17 Deviator stress, drained triaxial compression tests at different strain rates, 17.2 MPa initial effective confining pressure 277

Figure 7-18 Volumetric strain at failure, drained triaxial compression tests at different strain rates, 17.2 MPa initial effective confining pressure 279

Figure 7-19 Axial strain at failure, drained triaxial compression tests at different strain rates, 17.2 MPa initial effective confining pressure 280

Figure 7-20 Grain size analysis, drained and undrained compression tests at different strain rates, dense Cambria sand 283

Figure 8-1 Definitions of particle breakage factors by Marsal, Lee & Farhoumand, and Hardin 289

Figure 8-2 Grain size distribution curves, drained triaxial

compression tests, dense Cambria sand 294

Figure 8-3 Grain size distribution curves, undrained triaxial compression tests, dense Cambria sand 295

Figure 8-4 Grain size distribution curves, drained triaxial extension tests, dense Cambria sand 296

Figure 8-5 Grain size distribution curves, undrained triaxial extension tests, dense Cambria sand 297

Figure 8-6 Marsal's particle breakage factor B related to p', drained and undrained triaxial compression and extension tests, dense Cambria sand 300

Figure 8-7 Hardin's relative breakage B_r related to p', drained and undrained triaxial compression and extension tests, dense Cambria sand 301

Figure 8-8 Lee & Farhoumand's D_{15} ratio breakage factor related to p', drained and undrained triaxial compression and extension tests, dense Cambria sand 302

Figure 8-9 $(1-D_{15f}/D_{15i})$ breakage factor related to p', drained and undrained triaxial compression and extension tests, dense Cambria sand 303

Figure 8-10 Effect of stress path on particle breakage between drained and undrained tests, dense Cambria sand 306

Figure 8-11 Marsal's particle breakage factor B related to void ratio, drained and undrained triaxial compression and extension tests, dense Cambria sand 307

Figure 8-12 Hardin's relative breakage factor B_r related to void ratio, drained and undrained triaxial compression and extension tests, dense Cambria sand 308

Figure 8-13 Lee & Farhoumand's D_{15} ratio breakage factor related to void ratio, drained and undrained triaxial compression and extension tests, dense Cambria sand . . . 309

Figure 8-14 $(1-D_{15f}/D_{15i})$ breakage factor related to void ratio,

drained and undrained triaxial compression
and extension tests, dense Cambria sand 310

Figure 8-15 Marsal's particle breakage factor B related to energy,
drained and undrained triaxial compression
and extension tests, dense Cambria sand 317

Figure 8-16 Hardin's relative breakage factor B_r related to energy,
drained and undrained triaxial compression
and extension tests, dense Cambria sand 318

Figure 8-17 Lee & Farhoumand's D_{15} ratio breakage factor related to energy,
drained and undrained triaxial compression
and extension tests, dense Cambria sand 319

Figure 8-18 $(1-D_{15f}/D_{15i})$ breakage factor related to energy,
drained and undrained triaxial compression
and extension tests, dense Cambria sand 320

Figure 8-19 Photograph of thin-sections of Cambria sand
before and after shearing 322

Figure 8-20 Photograph of thin-sections of quartz sand
before and after shearing 323

Figure 8-21 Actual B_{10} crushing curve with hyperbolic prediction,
drained and undrained triaxial compression and
extension tests, dense Cambria sand 326

Figure 8-22 Predicted permeability on a drained triaxial
compression test from energy and Hazen
permeability equation dense Cambria sand 328

Figure 8-23 Grain size curves and hyperbolic modelled
predictions for some drained triaxial
compression tests, dense Cambria sand 330

Figure 8-24 Marsal's breakage factor B, effect of strain localization
on crushing curve, extension tests on dense Cambria sand 332

Figure 8-25 Hardin's relative breakage factor B_r, effect of strain
localization on crushing curve, extension tests
on dense Cambria sand 333

Figure 8-26 Lee & Farhoumand's D_{15}breakage factor, effect of strain localization on crushing curve, extension tests on dense Cambria sand 334

Figure 8-27 B_{10} breakage factor, effect of strain localization on crushing curve, extension tests on dense Cambria sand 335

Figure 9-1 Soil containment cell, one-dimensional compression tests . . 340

Figure 9-2 Piston adapter, one-dimensional compression tests 341

Figure 9-3 One-dimensional compression testing system, assembled apparatus, strain gage locations, and specimen 342

Figure 9-4 *Loading system stiffness displacment correction* curve, one-dimensional compression test 347

Figure 9-5 Axial stress vs. axial strain, one-dimensional compression tests, Cambria sand 350

Figure 9-6 Axial stress vs. axial strain, one-dimensional compression tests, quartz sand 351

Figure 9-7 Axial stress vs. axial strain, one-dimensional compression tests, Sacramento River sand 352

Figure 9-8 Void ratio vs. axial stress, one-dimensional compression tests, Cambria sand a. semilog scale b. linear scale 354

Figure 9-9 Void ratio vs. axial stress, one-dimensional compression tests, quartz sand 355

Figure 9-10 Void ratio vs. axial stress, one-dimensional compression tests, Sacramento River sand 356

Figure 9-11 Photograph of thin-section showing Cambria sand after shearing, one-dimensional compression test 359

Figure 9-12 Photograph of thin-section showing quartz sand after shearing, one-dimensional compression test 360

Figure 9-13 Results of numerical analysis, circumferential strain

vs. height of specimen, one-dimensional compression test . 363

Figure 9-14 Total stress K_o vs. axial stress, one-dimensional compression tests, Cambria sand 365

Figure 9-15 Total stress K_o vs. axial stress, one-dimensional compression tests, quartz sand 366

Figure 9-16 Total stress K_o vs. axial stress, one-dimensional compression tests, Sacramento River sand 367

Figure 9-17 Incremental stress K_o vs. axial stress, one-dimensional compression tests, Cambria sand 371

Figure 9-18 Incremental stress K_o vs. axial stress, one-dimensional compression tests, quartz sand 372

Figure 9-19 Incremental stress K_o vs. axial stress, one-dimensional compression tests, Sacramento River sand 373

Figure 9-20 Total stress K_o vs. void ratio, one-dimensional compression tests, Cambria sand 374

Figure 9-21 Total stress K_o vs. void ratio, one-dimensional compression tests, quartz sand 375

Figure 9-22 Total stress K_o vs. void ratio, one-dimensional compression tests, Sacramento River sand 376

Figure 9-23 Radial stress vs. axial stress, one-dimensional compression tests, Cambria sand 378

Figure 9-24 Radial stress vs. axial stress, one-dimensional compression tests, quartz sand 379

Figure 9-25 Radial stress vs. axial stress, one-dimensional compression tests, Sacramento River sand 380

Figure 9-26 Deviator stress vs. strain, loading-unloading-reloading test for determination of elastic parameters dense Cambria sand 383

Figure 9-27 Volumetric strain vs. strain, loading-unloading-reloading test for determination of elastic parameters dense Cambria sand 384

Figure 9-28 Elastic modulus, loading-unloading-reloading test for determination of elastic parameters dense Cambria sand 385

Figure 9-29 Poisson's ratio, loading-unloading-reloading test for determination of elastic parameters dense Cambria sand 386

Figure 9-30 Elastic K_o and Jaky's K_o, loading-unloading-reloading test for determination of elastic parameters dense Cambria sand 387

Figure 10-1 Dilatancy corrected friction angles using Bishop's method, drained triaxial compression and extension tests on dense Cambria sand 395

Figure 10-2 Dilatancy corrected friction angles using Rowe's method, drained triaxial compression and extension tests on dense Cambria sand 397

Figure 10-3 Casagrande critical state theory, under shearing loose sands compress and dense sands dilate to critical density (Casagrande, 1940) 400

Figure 10-4 Rutledge hypothesis, normally consolidated clays indicate parallel strength and consolidation lines (from Rutledge, 1947) 401

Figure 10-5 Roscoe, Schofield, and Wroth critical state theory, drained and undrained tests on Weald clay, Upper diagram shows critical state line on p'-q diagram, lower diagram indicates unique critical void ratio line (from Roscoe, et al, 1958) 403

Figure 10-6 Seed and Lee critical state theory, left diagrams show drained tests with zero volumetric strain at failure, right diagrams show undrained tests with confining pressure at failure, both appear on critical void ratio line. (from Seed and Lee, 1967) 404

Figure 10-7 Problem of evaluation of critical void ratio at high pressures, critical state soil mechanics, drained triaxial compression tests, four densities of Sacramento River sand 407

Figure 10-8 Problem of evaluation of critical confining pressure at high pressures, critical state soil mechanics, drained triaxial compression tests, four densities of Sacramento River sand 408

Figure 10-9 Critical void ratio lines, critical state in drained and undrained triaxial compression, dense Cambria sand . 410

Figure 10-10 q/p' vs. rate of dilation at failure, drained triaxial compression and extension, dense Cambria sand 411

Figure 10-11 Effective stress path, Cambridge p'-q, drained triaxial compression and extension, dense Cambria sand 412

Figure 10-12 Effective stress path, Cambridge p'-q, undrained triaxial compression and extension, dense Cambria sand 413

Figure 10-13 Void ratio related to stress, drained and undrained triaxial compression tests, Sacramento River sand (from Lee, 1965) 415

Figure 10-14 Void ratio vs. stress, different tests on Cambria sand 417

Figure 10-15 Void ratio vs. stress, different tests on quartz sand 420

Figure 10-16 Void ratio vs. energy at failure, drained and undrained triaxial compression tests, Sacramento River sand (from Lee, 1965) 424

Figure 10-17 Void ratio vs. energy at failure, different tests on Cambria sand 425

Figure 10-18 Maximum deviator stress vs. energy, drained and undrained triaxial compression, Sacramento River sand (from Lee, 1965) 427

Figure 10-19 Maximum deviator stress vs. energy at failure, drained and undrained triaxial compression,

dense Cambria sand 428

Figure 10-20 Breakdown of total energy to failure, drained and undrained triaxial compression tests, dense Cambria sand . 431

Figure 10-21 Breakdown of total energy to failure, drained and undrained triaxial extension tests, dense Cambria sand . . . 432

LIST OF TABLES

Manuscript

Table 7.1 Effects of strain rate variations in undrained triaxial compression tests on dense Cambria sand at 34.0 MPa confining pressure 273

Table 7.2 Effects of strain rate variations in drained compression on dense Cambria sand at 34.0 Mpa confining pressure 281

Appendix B

Table 1 Basic testing parameters in triaxial compression tests 470

Table 2 Basic testing parameters in triaxial extension tests 473

Table 3 Other testing information about triaxial compression tests 477

Table 4 Other testing information about triaxial extension tests 480

Table 5 Summary of results from drained triaxial compression tests . . . 483

Table 6 Summary of results from undrained triaxial compression and other tests 485

Table 7 Summary of results from drained triaxial extension tests 487

Table 8 Summary of results from undrained triaxial extension and other tests 490

Table 9 Void ratios in triaxial compression tests 491

Table 10 Void ratios in triaxial extension tests 494

Table 11 Failure energy in drained triaxial compression tests 497

Table 12 Failure energy in undrained triaxial

compression and other tests 499

Table 13 Failure energy in drained triaxial extension tests 501

Table 14 Failure energy in undrained triaxial extension and other tests 504

Table 15 End of test energy in triaxial compression tests 505

Table 16 End of test energy in triaxial extemsion tests 508

Table 17 Stress-dilatancy in triaxial compression tests 512

Table 18 Stress-dilatancy in triaxial extension tests 514

Table 19 Crushing parameters in triaxial compression tests 516

Table 20 Crushing parameters in triaxial extension tests 519

Table 21 Soil compressibility and B-values 522

Table 22 Derived elastic parameters from test CDLU3 for Cambria sand 523

Table 23 Sieve analyses for drained triaxial compression tests 524

Table 24 Sieve analyses for undrained triaxial compression tests 526

Table 25 Sieve analyses for drained triaxial extension tests 527

Table 26 Sieve analyses for undrained triaxial extension tests 531

Table 27 Sieve analyses for other tests 532

Table 28 Initial gradation of Cambria sand 533

Appendix C

Tables 1 to 29 Tabulation of individual test results for drained triaxial compression 534

Appendix D

Tables 1 to 22 Tabulation of individual test results for undrained triaxial compression 564

Appendix E

Tables 1 to 5 Tabulation of individual test results for drained/undrained stability tests in triaxial compression 587

Appendix F

Tables 1 to 24 Tabulation of individual test results for successful drained uniform strain triaxial extension tests 593

Appendix G

Tables 1 to 22 Tabulation of individual test results for drained conventional triaxial extension tests 620

Appendix H

Tables 1 to 14 Tabulation of individual test results for drained uniform strain triaxial extension tests with strain localization 644

Appendix I

Tables 1 to 5 Tabulation of individual test results for successful undrained uniform strain triaxial extension tests 659

Appendix J

Tables 1 to 8 Tabulation of individual test results for undrained uniform strain triaxial extension tests with strain localization 665

Appendix K

Tables 1 to 4 Tabulation of individual test results for successful drained/undrained uniform strain stability tests in triaxial extension 674

Appendix L

Tables 1 to 3 Tabulation of individual test results for isotropic compression/ B-value tests 679

Appendix M

Tables 1 to 7 Tabulation of individual test results for one-dimensional compression tests on three sands 698

Appendix N

Table 1 Tabulation of individual test results for drained triaxial compression loading/unloading test 712

ABSTRACT OF THE DISSERTATION

Instability and Behavior
of
Granular Materials
at
High Pressures

by

Jerry A. Yamamuro
Doctor of Philosophy in Civil Engineering
University of California, Los Angeles, 1993
Professor Poul V. Lade, Chair

This study presents the results of an extensive experimental investigation of granular materials at high pressures. Among the many types of experiments performed are drained and undrained triaxial compression and extension tests with an overall confining pressure range of 0.25 to 68.9 MPa. One-dimensional compression tests up to 900 MPa axial stress level were also performed.

Strain localization was studied in triaxial extension and it was found that necking initiates at very small strains. A method was developed to enforce uniform strains in cylindrical triaxial extension tests.

Drained and undrained stress-strain behavior from low to high pressures in triaxial extension and compression was examined on the basis of an extensive series of experiments.

Instability of granular materials at high pressures was demonstrated in compression and extension, and the location of the instability line was experimentally shown to coincide with the top of the effective stress path from undrained tests.

Skempton's pore-pressure parameter B was determined at high pressures and also found to be predictable. Strain-rate effects in granular materials at high pressures in drained and undrained conditions were evaluated. The effective-stress principle was experimentally examined at high pressures.

Particle breakage at high pressures was studied, and a correlation with input energy was found. A new particle breakage parameter and an analytical procedure were proposed to allow direct correlations with changes in soil permeability.

One-dimensional compression tests at very high pressures were performed, and these resulted in large reductions in void ratio. Values of K_o, the coefficient of earth pressure at rest, were obtained and found to be constant at high pressures. The elastic modulus and Poisson's ratio were determined at several high-pressure levels.

Correlations of high-pressure soil behavior with stress dilatancy, critical state, and input energy were studied.

CHAPTER 1 - INTRODUCTION TO INSTABILITY

1.1 Significance of Instability in Soils

Instability is defined as the inability to carry or sustain a given load, resulting in large strains that can eventually lead to failure. Instability in saturated, cohesionless soils is a demonstrated phenomenon in which soils may exhibit catastrophic characteristics similar to failure, but well within the established effective stress failure surface. Events triggering instability can be small in magnitude, such as small seismic occurrences, wave action, vibration from machinery, or volumetric creep. Large submarine slope failures, and earth dam failures have been attributed to soil instability. Current geotechnical engineering practice designs on the basis of either total stresses or effective stresses. Total stress analysis tends to be much too conservative, and underestimates the true strength of the soil. Under undrained conditions, effective stress design can significantly overestimate the resistance of cohesionless soil to liquefaction type failures. The condition of soil instability in loose soils is located between the two analysis methods. Therefore, it is very important to study, understand, and be able to predict this behavior, to prevent catastrophic events related to this phenomenon.

1.2 Instability of Granular Materials

When interpreting the results from triaxial tests, there are two commonly utilized criteria to define failure. They are:

1. Maximum stress difference $(\sigma_1 - \sigma_3)_{max}$.
2. Maximum effective principal stress ratio (σ'_1/σ'_3).

During drained tests the two criteria are achieved simultaneously. However, during undrained tests the two criteria do not occur simultaneously. During undrained tests when the soil is volumetrically contractive, the maximum stress difference is reached much earlier than the maximum effective stress ratio. This is caused by a rapid rise in pore pressures. In undrained tests under dilating soil conditions, the maximum deviator stress is reached after the maximum effective stress ratio is reached. Typically, the maximum stress difference is used in total stress analysis and the maximum effective stress ratio is used in effective stress analysis (Seed, et al, 1960; Whitman, 1960).

1.3 Stability Postulates

Stability as formulated by Drucker (1951, 1956, 1959) contains two elements as expressed by plastic work increments.

$$dW_p - dW_p^* = (\sigma_{ij} - \sigma_{ij}^*) \cdot \dot{\epsilon}_{ij}^p \geq 0 \qquad (1.1)$$

$$d^2W_P = \dot{\sigma}_{ij} \bullet \dot{\epsilon}^P_{ij} \geq 0 \qquad (1.2)$$

σ_{ij} - *a stress state on yield surface*
σ^*_{ij} - *a stress state inside yield surface*
$\dot{\sigma}_{ij}$ - *stress increment starting at* σ_{ij}
causing plastic strain increment $\dot{\epsilon}^P_{ij}$

Equation 1.1 is commonly referred to as stability in the large and implies that the yield surface must be convex. Equation 1.2 is referred to as stability in the small, and is fulfilled if the plastic strain increment vector is normal to the yield surface. This implies that the plastic potential surface is identical to the yield surface, so that when yielding occurs, the plastic strain increment is normal to the yield surface. Therefore, Drucker's stability postulates imply associated flow rules, and are applicable for solid metals, which can be reasonably characterized by associated flow.

Equation 1.2 also has often been taken to define stable and unstable behavior. If the condition is satisfied for any stress increment, then the material is unconditionally stable. The material may be conditionally stable, if Equation 1.2 is fulfilled for some stress increments and not for others. The material will be completely unstable, if Equation 1.2 is not satisfied for all possible stress increments. Equation 1.2 is always negative for the condition when the failure surface is reached, and results in complete instability.

Bishop and Hill (1951) and Hill (1958) extended the condition for stability slightly beyond Drucker by expressing it in terms of total strain increments.

$$d^2W_p = \dot{\sigma}^t_{ij} \cdot (\dot{\epsilon}^e_{ij} + \dot{\epsilon}^p_{ij}) - \dot{\sigma}_{ij} \cdot \dot{\epsilon}^e_{ij} + \dot{\sigma}_{ij} \cdot \dot{\epsilon}^p_{ij} \geq 0 \qquad (1.3)$$

$\dot{\epsilon}^t_{ij}$ - *total strain increment*
$\dot{\epsilon}^e_{ij}$ - *elastic strain increment*

Stability postulates developed by Drucker, and by Bishop and Hill provide sufficient conditions to ensure stability. However, theoretical considerations by Mroz (1963) and Mandel (1964) have suggested that they are not necessary considerations for stability.

Experimental evidence from several soils has indicated that conventional associated flow rules consistently overpredict dilation, which is indicated by the condition that the plastic strain increment is not normal to the yield surface. Therefore, proper soil constitutive models need to incorporate nonassociated flow rules, in which there is a separate plastic potential surface, which is not coincidental with the yield surface.

1.4 Consequences of Nonassociated Flow

A typical pattern of yield surfaces for an isotropic soil in the triaxial plane is shown in Figure 1-1. It exhibits in three dimensions, asymmetric tear drop shapes. For isotropic materials the yield surface crosses the hydrostatic axis at right angles, bend smoothly back toward the origin, and cross the failure surface at sharp angles.

Plastic potential surfaces for nonassociated flow are similarly shaped as yield surfaces, except they cross the yield surface. Experimental evidence for granular materials indicate that they are asymmetrically shaped, pointed near the ends, and

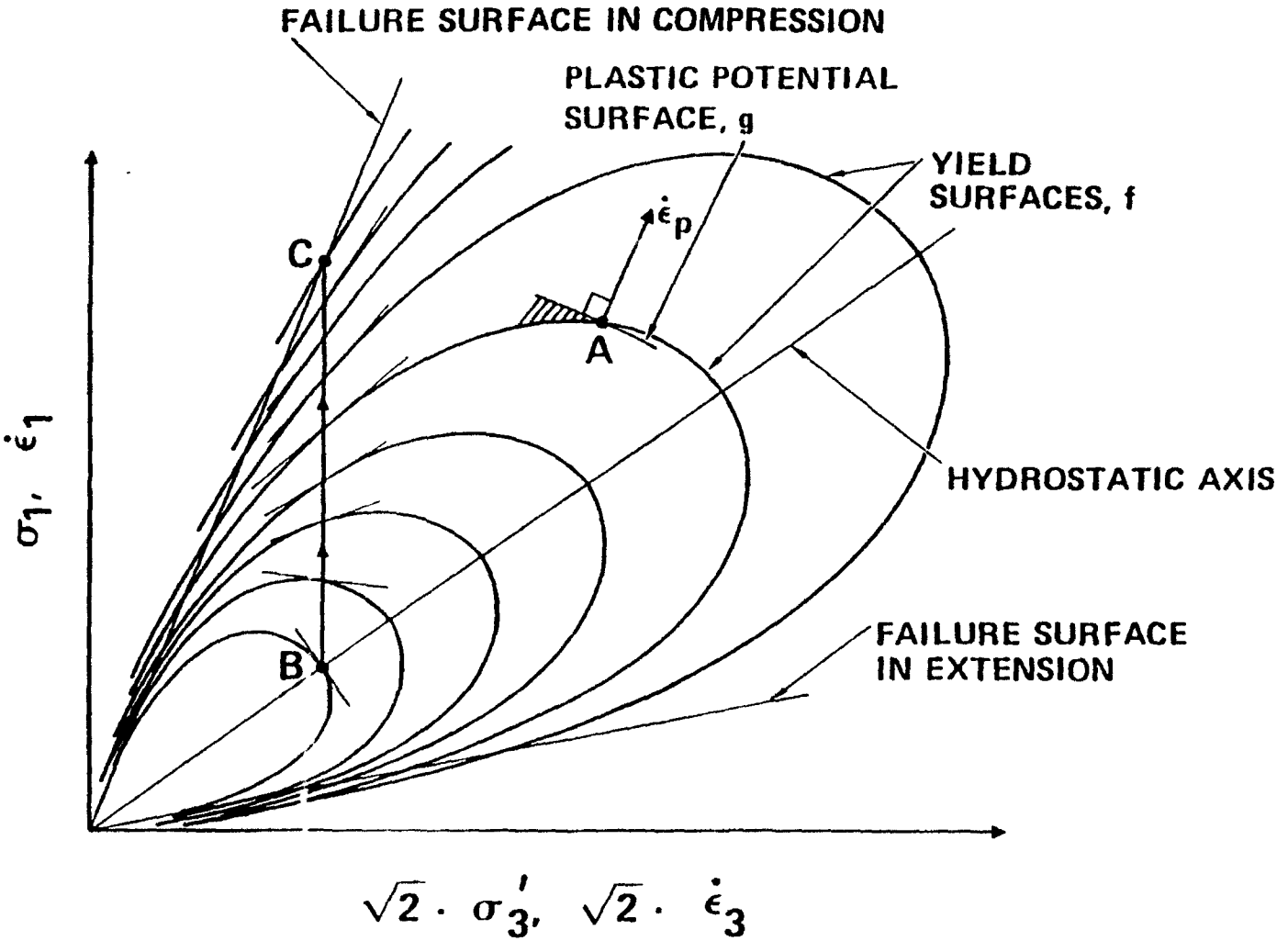

Figure 1-1 Pattern of Yield Surfaces for Isotropic Soils. Stress Path for Conventional Triaxial Compression Test (BC).

shaped like cigars. A typical plastic potential surface is shown crossing the yield surface at point A, on Figure 1-1.

At point A in the shaded wedge region between the yield surface and the plastic potential surface is an area where Equation 1.2 is not fulfilled, since the scalar product is negative. Drucker's stability postulate would indicate that the material could exhibit unstable behavior, since the scalar product is negative. However, drained tests conducted at low pressures clearly indicate that this material is completely stable. The deviator stress can be further increased to produce additional plastic strains without instability occurring.

Instability may occur when the slope of the yield surface is inclined toward the origin. In this condition of loading, plastic strains may occur under decreasing stresses. In other words, inside the failure surface, and under loading conditions, the material may become unstable, and not be able to maintain the current deviator stress. Figure 1-1 shows a typical triaxial compression test. Shearing of the specimen occurs between points B and C (Lade, 1992). As shearing commences, the slope of the yield surface is similar to point A and the material is stable. As the deviator stress increases, the slope changes and starts to point toward the origin, and finally the specimen reaches failure at point C. It is in the region of high deviator stresses before failure, where the yield surface slopes toward the origin, that instability could occur. This region is shown schematically in Figure 1-2 (Lade, 1992).

In this region, and with the condition of nonassociated flow, Equation 1.2 is not satisfied. The shaded wedge area on Figure 1-2 is between the yield surface

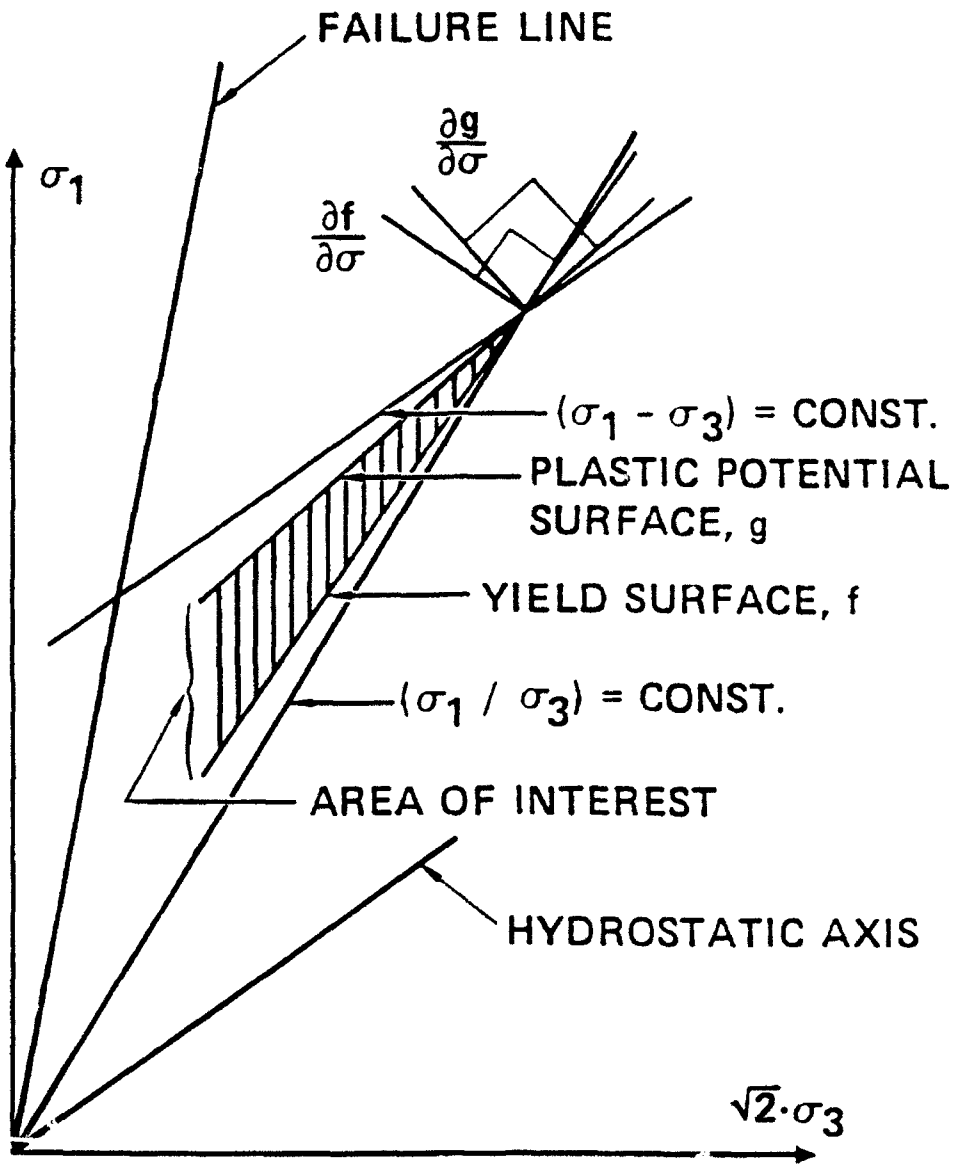

Figure 1-2 Wedge-Shaped Region of Stress Paths with Decreasing Stresses in which Soils with Nonassociated Flow may be Unstable During Hardening Inside the Failure Surface.

and the plastic potential surface. It is located below the line of constant deviator stress, which is parallel to the hydrostatic axis, and above the line of constant principal effective stress ratio. All stresses are decreasing in the region, including deviator stress and confining pressure. However, the principal effective stress ratio is increasing, which indicates a loading condition. The material may become unstable in this region.

1.5 Nonassociated Flow in Granular Materials

Under drained conditions, nonassociated flow is demonstrated in a drained triaxial compression test on fine silica sand as shown in Figure 1-3 (Lade, 1992). A stress path inside the failure surface was followed, under primary loading conditions, but with decreasing deviator stress and confining pressure as shown in Figure 1-3(b). The direction of the plastic strain increment vector is uniquely determined from the state of stress, and is independent of the stress path (Poorooshasb, Holubec, and Sherbourne, 1966, Lade and Duncan, 1976). The stress path is steep enough that it creates an obtuse angle with the plastic strain increment vector. Therefore, Equation 1.2 is violated. Large plastic strains are occurring as shown in Figure 1-3(a) between points B and C. This occurs when the yield surface is being pushed outward, which means that the yield surface has to be steeper than the stress path. If associated flow was being exhibited, then the yield surface would be less steep than the stress path. However, the stress path would be inside the yield surface, and corresponding to elastic unloading. This is not indicated in Figure 1-3(a), which shows large plastic strains.

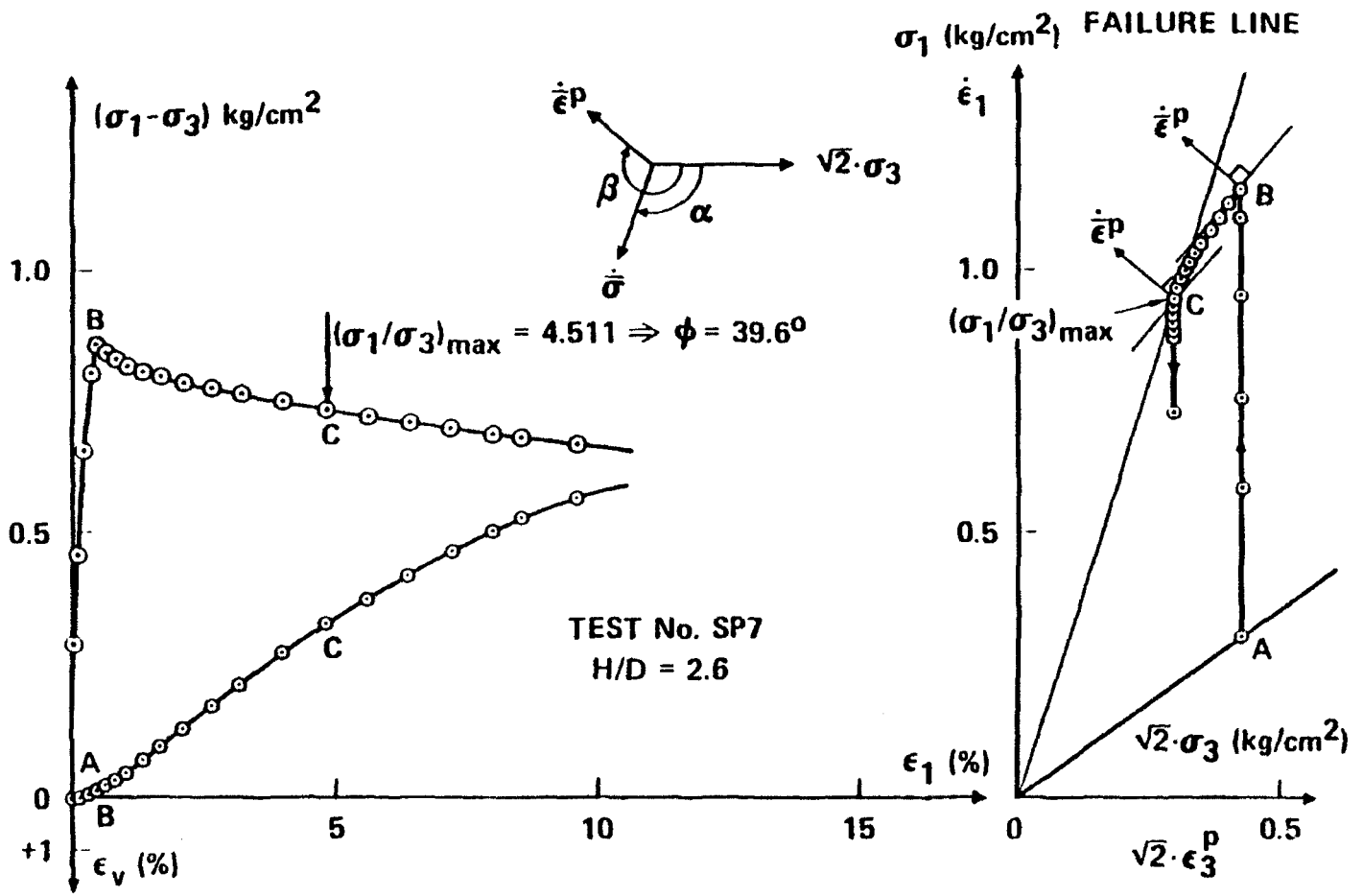

Figure 1-3 (a) Stress-Strain and Volume Change Curves, and (b) Stress Path and Plastic Strain Increment Vectors for Test on Fine Silica Sand.

To demonstrate nonassociated flow and instability under undrained conditions, a typical undrained stress path under high confining pressure is shown in the triaxial plane on Figure 1-4 (Lade, 1992). The strain increments at various points are overlaid on the stress path to evaluate the directions of the plastic potential, which by definition is perpendicular to the plastic strain increment vector directions. Undrained tests have no volumetric strain, which results in the total strain increment vector direction being perpendicular to the hydrostatic axis at all points on the stress path. This is shown on Figure 1-4. The diagram also shows that volumetric compression is indicated by a strain increment vector that points away from the origin, while volumetric dilation indicates a strain increment vector pointing toward the origin. The elastic strain increment vector direction is dependent on the value of Poisson's ratio. Without loss of generality with regard to the final conclusions, it is assumed that the elastic strain increment vector is parallel to the stress increment vector, which corresponds to a value of Poisson's ratio of zero. At the three different points on Figure 1-4, the directions of the plastic strain increment vector are obtained through vectoral subtraction of the elastic strain increment vector from the total strain increment vector. At point A, depending on the relative magnitudes of the total and elastic strain increment vectors, associated flow or nonassociated flow is possible and nonassociated flow is shown on the diagram. Stability is obtained along the stress path until point B is reached. At points B and C nonassociated flow is clearly demonstrated, irrespective of magnitude of the elastic and total strain increments. Even in the limiting case of no elastic strains, the plastic strain increment direction would be

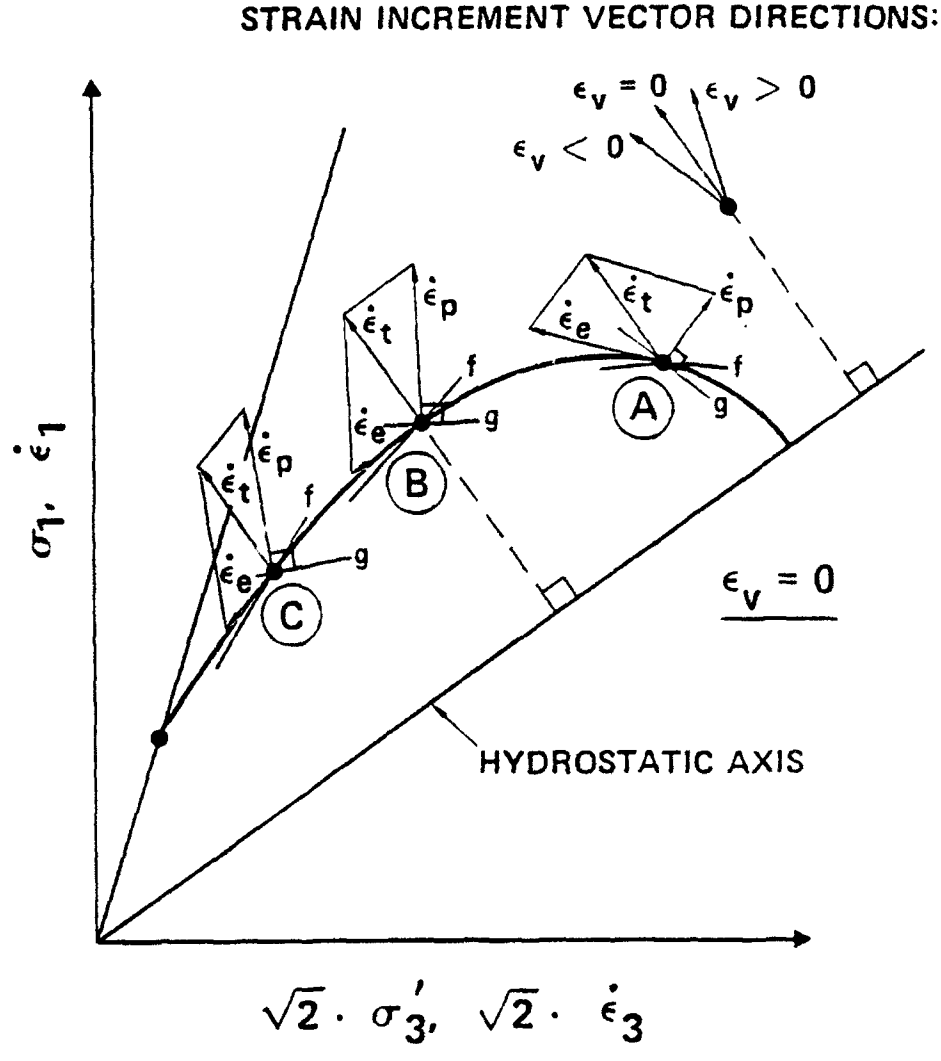

Figure 1-4 Evaluation of Relative Inclinations of Yield (f) and Plastic Potential (g) Surfaces Along Undrained Effective Stress Path.

perpendicular to the hydrostatic axis. This still indicates nonassociated flow, because as shown earlier the yield surface must be steeper than the effective stress path.

1.6 Instability in Drained Triaxial Compression Under Low Confining Pressures

Low pressure, drained, triaxial compression tests were performed to investigate stability in granular materials (Lade, et al, 1987, 1988; Lade and Pradel, 1990). Stress control tests were performed to achieve stress paths as shown in Figure 1-5, which are inside the failure surface. A series of triaxial compression tests were performed under fully drained conditions, and within the region of potential instability, where Equation 1.2 is less than zero. No instability was observed. However, nonassociated flow was again demonstrated. Therefore, Drucker's stability postulate was violated. To investigate whether dilative or compressive volume change tendencies were critical for instability in granular materials, a second series of drained tests was performed on sand which would compress under shearing. Stress paths similar to the first series of tests were followed. Again, Drucker's postulate was violated with stable behavior being observed for all tests.

The following conclusions can be made from these two series of drained tests. Stable behavior is always observed regardless of:

1. The sign of the second increment of work.
2. Whether the volume changes are compressive or dilative.

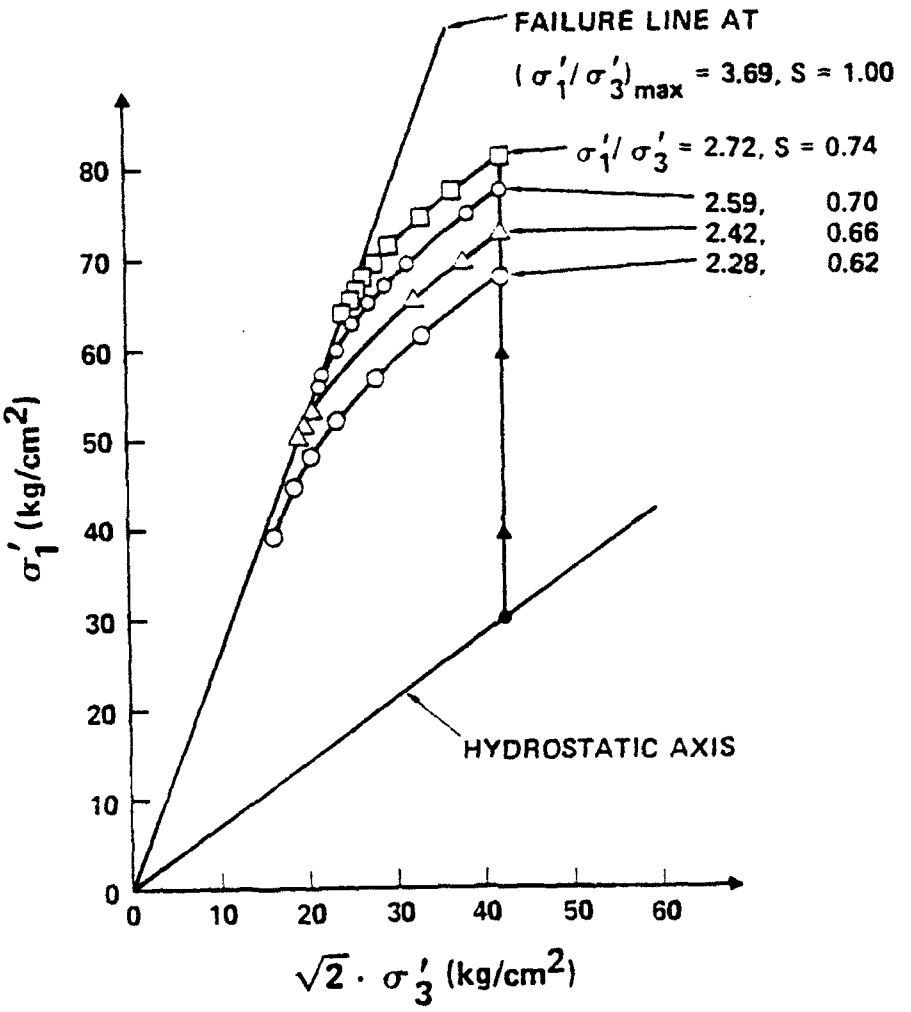

Figure 1-5 Effective Stress Paths for Stress-Controlled Triaxial Compression Tests on Loose Sacramento River Sand.

3. The sign and direction of stress increments.

When located inside the failure surface, in a region of potential instability as defined by Equation 1.2, and under fully drained conditions, instability is not observed. Therefore, Drucker's stability postulate is not a necessary condition for stability.

1.7 Instability in Undrained Triaxial Compression Under Low Confining Pressures

Under undrained conditions, fully saturated soils that tend to compress during shearing may become unstable inside the failure surface, which could lead to a liquefaction type failure. A series of undrained, stress controlled tests were performed on granular material that would compress during shearing (Lade, et al, 1988). Similar stress paths were followed as was shown in Figure 1-2. The actual stress paths are shown on Figure 1-5 (Lade, 1992). Under drained conditions, each test was isotropically consolidated and sheared to a different stress level S, which represents an indication of how close the stress condition is to failure (1.00 being at failure). At this stress level the drainage valve was closed, and in each case instability developed from increasing pore pressures as shown in Figure 1-6. Volumetric creep in a compressive material resulted in pore pressure increase, which in undrained conditions led to the inability of the soil to sustain the vertical load. The large plastic strains along the undrained stress path could not be caused by creep or viscous flow (Lade, et al, 1988). The undrained stress paths again exhibited nonassociated flow, and showed plastic volumetric compression, even

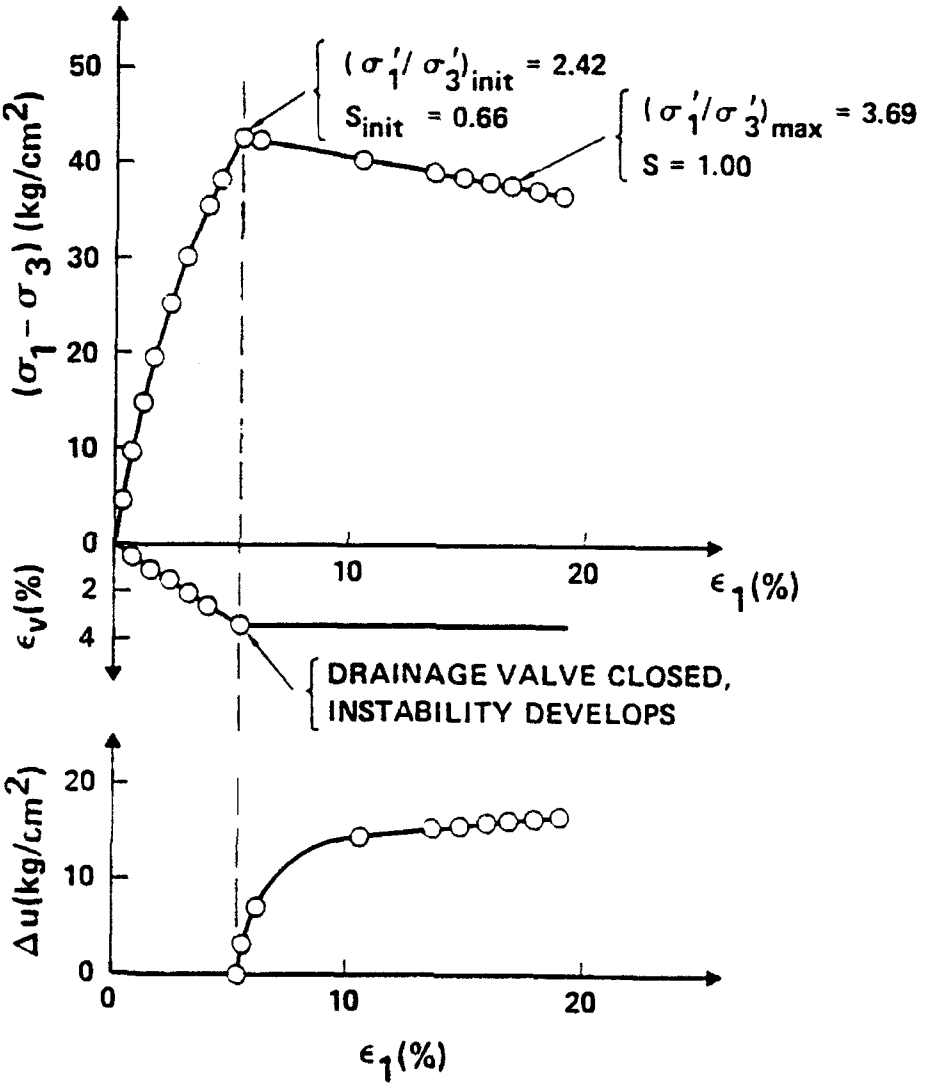

Figure 1-6 Stress-Strain, Volume Change, and Pore Pressure Relations in Stress-Controlled Triaxial Compression Test on Loose Sacramento River Sand.

though total volumetric strain was zero.

The undrained stress paths so far discussed can follow only one direction, when performed on fully saturated specimens. To investigate different stress path directions, a series of tests on unsaturated soils in undrained conditions were performed with decreasing degrees of saturation (Lade and Pradel, 1990). A controlled amount of air was introduced into the specimens to point the stress paths in different directions within the shaded wedge in Figure 1-2. All tests indicated unstable behavior until the degree of saturation is lowered below a certain critical level. Below this level the specimens exhibit stable behavior.

The conclusions are that changing drainage conditions from drained to undrained, and if the material is fully or nearly saturated, then the specimen can demonstrate unstable behavior.

1.8 Conditions of Instability

Arguments and experimental evidence provided by Lade, et al (1987, 1988), and Lade and Pradel (1990) indicate the conditions for unstable behavior for soils that exhibit nonassociated flow. Instability occurs when:

$$\dot{\sigma}_{ij} \cdot \dot{\epsilon}^{c}_{ij} < 0 \qquad (1.4)$$

and

$$\frac{\partial f}{\partial W_p} < 0 \qquad (1.5)$$

which indicates that softening happens after failure. This condition is also implied by Drucker's and Hill's stability conditions.

Equation 1.4 can be combined with the following to obtain instability within the failure surface.

$$\frac{\partial g}{\partial \sigma_{ij}} \cdot \delta_{ij} > 0 \qquad (1.6)$$

δ_{ij} = a vector on the hydrostatic axis.

and

$$\frac{\partial f}{\partial \sigma_{ij}} \cdot \delta_{ij} < 0 \qquad (1.7)$$

Equation 1.6 states the condition of plastic volumetric compression under drained conditions, or a tendency for plastic compression under undrained conditions, when total volumetric strain is zero. Equation 1.7 states the condition that the yield surface must open up in the outward direction of the hydrostatic axis.

In conclusion, the above conditions state that instability is possible in the shaded wedge shown on Figure 1-2, when plastic volumetric strains are compressive or show the tendency for compression under undrained conditions.

1.9 Location of the Region of Instability

Under undrained conditions, the condition of instability may be reached, where the current state of stress cannot be maintained. That stress state corresponds to the top of the current yield surface as shown on Figure 1-7, on

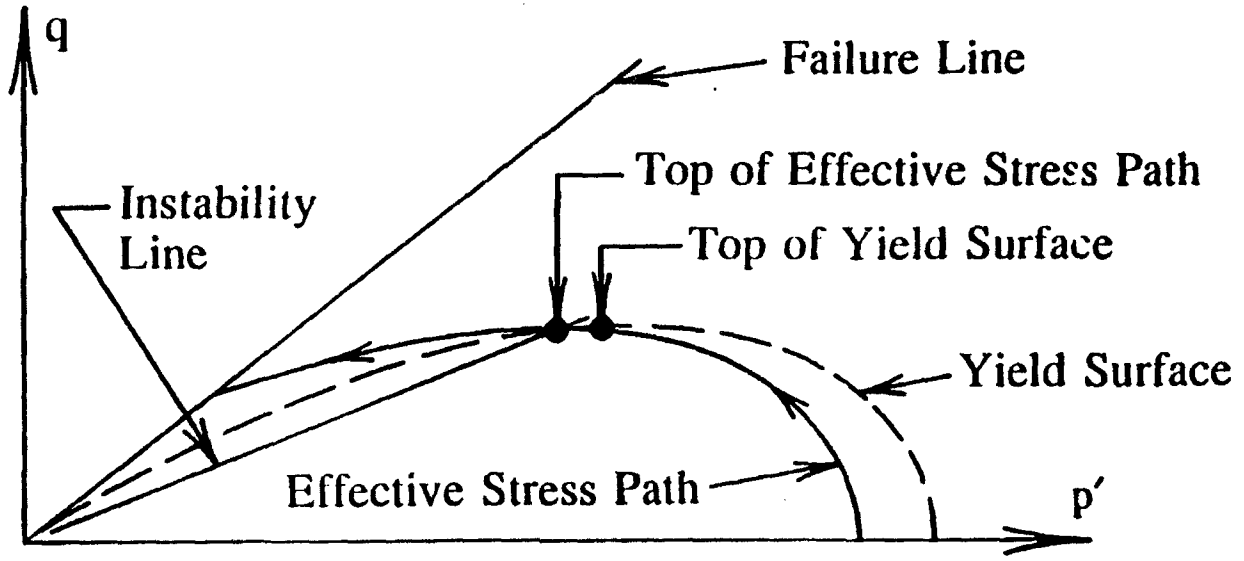

Figure 1-7 Location of Instability Line for Loose Sand.

which the vertical axis represents the stress difference, q, and the horizontal axis represents the effective mean normal stress, p'. Beyond the top point, the soil can deform plastically under decreasing stresses. The top of the effective stress path corresponds to the maximum deviator stress, and occurs slightly after the top of the yield surface, because it includes the effect of the elastic strain energy release, expressed in Equation 1.3. Therefore, a line connecting the tops of the effective stress paths form a lower limit of the instability region for undrained conditions. Experimental evidence indicates that this line is straight, and appears to intersect the origin. The upper limit of the instability region is the drained failure surface.

1.10 Needs for High Pressure Testing

There are several sound reasons to perform testing at higher-than-normal pressures. In the past most of the research performed in the field of soil mechanics has focused on the behavior under low pressures, where most geotechnical problems arise, and these conventional pressures are within the pressure limits of most of the conventional triaxial cells in use. However, there are many practical geotechnical problems that do fall into the category of high pressures. High earth dams, deep mine shafts, and tunnels may have pressures up to 70 kg/cm^2. Deep wells may experience pressures up to 700 kg/cm^2, and soil under the tips of deep driven pile foundations may experience pressures up to 3,500 kg/cm^2, (Murphy, 1987). Pressures that soils experience, when subjected to explosions from conventional or strategic ordnance, are higher yet. Additionally, many geological and seismic concerns focus on pressures deeper

under the surface of the earth. Understanding the behavior of soils under high pressure is fundamental to assisting in the solution to these types of geotechnical engineering and geological problems.

As discussed in the previous section, one of the requirements to achieve instability in granular materials is volumetric compression. This can be achieved by using very loose sands at low confining pressures, or dense soils at high confining pressures. In addition to the fact that the focus of this study is instability in soils, high pressure was selected for the following reasons. Testing very loose soils at low confining pressures creates more experimental scatter than usually observed at high pressures. Small variations in void ratio and effective confining pressure occurring at low pressures and loose soils, can make significant differences in experimental results. However, at high pressures these small variations in void ratio and confining pressure do not make a significant difference in the results. At low pressures anisotropy is a major component in test results that cannot be eliminated. At high pressures the natural anisotropic fabric in the soil, caused from creating a specimen in a gravitational field, is effectively eliminated. True isotropy is possible at high pressures. Another advantage of testing at high pressures is that soil density tends to become uniform at high pressures. Therefore, the assumption of isotropy and uniform density is best achieved at high pressures. At high confining pressures the quantities that are measured (load, pressure, displacement) are much larger, and can more easily be measured, and in conjunction with modern computer control and data aquisition systems, can create a set of highly consistent experimental data.

1.11 Evolved Overall Research Goals

The main goal of this research is to thoroughly examine the stability of granular materials at high confining pressures. Special emphasis was placed in the area of triaxial extension. Other areas of interest include the general behavior of granular soils at high pressures.

The experimental research program included the following basic elements:

1. Modify existing hardware, instrumentation, and control software to accomplish the following.

2. Perform a series of high pressure, drained triaxial compression tests to fully establish the behavior in triaxial compression as a basis of comparison with triaxial extension.

3. Perform a series of high pressure, undrained triaxial compression tests to fully establish the undrained behavior in compression, and the location of the instability line as a basis of comparison with triaxial extension.

4. Perform a series of high pressure, stress control, stability tests in compression as discussed in Section 1.2 to validate findings at low confining pressures, and provide a basis for comparison with tests in triaxial extension.

5. Perform a series of high and low pressure, drained triaxial extension tests to fully establish the behavior in drained extension.

6. Perform a series of high pressure, undrained triaxial extension tests to fully establish the undrained behavior in extension, and the location of the instability line in extension.

7. Perform a series of high pressure, stress control, stability tests as discussed in Section 1.2 in extension to establish instability behavior in extension.

8. Design and fabricate a device to perform one-dimensional co.npression tests at extremely high pressures on smaller specimens to achieve near zero void ratio conditions. Instrument the device with strain gages to indirectly measure lateral soil stresses.

9. Perform a series of one-dimensional compression tests on Cambria sand, quartz sand, and Sacramento River sand.

Overall goals of the experimental program was to provide information that will give insight into the following areas:

1. Establishing the exact shape of the drained and undrained failure

envelopes from low to high pressures for the granular material tested in triaxial compression and extension. This is important for the study of failure criteria.

2. Establishing the validity of nonassociated flow and its consequences in the form of instability in both compression and extension at high pressures.

3. Establishing predictive capability in the area of particle crushing and its correlation with plastic work.

4. Establishing predictive capability in the overall area of instability.

5. Establish general soil behavior at high pressures.

CHAPTER 2 - LITERATURE REVIEW

2.1 Review of Prior Investigations at High Pressures and Particle Breakage

Past research into the area of high pressure testing falls into two broad categories.

1. High pressure testing on rocks.
2. High pressure testing on soils.

The high pressure testing of rocks and minerals has a long history, actually much longer than soils, but will not be covered in this review, since the focus of this research is on soils.

High pressure testing of soils apparently started with Terzaghi and Peck (1948), when they performed confined compression tests (one-dimensional) on sand and sand mica at pressures up to 1,000 kg/cm^2. At high pressures, they were able to obtain displacements similar to those obtained for a normally consolidated clay settlement curve. They attributed these large displacements to grain crushing.

Golder and Ackroyd (1954) performed triaxial compression tests at confining pressures up to 70 kg/cm^2 on soft rock, crushed rock, and sand-clay mixtures. Their results indicated that the Mohr-Coulomb failure envelope was linear from very low pressures. Unfortunately, no stress-strain information or volume change data was included in their results.

Roberts and de Souza (1958) performed confined compression tests on sand and ground quartz, and observed that large displacements occur after a "critical pressure" is applied. They concluded that particle breakage was the main source. The chief factor controlling the "critical pressure" was the initial void ratio.

Hendron (1963) performed confined compression tests on four different sands at vertical pressures up to 230 kg/cm^2, and found that as void ratio decreased, the compressibility of the sand decreased. He also performed cyclic tests and correlated his results with energy dissipation. Later that year he (Hendron, et al 1963) reportedly performed statistical analysis on grain size distributions of the sands before, and after testing, and concluded that particle breakage decreases with increasing specific surface area. Their conclusions also were that as grain size and uniformity increases, the amount of particle crushing increases. Hendron (1963) found that Jaky's equation (Equation 9.4) is not always a good estimate of K_o, the ratio of the effective horizontal stress to the effective vertical stress, and as stresses increase the effect of initial void ratio can be eliminated.

Vesic and Barksdale (1963) performed drained triaxial compression tests on Chattahoochee River sand at confining pressures up to 700 kg/cm^2, and found that the Mohr-Coulomb failure envelope was curved, but past a certain pressure the failure envelope appeared to be straight. They also found that significant amounts of particle breakage had occurred from analyzing the grain size distribution curves.

Hirschfeld and Poulos (1963) performed drained triaxial compression tests on Cannonsville silt and sand at confining pressures up to 40 kg/cm^2, and they

also found that the failure envelope was curved. They attributed this to volume change in the specimen, of which particle breakage was a factor. They used the stress-dilatancy formula developed by Rowe (1962) to remove the dilational component of the friction angle. The following discussion by Rowe (1963) indicated that some of the volume change they experienced may be related to membrane penetration.

Hall and Gordon (1963) performed large-scale (15 and 30 cm. diameter) drained and undrained triaxial compression tests on clayey-sand/gravel and gravel/boulder material for Oroville Dam at confining pressures up to 45 kg/cm^2. Their undrained tests probably cannot be heavily relied upon, because their specimens were not fully saturated, and because membrane penetration occurred in the coarser grained material. However, their drained tests showed a curved Mohr-Coulomb failure envelope, of which the decrease in friction angle was related to particle breakdown, with most of the breakdown occurring during shearing, as opposed to consolidation or placement. Also, they found that well-graded soils have less particle degradation than uniform soils.

Leslie (1963) performed large-scale drained triaxial (30 cm. diameter) compression tests on several gravel materials up to 45 kg/cm^2 confining pressure, and obtained the same conclusions as Hall and Gordon.

Bishop, Webb, and Skinner (1965) performed drained and undrained triaxial compression tests on Ham River sand and London clay up to 70 kg/cm^2 confining pressure, and they observed that the failure envelope curved substantially from low to high pressures. They also noted that the significant

structural breakdown of particles controlled the undrained behavior, with a large pore pressure buildup that resulted in deviations from the theory of critical state (Roscoe, Schofield, and Wroth, 1958). They observed that the peak deviator stress does not coincide with the critical state line. Bishop (1966), in his Rankine Lecture, discussed that their ongoing research showed that the curvature of the failure envelope depends on density, with higher density producing envelopes of higher curvature. He also noted, that whether the initial density was loose or dense, the friction angles appear to be nearly the same at high pressures, which he related directly to the fact that the rates of dilation at failure coincide. He also noted that particle breakdown could possibly cause soil to become unstable under shock loads, due to large pore pressure rise. Finally, he pointed out that particle breakdown occurred mainly during shearing, as opposed to consolidation.

Marsal (1967) performed large-scale (113 cm. diameter) drained triaxial compression tests on three different gradations of coarse rock and sand with confining pressures up to 25 kg/cm^2, and observed the curved failure envelope, which he stated was caused primarily by particle fragmentation. He also proposed a particle breakage factor B, which was based on the change in the grain size distribution curve before and after testing.

Lee and Farhoomand (1967) performed isotropic and anisotropic drained compression triaxial tests on granite gravel at confining pressures up to 140 kg/cm^2 and found that compression is accompanied by significant particle breakage. They concluded that there are larger amounts of breakage for: coarse soils than fine soils; angular particles than rounded particles; uniform soil than

well-graded soils for same maximum particle size. They also noted that particle breakage continued over time at high static pressures, but with decreasing rates. They proposed another measure of particle crushing, based upon the grain size distribution curve ($D_{15initial}/D_{15final}$) to be used with earth dam filters.

Lee and Seed (1967) reported performing a series of drained triaxial compression tests on Sacramento River sand at four different void ratios, and dense Ottawa sand at confining pressures up to 140 kg/cm^2. They also noted the curved Mohr-Coulomb failure envelope, and hypothesized that the friction angle is composed of three basic components: sliding friction, dilatancy, and particle crushing/rearranging. Sliding friction was considered constant throughout all pressures. Dilatancy at low pressures causes large increases in the friction angle. At medium pressures, the dilatancy effect on the friction angle is reduced, but partially offset by rearranging of particles and particle crushing. At high pressures, the dilatancy effect is gone, but rearranging and crushing keep the friction angle constant, or slightly increasing, and above the sliding friction value. They performed corrections on the friction angles by using the two stress-dilatancy theories developed by Bishop (1954) and Rowe (1962). Lower friction angles resulted by using the Rowe method. They also proposed a variation in the theory of critical state, by defining the critical confining pressure as the confining pressure at failure, that produces no volume change. In a companion article Seed and Lee (1967) presented a series of undrained, triaxial compression tests on Sacramento River sand at four different void ratios and confining pressures up to 30 kg/cm^2. They performed tests with low back pressure, in which the pore water was allowed

to cavitate, as well as with high back pressure resulting in no cavitation. Although no stress-strain or pore pressure information was given, their results led them to propose a variation in the theory of critical state (Roscoe, Schofield, and Wroth, 1958) in which the undrained tests can be predicted from the drained tests. Their theory was based upon establishing that critical state occurred at failure conditions with zero volume change for the drained tests. Failure is defined to occur at the maximum effective principal stress ratio for the undrained tests with the effective confining pressure at failure defined as the critical confining pressure. With these definitions they found that the void ratio-critical confining pressure relationship for both drained and undrained tests yielded one single curve. Using this curve, which is defined from drained tests, it was possible to predict undrained behavior in the corresponding range of confining pressures.

Vesic and Clough (1968) performed a series of drained, triaxial compression tests on Chattahoochee River sand at confining pressures up to 633 kg/cm^2. Their tests were performed with either constant confining pressure, or at constant mean normal stress. They noted that the axial strains at failure first increase, and then decrease as the mean normal stress increases to high values. They concluded that at low pressure there was little particle crushing, but at elevated pressures there was intense crushing until a "breakdown stress" is reached. The "breakdown stress" is defined as the stress required to remove all effects of initial void ratio. They also concluded that at higher pressures beyond the "breakdown stress" the material behaved like a linearly deformable solid, with the modulus proportional to the mean normal stress. They stated that the friction angle decreases with increasing

pressure, and attains the basic interparticle friction angle at the "breakdown stress". However, their friction angle data seems to have substantial experimental scatter.

Barden, Ismail, and Tong (1969) performed plane strain tests on bronze ballotini, Welland River sand and crushed feldspar at confining pressures up to 70 kg/cm^2. They found that at higher pressures the dilatancy was suppressed by particle breakage and dense specimens started behaving similar to loose ones at low pressures.

Tai (1970) performed drained and undrained triaxial compression tests on Chattahoochee River sand and Ottawa sand with confining pressures up to 315 kg/cm^2 at three different densities. He noted that the curvature in the Mohr-Coulomb failure envelope is more curved for dense specimens. The drained tests had large axial strains at failure. Extensive particle breakage occurred during isotropic compression and shearing. He concluded that the "breakdown stress" concept that Vesic and Clough (1968) identified does exist, but it is different for different sands, and different densities. Again, the "breakdown stress" is defined as the pressure at which initial void ratio has no effect on friction angle, and it coincides with the end of any dilatancy effects, beyond which the friction angle is constant. Ottawa sand has stronger particles than Chattahoochee sand, and it had a higher "breakdown stress". The undrained tests showed much lower maximum deviator stresses than the drained tests. However, the axial strain to maximum principal effective stress ratio was larger than to the maximum deviator stress for the higher pressure tests. The friction angles, based upon maximum deviator stress and maximum principal effective stress ratio, were not the same. The friction

angle computed from the effective stress ratio was greater. It was also noted that pore pressures in the higher presssure tests always increased.

Murphy (1970) tested quartz, feldspar, calcite, and chlorite mineral sands in drained triaxial compression at confining pressures up to 3,150 kg/cm^2. He experimented extensively with different methods of providing frictionless ends, and concluded that at very high pressures the effects of end restraint on shear strength is not significant, if properly corrected for. He found that at very high pressures particle degradation is the most significant factor influencing the soil behavior. Therefore, mineral particle strength correlated well with the strength. He also noted that at very high pressures the behavior of the soil starts to be similar to the parent rock. Smaller grain size gave higher friction angles. The presence of water tends to weaken the soil with friction angles being higher for tests performed with dry sands. Electron micrograph examination of chlorite sands showed that the structure of the particle assembly after consolidation was of a "cardhouse" nature, which densifies substantially during shear. He hypothesized dividing the Mohr-Coulomb failure envelope into three regions: the pre-breakdown region; the region of linearity; and the post-linearity region. In the pre-breakdown region the strength of the soil is influenced by initial density. In the linear region the degradation components of shear strength replace the rearranging component. Beyond the linear region, he stated that particle crushing during consolidation results in a reduction of the friction angle.

Murphy (1971) reported additional results from his prior work (Murphy, 1970) on quartz, feldspar, calcite, and chlorite mineral sands and rocks at

confining pressures up to 3,150 kg/cm^2. His conclusions were that at very high pressures, there are strong inter-relationships between shear strength, compressibility and mineralogical hardness. He also stated that at some stress level, it may be possible to evaluate the behavior of rock by means of testing sand with identical parentage.

Billam (1971) performed drained triaxial compression tests on granulated chalk, crushed anthracite, and limestone sand at confining pressures up to 102 kg/cm^2. He found that the axial strain at failure first increases, but at high pressures starts to decrease. His results also showed that the friction angle decreases until it reaches a level, at which it appears to remain constant. He showed that the dilatancy rate at failure first decreases (compression), then starts to increase at high pressures. He noted that during the initial portion of shearing, the specimen may actually not expand, but contract slightly in the lateral direction. Another conclusion was that grain crushing at high pressures is directly related to grain strength.

Miura and Yamanouchi (1973) performed drained triaxial compression tests, and long-term isotropic consolidation tests on Toyura standard sand at confining pressures up to 500 kg/cm^2. The isotropic compression tests showed that for the lower pressures it was possible to achieve full secondary consolidation. However, at high pressures the sand was still exhibiting decreasing void ratio after 24 days, due to continued particle crushing. They concluded that the effect of initial density decreased as confining pressure increased, but there was still a small effect, even at their highest pressures. The Mohr-Coulomb failure envelope was

substantially curved at low pressures, and ended up as essentially a straight line. Their figures also showed that volumetric strain during shear decreases at high confining pressures. They noted that dry specimens appear stronger than saturated specimens, and that pore water aids in particle crushing. They suggested that bonds develop at particle contacts, when pore water was present.

Lo and Roy (1973) performed drained triaxial compression tests on aluminum oxide sand, quartz sand and limestone sand at confining pressures up to 112 kg/cm^2. They found that the soil behavior was governed by particle degradation. Their results showed that the friction angle decreased with increasing confining pressure, but the rate of decrease decreases with lower grain strength.

Miura and Ohara (1979) performed drained, triaxial compression tests on dense, decomposed granite at low confining pressures up to 3.0 kg/cm^2 to investigate particle crushing. They concluded that there was a strong correlation between particle crushing, as measured by an estimated increase in particle surface area, with the amount of plastic work dissipated in the specimen.

Charles and Watts (1980) performed large-scale (23 cm. diameter) drained, triaxial compression tests on a variety of very dense rockfill materials at confining pressures of 7.0 kg/cm^2. They found that the Mohr-Coulomb envelope was highly curved at low pressures, and concluded that earth dams could be built with steeper slopes, because the friction angle is so much higher at low normal stresses due to the dilatancy effect.

Miura, Murata, and Yasufuku (1984) analyzed previously performed tests

and performed some multi-step stress path tests in triaxial compression and extension at apparent confining pressures up to 150 kg/cm^2 to determine yield surface locations. Unfortunately, no specific test data, such as stress-strain or volumetric strain information was included.

Hardin (1984) extensively analyzed existing published data on particle breakage, and derived three parameters called breakage potential, total breakage and relative breakage. These parameters are all based on the grain size distribution curve. Breakage potential is defined as the area between the #200 sieve (silt size) and the initial grain size curve normalized to the area of one log cycle. It represents the potential, if all of the grains were crushed to pass through the #200 sieve. The total breakage is the area between the initial grain size curve and the final grain size curve, after stress is applied. This represents the total amount of breakage occurring between the initial and final conditions. Relative breakage is defined as the total breakage divided by the breakage potential. Hardin concluded from his analysis that relative breakage is a reasonable measure of particle breakage, because it is not sensitive to particle size as other investigators' breakage factors tend to be.

Murphy (1987) re-reported much of his prior work (Murphy, 1970; Murphy, 1971) with additional conclusions. He concluded that the Mohr-Coulomb failure envelope is continually curved even at confining pressures near 3,150 kg/cm^2 for feldspar, chlorite, and calcite. However, his conclusions were based upon only three different tests (confining pressures of 2 kg/cm^2, 315 kg/cm^2, and 3,150 kg/cm^2) for each mineral. Another observation at very high pressures was that

there is a fixed volumetric change capacity in a soil, and most of it occurs during isotropic consolidation. He further stated that the mineral friction angle increases with increasing pressure, which should increase the friction angle of a soil at high pressures.

Colliat-Dangus, Desrues, and Foray (1988) performed drained triaxial compression tests on loose and dense calcareous sand and siliceous sand at confining pressures up to 100 kg/cm^2. They experimented with lubricated ends and specimen height-to-diameter ratios, and they concluded that to attain uniform strains, lubricated ends were required and a height-to-diameter ratio of one was recommended. They reported that soil creep increased with increasing confining pressure, and was associated with particle breakdown. They also found that volumetric strains first increase with increasing confining pressure, and then start to decrease at high pressures. The friction angles were found to decrease with decreasing rate of dilation, but then start to increase after reaching a minimum value. They proposed a crushing coefficient C_c defined as 1/10 in the percentage finer between the D_{10} before and after the application of stress.

In summarizing the prior work, it is obvious that high pressure testing of soils has been performed and the results examined by many investigators. However, virtually all of prior investigations involved only drained compression tests. There were only two substantial investigations examining undrained behavior at high pressures (Seed and Lee, 1967, Tai, 1970). The regular use of lubricated ends did not start until in the 1970's, so the possibility of nonuniform strains exist, and this should be considered when examining prior work. Further,

effects of membrane penetration on volumetric strains in drained tests, and on pore pressures in undrained tests may also be present. Membrane penetration occurs when a relatively coarse sand is tested. The rubber membrane surrounding the specimen penetrates into the voids between the grains at the perimeter of the sample for varying effective confining pressure. This penetration increases the volume change during the isotropic consolidation portion of all tests, but more importantly, the pore pressure response is buffered during undrained tests (Lade and Hernandez, 1977). At high confining pressures, the membrane eventually stops penetrating into the soil when an upper pressure limit is reached. However, low pressure undrained tests can be seriously affected. Frydman, Zeitlen, and Alpan (1973) state that membrane penetration is not significant for soils with average grain sizes smaller than 0.1 to 0.2 mm. Both sands used by Tai (1970) in his undrained tests were rather coarse. Therefore, the results of the low pressure undrained tests may have exhibited pore pressures that were directly influenced by membrane penetration. The stresses in all his high pressure tests could also have been affected, since the isotropic volumetric change must be corrected to account for membrane penetration. Lubricated ends were not employed in his tests.

Seed and Lee (1967) used a finer sand, which should limit membrane penetration effects in their undrained tests. However, their reported undrained tests had a maximum initial confining pressure of only 30 kg/cm^2. They also did not use lubricated ends in their drained or undrained tests.

2.2 Review of Prior Investigations Involving Extension Testing on Granular Materials

There have been many investigations of soil behavior in extension. Most of them were performed to evaluate failure criteria.

Bishop and Eldin (1953) performed a series of drained and undrained, cylindrical triaxial compression tests, as well as a series of drained triaxial extension tests on well graded Brasted sand at low confining pressures, to study the effects of stress history and porosity. They found much more scatter in the extension tests, but observed that the friction angles were approximately the same as in the compression tests. However, they felt these results were not totally conclusive.

Kirkpatrick (1957) performed drained, cylindrical, triaxial compression and extension tests on Loch Aline sand at low confining pressures to investigate the Mohr-Coulomb, Extended Von Mises, and Tresca failure criteria. His test results showed that the friction angles in compression and extension were approximately the same.

Roscoe, Schofield and Thurairajah (1963) performed low confining pressure, drained, cylindrical triaxial compression and extension tests on Leighton Buzzard sand, to investigate a yield criterion. When their results were analyzed using conventional methods assuming uniform strain conditions (strains based on overall length and stresses based upon the assumption of deformation of a right cylinder), the friction angles were approximately the same. However, they also performed some "special" tests, in which they were able to accurately measure the specimen

dimensions at all points during the test. It should be noted that no lubricated ends were employed. In compression the sample "bulged", and in extension the specimen "necked". The assumption of uniform strains utilized in the conventional area correction formula cannot be correct in obtaining the true stresses in the specimens. However, for the compression tests they concluded that the conventional area correction method assuming uniform strains was approximately correct, even though it tended to overestimate the stresses in the center of the specimen. When they corrected the areas in the extension tests, they found that the stresses in the soil in the necked region were still increasing, and the specimens had not failed. If the conventional area correction method is employed, the stresses are underestimated. Therefore, their conclusions were that it was not possible to evaluate the different yield criteria until a testing method was developed, which resulted in uniform strains.

Cornforth (1964) performed low pressure, drained, cubical triaxial compression, extension and plane strain tests on Brasted sand, to investigate strain conditions in three dimensions. He found that the friction angle in plane strain was larger than in triaxial compression for all porosities. He also found that the triaxial extension tests had lower friction angles than the compression tests at high porosities, but higher values at low porosities. There was considerable scatter in the extension tests. He concluded that plane strain friction angles were higher than compression or extension friction angles, and the friction angles in compression and extension were approximately equal.

Barden and Khayatt (1966) performed drained, cylindrical, triaxial

compression and extension tests on River Wellend sand at low confining pressures, to investigate failure criteria. They modified a standard triaxial testing apparatus to incorporate the use of larger diameter specimens (10 cm.), performed tests at two different heights (10cm. and 20 cm.), and they found that the friction angles for extension were greater than for compression for the same initial porosity. They noted that there were more nonuniform strains in the taller extension specimens than in the shorter specimens. Their conclusion was that the Mohr-Coulomb failure criterion was more applicable than the Extended Von Mises, or the Extended Tresca failure criteria.

Ko and Scott (1967) performed low pressure, drained, cubical triaxial compression tests on Ottawa sand in a newly developed cubical testing device. Their results came out very different when compared with results of conventional cylindrical triaxial tests. Some of this was apparently due to the testing apparatus.

Green and Bishop (1969) performed low pressure, drained, cylindrical and cubical triaxial compression, plane strain, and extension tests on Ham River sand. Their cubical results showed that the friction angle increases from compression to plane strain, and then drops slightly at extension. Their cylindrical triaxial extension tests experienced nonuniform strains, and they applied an area correction. Even with the correction the cylindrical extension friction angles were lower than the cubical extension friction angles.

Proctor and Barden (1969) performed low pressure, drained, cylindrical, and cubical triaxial tests in compression, plane strain, and extension. Their cubical results showed that the friction angle increases from compression to plane strain,

and then drops slightly in extension. Their cylindrical triaxial extension tests had friction angles much lower than their cubical counterparts. They also showed that the average error in conventional extension tests is five times greater than in compression, so scatter in extension is to be expected.

Sutherland and Mesdary (1969) performed low pressure, drained, cubical triaxial compression, extension, and plane strain tests on Loch Aline sand to investigate the effect of the intermediate principal stress. They found that the friction angle in plane strain was higher than in triaxial compression. They also found that the friction angle for extension was approximately the same as in compression.

Green (1971) performed both cylindrical and cubical, drained, triaxial compression and extension tests on Ham River sand. His results showed that the friction angle increases from triaxial compression to plane strain conditions. There was substantial scatter in his friction angles from plane strain to extension. In extension, most of his values of friction angle are above plane strain. However, his interpretation of the results concluded that the friction angle did not change from plane strain to extension. The cylindrical triaxial compression tests agreed well with the cubical triaxial compression tests. However, the cylindrical triaxial extension tests were lower than his cubical triaxial extension tests.

Barden and Proctor (1971) performed low pressure, drained, cubical triaxial compression, plane strain and extension tests on River Wellend sand, crushed feldspar, and bronze ballotini. They also performed cylindrical triaxial extension tests. They concluded that triaxial compression friction angles were lower than

plane strain, but triaxial extension was unresolved. They noted that the published results are quite varied, and concluded that compression and extension probably had the same friction angle.

Lade and Duncan (1973) performed low pressure, drained, cubical triaxial compression, plane strain and extension tests on Monterey No. 0 sand. Their results show that plane strain has a much higher friction angle than in compression. From plane strain the friction angle decreases slightly in extension, but it is greater than in compression.

Reades and Green (1976) performed low pressure, drained, cubical triaxial compression, plane strain, and extension tests on Ham River sand. They also performed conventional triaxial extension tests on cylindrical and cubical specimens. Their cubical triaxial results indicated that the friction angle increases from compression to plane strain, and continued to increase into extension. In the conventional extension tests necking was observed, and the stresses were approximately corrected by using a ratio of the average area of the neck to the average area of the specimen. The cubical extension tests had higher friction angles than the corrected conventional triaxial extension tests by as much as six degrees.

Oda, Koishikawa, and Higuchi (1978) performed low pressure, drained, cubical triaxial compression and plane strain tests on Toyoura sand to study anisotropy. Their results showed that the friction angle for plane strain was not always greater than that in compression, due to anisotropy in the soil fabric.

Yamada and Ishihara (1979) performed low pressure, drained, cubical

triaxial compression, plane strain, and extension tests on Fuji River sand. They observed that at failure the ratio of octahedral shear stress to effective mean normal stress increased from compression to plane strain, and further decreased to extension. They stated that this corresponded well with the failure criterion established by Lade and Duncan (1975).

Lade (1982) performed low pressure, drained, cylindrical and cubical triaxial compression and extension tests on loose and dense Monterey and Santa Monica Beach sand. The results in extension indicate that the friction angles with strain localization are up to ten degrees less than with uniform strains and fall roughly near the compression friction angles. There is also wide scatter in the data. In a dilatant specimen the volume change would tend to be more compressive in the specimens with strain localization, because it causes most of the volume change to occur in the region of localization, which is usually a small part of the specimen. The strain to failure was observed to be less when strain localization occurred.

Nakai and Matsuoka (1983) performed low pressure, drained, cylindrical and cubical triaxial compression, plane strain, and extension tests on Toyoura sand. They reported that the friction angles increased from compression to plane strain, and then decreased to a value slightly higher than the compression values for the extension case. They indicated that their cylindrical triaxial compression and extension tests approximately agreed with their cubical tests.

Ochiai and Lade (1983) performed low pressure, drained, cubical triaxial compression, plane strain, and extension tests on Cambria sand. Their results

indicated that cross-anisotropy does influence the value of friction angles. However, the variation is fairly uniform from compression through plane strain, and into extension. Therefore, assumption of isotropic conditions in a failure criterion may still be applicable for cross-anisotropic soils.

Lam and Tatsuoka (1988a, 1988b) performed low pressure, drained, cylindrical triaxial compression and extension tests on Toyoura sand to evaluate effects of anisotropy and height-to-diameter ratios on the friction angle. Necking in the cylindrical extension tests occurred, and stresses were corrected by analyzing the area of the neck photographically. Their conclusion was that the failure mode controlled the strength in triaxial extension. They felt that the failure mode was controlled by height-to-diameter ratio, boundary conditions (flexible or rigid), and other unknown factors. Overall the friction angles increased from compression to plane strain, and further increased to extension. However, anisotropy played a large role in the relative friction angle change.

Wu and Kolymbas (1990) performed low pressure, drained cylindrical triaxial extension tests on Karlsruhe medium sand. They observed that for low pressures, corrections involving piston friction, membrane stiffness, influence of gravity, lubricated ends were significant in the final results. They observed necking in all of their extension tests. They made area corrections based on measurements of the deformed specimens. Their corrected friction angles resulted in the conclusion that extension produces higher friction angles than compression.

Triaxial extension at low pressures has been the subject of investigations by many investigators. Almost all investigators were investigating failure criteria.

Roscoe, Schofield and Thurairajah (1963) convincingly showed that the conventional triaxial extension test has substantially more strain localization than triaxial compression, and the results could not be relied upon, when evaluating failure criteria. This realization resulted in many investigators developing cubical triaxial testing apparatus, in which the full range of the effect of the intermediate principal stress could be investigated. Additionally, most of the cubical apparatuses developed enforced uniform strains by employing rigid boundary conditions around the specimen. Even with the cubical triaxial equipment, most investigators still performed conventional extension and compression tests to check their cubical tests results. Most of the investigators who used cylindrical extension tests admitted that nonuniform strains occurred in the specimens. Some applied some type of area correction. The area corrections that are commonly applied are usually expressed as ratios of the necked area to the average specimen area. These corrections may not truly represent the specimen stresses and strains. Lade (1982) showed that when strain localization occurs, virtually all of the shearing occurs in the localized zone, which may be a very small part of the specimen. This results in substantial errors in volumetric, and principal strains. Proctor and Barden (1969) showed that the triaxial extension test results are subject to five times greater error due to typical experimental errors than for the corresponding compression test. In combination with the approximate area corrections that are commonly employed, this results in the conclusion that the conventional cylindrical triaxial extension test is not a reliable means to determine soil behavior in extension.

Results obtained from low pressure, cubical triaxial testing apparatuses are in more general agreement, than cylindrical extension tests. With a few exceptions most investigators have determined that in the low pressure range the friction angle increases from compression to a high value around plane strain conditions, and it then decreases perhaps slightly to extension.

CHAPTER 3 EXPERIMENTAL PROCEDURES

The experimental procedures discussed in this chapter are related to the drained and undrained triaxial compression and extension tests, which comprise the bulk of the experimental work. The experimental equipment and procedures utilized for the high pressure one-dimensional compression tests is discussed in Chapter 9.

3.1 UCLA High Pressure Testing Facility

From 1987 to the present a high pressure testing facility has been developed and continuously refined at University of California, Los Angeles under the support of the Air Force Office of Scientific Research (Chamieh, 1990; Yamamuro, 1990). The basic components of the system consists of a one meganewton loading frame, high pressure triaxial cell, two axes of motion control, instrumentation, signal conditioning and microcomputer as shown in Figure 3-1.

The two axes of control consist of hydraulic cylinders that are actuated by stepping motors through reduction gears and ball-screw jacks. The whole system is close-loop-controlled by a microcomputer, which operates an analog-to-digital converter for data aquisition, and a stepping motor controller to control the stepping motors, all operated by custom control programs. This process is depicted in Figure 3-2. Load is measured by either a 25, 50 or 100 ton load cell, displacement by an LVDT, and cell and pore pressures by 1,000 bar pressure

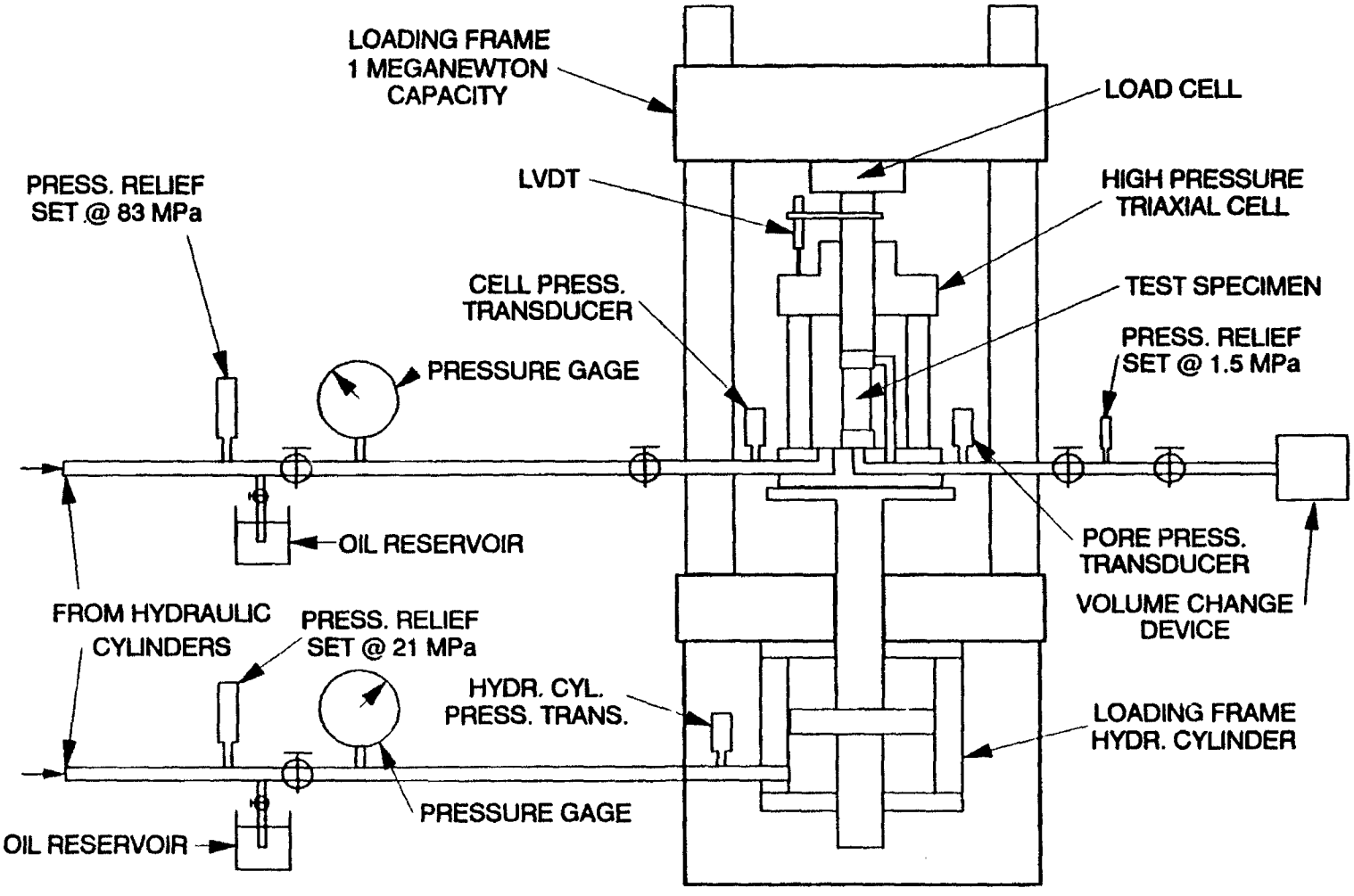

FIGURE 3-1 HIGH PRESSURE TESTING LOADING SYSTEM

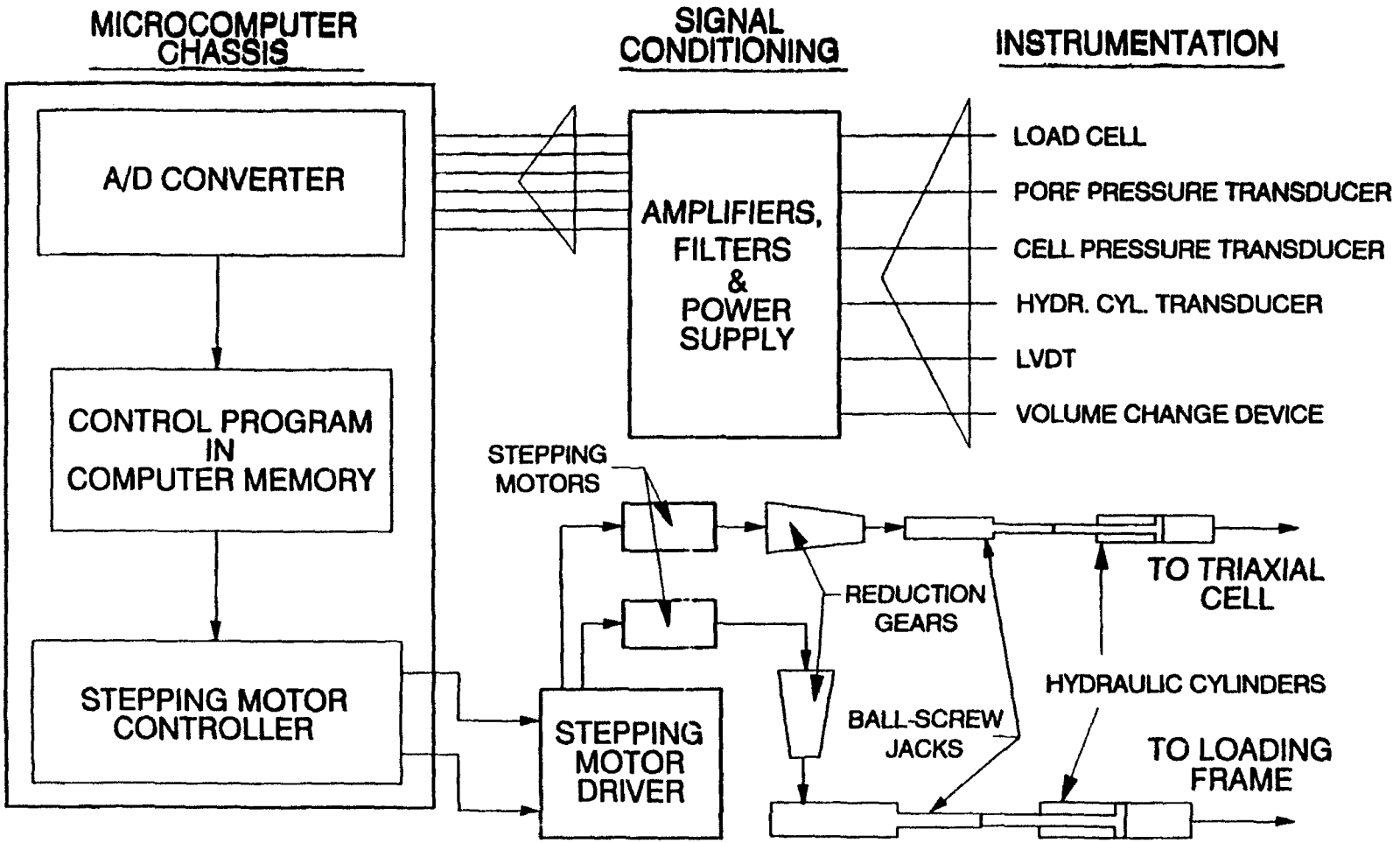

FIGURE 3-2 HIGH PRESSURE TESTING SYSTEM-PROCESS CONTROL FLOW

transducers. All instrumentation signals are conditioned through amplifiers and active filters before entering the microcomputer. The first control axis operates the true vertical stress or strain, by feeding hydraulic fluid into the loading frame's hydraulic cylinder, which raises or lowers the table on the frame. The second control axis operates the total confining pressure, by feeding hydraulic fluid into the high pressure triaxial cell. The high pressure triaxial cell and instrumentation can test the specimens in compression or extension, and has experienced confining pressures of up to 100 MPa. Custom control software has been developed to perform a wide variety of tests under both true strain and true stress control. Chamieh (1990) and Yamamuro (1990) have extensively documented the original high pressure testing system.

3.2 Modifications in Existing Testing Equipment and Software

Some of the original equipment was modified to improve the system and extend its capabilities. The signal conditioning system (instrumentation amplifiers and regulated power supply for excitation voltage) was replaced with a Measurements Group Model 2120A system and Analog Devices active filters were installed to improve the resolution capability of the data acquisition system. In addition to this, the testing hardware had to be modified to permit testing of specimens in extension. To accomplish this, a device had to be designed and fabricated to connect the piston to the specimen to allow an upward force to be applied to the specimen. The device also had to allow the specimen to freely deform downward during isotropic compression preceding shearing in extension.

The device is shown in Figure 5-20 in Chapter 5 where it will be described in further detail. Additionally, the cap and base for the specimen were modified. This is shown in Figure 5-21, also in Chapter 5.

Software modifications include rewriting the existing triaxial compression computer control programs to perform testing in triaxial extension under both drained and undrained conditions with strain control. Stability testing control programs were developed for both triaxial compression and extension. The stability test control programs are performed under both drained and undrained conditions, and with both stress and strain control. In addition to these control programs, special purpose control programs were developed to perform very low strain rate tests, isotropic loading and unloading tests, shearing loading and unloading tests, as well as control programs for testing and evaluation of Skempton's pore pressure parameter, B, at high pressures.

3.3 Granular Materials Used for Testing and Test Specimen Preparation

The soil used for the majority of the tests conducted in this investigation is a uniform Cambria sand consisting of rounded grains with diameters between 0.83 and 2.00 millimeters. Specific initial gradation information is given in Appendix B. Cambria sand is composed of more than one mineral constituent. The Cambria sand was analyzed for its mineral constituents by the Gazzi-Dickinson point count method (Ingersoll, et al, 1984) in which 300 separate points on a slide-mounted thin section of the sand are individually identified under a light polarizing microscope. Of the 300 identified points 54 percent were determined to be quartz

grains, 39 percent were lithic (rock) grains, and the remaining 7 percent were either feldspar, mica, calcite, or dense accessory minerals. Chert made up the majority (88 percent) of the quartz grains. Sedimentary lithic grains made up 60 percent of the lithic grains. These consisted of small quartz fragments embedded in a clay (shale) matrix. Metamorphic and volcanic lithic fragments accounted for the remaining lithic grains. The maximum void ratio was determined to be 0.783, the minimum void ratio was 0.493, and the specific gravity was 2.69. Void ratios for all specimens averaged 0.525 corresponding to a relative density of 89%.

In addition to the tests on Cambria sand, five high pressure triaxial compression tests were performed using a uniform quartz sand consisting of subangular grains with diameters between 0.60 and 1.70 millimeters. The Gazzi-Dickinson point count method indicated that this quartz sand is composed of approximately 80 percent quartz and 20 percent feldspar. The maximum void ratio was determined to be 1.073, the minimum void ratio was 0.655, and the specific gravity was 2.65. Void ratios for the quartz sand averaged 0.685 corresponding to a relative density of 93%.

Specimens were created by dry pluviation from a height of 40 centimeters. All specimens created were of cylindrical shape and averaged approximately 7.1 centimeters (2.8 inches) in diameter. The triaxial compression test specimens averaged approximately 17.8 centimeters (7.0 inches) in height for a height-to-diameter ratio of 2.5. A few tests at the highest confining pressures were created with heights that averaged approximately 13.0 centimeters (5.1 inches) for a height-to-diameter ratio of 1.8. The triaxial extension test specimens were created

with heights that averaged 13.0 centimeters (5.1 inches) for a height-to-diameter ratio of 1.8.

3.4 Membranes and O-Rings

All cylindrical membranes encasing the test specimens were made of latex rubber and measured 7.1 centimeters in diameter (2.8 inch) and 30.5 centimeters (12 inch) in length and were cut to proper length for the specimen height. The membranes for the triaxial compression tests were all 0.635 mm (0.025 inch) in thickness. The number of membranes used to prevent punctures by the sand grains ranged between three and five depending on confining pressure. Triaxial extension tests utilized both the 0.635 mm and 0.304 mm (0.012 inch) thick latex membranes. The number of membranes used in the extension tests depended on the number of layers of uniform strain plates used and the confining pressure. This is further discussed in Chapter 4. Generally, four O-rings each on the cap and base were adequate to attach the membranes without leakage. The O-rings were installed on the outside of all membranes.

Membranes could be reused after high pressure tests depending on the confining pressure of the test. The inside membrane was usually punctured too much to be of any further use, and it was discarded. Generally, the second membrane had some small punctures, but it could be used again as a padding layer in a subsequent test. All other membranes could be reused, either as the inside membrane or as outer membranes.

The O-rings which seal between the triaxial cell wall and the triaxial cell cap and base, the specimen base and the triaxial cell base, and the bottom drain line

to the triaxial cell base were periodically replaced to ensure proper sealing at high pressures. Actually, no leaks at these O-ring connections was ever observed, but damage, stretching, and flattening of the O-rings were visible after a few tests. A replacement frequency of approximately ten to fifteen tests would seem reasonable.

The control program calculating the stresses automatically corrected for the load absorbed by the stiffness of the combined latex membranes. A modulus of 14 kilograms per square centimeter and a Poisson's ratio of 0.5 were assumed for the latex rubber membranes.

3.5 Lubricated Ends

The use of lubricated caps and bases is necessary to reduce end friction to a minimum and to maintain uniform strains in the specimen. The type of lubricated ends evolved through extensive experimentation, and those needed for high pressure triaxial compression tests are different from those used for triaxial extension tests.

High pressure triaxial compression tests simply require sufficient thickness in the lubricated end, such that at high pressures and with very high deviator stresses, the sand grains do not penetrate easily through the lubricated ends to create friction on the surface of the cap and base. The type of lubricated ends that ensure deformation as a right cylinder in triaxial compression were made from two layers of latex rubber 0.635 mm in thickness (0.025 inch) and 7.1 centimeters in diameter (2.8 inch) placed on the cap and base. A thin layer of Dow Corning High

Vacuum Grease is applied to the surface of the cap and base and between the latex rubber sheets to provide some lubrication, but mainly to ensure no air is trapped between the lubricating rubber sheets.

High pressure triaxial extension tests require substantially different lubricated ends, because of the nature of the test. The standard triaxial extension test has a decreasing vertical stress as opposed to the compression test. This condition leads to unloading of the lubricated ends, and at high confining pressures the membranes surrounding the specimen will laterally intrude under the cap, and buckle the lubricated ends, separating the cap from the specimen as shown in Figure 3-3. This type of testing phenomenon is actually difficult to detect, because as the confining pressure is lowered after conclusion of the test, the separated cap and external membranes return to their original locations. A typical stress-strain curve and volumetric strain curve showing the effect of cap separation are compared with similar curves for a correct test in Figure 3-4. The curves appear reasonable except for the extremely low post-failure residual strength and the low volumetric strains after cap separation. To overcome the problem of cap separation, lubricated ends slightly smaller than the diameter of the specimen were employed. Thus, an annular ring of soil is butted directly against the metal surface of the cap, which forms a protective barrier of soil around the lubricated ends. Some extension tests were performed without lubricated ends. Since full-width lubricated ends cannot be used, some friction will develop between the cap and soil. However, since the vertical stress is constantly decreasing during an extension test until failure, the amount of friction

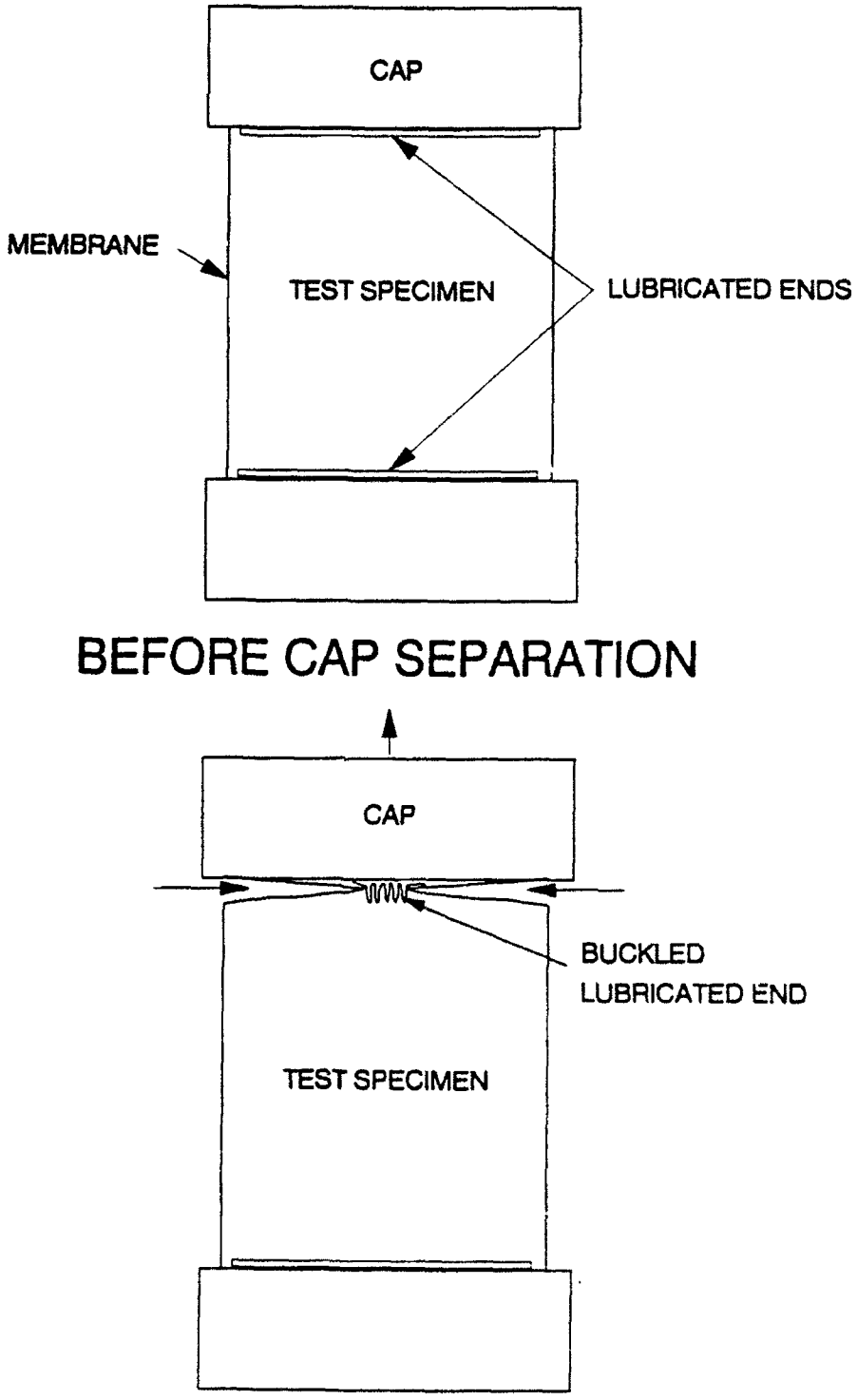

FIGURE 3-3 DIAGRAM DEMONSTRATING
EFFECTS OF CAP SEPARATION IN EXTENSION TEST

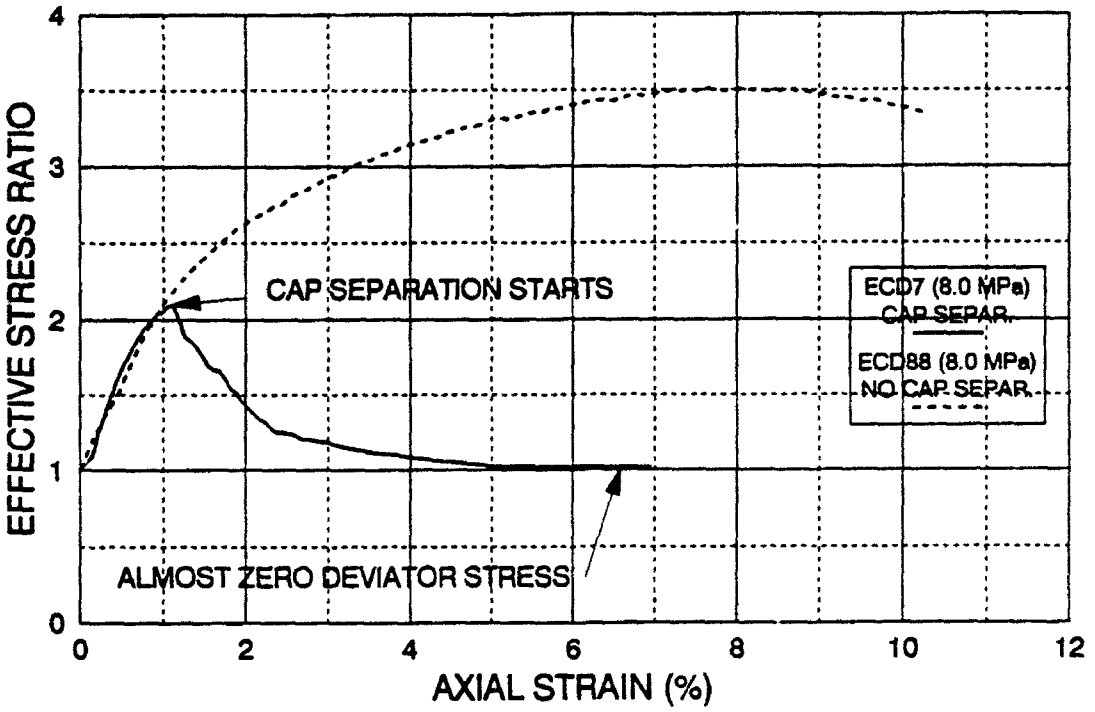

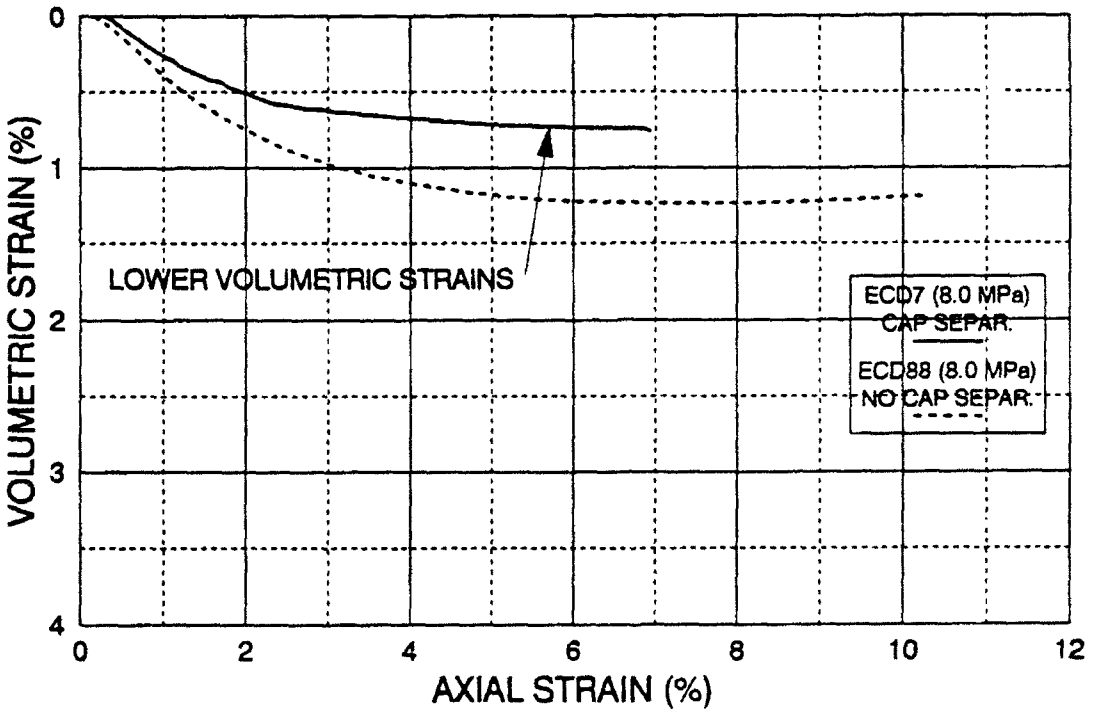

FIGURE 3-4
EXTENSION TEST EXPERIENCING CAP SEPARATION
DEVIATOR STRESS AND VOLUMETRIC STRAIN
DENSE CAMBRIA SAND

is not nearly as large as in compression tests. In addition, by using the methods discussed in Chapter 4 uniform strains in triaxial extension tests can be assured. The method developed for lubricated ends employed a single layer of latex rubber 0.635 mm in thickness (0.025 inch), and 4.6 centimeters in diameter (1.8 inch) placed on the cap and base. A thin layer of Dow Corning High Vacuum Grease is applied to the surfaces of the cap and base before the latex rubber sheets are placed to provide some lubrication, but mainly to ensure that no air is trapped within the lubricated ends.

3.6 Saturation

All specimens used in triaxial compression and extension tests were fully saturated prior to testing. After the specimen is created in a dry state, the triaxial cell is assembled around the specimen, and the cell is filled with hydraulic fluid, a small holding confining pressure is applied to the dry specimen. Then CO_2 is forced through the specimen from the bottom drainage line and out the top drainage line evacuating all the air from the dry specimen (Lade and Duncan, 1973). This is performed for approximately twenty minutes. Then water is fed into the specimen through the bottom drainage line under a small gravity head, and out the top drainage line flushing out the CO_2. A minimum of one liter of water in excess of the volume of the voids in the specimen is percolated through the specimen. Then, maintaining the same effective holding confining pressure, the cell pressure and backpressure are increased to force any remaining CO_2 into solution (Black and Lee, 1973). Typically, the backpressure was 0.517 MPa (75

psi), but it did occasionally vary from this value.

3.7 Membrane Penetration

Membrane penetration is caused by the cell fluid surrounding the specimen pushing the latex rubber membranes into the spaces between the sand grains on the external surface of the specimen. Membrane penetration is a testing error that increases the measured volume change in the specimen during isotropic consolidation, and more severely buffers the generated pore pressures in undrained tests. Coarse sands are most affected. Fine sands are not significantly affected by membrane penetration effects.

Membrane penetration for the coarse Cambria sand has been examined in a prior study (Chamieh, 1990). Isotropic compression tests were performed in which both axial and volumetric strain were measured. The results are shown on Figure 3-5. The total measured volumetric strain is plotted along with the assumed isotropic volumetric strain, based upon three times the measured axial strain (assumed isotropy). The difference should be the membrane penetration. As can be observed, the two curves become parallel as the effective confining pressure increases, which suggests that membrane penetration effectively stops at confining pressures above approximately 2 MPa. The physical interpretation of this effect is that, beyond a certain threshold cell pressure for a given sand, the membranes surrounding the specimen cannot be pushed further into the void spaces between sand grains as the confining pressure increases. The volume correction for drained tests using cylindrical specimens of 7.1 centimeter (2.8 inch)

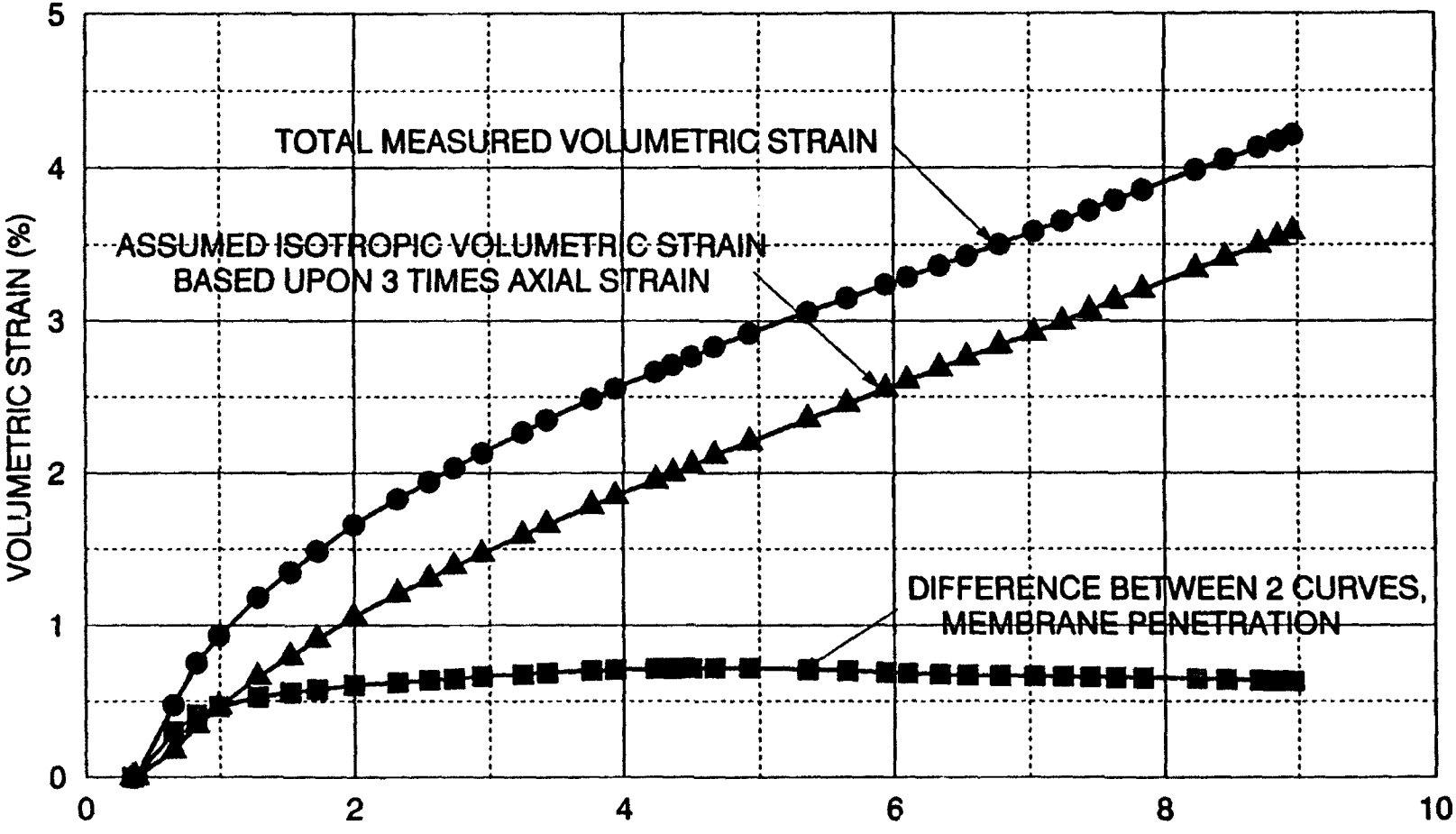

FIGURE 3-5 MEMBRANE PENETRATION EFFECTS
ISOTROPIC COMPRESSION TEST
DENSE CAMBRIA SAND

diameter, and 17.8 centimeter (7.0 inch) height, is approximately ten cubic centimeters. This correction is applied to the isotropic compression volume change. Undrained tests in which the effective confining pressure falls below 2.0 MPa are subject to membrane penetration effects, and therefore, do not produce reliable results in the low effective confining pressure range.

3.8 Detailed Testing Procedures for Triaxial Compression Tests

This section gives detailed documentation of the developed testing procedures utilized to assemble the specimen and triaxial cell, perform a high pressure triaxial compression test, and then to disassemble the test setup.

1. Prepare full lubricated ends, as previously discussed, and install on cap and base. Use the cap and base designed for triaxial compression. Cap top drain port on the specimen cap.

2. Attach specimen base to triaxial cell base. Install one latex membrane (0.635 mm thickness) on base with one O-ring, and place specimen mold over base and membrane.

3. Apply vacuum from vacuum pump to mold to pull membrane into position. Above the mold place mold extension rings, pluviation tube, and No. 4 U.S. sieve.

4. Weigh amount of soil on scale for the void ratio and size of specimen desired. Rain in soil through sieve.

5. Smooth top surface of soil and place top cap on specimen and attach membrane with one O-ring. Close large top drain valve on at the base of the cell. Pull vacuum on specimen through bottom drain line. Remove mold from specimen.

6. Measure specimen diameter at top, middle, and bottom locations. Measure height in two locations. Check height around specimen to ensure that the cap is perfectly level. Level cap as necessary.

7. Close large bottom drain valve trapping vacuum within specimen. Use vacuum pump and the membrane stretcher to install remaining membranes over the first membrane. Use O-ring stretcher to install four O-rings each on the cap and base. The O-ring on the first membrane can be removed to provide adequate room for the four O-rings on the cap.

8. Reconnect vacuum pump to bottom drain line and pull vacuum on specimen. Connect top drain line to the triaxial cell base. Quickly remove cap covering the top drain port on the specimen cap, and place a finger over the port to allow the vacuum to recover. Quickly connect top drain line to top drain port in cap and tighten. Remeasure specimen to ensure

the specimen has not been affected by the procedure.

9. Close the top and bottom large drain valves, trapping vacuum inside the specimen, and turn off vacuum pump. Place cell wall over specimen. Using the two overhead pulleys, lift the triaxial cell cap with the connection chains through the 2/3 and 6/7 bolt holes until it is over the cell wall. Carefully lower triaxial cell cap onto the cell wall. Rotate cap and wall to ensure that the O-rings are properly seated.

10. Place washers over all bolt holes on triaxial cell cap. Put bolts in bolt holes identified by bolt hole number, and finger tighten. Be sure to install the wire rope lifting loops around the 2/4 and 6/7 bolts. Using the ratchet wrench with the handle extension, tighten bolts alternately to evenly compress O-rings.

11. Start filling triaxial cell with water soluble oil by applying air pressure to the holding reservoir. Connect overflow line to the triaxial cell top drain port and place overflow container under overflow line. Progress of the filling operation can be observed through the piston hole in the top cap. When the specimen is fully covered with fluid, the piston may be installed by gently tapping on the exposed end until it slides through the seal. Install piston with the threaded end out of the triaxial cell. Gently lower the piston until it is in contact with the specimen.

12. When fluid flows out the overflow line into the overflow container decrease, but maintain the air pressure in the holding reservoir to about 0.048 MPa (7 psi) to hold the specimen. Close overflow valve, and remove overflow line.

13. Open top and bottom drain valves releasing vacuum from specimen. Connect CO_2 line to bottom drain line and flow gaseous CO_2 through the specimen at a pressure of about 0.01 MPa (1.5 psi). Connect top drain line to bubble chamber. Saturate specimen with CO_2 for approximately 20 minutes. Connect specimen through bottom drain line to water line. Feed water through specimen until over one liter of water has been pushed out through the top drain line.

14. Reduce pressure on volume change device to zero. Connect volume change device to specimen by opening both the small top and bottom drain line three-way valves simultaneously.

15. Connect overhead pulleys to wire rope lifting loops. Remove the two triaxial cell retaining bolts under the assembly table. Carefully lift triaxial cell to the exact center of the loading frame table keeping the cell level at all times. Connect the instrumentation cables to the cell and pore pressure transducers. Install the LVDT holder onto the piston.

16. Use the STEPPER.EXE program to actuate stepping motor number one to push the hydraulic cylinder that moves the loading frame table up, such that the piston is just short of making contact with the load cell.

17. Using the CALFAC.EXE program to get the initial load cell and LVDT readings. Increase the cell and back pressures in 0.069 MPa (10 psi) increments with the final initial effective confining pressure being 0.069 MPa (10psi). Allow the backpressure to saturate the specimen for a minimum of twenty minutes.

18. Perform the B-value test to check the degree of saturation using the pressure transducer on the volume change device. Use a minimum cell pressure increment of 0.069 MPa (10 psi).

19. After reducing the pressure at the conclusion of the B-value test, take new load cell and LVDT readings from CALFAC.EXE. The difference between these readings and the first set of readings is the net initial load cell reading and the GAP, respectively.

20. Use MENU.EXE to input the type of test, test identification, the specimen diameter, the specimen height, the initial cell pressure, the initial back pressure, the shearing strain rate, the type of consolidation, the final total consolidation pressure, the consolidation stress rate, and any changes

in the instrumentation calibration factors.

21. Execute the appropriate test control program. Input the GAP, the initial load cell force, the initial pointer direction on the volume change device, the membrane penetration volume correction. When ready, close the vent valve to the holding reservoir and press F2 to start the test under computer control. The control program will query the user, if other information is required, depending on the type of test.

22. During the test any change in pointer direction on the volume change device change is preceded by pressing F7. Different test control programs may require different responses by the user during its operation.

23. After the test is completed, the user presses F10 to terminate control program execution. Close both top and bottom drain valves to hold specimen.

24. The user can lower the cell pressure using the STEPPER.EXE to actuate the stepping motors. When the cell pressure is low enough, open vent valve to holding reservoir.

25. Disconnect the pressure transducer cables and remove the LVDT holder. Using the overhead pulleys, lower the cell down to the assembly table.

With the triaxial cell held just above the blocks on the table, screw in the holding bolts from beneath the assembly table. Finish lowering the triaxial cell to the blocks.

26. Apply air pressure through the triaxial cell overflow port at about 0.048 MPa (7 psi) to force the cell fluid back into the holding reservoir.

27. Remove piston. Remove triaxial cell bolts by alternately loosening to evenly decompress O-ring. Using the overhead pulleys and connection chains (through 2/3 and 6/7 bolt holds), lift cell cap from cell wall. Lift off cell wall.

28. Measure specimen height and diameter as required. With vacuum pump providing suction on specimen through bubble chamber, remove top drain line and place cap over drain port in specimen cap. Disconnect specimen base from triaxial cell base. Remove membranes from specimen and save specimen in soil drying tray.

29. Use STEPPER.EXE to move hydraulic cylinders to the starting position for the next test. Drain off accumulated water in the volume change device. Disconnect the volume change device using the small three-way valves. Blow out drain lines with compressed air.

3.9 Detailed Testing Procedures for Triaxial Extension Tests

This section presents a detailed documentation of the developed testing procedures utilized to assemble the specimen and triaxial cell, perform a high pressure triaxial extension test, and then to disassemble the test setup. See Figure 3-6.

1. Steps 1 through 6 in Section 3.8 is the same for high pressure extension tests except that the triaxial extension cap and bases are to be used, and partially lubricated ends, as previously discussed, are to be used.

2. Apply a layer of Dow Corning High Vacuum Grease on the outside of the inner membrane. Place first layer of steel plates over membrane, spaced apart enough to allow for movement from isotropic compression and shearing without touching. The plates will stick to the vacuum grease and should stay in place for the next step. See Chapter 4 for discussion of the technique and application of steel plates in the uniform strain extension tests. Use the vacuum pump and the membrane stretcher to place a 0.304 mm (0.012 inch) thick latex membrane over the first layer of plates. Apply a layer of vacuum grease over this membrane, and then place the second layer of steel plates. When all the layers of steel for that particular test are installed, install the sealing layers of membranes (0.635 mm thickness) over all the inner layers.

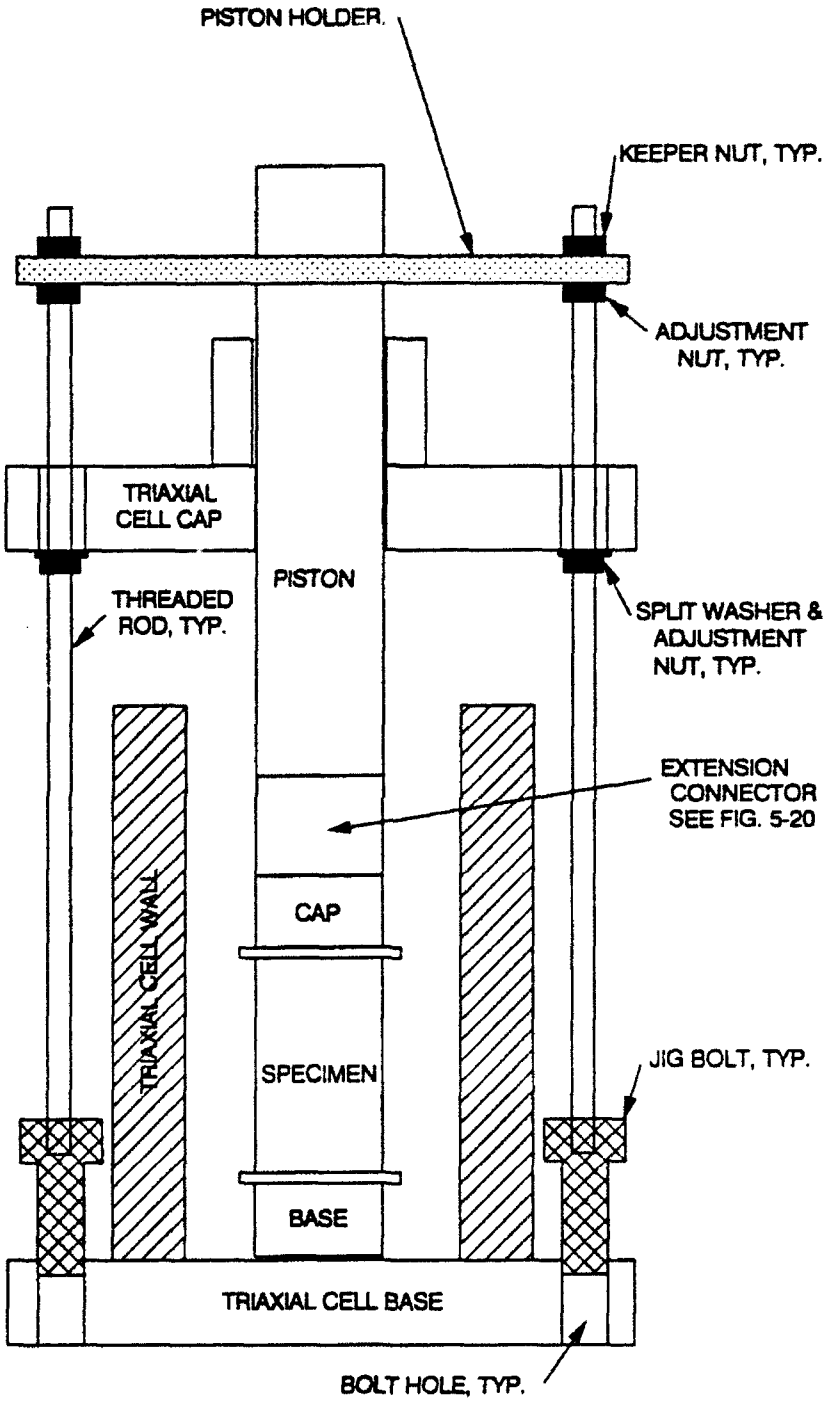

TRIAXIAL EXTENSION TEST SETUP

NOT TO SCALE
FIGURE 3-6

3. Step 8 in Section 3.8 is the same for high pressure extension tests.

4. Close the top and bottom drain valves, trapping the vacuum inside the specimen, and turn off vacuum pump. Place extension test connector on top of specimen cap. Screw the extension connector plug into specimen cap allowing enough slack to provide enough space for movement during isotropic compression with an additional 1.5 millimeters (0.06 inch) to allow piston friction stabilization. Record this dimension. Install triaxial cell wall over specimen.

5. Install the extension test jig bolts in bolt holes 1, 4 and 6. Screw threaded rod into jig bolts. Move vertical position adjustment nuts to the proper height on the threaded rod, which will allow enough working room between the triaxial cell cap and cell wall. Place split washers on adjustment nuts. Use overhead pulleys to lift triaxial cell top cap with the connection chains through the 2/3 and 5/7 bolt holes until it is over the threaded rods. Carefully lower triaxial cell cap, allowing the threaded rods to pass through the 1, 3 and 5 bolt holes until it rests on the split washers atop the adjustment nuts. Insert the piston with the threaded end down into the triaxial cell top cap by gently tapping it through the piston seal. Adjust location of piston holder adjustment nuts on the threaded rods, such that piston will be above specimen. Slide the piston holder over the threaded rods until it contacts the nuts. Clamp the piston holder onto the

piston with a hex wrench to rigidly attach it to the piston. Lower piston until it is suspended slightly above the extension connector by turning the piston holder adjustment nuts. Use the extension connector tool to grab the connector. Rotate the extension connector against the threads on the end of the piston until it threads onto the piston. This may take several minor adjustments to the vertical alignment of the cell cap. Thread the piston holder keeper nuts down on top of the piston holder to rigidly fix the piston in place. After the extension connector is fully screwed onto the piston, carefully lower the triaxial cell cap down to the cell wall by turning the vertical adjustment nuts. After contact with the cell wall is made, remove the split washers, and slightly rotate cap and wall to ensure that the O-rings are properly seated.

6. Place washers over bolt holes 2, 3, 5, 7 and 8 on triaxial cell cap. Put bolts in these bolt holes and finger tighten. Be sure to install the wire rope lifting loops around the 2/3 and 6/7 bolts. Using the ratchet wrench with the handle extension, tighten bolts alternately to evenly compress O-rings.

7. Start filling triaxial cell with water soluble oil by applying air pressure in the holding reservoir. Connect overflow line and place overflow container under overflow line.

8. When fluid flows out the overflow line into the overflow container loosen

the piston holder with the hex wrench, and carefully lower the piston until the extension connector makes contact with the specimen cap. Lower the air pressure in the holding reservoir to about 0.048 MPa (7 psi), close overflow valve, and remove overflow line. Remove piston holder from threaded rods. Remove threaded rods and jig bolts. Place washers on remaining bolt holes, and using the ratchet wrench with the handle extension, tighten bolts alternately to evenly compress O-rings.

9. Steps 13 through 19 in Section 3.8 is the same for high pressure extension tests.

10. Step 20 in Section 3.8 is the same for high pressure extension tests, except the amount of slack between the extension connector and the specimen cap is a required input by the extension test control program.

11. Steps 21 through 25 in Section 3.8 is the same for high pressure extension tests.

12. Remove all bolts and their associated washers. Install jig bolts, and threaded rod with split washers on the vertical adjustment nuts. Install piston holder and clamp firmly down onto piston with hex wrench. Install lifting chains through the 2/3 and 5/7 bolt holes, and using the overhead pulleys carefully lift the triaxial cell cap and piston up a distance less than

the slack distance between the extension connector and the specimen cap. Move the retaining nuts under the piston holder as it is moved upward. Using the extension connector tool, loosen the extension connector until it makes contact with the specimen cap. Again, lift the cell cap and piston up a distance less than the slack distance, and loosen the extension connector. Repeat this procedure until the extension connector is loose from the piston. Remove the piston from the cell cap. Remove the split washers and the threaded rods. Remove the triaxial cell cap. Remove the cell wall.

13. Steps 27 through 28 in Section 3.8 is the same for high pressure extension tests.

CHAPTER 4 - STRAIN LOCALIZATION AND NONUNIFORM STRAINS

4.1 Introduction

Analyses of most laboratory tests on soils assumes that the soil matrix can be accurately represented as a continuum, and that the soil deforms such that uniform strain conditions exist throughout the specimen. Specifically, in cylindrical compression and extension triaxial testing, the specimen is assumed to deform as a right cylinder, such that all parts of the specimen participate equally in the overall global strains. If the specimen does not behave in this manner, the computations of axial strain, volumetric strain, and global stresses are not entirely correct.

Strain localization occurs when most of the deformations are located within a small portion of the specimen. Shear planes are a common example of strain localization. Generalized strain is the opposite condition of localized strain, and occurs when the entire specimen is participates equally in the global strains. However, nonuniform strains can occur that are in a generalized strain condition, in which all parts of the specimen are participating, but the contributions are not uniform between portions. This condition may occur in triaxial compression tests as exemplified by "bulging" or "barreling".

4.2 Desirability of Maintaining Uniform Strains in Soil Testing

Whether test results that exhibit either strain localization or uniform strains

more accurately represents the true field condition of soils is pertinent to laboratory testing philosophy. It is true that in natural deposits of soils there are widely varying conditions, which may lead to failure by shear plane development. However, finite element codes with appropriate constitutive models successfully predict shear plane development using results from tests exhibiting uniform strain conditions. The key point is that adequate discretization of the finite element grid is required where the weaker soils exist or where stress concentrations occur. The weaker portions of the soil deposit must be represented by different soil parameters obtained from different uniform strain tests for the stress and material conditions of that portion of the deposit. A single test result in which strain localization occurs does not represent an entire field deposit. If a shear plane is to occur through an element in which weak soil resides or in which stress concentrations occur, then displacement compatability within the finite element code requires that adjacent elements along the shear plane must also have weak soils, otherwise the shear plane will not propagate. Therefore, traditionally laboratory testing in soil mechanics seeks uniform strain conditions to most accurately represent soils in field conditions. These uniform strain tests need to be performed for each soil type and each different field condition to accurately represent the entire field deposit.

4.3 Review of Strain Localization in Low Pressure Triaxial Compression

Nonuniform density in a soil specimen may cause strain localization. Since the lower density regions within a specimen have lower shear strength, strains will

tend to accumulate here, rather than in the denser portions of the specimen, and at low confining pressures may cause shear planes. Shear planes result in a rapid decrease in the load carrying capacity of the specimen, and a decrease in volumetric strain, because only a small portion of the specimen is participating in the shearing. Shear planes occur after failure in triaxial compression.

At low confining pressures in triaxial compression, the specimen will tend to dilate during shearing. As the soil dilates the density decreases, which accentuates the nonuniform density and may precipitate the development of strain localization in the form of shear planes (Lade, 1982). Compressive volumetric soil behavior during shear has the opposite effect. The lower density portions will compress and increase in strength. Eventually, the specimen will tend toward uniform density and uniform strains.

If there is sliding friction between the specimen and its cap or base, such as when lubricated ends are not employed, nonuniform strains may result. These nonuniform strains are different than shear planes, in that the specimen is undergoing generalized strains, but that different portions are undergoing different relative amounts of the total strain. At larger axial strains, the specimen appears as bulged outward in the middle portion of the specimen and is smaller in diameter at the ends. This deformation invalidates the assumption of deformation as a right cylinder. The friction between the cap and base results in shear stresses being developed, which acts with the same effect as a slightly higher confining pressure being applied to the entire specimen (Lee, 1978). The effect of this is to actually slightly increase the load carrying capacity of the specimen and the

steepness of the stress-strain curve, and it generally results in a smaller axial strain-to-failure. The specimen also has more compressive volumetric strain behavior. It is theoretically possible to analytically correct the stresses caused from tests exhibiting nonuniform strain conditions by utilizing nonuniform strain distributions, such as a parabolic distribution (Murphy, 1970). However, the relative strain distribution between the ends and middle of the specimen must be known or assumed. Stresses and strains from tests experiencing shear planes cannot be accurately corrected, because the strains are too highly localized, and their exterior shape does not necessarily reflect the strain conditions within the specimen.

4.4 Observations in High Pressure Triaxial Compression Tests

Drained, triaxial compression tests were performed between effective confining pressures of 2.22 MPa and 52.0 MPa. Undrained, triaxial compression tests were performed between initial effective confining pressures of 6.45 MPa and 68.92 MPa. These tests are presented in great detail in other pertinent chapters. However, observations relating to strain localization are discussed here.

Only the drained tests at a confining pressure of 2.22 MPa and the undrained tests up to initial confining pressures of 16.9 MPa show any dilatant tendencies. The remainder of the tests at higher confining pressures generally exhibited extreme compressive behavior, which would indicate that strain localization in the form of shear planes should not develop, and indeed none were ever observed.

The Cambria sand is rather coarse and it exhibits a dark color, which makes visual identification of shear planes very difficult. Additionally, several thicknesses of membranes are used to prevent leakage during high pressure tests. At the conclusion of the test, when the cell pressure has been brought down, and the triaxial cell disassembled, several membranes must be removed from the specimen without disturbance to visually inspect the specimen. All of these factors make identification of shear planes difficult. The softening regimes of the drained tests do not indicate any rapid decrease in deviator stresses that would indicate shear plane development.

Many different types of lubricated ends and techniques were employed to obtain uniform strain conditions for the high pressure triaxial compression tests. As discussed in Section 3.5, at high pressures the most successful lubricated ends simply provide enough separation between the sand and the surface of the cap/base, such that under high deviator stresses and large axial strains to failure, the grains cannot fully penetrate through the lubricated ends to generate friction on the surface of the cap or base. The axial strains to failure in the drained triaxial compression tests were large, typically well over thirty percent, which makes uniform strains difficult to achieve unless the lubricated ends perform well. The axial strains for the undrained tests were smaller, typically between fifteen and thirty percent.

Prior to successfully finding lubricated ends that worked well over a large range of axial strains, some nonuniform strains were experienced in the form of slight bulging or "barreling" of the specimen, caused by nominal friction on the cap

and base. These conditions occurred in the high pressure drained triaxial compression tests that had high deviator stresses and the largest axial strains at failure, approaching forty percent. These tests were between 5.8 and 26.0 MPa confining pressure. Analytical strain corrections based upon nonuniform strain distributions are difficult, since the ends of the specimen are not fully restrained. This results in an undefined level of sharing of strains between the ends and the middle of the specimen. Therefore, analytical nonuniform strain corrections were not performed on these test results. After lubricated ends were successfully developed that performed over a large strain and pressure range, uniform strains were obtained and "barreling" was no longer a problem. Figure 4-1 shows uniform strain specimens obtained at 52.0 MPa confining pressure.

None of the undrained tests exhibited "barreling", because they required much lower deviator stresses, and smaller axial strains to produce failure. Figure 4-2 shows uniform strains obtained in undrained compression tests.

In conclusion, high pressure triaxial compression tests did not experience significant strain localization, especially when successful lubricated ends were utilized.

4.5 Review of Strain Localization in Low Pressure Triaxial Extension

Strain localization effects as previously discussed for triaxial compression tests is much more pronounced in triaxial extension. Therefore, the effect of nonuniform density, dilatant behavior, and boundary conditions are similar, but greater in magnitude than in triaxial compression tests. However, the effect of

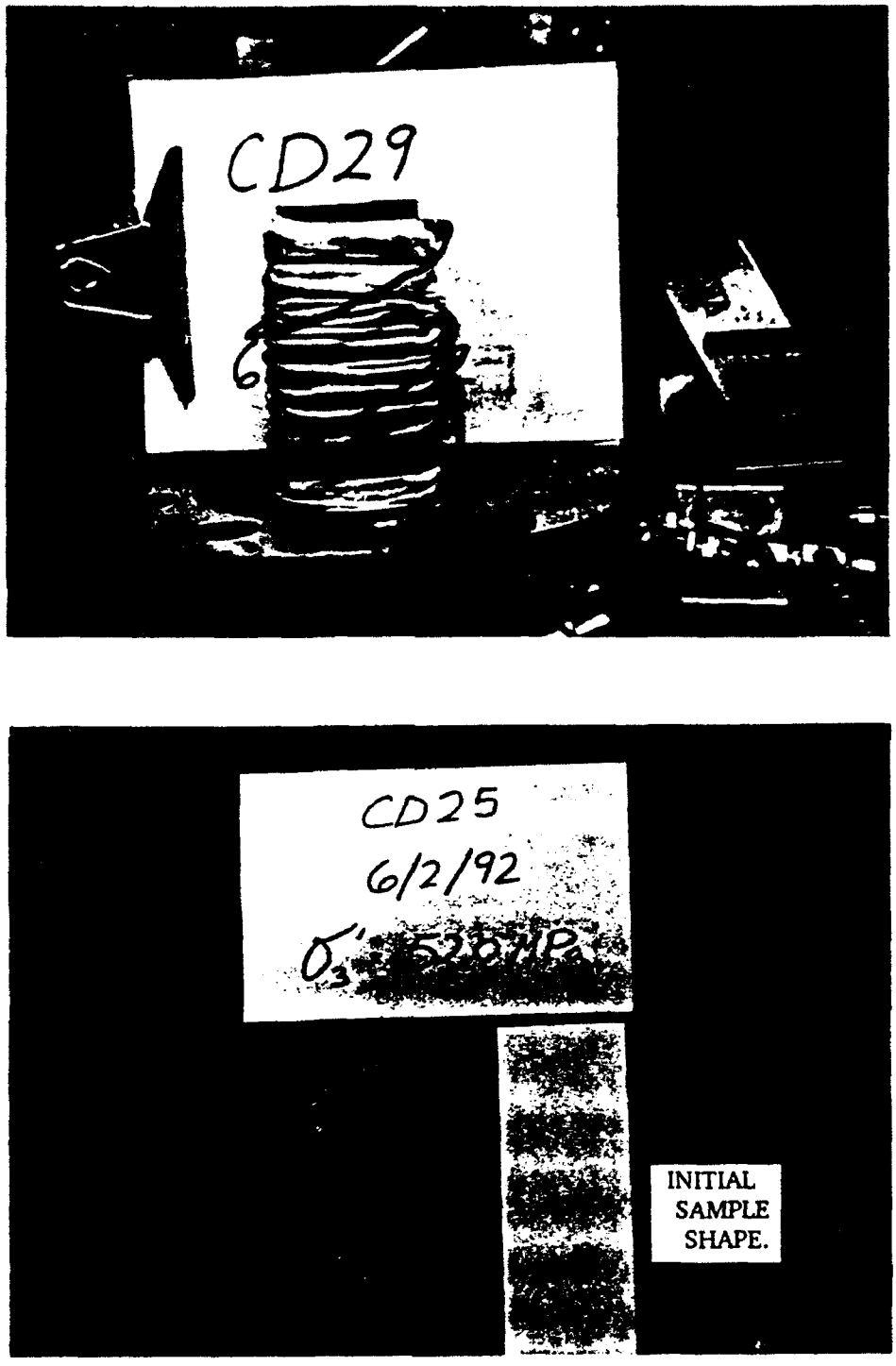

Figure 4-1 Photographs Exhibiting Test Specimens Showing Uniform Strain Conditions after 52.0 MPa Drained Triaxial Compression Tests. (Top) Inside membranes. (Bottom) Removed from membranes.

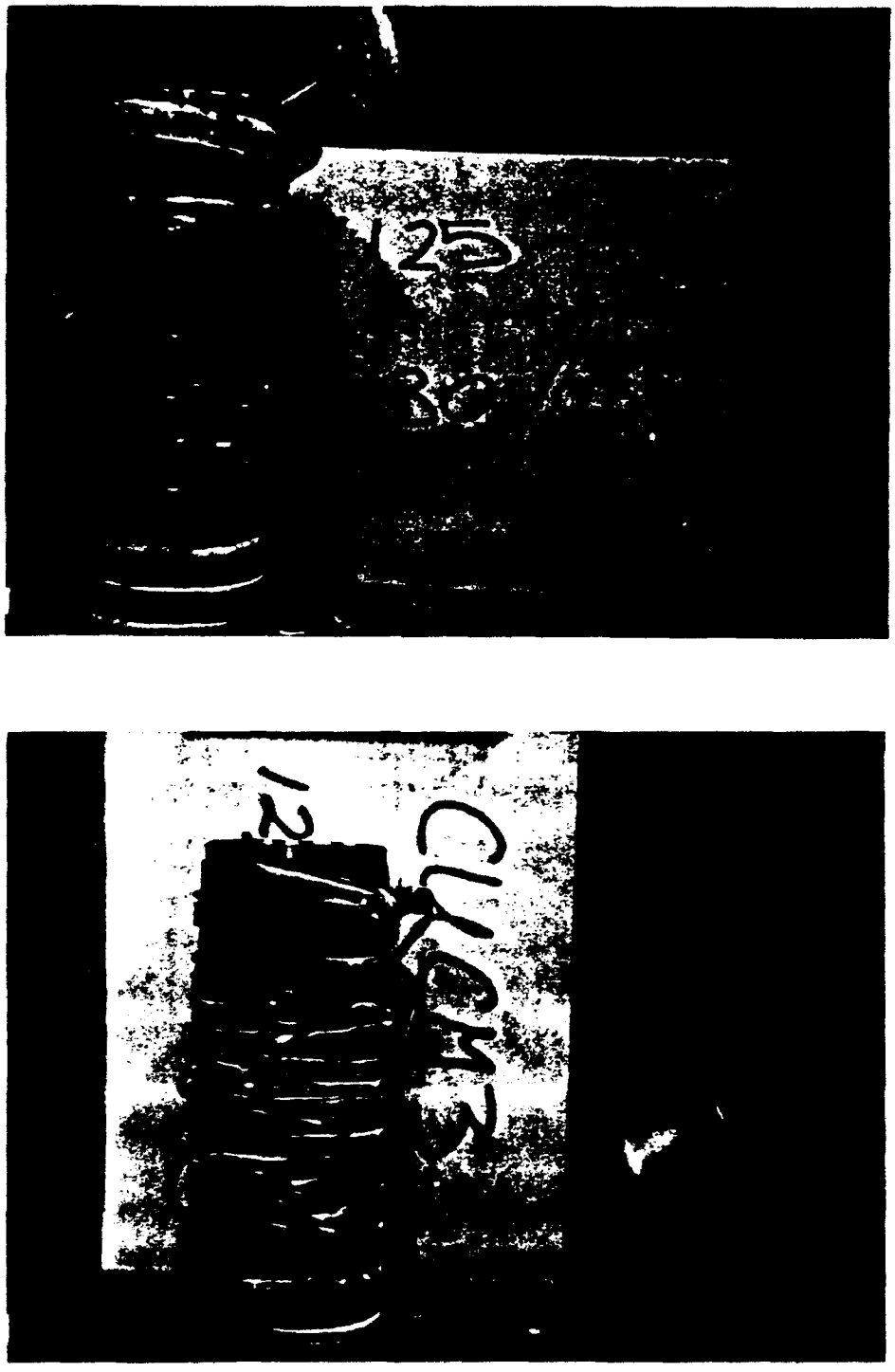

Figure 4-2 Photographs Exhibiting Two Test Specimens Showing Uniform Strain Conditions after Undrained Triaxial Compression Tests.

strain localization on the strength of soil in extension is much greater than in compression. Friction angles showing differences of as much as ten degrees (Lade, 1982) have been reported between test results with strain localization as opposed to uniform strain conditions. When shear planes develop at low pressures, the bulk of the shearing and dilation is occurring along the shear plane. The rest of the specimen is undergoing elastic compression, which causes the volumetric strains appear to be much more compressive. Strain localized test results also show a tendency for steeper stress-strain curves, and smaller strains-to-failure. Results tend to be highly scattered, but with shear strengths that are always lower in strain localized tests than in uniform strain tests. It appears that in extension, the occurrance of strain localization severely affects failure, whereas in compression it does not (Lam and Tatsuoka, 1988b). Strain localized extension tests appear to have approximately the same shear strengths as comparable compression tests, whereas uniform strain extension tests appear to have higher strengths (Green, 1971, Lade and Duncan, 1973, Lam and Tatsuoka, 1988b, Proctor and Barden, 1969, Reades and Green, 1976, Wu and Kolymbas, 1991).

4.6 Observations in Conventional High Pressure Triaxial Extension Tests

Conventional drained extension tests were performed between confining pressures of 0.25 and 52.0 MPa. The term conventional refers to the fact that the specimen is covered only with flexible latex rubber membranes, and not surrounded by any rigid boundaries except the cap and base. Undrained extension tests, which suffered from strain localization, were performed between initial

confining pressures of 12.0 and 68.0 MPa. The extension test as described here consists of drained isotropic consolidation followed by shearing with constant effective confining pressure. The shearing consists of decreasing the vertical stress, by raising the piston under axial strain control. The drained tests allow the specimens to change in volume through a volume change measuring device. The undrained tests prevent the volume of the specimens from changing by closing the drainage valves at the initiation of shearing. The induced pore pressures are measured by a pressure transducer. Tests performed below 2 MPa were conducted in a conventional low pressure triaxial cell. Higher pressure tests were performed in the high pressure triaxial cell.

4.6.1 Observations from Conventional Drained Extension Tests

After the first few conventional drained extension tests had been performed, it became very apparent that strain localization, in the form of necking occurred, at all confining pressures and in all tests. Figure 4-3 shows a photograph of a typical conventional extension test specimen after shearing. Strain localization occurred regardless of whether the volumetric strain tendency was dilatant or compressive. The location of necking varied within the specimen, but most were located in the middle two-thirds of the specimen. The stresses and strains for these conventional drained strain localized extension tests were calculated based upon uniform strain assumptions.

Stress-strain characteristics from conventional drained extension tests are shown on Figures 4-4 and 4-5. These diagrams display the effective principal

Figure 4-3 Photograph Exhibiting Test Specimen Showing Strain Localization in a Drained Triaxial Extension Test.

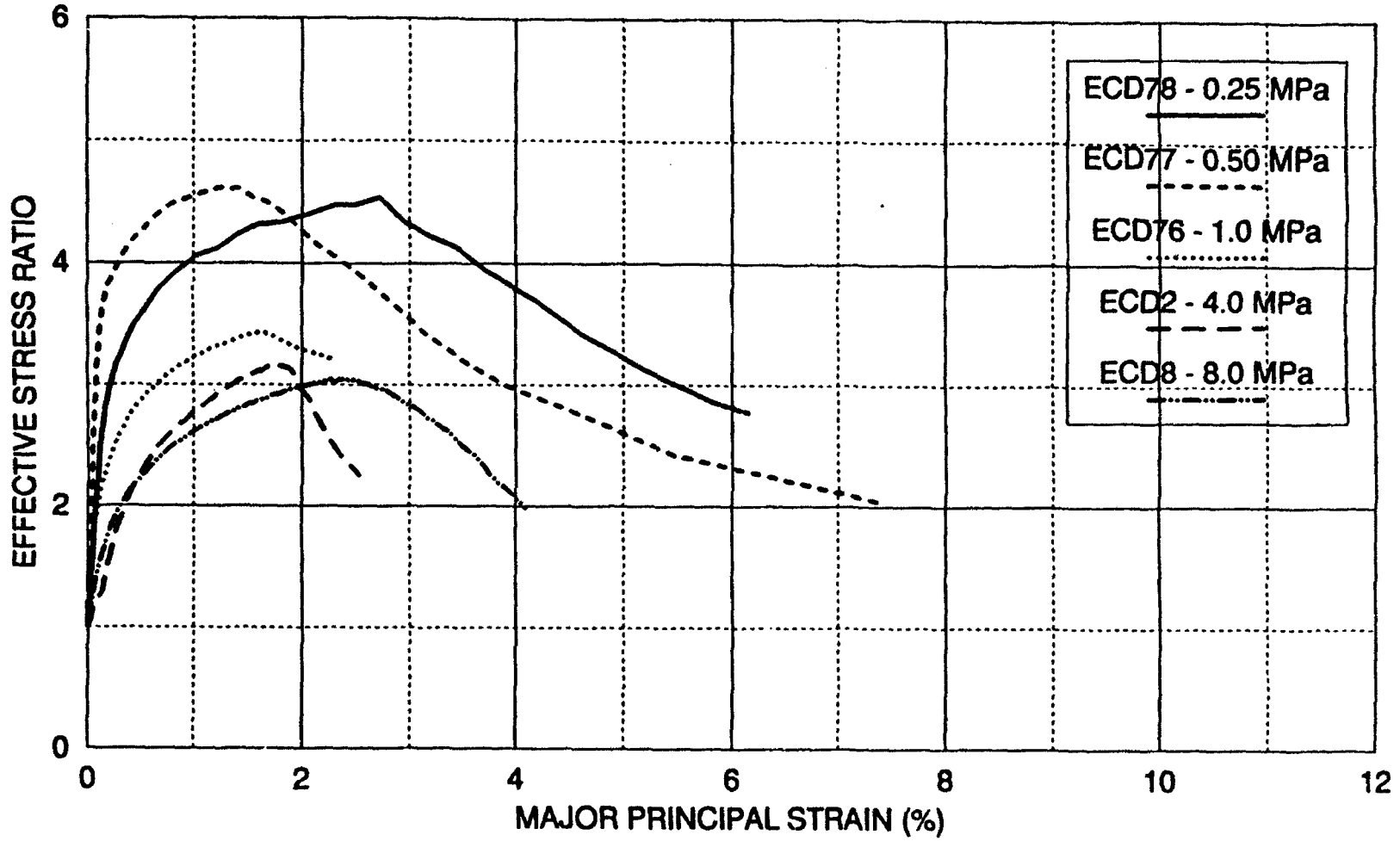

FIGURE 4-4 - STRESS RATIO 0.25 TO 8.0 MPa
CONVENTIONAL DRAINED TRIAXIAL EXTENSION
DENSE CAMBRIA SAND

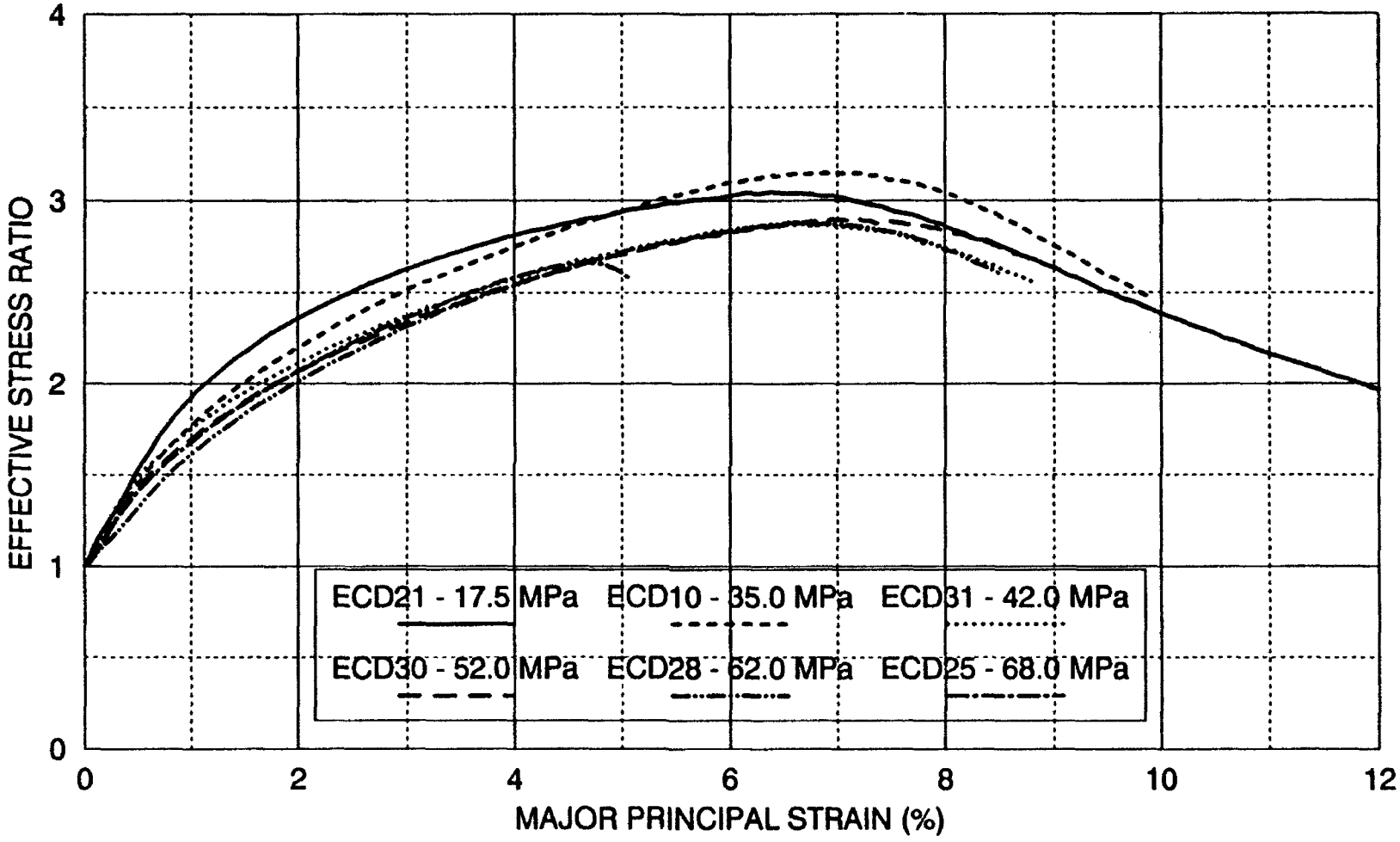

FIGURE 4-5 - STRESS RATIO 17.5 TO 68.0 MPa
CONVENTIONAL DRAINED TRIAXIAL EXTENSION
DENSE CAMBRIA SAND

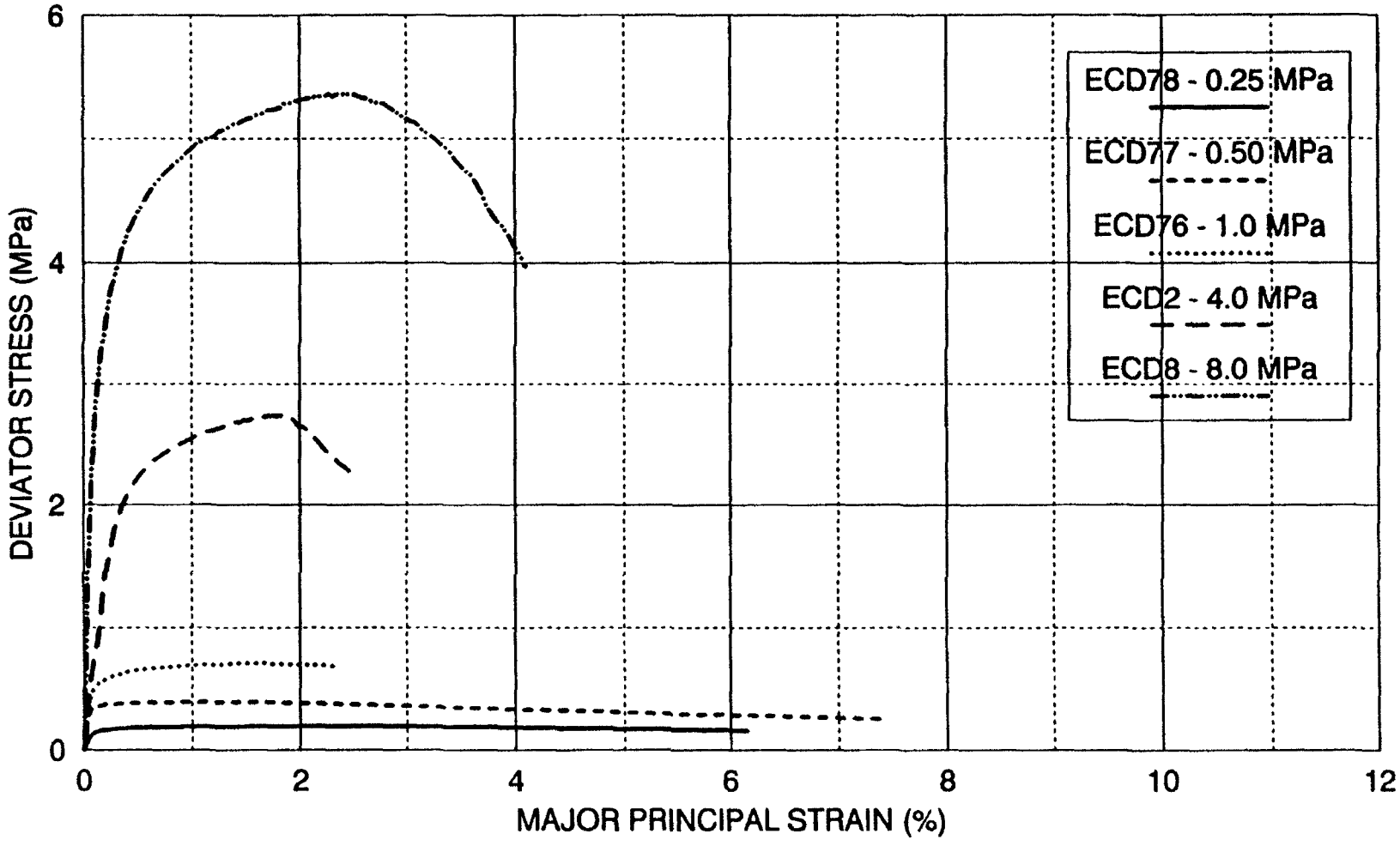

FIGURE 4-6 - DEVIATOR STRESS 0.25 TO 8.0 MPa
CONVENTIONAL DRAINED TRIAXIAL EXTENSION
DENSE CAMBRIA SAND

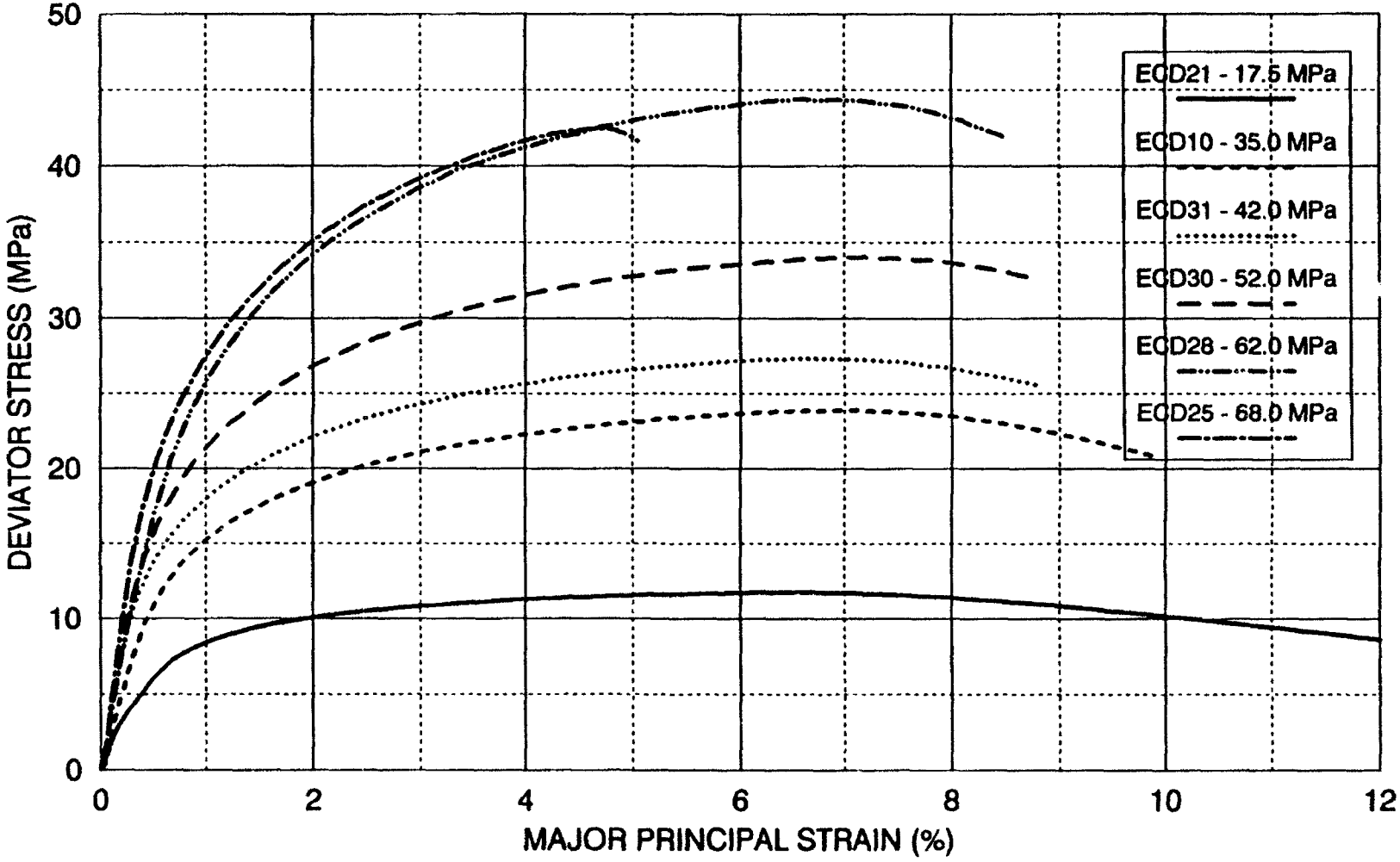

FIGURE 4-7 - DEVIATOR STRESS 17.5 TO 68.0 MPa
CONVENTIONAL DRAINED TRIAXIAL EXTENSION
DENSE CAMBRIA SAND

stress ratio plotted against the major principal strain (ϵ_1). The deviator stresses are displayed on Figures 4-6 and 4-7. These figures clearly indicate the large amount of scatter in test results, induced largely from strain localization effects. The results indicate considerable scattered crossing of stress-strain curves between tests of different confining pressures. For example the 0.5 MPa test has a higher maximum effective stress ratio than the the 0.25 MPa test, and the strain to failure is lower. Also, the initial slope 0.25 MPa on the effective stress curve is less steep than than 0.5 MPa test. Other examples of inconsistent stress-strain behavior are easily observed on these figures. The steep declines in strength after peak failure clearly indicate that strain localization is dominating and, in fact, producing the failure condition. The higher pressure tests tend to show less scatter than the lower pressure tests. This can be explained by the argument presented in Section 4.3, in which it was stated that with increasing dilatant volumetric tendency at low confining pressures the strain localization tendencies increase and they become more erratic. As discussed in Section 1.10, high pressures tend to create uniform density and true isotropy. This would explain the more consistent stress-strain behavior at the higher pressures.

The volumetric strains for the tests are shown on Figures 4-8 and 4-9. They also show considerable scatter and crossing of curves. The lower pressure tests more clearly show the effect of strain localization. The higher pressure tests appear to exhibit a more uniform pattern as was indicated for the stress-strain behavior. After strain localization occurs, there is a break in the slope of the volumetric strain curves, which is characterized by flattening or a reduction in

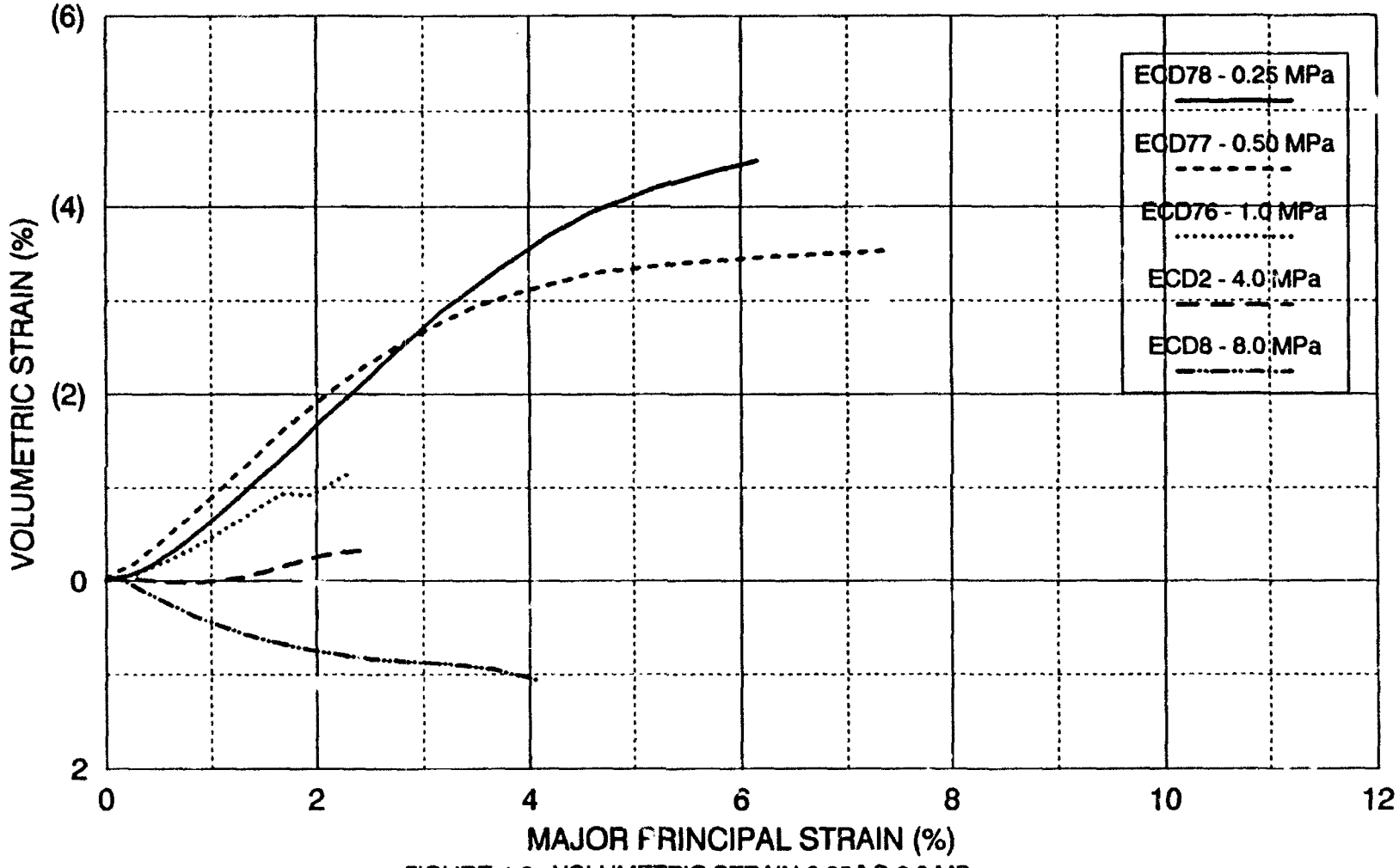

FIGURE 4-8 - VOLUMETRIC STRAIN 0.25 TO 8.0 MPa
CONVENTIONAL DRAINED TRIAXIAL EXTENSION
DENSE CAMBRIA SAND

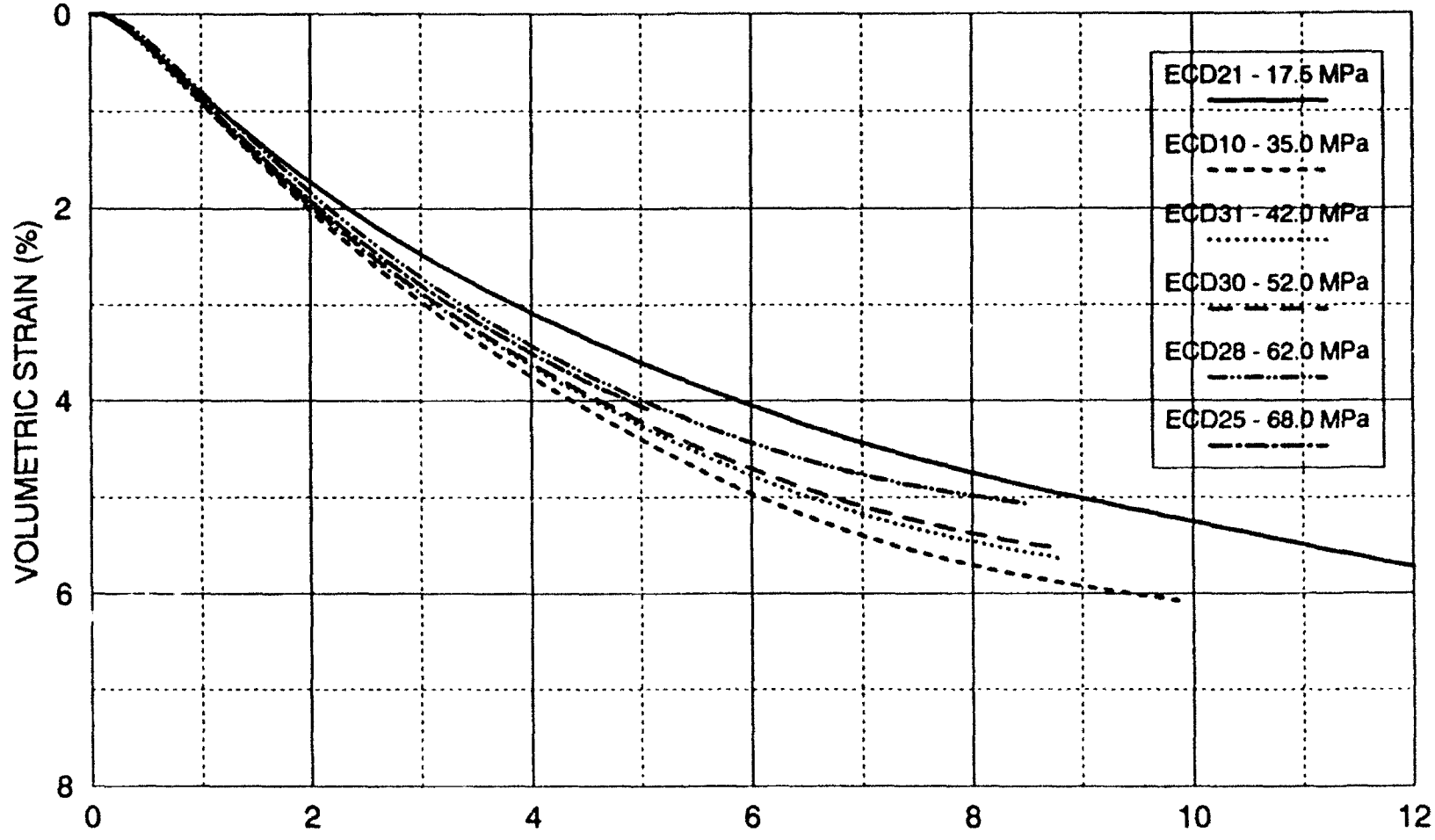

FIGURE 4-9 VOLUMETRIC STRAIN 17.5 TO 68.0 MPa
CONVENTIONAL DRAINED TRIAXIAL EXTENSION
DENSE CAMBRIA SAND

volume change tendencies. This is observed in all tests on Figure 4-8. A break in the slope of the volumetric strain curve is not apparent at higher confining pressures (Figure 4-9), because much of the volumetric compression is caused by particle breakage and rearranging. At high pressures particle breakage and rearranging continues, even after strain localization occurs, but not in as large a quantity as under uniform strain conditions. Comparisons with successful uniform strain drained extension tests will be discussed in a later section in this chapter.

4.6.2 Observations from Undrained Strain Localized Extension Tests

A series of undrained extension tests were performed, in which strain localization occurred. These tests were not truly conventional tests, since they were performed with an early, but not entirely successful version of the method eventually employed to enforce uniform strains. Therefore, strain localization occurred, but probably was not quite as pronounced as would be expected in true conventional undrained extension tests.

The stress-strain characteristics are displayed on Figure 4-10, which shows the effective principal stress ratio plotted against the major principal strain (ϵ_1). The deviator stresses are shown on Figure 4-11 plotted against the major principal strain. As confining pressure increases, the maximum effective stress ratios first decrease slightly at the 17.6 MPa test, and then increases in the 26.0 MPa test, but then again decreases to the highest confining pressure test 68.0 MPa. This scattered, inconsistent pattern does not seem reasonable and would appear to be due to strain localization. The strains to failure increase, and then remain fairly

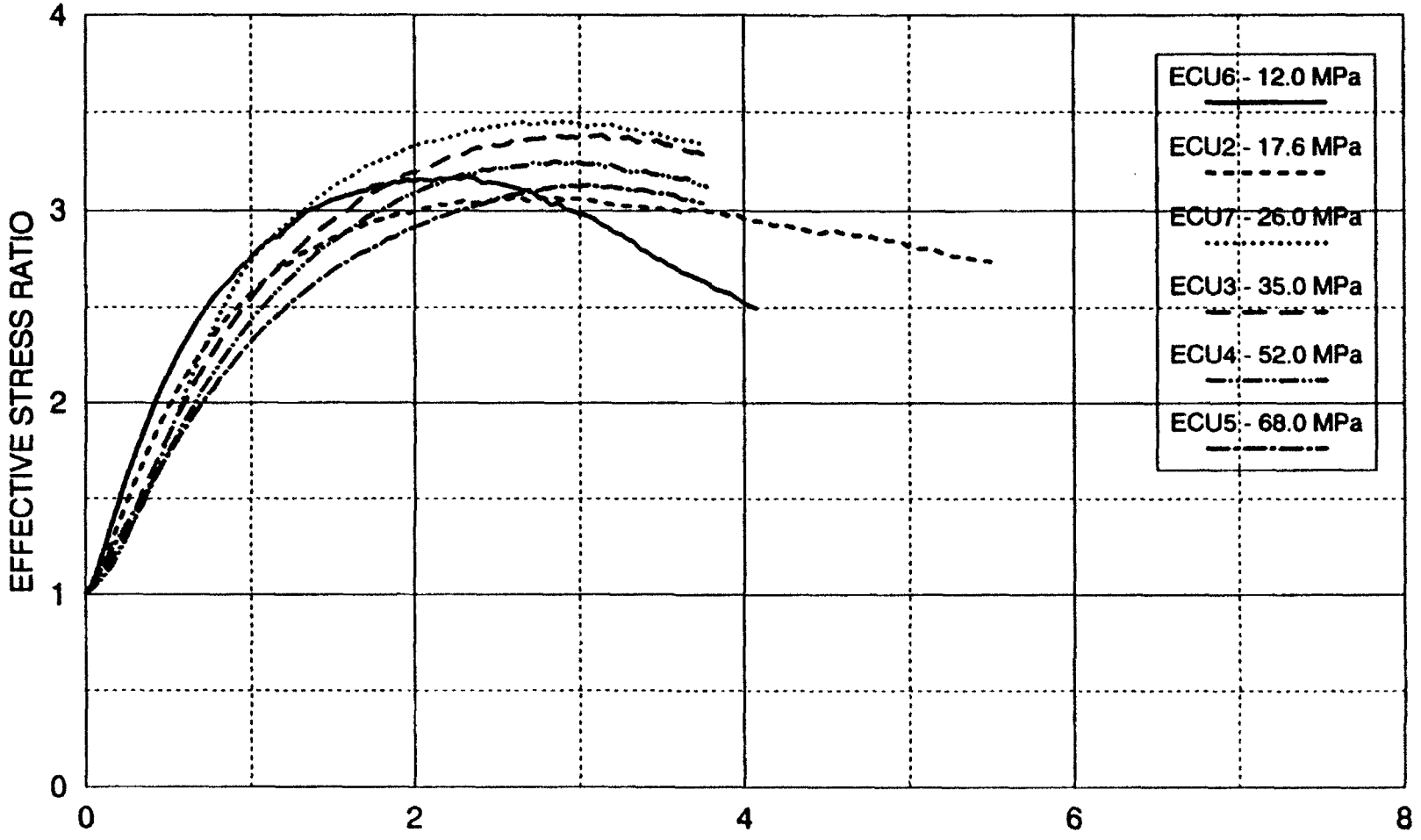

FIGURE 4-10 - EFFECTIVE STRESS RATIO
STRAIN LOCALIZED UNDRAINED TRIAXIAL EXTENSION
DENSE CAMBRIA SAND

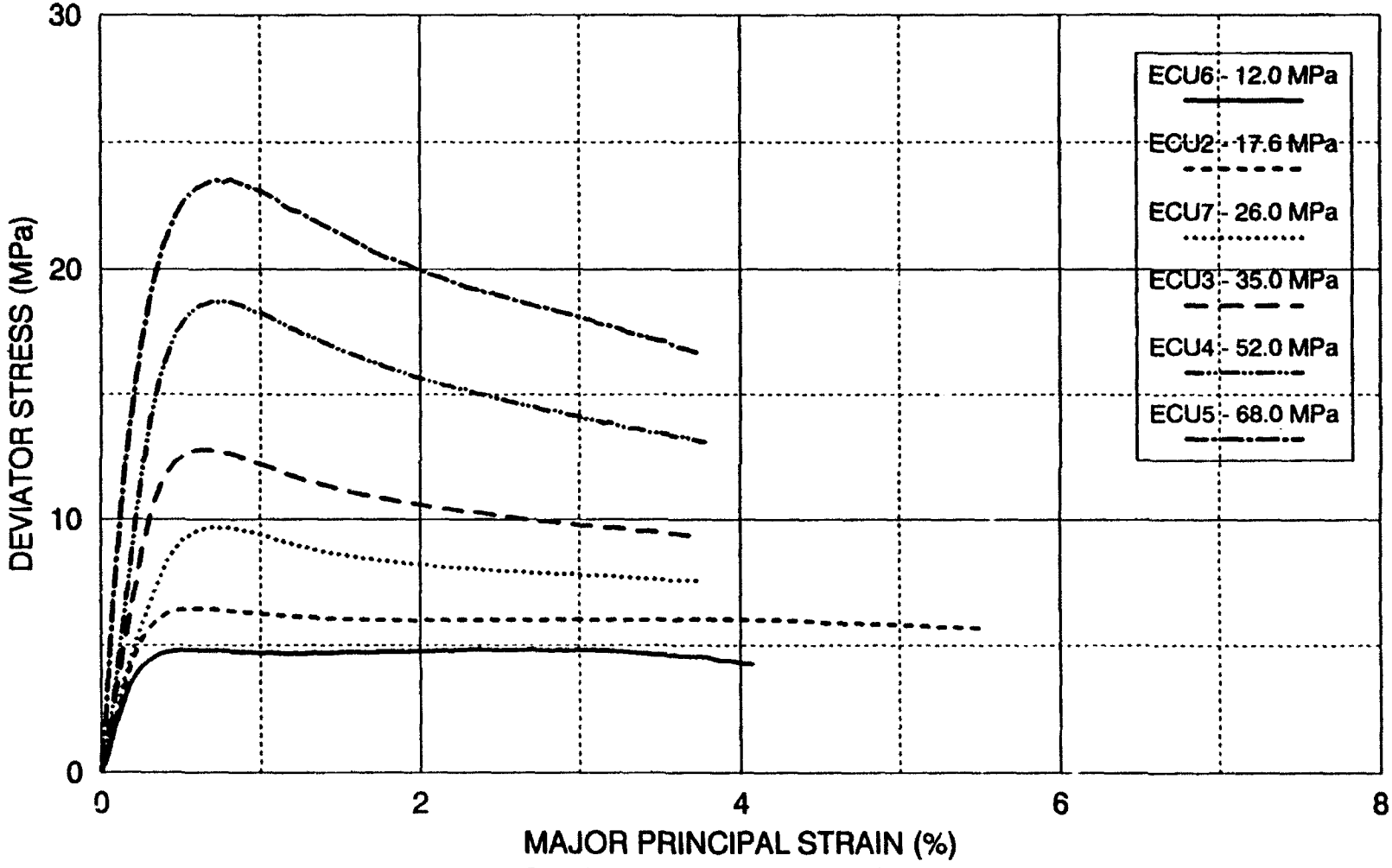

FIGURE 4-11 - DEVIATOR STRESS
STRAIN LOCALIZED UNDRAINED TRIAXIAL EXTENSION
DENSE CAMBRIA SAND

constant with increasing consolidation pressure. The deviator stresses appear to present a reasonable pattern with both increasing maximum deviator stress, and strain to maximum deviator stress, at and above the 17.6 MPa test. However, this reasonable pattern of behavior in the deviator stresses occurs at very low strains values, where significant effects of strain localization have not yet dominated the results. The maximum values of effective stress ratio decline at the higher confining pressures, because at the larger principal strain values, localization is more severely affecting the deviator stresses, which in turn lowers the effective stress ratio.

The effective stress paths for the strain localized undrained extension tests are shown on Figure 4-12. The stress paths are shown on the Cambridge p'-q diagram, in which the stress difference, q (deviator stress), is plotted on the vertical axis, and the effective mean normal stress, p', is shown on the horizontal axis. The total stress path of the test is represented by a line descending from the horizontal axis on a three to one slope. The magnitudes of the pore pressures are indicated by the horizontal distance between this line and the effective stress path. The test results generally show a reasonable general pattern of behavior for high pressure undrained tests. As the initial confining pressure is increased, an increase in pore pressure is observed. The stress difference reaches a maximum, and then decreases to the effective stress failure envelope. The pore pressures are shown on Figure 4-13, in which the pore pressures are indicated on the vertical axis and the major principal strain is shown on the horizontal axis. As with the effective stress paths, the pore pressures show a reasonable general pattern of behavior.

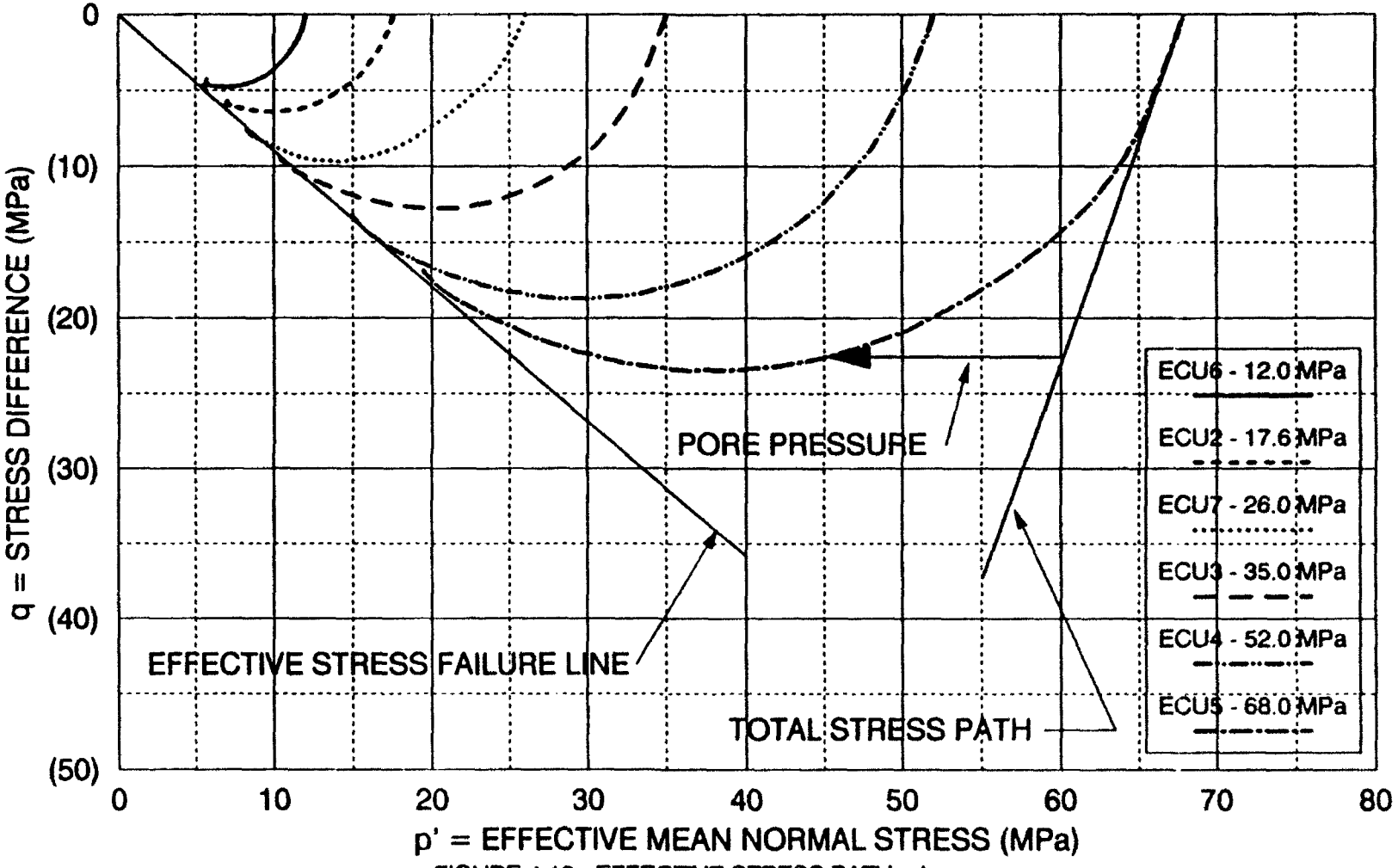

FIGURE 4-12 - EFFECTIVE STRESS PATH p'-q
STRAIN LOCALIZED UNDRAINED TRIAXIAL EXTENSION
DENSE CAMBRIA SAND

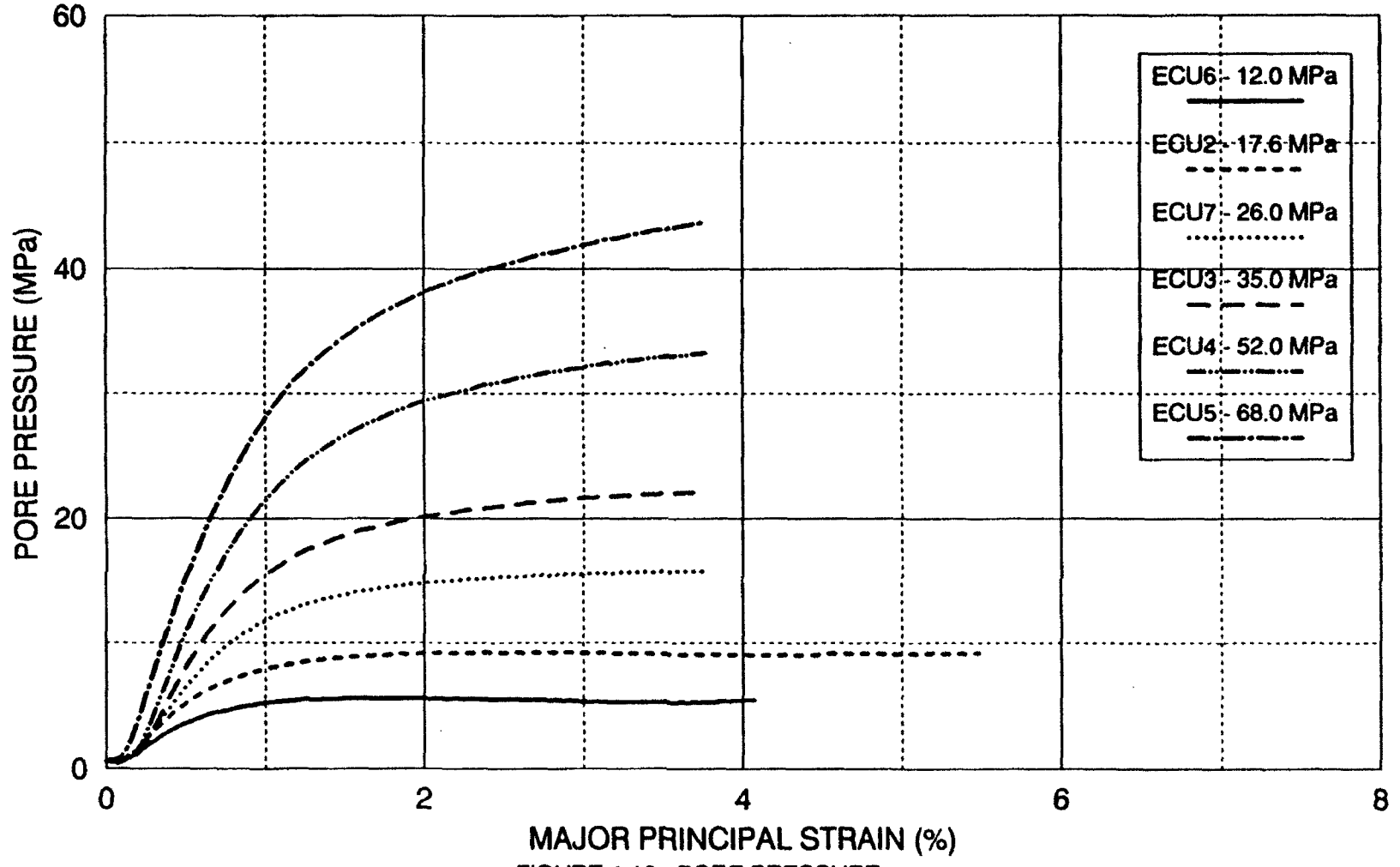

FIGURE 4-13 - PORE PRESSURE
STRAIN LOCALIZED UNDRAINED TRIAXIAL EXTENSION
DENSE CAMBRIA SAND

Comparisons with successful uniform strain undrained extension tests will be discussed in a later section of this chapter.

4.7 Progression of Strain Localization at High Pressures

Since strain localization appears to dominate the conventional triaxial extension tests, a series of seven conventional drained extension tests were performed at a confining pressure of 17.5 MPa to attempt to determine the progression of strain localization during the shearing phase of the test. The tests were performed under identical conditions, except that each of the seven tests was stopped at a different axial strain value. After the shearing was stopped, the confining pressure was removed and the specimens were held on vacuum. The triaxial cell was disassembled and the specimen diameters were carefully measured at a minimum of eleven different locations along the length of the specimens. Two additional tests at 52.0 MPa confining pressure were also included to see the effect of confining pressure on strain localization.

The results are depicted on Figure 4-14, which shows the area ratio of the different specimens plotted against axial strain. The area ratio is defined as the minimum cross-sectional area of the neck divided by the average cross-sectional area of the specimen. A value of 1.0 would indicate deformation under completely uniform strain conditions, whereas lower values would indicate a measure of strain localization. Many investigators have in the past used this quantity or other similar variations as a means of correcting the failure stress level to obtain a "uniform strain" value at failure (e.g. Reades and Green, 1976, Lam and Tatsuoka,

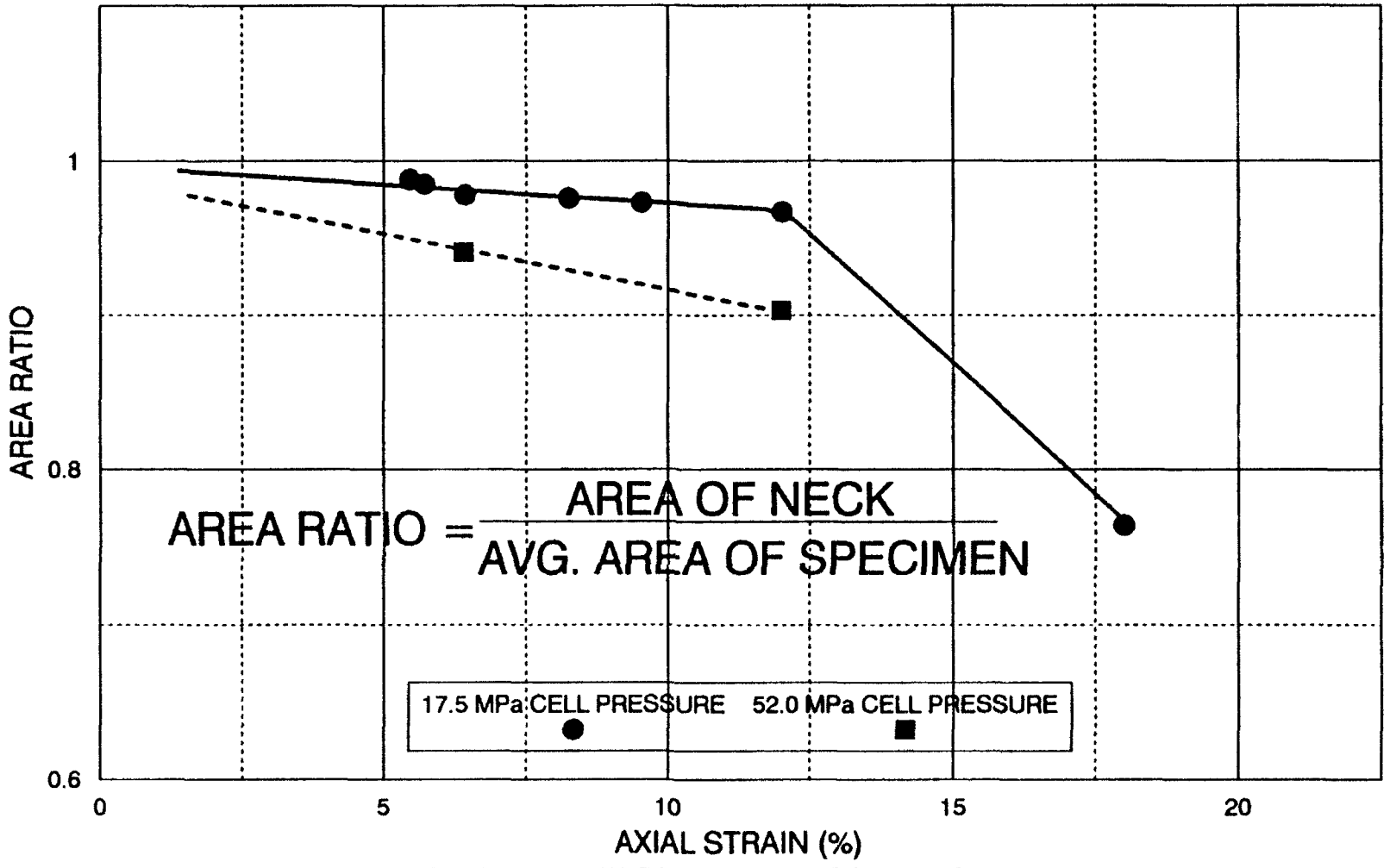

FIGURE 4-14 - AREA RATIO: STRAIN LOCALIZATION
CONVENTIONAL DRAINED TRIAXIAL EXTENSION
DENSE CAMBRIA SAND

1988, Wu and Kolymbas, 1991). The figure clearly shows that at low axial strain values, the necking appears to progress slowly, but as shearing continues to larger axial strains, the decrease in cross-sectional area at the neck progresses very quickly. Since failure for these tests generally occurs later in the test, this clearly indicates that strain localization initiates well in advance of failure. It also appears that the two curves extrapolate on converging lines that point toward zero axial strain. This would signify that necking initiates very early in the test, possibly near the very beginning. Another implication from this diagram is shown by the relative position of the 52.0 MPa line and the 17.5 MPa line. They indicate that increasing levels of isotropic compression tends to enhance the occurrence and magnitude of strain localization. Increasing levels of isotropic compression tend to decrease any initial variations in density within the specimen, and the specimen tends toward uniform density. These effects should create a condition where strain localization would not occur. However, during the process of producing uniform density, geometric irregularities in the shape of the specimen are likely created due to the compression of the looser zones. These geometric deformities may lead to earlier and larger formations of strain localization exhibited during the shearing phase.

Figure 4-15 shows typical stress-strain curves for several different drained extension tests at 17.5 MPa confining pressure. As can clearly be seen, failure in the form of peak deviator stresses can and does occur at any axial strain value. The instability and unpredictability of the conventional extension test is clearly demonstrated.

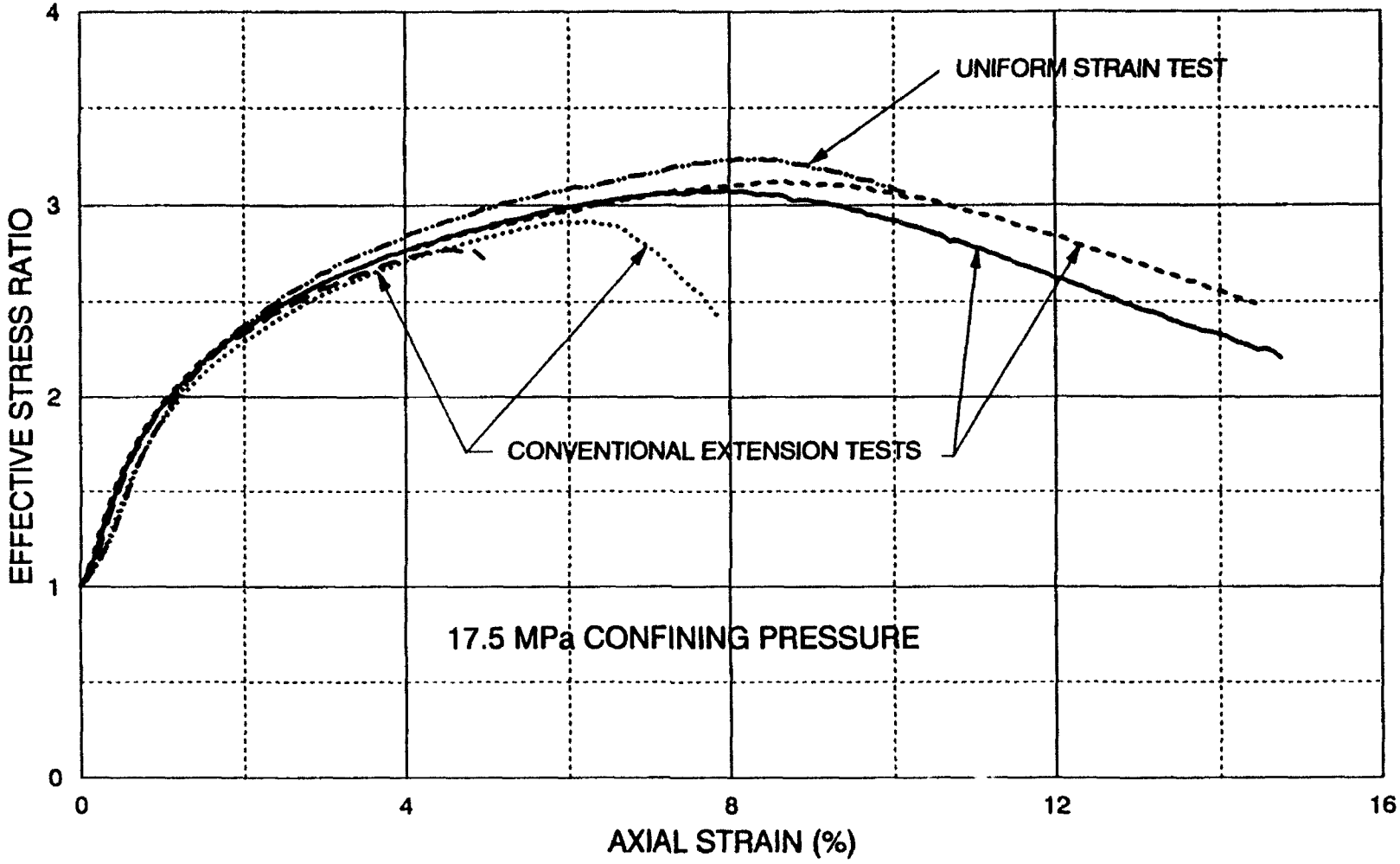

FIGURE 4-15 - STRESS RATIO AT 17.5 MPa
SEVERAL DIFFERENT DRAINED EXTENSION TESTS
DENSE CAMBRIA SAND

Experimental results clearly indicate that the conventional triaxial extension tests are inherently unstable, and failure is totally dominated by strain localization. The obvious conclusion appears to be that the conventional triaxial extension test should not be used to evaluate strength of soils in extension. The assumptions of uniform strains are violated almost from the beginning of the test, and unless accurate corrections are applied, the calculated failure stresses based upon uniform strain assumptions are much too low. Even correcting the stresses by an area correction method does not correct the inaccurate volumetric strains. Roscoe, Schofield and Thurairajah in 1963, concluded that the conventional extension test could not be used to evaluate failure criteria, because of the strain localization problems. They also concluded that a more reliable testing method needed to be developed to ensure uniform strain conditions. Since 1963 many investigators have developed three-dimensional testing devices, which do enforce uniform strains in the specimen. However, many investigators are still using the conventional triaxial extension tests to aid in the investigation of failure criteria.

Figures 4-16 and 4-17 provide reasons why the conventional triaxial extension test is inherently unstable. Figure 4-16 shows a typical compression test for any type of material. The material is divided into sections, with section 3 initially having a slightly smaller diameter as shown in the diagram on the left side of the figure. This could represent a geometric defect or a material defect, such as lower density or strength. Compressive load is then applied as shown on the right side of the figure. The initial stresses in section 3 are larger than in the surrounding sections, because the cross-sectional area is smaller. Therefore, the

COMPRESSION TEST

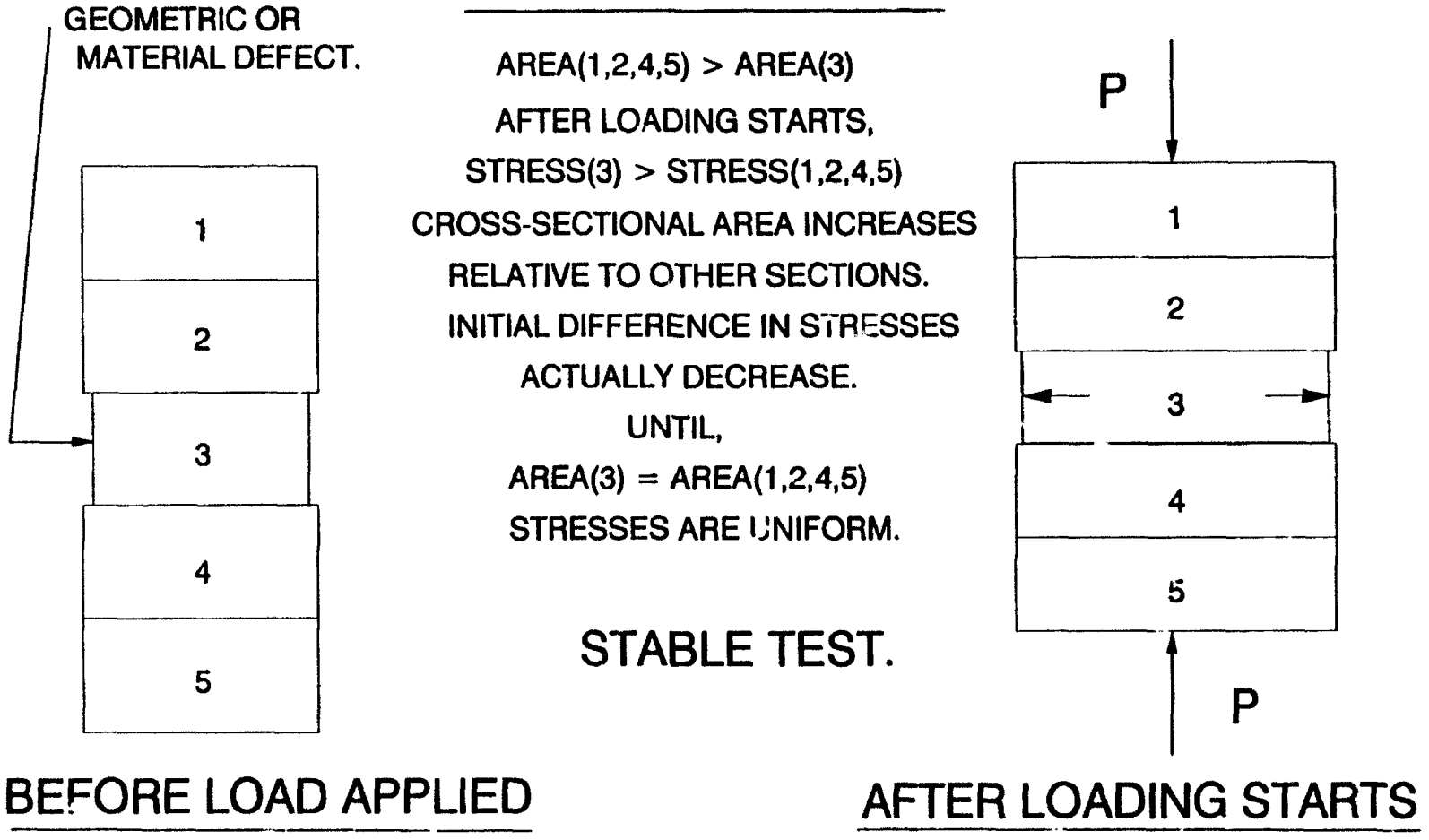

FIGURE 4-16 - DIAGRAM SHOWING COMPRESSION TEST
IS A STABLE TEST

TENSION TEST (EXTENSION)

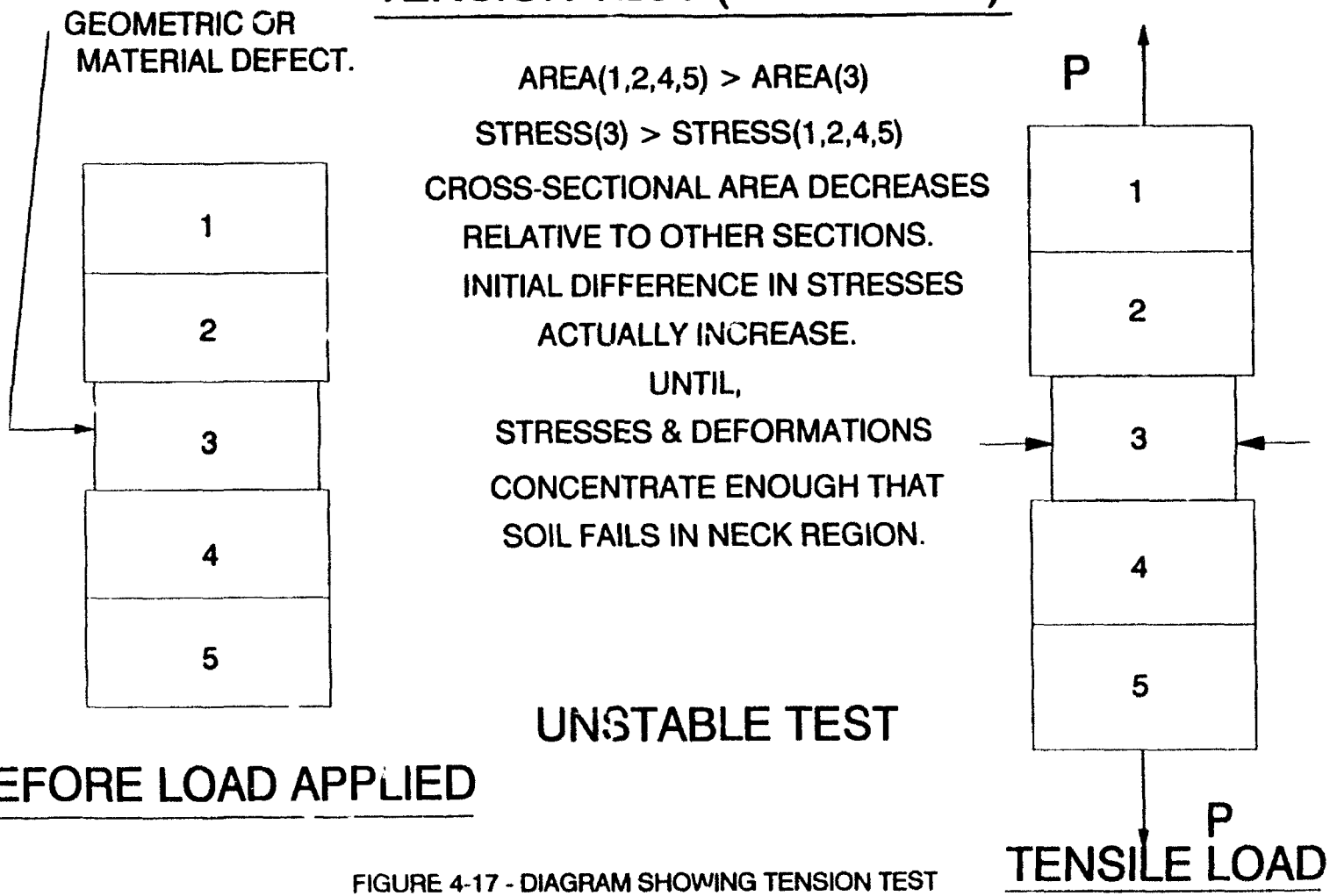

FIGURE 4-17 - DIAGRAM SHOWING TENSION TEST IS AN UNSTABLE TEST.

strains in both the vertical and horizontal directions in section 3 are relatively larger than in surrounding sections. As loading progresses, the difference in the initial stress state between section 3 and the other sections is actually decreasing, even though the total stresses are increasing. Eventually, the outward directed lateral strains in section 3 are large enough that the cross-sectional areas become equal to those in the surrounding sections. At this point the stresses are equal in all of the sections. Thus, in a compression test the initial concentration of stresses at a geometric or material defect distribute and the stress distribution tends toward a uniform stress condition. Therefore, a compression test can be considered a stable test, excluding instability by a buckling condition. Figure 4-17 depicts a tension test (extension for soils). The specimen has an assumed geometric or material defect in section 3 just as assumed for the compression specimen. When the upward load is applied, the initial vertical stress in section 3 is larger than in the surrounding sections, owing to its smaller cross-sectional area. Correspondingly, the vertical and lateral strains are also larger. However, these larger lateral strains are directed inward, thus decreasing the cross-sectional area. As upward loading progresses, the inward directed lateral strains continue to decrease the cross-sectional area in section 3 at a faster rate than in the surrounding sections. Thus, the initial difference in stresses between section 3 and the others increases very rapidly. Eventually, the material fails in the region of section 3, well in advance of the material in the other sections of the specimen. Therefore, in a tension test (extension in soils) the highest stresses are produced and concentrated in the weakest part of the specimen to form highly nonuniform

strain conditions. Therefore, the conclusion is that the conventional triaxial extension test is inherently unstable by its very nature. The only possible way to acquire uniform strains in a conventional triaxial extension test is to create a perfectly isotropic, uniform specimen with no geometric or material defects, and then apply loads to the specimen in a perfectly uniform fashion. Even for this idealized condition, such a test would then only be conditionally stable. Any small variation in the stress or strain distribution within the specimen will create an opportunity for strain localization to initiate. This unstable nature of the test itself explains the wide scatter in experimental results in conventional triaxial extension tests. Since perfection in creating a specimen is very difficult, the conventional extension test does not appear to provide a reliable means to determine soil properties in extension.

4.8 Enforcing Uniform Strains in Triaxial Extension

Since the conventional triaxial extension test does not produce uniform stresses and strains due to strain localization, it became apparent that uniform strains had to be enforced, otherwise material properties could not be properly assessed. To enforce uniform strains, a modification in the conventional extension test had to be explored. Obviously, necking in the conventional extension test is allowed by the flexible boundary condition provided by the latex membranes surrounding the specimen. The flexible membranes do not provide any means to redistribute the concentrated stresses and strains at the neck location to the soil in the rest of the specimen. Therefore, the approach undertaken was to provide

some form of external support to the soil in the horizontal direction that would be flexurally rigid. This would tend to redistribute the stress and strain concentration at the neck location. However, the system would also have to be able to move with the specimen throughout both the isotropic compression phase (decreasing specimen diameter and length), and the shearing phase (increasing specimen length and decreasing diameter). Additionally, no friction between the soil and the uniform strain enforcement system could be tolerated, since the vertical forces on the soil are measured externally by a load cell, and the magnitude of any frictional restraint could not be measured. This would lead to incorrect deviator stresses, because the frictional forces are part of the measured load.

Various methods were developed and tested. Initially, 3.2 millimeter (1/8 inch) square, stainless steel bars were glued to a thick rubber jacket. The rods were spaced slightly apart to accomodate the decrease in specimen diameter due to isotropic compression and subsequent shearing. The "straightjacket" was then placed around the specimen, but outside the first layer of membranes containing the soil. Then additional membranes were placed over the "straightjacket" to seal the specimen. This method was based upon the concept that the confining pressure was being applied to the specimen through the "straightjacket". Therefore, the soil could not pull away from the rigid bars, and uniform strains would be enforced. However, when it was employed, additional problems arose. The height of the jacket had to be slightly less than the initial height of the specimen, so that it would not impede isotropic compression during which the specimen decreases in height. Once shearing started, necking would almost

immediately start at the unprotected gap between the top or bottom of the specimen and the "straightjacket". Often the specimen would fail more quickly with the "straightjacket" at lower stresses and lower axial strains, because the neck would be confined into a very small region near one end of the specimen. The conclusion regarding strain localization that can be made from this exercise is that the location of the strain localization in the extension test is not necessarily fixed in the specimen. The results from this unsuccessful attempt to enforce uniform strains support the hypothesis that the weakest part of the specimen is the location where strain localization will initiate.

The next series of efforts to enforce uniform strains evolved over several months using one basic concept. Small stainless steel or tempered steel plates were fabricated from shim stock (0.01", 0.025" and 0.032" thickness), and bent in such a manner that they would fit the contours of the cylindrical specimen as shown on Figure 4-18. Pieces located adjacent to the cap or base have one end bent so that a small section is perpendicular to the rest of the plate, such that the cell pressure will press onto this area and hold the plates firmly against the cap and base as the axial extension load is applied during shearing. The first layer of plates was placed over the specimen's first layer of membranes. The plates had spaces between them as shown on Figure 4-18. The vacuum grease under the plates functions to hold the plates onto the membrane surface until another membrane is placed over the first layer of plates. In addition, the grease acts to provide lubrication for easy sliding. The second membrane was also greased, and another layer of plates was placed in a spaced pattern that overlapped the pieces

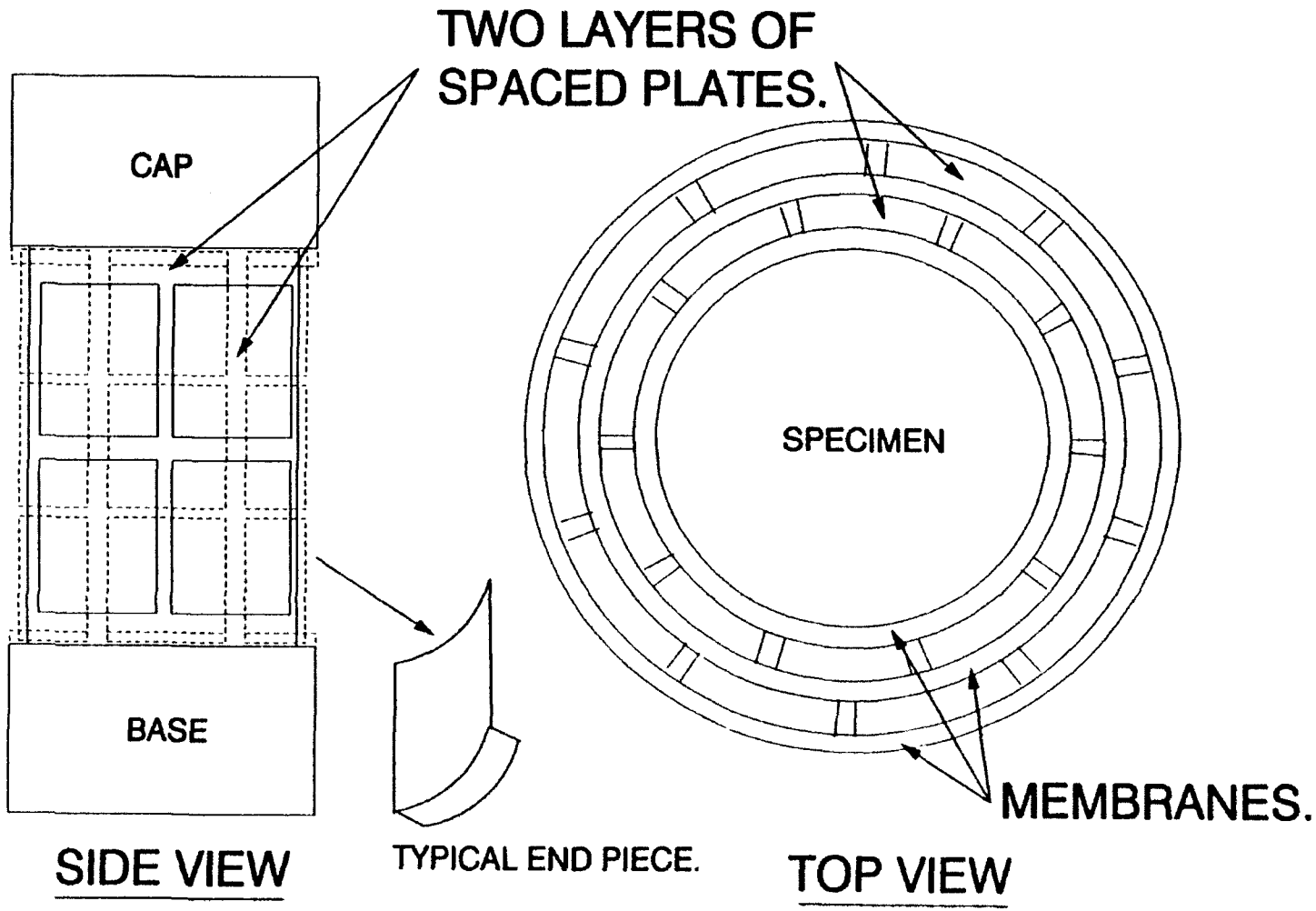

FIGURE 4-18 - METHOD USING STEEL PLATES FOR ENFORCING UNIFORM STRAINS IN EXTENSION.

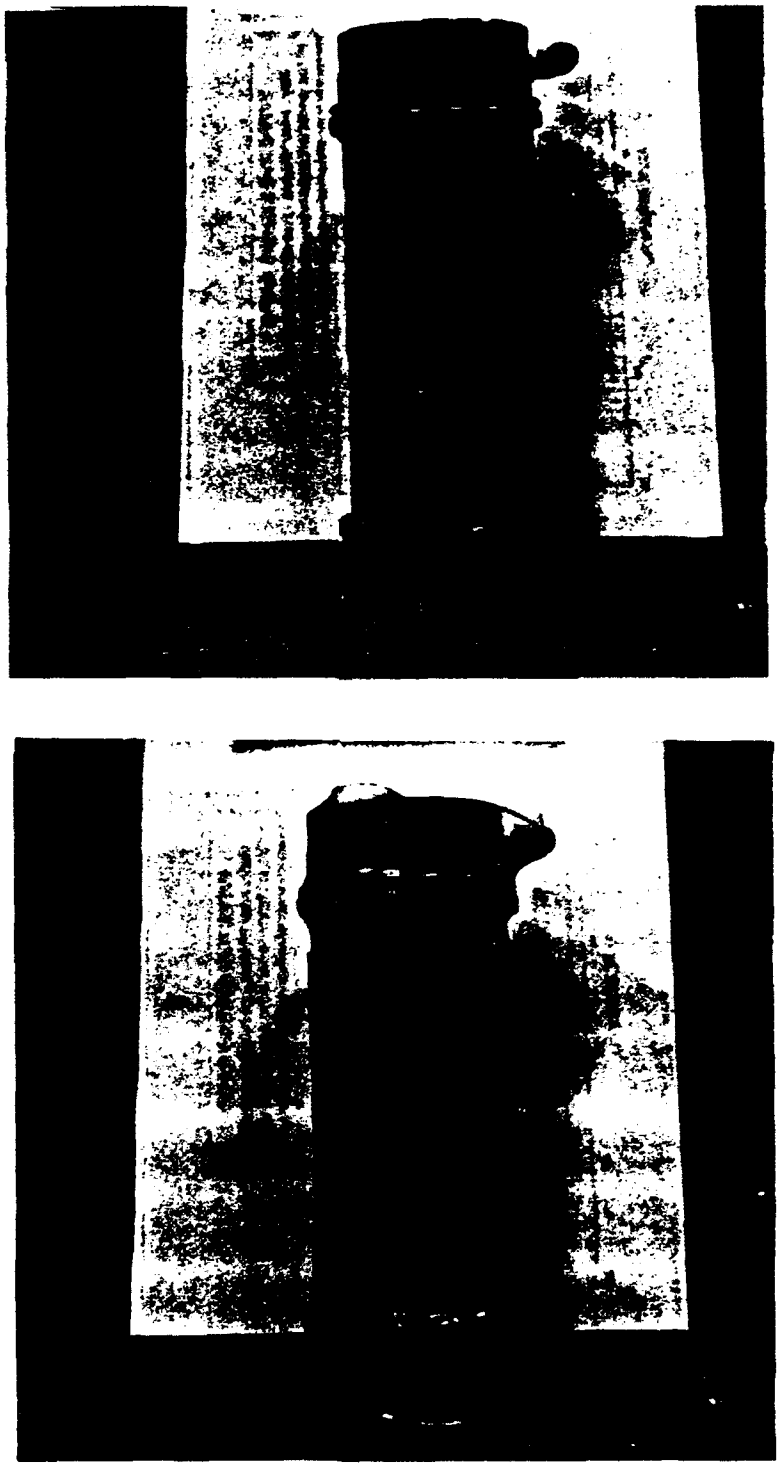

Figure 4-19 Photographs Showing Specimen Assembly Process with Plates to Enforce Uniform Strains in Extension. (Top) First Layer of Plates. (Bottom) Final Specimen before Testing.

in the first layer as shown on Figure 4-18. Additional layers of membranes and plates could be used to stiffen the resistance to bending. Lastly, two or three external membranes were placed to seal the specimen against the cell fluid. Figure 4-19 shows a photograph of an assembled specimen with plates. The conceptual basis of this method was that as confining pressure is applied to the specimen outside the plates and the outer membranes, the overlapped layers of plates will interlock under that pressure, and form a relatively rigid boundary around the specimen. Deformation from isotropic consolidation is accomodated through the spacing afforded between the plates. Since the plates are riding on greased membranes, and not actually in contact with each other, there was little or no friction induced. The major concern was to ensure that the soil grains do not penetrate the first layer of membranes, and directly induce friction between the soil grains and the first layer of plates. Therefore, adequate thickness of the first layer of membranes is essential. Extensive experimentation with this method was undertaken, trying different size plates, modification of the caps and bases to provide a seat on which the curved steel end plates could rest, different membrane thicknesses, and different plate placement patterns.

This method of utilizing small stainless steel plates appears to work very well in low confining pressures, with uniform strains being enforced. At high confining pressures, the inherent instability in the extension test makes uniform strains more difficult to achieve, since the stress magnitudes are very high. However, the use of the thicker tempered steel plates seemed to help achieve uniform strains at high pressures. This method was successful in achieving

uniform strain conditions in drained extension tests up to confining pressures of 52.0 MPa, and in undrained extension tests to initial confining pressures of 52.0 MPa.

There is one major drawback of the system regarding testing at high pressures. After the test is finished, and the confining pressure is lowered, visual inspection of the specimen does not yield much information regarding how uniform the specimen was during actual shearing. The stiff plates tend to elastically rebound at the lowered pressures, always creating a visual image of uniform strains. Therefore, test results must be evaluated carefully to see their consistency and reasonability. At low pressures, where visual inspection of the specimen during shearing is possible through a transparent triaxial cell wall, the effectiveness of the method enforcing uniform strains can be directly judged.

4.9 Comparison of Uniform Strain and Conventional Extension Tests

The uniform strain triaxial extension test results will be shown and discussed in greater detail in Chapter 5, however, comparisons are offered here between the conventional and uniform strain extension test. When the method is used properly, the adverse effects of strain localization in the test specimens can be negligible.

Figures 4-20, 4-21, 4-22, 4-23, 4-24, and 4-25 show comparisons between conventional drained extension tests, drained uniform strain extension tests, and when available, uniform strain extension tests, in which friction developed between the steel plates and soil grains. The drained extension tests shown on these figures

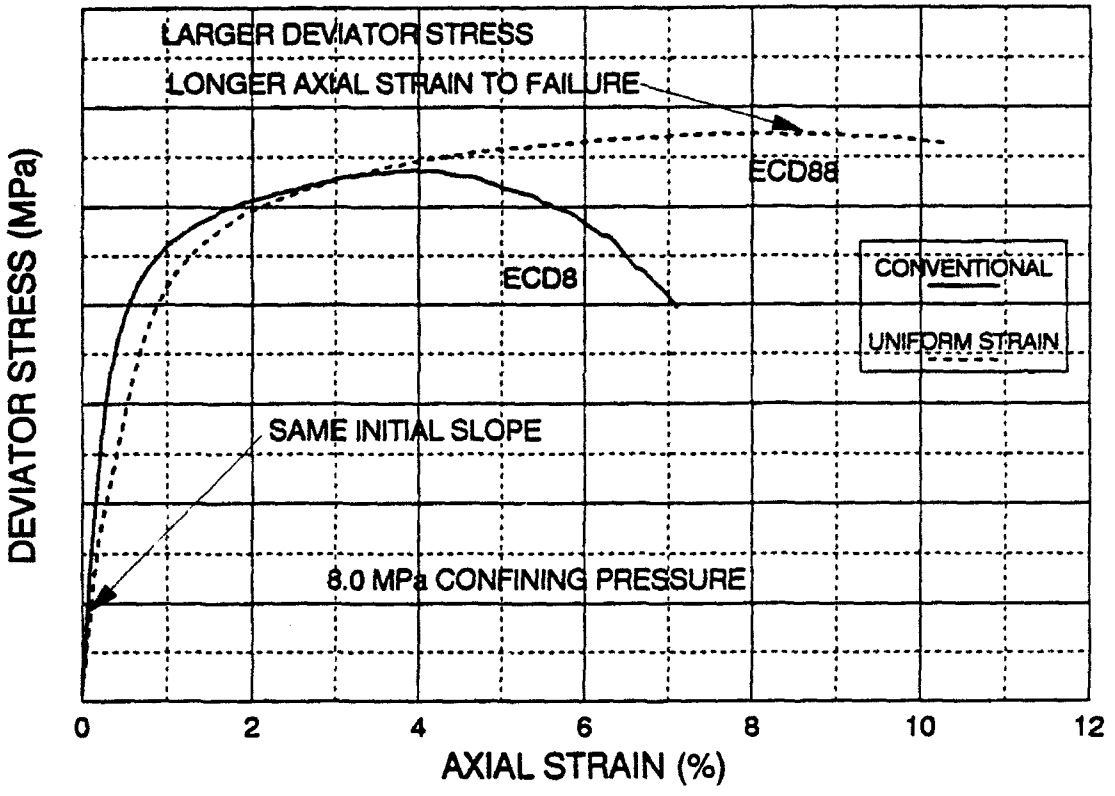

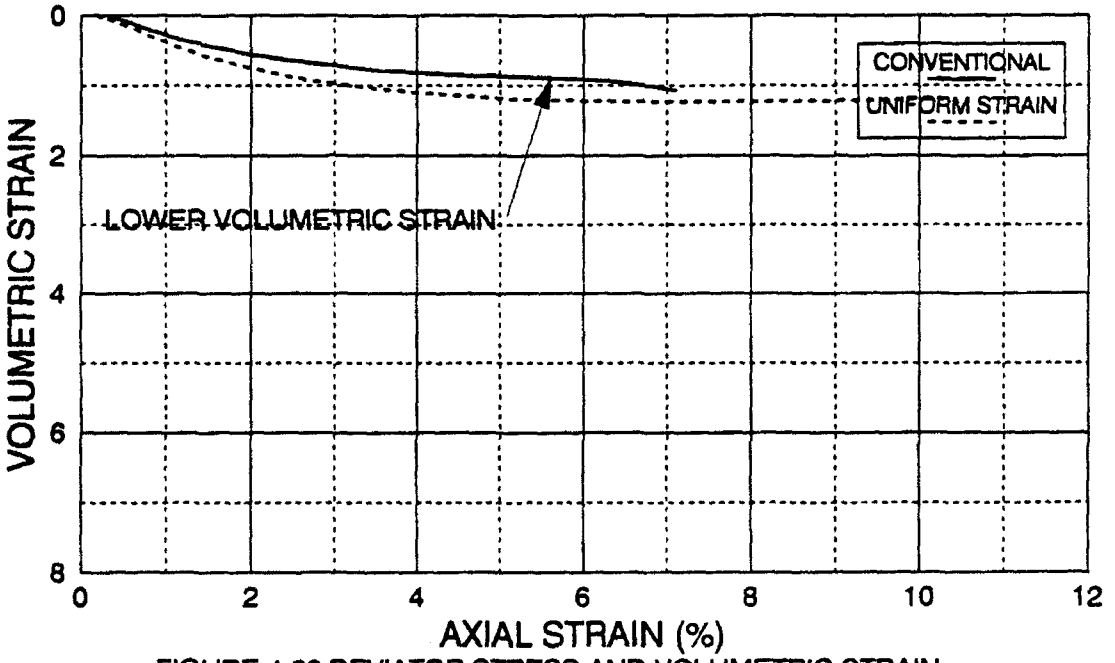

FIGURE 4-20 DEVIATOR STRESS AND VOLUMETRIC STRAIN
COMPARISON OF CONVENTIONAL & UNIFORM STRAIN
EXTENSION TESTS AT 8.0 MPA

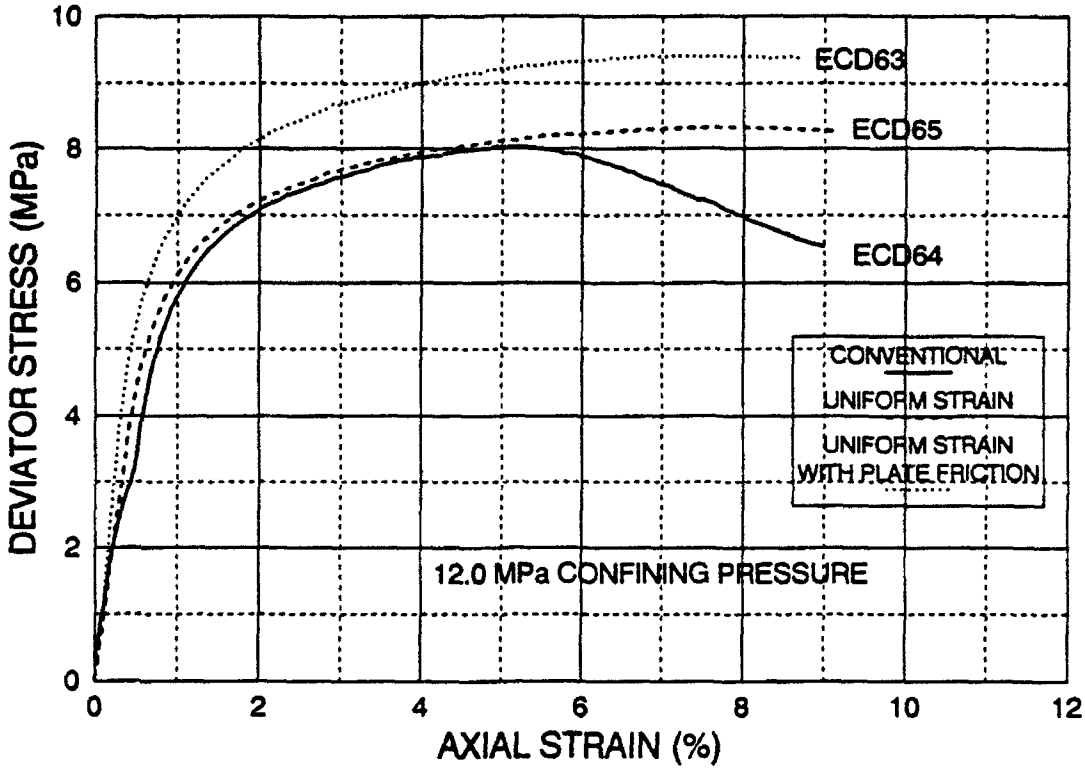

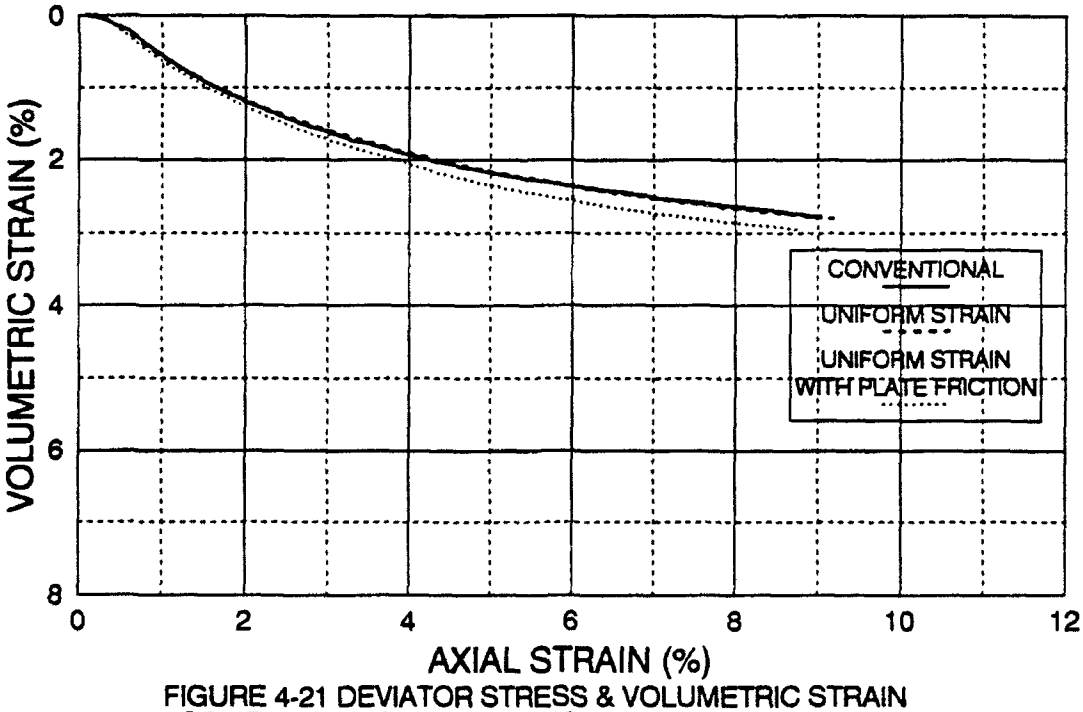

FIGURE 4-21 DEVIATOR STRESS & VOLUMETRIC STRAIN COMPARISON OF CONVENTIONAL, UNIFORM STRAIN, & UNIFORM STRAIN TESTS WITH PLATE FRICTION AT 12.0 MPA

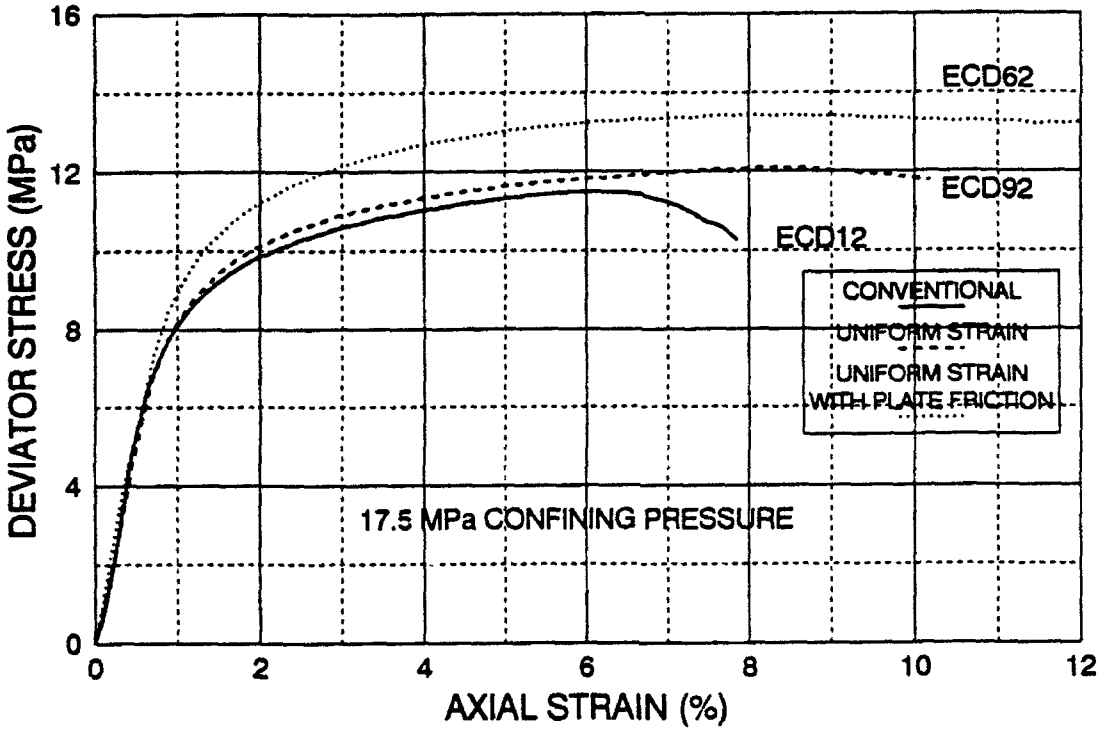

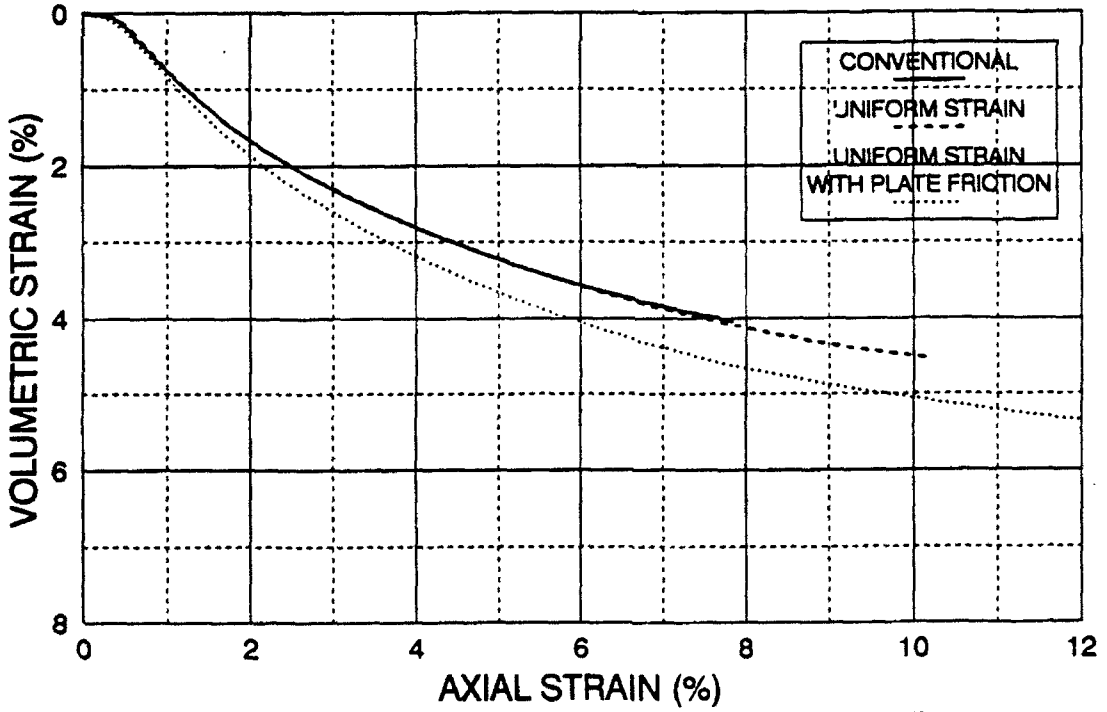

FIGURE 4-22 DEVIATOR STRESS AND VOLUMETRIC STRAIN
COMPARISON OF CONVENTIONAL, UNIFORM STRAIN,
& UNIFORM STRAIN TESTS WITH PLATE FRICTION AT 17.5 MPa

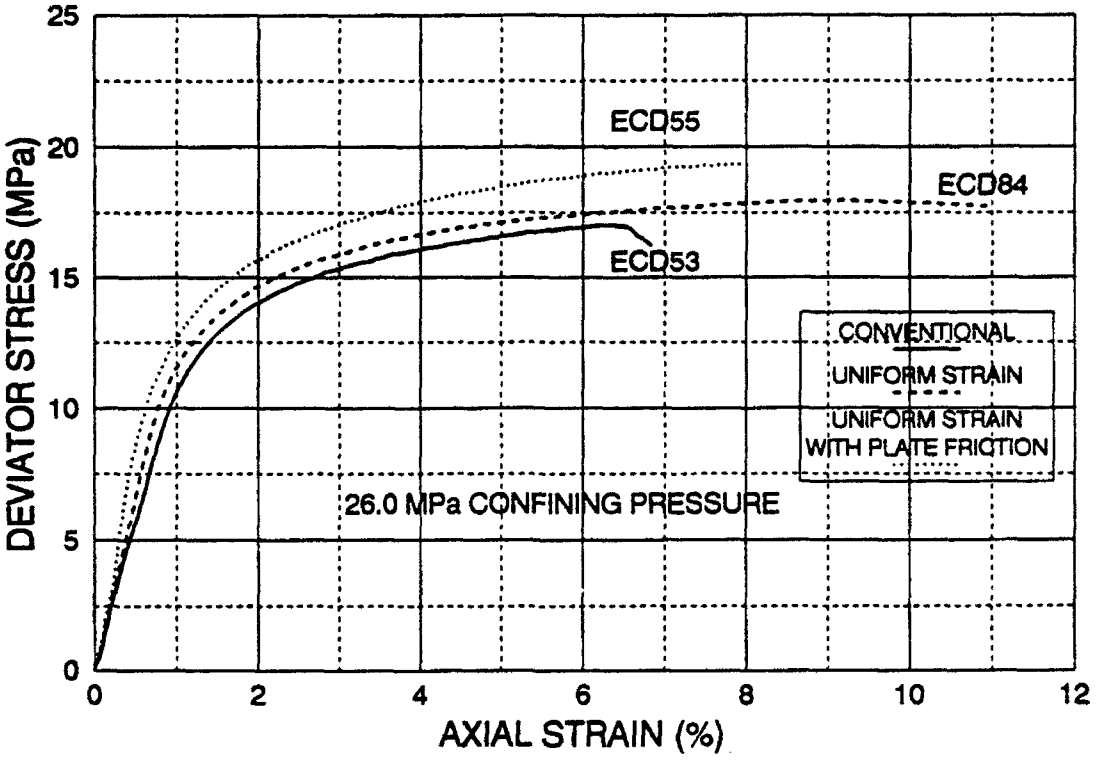

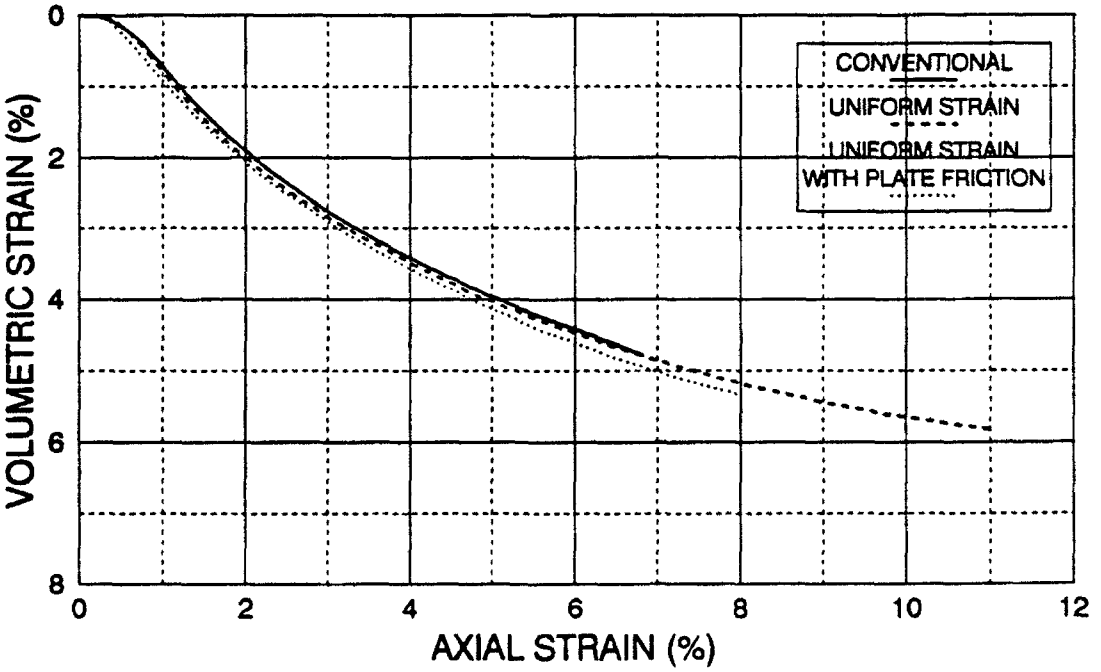

FIGURE 4-23 DEVIATOR STRESS AND VOLUMETRIC STRAIN
COMPARISON OF CONVENTIONAL, UNIFORM STRAIN,
& UNIFORM STRAIN TESTS WITH PLATE FRICTION AT 26.0 MPa

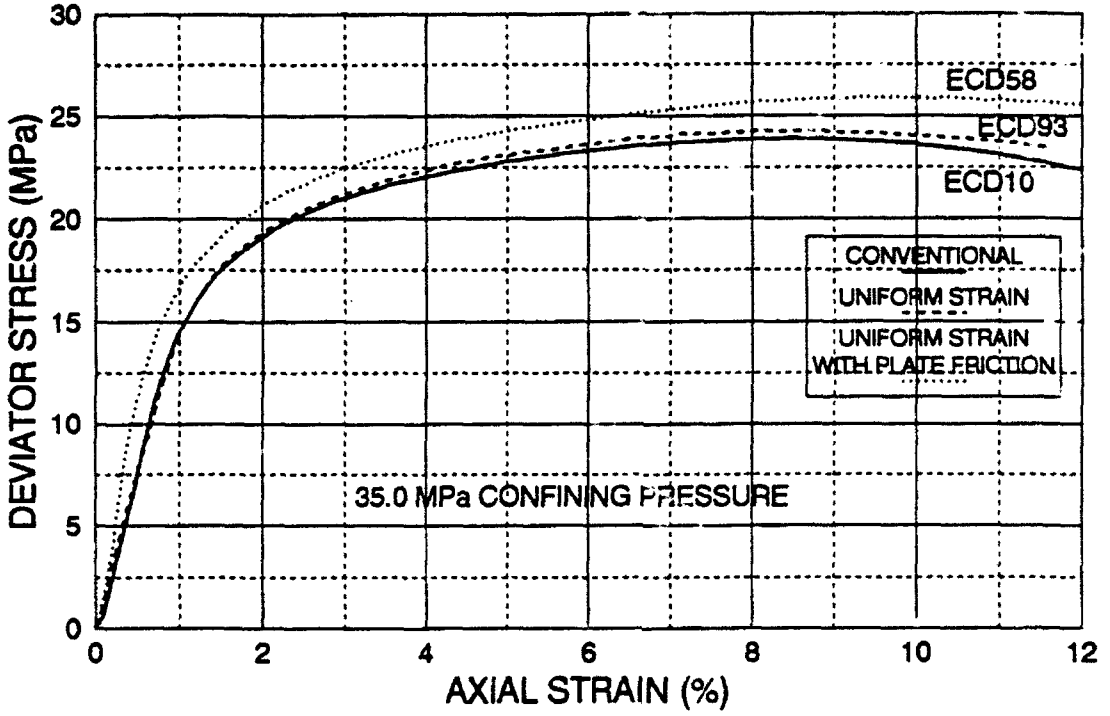

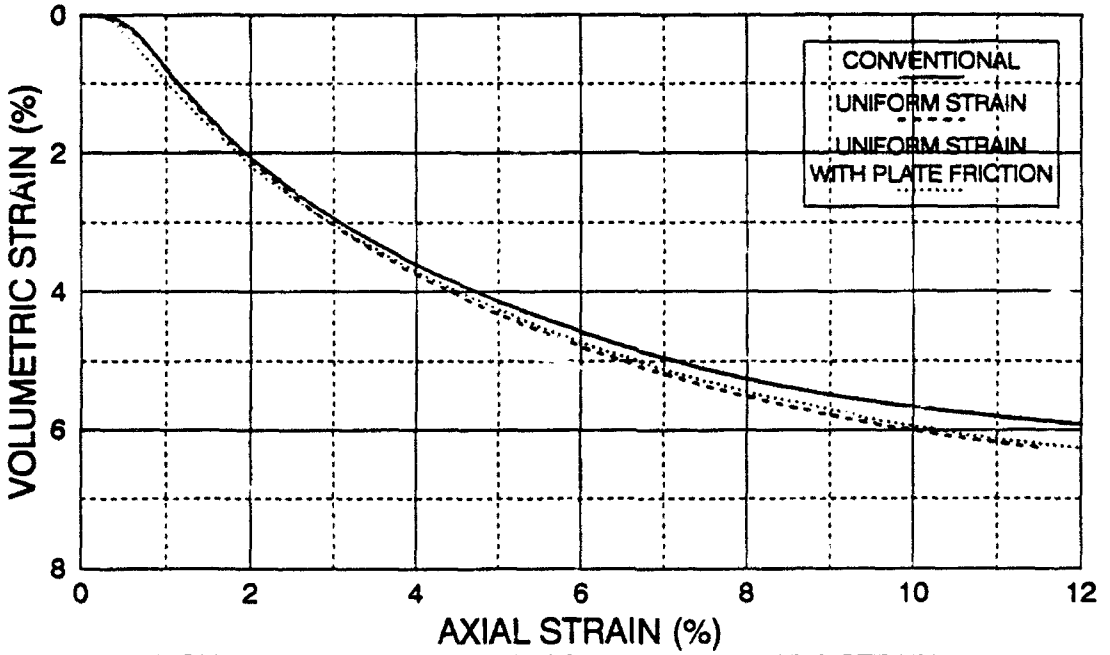

FIGURE 4-24 DEVIATOR STRESS AND VOLUMETRIC STRAIN COMPARISON OF CONVENTIONAL, UNIFORM STRAIN, & UNIFORM STRAIN TESTS WITH PLATE FRICTION AT 35.0 MPa

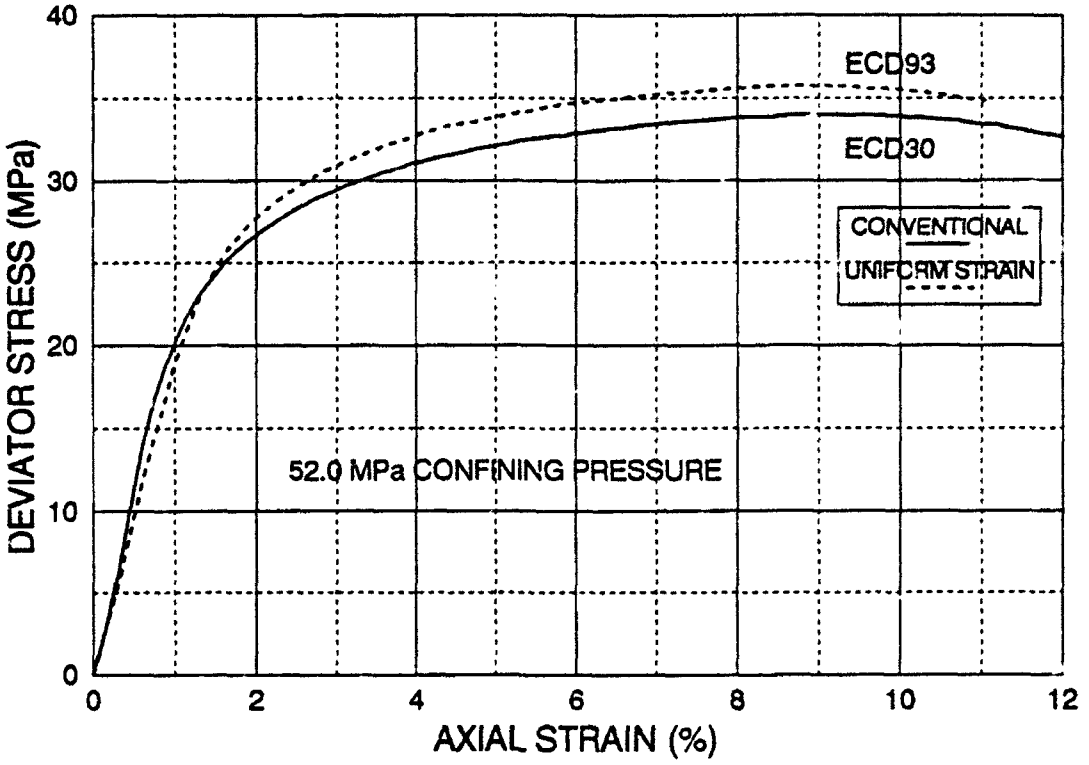

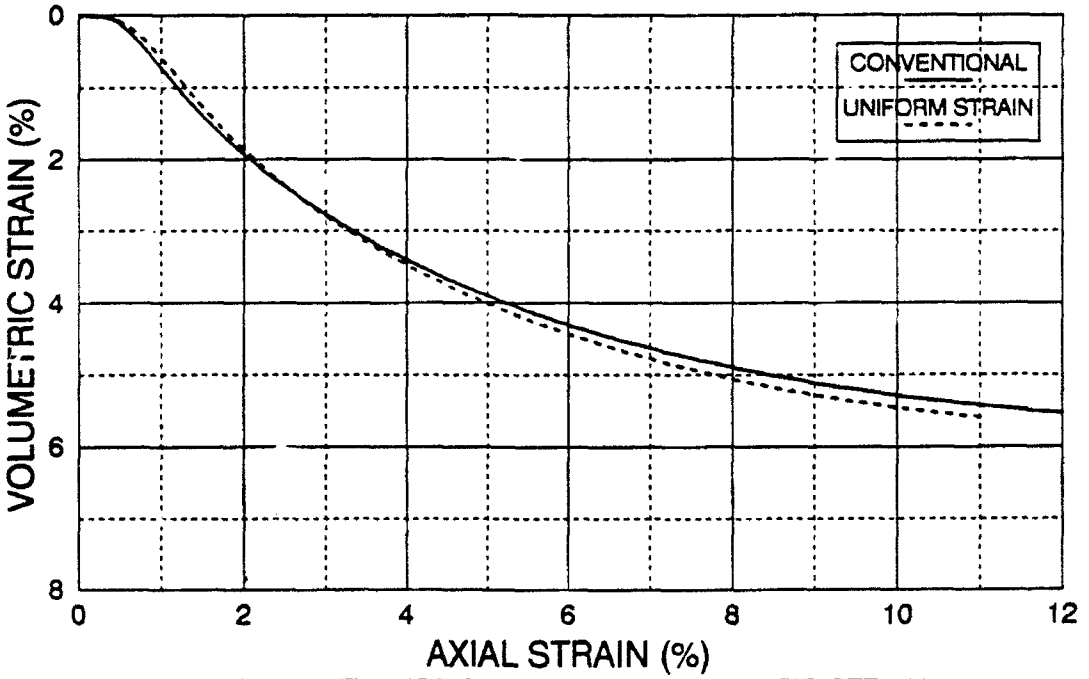

FIGURE 4-25 DEVIATOR STRESS AND VOLUMETRIC STRAIN COMPARISON OF CONVENTIONAL & UNIFORM STRAIN EXTENSION TESTS AT 52.0 MPa

were performed at confining pressures of 8.0, 12.0, 17.5, 26.0, 35.0 and 52.0 MPa, respectively. The deviator stresses and volumetric strains are shown plotted against axial strain (ϵ_3). Experience has shown that friction can develop between the soil grains and the first layer of steel plates when there is not adequate membrane thickness to prevent the grains from penetrating to the plate surface. The figures show test results in which it was determined that friction did occur. An excellent indicator that friction is occurring is the steepness of the slope of the stress-strain curve, which tends to be initially steeper than in the conventional or successful uniform strain test. The successful uniform strain extension tests indicate that no friction is developed on the plates, because the initial slope on the stress-strain curve is approximately equal or even sometimes less than the conventional extension test. If the plates were creating friction, the slope would have been steeper than in conventional extension tests.

As shown on the figures, the differences between successful uniform strain and conventional tests indicate that after a small axial strain, the deviator stresses in the uniform strain extension tests continue to increase above the conventional test to a higher ultimate value and to larger strains at failure. The separation point of the two curves probably coincides with the initiation of strain localization that eventually manifests itself to a degree that clearly affects the results. The volumetric strains tend to be slightly smaller for the conventional extension test at high pressures, because once strain localization develops, the major portion of the specimen undergoing shearing is in the region of the localization, thereby reducing the total volumetric strains. At high pressures this is slightly masked,

because particle breakage will continue throughout the specimen even after localization occurs, because of the high stress magnitudes. The uniform strain tests with plate friction tend to have higher volumetric strains, because the additional friction caused by soil shearing along the plates, creates additional shear stresses and strains within the specimen, which can result in higher volumetric strains.

Comparisons of undrained triaxial extension tests experiencing uniform strains and strain localization are shown on Figures 4-26, 4-27, 4-28, 4-29, 4-30, 4-31, 4-32, and 4-33. Deviator stresses and pore pressures are shown plotted against axial strain. Effective stress paths utilizing the Cambridge p'-q diagram are also shown. The 12.0 MPa initial confining pressure undrained extension tests shown on Figures 4-26 and 4-27 indicate initial contractive volumetric tendencies, while exhibiting dilational tendencies at larger strains, indicated by the decreasing pore pressures. The test that localized cannot keep dilating after strain localization occurs. The deviator stresses are higher in the successful uniform strain test, but with the same initial slope of the stress-strain curve, indicating little or no test interference by the method utilized to enforce uniform strains. The strain to maximum deviator stress and maximum effective stress ratio is larger for the uniform strain test. Since these tests exhibit dilatant tendencies, the difference in behavior is better revealed on the effective stress path shown. The successful uniform strain test exhibits strong dilatant tendencies as it approaches failure, but the strain localized test starts to dilate, and then localization initiates failure. The effective stress path loops around and down, whereas the successful uniform strain test has its deviator stress continuing to increase until failure is reached at a higher

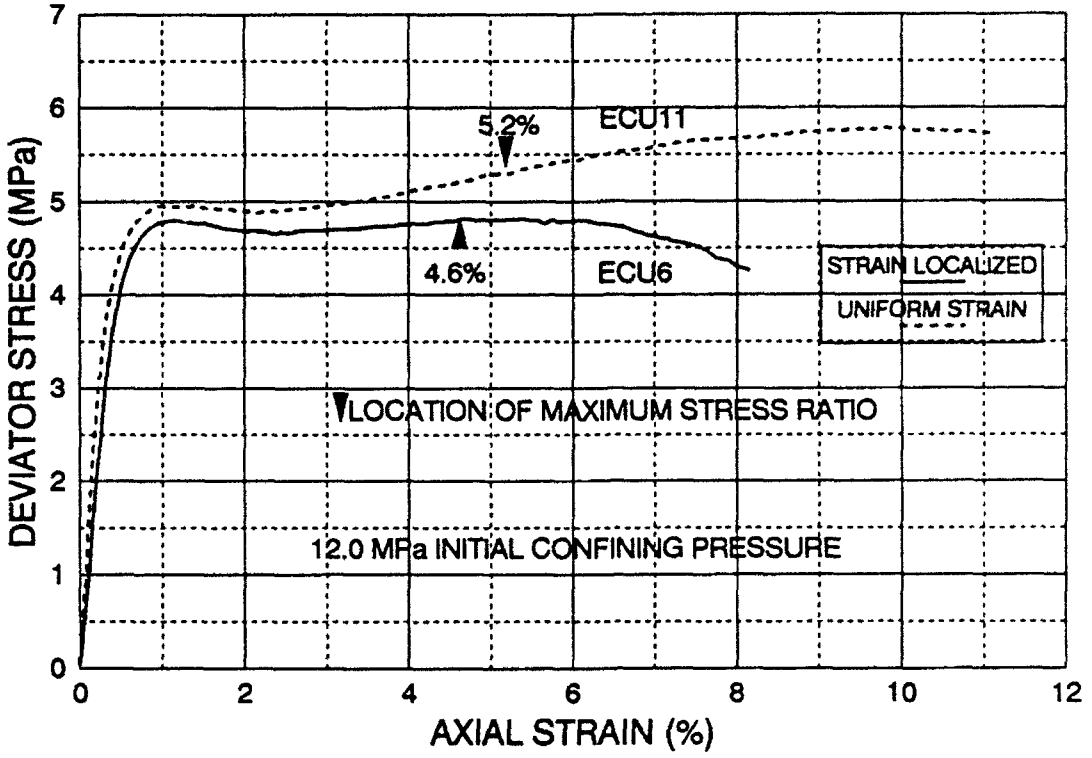

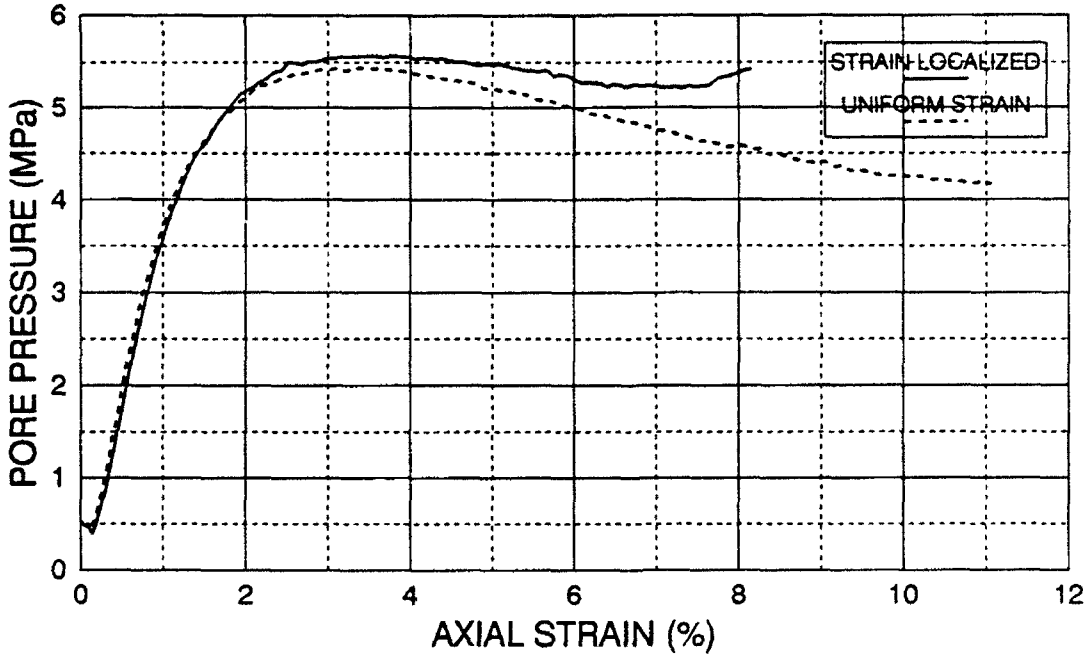

FIGURE 4-26 DEVIATOR STRESS AND PORE PRESSURE
COMPARISON OF STRAIN LOCALIZED & UNIFORM STRAIN
UNDRAINED EXTENSION TESTS AT 12.0 MPa

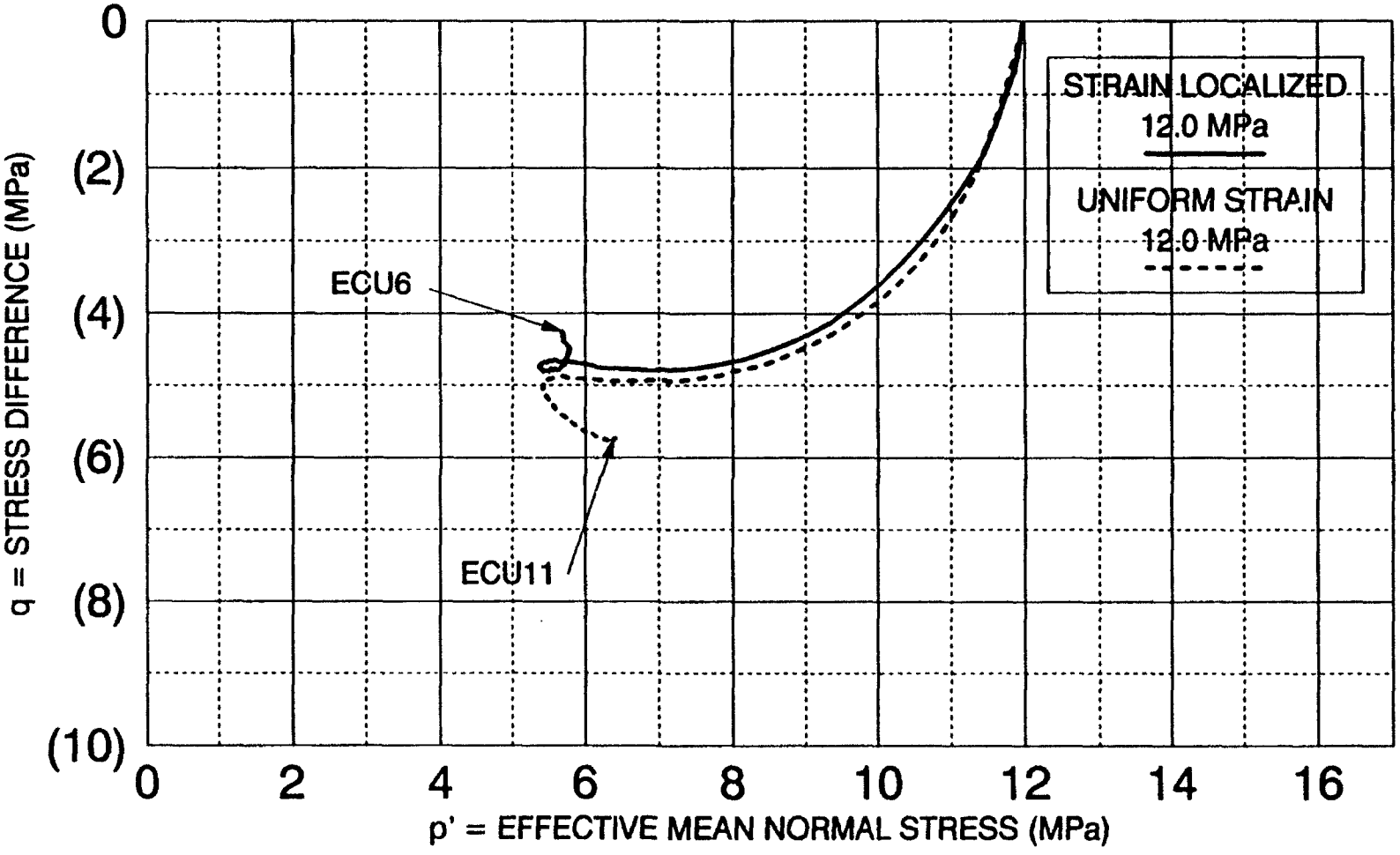

FIGURE 4-27 - EFFECTIVE STRESS PATH, CAMBRIDGE p'-q
COMPARISON OF STRAIN LOCALIZED & UNIFORM STRAIN
UNDRAINED EXTENSION TESTS

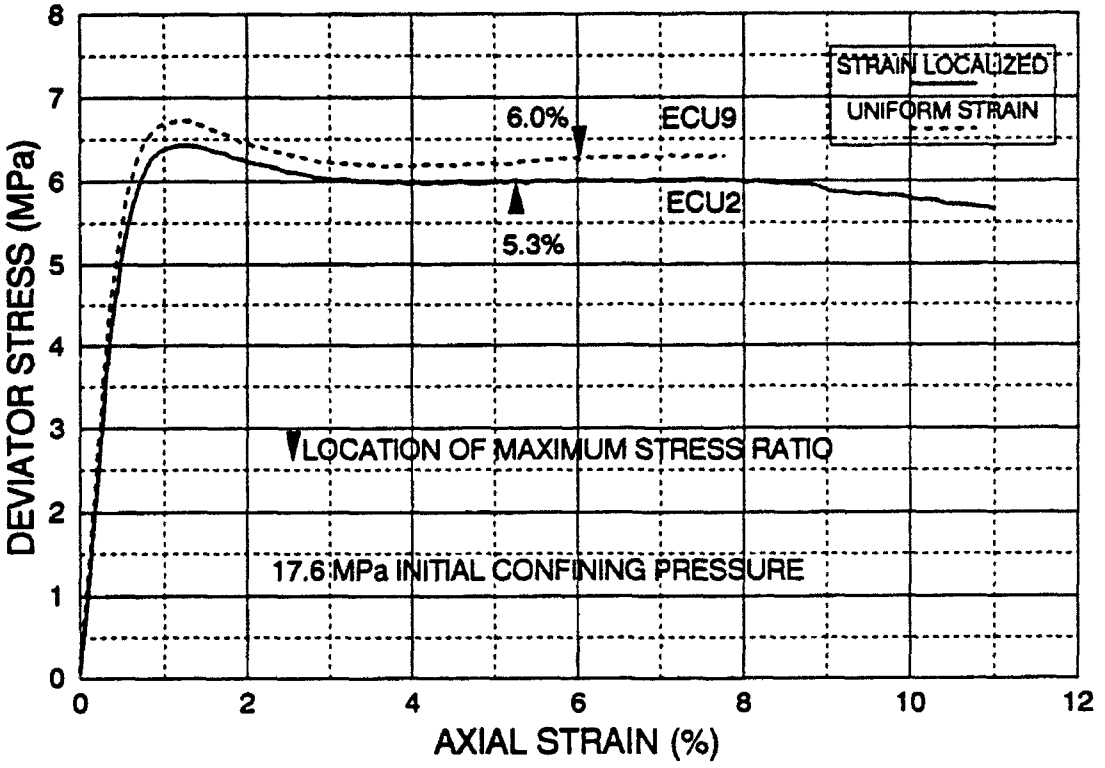

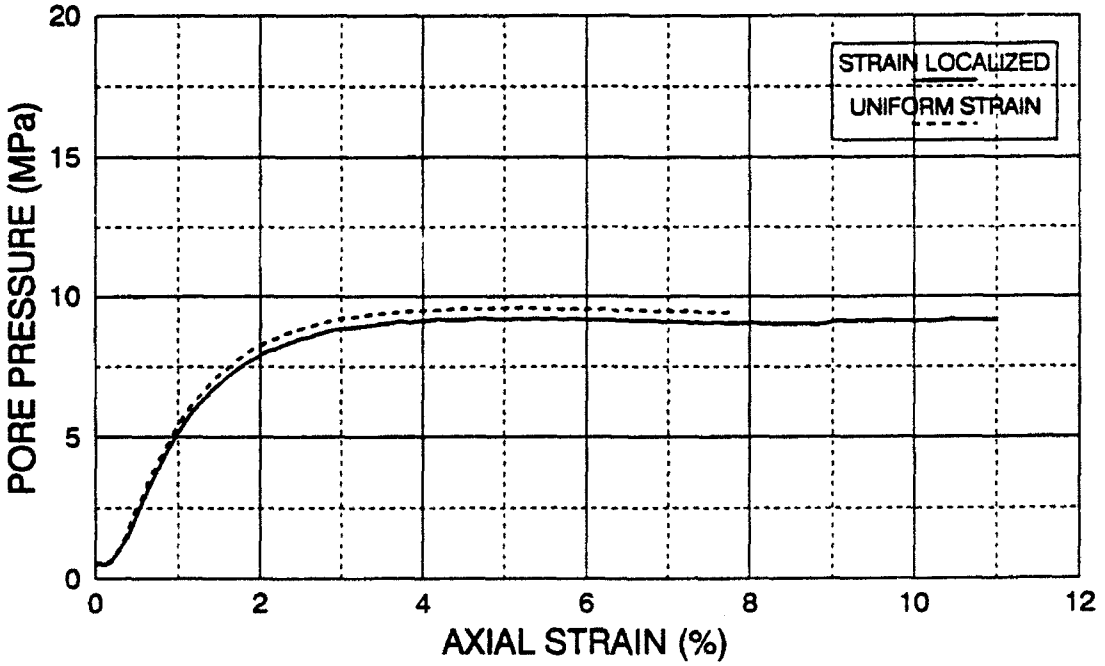

FIGURE 4-28 DEVIATOR STRESS AND PORE PRESSURE
COMPARISON OF STRAIN LOCALIZED & UNIFORM STRAIN
UNDRAINED EXTENSION TESTS AT 17.6 MPa

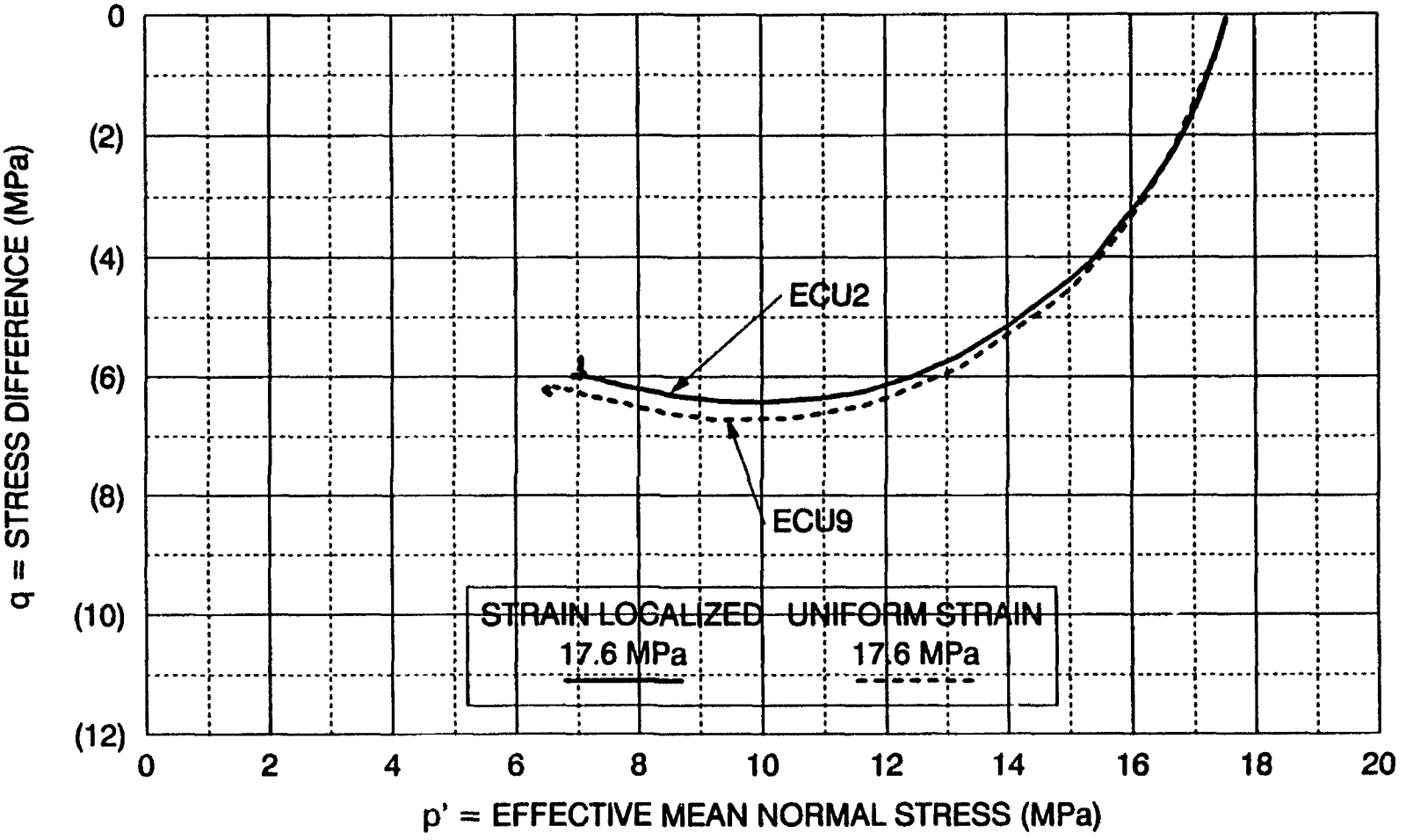

FIGURE 4-29 EFFECTIVE STRESS PATH, CAMBRIDGE p'-q
COMPARISON OF STRAIN LOCALIZED & UNIFORM STRAIN
UNDRAINED EXTENSION TESTS AT 17.6 MPa

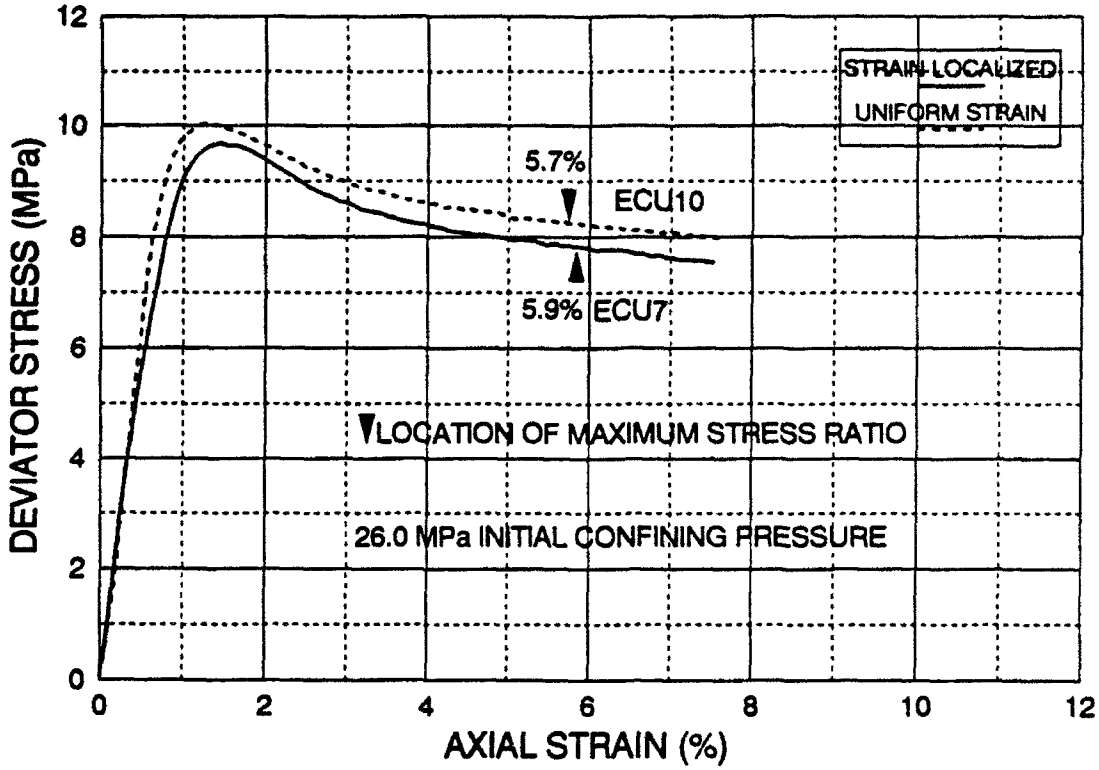

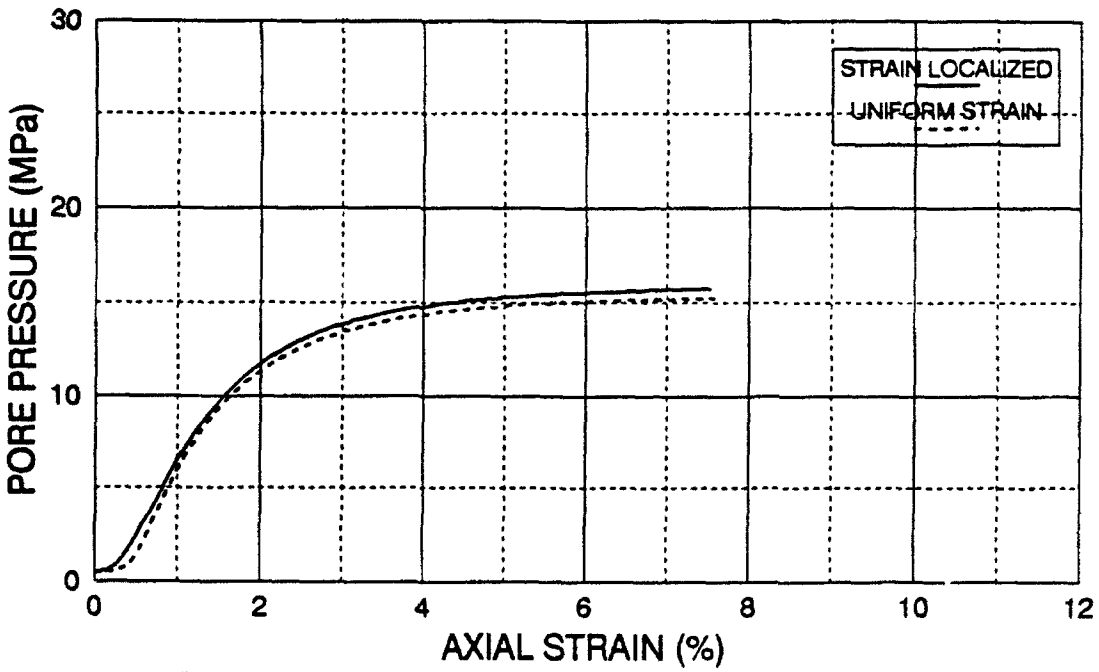

FIGURE 4-30 DEVIATOR STRESS AND PORE PRESSURE
COMPARISON OF STRAIN LOCALIZED & UNIFORM STRAIN
UNDRAINED EXTENSION TESTS AT 26.0 MPa

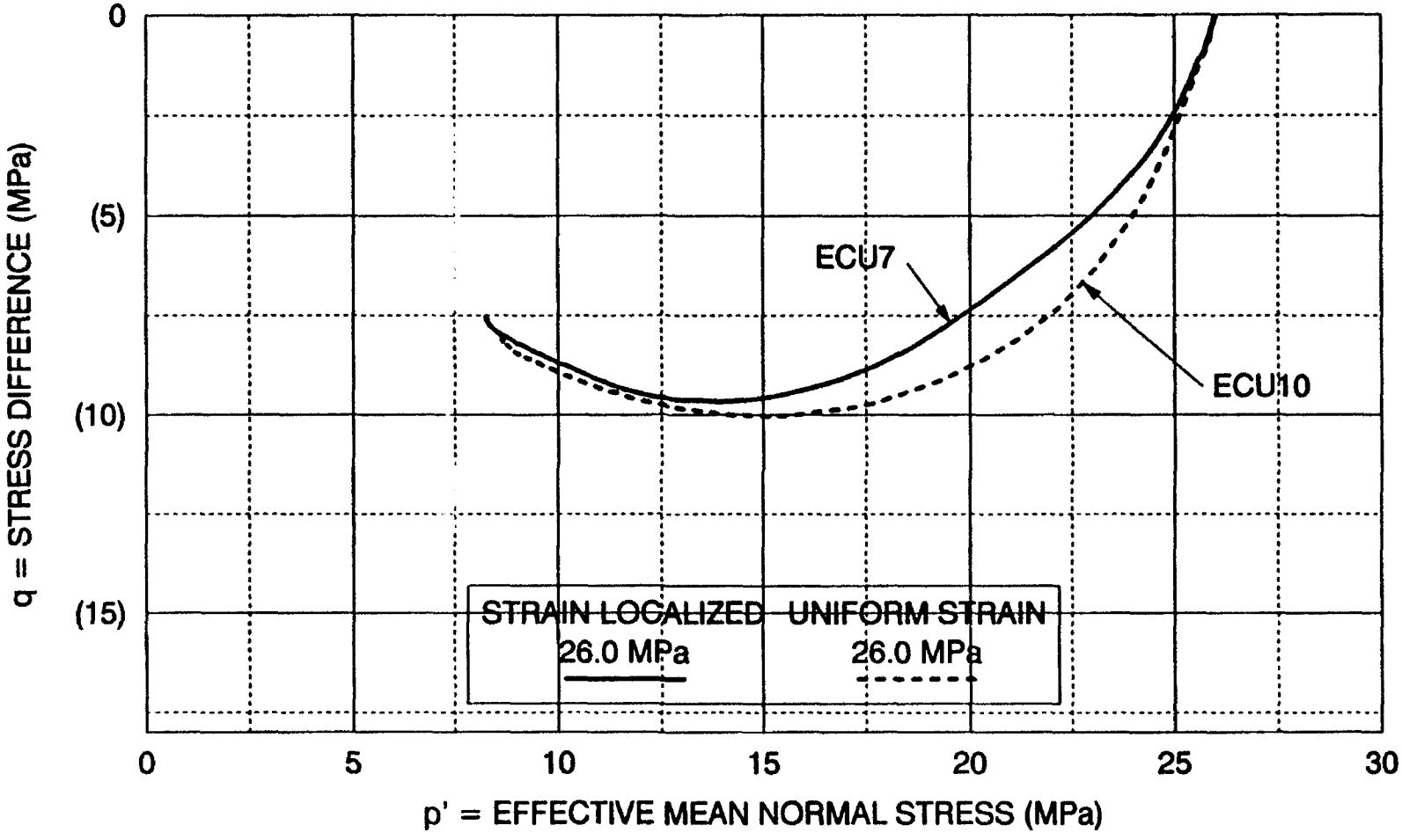

FIGURE 4-31 - EFFECTIVE STRESS PATH, CAMBRIDGE p'-q
COMPARISON OF STRAIN LOCALIZED & UNIFORM STRAIN
UNDRAINED EXTENSION TESTS AT 26.0 MPa

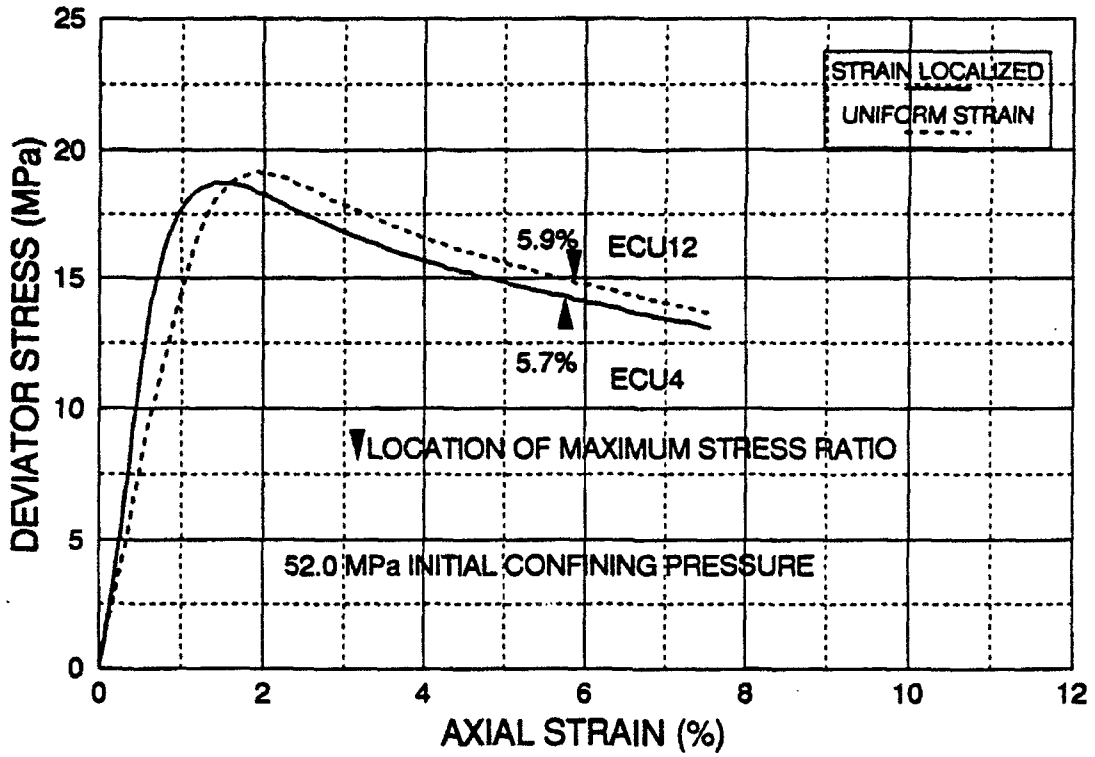

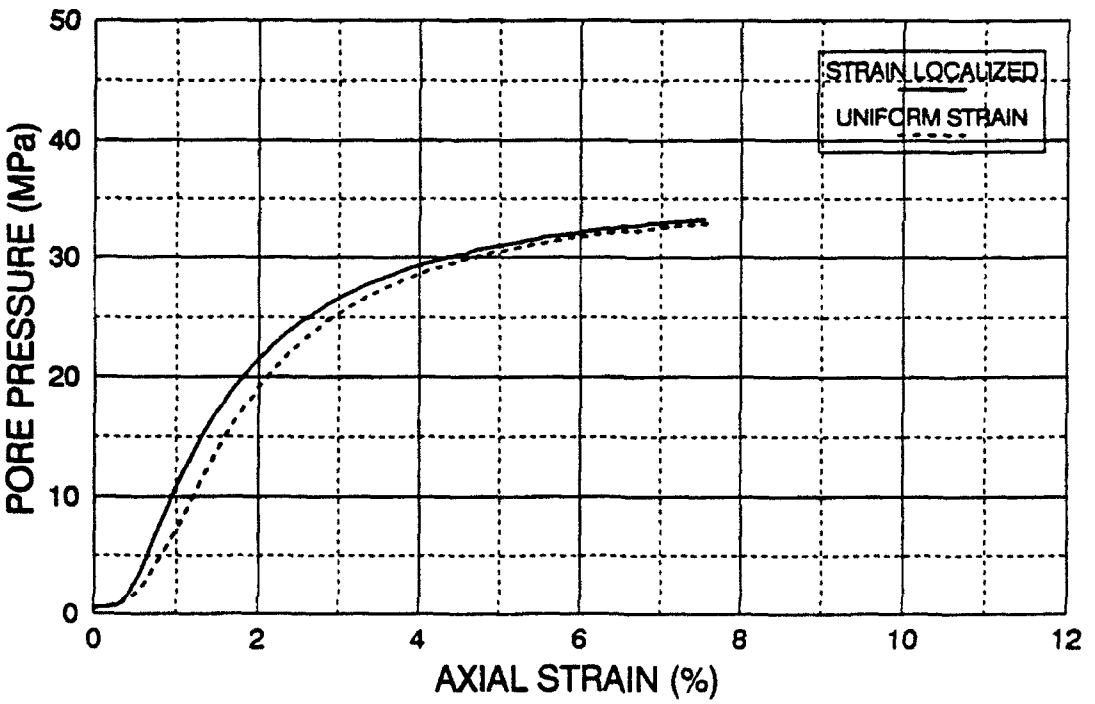

FIGURE 4-32 DEVIATOR STRESS AND PORE PRESSURE
COMPARISON OF STRAIN LOCALIZED & UNIFORM STRAIN
UNDRAINED EXTENSION TESTS AT 52.0 MPa

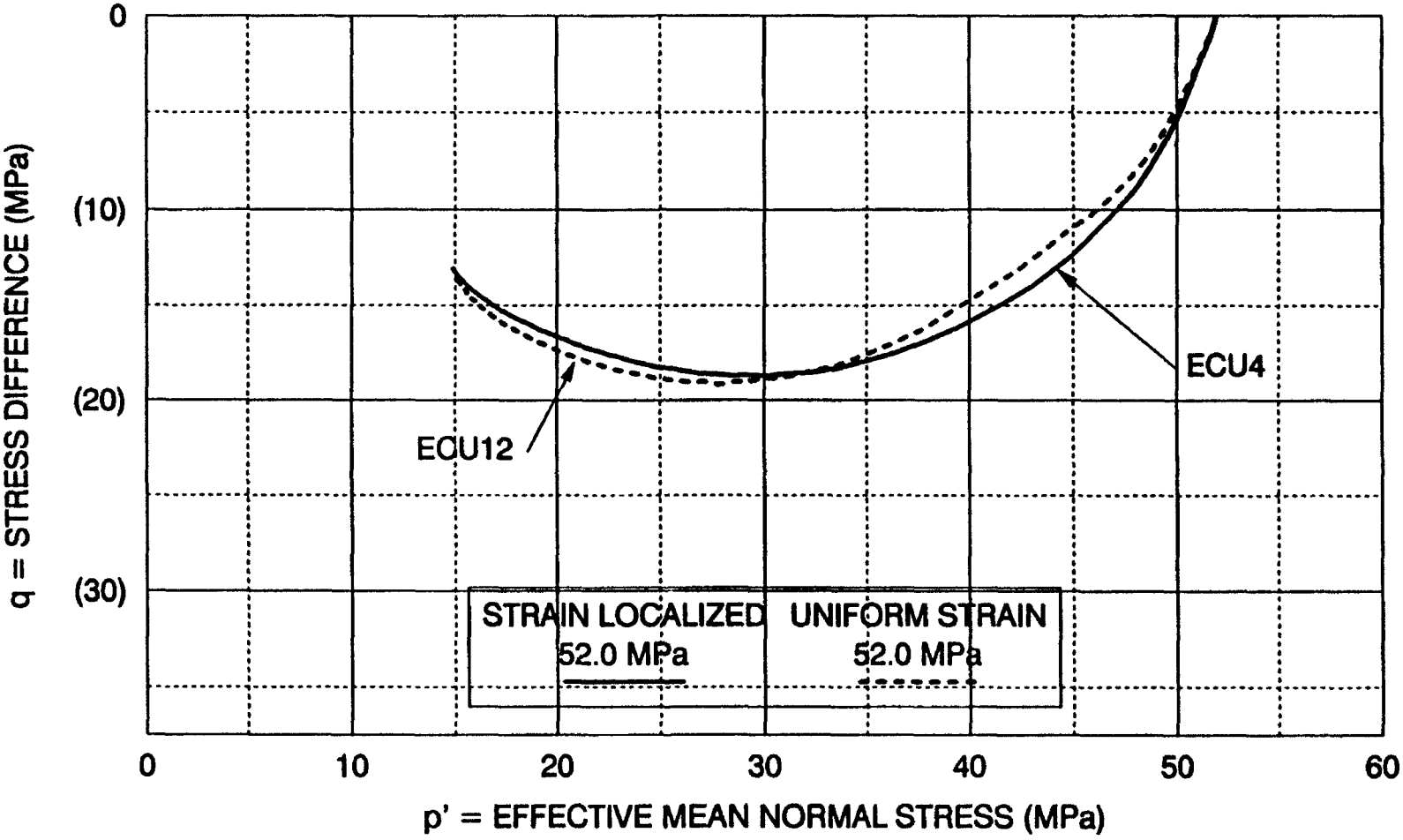

FIGURE 4-33 - EFFECTIVE STRESS PATH, CAMBRIDGE p'-q
COMPARISON OF STRAIN LOCALIZED & UNIFORM STRAIN
UNDRAINED EXTENSION TESTS AT 52.0 MPa

level. The remaining three sets of undrained test comparisons shown on Figures 4-28 through 4-33 indicate similar behavior patterns regarding deviator stresses and effective stress paths. The deviator stresses and maximum effective principal stress ratios are consistently larger for the successful uniform strain tests. Pore pressure development in tests with higher initial confining pressures are approximately the same for successful uniform strains and strain localized tests. Strain localized effective stress paths which exhibit dilation tend to fail during the increase in deviator stress caused by the dilatant behavior. Purely compressive effective stress paths with uniform strains exhibit a rounder curve, while the localized tests show a flat region on the stress path during hardening, indicating the probable development of strain localization.

The Mohr-Coulomb secant friction angles for both the drained, and undrained tests exhibiting uniform strains and strain localization are shown on Figure 4-34. The friction angles are plotted against the effective mean normal stress at failure. The friction angles for the conventional drained extension tests are consistently much lower than the uniform strain friction angles, and they exhibit considerably more scatter. Both show decreasing strength with increasing mean normal stress at failure. These results clearly show how strain localization dominates failure in extension. The friction angles for strain localized and successful uniform strain undrained extension tests also clearly indicate that there is a substantial strength decrease due to strain localization. The friction angles for the successful uniform strain tests indicate a fairly constant magnitude, whereas the localized tests indicate an inconsistent pattern.

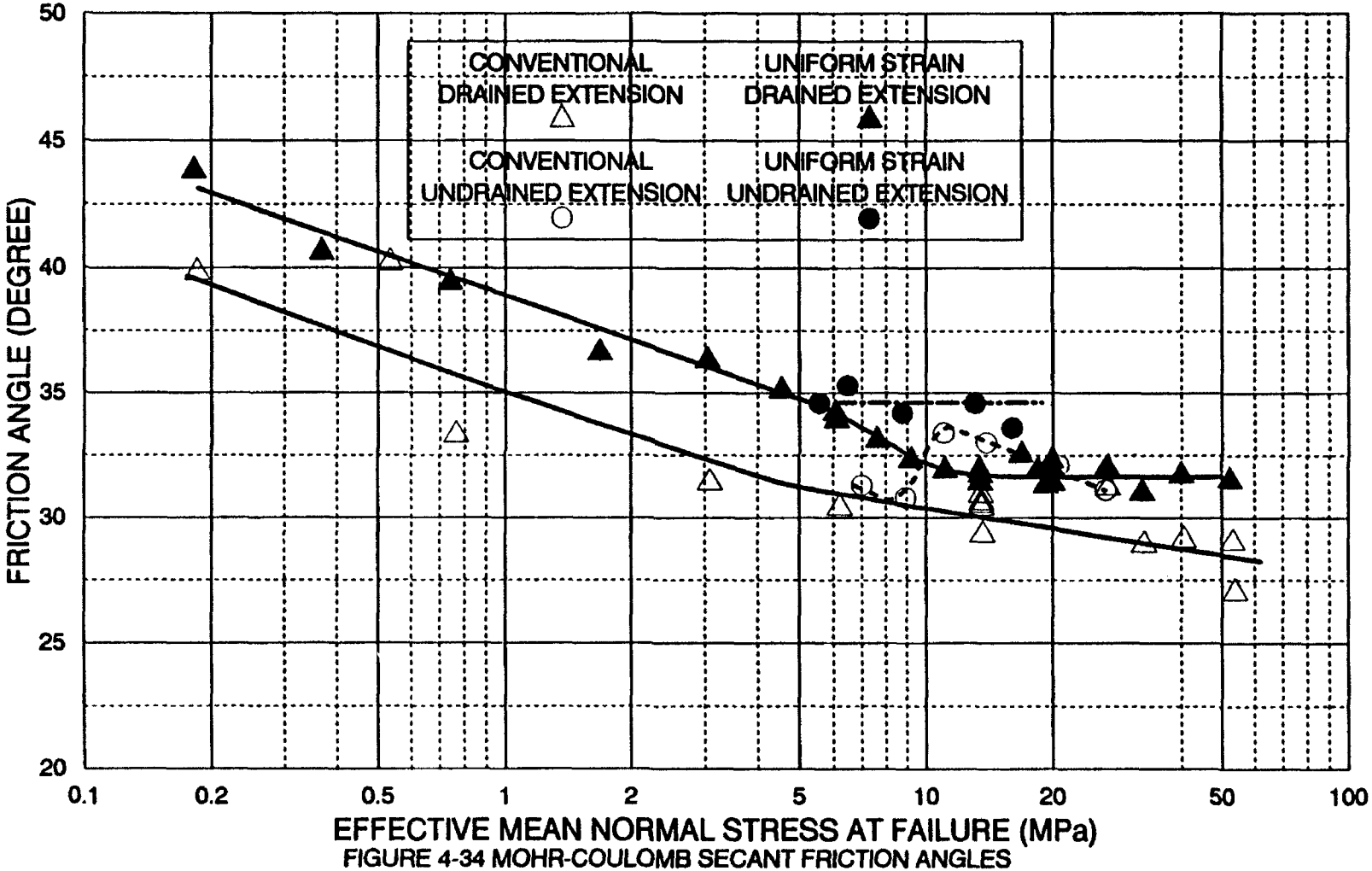

FIGURE 4-34 MOHR-COULOMB SECANT FRICTION ANGLES
DRAINED AND UNDRAINED EXTENSION TESTS
WITH & WITHOUT STRAIN LOCALIZATION ON DENSE CAMBRIA SAND

Volumetric strains at failure for uniform strain and conventional drained extension tests are shown on Figure 4-35. They are plotted against mean normal stress at failure. Close examination indicates that there are generally slightly higher compressive volumetric strains at failure for uniform strain tests, when compressive volumetric behavior is exhibited.

The major principal strains at effective stress failure for drained conventional tests, drained uniform strain tests, undrained strain localized tests, and undrained successful uniform strain tests are shown on Figure 4-36. They are plotted against mean normal stress at failure. Generally there are larger principal strains to failure in the drained uniform strain tests, when in the compressive volumetric region. There is much more scatter in tests experiencing strain localization.

4.10 Discussion

Strain localization dominates the results from conventional triaxial extension test. Scatter in conventional drained and undrained extension tests is very large. Failure was precipitated by strain localization in every conventional extension test performed. It is concluded that the conventional extension test is inherently unstable, because it concentrates stresses at the weakest point (geometric, or strength) in the test specimen, as opposed to compression tests, which tend to redistribute the higher stresses at inhomogeneities throughout the specimen. Strain localization appears to begin very early in shearing, and increasing isotropic consolidation pressures appear to accelerate its formation.

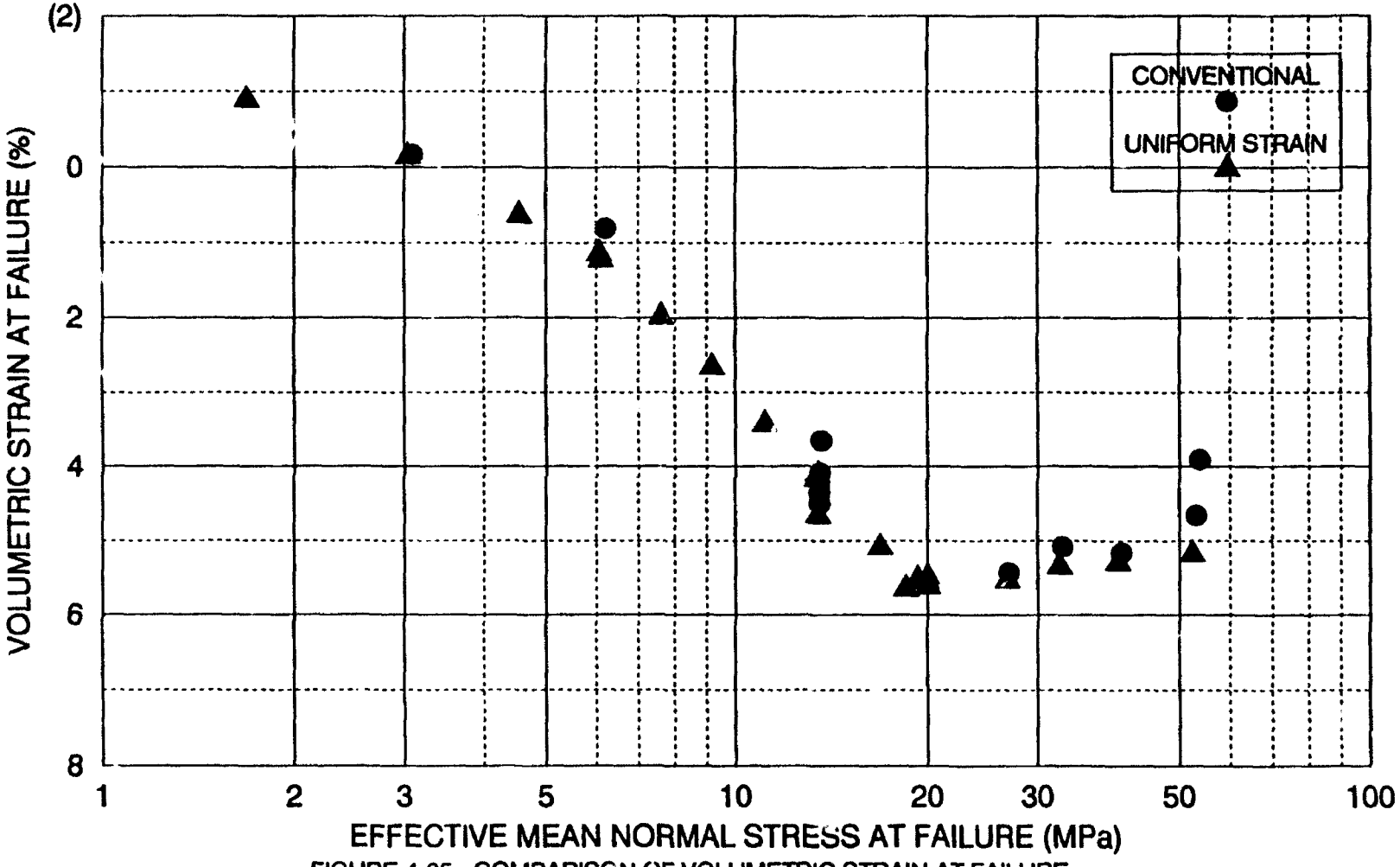

FIGURE 4-35 - COMPARISON OF VOLUMETRIC STRAIN AT FAILURE
CONVENTIONAL AND UNIFORM STRAIN EXTENSION TESTS
DENSE CAMBRIA SAND

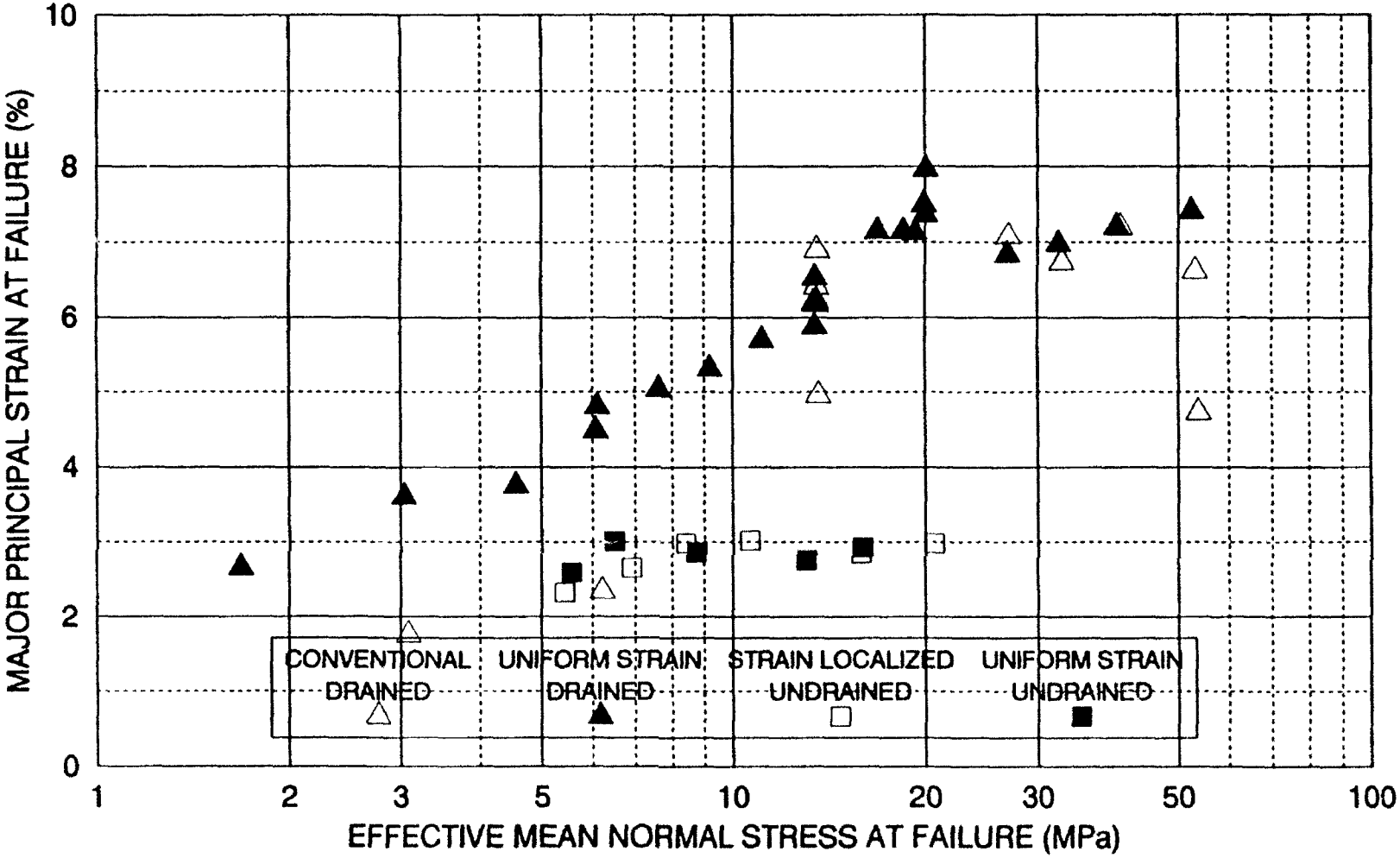

FIGURE 4-36 - COMPARISON OF PRINCIPAL STRAIN AT FAILURE
ALL CONVENTIONAL AND UNIFORM STRAIN EXTENSION TESTS
DENSE CAMBRIA SAND

An experimental method has been developed to enforce uniform strains in the conventional extension test using a cylindrical specimen. The method successfully enforces uniform strains over a wide confining pressure range without induced friction.

Comparison of successful uniform strain extension tests with conventional extension tests indicate that maximum deviator stresses are larger, the volumetric strains are generally slightly larger in the volumetric compressing region, and the strains to failure are generally larger. Using this method to enforce uniform strains is preferable over correcting the results of conventional extension tests using an area correction technique, since the method proposed here is direct, more reliable, and volumetric strains are correct.

CHAPTER 5 - STRESS-STRAIN BEHAVIOR IN TRIAXIAL COMPRESSION AND EXTENSION AT HIGH PRESSURES

5.1 Triaxial Compression Tests

Series of both drained and undrained triaxial compression tests were performed on Cambria sand at various confining pressures between 2.1 and 68.9 MPa, to establish the shape of the total and effective stress failure envelopes, and to ascertain the general soil behavior in triaxial compression. Four drained compression tests from a prior study of Cambria sand performed at low confining pressures (0.05 to 0.4 MPa) are included in the Appendix to extend the range of confining pressures at the lower end. Additionally, five drained triaxial compression tests on quartz sand were performed with confining pressures between 12.0 and 52.0 MPa.

The triaxial compression tests consist of a drained isotropic consolidation phase followed by a shearing phase performed under axial strain control. Shearing is accomplished by moving the loading table up creating an increasing vertical load on the specimen. Total confining pressure is maintained constant for both drained and undrained tests. Undrained triaxial compression tests with total stress paths that varied from this conventional testing method are described in Chapter 7. Drained tests allow the specimen to experience volume change measured by a volume change device. Undrained tests do not allow any volume change to occur due to closure of the drainage valves, and the induced pore pressures are measured on a pressure transducer. Failure is defined to occur at the maximum

effective principal stress ratio in all tests.

The equations to compute axial strain, volumetric strain, cross-sectional area correction, deviator stress, effective principal stress ratio, effective mean normal stress, and Mohr-Coulomb secant friction angle for triaxial compression are included in Appendix A.

5.2 Results from Drained Triaxial Compression Tests

Figure 5-1 and 5-2 show the drained triaxial compression stress-strain characteristics of dense Cambria sand at confining pressures between 2.1 and 52.0 MPa. Figure 5-3 shows the stress-strain curves for the five drained triaxial compression tests performed on quartz sand. The effective principal stress ratios are plotted against axial strain (ϵ_1). The effective principal stress ratio, a nondimensional normalized stress parameter, is utilized so that similarities and differences in the shapes of the stress-strain curves can be examined more easily over the wide confining pressure ranges. It is different from a true stress-strain curve, for which the deviator stress is utilized, because the normalization by the effective minor principal stress creates flatter initial slopes with increasing confining pressure. A true stress-strain curve would indicate an increasing modulus with increasing confining pressure. The deviator stresses for dense Cambria sand are shown on Figures 5-4 and 5-5, while the deviator stresses for dense quartz sand are indicated on Figure 5-6. The volumetric strains for the same tests are given on Figure 5-7 and 5-8 for dense Cambria sand, and Figure 5-9 for dense quartz sand.

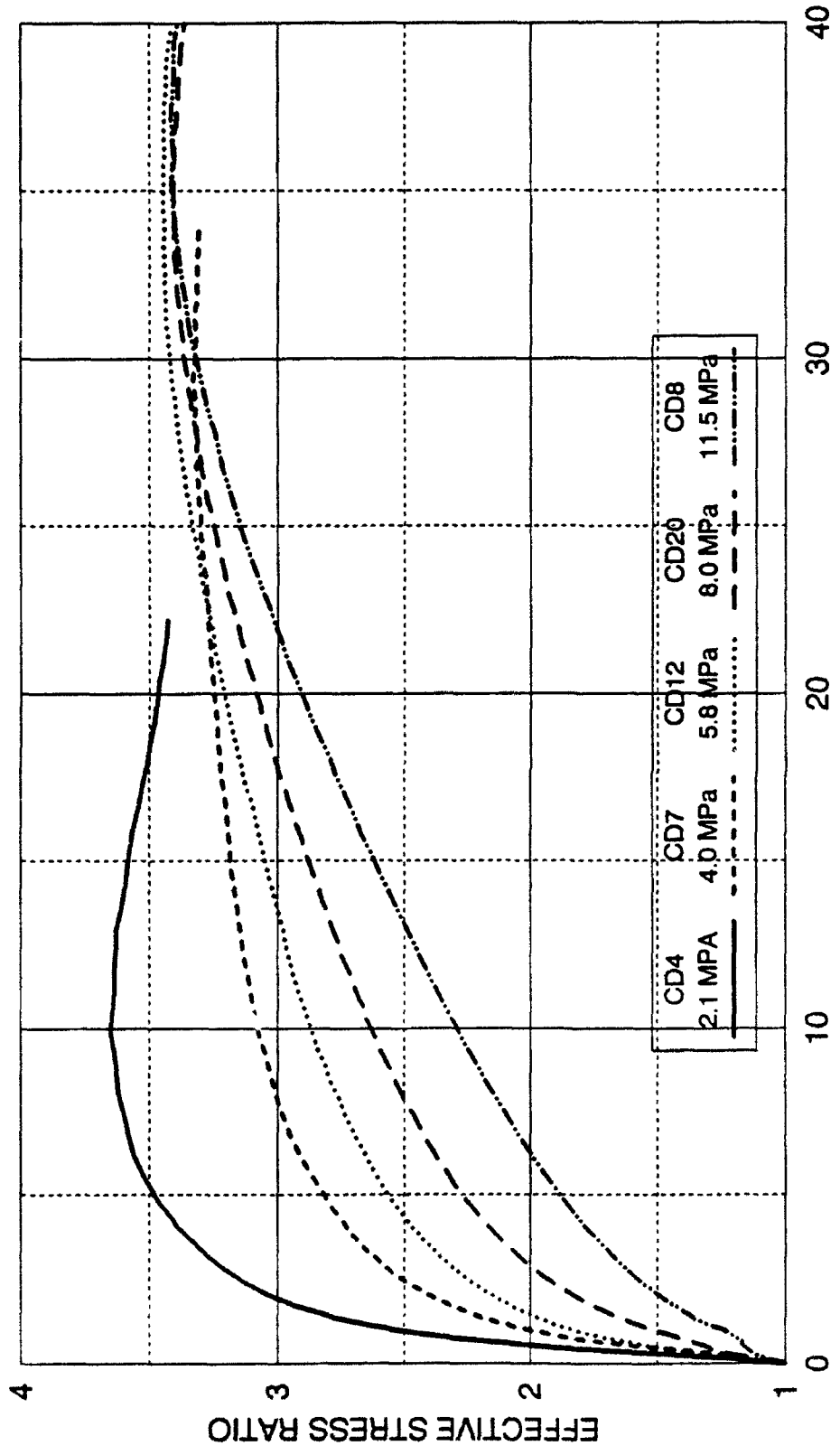

FIGURE 5-1 EFFECTIVE STRESS RATIO 2.1 TO 11.5 MPa
DRAINED TRIAXIAL COMPRESSION
DENSE CAMBRIA SAND

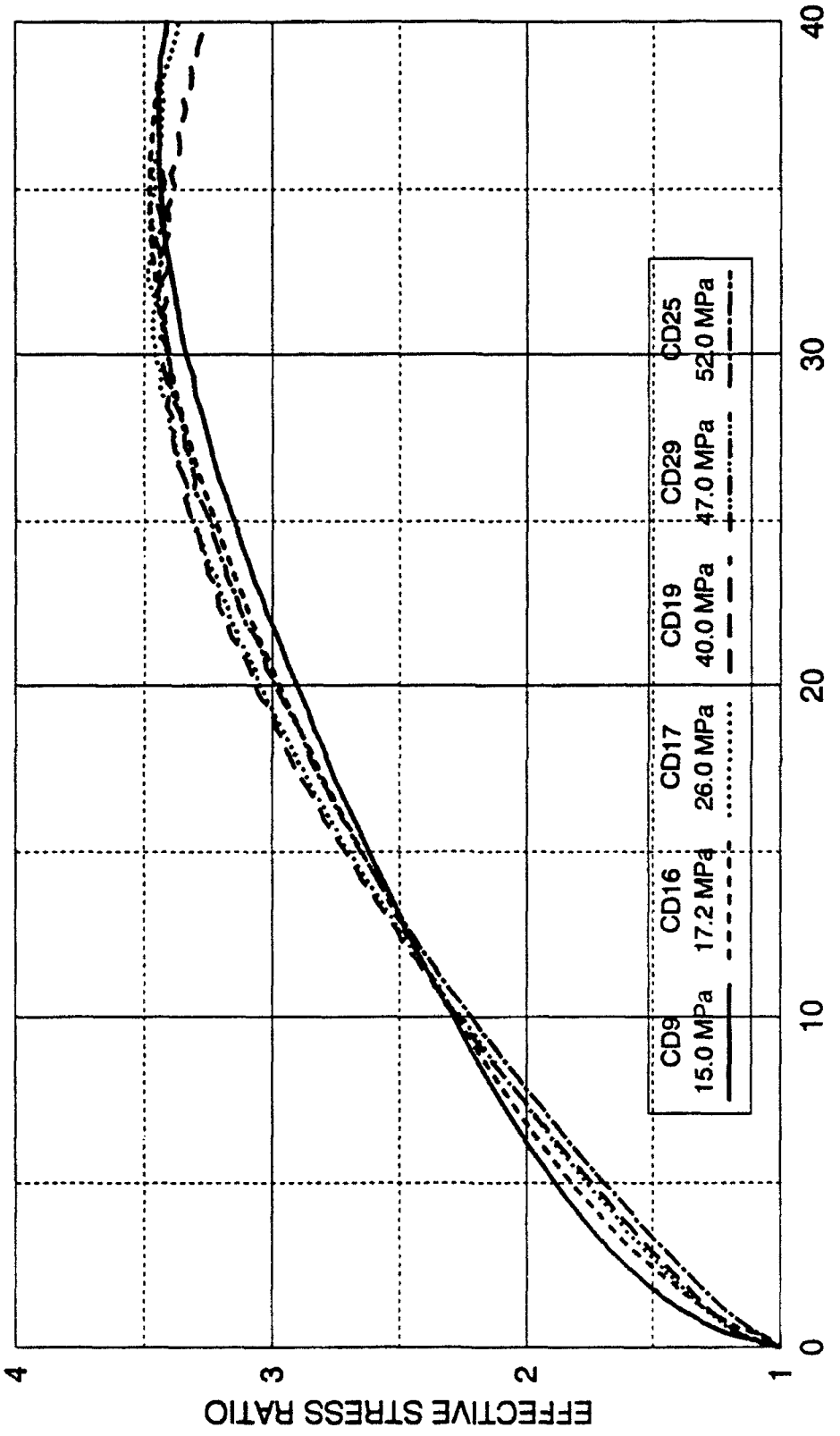

FIGURE 5-2 EFFECTIVE STRESS RATIO 15.0 TO 52.0 MPa
DRAINED TRIAXIAL COMPRESSION
DENSE CAMBRIA SAND

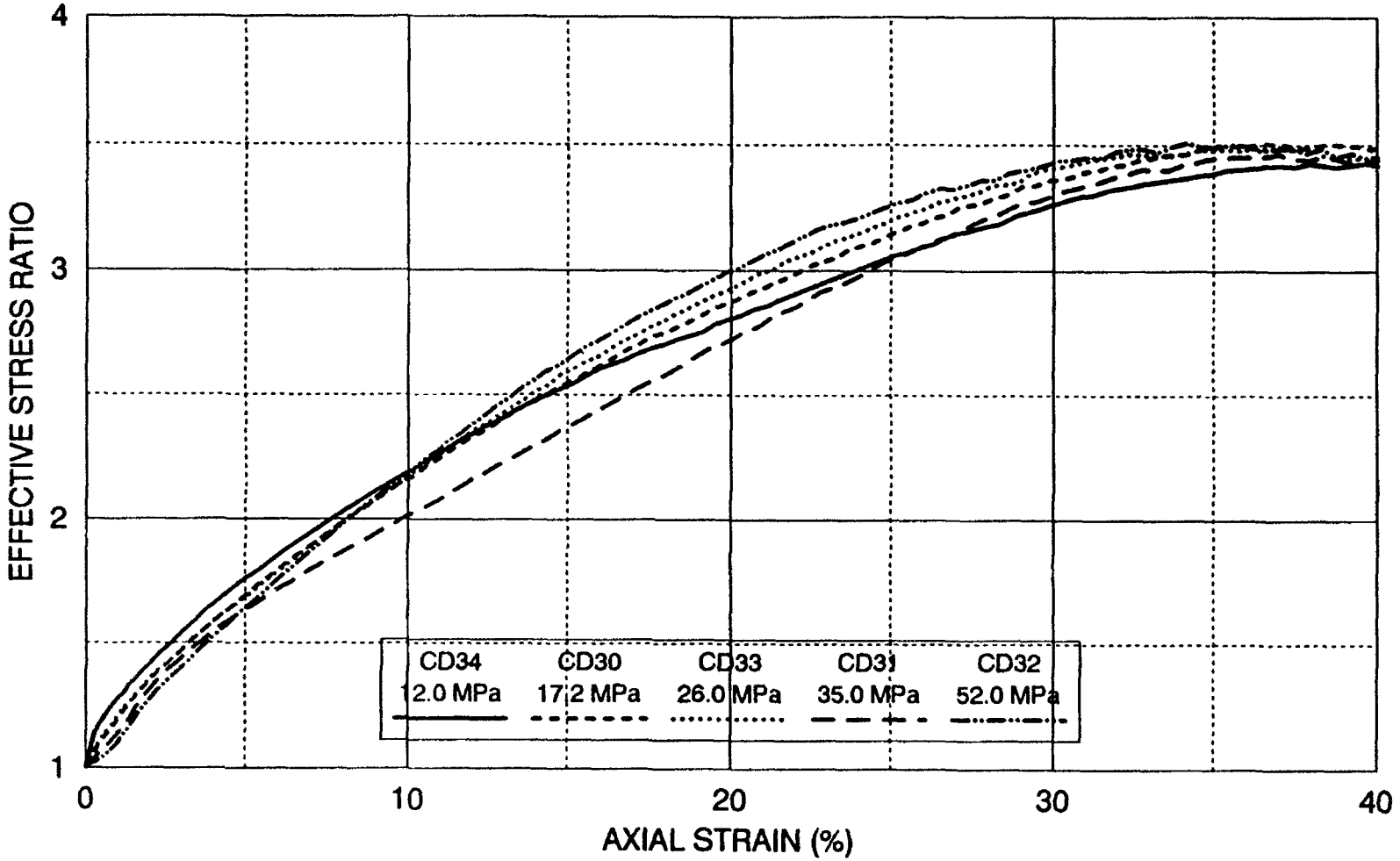

FIGURE 5-3 EFFECTIVE STRESS RATIO 12.0 TO 52.0 MPa
DRAINED TRIAXIAL COMPRESSION
DENSE QUARTZ SAND

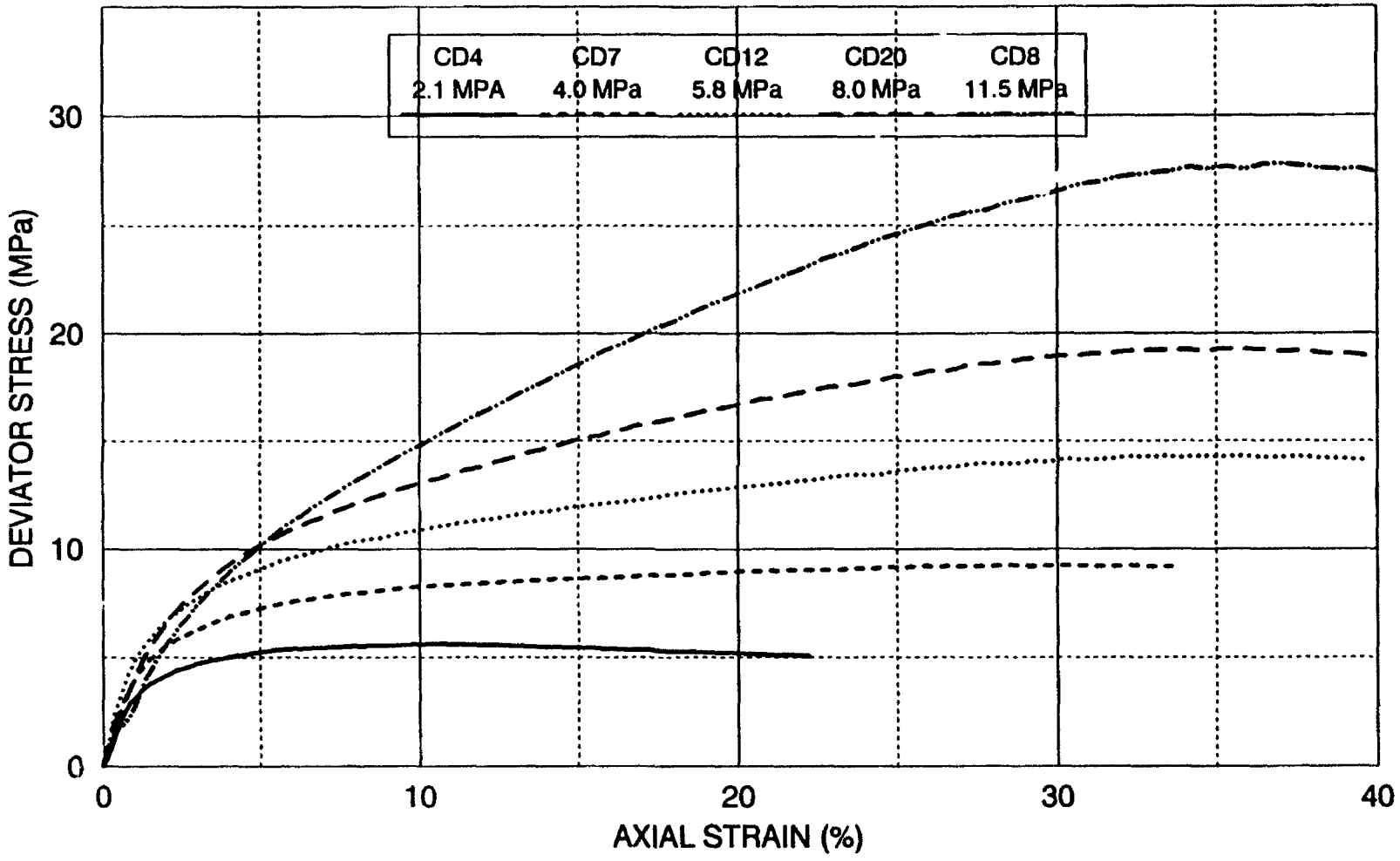

FIGURE 5-4 DEVIATOR STRESSES 2.1 TO 11.5 MPa
DRAINED TRIAXIAL COMPRESSION
DENSE CAMBRIA SAND

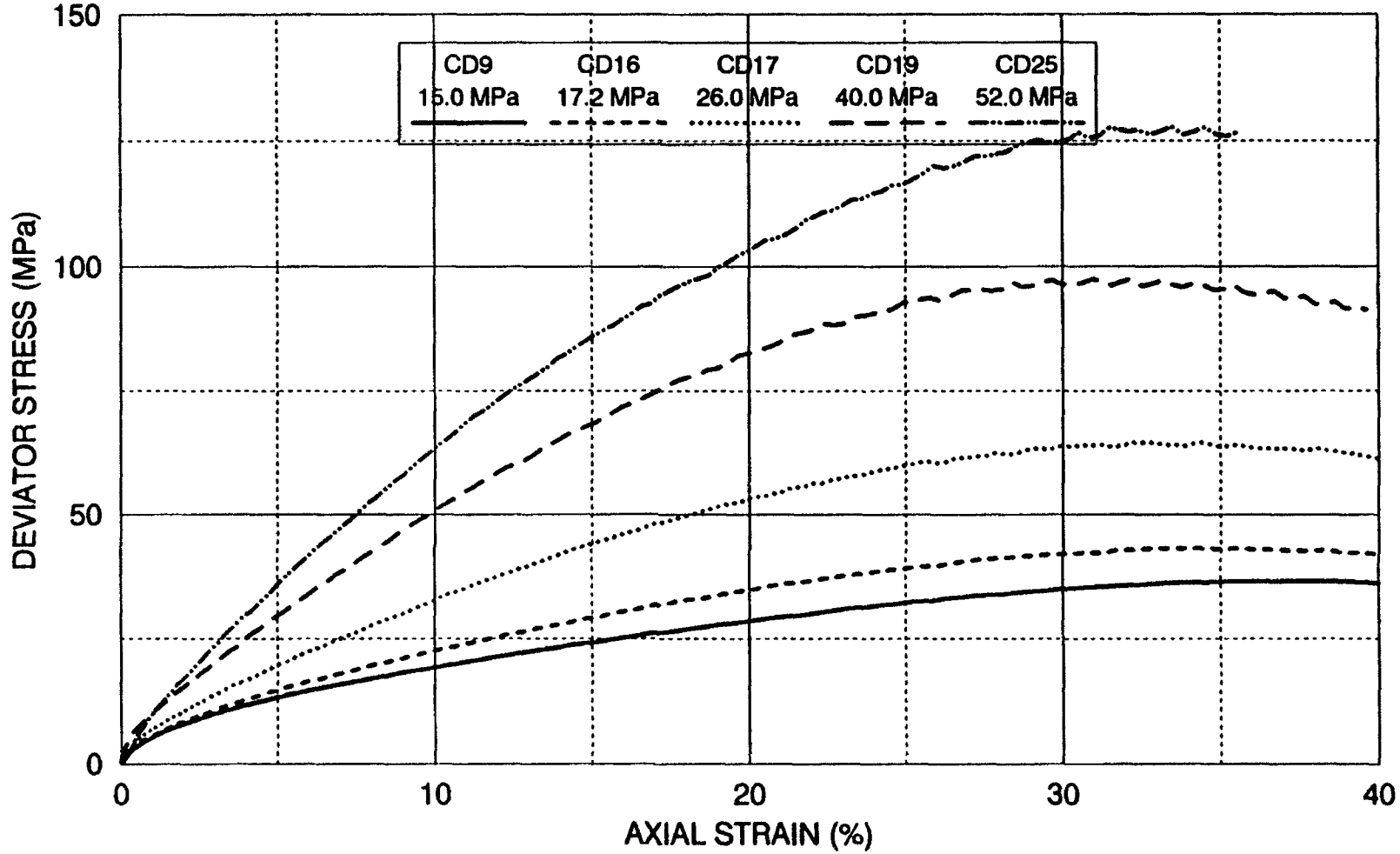

FIGURE 5-5 DEVIATOR STRESS 15.0 TO 52.0 MPa
DRAINED TRIAXIAL COMPRESSION
DENSE CAMBRIA SAND

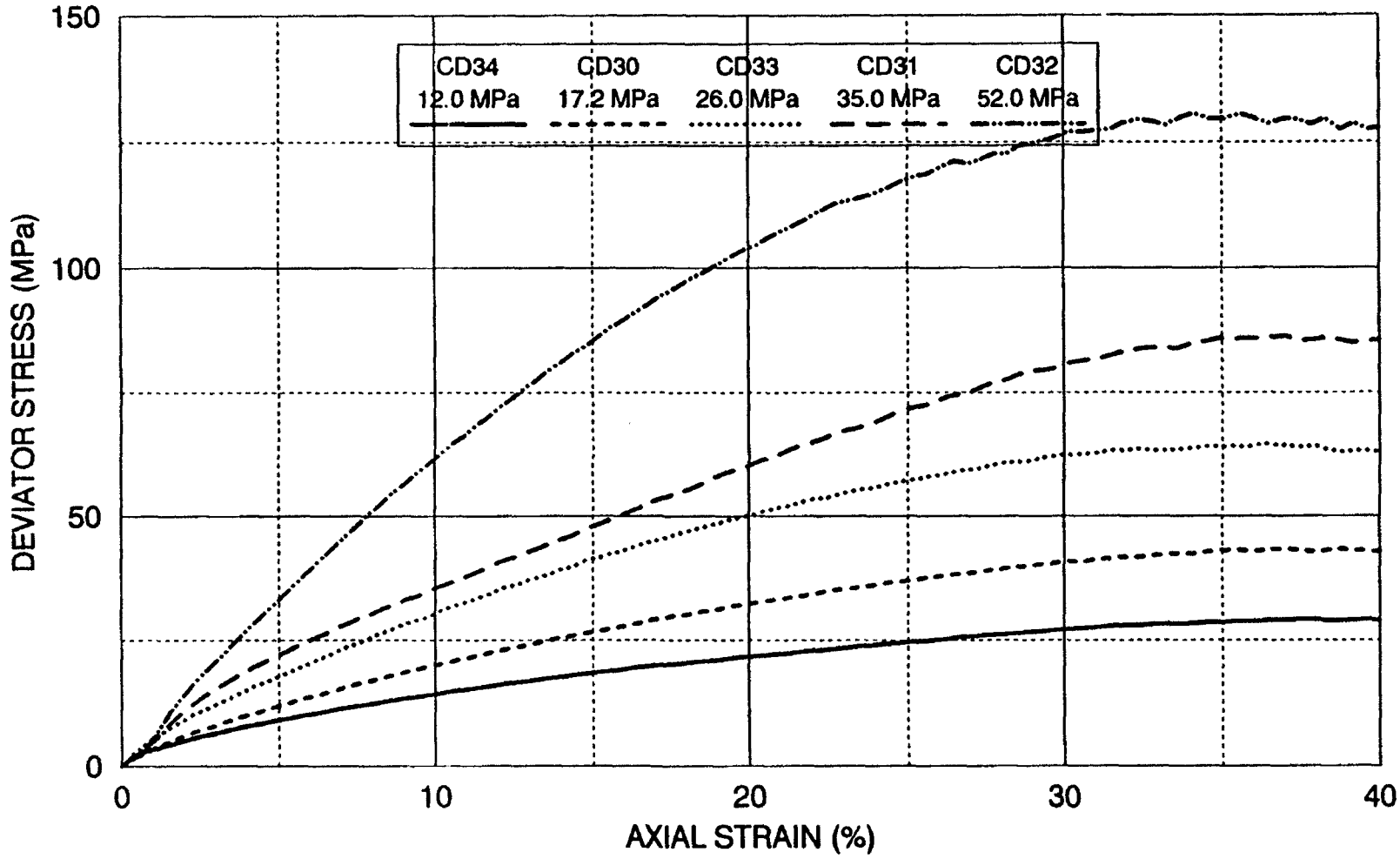

FIGURE 5-6 DEVIATOR STRESS 12.0 TO 52.0 MPa
DRAINED TRIAXIAL COMPRESSION
DENSE QUARTZ SAND

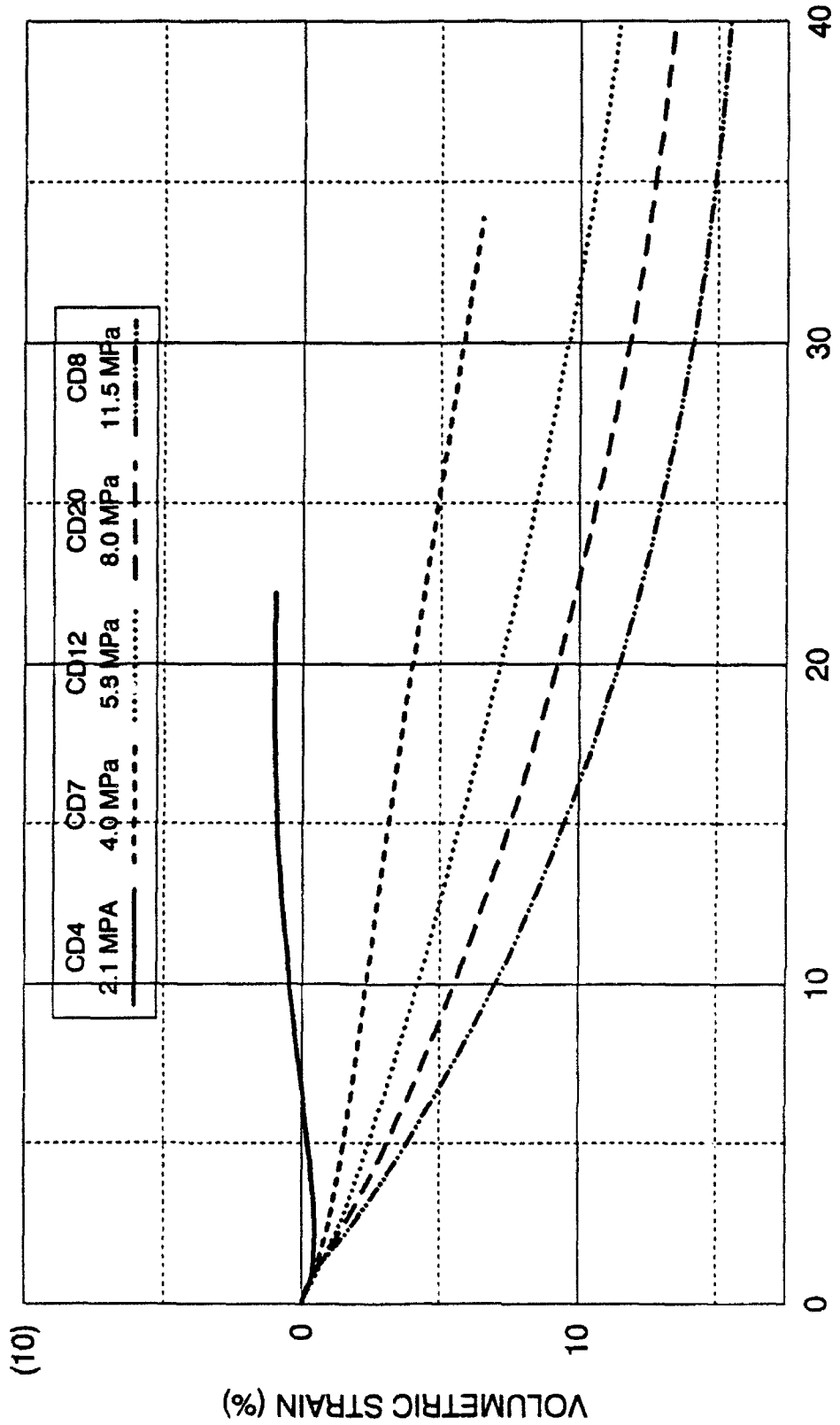

FIGURE 5-7 VOLUMETRIC STRAIN 2.1 TO 11.5 MPa
DRAINED TRIAXIAL COMPRESSION
DENSE CAMBRIA SAND

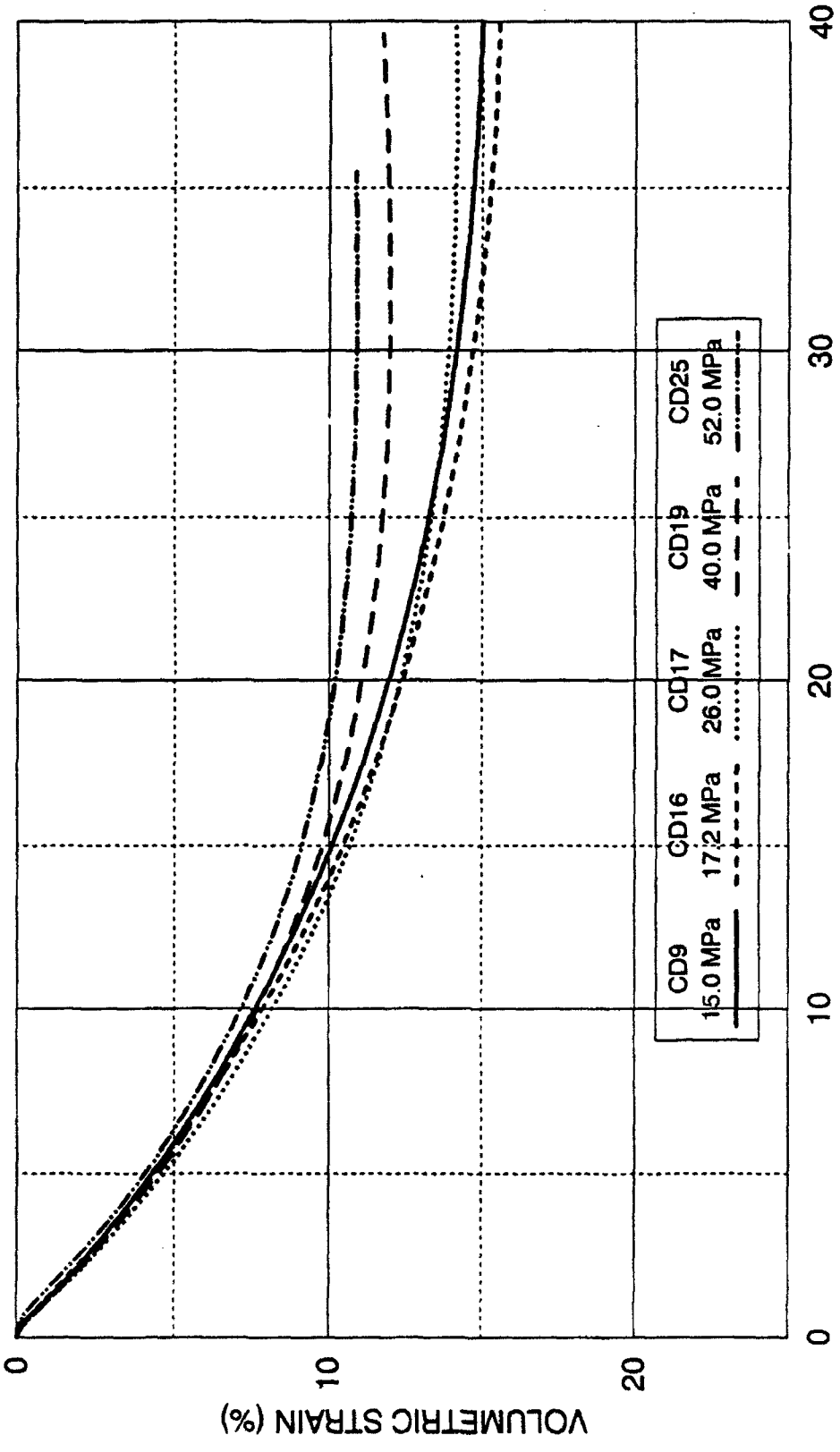

FIGURE 5-8 VOLUMETRIC STRAIN 15.0 TO 52.0 MPa
DRAINED TRIAXIAL COMPRESSION
DENSE CAMBRIA SAND

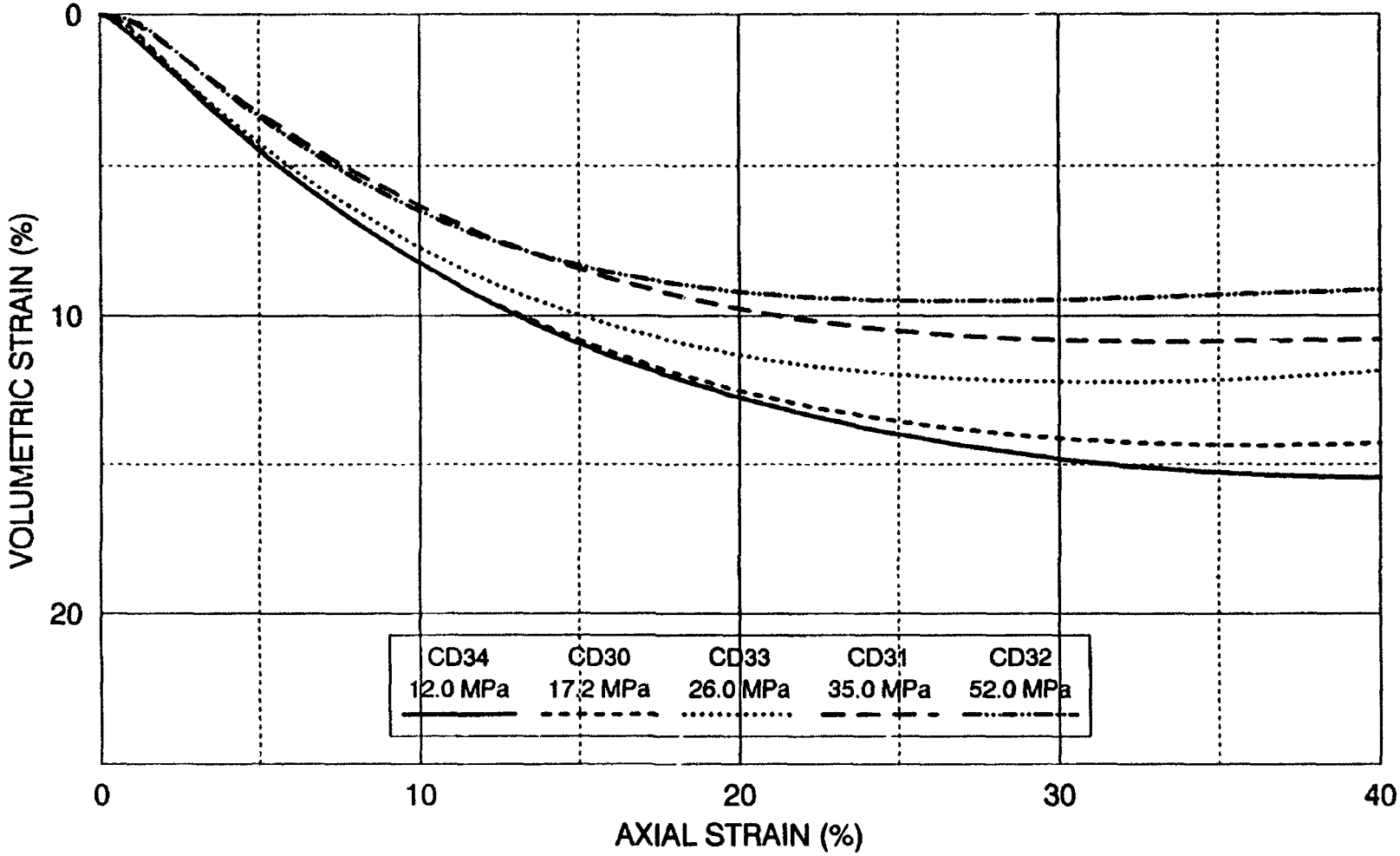

FIGURE 5-9 VOLUMETRIC STRAIN 12.0 TO 52.0 MPa
DRAINED TRIAXIAL COMPRESSION
DENSE QUARTZ SAND

The lowest confining pressure test (2.1 MPa), exhibits a stress ratio-strain curve that rises quickly, and curves over to its maximum value, which also represents the largest magnitude for all the tests. The strain to failure is relatively small, and the volumetric strains (Figure 5-7) are dilatant after an initial small compressive change. As the confining pressure increases beyond 2.1 MPa, the initial slopes of the stress ratio-strain curves tends to flatten, with decreasing maximum effective stress ratios, and with increasing magnitudes of volumetric compression. This flattening is especially noticeable in the higher confining pressure tests, where the stress ratio-strain curve is characterized by three almost linear sections. There is an initial steep portion, a very long middle flatter portion, and an almost horizontal portion near the failure stress. This flattening is caused by continual breakdown of load-bearing particle groups in the specimen by crushing and particle reorientation during increasing load (Billam, 1971). This is evidenced by examining the volumetric strain curves, which indicates that even at the conclusion of the 4.0 MPa test, the slope of the volumetric strain curve does not appear to be decreasing. This indicates that particle breakage and rearranging is continuing unabated even at the end of the test, well past failure. The axial strains to failure are seen to also dramatically increase with increasing confining pressure. However, the trend of decreasing maximum principal stress ratio with increasing confining pressure changes at the 5.8 MPa test from which the strength starts to increase slightly again. The initial slope of the stress-strain curve continues to flatten with increasing confining pressure. The volumetric strains continue to show increasing amounts of compression. This trend continues until

the 8.0 MPa test, where the magnitude of the maximum principal stress ratio stabilizes. Beyond this confining pressure the maximum principal effective stress ratio remains fairly constant up to the maximum confining pressure employed (52.0 MPa). Also at this confining pressure level (8.0 MPa), the slope of the volumetric strain curve at failure (rate of dilation) starts to decrease.

The trend showing continued flattening of the stress-strain curve continues through the 15.0 MPa test. Above this level the 17.2 MPa test is seen to cross over the stress-strain curve of the 15.0 MPa test (at about 11%), even though it started with an initially flatter slope. The reason for this is found by examining the volumetric strain curves. The volumetric strains for the 17.2 MPa test are very close to the values measured in the 15.0 MPa test, and they are the maximum amount measured for any compression test. Essentially, this pressure represents the point where the specimen will not volumetrically compress further during shearing. This is evidenced by the rate of dilation at failure, which is near zero. This is because increasing amounts of volumetric compression occurs during isotropic compression resulting in severely reduced void ratio after consolidation. Since the specimen has already been compressed, shearing results in less additional compression. This effect becomes increasingly pronounced with increasing confining pressures. Having reached the compressibility limit for this given stress state creates a stronger specimen, which results in the steepening of the stress ratio-strain curve at higher confining pressures. However, the effective stress ratios at failure are essentially the same. The 17.2 MPa test reaches failure at an axial strain and a volumetric strain, which are the largest of any test.

This general trend continues through the 26.0, 40.0, and 52.0 MPa tests. Initially, the slope of the stress ratio-strain curve is slightly flatter as the confining pressure increases. However, they quickly steepen and cross over lower confining pressure tests, then flatten out near the top, and culminate with nearly the same maximum principal stress ratio. These tests also indicate that the volumetric and the axial strains at failure are now decreasing with increasing confining pressure. The specimens in the 26.0, 40.0, 52.0 MPa tests have essentially reached a maximum state of volumetric compression at failure for a particular mean normal stress, with no further compressive volumetric strains. In fact, the tests generally dilate slightly after failure as the deviator stress starts to decrease during softening. This would tend to suggest that there is a minimum void ratio for a given mean normal stress during this type of test.

Examining the stress-strain curves and the volumetric strain curves for the five tests performed utilizing quartz sand, indicates that the trends discussed thus far for Cambria sand are also generally exhibited by the quartz sand. The stress-strain trends are the same, except in the 35.0 MPa test, whose slope is initially slightly less, but eventually fails at the same stress level. This could be caused by experimental scatter. The volumetric strains also show the trend of decreasing volumetric strains at failure as confining pressure increases.

Careful examination of the volumetric strain curves indicate a slight hesitation in the development of volumetric strains at the beginning of shearing. This is most likely caused by volumetric creep that occurs between the isotropic consolidation and shearing phase of the test. After isotropic consolidation, the

piston must be lowered into contact with the top cap of the specimen to begin the shearing phase. With the current testing system this cannot be accomplished instantaneously. Generally, lowering the piston into contact with the specimen takes between 15 and 20 minutes. During this delay the specimen undergoes volumetric creep, which is not insubstantial (up to a few cubic centimeters). This creep tends to initially buffer the initial volumetric strain response during shearing.

After the creep effects are overcome, the volumetric strain curves for the 15.0 through 52.0 MPa confining pressure tests have very steep slopes. In fact, tangents to the curves would indicate slopes in excess of unity. This indicates that the horizontal strains near the beginning of the test are actually positive, corresponding to compression or inward movement. The specimen, after isotropic compression, is in a volumetrically collapsing state moving inward in all three directions. This is caused by the massive amount of rearranging and particle crushing during the initial application of shear stresses. This condition corresponds to a negative Poisson's ratio. Eventually, as the specimens densify the horizontal strains change direction and move outward.

At the highest confining pressure employed, 52.0 MPa, there was considerable difficulty in achieving good test results due to lateral slipping of the specimen between the cap and base on the lubricated end. Just prior to shearing, the control program lowers the piston until it achieves contact with the specimen cap. The piston contact area is designed to cover the majority of the cap surface area. However, if the contact between the piston and cap is not perfectly horizontal, a small horizontal force is imparted into the specimen. With functional

lubricated ends, there is a tendency for the specimen to slip laterally off the cap and base, and the specimen eventually fails by buckling into an S-shape. The main reason why this difficulty occurs at high confining pressures is that a very large amount of isotropic compression occurs during which the specimen cap may not remain perfectly horizontal. The vertical deformation due to isotropic compression for the taller specimens (17.8 centimeter) is in excess of one centimeter. Another factor which exacerbates the problem is that under high confining pressures, the specimen is extremely rigid and resists the initial deformations, which would help anchor the specimen to the cap by allowing the cap to straighten slightly into a fully horizontal position. To overcome this problem, it is possible to change the height-to-diameter ratio by changing the specimen height from 17.8 centimeters to 13.0 centimeters, which reduces the magnitude of the deformation associated with the isotropic compression. Successful tests were performed using this procedure. Unfortunately, the character of the stress strain curve changes slightly, as shown on Figure 5-10, where stress-strain and volumetric strain curves are shown for a tall specimen that buckled, a tall specimen that did not buckle, and a short specimen. The buckled specimen is seen to have multiple changes in curvature in the stress-strain curve, and much lower compressive volumetric strains than the successful tests. The tall specimen (H/D ratio of 2.5) shows a stress-strain curve for which failure occurs at a smaller axial strain than in the shorter specimen (H/D ratio of 1.8). However, the volumetric strain curves from the two tests are essentially the same.

Friction angles, volumetric and axial failure strains will be discussed in the

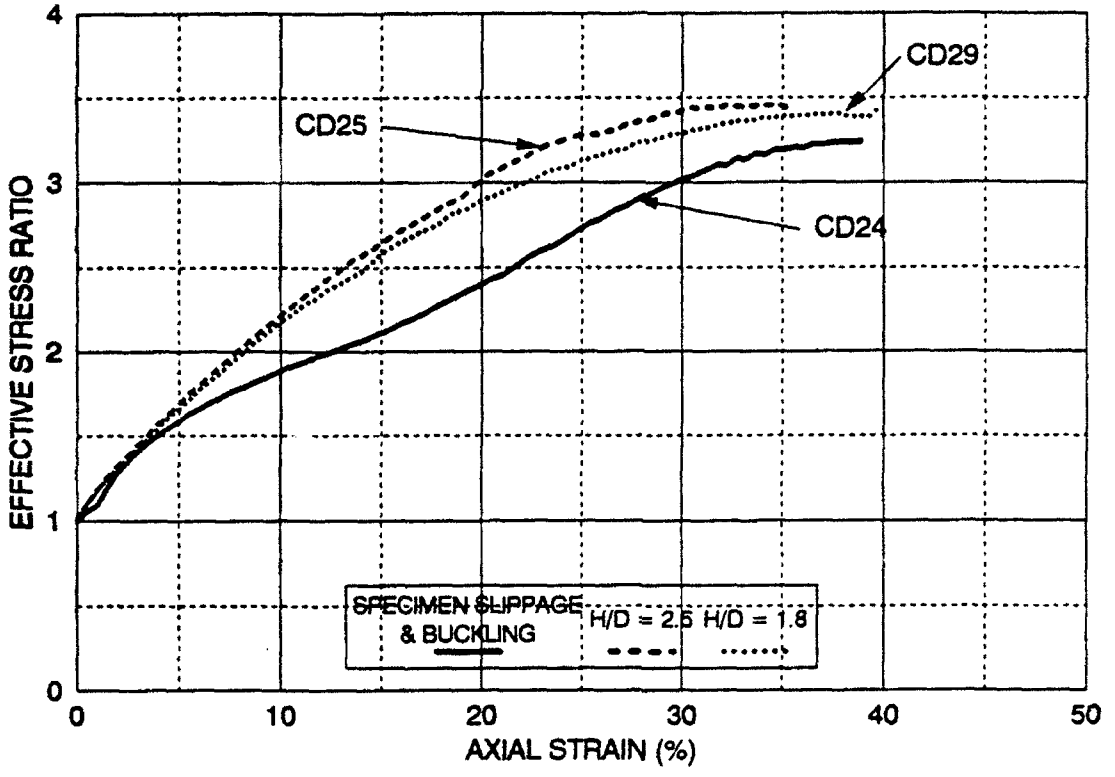

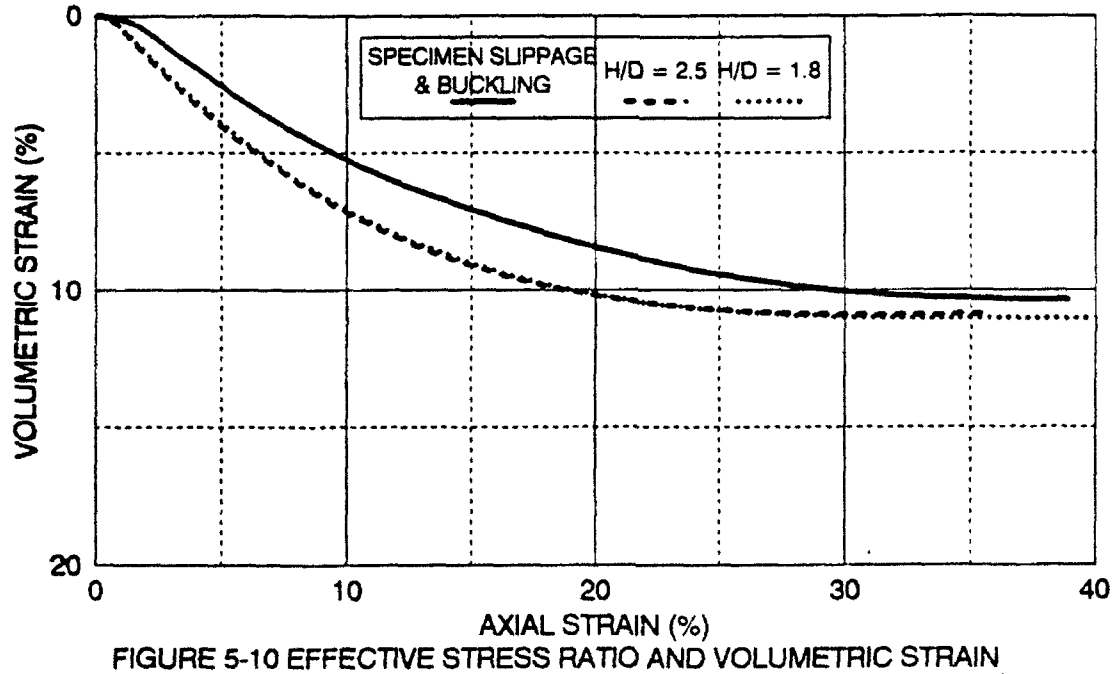

FIGURE 5-10 EFFECTIVE STRESS RATIO AND VOLUMETRIC STRAIN BUCKLING, SLIPPAGE AND EFFECT OF HEIGHT-TO-DIAMETER RATIO 52.0 MPa DRAINED TRIAXIAL COMPRESSION TESTS

following sections.

5.3 Results from Undrained Triaxial Compression Tests

The undrained triaxial compression stress-strain characteristics are shown on Figures 5-11 and 5-12, where the maximum effective principal stress ratios and the deviator stresses are plotted against axial strains (ϵ_1). The lowest initial confining pressure test (6.4 MPa) has its effective stress ratio curve commencing with a steep initial slope, which then rises up smoothly to its maximum value, the lowest value of all the undrained tests. It was not possible to perform undrained triaxial compression tests with lower initial confining pressures, because the large grain size of the Cambria sand would result in membrane penetration and this would affect the pore pressure response, as was discussed in Chapter 3. As the initial confining pressure increases, the initial slopes of the effective principal stress ratio curves become progressively flatter. The maximum effective principal stress ratios also increase, and they stabilize near a maximum value in the 34.0 MPa test. The top portion of the effective stress ratio-strain curves are all very flat over a large axial strain range. Careful examination indicates that the effective stress ratio-strain curve for the 68.9 MPa test is seen to cross the 52.0 MPa test at very low axial strain values. This is not considered significant. The crossing is most likely caused by slightly nonhorizontal settlement of the specimen cap during the large isotropic consolidation phase, causing the piston to initially have slightly uneven contact with the cap. Assuring that the specimen will consolidate evenly in the vertical direction is difficult, since it only takes a variation of about 0.025

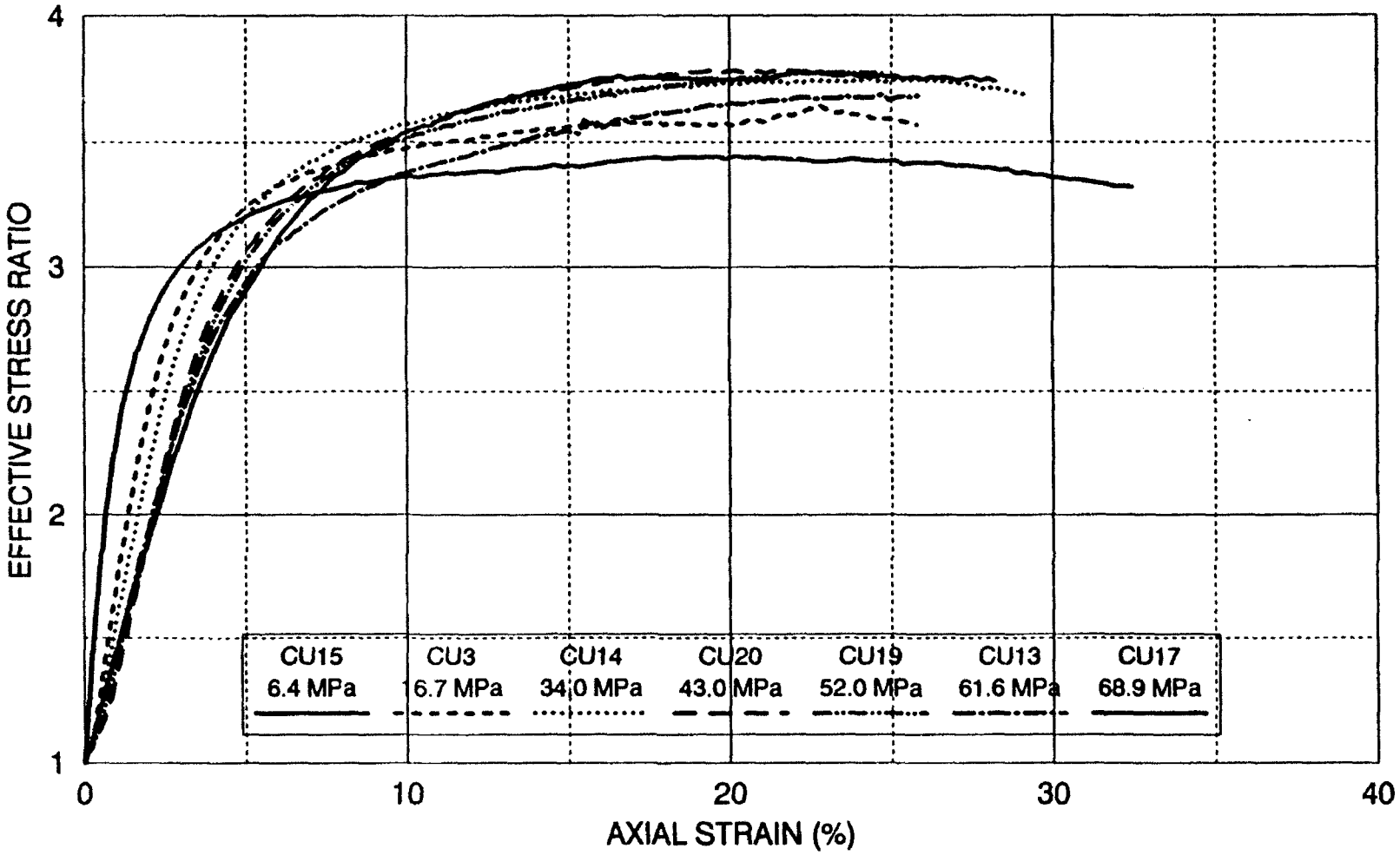

FIGURE 5-11 EFFECTIVE STRESS RATIO 6.4 TO 68.9 MPa
UNDRAINED TRIAXIAL COMPRESSION
DENSE CAMBRIA SAND

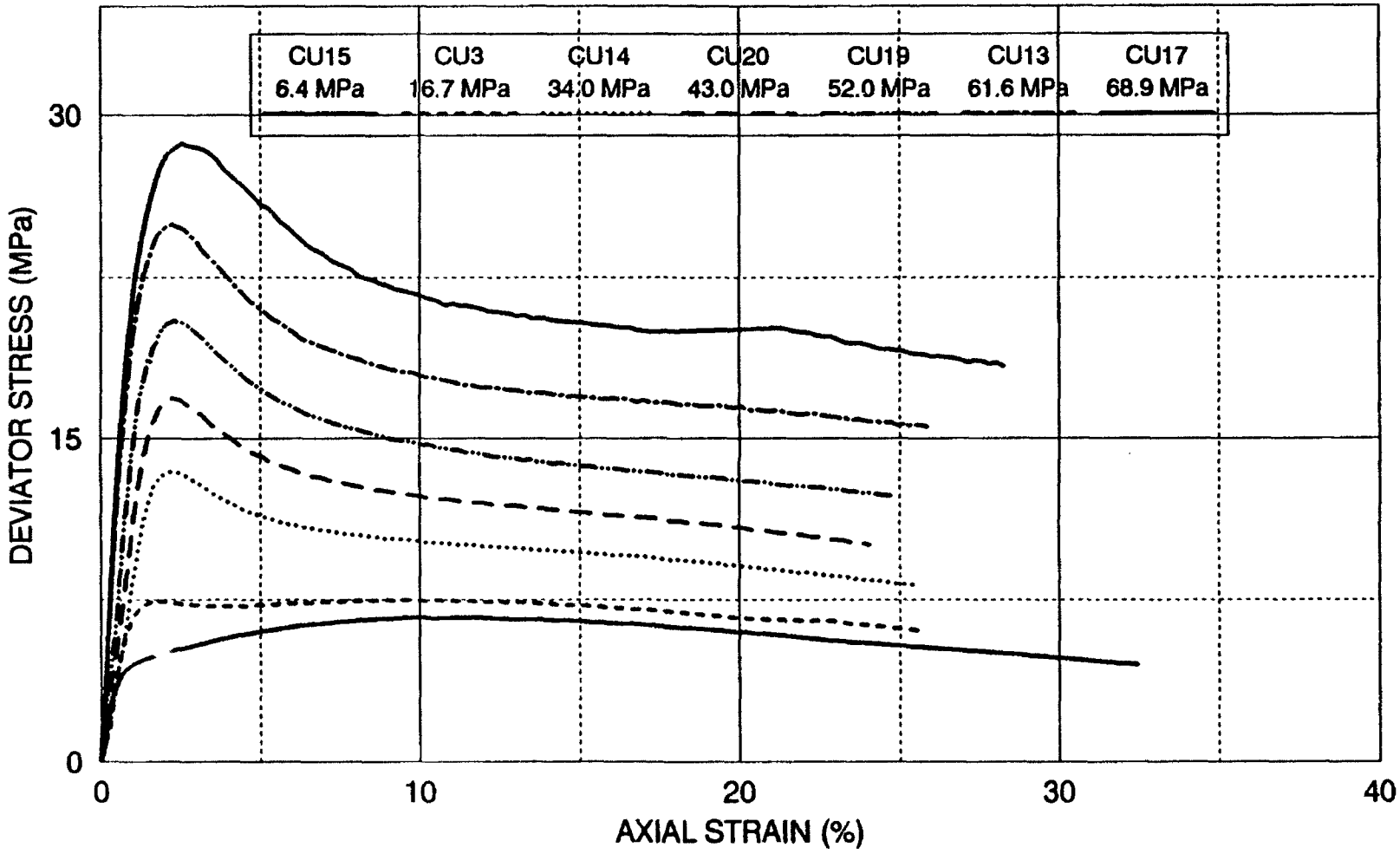

FIGURE 5-12 DEVIATOR STRESS 6.4 TO 68.9 MPa
UNDRAINED TRIAXIAL COMPRESSION
DENSE CAMBRIA SAND

centimeters of a total settlement of over one centimeter to have these types of effects produced in the tests. Another possible factor for the crossing of the stress-strain curves is based upon small variations in lubricated end thicknesses.

The deviator stresses shown on Figure 5-12 indicate initially steeper slopes on the stress-strain curve with increasing initial confining pressure. At low initial confining pressures, such as in the 6.4 MPa test, the maximum deviator stress occurs at larger strain values. The test at 16.7 MPa shows a pattern of behavior with deviator stress increasing to a peak, then decreasing, and eventually it rises again to a maximum at failure, after which it declines again. This occurs as a result of the volume change tendency of the specimen. The specimen first wants to compress, causing pore pressures to rise, and this decreases the deviator stress. Then the specimen wants to dilate, causing the pore pressures to drop, and this causes the deviator stress to increase again. Eventually, the specimen reaches effective stress failure after which the deviator stress decreases as the specimen softens.

Pore pressures are shown on Figure 5-13. All tests show tendencies for overall net compressive volumetric behavior, since the pore pressures are all positive. As the initial confining pressure reaches 34.0 MPa, the maximum deviator stresses start to occur at very low axial strain values as indicated on Figure 5-12. The strain to maximum deviator stress then gradually increases with continued increasing initial confining pressure. Large, quickly developing pore pressures cause the deviator stresses to peak very early in the test due to the rapidly decreasing effective confining pressures in the specimen. The deviator

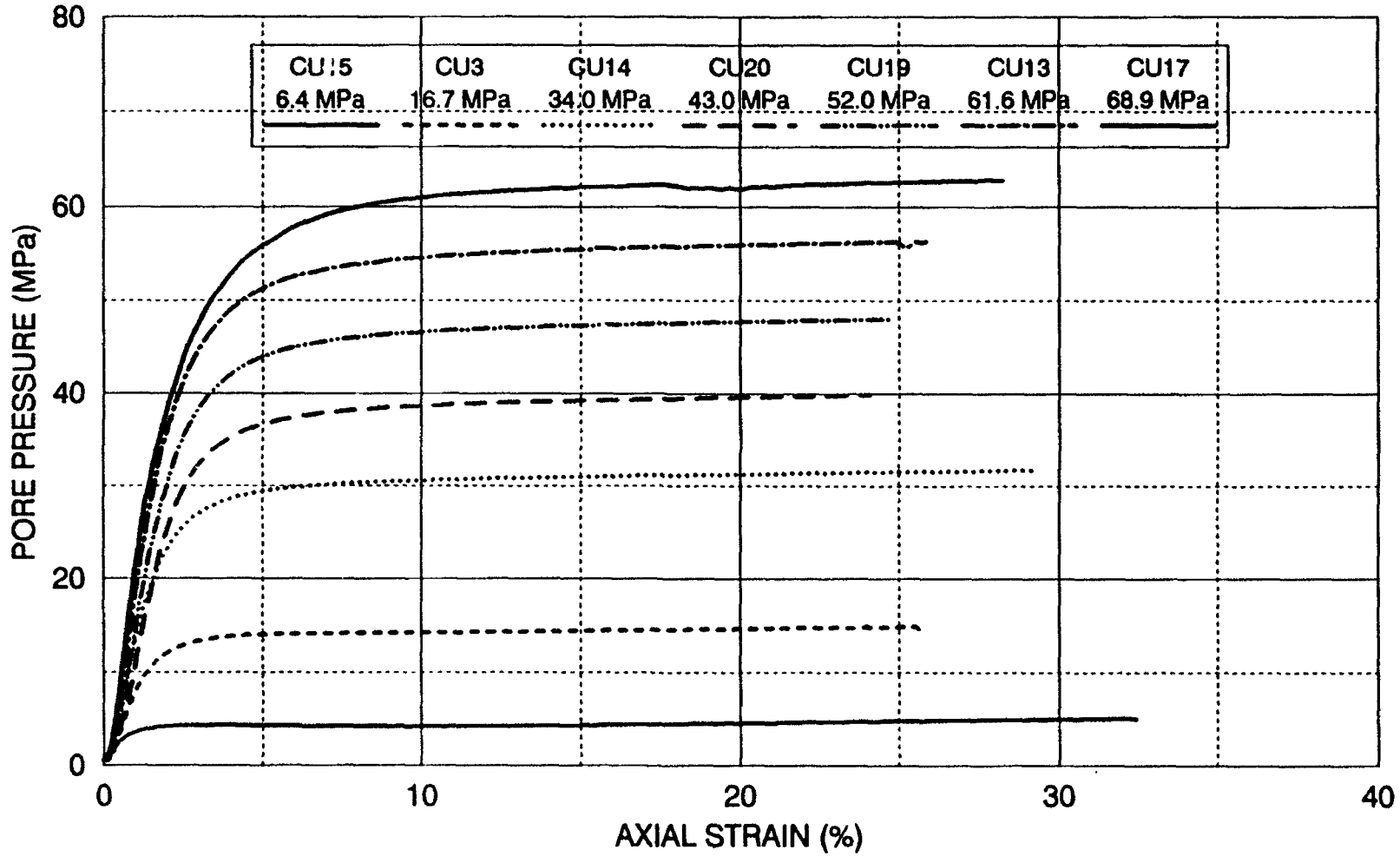

FIGURE 5-13 PORE PRESSURE 6.4 TO 68.9 MPa
UNDRAINED TRIAXIAL COMPRESSION
DENSE CAMBRIA SAND

stresses then continue to decline until the end of the test. However, since the pore pressures are large, and continue to increase throughout the higher initial confining pressure tests, the effective stress ratio continues to increase until it reaches a maximum value at much larger axial strains as was shown on the effective stress ratio curve.

Close inspection of the pore pressure curves associated with the higher confining pressure tests indicate a slightly buffered pore pressure development at the immediate onset of shearing. This is the same effect causing the slight delay in the volume change response observed in the drained tests. Again, this was due to the volumetric creep effects between the isotropic consolidation phase and the starting of the shearing phase.

The effective stress paths for the undrained tests are shown on the Cambridge p'-q diagram in Figure 5-14. Plotted on the vertical axis is the stress difference (deviator stress) against the effective mean normal stress on the horizontal axis. Undrained tests with constant total confining pressure have total stress paths indicated by a line rising on a 3 on 1 slope during loading, and coming back down the line during softening or unloading. The effective stress path for undrained tests indicate the magnitude of pore pressures by the horizontal distance between the total stress path line, and the effective stress path. The higher initial confining pressure undrained tests (above 16.7 MPa) result in effective stress paths that rise up, but move toward the origin due to increasing pore pressures. The effective stress paths then reach maximum values of deviator stress, and then move downward with decreasing deviator stresses and continued

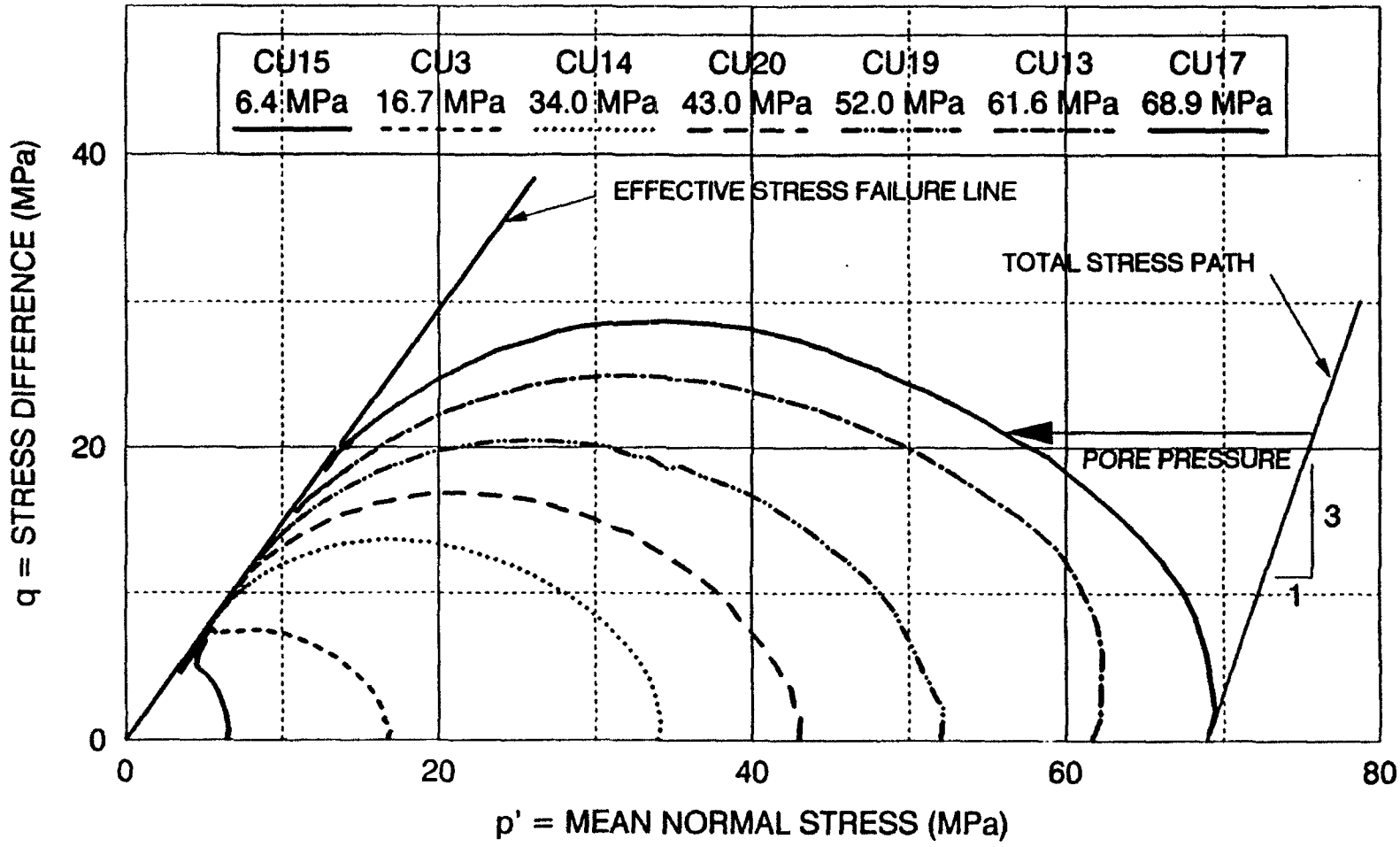

FIGURE 5-14 EFFECTIVE STRESS PATH - CAMBRIDGE p'-q
UNDRAINED TRIAXIAL COMPRESSION
DENSE CAMBRIA SAND

decreasing effective mean normal stresses until they intersect the effective stress failure envelope. The lower pressure undrained tests indicate effective stress paths that also move upward, and toward the origin. However, in such a test, the specimen indicates a tendency to dilate, resulting in a pore pressures decrease which causes the specimen to gain strength and the stress path to continue upward with increasing deviator stresses and effective mean normal stresses. The deviator stress finally reaches its maximum value at the effective stress failure envelope.

5.4 Discussion of Triaxial Compression Tests

Figure 5-15 displays the rate of dilation at failure plotted against the effective mean normal stress at failure for the drained triaxial compression tests. The rate of dilation at failure is the tangential slope of the volumetric strain-axial strain (ϵ_3) curve at failure. Under low confining pressures the specimens are dilating, resulting in negative volumetric strains. Therefore, the rate of dilation is negative. As the confining pressures increase, the effective mean normal stress at failure also increases, and the specimens start undergoing volumetric compression at an increasing rate, which increases the magnitude of the rate of dilation (more positive or increasing compression). Much of this increase in the rate of dilation is due to particle crushing and grain rearrangement. The rate of dilation at failure continues to increase (more positive or increasing compression) until the effective mean normal stress at failure reaches a value of approximately 8 MPa, where it reaches a maximum value. Then it starts to decrease (more negative or increasing dilatancy) until it reaches zero at the highest mean normal stresses achieved in the

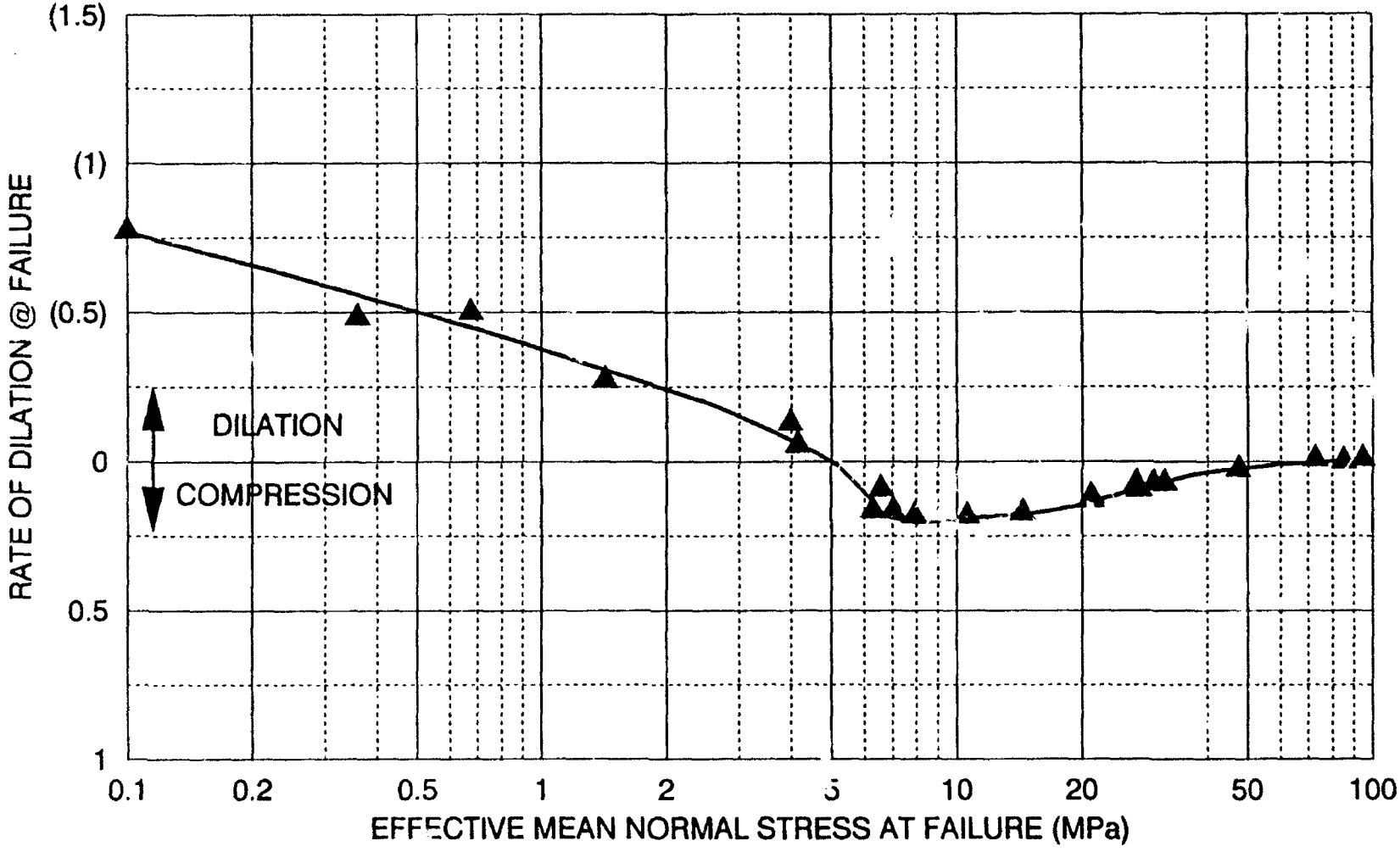

FIGURE 5-15 RATE OF DILATION AT FAILURE
DRAINED TRIAXIAL COMPRESSION
DENSE CAMBRIA SAND

testing program. These high pressure tests which exhibit a rate of dilation at failure that is close to zero, exhibit a slight amount of dilation during softening, when the mean normal stress decreases from the maximum value. This slightly increases the void ratio. This observation would indicate that there is a fixed amount of total volumetric compression in a specimen, for a given maximum effective mean normal stress, which coincides with failure. At lower pressures the majority of volumetric strains occur in the shearing phase, and not in the isotropic consolidation phase. Also, at lower pressures the rate of dilation at failure is large (highly compressive), and compressive volumetric strains are still increasing well after failure, due to continued particle breakage beyond failure. As confining pressures increase, the proportion changes until eventually the majority of volume change occurs during isotropic consolidation, and the volume change measured during shearing actually decreases. This is shown on Figure 5-16, which displays the volumetric strain at failure plotted against the effective mean normal stress at failure. This figure clearly shows that volumetric strains during shearing start to decrease from a maximum of 15% at about 30 MPa. Eventually, the combined consolidation and shearing volume change reaches a limit for a given maximum effective mean normal stress, indicated by the near zero rate of dilation at failure. As the confining pressure continues to increase, the maximum mean normal stress increases, since it always occurs at failure. Therefore, for each increase in maximum mean normal stress, there appears to be a corresponding increase in total volume reduction capacity of the specimen. Possibly, this general trend would continue with increasing confining pressure, until a near zero void ratio is

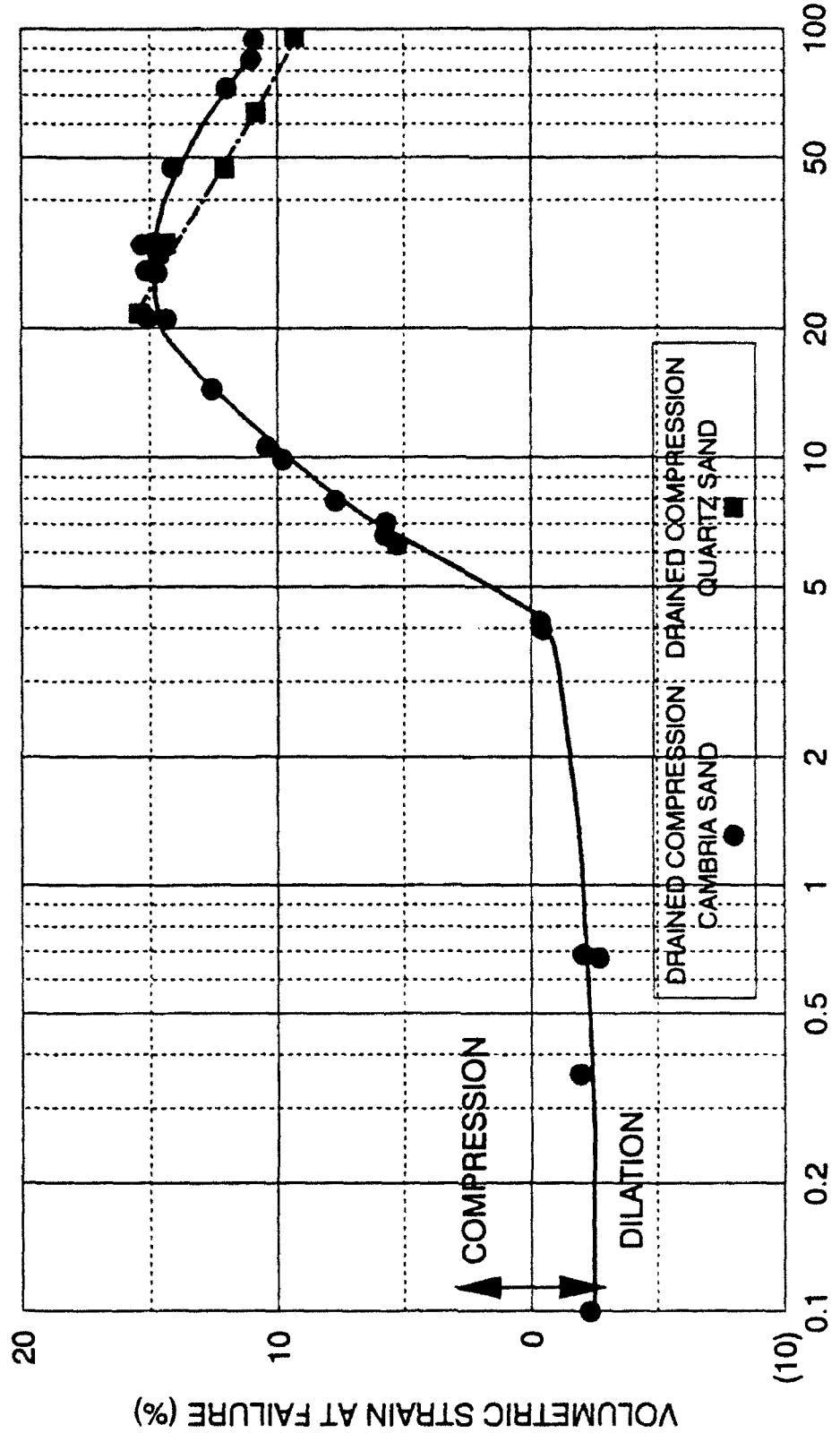

FIGURE 5-16 VOLUMETRIC STRAIN AT FAILURE
DRAINED TRIAXIAL COMPRESSION
DENSE CAMBRIA SAND AND DENSE QUARTZ SAND

achieved. The capacity of the loading frame was reached in the 52.0 MPa drained compression test for the size of specimen used in this experimental program. The five triaxial compression tests on quartz sand exhibit the same volumetric behavior as the Cambria sand.

The axial strains to failure are shown on Figure 5-17, plotted against effective mean normal stress at failure. The general shape of the curve looks very similar to the volumetric strain at failure curve. The drained tests exhibit low values of strain to failure at low effective mean normal stresses. They increase slowly until around 4 MPa, where they start to increase rapidly. This corresponds to the approximate stress magnitude where volumetric strain switches from dilation to compression. The strains to failure quickly increase as particle breakage, and large volumetric compression becomes significant and have important effects on the stress-strain behavior. Eventually, at a stress around 30 MPa the strain to failure reaches a peak of approximately 36%. Then the strains to failure start to decrease in magnitude. The maximum strain to failure occurs at the same effective mean normal stress at failure, as the maximum volumetric strain at failure, as shown on Figure 5-16. Below this stress value the volumetric and axial strains at failure are increasing, and afterward they decrease. This magnitude also appears to relate with a rate of dilation approaching zero as shown on Figure 5-15. As the magnitude of the isotropic consolidation gets larger, there is less volume change available during shear. Therefore, the specimens start to fail earlier when they reach this level, but the maximum effective principal stress ratio is not affected. The undrained axial strains at failure initially reach approximately

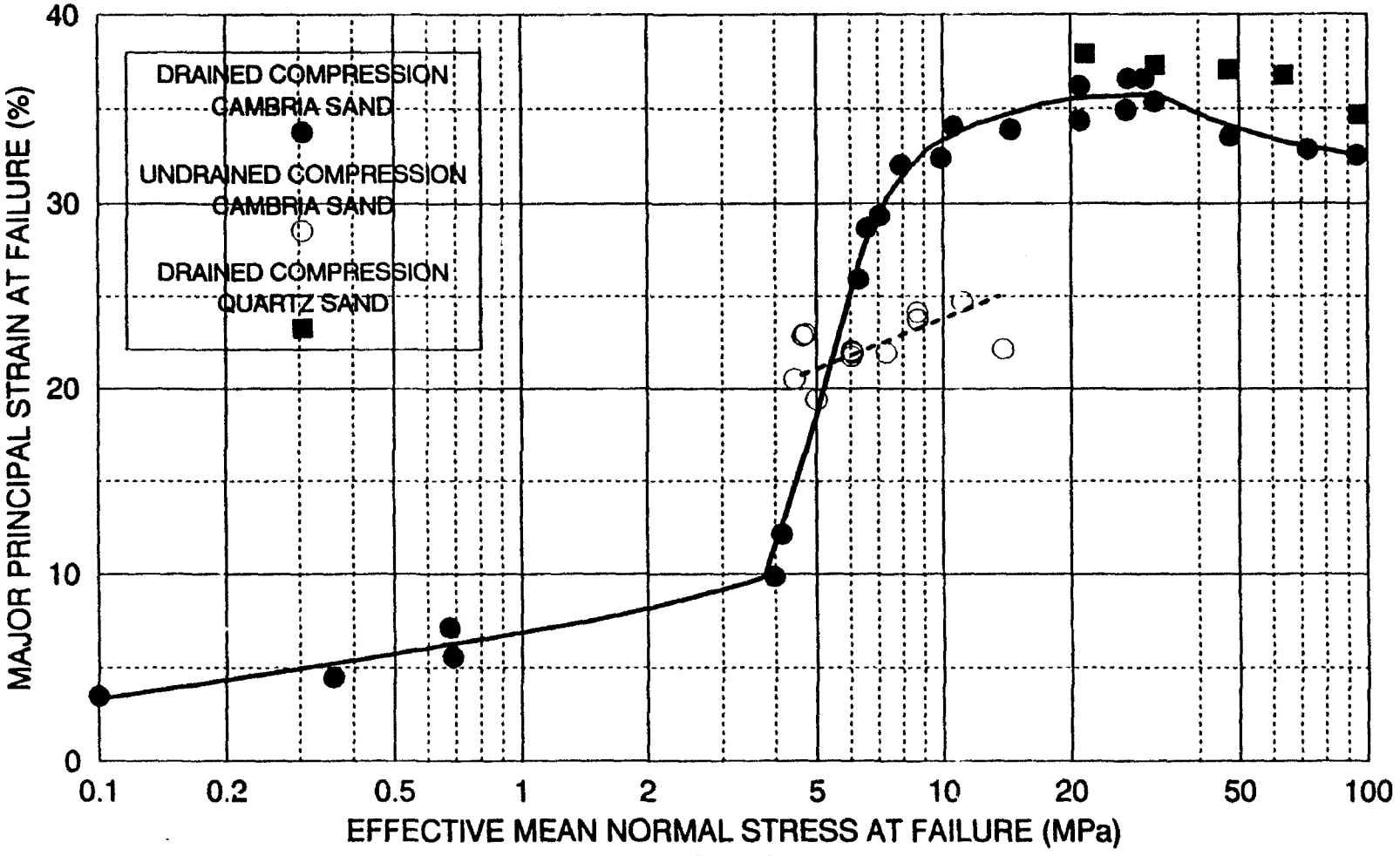

FIGURE 5-17 MAJOR PRINCIPAL STRAIN AT FAILURE
DRAINED AND UNDRAINED TRIAXIAL COMPRESSION
DENSE CAMBRIA SAND AND DENSE QUARTZ SAND

around twenty percent for low consolidation pressures, and they increase slightly, but never reach as high values as observed in the drained tests.

The drained and undrained Mohr-Coulomb secant friction angles for both the Cambria and quartz sand are shown on Figure 5-18, plotted against effective mean normal stress at failure. As the confining pressure and effective mean normal stress at failure increases, the drained friction angle first decreases. The friction angle appears to reach a low value around 8 MPa, it then increases slightly with increasing stress magnitude, and finally stabilizes at a constant value beyond effective mean normal stresses at failure between 20 and 30 MPa . This is the approximate effective mean normal stress at failure, where the greatest axial strain to failure and volumetric strain at failure also occurs. The friction angle then stays constant up to the highest mean normal stress encountered, 94 MPa.

The variation in friction angle from the drained tests bears a strong resemblance to the variation in rate of dilation at failure shown on Figure 5-15. This suggests a direct relationship between the secant friction angle and the rate of dilation over all pressure ranges. This has been proposed by other investigators (Rowe, 1964, Bishop, 1954, and Taylor, 1948). However, their conclusions regarding the effects of dilatancy on strength were developed for low confining pressure applications. The topic of stress-dilatancy is discussed at great length in Chapter 10. The increases in friction angle from its low value at 8 MPa to its stable value at higher stresses, appears to relate to the increasing volumetric dilatancy shown on Figure 5-15. Specimens tested in the range between 10 and 50 MPa experienced some slight bulging in the deformation patterns, which

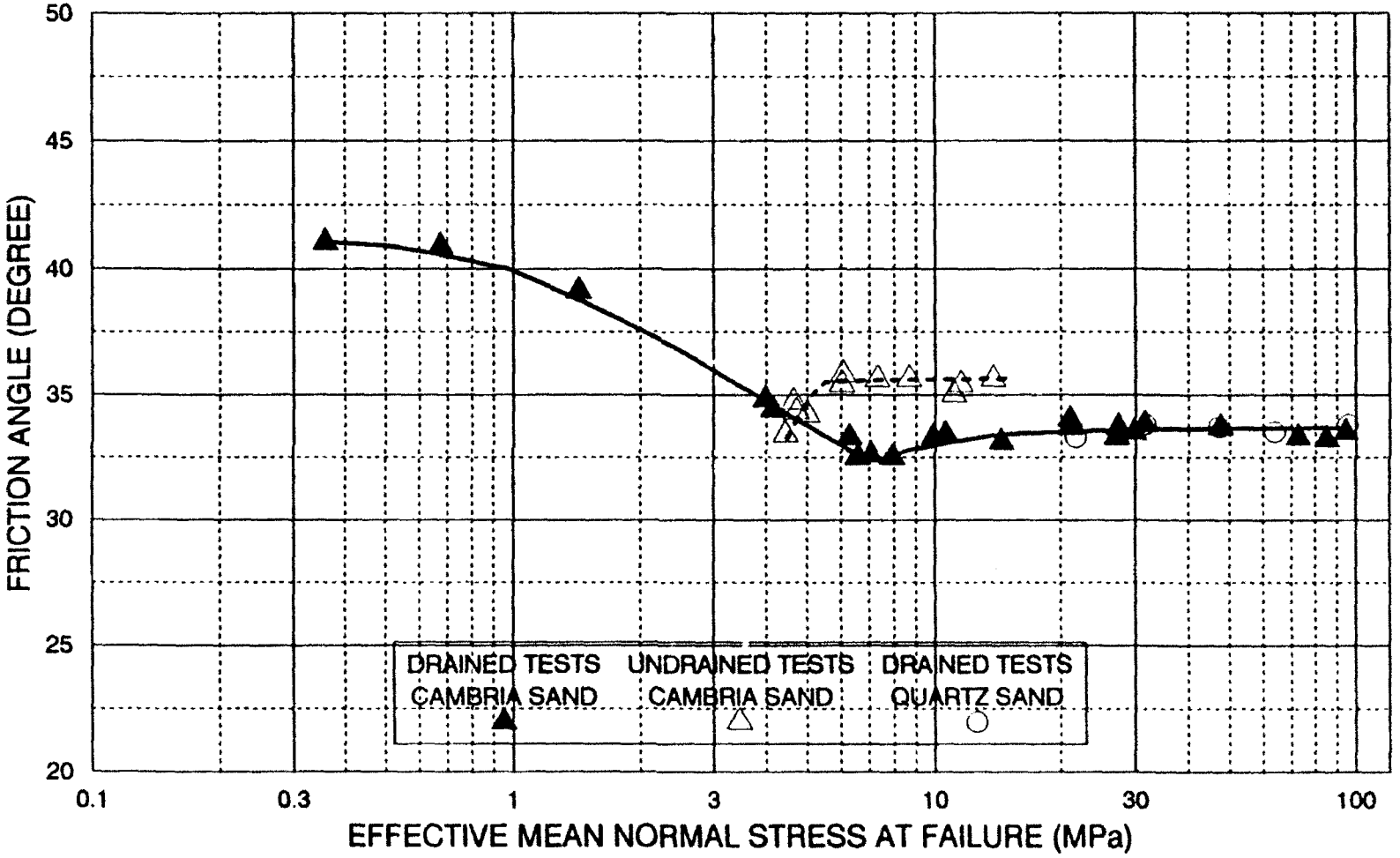

FIGURE 5-18 MOHR-COULOMB SECANT FRICTION ANGLES
DRAINED & UNDRAINED COMPRESSION
DENSE CAMBRIA SAND & DENSE QUARTZ SAND

could account for the friction angle increase in this zone. Therefore, the true friction angle in this stress region may be slightly less, corresponding even more closely to the shape of the rate of dilation diagram. However, corrections for these nonuniform strains was not performed, because the bulging was not excessive, and the relation between the amount of sharing of strains between the end and center portions of the specimen is not really known (Chapter 3). Full uniform strains in the test specimens were achieved below and above this mean normal stress range.

The undrained failure envelope is also shown on Figure 5-18. At lower stress levels, the friction angles are similar to the drained friction angles, when plotted against effective mean normal stress at failure. As the pressure level increases, particle crushing during isotropic consolidation starts to play an important role. The effective stress friction angle quickly increases, because the initially dense uniform sand becomes altered. At high confining pressures, as shown on Figure 5-14, the effective stress path that a specimen follows during an undrained test is completely different from the drained tests. The specimen first undergoes a large isotropic consolidation under drained conditions. Particle breakage and rearranging during consolidation changes the sand from its initial dense uniform state into a sand that is even denser, thus creating a well-graded, stronger sand. The specimen is then turned undrained as the shearing phase commences. The pore pressures rise very quickly, and the effective confining pressure drops down to low values. The effect of this effective stress path is to create a specimen with a stronger sand, which near failure is sheared under rather low effective confining pressures. It is therefore understandable that the friction

angles from the undrained tests, initially consolidated to high confining pressures, are measurably larger than the drained friction angles at the same effective mean normal stress at failure. The undrained friction angles appear to be relatively constant, as the initial confining pressure continues to increase. As was previously stated, undrained tests initiated at initial confining pressures below 6.4 MPa were not performed, due to adverse membrane penetration effects.

Figure 5-19 displays the drained and undrained void ratios at failure plotted against effective confining pressure at failure. Also shown is the isotropic consolidation line. The relative amounts of volume change that occur during isotropic consolidation and shearing are shown for the full range of confining pressures. At high confining pressures, the drained tests do not appear to be reaching significantly lower void ratios, even with relatively large increases in stress level, i.e. there appears to be a lower limit of void ratio the sand can reach. Since the undrained tests reach their void ratio at failure at the conclusion of the isotropic consolidation phase, the undrained tests with the highest initial confining pressure test (68.9 MPa) cannot reach the void ratios of the drained test with the highest confining pressure (52.0 MPa).

5.5 Triaxial Extension Tests

As previously discussed in Chapter 3, the triaxial apparatus used for the compression tests was modified to permit performance of tests in extension. The triaxial cell piston was threaded to allow attachment of a specially fabricated fixture, that connects the top cap of the specimen to the piston, so an upward force

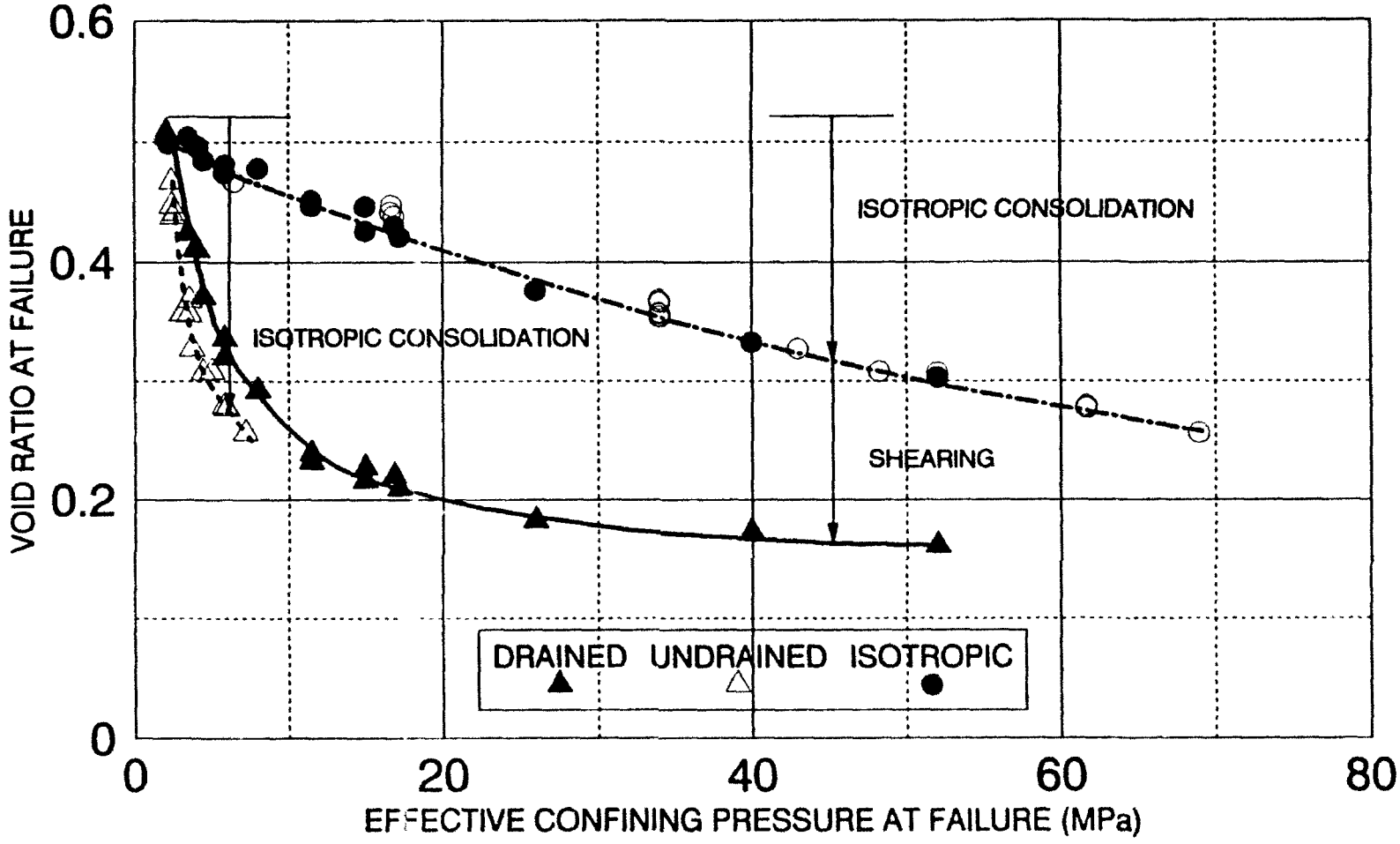

FIGURE 5-19 - VOID RATIO AT FAILURE
DRAINED AND UNDRAINED TRIAXIAL COMPRESSION TESTS
DENSE CAMBRIA SAND

can be applied to the specimen. This fixture and setup are shown on Figures 5-20 and 5-21. The fixture is designed such that there is up to 1.9 centimeters of free downward movement, which allows unrestrained isotropic compression of the specimen, even at high confining pressures. The upward force is generated from the cell pressure acting vertically upward on the bottom area of the piston (7.6 centimeter diameter). Since the area of the piston is larger than the diameter of the specimen, there is sufficient force available to fail the specimen in extension. After isotropic consolidation, the loading frame table is moved downward, which has the effect of moving the piston upward until contact between the extension connector and the cap plug is made. At this point the shearing is started.

A series of both drained and undrained, uniform strain, triaxial extension tests were performed at various initial confining pressures to establish the shapes of the total and effective stress failure envelopes in extension, the location of the instability line in extension, and to ascertain the general soil behavior in triaxial extension. All tests consisted of a drained isotropic consolidation phase followed by shearing under axial strain control accomplished by raising the piston, thus creating a negative vertical deviator stress. The total confining pressure is maintained at a constant value for both drained and undrained tests. Drained tests allow volumetric change to occur and be measured by a volume change device. Undrained tests do not allow volume change to occur due to closure of the drainage valves, and the induced pore pressures are measured on a pressure transducer. Failure for all tests was taken to occur at the maximum effective principal stress ratio. The equations to compute axial strain, volumetric strain,

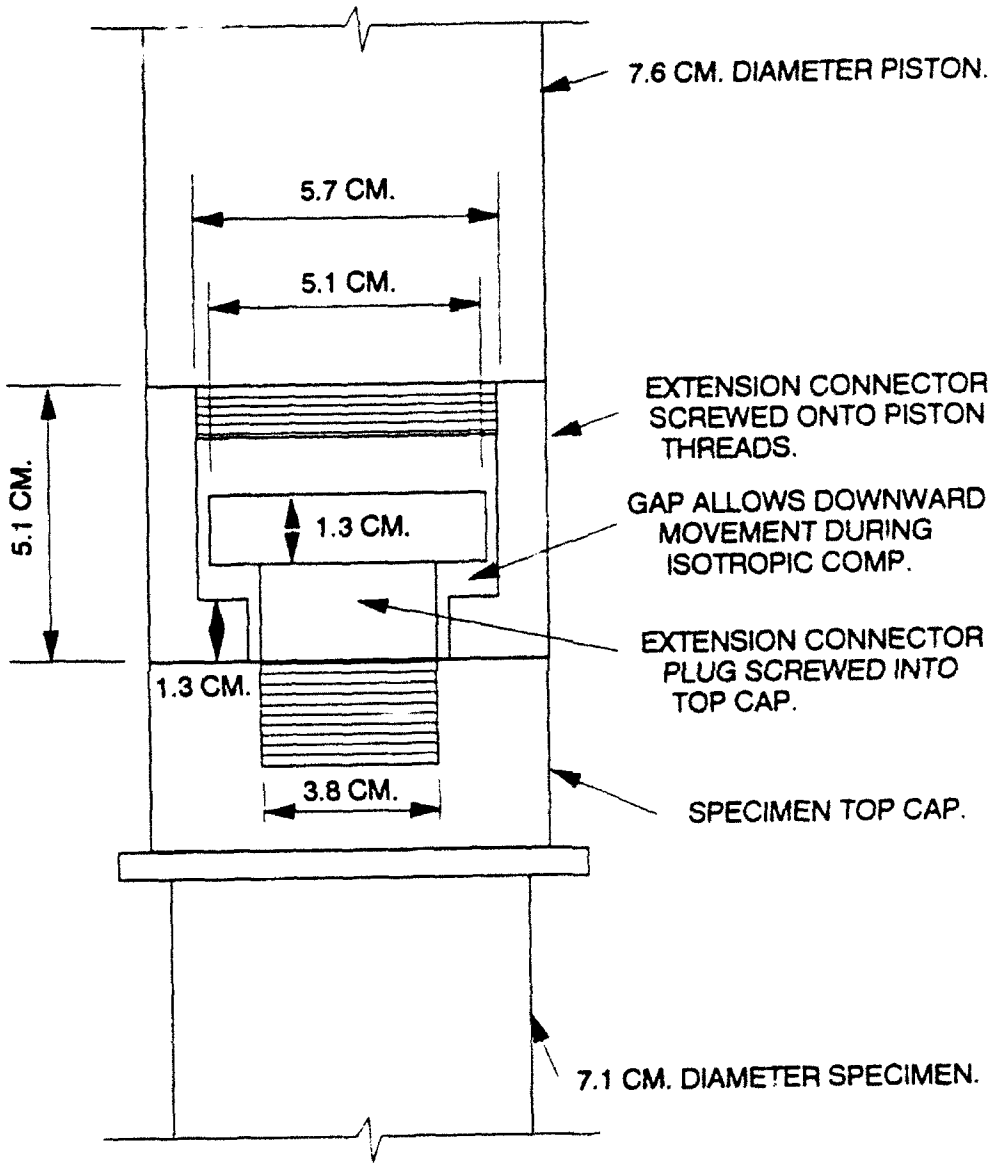

FIGURE 5-20

EXTENSION CONNECTOR

NOT TO SCALE

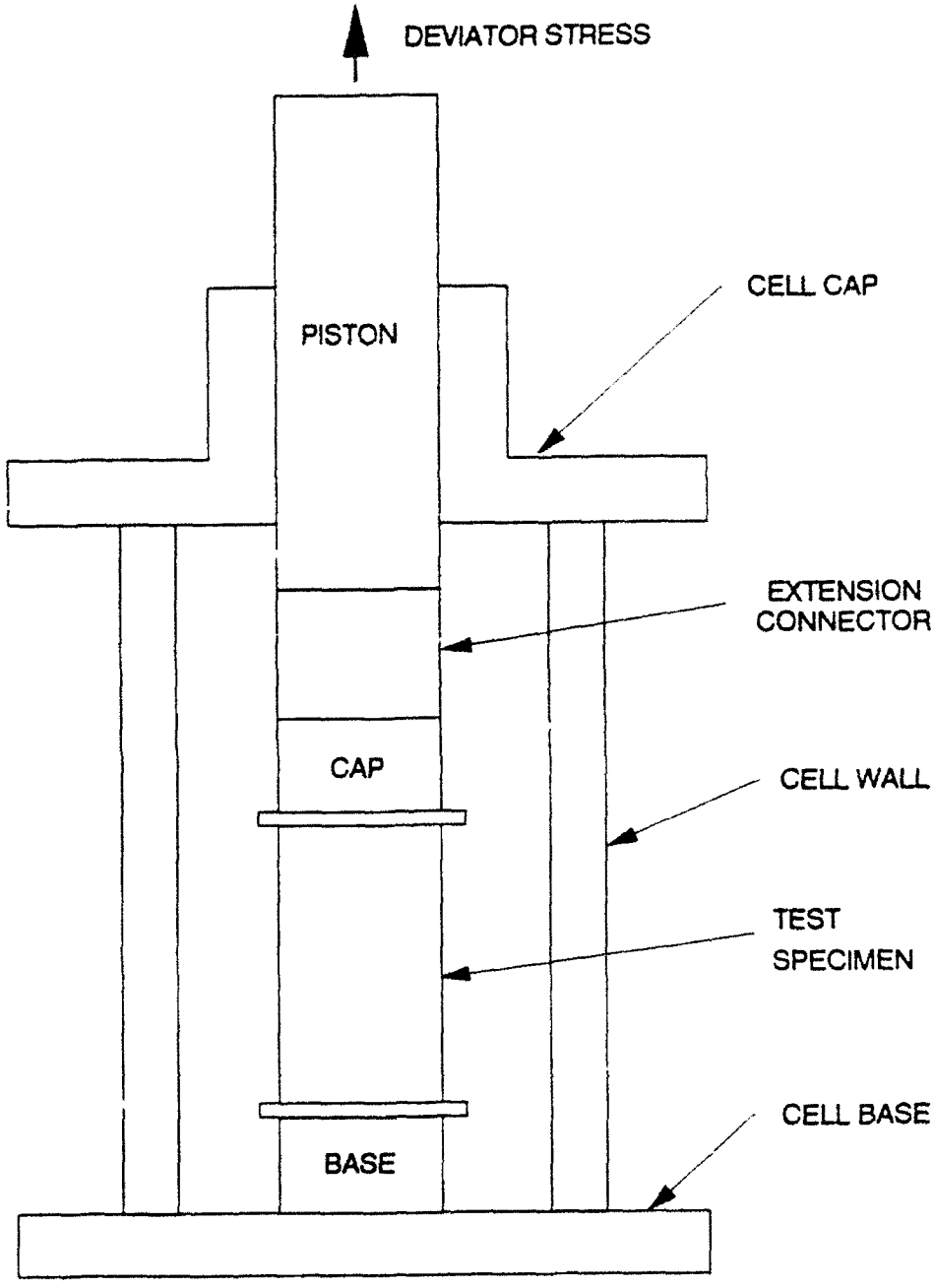

FIGURE 5-21

EXTENSION TEST

NOT TO SCALE

cross-sectional area correction, deviator stress, effective principal stress ratio, effective mean normal stress, and Mohr-Coulomb secant friction angle the for triaxial extension are included in Appendix A.

5.6 Results from Drained Uniform Strain Extension Tests

Tests were conducted using the method developed in Chapter 4 to enforce uniform strains on cylindrical specimens in extension. The tests were performed between 0.25 and 52.0 MPa confining pressure. The stress-strain characteristics are shown on Figures 5-22 and 5-23, in which the effective principal stress ratio is plotted against the major principal strain (ϵ_1), allowing comparisons between the shapes of the stress-strain curves of different confining pressures. The results are similar in nature to the drained triaxial compression tests previously discussed. The initial slope of the stress ratio-strain curve is steepest at low confining pressure. The maximum value of effective stress ratio is greatest at low confining pressures. As the confining pressure increases, the slopes of the stress ratio-strain curves decrease, and the magnitude of the maximum effective principal stress ratio decreases quickly. The maximum effective stress ratio continues to decline with increasing confining pressure until the 14.5 Mpa test is reached. At this confining pressure the effective stress ratio appears to stabilize at a minimum value, and remains constant throughout the rest of the confining pressure range used in the experimental program. There is some inherent scatter in the results of extension tests as discussed in Chapter 4. The constant value of maximum effective stress ratio is different from that obtained from the drained triaxial compression tests.

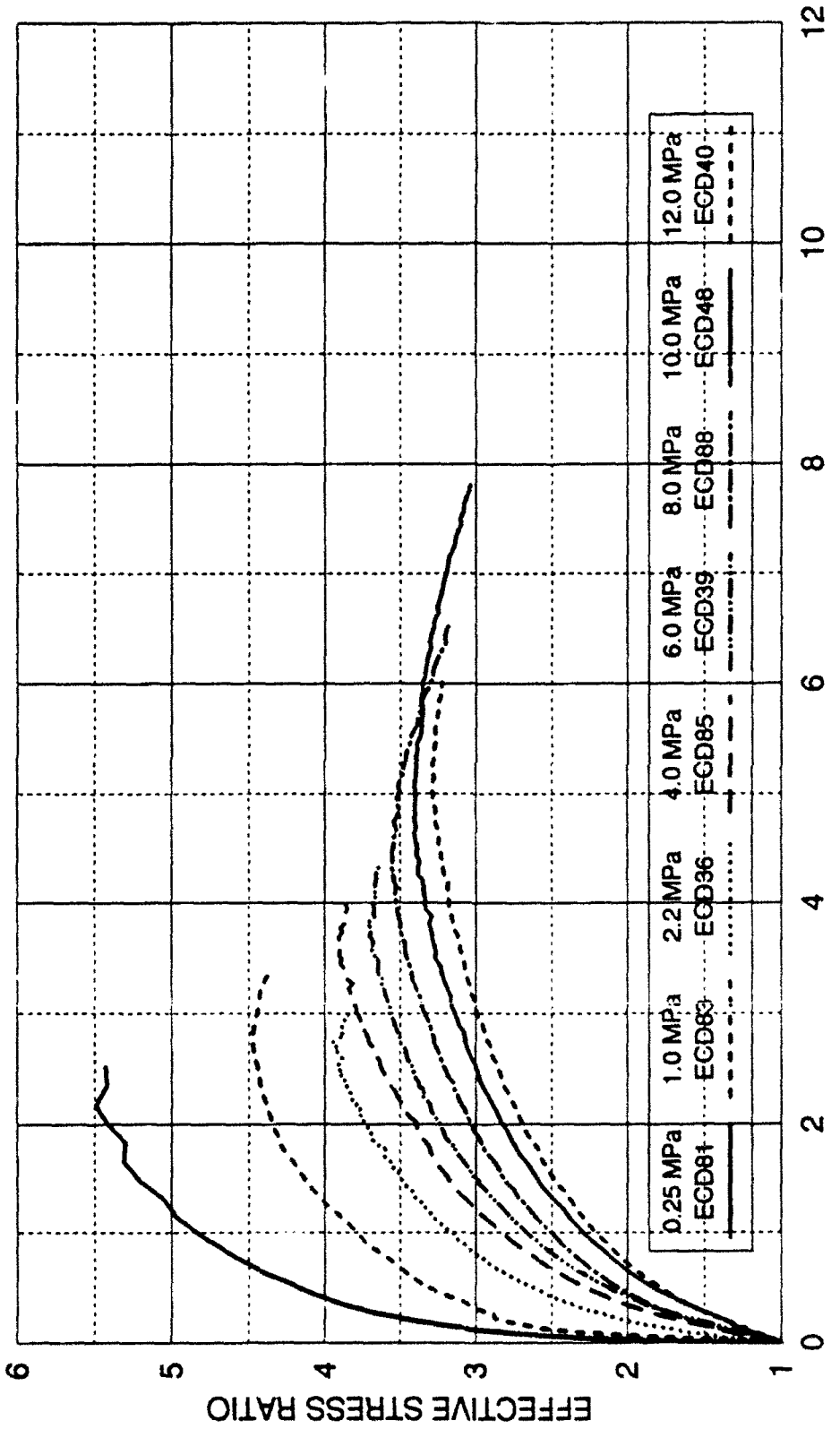

FIGURE 5-22 EFFECTIVE STRESS RATIO 0.25 TO 12.0 MPa
DRAINED TRIAXIAL EXTENSION
DENSE CAMBRIA SAND

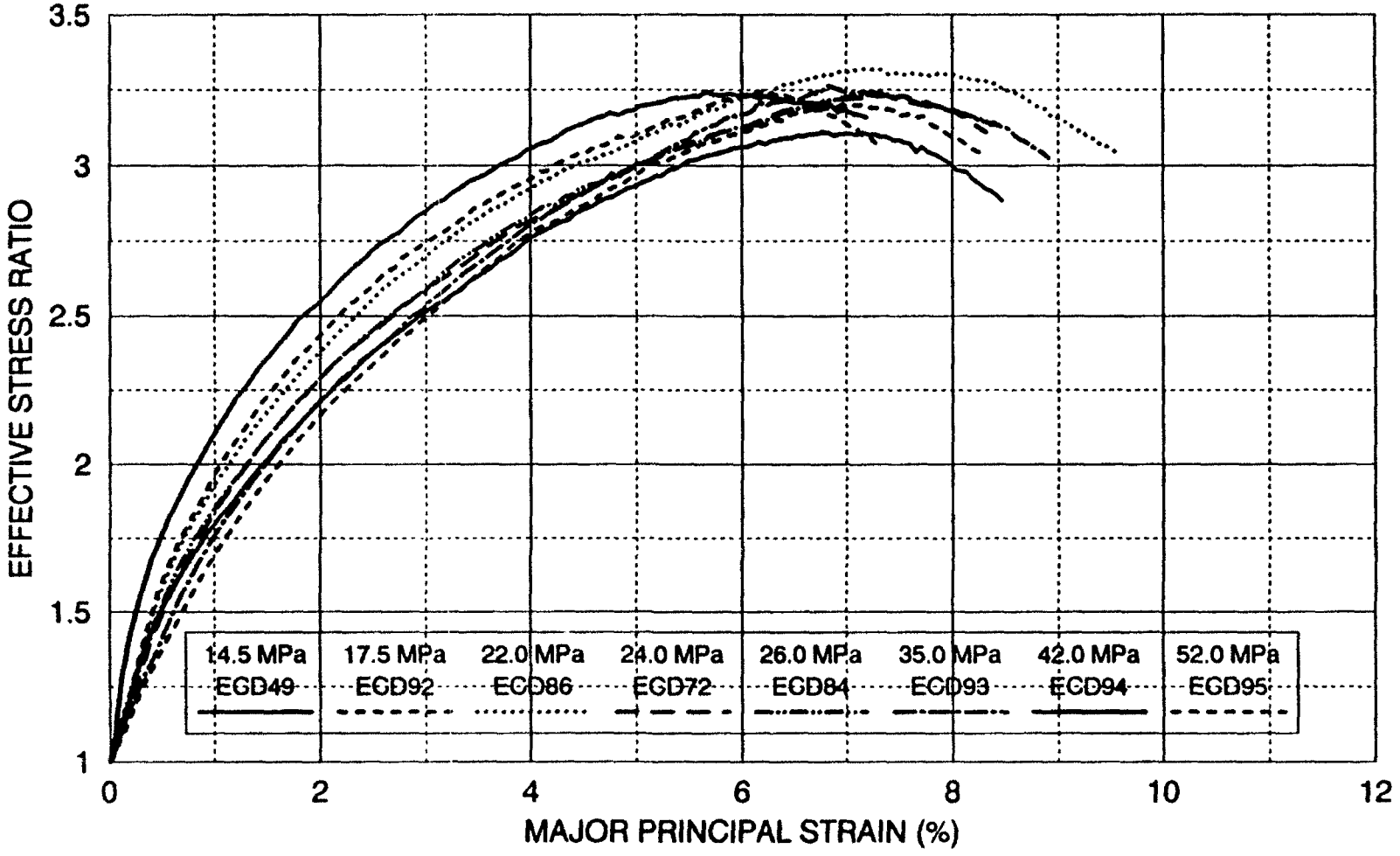

FIGURE 5-23 EFFECTIVE STRESS RATIO 14.5 TO 52.0 MPa
DRAINED TRIAXIAL EXTENSION
DENSE CAMBRIA SAND

In the compression tests the maximum effective stress ratio showed a decrease in magnitude, and this was followed by an increase as the confining pressure continued to increase to yet higher levels.

Deviator stresses are shown on Figures 5-24 and 5-25 plotted against major principal strains. They indicate increasing deviator stresses with increasing confining pressure. The curves are very rounded and smoothly increase up to their maximum value, and then decrease slightly after failure. This is markedly different from the behavior obtained in the conventional extension tests in which there are precipitous strength reductions after strain localization occurs as discussed in Chapter 4. The shapes of extension test curves are also different from the shapes of the compression test curves. The latter displayed curves characterized by three almost linear portions.

The major principal strains to failure are seen to increase with increasing confining pressure. Eventually, they appear to become constant at higher confining pressures.

The volumetric strains are displayed on Figures 5-26 and 5-27. The low pressure tests indicate dilation. As with the triaxial compression tests, the volume changes moves toward compression as the confining pressures increase. For any given confining pressure, the extension tests are more dilatant than the compression tests. The main reason for this is that the total stress path in drained extension with constant cell pressure have decreasing mean normal stresses, as opposed to compression tests in which the mean normal stress increases in tests with constant cell pressure. This tends to increase the volumetric dilatant

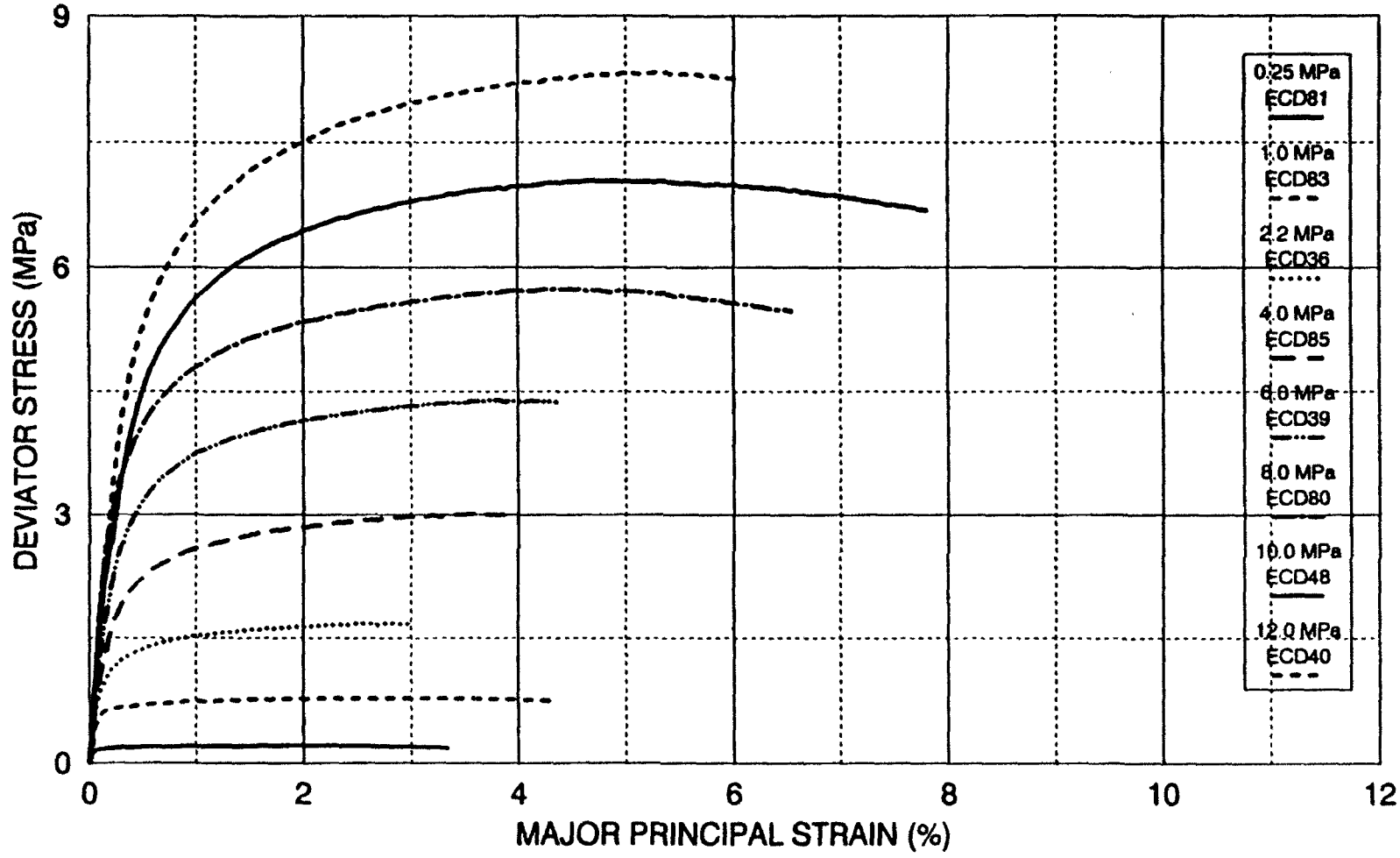

FIGURE 5-24 DEVIATOR STRESS 0.25 TO 12.0 MPa
DRAINED TRIAXIAL EXTENSION
DENSE CAMBRIA SAND

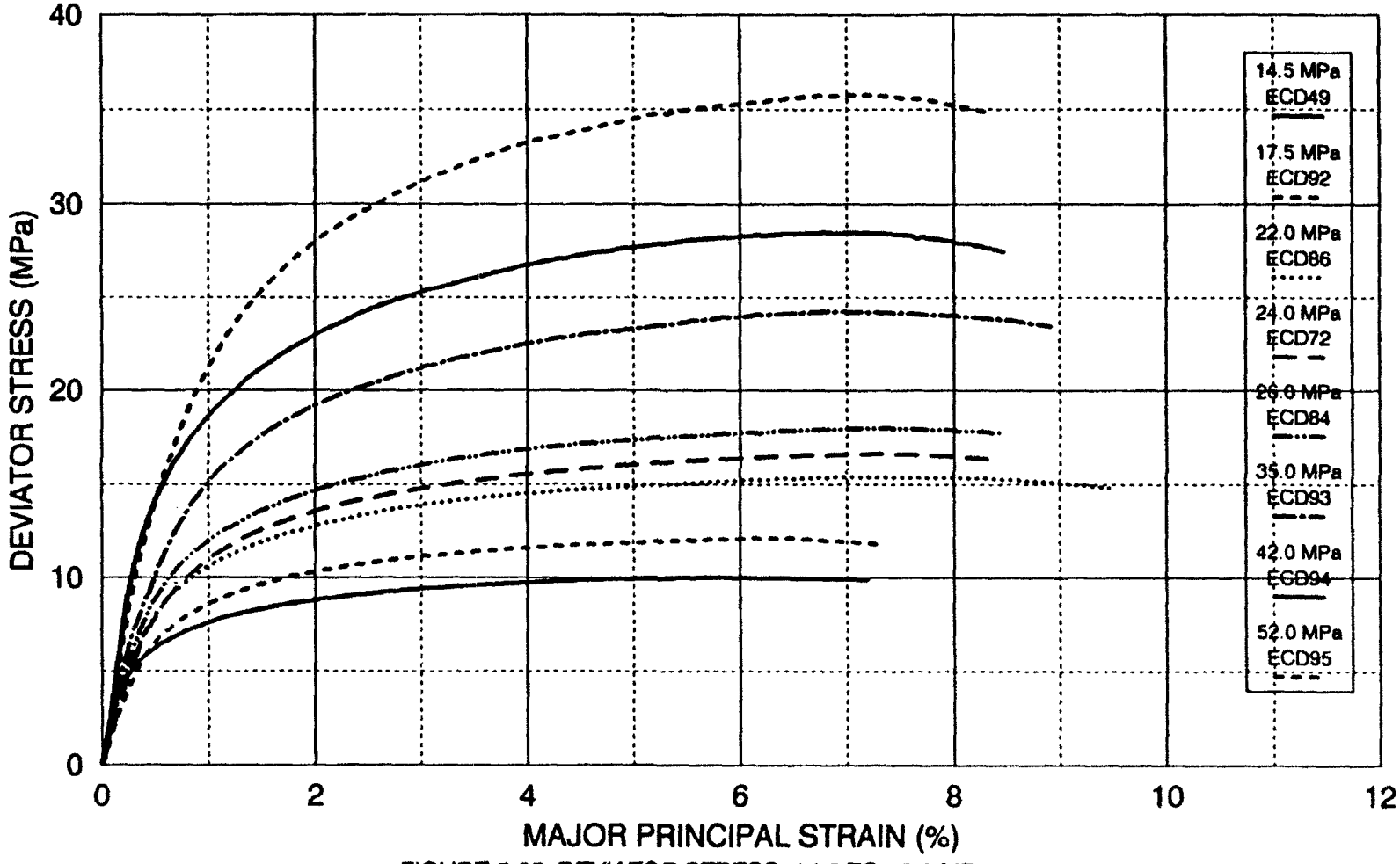

FIGURE 5-25 DEVIATOR STRESS 14.5 TO 52.0 MPa
DRAINED TRIAXIAL EXTENSION
DENSE CAMBRIA SAND

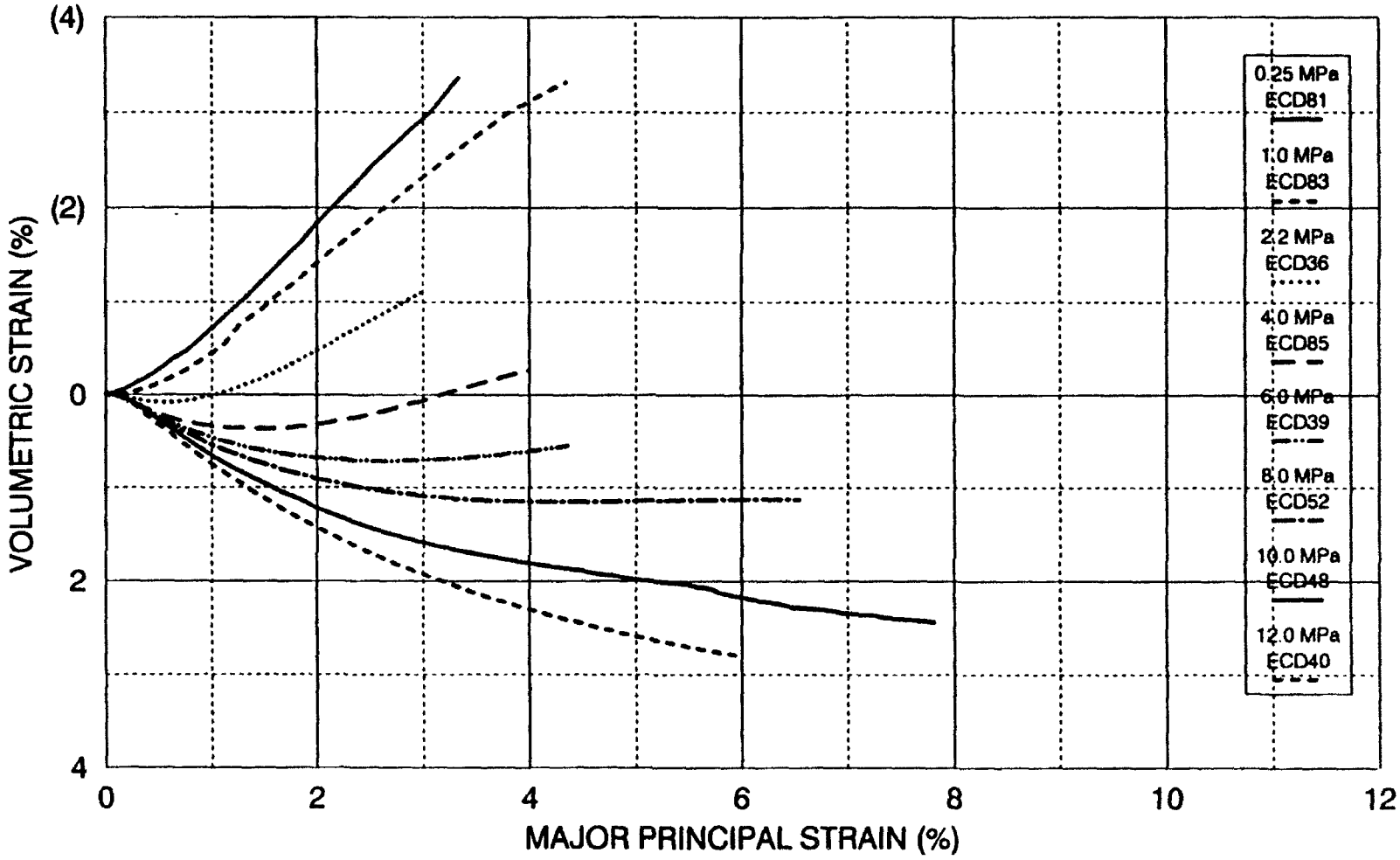

FIGURE 5-26 VOLUMETRIC STRAIN 0.25 TO 12.0 MPa
DRAINED TRIAXIAL EXTENSION
DENSE CAMBRIA SAND

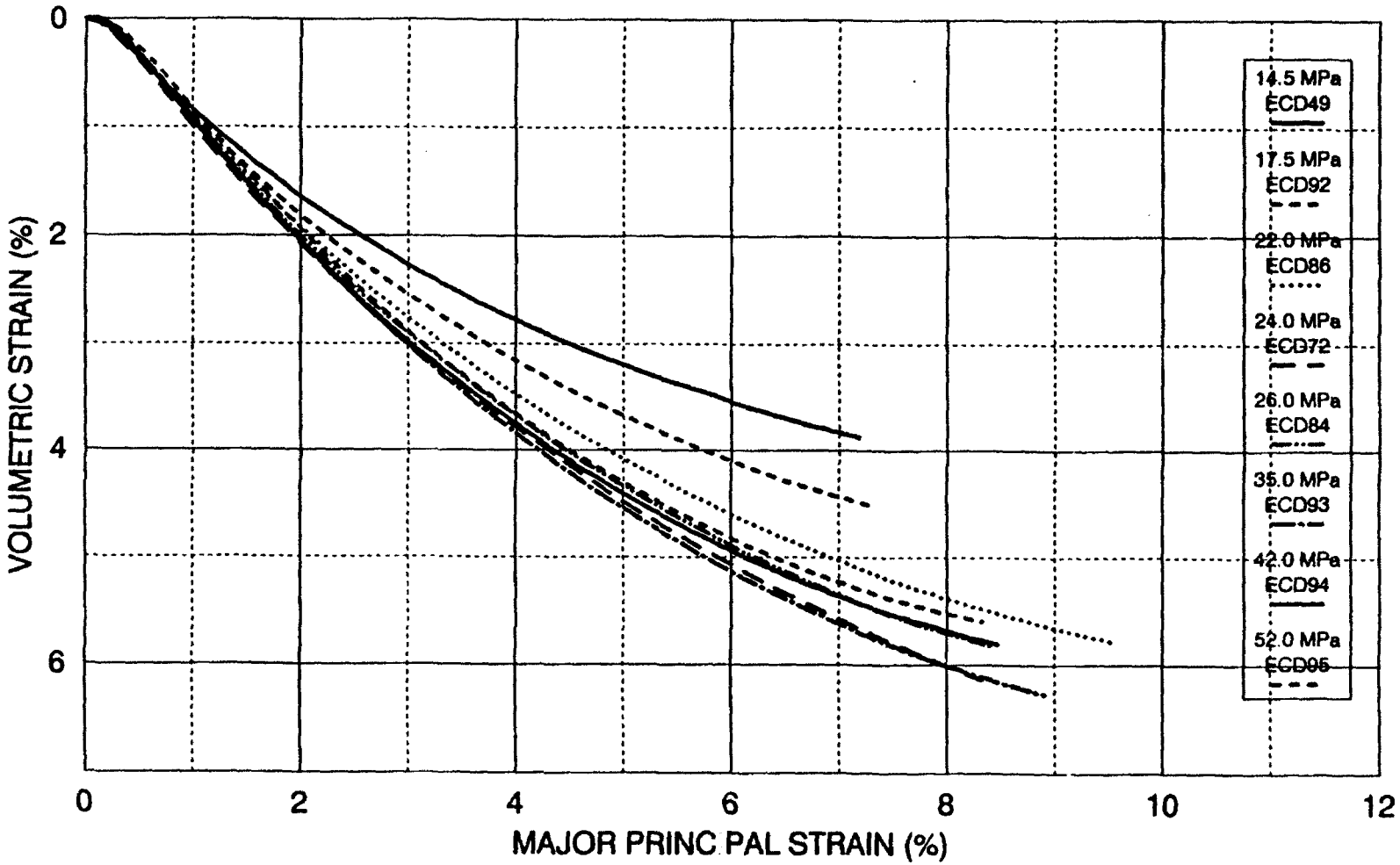

FIGURE 5-27 VOLUMETRIC STRAINS 14.5 TO 52.0 MPa
DRAINED TRIAXIAL EXTENSION
DENSE CAMBRIA SAND

tendency in extension. As the confining pressure continues to increase, the volumetric strains continue to become more compressive. At high confining pressures the volumetric strains at failure tend to become constant before they decrease slightly at yet higher confining pressures. A similar pattern was also observed in triaxial compression tests.

The higher confining pressure extension tests exhibit slightly buffered volumetric strain response at the onset of shearing. This was explained for the triaxial compression tests as being caused by volumetric creep occurring between the isotropic consolidation phase and the initiation of shearing.

5.7 Results from Undrained Uniform Strain Extension Tests

A series of undrained uniform strain triaxial extension tests was performed with the purpose of determining the effective stress failure envelope, and the location of the instability line in extension. The tests were performed with initial confining pressures between 12.0 and 52.0 MPa. Uniform strains were enforced using the method described in Chapter 4. The effective principal stress ratios are plotted against major principal strain (ϵ_1) in Figure 5-28. As with the drained extension and compression tests, the initial slopes on the effective stress ratio curves decrease with increasing confining pressure. The maximum effective stress ratios tended to be relatively constant throughout the confining pressure range tested, which is similar to results from the undrained triaxial compression tests. This is quite different from the undrained extension tests with strain localization, which exhibited considerable scatter. The major principal strain to failure was

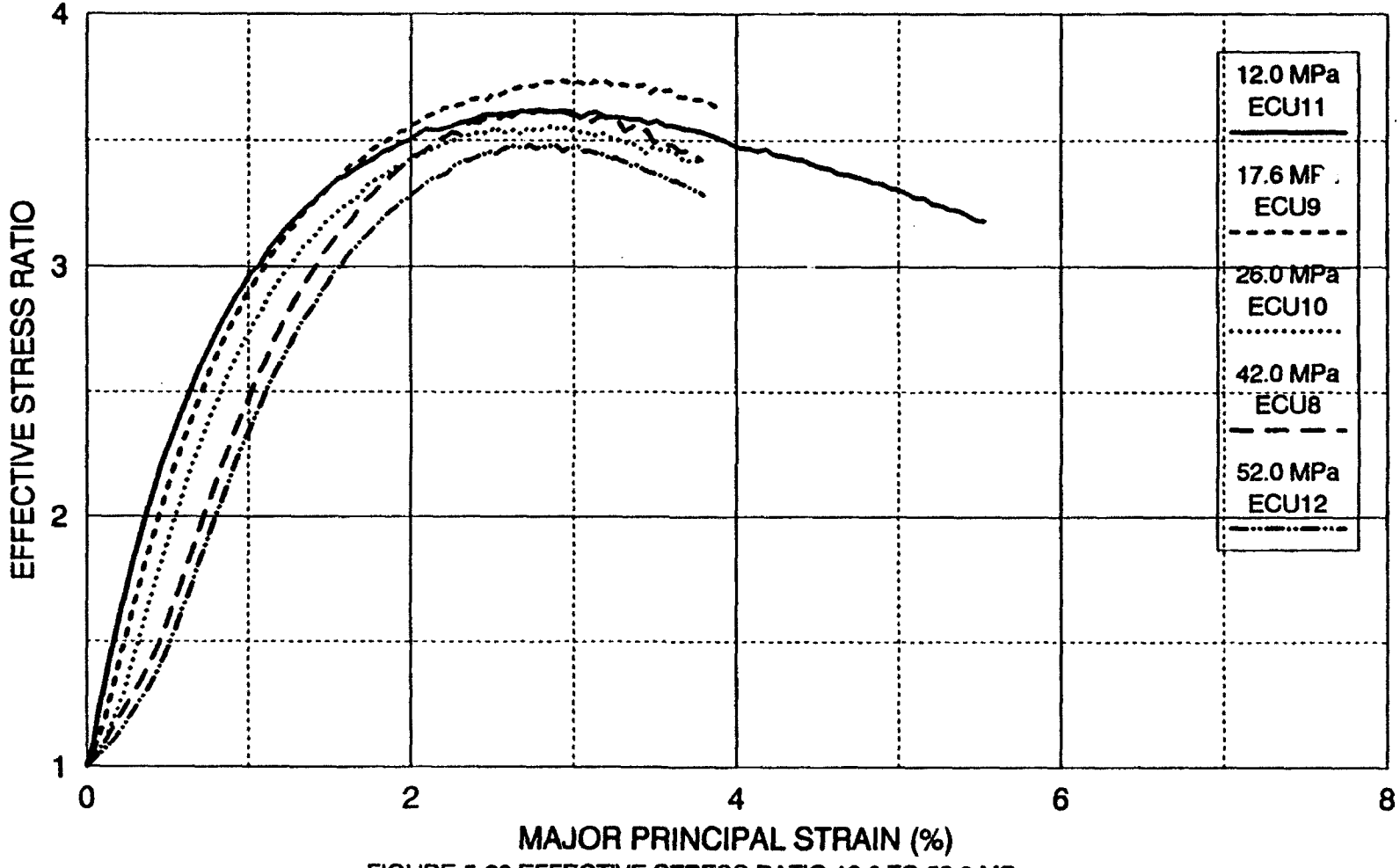

FIGURE 5-28 EFFECTIVE STRESS RATIO 12.0 TO 52.0 MPa
UNDRAINED TRIAXIAL EXTENSION
DENSE CAMBRIA SAND

essentially the same for all tests. This pattern is also similar to that observed in the undrained compression tests, in which there were only relatively small changes in strain to failure when compared to the drained tests. The deviator stresses are shown on Figure 5-29. They show consistent behavior with increasing maximum deviator stresses with increasing confining pressure. The 12.0 MPa test exhibits first compressive, and then dilatant volumetric tendencies, as shown by the deviator stress and the pore pressure variation as indicated on Figure 5-30. The pore pressure initially increases and then later decreases, which causes the deviator stress to initially decrease, and then later increase. Beyond this behavior at low consolidation pressure, the maximum deviator stresses occur at low strain values, which consistently, but gradually increases as the initial confining pressure increases. The higher confining pressure tests show declining deviator stresses after failure, but in a slightly different pattern than observed in undrained compression. After the maximum deviator stress is achieved in extension, it declines initially with a more gradual slope. Another difference is that, after failure at the maximum effective stress ratio shown in Figure 5-28, the deviator stress declines more steeply than in undrained compression. These differences can be explained by the pore pressure behavior. At high consolidation pressures in extension, the pore pressures do not develop quite as rapidly as in compression, most likely due to less particle crushing at the onset of shearing. The pore pressure behavior is related to the different total stress path in extension, which has declining values of mean normal stress. This results in the more gentle decline from the maximum deviator stress. The second difference indicating a more rapid

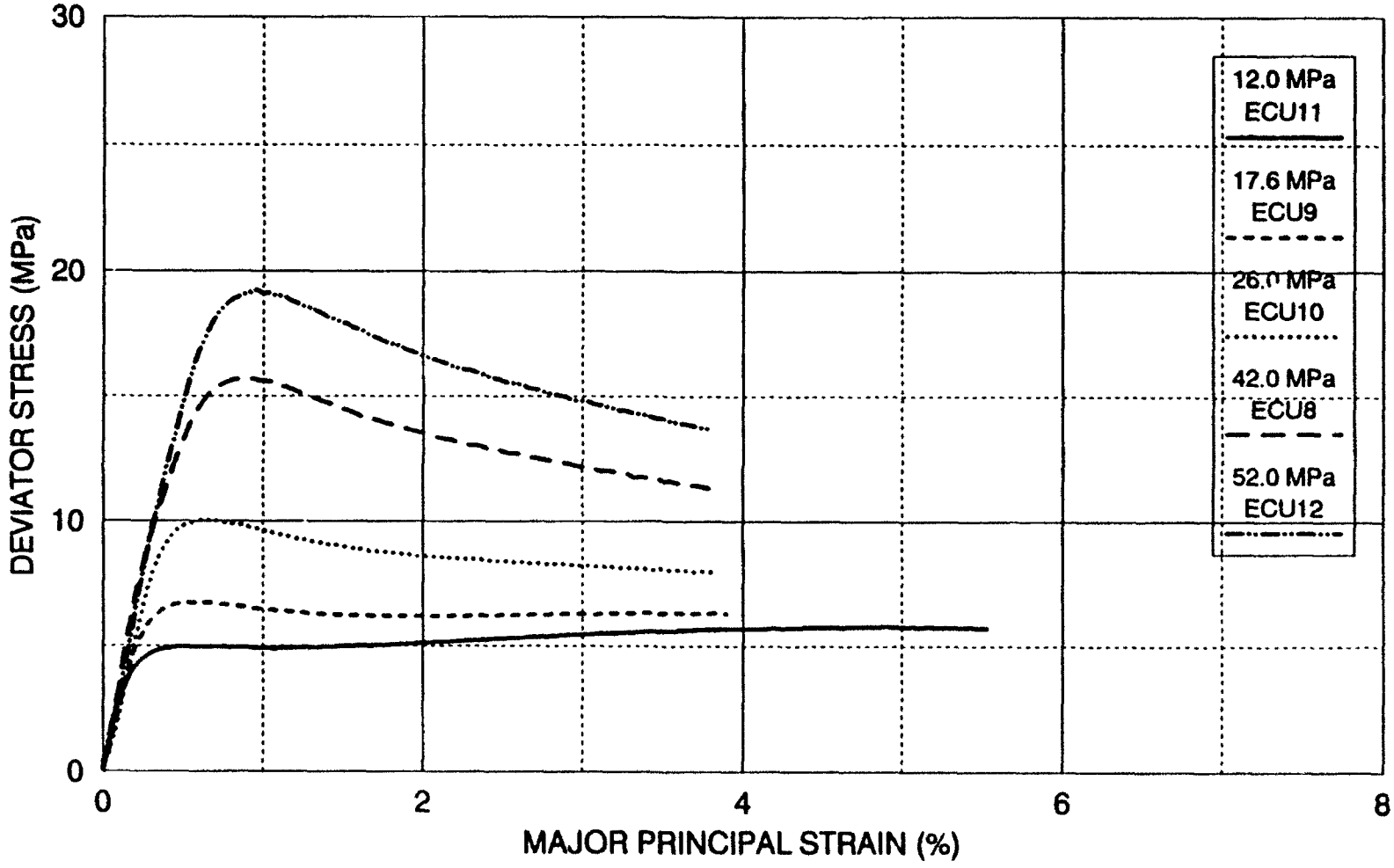

FIGURE 5-29 DEVIATOR STRESS 12.0 TO 52.0 MPa
UNDRAINED TRIAXIAL EXTENSION
DENSE CAMBRIA SAND

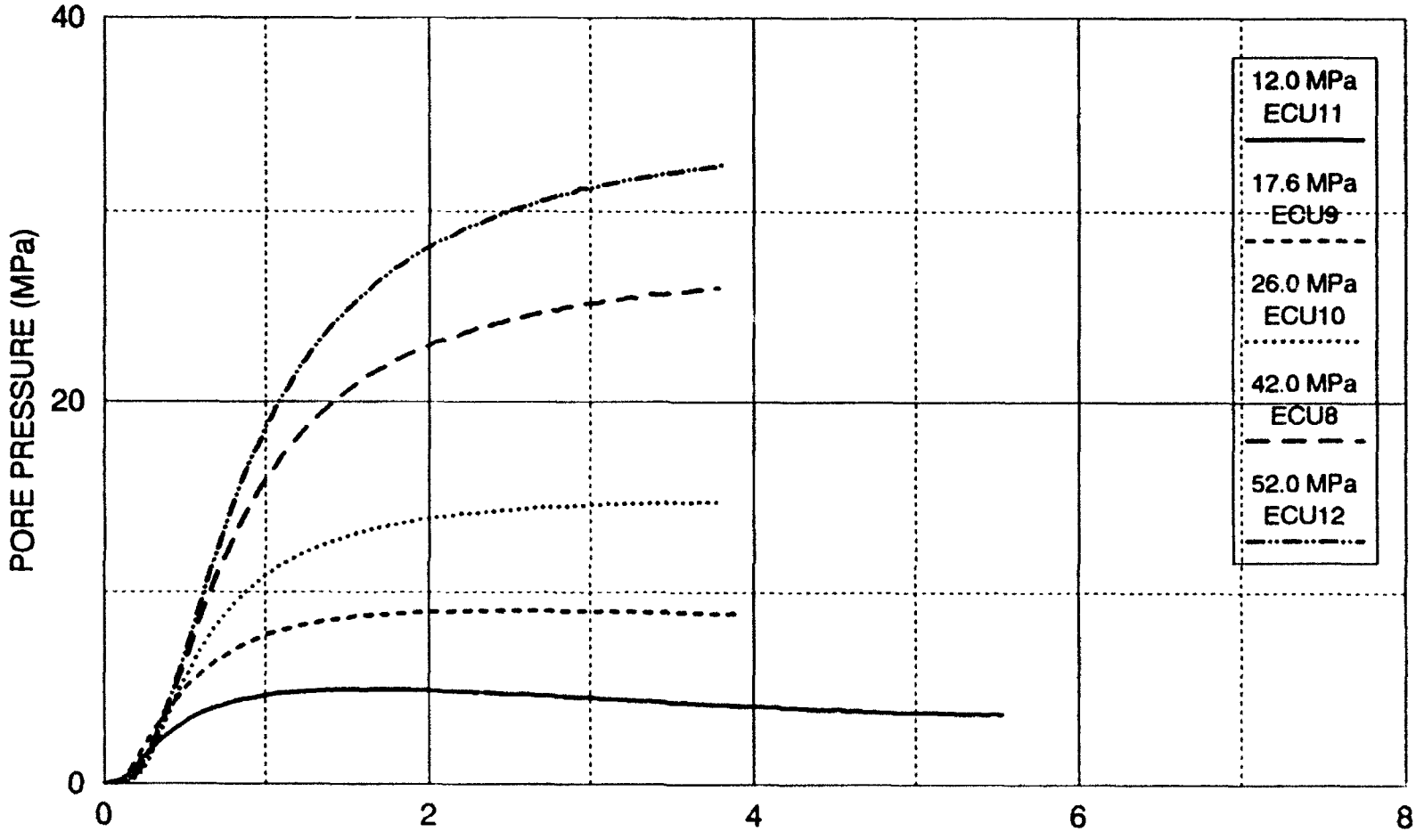

FIGURE 5-30 PORE PRESSURE 12.0 TO 52.0 MPa
UNDRAINED TRIAXIAL EXTENSION
DENSE CAMBRIA SAND

after failure is again related to the pore pressure pattern. The pore pressures continue to rise more rapidly in extension after failure, resulting in a rapid decline in deviator stress. This depresses the effective stress ratio after failure more quickly than in compression. This again is related to the fact that overall particle crushing in extension is less. It has not ceased but continues after failure. As was discussed for undrained compression, the initial pore pressure response is slightly buffered due to volumetric creep occurring between isotropic consolidation and initiation of shearing.

The effective stress paths on the Cambridge p'-q diagram are shown on Figure 5-31. This diagram displays the stress difference on the vertical axis and the effective mean normal stress on the horizontal axis. The effective stress paths show similar patterns as obtained from the undrained tests with strain localization described in Chapter 4. However, the maximum deviator stresses are slightly larger, which moves the instability line up, and the effective stress failure line is also steeper, indicating a higher effective stress friction angle. The effect of the slower rising pore pressures is seen on the effective stress paths with the slowly declining deviator stresses after the maximum has been reached. This tends to create a very flat top on the effective stress path in extension at high pressures.

5.8 Comparisons Between Extension and Compression Tests

The major principal strains to failure (ϵ_1) for drained and undrained, uniform strain, triaxial extension tests are shown on Figure 5-32, plotted against effective mean normal stress at failure. Results from drained and undrained

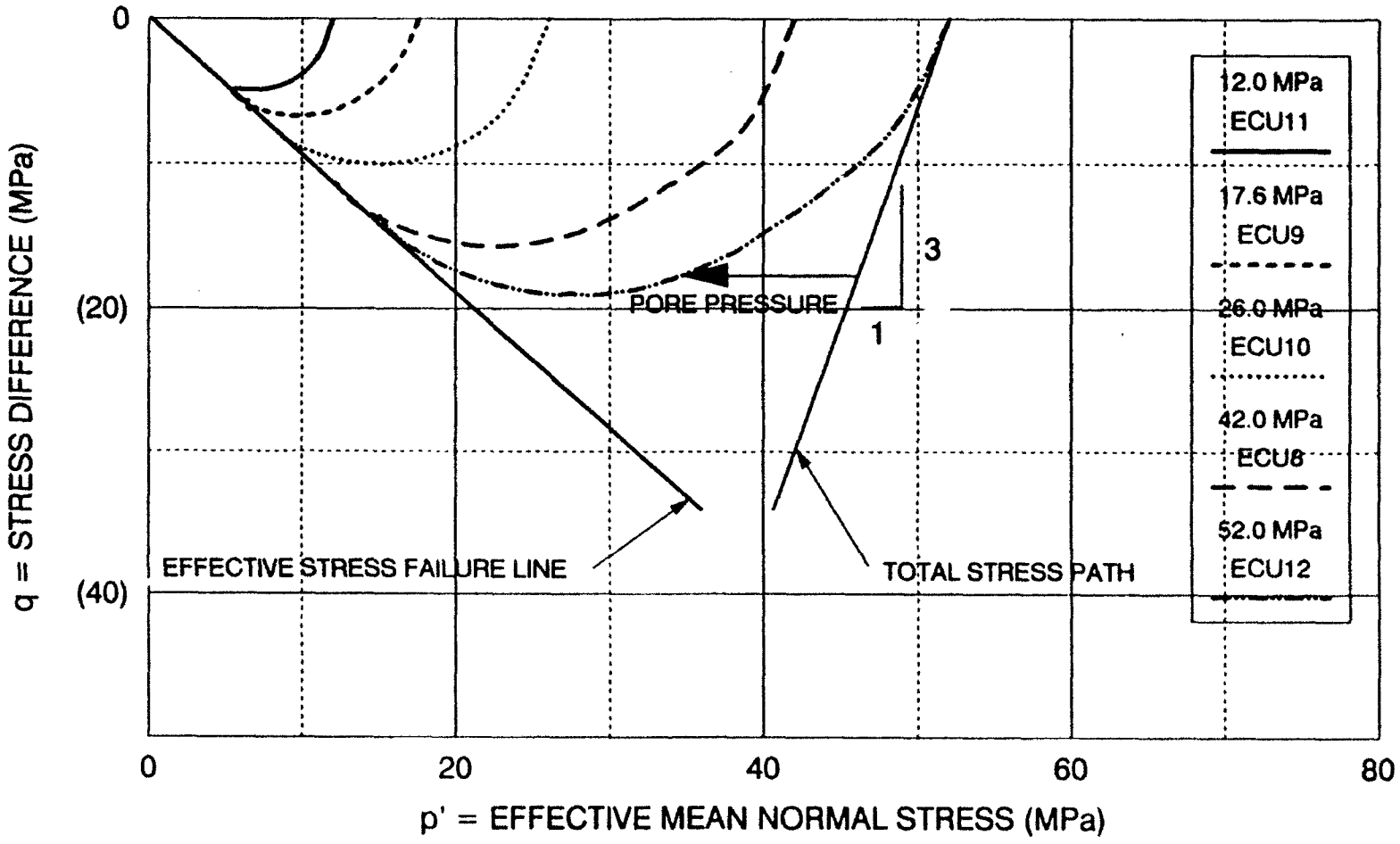

FIGURE 5-31 EFFECTIVE STRESS PATHS, CAMBRIDGE p-'q
UNDRAINED TRIAXIAL EXTENSION 12.0 TO 52.0 MPa
DENSE CAMBRIA SAND

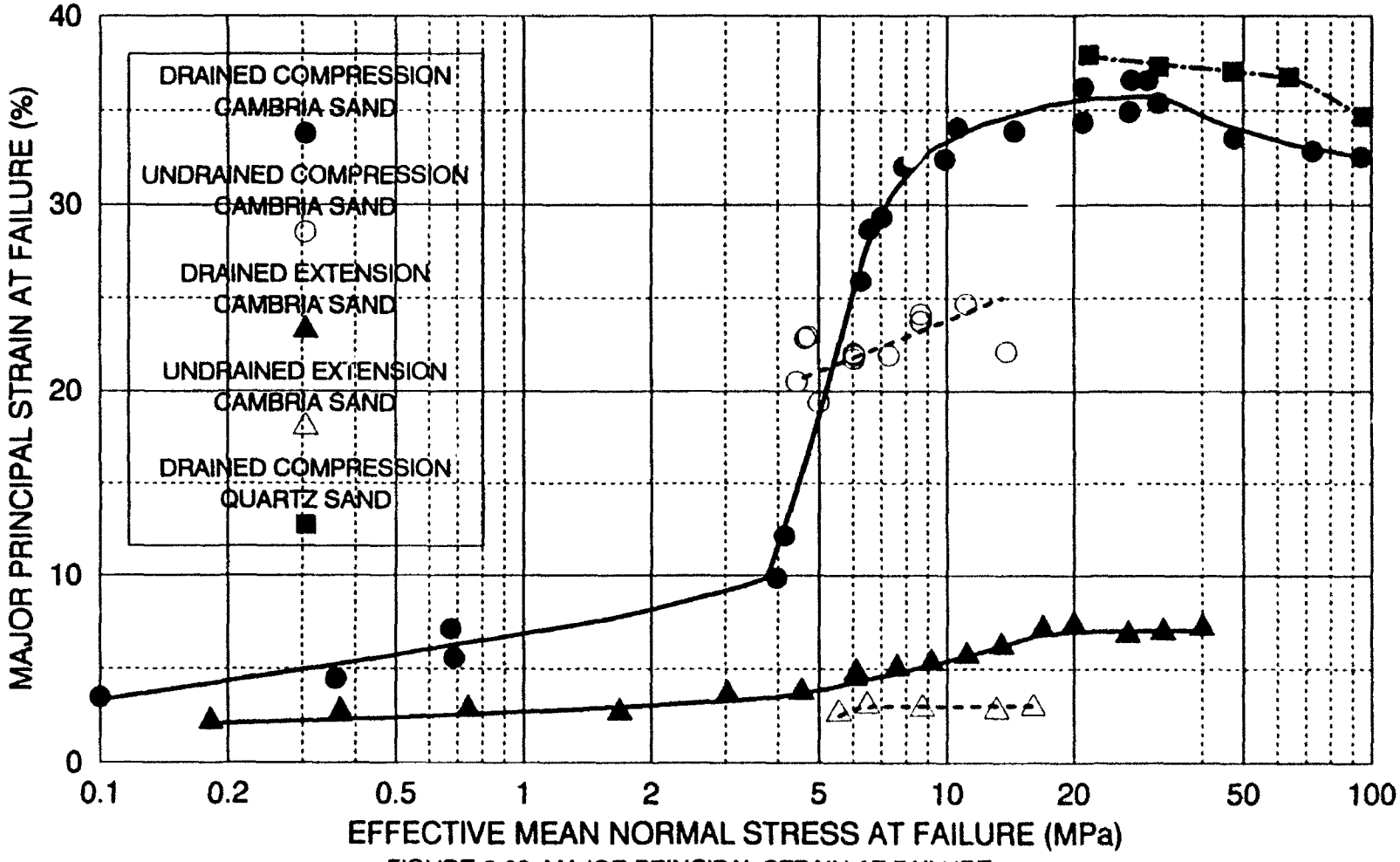

FIGURE 5-32 MAJOR PRINCIPAL STRAIN AT FAILURE
DRAINED & UNDRAINED COMPRESSION & EXTENSION
DENSE CAMBRIA SAND AND DENSE QUARTZ SAND

triaxial compression tests are also displayed on the diagram for comparison. Drained extension tests at low stresses result in strains to failure that are small and gradually increase with increasing confining pressure. At stresses between 20 and 40 MPa the strains to failure stabilize at a relatively constant value. This is also the same general stress level in compression, where the maximum strain to failure occurred. The strains to failure in compression are always consistently higher than extension in both drained and undrained tests. The difference between compression and extension is relatively small at low stress magnitudes, but increases with increasing stress magnitude. The compression curve has a major break in slope at around 4 MPa, from which the strains to failure increase dramatically with further increases in stress magnitude. This was previously noted as the stress magnitude where the volumetric strain at failure changes from dilatant to compressive behavior (See Figure 5-16). Careful examination of the extension line in Figure 5-32 indicates that its slope increases slightly at 4 MPa, but not nearly as much as in the compression tests. This stress magnitude corresponds to a sudden rapid increase in particle breakage as shown on Figure 5-33. This diagram exhibits Hardin's relative crushing parameter (Hardin, 1985) plotted against the effective mean normal stress at failure. The crushing curve for compression rapidly increases in slope, and deviates from the extension line at the 4 MPa stress level. Particle crushing will be examined closely in Chapter 8.

The strains to failure in undrained extension may increase slightly from a low stress magnitude, but then remain relatively constant. This is somewhat the same behavior as in undrained compression, where the strains to failure increase

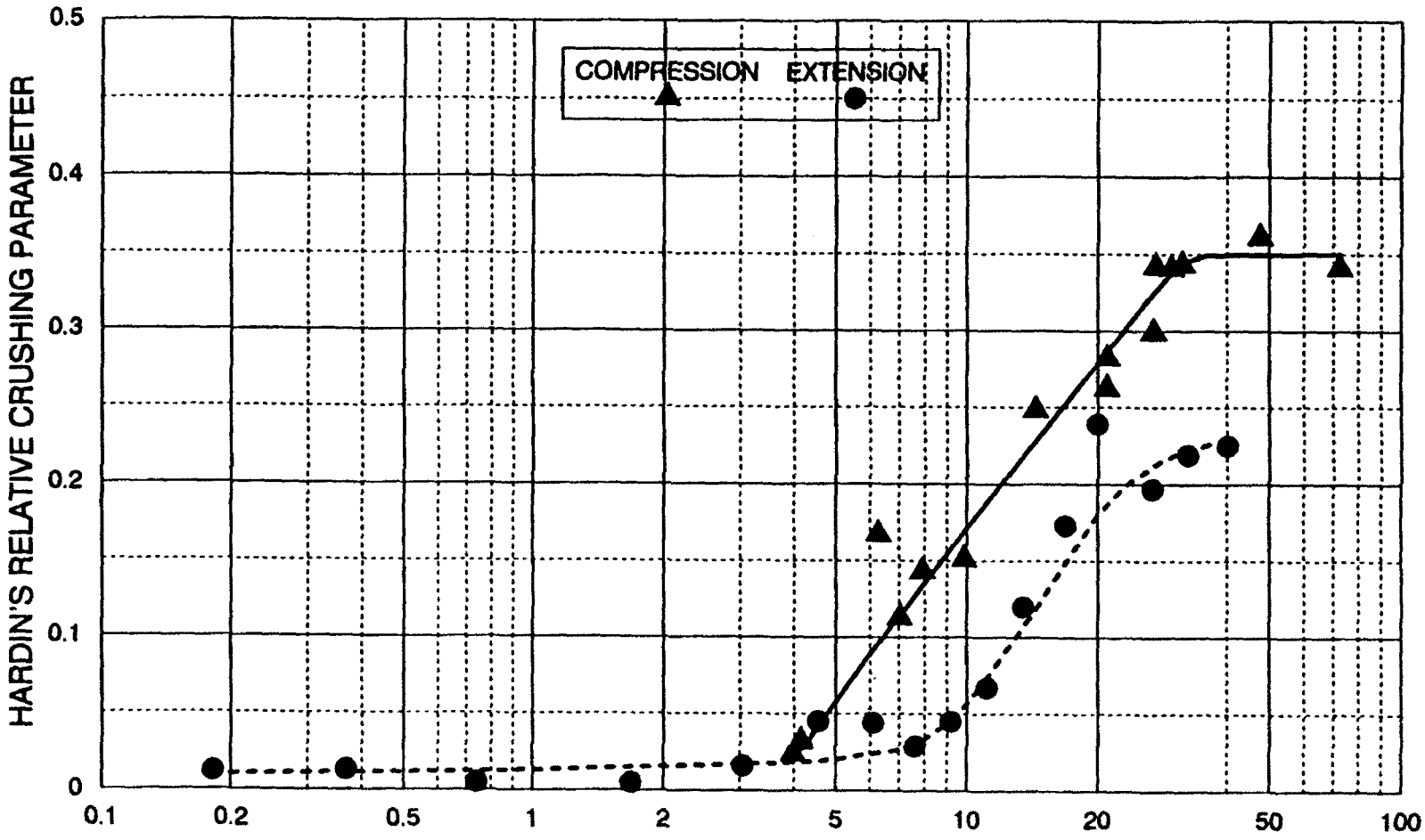

FIGURE 5-33 HARDIN'S RELATIVE CRUSHING
DRAINED TRIAXIAL COMPRESSION AND EXTENSION
DENSE CAMBRIA SAND

only slightly compared with the drained strains to failure.

Volumetric strains at failure for the drained, uniform strain, extension tests are plotted against effective mean normal stress at failure in Figure 5-34. Results from drained compression tests are also shown on the diagram for comparison. At low stress magnitudes the extension and compression volumetric strains at failure are essentially on a single line. The volumetric strains gradually increase with increasing stresses until around 4 MPa, where the compression tests separate from the extension tests and show more rapidly increasing volumetric strains at failure, as compared to the extension tests. This also is the stress magnitude from which the axial strains at failure increase rapidly in drained compression tests, whereas they increase more modestly in drained extension tests. As with axial strains to failure, this behavior can be related to directly to the rapidly increasing amount of particle breakage and rearranging that starts at this stress magnitude. It was also noted earlier that this stress magnitude corresponds to zero volumetric strain at failure. Beyond this stress level the volumetric strains at failure increase for both compression and extension until the 20 to 30 MPa mean normal stress magnitude is reached, where a maximum is reached for both compression and extension. At higher stress magnitudes the compressive volumetric strain decreases, but the extension volumetric strains seem to be relatively constant, possibly reducing slightly. Extrapolation of the volumetric strain at failure curves for extension and compression to much higher stress magnitudes appears to indicate that both the compression and extension curves might eventually join together and approach zero.

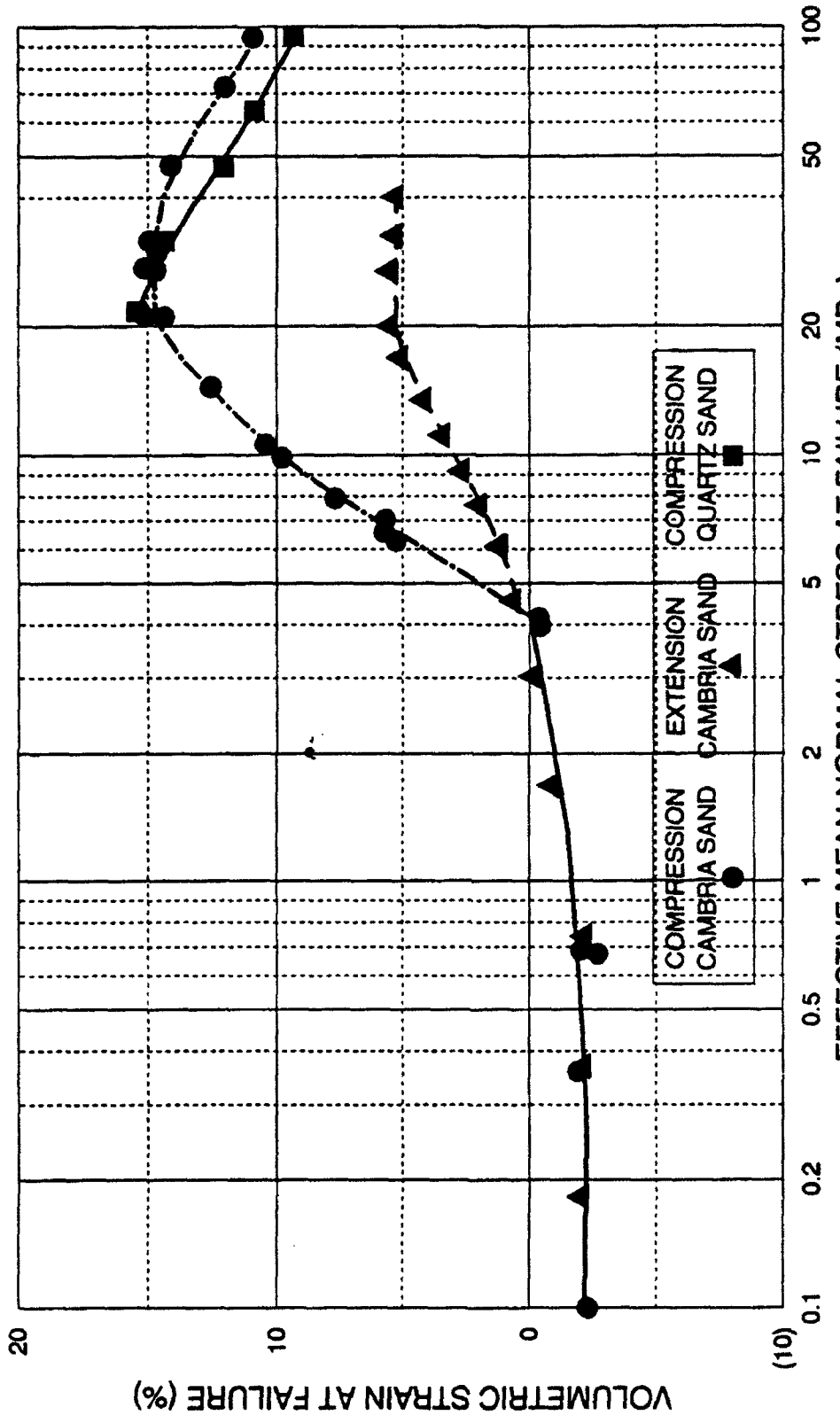

FIGURE 5-34 VOLUMETRIC STRAIN AT FAILURE
DRAINED COMPRESSION AND EXTENSION
DENSE CAMBRIA SAND AND DENSE QUARTZ SAND

The rates of dilation at failure for drained tests in extension are shown on Figure 5-35, plotted against effective mean normal stress at failure. The compression test results are also plotted for comparison purposes. The rate of dilation at failure is defined as the slope of the volumetric strain-principal strain (ϵ_1) curve at failure. Negative values indicate dilatant behavior and positive values indicate compressive behavior. At low stress magnitudes the rates of dilation in extension are significantly lower (more dilatant or more negative) than in compression. As the mean normal stress at failure increases, the rate of dilation increases (more positive indicating more volumetrically contractive behavior) as also was found in compression. The compression tests reach a maximum rate of dilation around 8 MPa, but the rate of dilation in extension continues to increase to higher values, and reaches a maximum value somewhere between 20 and 40 MPa. The extension and compression curves cross each other between 8 and 10 MPa. At the highest stress magnitude test in extension the results indicate that the rate of dilation is beginning to decrease slightly (more dilatant). This is similar to the behavior in compression. The extension rate of dilation curve appears to linger near its maximum value for a much larger span of stresses than in compression. This may be due to the smaller amount of total particle breakage and rearranging in extension than observed in compression, as shown on Figure 5-33. By the time failure occurs for the high confining pressure compression tests, the Cambria sand is densified to a maximum level, whereas in extension the sand particles are still undergoing some particle crushing. This is evidenced by the decreasing rates of dilation at failure (more dilatant). Explanations accounting for less particle

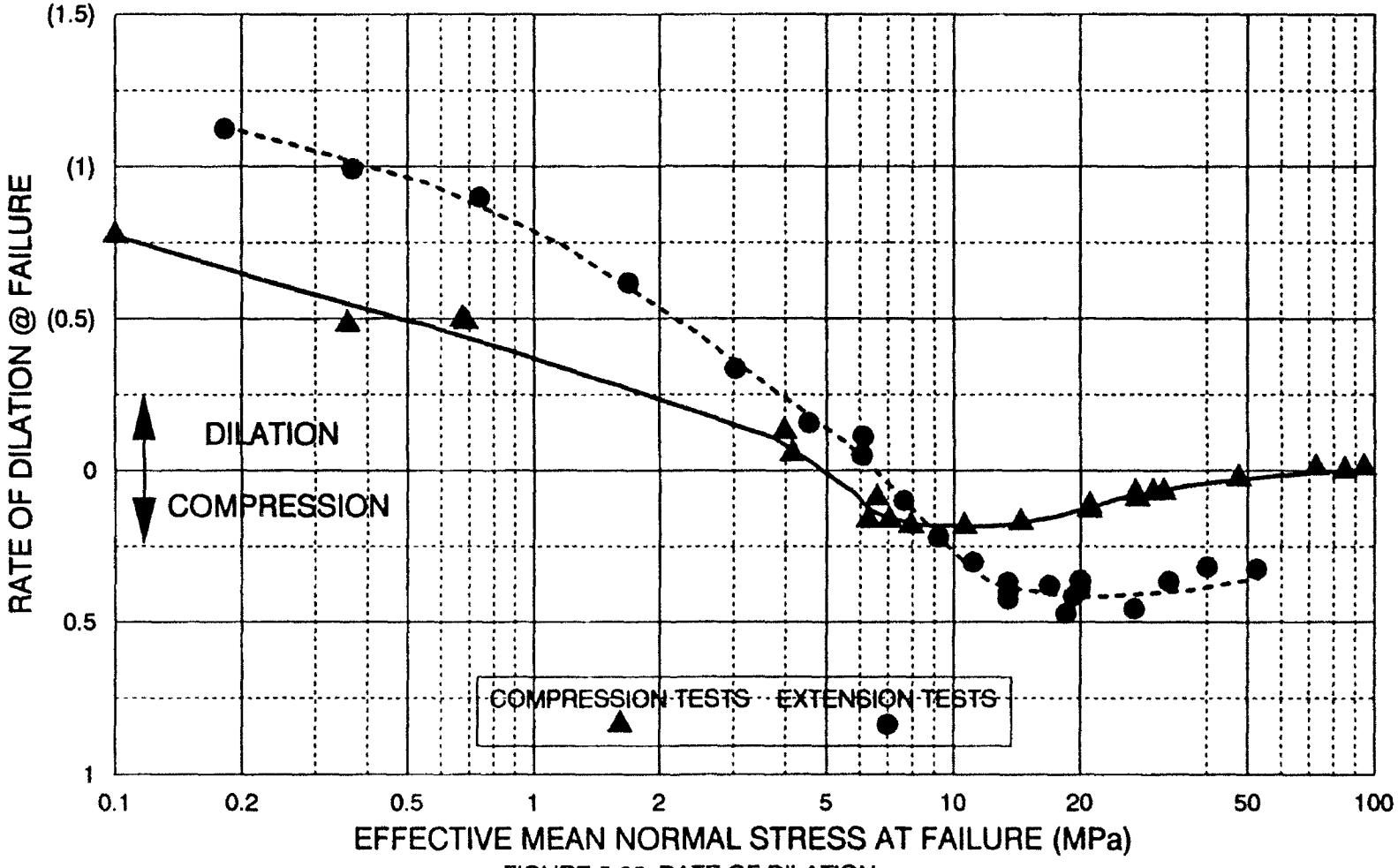

FIGURE 5-35 RATE OF DILATION
DRAINED TRIAXIAL COMPRESSION AND EXTENSION
DENSE CAMBRIA SAND

crushing in extension are attributed to the effects of different total stress paths resulting in a decreasing mean normal stress in extension as the shearing progresses. Another identified explanation is that the principal strains to failure are much smaller in extension. Particle breakage will be discussed in much greater detail in Chapter 8.

The Mohr-Coulomb secant friction angles in both drained extension and drained compression are plotted against the effective mean normal stress at failure in Figure 5-36. This figure is strikingly similar to the rate of dilation at failure diagram (Figure 5-35) in both shape and trends. This suggests a direct correlation between the friction angle and the volume change characteristics of the material over the entire pressure range. At low stress magnitudes the extension friction angles are higher than in compression. As the mean normal stress at failure increases, the two curves converge and eventually cross each other at around 9 MPa. This is the same stress magnitude where the two curves crossed on the rate of dilation diagram. At and above this stress magnitude, the friction angle in compression is higher than in extension, due to the more intense and increasing densification from particle breakage and rearranging occurring in compression. In extension the material is still crushing during shearing, and it has not approached a zero rate of dilation at failure. In compression the zero rate of dilation at failure was associated with the maximum densification possible for a particular high stress state. This compressibility limit is indicated by post-failure (decreasing mean normal stress) dilation, while at lower confining pressures the specimen will continue to volumetrically compress beyond failure. The zero rate of dilation at

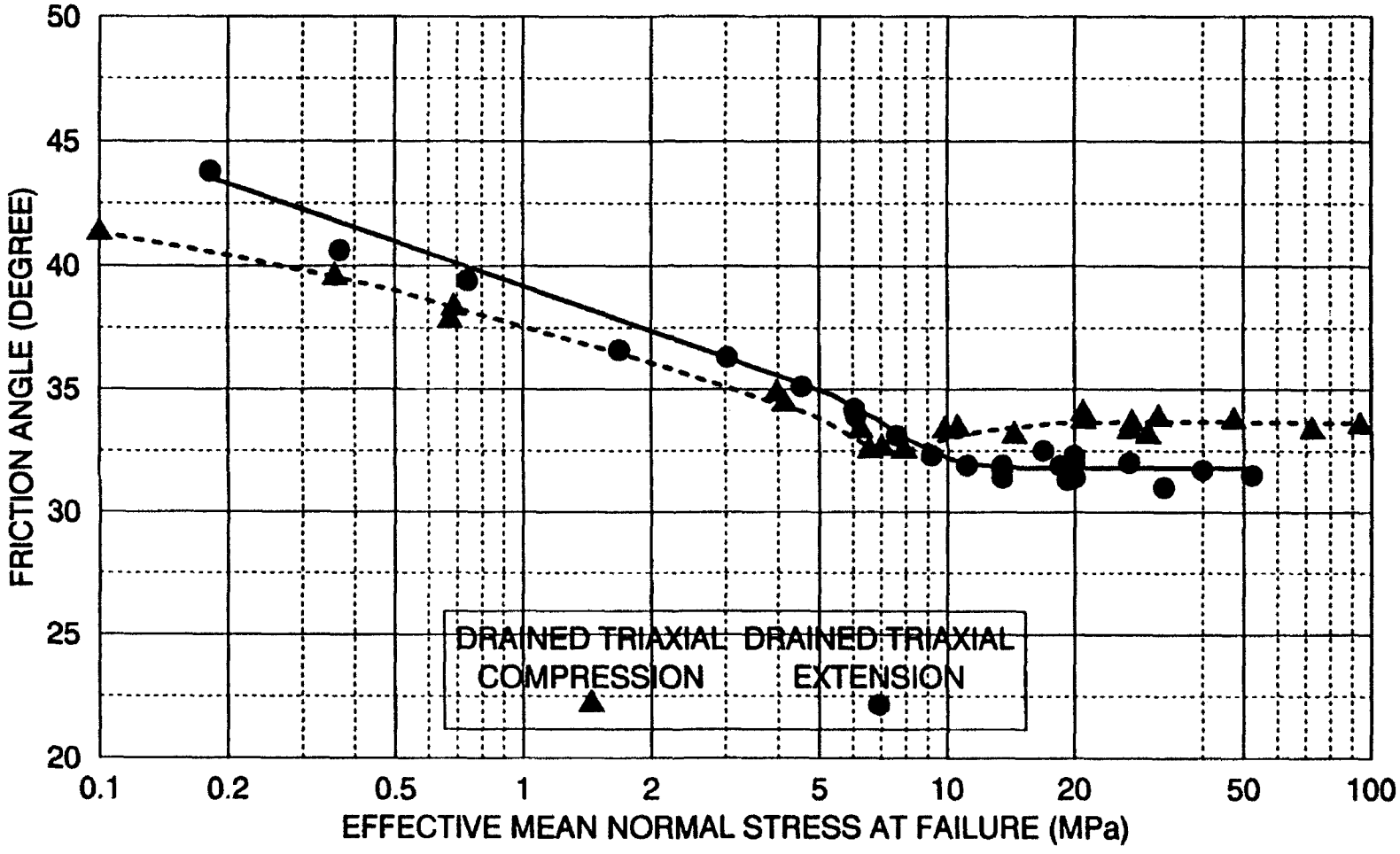

FIGURE 5-36 MOHR-COULOMB SECANT FRICTION ANGLES
DRAINED TRIAXIAL COMPRESSION & EXTENSION
DENSE CAMBRIA SAND

failure also represents the stress magnitude in which the friction angle increases and maintains a constant value. As shown on Figure 5-36, the friction angle in compression stabilizes at about 30 MPa, because the particle breakage and rearranging has ceased. The friction angles in extension appear to stabilize at a constant level below the level in compression. This is also supported by the pattern of rates of dilation at failure. Presumably, if uniform strain extension tests could have been performed at much higher stress levels, and the rates of dilation start approaching zero, then the friction angle in extension would increase up toward the compression values. This would occur only when the amount of particle crushing had increased to the maximum possible for a given high stress magnitude. Figure 5-33 clearly shows that above the 30 MPa stress magnitude particle crushing is continuing in extension, while it has stabilized in compression. The trends of the crushing curves also show that there is still considerably more particle crushing required in extension to reach the stabilized level that was achieved in compression. This indicates that the friction angle in extension may remain lower than compression out to much higher stress levels.

The undrained Mohr-Coulomb secant friction angles are shown on Figure 5-37, plotted against the effective mean normal stress at failure. The undrained compression friction angles are also included on the diagram. The undrained friction angles in extension are relatively constant and very similar to the undrained compression friction angles. Both sets of friction angles are larger than the corresponding drained friction angles in either extension or compression for a given effective mean normal stress at failure. This would seem reasonable, since

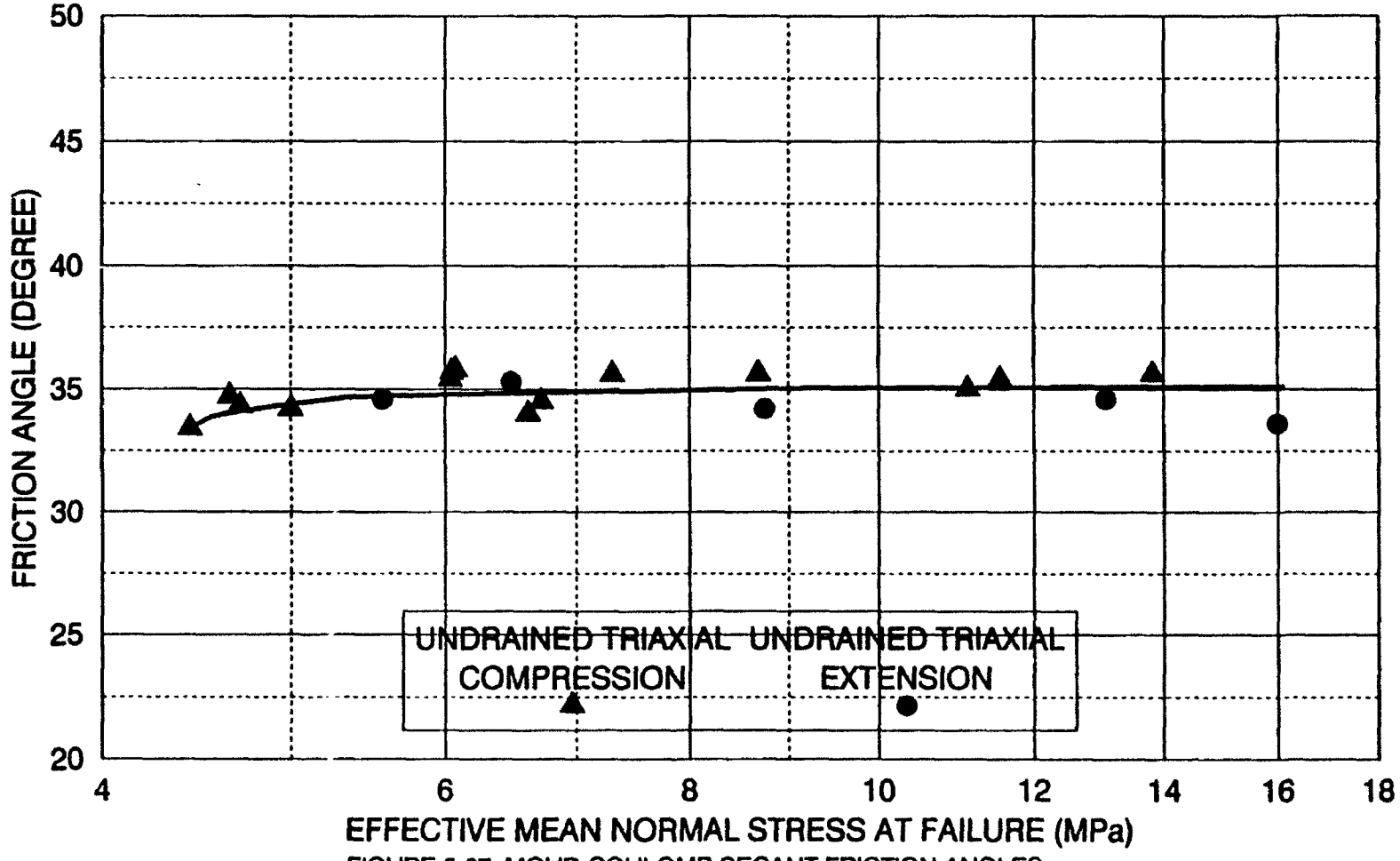

FIGURE 5-37 MOHR-COULOMB SECANT FRICTION ANGLES
UNDRAINED TRIAXIAL COMPRESSION & EXTENSION
DENSE CAMBRIA SAND

the undrained friction angles at high pressures appear to be controlled by the isotropic consolidation stress magnitudes, which are the same for both compression and extension. As previously discussed for undrained compression, the heavy isotropic consolidation physically changes the sand, due to large amounts of particle crushing before shearing begins. This eventually results in higher friction angles for the undrained condition, when the pore pressure rapidly increases and therefore decreases the effective confining pressure in the specimen to very low levels.

The void ratios at failure in drained and undrained extension tests are plotted against effective mean normal stress at failure on Figure 5-38. The drained and undrained compression tests are also shown for comparison, along with the isotropic consolidation line. The relative change in void ratio between the isotropic consolidation phase and the shearing phase is shown. The undrained and drained extension lines have similar patterns as the compression tests with the undrained line located below the drained line, indicating more volumetric compression in the undrained tests as opposed to the drained tests when compared on the basis of effective mean normal stress at failure. The extension curves are located above the compression curves, which indicates less volumetric contraction in the extension tests than in the compression tests. This is due to less particle breakage and rearranging, which results in higher void ratios. The drained compression and extension curves appear to each have a break in the slope. The breaks in slope are located at different stress levels, and are associated with the more intense particle crushing and rearranging initiating at that stress level. As

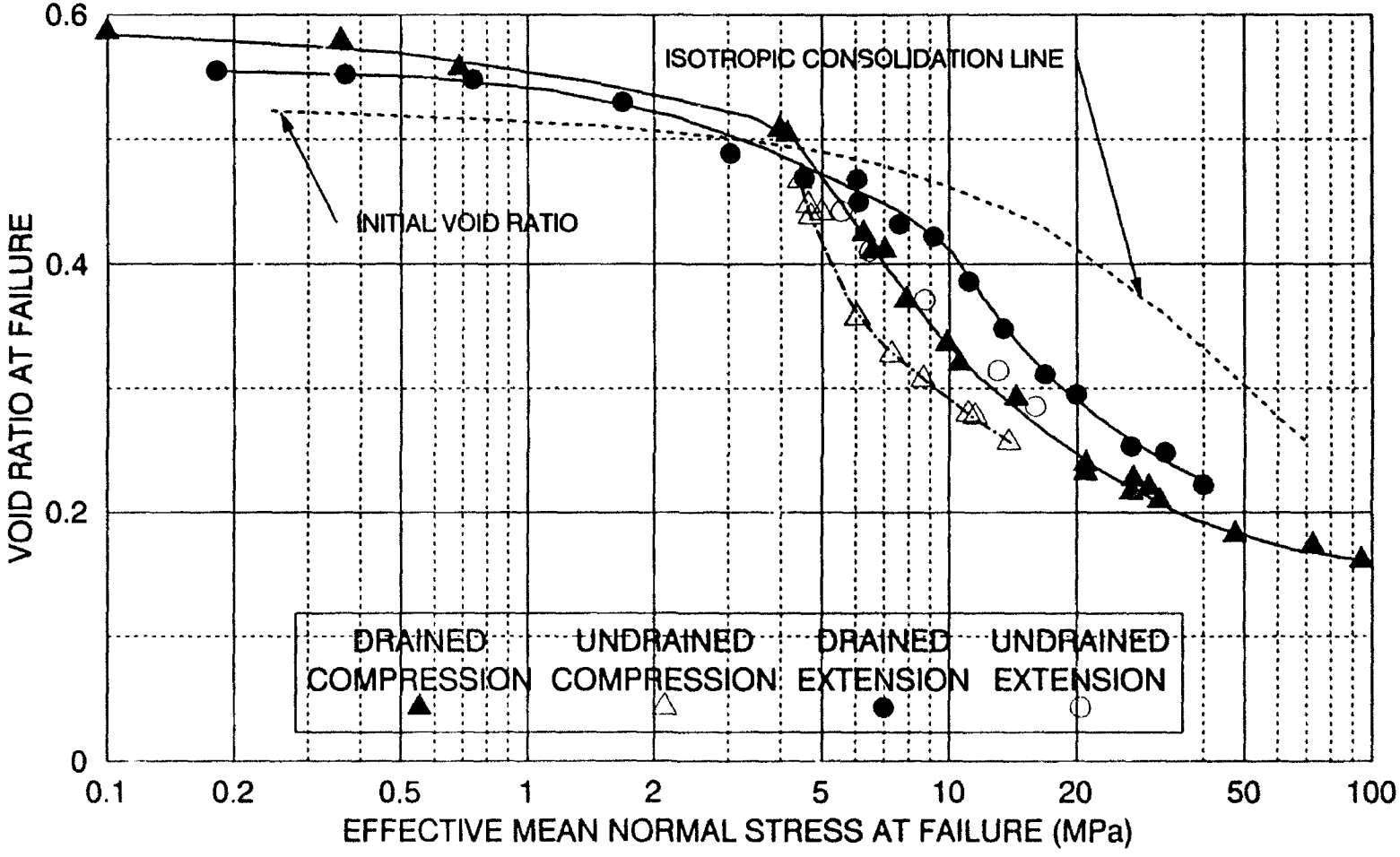

FIGURE 5-38 - VOID RATIO AT FAILURE
DRAINED & UNDRAINED COMPRESSION & EXTENSION
DENSE CAMBRIA SAND

the effective mean normal stress at failure increases to higher levels, all curves appear to run almost parallel to each other, but with the extension curves very slightly steeper than the compression curves. This indicates that the compression and extension void ratio lines may possibly converge at some higher stress magnitude.

5.9 Repeatability and Experimental Scatter

It was previously stated in Chapter 1 that testing at high pressures provides advantages regarding repeatability and scatter. This assertion was based on the observations that variations in initial void ratio and effects of anisotropy are much reduced at high pressures. Additionally, the confining pressures can be controlled to a relatively higher degree of precision than at low pressures. Once the procedural problems of membrane leaks and nonuniform strains are solved, the tests tend to be very repeatable, especially in triaxial compression. Figures 5-39 and 5-40 show some repeated tests for drained and undrained triaxial compression. There does appear to be very good general overall repeatability in results.

There were not many repeated tests in compression or extension, because of the basic testing philosophy used in this experimental program. There are two general philosophies governing experimental programs. According to one philosophy each experiment is painstakingly repeated until validity of the results and the magnitude of the experimental scatter are determined. The principal limitation of this method is that much of the effort in the experimental program

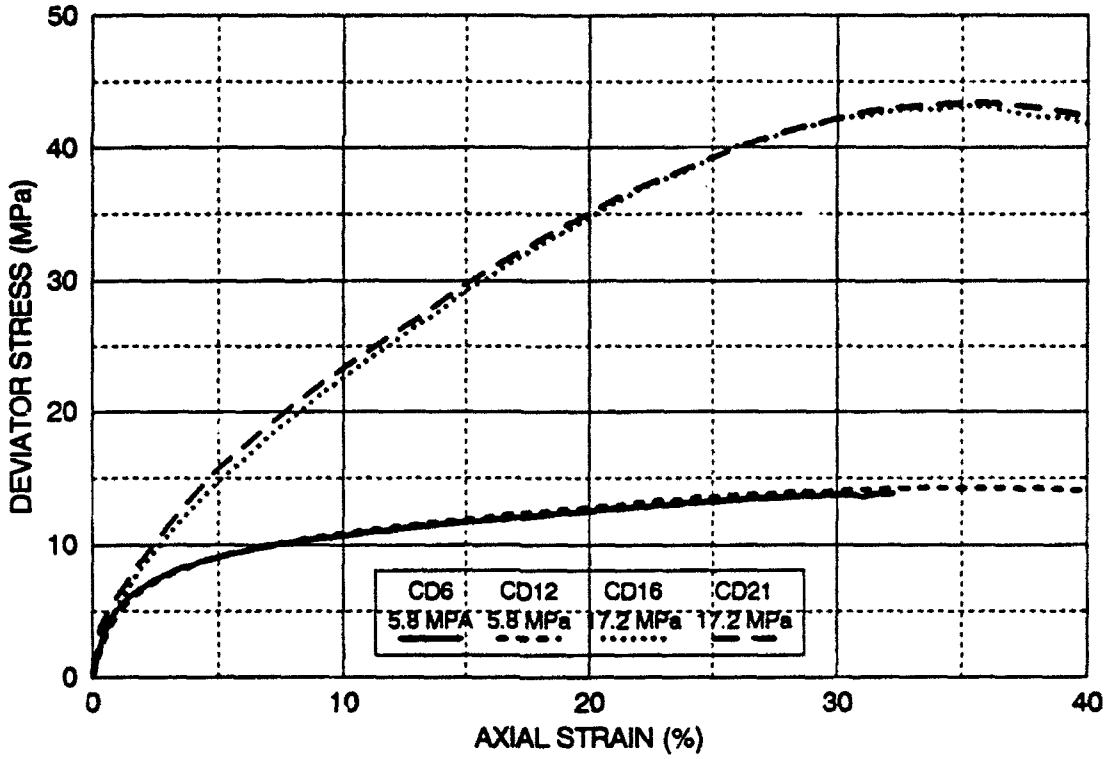

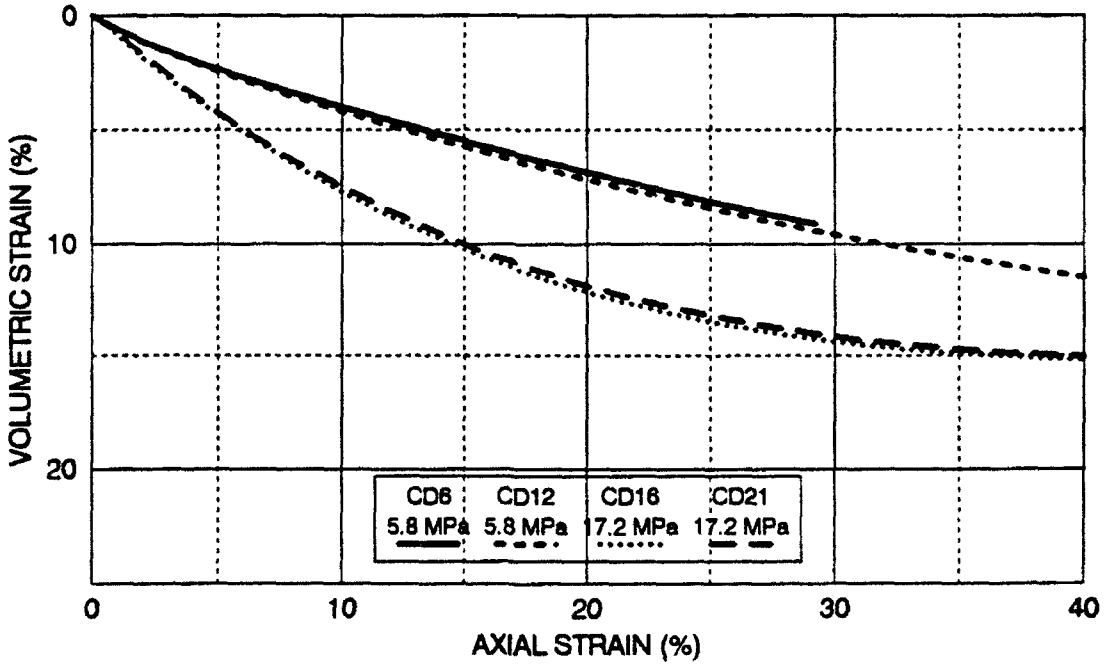

FIGURE 5-39 5.85 & 17.23 MPa DRAINED TESTS
REPEATABILITY IN DRAINED TRIAXIAL COMPRESSION
DENSE CAMBRIA SAND

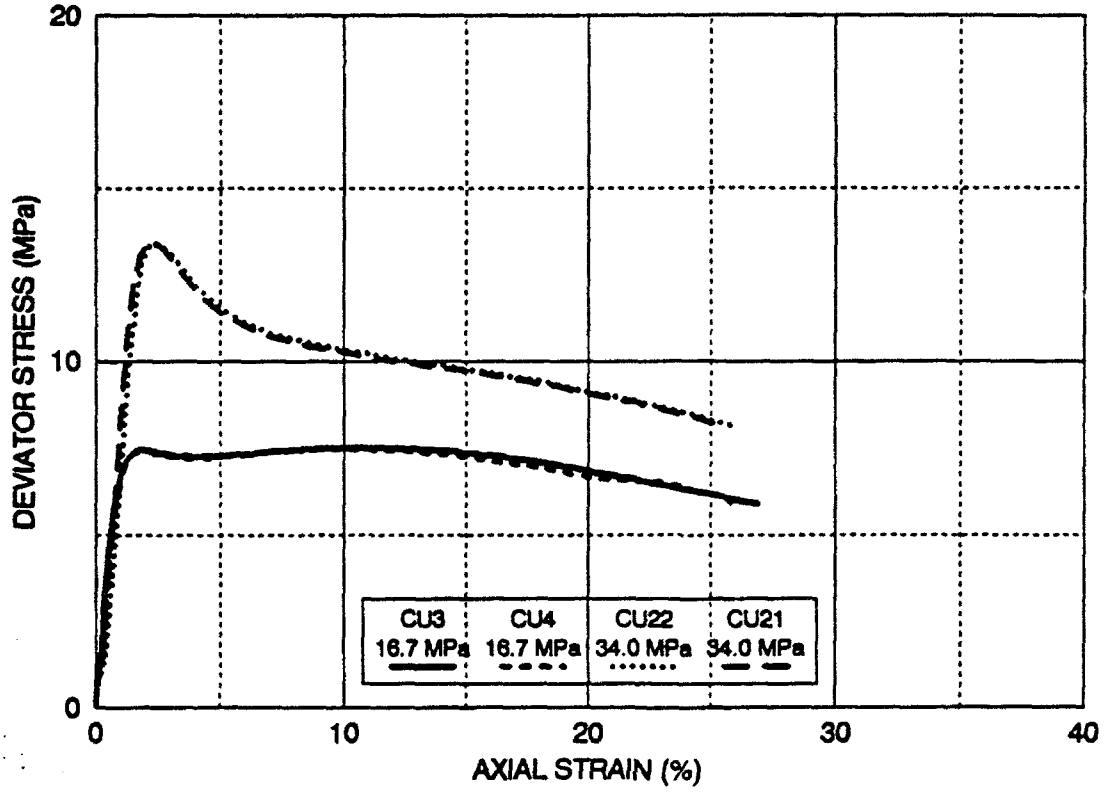

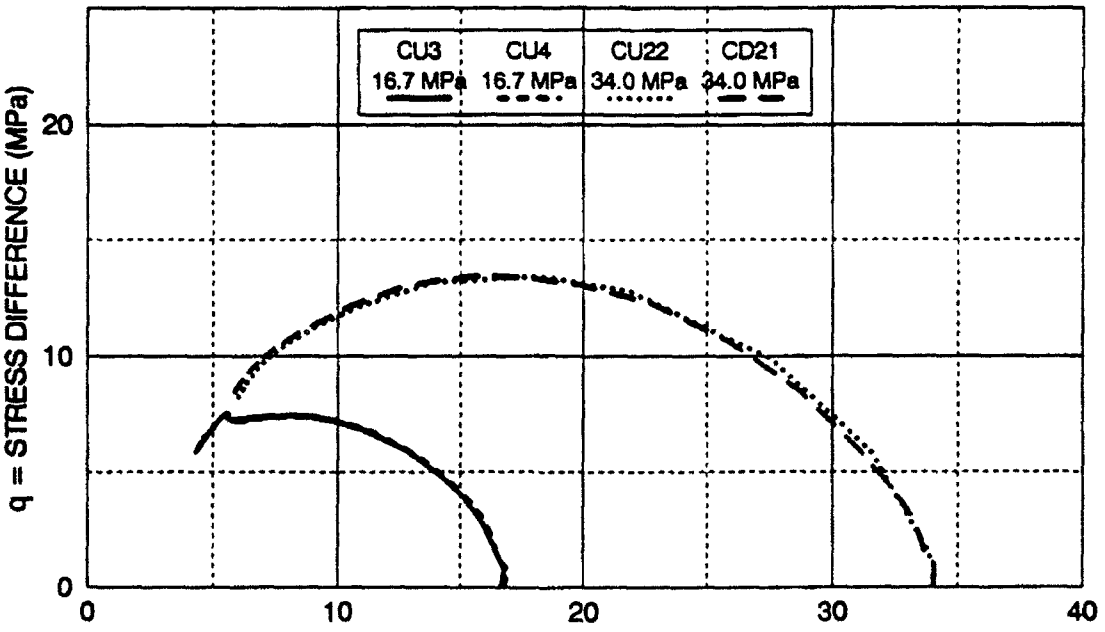

FIGURE 5-40 16.7 AND 34.0 MPa UNDRAINED TESTS
REPEATABILITY IN UNDRAINED TRIAXIAL COMPRESSION
DENSE CAMBRIA SAND

is expended performing repetitive experimentation. Another possible disadvantage of this philosophy is that embedded systematic errors within the experimental results may not be obvious to the observer, since the same experiments are repeated, resulting in the same systematic errors. The second experimental philosophy is to perform a series of experiments varying the testing parameter whose effect is being investigated. The experimental results will generally form some sort of pattern of behavior. The pattern itself is a form of confirmation of the validity of individual experimental results. If the results of an experiment do not fit into the pattern of behavior, then it may be performed again to confirm or deny the individual result or the established pattern. Additionally, selective repetitive experiments may be performed to address the issue of quantifying scatter. The principal advantage of the second philosophy over the first philosophy is that more overall progress in the experimental program is achieved with the same amount of effort. Also, systematic errors tend to be more easily discovered in the second approach because the total variation in the experimental parameters is larger, which results in the systematic error either increasing or decreasing to a point of being more readily obvious to the observer. The experimental program described here utilizes this second experimental philosophy.

Triaxial extension is a different case than compression. It has been shown in Chapter 4 that the conventional triaxial extension test is an inherently unstable test, which explains the wide degree of scatter in test results reported by prior investigators. Enforcing uniform strains by the methods developed in Chapter 4, produce results which are much more consistent and reasonable in most respects.

However, enforcing uniform strains at high pressures is still very difficult, because the inherent instability in the test is amplified at high pressures. Many more tests were performed to achieve the results included in this thesis. Experimental scatter is not possible to evaluate effectively in extension, since one test may completely fail, and another may be successful. Evaluation of the test results must be carefully performed. The mode of failure must be carefully considered, along with the trends established by other tests.

Proctor and Barden (1969) showed that the cylindrical triaxial extension test suffers from additional basic experimental scatter, much greater than experienced in triaxial compression. By assuming a certain percentage measurement error in load, specimen height, and cross-sectional area, they demonstrated that the triaxial extension test suffers from five times greater error than the triaxial compression test, when the same errors are used in the computations. This results in a substantially larger amount of uncertainty in extension than in compression. If there is an uncertainty of 0.5 degrees in the friction angle in compression, then the uncertainty could be as high as 2.5 degrees in triaxial extension. Another experimental measurement problem in the test setup is based on the fact that the deviator stress in extension is created by the uplift force on the piston provided by the confining pressure. As shearing in extension progresses, the actual load measured by the load cell from the maximum measured at the end of istropic consolidation. This is due to the soil absorbing the load as a negative deviator stress. Using this setup, the instrumentation and data acquisition systems provide the highest level of resolution and accuracy at the

highest load encountered, which unfortunately is at the beginning of shearing. When failure occurs, the instrumentation provides less resolution and accuracy, depending on the size of the deviator stress, and the overall capabilities of the system. Triaxial compression does not suffer from this additional induced error. Regardless, it appears that extension always has more scatter in test results compared to compression. The uniform strain extension tests reported in this chapter do exhibit more scatter than comparable compression tests. The experimental error in extension is estimated to be approximately 2 degrees in the friction angle, whereas in compression it is estimated to be between 0.5 and 1 degree.

CHAPTER 6 - SOIL INSTABILITY IN TRIAXIAL COMPRESSION AND EXTENSION AT HIGH PRESSURES

6.1 Instability of Soils at High Pressures

Instability is defined as the inability to carry or sustain a given load, resulting in large strains. The characteristics of instability are similar to failure, but it can occur well within the established effective stress failure envelope. Submarine slopes and mine tailings dams have experienced catastrophic failures due to soil instability. Mechanisms triggering instability can be small in magnitude, such as small seismic events, wave action, vibration from machinery, or volumetric creep. The general requirements for occurrence of instability are: near fully saturated conditions; cohesionless soils; volumetric compressive tendency; and undrained conditions. Prior studies of instability at low confining pressures were studied for low soil densities (Lade, et al, 1988). Dense sand can be used at high confining pressures for the investigation of instability, since at high pressures even dense sands will exhibit volumetric compression.

6.2 Location of the Instability Region at High Pressures

As stated in Section 1.9, the instability region is represented by a wedge shaped area with its upper bound being the effective stress failure line. The lower bound is a line that joins the tops of the effective stress paths (Cambridge p'-q diagram) of undrained tests, corresponding to the maximum deviator stresses. The compression and extension instability regions for dense Cambria sand are shown

on Figure 6-1. The figure shows the effective stress paths plotted on the Cambridge p'-q diagram for some of the undrained compression and extension tests performed on dense Cambria sand. These test results were discussed in detail in Chapter 5

The instability lines are again shown on Figure 6-2. Plotted on this diagram are the individual points representing the points of maximum stress difference on the effective stress paths from the previous figure. The maximum deviator stress is plotted against the effective mean normal stress at the maximum deviator stress. As can be seen, both instability lines pass through the origin. A few of the lower pressure compression and extension tests have dilatant tendencies, and therefore, do not fall on the instability line. The remaining tests, which show compressive volumetric tendencies, fall close to the instability lines. The diagram indicates the q/p' ratios for compression and extension, and the corresponding Mohr-Coulomb friction angles of the instability lines. A linear regression through the origin was performed on all points except those associated with dilating tests. The compression instability friction angle is 20.6 degrees (q/p' = 0.798), and the extension instability friction angle is 23.0 degrees (q/p' = 0.692).

The bottom of the wedge shaped instability region near the origin is bounded by a horizontal line, which would ideally represent an effective stress path that would reach its maximum deviator stress at the instability line, and maintain this stress level (horizontal) until it intersects the effective stress failure line. This horizontal line is also the upper bound of the temporary instability region as shown on Figure 6-3 for dense Cambria sand. The temporary instability

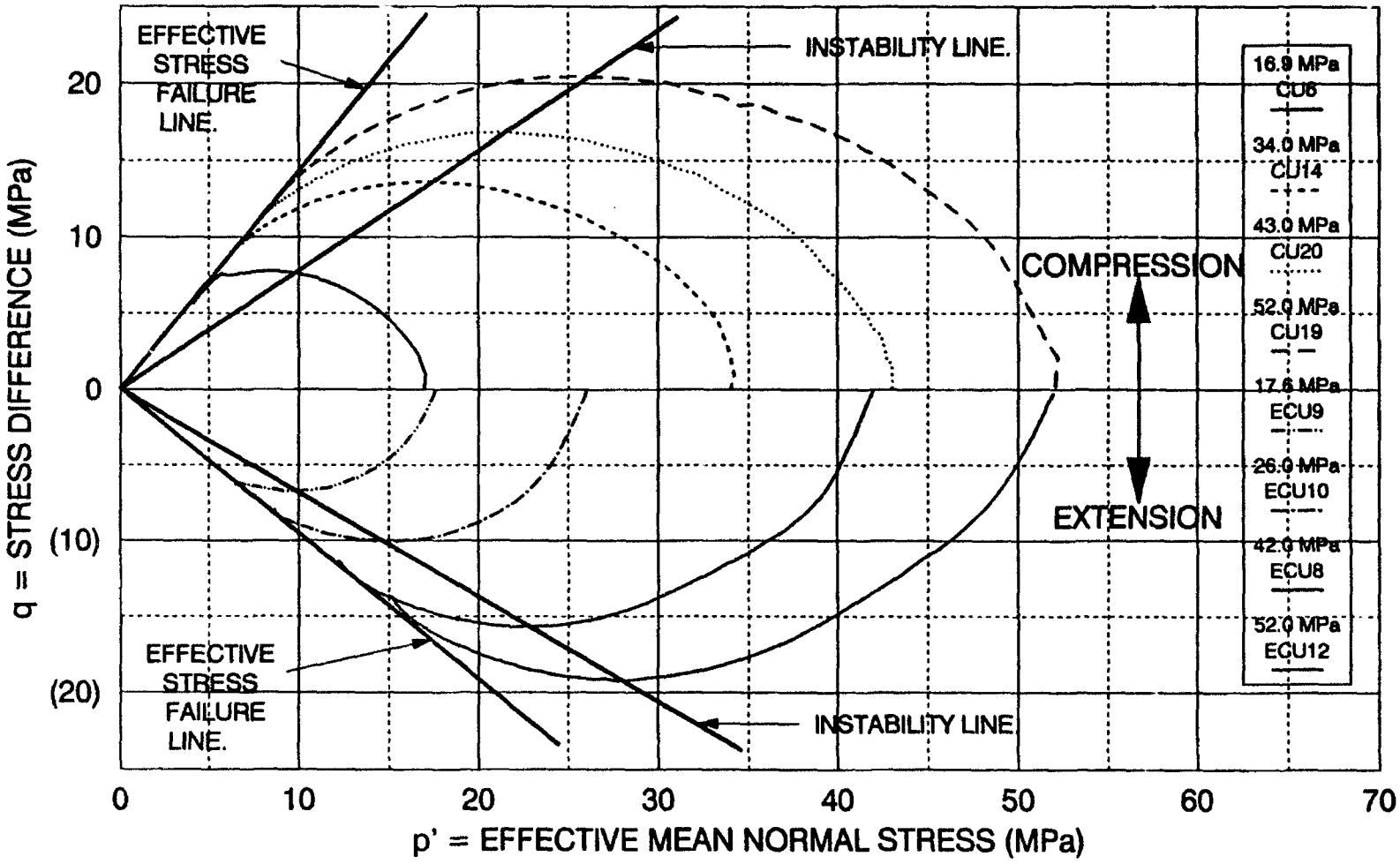

FIGURE 6-1 INSTABILITY LINES & FAILURE LINES, CAMBRIDGE p'-q
UNDRAINED TRIAXIAL EXTENSION & COMPRESSION
DENSE CAMBRIA SAND

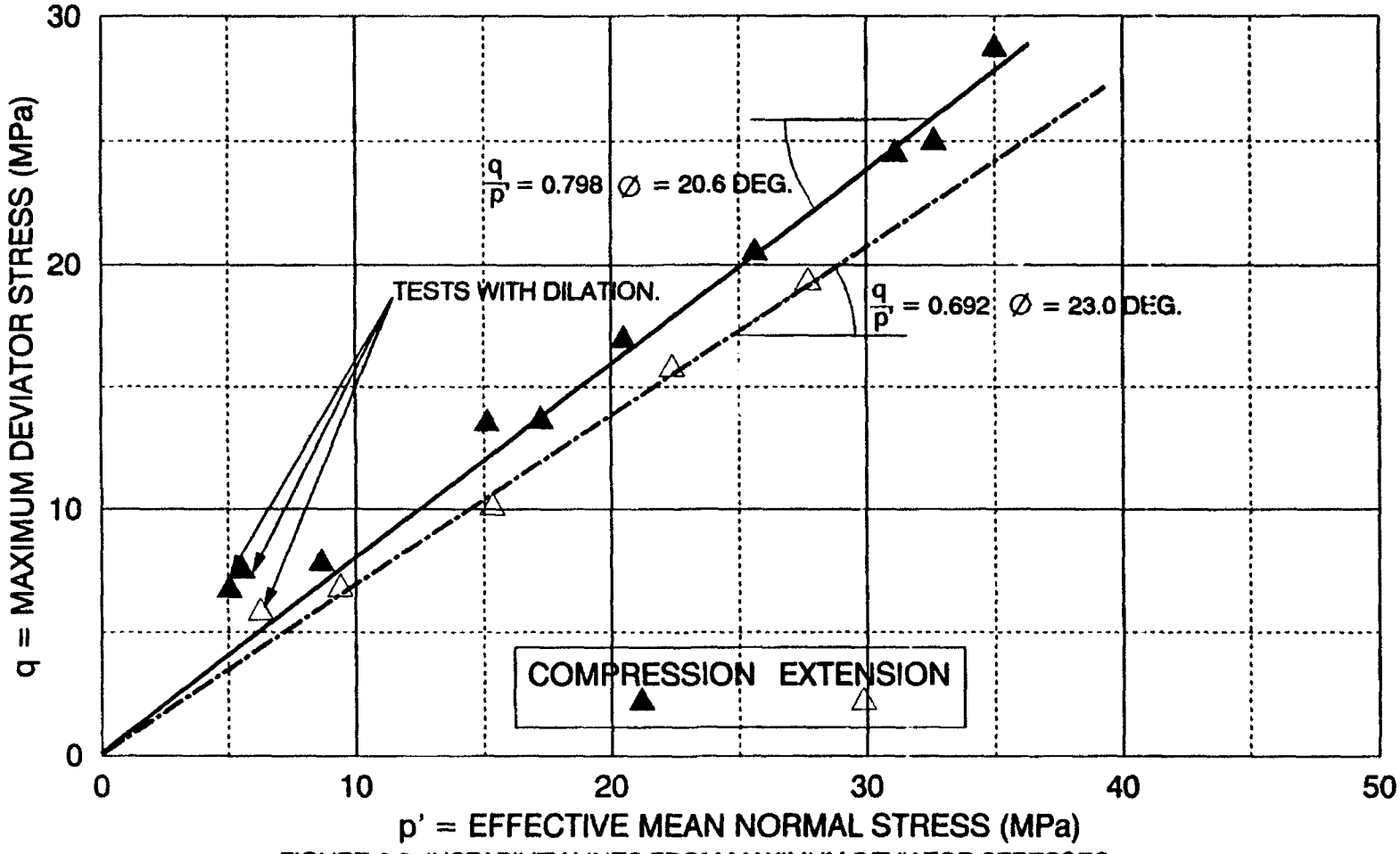

FIGURE 6-2 INSTABILITY LINES FROM MAXIMUM DEVIATOR STRESSES
FROM UNDRAINED COMPRESSION AND EXTENSION TESTS
DENSE CAMBRIA SAND

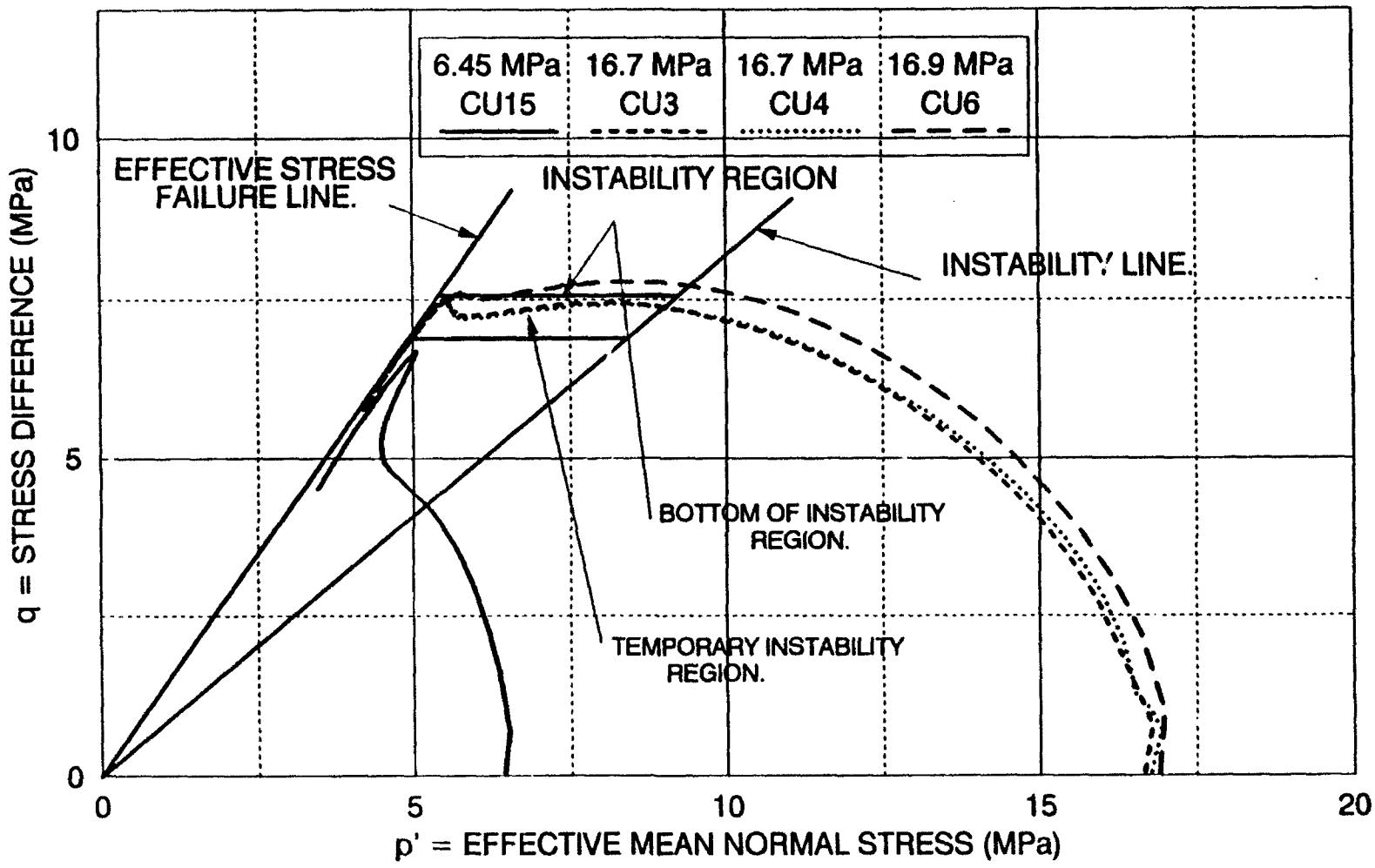

FIGURE 6-3 TEMPORARY INSTABILITY ZONE
LOW PRESSURE UNDRAINED COMPRESSION TESTS
DENSE CAMBRIA SAND

region is a narrow zone, in which the soil experiences initial compressive volumetric behavior after the first peak deviator stress, causing decreasing stresses and instability. However, as the stresses in the soil move toward failure, the soil begins to exhibit dilatant tendencies, and this decreases the pore pressures. This stabilizes the soil with an increasing capability to carry larger deviator stresses above the initial peak, prior to reaching failure (Castro, 1969). Figure 6-3 shows the lower pressure undrained compression tests on Cambria sand which bound this threshold. The two tests conducted with initial confining pressure near 16.7 MPa exhibit behavior that classifies them as within the temporary instability region, since the deviator stresses reach an initial peak, then decreases before rising again above the first peak. The test with an initial confining pressure of 16.9 MPa indicates general compressive behavior beyond the initial maximum deviator stress with a slight tendency to dilate, but the deviator stress never increases above the initial maximum value. Therefore, the lower limit of the instability region must be located between the stress paths of these two different initial confining pressures, and it is estimated to be at a deviator stress of approximately 7.5 MPa. The lower boundary of the temporary instability region is a horizontal line at which the "proper" stress path would not exhibit any initial drop in deviator stress, but would become horizontal before continuing upwards toward failure. This represents a condition where the volumetrically dilatant tendencies of the soil are strong enough so the soil never becomes unstable. The test with an initial confining pressure of 6.45 MPa shows a stress path with this general behavior. The overall behavior is compressive, but dilation in the specimen occurs before an

initial peak in the deviator stress is created. However, it does not become horizontal before rising up to failure. At higher stress magnitudes the soil would have more compressive tendencies and a flat region would be formed before dilation would cause it to rise up to failure. A test with the required effective stress path that would represent the lower limit of the temporary instability region is estimated to produce a deviator stress of approximately at the 7.0 MPa in triaxial compression.

Effective stress paths for the lower pressure, undrained triaxial extension tests are shown on Figure 6-4. The two effective stress paths shown on this figure effectively bound the lower limit of the instability region. The test with an initial confining pressure of 17.6 MPa exhibits generally compressive volumetric tendencies beyond the initial maximum deviator stress resulting in a deviator stress that declines, and never exceeds the initial maximum prior to failure. This test does exhibit slightly dilatant tendencies near failure, but the increase in deviator stress is small. Close examination of the test with an initial confining pressure of 12.0 MPa indicates a very small amount of temporary instability, with a small decrease in deviator stress before dilatant behavior increases it to a higher level and eventual failure. Therefore, the lower boundary of the instability region falls between the stress paths of these two tests, and it is estimated to be approximately at the 6.0 MPa deviator stress level. Since the 12.0 MPa test indicates only very slight temporary instability characteristics, the lower boundary of the temporary instability region is located only slightly beneath this stress path. The 4.5 MPa deviator stress level is estimated to be the lower boundary of the temporary

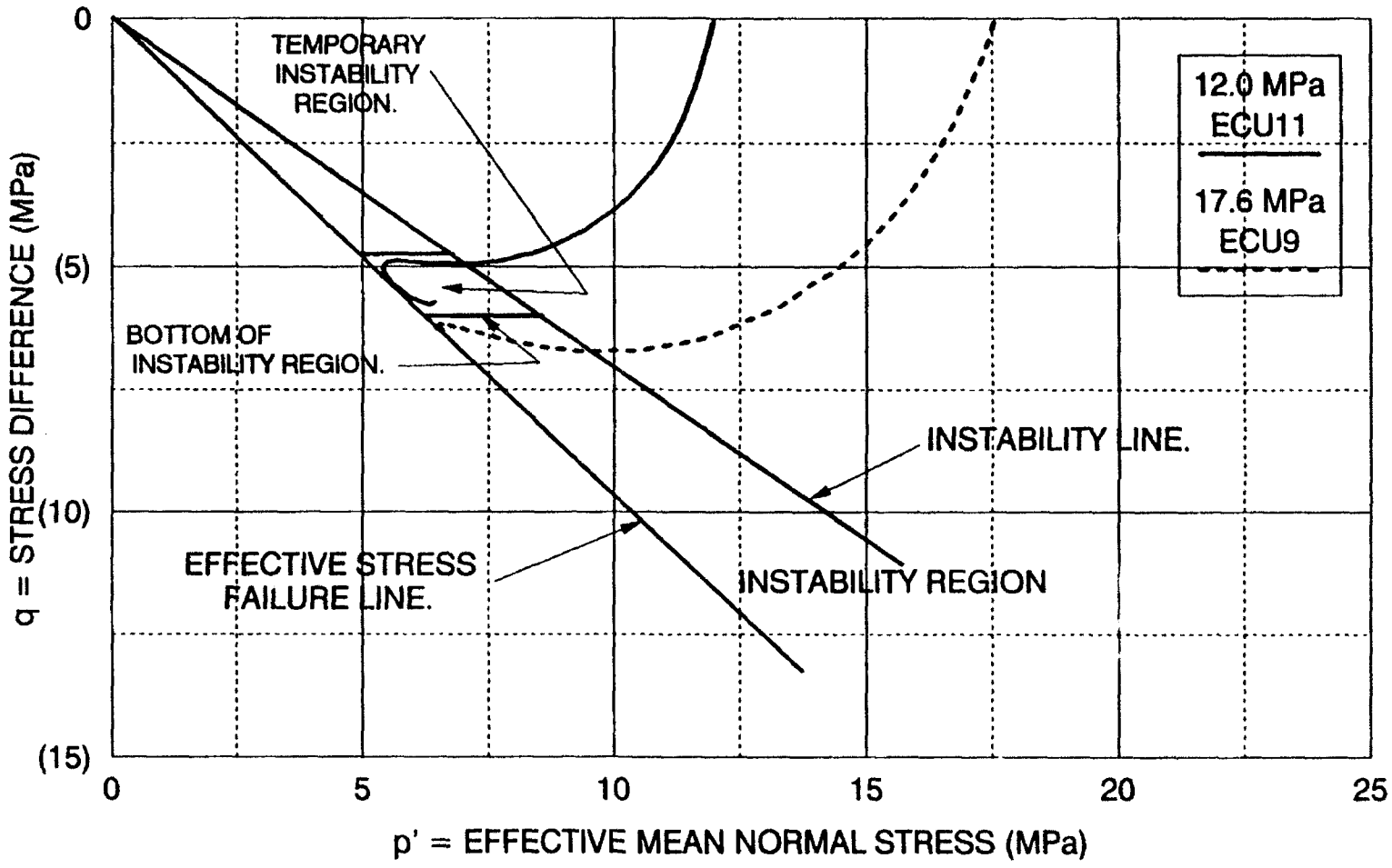

FIGURE 6-4 TEMPORARY INSTABILITY ZONE
LOW PRESSURE UNDRAINED EXTENSION TESTS
DENSE CAMBRIA SAND

instability region. The temporary instability region appears to be larger in extension than in compression. This might be due to the fact that there is more particle crushing in compression than in extension, which may suppress the dilatant behavior in triaxial compression.

The instability and temporary instability regions in both compression and extension are shown on Figures 6-5 and 6-6 superimposed on the effective stress paths for several undrained compression and extension tests. All boundaries of the instability region have now been established and indicated on the figures, including the temporary instability regions.

Tests whose stress paths venture into the indicated instability regions should exhibit instability, if undrained conditions are imposed.

6.3 Instability Test Procedures

The sand used for the instability investigation was Cambria sand and specimens were prepared as described in Chapter 3. Height-to-diameter ratios for all compression test specimens was 2.5 to 1. The height-to-diameter ratios for all extension test specimens was 1.8 to 1. The techniques to enforce uniform strains in triaxial extension tests, described in Chapter 4, was used in all extension instability tests.

Special computer control programs were developed to perform the instability tests in both compression and extension. The programs were written to initiate each test with standard drained isotropic consolidation to a specified confining pressure. Constant total cell pressure was maintained throughout the

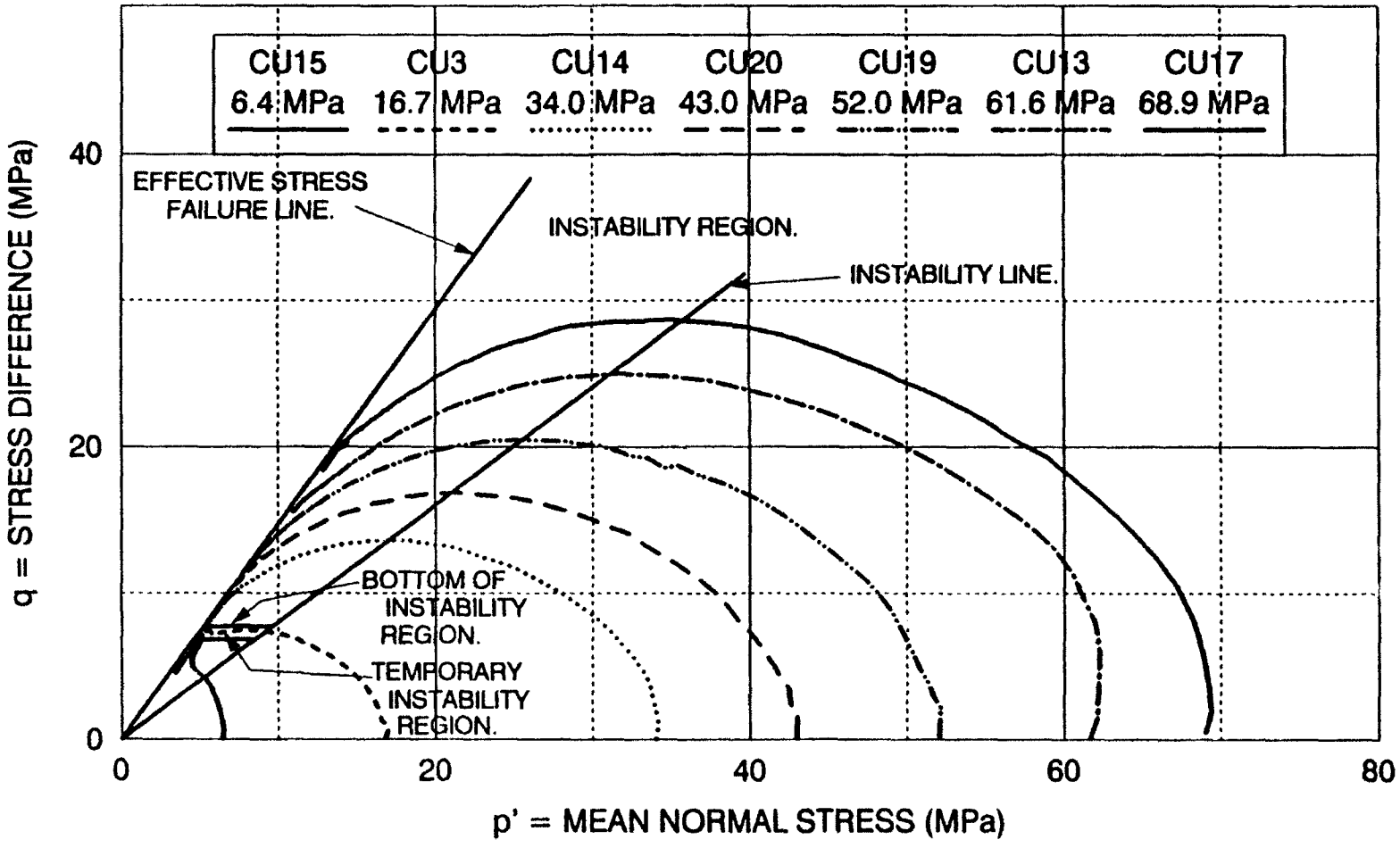

FIGURE 6-5 INSTABILITY AND TEMPORARY INSTABILITY REGION, CAMBRIDGE p'-q
UNDRAINED TRIAXIAL COMPRESSION
DENSE CAMBRIA SAND

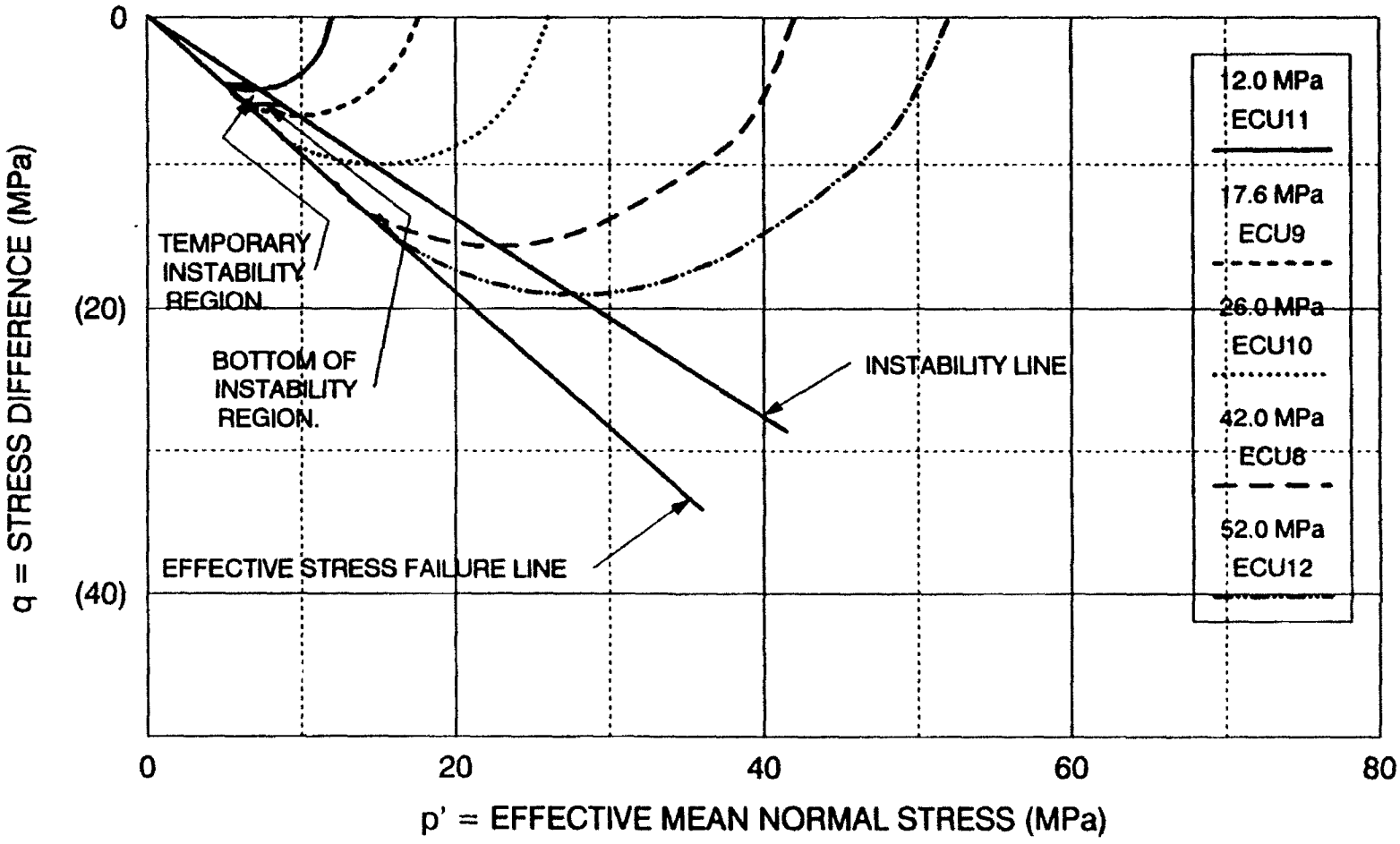

FIGURE 6-6 INSTABILITY AND TEMPORARY INSTABILITY REGIONS, CAMBRIDGE p-'q
UNDRAINED TRIAXIAL EXTENSION
DENSE CAMBRIA SAND

duration of the test. Drained shearing was then performed under strain control conditions, until a user-specified effective principal stress ratio was attained. At that time the specimen is turned into an undrained state by closing the drainage valves on the triaxial cell, and the program switches to stress control. The control program attempts to maintain the deviator stress at a constant level. If the specimen exhibits instability, then the stepping motor controlling the vertical deviator stress should increase to its maximum speed, as it attempts to hold the deviator stress level constant. If the behavior is stable the stepping motors should have little difficulty in maintaining the deviator stress level constant.

6.4 Results of Triaxial Compression Instability Tests

The experimental program in triaxial compression consisted of five tests. All tests were performed with drained shearing to different stress ratios, where undrained conditions were imposed. Four tests were performed at an initial confining pressure of 17.2 MPa, and one test was conducted at 26.0 MPa. Three specimens were sheared to different stress levels within the defined instability region. These tests should immediately exhibit unstable behavior when undrained conditions were imposed. Two tests were sheared to stress ratios that were below the instability line of the established instability region for compression. It was expected in these two tests that, if undrained conditions were imposed on the specimen, undrained volumetric creep would increase the pore pressures, and cause the stress condition to move toward the instability line. If the creep-generated pore pressures were large enough, then the specimen may become

unstable, and the absolute location of the instability line in compression would be experimentally ascertained.

The effective stress paths for three tests are shown on Figure 6-7, with the stress difference on the vertical axis plotted against the effective mean normal stress. The three tests that were sheared to stress levels inside the established instability region will are discussed first. The three tests were sheared to effective stress ratios of 2.30, 2.67, and 3.20. A failure effective stress ratio of approximately 3.50 was obtained for a drained compression test at this effective confining pressure. Upon closure of the drainage valves in each of the three tests, the pore pressures started to rise rapidly, as shown on Figure 6-8, resulting in a rapidly declining effective confining pressure. This in turn caused the deviator stresses to decrease, as shown on Figure 6-9. In all three tests instability is induced by the imposed undrained conditions, since the stress states are already inside the instability region. Even though the computer control program attempts to maintain constant deviator stress, the stepping motors cannot produce a large enough axial deformation rate to successfully maintain sufficient load, and the motors quickly reach their maximum possible speed. Therefore, the deviator stresses decrease rapidly in magnitude after the onset of instability, as shown on Figure 6-9. The instability is produced very quickly, since the deviator stress curves have relatively sharp peaks at the point where undrained conditions are imposed. The deviator stresses in the three tests shown on Figure 6-9 all overlay each other within the first 11 percent of axial strain indicating excellent repeatability of test results. The pore pressures for the three tests shown on Figure

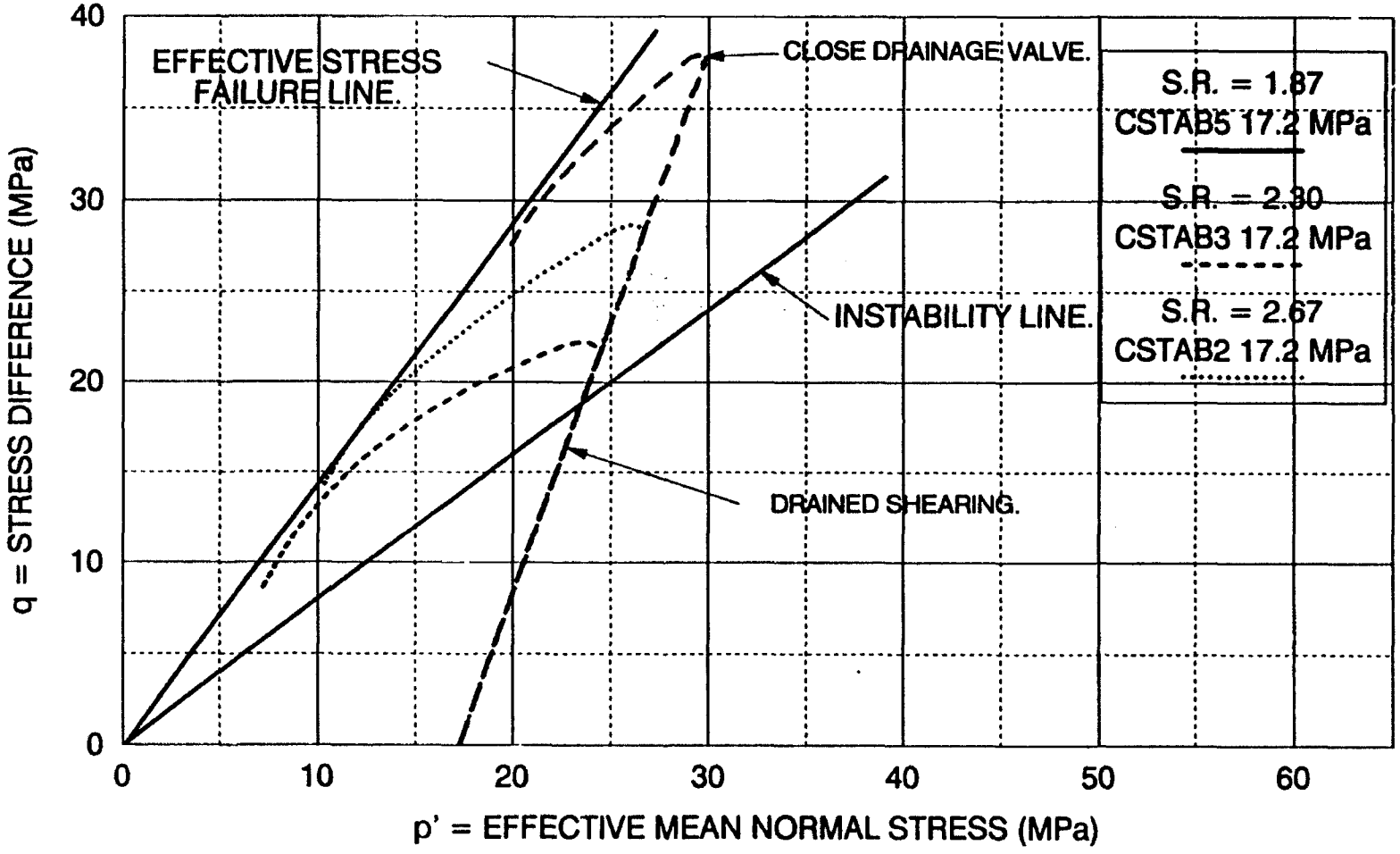

FIGURE 6-7 INSTABILITY TESTS INSIDE INSTABILITY REGION, CAMBRIDGE p'-q
DRAINED-UNDRAINED STABILITY COMPRESSION TESTS
DENSE CAMBRIA SAND

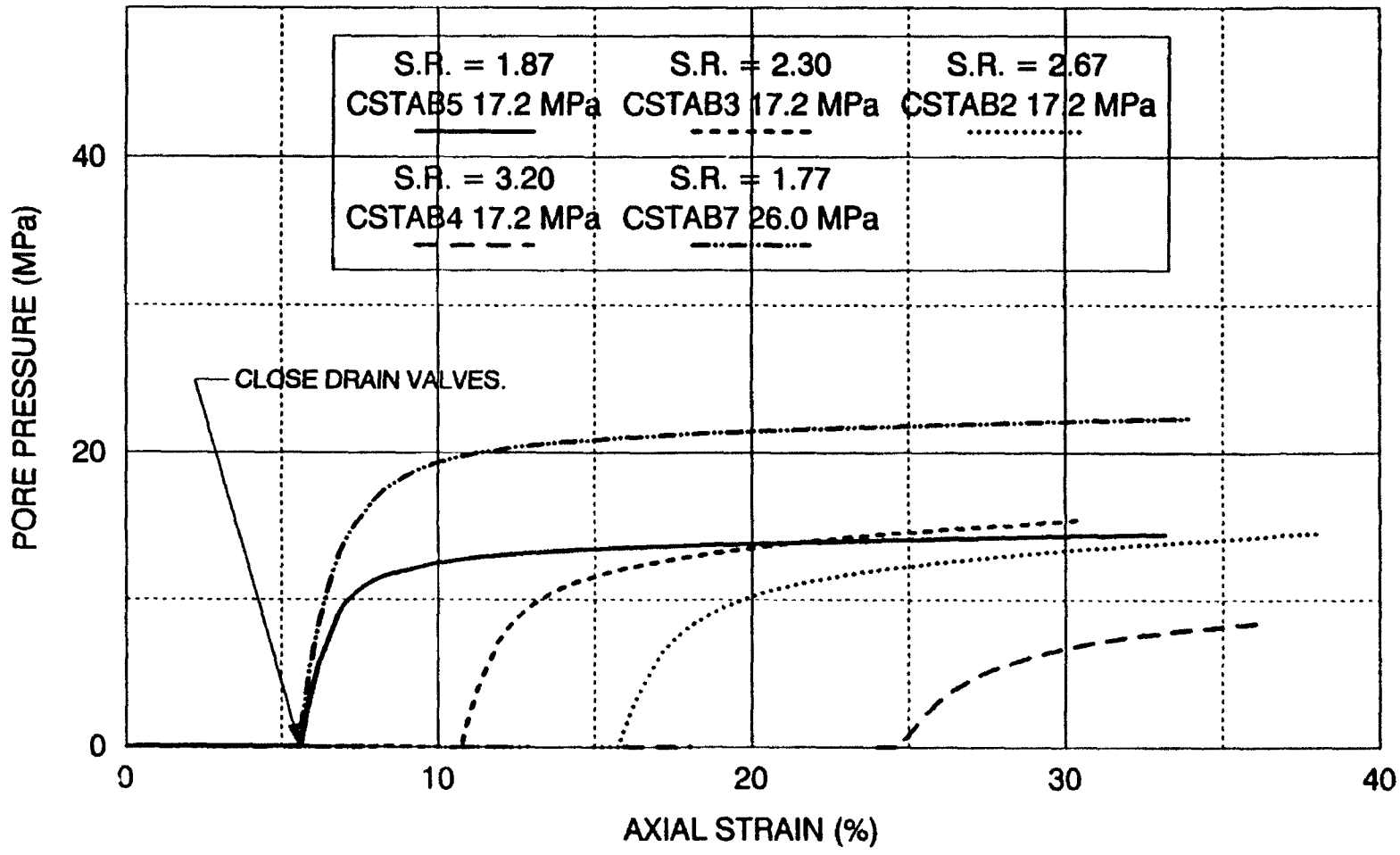

FIGURE 6-8 PORE PRESSURE
DRAINED-UNDRAINED COMPRESSION STABILITY TEST
DENSE CAMBRIA SAND

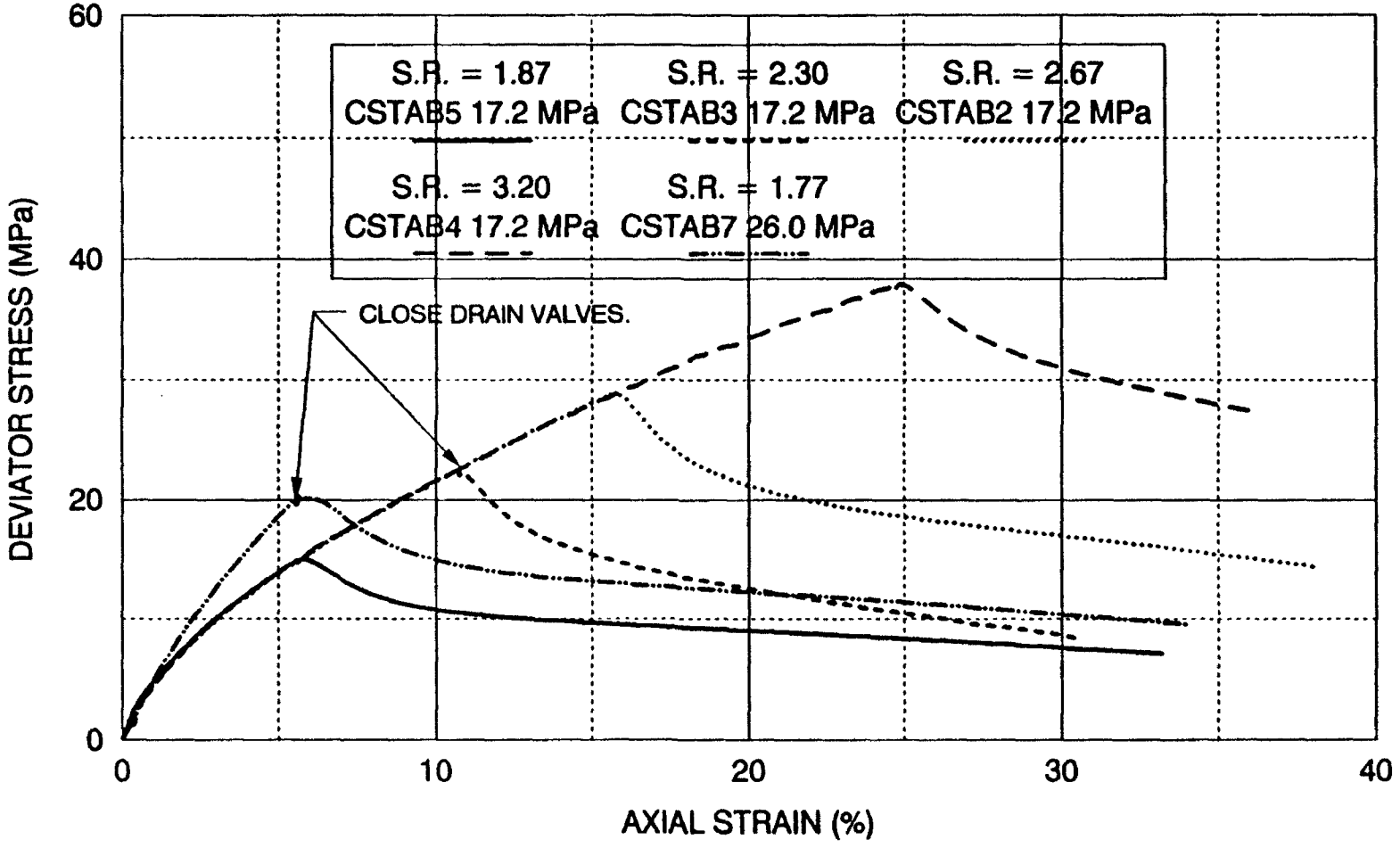

FIGURE 6-9 DEVIATOR STRESS
DRAINED-UNDRAINED COMPRESSION STABILITY TESTS
DENSE CAMBRIA SAND

6-8 indicate rapid pore pressure development after the drainage valves are closed. However, the rate of pore pressure generation decreases, as the stress ratio increases following initiation of undrained conditions. This is due to the closer proximity of the effective stress failure surface. The variation of the effective stress ratios are shown on Figure 6-10. When the drainage valves are closed, the effective stress ratios rise very quickly, due to the rising pore pressures, and effective stress failure eventually occurs at higher axial strains. However, the 2.30 stress ratio test appears to fail at a lower maximum stress ratio and axial strain magnitude than the other two tests. This was due to some observed slippage between the specimen and its cap and base. This occurred after the specimen became unstable. Close examination of the figures indicates that the measured deviator stresses and generated pore pressures for this test deviate from the established pattern of the other two tests.

The volumetric strains are shown on Figure 6-11. The volumetric strains of the three tests also overlay each other until the drainage valves are closed at different axial strain levels, which again indicates good repeatability in test results. After closure, volumetric strains cease. The effective stress paths of the three tests (Figure 6-7) indicate increasing steepness of the stress path as the stress level increases, in which undrained conditions were induced. This is indicative of the proximity to the effective stress failure surface, and it is similar to the steepness of the slopes of effective stress paths from the standard undrained compression tests.

Now that instability is clearly demonstrated within the established triaxial

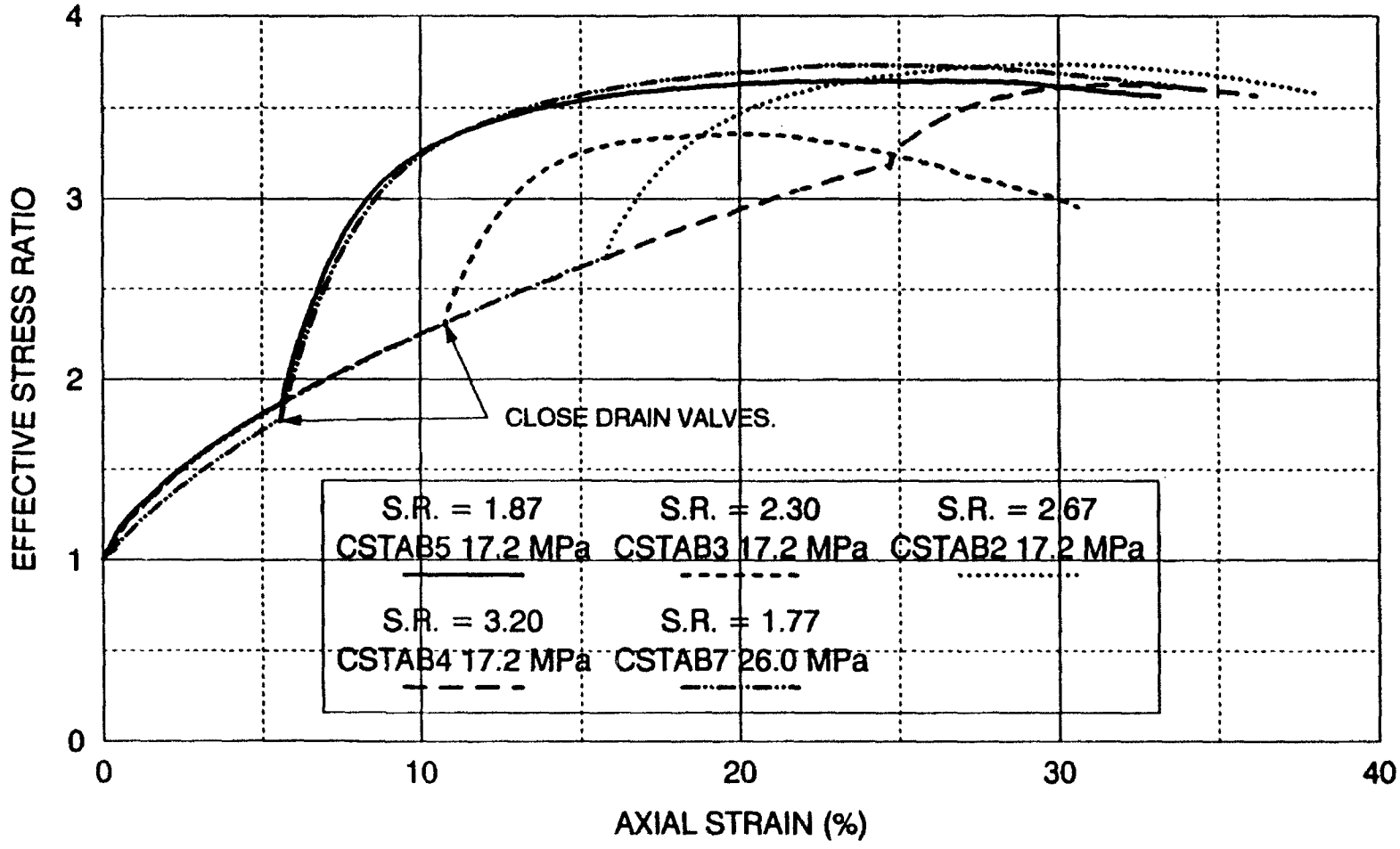

FIGURE 6-10 EFFECTIVE STRESS RATIO
DRAINED-UNDRAINED COMPRESSION STABILITY TESTS
DENSE CAMBRIA SAND

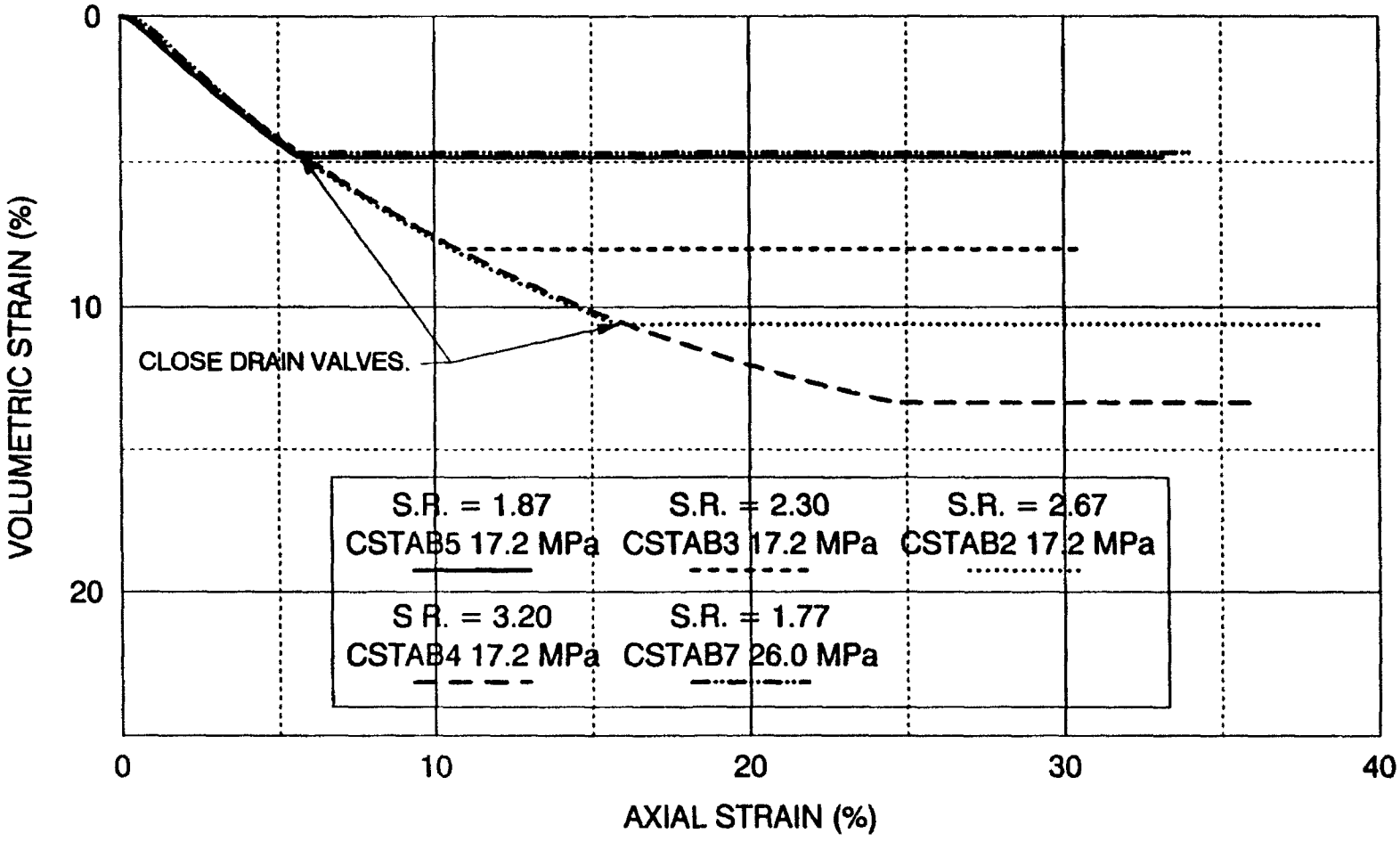

FIGURE 6-11 VOLUMETRIC STRAINS
DRAINED-UNDRAINED COMPRESSION STABILITY TESTS
DENSE CAMBRIA SAND

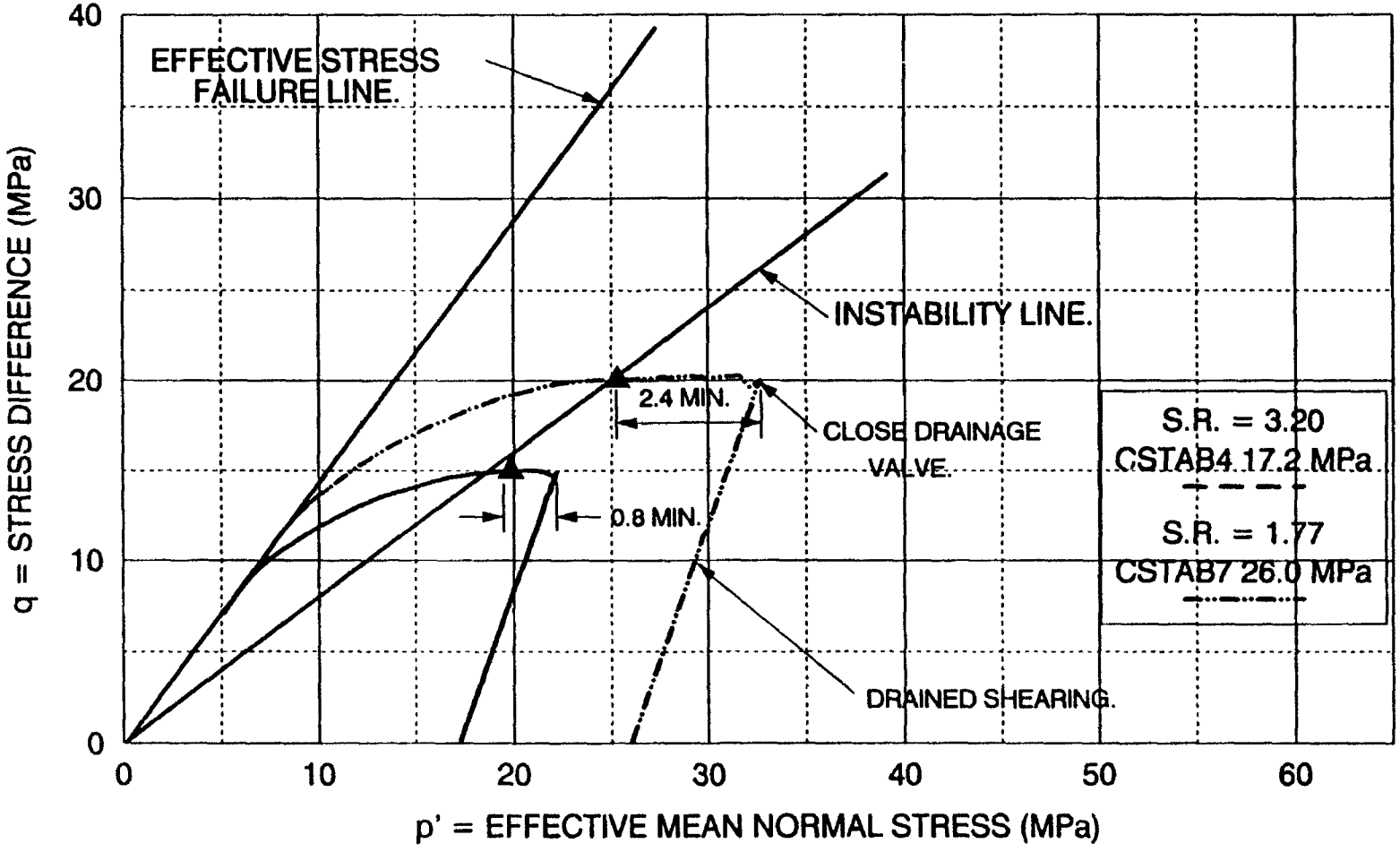

FIGURE 6-12 INSTABILITY TESTS CREEPING INTO INSTABILITY REGION, CAMBRIDGE p'-q
DRAINED-UNDRAINED STABILITY COMPRESSION TESTS
DENSE CAMBRIA SAND

compression instability region, an attempt was made to directly confirm the location of the instability line through other types of instability tests. Two tests, consolidated to 17.2 and 26.0 MPa, were sheared under drained conditions to effective stress ratios of 1.87 and 1.77, respectively. These stress levels correspond to locations well outside the established instability region as shown on Figure 6-12. When the desired stress ratio was attained, the drainage valves were closed, and the deviator stresses were held constant. There was a temporary slight drop in deviator stress, due to a slight delay as the computer stress control algorithm adjusted itself to the new conditions after switching from strain control. However, the computer control program quickly corrects the stress level back to the proper level and maintains it constant thereafter. The two tests indicate that upon closure of the drainage valves, pore pressures are generated due to prevented volumetric creep under the undrained conditions. However, outside of the instability region the deviator stresses can easily be maintained by the computer with no increase in speed from the stepping motors. As the stress state approaches the instability line, the deviator stresses become very difficult to maintain, and the stepping motors increase speed to their maximum. Instability results. Examination of the deviator stresses, pore pressures, effective stress ratios, and volumetric strains on the figures indicate behavior similar to the previously discussed test. Only the 26.0 MPa test is different, because of the difference in the initial confining pressure.

Analyses were performed to determine the exact stress conditions at which instability is initiated. Figures 6-13 and 6-14 show axial displacement-time curves for the two creep-instability tests performed. The diagrams indicate two different

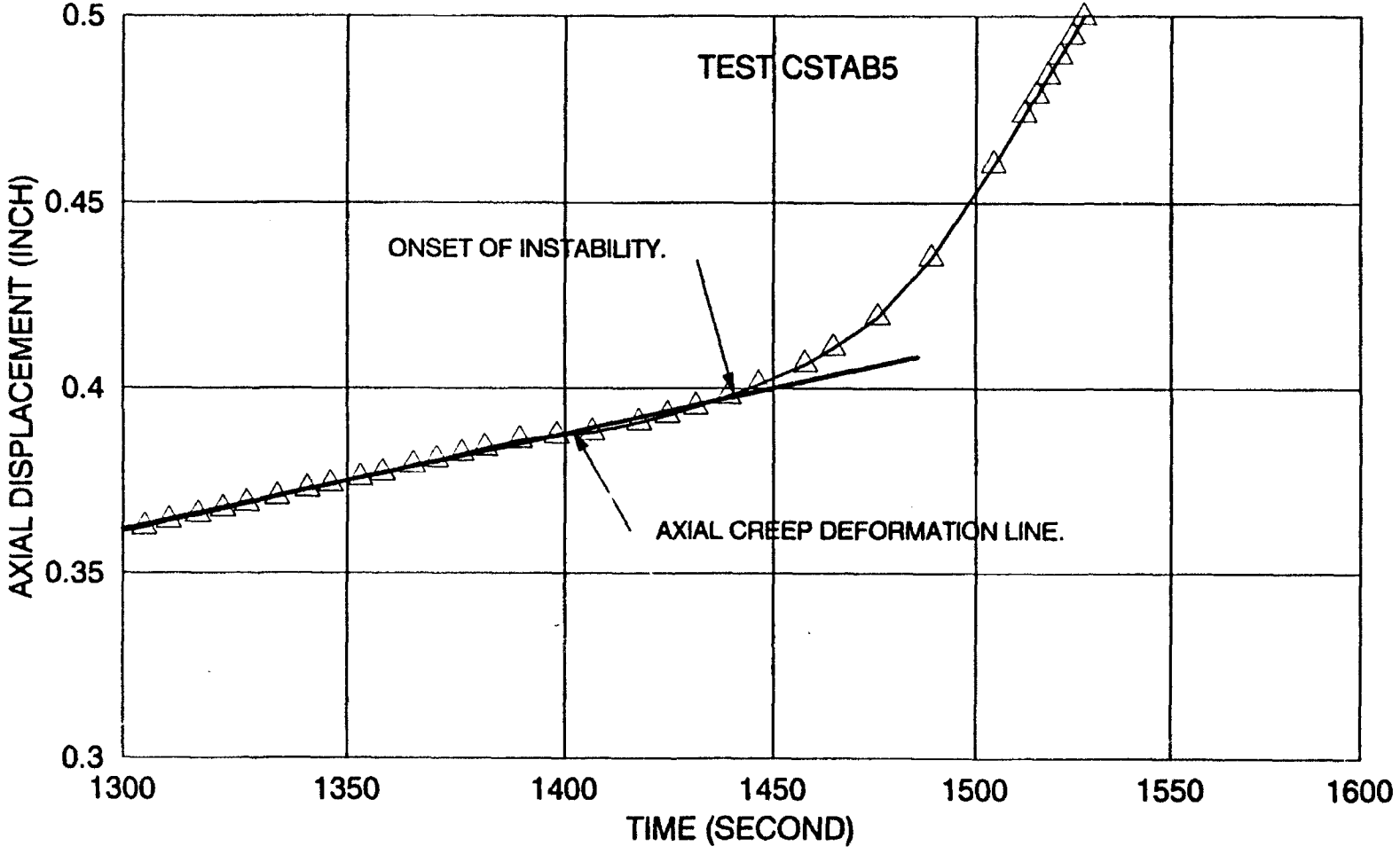

FIGURE 6-13 POINT OF INSTABILITY
DRAINED-UNDRAINED COMPRESSION STABILITY TEST
DENSE CAMBRIA SAND

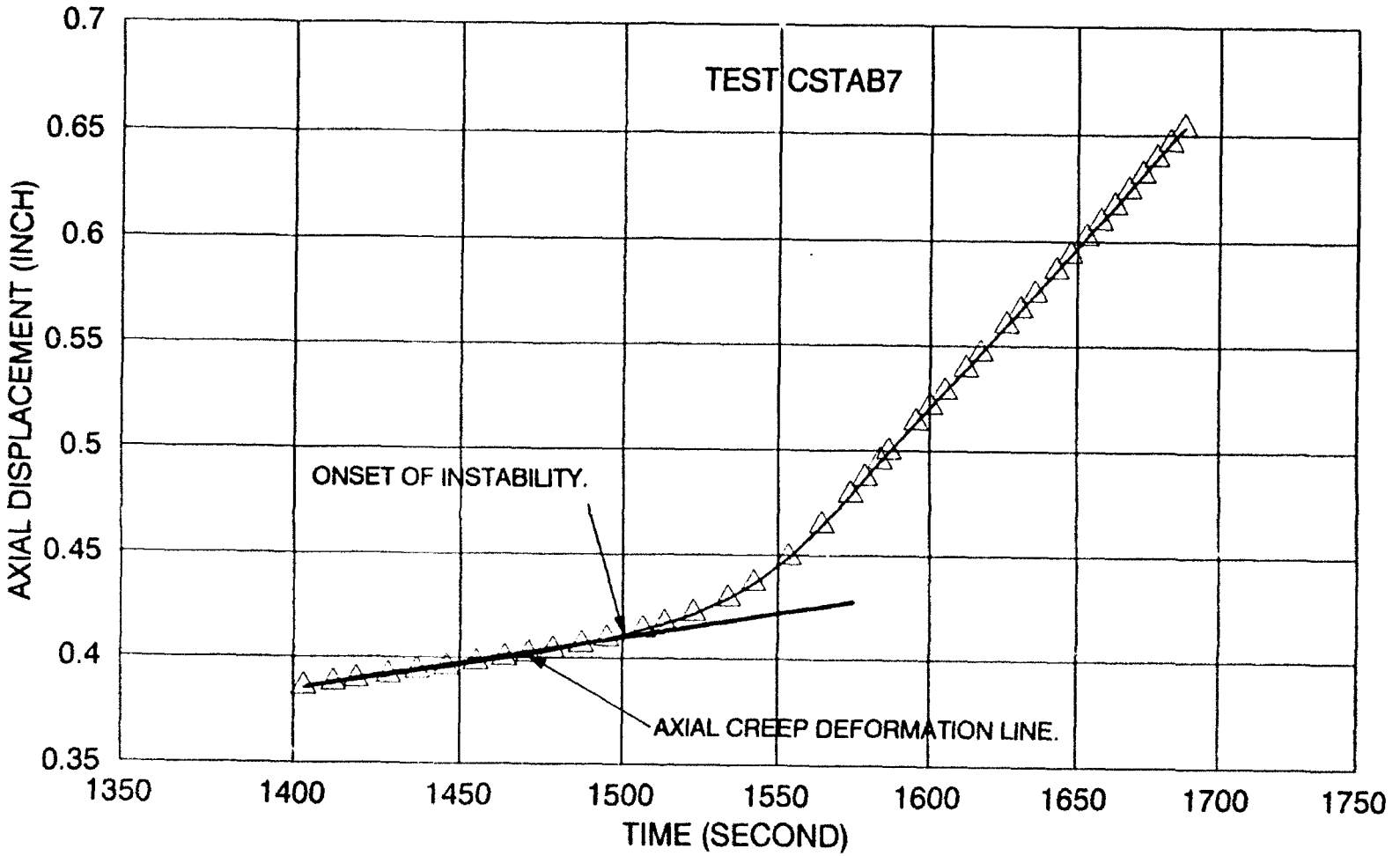

FIGURE 6-14 POINT OF INSTABILITY
DRAINED-UNDRAINED COMPRESSION STABILITY TEST
DENSE CAMBRIA SAND

slopes which display conditions before and after instability develops. The flatter section occurs during the undrained creep portion with constant deviator stress. Once instability starts developing, the axial deformation rate increases, as the computer tries to maintain constant deviator stress. The point of departure from the creep line is the time at which instability starts. Once the time at which instability initiates is determined, then the effective mean normal stress can be cross-referenced from the computer generated test data file. The points of instability for the two tests are indicated on the effective stress paths in Figure 6-12 as triangular symbols. They fall very close to the location of the instability line previously established from the undrained compression tests. The location of the instability line in compression has therefore been experimentally confirmed. The time for the undrained creep to move the stress states to the instability line for the two tests is also shown on Figure 6-12.

The maximum effective stress ratio for the test with significant undrained creep appears to be slightly larger than the rest of the instability tests, whose maximum stress ratios are approximately equal to those from the conventional undrained compression tests. The time effects from the undrained creep appears to increase the effective stress friction angle, but time does not have any effect on the actual location of the instability line (Yamamuro and Lade, 1993b).

6.5 Results of Triaxial Extension Instability Tests

An experimental program similar to that in triaxial compression was performed to investigate instability in triaxial extension. Following the drained

isotropic consolidation phase, the specimens are sheared under drained conditions to different stress ratios. At the respective stress levels the specimens are turned undrained, by closure of the drainage valves, and the deviator stresses are held constant by the computer. Two tests were performed at an initial confining pressure of 17.6 MPa, and sheared to stress ratios of 2.40 and 2.90. This placed them within the established triaxial extension instability region. After the specimens were turned undrained in these two tests, pore pressures started generating, causing the deviator stresses to decrease. The rate of pore pressure generation is slower in extension than in compression, but the results are the same. Instability developed in both cases as shown on Figure 6-15 in which the effective stress paths are shown. Figure 6-16 shows that the deviator stresses cannot be maintained by the computer and stepping motors after instability develops, and in fact rapid decreases in the deviator stresses occur. Also plotted on Figure 6-16 is a standard drained extension test at approximately the same confining pressure as in two of the tests. This figure indicates good repeatability in test results. The deviator stresses decrease after instability develops, because of the rise in pore pressures. The rising pore pressures are depicted on Figure 6-17 plotted against major principal strain. The figure indicates that the lower stress level test has a higher rate of pore pressure generation. Again, this is the the effect of the increased distance from the effective stress failure line. The variations in effective principal stress ratios are shown on Figure 6-18 plotted against major principal strain. As soon as the specimens are turned undrained, the effective stress ratio rapidly increases due to the rising pore pressures until effective stress

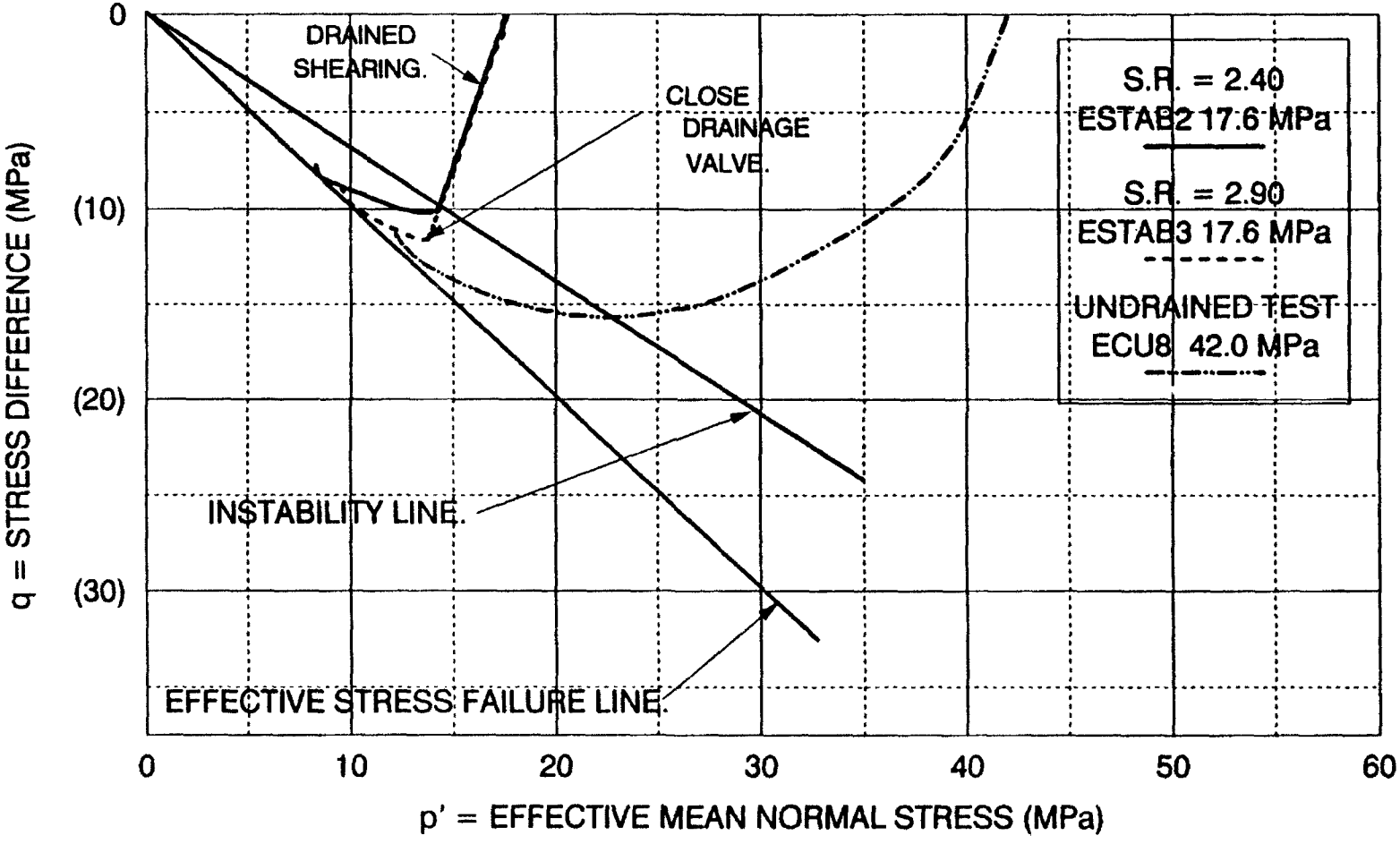

FIGURE 6-15 INSTABILITY TESTS WITHIN INSTABILITY REGION, CAMBRIDGE p'-q
DRAINED-UNDRAINED STABILITY EXTENSION TESTS
DENSE CAMBRIA SAND

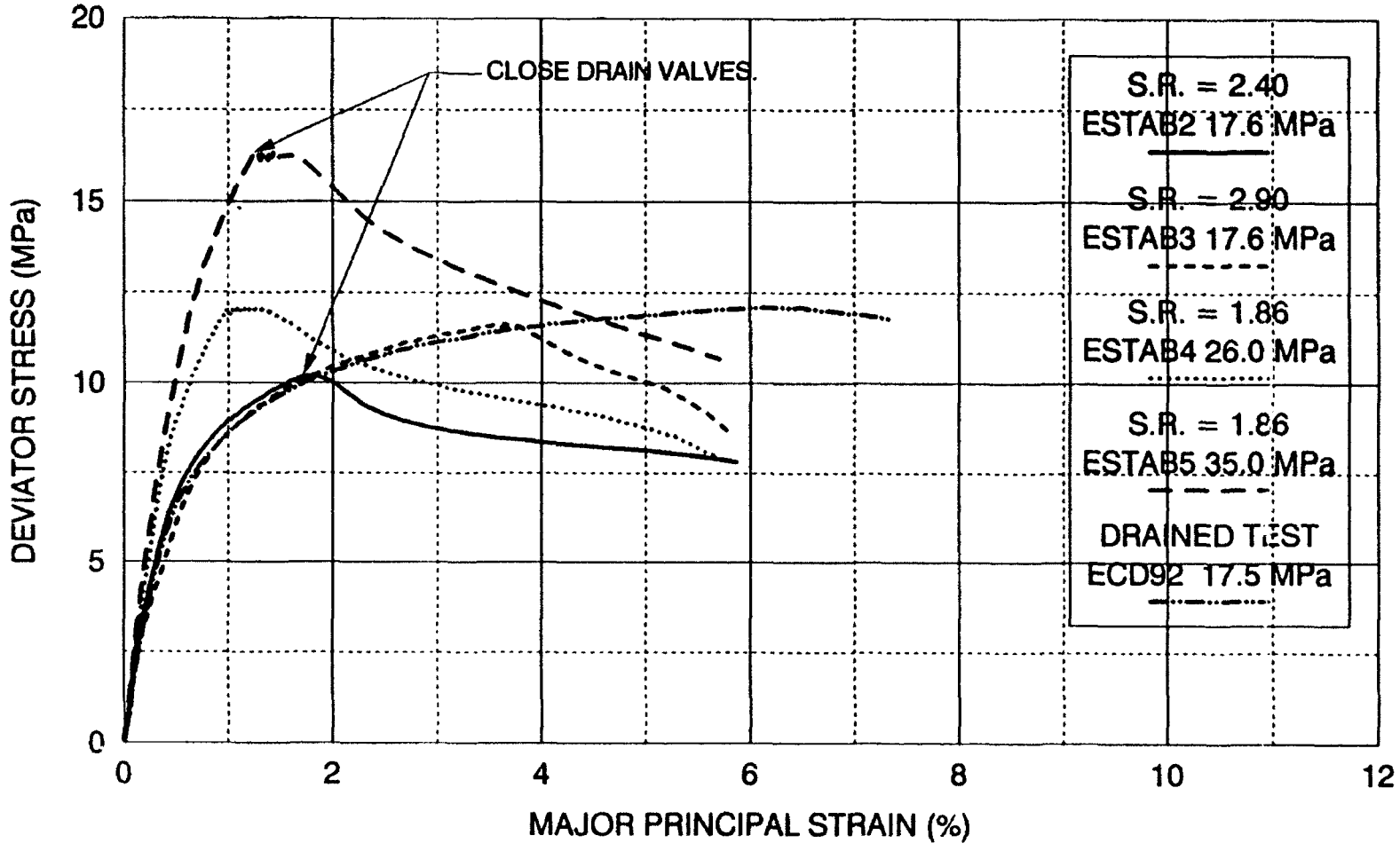

FIGURE 6-16 DEVIATOR STRESS
DRAINED-UNDRAINED EXTENSION STABILITY TESTS
DENSE CAMBRIA SAND

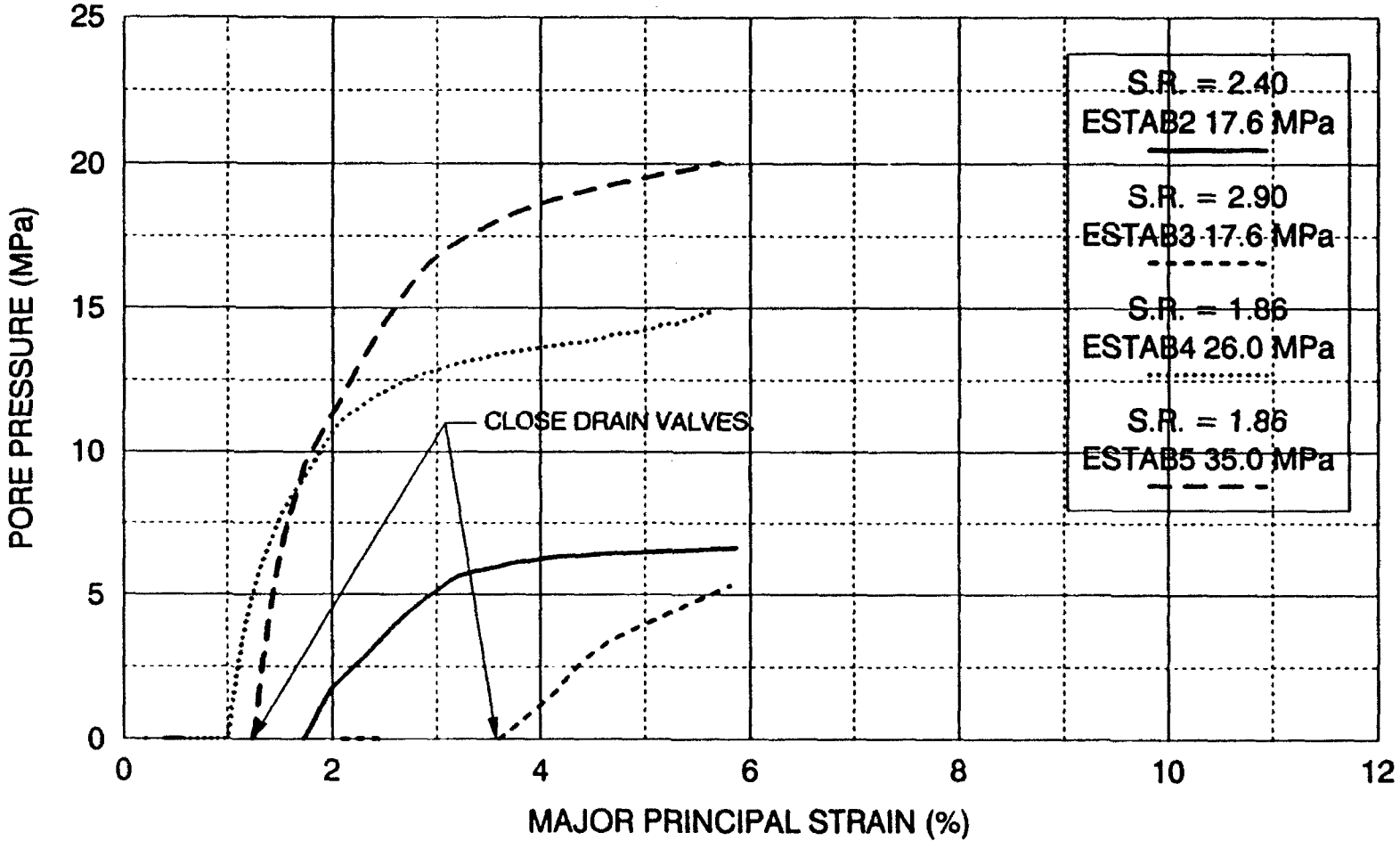

FIGURE 6-17 PORE PRESSURE
DRAINED-UNDRAINED EXTENSION STABILITY TESTS
DENSE CAMBRIA SAND

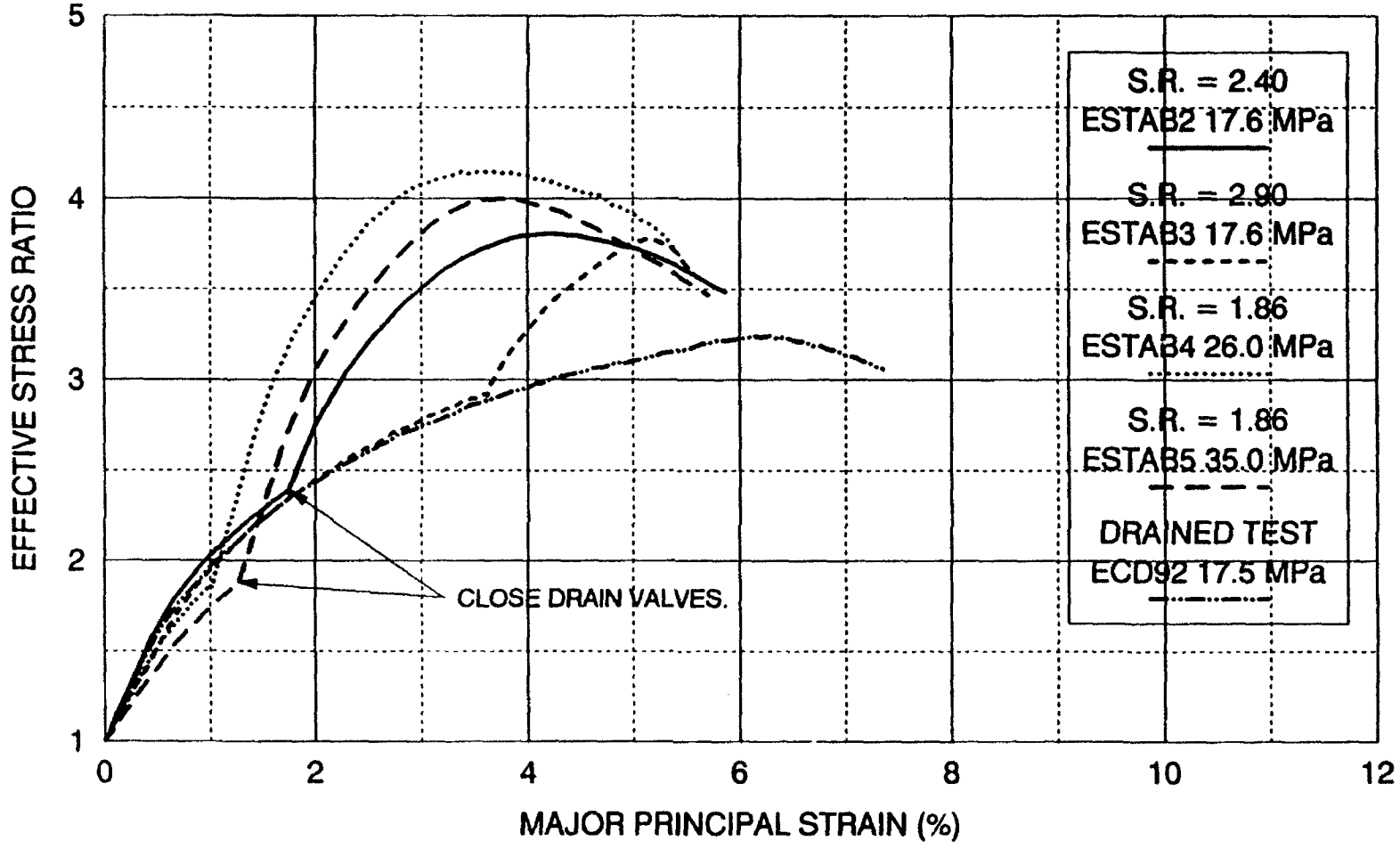

FIGURE 6-18 EFFECTIVE STRESS RATIO
DRAINED-UNDRAINED EXTENSION STABILITY TESTS
DENSE CAMBRIA SAND

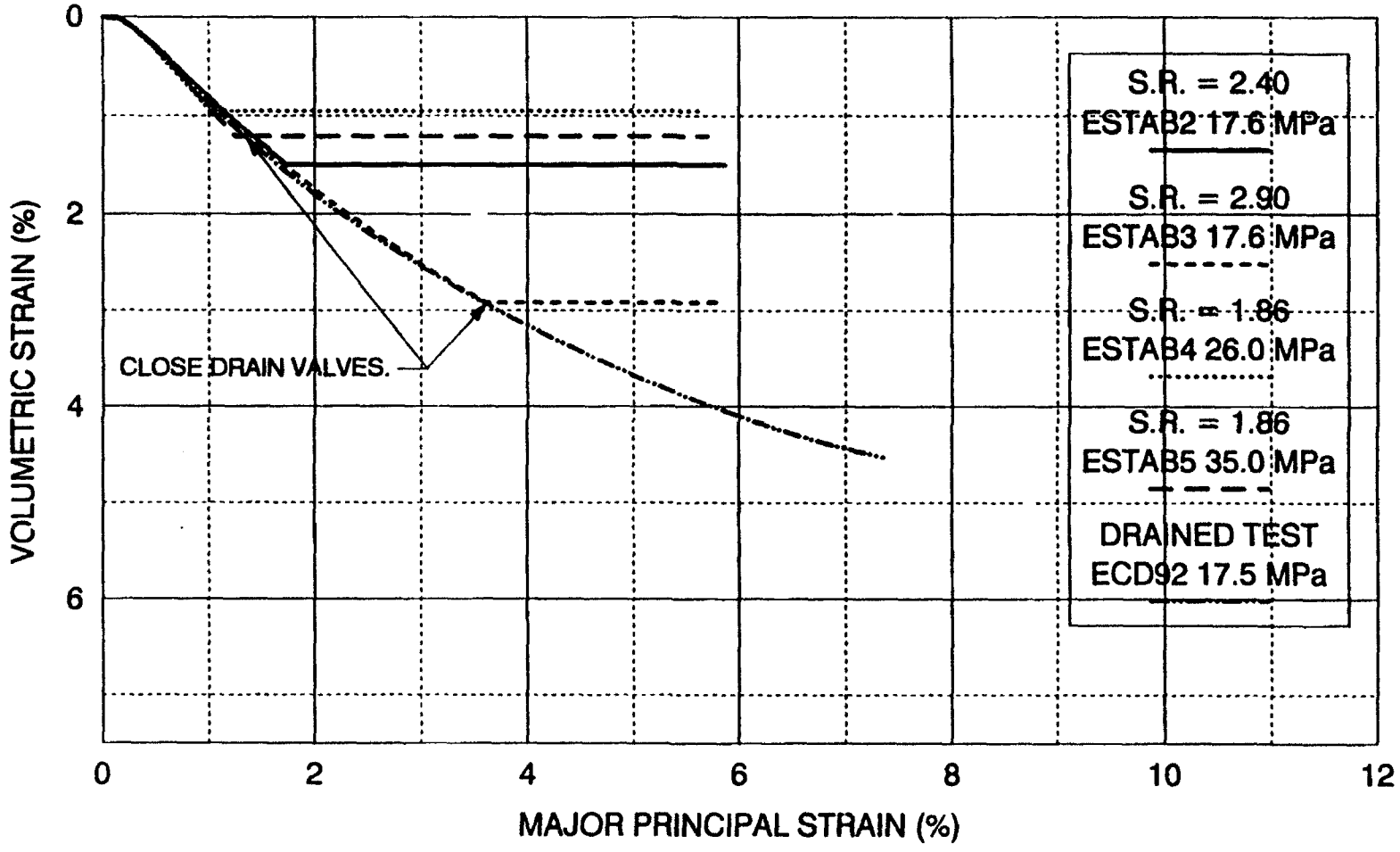

FIGURE 6-19 VOLUMETRIC STRAINS
DRAINED-UNDRAINED EXTENSION STABILITY TESTS
DENSE CAMBRIA SAND

failure is achieved. The volumetric strains are shown on Figure 6-19. This diagram indicates the different levels of shearing before undrained conditions are imposed, as well as the excellent repeatability of the test results. No volumetric strains occur after undrained conditions are imposed.

Two additional instability tests were performed with initial confining pressures of 26.0 and 35.0 MPa. The specimens in these two tests were both sheared under drained conditions to stress ratios of 1.86, before being turned undrained. This stress ratio corresponds to a stress state that is well outside the established instability region in triaxial extension. The computer control program maintained constant stress state at this condition. As with the analagous compression tests, prevented undrained volumetric creep caused the pore pressures to increase, moving the effective stress paths toward the instability region as shown on Figure 6-20. The deviator stresses were maintained at the proper stress level, until the proximity of the instability region was approached. When the stress states moved inside the instability region the deviator stresses could not be maintained, and the motors quickly achieved their maximum speeds. Shown on Figures 6-21 and 6-22 are the axial deformations plotted against time. The lower section of the curve represents the portion of the test corresponding to undrained creep with constant deviator stress, while the steeper section represents the axial deformations after instability is initiated. When the deformations depart from the creep line, the time of initial instability is established. The stress states corresponding to this time are shown on Figure 6-20, as triangular symbols. They fall essentially on the instability line previously established from the standard

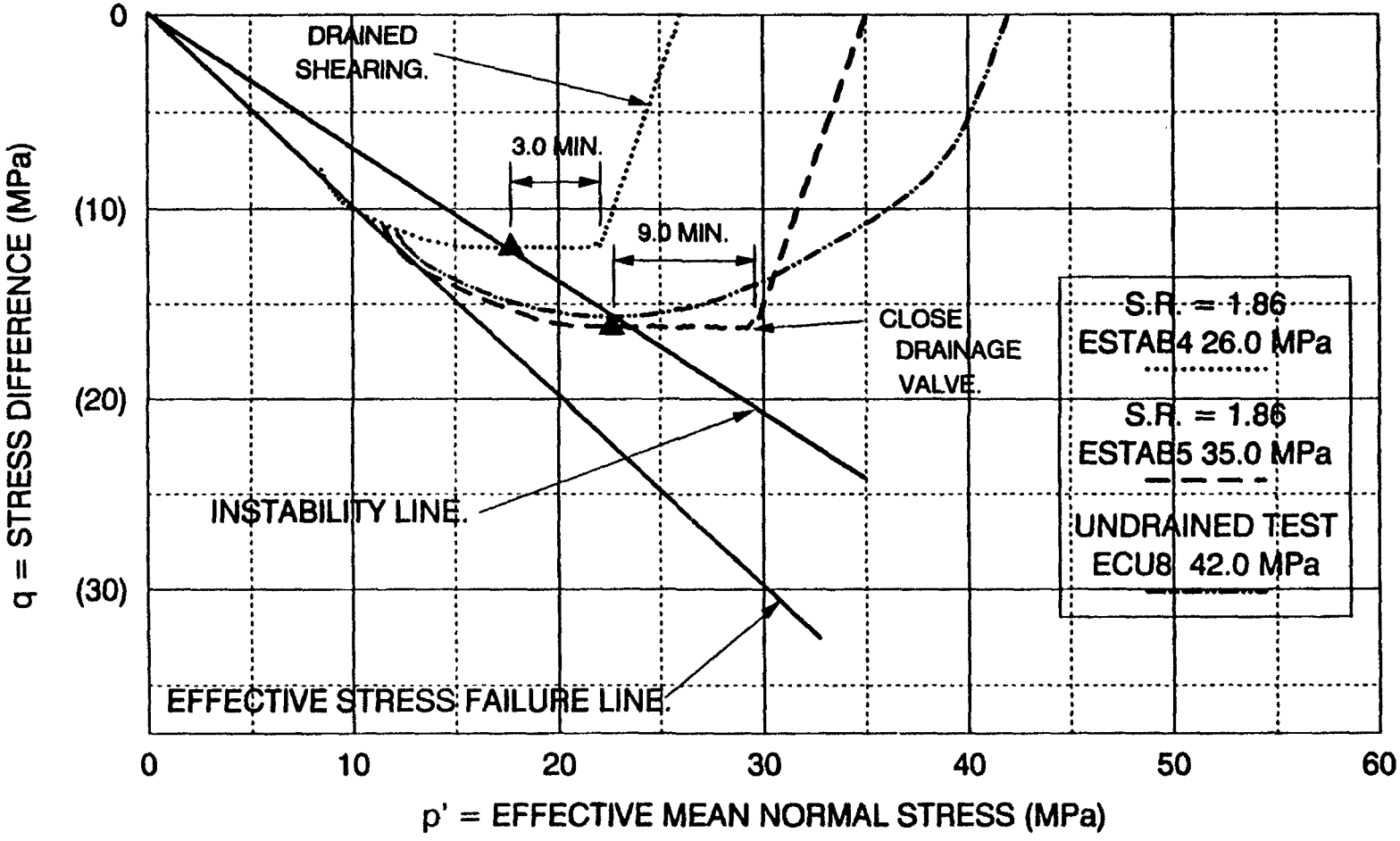

FIGURE 6-20 INSTABILITY TESTS CREEPING INTO INSTABILITY REGION, CAMBRIDGE p'-q DRAINED-UNDRAINED STABILITY EXTENSION TESTS DENSE CAMBRIA SAND

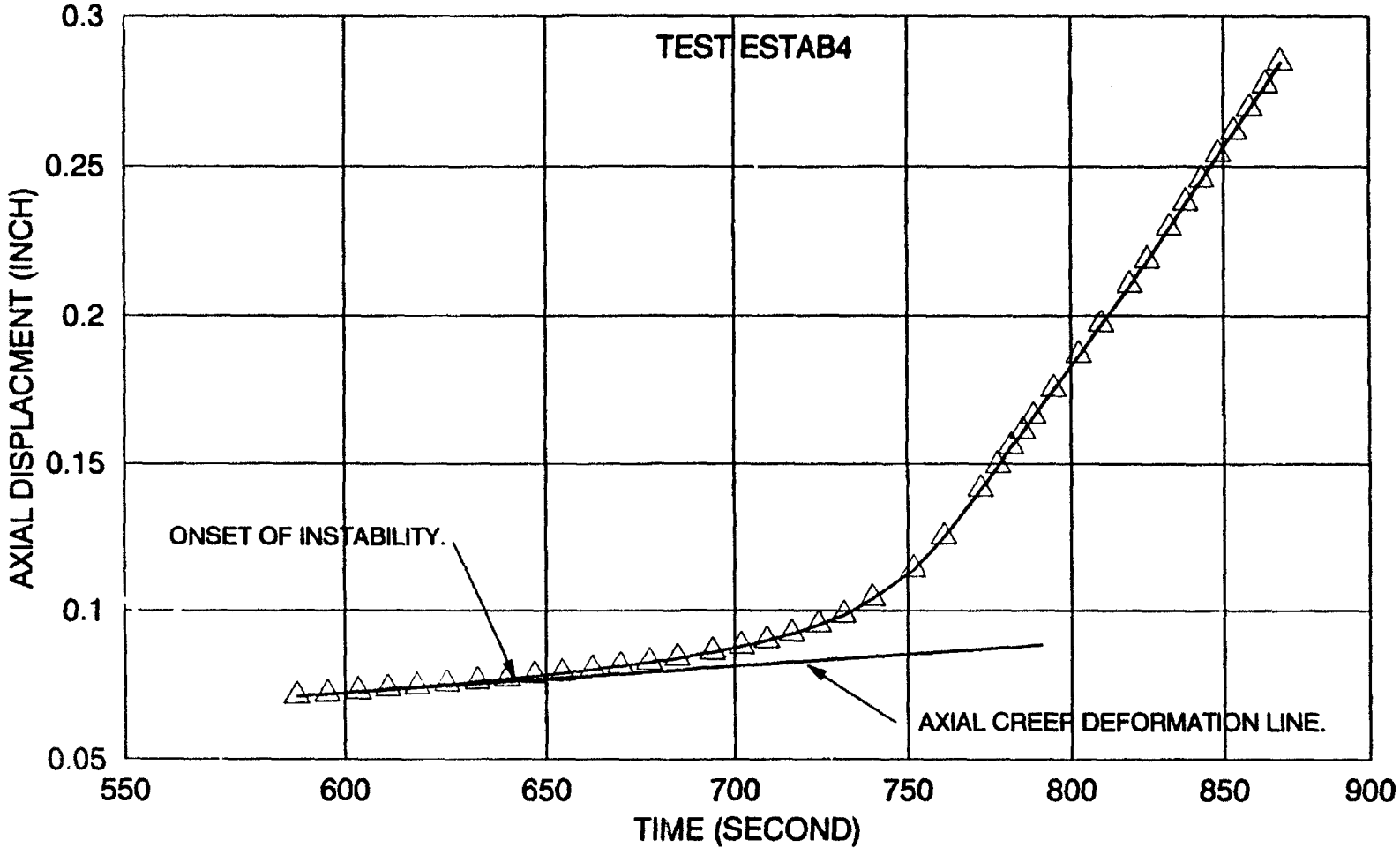

FIGURE 6-21 POINT OF INSTABILITY
DRAINED-UNDRAINED EXTENSION STABILITY TEST
DENSE CAMBRIA SAND

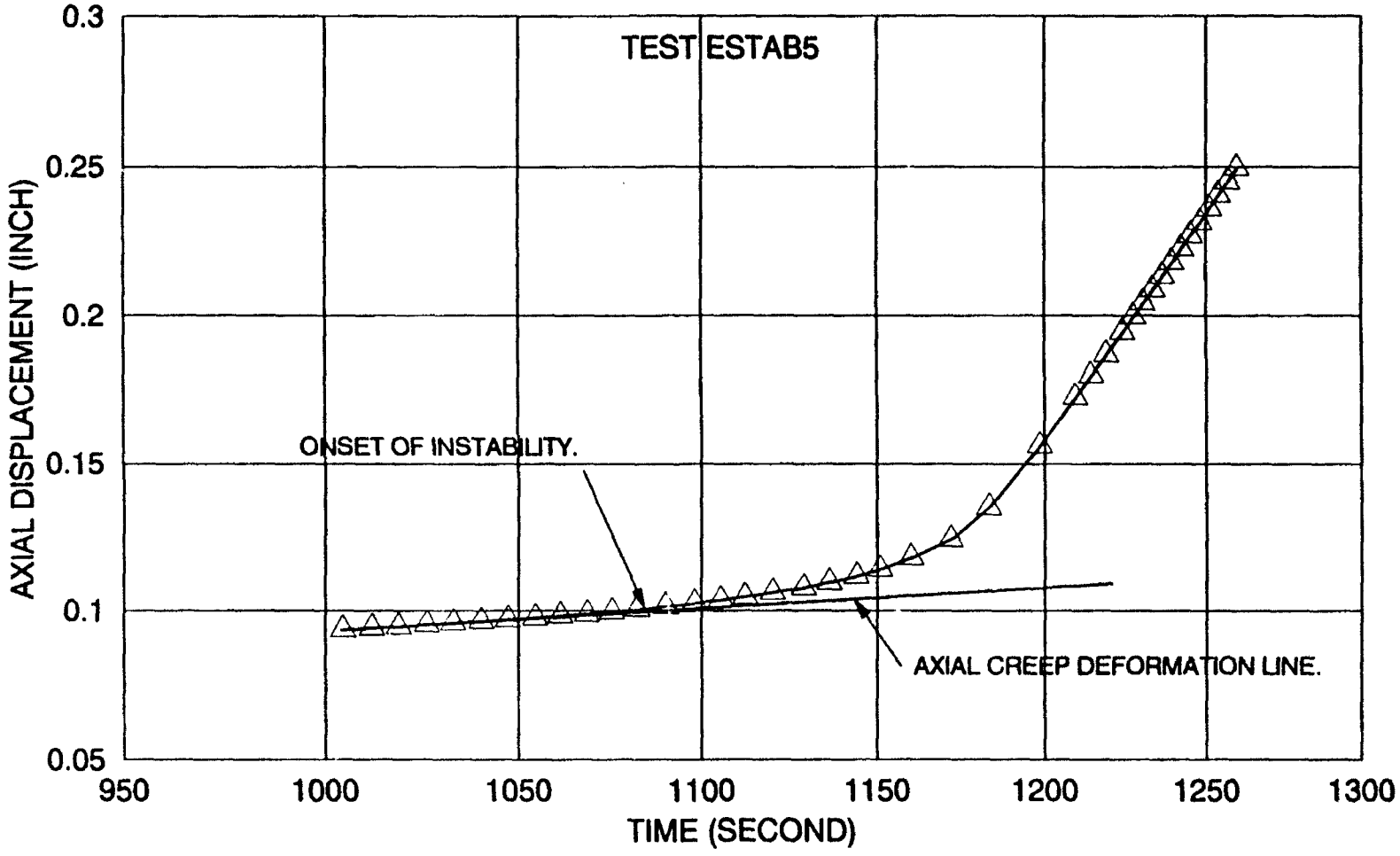

FIGURE 6-22 POINT OF INSTABILITY
DRAINED-UNDRAINED EXTENSION STABILITY TEST
DENSE CAMBRIA SAND

undrained extension tests. Therefore, the absolute location of the instability line in extension is experimentally confirmed. The time for the undrained creep to move the stress point to the instability region is also shown on the figure. These times appear to be larger in extension than in compression. This is due to less particle crushing in extension resulting in lower pore pressure generation. The effective stress paths of the instability tests are flatter in extension than compression. An effective stress path of standard undrained compression and extension tests are also shown on Figures 6-15 and 6-20. As exhibited in compression, the stress paths for the instability extension tests tend to follow the effective stress paths of the corresponding standard undrained extension tests, and these tend to be very flat in the extension instability region.

As was exhibited in the compression tests, the maximum effective stress ratios in extension tests indicate that tests undergoing substantial undrained creep had much higher magnitudes as shown on Figure 6-18 . The effective stress friction angle corresponding to the stress ratio of 4.14 is more than three degrees larger than the corresponding standard undrained extension tests. As was discussed for compression, these time effects associated with the undrained creep do not appear to affect the location of the instability line (Yamamuro and Lade, 1993b).

6.6 Discussion

The location of the instability regions for dense Cambria sand in both compression and extension have been established by performing high pressure

undrained tests. They are located between the effective stress failure line, and a line connecting the peak deviator stresses on the effective stress paths. The temporary instability regions also have been established by performing lower pressure undrained tests. It is located below the bottom of the wedge shaped instability region between two parallel horizontal lines at different stress magnitudes. The bottom of the instability region is the upper stress line, and it is represented by a stress path which rises up to a maximum deviator stress value from which it does not vary until after failure. The lower horizontal stress line represents an undrained stress path that exhibits overall compressive behavior, but dilates during the latter portion of the test. The deviator stress rises to a horizontal constant as it compresses, and then eventually dilatancy increases the deviator stress upward to effective stress failure.

Instability in dense Cambria sand at high pressures has been demonstrated by performing instability tests in both compression and extension. In these tests specimens are sheared under strain controlled, drained conditions to stress levels within the established instability regions. Then the specimens are turned undrained, by closure of the drainage valves, and the computer attempts to maintain constant deviator stresses. Pore pressures quickly generate in the specimen thus decreasing the deviator stresses. The specimens become unstable, and the computer controlled stepping motors cannot load the specimen quickly enough to maintain constant deviator stresses, and eventually they reach effective stress failure.

The location of the instability lines in compression and extension, as derived

above, has been directly proved by experiments. Tests similar to those just described above were performed in which the stress levels attained under stable drained conditions are well outside of the established instability region. After being turned undrained, pore pressures develop due to prevented volumetric creep, but the computer can easily keep the deviator stresses constant, indicating stability. However, as the effective stress paths move across to the location of the instability lines, the specimens become unstable with continued increasing pore pressures. Since the computer cannot maintain the stress level, the deviator stresses start decreasing, until failure is eventually reached.

Higher effective stress friction angles were exhibited in both compression and extension for tests which underwent significant amounts of undrained creep. The time effects associated with the undrained creep does not affect the location of the instability line.

CHAPTER 7 - THE B-VALUE, THE EFFECTIVE STRESS PRINCIPLE, AND STRAIN RATE EFFECTS AT HIGH CONFINING PRESSURES

7.1 Introduction

Skempton (1954) developed an expression for the increment in pore pressure in terms of the total stress changes, and the pore pressure coefficients B and A as shown by Equation 7.1.

$$\Delta u = B \cdot \Delta\sigma_3 + \bar{A} \cdot (\Delta\sigma_1 - \Delta\sigma_3) \qquad (7.1)$$

Δu - *change in pore pressure.*
B - *pore pressure coefficient B.*
$\Delta\sigma_3$ - *change in minor principal stress.*
$\bar{A}$ - *pore pressure coefficient A·B.*
$\Delta\sigma_1$ - *change in major principal stress.*

This expression can be reduced in form by assuming a stress difference of zero, and this version is commonly used in soil testing to evaluate the level of saturation within a specimen prior to shearing as shown by Equation 7.2.

$$B = \frac{\Delta u}{\Delta\sigma_{cell}} \qquad (7.2)$$

$\Delta\sigma_{cell}$ - *change in cell pressure.*

At low confining pressures, the B-value is close to unity when the specimen is fully saturated, and thus the readily measured B-value can be used to infer the degree of saturation. However, at high confining pressures, the B-value is much less than

unity due to decreasing soil compressibility in the soil skeleton, and this reduces the pore pressure response, despite full saturation

The B-value in Equation 7.1 can also be represented by the following equation from Lade and Hernandez (1977).

$$B = \frac{(m_v + \frac{f_m}{V_o})}{(m_v + \frac{f_m}{V_o}) + n \cdot S \cdot C_w + n \cdot \frac{1-S}{u_2} + \frac{f_s}{V_o}} \qquad (7.3)$$

n - soil porosity.
C_w - compressibility of water ($4.75X10^{-5}$ 1/KPa).
S - degree of saturation of soil.
u_2 - absolute pressure in pore fluid after application of cell pressure increment.
m_v - volumetric compressibility of soil skeleton.
V_o - total volume of specimen.
f_s - volumetric flexibility of pore pressure measuring syster
f_m - volumetric flexibility of membrane around specimen.

The term in the parentheses in Equation 7.3 represents the slope of the measured volumetric strain-effective confining pressure curve (Lade and Hernandez, 1977). All other parameters are easily derivable from the particular testing conditions and equipment. Using Equation 7.3, the degree of saturation may be ascertained for a measured B-value.

The first part of this chapter examines the determination and interpretation of B-values for a granular material at confining pressures up to 69 MPa (Yamamuro and Lade, 1993c).

The second part of this chapter examines the factors that affect the uniqueness of the effective stress path in high pressure undrained tests on soil based upon the effective stress principle (Yamamuro and Lade, 1992a), which

states that the effective stress in the soil skeleton equals the total stress minus the pore pressure as shown by Equation 7.4.

$$\sigma_{effective} = \sigma_{total} - u \tag{7.4}$$

$\sigma_{effective}$ = effective stress.
σ_{total} = total stress.
u = pore pressure.

This expression indicates that an undrained test on a fully saturated soil tested at low confining pressures, where B is close to unity, produces an effective stress path that is independent of the externally imposed total stress path. However, since the value of B decreases significantly with increasing confining pressure, Skempton's equation would indicate that the effective stress path consequently may be affected by the direction of the total stress path. This effect would be expected to be most pronounced at high confining pressures.

The third part of this chapter examines how the variation in strain rate on cohesionless soils at high confining pressures affect soil instability and general soil behavior (Yamamuro and Lade, 1993b).

7.2 Soil and Testing Procedures

Cambria sand was used in this investigation and specimens were prepared as described in Section 3.3 with a height-to-diameter ratio of 2.5. The B-value was checked for each specimen at low confining pressures through the pressure transducer on the volume change measuring device before the test commenced, and a minimum value of 0.979 was obtained. This B-value corresponds to a degree of saturation of approximately 99.9%. As will be further discussed, this

degree of saturation was obtained using Equation 7.3 with the known specimen and equipment parameters.

As was discussed in Section 3.1 and 3.2, the cell pressure in the high pressure triaxial system is generated by a complex mechanically-linked system. Therefore, the application of cell pressure cannot be instantaneous, but tends to occur along a ramp. The importance of this condition is discussed later. The cell and pore pressures at high cell pressures are measured by the two identical pore pressure transducers attached close to the base of the triaxial cell.

7.3 Tests to Determine B-Values at High Confining Pressure

The tests to determine B-values at high pressures were performed during isotropic compression at ten different levels of effective confining pressures up to a maximum of 69.0 MPa. Two experiments with essentially the same results were performed. The results of one of these experiments is shown on Figure 7-1.

When the confining pressure desired for a B-value test had been reached, the cell pressure was held constant for a minimum of 30 minutes to allow as much of the creep in the soil to be eliminated as possible. The drainage valves were then closed, and the confining pressure was increased by 0.75 MPa above its initial value, and held constant for 20 minutes, while the pore pressure was continuously monitored. The confining pressure was then reduced to its original value, and the drainage valves were opened. After this B-value test, the confining pressure was raised to the next level at which a B-value test was desired. Following the last test at 69.0 MPa, the confining pressure was reduced to zero.

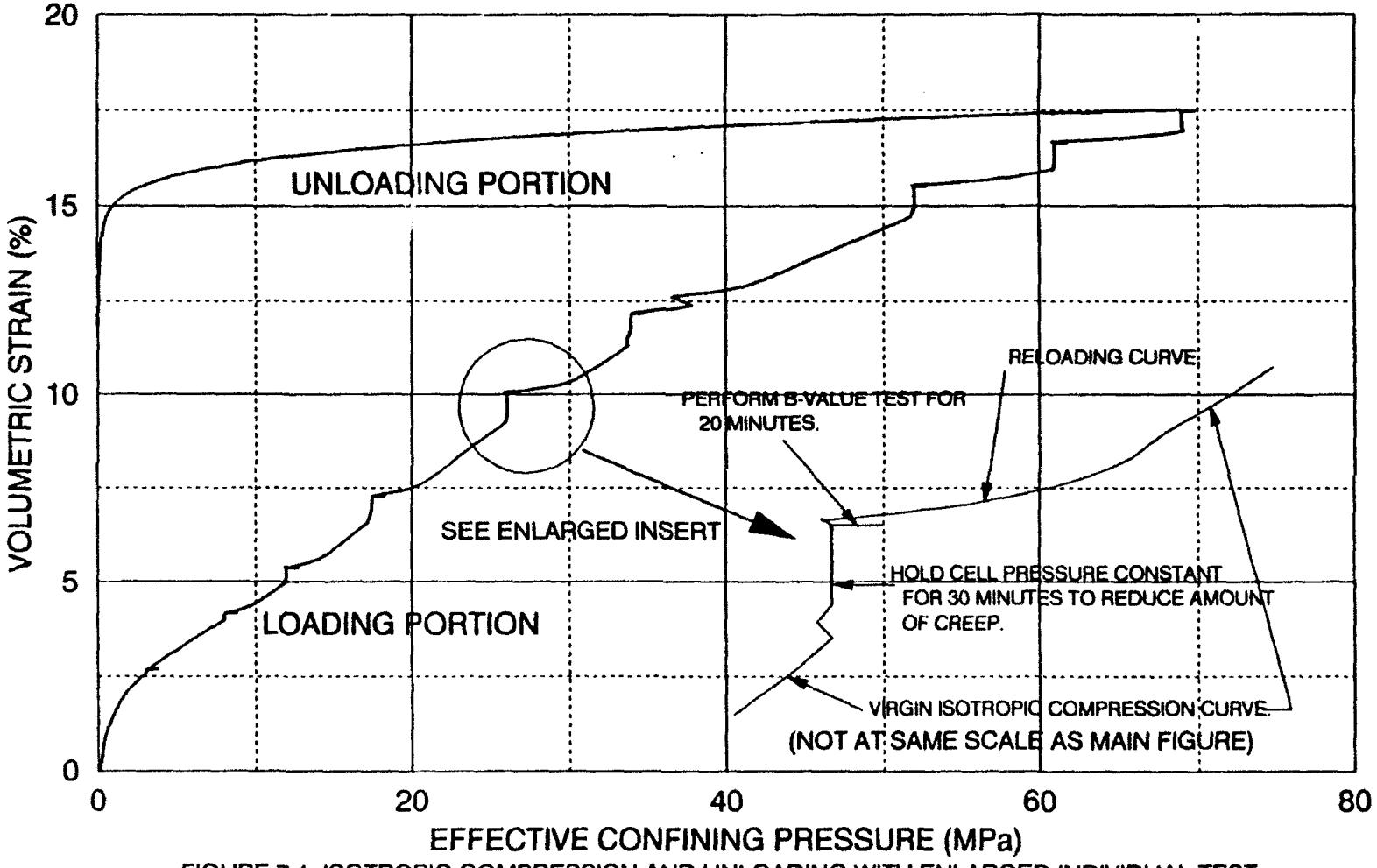

FIGURE 7-1 ISOTROPIC COMPRESSION AND UNLOADING WITH ENLARGED INDIVIDUAL TEST LOCATIONS OF B-VALUE TESTS
DENSE CAMBRIA SAND

As indicated on the insert in Figure 7-1, the B-value tests were actually performed for conditions where the soil undergoes reloading rather than virgin compression. Thus an elastic response of the soil would be expected during the B-value tests.

The experimental B-values from the tests were calculated from the Skempton pore pressure equation (Equation 7.1) in its reduced form for zero stress difference (Equation 7.2).

Application of the increment of cell pressure (0.75 MPa) took approximately 140 seconds, as indicated on Figure 7-2. The initial conditions for the B-value determination corresponded to the values of cell pressure and pore pressure obtained during the very beginning of the test immediately following the closure of the drainage valves. Considerable amounts of volumetric soil creep are produced under high confining pressures, due to particle breakage and rearranging. B-values measured during the initial stages of the test are typically greater than unity. The B-value decreases below unity during the period of application of the increment in confining pressure. Due to continued creep from particle crushing during the 20 minute period where the cell pressure is held constant, the B-value again increases to values substantially above unity. Figure 7-3 shows that B-values as high as 3.8 were obtained after 20 minutes for the highest confining pressure of 69.0 MPa. To obtain the B-value corresponding to zero elapsed time for a particular effective confining pressure, the creep response curve is projected back to the start of the test as indicated on Figure 7-2. The variation of these instantaneous B-values with effective confining pressure are also

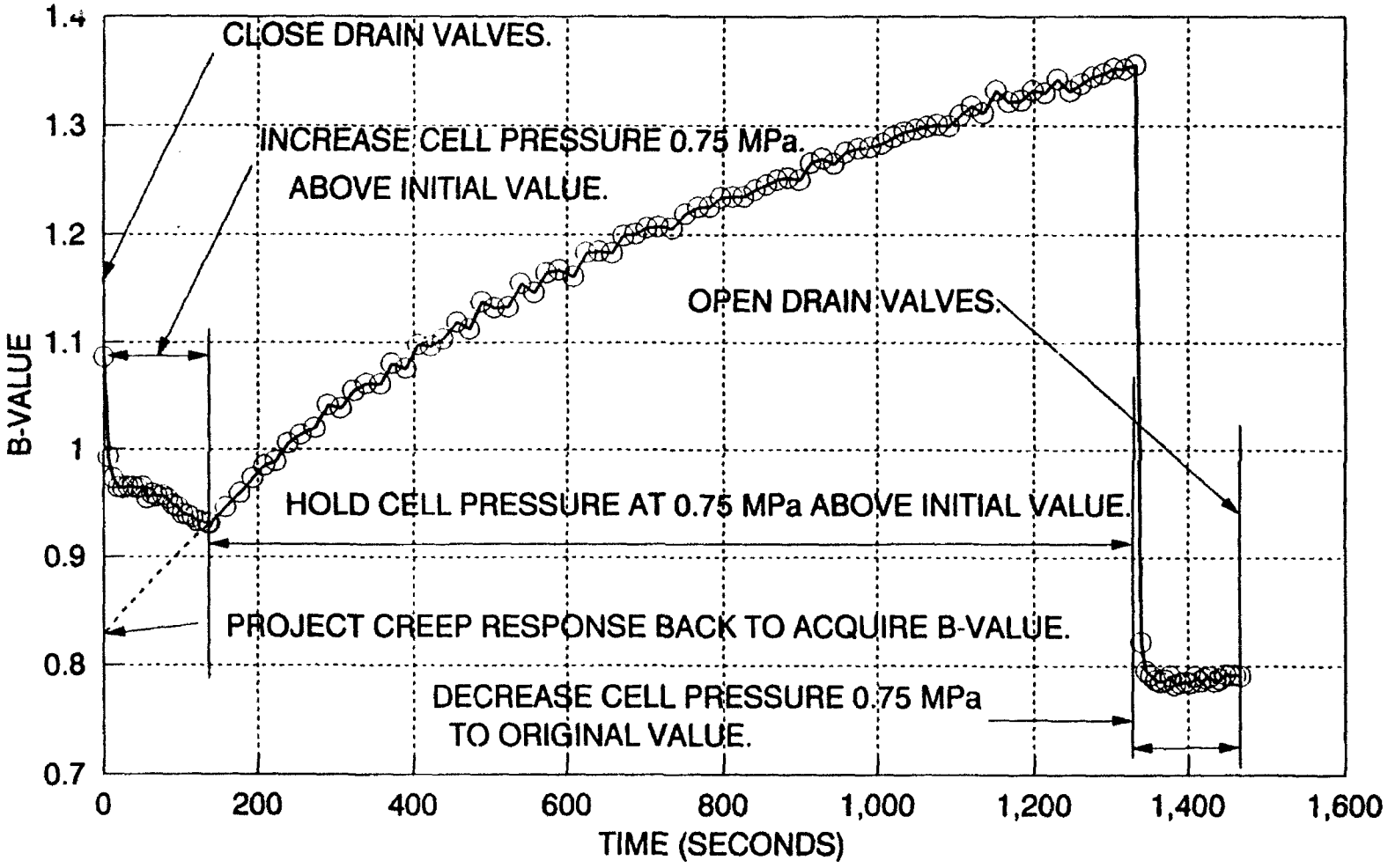

FIGURE 7-2 VARIATION IN B-VALUES DURING INDIVIDUAL B-VALUE TEST
AT 12.0 MPa EFFECTIVE CONFINING PRESSURE
DENSE CAMBRIA SAND

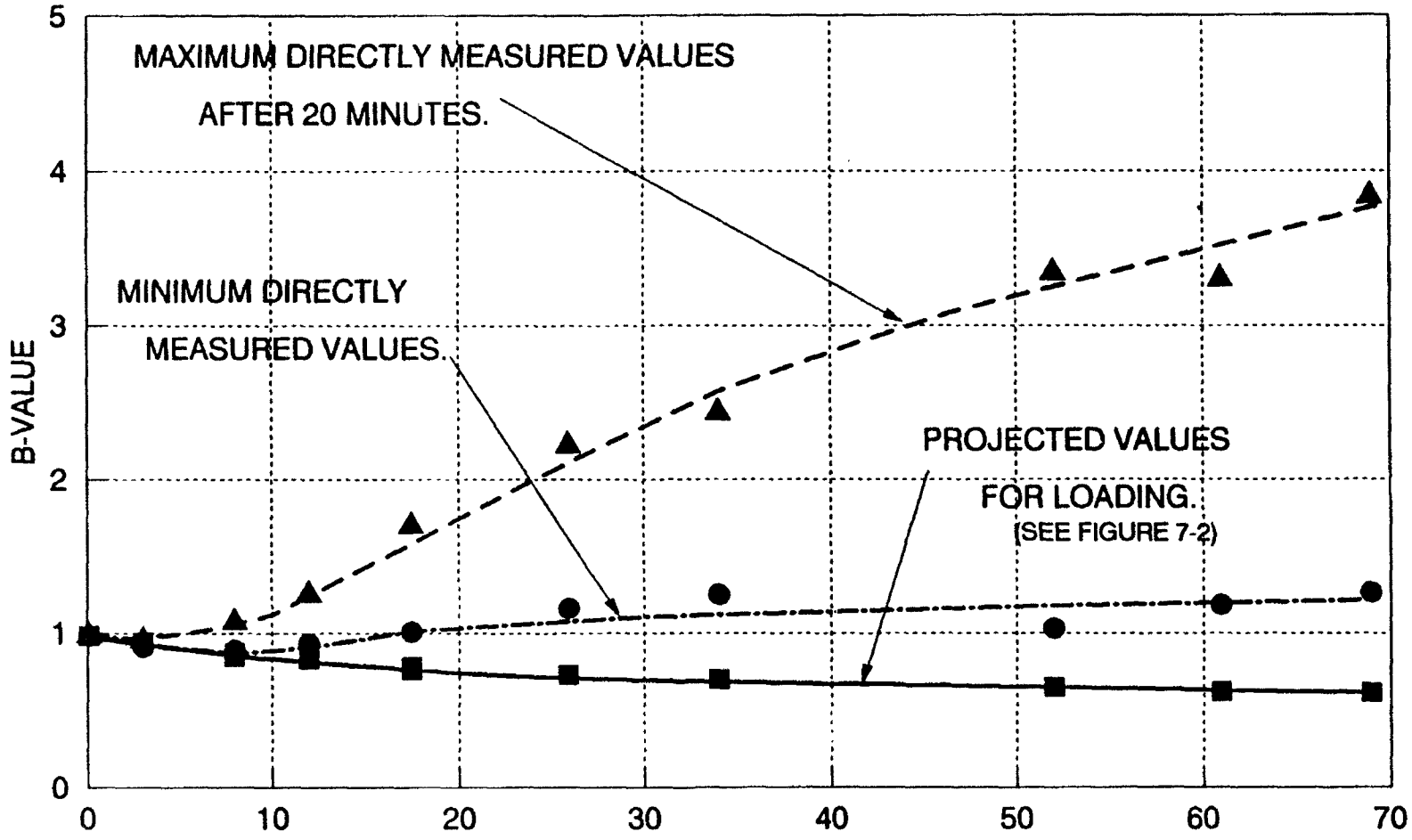

FIGURE 7-3 VARIATION OF MEASURED AND PROJECTED B-VALUES
OVER DIFFERENT CONFINING PRESSURES
DENSE CAMBRIA SAND

shown on Figure 7-3. These values are free of creep effects, and should be predictable from considerations involving time-independent elastic behavior. Predictions are discussed later.

The B-values for the unloading portion shown in Figure 7-2 were obtained directly from the pore pressure response in the last few time increments at the end of the test. Since the soil was being unloaded, its tendency to creep was much reduced, and the calculated B-values for unloading need no adjustment.

The experimental reloading B-values range from 0.98 at an effective confining pressure of 0.07 MPa to approximately 0.61 at 69.0 MPa as shown on Figure 7-4. During unloading, the measured B-values range between 0.98 at 0.07 MPa to approximately 0.47 at 69.0 MPa. The experimental B-values corresponding to reloading and unloading appear to be close together at low effective confining pressures and deviate at higher pressures. The difference between the curves is explained based on the fact that at higher pressures the soil compressibility is very small, and the relative difference between soil compressibilities on the virgin curve, the reloading curve, and the unloading curve becomes larger as shown on Figure 7-5. The peculiar dip on the soil compressibility curve for virgin loading is considered to be the result of the fact that the Cambria sand used in all of the tests is composed of many mineral components, and it was observed that the weaker components (sedimentary lithic grains) crush earlier than the harder components (quartz-feldspar grains). This effect has been observed in th isotropic consolidation curves in all tests using Cambria sand, while it is not observed in tests using single mineral sands, such as quartz.

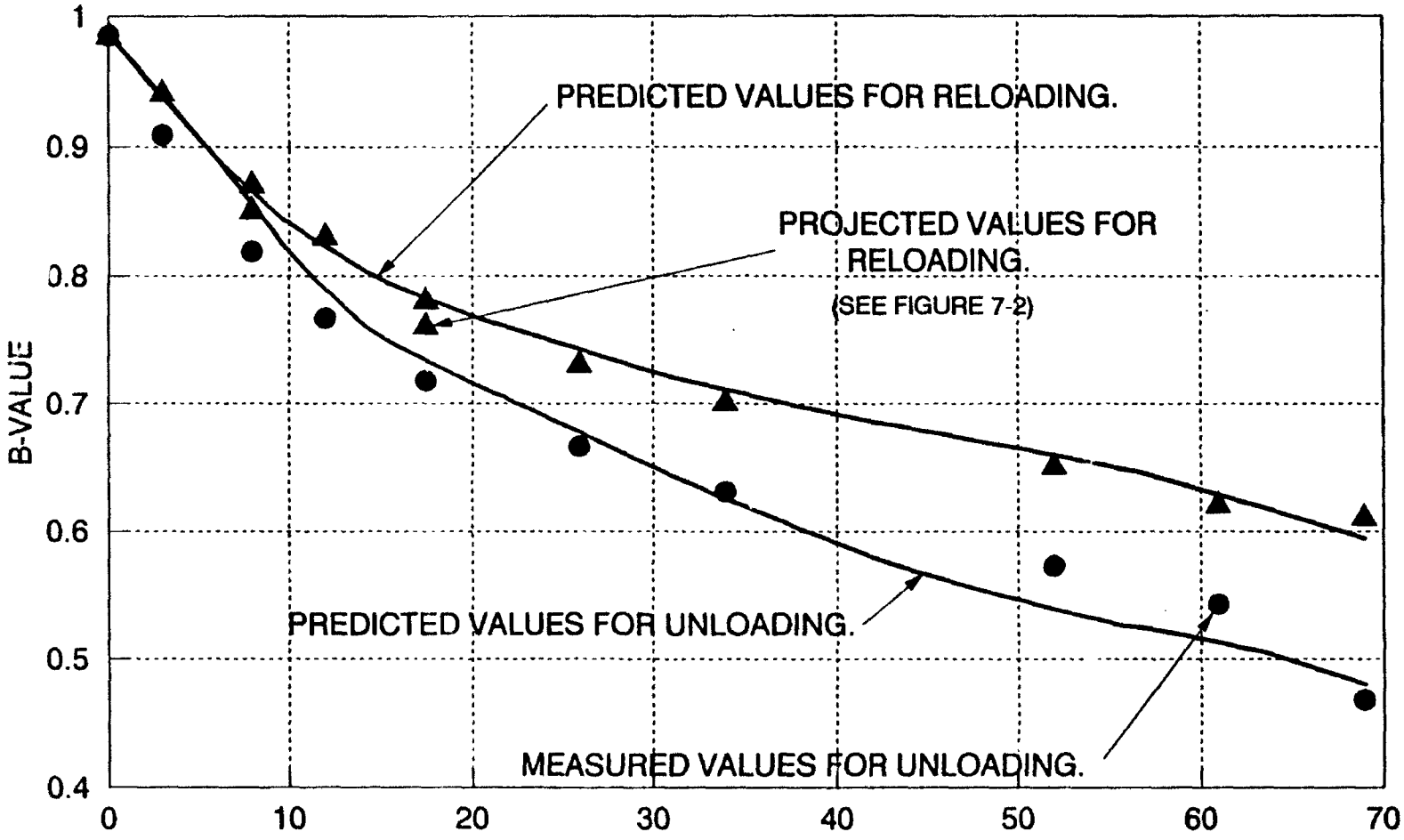

FIGURE 7-4 EXPERIMENTAL & PREDICTED B-VALUES
FOR RELOADING AND UNLOADING CONDITIONS
DENSE CAMBRIA SAND

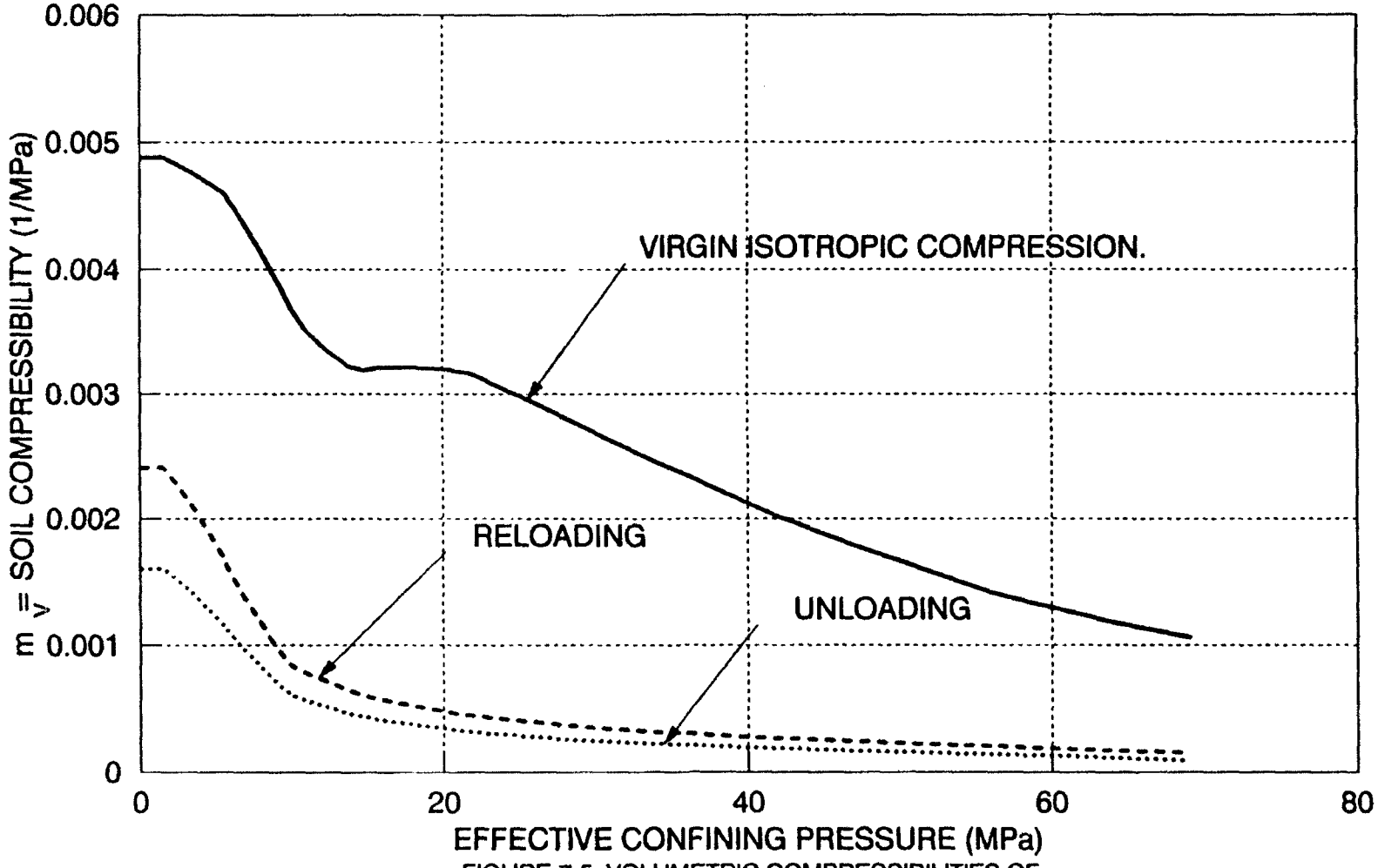

FIGURE 7-5 VOLUMETRIC COMPRESSIBILITIES OF VIRGIN ISOTROPIC COMPRESSION, RELOADING AND UNLOADING CONDITIONS FOR DENSE CAMBRIA SAND

7.4 B-Value Predictions

For the initial B-value test performed at an effective confining pressure of 0.07 MPa, the pore pressure was measured through a volume change measuring device, and membrane penetration effects were present. Therefore, all the terms in Equation 7.3 had non-zero values. Based upon determination of all the appropriate values, and the measured minimum B-value of 0.979, the degree of saturation of the soil specimen was calculated to be in excess of 99.9%. Therefore, the specimen was assumed to be fully saturated for B-value tests performed at higher pressures.

The pore pressures obtained in the high pressure tests were measured by a pressure transducer mounted directly on the stainless steel base of the triaxial cell. The pore pressure measuring system flexibility was therefore negligible.

The term in the parenthesis in Equation 7.3, which is represented by the slope of the volumetric strain-confining pressure curve, includes the effect of membrane penetration on the B-value (Lade and Hernandez, 1977). No further correction to the B-value is necessary. Additionally, extensive high pressure testing experience with the equipment and the Cambria sand has shown that membrane penetration effects are negligible at confining pressures beyond approximately 2.0 MPa (Chamieh, 1990), as was discussed in Chapter 3. Therefore, most of the terms in Equation 7.3 drop out, and it reduces to the following much simpler expression (Skempton, 1954).

$$B = \frac{m_v}{m_v + n \cdot C_w} \qquad (7.5)$$

in which only the soil skeleton volumetric compressibility, m_v, the soil porosity, n, and the compressibility of the pore water C_w, affect the B-value. All B-values at effective confining pressures above 2.0 MPa were calculated using Equation 7.5.

Appropriate values of m_v were determined from Figure 7-5 for calculation of the B-values shown on Figure 7-4. It may be seen from Figure 7-4 that the predicted B-values correspond very well with those experimentally measured in the entire range of effective confining pressures. Thus, it is possible to evaluate the B-values at high confining pressures using the procedure proposed here.

7.5 The Effective Stress Principle at High Pressures

The next step in the investigation was to determine the effect of lower B-values and total stress paths on the effective stress path during undrained shearing. Three undrained triaxial compression tests were performed with three different total stress paths as shown on Figure 7-6 in the upper left-hand corner. The tests were all initially isotropically consolidated to 34.0 MPa prior to shearing at which the B-value was earlier determined to be 0.7 for a fully saturated specimen. For this magnitude of B-value, the pore pressure equation developed by Skempton (Equation 7.1) suggests that the effective stress path is influenced by the externally imposed total stress path as indicated in Figure 7-6. The two tests characterized by total stress paths with constant cell pressure and constant total mean normal stress were performed with an axial deformation rate of 2.54

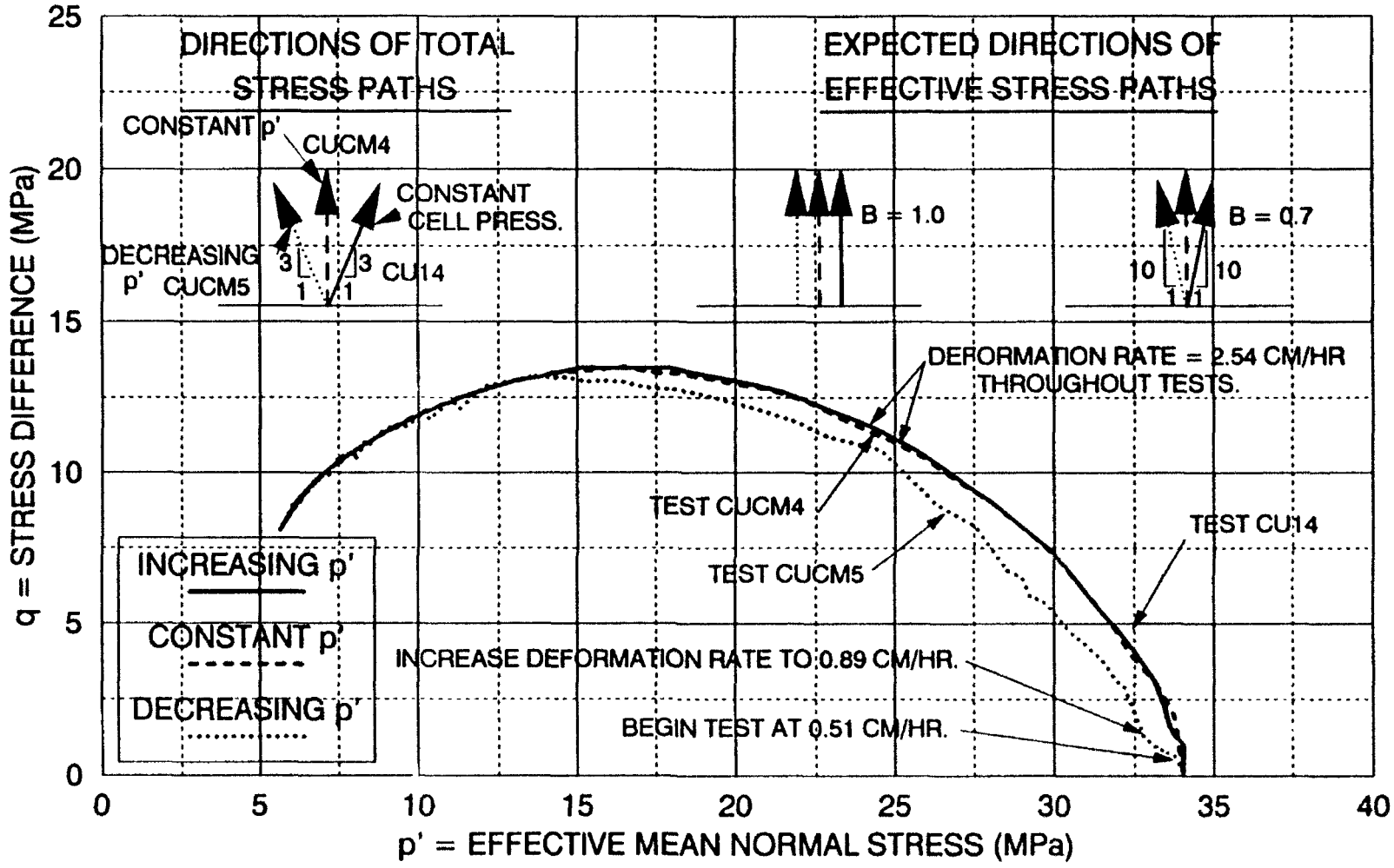

FIGURE 7-6 EFFECTIVE STRESS PATHS, CAMBRIDGE p'-q, FOR DIFFERENT TOTAL STRESS PATHS, AND DIFFERENT EXPECTED DIRECTIONS AT 34.0 MPa CONFINING PRESSURE DENSE CAMBRIA SAND

centimeters per hour (1.0 inch per hour). No detectable difference in effective stress paths beyond normal experimental scatter was observed. The reason for this is believed to be related to the fact that after the onset of shearing after isotropic compression to high pressures, the soil is initially in a volumetrically collapsing or rapidly densifying state, with large amounts of particle crushing and rearranging occurring from small changes in stress. The pore pressures generated from this condition accumulate rapidly, and appear to be similar for different total stress paths. The differences in increments of total confining pressure, between the different total stress paths do not seem to influence the rate of pore pressure generation and hence, the effective stress path. Previous experience from drained high pressure triaxial compression tests indicate that the rate of densification decreases with increasing axial strain, but continues well past the maximum stress difference. In the undrained triaxial compression tests performed here the peak stress difference value is reached at about 2 percent axial strain. Therefore, it is possible that the effect of the lower B-value on the effective stress path is probably hidden beyond the peak stress difference, where it is not easily detected.

The third total stress path with decreasing mean normal stress was performed, but starting at an axial deformation rate of 0.51 centimeters per hour (0.20 inch per hour). The reason to decrease the deformation rate was to allow the computer control adequate response time to decrease the cell pressure, which is required to be rapid in the test requiring a decrease in mean normal stress at the onset of shearing. Shortly after the start of shearing it was noticed that the effective stress path was rapidly departing from the two previous effective stress

paths. At this time the axial strain rate was increased to 0.89 centimeters per hour (0.35 inch per hour). As a consequence, the effective stress path changed direction, and moved upward as shown at the bottom of Figure 7-6. At high pressures volumetric soil creep caused by particle crushing and skeleton collapse is apparently a major factor in the generation of pore pressures. Axial strain rate during loading therefore plays a major role in the soil response, and the subsequent effective stress path obtained from undrained tests. As previously discussed in Chapter 5, both undrained and drained tests exhibit effects from creep between the isotropic consolidation and the shearing phases. The short time to lower the piston into contact with the specimen allows volumetric creep. This buffers the initial pore pressure response of the specimen. It creates a temporary elastic response in the specimen, which in turn causes the effective stress path in undrained tests to temporarily stray toward the total stress path. The effective stress path quickly returns to the normal undrained stress path as soon as pore pressures start to develop.

To study the influence of B-value and total stress path on the effective stress path in undrained tests, it is necessary to avoid volumetric soil creep associated with particle crushing at high pressures. Tests should be performed at lower effective confining pressures. However, at low pressures the deviation of the B-value from unity is relatively small. Therefore, the magnitude of the B-value and the direction of the total stress path would be expected to have little effect on the effective stress path.

7.6 Previous Studies of Strain Rate Effects in Cohesionless Soils

Several investigators have studied the effect of strain rate on the behavior of cohesionless soils. Casagrande and Shannon (1948) apparently were the first to study the effect of strain rate on the strength of soil. They performed drained triaxial compression tests (vacuum triaxial) on dense sand at low confining pressures (0.3 to 0.9 kg/cm^2) with times to failure varying between 0.03 and 2,100 seconds. They found that the compressive strength increased by about 10%, but the initial modulus of deformation did not change. Seed and Lundgren (1954) performed drained and undrained tests on dense sand at low confining pressures (2.0 kg/cm^2) with times to failure varying between 0.02 and 900 seconds. They discovered that drained tests on saturated sands at high strain rates did not have sufficient time to adequately drain, and consequently approached undrained conditions. This resulted in compressive strength increases of 15 to 20 percent, as well as increases in the initial modulus of deformation. This behavior may be related to generation of negative pore pressures resulting from a tendency of the sand to dilate. Nash and Dixon (1961) performed undrained tests on sand at low consolidation pressures (0.1 kg/cm^2) using strain rates varying from 2 percent per minute to 8,000 percent per minute. Their results showed decreasing maximum deviator stresses and lower moduli of deformation with increasing strain rates. Whitman and Healy (1962) performed drained (vacuum triaxial) and undrained tests on dense and loose sands at low confining pressures (0.7 kg/cm^2) with times to failure varying from 0.005 to 300 seconds. At high strain rates and drained conditions they found that the compressive strength increased about 10 percent.

However, at lower strain rates and drained conditions, they found that the compressive strengths actually decreased slightly with increasing strain rate. The compressive strength essentially did not vary with strain rate in their undrained tests. Lee, et al. (1969) performed drained (dry) and undrained tests on dense and loose sands at low to moderate confining pressures (1.0 to 15 kg/cm^2) with strain rates varying from 0.018 percent per minute to 15,000 percent per minute. Their drained compressive strengths increased up to 20 percent for the higher confining pressures, and the modulus of deformation also increased with increasing strain rate. They also found that the compressive strength increased in their undrained tests, but their method of performing the undrained tests leaves their results open to interpretation.

As can be deduced from the above review of results from prior investigations, there appear to be contradictory opinions regarding effects of strain rate on the behavior of cohesionless soils. Most of the drained compression tests were performed dry, which results in negligible development of pore pressures during transient loading, but this technique does not yield information about volume changes in the soil. This information would seem critical to determine the basic mechanisms of strain rate effects. In addition, all but a few tests performed by Lee, et al. (1969) were conducted at low confining pressures, where the effects of dilatancy, small changes in void ratio, and small differences in effective confining pressure can create sufficient scatter in the test results to disguise the true effects of strain rate in the behavior of cohesionless soil.

Measuring volumetric strains on saturated specimens at transient strain rates

centimeters per hour (1.0 inch per hour). No detectable difference in effective stress paths beyond normal experimental scatter was observed. The reason for this is believed to be related to the fact that after the onset of shearing after isotropic compression to high pressures, the soil is initially in a volumetrically collapsing or rapidly densifying state, with large amounts of particle crushing and rearranging occurring from small changes in stress. The pore pressures generated from this condition accumulate rapidly, and appear to be similar for different total stress paths. The differences in increments of total confining pressure, between the different total stress paths do not seem to influence the rate of pore pressure generation and hence, the effective stress path. Previous experience from drained high pressure triaxial compression tests indicate that the rate of densification decreases with increasing axial strain, but continues well past the maximum stress difference. In the undrained triaxial compression tests performed here the peak stress difference value is reached at about 2 percent axial strain. Therefore, it is possible that the effect of the lower B-value on the effective stress path is probably hidden beyond the peak stress difference, where it is not easily detected.

The third total stress path with decreasing mean normal stress was performed, but starting at an axial deformation rate of 0.51 centimeters per hour (0.20 inch per hour). The reason to decrease the deformation rate was to allow the computer control adequate response time to decrease the cell pressure, which is required to be rapid in the test requiring a decrease in mean normal stress at the onset of shearing. Shortly after the start of shearing it was noticed that the effective stress path was rapidly departing from the two previous effective stress

paths. At this time the axial strain rate was increased to 0.89 centimeters per hour (0.35 inch per hour). As a consequence, the effective stress path changed direction, and moved upward as shown at the bottom of Figure 7-6. At high pressures volumetric soil creep caused by particle crushing and skeleton collapse is apparently a major factor in the generation of pore pressures. Axial strain rate during loading therefore plays a major role in the soil response, and the subsequent effective stress path obtained from undrained tests. As previously discussed in Chapter 5, both undrained and drained tests exhibit effects from creep between the isotropic consolidation and the shearing phases. The short time to lower the piston into contact with the specimen allows volumetric creep. This buffers the initial pore pressure response of the specimen. It creates a temporary elastic response in the specimen, which in turn causes the effective stress path in undrained tests to temporarily stray toward the total stress path. The effective stress path quickly returns to the normal undrained stress path as soon as pore pressures start to develop.

To study the influence of B-value and total stress path on the effective stress path in undrained tests, it is necessary to avoid volumetric soil creep associated with particle crushing at high pressures. Tests should be performed at lower effective confining pressures. However, at low pressures the deviation of the B-value from unity is relatively small. Therefore, the magnitude of the B-value and the direction of the total stress path would be expected to have little effect on the effective stress path.

would be impossible. The experimental program presented here concentrated on low to moderately fast strain rates normally used in static testing, where conditions permit better control and measurement of all soil parameters. The strain rates selected for this study fall in the low end of the ranges previously studied. Employing high confining pressures was necessary to achieve the instability conditions (requiring volume compression in dense sands), but also has the benefit of providing results with a high degree of consistency and repeatability. These qualities are necessary to carefully study quantities that may not show easily measurable differences, as encountered in studying strain rate effects in cohesionless soils.

7.7 Strain Rate Effects in Undrained Triaxial Compression Tests

To study the effects of strain rate on the location of the instability line, seven undrained triaxial compression tests were performed. All specimens were isotropically consolidated to an effective confining pressure of 34.0 MPa and allowed to remain at this pressure for 20 minutes before the drainage valves were closed and shearing begun. The total confining pressure was maintained constant throughout each test. Shearing was performed at seven different strain rates varying from a lower value of 0.0042 percent per minute to the highest value of 0.74 percent per minute. All except one specimen was sheared beyond failure as defined by the maximum effective principal stress ratio. The tests performed at strain rates of 0.0042 and 0.0045 percent per minute aborted after 18 and 58 hours of shearing (4.4% and 14.7% axial strain), respectively, due to technical

limitations of the equipment for long-term testing. This test was repeated several times with the same unfortunate results. The high pressure testing system was not originally designed for low strain rates, because the design intent was to study instability, which requires faster strain rates to demonstrate the occurrence of instability. The slow test required that the computer operate the stepping motors in an intermittent fashion, which increases the required number of computer-generated I/O commands to the peripheral hardware to the point, where over a period of a few days, the computer eventually makes an I/O error, causing the stepping motors to cease functioning. However, all the specimens were sheared well beyond the maximum deviator stress required to study the location of the instability line.

The stress-strain and pore pressure relations from the undrained triaxial compression tests are shown on Figures 7-7 and 7-8, and the corresponding effective stress paths are presented on the Cambridge p'-q diagram as shown on Figure 7-9. The diagrams clearly show that the soil behavior was affected by the different strain rates. The higher strain rates produced stress paths that are located above the stress paths corresponding to the lower strain rates as shown on Figure 7-9. The reason for the different effective stress paths is that the different strain rates generate different pore pressures as shown on Figure 7-8. As the strain rate decreases, the generated pore pressures are significantly greater. The effect of the larger pore pressures is to lower the effective confining pressure in the specimen enough that the magnitude of the maximum deviator stress as well as the entire stress path is lowered as shown on Figures 7-7 and 7-9. The effective

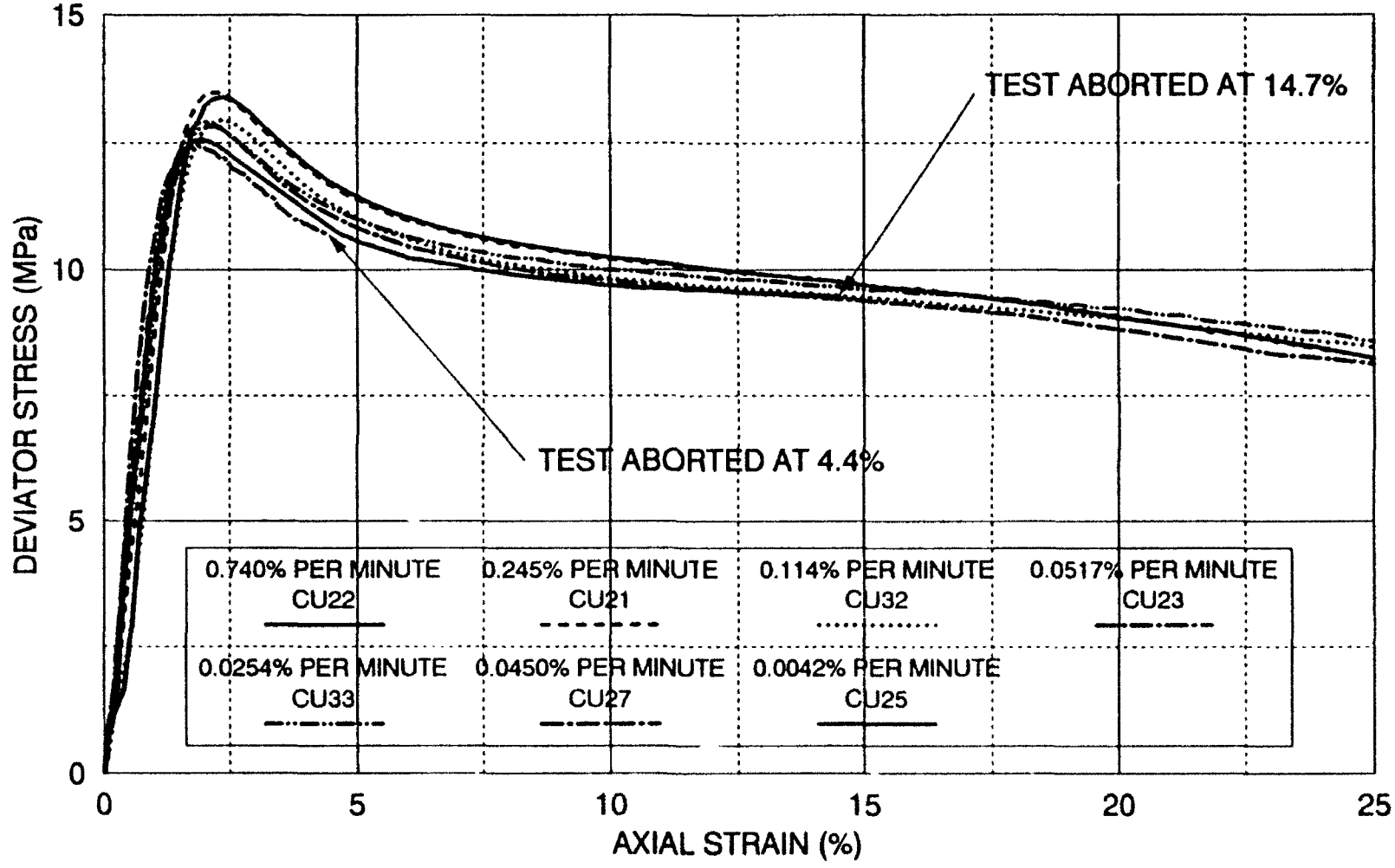

FIGURF 7-7 DEVIATOR STRESS
UNDRAINED TRIAXIAL COMPRESSION TESTS AT DIFFERENT STRAIN RATES
INITIAL EFFECTIVE CONFINING PRESSURE 34.0 MPa

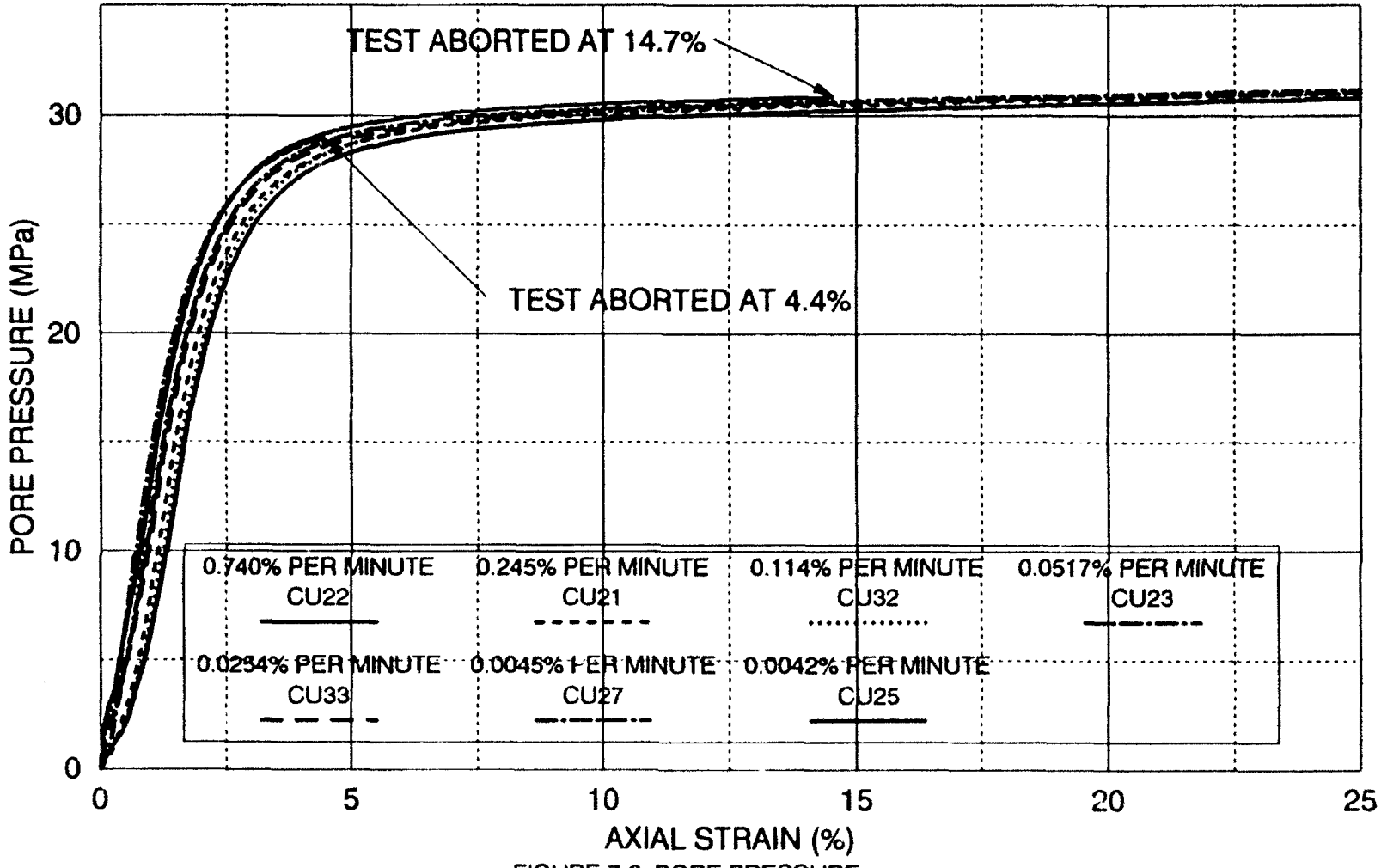

FIGURE 7-8 PORE PRESSURE
UNDRAINED TRIAXIAL COMPRESSION TESTS AT DIFFERENT STRAIN RATES
INITIAL EFFECTIVE CONFINING PRESSURE 34.0 MPa

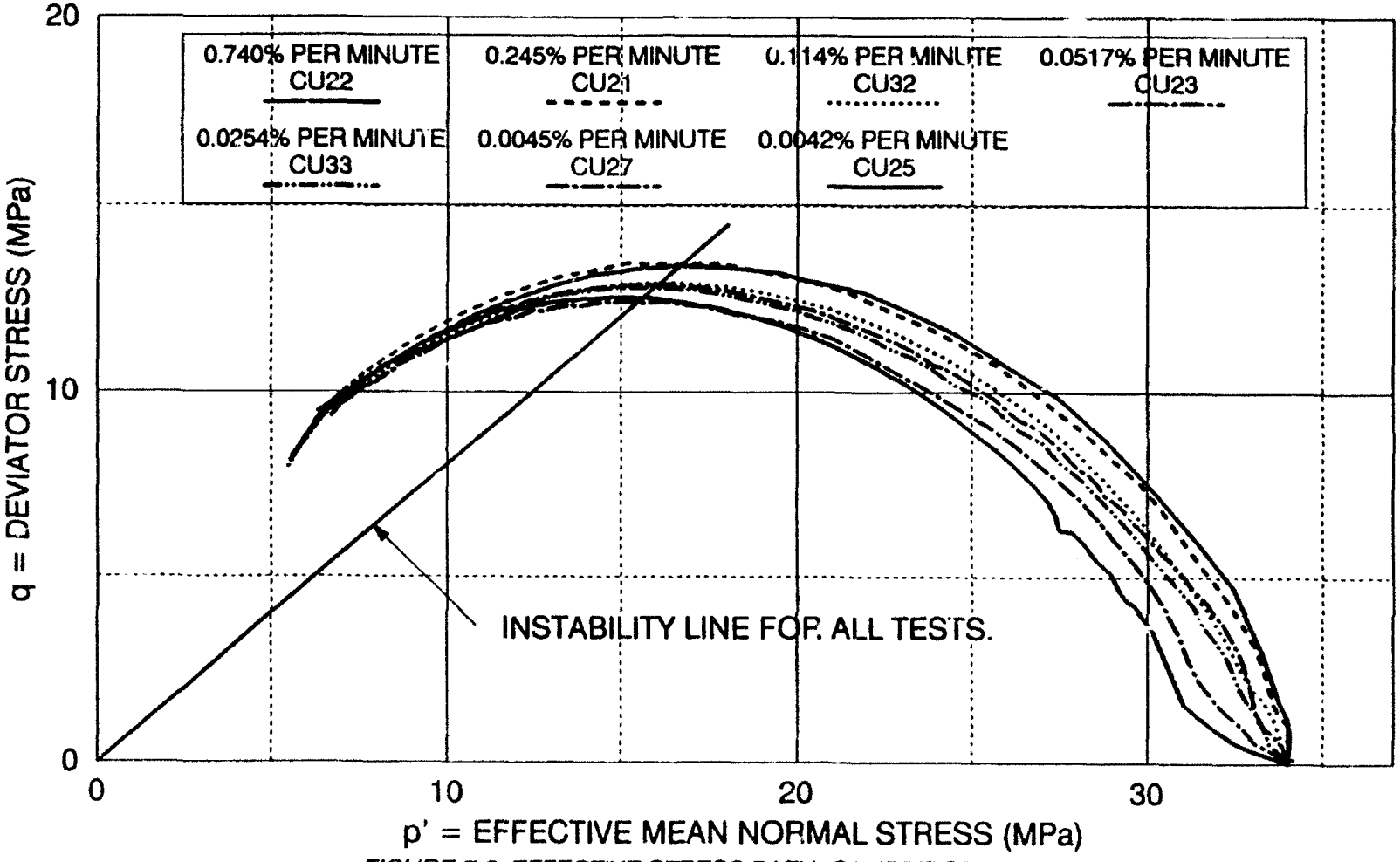

FIGURE 7-9 EFFECTIVE STRESS PATH, CAMBRIDGE p'-q
UNDRAINED TRIAXIAL COMPRESSION TESTS AT DIFFERENT STRAIN RATES
INITIAL EFFECTIVE CONFINING PRESSURE 34.0 MPa

confining pressures at maximum deviator stress for the different tests vary from 11.06 MPa to 12.23 MPa from the lowest to the highest strain rates. This explains why the maximum deviator stress increased with strain rate from 12.56 MPa to 13.48 MPa, as shown on Figure 7-10. For high confining pressures, it seems reasonable to hypothesize that the main reason for the higher pore pressures generated at low strain rates is that more time is available for particle crushing and rearranging to occur during the shearing process. This would have resulted in more volumetric compression, but since the tests were undrained, higher pore pressures were induced instead. At higher strain rates, less time is allowed for particle crushing and rearranging to occur, and this causes the specimen to be less compressive, and thereby, lower pore pressures are produced, and higher deviator stresses are obtained. This mechanism of strain rate effect was also hypothesized by Nash and Dixon (1961). The difference in pore pressure generation between low and high strain rates is most noticeable during the initial stages of shearing in the high pressure tests as shown on Figure 7-9. Much of the particle crushing and rearranging occurs early in the test, before the effective stresses in the specimen decrease due to the pore pressure increase. However, the lower strain rate tests always have slightly larger pore pressures throughout the test, since the rate of particle crushing decreases, but never actually stops in these tests. Figure 7-7 shows that the axial strain at maximum deviator stress increases as the strain rate increases. Similar trends were observed in results of drained tests performed by Whitman and Healy (1962), and by Casagrande and Shannon, (1948).

Close examination of the deviator stresses on Figure 7-7 shows that

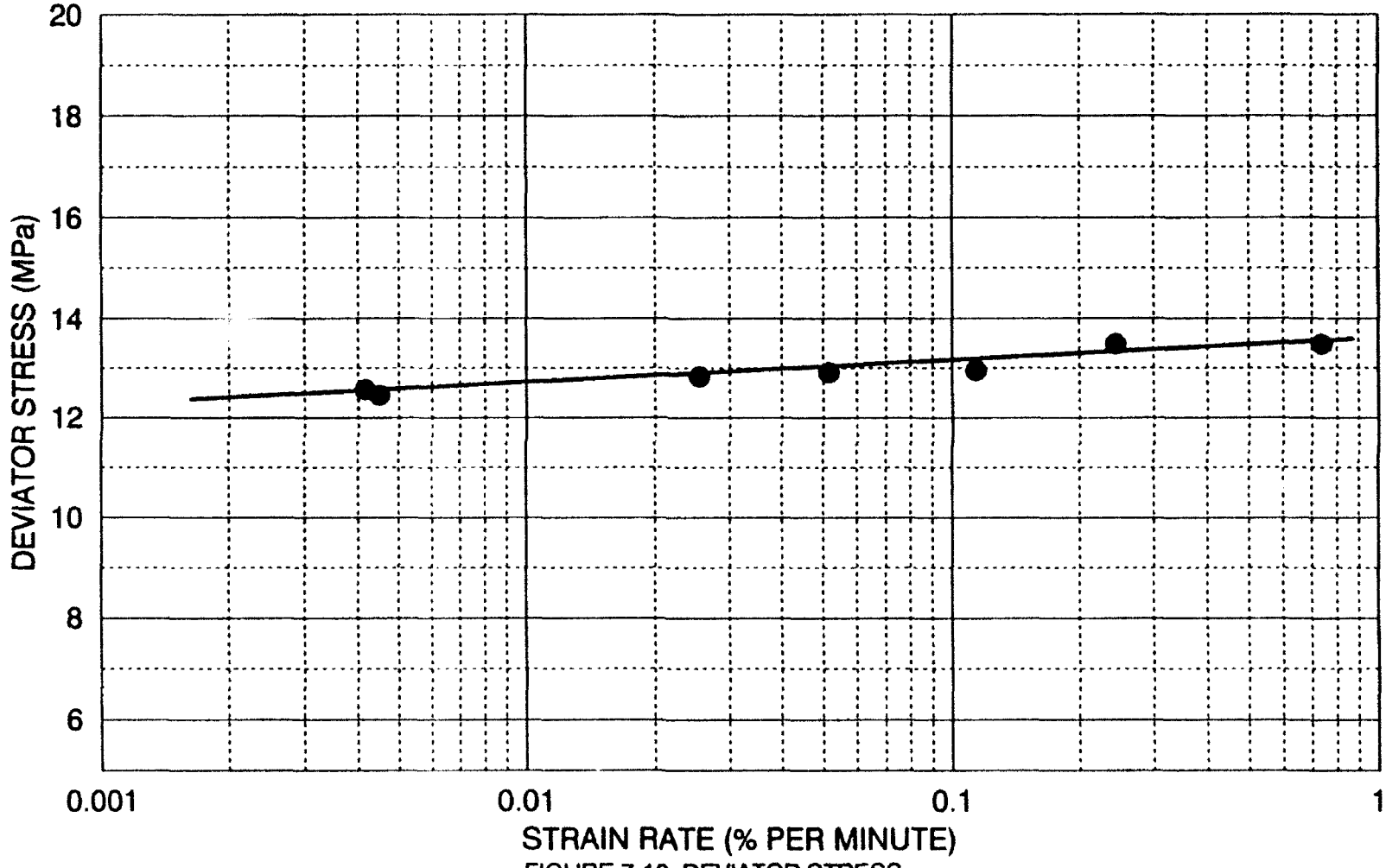

FIGURE 7-10 DEVIATOR STRESS
UNDRAINED TRIAXIAL COMPRESSION TESTS AT DIFFERENT STRAIN RATES
34.0 MPa INITIAL EFFECTIVE CONFINING PRESSURE

regardless of the strain rate, the deviator stresses eventually reach a common value at approximately 25 percent axial strain. This, along with the fact that the effective confining pressures decrease with decreasing strain rate as shown on Figure 7-14, account for the increase in the effective principal stress ratios as shown on Figure 7-11. The effective stress friction angle computed from the maximum effective principal stress ratio varies between 36.2 degrees for the 0.0254 percent per minute test and 34.5 degrees for the 0.74 percent per minute test as shown on Figure 7-12. Observations also indicate that the axial strain at effective stress failure increases with decreasing strain rate as shown on Figure 7-13. A summary of the effects of strain rate on the soil behavior in undrained tests at high confining pressures is presented in Table 7.1.

The effect of strain rate on the location of the instability line appears to be negligible as shown on Figure 7-9. All maximum deviator stresses essentially fall on the same instability line regardless of strain rate, because the larger pore pressures in the slower tests reduce the deviator stress, and at the same time push the effective stress path towards the origin, thus keeping the maximum deviator stress on the same line. The axial strain to the instability line increased with increasing strain rate from 1.84 to 2.38 percent.

7.8 Strain Rate Effects in Drained Triaxial Compression Tests

Three drained triaxial compression tests were performed to investigate the mechanism of particle crushing and rearranging, that was proposed from the results of the undrained tests as influenced by strain rate effects. It was suggested

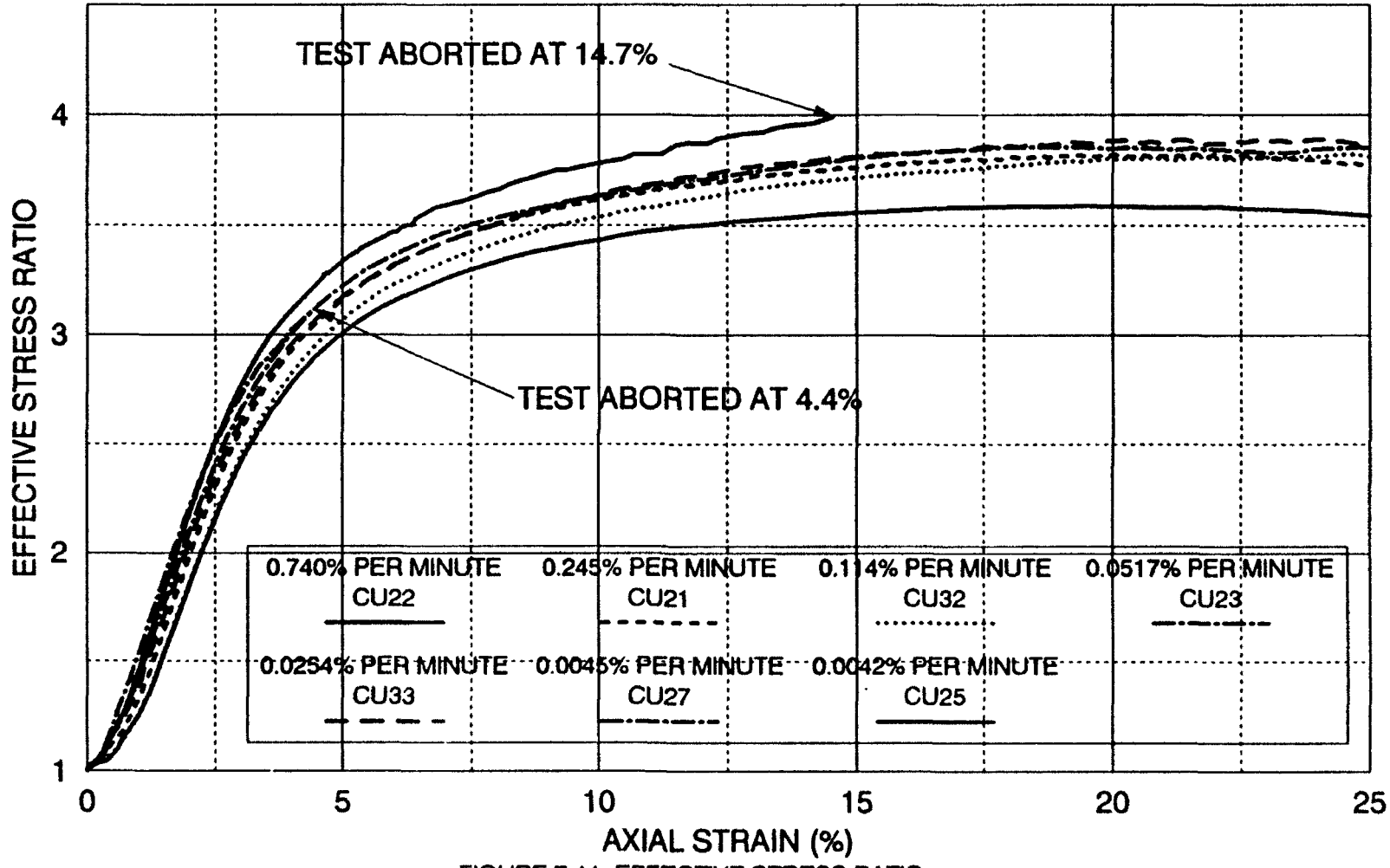

FIGURE 7-11 EFFECTIVE STRESS RATIO
UNDRAINED TRIAXIAL COMPRESSION TESTS AT DIFFERENT STRAIN RATES
INITIAL EFFECTIVE CONFINING PRESSURE 34.0 MPa

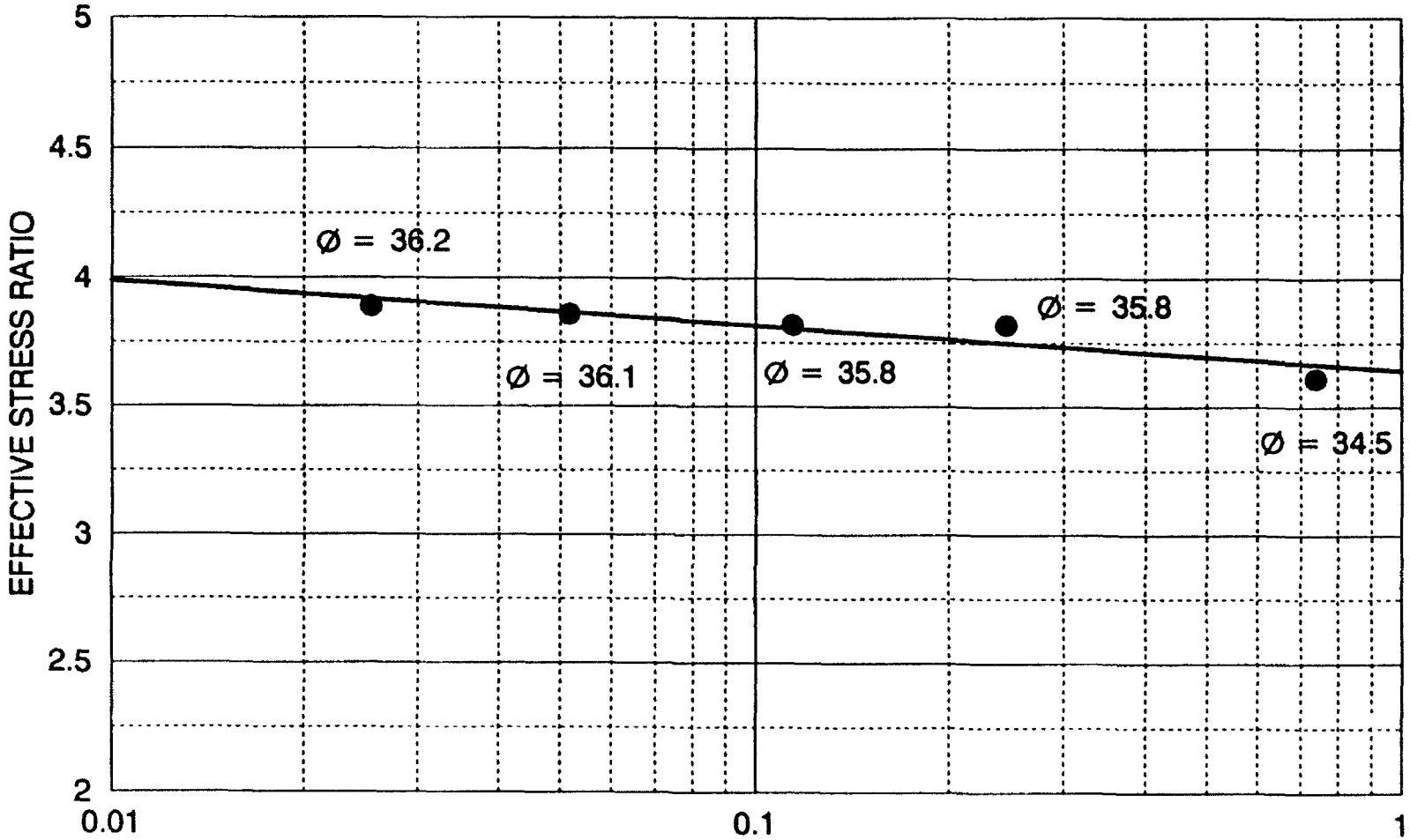

FIGURE 7-12 EFFECTIVE STRESS RATIO
UNDRAINED TRIAXIAL COMPRESSION TESTS AT DIFFERENT STRAIN RATES
34.0 MPa EFFECTIVE CONFINING PRESSURE

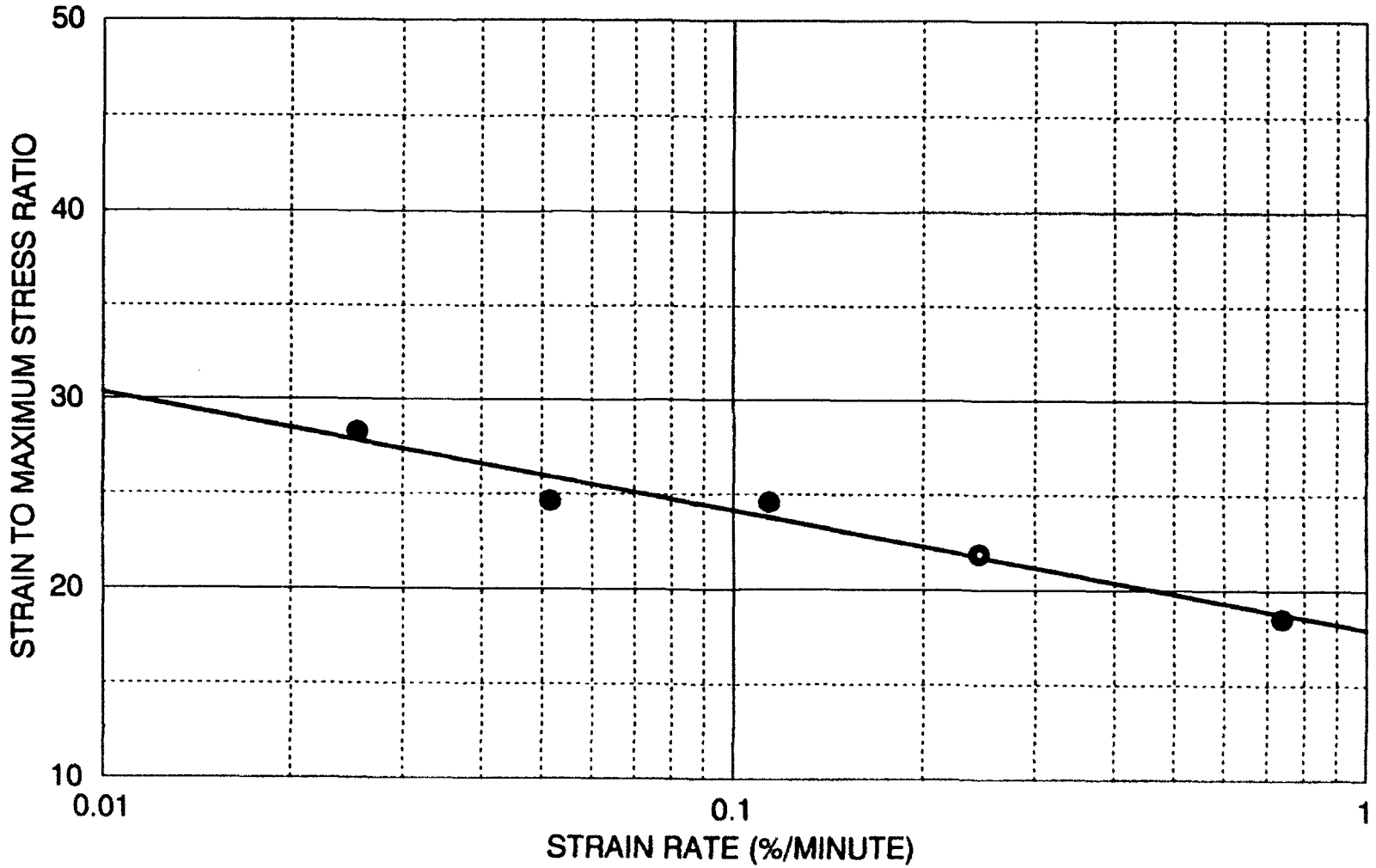

FIGURE 7-13 AXIAL STRAIN TO MAXIMUM STRESS RATIO
UNDRAINED TRIAXIAL COMPRESSION TESTS AT DIFFERENT STRAIN RATES
34.0 MPa EFFECTIVE CONFINING PRESSURE

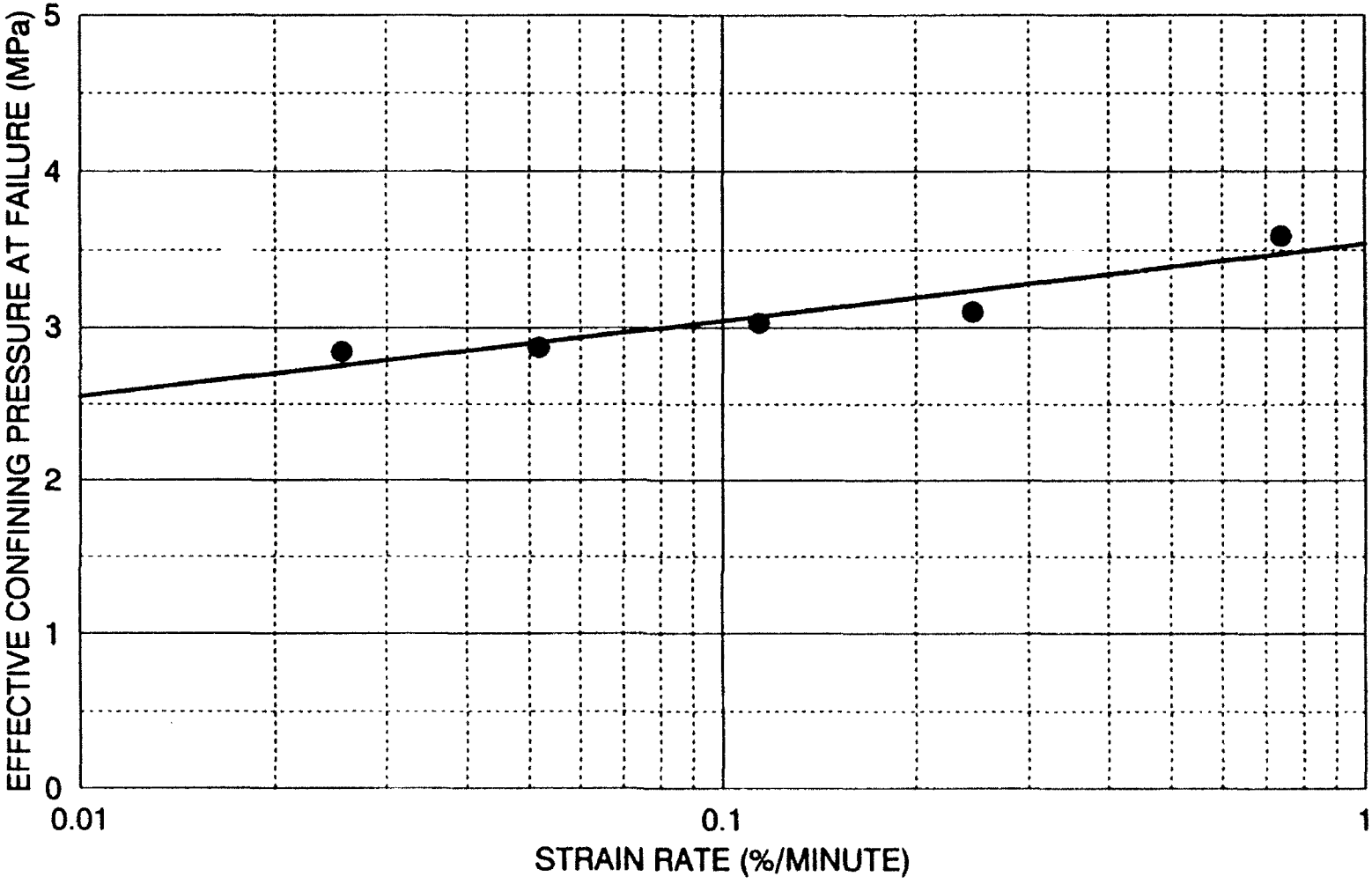

FIGURE 7-14 EFFECTIVE CONFINING PRESSURE
UNDRAINED TRIAXIAL COMPRESSION TESTS AT DIFFERENT STRAIN RATES
34.0 MPa INITIAL EFFECTIVE CONFINING PRESSURE

STRAIN RATE (%/MINUTE)	MAXIMUM DEVIATOR STRESS (MPa)	AXIAL STRAIN AT INSTABILITY LINE	FRICTION ANGLE (DEGREE)	AXIAL STRAIN AT FAILURE (%)	EFFECTIVE CONFINING PRESSURE AT FAILURE (MPa)
0.0042% TO 0.74%	12.56 TO 13.48	1.84 TO 2.38%	36.2 TO 34.5	18.5 TO 28.3%	2.8 TO 3.6 MPa
+17,800%	+7.3%	+29%	-4.7%	+53%	+29%

TABLE 7.1 EFFECTS OF STRAIN RATE VARIATIONS IN UNDRAINED TRIAXIAL COMPRESSION TESTS ON DENSE CAMBRIA SAND AT 34.0 MPa CONFINING PRESSURE

that fracturing and rearranging soil grains require time, and that increased strain rate allows less time, and therefore, results in decreasing amounts of particle crushing and consequent rearranging. In a drained test the specimen would consequently be less compressive and its strength would possibly increase with increasing strain rate. Thus, strain rate should affect particle crushing and rearranging, and differences should be noticed in the volumetric strains during drained tests.

All specimens were isotropically consolidated to an effective confining pressure of 17.2 MPa and allowed to remain at this pressure for 15 minutes prior to shearing. The effective confining pressure was maintained constant throughout each test. Shearing was performed at three different strain rates varying between a lower value of 0.0517 percent per minute and an upper value of 0.74 percent per minute. All specimens were sheared beyond the maximum deviator stress.

The stress-strain and volume change curves for the three drained tests are shown on Figures 7-15 and 7-16. The deviator stresses show small increases with increasing strain rate. At failure they range from 42.72 MPa to 43.40 MPa from the lowest to highest strain rates, as indicated on Figure 7-17. These increases are small and could conceivably be within the overall experimental scatter. The corresponding friction angles increase slightly from 33.6 to 33.9 degrees. Increases in maximum deviator stresses with strain rate during drained tests have been reported by, Casagrande and Shannon (1948); Whitman and Healy (1962); Seed and Lundgren (1954); Lee et al. (1969). However, most of these investigations were performed on dry sand, and volume changes were not reported. Only Seed

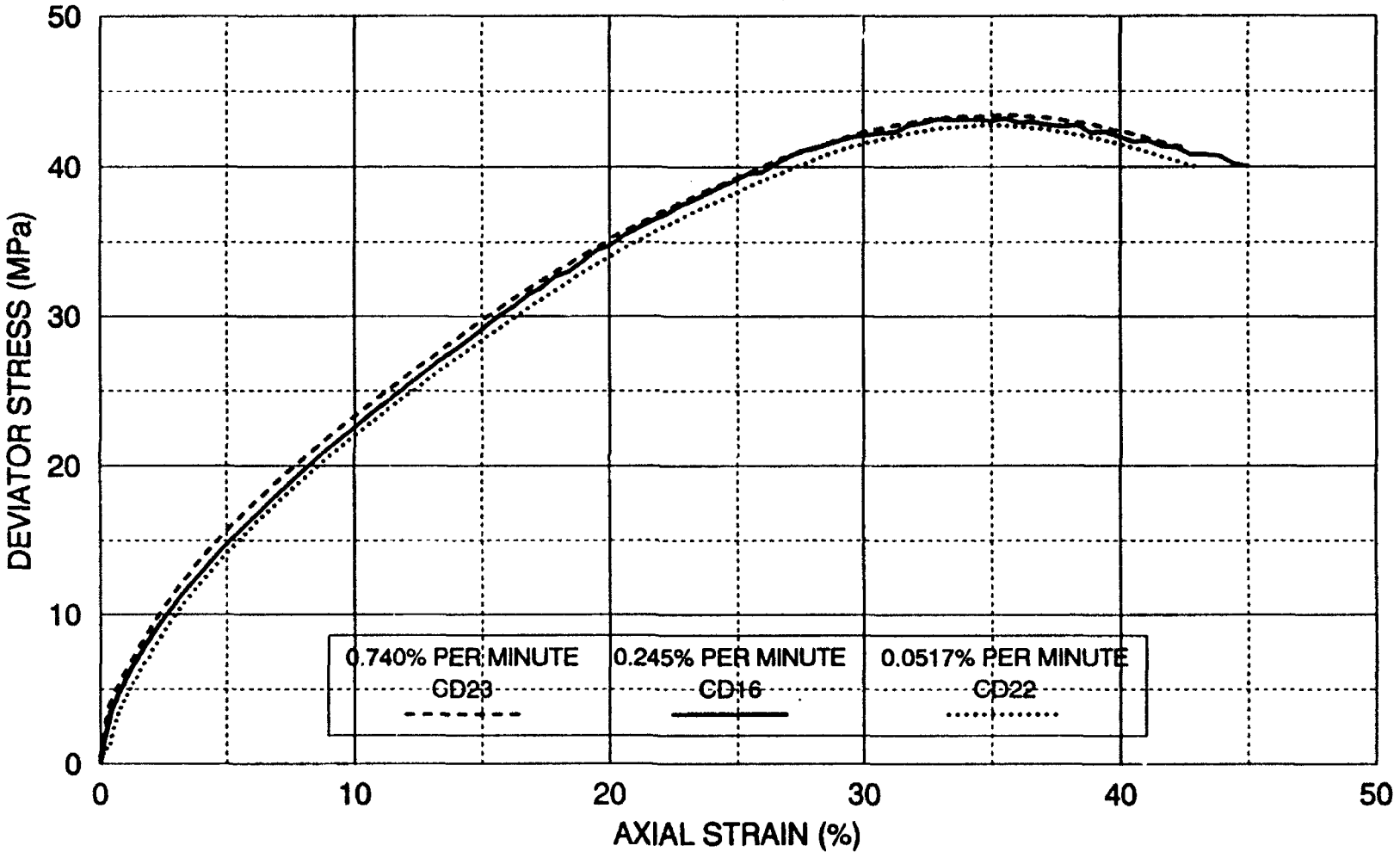

FIGURE 7-15 DEVIATOR STRESS
DRAINED TRIAXIAL COMPRESSION TESTS AT DIFFERENT STRAIN RATES
17.2 MPa INITIAL EFFECTIVE CONFINING PRESSURE

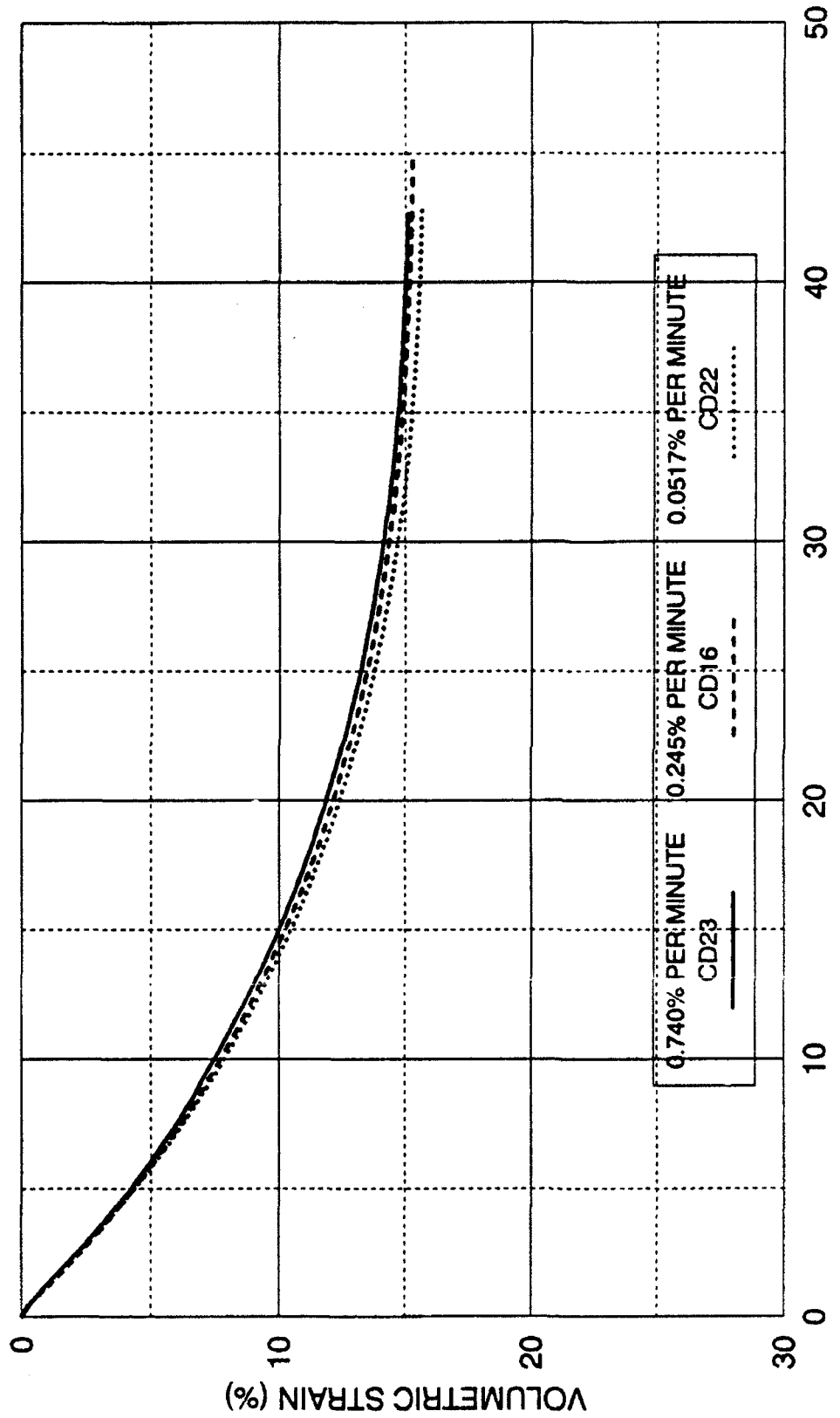

FIGURE 7-16 VOLUMETRIC STRAIN
DRAINED TRIAXIAL COMPRESSION TESTS AT DIFFERENT STRAIN RATES
17.2 MPa INITIAL EFFECTIVE CONFINING PRESSURE

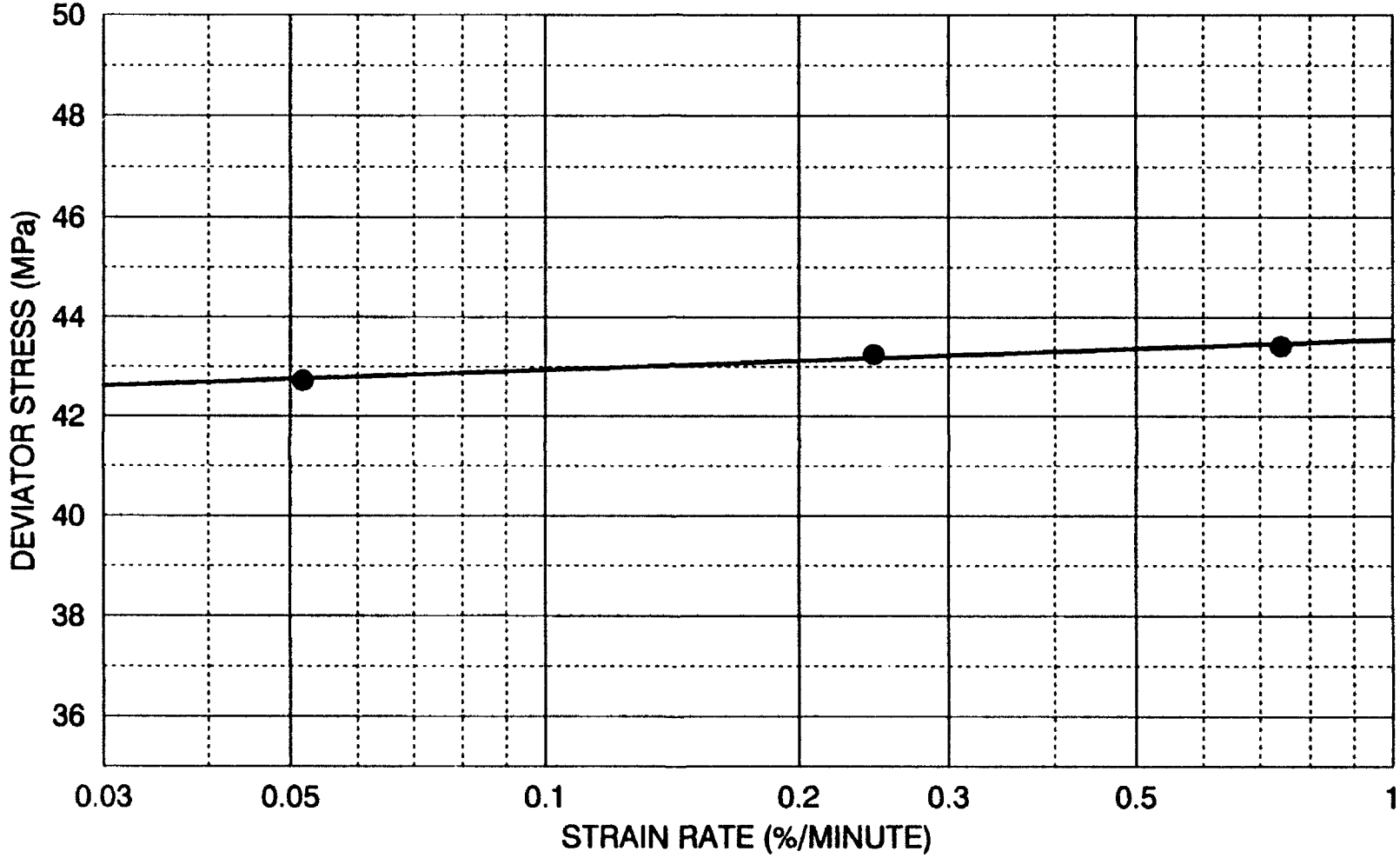

FIGURE 7-17 DEVIATOR STRESS
DRAINED TRIAXIAL COMPRESSION TESTS AT DIFFERENT STRAIN RATES
17.2 MPa INITIAL EFFECTIVE CONFINING PRESSURE

and Lundgren (1954) employed saturated specimens, but they could not be considered fully drained under the rapid loading conditions.

The reason for the increase in deviator stress and friction angle would appear to be related to the volume changes during shearing as shown on Figures 7-16 and 7-18. The increases in volumetric strain are small, but definitely measurable. Higher strain rates induce volume changes that are slightly less compressive than in the slower tests. These smaller amounts of volumetric compression change make the specimens appear more dilatant, and they consequently exhibit a slightly higher strength. These small changes in volumetric strain, and the corresponding small changes in the maximum deviator stresses are relatively insignificant for the drained tests. However, similar small volume change tendencies translate into much more significant pore pressure differences in the undrained tests, as previously discussed.

The axial strain to failure for the drained tests increase with increasing strain rate as shown on Figure 7-19. This agrees with results from Casagrande and Shannon (1948) and Whitman and Healy (1962). These results are unlike the drained test results of Lee et al. (1969), which show a decrease in axial strain to maximum deviator stress with increasing strain rate during drained tests. An analysis of strain rate effects on the soil behavior in drained tests obtained here is presented in Table 7.2. The variations in the quantities obtained for the drained tests are very small, but measurable. This may explain the scatter in results from previous investigations. Since they were performed at low confining pressures, these small variations in quantities may be within normal experimental scatter.

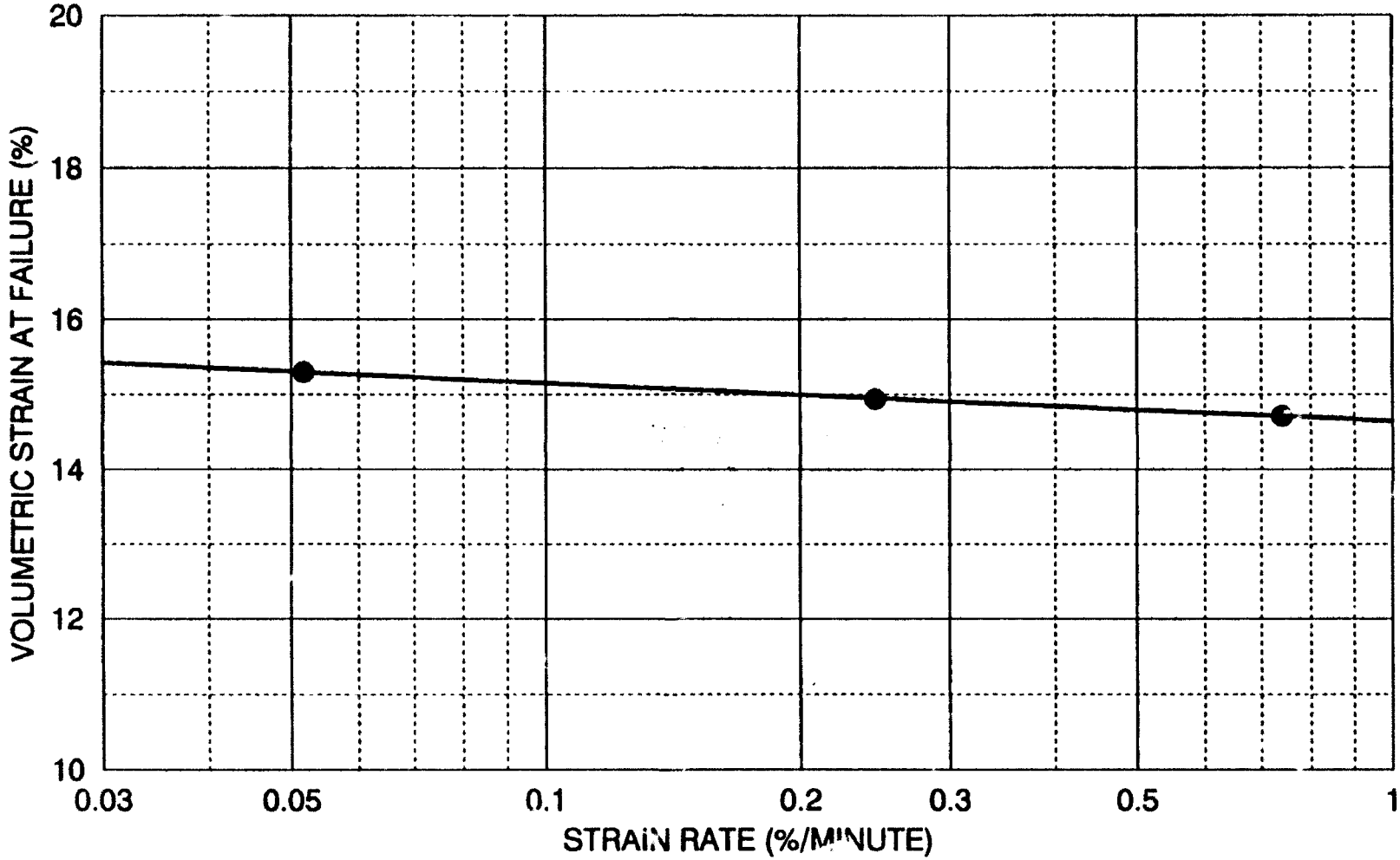

FIGURE 7-18 VOLUMETRIC STRAIN AT FAILURE
DRAINED TRIAXIAL COMPRESSION TESTS AT DIFFERENT STRAIN RATES
17.2 MPa INITIAL EFFECTIVE CONFINING PRESSURE

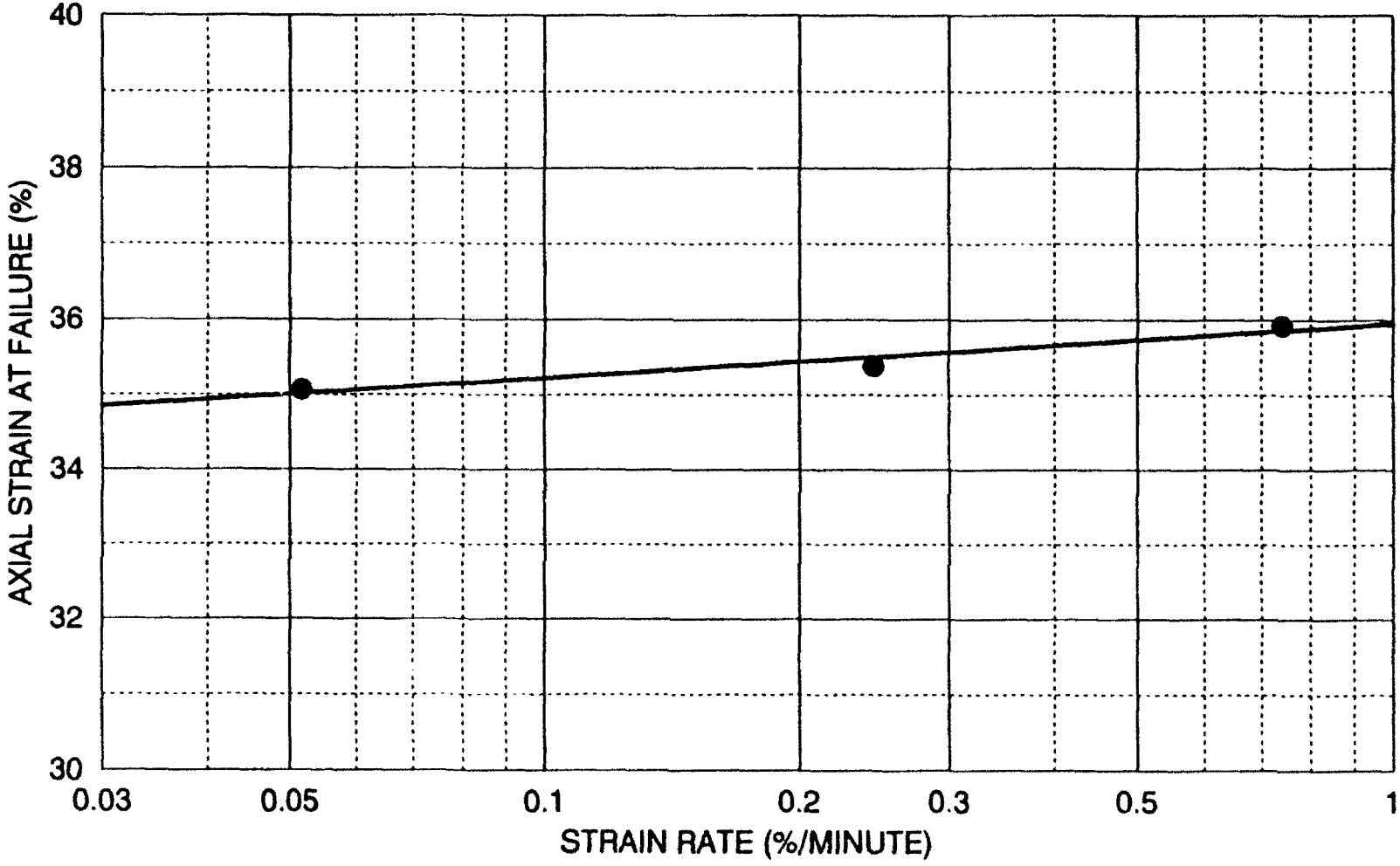

FIGURE 7-19 AXIAL STRAIN AT FAILURE
DRAINED TRIAXIAL COMPRESSION TESTS AT DIFFERENT STRAIN RATES
17.2 MPa INITIAL EFFECTIVE CONFINING PRESSURE

STRAIN RATE (%/MINUTE)	MAXIMUM DEVIATOR STRESS (MPa)	FRICTION ANGLE (DEGREE)	AXIAL STRAIN AT FAILURE (%)	VOLUMETRIC STRAIN AT FAILURE (%)
0.0517% TO 0.74%	42.72 TO 43.40	33.6 TO 33.9	35.1 TO 35.9%	15.3 TO 14.7%
+1,430%	+1.6%	+0.8%	+2.3%	-3.9%

TABLE 7.2 EFFECTS OF STRAIN RATE VARIATIONS IN DRAINED COMPRESSION ON DENSE CAMBRIA SAND AT 34.0 MPa CONFINING PRESSURE

It is concluded that testing at high confining pressures at slower strain rates enhanced the consistency of the results presented here.

7.9 Grain Size Analysis

Sieve analyses were performed on all specimens after testing to determine if the additional particle crushing could be detected from their grain size distributions, and their results are shown on Figure 7-20. Significant particle crushing occurred in all tests, as evidenced by the relative location of the original uniform gradation and the final gradations. The results of the grain size analyses were inconclusive. As can be seen all drained tests produced grain size curves that were close to each other. Similar results were obtained from the undrained tests, except the 0.0042 percent strain rate test, which was terminated at 14.7 percent. The amount of particle crushing is directly related to the extent to which the specimen is sheared. The drained tests were not terminated at the same axial strain, and therefore exhibit different amounts of particle crushing. The differences are within the experimental scatter for a sieve analysis. The undrained test terminated early at 14.7 percent also clearly indicates this behavior, with its gradation curve being noticably offset from the other undrained tests. The possible variations in grain size distributions that may occur early in the tests, where the soil behavior is noticably different, will not be properly reflected at the end of the tests. In addition, the differences in volume change that occurred between the drained tests were relatively small, and any variation in grain size distribution would have been very small.

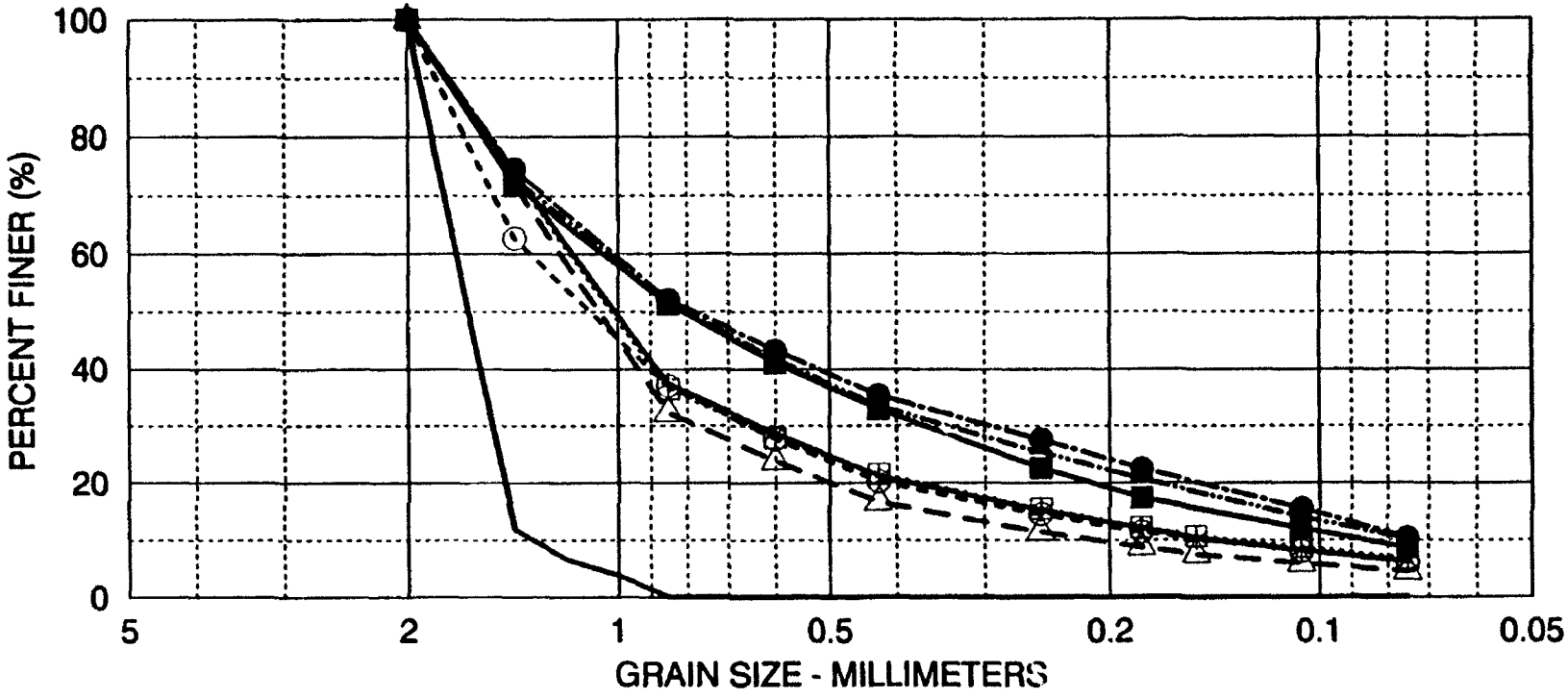

FIGURE 7-20 GRAIN SIZE ANALYSIS
DRAINED AND UNDRAINED COMPRESSION TESTS AT DIFFERENT STRAIN RATES
DENSE CAMBRIA SAND

7.10 Conclusions

B-values can be reliably measured and predicted at high confining pressures. However, evaluating the degree of saturation through B-value measurements is complicated because of creep effects that granular materials exhibit at high confining pressures. Since the flexibility of the pore pressure measuring system, the soil compressibility, and the membrane flexibility can be relatively easily evaluated at low confining pressures without the added complication of creep effects, it is preferable to check the degree of saturation of a triaxial specimen of granular material at low effective confining pressure, before consolidating the specimen to higher pressures.

Experiments and analyses have been performed to study the role of soil stiffness at low and high confining pressures on the influence of total stress path on the effective stress path in undrained tests. This influence is known to be negligible at low confining pressures, where the soil stiffness is low. The soil stiffness increases with increasing confining pressure, and Skempton's pore pressure equation (Equation 7.1) indicates that the effective stress path direction should be affected by the externally imposed total stress path direction for high soil stiffnesses. High confining pressure undrained triaxial tests indicate that the effective stress path is not affected by the total stress paths, and the expected effect is overshadowed by volumetric soil creep caused by particle crushing at high confining pressures. The axial deformation rate has a significant effect on the direction of the effective stress path.

The effect of strain rate on the location of the instability line appears to be

negligible. As strain rates decrease, the tendency is for the high point on the effective stress path to follow the instability line down toward the origin as was shown on Figure 7-9.

The magnitude of the strain rates used in this study were within the range of normal static testing strain rates, and were within the lower ranges of strain rates used by prior investigators. The mechanism that governs strain rate effects in granular soils at high pressures relates to particle crushing and rearranging, and consequent volume change tendencies in the soil during shearing. Higher strain rates do not allow as much time for particle crushing and rearranging, and this makes the soil appear less compressive or more dilatant, resulting in higher strengths. It is very likely that the same mechanism operates at low confining pressures, where particles would not have adequate time to efficiently rearrange during rapid loading, which results in the soil's appearing more dilatant, and noticeably stronger.

Strain rate effects are measurable in cohesionless soils. The effects in drained tests are not found to be significant. However, the experimental results indicate that the effects are magnified in undrained tests, because the small tendencies for volume changes caused by particle crushing and rearranging result in large pore pressure differences.

Specifically, the following strain rate effects were found for drained and undrained conditions:

As strain rate increases in drained conditions:

1. Friction angles and maximum deviator stresses increase

slightly.

2. Volumetric compression decreases slightly.

3. Axial strain-to-failure increases slightly.

As strain rate increases in undrained conditions:

1. Maximum deviator stress increases.

2. Axial strain at maximum deviator stress increases.

3. Pore pressures decrease significantly.

4. Effective stress friction angle decreases significantly.

5. Axial strain at maximum effective principal stress ratio increases significantly.

6. Effective confining pressure at failure decreases significantly.

CHAPTER 8 - PARTICLE BREAKAGE AT HIGH PRESSURES

8.1 - Introduction

Virtually all previous researchers in the field of high pressure testing have noted that there is considerable particle breakage during testing at high pressures (Terzaghi and Peck, 1948; Roberts and deSouza, 1958; Hendron, 1963; Vesic and Barksdale, 1963; Hirschfield and Poulos, 1963; Hall and Gordon, 1963; Leslie, 1963; Bishop, et al, 1965; Bishop, 1966; Marsal, 1967; Lee and Farhoomand, 1967; Lee and Seed, 1967; Vesic and Clough, 1968; Barden, et al, 1969; Marachi, et al, 1969; Tai, 1970, Murphy, 1970; Billam, 1971; Murphy, 1971; Becker, et al, 1972; Miura and Yamanouchi, 1973; Lo and Roy, 1973; Miura and Ohara, 1979; Hardin, 1984, Murphy, 1987; Colliat-Dangus, et al, 1988; Chamieh, 1990).

As discussed in Chapter 5, particle crushing is perhaps the most significant phenomenon occurring at high pressures that affects the overall soil behavior. This chapter attempts to quantify the particle breakage and relate the amount of breakage with various soil parameters including energy. Also, a method is proposed to predict the amounts of particle crushing.

8.2 Measures of Particle Breakage

There have been considerable attempts by various investigators to quantify particle breakage. All developed methods are empirical in nature and are based upon changes in particle sizes as the key measurement. Some particle breakage

indices are based upon a single particle size, while others are based upon aggregate changes in the overall grain size distribution. The most widely used particle breakage indices are the ones developed by Marsal, 1967, Lee and Farhoomand, 1967, and Hardin, 1984.

Marsal created his measure of particle breakage while investigating earth and rockfill dams. While he was performing large-scale triaxial compression tests, he noticed significant amounts of particle breakage, which resulted in the development of his breakage index, B. His method involves the change in particle sizes in the grain size distribution. A difference in percentage retained is computed for each sieve size. This difference will either be positive or negative. Marsal's breakage factor, B, is the sum of the differences of the same sign. This is depicted on Figure 8-1. The lower limit of this index is zero percent and it has a theoretical upper limit of 100 percent.

Lee and Farhoomand created their measure of particle crushing while investigating earth dam filter material. Their concern was whether extensive particle crushing could effectively plug dam filters. They performed a series of isotropic and proportional loading tests. Their measure consists of examining a single particle size on the grain size distribution. They chose the particle size at 15 percent finer as shown on Figure 8-1. This was chosen because gravel filter drainage requirements are commonly based upon this particle size. Their measure is $D_{15(initial)}/D_{15(final)}$. The lower limit of this index is unity and there is no upper limit.

Hardin's measure of particle breakage is based upon changes in the entire

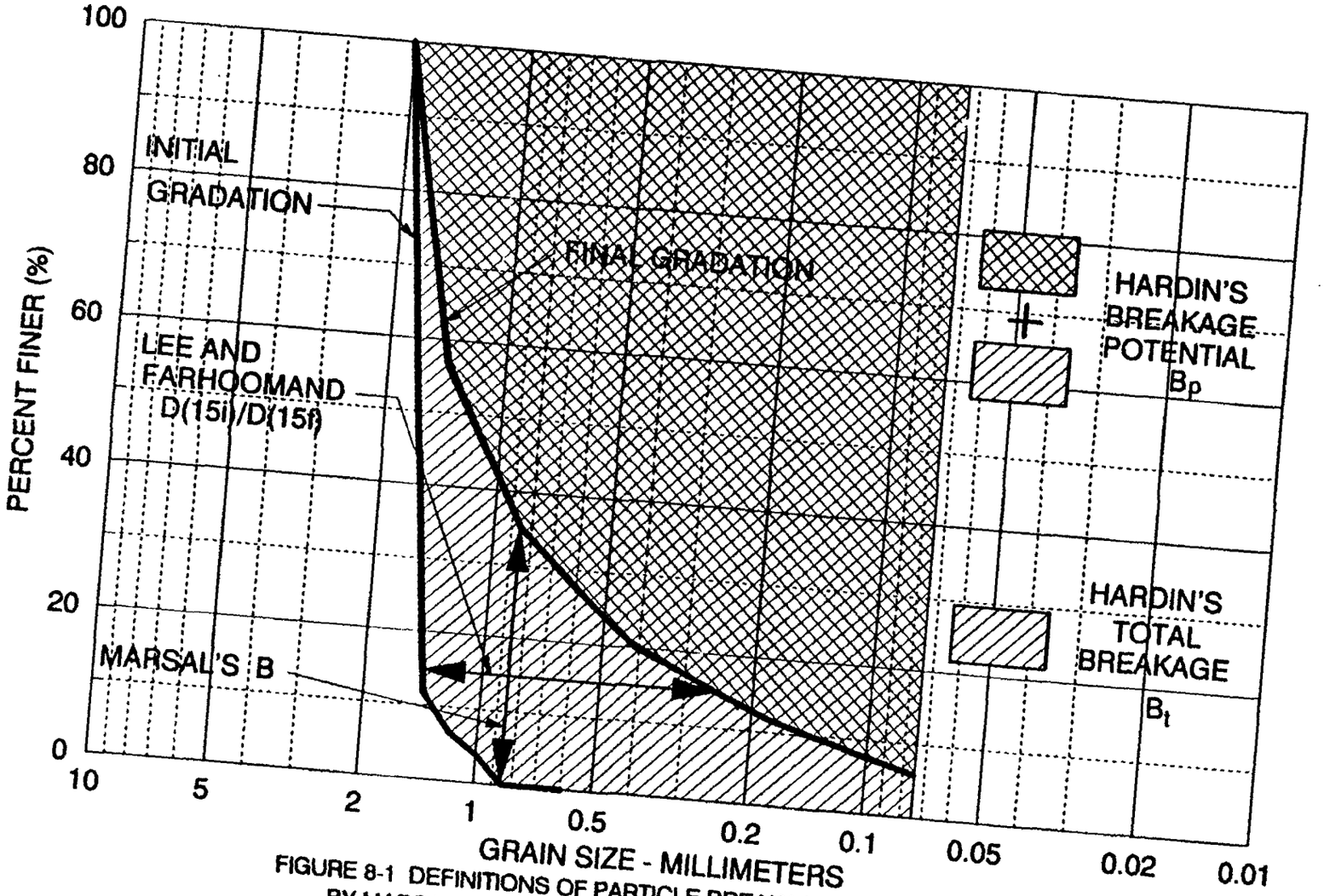

FIGURE 8-1 DEFINITIONS OF PARTICLE BREAKAGE FACTORS
BY MARSAL, LEE AND FARHOOMAND, AND HARDIN

particle size distribution. He defined three different quantities. Breakage potential, B_p, is the area between the original grain size distribution curve of the soil and the No. 200 sieve size, as shown in Figure 8-1. He limited the size to the No. 200 U.S. sieve size, because of the difficulty in crushing particles below this size, and also because it is difficult to obtain particle size distributions below this size using sieve analyses (a hydrometer test is usually required) size, and because soil behavior will not be significantly affected by crushing below this size. The breakage potential represents the total possible gradation change of a soil if it is crushed from its originial gradation to below the No. 200 sieve size. Total breakage, B_t, is defined as the area between the original grain size distribution curve and the final grain size distribution curve as shown on Figure 8-1. Relative Breakage, B_r, is defined as the ratio of total breakage divided by the potential breakage (B_t/B_p). Relative breakage has a lower limit of zero and a theoretical upper limit of unity.

8.3 Factors Affecting Particle Breakage

There are several factors that affect the amount of particle breakage (Lee and Farhoomand, 1967; Hardin, 1984). The stress level and stress path affect the amount of particle crushing. The higher the stress level, and the longer the stress path lingers in regions of high stress levels, the larger amounts of particle breakage are generated. However, another factor is time. The quantity of particle breakage is a function of time. Even under constant stress levels, particle breakage will continue, but at a decreasing rate.

As particle size increases, particle crushing also increases. This is due to the fact that larger particles have a higher probability that there is a defect within the particle that will cause breakage. Smaller particles are generally created from larger particles fracturing along these defects. As this process continues, there are fewer defects in the subdivided particles, so it is less likely that particles will fracture as they become smaller.

Increasing particle angularity increases particle breakage. Angular particles break more easily, because stresses can concentrate along their narrow dimension, thus fracturing the particle. Also, stresses can concentrate at angular contact points causing the points to fracture.

Well graded soils do not break down as easily as uniform soils. Also, as relative density increases, the amount of particle breakage decreases. Both these factors are based upon the fact that with more particles surrounding each particle, the average contact stresses tend to be decreased.

Increasing mineral hardness decreases the amount of particle crushing. The harder or stronger particle materials show smaller amount of breakage for a given stress.

8.4 Reasons to Quantify Crushing

Other than the need to have measurements of particle breakage that are numerically specific, such that reasonable comparisons can be made to determine quantitatively the extent of crushing, there do not appear to be many purposes for particle crushing parameters. The reason for this lack of need is that correlations

of particle crushing parameters with basic soil properties do not yield solid relationships. Virtually all the measures of particle crushing are relating the particle size distribution before and after shearing. Since a particular soil represented by a specific gradation curve can have any number of different densities from that same gradation, the particle breakage parameters do not form any consistent pattern with shear strength or volume change characteristics of a given soil.

The one area where crushing indices could have significant application is in the area of soil permeability. Lee and Farhoomand investigated whether particle crushing in earth dams could be detrimental to gravel drains and soil filters. There are a number of empirical correlations of grain size with permeability (Duncan, et al, 1972). One of the most widely used empirical correlations that relates particle grain size with permeability is Hazen's formula shown as Equation 8.1.

$$k = 100 \cdot (D_{10})^2 \qquad (8.1)$$

k - permeability coefficient (cm/sec).
D_{10} - grain size(cm) represented by 10 percent of material being smaller by weight.

This relationship was obtained by Hazen on tests with sharp filter sand, where the D_{10} sizes were between 0.1 and 0.3 millimeters, and the coefficient of uniformity was less than five. The change in permeability of a sand can be determined with this relationship before and after crushing.

With permeability correlations in mind a new particle crushing parameter is proposed based upon the D_{10} size. It is defined in Equation 8.2. The formulation of this particle breakage parameter is based upon having the lower

limit being zero, when there is no particle breakage, and having the upper limit being unity at infinite particle breakage. The usefulness of this formulation will be discussed later.

$$B_{10} = 1 - \frac{D_{10f}}{D_{10i}} \qquad (8.2)$$

B_{10} = particle breakage factor.
D_{10f} = 10 percent finer by weight grain size of crushed soil.
D_{10i} = 10 percent finer by weight grain size of original soil.

Permeability correlations using a single grain size are generally best suited for soils with uniform gradations. Permeability correlations utilizing multiple grain sizes are better suited for well-graded soils.

8.5 Observations at High Pressures

The tests on dense Cambria sand described in previous chapters exhibited various amounts of particle crushing. The tests included undrained and drained tests in triaxial compression and extension. After the specimens were sheared, the specimens were generally saved, and sieve analysis was performed on the dried soil to evaluate the grain size distribution. Results of the sieve analyses for all the individual tests are included in the Appendix. The results of a few of these sieve analyses are shown on Figures 8-2, 8-3, 8-4 and 8-5 for drained triaxial compression, undrained triaxial compression, drained triaxial extension, and undrained triaxial extension, respectively. The diagrams depict the percent finer plotted against the particle grain size. Also, shown on the diagrams is the initially very uniform gradation for the Cambria sand. It can be concluded from the

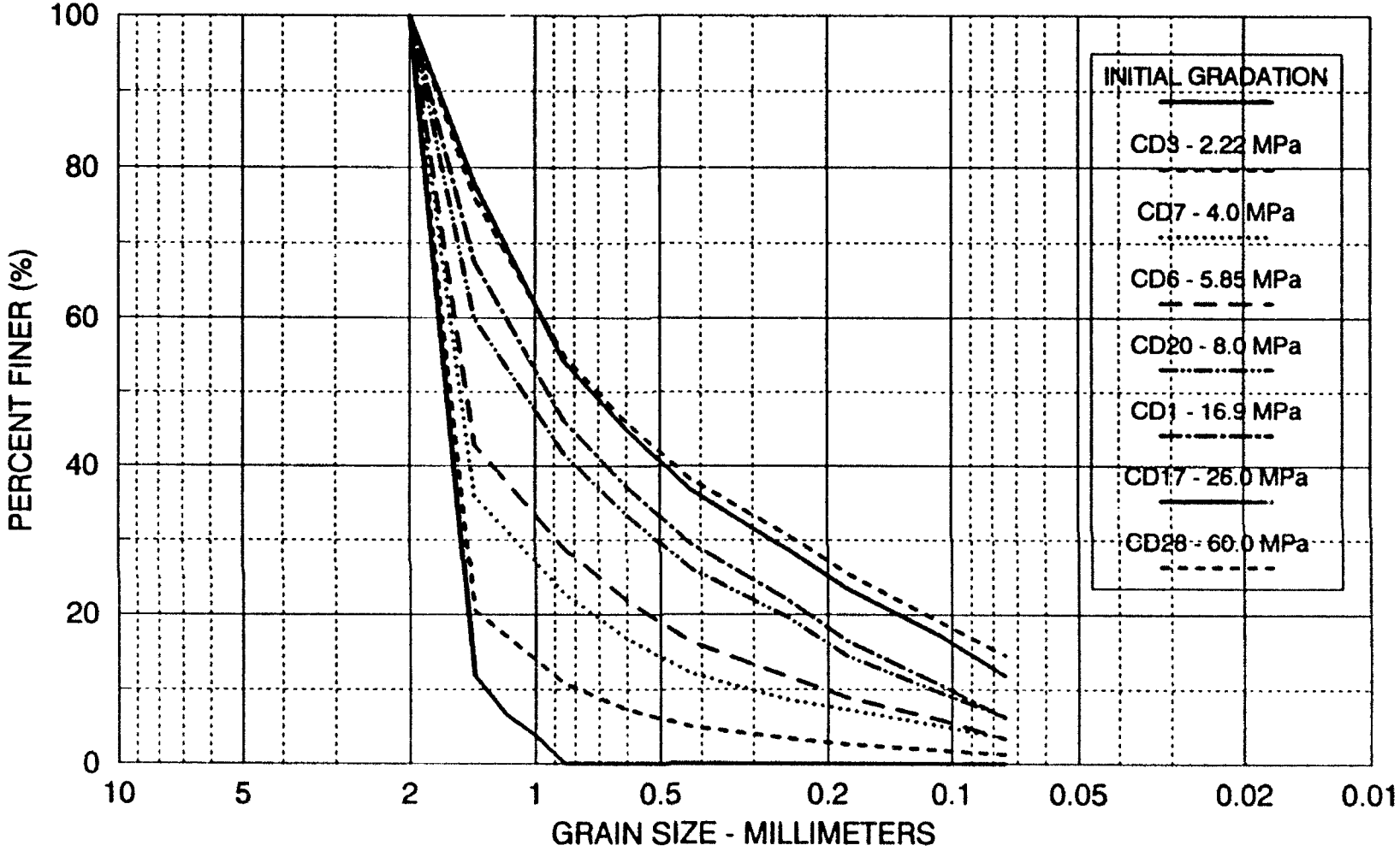

FIGURE 8-2 GRAIN SIZE DISTRIBUTION CURVES
DRAINED TRIAXIAL COMPRESSION TESTS
DENSE CAMBRIA SAND

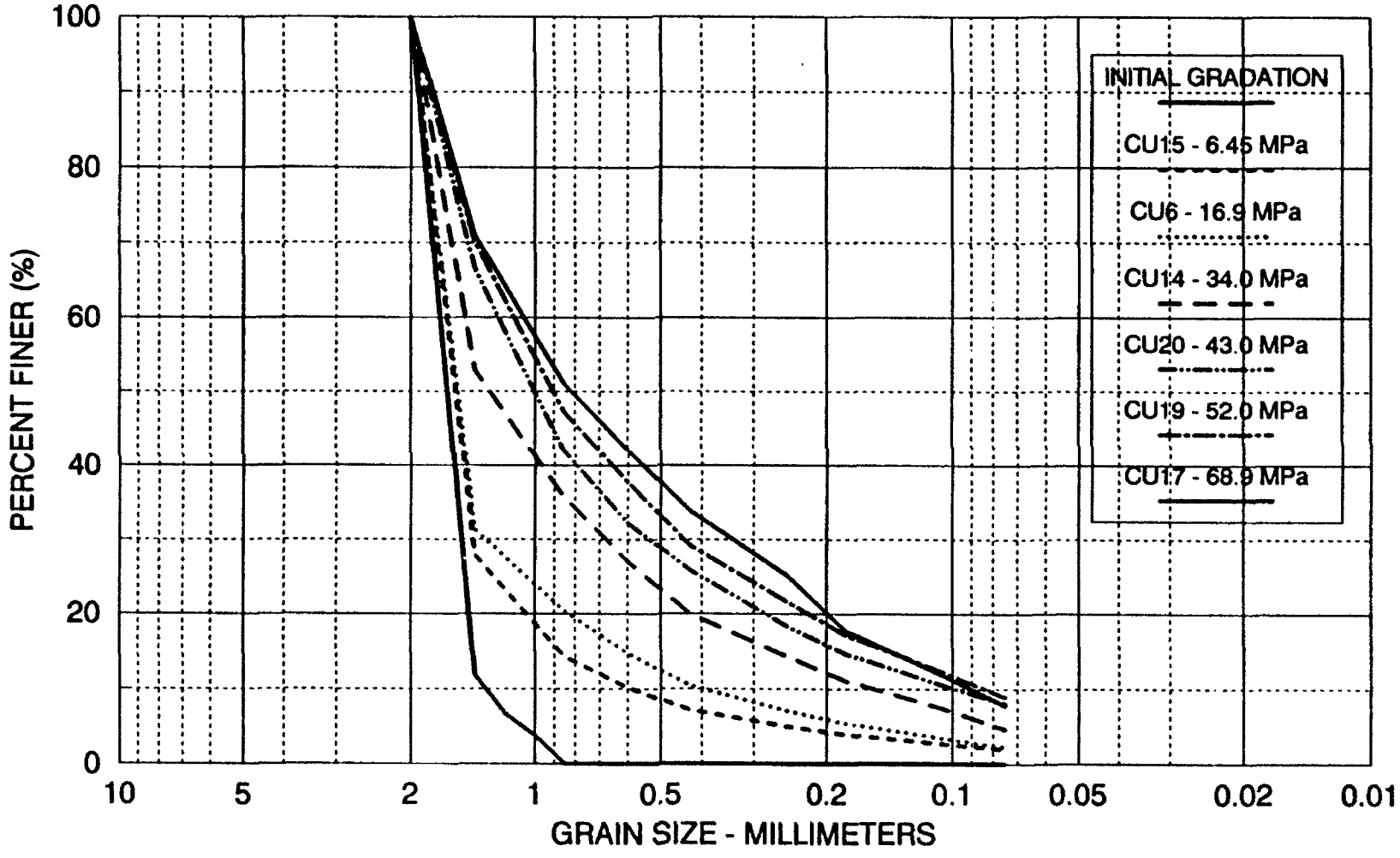

FIGURE 8-3 GRAIN SIZE DISTRIBUTION CURVES
UNDRAINED TRIAXIAL COMPRESSION TESTS
DENSE CAMBRIA SAND

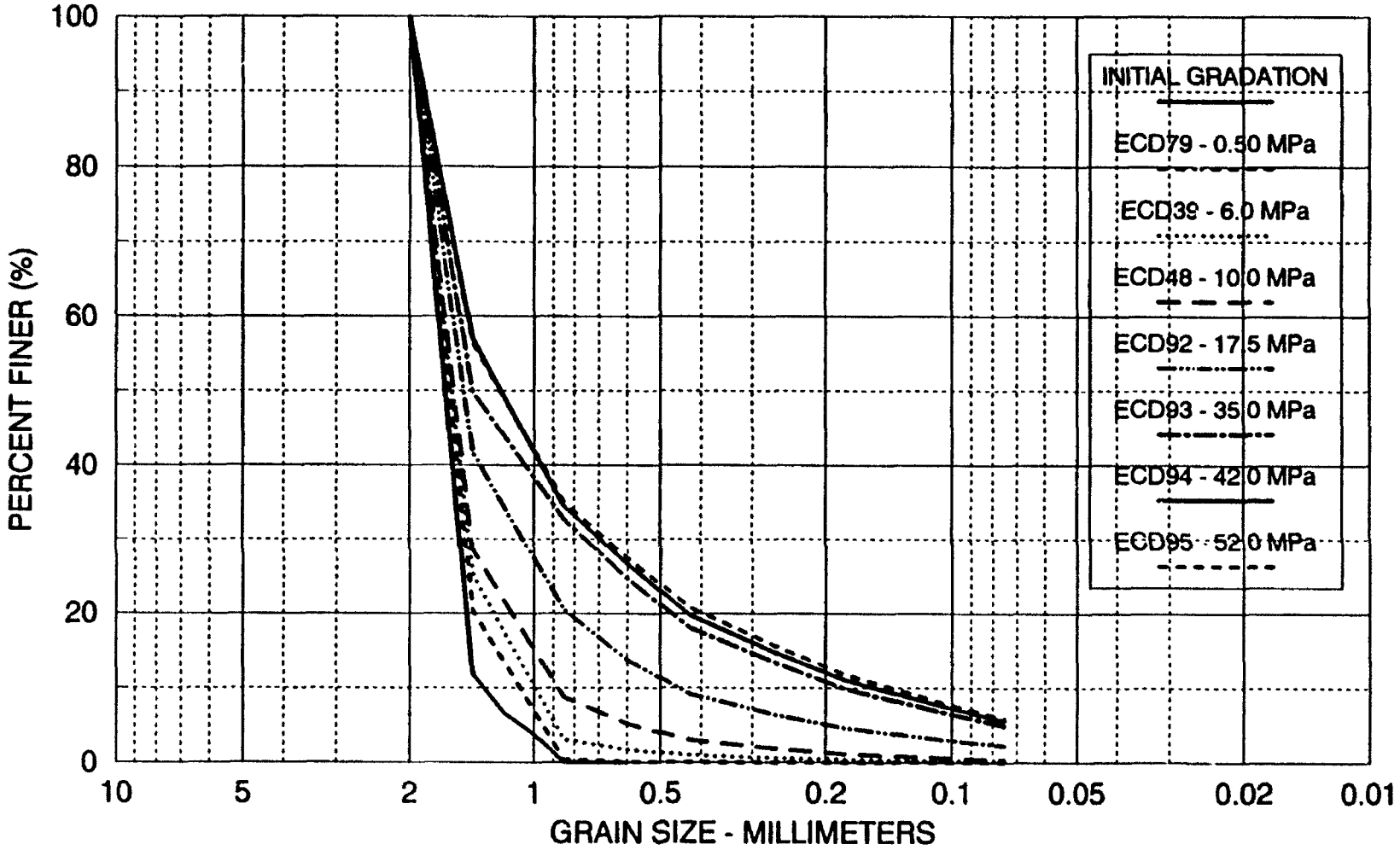

FIGURE 8-4 GRAIN SIZE DISTRIBUTION CURVES
DRAINED TRIAXIAL EXTENSION TESTS
DENSE CAMBRIA SAND

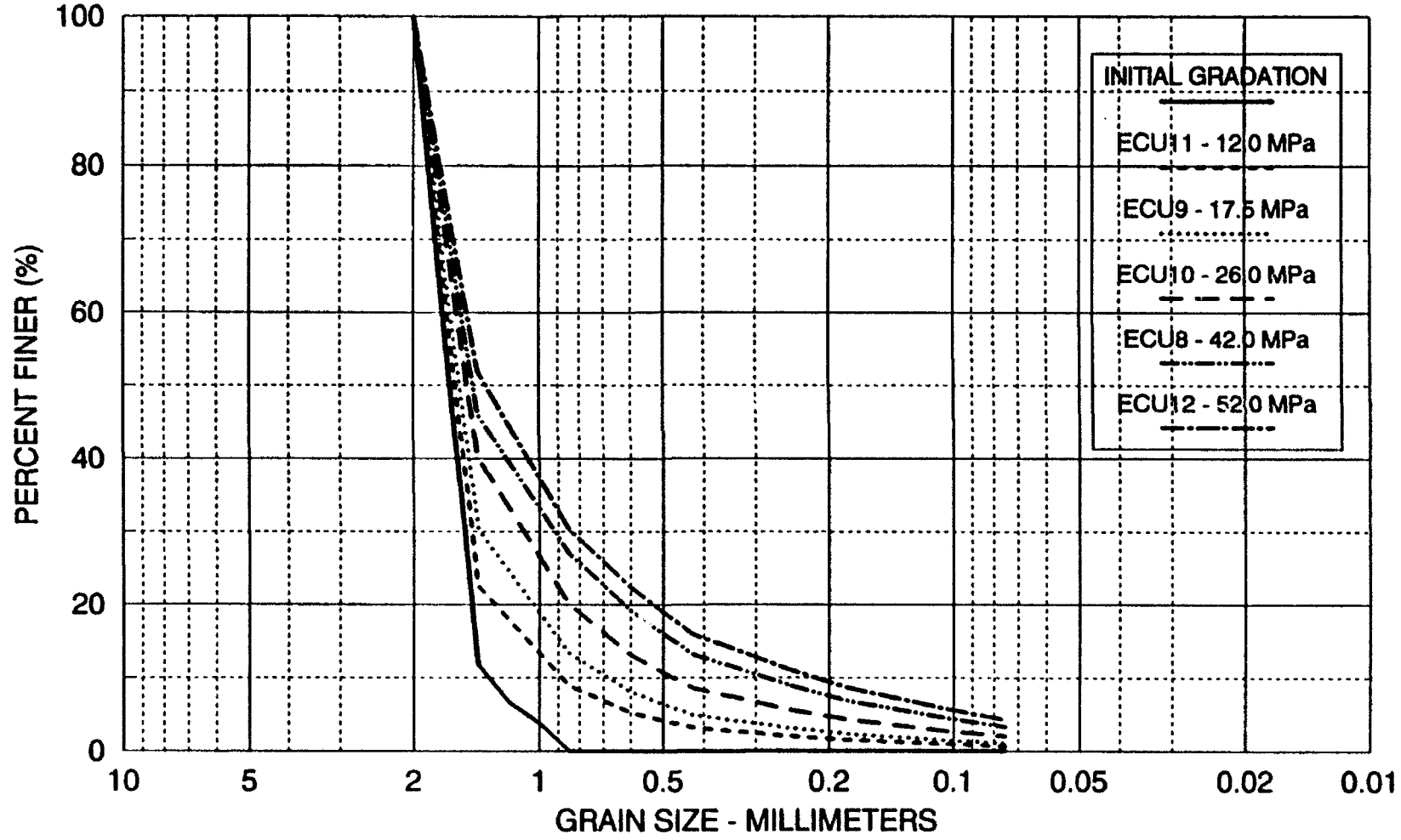

FIGURE 8-5 GRAIN SIZE DISTRIBUTION CURVES
UNDRAINED TRIAXIAL EXTENSION TESTS
DENSE CAMBRIA SAND

different types of tests, that particle crushing increases with increasing initial confining pressure. The gradations all move toward a well-graded condition. Generally, the high pressure drained tests have more particle crushing than the high pressure undrained tests for similar initial effective confining pressures. This was evident from visual examination of the sheared specimens after the tests were completed. The high pressure drained test specimens tend to resemble solid rocks, and are often recoverable as a single piece. The undrained tests, which must maintain the void ratio of consolidation during shearing, pour out of the membranes as individual grains. Of course this is partly due to the low effective confining pressure at the end of a high pressure undrained test. Undrained tests do not exhibit as much crushing in the shearing phase, since the stress levels are much lower than in the drained tests with the same initial consolidation pressure. Another observation from the gradation curves indicates that extension tests do not exhibit as much particle crushing as compression tests. This will be discussed in more detail in later sections.

The four particle breakage factors discussed thus far, the Marsal B, the Lee and Farhoomand D_{15f}/D_{15f}, the Hardin relative breakage B_r, and the proposed B_{10} have been calculated for many of the compression and extension tests performed. These calculated values for individual tests are included in the Appendix. It should be noted that a linear interpolation was performed between sieve sizes in the calculation of the particle breakage factors. Also, some linear extrapolation was required to find the D_{15f} and D_{10f} sizes in a few of the very heavily crushed drained compression tests, because occasionally more than 15 percent was finer than the

No. 200 sieve size. The D_{15i} value was determined to be 1.41 millimeters for Cambria sand. The D_{10i} value was determined to be 1.32 millimeters. The potential breakage factor, B_p, was determined to be 1.296 for Cambria sand. Figures 8-6, 8-7, 8-8 and 8-9 indicate the particle breakage factors by Marsal, Hardin, Lee and Farhoomand, and the new B_{10}, respectively. The breakage factors are plotted against the effective mean normal stress at failure, so comparisons between extension and compression can be analyzed. The relationship between these two variables is not totally accurate, because the mean normal stress at failure does not necessarily represent the state of particle breakage at the conclusion of the test. However, the general trends can be established. As can be seen from all four figures, particle crushing increases with increasing mean normal stress at failure.

Particle breakage is more extensive in triaxial compression than in triaxial extension tests. This is primarily due to the direction of the total stress path in extension, which has decreasing mean normal stress during loading, as opposed to compression, which has increasing mean normal stress during loading. Also, the stresses and strains are much smaller in extension than in compression. All four figures clearly indicate that the rate of particle crushing is reduced in the drained compression and extension tests at the larger effective mean normal stresses at failure. As discussed in Chapter 5, this is in the region where volumetric and principal strains to failure are decreasing, and the material is approaching a compressibility limit for a given maximum stress magnitude. This is also reflected in the grain size distribution curves, which indicate that at higher pressures there

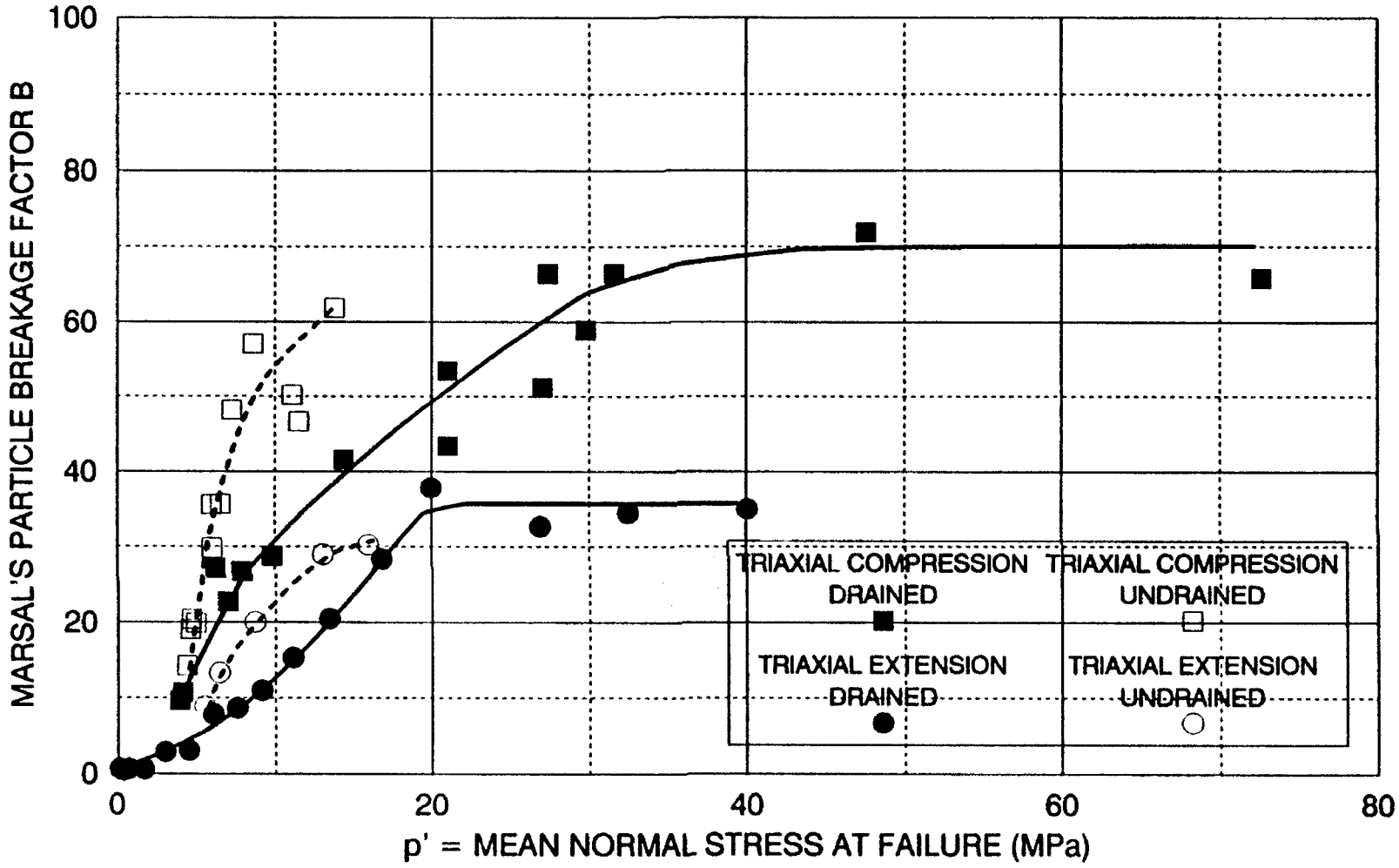

FIGURE 8-6 MARSAL'S PARTICLE BREAKAGE FACTOR B RELATED TO p'
DRAINED AND UNDRAINED TRIAXIAL COMPRESSION AND EXTENSION TESTS
DENSE CAMBRIA SAND

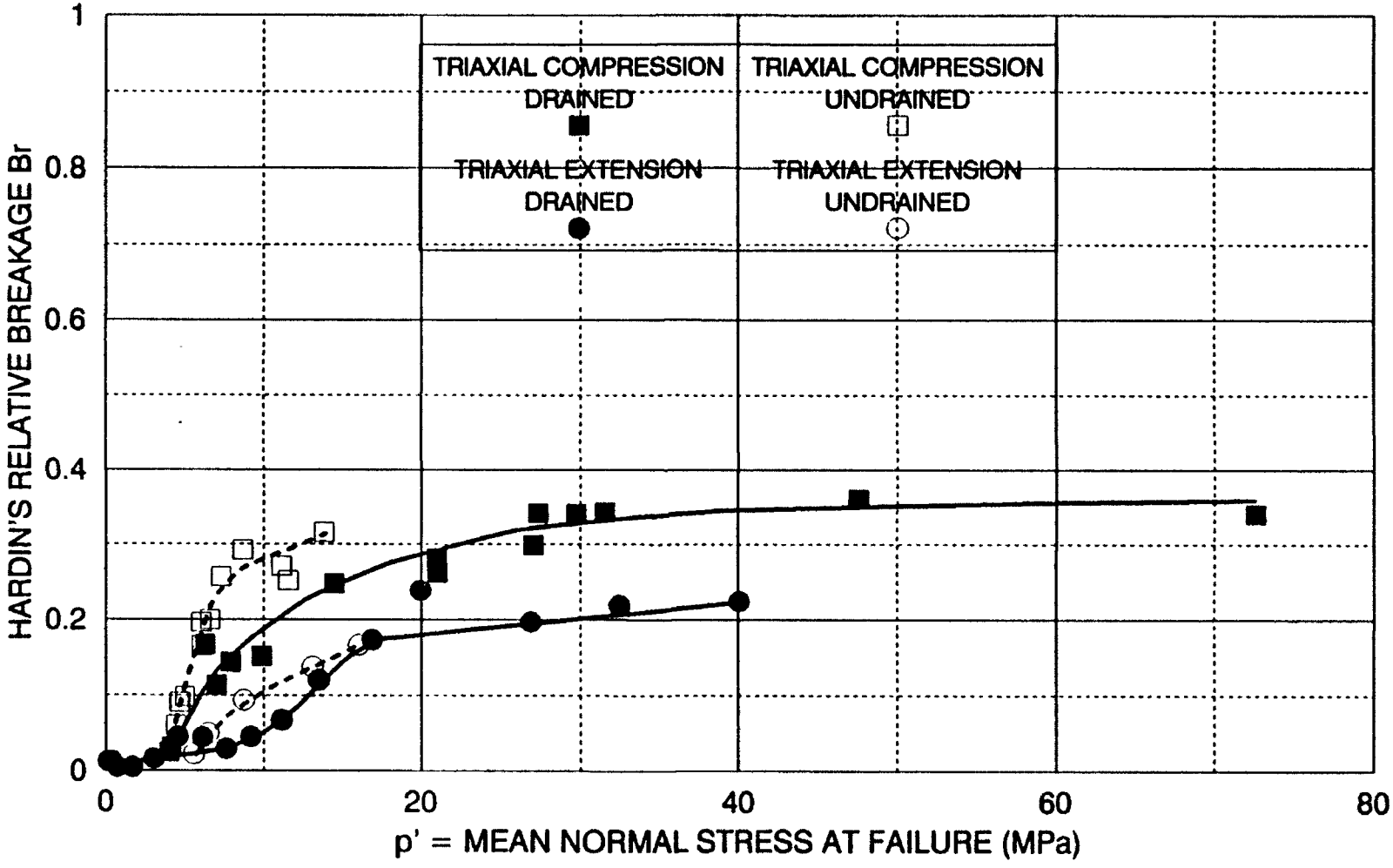

FIGURE 8-7 HARDIN'S RELATIVE BREAKAGE Br RELATED TO p'
DRAINED AND UNDRAINED TRIAXIAL COMPRESSION AND EXTENSION TESTS
DENSE CAMBRIA SAND

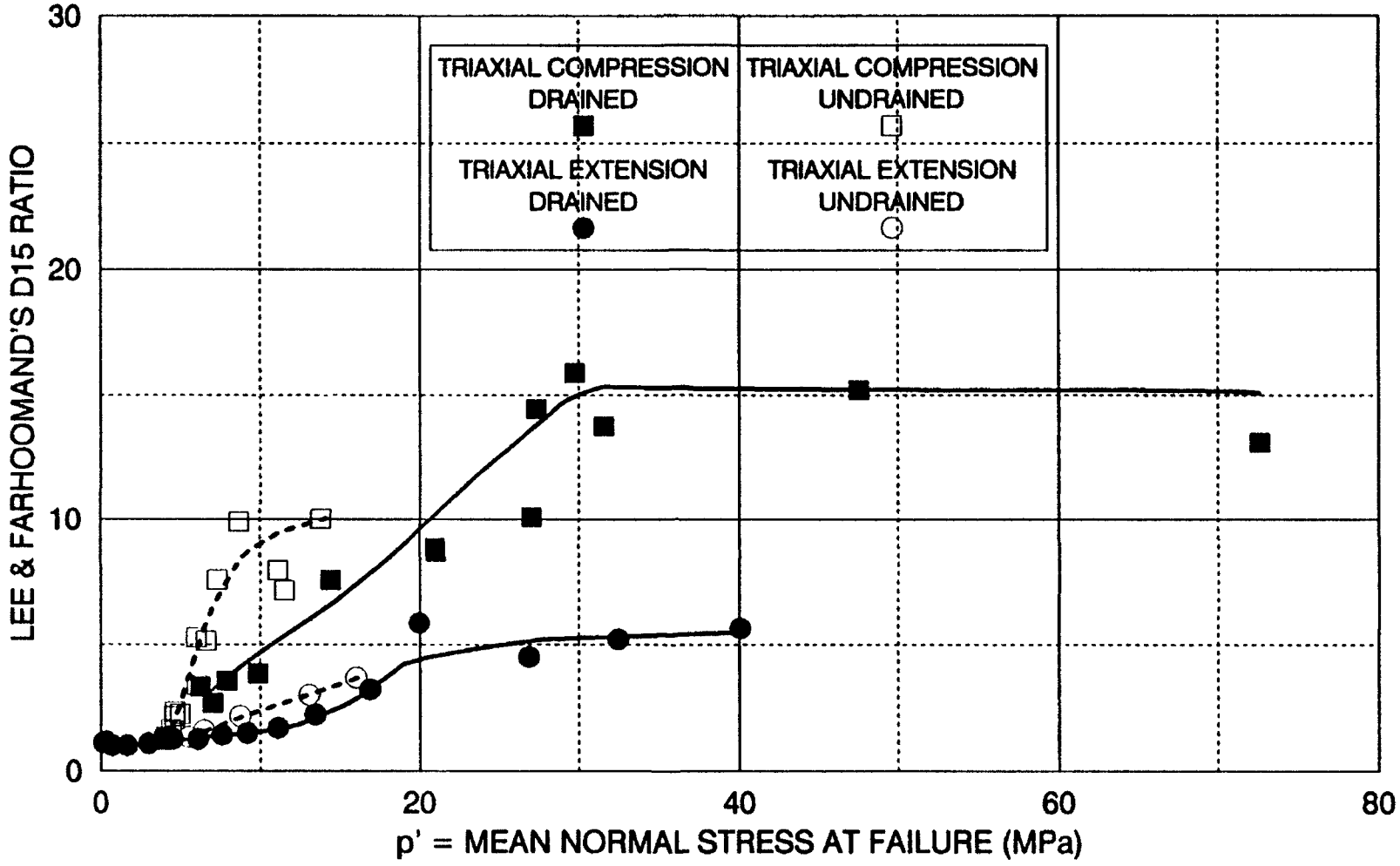

FIGURE 8-8 LEE & FARHOOMAND'S D15 RATIO RELATED TO p'
DRAINED AND UNDRAINED TRIAXIAL COMPRESSION AND EXTENSION TESTS
DENSE CAMBRIA SAND

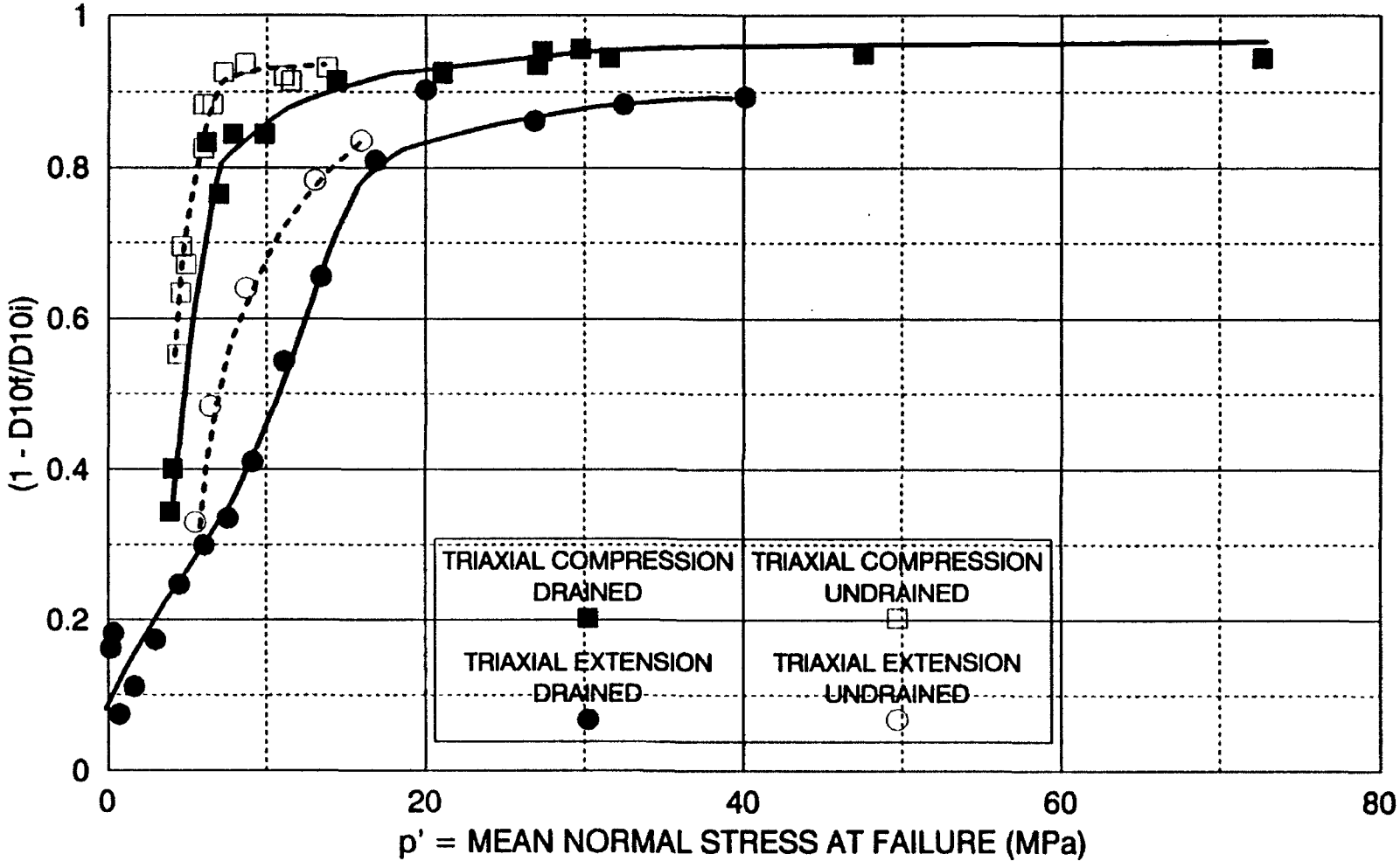

FIGURE 8-9 B10 = (1 - D10f/D10i) RELATED TO p'
DRAINED AND UNDRAINED TRIAXIAL COMPRESSION AND EXTENSION TESTS
DENSE CAMBRIA SAND

is not a substantial change in the final particle size distribution, even when large increases in stress magnitudes are applied. The grain size distribution curve appears to be approaching what would be considered a practical maximum density curve for this given sand. As particle crushing approaches these limits, the void spaces are greatly decreased in volume. The individual particles are packed so tightly and mutually supported at enough contact points that particle breakage slows significantly. At these stress levels particle rearranging may be as significant as particle breakage.

Another observation in both extension and compression clearly indicates that particle crushing is substantially higher in undrained tests, as opposed to drained tests, when compared on the basis of the effective mean normal stress at failure. This is due to the effect of the stress path that undrained tests follow at high pressures. Typically, for a specific mean normal stress at failure the undrained tests undergo a much higher degree of isotropic consolidation, where significant particle breakage occurs as shown on Figure 8-10. The isotropic consolidation stress path follows the horizontal axis at zero stress difference. Once shearing begins, the pore pressures rapidly build up, and the effective mean normal stress at failure is decreased to a much lower magnitude on the effective stress failure line. The drained test, with the same mean normal stress at failure, does not ever venture into these regimes of high stress magnitudes. The effective mean normal stress at failure does not really reflect the effect of stress path on particle crushing. It is therefore not a good basis for comparison of crushing between different types of tests.

The void ratio at failure is shown plotted on Figures 8-11, 8-12, 8-13 and 8-14 against the four particle breakage factors of Marsal, Hardin, Lee and Farhoomand, and the proposed B_{10}. They all clearly indicate a direct relationship between particle crushing and the void ratio at failure. The obvious reason is that at high pressures particle breakage is the major component in the total volume change of the material. Therefore, the void ratios are directly linked to particle crushing. These diagrams also indicate that particle breakage is much greater in compression than extension. However, using this comparison, the drained and undrained tests generally tend to occur on the same line as opposed to comparing the breakage factors on the basis of the effective mean normal stress at failure. The effect of stress path apparently is included in the void ratio at failure.

8.6 Discussion of Different Crushing Parameters

The different crushing parameters, which were developed for different applications, indicate different amounts of scatter, even though they are computed from the same grain size distribution data. There are specific reasons for the amounts of scatter in the figures thus far presented.

The Marsal breakage factor, B, is calculated from the changes in the amounts of material retained on each sieve size. This breakage factor was developed for use with rockfill and gravel size material in earth dams, in which particle breakage is important, but changes in gradation are not extremely large. Theoretically all of the sieve sizes are included in the computation of this breakage factor. However, when particle crushing is very large, there tends to be very little

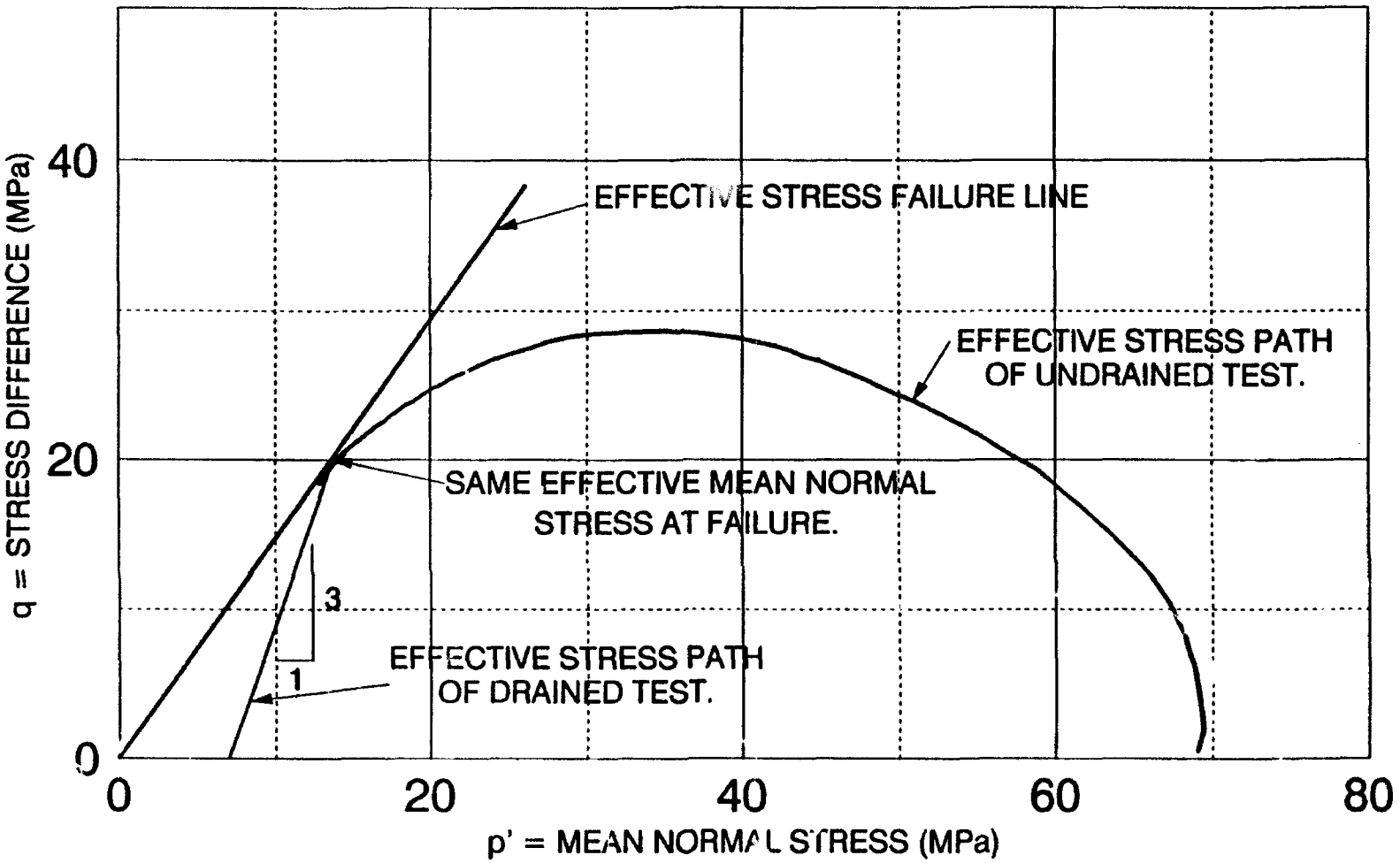

FIGURE 8-10 EFFECT OF STRESS PATH ON PARTICLE BREAKAGE
BETWEEN DRAINED AND UNDRAINED TESTS
DENSE CAMBRIA SAND

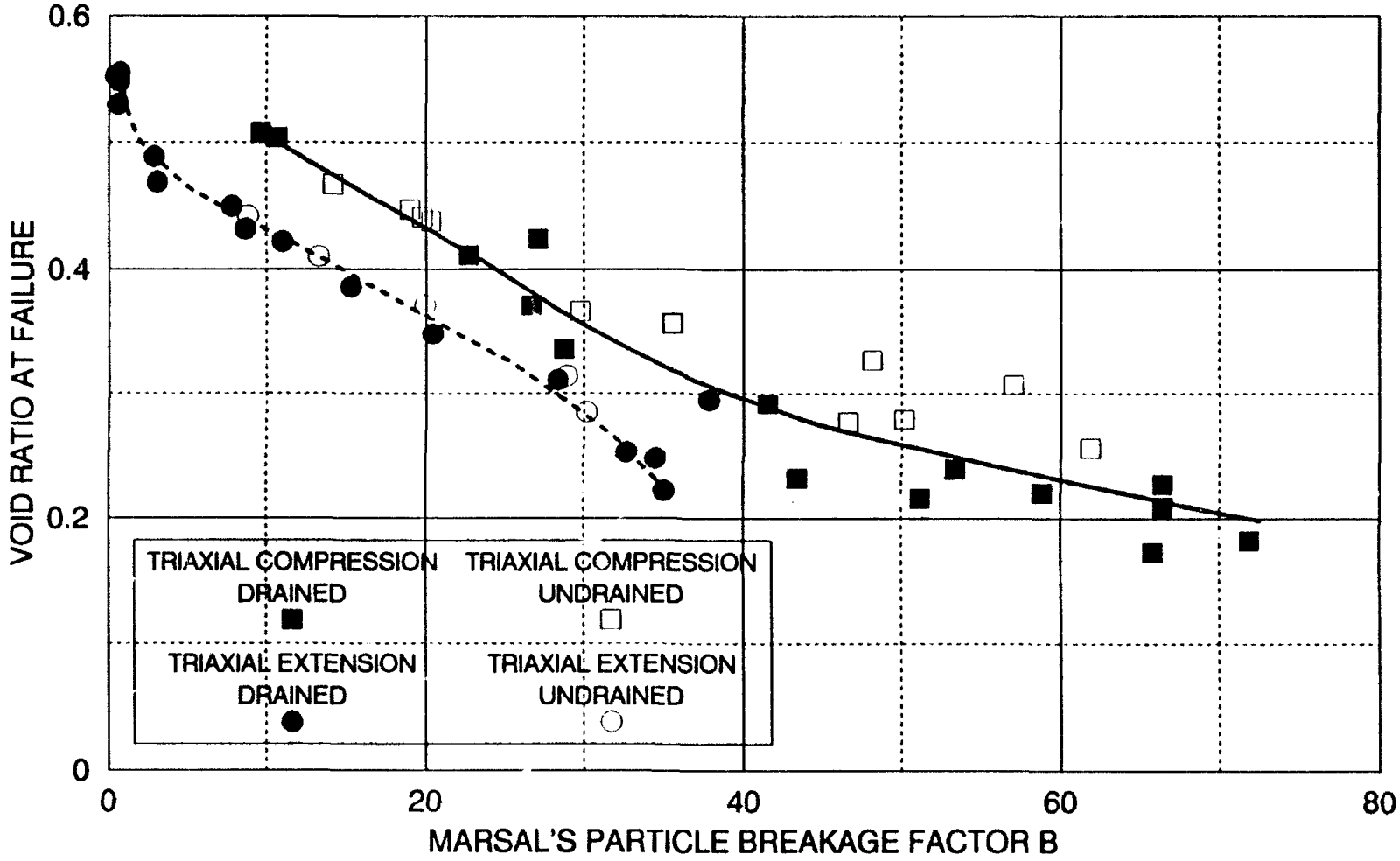

FIGURE 8-11 MARSAL'S PARTICLE BREAKAGE FACTOR B RELATED TO VOID RATIO
DRAINED AND UNDRAINED TRIAXIAL COMPRESSION AND EXTENSION TESTS
DENSE CAMBRIA SAND

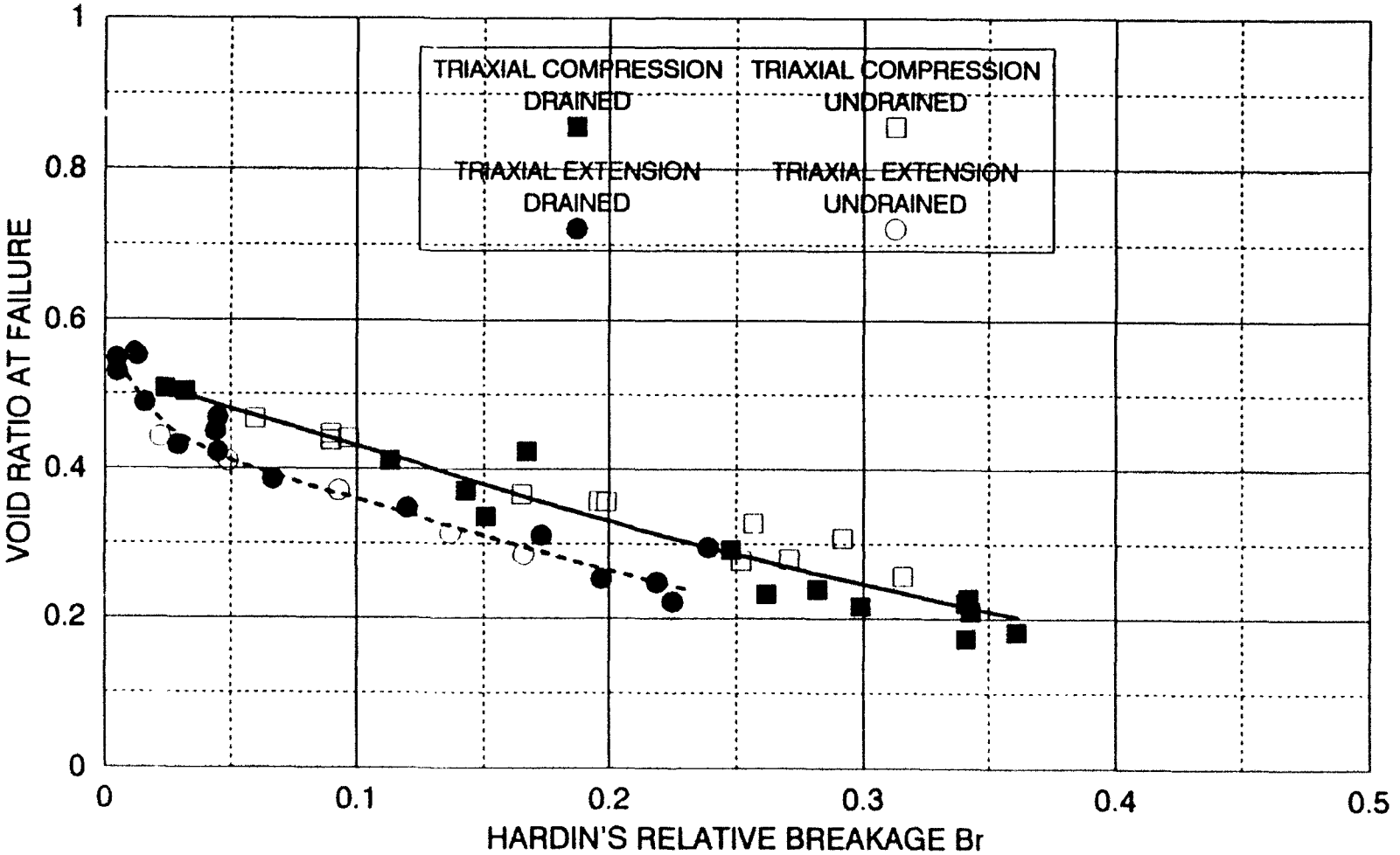

FIGURE 8-12 HARDIN'S RELATIVE BREAKAGE FACTOR Br RELATED TO VOID RATIO
DRAINED AND UNDRAINED TRIAXIAL COMPRESSION AND EXTENSION TESTS
DENSE CAMBRIA SAND

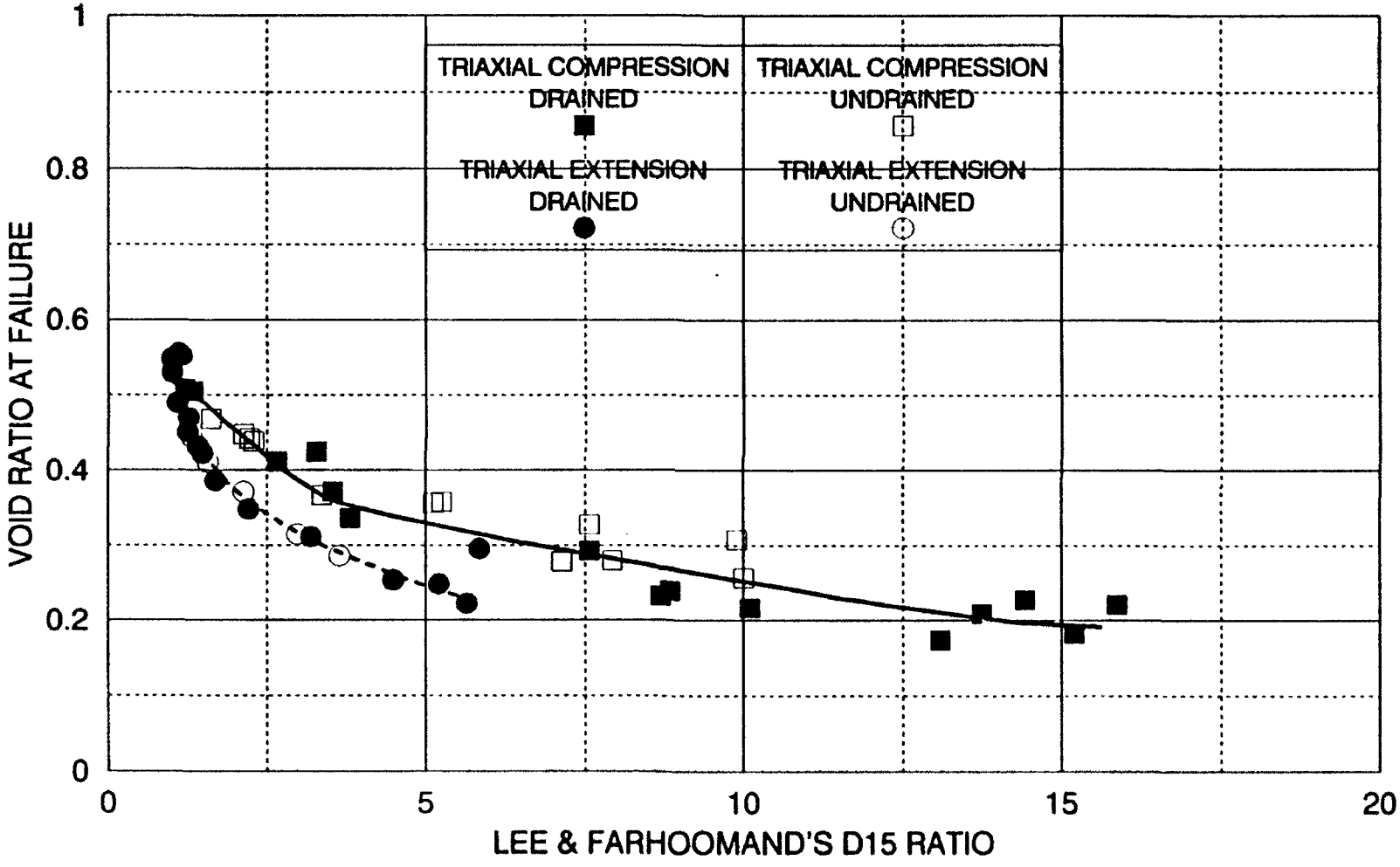

FIGURE 8-13 LEE & FARHOOMAND'S D15 RATIO BREAKAGE FACTOR RELATED TO VOID RATIO
DRAINED AND UNDRAINED TRIAXIAL COMPRESSION AND EXTENSION TESTS
DENSE CAMBRIA SAND

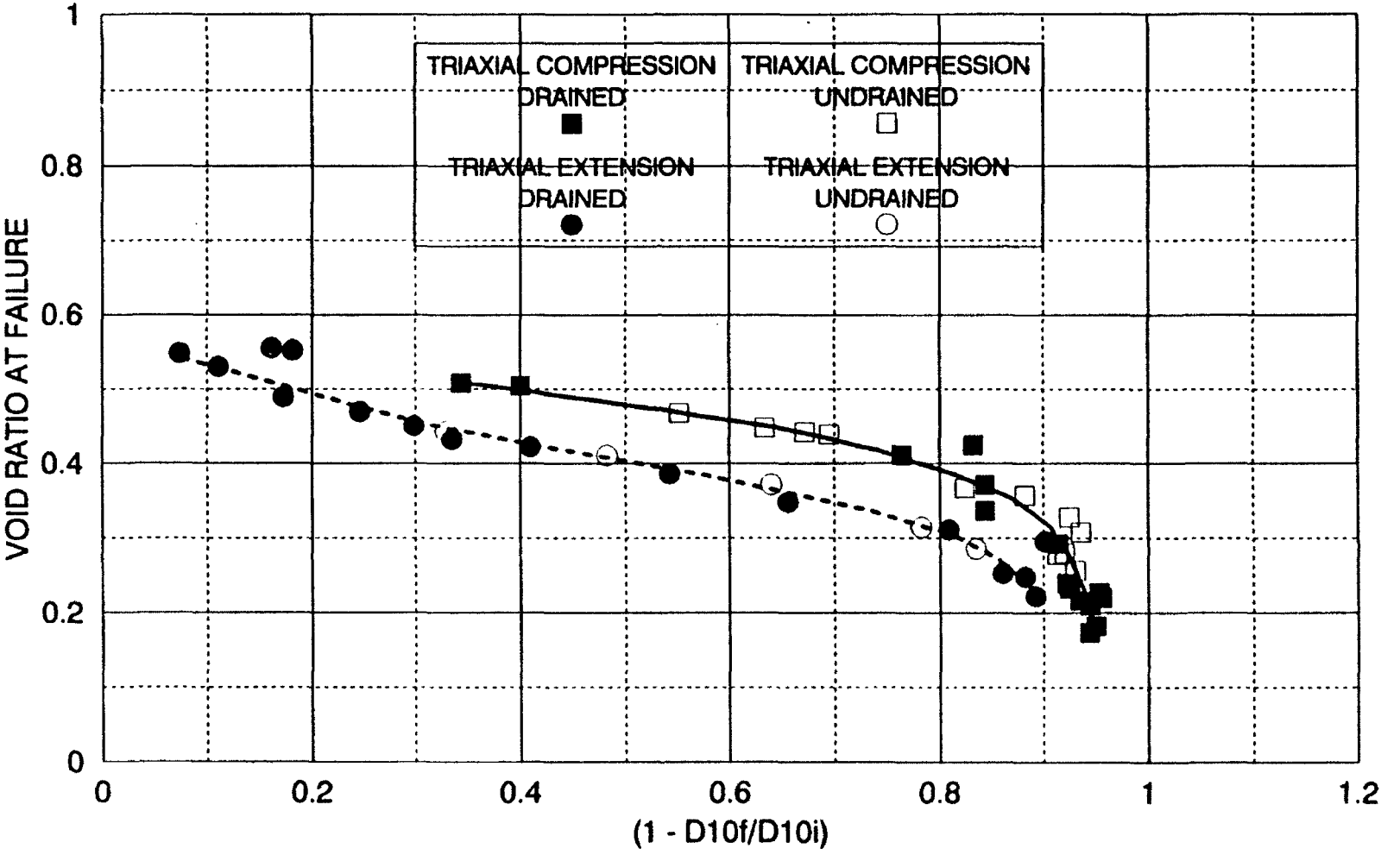

FIGURE 8-14 B10 = (1 - D10f/D10i) FACTOR RELATED TO VOID RATIO
DRAINED AND UNDRAINED TRIAXIAL COMPRESSION AND EXTENSION TESTS
DENSE CAMBRIA SAND

material left on the original sieve sizes for comparison. Often with the originally uniform Cambria sand, the differences in the initial and final gradations almost do not overlap and only one or two sieve sizes can be used in the computation of Marsal's breakage factor. This situation tends to create additional scatter in the magnitude of B for tests in which the soil was extensively crushed.

The particle breakage factor of Lee and Farhoomand, D_{15i}/D_{15f}, which was originally developed to evaluate gravel filters in earth dams, exhibits some scatter, because the ratio is based on a single grain size. A breakage factor based upon a single grain size does not spread out the error in the sieve analysis, which has inherently large errors. Another reason for the scatter is that the ratio places the final D_{15f} grain size in the denominator. When there is significant particle crushing, the D_{15} grain size after shearing is very small. Any small differences in magnitude of this size, as one could expect in the sieve analysis, gets amplified by the division of a small number into a larger one, and additional sensitivity appearing as scatter is obtained.

Hardin's relative breakage factor, B_r, is based upon the area between the original and final grain size curves, normalized by the area between the original grain size curve and the No. 200 sieve size. Since all sieve sizes are involved in this area calculation, any small errors between sieve sizes is not amplified, and indeed this breakage factor does not appear to exhibit much scatter.

The proposed particle breakage factor, B_{10}, is based upon only one grain size, but the ratio of the diameters is inverse of that proposed by Lee and Farhoomand. This tends to stabilize any small errors in the evaluation of the

crushing parameter. Also, since the crushing parameter has a lower limit of zero and an upper limit of unity, the scatter in results is limited. Consequently, there is little scatter in the results. However, one problem occurred for tests that experienced very large amounts of particle breakage. The sieve analyses were performed with the smallest sieve size being the No. 200 sieve. Some tests had more than 10 percent passing the No. 200 sieve. Therefore, for a few tests some values of D_{10} had to be obtained through linear extrapolation. This problem was also experienced with the Lee and Farhoomand particle breakage factor.

8.7 Effects of Particle Crushing on the Stress-Strain Behavior

Parts of this discussion was previously presented in Chapter 5, but the importance of particle crushing on the overall behavior of soils at high pressures is further discussed here. The effect of particle crushing is substantial on the stress-strain behavior of granular materials at high pressures. The crushing curves plotted against effective mean normal stress at failure (Figures 5-32 & 5-34) clearly show that the large increase in the principal strain to failure and volumetric strain at failure for drained compression tests starting at 4 MPa is directly related to increased particle crushing. This also explains why the extension test strains to failure do not increase as much as strains to failure in compression. When the rate of particle crushing starts to decrease, the strains to failure and volumetric strains at failure also start to decrease.

The normalized stress-strain curve for high pressure drained compression tests is composed of three line segments (Figures 5-1 & 5-2). The flattening of the

middle segment is directly related to the extent of particle crushing. While significant particle crushing is occurring, the segment becomes very flat, but when particle crushing nears its ultimate value, the steepness of the normalized stress-strain curve increases.

The drained Mohr-Coulomb secant friction angles in the high pressure drained compression and extension tests are directly related to the rate of dilation at failure (Figures 5-35 & 5-36), which at high pressures is directly related to the extent of particle crushing. The drained friction angle decreases to a minimum value as the volumetric strain changes and moves out of the initial dilatancy region. This occurs as particle crushing is rapidly increasing. Then as the rate of particle crushing decreases at higher confining pressures, the friction angle increases slightly to a stable value, at which the particle crushing has reached its ultimate value for that particular mean normal stress level. This is the reason the drained extension friction angle at high pressures is smaller than in compression. Until the densification caused by the level of particle breakage in extension increases to the level of those experienced in compression, the drained friction angle in extension probably will not increase appreciably, and it will remain lower than that in compression.

The undrained friction angles in high pressure compression and extension tests are higher than the drained values at the same mean normal stress at failure. This is due to the effect of the differences in stress paths, as was shown on Figure 8-10. The large amount of particle breakage occurring and the resulting densification from the high stress levels experienced during isotropic compression

directly related to the extent of particle crushing. While significant particle crushing is occurring, the segment becomes very flat, but when particle crushing nears its ultimate value, the steepness of the normalized stress-strain curve increases.

The drained Mohr-Coulomb secant friction angles in the high pressure drained compression and extension tests are directly related to the rate of dilation at failure, which at high pressures is directly related to the extent of particle crushing. The drained friction angle decreases to a minimum value as the volumetric strain changes and moves out of the initial dilatancy region. This occurs as particle crushing is rapidly increasing. Then as the rate of particle crushing decreases at higher confining pressures, the friction angle increases slightly to a stable value, at which the particle crushing has reached its ultimate value for that particular mean normal stress level. This is the reason the drained extension friction angle at high pressures is smaller than in compression. Until the densification caused by the level of particle breakage in extension increases to the level of those experienced in compression, the drained friction angle in extension probably will not increase appreciably, and it will remain lower than that in compression.

The undrained friction angles in high pressure compression and extension tests are higher than the drained values at the same mean normal stress at failure. This is due to the effect of the differences in stress paths, as was shown on Figure 8-10. The large amount of particle breakage occurring and the resulting densification from the high stress levels experienced during isotropic compression

creates higher undrained friction angles. The corresponding drained tests must create most of their densification during the shearing phase.

8.8 Particle Breakage Factors Correlated with Energy

It was pointed out that using the effective mean normal stress at failure to correlate test results with the particle breakage factors was not satisfactory, because it was demonstrated that there did not appear to be any commonality between undrained tests, drained tests, extension tests and compression tests. Most standard soil mechanics parameters derived from analysis of data from testing do not effectively reflect the amount of particle breakage, such that all types of tests can be directly related. It has been shown that increases in confining pressure as well as shearing the soil to larger strain levels increase the amount of particle breakage. With this in mind, the magnitude of energy input into the specimen during the tests would seem to be a more appropriate parameter to use for correlation with particle breakage. The reason for this is based upon the fact that computations of energy incorporate the magnitudes of both stresses and strains, both of which greatly affect the amount of particle crushing. A form of this correlation has previously been proposed by Miura and Ohara in 1979. However, they proposed using plastic work instead of total input energy, and they extracted the elastic energy from the total energy to obtain the plastic work. The amount of elastic energy in tests where particle crushing is significant is very small compared to the magnitude of plastic work, such that there is little difference between the two quantities. Using total energy input simplifies the computational

procedure considerably. The total amount of energy input into a specimen during a triaxial test is the sum of energy input during the isotropic consolidation phase and the shearing phase as shown in Equation 8.3.

$$E_T = E_C + E_S \qquad (8.3)$$

E_T - *total energy input into specimen.*
E_C - *energy input during consolidation.*
E_S - *energy input during shearing.*

During consolidation the amount of input energy is created by the increase in cell pressure resulting in volumetric strains. During drained shearing the input energy is generated by two components: The cell pressure and volumetric strain, and the deviator stress with the resulting axial strain as shown in Equation 8.4. Undrained tests do not experience volumetric strains, so there is no contribution from that component.

$$E_T = \sum_{0}^{\sigma_C} \overline{\sigma}_C \cdot \dot{\epsilon}_V + \left[\sum_{0}^{EOT} (\sigma_1 - \sigma_3) \cdot \dot{\epsilon}_A + \sum_{0}^{EOT} \overline{\sigma}_C \cdot \dot{\epsilon}_V \right] \qquad (8.4)$$

σ_C - *final cell pressure.*
$\overline{\sigma}_C$ - *average cell pressure over increment.*
$\dot{\epsilon}_V$ - *volumetric strain increment.*
EOT - end of test.
$(\sigma_1 - \sigma_3)$ - *average deviator stress over increment.*
$\dot{\epsilon}_A$ - *axial strain increment*
(ϵ_1 *in compression,* ϵ_3 *in extension*).

Input energy for tests in extension use the same method as represented in Equation 8.4. The correlation with particle crushing necessitates that energy computations be performed and accumulated from the beginning to the end of the test. The input energies were calculated for all tests for which particle breakage factors were

calculated. The values for energy of consolidation, energy from volumetric strains, and energy obtained from the axial strains are included in the Appendix. The total input energies were calculated and accumulated from the full original data files that contained hundreds of data points recorded by the data acquisition system. Therefore, some small variations are to be expected if calculations of energy are performed using the more limited number of points provided by the test data in the Appendix.

The four particle breakage factors by Marsal, Hardin, Lee and Farhoomand, and the proposed B_{10} are plotted against total input energy and shown on Figures 8-15, 8-16, 8-17 and 8-18, respectively. As can be readily seen, the correlation of crushing parameters with total input energy is excellent and relates all the different types of tests, drained and undrained compression and extension, with one unique curve. There is some scatter with the Marsal parameter and with the Lee and Farhoomand parameter, for reasons previously discussed, but the Hardin relative breakage parameter, B_r, and the proposed parameter, B_{10}, show unique correlations within the normal scatter obtained in a sieve analysis.

8.9 Evaluation of Particle Breakage on a Grain Level

Thus far the analysis of particle breakage has taken the form of relating the empirical particle breakage factors, derived from the change in particle sizes, with soil parameters obtained on a macro-level, such as effective mean normal stress at failure, void ratio, and input energy. The qualitative mechanics on a micro-level needs to be ascertained to observe if the correlations explored thus far are

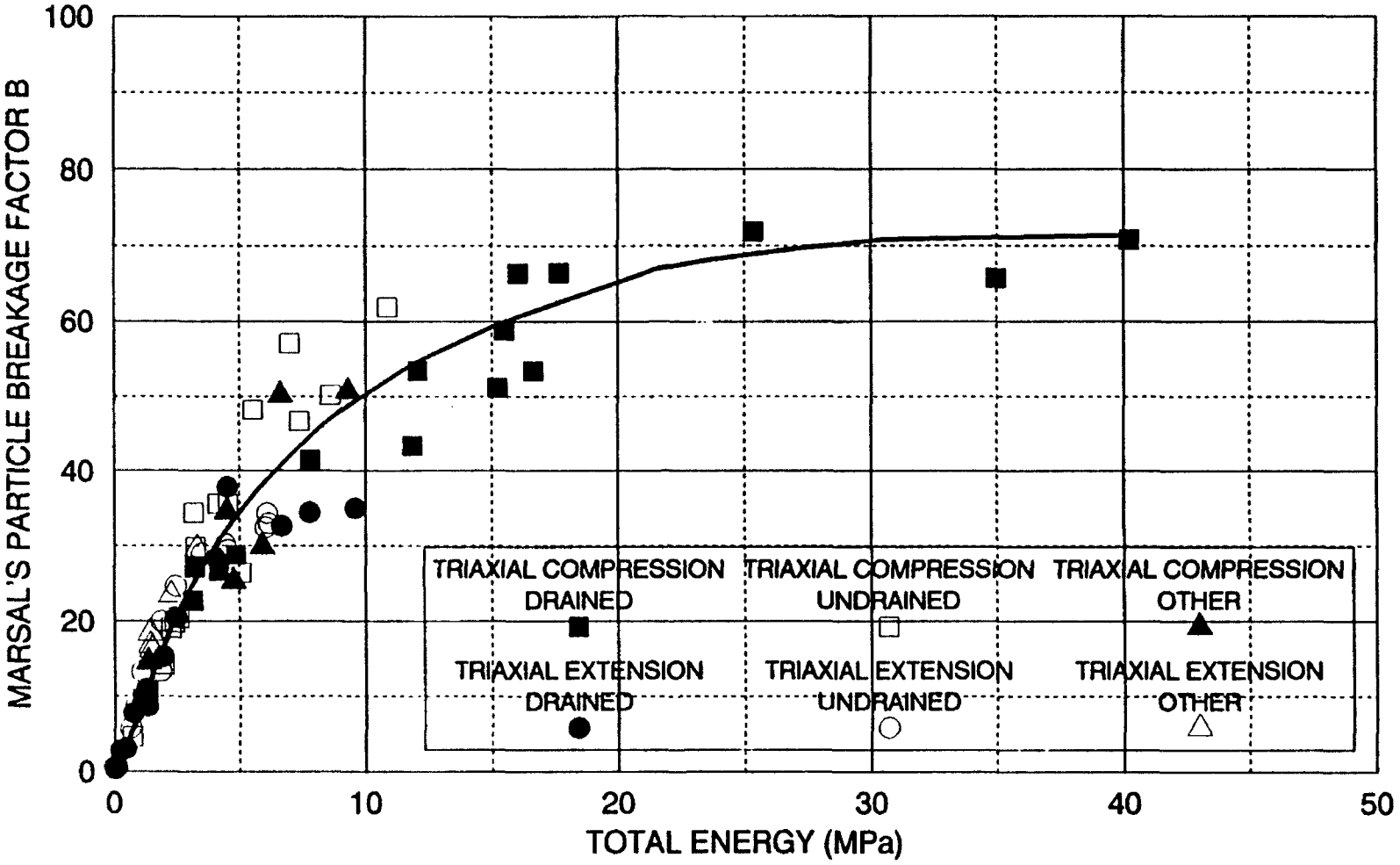

FIGURE 8-15 MARSAL'S PARTICLE BREAKAGE FACTOR B RELATED TO ENERGY
DRAINED AND UNDRAINED TRIAXIAL COMPRESSION AND EXTENSION TESTS
DENSE CAMBRIA SAND

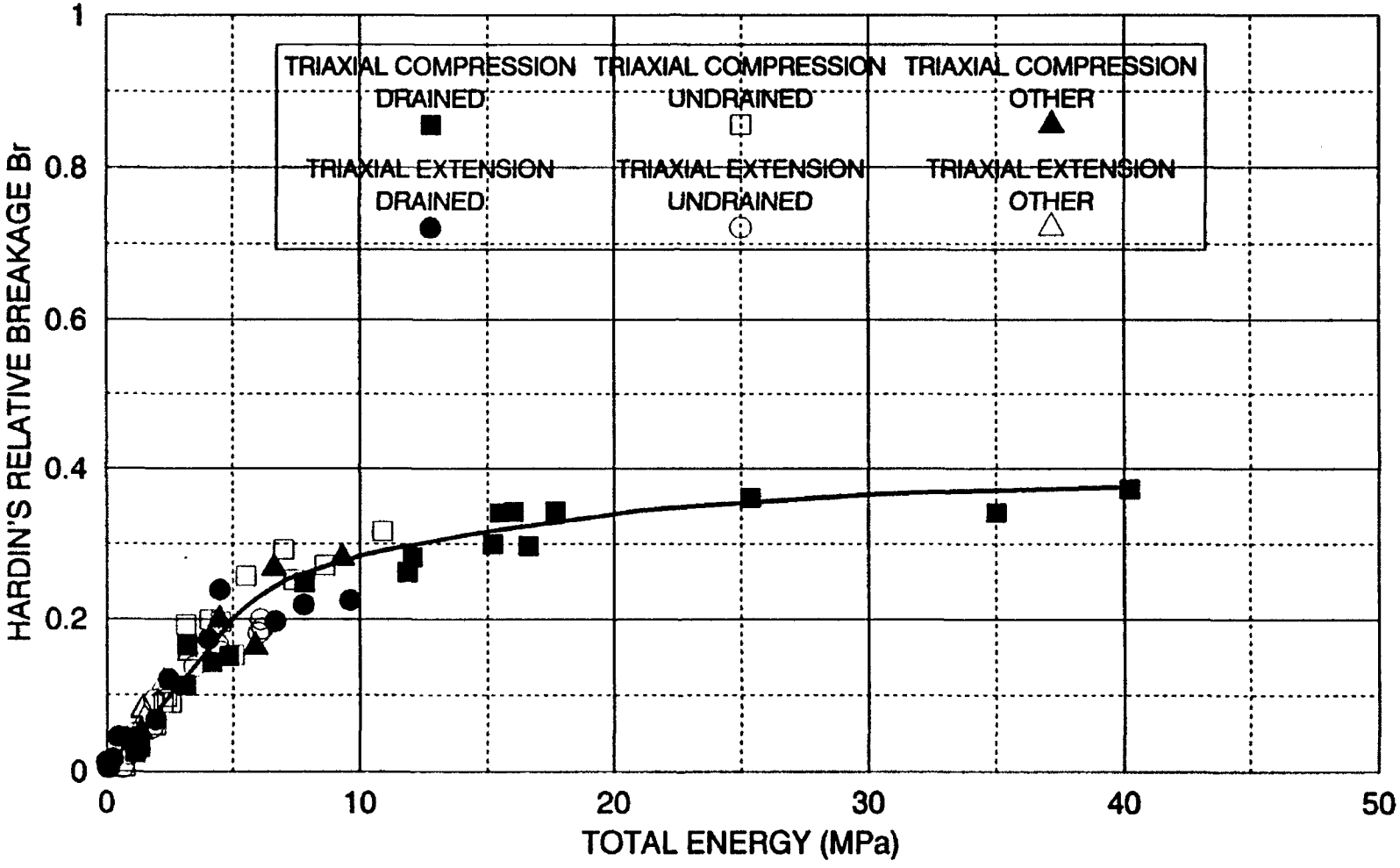

FIGURE 8-16 HARDIN'S RELATIVE BREAKAGE Br RELATED TO ENERGY
DRAINED AND UNDRAINED TRIAXIAL COMPRESSION AND EXTENSION TESTS
DENSE CAMBRIA SAND

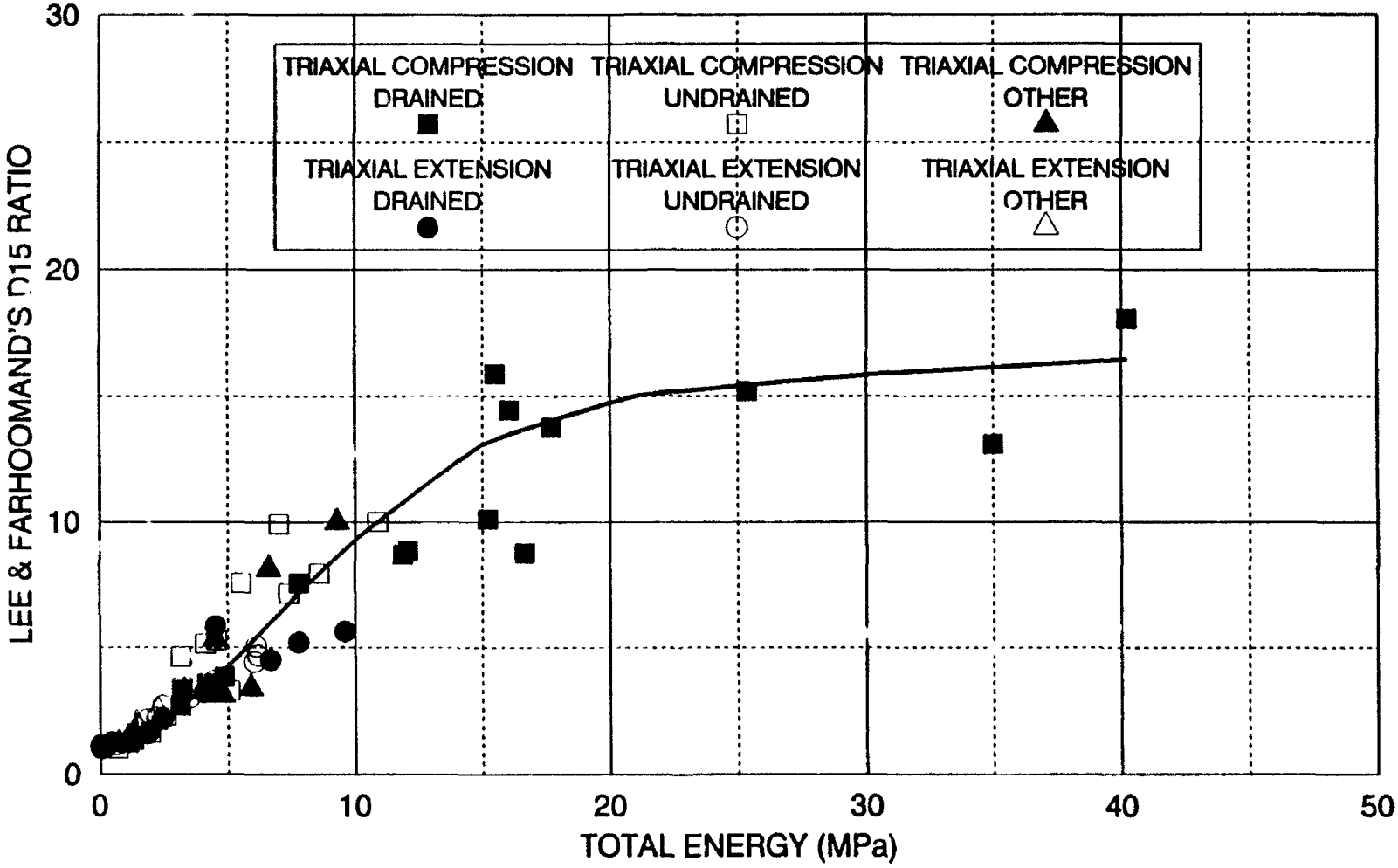

FIGURE 8-17 LEE & FARHOOMAND'S D15 RATIO BREAKAGE FACTOR, RELATED TO ENERGY
DRAINED AND UNDRAINED TRIAXIAL COMPRESSION AND EXTENSION TESTS
DENSE CAMBRIA SAND

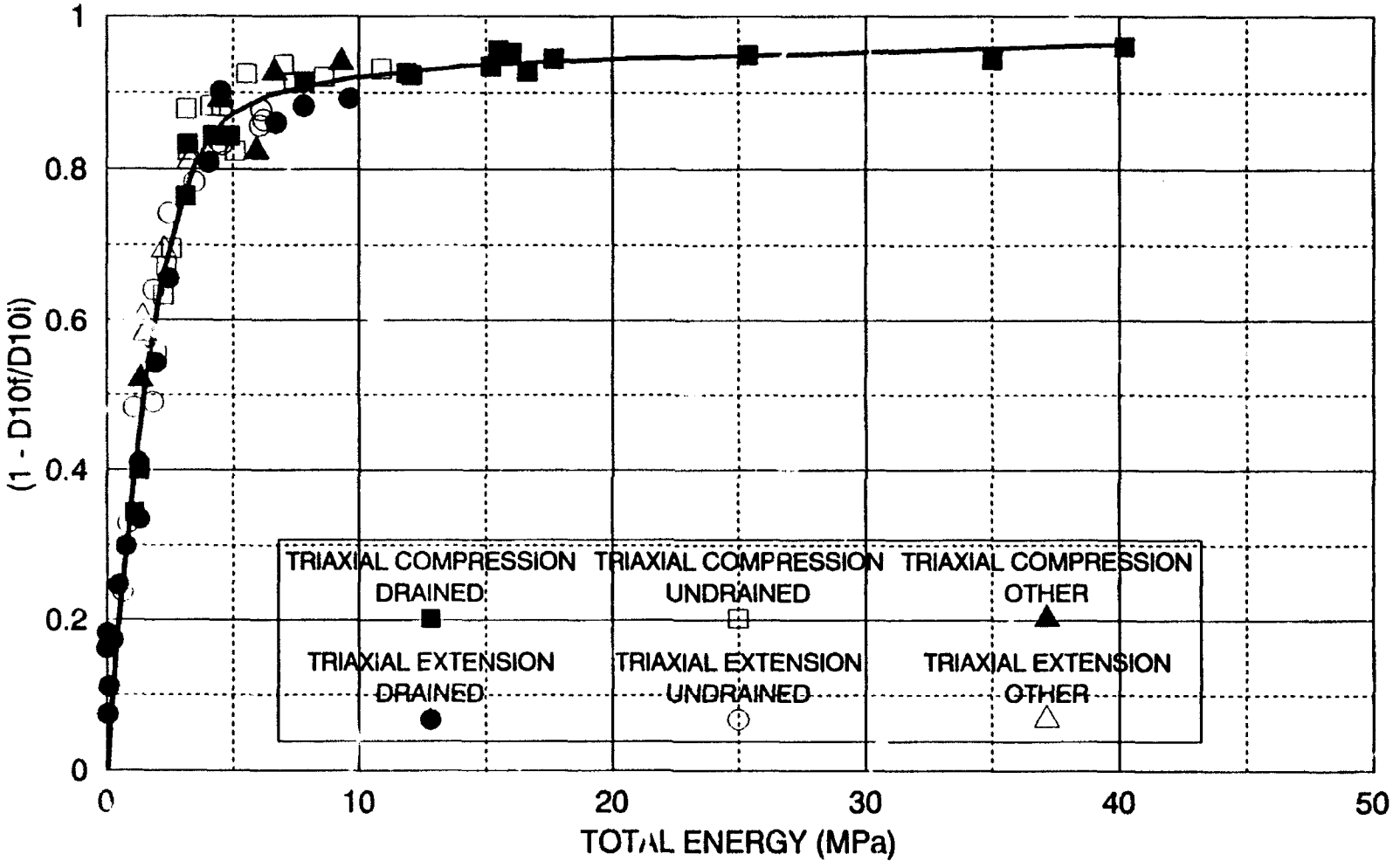

FIGURE 8-18 B10 = (1 - D10f/D10i) BREAKAGE FACTOR RELATED TO ENERGY
DRAINED AND UNDRAINED TRIAXIAL COMPRESSION AND EXTENSION TESTS
DENSE CAMBRIA SAND

generally applicable to all soils.

With the assistance from the Department of Earth and Space Sciences at University of California, Los Angeles, thin-section slides were made from the original and sheared Cambria sand. The thin-sections of the crushed material are made by impregnating the larger pieces of compressed sand with expoxy resin. After the saturated pieces are cured, they are sliced into flat sections. These flat sections are mounted onto the surface of a glass slide, where they are ground down to a thickness of approximately 0.03 millimeters. At this thickness the thin-section is translucent, and it may be examined under a light-polarizing microscope, in which minerology and structure may be evaluated.

Since the Cambria sand is composed of many mineral constituents (Chapter 3), some particles are significantly harder than other particles. The sheared Cambria sand thin-section was obtained from a drained triaxial compression test with a confining pressure of 17.2 MPa. Since Cambria sand is composed of many minerals of different hardnesses, a sand that is composed of particles of similar mineral hardnesses was also evaluated. A quartz sand that contained some feldspar was tested in a series of five drained triaxial compression tests. Thin-sections were made of the sand before and after shearing. The post-sheared specimen was obtained from a drained triaxial compression test performed at a confining pressure of 52.0 MPa.

Photographs of the thin-sections of the Cambria and quartz sand both before and after shearing are shown in Figures 8-19 and 8-20, respectively. The thin-sections of Cambria sand, shown on Figure 8-19, indicate that compression and

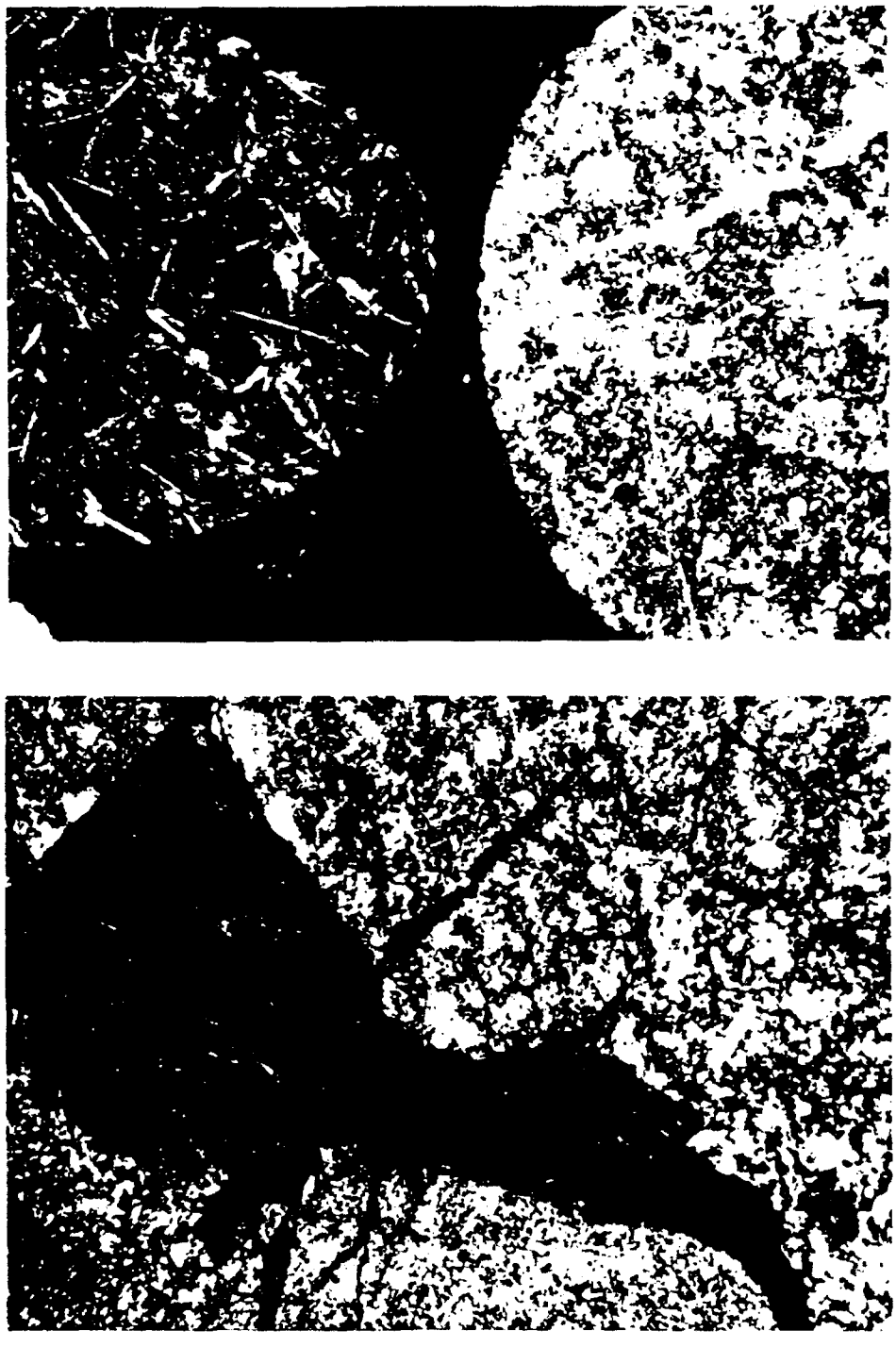

Figure 8-19 Photographs of Thin Sections of Cambria Sand before and after Shearing.

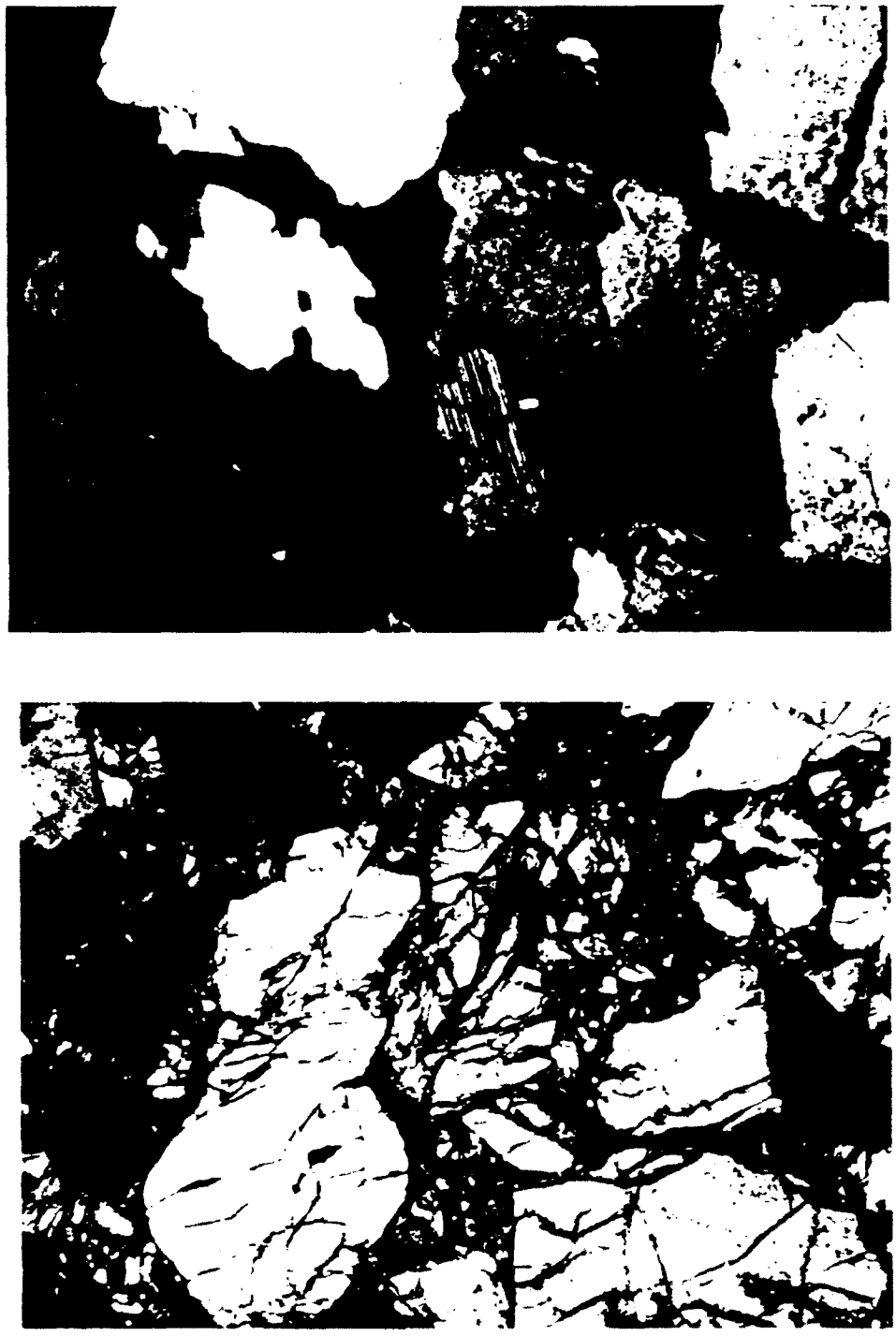

Figure 8-20 Photographs of Thin Sections of Quartz Sand before and after Shearing.

densification take the form of softer grains being plastically deformed and squeezed into the void spaces between harder grains. There does not seem to be much evidence of particle fracturing and rearranging into void spaces.

The thin-sections of the quartz sand, shown on Figure 8-20, indicate that particle fracturing and rearranging is the predominant form of densification for this sand. The plastic deformations seen in the Cambria sand thin-sections is not apparent in the quartz sand. This stems from the fact that the quartz and feldspar grains have similar mineral hardness.

The apparent lack of visible pore spaces on the thin-sections does not result in the conclusion that there is very little residual porosity. Under this level of grain crushing, the large pore spaces are filled, but there is still substantial amounts of "micro porosity" within the specimen. Microporosity is porosity in cracks and fissures within and around grain structures. Thin-sections are approximately 0.03 milimeters thick. Therefore, if grains are smaller than this dimension, then there may be actual void spaces above and below the grains shown on the slide.

Even though there are apparent differences in the mechanisms of volumetric compression on the grain level between the two sands, either can be treated with the macro-correlations examined here. Energy computations are global in nature, and it is independent of how the strains are achieved.

8.10 Using the B_{10} Particle Breakage Factor to Obtain Permeability

As discussed in Section 8.4, particle crushing indices could possibly be used

to determine the permeability of granular materials. The correlation of particle breakage factors with total energy input could potentially be used for a evaluation of permeability of soils in earth dams or other earth structures in which the effect of particle breakage on permeability is important for the purposes of seepage analysis. In a finite element analysis of any earth structure, the stresses and strains in each element are known throughout loading. Thus the total energy input can easily be computed for each element. With particle breakage being directly related to energy, the particle breakage factor can be estimated from calculated energy. This was the reason to propose the new crushing parameter, B_{10}, based upon the D_{10} particle size, which relates directly to Hazen's permeability equation expressed by Equation 8.1. The value of B_{10} is zero at zero energy input, and it approaches unity as the energy input goes to infinity. A hyperbolic curve fit function works very well for this type of data distribution, and it is expressed in the form of Equation 8.5. Figure 8-21 shows the actual B_{10} particle breakage curve and the hyperbolic fit. Points were selected for the hyperbolic fit to provide a close fit in the initial 10 MPa of input energy, where most geotechnical engineering would occur.

$$B_{10} = \frac{E_T}{a + b \cdot E_T} \qquad (8.5)$$

B_{10} - *particle breakage factor based on* D_{10}.
E_T - *total energy input into specimen.*
a,b - *hyperbolic curve fit parameters.*

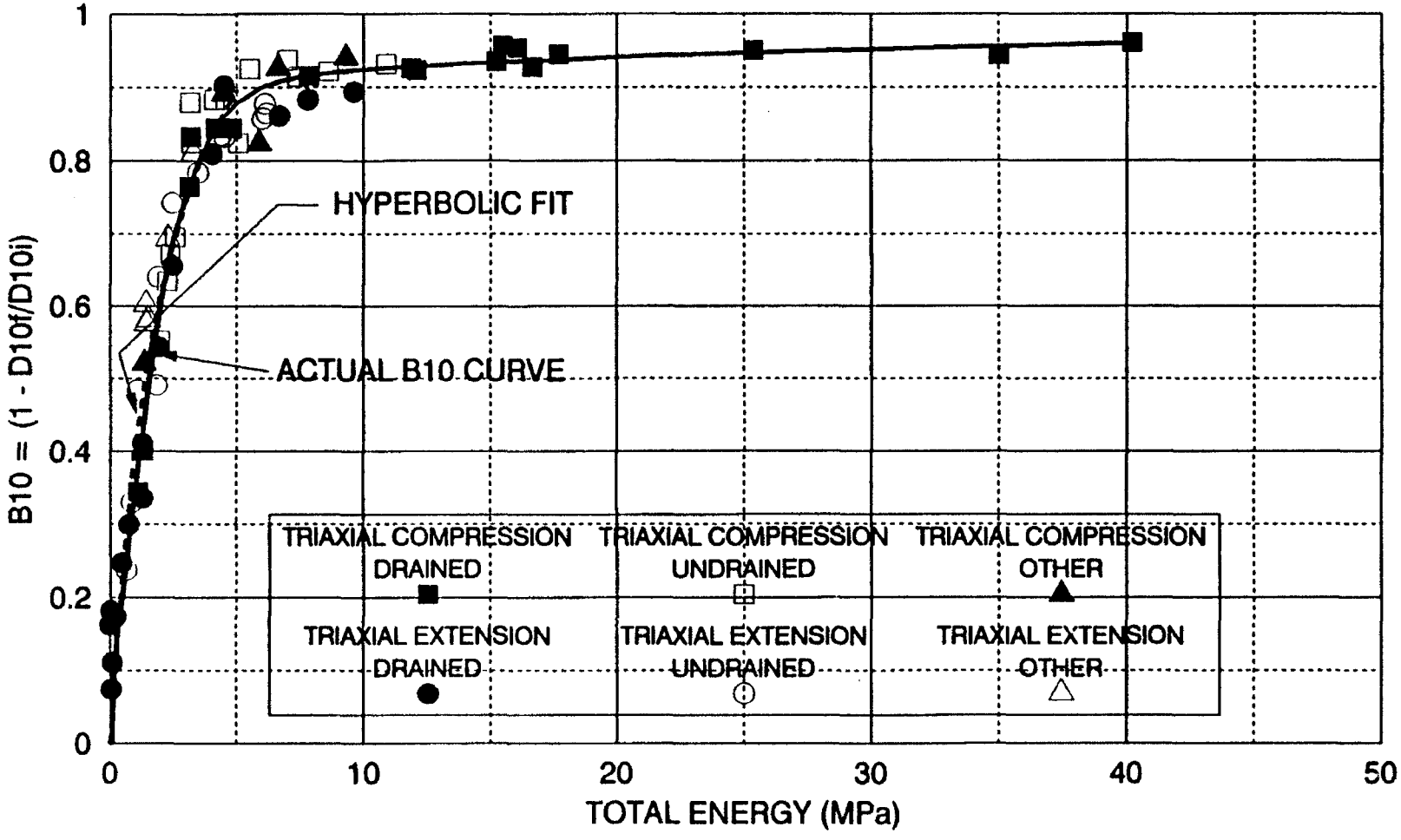

FIGURE 8-21 ACTUAL B10 CRUSHING CURVE WITH HYPERBOLIC FIT
DRAINED AND UNDRAINED TRIAXIAL COMPRESSION AND EXTENSION TESTS
DENSE CAMBRIA SAND

The hyperbolic curve fit parameters a and b need to be determined. Parameter b is always unity, because the asymptotic limit of B_{10} is always unity. Testing data is required to determine parameter a. For Cambria sand the a parameter was calculated to be 0.747. After the variables in Equation 8.5 are obtained, the total input energy directly yields the particle breakage factor. The particle breakage factor in turn yields the D_{10f} grain size as expressed by Equation 8.2. The D_{10f} particle size then directly yields the permeability from Equation 8.1. Using the proposed method just outlined, the predicted changes in permeability of Cambria sand during a typical drained triaxial compression test is depicted on Figure 8-22. This test had an effective confining pressure of 26.0 MPa. As can be seen, the largest decrease in permeability occurs during the isotropic consolidation phase, where it decreases from 1.75 to 0.24 cm/sec. This is due to the sensitivity of the Hazen equation to the squared D_{10} grain size. Note the vertical line segment at the end of consolidation. This decrease in permeability is due to soil creep, during the time the piston is being lowered into contact with the specimen. During the shearing phase the permeability further decreases, but the rate of permeability decrease rapidly slows down, because the rate of particle crushing decreases near the end of the test, even though the input energy continues to increase. The Hazen formula for permeability is only applicable for sands with coefficients of uniformity less than five. Near the end of the test the heavily crushed Cambria sand has a coefficient of uniformity much greater than five. However, this is just an illustration of how the proposed process would work.

There are other correlations relating permeability with grain size (Duncan,

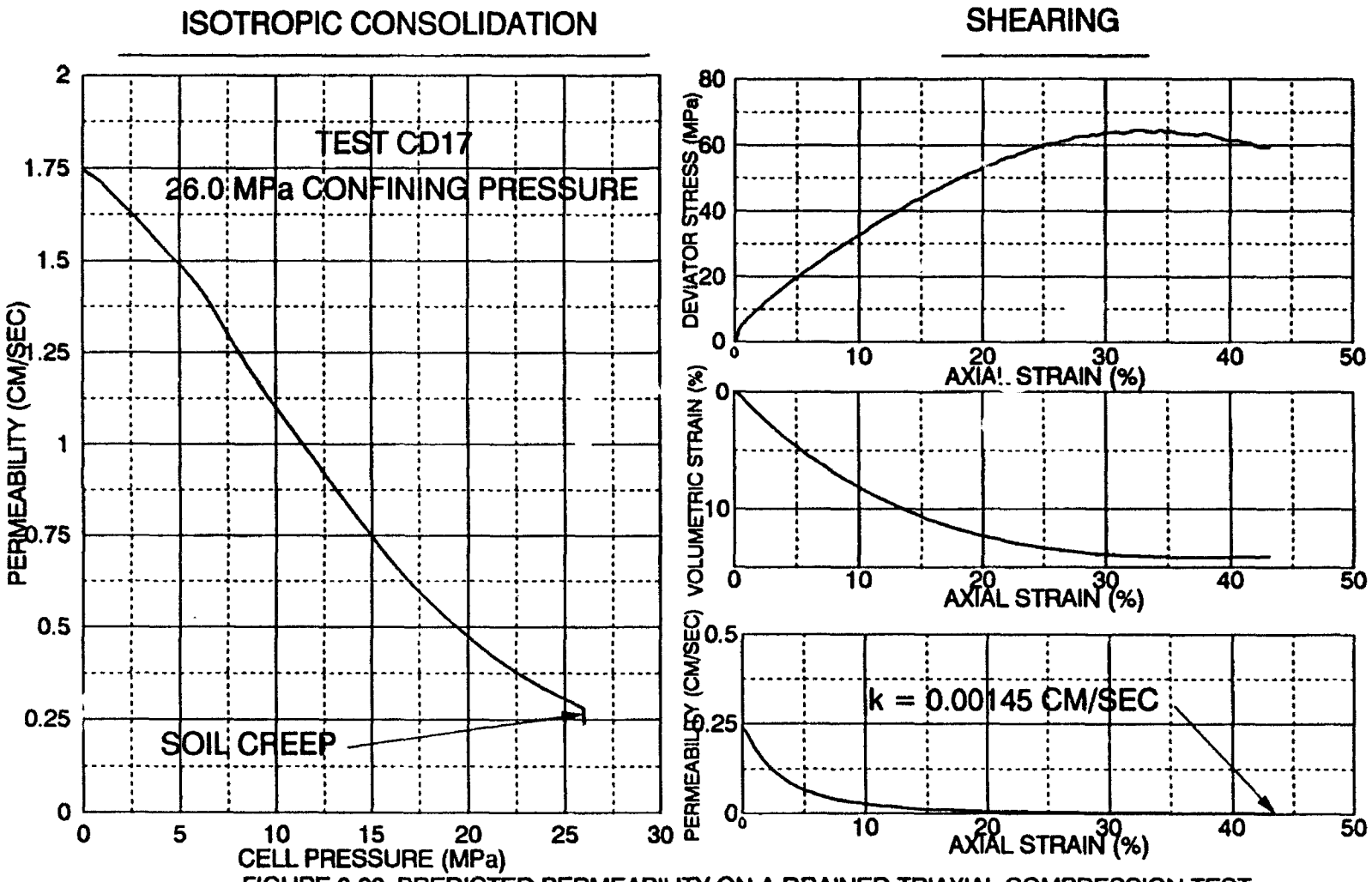

FIGURE 8-22 PREDICTED PERMEABILITY ON A DRAINED TRIAXIAL COMPRESSION TEST FROM ENERGY & HAZEN PERMEABILITY EQUATION DENSE CAMBRIA SAND

et al, 1972). Some relate the D_{50} grain size, while others use a grain size dependent on other factors. This is easily accomodated by changing the B_{10} particle breakage factor to relate a different grain size with energy.

Grain size distributions of the type shown in Figures 8-2, 8-3, 8-4, and 8-5 can also be modelled with a hyperbolic curve, similar to the crushing index-total energy curve. By inverting the scale on the vertical axis, so that it is increasing downward, and adjusting the location of the asymptotic level on the horizontal axis, it is possible to create a family of curves that are sensitive to the particle breakage parameter. If the particle breakage parameter is based upon a single grain size, then the grain size distribution can easily be reconstructed. Being able to predict the grain size curve is very useful for permeability correlations based on multiple grain sizes. Figure 8-23 shows a series of actual grain size distributions with hyperbolic predicted fits. Grain size curves that exhibit reverse curvatures cannot be modelled in this way, and a different mathematical representation of the grain size curve needs to be found.

8.11 Effect of Strain Localization on Particle Breakage

Strain localization that occurred in drained and undrained extension tests could have an effect on the extent of particle crushing. The assumption of uniform strain conditions biases the computed stresses downward, when compared with the real stresses in the region of the localization. The computed axial strains in the region of the localization are also too low, when compared with the actual strains. Therefore, the actual amount of energy in the strain localized region is much

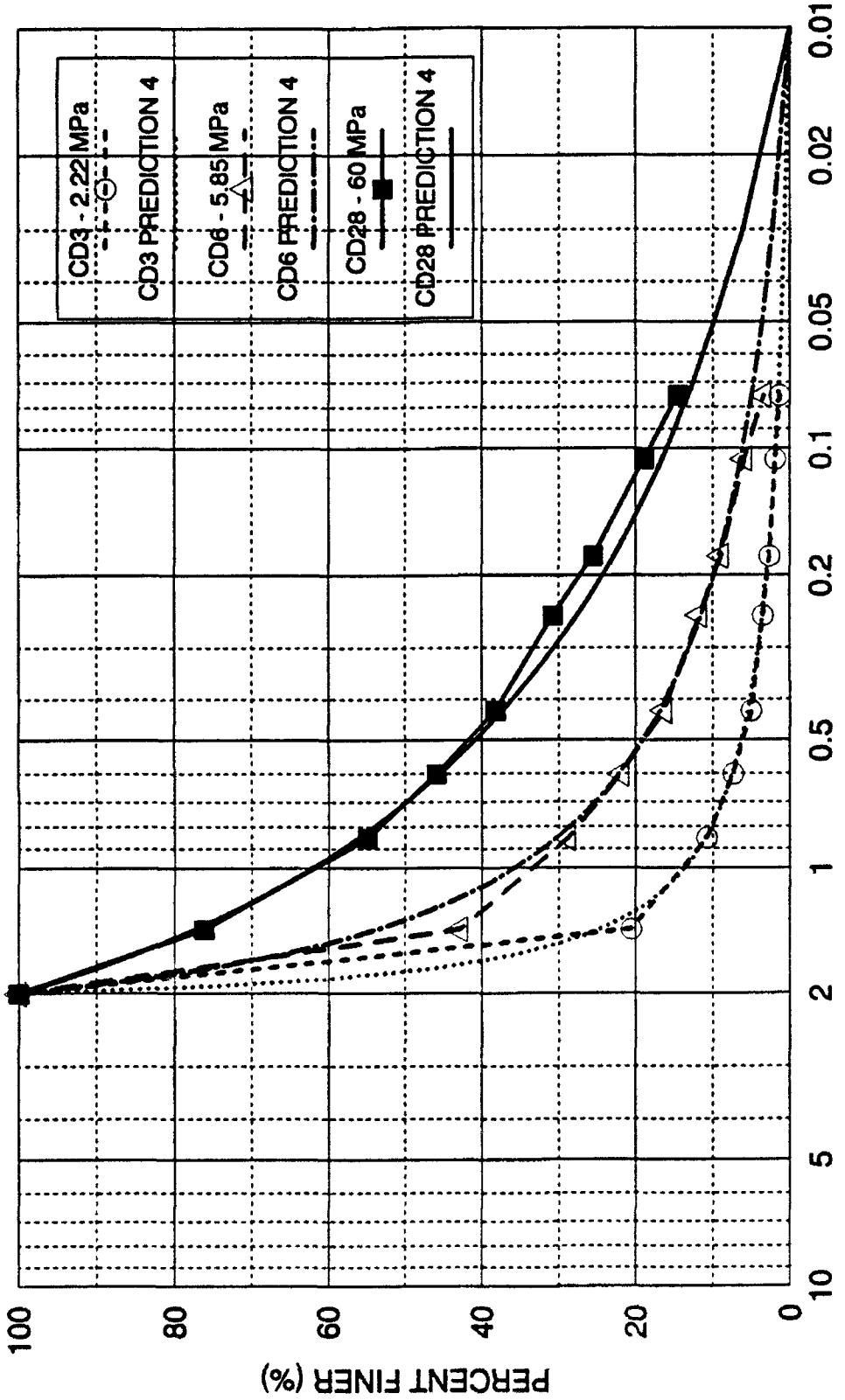

FIGURE 8-23 GRAIN SIZE CURVES AND HYPERBOLIC MODELLED PREDICTIONS FOR SOME DRAINED TRIAXIAL COMPRESSION TESTS DENSE CAMBRIA SAND

higher, and particle breakage should be higher in that region. This is indeed the case. Visual observation of severely necked specimens indicates that particle crushing is much more intense in the region of the neck. Observations indicated that within the region of the neck, there is a much higher quantity of very fine particles after shearing, and it appears almost as if a clay or silt were added to the sand. These characteristics are not exhibited in the rest of the specimen. However, few tests were allowed to continue well after the neck was formed. Therefore, the differences in crushing generated by the localization may not be large. The increased particle crushing within the localized region could be more than offset by the lesser amount of particle breakage occurring in the remainder of the specimen, since it is not fully participating in the overall strains. The necked region is volumetrically much smaller in comparison with the rest of the specimen.

Figures 8-24, 8-25, 8-26, and 8-27 show correlations between particle breakage factors and energy input for extension tests that exhibited strain localization. Sieve analyses were performed on the specimens, and the particle breakage factors were calculated. Also shown are the lines representing the particle crushing curves from the tests in which strain localization did not occur. In general, the strain localized tests tend to fall beneath the line, indicating that there is overall less particle fracturing in strain localized tests. Also it appears that results from tests with higher stress magnitudes deviate the most. This indicates that the stress/strain computation error from uniform strain assumptions combined with the small-sized localized neck region create a condition where less particle

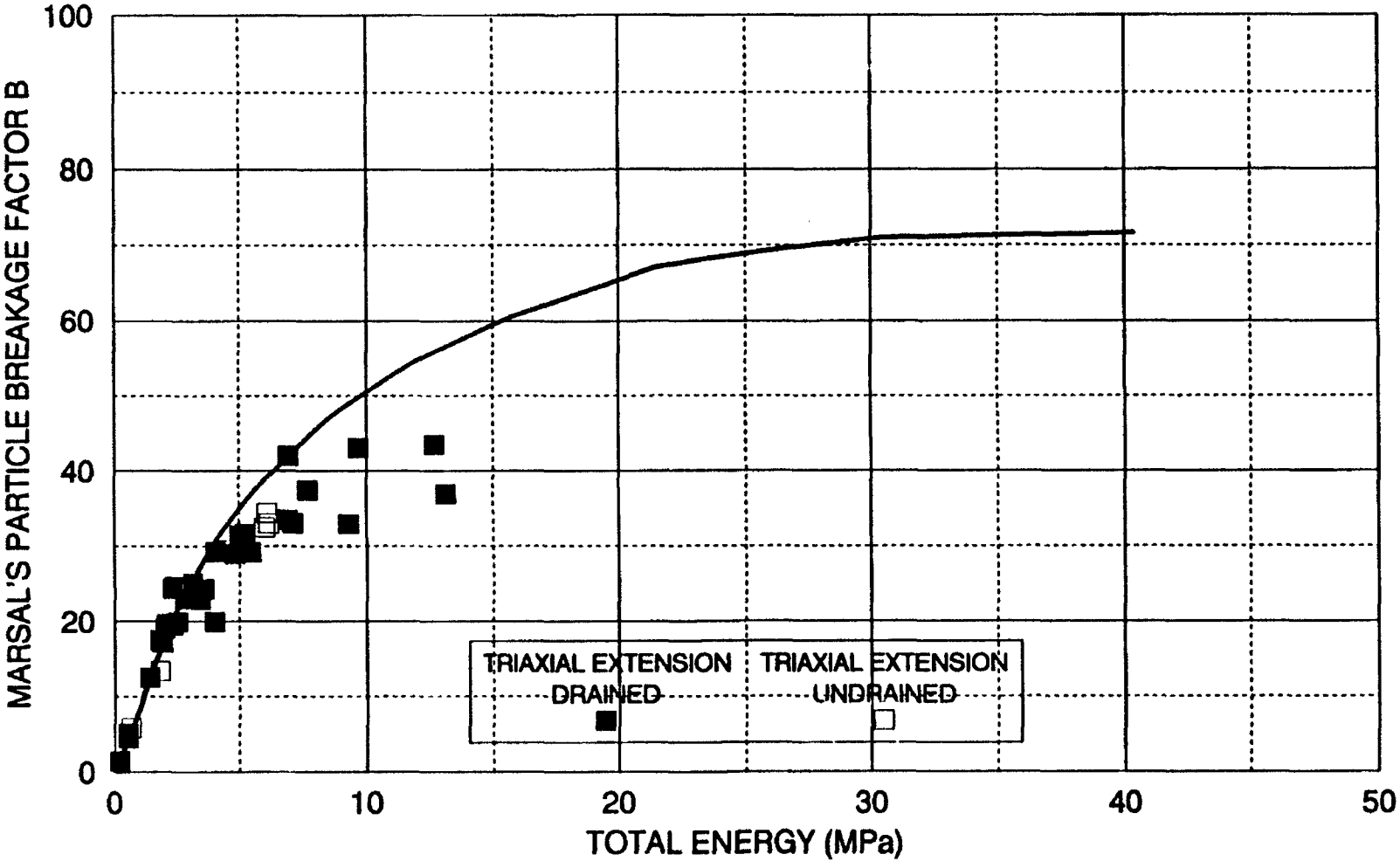

FIGURE 8-24 MARSAL'S BREAKAGE FACTOR B
EFFECT OF STRAIN LOCALIZATION ON CRUSHING CURVE
EXTENSION TESTS ON DENSE CAMBRIA SAND

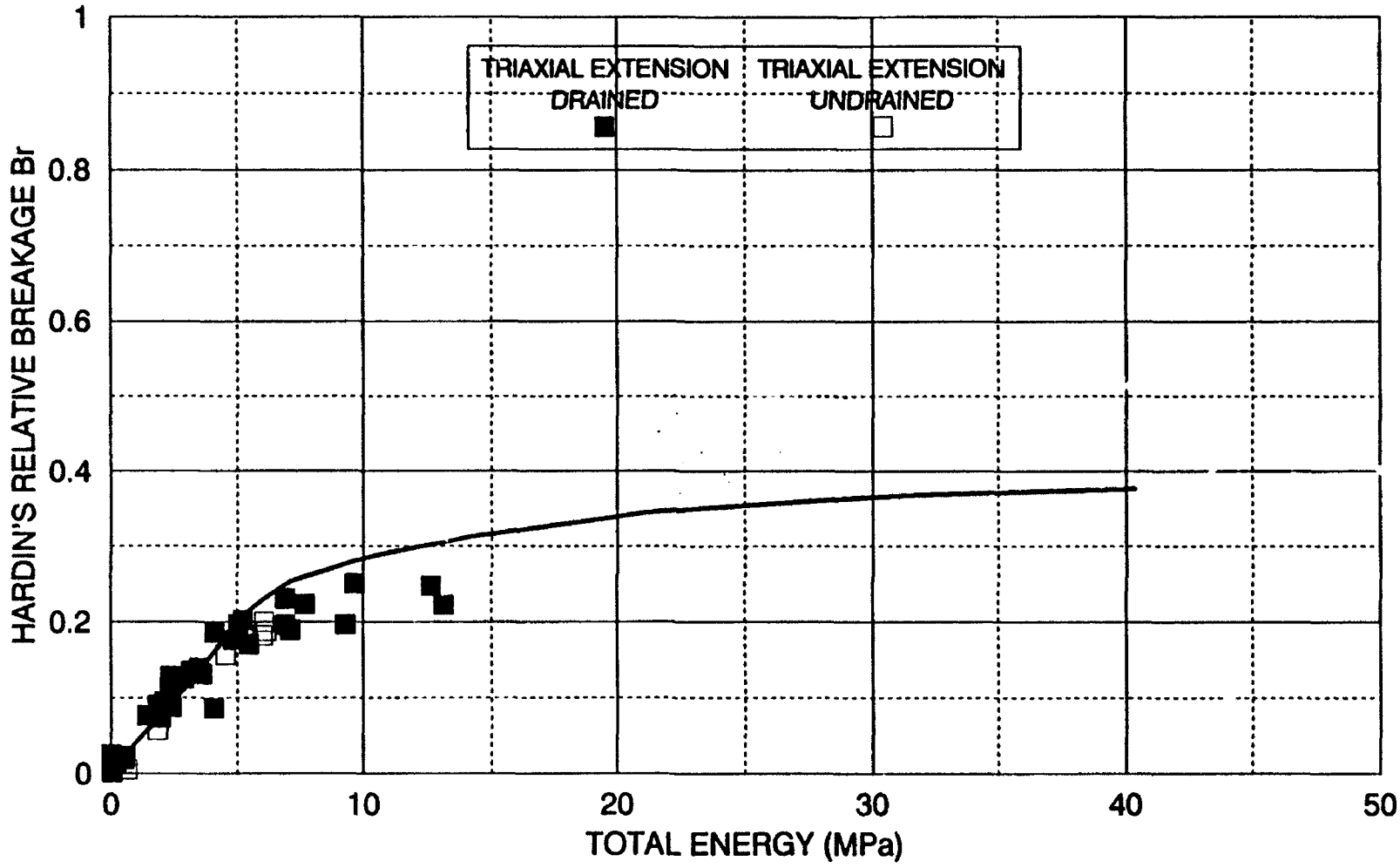

FIGURE 8-25 HARDIN;S RELATIVE BREAKAGE FACTOR Br
EFFECT OF STRAIN LOCALIZATION ON CRUSHING CURVE
EXTENSION TESTS ON DENSE CAMBRIA SAND

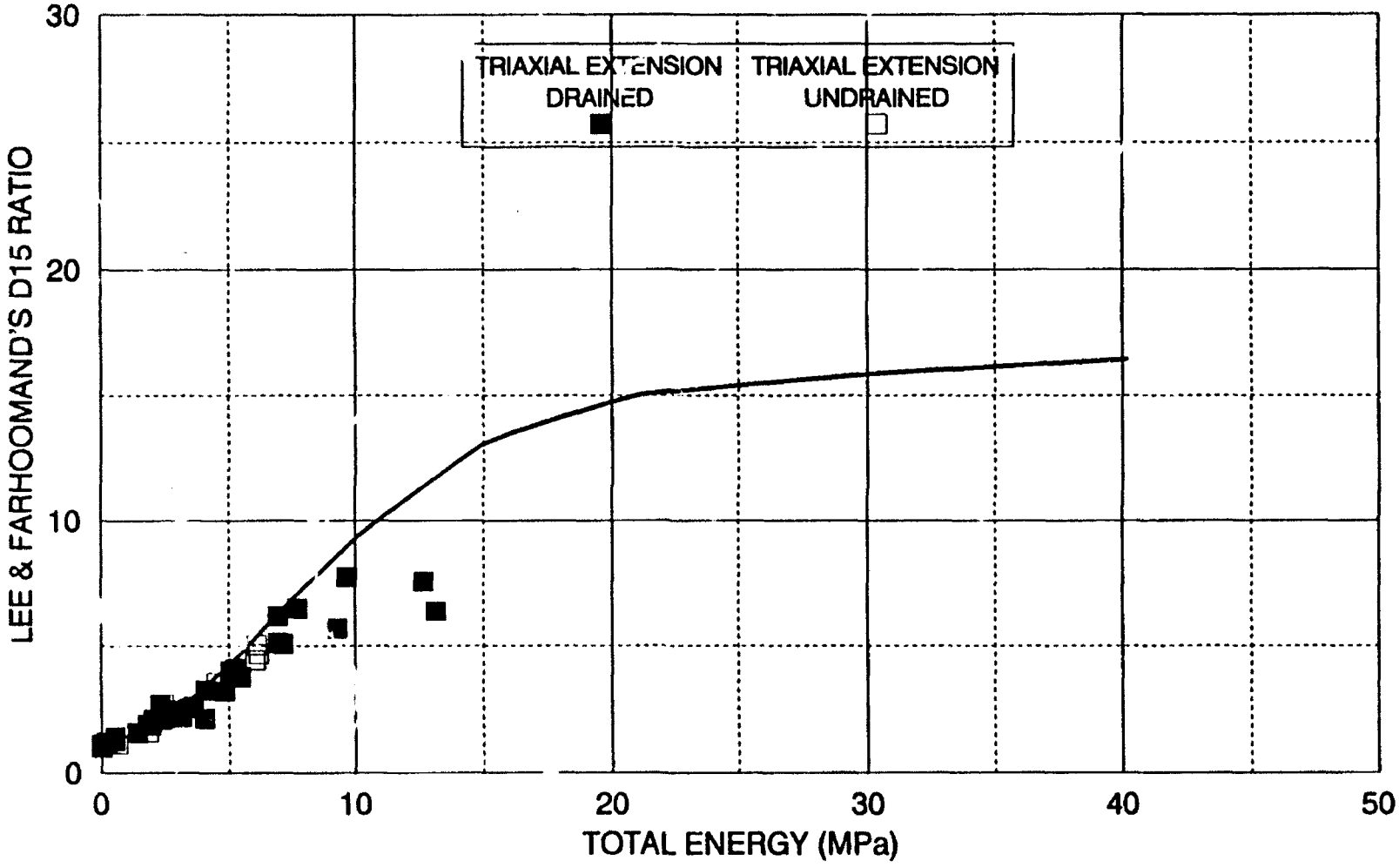

FIGURE 8-26 LEE & FARHOUMAND'S D15 RATIO BREAKAGE FACTOR
EFFECT OF STRAIN LOCALIZATION ON CRUSHING CURVE
EXTENSION TESTS ON DENSE CAMBRIA SAND

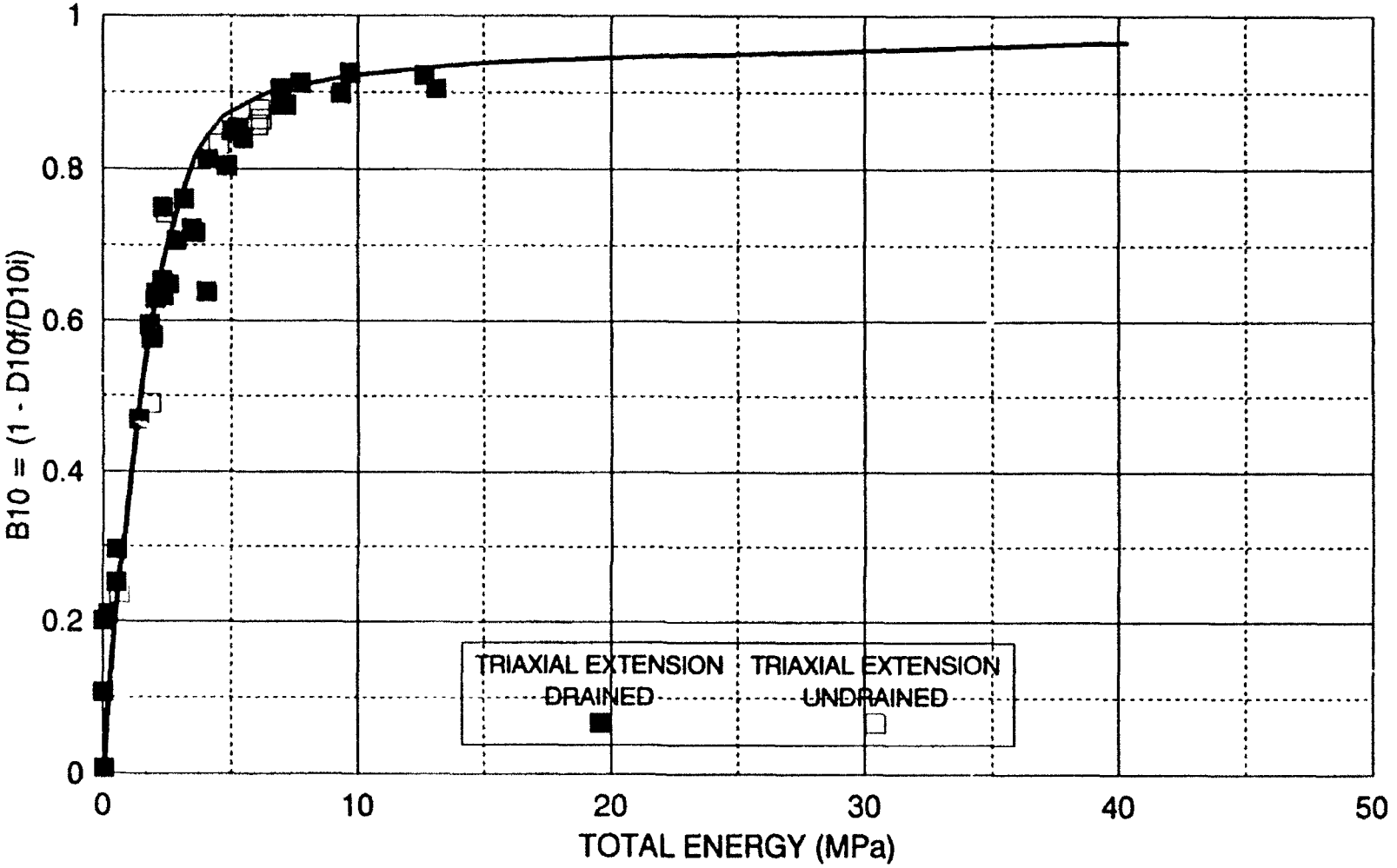

FIGURE 8-27 B10 BREAKAGE FACTOR
EFFECT OF STRAIN LOCALIZATION ON CRUSHING CURVE
EXTENSION TESTS ON DENSE CAMBRIA SAND

breakage is exhibited in strain localized tests.

8.12 Conclusions

Grain size distributions based upon sieve analyses were evaluated on many high-pressure drained and undrained triaxial compression and extension test specimens after shearing. Different particle breakage factors that were devised by Marsal, Lee and Farhoomand, Hardin, and a newly proposed particle breakage factor B_{10} have been computed from these grain size distribution curves. Correlations with standard soil mechanics parameters, including effective mean normal stress at failure and void ratio at failure, have been examined without finding a single unifying variable. However, it was determined that triaxial compression tests exhibited higher amounts of particle crushing than triaxial extension tests. Also, particle crushing was seen to increase most at moderate pressure levels, whereas the amounts occurring at high stress magnitudes appear to become constant. Input energy was examined and found to produce unique correlations with all particle breakage factors. These correlations encompass all types of tests, because the computations of energy, from the stresses and strains in the test, include the effects of stress path and type of test.

Thin sections of sheared specimens were obtained and it was observed that there are different mechanisms of volumetric compression on the grain level. The Cambria sand has its weaker components being squeezed into void spaces between stronger components. Quartz sand, being of uniform hardness, fractures and rearranges. However, correlating particle crushing with input energy is valid for

either case.

The proposed particle breakage factor B_{10} was designed to correlate with Hazen's permeability equation (Equation 8.1) and to provide an easy hyperbolic curve fit. B_{10} combined with the correlation with energy yields a proposed procedure to calculate permeabilty. This could be useful in applications where particle breakage could affect quantities of seepage, such as in the design of earth dams. Also, it was shown that particle grain size distributions similar to the ones found for Cambria sand could be represented by a hyperbolic fit, which could be useful in conjunction with permeability relations that require multiple grain sizes in their formulation.

It was found that extension tests experiencing strain localization had lower amounts of particle crushing, when energy was computed based on the assumptions of uniform strains.

CHAPTER 9 - ONE-DIMENSIONAL COMPRESSION TESTING AND ELASTIC PARAMETERS

9.1 Introduction

In the course of attempting to fully understand the behavior of granular materials at high pressures, an additional experimental program was undertaken to attempt to gain insight into soil behavior at pressures well beyond those employed in the triaxial compression and extension tests thus far discussed (maximum confining pressure 70 MPa). To obtain the desired much higher stress levels with the existing loading frame and equipment it was decided to perform one-dimensional tests on smaller specimens. These tests were performed on cylindrical specimens with diameters of 1.5 inches. The one meganewton capacity of the loading system could produce axial stresses up to approximately 900 MPa corresponding to vertical stresses to 55 kilometers (34 miles) beneath the ground surface.

9.2 One-Dimensional Testing Equipment and Control Software

The design of the soil-containment cell for one-dimensional testing was determined by the test specimen size. The specimen size was determined by balancing the desire to test specimens that were large enough to obtain good experimental measurements, but small enough that the capacity of the loading system could create conditions of high stress. Other considerations included that

normal structural steels have yield stresses lower than the stress conditions required. The steel selected was 300M VAR, which can be heat-treated after machining to yield stresses in excess of 1,700 MPa. It also was desirable to have the containment cell small enough to fit inside the existing high-pressure triaxial cell for reasons of safety. The final design of the containment cell and piston is shown on Figure 9-1. The specimen diameter is 3.81 centimeters (1.5 inch). The specimen height is variable. A special adapter was also fabricated for transition between the existing high-pressure triaxial cell piston and the one-dimensional testing piston as shown on Figure 9-2. The soil containment cell is recessed on the ends to allow it to sit on the existing specimen base within the high-pressure triaxial cell. The piston is slightly smaller in diameter than the bore in the containment cell to accomodate its elastic radial expansion under high loading conditions.

To determine lateral stresses in the soil containment vessel created by the soil as it is loaded, the circumferential strains in the cell were measured. The containment cell was instrumented by installing strain gages in two half-bridge configurations on opposite sides of the cell at the approximate final specimen mid-height location. The assembled testing apparatus is shown on Figure 9-3. The strain gages installed were Measurements Group Inc. CEA 350 ohm gages with a 2.12 gage factor. Each half-bridge arrangement consisted of an active gage installed in the circumferential direction at the correct height and a compensation gage installed near the top of the containment cell perpendicular to the active gage. Two half-bridges were used so that the outputs could be compared to

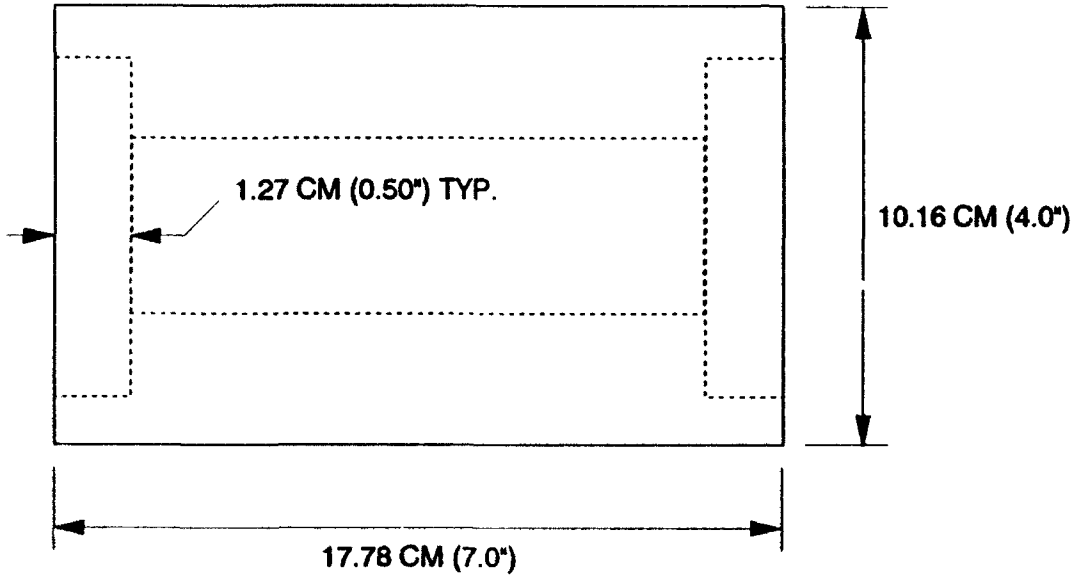

CELL

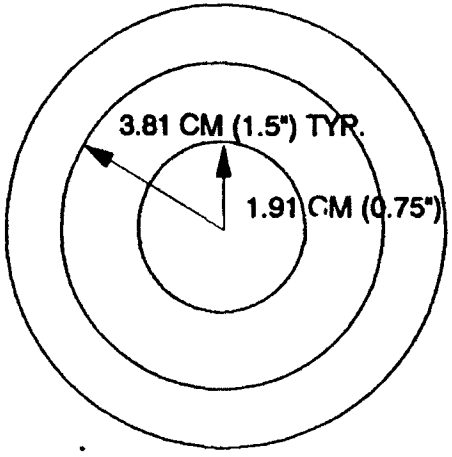

END VIEW

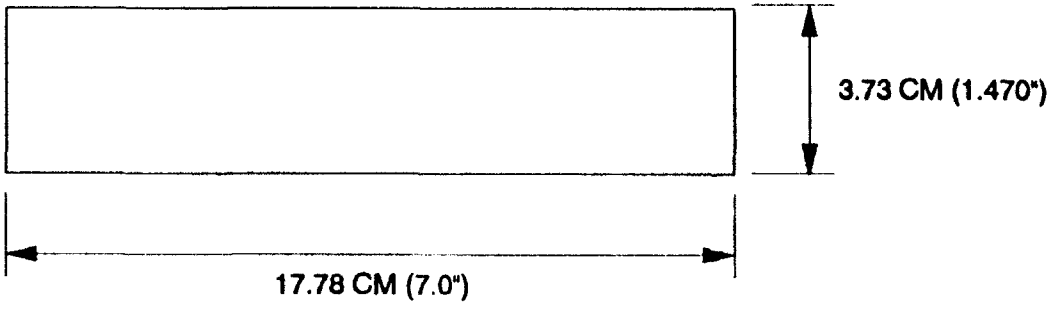

PISTON

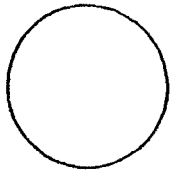

END VIEW

FIGURE 9-1 SOIL CONTAINMENT CELL
ONE-DIMENSIONAL COMPRESSION TESTS

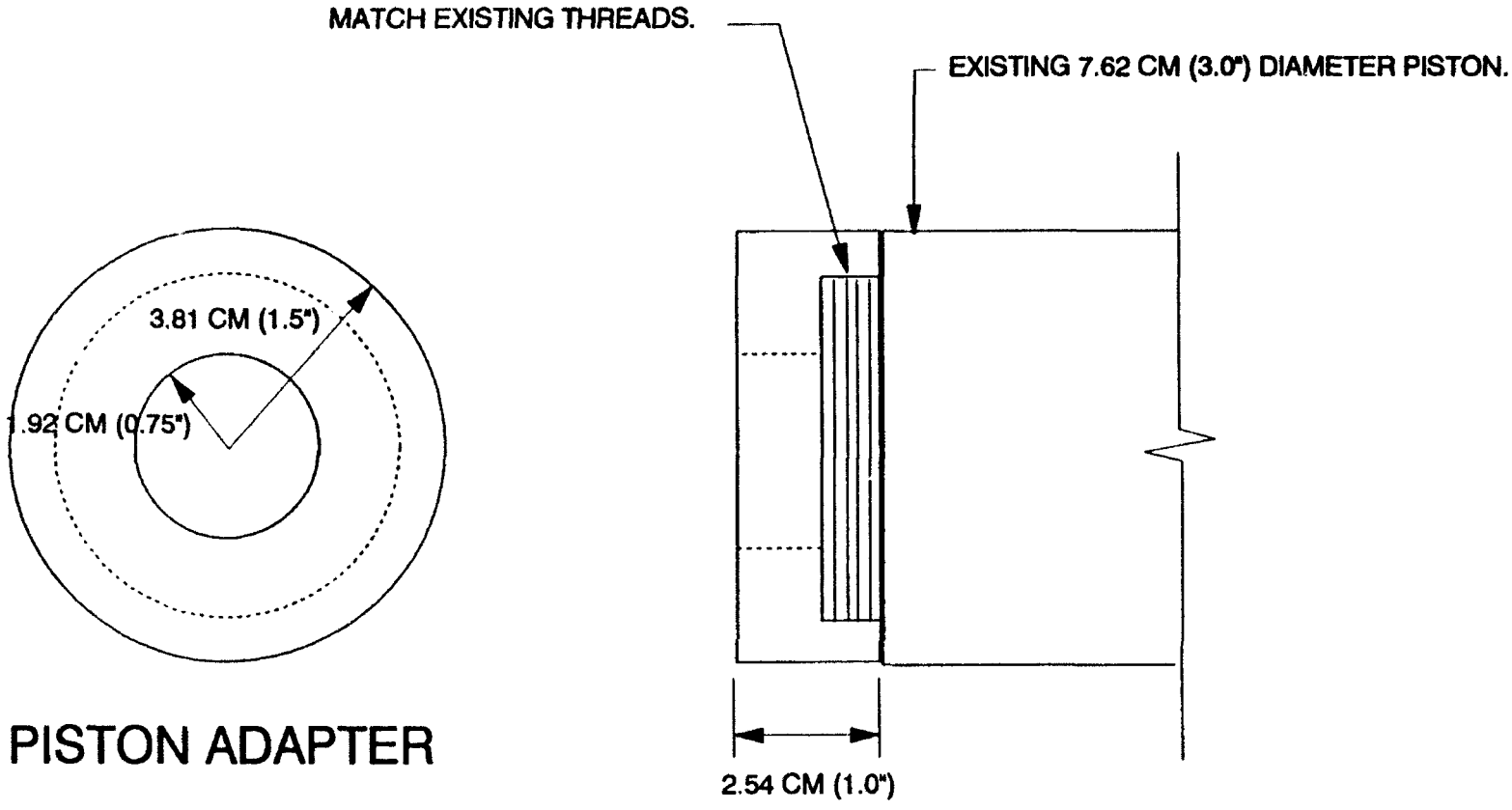

FIGURE 9-2 PISTON ADAPTER
ONE-DIMENSIONAL COMPRESSION TESTS

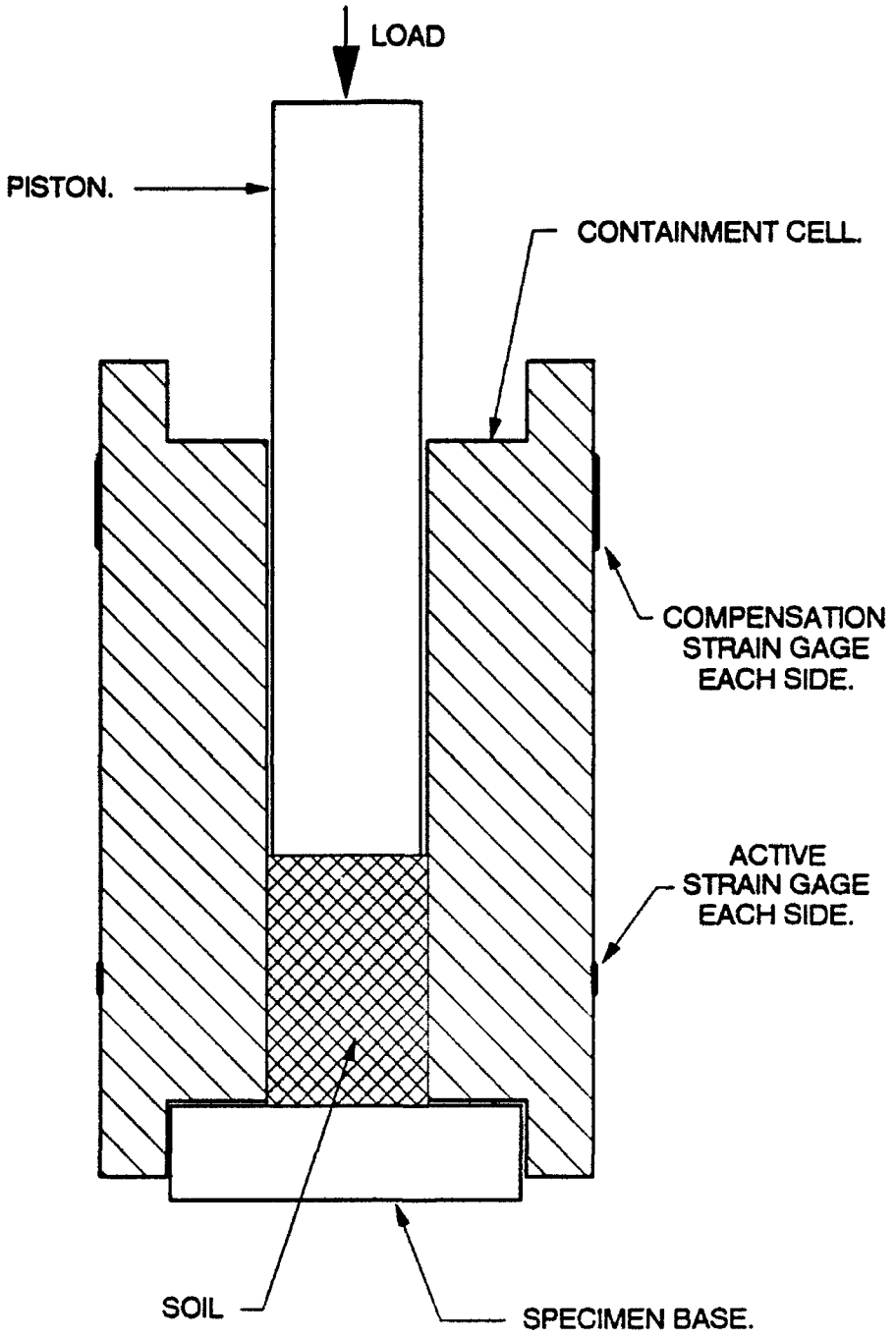

ONE-DIMENSIONAL TEST

NOT TO SCALE

FIGURE 9-3 ONE-DIMENSIONAL COMPRESSION TESTING SYSTEM
ASSEMBLED APPARATUS, STRAIN GAGE LOCATIONS, AND SPECIMEN

evaluate the consistency and repeatability of the strain measurement system. Since it is not possible to directly calibrate the strain gages, BLH Electronics, Inc. Model 1200 Digital Strain Indicators were employed to measure the half-bridge microstrain outputs. They were calibrated just prior to the testing. A hole had to be drilled in the high-pressure triaxial cell base under the specimen base and a specimen base was modified to allow the entry of the instrumentation cables into the triaxial cell.

A relatively simple computer control program, 1DTEST.EXE, was created to operate the vertical-motion stepping motor at a user-specified rate with options to change the motor speed during the test. The vertical load, the vertical deformation, and the test time were measured and recorded in a data file. The values were also echoed on the monitor, which allowed the manually measured strains of the strain gages to be time-synchronized with the information in the data file.

9.3 One-Dimensional Testing Procedures

The developed experimental procedure for the one-dimensional testing is relatively simple.

1. Feed the instrumentation cables through the triaxial cell base and connect them to the BLH digital strain indicators.

2. Install specimen base and place soil containment cell on base.

3. Dry pluviate the soil into the cell to the desired void ratio. Be sure the top of the specimen is level.

4. If a test is to be performed with a specimen in a wet condition, then pour water into the containment cell. The weight of the cell is sufficient to seal along the base and prevent water from draining out of the specimen from the bottom of the cell.

5. Wrap piston with teflon sheets and insert into cell until in full contact with the specimen. Measure height of specimen relative to benchmark outside of containment cell.

6. Assemble the high-pressure triaxial cell. Insert triaxial cell piston into cell with special adapter screwed onto end of piston. Remeasure height of specimen relative to external benchmarks outside of triaxial cell.

7. Lift triaxial cell into loading frame with electric pulleys.

8. Install LVDT and remeasure the height of the specimen relative to benchmark outside of containment cell.

9. Take base strain readings and start computer control program. Establish time synchronization between computer data acquisition and manual

readings on the BLH strain-gage indicators. Decrease vertical deformation rate as the load approaches the maximum value, because the stresses increase very rapidly near the end of the test.

10. When loading system capacity is reached, stop stepping motor and reverse direction for unloading branch of test.

11. After load is taken to zero, remove the triaxial cell from the loading frame and disassemble. The specimen generally needs to be forceably extruded from the soil containment cell.

9.4 Sands Tested and Corrections to Data

For the purpose of gaining further understanding of the behavior of soils at very high pressures, one-dimensional tests were performed on three different sands. The three sands used in this investigation were Cambria sand, quartz sand, and Sacramento River sand. Different initial void ratios were used in tests on Cambria sand and quartz sand to evaluate effects of initial void ratio. Due to lack of sufficient quantity of Sacramento River sand, only one initial void ratio was used for this sand. A large number of tests was not deemed necessary in this experimental program, since the object of the program was to gain additional insights into the general behavior of these sands at higher stress levels beyond the triaxial testing already performed. The initial heights of the specimens were determined from the desired initial void ratio and the final dimension of the

specimen after testing, such that the active strain gages would be located near the center of the specimen at that time. Since the active strain gages were placed 2.5 centimetes (1 inch) above the specimen base, the final specimen height was desired to be approximately 5.0 centimeters (2 inches).

The Cambria and quartz sands were loaded in a wet condition. The Sacramento River sand was sheared in a dry condition, because it was feared that adding water to such a fine sand could cause a slurry of sand would flow into the space between the piston and cell. This could cause loss of material and inaccuracy of the volume of the specimen during shearing. The injection of material into that space could also bind the piston creating errors, in the true load applied to the specimen.

Since a smaller specimen is used and the stiffness of the specimen is very high at large stress levels, accurate determination of the vertical deformation is essential to accurately estimate the void ratio. A correction to the axial deformation of the specimen for the elastic compression of the loading system was necessary to ensure this accuracy. A test was performed up to the maximum capacity of the loading system to obtain a displacement correction curve as shown on Figure 9-4. In the analysis of the data, the vertical displacement data are corrected according to this curve by one of five linear fits, as a function of the vertical load. The analysis of these one-dimensional tests assumes that the cross-sectional area of the specimen does not change from the initial condition. This is a reasonable assumption, because the measured radial strains are very small (maximum near 0.33%).

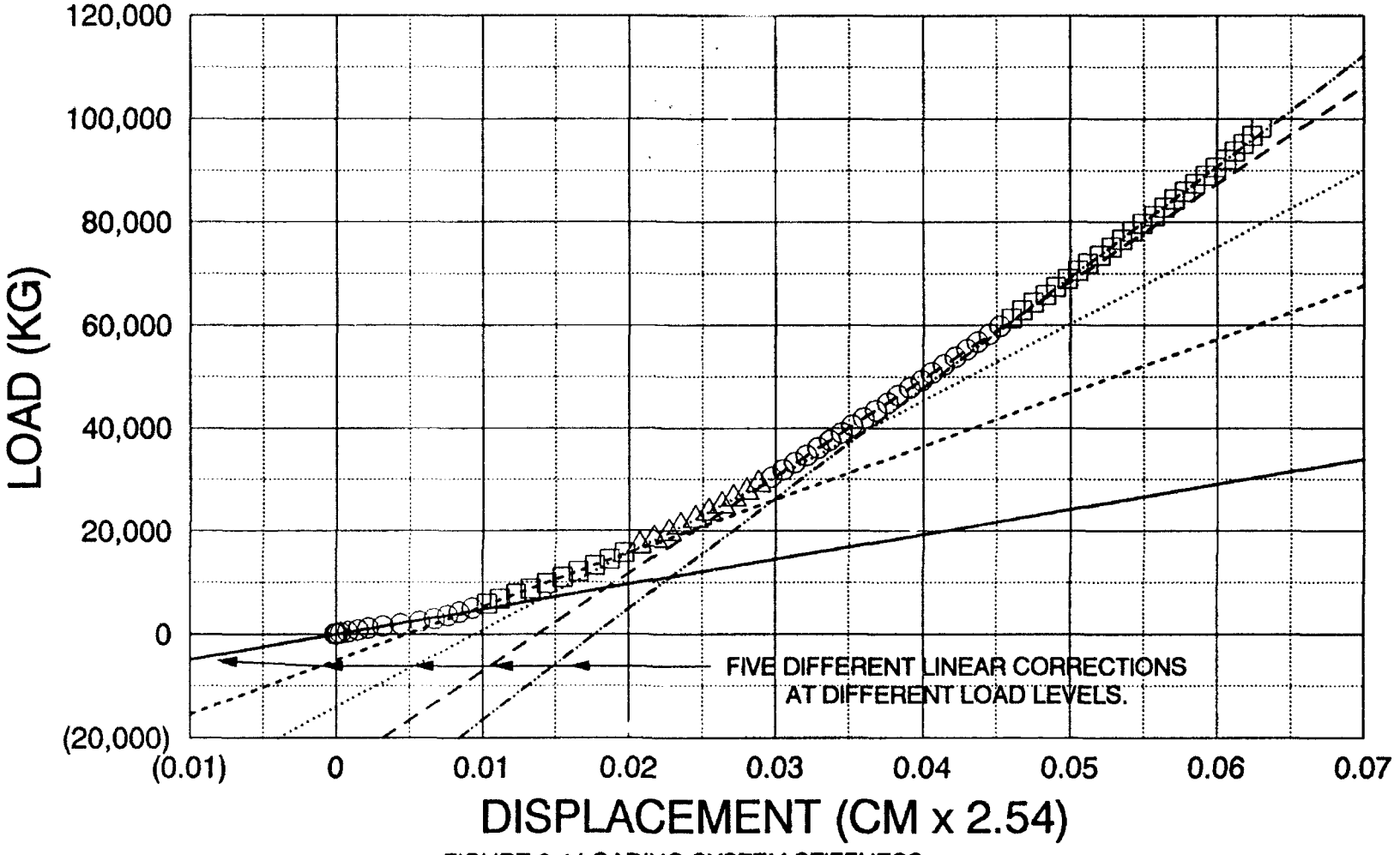

FIGURE 9-4 LOADING SYSTEM STIFFNESS
DISPLACEMENT CORRECTION CURVE
ONE-DIMENSIONAL COMPRESSION TESTS

It was realized before and during testing that sidewall friction between the soil grains and the wall of the containment cell would be present. Friction would tend to reduce the effective vertical stress within the specimen below that actually applied by the piston at the top of the specimen. The maximum stress would be located at the top of the specimen and the lowest stress condition would be at the bottom of the specimen. This also would tend to decrease the horizontal stresses applied by the soil to the cell wall. These stress decreases would then probably not allow full compression of the soil for a given externally applied load. The magnitude and effects of this friction were not known before actual testing. Therefore, tests with full-friction and reduced-friction were performed to evaluate the overall effects of friction.

The full-friction tests were performed with direct soil-cell wall contact with no attempt to reduce the friction. The reduced-friction tests were performed by applying a layer of graphite-based grease on the inner surface of the soil containment cell prior to pluviation of the sand. After the soil was pluviated, the piston was used to tamp the soil and force the sand grains outward through the grease and into contact with the cell wall. The grease was expected to mix with the soil matrix at the soil-cell wall interface as the grains were crushed, and provide a much reduced friction coefficient. As the tests indicated, this method did substantially reduce the amount of sidewall friction. At the end of a one-dimensional compression testm there was a residual circumferential strain, which represents a radial stress that is locked into the specimen. If the maximum force to extrude the specimen at that time is measured, then a friction force can be

obtained for that radial stress. This evaluation was performed for both the full-friction and reduced-friction tests. Full-friction tests had maximum extrusion forces between 25 and 50 tons, often without the full height of the specimen acting, because the capacity of the hydraulic jack used in the extrusion process required removal of some of the specimen to stay within the system capacity. The reduced-friction tests experienced maximum extrusion forces that varied between 5 and 13 tons, but all with full specimen heights. The results of these friction indicators show that the coefficient of friction was approximately 2.7 for full-friction tests and 0.45 with the reduced-friction tests. Whether the relationship between these friction coefficients at low pressures relates to the friction at high pressures is uncertain. Even though the sidewall friction is still substantial, this represents an 83 percent reduction in sidewall friction. As is demonstrated below, the changes that this substantial reduction in sidewall friction creates were not great. Therefore, it is maintained that reduction in friction toward zero is not likely to further change the current results substantially.

9.5 Experimental Results from One-Dimensional Compression Tests

The loading and unloading axial stress-strain curves for Cambria, quartz and Sacramento River sands are shown on Figures 9-5, 9-6, and 9-7, respectively. Obviously, in one-dimensional tests there is no failure condition, since it is a fully confined test, and the test is terminated at the maximum load level of the loading system. The figures clearly show that the soil stiffness continually increases as strain level increases in all tests. Specimens with lower initial densities specimens

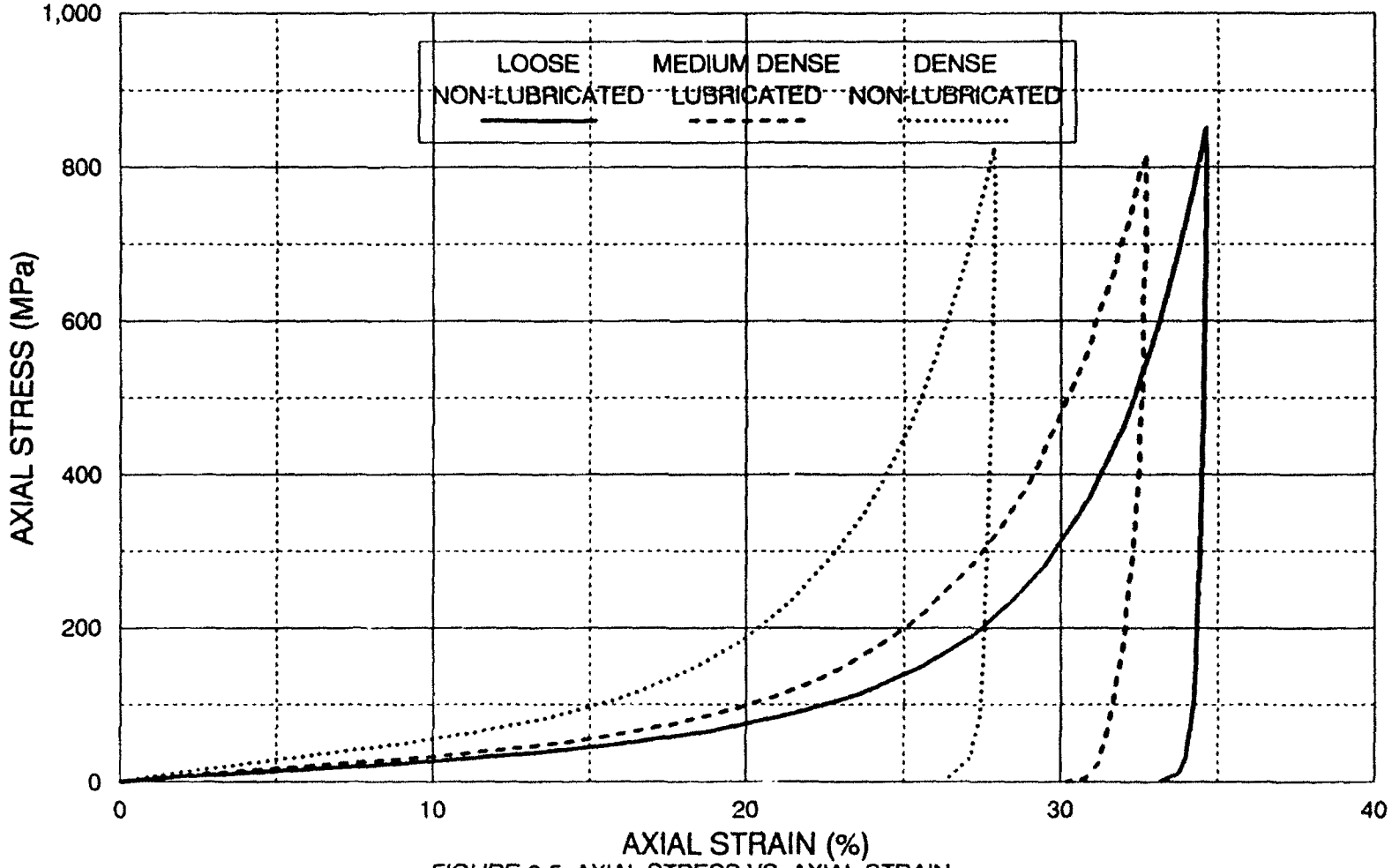

FIGURE 9-5 AXIAL STRESS VS. AXIAL STRAIN
ONE-DIMENSIONAL COMPRESSION TESTS
CAMBRIA SAND

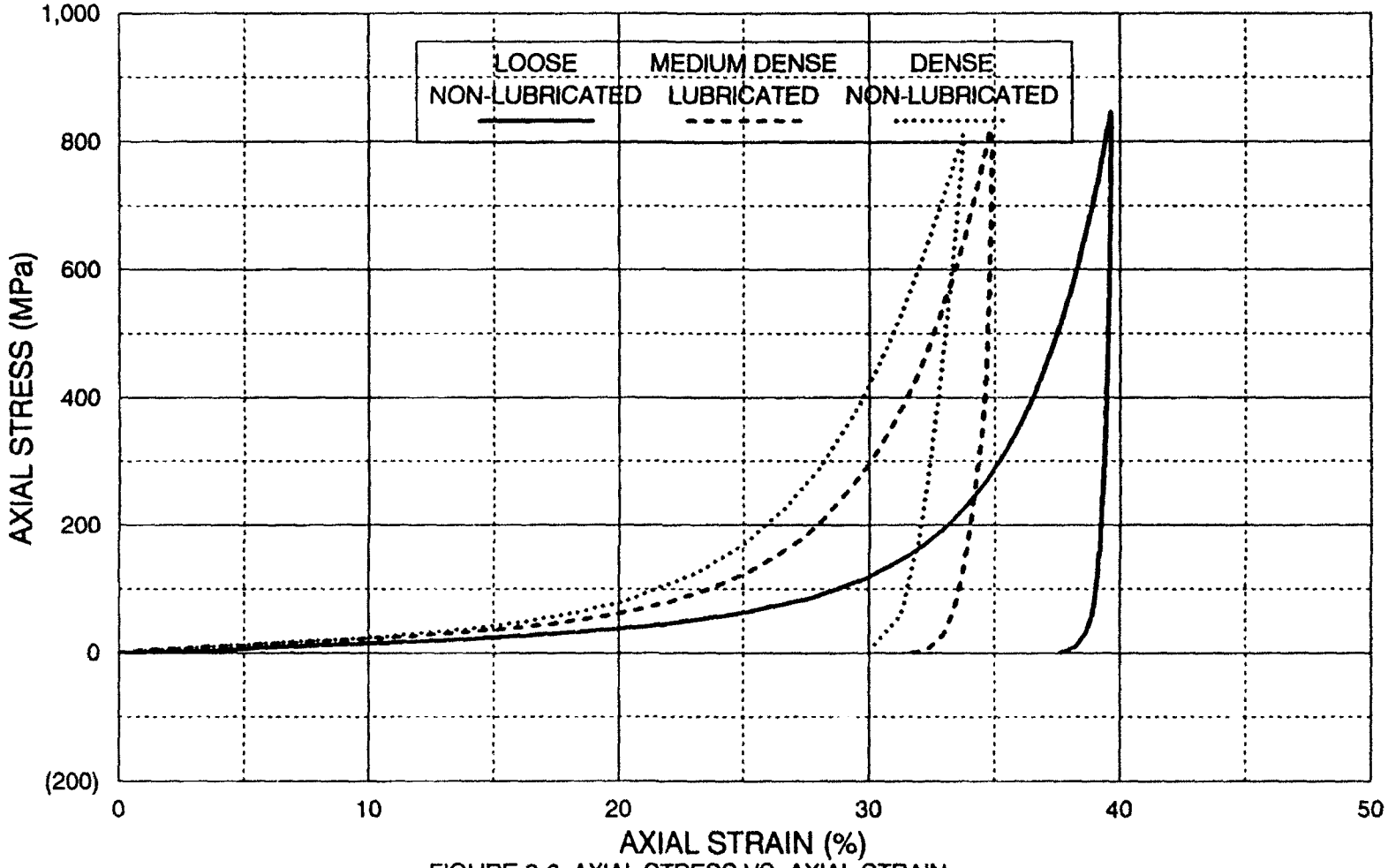

FIGURE 9-6 AXIAL STRESS VS. AXIAL STRAIN
ONE-DIMENSIONAL COMPRESSION TEST
QUARTZ SAND

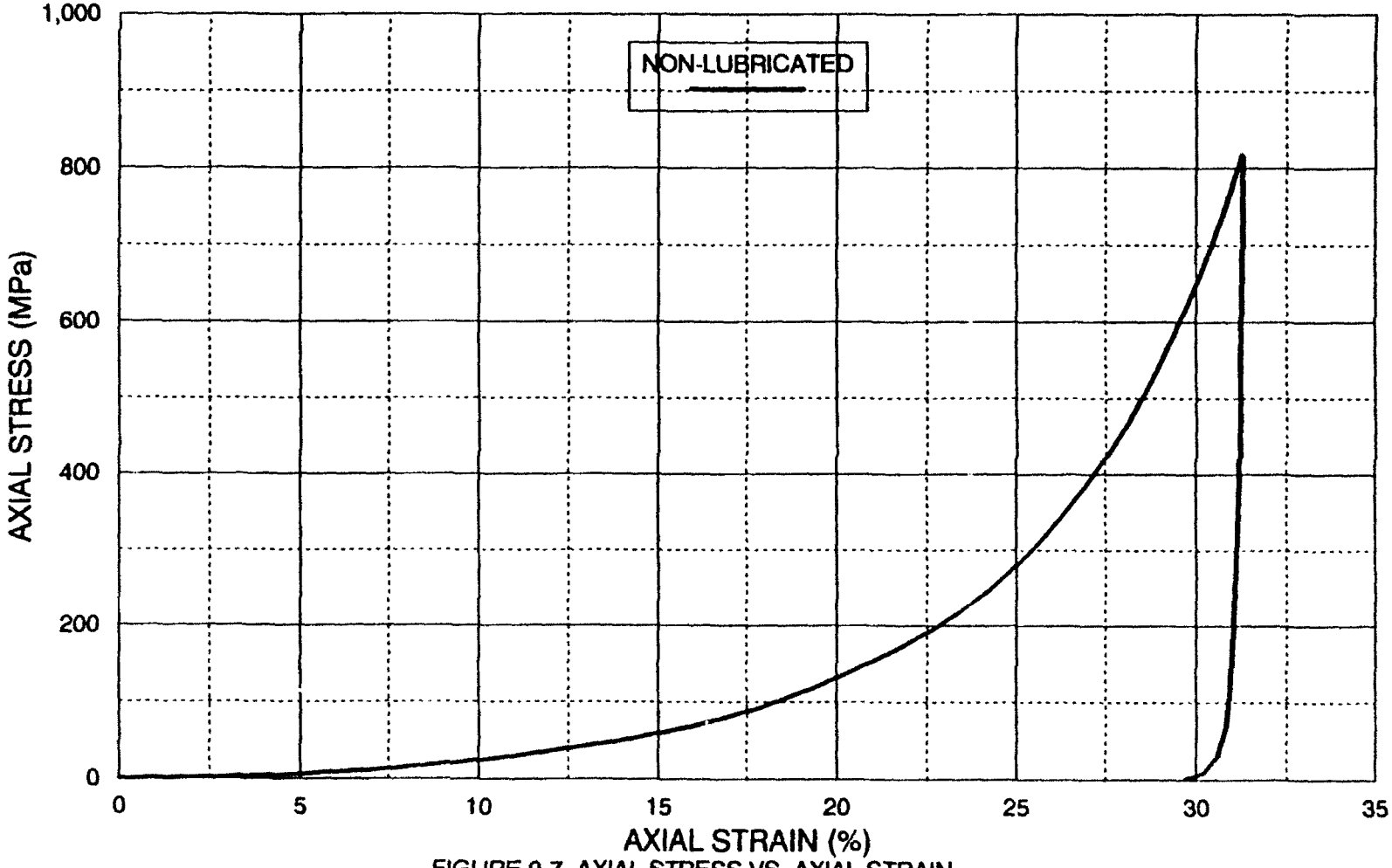

FIGURE 9-7 AXIAL STRESS VS. AXIAL STRAIN
ONE-DIMENSIONAL COMPRESSION TEST
SACRAMENTO RIVER SAND

experienced larger strains at the maximum stress condition than did denser specimens. The shapes of the high stress parts of the stress-strain curves appear almost identical. Additional strains are required to reach equivalent densities for initially loose specimens, as compared to the initially dense test specimens. The effect of lubrication results in less change in the stress-strain curves for either the Cambria or quartz sands.

The void ratios plotted against axial stress for Cambria, quartz and Sacramento River sands are shown on Figures 9-8, 9-9, and 9-10, respectively. When viewed on a semilogarithmic plot as shown on Figure 9-8a, they indicate that the void ratio at low pressures and low stress magnitudes did not change much until a certain stress level was reached, and then large volume reductions occurred as particle breakage and rearranging increased rapidly. When viewed on a linear plot as shown on Figure 9-8b, the void ratio is seen to change most rapidly at low stress levels. The minimum void ratios achieved in the tests which all ended at the same maximum pressure were the lowest for Cambria sand; quartz sand was in between, and Sacramento River sand had the highest minimum void ratio. This can be explained by the fact that Cambria sand has many softer components, while the quartz sand consists of grains with high hardness and no soft components. The Sacramento River sand is the most difficult to crush because of its fineness. In addition, the test on Sacramento River sand was performed in a dry state. Both of these factors have been identified as making a sand less susceptible to particle crushing (Lee and Farhoomand, 1967; Murphy, 1970; Miura and Yamanouchi, 1973; Pittman and Larese, 1991). Another conclusion that can

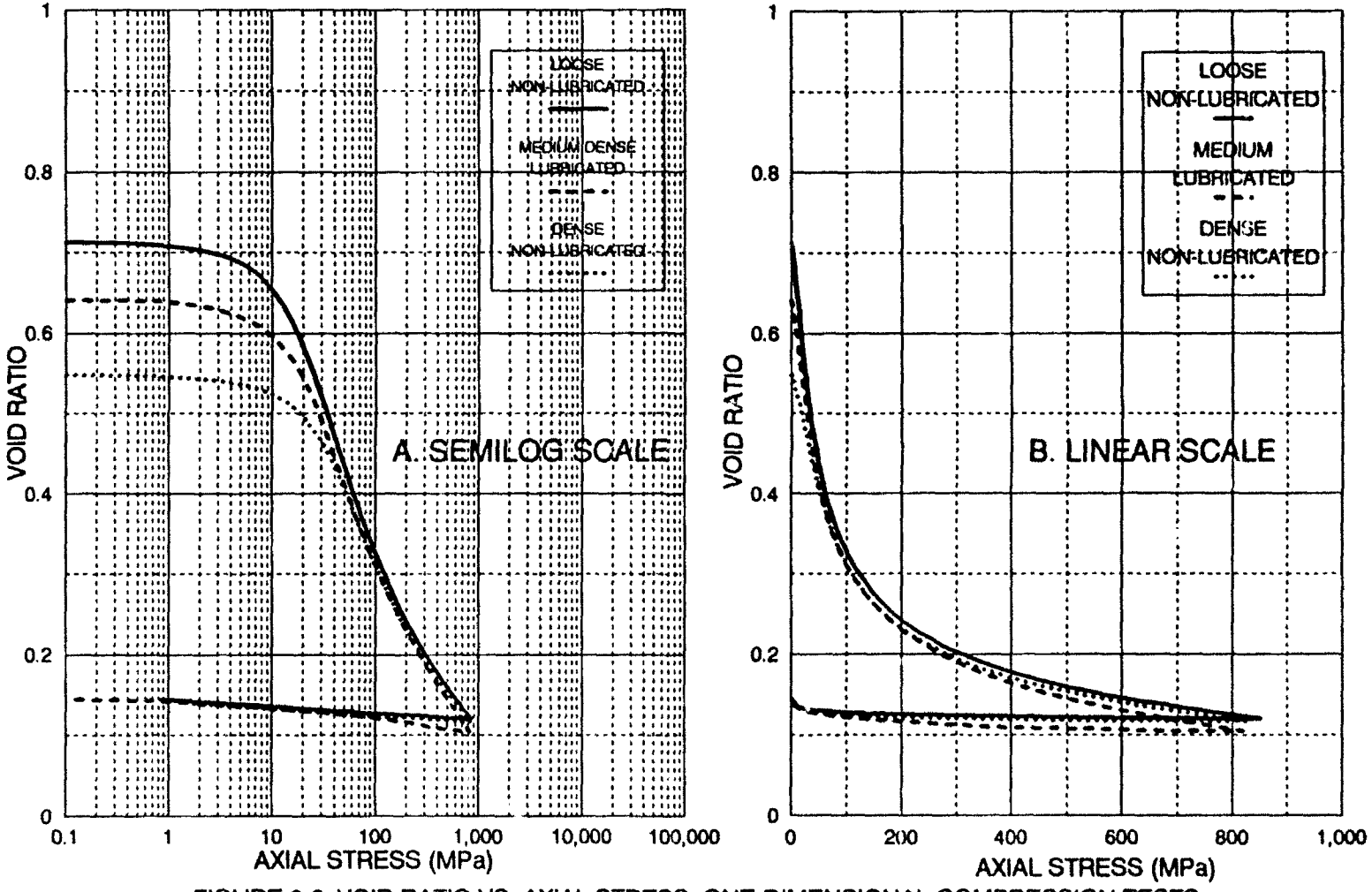

FIGURE 9-8 VOID RATIO VS. AXIAL STRESS, ONE-DIMENSIONAL COMPRESSION TESTS, CAMBRIA SAND, A. SEMILOG SCALE, B. LINEAR SCALE.

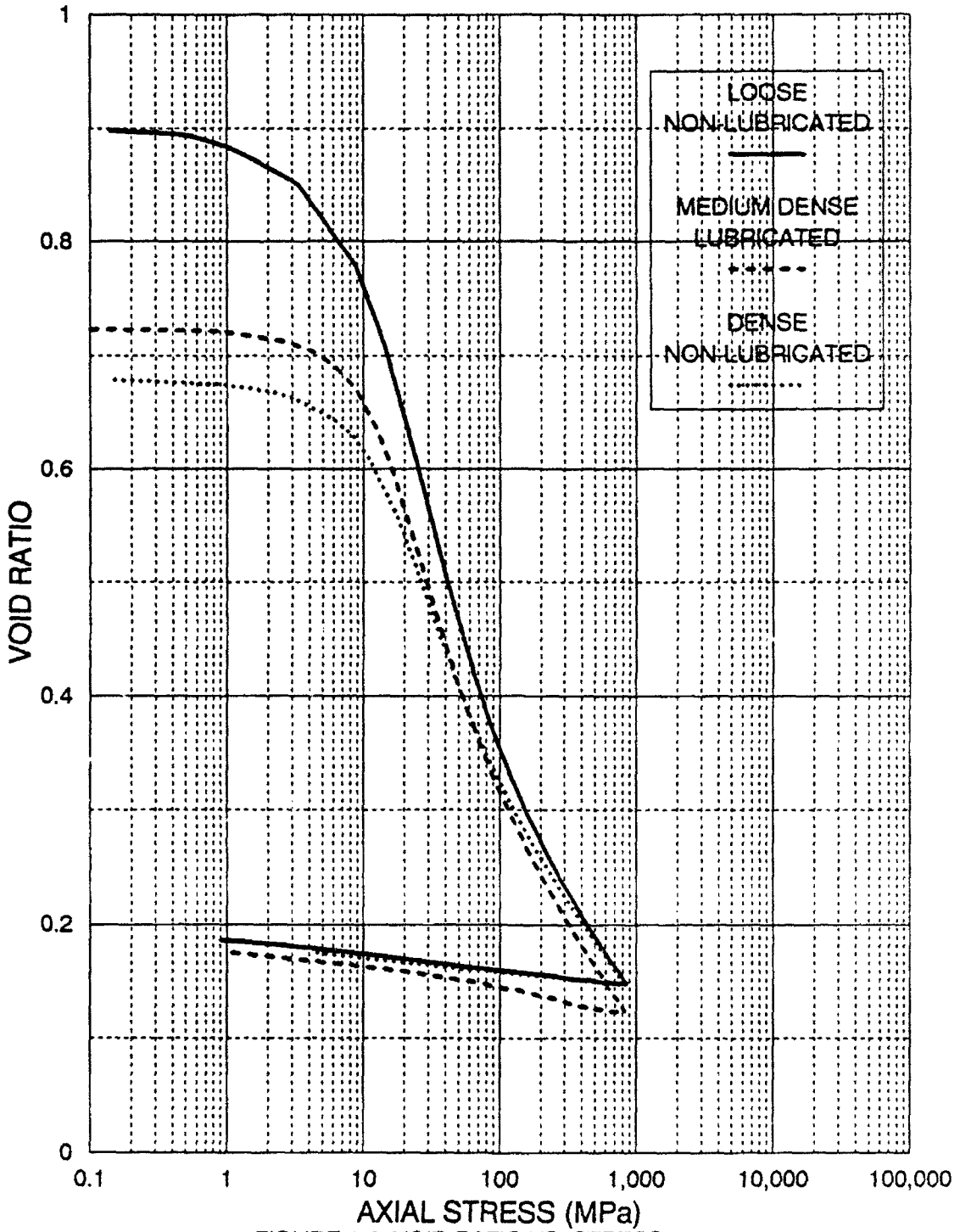

FIGURE 9-9 VOID RATIO VS. STRESS
ONE-DIMENSIONAL COMPRESSION TEST
QUARTZ SAND

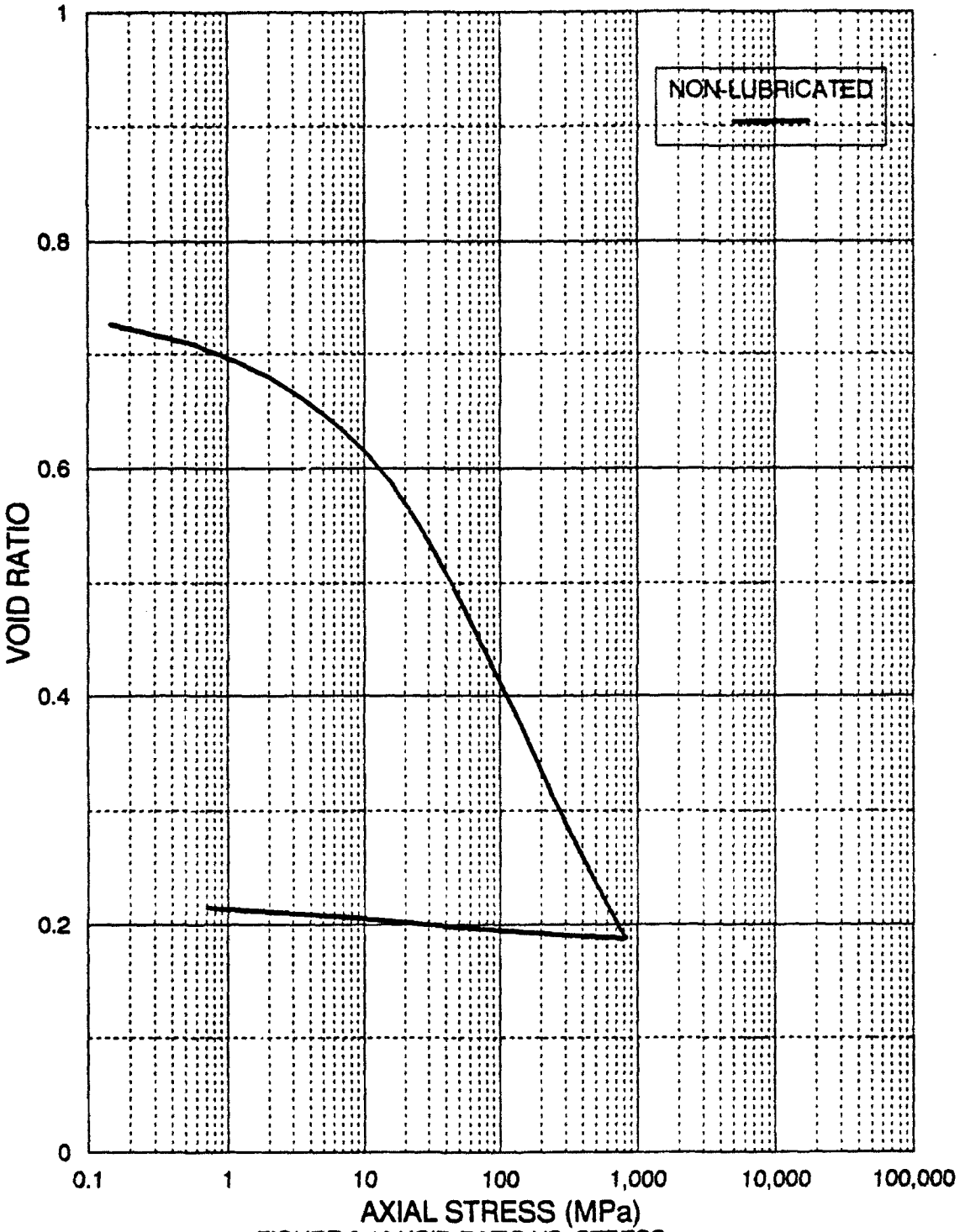

FIGURE 9-10 VOID RATIO VS. STRESS
ONE DIMENSIONAL COMPRESSION TESTS
SACRAMENTO RIVER SAND

be made from these figures is that the effect of initial void ratio is eliminated after a certain stress level has been reached. The loose, medium, and dense curves tend to merge together for both the Cambria sand and the quartz sand. The curves for the Cambria sand merge together at a lower stress level than those for the quartz sand for the same reasons that its minimum void ratio is lower for the Cambria sand than for the quartz sand.

The effect of lubrication in the reduced-friction tests has measurable results in terms of void ratio variation. Though not large, there is a slight increase in the slope of the void ratio curves, and this results in the minimum void ratio being reduced. Since the large decrease in friction (83 percent) resulted in a decrease in void ratio by only a relatively small amount, it would appear that further reduction in friction would not likely reduce the minimum void ratio much further. Small effects of lubrication are observed on the unloading part of the void ratio curves. The unloading curves for the lubricated specimens appear slightly rounded, whereas the nonlubricated unloading branches appear linear. It was noted through the loading phase that the lubrication had the effect of creating an uneven loading pattern. The vertical load was observed to oscillate about a smooth loading curve. This was not observed in the full-friction tests. Apparently, the vertical stress increases to a level at which the sidewall-friction is overcome, at which point, the specimen breaks free and the load momentarily drops before recovering. This effect is probably the cause of the nonlinear unloading branch. As the load is quickly decreased during unloading, the specimen undergoes periodic releases in a slightly irregular fashion.

9.6 Appearance of Sheared Specimens

The appearance of the sheared specimens after being extruded from the soil containment cell is striking. The specimens are extremely dense and resemble sandstones. The densification appears to be visually greater than in the triaxial compression tests, as also indicated by the lower void ratios. Thin sections of the compressed Cambria and quartz sands are shown on Figures 9-11 and 9-12, respectively. However, the thin sections from full-friction tests appear very similar to either the reduced-friction tests or the thin sections sheared in triaxial compression, shown in Chapter 8. The outer layer of soil adjacent to the cell wall has been so heavily sheared that there does not appear to be any observable grain structure left. The material appears to be powder. This layer is very thin (0.05 cm). Throughout the rest of the specimen, there is a definable grain structure, though heavily crushed and compressed. The grease used in reduced-friction tests appears as a thin layer of reflective black graphite within the thin heavily sheared outer layer of the sheared specimen.

9.7 K_o at High Pressures

The purpose of installing the strain gages on the one-dimensional soil containment cell was to possibly infer soil stress conditions from the measured circumferential strains at very high pressures. Thereby, K_o, the coefficient of earth pressure at rest, can be determined at high pressures. The measured values of microstrain were generally very consistent between the two half-bridge installations, rarely varying more than a few microstrain (10^{-6} cm/cm) from each

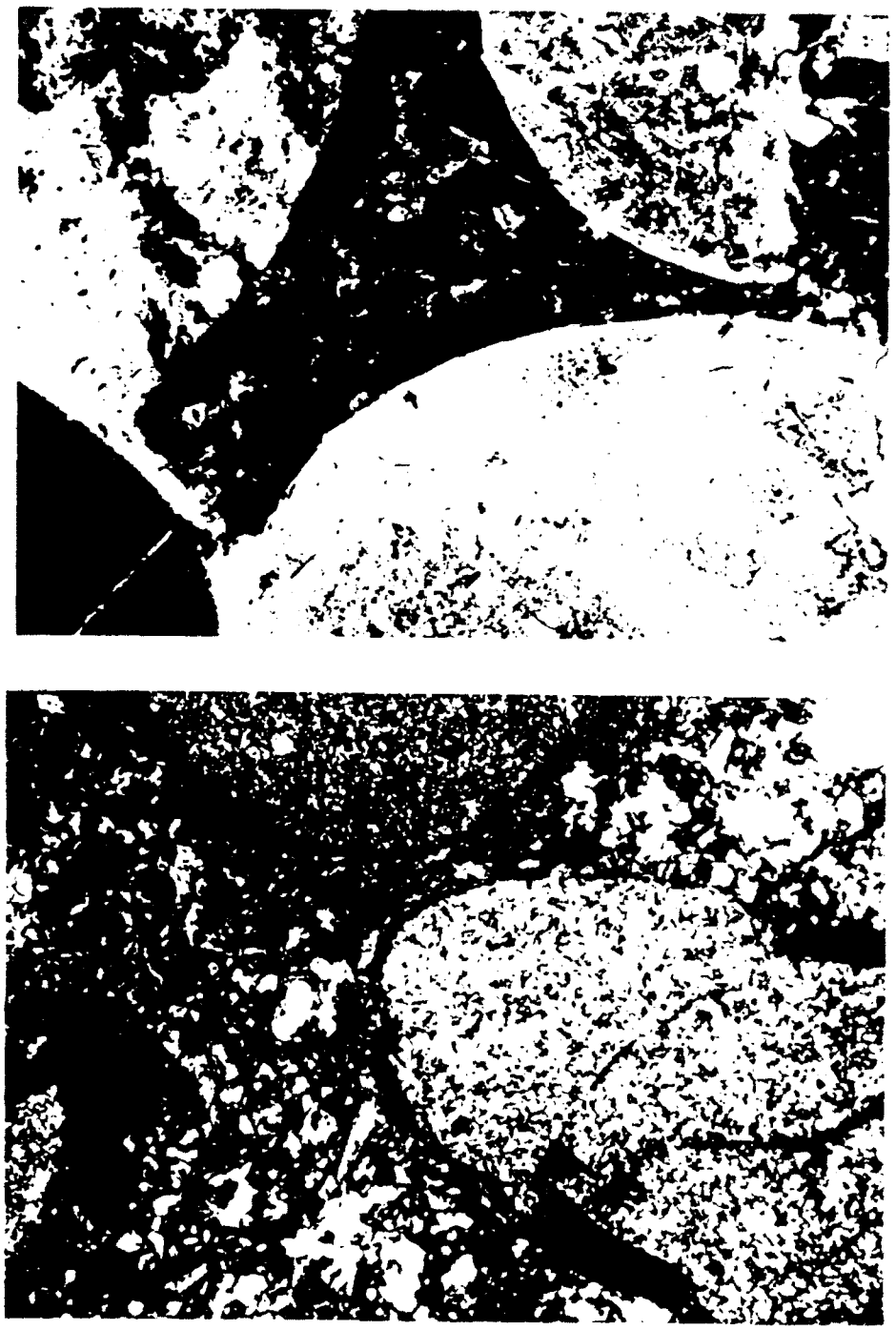

Figure 9-11 Photographs of Thin Section Showing Cambria Sand after Shearing, One-Dimensional Compression Test.

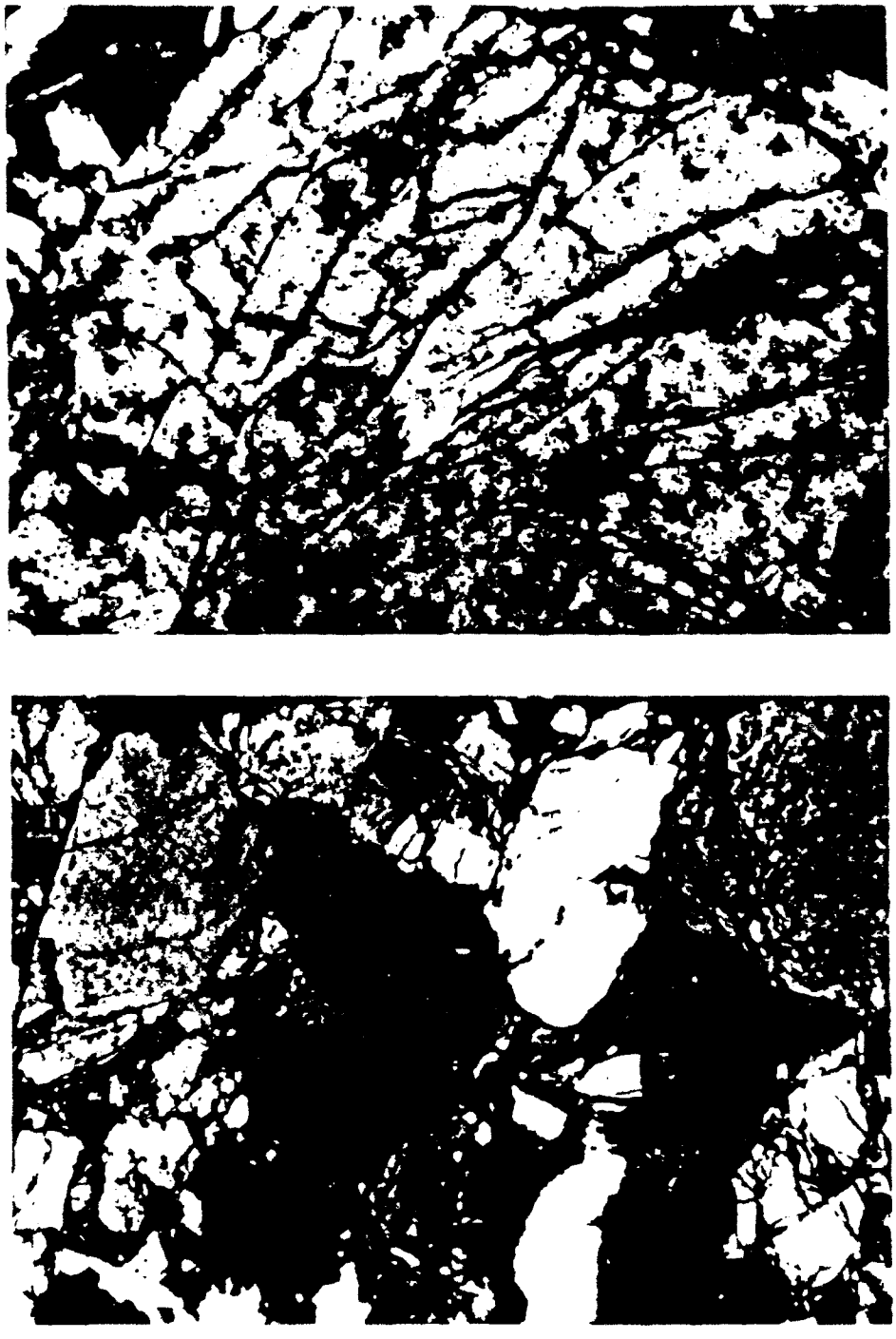

Figure 9-12 Photographs of Thin Section Showing Quartz Sand after Shearing, One-Dimensional Compression Test.

other. Since the shape of the containment cell is not a uniform thick-walled tube and the specimen is not applying internal stresses throughout the height of the cell, a closed-form elastic solution could not be used to evaluate the relationship between the measured strains and the internal soil stresses. Therefore, a numerical analysis was performed to evaluate the soil stress conditions that corresponded to the measured strains.

Several assumptions were made in the numerical analysis. The containment cell was assumed to be axi-symmetric, the internal stresses were assumed to be uniform over the entire active length of the specimen, the soil stresses only acted in the radial direction, and the stresses experienced by the cell were assumed to be within its elastic range. For steel, the elastic modulus was assumed to be 199,860 MPa and Poisson's ratio was assumed to be 0.27. A commercial explicit finite-difference numerical-analysis program, FLAC (Fast Lagrangian Analysis of Continua), was used in the analysis. Before the analysis of the actual containment cell was performed, a uniform cylinder was analyzed with full internal pressure. Since a closed-form solution is available for this case (Roark and Young, 1982), the numerical analysis program and discretization procedure could be evaluated. The results of this elastic analysis indicate that the numerical solution showed strain levels that were 0.6 percent below those from the closed-form solution. This was deemed to be adequate to achieve reasonable accuracy for the soil stresses.

The actual containment cell was discretized into 480 zones for the numerical routine and the analysis was performed for specimen heights between 8.89 centimeters (3.5 inches) and 4.44 centimeters (1.75 inches). A unit MPa

internal radial stress was assumed. In this way, K_o could be determined as the specimen deformed. The assumed displacement boundary condition was zero vertical displacement on the bottom of the cell. Figure 9-13 displays the results in the form of specimen height versus circumferential strain at the location of the strain gage. The inferred internal radial stress is simply equal to the ratio of the measured strain divided by the calculated strain for the unit stress for a given specimen height in units of MPa.

There are several definitions of K_o. Terzaghi (1920) defined it as expressed in Equation 9.1, while he was studying the importance of no lateral movement of retaining walls in sands and clays.

$$K_o = \frac{\sigma_h}{\sigma_v} \qquad (9.1)$$

σ_h = *total horizontal soil pressure.*
σ_v = *total vertical soil pressure.*

Bishop (1958) defined K_o more precisely. He stated that the coefficient of earth pressure at rest is the ratio of the lateral to vertical effective stresses in a consolidated soil under the condition of no lateral deformations. Also, he stated a condition where these were principal stresses with no shear stresses being applied on the principal planes as indicated in Equation 9.2.

$$K_o = \frac{\sigma'_h}{\sigma'_v} \qquad (9.2)$$

σ'_h = *effective horizontal stress.*
σ'_v = *effective vertical stress.*

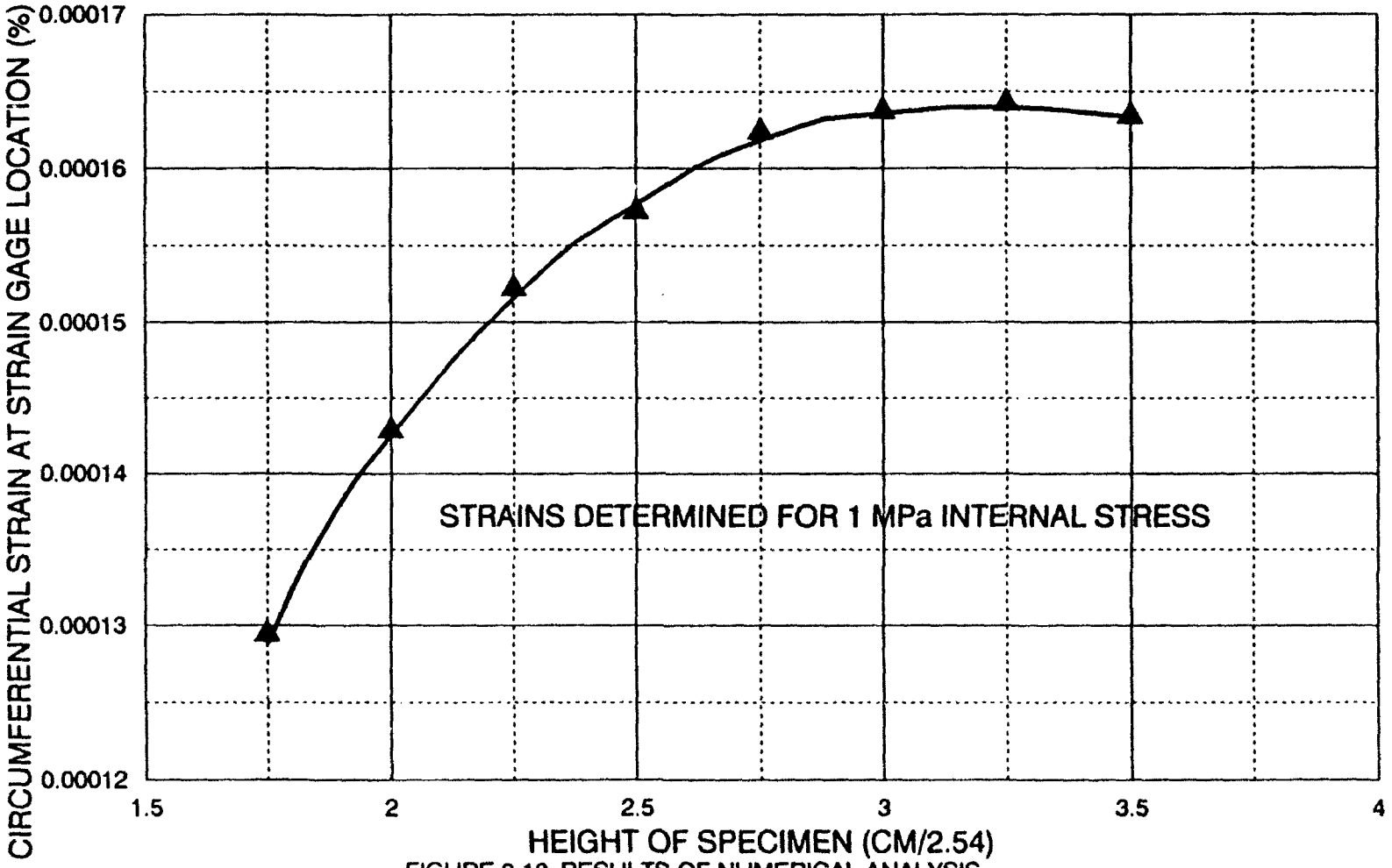

FIGURE 9-13 RESULTS OF NUMERICAL ANALYSIS
CIRCUMFERENTIAL STRAIN vs. HEIGHT OF SPECIMEN
ONE-DIMENSIONAL COMPRESSION TESTS

$$K_o = \frac{\Delta\sigma'_h}{\Delta\sigma'_v} \qquad (9.3)$$

$\Delta\sigma'_h$ = *horizontal stress increment.*
$\Delta\sigma'_v$ = *vertical stress increment.*

Andrawes and El-Sohby (1973) further refined the definition of K_o by stating that it should be expressed in stress increments to remove any effects of stress history on the soil as shown above in Equation 9.3. Figures 9-14, 9-15 and 9-16 indicate the values for K_o related to axial stress for the three sands. The definition of K_o used for these figures is as expressed in Equations 9.1 or 9.2, since in this case the total and effective stresses are the same. By definition the radial strains in a one-dimensional test should be zero. However, this is not possible, since strains are necessary to infer the horizontal stresses. The radial strain values experienced during the highest stresses are very low (maximum 0.33 percent). Andrawes and El-Sohby (1973) concluded that small strain deviations from zero would not significantly affect the resulting values of K_o. Also shown on the figures is the value of K_o calculated based upon Jaky's equation, which is an empirical correlation with the Mohr-Coulomb secant friction angle that is widely used at low confining pressures. Jaky's formulation for K_o is expressed in Equation 9.4. The friction angles are those obtained from the triaxial compression tests.

$$K_o = 1 - \sin\phi \qquad (9.4)$$

K_o = *coeffcient of earth pressure at rest.*
ϕ = *Mohr-Coulomb secant friction angle of the soil.*

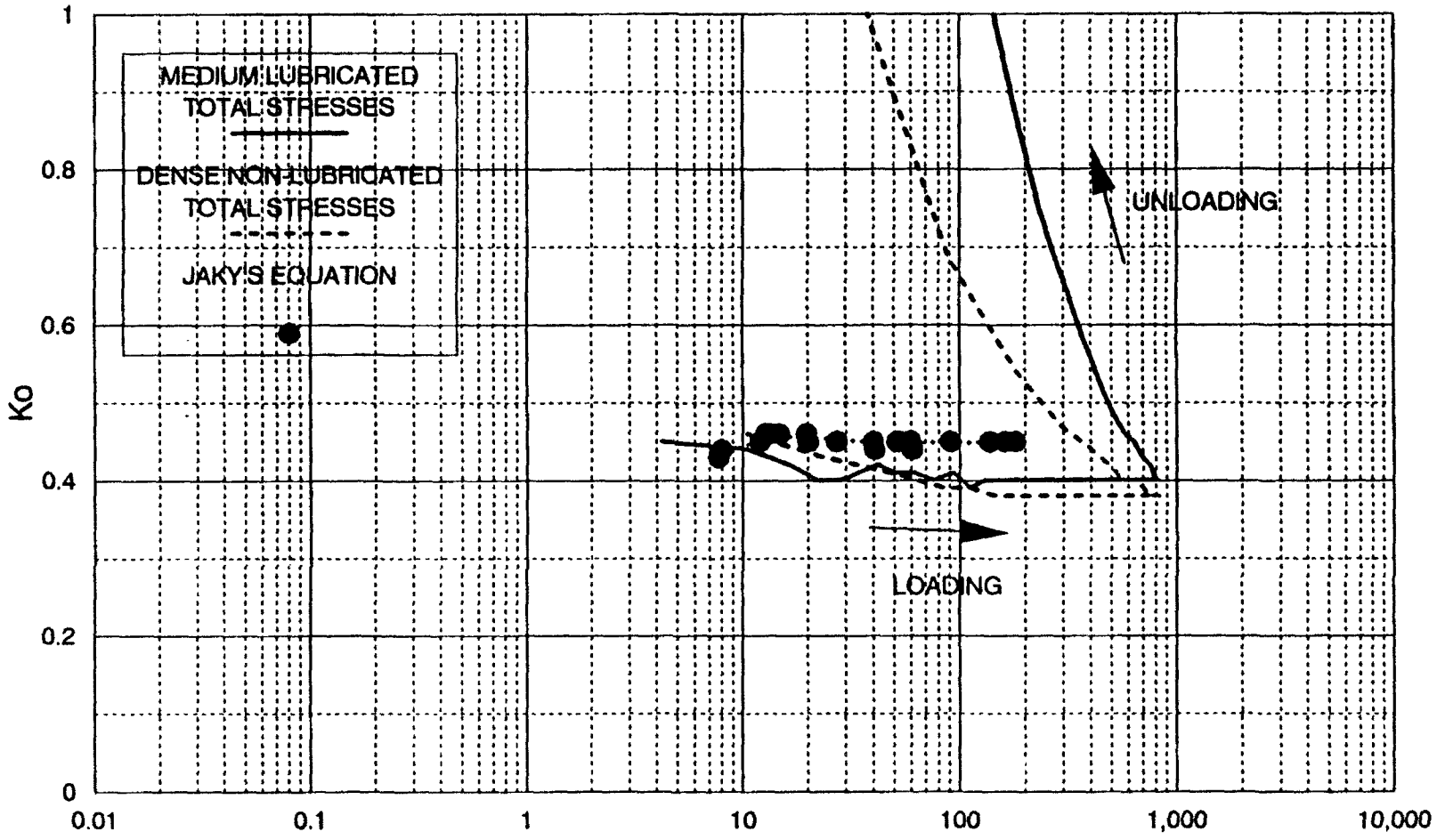

FIGURE 9-14 TOTAL STRESS Ko vs. AXIAL STRESS
ONE-DIMENSIONAL AND TRIAXIAL COMPRESSION TESTS
CAMBRIA SAND

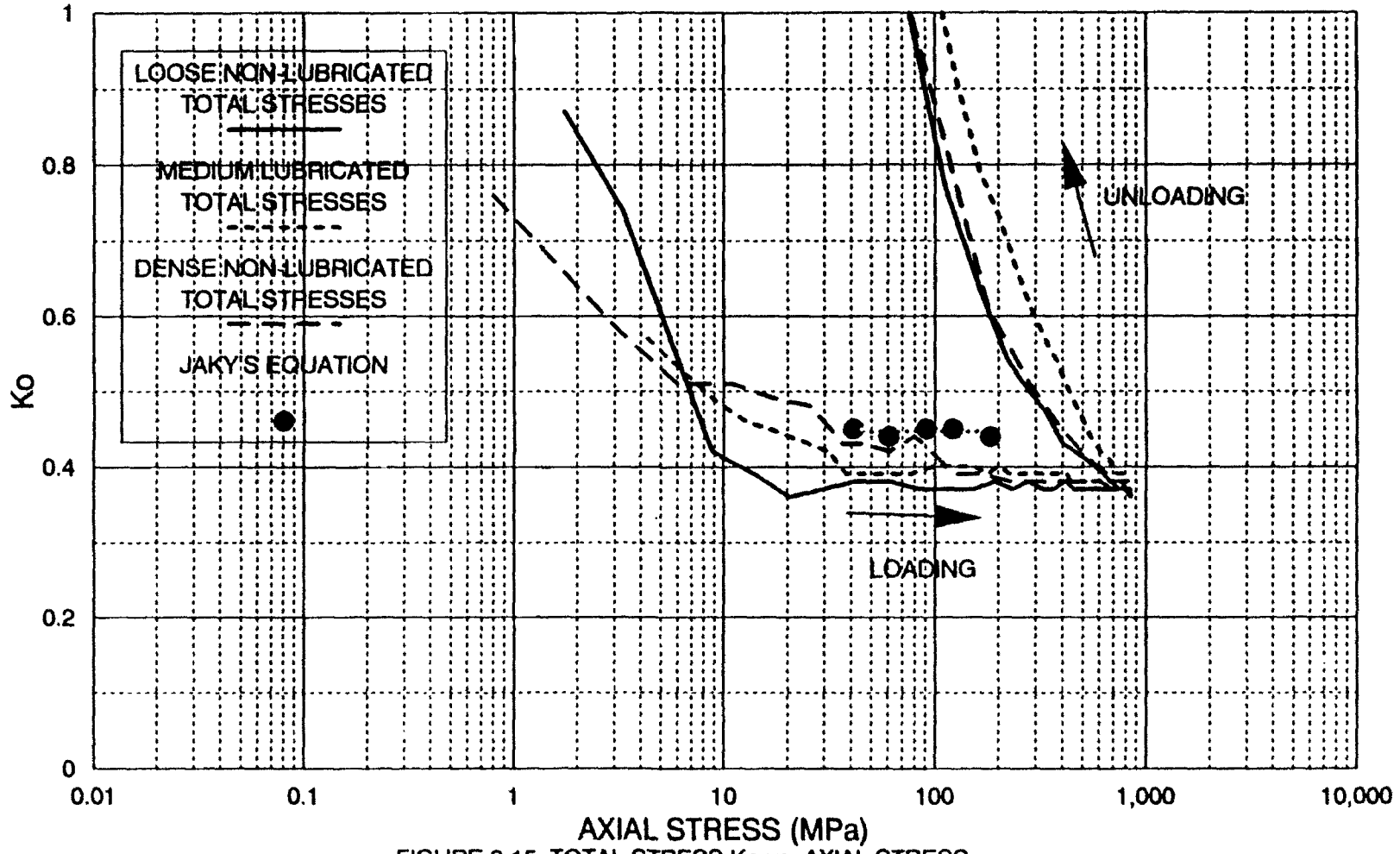

FIGURE 9-15 TOTAL STRESS Ko vs. AXIAL STRESS
ONE-DIMENSIONAL AND TRIAXIAL COMPRESSION TESTS
QUARTZ SAND

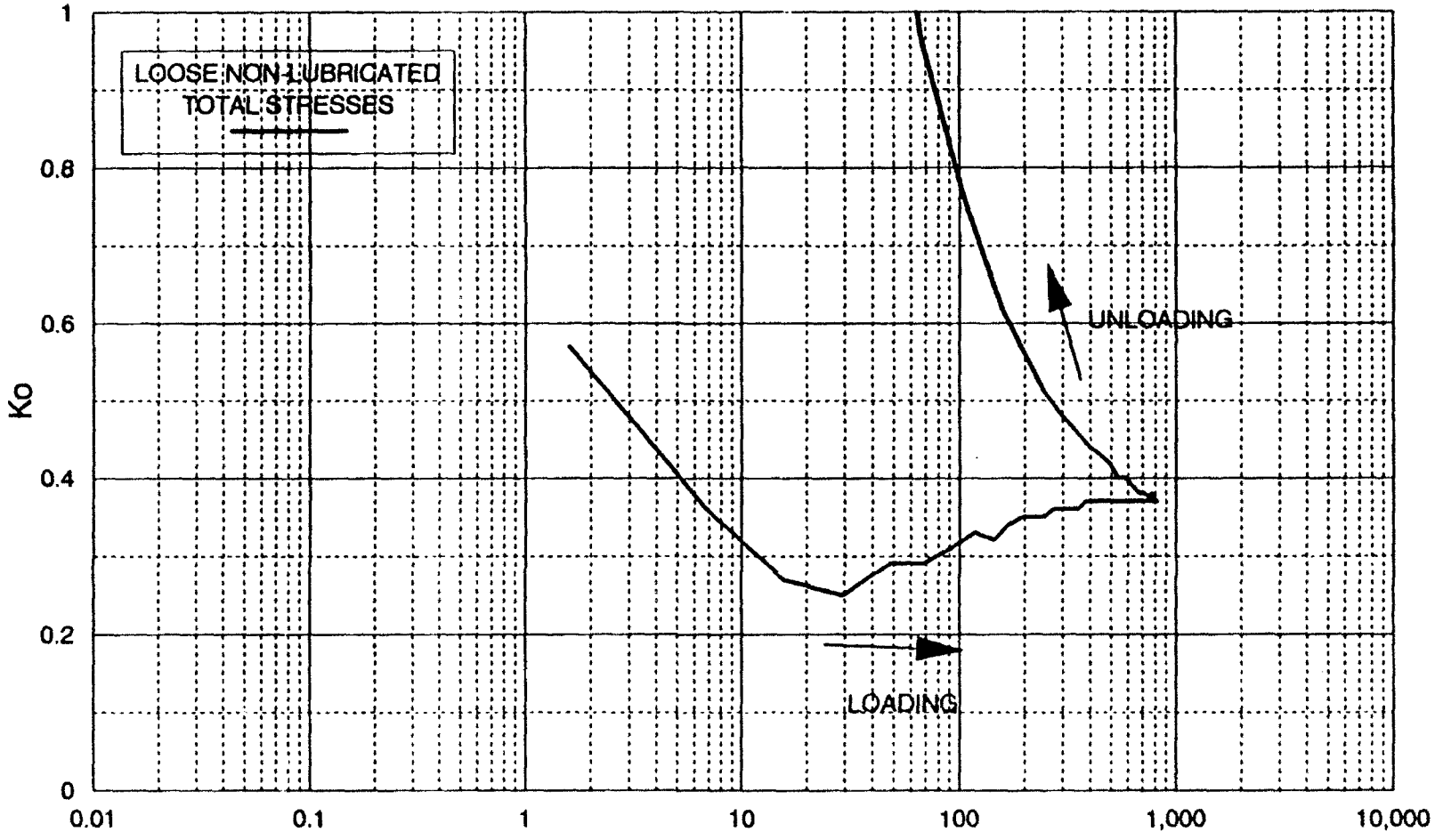

FIGURE 9-16 TOTAL STRESS Ko vs. AXIAL STRESS
ONE-DIMENSIONAL COMPRESSION TESTS
SACRAMENTO RIVER SAND

There were some problems with the instrumentation and not all tests yielded reliable results. As can be seen from the plots, the value of K_o is a maximum at low pressures and decreases with increasing axial stresses. The magnitude then appears to stabilize at a constant value at higher stresses. The measured K_o values for Cambria sand stabilizes at values between 0.38 and 0.40, quartz sand between 0.37 and 0.39, and Sacramento River sand around 0.37. These values appear to be reasonable for K_o at high pressures. Hendron (1963) obtained values of K_o between 0.33 and 0.43 for four different dense sands tested to axial stresses of 23.4 MPa (3,400 psi). It is apparent that Jaky's formulation (Equation 9.4) tends to overpredict the value of K_o. At low pressures the friction angle increases with decreasing void ratio. However, at high pressures the friction angle becomes constant with decreasing void ratios.

Sidewall friction does slightly affect the results regarding K_o. Close examination of the diagrams indicates that the reduced-friction tests had slightly higher values of K_o, but they were still within the experimental scatter. Apparently, the effect of friction is to reduce the vertical stresses applied to the specimen. This results in corresponding lower horizontal stress. Therefore, the net effect on K_o is negligible. However, it must be stated that the circumferential strain values obtained from the numerical analysis were correct. Since there is friction, the internal normal stress distribution is not uniform as assumed, but it decreases from the top to the bottom of the specimen. A decreasing normal stress distribution would lower the calculated value of the horizontal stress, and hence the magnitude of K_o. Another effect attributable to friction is the curious dip in the

K_o curve for the Sacramento River sand at lower stresses. A possible explanation is that the very fine Sacramento River sand does not compress and crush as easily at low stresses, and the densification is primarily due to rearranging. The friction prevents the compaction process until the axial stress is at a sufficiently high level to overcome the sidewall friction. Therefore, the horizontal stress development tends to lag behind the vertical stresses until higher stresses are reached. At the higher stresses, the value of K_o stabilizes and moves toward a constant value. Another possible reason may be the fine grain size of the Sacramento River sand. The sand did tend to push upward into the annular space between the piston and cell wall possibly creating friction, which would increase the measured vertical stress. This sand was the only sand for which this problem occurred.

The effect of the initial density follows a pattern of behavior that is consistent with prior studies. The plots clearly show that soils with lower initial densities have higher values of K_o. The magnitude of K_o then decreases as the axial stress increases. However, it is interesting to see how the relative values of K_o for different initial densities change with increasing axial stress level. Jaky's K_o formulation (Equation 9.4) for low pressures would indicate that the value of K_o should be higher for low density sands, since the friction angle of a sand is lower at low densities. This is correct for the initial void ratio at the lowest stress conditions. However, as the axial stress level increases, the sand starts to densify quickly due to particle rearranging and crushing, and K_o decreases much more rapidly for the medium and loose sands than for the dense sand, and this results in lower K_o values for the loose sand when still at relatively low stress values.

Figures 9-14 and 9-15 clearly indicate that the different density K_o curves cross each other. This phenomenon can be explained from the fact that at high axial stress levels the soil is undergoing large amounts of densification and is highly compressible, and it does not generate as large an amount of radial stress for a given axial stress. In other words the specimen is in a partially volumetrically collapsing state. The horizontal stresses do increase, but not as fast as the vertical stresses. Eventually, the specimen densifies to conditions that are independent of the initial density. Similar behavior was observed in high pressure triaxial compression tests on the Cambria and quartz sands. The magnitude of the volumetric strains at the onset of the shearing phase are so large that it was shown (Chapter 5) that the radial strains in the specimen are contractive. It would seem that Jaky's formulation for K_o is not valid at axial stress levels where significant amounts of particle crushing occurs.

Figures 9-17, 9-18 and 9-19 show K_o related to axial stress for the three sands, but using the incremental stress definition expressed by Equation 9.3. As can be seen there is quite a substantial variation in the magnitude of K_o when expressed in this manner. However, the large variations do tend to oscillate about the total stress value of K_o, which indicates that the total stress or effective stress methods are reasonable representations for this type of test. It also appears that the oscillations are larger for the reduced-friction tests, especially at high stress levels. This indicates that the lubrication is working. During the reduced-friction tests the vertical loads were seen to rise in an irregular manner. This is associated with the specimen periodically breaking loose from sidewall friction and further

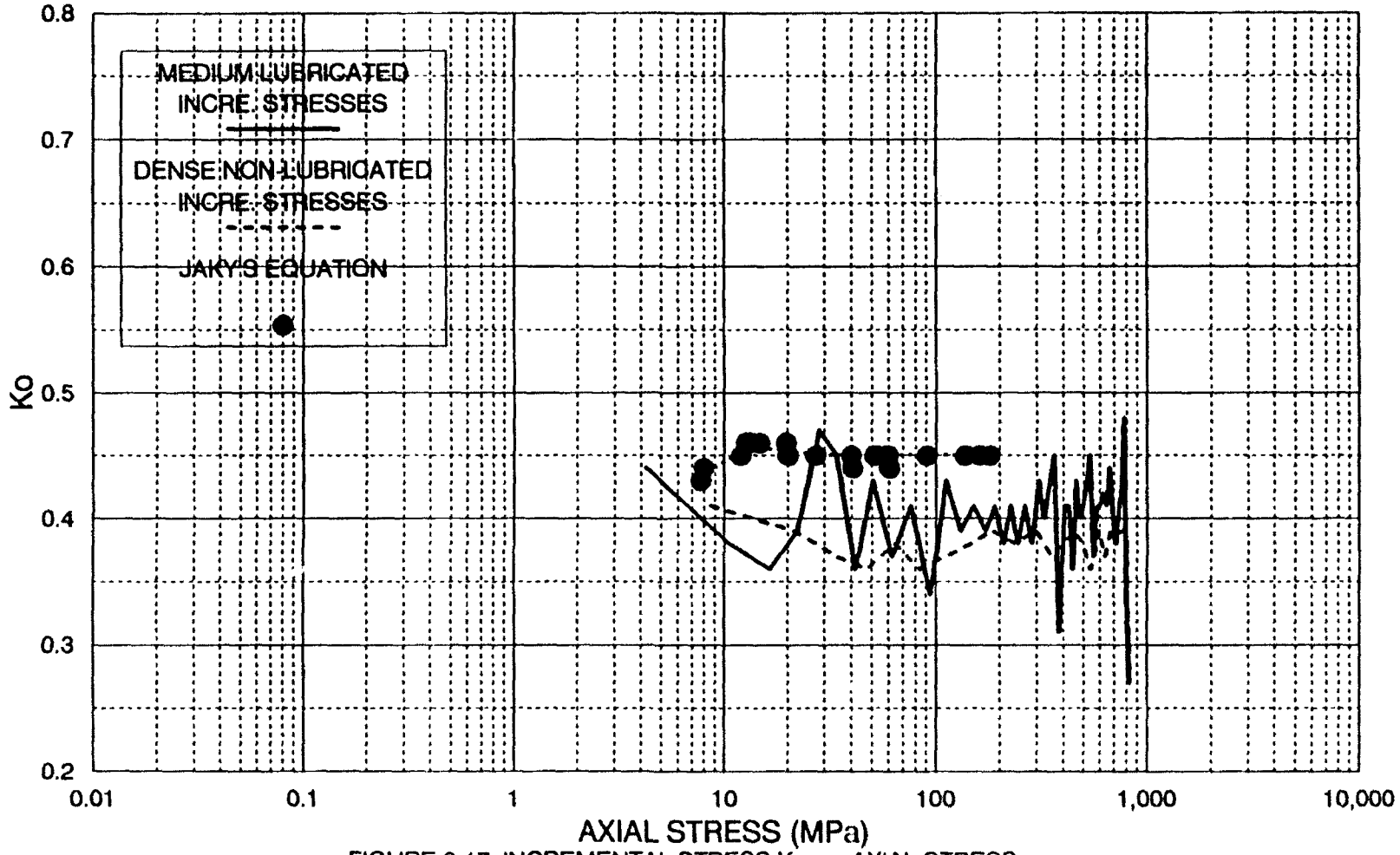

FIGURE 9-17 INCREMENTAL STRESS Ko vs. AXIAL STRESS
ONE-DIMENSIONAL AND TRIAXIAL COMPRESSION TESTS
CAMBRIA SAND

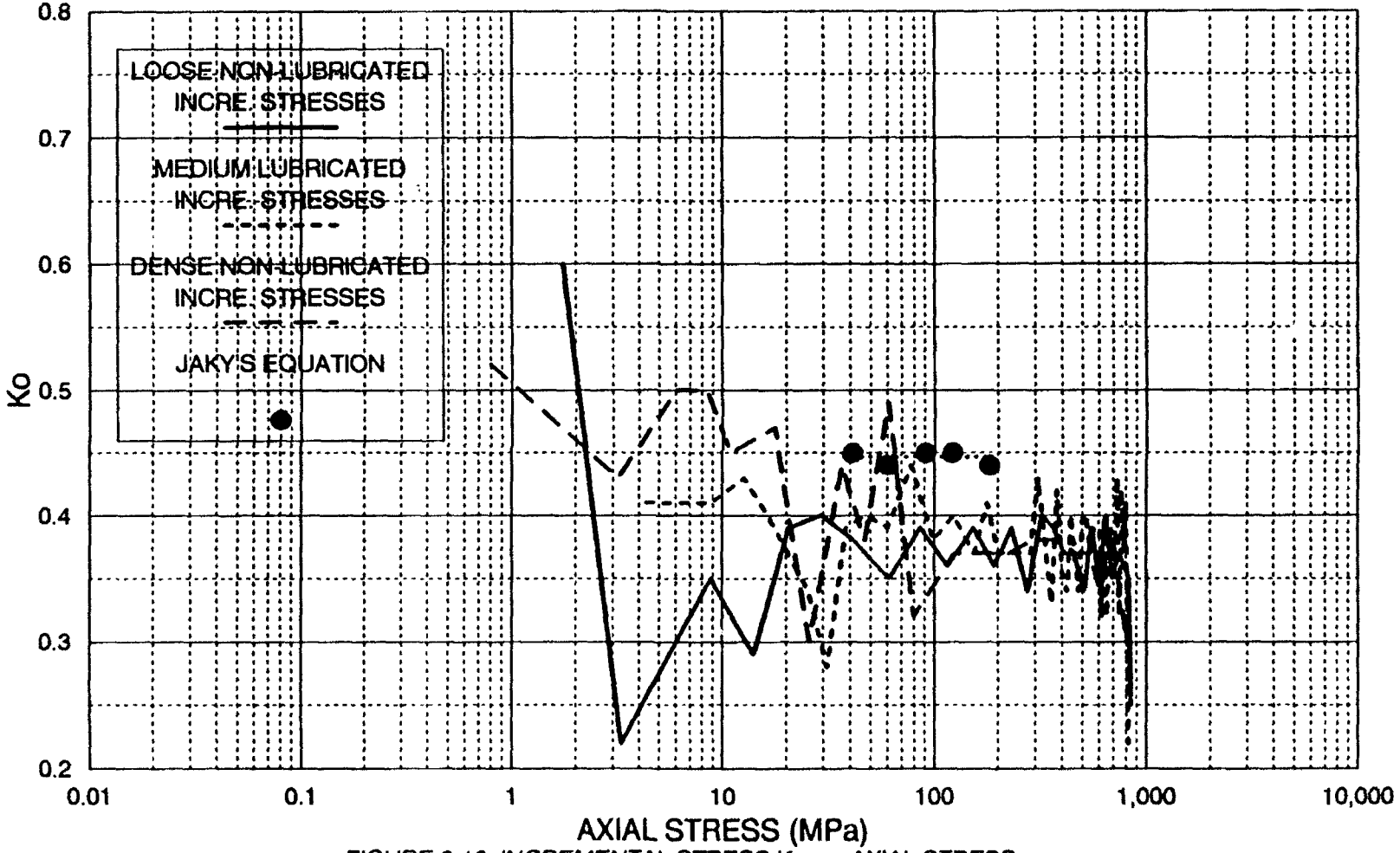

FIGURE 9-18 INCREMENTAL STRESS Ko vs. AXIAL STRESS
ONE-DIMENSIONAL AND TRIAXIAL COMPRESSION TESTS
QUARTZ SAND

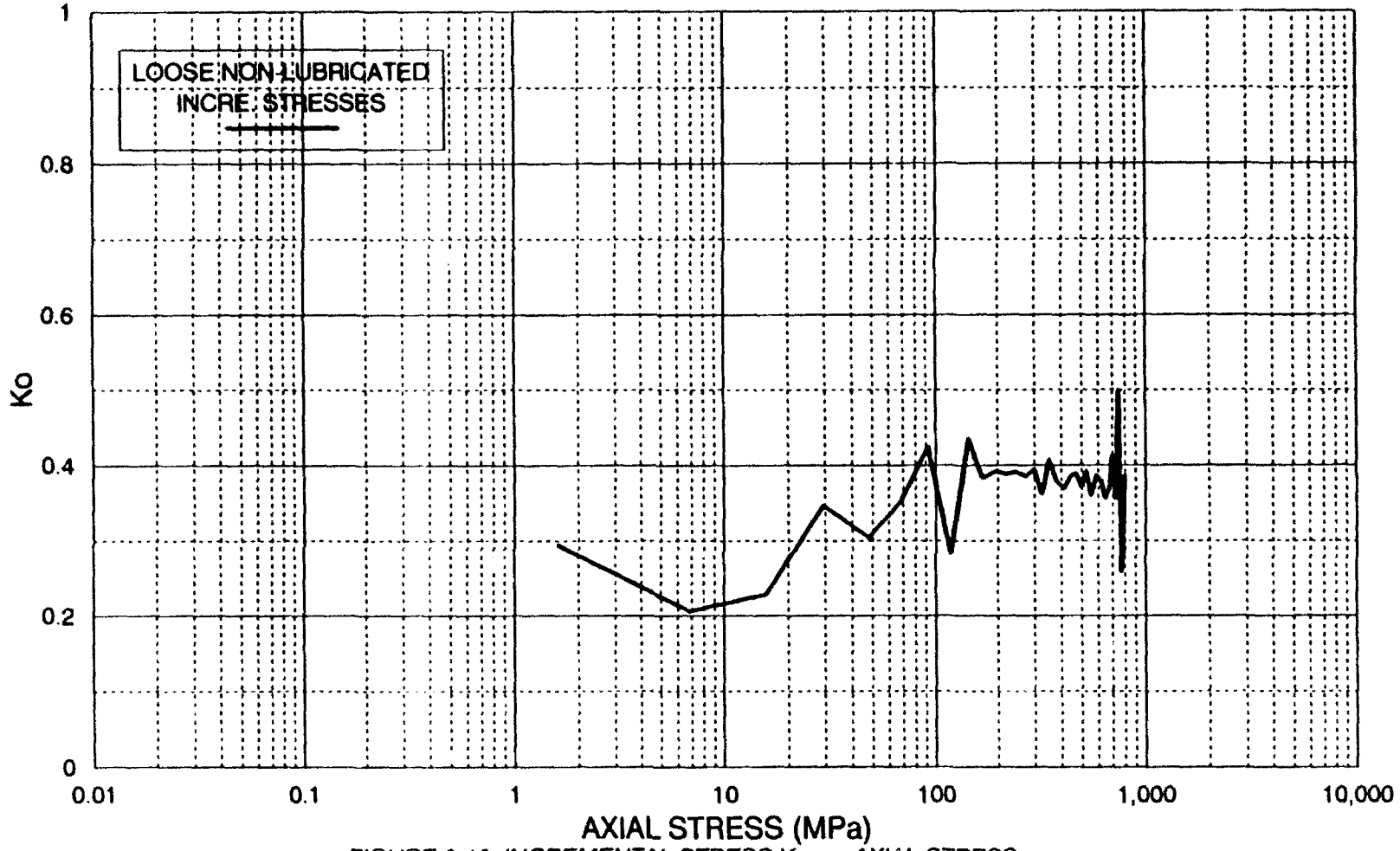

FIGURE 9-19 INCREMENTAL STRESS Ko vs. AXIAL STRESS
ONE-DIMENSIONAL COMPRESSION TESTS
SACRAMENTO RIVER SAND

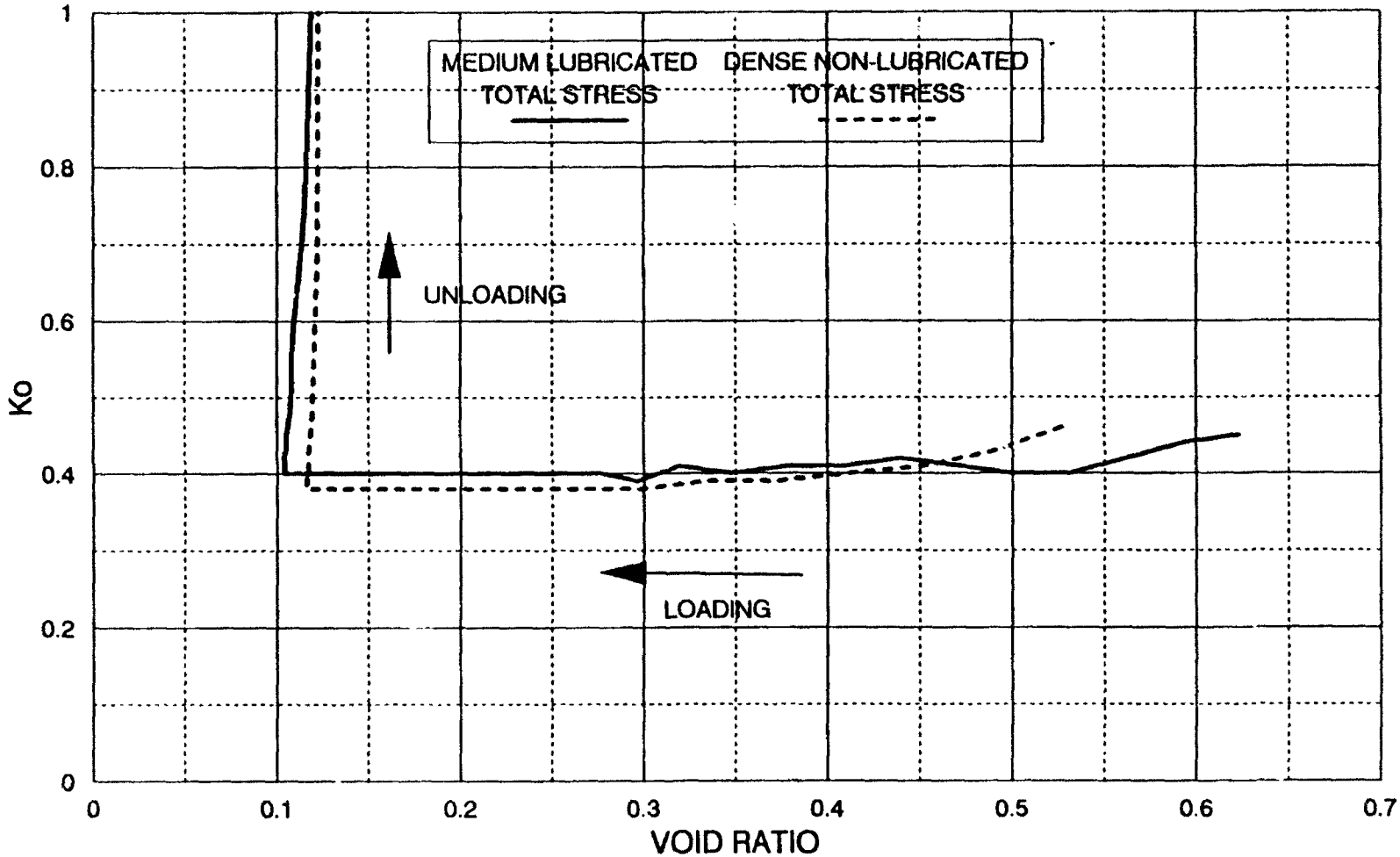

FIGURE 9-20 TOTAL STRESS Ko vs. VOID RATIO
ONE-DIMENSIONAL COMPRESSION TESTS
CAMBRIA SAND

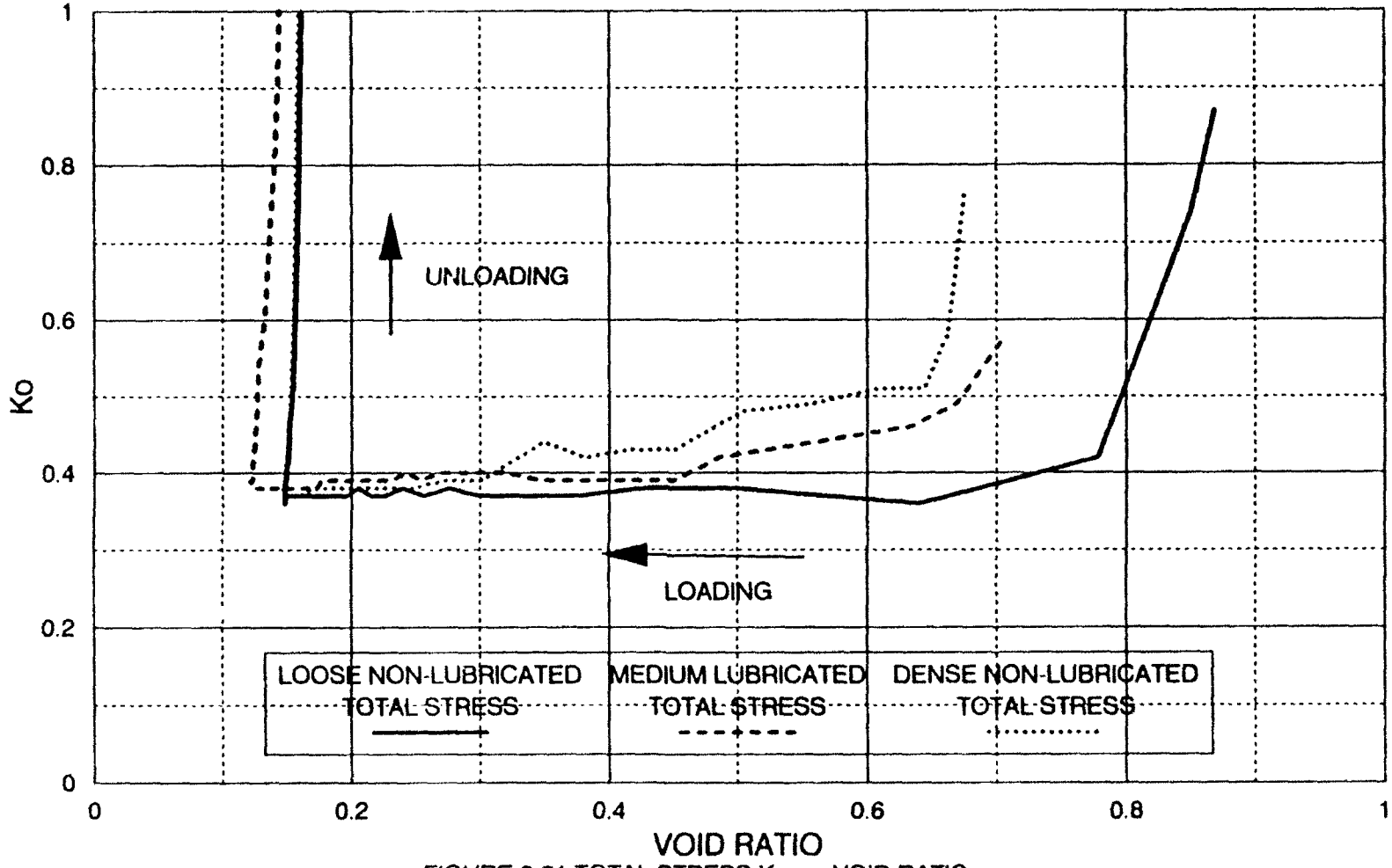

FIGURE 9-21 TOTAL STRESS Ko vs. VOID RATIO
ONE-DIMENSIONAL COMPRESSION TESTS
QUARTZ SAND

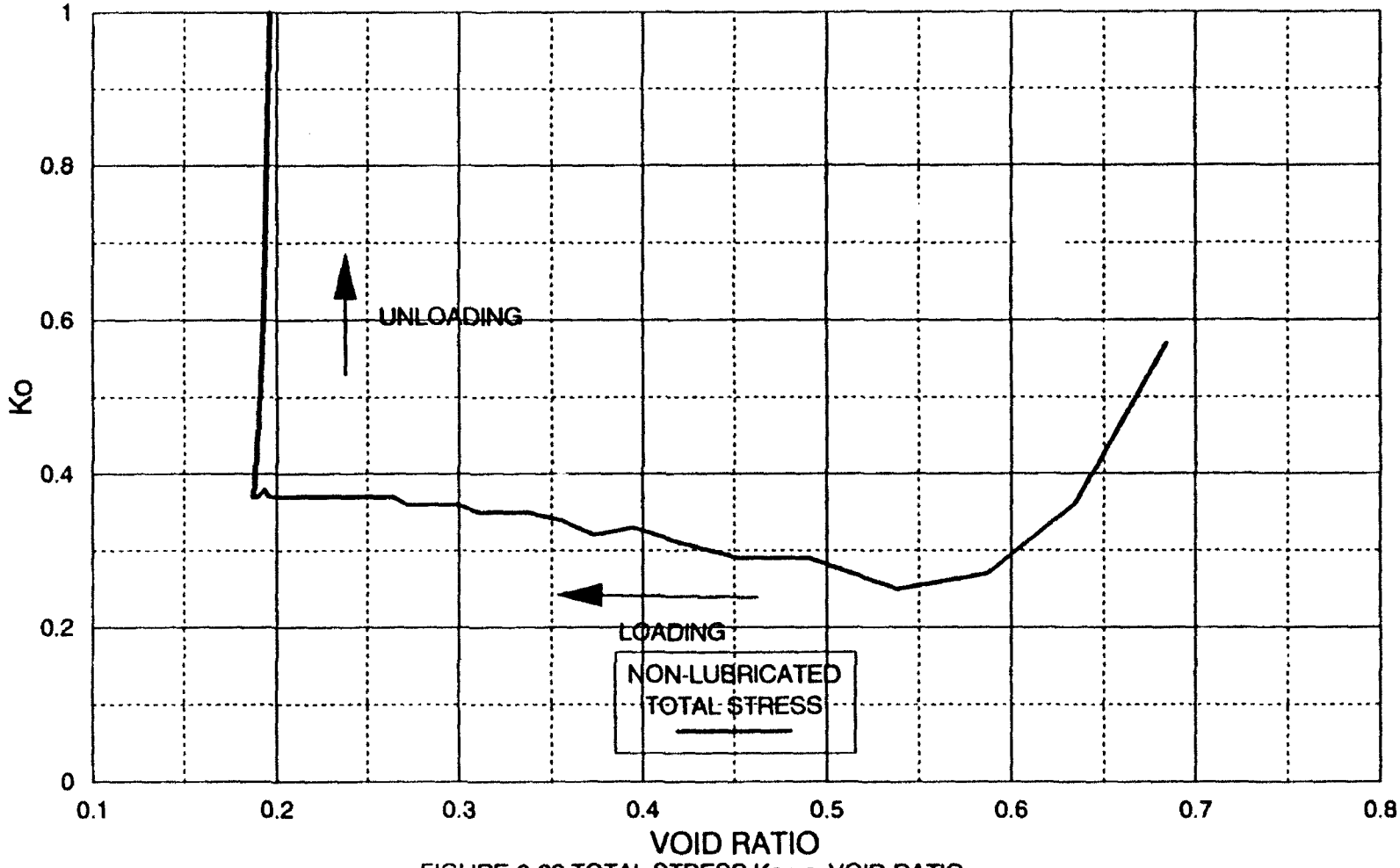

FIGURE 9-22 TOTAL STRESS Ko vs. VOID RATIO
ONE-DIMENSIONAL COMPRESSION TESTS
SACRAMENTO RIVER SAND

densifying. The circumferential strains were not seen to oscillate in this manner, since the horizontal stresses tend to be locked-in and demonstrate an insensitivity to small variations in vertical stress.

Figures 9-20, 9-21 and 9-22 display the value of K_o related to the void ratio for Cambria, quartz and Sacramento River sand, respectively. The effect of initial void ratio is clearly indicated on these diagrams. The different density curves initially have large values of K_o, but then merge together at high axial stress levels as the effect of initial void ratio is eliminated. The magnitude then stays relatively constant at high axial stress levels during further large reductions in void ratio. The values of K_o for the higher void ratios are typical of values obtained by other researchers (e.g. Hendron, 1963). Again, these figures show results that appear contrary from what might be expected from Jaky equation at high pressures, since K_o for the loose sand should be the largest, followed by the medium, and then the dense sand.

Figures 9-23, 9-24 and 9-25 show the radial stress plotted against the axial stress for the three sands. Most of the loading portions of the curves appears almost linear, which is expected owing to the fact that K_o appears constant at high pressures. The effect of sidewall friction does not seem to be significantly affecting the slopes of the loading curves. Since there is a limited number of data points available at the low stress conditions, the curvature at low stresses is not well defined.

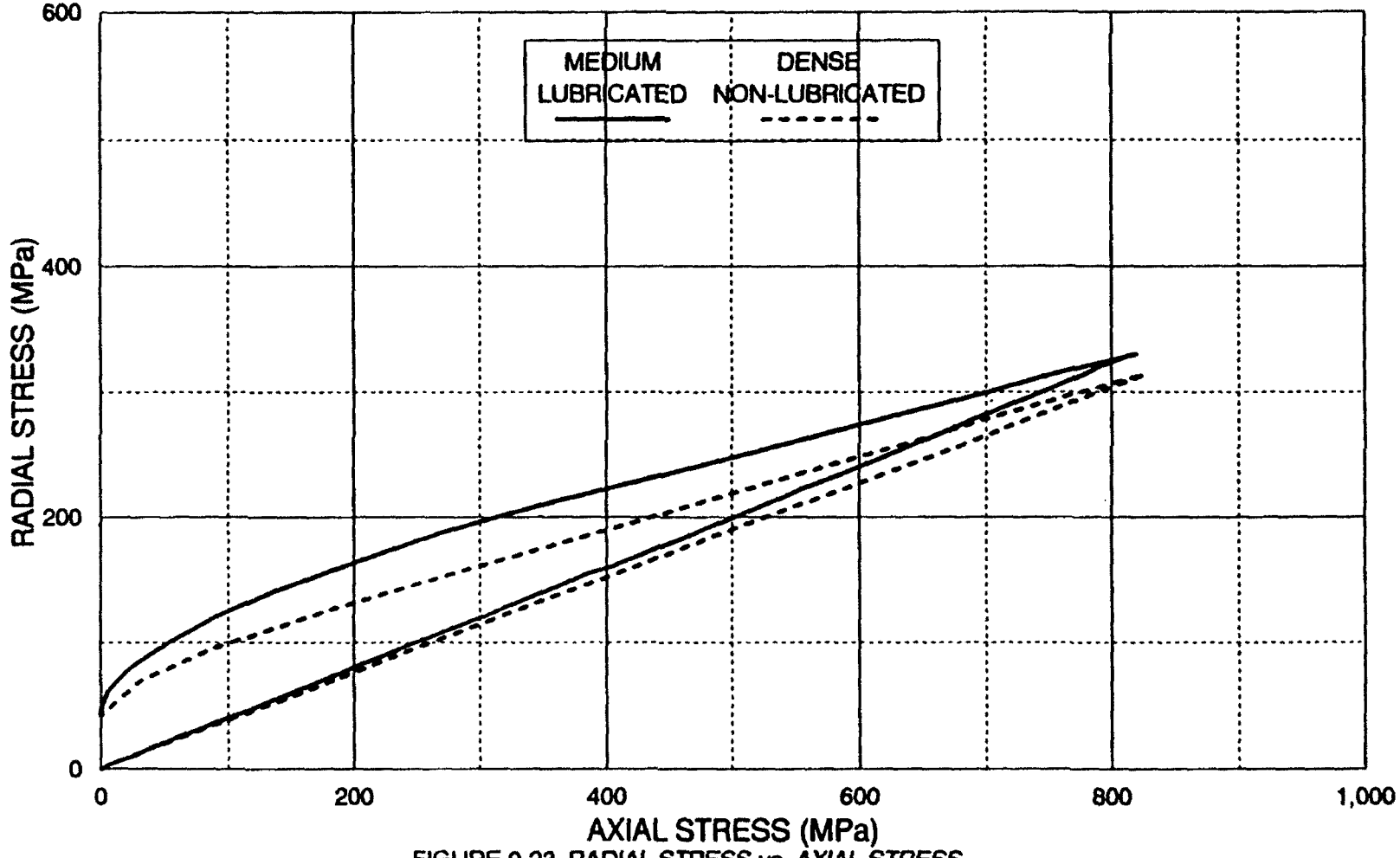

FIGURE 9-23 RADIAL STRESS vs. AXIAL STRESS
ONE-DIMENSIONAL COMPRESSION TESTS
CAMBRIA SAND

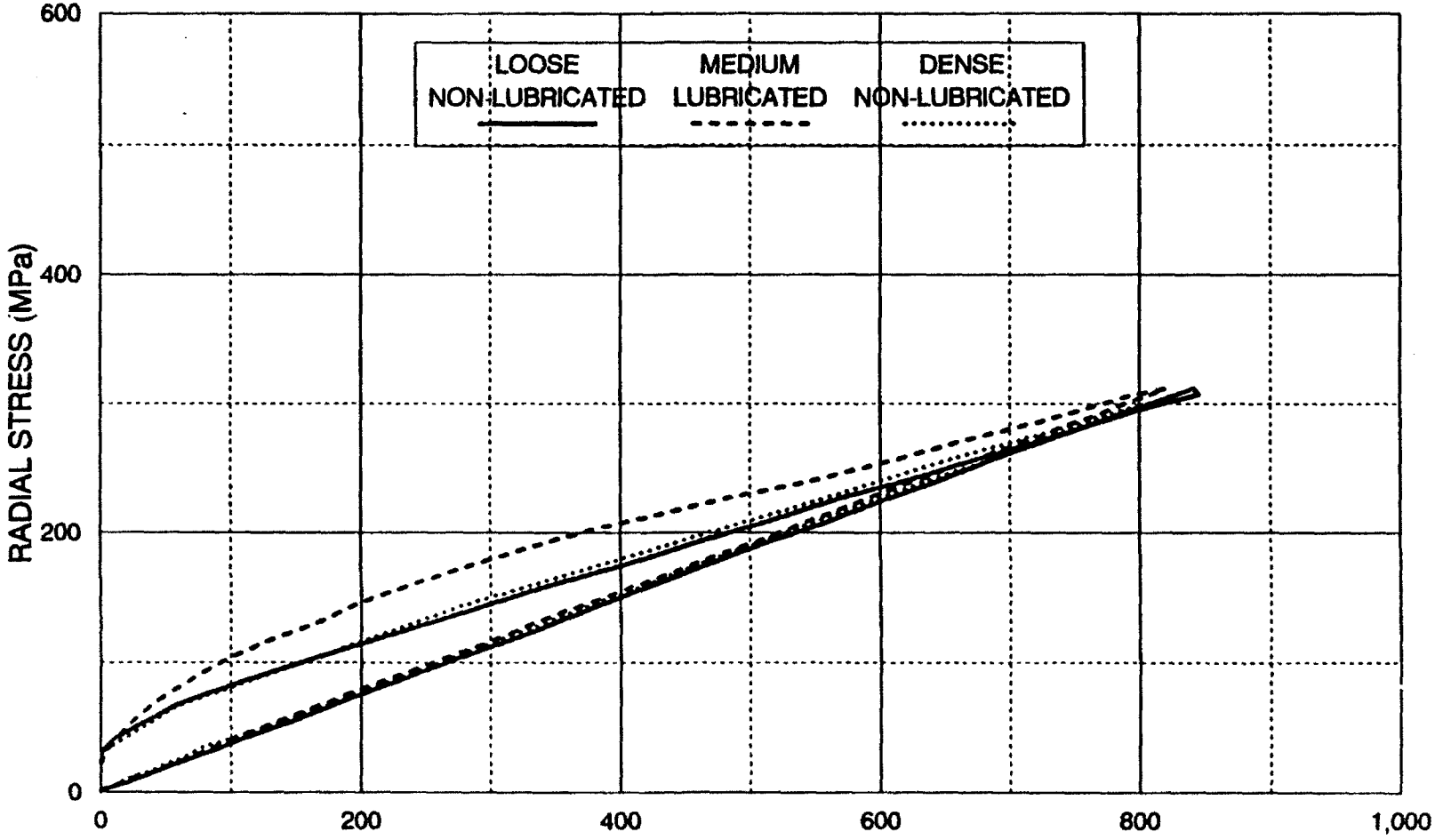

FIGURE 9-24 RADIAL STRESS vs. AXIAL STRESS
ONE-DIMENSIONAL COMPRESSION TEST
QUARTZ SAND

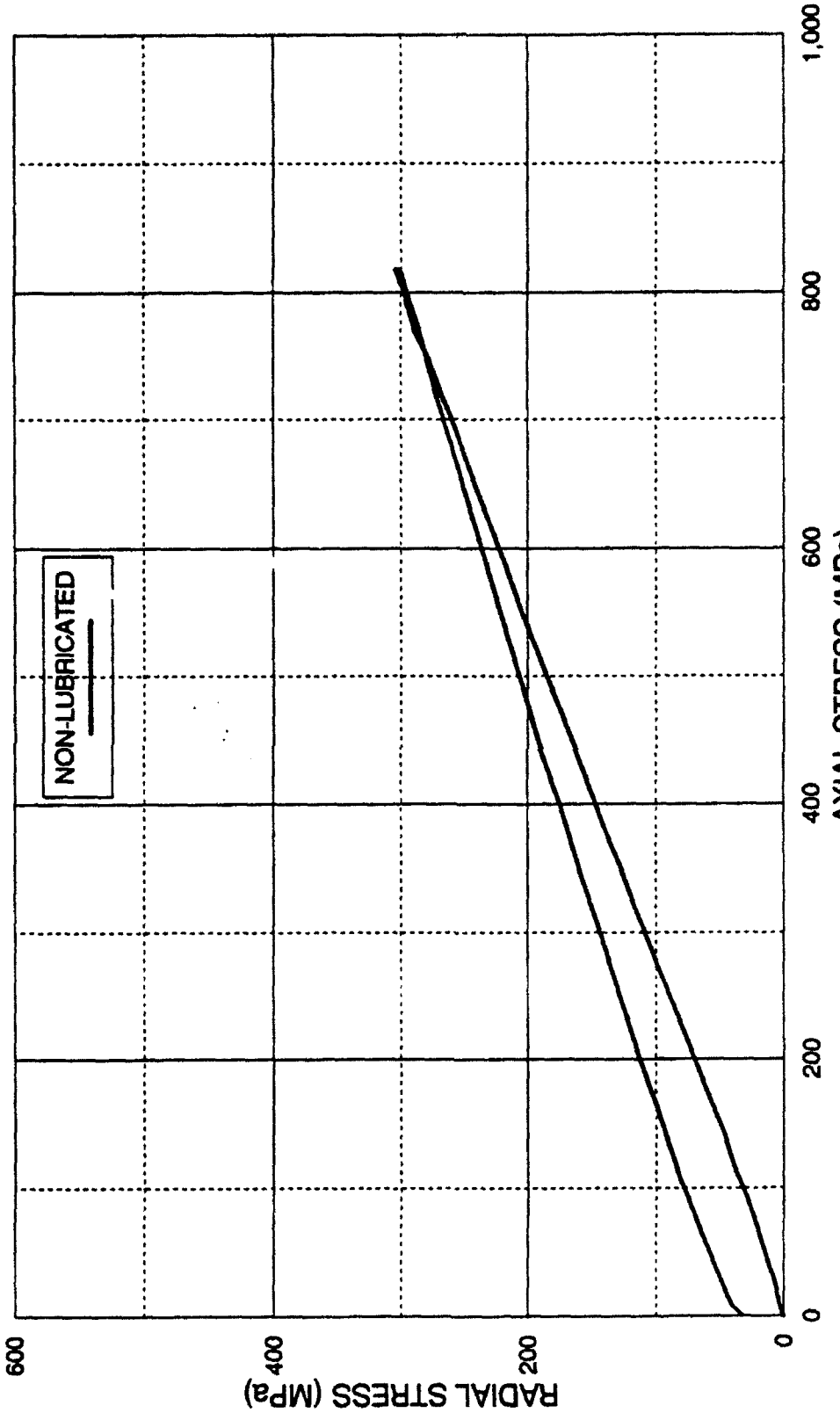

FIGURE 9-25 RADIAL STRESS vs. AXIAL STRESS
ONE-DIMENSIONAL COMPRESSION TEST
SACRAMENTO RIVER SAND

9.8 Elastic Parameters for Cambria Sand

To quantify the elastic parameters for Cambria sand (i.e. the elastic modulus and Poisson's ratio) a special test was performed. It consisted of a drained triaxial compression test, which would load, unload, reload, and then unload the test specimen at specified confining pressures. Since the specimen did not need to be sheared to failure, one specimen could be used to evaluate the elastic parameters at several different confining pressures. The effective confining pressures selected were 4.0, 8.0, 16.0, 32.0, and 64.0 MPa. The test consisted of a repeated pattern of loading, unloading, reloading and unloading cycles at different confining pressures.

A special control program was created to allow user control of the loading and unloading process, while the load cell, LVDT, volume change device, and cell/pore pressure transducers were being monitored by the data acquisition system and values recorded in a data file. Analysis of the data was after the test was concluded. A major consideration for the loading and unloading test would be the evaluation of the triaxial cell seal friction. Testing experience has determined that the seal friction is constant at constant cell pressure and constant deformation rate. Therefore, the seal friction during the loading cycle could be estimated by pulling the piston well away from the specimen during the unloading phase before changing directions, such that the piston friction had an opportunity to stabilize and could be estimated from the difference between the piston uplift force and the load cell reading. The unloading seal friction could be estimated as the piston lost contact with the specimen during unloading, and it was also

calculated as the difference between the piston uplift force and the load cell reading. Since the displacement during a typical loading/unloading cycle to evaluate the elastic parameters was very small, lubricated ends were not employed. It was anticipated that the lubricated end stiffness would tend to be incorporated and adversely affect the final results.

In the analysis of the test data, corrections for the loading system flexibility were made to the displacements based upon a correction curve obtained by performing a test without a specimen in the cell and increasing the cell pressure and load, causing the loading system to deform. The stress-strain curves for the loading and unloading cycles for the five confining pressures is shown on Figure 9-26, which displays the deviator stress plotted against the axial strain. Derivation of the elastic modulus is accomplished by measuring the initial slope of the reloading stress-strain curve at each confining pressure. The volumetric strains for the five confining pressures are shown on Figure 9-27. Estimating Poisson's ratio is accomplished by measuring the initial slope of the volumetric strain curve during reloading and utilizing Equation 9.5.

$$\nu = \frac{1}{2} - \frac{\Delta \epsilon_v}{2 \cdot \Delta \epsilon_1} \qquad (9.5)$$

ν = *Poisson's ratio.*
$\frac{\Delta \epsilon_v}{\Delta \epsilon_1}$ = *Slope of volume change curve during reloading.*

The measured values of elastic modulus for Cambria sand at the five different confining pressures are shown on Figure 9-28. The elastic modulus increases with increasing confining pressure and appears to increase in a linear fashion on the the

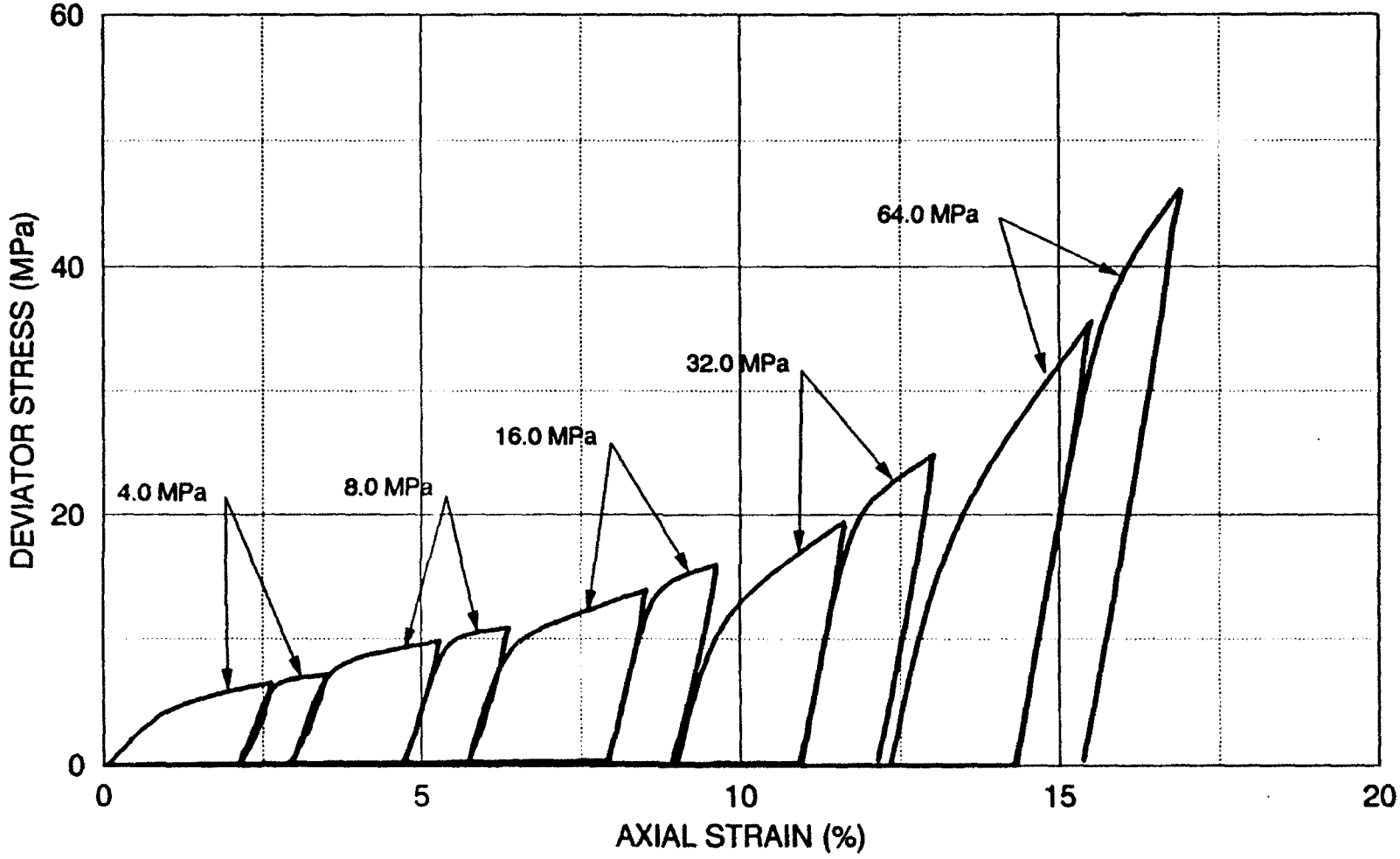

FIGURE 9-26 DEVIATOR STRESS vs. STRAIN
LOADING-UNLOADING-RELOADING TEST FOR DETERMINATION OF ELASTIC PARAMETERS
DENSE CAMBRIA SAND

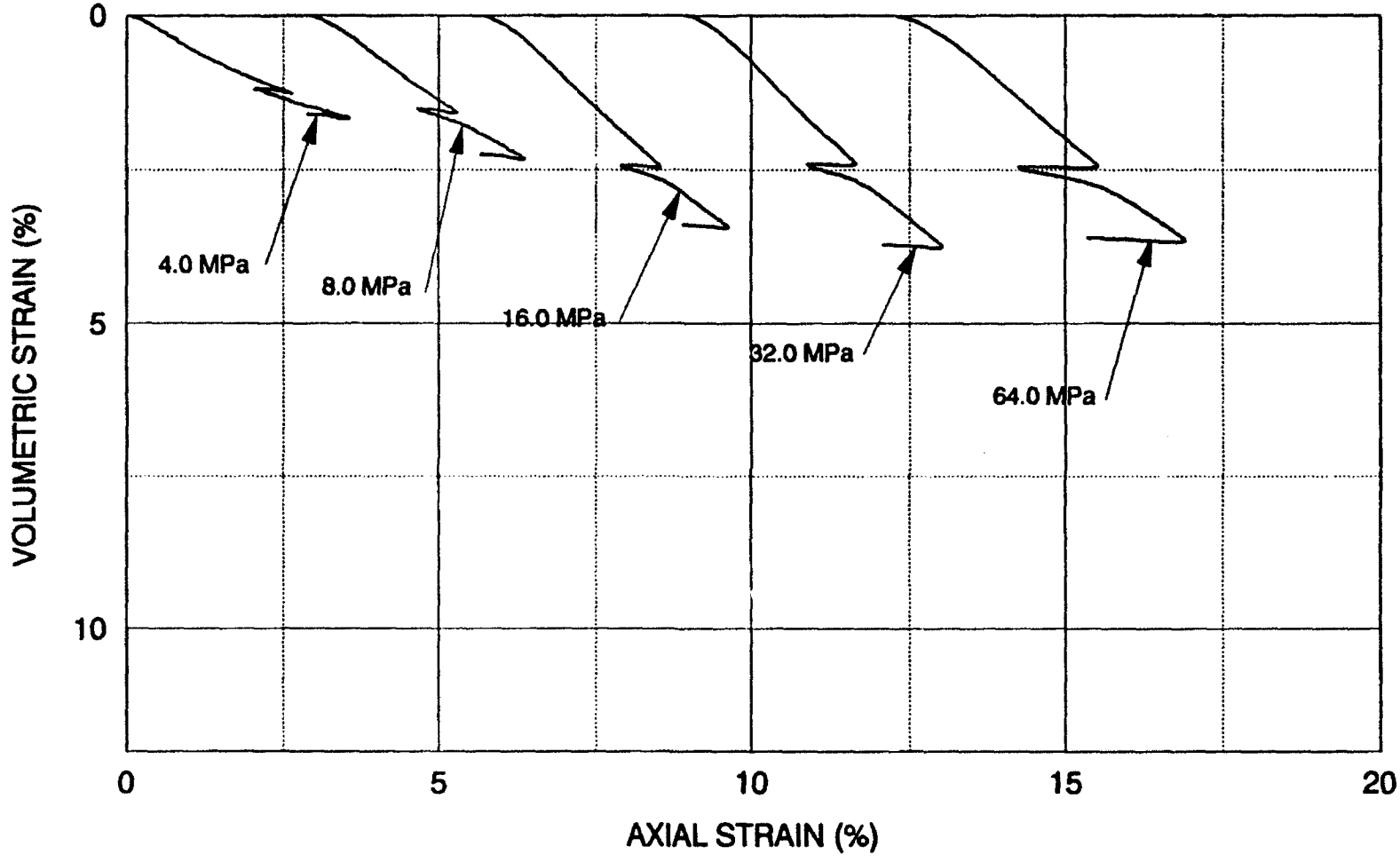

FIGURE 9-27 VOLUMETRIC STRAIN vs. STRAIN
LOADING-UNLOADING-RELOADING TEST FOR DETERMINATION OF ELASTIC PARAMETERS
DENSE CAMBRIA SAND

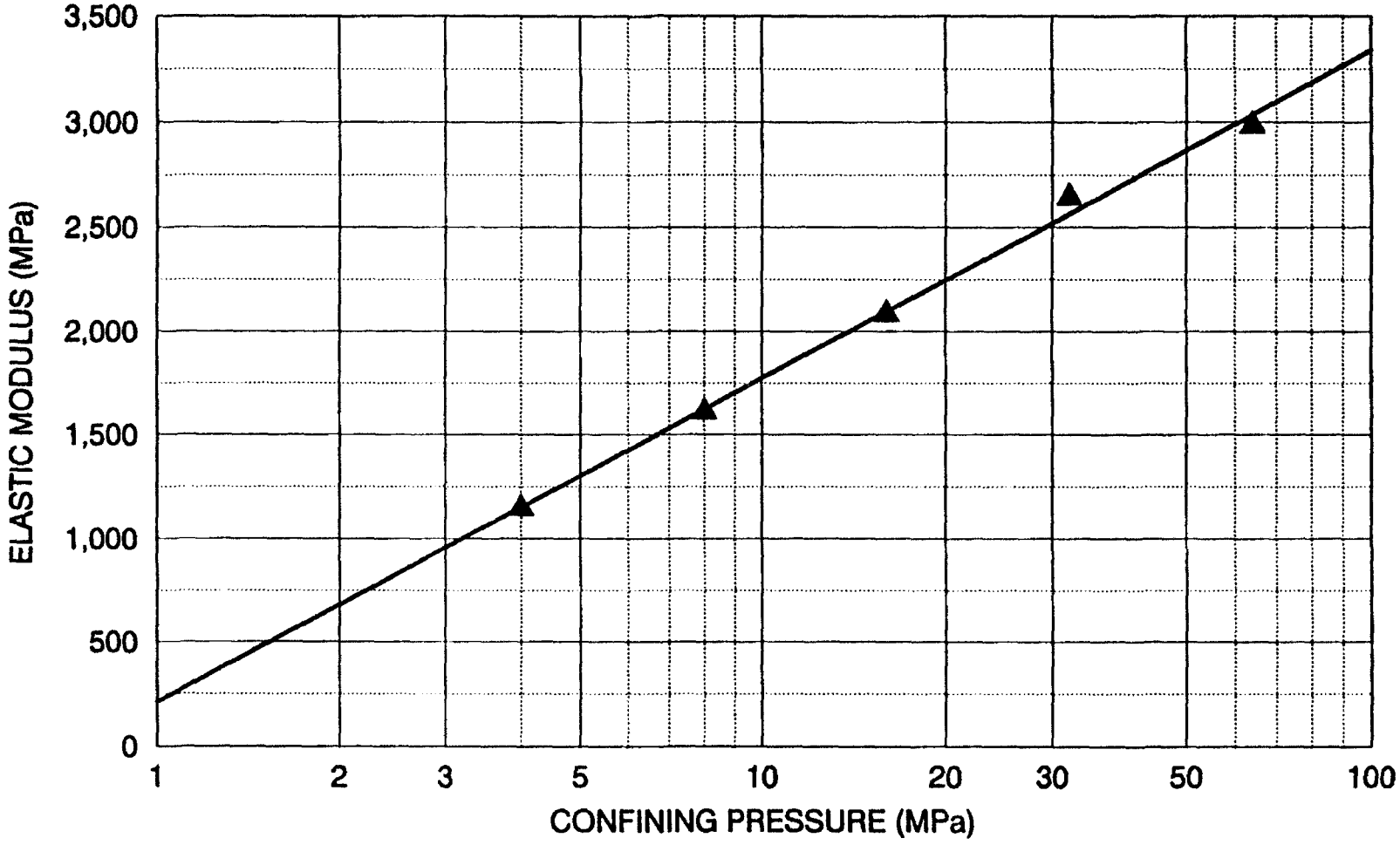

FIGURE 9-28 ELASTIC MODULUS
LOADING-UNLOADING-RELOADING TEST FOR DETERMINATION OF ELASTIC PARAMETERS
DENSE CAMBRIA SAND

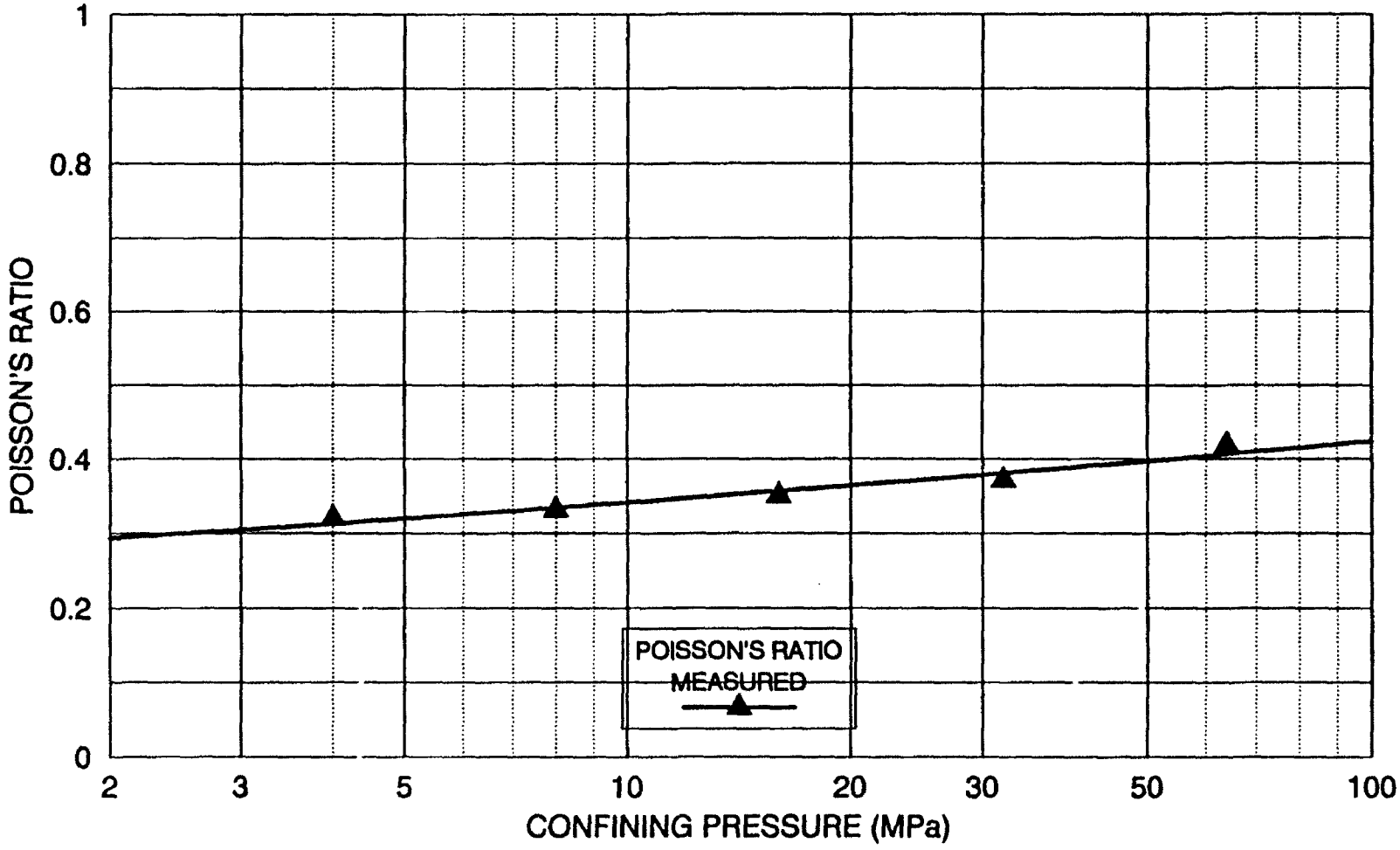

FIGURE 9-29 POISSON'S RATIO
LOADING-UNLOADING-RELOADING TEST
DENSE CAMBRIA SAND

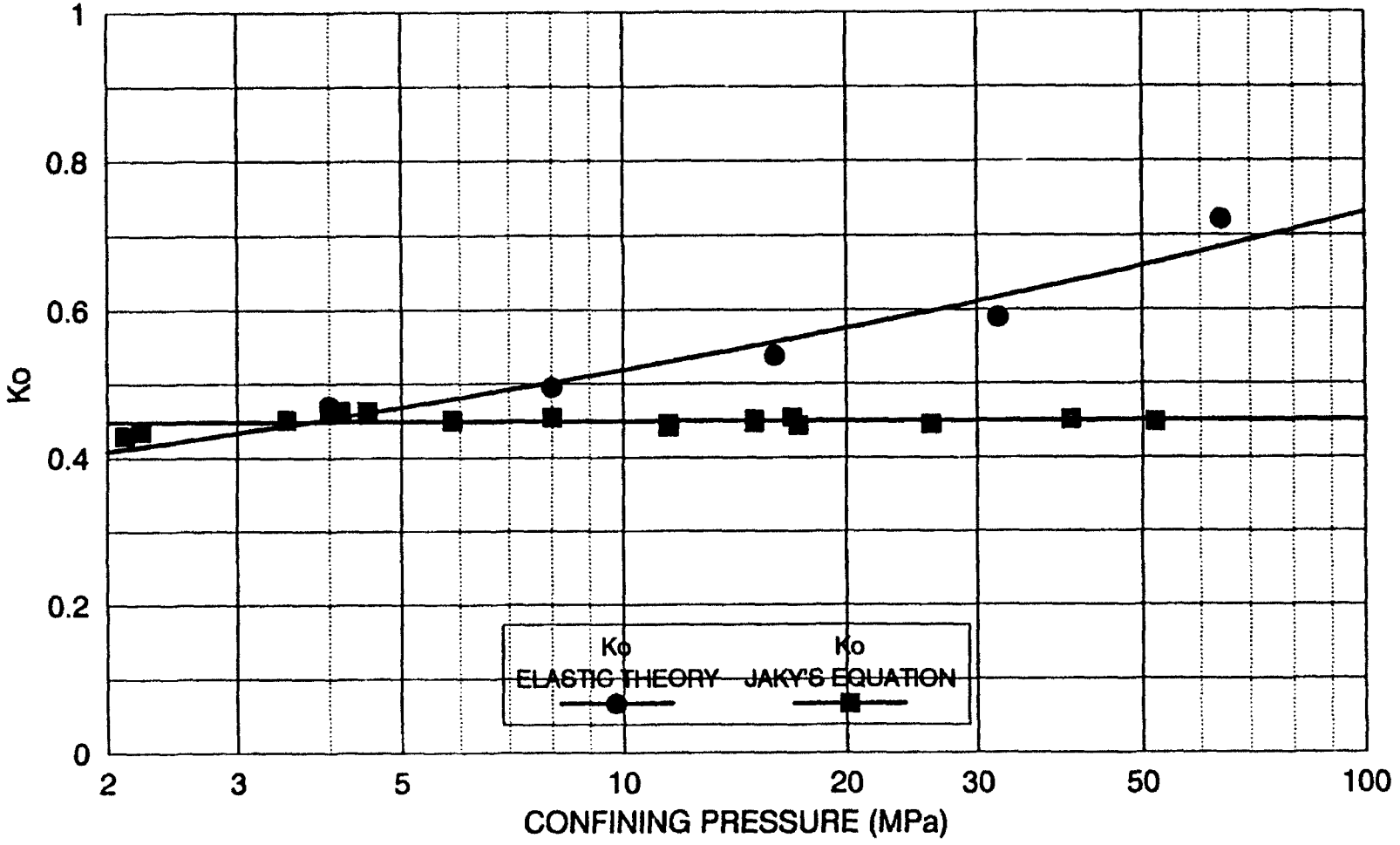

FIGURE 9-30 ELASTIC Ko AND JAKY'S Ko
LOADING-UNLOADING-RELOADING TEST
DENSE CAMBRIA SAND

$$K_0 = \frac{\nu}{1 - \nu}$$

$$K_0 = \frac{\sigma_3}{\sigma_1} \qquad (9.6)$$

ν = *Poisson's ratio.*

semilog plot. Poisson's ratio is shown on Figure 9-29. Poisson's ratio also appears to increase linearly on a semilog plot with increasing confining pressure. An elastic K_o can be calculated from elastic theory as represented by Equation 9.6. It is also shown on Figure 9-30. The elastic K_o, based on the elastic Poisson's ratio, also indicates an increasing trend with increasing confining pressure. Also shown on Figure 9-30 is K_o as computed by Jaky's equation represented by Equation 9.4. Based upon Jaky's equation, K_o would be relatively constant, because the friction angle in compression at high pressures is relatively constant.

9.9 Conclusions

A one-dimensional testing apparatus has been developed to test soils to pressures up to 900 MPa axial stresses. The soil containment cell was instrumented with strain gages to measure circumferential strains such that lateral soil stresses could be inferred from the elastic expansion of the cell wall.

Three different sands, Cambria sand, quartz sand, and Sacramento River sand, were tested at different initial densities. Full-friction and reduced friction (83 percent less friction) one-dimensional compression tests were performed to evaluate the effect of sidewall friction on test results. It was found that there was a very small effect, and effects of further friction reduction would not cause additional significant changes in the results. Void ratio reductions were very large

at high stresses. Test specimens started with initial void ratios ranging from 0.90 to 0.54, and finished with void ratios of 0.10 to 0.13 for the Cambria and quartz sands, respectively. The effect of initial void ratio clearly disappears at higher stresses.

To estimate horizontal stresses, a numerical analysis of the soil containment cell was performed to produce the elastic circumferential strains for different specimen heights. Horizontal soil stresses were estimated from this analysis and the values of K_o were established for the three sands at different initial densities. K_o was found to decrease with increasing axial stress and then remain contant for further increases in stresses or further reductions in void ratio. The total or effective stress (Equation 9.1, 9.2) definition of K_o was deemed preferable to the incremental stress (Equation 9.3) definition, since it appears more stable and the effect of stress history is insignificant in these tests. The calculations of Jaky's equation appear to be valid at low pressures, but do not match the measured values at higher pressures. As the void ratios decrease, relative positions of the loose and dense K_o curves change locations, with the loose curve indicating lower values of K_o than the dense curve.

A special test consisting of a series of five loading, unloading, reloading and unloading cycles at different confining pressures was performed to establish the elastic modulus and Poisson's ratio for Cambria sand. It was found that the elastic modulus and Poisson's ratio increased linearly on a semilog plot against confining pressure.

CHAPTER 10 - GENERAL SOIL BEHAVIOR AT HIGH PRESSURES

10.1 Introduction

The discussion in previous chapters has focused on the experimental methods used in the investigations, the experimental results, and their interpretation within the context of the individual topics of each chapter. The present chapter attempts to examine the overall qualitative and quantitative behavior of granular materials from low to high pressures to try to establish any unifying behavioral patterns. This could advance the development of an encompassing set of principles, which might be applicable to all soil behavior. The experimental results are carefully examined to determine how they correlate with widely used theories and concepts to describe general soil behavior. The theories that will be examined are the theories of stress dilatancy, critical state soil mechanics, and the Rutledge Hypothesis. Additionally, since the bulk of the experimental testing contained within this thesis represents only one sand and one void ratio, data from other investigators are included to evaluate the effect of variations in the initial void ratio. This should broaden the scope of any conclusions.

10.2 Stress Dilatancy

Dilatancy or expansion during shearing is a fundamental characteristic of soils. It generally occurs in drained dense sand condition at low confining

pressures. If the soil particles are arranged in a dense, well-packed configuration, the particles must move around each other as shearing deforms the particle arrangement. As the particles move around each other, the overall volume of the soil must increase. This occurs when confining pressures are low. High confining pressures may not allow the particle arrangement to expand, and thus particles may instead fracture during shearing.

In granular cohesionless materials the shear strength is mobilized from two basic sources. The first source is comprised of the frictional energy required for grains to slide over each other, the energy expended for rearrangement of the particles, and the energy consumed in particle breakage. The second source of shearing strength is the energy required for the soil to undergo dilation. Dilation adds strength to a soil, and causes low pressure drained tests to exhibit an accentuated peak in their stress-strain curve. This added strength also results in the curvature in the drained Mohr-Coulomb failure envelope at low pressures.

Taylor (Taylor, 1948) proposed a relation for direct shear tests that would provide a correction for the dilatancy effect, and result in the real Mohr-Coulomb friction angle. It is shown as Equation 10.1.

$$\tan \phi_f = \frac{\tau}{\sigma_n} - \frac{\delta V}{\delta \Delta} \qquad (10.1)$$

ϕ_f - *true friction angle of soil.*
τ - *measured total shear stress.*
σ_n - *applied normal stress.*
δV - *change in volume of specimen.*
$\delta \Delta$ - *change in horizontal deformation.*

The ratio $\delta V/\delta\Delta$ corresponds to the slope of the volume change curve in the direct shear test. The peak value of this ratio occurs simultaneously with the peak value of the measured shear stress.

Bishop (Bishop, 1954) proposed another correction for the dilatancy effect in soils occurring in triaxial compression tests. Based upon overall energy considerations, he separated the deviator stress into a component at constant volume and another portion created from energy for the specimen to expand against the confining pressure. He found that the added deviator stress due to dilation in triaxial compression was related to the rate of dilation as shown in Equation 10.2. This expression can be modified to treat the triaxial extension case.

$$\sigma_{de} = \sigma_3 \cdot \frac{\dot{\epsilon}_v}{\dot{\epsilon}_1} \qquad (10.2)$$

σ_{de} - *added deviator stress due to expansion in compression.*
σ_3 - *confining pressure (minor principal stress).*
$\frac{\dot{\epsilon}_v}{\dot{\epsilon}_1}$ - *rate of dilation ($\dot{\epsilon}_1$ - major principal strain).*

Rowe (Rowe, 1962, Rowe, et al, 1964) proposed a different dilatancy correction factor for axisymmetric triaxial tests and the direct shear test. He based his correction on analyzing the geometry of the deformation of an assembly of rigid spheres. The correction relates the measured principal stress ratio, the measured rate of dilation, and the dilatancy corrected friction angle. The dilatancy corrected friction angle is the basic interparticle friction angle at low confining pressures. Equation 10.3 represents the dilatancy correction for cylindrical triaxial compression tests.

$$\frac{\sigma_1}{\sigma_3} = \left(1 - \frac{\dot{\epsilon}_v}{\dot{\epsilon}_1}\right) \cdot \tan^2\left(45 + \frac{\phi_f}{2}\right) \qquad (10.3)$$

$\frac{\sigma_1}{\sigma_3}$ - *principal stress ratio.*
$\frac{\dot{\epsilon}_v}{\dot{\epsilon}_1}$ - *rate of dilation* ($\dot{\epsilon}_1$ - *major principal strain*).
ϕ_f - *dilatancy corrected friction angle.*

Equation 10.4 represents the dilatancy correction for cylindrical triaxial extension tests.

$$\frac{\sigma_1}{\sigma_3} = \left(1 - \frac{\dot{\epsilon}_v}{\dot{\epsilon}_3}\right) \cdot \tan^2\left(45 + \frac{\phi_f}{2}\right) \qquad (10.4)$$

$\frac{\sigma_1}{\sigma_3}$ - *principal stress ratio.*
$\frac{\dot{\epsilon}_v}{\dot{\epsilon}_3}$ - *rate of dilation* ($\dot{\epsilon}_3$ - *minor principal strain*).
ϕ_f - *dilatancy corrected friction angle.*

Rowe developed another expression for direct shear tests, but it is not presented here. The quantity represented in the first parenthesis is the dilatancy correction, and the value in the second parenthesis is the basic frictional strength component. He determined that the dilatancy correction is composed of two parts. In addition to the component comprised of the energy required to expand against the confining pressure, there is a component according to which energy is dissipated from friction as the mass of particles expands.

10.3 Observations at High Pressures Regarding Stress-Dilantancy

It was shown in Chapter 5 that the volume change tendency (rate of

dilation) at failure appears to be directly related to the friction angle of the soil at both low and high pressures. As the amount of volumetric dilatancy at failure decreases, the strength decreases, and as it increases, the strength increases. However, the stress-dilatancy theories by Taylor, Bishop, and Rowe were developed for low pressure applications, where particle crushing was not significant.

Bishop's dilatancy correction method was utilized to calculate the dilatancy corrected friction angles for drained compression and extension tests on Cambria sand. Equation 10.2 was modified for the constant cell pressure extension case using the same assumptions Bishop utilized in deriving his equation for compression. The extension dilatancy correction is represented by Equation 10.5.

$$-\sigma_{de} = \sigma_1 \cdot \frac{\dot{\epsilon}_v}{\dot{\epsilon}_3} \qquad (10.5)$$

$-\sigma_{de}$ = added deviator stress due to expansion in extension.
σ_1 = confining pressure (major principal stress).
$\frac{\dot{\epsilon}_v}{\dot{\epsilon}_3}$ = rate of dilation ($\dot{\epsilon}_3$ = minor principal strain).

The results of the analyses of the extension tests are displayed on Figure 10-1. The dilatancy corrected friction angles for both compression and extension are plotted against the effective mean normal stresses at failure in this figure. The dilatancy corrected friction angle in compression decreases slightly from its highest value at low stresses. It reaches a low point at approximately 7 to 8 MPa, which was the stress level where the rate of dilation at failure was the highest (most compressive) in the compression tests. As the stress magnitudes continue to

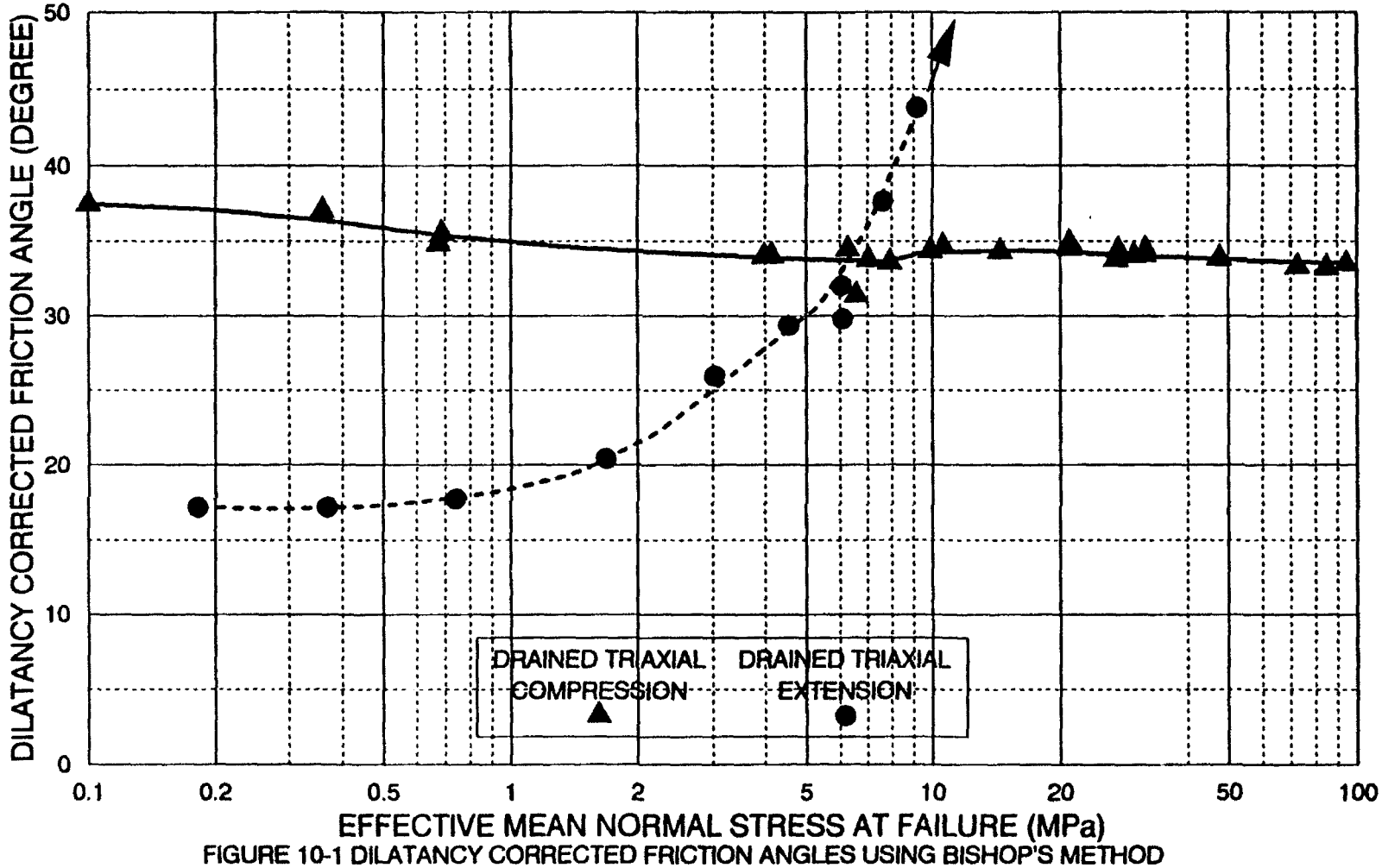

FIGURE 10-1 DILATANCY CORRECTED FRICTION ANGLES USING BISHOP'S METHOD
DRAINED TRIAXIAL COMPRESSION & EXTENSION
DENSE CAMBRIA SAND

increase, the friction angles increase slightly before decreasing slightly to a constant level at the highest pressure levels. Overall the dilatancy corrected friction angle in compression is relatively stable. In extension the dilatancy corrected friction angle is very peculiar. At low pressures the dilatancy correction is excessive and it depresses the friction angle to a very low value. At higher pressures the correction is excessive and it amplifies the friction angle to extremely high values. Obviously, the derived dilatancy correction for extension is not reasonable. The problem appears to be in the assumption that the additional deviator stress is created by the work of the specimen expanding against the confining pressure. In the constant cell pressure extension test the confining pressure is the major principal stress. Therefore, the change in deviator stress is relatively large. Since the friction angle in extension is very sensitive to relatively small changes in the deviator stress, the results appear to be exaggerated in most cases where there are large amounts of volumetric dilation or contraction.

The results of using Rowe's dilatancy correction method (Equations 10.3 and 10.4) on the same test results are shown on Figure 10-2. They are plotted against effective mean normal stress at failure. They indicate that the adjusted friction angles at low stress levels in extension are larger than in compression. As the mean normal stress at failure increases, the two lines are seen to merge together and then separate at a stress of about 4 MPa. Beyond this stress both corrected friction angles increase as the rates of dilation increase (more compressive) in both compression and extension due to increasing amounts of particle crushing and rearranging. The adjusted friction angles in compression

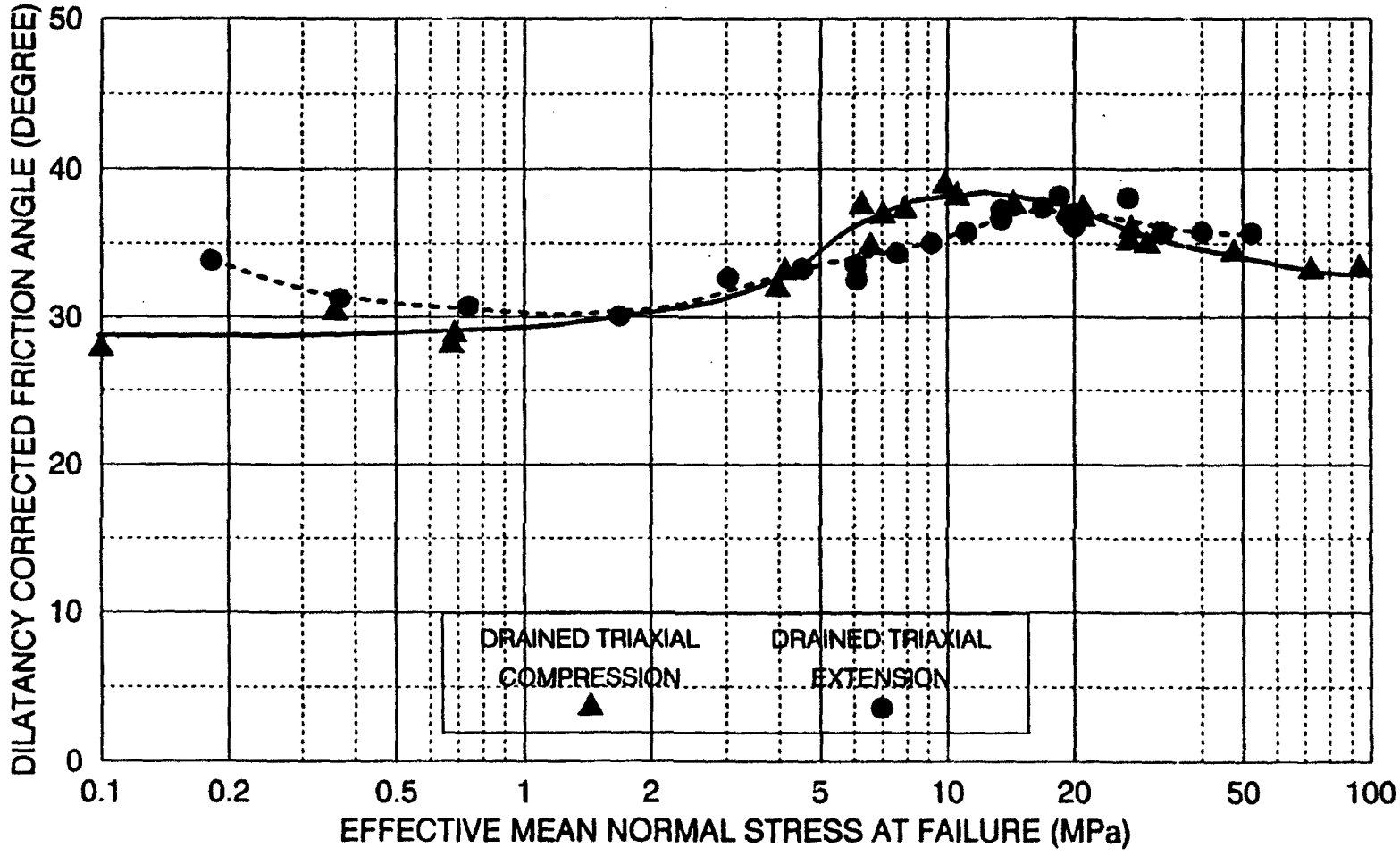

FIGURE 10-2 DILATANCY CORRECTED FRICTION ANGLES USING ROWE'S METHOD
DRAINED TRIAXIAL COMPRESSION & EXTENSION
DENSE CAMBRIA SAND

appear to be larger than in extension, because the larger amounts of particle crushing in compression create larger rates of dilation at failure (more compressive). As the stress level continues to increase, the dilatancy corrected friction angles start decreasing at the same time as particle crushing and rates of dilation start to decrease. Adjusted friction angles reach approximately the same level in compression and extension, but at different stress magnitudes. This is due to the rates of dilation reaching a peak at different stress magnitudes. At high stresses the corrected friction angles appear to be slightly higher in extension than in compression.

The general concept of stress-dilatancy, that soils are stronger when they exhibit dilatant behavior, and weaker when they exhibit volumetrically compressive behavior, has been shown to be essentially correct by experimental observations at high pressures as discussed in Chapter 5. However, since the evaluated methods for dilatancy correction were developed for low pressure applications without the influence of large amounts of particle crushing, their validity at high pressures appears to be questionable. Both methods show rather large variations in the dilatancy corrected friction angles, and these tend to follow the relative amounts of particle crushing at failure in the soil for a particular stress condition. The basic friction angle of a material would not be expected to change in such an inconsistent manner. On the assumption that the dilatancy corrected friction angle and the basic material friction angle should be approximately equal and should not change significantly with stress magnitude, the method proposed by Bishop for compression may be more correct than the method proposed by Rowe at high

pressures. However, the derived formulation in extension based upon Bishop's compression method is clearly incorrect, and the method proposed by Rowe is preferred.

10.4 Critical State Soil Mechanics

The concept of critical state was originally described by Casagrande in 1936 (Casagrande, 1940). In drained tests on cohesionless soil he observed that loose soils contract and dense soils expand upon application of shear stresses as shown on Figure 10-3. He noted that eventually both dense and loose soils reach a density where the applied shear stresses remain fixed at constant volume. Casagrande identified this density as the critical density (critical void ratio). At this time he did not relate undrained behavior to critical state.

Rutledge (Rutledge, 1947) found that for normally consolidated saturated clays, the compressive strength is dependent only on the void ratio at failure. This is exemplified by the consolidation and the compressive strength lines being parallel on a semi-logarithmic plot as shown on Figure 10-4. The significance of this observation was that strength predictions for a particular normally consolidated clay could be made from a consolidation test and a single undrained triaxial compression test. Additionally, since normally consolidated clays usually reach effective stress failure at the maximum deviator stress, the Mohr-Coulomb effective stress friction angle can be inferred from this figure.

Roscoe, Schofield and Wroth (Roscoe, et al, 1958) extended this concept. They observed that clays exhibited converging loading paths onto a critical void

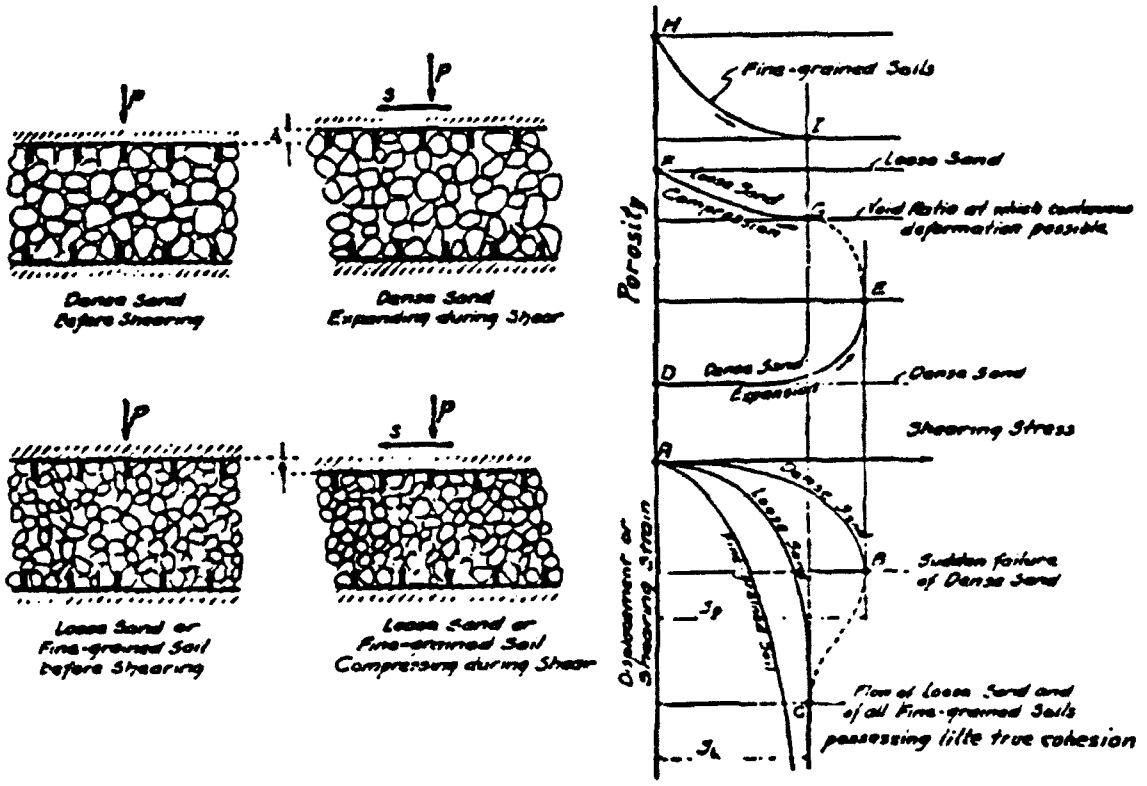

Figure 10-3 Casagrande Critical State Theory
Under Shearing Loose Sands Compress and Dense
Sands Dilate to Critical Density
(from Casagrande, 1940)

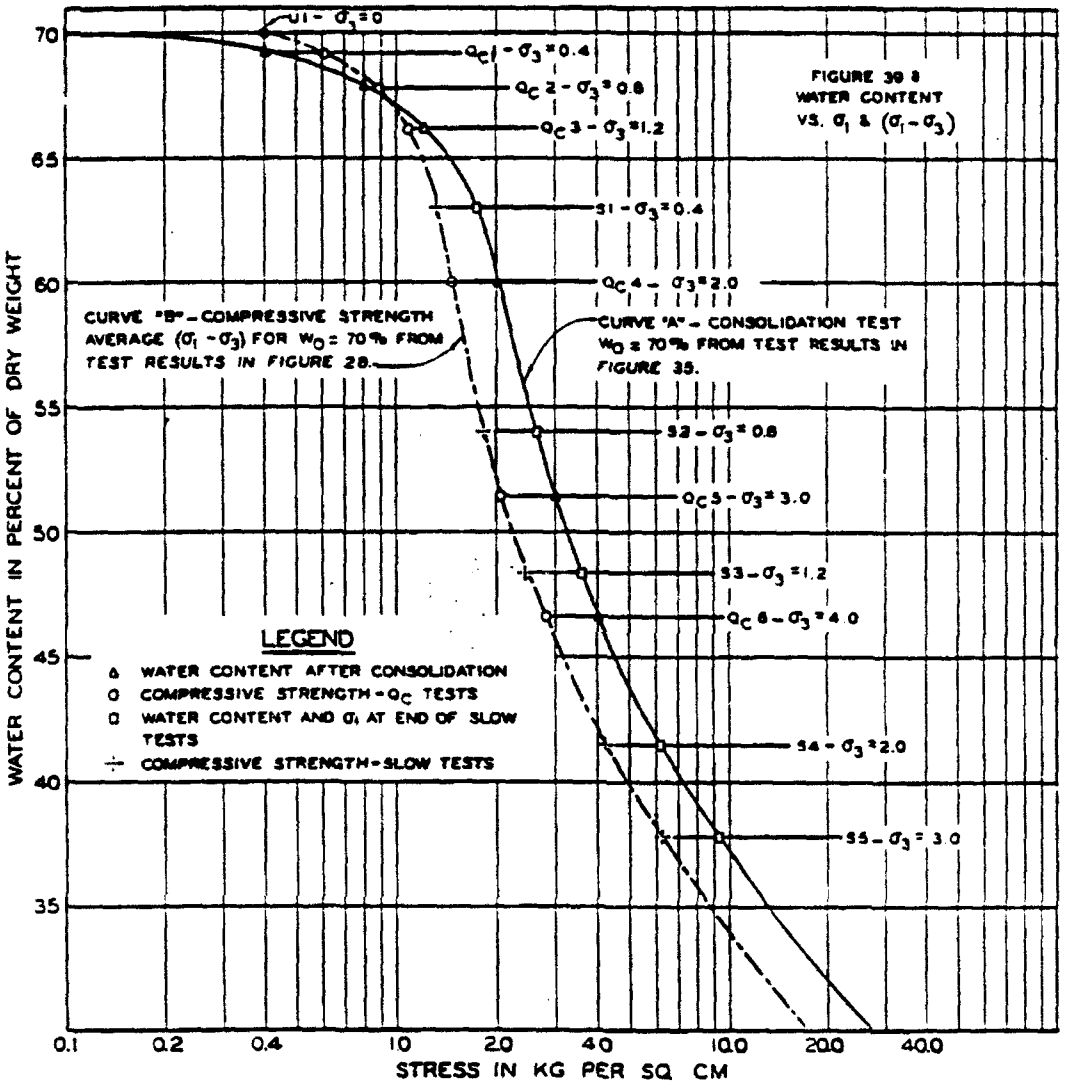

Figure 10-4 Rutledge Hypothesis
Normally Consolidated Clays Indicate Parallel
Compressive Strength and Consolidation Lines
(from Rutledge, 1947)

ratio line at large strains within a characteristic yield surface. The critical void ratio line is characterized by continued straining resulting in constant stress without change in void ratio. This line on the Cambridge p'-q diagram passes through the points of maximum stress difference as shown on Figure 10-5. This observation was made for both drained and undrained conditions. These concepts are the basis for the original Cam-Clay constitutive model for cohesive soils. They also showed results of tests on silts, steel balls, and glass beads, which also showed that the concept of a critical void ratio line and a characteristic yield surface was reasonable for cohesionless soils, although the scatter was larger than with clays. This characteristic behavior formed part of the original Granta gravel constitutive model for cohesionless soils.

Seed and Lee (Lee and Seed, 1967; Seed and Lee, 1967) modified the previously defined concept of critical state. They performed drained and undrained tests on four different densities of Sacramento River sand. They defined the critical state as the combination of the (critical) void ratio after consolidation and the (critical) confining pressure at which zero total volume change was obtained at failure, as shown on Figure 10-6. Failure was defined as the maximum effective stress ratio, as opposed to the maximum stress difference.

10.5 Observations at High Pressures Regarding Critical State

The correlations of critical state soil mechanics with experimental results obtained at high confining pressures will be discussed in the reverse order of their presentation in the previous section. Observations at high pressures will not be

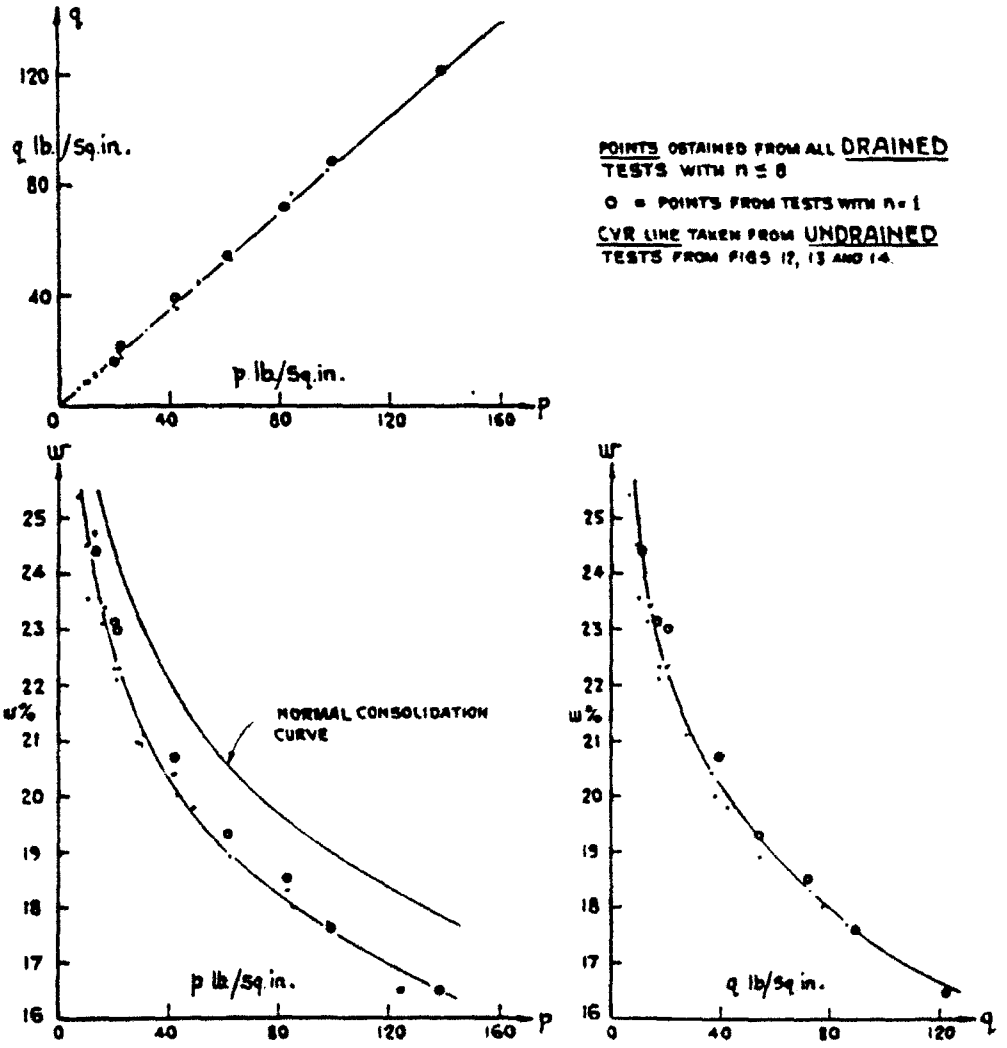

Figure 10-5 Roscoe, Schofield and Wroth Critical State Theory
Drained and Undrained Tests on Weald Clay
Upper Diagram Shows Critical State Line on p'-q Diagram
Lower Diagrams Indicates Unique Critical Void Ratio Line
(from Roscoe, et al, 1958)

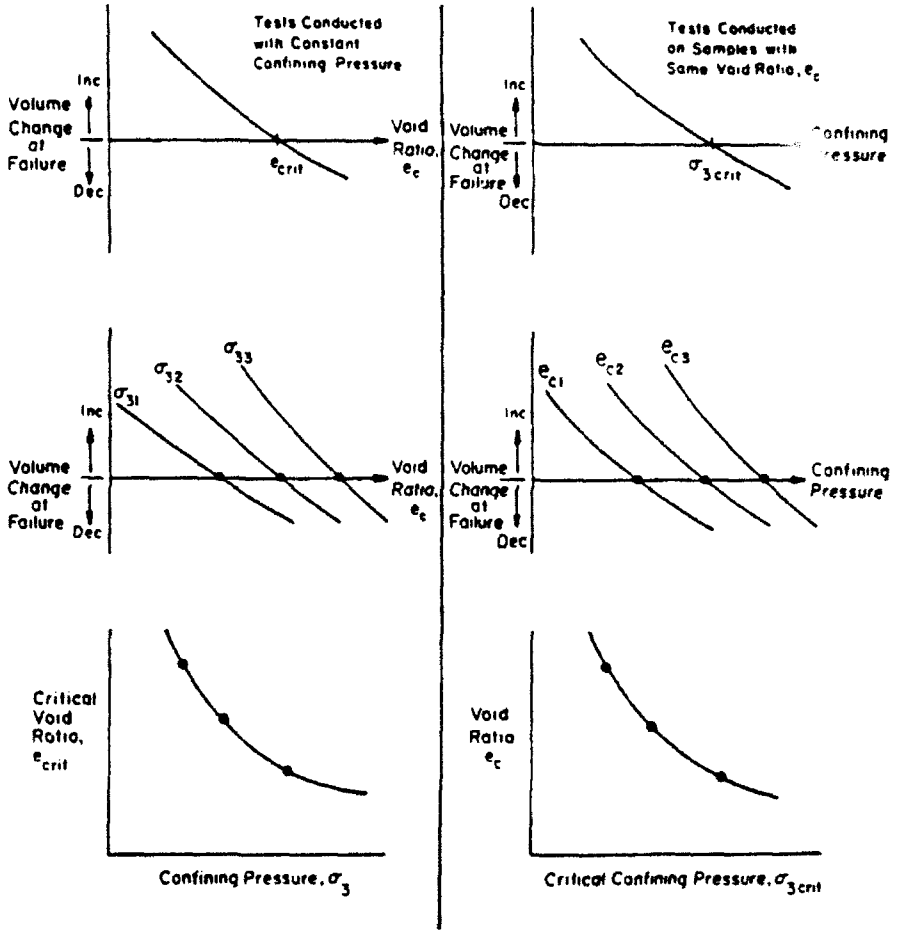

Figure 10-6 Seed and Lee Critical State Theory
Left Diagrams Show Drained Tests with Zero Volumetric Strain at Failure
Right Diagrams Show Undrained Tests with Confining Pressure at Failure
Both Appear on Unique Critical Void Ratio Line
(from Seed and Lee, 1967)

considered in view of Casagrande's observations on critical state, because he only discussed drained tests. The primary value of critical state soil mechanics is its ability to predict undrained behavior from drained test results, i.e. to unify the soil behavior within one framework.

The Seed and Lee (1967) approach to critical state, which relates the critical confining pressure uniquely with the void ratio after consolidation was shown to be valid for Sacramento River sand at confining pressures up to 3 MPa. At high pressures there are two principal deviations from the observed behavior pattern at low pressures. The first deviation is based upon the method they proposed to estimate the location of the critical void ratio-critical confining pressure line. Their technique consisted of performing drained tests and vary the consolidation void ratio with constant confining pressure or vary the confining pressure with constant consolidation void ratio. This method is depicted on Figure 10-6. It makes it possible to estimate the critical void ratios (zero total volumetric strain at failure) and the critical confining pressures to establish the critical void ratio line. Many prior investigators in the field of high pressure behavior of soils (Hendron, 1963, Vesic and Clough, 1968, Murphy, 1970, Tai, 1970) have noted that for a given sand the effect of initial void ratio is eliminated beyond a certain stress level. The one-dimensional compression tests discussed in Chapter 9, which were performed at different initial void ratios, clearly supports the hypothesis that the effects of initial void ratios are eventually eliminated at high stress levels. The implications of this observation is profound for the Seed and Lee approach to critical state for applications at high pressures. Seed and Lee's method to determine the location

of the critical void ratio line will cease to function, when the effect of initial void ratio is eliminated, because when the stresses are high enough, there is only one possible void ratio of consolidation at that stress level for a given sand. These void ratios will all result in large compressive volumetric strains at high stresses, not zero volumetric strain at failure. Figures 10-7 and 10-8 indicate this problem using test data for four densities of Sacramento River sand (Lee, 1965) tested to maximum confining pressures of 13.73 MPa. These figures show the volumetric strain at failure plotted against void ratio of consolidation and effective consolidation pressure, respectively. Figure 10-7 indicates the critical void ratios derived for the different pressure levels. It is possible to ascertain from both Figures 10-7 and 10-8 that as the confining pressure increases, the void ratio of consolidation and the volumetric strain at failure start converging. This is the effect of the reduced influence of initial void ratio. Therefore, as the stresses increase from this to higher levels, it will not be possible to identify the location of the critical void ratio line from drained test results. Essentially, the Seed and Lee definition of critical state, zero volume change at failure, is not possible to achieve at high pressures, whereas the definition is reasonable at low pressures.

The second deviation from Seed and Lee's version of critical state at high pressures stems from the fact that the critical void ratio line is not unique for both drained and undrained test results. In the previous paragraph it was shown that the location of the critical void ratio line could not be ascertained from drained tests at high pressures. However, by definition undrained tests should be located on the critical void ratio line, due to the fact that they are constant volume tests.

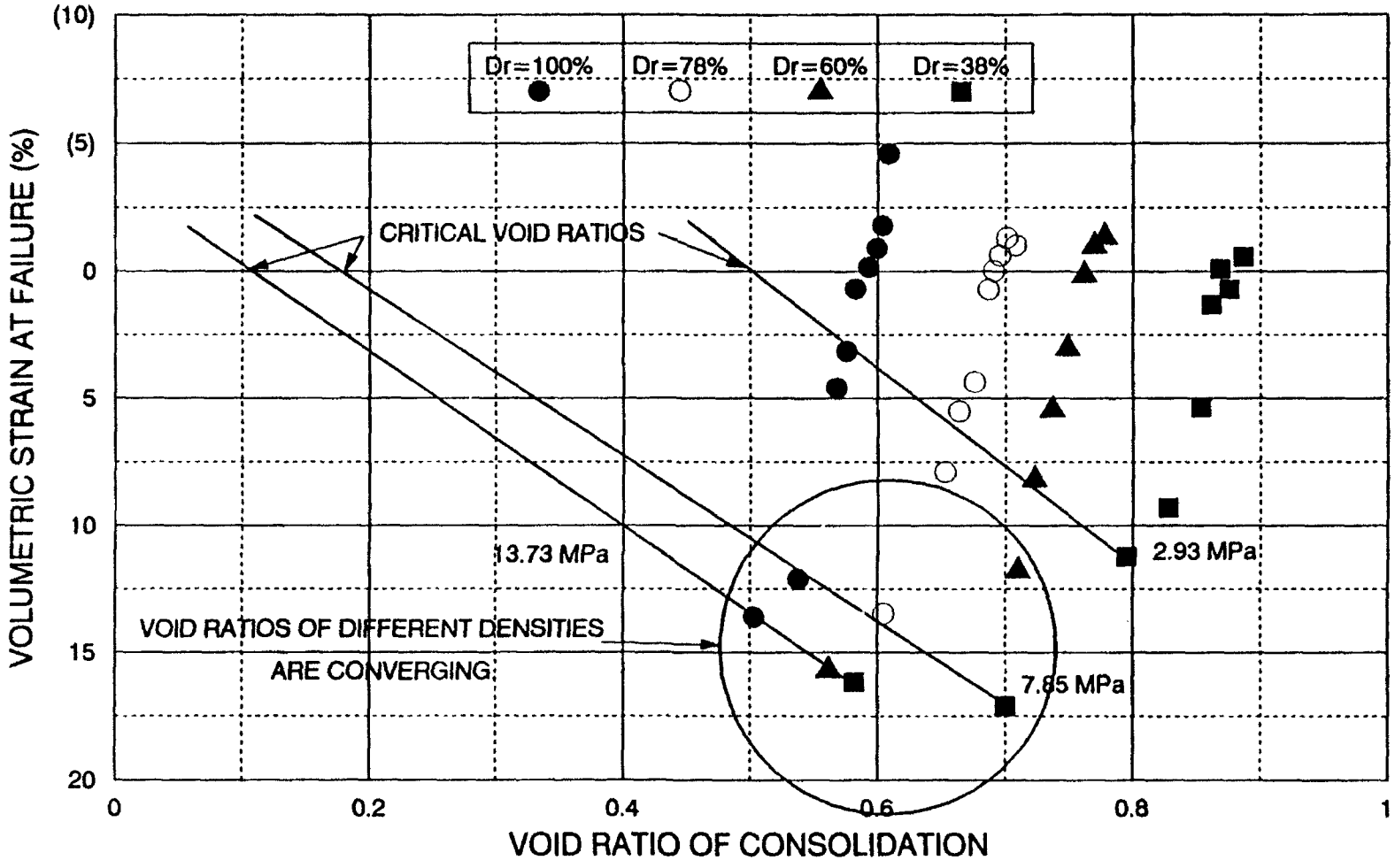

FIGURE 10-7 PROBLEM OF EVALUATION CRITICAL VOID RATIO AT HIGH PRESSURES
CRITICAL STATE SOIL MECHANICS, DRAINED TRIAXIAL COMPRESSION TESTS
FOUR DENSITIES OF SACRAMENTO RIVER SAND

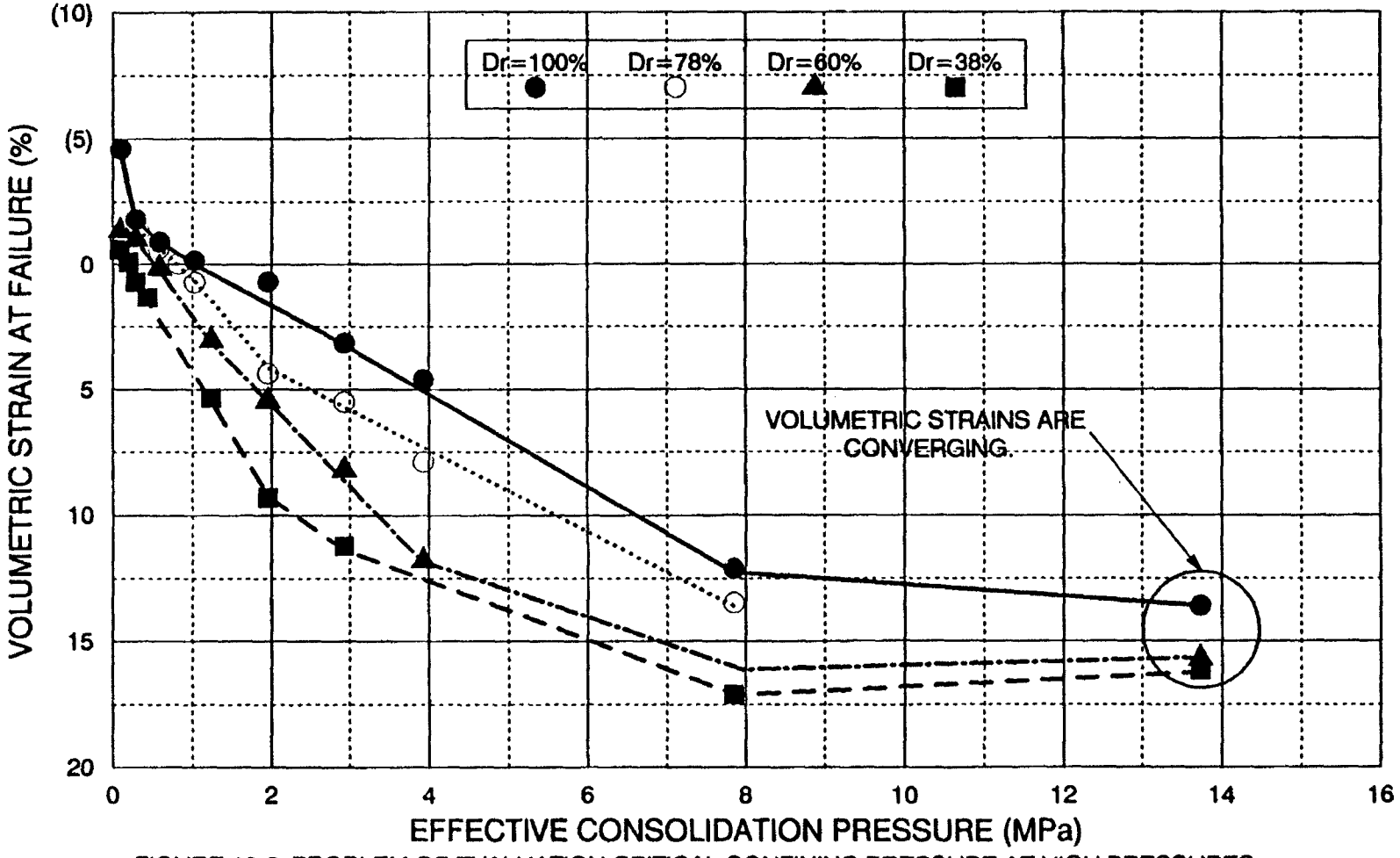

FIGURE 10-8 PROBLEM OF EVALUATION CRITICAL CONFINING PRESSURE AT HIGH PRESSURES
CRITICAL STATE SOIL MECHANICS, DRAINED TRIAXIAL COMPRESSION TESTS
FOUR DENSITIES OF SACRAMENTO RIVER SAND

Therefore, the undrained effective confining pressure at failure should be the critical confining pressure, and the critical void ratio line can consequently be determined at high pressures from results of the undrained tests. However, the use of the undrained tests to evaluate the critical void ratio line, obviates the value of critical state soil mechanics, since the prediction of undrained tests from results of drained tests was the main usefulness of this theory. Figure 10-9 displays results from high pressure drained and undrained triaxial compression tests on Cambria sand with the consolidation or critical void ratio on the vertical axis and the effective or critical confining pressure on the horizontal axis. The line indicating the undrained tests is by definition the critical void ratio line. As can be seen, the drained tests do not coincide with this line. This clearly indicates that the Seed and Lee version of critical state is not applicable at high pressures.

The Roscoe, Schofield and Wroth (1958) defines the critical state as the condition at large strains, where there is no further changes in void ratio, stress difference and mean normal stress. Critical state is achieved along a line on the Cambridge p'-q diagram that originates from the origin and whose slope is defined as M (= q/p'). The results of the high pressure drained compression and extension tests were analyzed to determine the appropriate value of M at zero rate of dilation as shown on Figure 10-10. The derived critical state lines, M-lines, are shown on Figure 10-11 with some stress paths obtained from drained compression and extension tests. The concept of critical state appears to work well for the drained tests. This has been reported previously (Coop, 1990; Wood, 1990). However, on Figure 10-12 the same M-lines are shown with effective stress paths

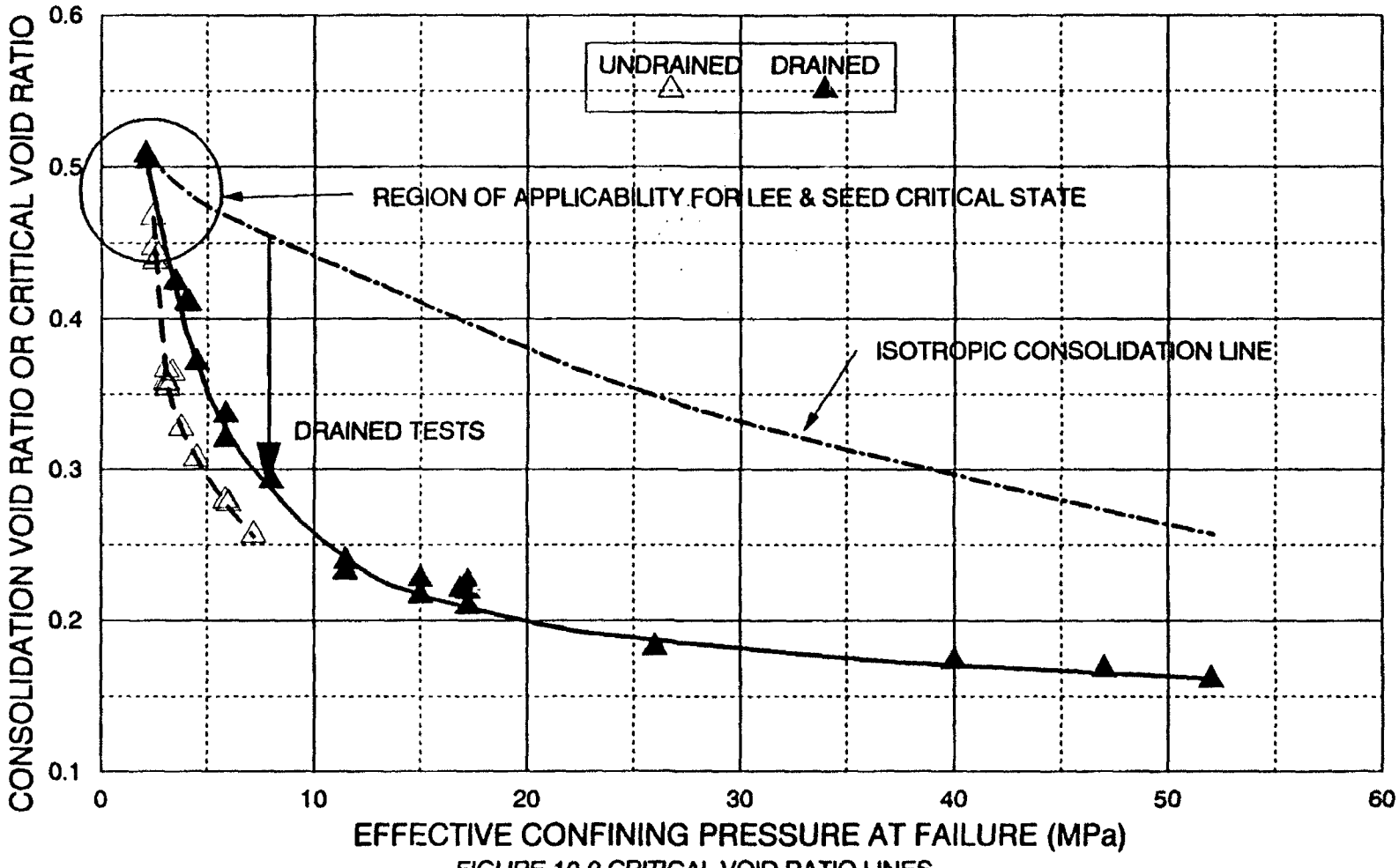

FIGURE 10-9 CRITICAL VOID RATIO LINES
CRITICAL STATE IN DRAINED AND UNDRAINED TRIAXIAL COMPRESSION
DENSE CAMBRIA SAND

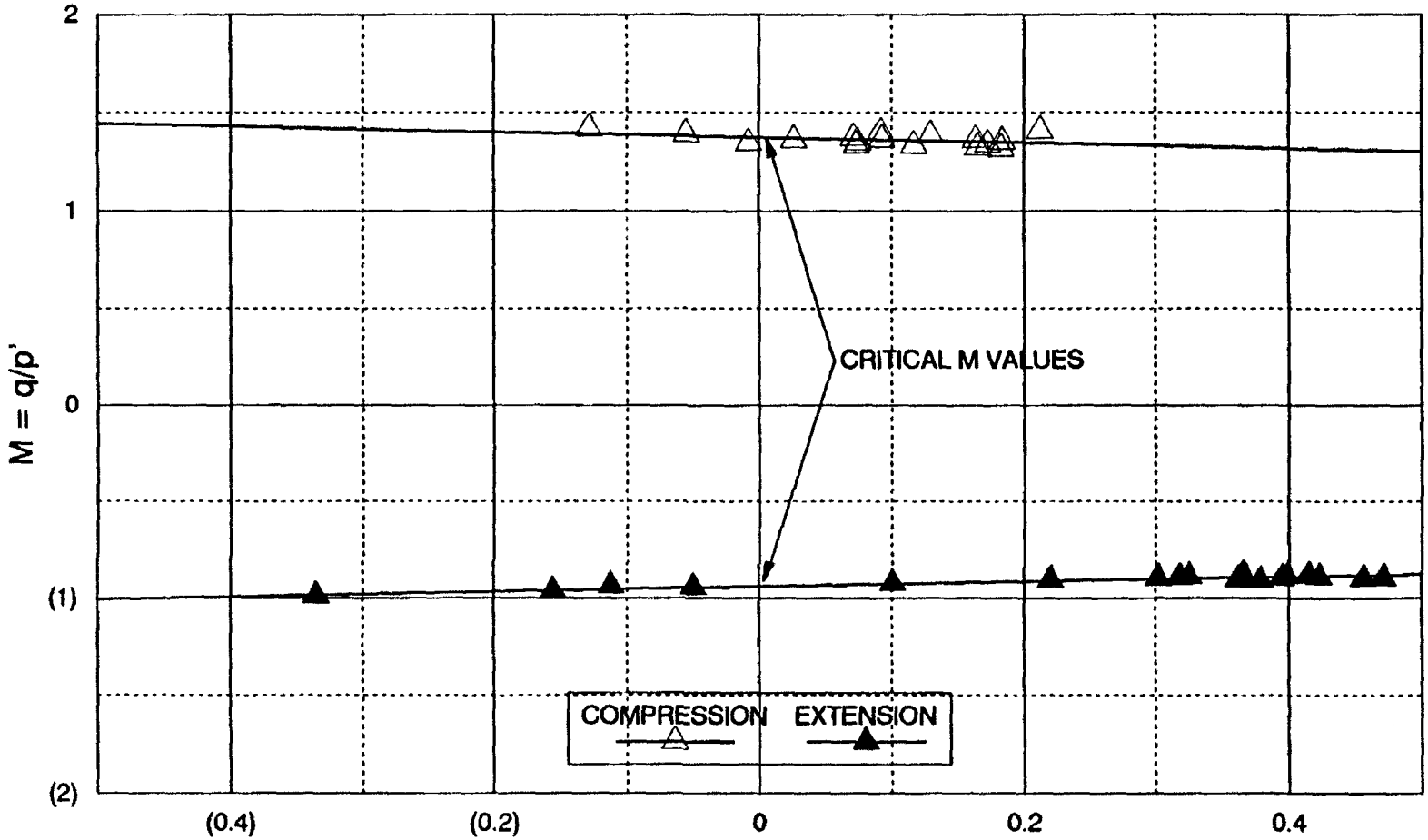

FIGURE 10-10 q/p' vs. RATE OF DILATION AT FAILURE
DRAINED TRIAXIAL COMPRESSION
DENSE CAMBRIA SAND

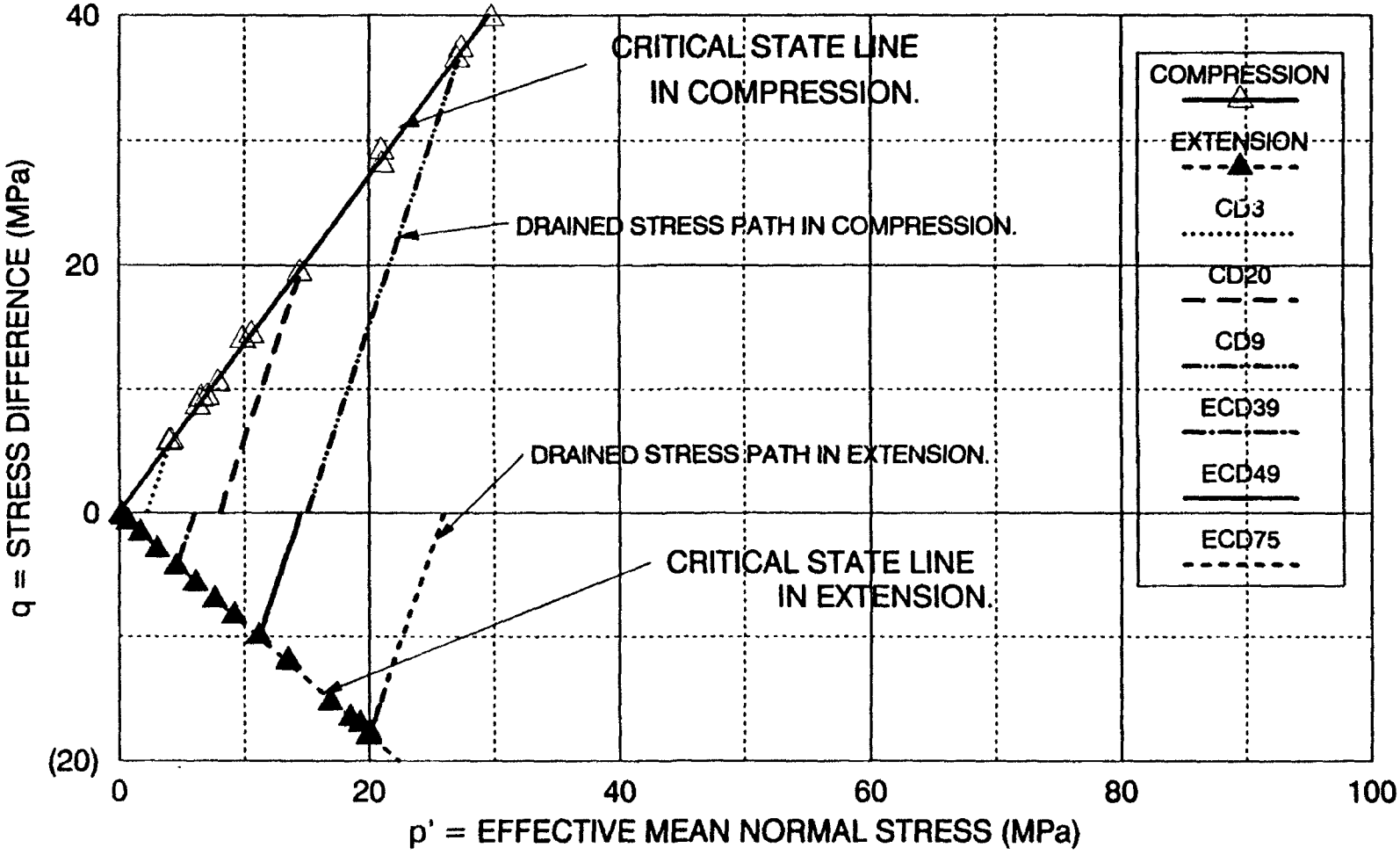

FIGURE 10-11 EFFECTIVE STRESS PATH, CAMBRIDGE p'-q
DRAINED TRIAXIAL COMPRESSION AND EXTENSION
DENSE CAMBRIA SAND

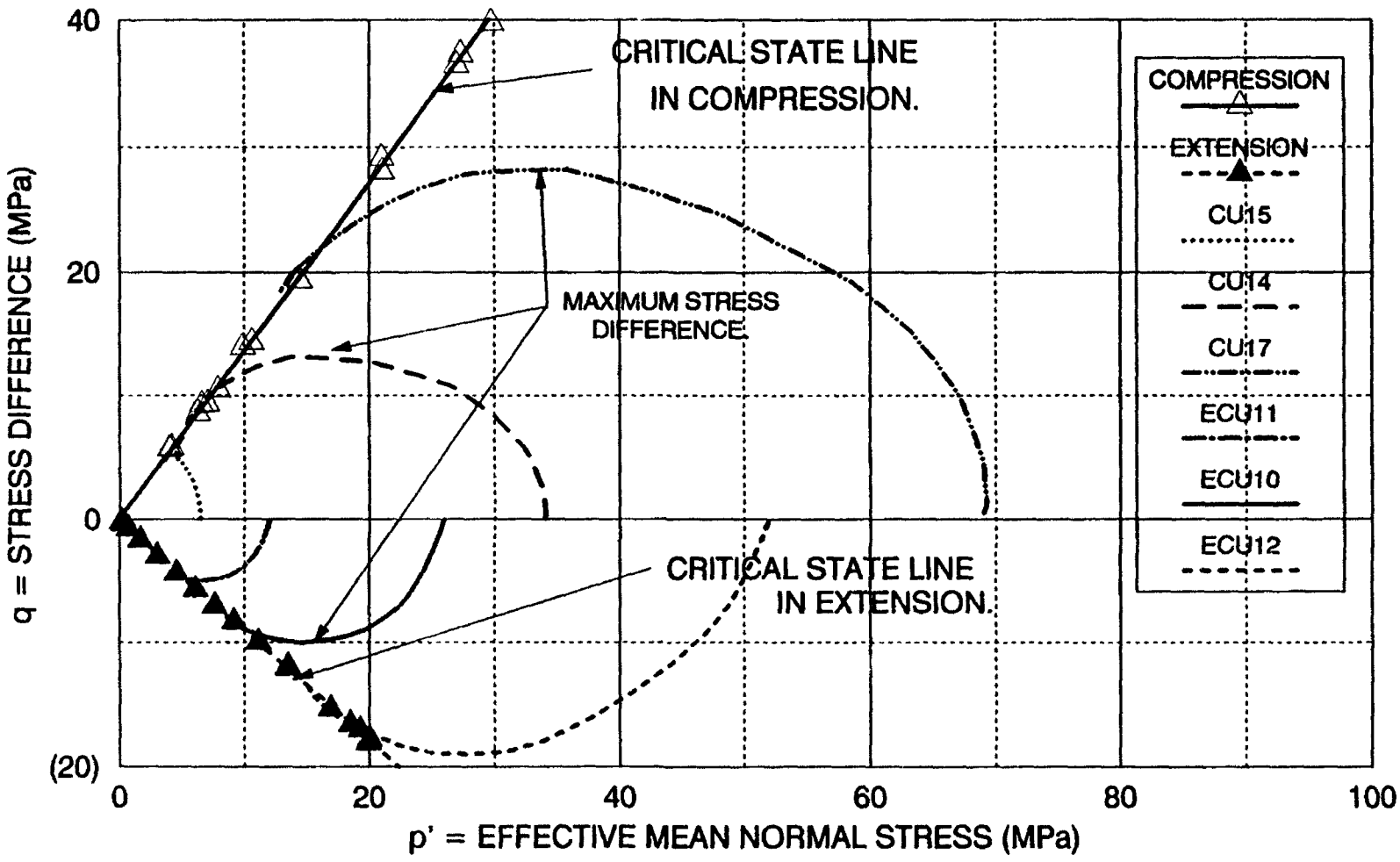

FIGURE 10-12 EFFECTIVE STRESS PATH, CAMBRIDGE p'-q
UNDRAINED TRIAXIAL COMPRESSION AND EXTENSION
DENSE CAMBRIA SAND

from some undrained triaxial compression tests performed at high pressures. The undrained stress paths all eventually end on the established M-lines as they approach effective stress failure at large strains. However, their maximum stress differences do not always end up near the critical state line, as suggested by the Roscoe, et al. definition of critical state. At lower pressures the undrained stress paths achieve the maximum stress difference simultaneously with intersecting the critical state line. However, at higher pressures the maximum stress difference occurs well inside the critical state line. This line connecting the maximum stress differences of undrained tests is the instability line. It has been shown to not coincide with the critical state line at high pressures in Chapter 6. The definition of critical state by Roscoe, Schofield and Wroth, that the maximum stress difference coincides with the critical state line is not correct for undrained tests on cohesionless soils at high confining pressures.

The Rutledge Hypothesis (1947) stated that the isotropic consolidation and strength lines are parallel was shown on Figure 10-4. This was generally considered only applicable to normally consolidated clays. It was not considered valid for granular materials at lower pressures, because the isotropic consolidation and strength lines cross, and they do not become parallel as shown on Figure 10-13 for drained and undrained triaxial compression tests on Sacramento River sand (Lee, 1965). On this figure strength lines for three different void ratios are shown along with two isotropic consolidation lines on a semi-logarithmic plot. As can be seen the strength and isotropic consolidation lines for the range of pressures tested are not parallel, as opposed to normally consolidated clay in Figure 10-4. The

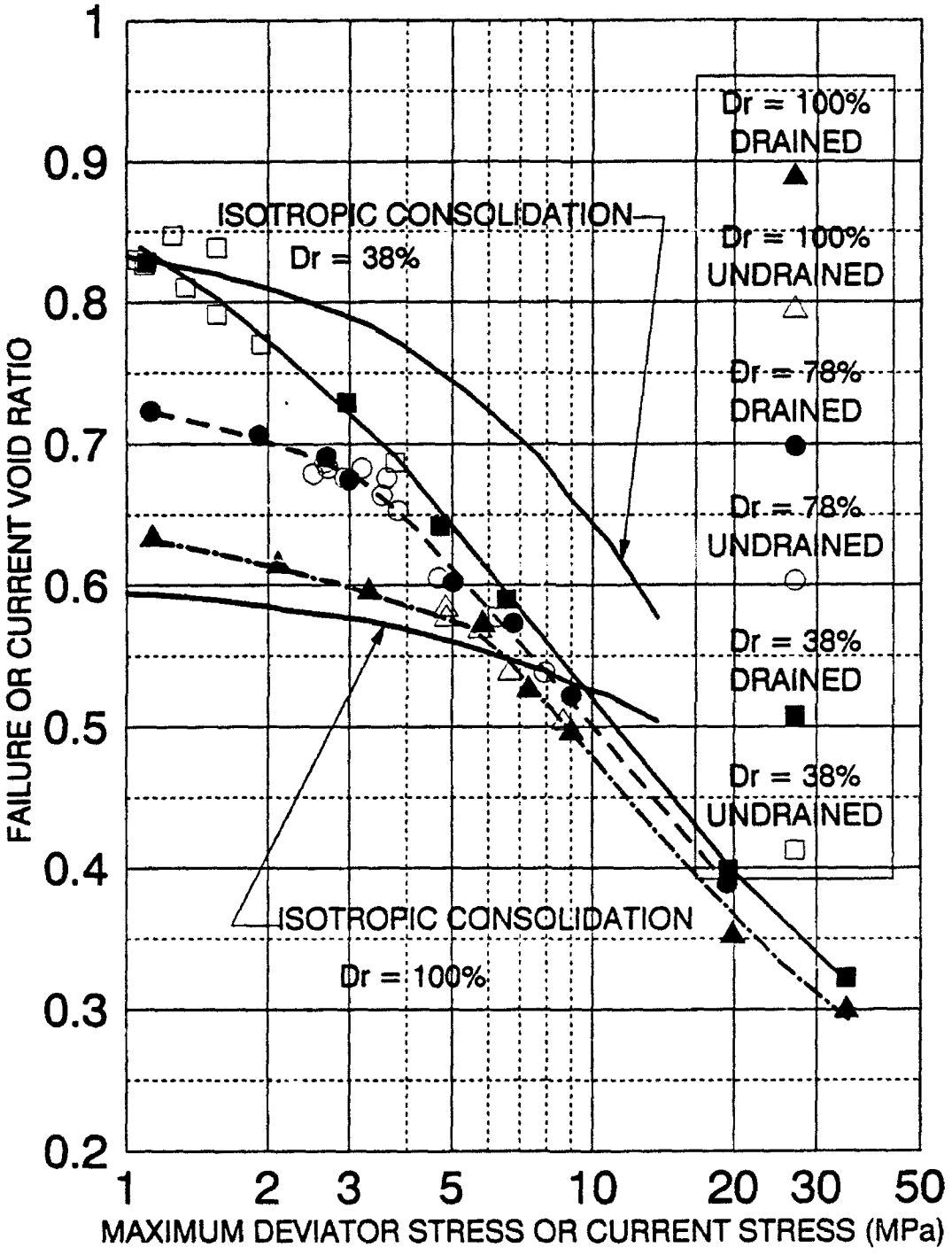

FIGURE 10-13 - VOID RATIO RELATED TO STRESS
DRAINED & UNDRAINED TRIAXIAL COMPRESSION TESTS
SACRAMENTO RIVER SAND (from LEE, 1965)

consolidation and strength lines for loose Sacramento River sand (D_r=38%) may tend toward being parallel at the highest pressures, but the strength line and the consolidation line for the dense sand are definitely not parallel. However, close examination of Figure 10-4 indicates that the consolidation and strength lines for the clay do cross near the very top of the two curves. This may be the effect of a slightly overconsolidated condition in the clay at low stresses. Another observation from Figure 10-13 is that the maximum deviator stresses for both drained and undrained tests appear on the same lines for each initial void ratio, when void ratio at failure is used as an independent variable. Another observation from this diagram is that as the stress magnitude increases the effect of initial void ratio is reduced, as evidenced by the decreasing distance between the two isotropic consolidation lines. At the highest stress magnitudes the strength lines corresponding to different initial void ratios tend to become parallel and very closely spaced.

When stresses are increased to much higher levels than in Lee's tests on Sacramento River sand, the behavior starts to resemble that of normally consolidated clay as evidenced in Figure 10-14. This figure represents tests performed on Cambria sand in both triaxial compression and extension in drained and undrained conditions. Also shown on the diagram are the results of the three one-dimensional compression tests performed at different initial void ratios and an isotropic consolidation test. Shown on the horizontal axis is either the maximum deviator stress or current axial stress for the strength lines or the confining pressure for the isotropic consolidation line. The vertical axis indicates either the

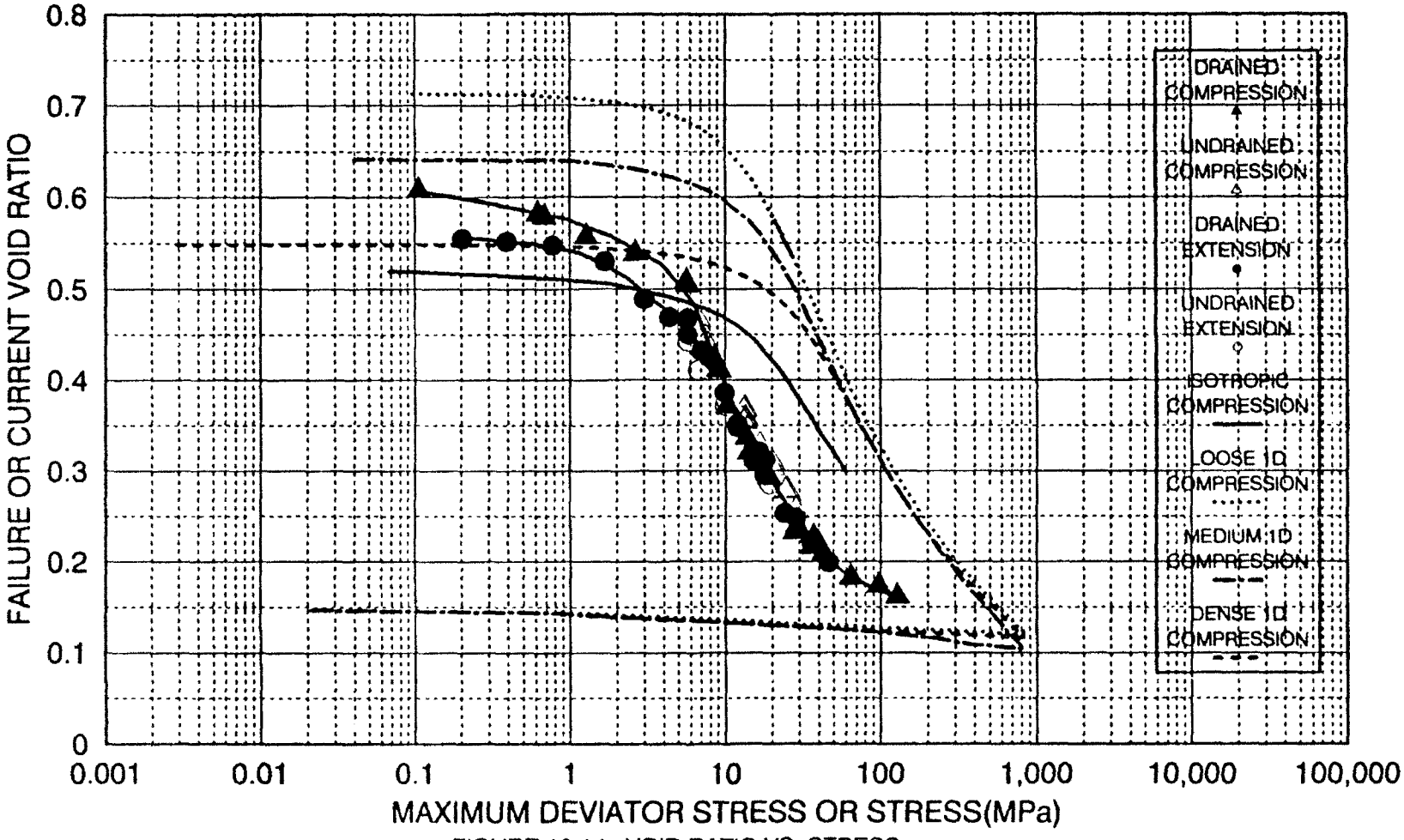

FIGURE 10-14 VOID RATIO VS. STRESS
DIFFERENT TESTS
CAMBRIA SAND

void ratio at failure for the triaxial compression and extension tests or the current void ratio in the one-dimensional compression tests and isotropic consolidation tests. As can be seen, at lower pressures the drained extension and compression strength lines are at different locations with the compression deviator stresses being higher than those in extension. At deviator stresses of 8 to 10 MPa the two strength lines join together and essentially form a unique line of maximum deviator stresses for all four types of triaxial tests. This behavior is maintained throughout the highest stress levels achieved during triaxial testing. Apparently at high pressures there is a unifying influence based upon void ratio at failure, which results in all triaxial extension and compression tests under both drained and undrained conditions being on the same line. Close examination of the individual test results indicates that the undrained tests may have slightly higher deviator stresses than comparable drained tests. This is attributed to the creep effects associated with the time to lower the piston into contact with the specimen. The drained tests are relatively unaffected, because their maximum deviator stresses are achieved at large axial strains, typically greater than 30 percent. However, the undrained tests may be more affected by the creep, because the maximum deviator stresses are achieved at very low axial strains, typically less than two percent. This effect was discussed in Chapter 7.

At high stress magnitudes the one-dimensional compression tests form a line parallel to the triaxial compression and extension strength line. The isotropic consolidation line also eventually tends toward becoming parallel to the strength lines at high stresses. A quasi-overconsolidation pressure based upon drawing two

lines tangent to the two different slopes on the isotropic consolidation line may be inferred. This overconsolidation pressure appears to correspond to a deviator stress at which the extension and compression lines join together. This also corresponds to the stress where the rates of dilation and the friction angles in compression and extension are equal as discussed in Chapter 5. The principal interesting aspect of this unifying behavioral correlation, which appears for both Cambria sand and Sacramento River sand, is that the maximum deviator stresses in the drained tests are associated with failure, but most of the undrained tests have their maximum deviator stresses occurring well inside the failure surface. The Rutledge Hypothesis for normally consolidated clays may be used to infer the effective stress friction angle from the maximum deviator stress, because it occurs simultaneously with the maximum effective stress ratio. This is only true for normally consolidated clays. As was shown in Chapter 5, the maximum effective stress ratio in granular materials at high pressures occurs well after the maximum deviator stress.

Figure 10-14 shows that the triaxial strength and the one-dimensional compression lines curve outward near the bottom at high stress magnitudes. This is caused by decreasing compressibility of the specimens at these higher stresses. The points on the triaxial strength line at high stresses correspond to drained compression tests with near zero rates of dilation at failure. This condition produces stresses being increased with smaller reduction in void ratio. Hence, the line tends to curve outward slightly.

Tests on quartz sand are shown on Figure 10-15. Three one-dimensional

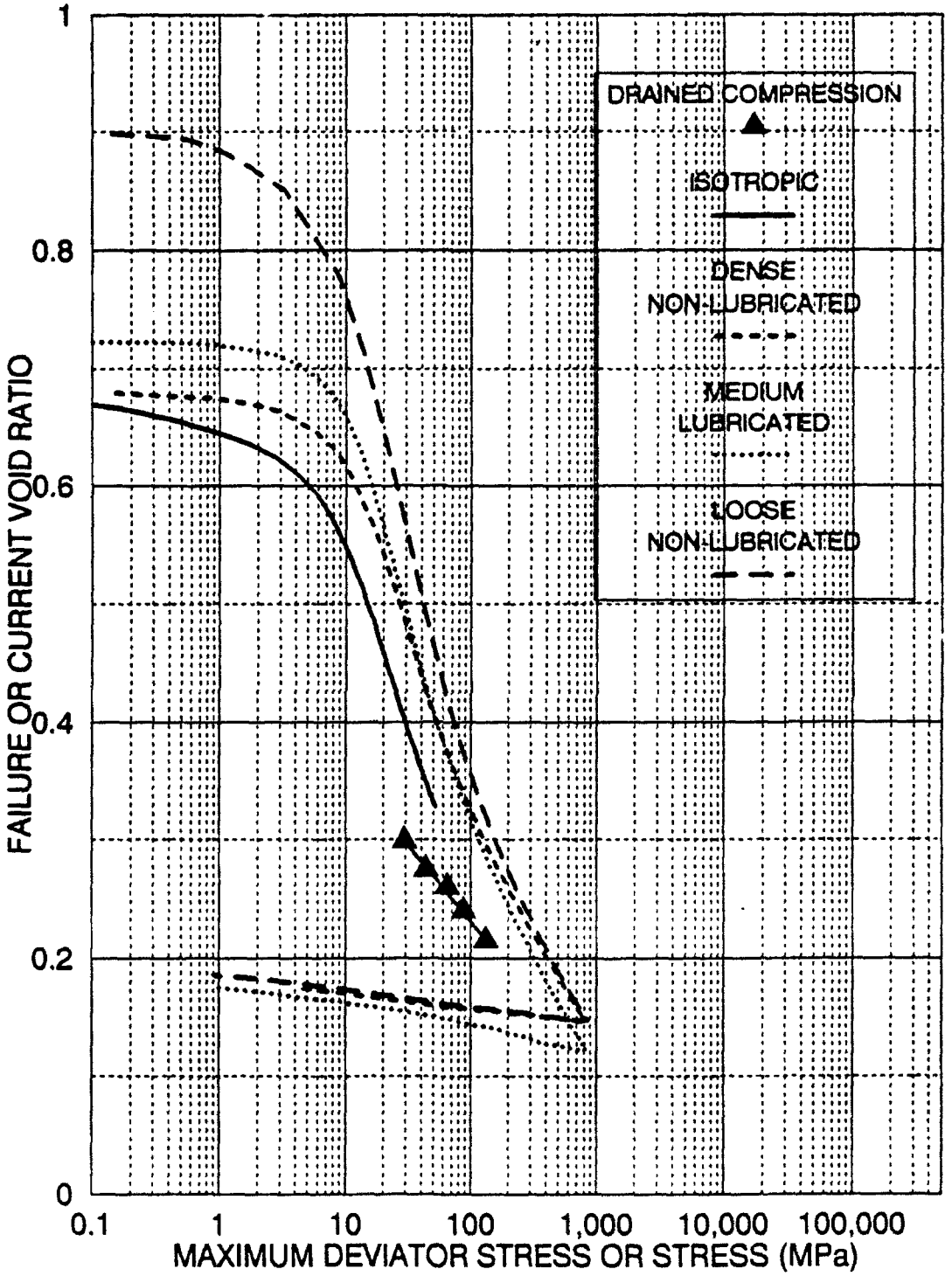

FIGURE 10-15 VOID RATIO VS. STRESS
DIFFERENT TESTS
QUARTZ SAND

compression tests and one isotropic consolidation test are shown along with points from the five drained triaxial compression tests performed on quartz sand. They are plotted with the failure or current void ratio on the vertical axis and current axial stress, maximum deviator stress or consolidation stress on the horizontal axis. As with the Cambria sand, the one-dimensional compression and isotropic consolidation lines tend to become parallel at high stress magnitudes. The points indicating the maximum deviator stresses for the five drained triaxial compression tests do not appear to be exactly parallel with the isotropic consolidation and one-dimensional compression lines. However, these tests were performed at stress magnitudes corresponding to the lower outwardly curved portion on the Cambria sand triaxial strength line with near zero rates of dilation at failure. The outwardly curved portion tends to not be exactly parallel to the other lines in both sands.

The critical state theories of Seed and Lee, Roscoe et al., and Rutledge have been examined in view of results of high pressure tests. The Seed and Lee approach does not appear to correlate well with high pressure data, because of an inability to predict the location of the critical void ratio line at high pressures. Their method also clearly does not provide a unique critical void ratio line for both drained and undrained test results at high pressures. The Roscoe, Schofield and Wroth approach to critical state fails to account for the fact that effective stress paths for high pressure undrained triaxial compression tests do not achieve their maximum stress difference near the critical state line. The Rutledge Hypothesis appears to work at high pressures, with the strength lines from the drained and

undrained triaxial compression and extension tests merging into one unique line. This strength line becomes parallel with the lines from one-dimensional compression tests, and isotropic consolidation tests. The main difference between this correlation and the Rutledge Hypothesis is that the effective stress friction angle of the undrained tests cannot be calculated from the parallel lines, since the maximum deviator stress on the strength line does not correspond to failure.

10.6 Experimental Results and Correlations with Energy

Continuing to search for unifying concepts or parameters in the behavior of granular materials, the experimental data from tests on Cambria sand and Sacramento River sand (Lee, 1965) was analyzed to calculate the total energy input into the specimen until effective stress failure was reached. The total amount of energy to failure that is input into a specimen during a triaxial test is the sum of energy input during the isotropic consolidation phase and the shearing phase to failure as shown in Equation 10.6.

$$E_T = E_C + E_S \qquad (10.6)$$

E_T - *total energy input into specimen to failure.*
E_C - *energy input during consolidation.*
E_S - *energy input during shearing to failure.*

During consolidation the amount of input energy is created by the increase in effective cell pressure resulting in volumetric strains. During drained shearing the input energy is generated by two components: (1) The effective cell pressure and volumetric strain during isotropic consolidation, and from (2) the deviator stress,

which results in axial strains, creating additional input energy as calculated in Equation 10.7. Undrained tests do not experience volumetric strains, so there is no contribution from the latter component.

$$E_f = \sum_{0}^{\bullet_c} \bar{\sigma}_c \cdot \dot{\epsilon}_v + \left[\sum_{0}^{failure} (\sigma_1 - \sigma_3) \cdot \dot{\epsilon}_A + \sum_{0}^{failure} \bar{\sigma}_c \cdot \dot{\epsilon}_v \right] \quad (10.7)$$

σ_c - *final effective cell pressure.*
$\bar{\sigma}_c$ - *average effective cell pressure over increment.*
$\dot{\epsilon}_v$ - *volumetric strain increment.*
EOT - End Of Test.
$(\sigma_1 - \sigma_3)$ - *average deviator stress over increment.*
$\dot{\epsilon}_A$ - *axial strain increment.*

Input energy for tests in extension utilize the same computational method as expressed in Equations 10.6 and 10.7.

Input energy to failure were calculated for the drained and undrained triaxial compression data on Sacramento River sand (Lee, 1965) as shown on Figure 10-16. The failure or current input energy is plotted against failure or current void ratio. It appears that input energy to failure can also represent a unifying parameter. At stress magnitudes where initial void ratio still influences the soil behavior, both the drained and undrained tests of the same initial void ratio appear on the same lines. As the stress and input energy increase, the separate void ratio lines converge toward a single line for all triaxial compression tests. Using calculated input energies for experimental data on Cambria sand indicates that the drained and undrained triaxial compression tests also coincide on a unique line as shown on Figure 10-17. In addition to this observation, the drained and undrained extension tests also fall onto a unique, but separate line. The compression and extension lines are not coincidental, since the stress paths are

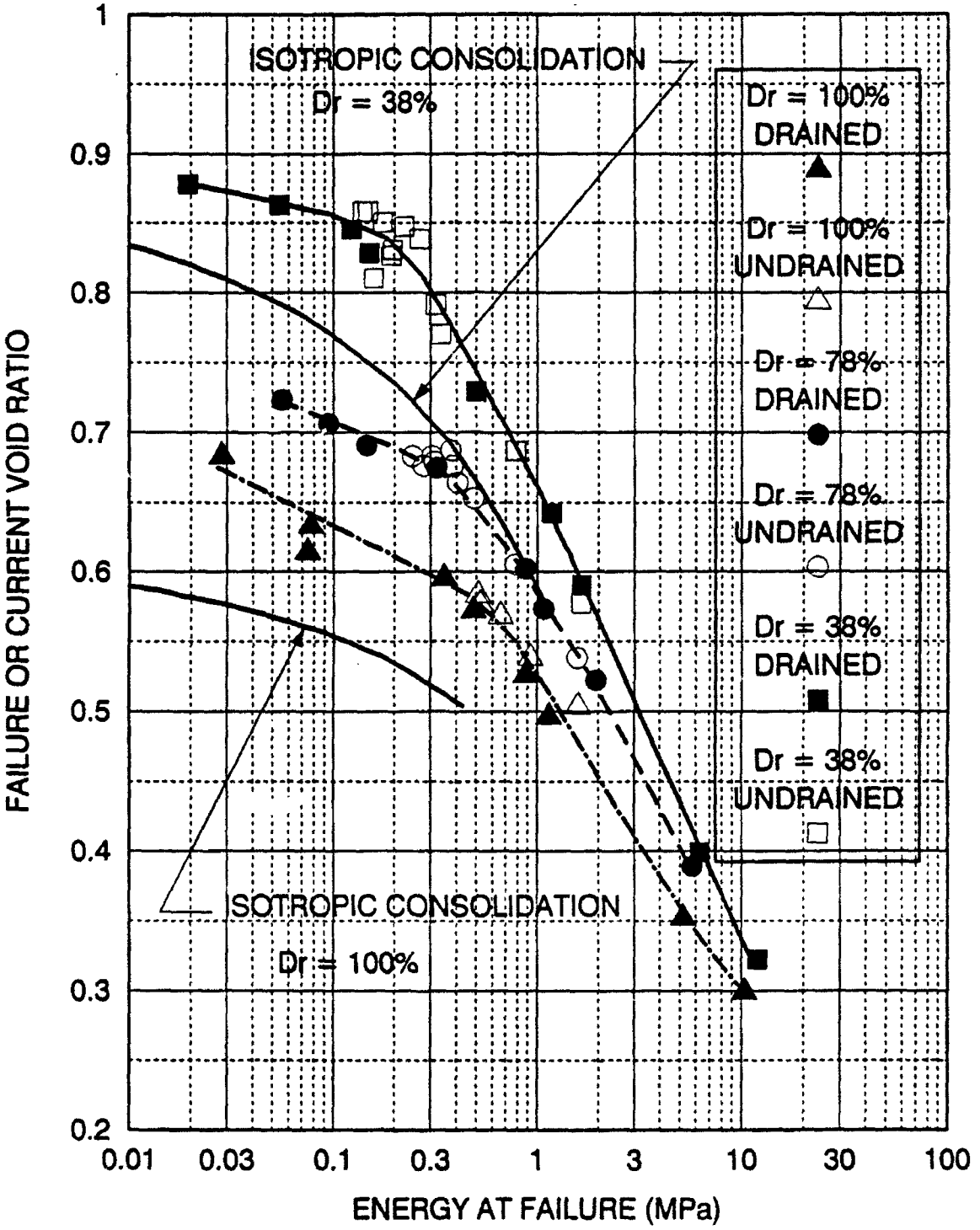

FIGURE 10-16 VOID RATIO VS. ENERGY AT FAILURE
DRAINED AND UNDRAINED TRIAXIAL COMPRESSION TESTS
SACRAMENTO RIVER SAND (from LEE, 1965)

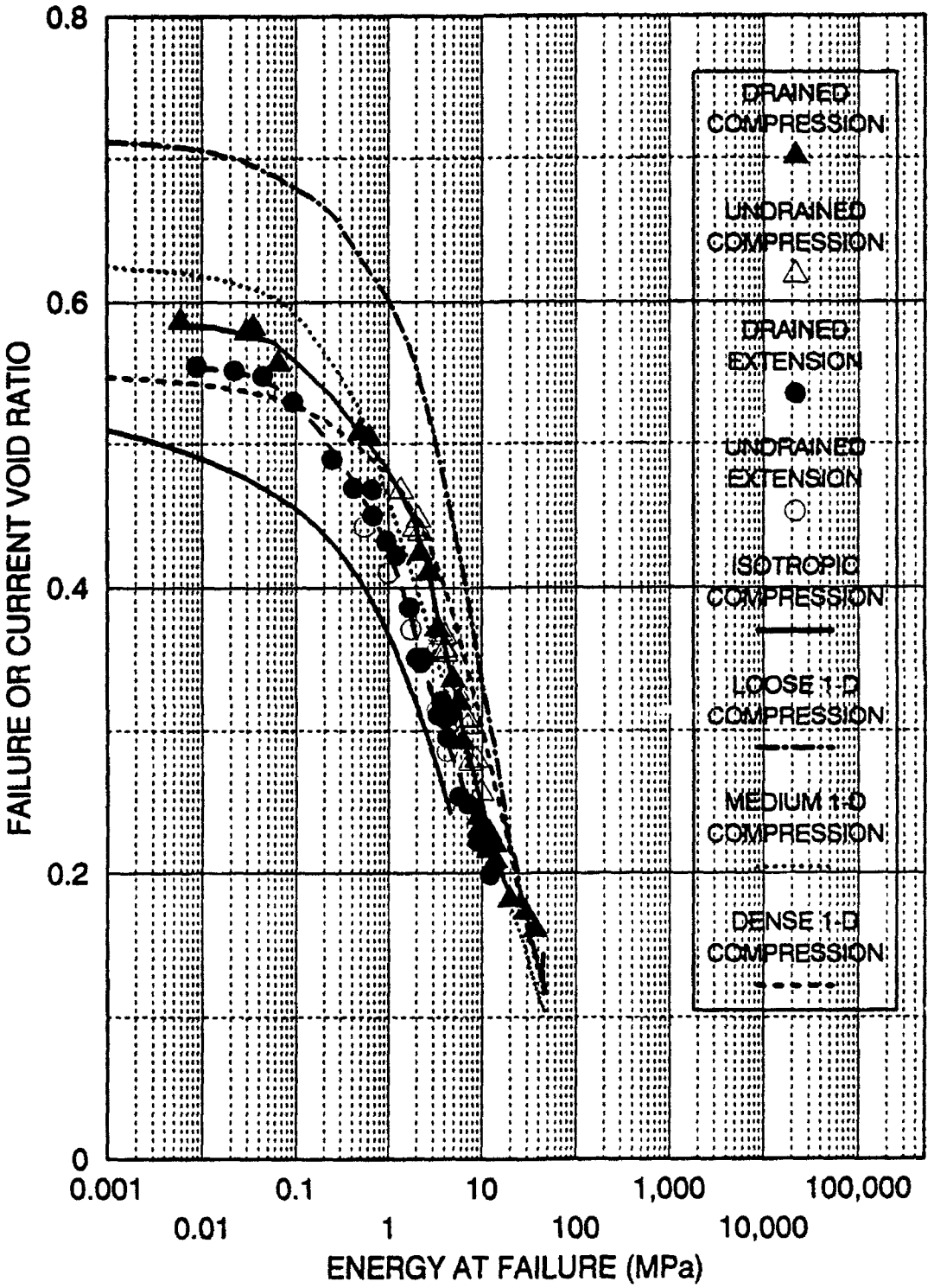

FIGURE 10-17 VOID RATIO VS. ENERGY AT FAILURE
DIFFERENT TESTS ON CAMBRIA SAND

considerably different, and therefore, the energy path to failure is different. The separate triaxial compression and extension lines appear to be converging at high stress or energy levels. The isotropic consolidation and one-dimensional compression lines tend to become parallel to the triaxial lines. However, the triaxial lines change their slopes at the highest input energy levels and cross the one-dimensional compression line. The principal reason for this is that triaxial tests are not fully confined tests, like the isotropic consolidation or one-dimensional compression tests. When these high pressure triaxial tests reach their compressibility limits for a given stress magnitude, the specimens do not volumetrically compress further, but they still absorb input energy by continuing to axially strain downward and radially outward against the cell fluid. Therefore, there is no further reduction in void ratio, but the levels of input energy increase. However, in the isotropic consolidation and one-dimensional compression tests, the soil is constrained by rigid boundary conditions, such that there is no further input energy accumulated once the volumetric strains cease.

Another correlation with input energy to failure was discovered in the drained and undrained triaxial compression tests on Sacramento River sand, and the drained and undrained triaxial compression and extension tests on Cambria sand. The results are displayed on Figures 10-18 and 10-19. Maximum deviator stress is plotted on the vertical axis against input energy to failure on the horizontal axis. The first impression is that the curves bears a striking similarity to a typical Mohr-Coulomb failure envelope with the higher density sand being located above the one with lower density. Another similarity with a typical failure

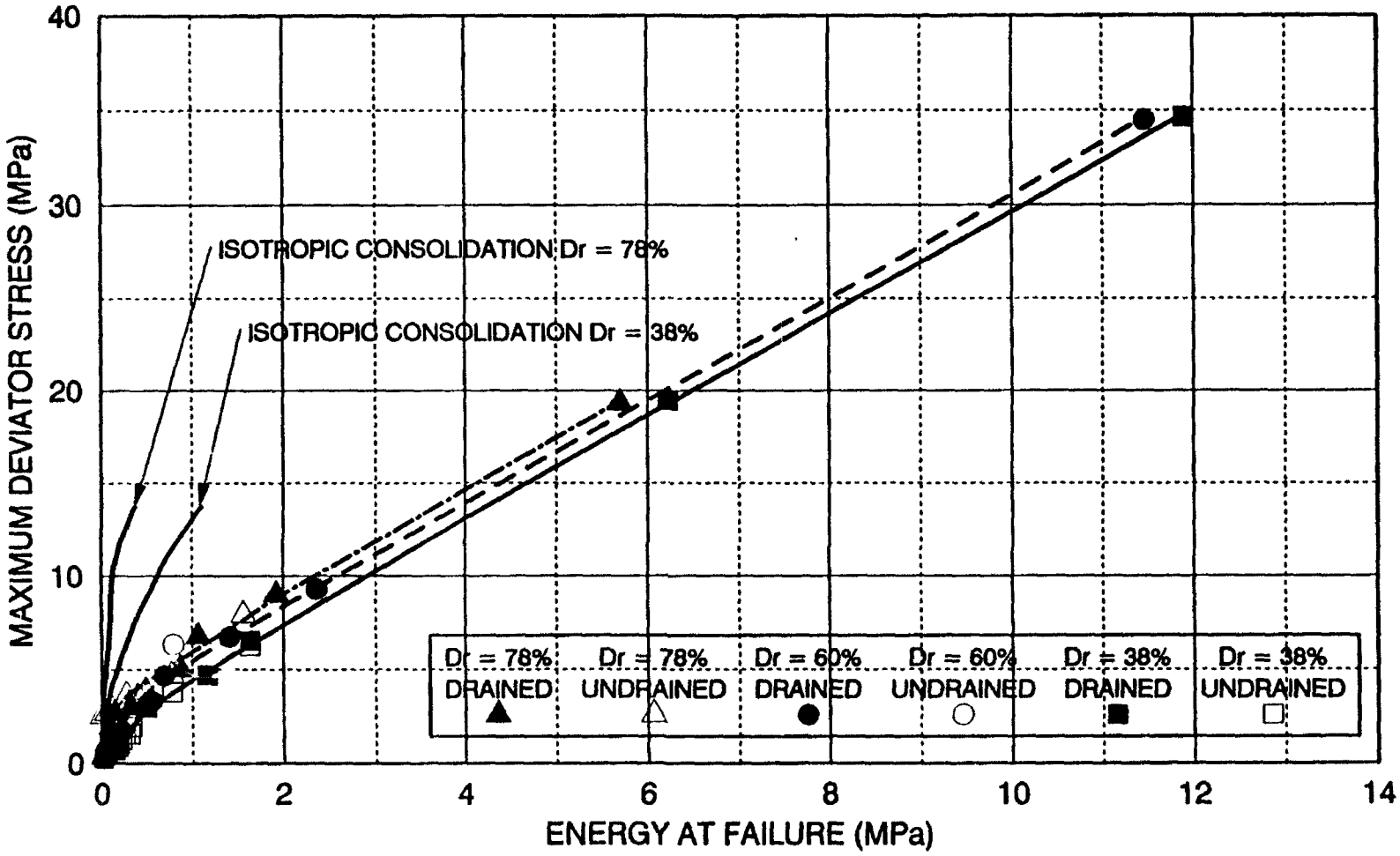

FIGURE 10-18 MAXIMUM DEVIATOR STRESS VS. ENERGY
DRAINED AND UNDRAINED TRIAXIAL COMPRESSION
SACRAMENTO RIVER SAND (from LEE, 1965)

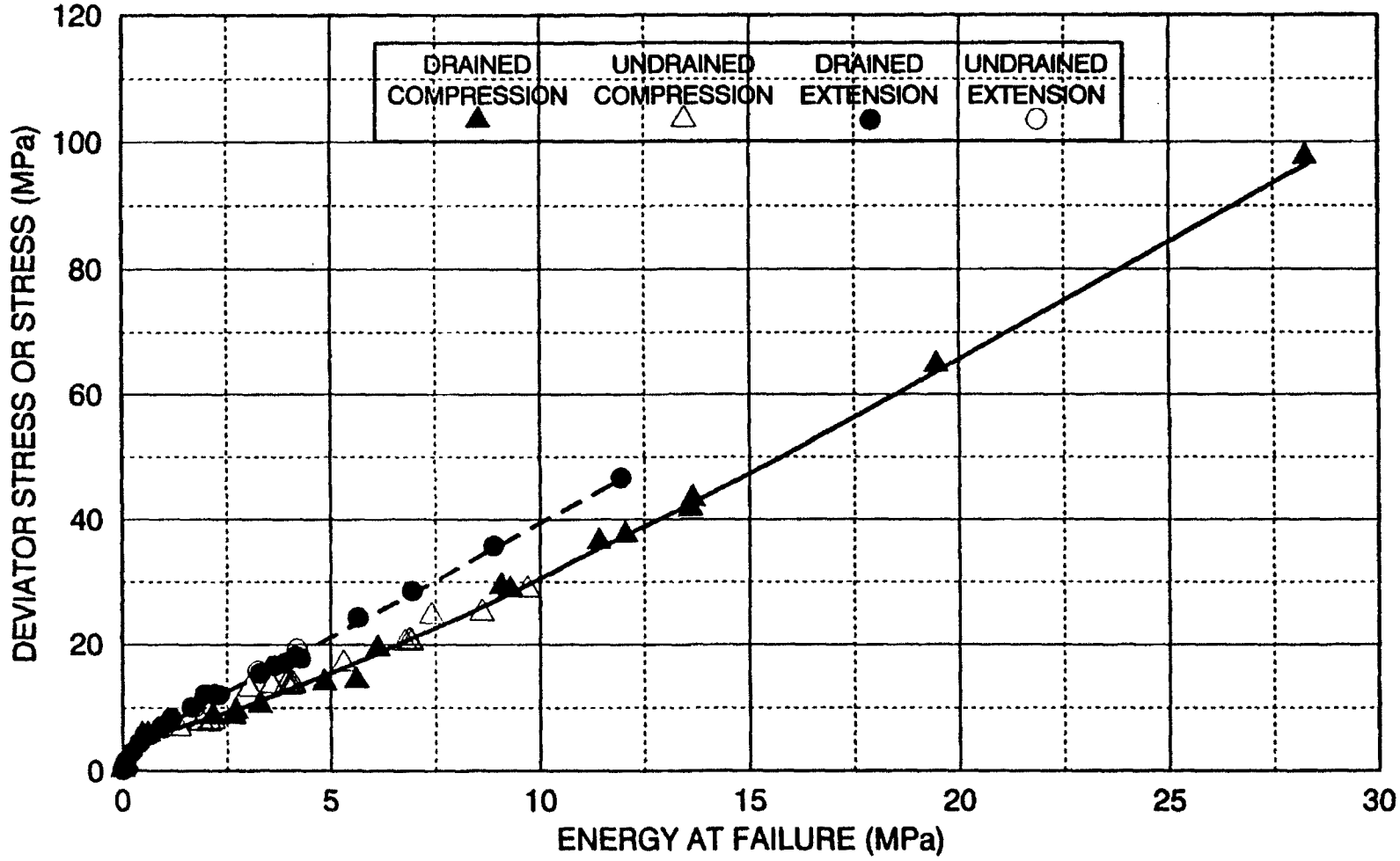

FIGURE 10-19 MAXIMUM DEVIATOR STRESS VS. ENERGY AT FAILURE
DRAINED AND UNDRAINED TRIAXIAL COMPRESSION AND EXTENSION TESTS
DENSE CAMBRIA SAND

envelope is the curvature near the origin, which appears to be caused by the effects of dilation. The deviator stresses at low stresses are enlarged by dilatancy effects. As can be seen on Figure 10-18, the different densities of Sacramento River sand appear on slightly different, but linear and parallel energy lines. The drained and undrained tests appear on the same density lines. There is a certain amount of apparent experimental scatter in the lowest pressure results. The deviator stresses at high stress levels appear to be similar in magnitude, but are slightly offset with the looser sands having higher energies at failure. This is caused by the reduced, but still present influence of initial void ratio. The total energy at failure is composed of portions from isotropic consolidation and shearing. Since the energy associated with isotropic consolidation is larger for looser sands, the offset between the energy lines is created. This is shown on Figure 10-18 by the two isotropic consolidation energy lines for 78 and 38 percent relative density. However, as the stress magnitude increases and the influence of initial void ratio is further reduced, the energy lines of different densities appear to merge. This is based on the fact that the energy derived from the volumetric strains in the denser sands are lower than in the looser sands, partially compensating for the initial difference in energy of consolidation. Beyond the stress level where initial void ratio is elminated, a small energy offset probably will persist, because the specimens will eventually fail near the same void ratio. Since the looser specimen will have had an overall larger reduction in volume and the stress-strain behavior will be identical, the total input energy will be slightly higher for the looser material. However, at these high stress levels, the relative difference

in energy contributed from the different levels of consolidation will be small compared with the total energy input.

Figure 10-19 shows the results from the tests on Cambria sand. Again, the general similarity to a typical Mohr-Coulomb failure envelope is evident. The drained and undrained tests appear on the same almost linear energy lines. The extension tests do not appear on the same line as the compression test, which is not unexpected, since the stress paths, and therefore, the energy paths to failure are different. The location of the compression energy line would indicate that it requires more energy to achieve the same deviator stress level as in extension. This is related to the larger amount of particle crushing and rearranging experienced in the compression tests. It is unexpected that the undrained maximum deviator stress appears on the same line as the drained tests when related to input energy at failure. The input energy at failure is associated with large axial strains (20 to 25 percent), while at high pressures the maximum deviator stress occurs at very small axial strains(1 to 2 percent).

Figures 10-20 and 10-21 display the breakdown of the total input energy into its separate components for drained and undrained triaxial compression and extension tests on dense Cambria sand. The energies of consolidation, volumetric strain during shearing, and deviator stress are shown by separate lines plotted against the maximum deviator stress. Both figures clearly show that beyond the dilatancy region the contributions are almost linear proportions relative to each other. The drained compression tests on Figure 10-20 indicate that the energy associated with the deviator stress is by far the largest component. The undrained

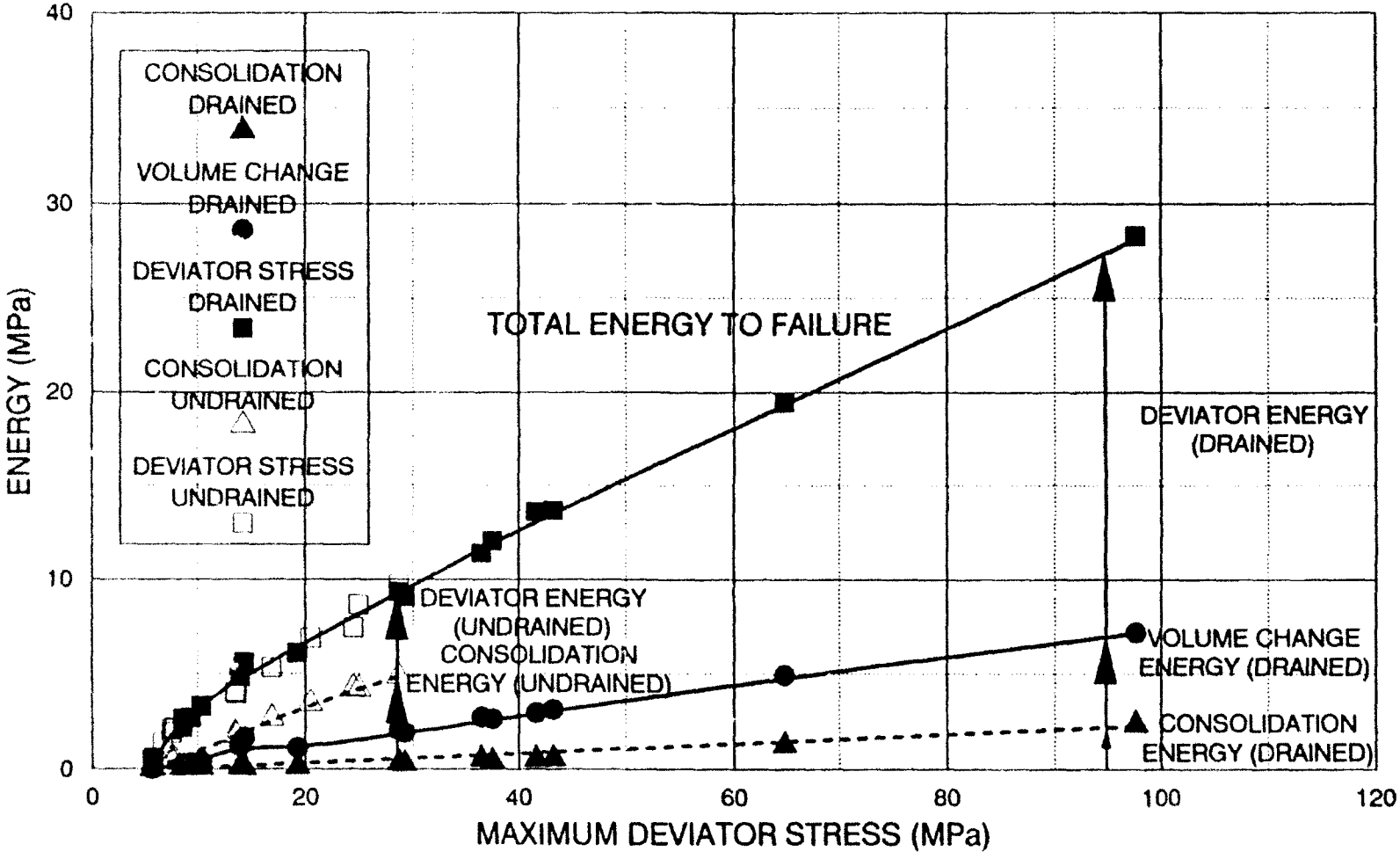

FIGURE 10-20 BREAKDOWN OF TOTAL ENERGY TO FAILURE
DRAINED AND UNDRAINED TRIAXIAL COMPRESSION TESTS
DENSE CAMBRIA SAND

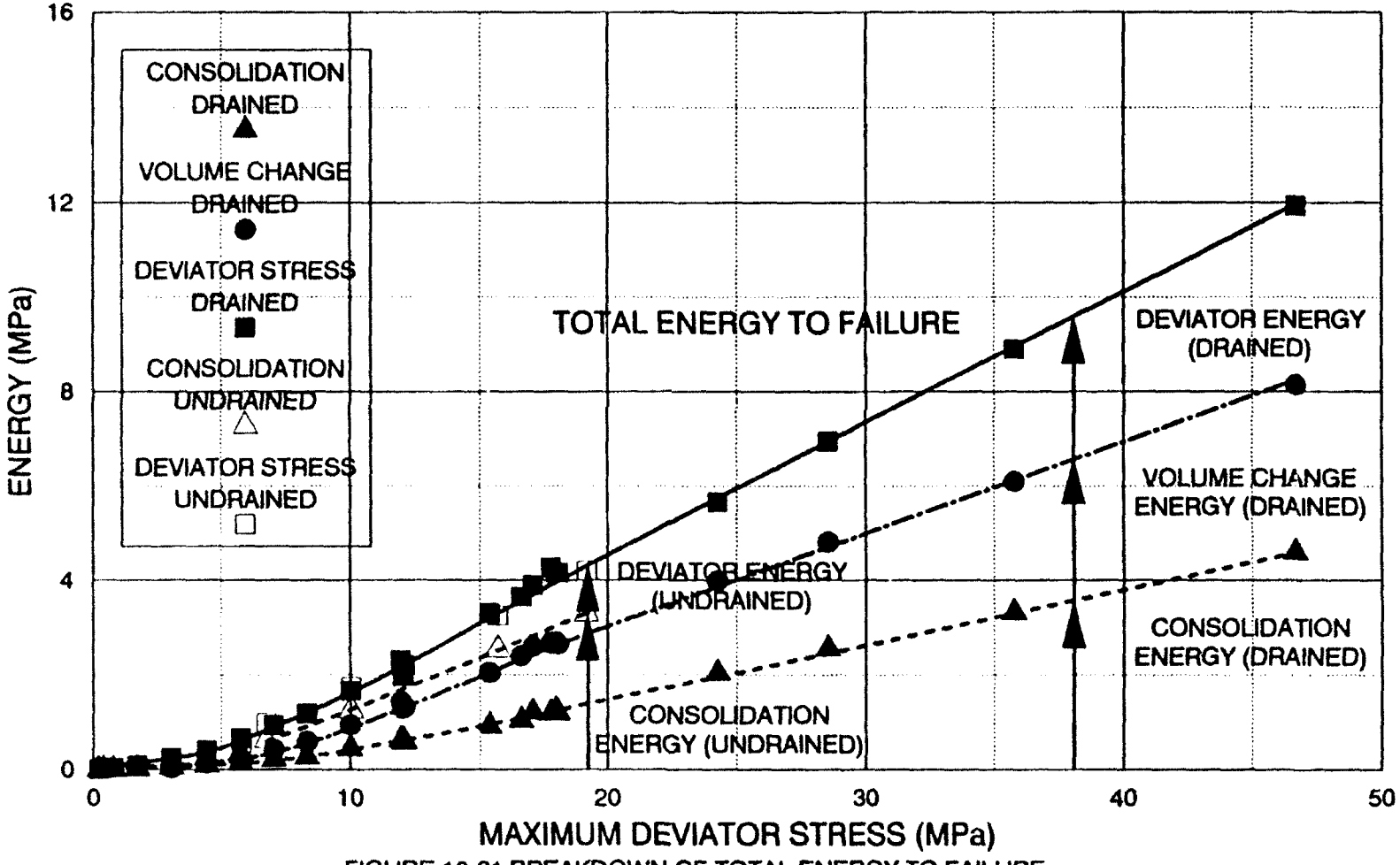

FIGURE 10-21 BREAKDOWN OF TOTAL ENERGY TO FAILURE
DRAINED AND UNDRAINED TRIAXIAL EXTENSION TESTS
DENSE CAMBRIA SAND

compression tests show their higher consolidation input energy, but smaller deviator stress contribution (about half) to appear on the same total energy to failure line as the drained tests. The drained extension tests on Figure 10-21 clearly show that the contribution of the energy associated with the deviator stress is lower in extension than in compression, sharing almost equally with consolidation and volumetric strain during shearing. The undrained tests again indicate the higher amount of consolidation energy and lower proportional contribution from the deviator stress.

10.7 Discussion

Stress dilatancy theories developed by Bishop (1954) and Rowe (1962, 1964) were examined for their applicability to experimental data collected on Cambria sand at high pressures. The analysis indicates that both methods of correcting for dilatancy effects on the friction angle are not effective for high pressures, if a result of constant friction angle is expected in both triaxial compression and extension. Bishop's dilatancy correction method, when extended to extension, appears to be incorrect, whereas Rowe's method is deemed more reasonable. However, Bishop's method in compression does provide a more constant friction angle throughout high pressures than Rowe's method. Both methods use the rate of dilation at failure as a means of correcting for dilatancy effects, which varies widely over the pressure range tested due to increasing and then decreasing levels of particle crushing. Since neither method was intended to cope with particle breakage and both were based upon the assumption that the soil

was actually dilating, it is unreasonable to assume their general applicability, especially at high pressures. However, the concept of stress-dilatancy is supported by the data, which indicates increasing strength with less compressive behavior.

Critical state soil mechanics theories by Rutledge, Roscoe et al., and Seed and Lee were evaluated for applicability to high pressures by comparing them with experimental data collected at high pressures. It was shown that the critical state theory by Seed and Lee does not apply well at high pressures, because the critical void ratio line cannot be determined from high pressure drained tests. In addition to this, the critical void ratio line is not unique for both drained and undrained tests at high pressures. The critical state theory by Roscoe et al. also does not apply well at high pressures, because undrained stress paths do not have their maximum stress difference coinciding with the critical state line. However, the Rutledge Hypothesis originally applied to normally consolidated clays, appears to apply to cohesionless soils at high pressures. Experimental data from Sacramento River sand and Cambria sand indicate a unifying behavior pattern from low to high pressures. At low pressures, where the effect of initial void ratio is present, the maximum deviator stresses from both drained and undrained triaxial compression tests fall onto separate but unique void ratio lines that move toward convergence as the stresses increase. At higher stresses, where the effect of initial void ratio is eliminated, the lines join together into a single line. This line represents maximum deviator stresses from triaxial compression and extension tests in both drained and undrained conditions. The main deviation from the Rutledge Hypothesis is that the effective stress friction angle from undrained tests cannot necessarily be

ascertained from the maximum deviator stress, since the maximum deviator stress does not occur at failure. A quasi-overconsolidation pressure can be estimated from the isotropic consolidation line, which appears to fall near a deviator stress level that represents the point where the extension and compression lines merge. The occurrence of maximum deviator stresses from drained and undrained tests on a unique line through the range from low to high pressures is unexpected, because the drained tests represent failure at large strains, while the undrained tests are generally significantly removed from failure at low strains. An undrained friction angle calculated from these values of deviator stress obtained from this line would be related to the instability line.

Input energy to failure appears to provide another unifying correlation for soil behavior at high pressures. When examined with experimental data from Sacramento River sand and Cambria sand, it was seen that input energy resulted in either the void ratio at failure or the maximum deviator stress appearing on unique almost straight lines for both drained and undrained conditions. The correlation of input energy to failure with maximum deviator stress strongly resembles a failure envelope. It possesses a dilating region at low energy levels and tends to be linear beyond it. At lower pressures and different initial densities, the void ratios at failure and maximum deviator stresses appear on separate lines that move closer together at higher pressures, as the influence of initial density is reduced. Extension tests appear on a unique, but separate line from the compression tests, because of stress path differences. The breakdown of the total input energy to failure into the relative contributions from consolidation,

volumetric strain during shearing, and deviator stress components indicate a linear relations with pressure.

CHAPTER 11 - CONCLUSIONS

11.1 Introduction

This study presents the results of an extensive experimental investigation of granular materials at high pressures. Among the many types of experiments performed are drained and undrained triaxial compression and extension tests with an overall confining pressure range of 0.25 to 68.9 MPa. One-dimensional compression tests up to 900 MPa axial stress level were also performed.

Major topics that were studied include: strain localization in triaxial extension tests; drained and undrained stress-strain and strength behavior from low to high pressures in triaxial extension and compression; instability of granular materials at high pressures in triaxial compression and extension; the determination of Skempton's pore pressure parameter B at high pressures; strain rate effects of granular materials at high pressures in drained and undrained conditions; examination of the effective stress principle at high pressures; particle breakage at high pressures; behavior of sands in one-dimensional compression tests at very high pressures; determination of values of K_o, the coefficient of earth pressure at rest, at high pressures; evaluation of the elastic modulus and Poisson's ratio at high pressure levels; and correlations of high pressure soil behavior with stress-dilatancy, critical state, and input energy.

11.2 Strain Localization (Chapter 4)

A series of conventional extension tests (tests with only membranes

surrounding the specimen) was performed. Strain localization severely affected the results of conventional triaxial extension tests, with failure being precipitated by necking in all tests performed (Figure 4-15). The conventional extension test was determined to be an inherently unstable test (Figure 4-17), because it concentrates the stresses (and therefore strains) at the weakest portion of the specimen, and it is not deemed to be an appropriate means to evaluate the strength characteristics of soil in extension.

A series of conventional extension tests was performed and terminated at different axial strains, whereupon the specimen was carefully measured. It was determined that strain localization developed very early in the extension test, possibly near zero axial strain (Figure 4-15). Increasing levels of isotropic consolidation was also seen to enhance the development of strain localization.

An experimental method was developed to enforce uniform strains in the cylindrical extension test. The method consists of encasing the test specimen with layers of overlapping small steel plates bent to fit the curvature of the specimen and sandwiched between greased membranes (Figure 4-18). Upon application of cell pressure, the plates interlock to form a flexurally rigid jacket, resulting in uniform strains being enforced. Friction is not induced because the plates can slide relative to each other on the greased membranes that separate them. Friction was shown to be insignificant, because the initial slope of the stress-strain curve is essentially the same as in conventional extension tests.

Drained uniform strain extension test results indicate that the volumetric strains (in the volumetrically compressing region) and the principal strains to

failure are generally larger than in conventional extension tests (Figures 4-35 and 4-36). Also, the effective stress friction angles are generally higher in both drained or undrained uniform extension tests, as compared with those from strain localized tests (Figure 4-34).

11.3 Stress-Strain Behavior at High Pressure (Chapter 5)

A series of drained and undrained triaxial compression and extension tests were performed to evaluate the stress-strain behavior of Cambria sand at high pressures (up to 68.9 MPa confining pressure). The normalized stress-strain curves from drained triaxial compression and extension tests were seen to become flatter with increasing confining pressure (Figures 5-1 and 5-22). The volumetric strains at failure and the principal strains to failure also increase with confining pressure (Figures 5-32 and 5-34), and this was attributed to increasing amounts of particle crushing and rearranging (Figure 5-33). As confining pressure continues to increase, the volumetric strains at failure and the principal strains to failure reach a maximum level, and start to decrease as particle crushing reaches a maximum level. This stress magnitude was seen to coincide with a steepening of the normalized stress-strain curve.

At high pressures the deviator stress curves from undrained triaxial compression and extension tests generally exhibit a maximum value at very low principal strain levels (Figures 5-12 and 5-29), but actually reach effective stress failure at large principal strains (Figures 5-11 and 5-23). This is caused by the rapid development of positive pore pressures (Figures 5-13 and 5-30).

The drained friction angles in triaxial compression and extension clearly relate directly to the rate of dilation at failure (Figures 5-35 and 5-36). As the confining pressure increases, the rate of dilation increases (increasing volumetric compression) due to higher levels of particle breakage resulting in more volumetric compression. At low pressures the soil is more dilatant at failure in extension, resulting in higher drained friction angles than in compression, but the two curves eventually cross. The stress at the crossing point correspond to the point where the drained friction angles in compression and extension are equal. As the stress magnitude increases and particle crushing slows down in compression, the friction angle increases up to a stable value where it remains constant, even at the highest stress magnitudes employed. In extension, where particle crushing is not as extensive, the rate of dilation at failure is observed to reach a maximum level (most compressive behavior), and the friction angle reaches a constant minimum value.

At high pressures the undrained friction angles in compression and extension are generally constant and of equal value, but at a higher value than obtained in the drained tests (Figure 5-37). This is the result of the sand being subjected to high stress regions, as was shown on the effective stress path (Figure 5-14).

11.4 Instability of Soils at High Pressures (Chapter 6)

Undrained tests in both triaxial compression and extension were used to establish the boundaries of the instability and the temporary instability regions for

dense Cambria sand (Figures 6-5 and 6-6). Instability for stress states inside the instability region was demonstrated by special tests (Figure 6-7 and 6-15). In these tests specimens were sheared under drained conditions into the instability region. The specimens were then rendered undrained and placed under stress control, and it was attempted to hold the deviator stress constant. All test specimens became unstable with increasing pore pressures, and eventually reached effective stress failure. These special tests were performed in both triaxial compression and extension.

The location of the instability line at high pressures was determined from experiments (Figure 6-12 and 6-20). Special tests were performed which brought the test specimens to stress states well outside the instability region under drained conditions. The specimens were then rendered undrained and the deviator stress was held constant. Volumetric soil creep at high pressures caused the pore pressures to increase, and this resulted in the effective stress path moving horizontally toward the instability line. When the instability line was crossed, the specimens became unstable, and eventually reached failure.

11.5 B-Values, The Effective Stress Principle, and Strain Rate Effects (Chapter 7)

Values of Skempton's pore pressure parameter B at high pressures were experimentally determined utilizing special isotropic compression tests (Figures 7-1 and 7-2). The B-values were found to be substantially below unity and depended on whether the soil was on the virgin consolidation or reloading curve. These results also were reliably predicted using a compressiblity equation (Figure 7-4).

The effective stress principle was examined at high pressures by performing undrained triaxial compression tests with three different total stress paths (Figure 7-6). Since the value of B is much less than unity, the effective stress paths should show effects of the varying total stress paths. However, it was found that the effects of volumetric soil creep overshadowed the potential effects of the changes in total stress path, and no conclusion could be reached regarding the uniqueness of the effective stress path at high pressures.

Since the effect of soil creep was observed to be substantial at high pressures, an investigation of the effect of strain rate on the location of the instability line was undertaken by performing a series of drained and undrained triaxial compression tests at different strain rates. The location of the instability line does not appear to be influenced by effects of strain rate (Figure 7-9). It was demonstrated that the undrained effective stress paths change, but the different maximum deviator stresses still fall on the same instability line. It was determined from drained conditions that increasing strain rate (Table 7.2) increases the deviator stress slightly, decreases the volumetric strains slightly, and increases the axial strains to failure slightly. The mechanism identified as causing strain rate effects at high pressures was the effect of increasing dilatancy (less time for particle crushing) with increasing strain rate. At high strain rates the soil does not have time to undergo as much particle breakage and rearranging as it can experience at lower strain rates. Even though the effects of strain rate was determined to be insignificant for drained tests, the effects on undrained tests was substantial (Table 7.1). It was found that decreasing strain rates in undrained

tests substantially reduces the maximum deviator stress, substantially increases the strain to effective stress failure, substantially increases pore pressures, substantially increases effective stress friction angles, and substantially decreases the effective confining pressures at failure.

11.6 Particle Breakage at High Pressures (Chapter 8)

Sieve analyses on many sheared specimens of Cambria sand were performed and grain size distributions were evaluated (Figures 8-2 through 8-5). Commonly used empirical particle breakage factors created by Marsal, by Lee and Farhoomand, and by Hardin were calculated based upon these grain size curves. It was found that triaxial compression tests had significantly more particle crushing than triaxial extension tests (Figures 8-6 through 8-9). Undrained tests appear to produce more particle breakage than drained tests, when results are compared on the basis of effective mean normal stress at failure. This was due to effects of stress path, and the effective mean normal stress at failure was not considered to be a good variable on which to base the comparison (Figure 8-10) of crushing. Void ratio at failure provided a better variable for comparison, since the drained and undrained tests appeared to be on the same lines (Figures 8-11 through 8-14). However, the extension and compression tests still appeared on different lines.

Total input energy was calculated at the end of the test and it was determined to be a unifying variable, with results of particle breakage parameters from drained and undrained triaxial compression and extension tests all appearing on a unique line (Figures 8-15 through 8-18).

Thin sections of sheared specimens were obtained and examined under a light polarizing microscope (Figures 8-19 and 8-20). Photographs of the thin-sections indicate that the mechanism of compaction was different in Cambria sand and in quartz sand. The Cambria sand, which is composed of grains of different hardnesses, experienced softer grains squeezing plastically between the harder grains. The quartz sand, whose grains are of more uniform hardness, experienced grain fracturing and rearranging. However, either can be treated using the total energy input as a unifying parameter.

A new particle breakage factor B_{10} was proposed, which facilitates the prediction of permeability based upon Hazen's permeability equation. When correlated with total input energy (Figure 8-21), this new breakage factor, which is based on the D_{10} particle grain size, was designed to be easily represented by a hyperbolic curve fit through its crushing curve. With this new particle breakage factor, it is possible to predict permeability based upon input energy into the soil. This proposed method is potentially useful in prediction of variations in permeability in earth dams or other geotechnical structures in which particle crushing occurs. Using a hyperbolic curve fit, it is also possible to predict some types of grain size distributions (Figure 8-23) after shearing and crushing.

Extension tests that exhibited strain localization were analyzed for total input energy and particle breakage factors were estimated from grain size distribution curves to ascertain the effect of strain localization on particle crushing. The input energy computations were made on the basis of stresses and strains calculated assuming uniform strain conditions. It was determined that tests

exhibiting strain localization had lower values of particle breakage than uniform strain tests (Figures 8-24 through 8-27).

11.7 One-Dimensional Compression Tests and Elastic Parameters (Chapter 9)

A high pressure one-dimensional compression testing apparatus was designed and fabricated (Figure 9-1 through 9-3) to test soil up to 900 MPa axial stress magnitudes. The soil containment cell was instrumented with strain gages to infer internal lateral normal soil stresses.

High pressure one-dimensional compression tests on Cambria sand, quartz sand, and Sacramento River sand were performed at different initial densities. Full-friction and reduced-friction tests were performed and friction was found to have only minor effects on the overall soil behavior. The effect of initial void ratio was seen to disappear at high stress magnitudes with initially loose sand eventually reaching the same density as initially dense sand (Figures 9-8 and 9-9).

Thin sections were made from sheared specimens from the one-dimensional compression tests, after the specimens were extruded from the soil containment cell. The photographs of the thin sections appeared very similar to those made from high pressure triaxial compression tests (Figures 9-11 and 9-12).

An elastic numerical analysis was performed so that measured strains on the soil containment cell could be converted into appropriate values of internal lateral normal soil stresses. Thus K_o could be estimated at high pressures. It was found that K_o decreased from low pressures to constant values at high pressures that ranged between 0.37 and 0.40 for the three sands tested (Figures 9-14 through 9-

16). Jaky's equation for K_o appears valid at low pressures, but does not appear to be correct at high pressures. As the void ratio decreases under increasing axial stress, the relative positions of K_o curves from different initial densities indicate that looser soils have lower values of K_o than denser soils (Figures 9-20 and 9-21).

A special loading-unloading-reloading-unloading drained triaxial compression test was performed at five different confining pressures to obtain the elastic modulus and Poisson's ratio over a wide confining pressure range (Figures 9-26 and 9-27). It was determined that the elastic modulus and Poisson's ratio of Cambria sand increased linearly with the logarithm of confining pressure.

11.8 General Soil Behavior at High Pressures (Chapter 10)

An attempt was made to correlate high pressure experimental results with commonly used theories for soil behavior at lower pressures. The theories examined were the stress dilatancy theories by Bishop (1954) and Rowe (1962, 1964) and critical state theories by Seed and Lee (1967), Roscoe et al. (1958), and Rutledge (1947). Correlations with total input energy to failure were also presented.

The dilatancy correction equations by Bishop and Rowe ideally should result in a constant friction angle, which Rowe considered to be the basic interparticle friction angle. Both formulations for dilatancy correction involve the rate of dilation at failure. When high pressure test results are applied to Rowe's formulations for compression and extension, the friction angles that result exhibit a large increase at moderately high pressures before decreasing to a constant value

at the highest pressures employed (Figure 10-2). The constant friction angle occurs at a stress magnitude where particle crushing is rapidly increasing, and this results in increasing (more compressive) rate of dilation at failure. Bishop's dilatancy correction formulation for triaxial compression tests produces friction angles that exhibit a smoother and more constant value through high pressures. However, when an expression for triaxial extension was derived on the basis of his compression formulation, the reduced friction angles that resulted were apparently incorrect (Figure 10-1): The reduced friction angles at low pressures are much too low and at high pressures excessively large. Both Rowe's and Bishop's formulations for dilatancy corrections were formulated for low pressure applications, where little particle crushing occurs. Implicit in their derivations is the assumption that the soil actually does dilate, even though the expressions have been widely used for volumetrically contracting soils. However, the general concept of stress-dilatancy has been shown to be correct: A soil is measureably stronger when it exhibits more dilatant tendencies.

Seed and Lee's concept of critical state was shown to be inapplicable at high pressures, because the critical void ratio line could not be predicted from drained tests (Figures 10-7 and 10-8). The uniqueness of their critical void ratio line was not confirmed at high pressures, with drained and undrained tests not appearing on a unique line (Figure 10-9).

Roscoe, Schofield, and Wroth's concept of critical state was also shown to be inapplicable at high pressures. The critical state line was derived from drained tests, and indeed appears to work well for drained tests (Figure 10-11). However,

it was determined that the effective stress paths from high pressure undrained tests did not have their maximum stress differences occurring on the derived critical state line, as required by the their definition of critical state (Figure 10-12). A line passing through the maximum stress differences correspond to the instability line, not the critical state line.

The Rutledge Hypothesis appears to be valid for granular materials at high pressures. Originally it was only considered applicable to normally consolidated clays at low pressures. The line defined by plotting the void ratio at failure against the maximum deviator stress becomes parallel to the isotropic and one-dimensional compression lines at high pressures on a semilogarithic plot (Figures 10-13 and 10-14). At low pressures the effect of initial void ratio causes the maximum deviator stresses from drained and undrained tests to be on separate lines. As the effect of initial void ratio is reduced at higher stresses the strength lines start converging toward each other. At higher stresses yet, the strength lines for drained and undrained triaxial compression and extension tests all converge together onto a unique line. The implication of this is that the void ratio at failure essentially controls the strength of soils at high pressures. However, the principal difference with the Rutledge Hypothesis is that the effective stress friction angle for the undrained tests on sands cannot be inferred from the maximum deviator stress, since it occurs well away from effective stress failure condition.

Input energy to failure appears to be useful as a unifying variable when used for comparison with the void ratio at failure and the maximum deviator stress. The correlation with void ratio at failure appears very similar to the void

ratio-deviator stress correlation just stated, except the extension and compression tests appear on separate lines until high pressure levels are achieved (Figures 10-16 and 10-17). This is due to the effect of different stress paths, resulting in different amounts of input energy to failure. The correlation of input energy to failure with maximum deviator stress results in a linear relationship beyond the dilatancy region, and it appears very similar to a classic Mohr-Coulomb failure envelope (Figures 10-18 and 10-19). Extension and compression tests do not appear on a unique line due to stress path effects. Breaking down the total input energy into its separate components of consolidation energy, volumetric strain energy (drained tests only), and deviator stress energy indicates that beyond the dilatancy region the individual component energies appear almost to linearly increase with stress (Figures 10-20 and 10-21).

REFERENCES

Andrawes, K.Z., and El-Sohby, M.A., 1973, "Factors Affecting Coefficient of Earth Pressure K_0," *Journal of the Soil Mechanics and Foundations Division*, ASCE, Vol. 99, No. SM7, pp. 527-539.

Barden, L., and Khayatt, A.J., 1966, "Incremental Strain Rate Ratios and Strength of Sand in the Triaxial Test," *Geotechnique*, Vol. 16, No. 4. pp. 338-357.

Barden, L., Ismail, H., and Tong, P., 1969, "Plane Strain Deformation of Granular Material at Low and High Pressures," *Geotechnique*, Vol. 19, No. 4, pp. 441-452.

Barden, L., and Proctor, D.C., 1971, "The Drained Strength of Granular Material," *Canadian Geotechnical Journal*, August, pp. 372-383.

Becker, E., Chan, C.K., and Seed, H.B., 1972, "Strength and Deformation Characteristics of Rockfill Materials in Plane Strain and Triaxial Compression Tests," *Report No. TE 72-3*, University of California, Berkeley, October, 121 pp.

Billam, J., 1971, "Some Aspects of the Behaviour of Granular Materials at High Pressures," *Stress-Strain Behaviour of Soils*, Proceedings of the Roscoe Memorial Symposium, Cambridge University, March, pp. 69-80.

Bishop, A.W., and Eldin, A.K.G., 1953, "The Effect of Stress History on the Relation between Phi and Porosity in Sand," *Proceedings of the Third International Conference on Soil Mechanics and Foundation Engineering*, Vol. 1, August, Zurich, Switzerland, pp.100-105.

Bishop, A.W., 1954, Correspondence on "Shear Characteristics of a Saturated Silt, Measured in Triaxial Compression," *Geotechnique*, Vol. 4, pp. 43-45.

Bishop, A.W., 1958, "Test Requirements for Measuring the Coefficient of Earth Pressure at Rest," *Proceedings of the Brussels Conference on Earth Pressure Problems*, Vol. 1 pp. 2-14.

Bishop, A.W., Webb, D.L., and Skinner, A.E., 1965, "Triaxial Tests on Soil at Elevated Cell Pressures," *Proceedings of the Sixth International Conference on Soil Mechanics and Foundation Engineering*, Montreal, Canada, Vol.1, pp. 170-174.

Bishop, A.W., 1966, "The Strength of Soils as Engineering Materials," *Geotechnique*, Vol. 16, No. 2, June, pp. 91-130.

Bishop, J.F.W., and Hill R., 1951, "A Theory of the Plastic Distortion of a Polycrystaline Aggregate Under Combined Stresses," *Philosophical Magazine*, Vol. 42, No. 327, pp. 414-427.

Black, D.K., and Lee, K.L., 1973, "Saturating Laboratory Samples by Back Pressure," *Journal of the Soil Mechanics and Foundations Division*, ASCE, Vol. 99, No. SM1, pp. 75-93.

Casagrande, A., 1940 (originally published in 1936), "Characteristics of Cohesionless Soils Affecting the Stability of Slopes and Earth Fills," *Contributions to Soil Mechanics, 1925-1940*, Boston Society of Civil Engineers, pp. 257-276.

Casagrande, A., and Shannon W.L., 1948, "Strength of Soils Under Dynamic Loads." *Proceedings, American Society of Civil Engineers*, Vol. 74, No. 4, pp. 591-632.

Casagrande, A., 1979, "Liquefaction and Cyclic Deformation of Sands, A Critical Review," *Proceedings of the Sixth Panamerican Conference on Soil Mechanics and Foundation Engineering*, Lima, Peru, December 1979, Vol. II, pp. 80-133.

Castro, G., 1969, "Liquefaction of Sands," PH.D. Dissertation, Harvard University, pp.112.

Castro, G., Poulos, S.J., 1977, "Factors Affecting Liquefaction and Cyclic Mobility," *Journal of the Geotechnical Engineering Division*, ASCE, Vol. 103, No. GT6, pp. 501-516.

Chamieh, N.S., 1990, "Experimental Investigation of the Behavior and Stability of Granular Soils at High Pressure," Ph.D Dissertation, University of California, Los Angeles, 222 pp.

Charles, J.A., and Watts, K.S., 1980, "The Influence of Confining Pressure on the Shear Strength of Compacted Rockfill," *Geotechnique*, Vol. 30, No. 4, pp. 353-367.

Colliat-Dangus, J.L., Desrues, J., and Foray, P., 1988, "Triaxial Testing of Granular Soil Under Elevated Cell Pressure," *Advanced Triaxial Testing of Soil and Rock, ASTM STP 977*, ASTM, Philadelphia, pp. 290-310.

Coop, M.R., 1990, "The Mechanics of Uncemented Carbonate Sands," *Geotechnique*, Vol. XL, No. 4, December, pp. 607-626.

Drucker, D.C., 1951, "A More Fundamental Approach to Stress-Strain Relations," *Proceedings of the First Congress of Applied Mechanics*, pp. 487-491.

Drucker, D.C., 1956, "On Uniqueness in the Theory of Plasticity," *Quarterly of Applied Mathematics*, Vol. 14, pp. 35-42.

Drucker, D.C., 1959, "A Definition of Stable Inelastic Material," *Journal of Applied Mechanics*, Vol. 26, pp. 101-106.

Duncan, J.M., Witherspoon, P.A., Mitchell, J.K., Watkins, D.J., Hardcastle, J.H., and Chen, J.C., 1972, "Seepage and Groundwater Effects Associated with Explosive Cratering," *Report No. TE-72-2*, University of California, Berkeley, April, 191 pp.

Frydman, S., Zeitlen, J.G., and Alpan, I., 1973, "The Membrane Effect in Triaxial Testing of Granular Soils," *Journal of Testing and Evaluation*, Vol. 1, No. 1, January, pp. 37-41.

Fuller, W.B., and Thompson, S.E., 1907, "The Laws of Proportioning Concrete," *Transactions of the American Society of Civil Engineers*, ASCE, Vol. 58, December, pp. 67-172.

Ghiassian, H., 1988, "A Study of Shear Characteristics of Coarse Sand," Masters thesis, University of California, Los Angeles, 89 pp.

Golder, H.Q., and Ackroyd, T.N., 1954, "An Apparatus for Triaxial Compression Tests at High Pressures," *Geotechnique*, Vol. 4, pp. 131-136.

Green, G.E., 1971, "Strength and Deformation of Sand Measured in an Independent Stress Control Cell," *Stress-Strain Behaviour of Soils*, Proceedings of the Roscoe Memorial Symposium, Cambridge University, March, pp. 285-323.

Green, G.E., and Bishop, A.W., 1969, "A Note on the Drained Strength of Sand Under Generalized Strain Conditions," *Geotechnique*, Vol. 19, No. 1, pp. 144-149.

Hall, E.B., and Gordon, B.B., 1963, "Triaxial Testing with Large-Scale High Pressure Equipment," *Laboratory Shear Testing of Soils, ASTM STP 361*, ASTM, pp. 315-328.

Hardin, B.O., 1985, "Crushing of Soil Particles," *Journal of Geotechnical Engineering*, ASCE, Vol. 111, No. 10, October, pp. 1177-1192.

Hardin, B.O., 1987, "1-D Strain in Normally Consolidated Cohesionless Soils," *Journal of Geotechnical Engineering*, ASCE, Vol. 113, No. 12, pp. 1449-1467.

Hendron, A., 1963, "The Behavior of Sand in One-Dimensional Compression," Ph.D Dissertation, University of Illinois, 283 pp.

Hendron, A.J., Fulton, R.E., and Mohraz, B., 1963, "The Energy Absorption Capacity of Granular Materials in One Dimensional Compression," Report to Air Force Special Weapons Center, Kirtland Air Force Base, New Mexico, [as quoted by Tai (1970)].

Hill, R., 1958, "A General Theory of Uniqueness and Stability in Elasto-Plastic Solids," *Journal of Mechanics of Physical Solids*, Vol. 6, pp. 236-249.

Hirschfeld, R.C., and Poulos, S.J., 1963, "High-Pressure Triaxial Tests on a Compacted Sand and an Undisturbed Silt," *Laboratory Shear Testing of Soils, ASTM STP 361*, ASTM, pp. 329-339.

Ingersoll, R.V., Bullard, T.F., Ford, R.L., Grimm, J.P., Pickle, J.D., and Sares, S.W., 1984, "The Effect of Grain Size on Detrital Modes: A Test of the Gazzi-Dickinson Point-Counting Method," *Journal of Sedimentary Petrology*, Vol. 54, No. 1, March, pp. 103-116.

Kirkpatrick, W.M., 1957, "The Condition of Failure for Sands," *Proceedings of the Fourth International Conference on Soil Mechanics and Foundation Engineering*, Vol. 1, London, pp. 172-178.

Ko, H.Y., and Scott, R.F., 1967, "A New Soil Testing Apparatus," *Geotechnique*, Vol. 17, No. 1, pp. 40-57.

Kramer, S.L., and Seed, H.B., 1988, "Initiation of Soil Liquefaction Under Static Loading Condition," *Journal of Geotechnical Engineering*, ASCE, Vol. 114, No. 4, April, pp. 412-430.

Ladanyi, B., et al, 1967, "Discussion: Compressibility of Granular Soil," *Canadian Geotechnical Journal*, Vol. 4, No. 1, February, pp. 87-99.

Lade, P.V., and Duncan, J.M., 1973, "Cubical Triaxial Tests on Cohesionless Soil," *Journal of the Soil Mechanics and Foundations Division*, ASCE, Vol. 99, No. SM10, pp. 793-812.

Lade, P.V., and Duncan, J.M., 1975, "Elastoplastic Stress-Strain Theory for Cohesionless Soil," *Journal of the Geotechnical Engineering Division*, ASCE, Vol. 101, No. GT10, pp. 1037-1053.

Lade, P.V., and Duncan, J.M., 1976, "Stress-Path Dependent Behavior of Cohesionless Soil," *Journal of the Geotechnical Engineering Division*, ASCE, Vol. 102, No. 1, pp. 51-68.

Lade, P.V., and Hernandez, S.B., 1977, "Membrane Penetration Effects in Undrained Tests," *Journal of the Geotechnical Engineering Division*, ASCE, Vol. 103, No. GT2, pp. 109-125.

Murphy, D.J., 1987, "Stress, Degradation, and Shear Strength of Granular Material," *Geotechnical Modeling and Applications*, Sayed M. Sayed, ed., Gulf Publishing Co., Houston, pp. 181-211.

Nakai, T., and Matsuoka, H., 1983, "Shear Behaviors of Sand and Clay Under Three-Dimensional Stress Condition," *Soils and Foundations*, Vol. 23, No. 2, June, pp. 26-47.

Nash K.L., and Dixon R.K. 1961, "The Measurement of Pore Pressure in Sand Under Rapid Triaxial Tests." *Proceedings, Conference on the Pore Pressure and Suction in Soils*, Butterworths, pp.21-25.

Ochiai, H., and Lade, P.V., 1983, "Three-Dimensional Behavior of Sand with Anisotropic Fabric," *Journal of Geotechnical Engineering*, ASCE, Vol. 109, No. 10, October, pp. 1313-1328.

Oda, M., Koishikawa, I., and Higuchi, T., 1978, "Experimental Study of Anisotropic Shear Strength of Sand by Plane Strain Test," *Soils and Foundations*, Vol.18, No. 1, pp. 25-38.

Pittman, E.D., and Larese, R.E., 1991, "Compaction of Lithic Sands: Experimental Results and Applications," *The American Association of Petroleum Geologists Bulletin*, Vol. 75, No. 8, August, pp. 1279-1299.

Poorooshasb, H.B., Holubec, I., Sherbourne, A.N., 1966, "Yielding and Flow of Sand in Triaxial Compression: Part I," *Canadian Geotechnical Journal*, Vol. 3, No. 4, pp. 179-190.

Poulos, S.J., Castro, G., and France, J.W., 1985, "Liquefaction Evaluation Procedure," *Journal of Geotechnical Engineering*, ASCE, Vol. 111, No. 6, pp. 772-792.

Pradel D., and Lade, P.V. 1990, "Instability and Plastic Flow of Soils. II: Analytical Investigation." *Journal of Engineering Mechanics*, ASCE, Vol. 116, pp. 2550-2565.

Procter, D.C., and Barden, L., 1969, Discussion on: "A Note on the Drained Strength of Sand Under Generalized Strain Conditions," *Geotechnique*, Vol. 19, No.3, pp. 424-426.

Ramamurthy, T., and Rawat, P.C., 1973, "Shear Strength of Sand Under General Stress System," *Proceedings of the Eighth International Conference on Soil Mechanics and Foundation Engineering*, Vol. 1, pp. 339-342.

Reades, D.W., and Green, G.E., 1976, "Independent Stress Control and Triaxial Extension Tests on Sand," *Geotechnique*, Vol. 26, No. 4, pp. 551-576.

Roark R.J., and Young, W.C., 1982, *Formulas for Stress and Strain*, fifth edition, McGraw-Hill Book Co. pp. 504.

Roberts, J.E., and de Souza, J.M., 1958, "The Compressibility of Sand," *Proceedings, American Society for Testing Materials, Volume 58*, ASTM, Philidelphia, pp. 1269-1277.

Roscoe, K.H., Schofield, A.N., and Wroth, C.P., 1958, "On the Yielding of Soils," *Geotechnique*, Vol. 8, No. 1, March, pp. 22-53.

Rowe, P.W., 1962, "The Stress-Dilatancy Relation for Static Equilibrium of an Assembly of Particles in Contact," *Proceedings, Royal Society*, Series A, Vol. 269, No. 1339, London, October, pp. 500-527 [as quoted by Hirschfeld and Poulos (1963)].

Rowe, P.W., 1963, "Discussion: High-Pressure Triaxial Tests on a Compacted Sand and an Undisturbed Silt," *Laboratory Shear Testing of Soils, ASTM STP 361*, ASTM, pp. 340-341.

Rowe, P.W., Barden, L., and Lee, I.K., 1964, "Energy Components During the Triaxial Cell and Direct Shear Tests," *Geotechnique*, Vol. 14, No. 3, pp. 247-261.

Rowe, P.W., 1969, "The Relation Between the Shear Strength of Sands in Triaxial Compression, Plane Strain, and Direct Shear," *Geotechnique*, Vol. 19, No. 1, pp. 75-86.

Rutledge, P., 1947, "Cooperative Triaxial Shear Research Program," *Progress Report on Soil Mechanics Fact Finding Survey*, U.S. Army Corps of Engineers, Waterways Experiment Station.

Schimming B.B., Haas A.M., and Saxe H.C. 1966, "Study of Dynamic and Static Failure Envelopes." *Journal of the Soil Mechanics and Foundation Division*, ASCE, Vol. 92, No. SM2, pp. 105-124.

Schofield, A., and Wroth, P., 1968, *Critical State Soil Mechanics*, McGraw-Hill, pp. 19-21.

Seed H.B., and Lundgren R. 1954, "Investigation of the Effect of Transient Loading on the Strength and Deformation Characteristics of Saturated Sands." *Proceedings, American Society for Testing and Materials*, Vol. 54, pp. 1288-1306.

Seed, H.B., and Lee, K.L., 1967, "Undrained Strength Characteristics of Cohesionless Soils," *Journal of the Soil Mechanics and Foundations Division*, ASCE, Vol. 93, No. SM6, November, pp. 333-360.

Lade, P.V., 1982, "Localization Effects in Triaxial Tests on Sands," *Deformation and Failure of Granular Materials*, IUTAM, Symposium on Deformation and Failure of Granular Materials, August, pp. 461-471.

Lade P.V., and Tsai, J., 1985, "Effects of Localization in Triaxial Tests on Clay," *Proceedings of the 11th International Conference on Soil Mechanics and Foundation Engineering*, San Francisco, August, pp. 549-552.

Lade P.V., Nelson, R.B., and Ito, Y.M. 1987, "Nonassociated Flow and Stability of Granular Materials," *Journal of Engineering Mechanics*, ASCE, Vol. 113, No. 9, pp. 1302-1318.

Lade P.V., Nelson, R.B., and Ito, Y.M. 1988, "Instability of Granular Materials with Nonassociated Flow," *Journal of Engineering Mechanics*, ASCE, Vol. 114, No. 12, pp. 2173-2191.

Lade P.V., and Pradel, D. 1990, "Instability and Plastic Flow of Soils. I: Experimental Observations." *Journal of Engineering Mechanics*, ASCE, Vol. 116, No. 11, pp. 2532-2550.

Lade, P.V., 1992, "Static Instability and Liquefaction of Loose Fine Sandy Slopes." *Journal of Geotechnical Engineering*, ASCE, Vol. 118, No. 1, pp. 51-71.

Lam, W.K., and Tatsuoka, F., 1988a, "Triaxial Compressive and Extension Strength of Sand Affected by Strength Anisotropy and Sample Slenderness," *Advanced Triaxial Testing of Soil and Rock, ASTM STP 977*, ASTM, Philadelphia, pp. 655-666.

Lam, W.K., and Tatsuoka, F., 1988b, "Effects of Initial Anisotropic Fabric and σ_2 on Strength and Deformation Characteristics of Sand," *Soils and Foundations*, Vol. 28, No. 1, pp. 89-106.

Lee, K.L., 1965, "Triaxial Compressive Strength of Saturated Sand Under Seismic Loading Conditions," Ph.D. thesis, University of California, Berkeley.

Lee, K.L., and Farhoomand, I., 1967, "Compressibility and Crushing of Granular Soils in Anisotropic Triaxial Compression," *Canadian Geotechnical Journal*, Vol. 4, No. 1, February, pp. 68-86.

Lee, K.L., and Seed, H.B., 1967, "Drained Strength Characteristics of Sands" *Journal of the Soil Mechanics and Foundations Division*, ASCE, Vol. 93, No. SM6, November, pp. 117-141.

Lee, K.L., 1978, "End Restraint Effects on Undrained Static Triaxial Strength of Sand," *Journal of the Geotechnical Engineering Division*, ASCE, Vol. 104, No. GT6, pp. 687 704.

Lee K.L., Seed H.B., and Dunlop P. 1969, "Effect of Transient Loading on the Strength of Sand." *Proceedings, 7th International Conference on Soil Mechanics and Foundation Engineering*, Mexico, Vol. 1, pp. 239-247.

Leslie, D.D., 1963, "Large Scale Triaxial Tests on Gravelly Soils," *Proceedings of the Second Pan-American Conference on Soil Mechanics and Foundation Engineering*, Sao Paulo, Brazil, Vol. 1, pp. 183-202 [as quoted by Tai (1970)].

Lo, K.Y., and Roy, M., 1973, "Response of Particulate Materials at High Pressures," *Soils and Foundations*, JSSMFE, Vol. 13, No. 1, March, pp. 1-14.

Mandel, J., 1964, "Conditions de Stabilite et Postulat de Drucker," *Proceedings IUTAM Symposium on Rheology and Soil Mechanics*, pp. 58-68, (in French).

Marachi, N.D., Chan, C.K., Seed, H.B., and Duncan, J.M., 1969, "Strength and Deformation Characteristics of Rockfill Materials," *Report No. TE-69-5*, University of California, Berkeley, September, 139 pp.

Marsal, R.J., 1967, "Large Scale Testing of Rockfill Materials," *Journal of the Soil Mechanics and Foundations Division*, Vol. 93, No. SM2, March, pp. 27-43.

Matsuoka, H, and Ishizaki, H., 1981, Deformation and Strength of Anisotropic Soil," *Proceedings of the Tenth International Conference on Soil Mechanics and Foundation Engineering*, Vol. 1, pp. 699-702.

Miura, N., and Yamanouchi, T., 1973, "Compressibility and Drained Shear Characteristics of a Sand Under High Confining Pressures," *Technology Reports of the Yamaguchi University*, Vol. 1, No. 2, December, pp. 271-290.

Miura, N., and O-hara, S., 1979, "Particle Crushing of a Decomposed Granite Soil Under Shear Stresses," *Soils and Foundations*, JSSMFE, Vol. 19, No. 3, September, pp. 61-76.

Miura, N., Murata, H., and Yasufuku, N., 1984, "Stress-Strain Characteristics of Sand in a Particle-Crushing Region," *Soils and Foundations*, Vol. 24, No. 1, March, pp. 77-89.

Mroz, Z., 1963, "Non-associated Flow Laws in Plasticity," *Journal de Mechanique*, Vol. 2, No. 1. pp. 21-42.

Murphy, D.J., 1970, "Soils and Rocks: Composition, Confining Level and Strength," Ph.D. Dissertation, Duke University.

Murphy, D.J., 1971, "High Pressure Experiments on Soil and Rock," *Proceedings 13th Symposium on Rock Mechanics*, Illinois, pp. 691-714.

Skempton, A. W., 1954, "The Pore Pressure Coefficients A and B," *Geotechnique*, London, England, Vol. 4, pp. 143-147.

Skempton, A.W., 1961, "Effective Stress in Soils, Concrete, and Rocks," *Proceedings of the Conference on Pore Pressure and Suction in Soils*, Butterworths, pp. 4-16.

Sutherland, H.B., and Mesdary, M.S., 1969, "The Influence of the Intermediate Principal Stress on the Strength of Sand," *Proceedings of the Seventh International Conference on Soil Mechanics and Foundation Engineering*, Vol. 1, Mexico, pp. 391-399.

Tai, T., 1970, "Strength and Deformation Characteristics of Cohesionless Materials at High Pressures," Ph.D. dissertaion, Duke University.

Taylor, D.W., 1948, "*Fundamentals of Soil Mechanics*," Wiley, New York.

Terzaghi, K., 1920, "Old Earth Pressure Theories and New Test Results," *Engineering News Record*, Vol. 85, pp. 632.

Terzaghi, K., and Peck, R.B., 1948, *Soil Mechanics in Engineering Practice*, pp. 65-67.

Townsend, F.C., 1979, "Liquefaction Potential of a Sand Under Static and Dynamic Loadings," *Proceedings of the Sixth Panamerican Converence on Soil Mechanics and Foundation Engineering*, Lima, Peru, December, Vol. II, pp. 139-150.

Vesic, A.S., and Barksdale, R.D., 1963, "Discussion: Shear Strength at High Pressures," *Laboratory Shear Testing of Soils, ASTM STP 361*, ASTM, pp. 301-305.

Vesic, A.S., and Clough, G.W., 1968, "Behavior of Granular Materials Under High Stresses," *Journal of the Soil Mechanics and Foundations Division*, ASCE, Vol. 94, No. SM3, May, pp. 661-688.

Whitman R.V., and Healy K.A. 1962, "Shear Strength of Sands During Rapid Loadings." *Journal of the Soil Mechanics and Foundations Division*, ASCE, Vol. 88, No. SM 2, pp. 99-132.

Wu, W., and Kolymbas, D., 1991, "On Some Issues in Triaxial Extension Tests," *Geotechnical Testing Journal*, GTJODG, Vol. 14, No. 3, September, pp. 276-287.

Wood, D.M., 1990, *Soil Behaviour and Critical State Soil Mechanics*, Cambridge University Press, Cambridge, pp. 139-173.

Yamada, Y., and Ishihara, K., 1979, "Anisotropic Deformation Characteristics of Sand Under Three Dimensional Stress Conditions," *Soils and Foundations*, Vol. 19, No. 2, June, pp. 79-91.

Yamamuro, J.A., 1990, "Controlling High-Pressure Triaxial Tests Under Stress and Strain Control Using a Microcomputer," Masters thesis, University of California, Los Angeles, 287 pp.

Yamamuro, J.A., and Lade, P.V., 1992a, "The Effective Stress Path for Soil at High Pressure," *Proceedings of the 9th Engineering Mechanics Conference*, ASCE, College Station, Texas, May, pp. 729-732.

Yamamuro, J.A., and Lade, P.V., 1993b, "Effects of Strain Rate on Instability of Granular Soils," submitted to*Geotechnical Testing Journal*, ASTM.

Yamamuro, J.A., and Lade, P.V., 1993c, "B-Value Measurements for Granular Materials at High Confining Pressures," submitted to *Geotechnical Testing Journal*, ASTM.

TABLE OF CONTENTS OF APPENDICES

A. EQUATIONS USED IN DATA ANALYSIS 462

B. SUMMARY OF TESTING DATA 467

Description of Summary 468
Basic Testing Parameters in Triaxial Compression Tests 470
Basic Testing Parameters in Triaxial Extension Tests 473
Other Testing Information About Triaxial Compression Tests 477
Other Testing Information About Triaxial Extension Tests 480
Summary of Results from Drained Triaxial Compression Tests . . . 483
Summary of Results from Undrained
Triaxial Compression & Other Tests 485
Summary of Results from Drained Triaxial Extension Tests 487
Summary of Results from Undrained
Triaxial Extension & Other Tests 490
Void Ratios in Triaxial Compression Tests 491
Void Ratios in Triaxial Extension Tests 494
Failure Energy in Drained Triaxial Compression Tests 497
Failure Energy in Undrained Triaxial
Compression & Other Tests 499
Failure Energy in Drained Triaxial Extension Tests 501
Failure Energy in Undrained Triaxial
Extension & Other Tests 504
End of Test Energy in Triaxial Compression Tests 505
End of Test Energy in Triaxial Extension Tests 508
Stress-Dilatancy in Drained Triaxial Compression Tests 512
Stress-Dilatancy in Drained Triaxial Extension Tests 514
Crushing Parameters in Triaxial Compression Test 516
Crushing Parameters in Triaxial Extension Tests 519
Soil Compressibility and B-value 522
Derived Elastic Parameters from
Test CDLU3 for Cambria Sand 523
Sieve Analyses for Drained Triaxial Compression Tests 524
Sieve Analyses for Undrained Triaxial Compression Tests 526
Sieve Analyses for Drained Triaxial Extension Tests 527
Sieve Analyses for Undrained Triaxial Extension Tests 531
Sieve Analyses for Other Tests 532
Initial Gradation of Cambria Sand 533

C. DRAINED TRIAXIAL COMPRESSION TESTS 534

D. UNDRAINED TRIAXIAL COMPRESSION TESTS 564

E. DRAINED/UNDRAINED STABILITY TESTS IN TRIAXIAL COMPRESSION 587

F. SUCCESSFUL DRAINED UNIFORM STRAIN TRIAXIAL EXTENSION TESTS 593

G. DRAINED CONVENTIONAL TRIAXIAL EXTENSION TESTS 620

H. DRAINED UNIFORM STRAIN TRIAXIAL EXTENSION TESTS WITH STRAIN LOCALIZATION 644

I. SUCCESSFUL UNDRAINED UNIFORM STRAIN TRIAXIAL EXTENSION TESTS 659

J. UNDRAINED UNIFORM STRAIN TRIAXIAL EXTENSION TESTS WITH STRAIN LOCALIZATION 665

K. SUCCESSFUL DRAINED/UNDRAINED UNIFORM STRAIN STABILITY TESTS IN TRIAXIAL EXTENSION 674

L. ISOTROPIC COMPRESSION/B-VALUE TESTS 679

M. ONE-DIMENSIONAL COMPRESSION TESTS ON THREE SANDS 698

N. DRAINED TRIAXIAL COMPRESSION LOADING/UNLOADING TEST . . 712

APPENDIX A

EQUATIONS USED IN DATA ANALYSIS

A.1 Triaxial Compression Tests

The equations used in the triaxial compression tests in this study are as follows.

Major principal strain in compression.

$$\epsilon_1 = \frac{\Delta H}{H_c}$$

ϵ_1 = *axial strain.*
ΔH = *change in height.*
H_c = *height after consolidation.*

Area correction of test specimen in compression.

$$A = A_c \frac{1 - \epsilon_v}{1 - \epsilon_1}$$

A = *area of specimen.*
A_c = *area of specimen after consolidation.*
ϵ_v = *volumetric strain.*
ϵ_1 = *axial strain.*

Volumetric strain in compression.

$$\epsilon_v = \frac{\Delta V}{V_c}$$

ϵ_v = *volumetric strain.*
ΔV = *change in volume.*
V_c = *volume after consolidation.*

Deviator stress in compression.

$$\sigma_1 - \sigma_3 = \frac{P - F - M - PU}{A}$$

$\sigma_1 - \sigma_3$ = *deviator stress.*
P = *force measured by load cell.*
F = *piston friction.*
M = *force in membrane.*
PU = *uplift force on piston from cell pressure.*

Effective principal stress ratio in compression.

$$\frac{\sigma_1'}{\sigma_3'} = \frac{(\sigma_1 - \sigma_3) + (CP - U)}{(CP - U)}$$

$\frac{\sigma_1'}{\sigma_3'}$ = *effective stress ratio.*
$\sigma_1 - \sigma_3$ = *deviator stress.*
CP = *total cell pressure.*
U = *pore pressure.*

Effective mean normal stress in compression.

$$p' = \frac{(\sigma_1 - \sigma_3)}{3} + CP - U$$

P' = *effective mean normal stress.*
$\sigma_1 - \sigma_3$ = *deviator stress.*
CP = *total cell pressure.*
U = *pore pressure.*

Mohr-Coulomb, secant, effective stress friction angle in compression.

$$\sin \phi' = \frac{\frac{\sigma_1'}{\sigma_3'} - 1}{\frac{\sigma_1'}{\sigma_3'} + 1}$$

ϕ' = *effective stress friction angle.*
$\frac{\sigma_1'}{\sigma_3'}$ = *effective stress ratio.*

A.2 Triaxial Extension Tests

Minor principal strain in extension.

$$\varepsilon_3 = \frac{\Delta H}{H_c}$$

ε_3 = *axial strain.*
ΔH = *change in height(negative).*
H_c = *height after consolidation.*

Area correction for test specimen in extension.

$$A = A_c \frac{1 - \varepsilon_v}{1 - \varepsilon_3}$$

A = *area of specimen.*
A_c = *area of specimen after consolidation.*
ε_v = *volumetric strain.*
ε_3 = *axial strain(negative).*

Volumetric strain in extension.

$$\varepsilon_v = \frac{\Delta V}{V_c}$$

ε_v = *volumetric strain.*
ΔV = *change in volume.*
V_c = *volume after consolidation.*

Major principal strain in extension.

$$\varepsilon_1 = \frac{\varepsilon_v - \varepsilon_3}{2}$$

ε_1 = *major principal strain.*
ε_v = *Volumetric strain.*
ε_3 = *minor principal strain(negative).*

Deviator stress in extension.

$$\sigma_1 - \sigma_3 = \frac{P + F + M + PU}{A}$$

$\sigma_1 - \sigma_3$ = *deviator stress.*
P = *force(negative) measured by load cell.*
F = *piston friction.*
M = *force in membrane.*
PU = *uplift force on piston from cell pressure.*

Effective principal stress ratio in extension.

$$\frac{\sigma_1'}{\sigma_3'} = \frac{(CP - U)}{(CP - U) - (\sigma_1 - \sigma_3)}$$

$\frac{\sigma_1'}{\sigma_3'}$ = *effective stress ratio.*
$\sigma_1 - \sigma_3$ = *deviatorstress.*
CP = *total cell pressure.*
U = *pore pressure.*

Effective mean normal stress in extension.

$$p' = \frac{(\sigma_1 - \sigma_3)}{3} + CP - U$$

P' = *mean normal stress.*
$\sigma_1 - \sigma_3$ = *deviator stress(negative).*
CP = *total cell pressure.*
U = *pore pressure.*

Mohr-Coulomb, secant, effective stress friction angle in extension.

$$\sin \phi' = \frac{\frac{\sigma_1'}{\sigma_3'} - 1}{\frac{\sigma_1'}{\sigma_3'} + 1}$$

ϕ' = *effective stress friction angle.*
$\frac{\sigma_1'}{\sigma_3'}$ = *effective stress ratio.*

APPENDIX B

DESCRIPTION OF SUMMARY

The following appendices uses several letter code designations to decribe the type of test and the results. The first code is the test identification itself.

CD - Consolidated-Drained triaxial compression test with constant effective confining pressure.

CU - Consolidated-Undrained triaxial compression test with constant total confining pressure.

CUCM - Consolidated-Undrained triaxial compression test with either constant total mean normal stress or decreasing total mean normal stress.

CSTAB - Consolidated-Drained/Undrained stability test in triaxial compression with constant total confining pressure.

TCT - Low pressure triaxial compression tests with constant effective confining pressure performed by Brian D. Skyers.

ISO - Isotropic compression/B-value test.

ECD - Consolidated-Drained triaxial Extension test with constant effective confining pressure.

ECU - Consolidated-Undrained triaxial Extension test with constant total confining pressure.

ESTAB - Consolidated-Drained/Undrained stability test in triaxial extension with constant total confining pressure.

1D - One-Dimensional compression test. Following letters refer to type of sand employed in the test.

CDLU - Consolidated-Drained Loading/Unloading test in triaxial compression at five different confining pressures on Cambria sand.

The second letter code is employed in the tables in the following appendices to further describe the individual test.

CS - Cambria Sand was used in test.

G - Successful test.

BK - The test specimen buckled during test.

SL - The test specimen slipped on the lubricated ends during test.

Q - Quartz sand was used in test.

T - Test was terminated prior to failure.

U - Uniform strain extension test with steel plates surrounding specimen.

C - Conventional extension test with only membranes surrounding specimen.

UP - Extension test experiencing cap uplift problem.

B - Unsuccessful uniform strain extension test.

F - Extension test where friction between soil and steel plates was experienced.

APPENDIX B TABLE 1
BASIC TESTING PARAMETERS IN TRIAXIAL COMPRESSION TESTS

Test	Test Type	σ_{3i}' MPa	H/D	Deformation Rate cm/hr
	Drained Tests			
CD1	CS/G	16.89	2.50	2.54
CD3	CS/G	2.22	2.51	2.54
CD4	CS/G	2.11	2.50	2.54
CD5	CS/G	4.14	2.51	2.54
CD6	CS/G	5.85	2.49	2.54
CD7	CS/G	4.00	2.53	2.54
CD8	CS/G	11.48	2.53	2.54
CD9	CS/G	15.00	2.52	2.54
CD10	CS/G	15.00	2.54	2.54
CD12	CS/G	5.85	2.50	2.54
CD13	CS/G	4.50	2.51	2.54
CD14	CS/G	3.50	2.53	2.54
CD15	CS/G	11.50	2.50	2.54
CD16	CS/G	17.23	2.50	2.54
CD17	CS/G	26.00	2.50	2.54
CD19	CS/G	40.00	2.50	2.54
CD20	CS/G	8.00	2.51	3.81
CD21	CS/G	17.23	2.50	7.62
CD22	CS/G	17.23	2.50	0.53
CD23	CS/G	17.23	2.51	7.62
CD24	CS/BK	52.00	2.51	1.27
CD25	CS/G	52.00	2.50	2.54
CD27	CS/BK	60.00	2.50	2.54
CD28	CS/SL	60.00	1.86	2.54
CD29	CS/G	47.01	1.87	2.56
CD30	Q/G	17.23	1.86	2.54
CD31	Q/G	35.00	1.86	2.54

APPENDIX B TABLE 1
BASIC TESTING PARAMETERS IN TRIAXIAL COMPRESSION TESTS

Test	Test Type	σ_{3i}' MPa	H/D	Deformation Rate cm/hr
CD32	Q/G	52.00	1.86	2.54
CD33	Q/G	26.00	1.84	2.54
CD34	Q/G	12.00	1.83	2.54
TCT2	CS/G	0.39	2.50	
TCT3	CS/G	0.39	2.50	
TCT4	CS/G	0.20	2.50	
TCT6	CS/G	0.05	2.50	
TCT9	CS/G	0.20	2.50	
	Undrained Tests			
CU3	CS/G	16.68	2.52	2.54
CU4	CS/G	16.71	2.55	2.54
CU6	CS/G	16.89	2.53	2.54
CU12	CS/T	61.65	2.52	2.54
CU13	CS/G	61.65	2.50	2.54
CU14	CS/G	34.01	2.50	2.54
CU15	CS/G	6.45	2.50	2.54
CU17	CS/G	68.92	2.51	2.54
CU19	CS/G	52.00	2.51	2.54
CU20	CS/G	43.00	2.51	2.54
CU21	CS/G	34.01	2.51	2.54
CU22	CS/G	34.01	2.50	7.62
CU23	CS/G	34.01	2.50	0.55
CU25	CS/T	34.01	2.50	0.05
CU26	CS/T	34.01	2.50	0.53
CU27	CS/T	34.01	2.53	0.05
CU32	CS/G	34.01	2.50	1.16
CU33	CS/G	34.01	2.50	0.26
CU10	CS/T	34.01	NA	NA

APPENDIX B TABLE 1
BASIC TESTING PARAMETERS IN TRIAXIAL COMPRESSION TESTS

Test	Test Type	σ_{3i}' MPa	H/D	Deformation Rate cm/hr
CU16	CS/T	69.50	NA	NA
	Undrained Tests with Different Total Stress Paths			
CUCM1	CS/G	48.26	2.51	2.54
CUCM3	CS/G	52.00	2.51	2.54
CUCM4	CS/G	34.01	2.51	2.54
CUCM5	CS/G	34.01	2.50	0.64
	Drained/Undrained Stability Tests			
CSTAB2	CS/G	17.23	2.51	2.54
CSTAB3	CS/S	17.23	2.50	2.54
CSTAB4	CS/G	17.23	2.49	2.54
CSTAB5	CS/G	17.23	2.51	2.54
CSTAB6	CS/G	17.23	NA	NA
CSTAB7	CS/G	26.00	2.50	2.54
	Isotropic Compression/B-Value Tests			
ISO4	CS/G	NA	2.51	NA
ISO6	CS/G	NA	2.50	NA
ISO7	CS/G	NA	2.50	NA

APPENDIX B TABLE 2
BASIC TESTING PARAMETERS IN TRIAXIAL EXTENSION TESTS

Test	Test Type	σ_{11}' MPa	H/D	Deformation Rate cm/hr
	Successful Drained Uniform Strain Tests			
ECD36	CS/U/G	2.22	1.91	1.02
ECD39	CS/U/G	6.00	1.89	1.02
ECD40	CS/U/G	12.00	1.89	1.02
ECD48	CS/U/G	10.00	1.89	1.02
ECD49	CS/U/G	14.50	1.88	1.02
ECD50	CS/U/G	68.00	1.93	1.02
ECD52	CS/U/G	8.00	1.90	1.02
ECD54	CS/U/G	26.00	1.90	1.02
ECD70	CS/U/G	17.50	1.90	1.02
ECD72	CS/U/G	24.00	1.90	1.02
ECD74	CS/U/G	25.01	1.90	1.27
ECD75	CS/U/G	26.00	2.00	1.27
ECD79	CS/U/G	0.50	1.92	2.54
ECD81	CS/U/G	0.25	1.94	2.54
ECD83	CS/U/G	1.00	2.05	2.54
ECD84	CS/U/G	26.00	2.03	1.27
ECD85	CS/U/G	4.00	2.03	1.27
ECD86	CS/U/G	22.00	2.02	1.27
ECD87	CS/U/G	17.50	2.03	1.27
ECD88	CS/U/G	8.00	1.95	1.27
ECD92	CS/U/G	17.50	2.05	1.27
ECD93	CS/U/G	35.00	2.15	1.40
ECD94	CS/U/G	42.00	2.14	1.40
ECD95	CS/U/G	52.00	2.15	1.40
	Drained Conventional Tests with Strain Localization			
ECD2	CS/C	4.00	1.88	1.91

APPENDIX B TABLE 2
BASIC TESTING PARAMETERS IN TRIAXIAL EXTENSION TESTS

Test	Test Type	σ_{1i}' MPa	H/D	Deformation Rate cm/hr
ECD7	CS/C/UP	8.00	1.87	0.64
ECD8	CS/C	8.00	1.87	0.89
ECD9	CS/C	17.50	1.90	1.02
ECD10	CS/C	35.00	1.90	1.27
ECD11	CS/C	17.50	1.91	1.91
ECD12	CS/C	17.50	1.88	1.27
ECD15	CS/C/T	17.50	1.87	1.27
ECD16	CS/C	17.50	1.87	1.27
ECD17	CS/C	17.50	1.87	1.27
ECD18	CS/C/T	17.50	1.87	1.27
ECD19	CS/C/T	17.50	1.87	1.27
ECD20	CS/C/T	17.50	1.87	1.27
ECD21	CS/C	17.50	1.87	1.27
ECD25	CS/C	68.00	1.88	1.27
ECD28	CS/C	68.00	1.88	1.27
ECD29	CS/C	52.00	1.88	1.27
ECD30	CS/C	52.00	1.89	1.27
ECD31	CS/C	42.00	1.89	1.27
ECD76	CS/C	1.00	1.90	2.54
ECD77	CS/C	0.50	1.92	2.54
ECD78	CS/C	0.25	1.93	2.54
	Drained Uniform Strain Tests with Strain Localization			
ECD34	CS/U/B	4.00	1.88	1.02
ECD35	CS/U/B	4.00	1.88	1.02
ECD37	CS/U/B	8.00	1.90	1.02
ECD38	CS/U/B	17.50	1.90	1.02
ECD41	CS/U/B	17.50	1.90	1.02

APPENDIX B TABLE 2
BASIC TESTING PARAMETERS IN TRIAXIAL EXTENSION TESTS

Test	Test Type	σ_{1i}' MPa	H/D	Deformation Rate cm/hr
ECD42	CS/U/B	35.00	1.90	1.27
ECD43	CS/U/B	35.00	1.90	1.27
ECD55	CS/U/B/F	26.00	1.88	1.02
ECD58	CS/U/B/F	35.00	1.87	1.02
ECD62	CS/U/B/F	17.50	1.89	1.02
ECD63	CS/U/B/F	12.00	1.90	1.02
ECD65	CS/U/B	12.00	1.90	1.02
ECD66	CS/U/B	17.50	1.89	1.02
ECD73	CS/U/B	26.00	1.95	1.14
	Successful Undrained Uniform Strain Tests			
ECU8	CS/U/G	42.00	2.03	1.14
ECU9	CS/U/G	17.57	2.04	1.14
ECU10	CS/U/G	26.00	2.04	1.14
ECU11	CS/U/G	12.00	2.04	1.27
ECU12	CS/U/G	52.00	2.14	1.27
	Undrained Uniform Strain Tests with Strain Localization			
ECU2	CS/U/B	17.57	1.93	1.02
ECU3	CS/U/B	35.00	1.93	1.14
ECU4	CS/U/B	52.00	1.93	1.14
ECU5	CS/U/B	68.00	2.03	1.14
ECU6	CS/U/B	12.00	1.93	1.14
ECU7	CS/U/B	26.00	1.92	1.14
ECU13	CS/U/B	68.00	2.13	1.27
ECU14	CS/U/B	68.00	2.13	1.27

APPENDIX B TABLE 2
BASIC TESTING PARAMETERS IN TRIAXIAL EXTENSION TESTS

Test	Test Type	σ_{1i}' MPa	H/D	Deformation Rate cm/hr
	Successful Drained/Undrained Uniform Strain Stability Tests			
ESTAB2	CS/U/G	17.57	2.03	1.27
ESTAB3	CS/U/G	17.57	2.03	1.14
ESTAB4	CS/U/G	26.00	2.03	1.14
ESTAB5	CS/U/G	35.00	2.03	1.14

APPENDIX B TABLE 3
OTHER TESTING INFORMATION ABOUT TRIAXIAL COMPRESSION TESTS

Test	Test Type	Initial Volume cm^3	Weight of Soil gm	Backpressure MPa
	Drained Tests			
CD1	CS/G	705.32	1250.00	NA
CD3	CS/G	708.34	1260.00	NA
CD4	CS/G	704.91	1260.00	NA
CD5	CS/G	710.47	1260.00	NA
CD6	CS/G	710.97	1260.00	NA
CD7	CS/G	713.99	1260.00	NA
CD8	CS/G	718.56	1260.00	NA
CD9	CS/G	711.98	1275.00	NA
CD10	CS/G	717.43	1275.00	NA
CD12	CS/G	709.46	1260.00	NA
CD13	CS/G	711.99	1260.00	NA
CD14	CS/G	716.01	1260.00	NA
CD15	CS/G	711.48	1260.00	NA
CD16	CS/G	711.48	1260.00	NA
CD17	CS/G	713.00	1260.00	NA
CD19	CS/G	711.48	1260.00	NA
CD20	CS/G	707.84	1250.00	NA
CD21	CS/G	707.33	1250.00	NA
CD22	CS/G	707.34	1250.00	NA
CD23	CS/G	708.34	1250.00	NA
CD24	CS/BK	708.85	1250.00	NA
CD25	CS/G	707.33	1250.00	NA
CD27	CS/BK	707.33	1250.00	NA
CD28	CS/SL	510.47	900.00	NA
CD29	CS/G	510.31	900.00	NA
CD30	Q/G	505.76	800.00	NA
CD31	Q/G	504.78	800.00	NA
CD32	Q/G	504.78	800.00	NA

APPENDIX B TABLE 3
OTHER TESTING INFORMATION ABOUT TRIAXIAL COMPRESSION TESTS

Test	Test Type	Initial Volume cm^3	Weight of Soil gm	Backpressure MPa
CD33	Q/G	502.77	800.00	NA
CD34	Q/G	504.83	800.00	NA
TCT2	CS/G	767.24	1301.11	NA
TCT3	CS/G	744.28	1301.11	NA
TCT4	CS/G	752.64	1300.50	NA
TCT6	CS/G	749.68	1301.00	NA
TCT9	CS/G	751.43	1301.06	NA
	Undrained Tests			
CU3	CS/G	712.48	1249.38	0.55
CU4	CS/G	716.46	1260.00	0.52
CU6	CS/G	721.14	1270.00	0.34
CU12	CS/T	717.06	1260.00	0.45
CU13	CS/G	711.48	1260.00	0.45
CU14	CS/G	708.95	1260.00	0.45
CU15	CS/G	709.46	1260.00	0.55
CU17	CS/G	711.48	1260.00	0.55
CU19	CS/G	710.36	1250.00	0.45
CU20	CS/G	708.85	1250.00	0.45
CU21	CS/G	708.34	1250.00	0.52
CU22	CS/G	707.33	1265.00	0.14
CU23	CS/G	706.33	1260.00	0.33
CU25	CS/T	706.33	1250.00	0.48
CU26	CS/T	707.33	1250.00	0.48
CU27	CS/T	707.33	1250.00	0.52
CU32	CS/G	706.33	1220.00	0.52
CU33	CS/G	706.33	1220.00	0.52
CU10	CS/T	713.34	1260.00	0.52
CU16	CS/T	711.48	1260.00	0.52
	Undrained Tests with Different Total Stress Paths			

APPENDIX B TABLE 3
OTHER TESTING INFORMATION ABOUT TRIAXIAL COMPRESSION TESTS

Test	Test Type	Initial Volume cm^3	Weight of Soil gm	Backpressure MPa
CUCM1	CS/G	708.85	1250.00	0.52
CUCM3	CS/G	709.35	1250.00	0.45
CUCM4	CS/G	710.36	1250.00	0.52
CUCM5	CS/G	707.33	1250.00	0.52
	Drained/Undrained Stability Tests			
CSTAB2	CS/G	708.35	1250.00	0.52
CSTAB3	CS/SL	706.33	1250.00	0.52
CSTAB4	CS/G	706.16	1250.00	0.52
CSTAB5	CS/G	708.34	1250.00	0.52
CSTAB6	CS/G	706.33	1250.00	0.52
CSTAB7	CS/G	707.33	1250.00	0.52
	Isotropic Compression Tests			
ISO4	CS/G	708.34	1250.00	0.50
ISO6	CS/G	706.33	1250.00	0.48
ISO7	CS/G	707.33	1250.00	0.52

APPENDIX B TABLE 4
OTHER TESTING INFORMATION ABOUT TRIAXIAL EXTENSION TESTS

Test	Test Type	Initial Volume cm^3	Weight of Soil gm	Backpressure MPa
	Successful Drained Uniform Strain Tests			
ECD36	CS/U/G	521.91	920.00	NA
ECD39	CS/U/G	516.97	915.00	NA
ECD40	CS/U/G	517.47	915.00	NA
ECD48	CS/U/G	514.00	910.00	NA
ECD49	CS/U/G	514.50	910.00	NA
ECD50	CS/U/G	513.36	910.00	NA
ECD52	CS/U/G	519.44	910.00	NA
ECD54	CS/U/G	519.44	915.00	NA
ECD70	CS/U/G	532.88	940.00	NA
ECD72	CS/U/G	533.89	940.00	NA
ECD74	CS/U/G	534.89	940.00	NA
ECD75	CS/U/G	563.04	995.00	NA
ECD79	CS/U/G	566.28	995.00	NA
ECD81	CS/U/G	565.09	995.00	NA
ECD83	CS/U/G	513.06	900.00	NA
ECD84	CS/U/G	554.00	980.00	NA
ECD85	CS/U/G	555.31	980.00	NA
ECD86	CS/U/G	551.37	980.00	NA
ECD87	CS/U/G	554.00	980.00	NA
ECD88	CS/U/G	531.98	940.00	NA
ECD92	CS/U/G	559.26	990.00	NA
ECD93	CS/U/G	581.40	1030.00	NA
ECD94	CS/U/G	583.21	1030.00	NA
ECD95	CS/U/G	581.39	1030.00	NA
	Drained Conventional Tests with Strain Localization			NA
ECD2	CS/C	515.49	910.00	NA
ECD7	CS/C/UP	512.50	900.00	NA
ECD8	CS/C	512.52	900.00	NA

APPENDIX B TABLE 4
OTHER TESTING INFORMATION ABOUT TRIAXIAL EXTENSION TESTS

Test	Test Type	Initial Volume cm^3	Weight of Soil gm	Backpressure MPa
ECD9	CS/C	520.92	910.00	NA
ECD10	CS/C	520.92	920.00	NA
ECD11	CS/C	523.39	920.00	NA
ECD12	CS/C	515.00	910.00	NA
ECD15	CS/C/T	510.55	900.00	NA
ECD16	CS/C	511.54	900.00	NA
ECD17	CS/C	511.54	900.00	NA
ECD18	CS/C/T	511.54	900.00	NA
ECD19	CS/C/T	511.54	900.00	NA
ECD20	CS/C/T	510.55	900.00	NA
ECD21	CS/C	511.54	900.00	NA
ECD25	CS/C	515.49	910.00	NA
ECD28	CS/C	515.49	910.00	NA
ECD29	CS/C	514.50	910.00	NA
ECD30	CS/C	516.48	915.00	NA
ECD31	CS/C	517.47	920.00	NA
ECD76	CS/C	557.69	980.00	NA
ECD77	CS/C	566.01	995.00	NA
ECD78	CS/C	568.97	1000.00	NA
	Drained Uniform Strain Tests with Strain Localization			
ECD34	CS/U/B	513.52	910.00	NA
ECD35	CS/U/B	514.50	910.00	NA
ECD37	CS/U/B	520.92	915.00	NA
ECD38	CS/U/B	519.94	915.00	NA
ECD41	CS/U/B	518.45	915.00	NA
ECD42	CS/U/B	520.92	915.00	NA
ECD43	CS/U/B	520.92	910.00	NA
ECD55	CS/U/B/F	527.85	930.00	NA
ECD58	CS/U/B/F	526.85	930.00	NA

APPENDIX B TABLE 4
OTHER TESTING INFORMATION ABOUT TRIAXIAL EXTENSION TESTS

Test	Test Type	Initial Volume cm^3	Weight of Soil gm	Backpressure MPa
ECD62	CS/U/B/F	52w87	930.00	NA
ECD63	CS/U/B/F	532.88	940.00	NA
ECD65	CS/U/B	532.88	940.00	NA
ECD66	CS/U/B	528.08	940.00	NA
ECD73	CS/U/B	534.89	940.00	NA
	Successful Undrained Uniform Strain Tests			
ECU8	CS/U/G	552.99	980.00	0.52
ECU9	CS/U/G	554.96	980.00	0.52
ECU10	CS/U/G	555.94	980.00	0.52
ECU11	CS/U/G	555.94	980.00	0.52
ECU12	CS/U/G	579.42	1025.00	0.53
	Undrained Uniform Strain Tests with Strain Localization			
ECU2	CS/U/B	527.34	928.00	0.52
ECU3	CS/U/B	524.46	920.00	0.52
ECU4	CS/U/B	524.46	930.00	0.52
ECU5	CS/U/B	551.02	968.50	0.52
ECU6	CS/U/B	525.44	925.50	0.52
ECU7	CS/U/B	579.42	1025.00	0.52
ECU13	CS/U/B	584.33	1030.00	0.52
ECU14	CS/U/B	580.54	1025.00	0.52
	Successful Drained/Undrained Uniform Strain Stability Tests			
ESTAB2	CS/U/G	553.34	980.00	0.52
ESTAB3	CS/U/G	554.00	980.00	0.53
ESTAB4	CS/U/G	553.20	980.00	0.52
ESTAB5	CS/U/G	554.19	980.00	0.53

APPENDIX P TABLE 5
SUMMARY OF RESULTS FROM DRAINED TRIAXIAL COMPRESSION TESTS

Test	Test Type	ϕ' degree	ϵ_{1f} %	ϵ_{vf} %	$(\sigma_1-\sigma_3)_f$ MPa	$(\sigma_1'/\sigma_3')_f$	p_f' MPa
CD1	CS/G	33.7	36.57	14.66	41.65	3.49	29.78
CD3	CS/G	34.4	12.14	-0.37	5.77	3.59	4.15
CD4	CS/G	34.8	9.87	-0.43	5.52	3.66	3.98
CD5	CS/G	32.5	28.68	5.74	8.61	3.32	6.56
CD6	CS/G	32.9	31.30	9.80	13.92	3.38	9.89
CD7	CS/G	32.6	29.33	5.69	9.36	3.34	7.04
CD8	CS/G	33.7	36.29	15.09	28.70	3.50	21.05
CD9	CS/G	33.3	36.79	14.72	36.45	3.43	27.04
CD10	CS/G	33.7	36.59	15.13	37.50	3.50	27.36
CD12	CS/G	33.4	34.08	10.43	14.33	3.45	10.59
CD13	CS/G	32.5	32.03	7.70	10.31	3.32	7.92
CD14	CS/G	33.3	25.91	5.28	8.54	3.44	6.28
CD15	CS/G	34.0	34.36	14.37	29.2[illegible]	3.54	21.02
CD16	CS/G	33.8	35.38	14.94	43.25	3.51	31.57
CD17	CS/G	33.7	33.53	14.11	64.74	3.49	47.60
CD19	CS/G	33.3	32.23	12.00	97.60	3.44	72.63
CD20	CS/G	33.1	33.90	12.56	19.28	3.41	14.43
CD21	CS/G	33.9	35.92	14.80	43.40	3.52	31.70
CD22	CS/G	33.6	35.00	15.30	42.47	3.48	31.47
CD23	CS/G	34.2	36.98	14.86	43.40	3.57	31.70
CD24	CS/BK	NA	NA	NA	NA	NA	NA
CD25	CS/G	33.5	32.54	10.91	127.90	3.46	94.57
CD27	CS/BK	NA	NA	NA	NA	NA	NA
CD28	CS/SL	NA	NA	NA	NA	NA	NA
CD29	CS/G	33.2	37.21	11.04	113.89	3.42	85.02
CD30	Q/G	33.8	37.30	14.37	43.27	3.51	31.66
CD31	Q/G	33.5	36.76	10.84	86.52	3.47	63.89
CD32	Q/G	33.8	34.68	9.31	130.85	3.51	95.69
CD33	Q/G	33.7	37.08	12.07	64.74	3.49	47.58

APPENDIX B TABLE 5
SUMMARY OF RESULTS FROM DRAINED TRIAXIAL COMPRESSION TESTS

Test	Test Type	ϕ' degree	ϵ_{1f} %	ϵ_{vf} %	$(\sigma_1-\sigma_3)_f$ MPa	$(\sigma_1'/\sigma_3')_f$	p_f' MPa
CD34	Q/G	33.3	37.93	15.42	29.19	3.43	21.73
TCT2	CS/G	37.8	7.12	-2.68	1.24	4.16	0.68
TCT3	CS/G	38.3	5.57	-2.03	1.28	4.26	0.69
TCT4	CS/G	37.9	4.74	-1.92	0.62	4.19	0.34
TCT6	CS/G	41.3	3.48	-2.30	0.19	4.88	0.10
TCT9	CS/G	39.5	4.47	-1.93	0.69	4.50	0.36

APPENDIX B TABLE 6
SUMMARY OF RESULTS FROM UNDRAINED TRIAXIAL COMPRESSION
& OTHER TESTS

Test	Test Type	ϕ' deg.	ϵ_{1f} / ϵ_{1dev} %	u_f /u_{dev} MPa	Max. Dev. Stress MPa	Max. Effect. Stress Ratio	p_f' MPa
CU3	CS/G	34.2	19.37/10.92	14.53/14.24	7.54	3.57	5.00
CU4	CS/G	34.7	22.85/8.84	14.76/14.18	7.49	3.65	4.65
CU6	CS/G	34.3	22.94/1.62	14.71/11.15	7.79	3.58	4.71
CU12	CS/T	35.4	17.30/2.50	56.09/39.15	24.47	3.75	11.54
CU13	CS/G	35.0	24.68/2.15	56.24/37.80	24.95	3.69	11.11
CU14	CS/G	35.4	21.72/1.88	31.33/22.47	13.61	3.75	6.04
CU15	CS/G	33.4	20.50/10.19	4.56/4.18	6.70	3.45	4.44
CU17	CS/G	35.6	22.12/2.52	62.28/44.02	28.68	3.78	13.83
CU19	CS/G	35.6	23.74/2.32	47.96/33.65	20.49	3.78	8.68
CU20	CS/G	35.6	21.92/2.36	39.69/28.60	16.90	3.79	7.31
CU21	CS/G	35.8	21.88/2.43	31.43/23.91	13.48	3.82	6.08
CU22	CS/G	34.5	18.52/2.38	30.55/1.92	13.47	3.61	6.72
CU23	CS/G	34.0	12.20/1.96	30.76/22.38	12.89	3.53	6.62
CU25	CS/T	NA	NA/1.95	NA/23.18	12.56	NA	NA
CU26	CS/T	36.0	24.64/2.03	31.14/22.53	12.91	3.86	5.59
CU27	CS/T	NA	NA/1.84	NA/23.42	12.45	NA	NA
CU32	CS/G	35.8	24.58/2.34	31.50/22.66	12.95	3.82	5.87
CU33	CS/G	36.2	28.27/2.12	31.15/23.25	12.83	3.89	5.63
CU10	CS/T	NA	NA/NA	NA/NA	NA	NA	NA
CU16	CS/T	NA	NA/NA	NA/NA	NA	NA	NA
	Undrained Tests with Different Total Stress Paths						
CUCM1	CS/G	35.6	23.73/2.47	43.73/25.18	20.18	3.79	8.69
CUCM3	CS/G	36.0	24.12/2.26	43.89/26.83	20.24	3.85	8.68
CUCM4	CS/G	35.7	22.04/2.05	28.46/18.14	13.50	3.80	6.05
CUCM5	CS/G	36.3	21.97/2.44	25.45/16.09	13.23	3.90	6.08

APPENDIX B TABLE 6
SUMMARY OF RESULTS FROM UNDRAINED TRIAXIAL COMPRESSION & OTHER TESTS

Test	Test Type	ϕ' deg.	ϵ_{1f} / ϵ_{1dev} %	u_f / u_{dev} MPa	Max. Dev. Stress MPa	Max. Effect. Stress Ratio	p_f' MPa
	Drained/Undrained Stability Tests						
CSTAB2	CS/G	35.3	29.96/15.69	13.84/0.52	28.96	3.73	11.86
CSTAB3	CS/SL	32.6	19.97/10.72	14.00/0.52	22.44	3.34	9.51
CSTAB4	CS/G	34.5	31.72/24.63	7.84/0.52	37.83	3.62	21.26
CSTAB5	CS/G	34.7	27.26/5.60	14.72/0.52	14.97	3.64	5.70
CSTAB6	CS/G	NA	NA/NA	NA/NA	NA	NA	NA
CSTAB7	CS/G	35.3	24.00/5.55	22.28/0.52	20.13	3.73	8.10
	Isotropic Compression Tests						
ISO4	CS/G	NA	NA/NA	NA/NA	NA	NA	NA
ISO6	CS/G	NA	NA/NA	NA/NA	NA	NA	NA
ISO7	CS/G	NA	NA/NA	NA/NA	NA	NA	NA

APPENDIX B TABLE 7
SUMMARY OF RESULTS FROM DRAINED TRIAXIAL EXTENSION TESTS

Test	Test Type	ϕ' degree	ϵ_{3f} %	ϵ_{vf} %	$(\sigma_1-\sigma_3)_f$ MPa	$(\sigma_1'/\sigma_3')_f$	p_f' MPa
	Successful Drained Uniform Strain Tests						
ECD36	CS/U/G	36.6	6.18	-0.89	1.68	3.96	1.68
ECD39	CS/U/G	35.1	6.86	0.64	4.39	3.71	4.55
ECD40	CS/U/G	32.3	7.95	2.66	8.33	3.29	9.19
ECD48	CS/U/G	33.1	8.07	1.99	7.05	3.41	7.62
ECD49	CS/U/G	31.9	7.91	3.43	10.01	3.24	11.13
ECD50	CS/U/G	31.5	9.63	5.18	46.69	3.19	52.44
ECD52	CS/U/G	34.2	7.82	1.15	5.74	3.56	6.07
ECD54	CS/U/G	31.4	10.30	5.62	17.78	3.17	20.05
ECD70	CS/U/G	31.4	8.37	4.67	11.96	3.17	13.49
ECD72	CS/U/G	31.9	8.63	5.65	16.61	3.24	18.50
ECD74	CS/U/G	31.3	8.73	5.52	17.07	3.16	19.29
ECD75	CS/U/G	32.3	9.43	5.55	18.07	3.29	19.93
ECD79	CS/U/G	40.6	7.55	-2.14	0.39	4.73	0.37
ECD81	CS/U/G	43.8	6.38	-2.04	0.20	5.49	0.18
ECD83	CS/U/G	39.4	7.82	-2.17	0.78	4.48	0.74
ECD84	CS/U/G	32.0	9.23	5.49	17.98	3.25	19.99
ECD85	CS/U/G	36.3	7.34	-0.14	3.01	3.91	3.04
ECD86	CS/U/G	32.5	9.18	5.09	15.37	3.32	16.87
ECD87	CS/U/G	31.7	7.64	4.11	12.04	3.21	13.48
ECD88	CS/U/G	33.9	8.37	1.23	5.74	3.52	6.11
ECD92	CS/U/G	31.9	8.21	4.18	12.10	3.24	13.46
ECD93	CS/U/G	32.0	8.11	5.54	24.26	3.26	26.89
ECD94	CS/U/G	31.0	8.59	5.35	28.52	3.12	32.46
ECD95	CS/U/G	31.7	9.10	5.30	35.79	3.21	40.09
	Drained Conventional Tests with Strain Localization						
ECD2	CS/C	31.3	3.66	-0.17	2.74	3.16	3.10
ECD7	CS/C/UP	NA	NA	NA	NA	NA	NA
ECD8	CS/C	30.4	3.95	0.82	5.37	3.05	6.20

APPENDIX B TABLE 7
SUMMARY OF RESULTS FROM DRAINED TRIAXIAL EXTENSION TESTS

Test	Test Type	ϕ' degree	ϵ_{3f} %	ϵ_{vf} %	$(\sigma_1-\sigma_3)_f$ MPa	$(\sigma_1'/\sigma_3')_f$	p_f' MPa
ECD9	CS/C	30.7	7.86	4.48	11.80	3.08	13.54
ECD10	CS/C	31.3	8.74	5.43	23.89	3.16	27.00
ECD11	CS/C	31.0	8.78	3.76	11.87	3.12	13.51
ECD12	CS/C	29.3	6.25	3.65	11.51	2.92	13.66
ECD15	CS/C/T	NA	NA	NA	NA	NA	NA
ECD16	CS/C	30.5	8.43	4.36	11.75	3.06	13.58
ECD17	CS/C	30.6	8.29	4.84	11.78	3.07	13.54
ECD18	CS/C/T	NA	NA	NA	NA	NA	NA
ECD19	CS/C/T	NA	NA	NA	NA	NA	NA
ECD20	CS/C/T	NA	NA	NA	NA	NA	NA
ECD21	CS/C	30.4	8.59	4.22	11.75	3.05	13.57
ECD25	CS/C	27.0	5.54	3.91	42.46	2.66	53.83
ECD28	CS/C	29.0	8.56	4.66	44.39	2.88	53.19
ECD29	CS/C	26.3	5.31	3.99	31.95	2.59	41.33
ECD30	CS/C	29.2	9.22	5.16	34.04	2.90	40.63
ECD31	CS/C	28.9	8.38	5.08	27.35	2.87	32.84
ECD76	CS/C	33.2	7.29	-0.92		3.42	0.76
ECD77	CS/C	40.1	3.59	-1.13		4.61	0.54
ECD78	CS/C	39.7	7.84	-2.42		4.53	0.19
	Drained Uniform Strain Tests with Strain Localization						
ECD34	CS/U/B	NA	NA	NA	NA	NA	NA
ECD35	CS/U/B	NA	NA	NA	NA	NA	NA
ECD37	CS/U/B	NA	NA	NA	NA	NA	NA
ECD38	CS/U/B	NA	NA	NA	NA	NA	NA
ECD41	CS/U/B	NA	NA	NA	NA	NA	NA
ECD42	CS/U/B	NA	NA	NA	NA	NA	NA
ECD43	CS/U/B	NA	NA	NA	NA	NA	NA
ECD55	CS/U/B/F	NA	NA	NA	NA	NA	NA
ECD58	CS/U/B/F	NA	NA	NA	NA	NA	NA

APPENDIX B TABLE 7
SUMMARY OF RESULTS FROM DRAINED TRIAXIAL EXTENSION TESTS

Test	Test Type	ϕ' degree	ϵ_{3f} %	ϵ_{vf} %	$(\sigma_1-\sigma_3)_f$ MPa	$(\sigma_1'/\sigma_3')_f$	p_f' MPa
ECD62	CS/U/B/F	NA	NA	NA	NA	NA	NA
ECD63	CS/U/B/F	NA	NA	NA	NA	NA	NA
ECD65	CS/U/B	NA	NA	NA	NA	NA	NA
ECD66	CS/U/B	NA	NA	NA	NA	NA	NA
ECD73	CS/U/B	NA	NA	NA	NA	NA	NA

APPENDIX B TABLE 8
SUMMARY OF RESULTS FROM UNDRAINED TRIAXIAL EXTENSION & OTHER TESTS

Test	Test Type	ϕ' deg.	ϵ_{3f} / ϵ_{3dev} %	u_f /u_{dev} MPa	Max. Dev. Stress MPa	Max. Effect. Stress Ratio	p_f' MPa
	Successful Undrained Uniform Strain Tests						
ECU8	CS/U/G	34.6	5.60/1.79	25.26/14.88	15.70	3.63	13.08
ECU9	CS/U/G	35.4	6.15/1.25	9.48/6.44	6.75	3.75	6.50
ECU10	CS/U/G	34.2	5.72/1.24	15.00/7.83	10.04	3.56	8.75
ECU11	CS/U/G	34.6	5.18/9.44	5.16/4.30	5.78	3.63	5.57
ECU12	CS/U/G	33.6	5.86/1.93	31.48/18.32	19.19	3.48	16.03
	Undrained Uniform Strain Tests with Strain Localization						
ECU2	CS/U/B	30.6	5.58/1.27	9.15/6.19	6.47	3.07	6.92
ECU3	CS/U/B	33.0	6.03/1.31	21.61/11.12	12.78	3.39	10.64
ECU4	CS/U/B	32.0	5.69/1.52	31.80/17.41	18.75	3.25	15.93
ECU5	CS/U/B	31.0	5.95/1.53	41.83/22.87	23.64	3.13	20.63
ECU6	CS/U/B	31.4	4.64/5.35	5.50/5.39	4.83	3.17	5.43
ECU7	CS/U/B	33.5	6.10/1.44	15.49/9.38	9.68	3.46	8.39
ECU13	CS/U/B	32.5	6.12/1.82	40.47/21.58	25.43	3.32	21.52
ECU14	CS/U/B	29.9	5.13/1.82	40.54/26.70	22.83	2.99	21.78
	Successful Uniform Strain Drained/Undrained Stability Tests						
ESTAB2	CS/U/G	35.7	7.01/1.96	6.85/0.52	10.19	3.81	8.48
ESTAB3	CS/U/G	35.6	7.38/4.29	4.74/0.53	11.62	3.78	10.14
ESTAB4	CS/U/G	37.7	6.42/1.06	13.97/0.52	12.01	4.14	9.38
ESTAB5	CS/U/G	36.9	6.20/1.26	18.74/0.53	16.23	4.00	12.59

APPENDIX B TABLE 9
VOID RATIOS IN TRIAXIAL COMPRESSION TESTS

Test	Test Type	$e_{initial}$	e_{consol}	e_{final}
	Drained Tests			
CD1	CS/G	0.518	0.430	0.220
CD3	CS/G	0.512	0.499	0.504
CD4	CS/G	0.505	0.502	0.508
CD5	CS/G	0.517	0.496	0.410
CD6	CS/G	0.518	0.481	0.336
CD7	CS/G	0.524	0.497	0.411
CD8	CS/G	0.534	0.451	0.232
CD9	CS/G	0.502	0.426	0.216
CD10	CS/G	0.514	0.446	0.227
CD12	CS/G	0.515	0.474	0.320
CD13	CS/G	0.520	0.485	0.371
CD14	CS/G	0.529	0.504	0.424
CD15	CS/G	0.519	0.447	0.239
CD16	CS/G	0.519	0.421	0.209
CD17	CS/G	0.522	0.376	0.182
CD19	CS/G	0.519	0.333	0.173
CD20	CS/G	0.523	0.478	0.292
CD21	CS/G	0.522	0.437	0.224
CD22	CS/G	0.522	0.439	0.219
CD23	CS/G	0.524	0.439	0.225
CD24	CS/BK	0.525	0.306	0.306
CD25	CS/G	0.522	0.303	0.161
CD27	CS/BK	0.522	0.290	0.290
CD28	CS/SL	0.526	0.296	0.296
CD29	CS/G	0.525	0.313	0.168
CD30	Q/G	0.675	0.489	0.275
CD31	Q/G	0.672	0.390	0.240
CD32	Q/G	0.672	0.339	0.215

APPENDIX B TABLE 9
VOID RATIOS IN TRIAXIAL COMPRESSION TESTS

Test	Test Type	$e_{initial}$	e_{consol}	e_{final}
CD33	Q/G	0.665	0.433	0.260
CD34	Q/G	0.672	0.536	0.299
TCT2	CS/G	0.586	0.573	0.615
TCT3	CS/G	0.539	0.526	0.557
TCT4	CS/G	0.557	0.552	0.582
TCT6	CS/G	0.550	0.550	0.586
TCT9	CS/G	0.554	0.549	0.579
	Undrained Tests			
CU3	CS/G	0.534	0.441	0.441
CU4	CS/G	0.530	0.447	0.447
CU6	CS/G	0.527	0.438	0.438
CU12	CS/T	0.531	0.277	0.277
CU13	CS/G	0.519	0.279	0.279
CU14	CS/G	0.514	0.357	0.357
CU15	CS/G	0.515	0.467	0.467
CU17	CS/G	0.519	0.256	0.256
CU19	CS/G	0.529	0.307	0.307
CU20	CS/G	0.525	0.327	0.327
CU21	CS/G	0.524	0.357	0.357
CU22	CS/G	0.504	0.368	0.368
CU23	CS/G	0.508	0.356	0.356
CU25	CS/T	0.520	0.340	0.340
CU26	CS/T	0.522	0.364	0.364
CU27	CS/T	0.522	0.364	0.364
CU32	CS/G	0.557	0.336	0.336
CU33	CS/G	0.557	0.340	0.340
CU10	CS/T	0.523	0.332	0.332
CU16	CS/T	0.519	0.235	0.235
	Undrained Tests with Different Total Stress Paths			

APPENDIX B TABLE 9
VOID RATIOS IN TRIAXIAL COMPRESSION TESTS

Test	Test Type	$e_{initial}$	e_{consol}	e_{final}
CUCM1	CS/G	0.525	0.308	0.308
CUCM3	CS/G	0.527	0.303	0.303
CUCM4	CS/G	0.529	0.354	0.354
CUCM5	CS/G	0.522	0.366	0.366
	Drained/Undrained Stability Tests			
CSTAB2	CS/G	0.524	0.427	0.276
CSTAB3	CS/SL	0.520	0.429	0.315
CSTAB4	CS/G	0.520	0.431	0.239
CSTAB5	CS/G	0.524	0.427	0.358
CSTAB6	CS/G	0.520	0.430	NA
CSTAB7	CS/G	0.522	0.392	0.327
	Isotropic Compression/B-Value Tests			
ISO4	CS/G	0.524	NA	NA
ISO6	CS/G	0.520	NA	NA
ISO7	CS/G	0.522	NA	NA

APPENDIX B TABLE 10
VOID RATIOS IN TRIAXIAL EXTENSION TESTS

Test	Test Type	$e_{initial}$	e_{consol}	$e_{failure}$
	Successful Drained Uniform Strain Tests			
ECD36	CS/U/G	0.526	0.516	0.530
ECD39	CS/U/G	0.520	0.479	0.469
ECD40	CS/U/G	0.521	0.461	0.422
ECD48	CS/U/G	0.519	0.461	0.432
ECD49	CS/U/G	0.521	0.435	0.386
ECD50	CS/U/G	0.518	0.265	0.199
ECD52	CS/U/G	0.535	0.485	0.468
ECD54	CS/U/G	0.527	0.388	0.310
ECD70	CS/U/G	0.525	0.417	0.351
ECD72	CS/U/G	0.528	0.400	0.321
ECD74	CS/U/G	0.531	0.384	0.308
ECD75	CS/U/G	0.522	0.389	0.312
ECD79	CS/U/G	0.531	0.519	0.552
ECD81	CS/U/G	0.528	0.524	0.555
ECD83	CS/U/G	0.533	0.515	0.548
ECD84	CS/U/G	0.521	0.370	0.295
ECD85	CS/U/G	0.524	0.487	0.489
ECD86	CS/U/G	0.513	0.382	0.311
ECD87	CS/U/G	0.521	0.408	0.351
ECD88	CS/U/G	0.522	0.468	0.450
ECD92	CS/U/G	0.520	0.407	0.348
ECD93	CS/U/G	0.518	0.326	0.253
ECD94	CS/U/G	0.523	0.319	0.248
ECD95	CS/U/G	0.518	0.290	0.222
	Drained Conventional Tests with Strain Localization			
ECD2	CS/C	0.524	0.498	0.500
ECD7	CS/C/UP	0.532	0.484	0.484
ECD8	CS/C	0.532	0.490	0.477

APPENDIX B TABLE 10
VOID RATIOS IN TRIAXIAL EXTENSION TESTS

Test	Test Type	$e_{initial}$	e_{consol}	$e_{failure}$
ECD9	CS/C	0.540	0.444	0.379
ECD10	CS/C	0.523	0.358	0.285
ECD11	CS/C	0.530	0.443	0.389
ECD12	CS/C	0.522	0.428	0.376
ECD15	CS/C/T	0.526	0.430	0.430
ECD16	CS/C	0.529	0.437	0.374
ECD17	CS/C	0.529	0.429	0.360
ECD18	CS/C/T	0.529	0.436	0.436
ECD19	CS/C/T	0.529	0.425	0.425
ECD20	CS/C/T	0.526	0.438	0.438
ECD21	CS/C	0.529	0.440	0.379
ECD25	CS/C	0.524	0.290	0.239
ECD28	CS/C	0.524	0.291	0.231
ECD29	CS/C	0.521	0.323	0.270
ECD30	CS/C	0.518	0.323	0.255
ECD31	CS/C	0.513	0.340	0.272
ECD76	CS/C	0.531	0.507	0.520
ECD77	CS/C	0.530	0.518	0.535
ECD78	CS/C	0.531	0.526	0.563
	Drained Uniform Strain Tests with Strain Localization			
ECD34	CS/U/B	0.518	0.489	0.489
ECD35	CS/U/B	0.521	0.501	0.501
ECD37	CS/U/B	0.531	0.479	0.479
ECD38	CS/U/B	0.529	0.441	0.441
ECD41	CS/U/B	0.524	0.415	0.415
ECD42	CS/U/B	0.531	0.349	0.349
ECD43	CS/U/B	0.540	0.373	0.373
ECD55	CS/U/B/F	0.527	0.374	0.374
ECD58	CS/U/B/F	0.524	0.341	0.341

APPENDIX B TABLE 10
VOID RATIOS IN TRIAXIAL EXTENSION TESTS

Test	Test Type	$e_{initial}$	e_{consol}	$e_{failure}$
ECD62	CS/U/B/F	0.533	0.420	0.420
ECD63	CS/U/B/F	0.525	0.444	0.444
ECD65	CS/U/B	0.525	0.454	0.454
ECD66	CS/U/B	0.511	0.422	0.422
ECD73	CS/U/B	0.531	0.394	0.394
	Successful Undrained Uniform Strain Tests			
ECU8	CS/U/G	0.518	0.314	0.314
ECU9	CS/U/G	0.523	0.410	0.410
ECU10	CS/U/G	0.526	0.371	0.371
ECU11	CS/U/G	0.526	0.442	0.442
ECU12	CS/U/G	0.521	0.285	0.285
	Undrained Uniform Strain Tests with Strain Localization			
ECU2	CS/U/B	0.529	0.429	0.429
ECU3	CS/U/B	0.533	0.340	0.340
ECU4	CS/U/B	0.517	0.293	0.293
ECU5	CS/U/B	0.530	0.279	0.279
ECU6	CS/U/B	0.527	0.452	0.452
ECU7	CS/U/B	0.521	0.149	0.149
ECU13	CS/U/B	0.526	0.263	0.263
ECU14	CS/U/B	0.524	0.185	0.185
	Successful Drained/Undrained Uniform Strain Stability Tests			
ESTAB2	CS/U/G	0.519	0.409	0.388
ESTAB3	CS/U/G	0.521	0.411	0.370
ESTAB4	CS/U/G	0.518	0.365	0.352
ESTAB5	CS/U/G	0.521	0.336	0.320

APPENDIX B TABLE 11
FAILURE ENERGY IN DRAINED TRIAXIAL COMPRESSION TESTS

Test	Test Type	Energy Consol. MPa	ϵ_v Energy to $(\sigma_1'/\sigma_3')_f$ MPa	$\sigma_1 - \sigma_3$ Energy to $(\sigma_1'/\sigma_3')_f$ MPa	Total Energy to $(\sigma_1'/\sigma_3')_f$ MPa
CD1	CS/G	0.53000	2.41800	10.65400	13.60200
CD3	CS/G	0.01850	-0.00816	0.60600	0.61634
CD4	CS/G	0.01500	-0.00911	0.46800	0.47389
CD5	CS/G	0.04580	0.23800	2.37000	2.65380
CD6	CS/G	0.09280	1.11200	3.65300	4.85780
CD7	CS/G	0.04400	0.27800	2.39100	2.71300
CD8	CS/G	0.29800	1.73300	7.26900	9.30000
CD9	CS/G	0.53000	2.20900	8.66800	11.40700
CD10	CS/G	0.39100	2.24100	9.41100	12.04300
CD12	CS/G	0.08880	1.56700	3.97100	5.62680
CD13	CS/G	0.05770	0.34700	2.88800	3.29270
CD14	CS/G	0.03670	0.18500	1.93800	2.15970
CD15	CS/G	0.27100	1.65500	7.15700	9.08300
CD16	CS/G	0.55700	2.57500	10.52900	13.66100
CD17	CS/G	1.26400	3.66800	14.52200	19.45400
CD19	CS/G	2.37500	4.79900	21.09700	28.27100
CD20	CS/G	0.12900	1.00700	4.98600	6.12200
CD21	CS/G	NA	NA	NA	NA
CD22	CS/G	NA	NA	NA	NA
CD23	CS/G	0.50180	NA	NA	NA
CD24	CS/BK	NA	NA	NA	NA
CD25	CS/G	3.43500	5.67000	26.87000	35.97500
CD27	CS/BK	NA	NA	NA	NA
CD28	CS/SL	NA	NA	NA	NA
CD29	CS/G	NA	NA	NA	NA
CD30	Q/G	1.03500	2.47500	10.63700	14.14700
CD31	Q/G	2.68700	3.79300	19.78200	26.26200

APPENDIX B TABLE 11
FAILURE ENERGY IN DRAINED TRIAXIAL COMPRESSION TESTS

Test	Test Type	Energy Consol. MPa	ϵ_v Energy to $(\sigma_1'/\sigma_3')_f$ MPa	$\sigma_1 - \sigma_3$ Energy to $(\sigma_1'/\sigma_3')_f$ MPa	Total Energy to $(\sigma_1'/\sigma_3')_f$ MPa
CD32	Q/G	4.03880	4.83800	29.62200	38.49880
CD33	Q/G	1.75300	3.14300	16.11200	21.00800
CD34	Q/G	0.55770	1.85200	7.45700	9.86670
TCT2	CS/G	0.00245	-0.01481	0.10787	0.09551
TCT3	CS/G	0.00245	-0.00946	0.07120	0.06418
TCT4	CS/G	0.00063	0.00435	0.02942	0.03441
TCT6	CS/G	0.00009	-0.00132	0.00709	0.00586
TCT9	CS/G	0.00063	-0.00453	0.03323	0.02934

APPENDIX B TABLE 12
FAILURE ENERGY IN UNDRAINED TRIAXIAL COMPRESSION & OTHER TESTS

Test	Test Type	Energy Consol. MPa	$\sigma_1 - \sigma_3$ Energy to $(\sigma_1 - \sigma_3)_{max}$ MPa	$\sigma_1 - \sigma_3$ Energy to $(\sigma_1'/\sigma_3')_f$ MPa	Total Energy to $(\sigma_1 - \sigma_3)_f$ MPa	Total Energy to $(\sigma_1'/\sigma_3')_f$ MPa
CU3	CS/G	0.5020	0.7710	1.3880	1.2730	1.8900
CU4	CS/G	0.4690	0.6100	1.6010	1.0790	2.0700
CU6	CS/G	0.5000	0.0955	1.6540	0.5955	2.1540
CU12	CS/T	4.2330	0.3990	3.1830	4.6320	7.4160
CU13	CS/G	4.1740	0.4020	4.4480	4.5760	8.6220
CU14	CS/G	1.7540	0.1820	2.1860	1.9360	3.9400
CU15	CS/G	0.1060	0.5810	1.2430	0.6870	.3490
CU17	CS/G	4.8460	0.5270	4.8530	5.3730	9.6990
CU19	CS/G	3.4080	0.2920	3.4730	3.7000	6.8810
CU20	CS/G	2.6360	0.2640	2.6840	2.9000	5.3200
CU21	CS/G	1.8460	0.2160	2.2010	2.0620	4.0470
CU22	CS/G	1.6900	0.1930	1.8950	1.8830	3.5850
CU23	CS/G	1.7780	0.1720	1.2510	1.9500	3.0290
CU25	CS/T	NA	NA	NA	NA	NA
CU26	CS/T	NA	NA	NA	NA	NA
CU27	CS/T	NA	NA	NA	NA	NA
CU32	CS/G	NA	NA	NA	NA	NA
CU33	CS/G	NA	NA	NA	NA	NA
CU10	CS/T	1.9090	NA	NA	NA	NA
CU16	CS/T	4.9320	NA	NA	NA	NA
	Undrained Tests with Different Total Stress Paths					
CUCM1	CS/G	3.3700	0.2800	3.4090	3.6500	6.7790
CUCM3	CS/G	3.4100	0.3020	3.5320	3.7120	6.9420
CUCM4	CS/G	1.8840	0.1890	2.2320	2.0730	4.1160
CUCM5	CS/G	1.8080	0.2180	2.1950	2.0260	4.0030

APPENDIX B TABLE 12
FAILURE ENERGY IN UNDRAINED TRIAXIAL COMPRESSION & OTHER TESTS

Test	Test Type	Energy Consol. MPa	$\sigma_1 - \sigma_3$ Energy to $(\sigma_1 - \sigma_3)_{max}$ MPa	$\sigma_1 - \sigma_3$ Energy to $(\sigma_1'/\sigma_3')_f$ MPa	Total Energy to $(\sigma_1 - \sigma_3)_f$ MPa	Total Energy to $(\sigma_1'/\sigma_3')_f$ MPa
	Drained/Undrained Stability Tests					
CSTAB2	CS/G	0.5636	NA	NA	NA	NA
CSTAB3	CS/SL	0.5382	NA	NA	NA	NA
CSTAB4	CS/G	0.5289	NA	NA	NA	NA
CSTAB5	CS/G	0.5807	NA	NA	NA	NA
CSTAB6	CS/G	0.5389	NA	NA	NA	NA
CSTAB7	CS/G	1.2100	NA	NA	NA	NA
	Isotropic Compression Tests					
ISO4	CS/G	NA	NA	NA	NA	NA
ISO6	CS/G	NA	NA	NA	NA	NA
ISO7	CS/G	NA	NA	NA	NA	NA

APPENDIX B TABLE 13
FAILURE ENERGY IN DRAINED TRIAXIAL EXTENSION TESTS

Test	Test Type	Energy Consol. MPa	ϵ_v Energy to $(\sigma_1'/\sigma_3')_f$ MPa	$\sigma_1 - \sigma_3$ Energy to $(\sigma_1'/\sigma_3')_f$ MPa	Total Energy to $(\sigma_1'/\sigma_3')_f$ MPa
	Successful Drained Uniform Strain Tests				
ECD36	CS/U/G	0.0157	-0.0200	0.0754	0.0911
ECD39	CS/U/G	0.1008	0.0382	0.3074	0.4082
ECD40	CS/U/G	0.2603	0.3217	0.9160	1.1763
ECD48	CS/U/G	0.2142	0.2001	0.7183	0.9325
ECD49	CS/U/G	0.4356	0.5042	1.2216	1.6572
ECD50	CS/U/G	4.5970	3.5400	7.3390	11.9360
ECD52	CS/U/G	0.1422	0.0923	0.5062	0.6484
ECD54	CS/U/G	1.1910	1.4760	3.0770	4.2680
ECD70	CS/U/G	0.6140	0.8252	1.6992	2.3132
ECD72	CS/U/G	1.0338	1.3640	2.6120	3.6458
ECD74	CS/U/G	1.2110	1.3910	2.6910	3.9020
ECD75	CS/U/G	1.1920	1.4540	2.9640	4.1560
ECD79	CS/U/G	0.0027	-0.0116	0.0188	0.0215
ECD81	CS/U/G	0.0007	-0.0056	0.0079	0.0086
ECD83	CS/U/G	0.0054	-0.0234	0.0382	0.0436
ECD84	CS/U/G	1.2530	1.4390	2.8990	4.1520
ECD85	CS/U/G	0.0454	-0.0067	0.1948	0.2403
ECD86	CS/U/G	0.9128	1.1297	2.3843	3.2971
ECD87	CS/U/G	0.6153	0.6779	1.3535	1.9688
ECD88	CS/U/G	0.1287	0.0984	0.5314	0.6601
ECD92	CS/U/G	0.5871	0.7383	1.6155	2.2026
ECD93	CS/U/G	2.0417	1.9540	3.6230	5.6647
ECD94	CS/U/G	2.5538	2.2650	4.4000	6.9538
ECD95	CS/U/G	3.3230	2.7780	5.5770	8.9000

APPENDIX B TABLE 13
FAILURE ENERGY IN DRAINED TRIAXIAL EXTENSION TESTS

Test	Test Type	Energy Consol. MPa	ϵ_v Energy to $(\sigma_1'/\sigma_3')_f$ MPa	$\sigma_1 - \sigma_3$ Energy to $(\sigma_1'/\sigma_3')_f$ MPa	Total Energy to $(\sigma_1'/\sigma_3')_f$ MPa
	Drained Conventional Tests with Strain Localization				
ECD2	CS/C	0.0425	-0.0071	0.0774	0.1199
ECD7	CS/C/UP	NA	NA	NA	NA
ECD8	CS/C	0.1285	0.0658	0.2556	0.3841
ECD9	CS/C	0.6059	0.7879	1.6085	2.2144
ECD10	CS/C	1.9500	1.9150	3.7250	5.6750
ECD11	CS/C	NA	NA	NA	NA
ECD12	CS/C	0.5659	0.6439	1.2615	1.8274
ECD15	CS/C/T	0.5737	NA	NA	NA
ECD16	CS/C	0.5604	0.7694	1.6427	2.2031
ECD17	CS/C	0.6204	0.8537	1.7047	2.3251
ECD18	CS/C/T	0.5731	NA	NA	NA
ECD19	CS/C/T	0.6578	NA	NA	NA
ECD20	CS/C/T	0.5381	NA	NA	NA
ECD21	CS/C	0.5507	0.7441	1.6314	2.1821
ECD25	CS/C	4.4750	2.6810	4.5610	9.0360
ECD28	CS/C	4.6610	3.1800	6.3330	10.9940
ECD29	CS/C	3.2100	2.0900	3.4550	6.6650
ECD30	CS/C	3.2170	2.6970	5.4060	8.6230
ECD31	CS/C	2.4410	2.1490	4.1370	6.5780
ECD76	CS/C	0.0059	-0.0092	0.0187	0.0246
ECD77	CS/C	0.0020	-0.0072	0.0097	0.0117
ECD78	CS/C	0.0007	-0.0067	0.0093	0.0100
	Drained Uniform Strain Tests with Strain Localization				
ECD34	CS/U/B	NA	NA	NA	NA
ECD35	CS/U/B	NA	NA	NA	NA
ECD37	CS/U/B	NA	NA	NA	NA

APPENDIX B TABLE 13
FAILURE ENERGY IN DRAINED TRIAXIAL EXTENSION TESTS

Test	Test Type	Energy Consol. MPa	ϵ_v Energy to $(\sigma_1'/\sigma_3')_f$ MPa	$\sigma_1 - \sigma_3$ Energy to $(\sigma_1'/\sigma_3')_f$ MPa	Total Energy to $(\sigma_1'/\sigma_3')_f$ MPa
ECD38	CS/U/B	NA	NA	NA	NA
ECD41	CS/U/B	NA	NA	NA	NA
ECD42	CS/U/B	NA	NA	NA	NA
ECD43	CS/U/B	NA	NA	NA	NA
ECD55	CS/U/B/F	NA	NA	NA	NA
ECD58	CS/U/B/F	NA	NA	NA	NA
ECD62	CS/U/B/F	NA	NA	NA	NA
ECD63	CS/U/B/F	NA	NA	NA	NA
ECD65	CS/U/B	NA	NA	NA	NA
ECD66	CS/U/B	NA	NA	NA	NA
ECD73	CS/U/B	NA	NA	NA	NA

APPENDIX B TABLE 14
FAILURE ENERGY IN UNDRAINED TRIAXIAL EXTENSION & OTHER TESTS

Test	Test Type	Energy Consol. MPa	$\sigma_1 - \sigma_3$ Energy to $(\sigma_1 - \sigma_3)_{max}$ MPa	$\sigma_1 - \sigma_3$ Energy to $(\sigma_1'/\sigma_3')_f$ MPa	Total Energy to $(\sigma_1 - \sigma_3)_f$ MPa	Total Energy to $(\sigma_1'/\sigma_3')_f$ MPa
	Successful Undrained Uniform Strain Tests					
ECU8	CS/U/G	2.5261	0.2096	0.7206	2.7357	3.2467
ECU9	CS/U/G	0.6154	0.0686	0.3680	0.6840	0.9834
ECU10	CS/U/G	1.2403	0.0882	0.4892	1.3285	1.7295
ECU11	CS/U/G	0.2851	0.4961	0.2540	0.7812	0.5391
ECU12	CS/U/G	3.2800	0.2555	0.9172	3.5355	4.1972
	Undrained Uniform Strain Tests with Strain Localization					
ECU2	CS/U/B	NA	NA	NA	NA	NA
ECU3	CS/U/B	2.0370	0.1250	0.6395	2.1620	2.6765
ECU4	CS/U/B	3.4140	0.2100	0.8912	3.6240	4.3052
ECU5	CS/U/B	4.6000	0.2950	1.2000	4.8950	5.8000
ECU6	CS/U/B	0.2832	0.2440	0.2107	0.5272	0.4939
ECU7	CS/U/B	1.2485	0.1030	0.4938	1.3515	1.7423
ECU13	CS/U/B	4.6620	0.3250	1.2720	4.9870	5.9340
ECU14	CS/U/B	4.6940	0.3090	1.0000	5.0030	5.6940
	Successful Drained/Undrained Uniform Strain Stability Tests					
ESTAB2	CS/U/G	0.5960	NA	0.6600	NA	1.5198
ESTAB3	CS/U/G	0.6069	NA	0.7746	NA	1.8950
ESTAB4	CS/U/G	1.2800	NA	0.6700	NA	2.1982
ESTAB5	CS/U/G	2.0140	NA	0.8850	NA	3.3231

APPENDIX B TABLE 15
E.O.T. ENERGY IN TRIAXIAL COMPRESSION TESTS

Test	Test Type	Energy Consol. MPa	ϵ_v Energy to E.O.T MPa	$\sigma_1 - \sigma_3$ Energy to E.O.T. MPa	Total Energy to E.O.T. MPa
	Drained Tests				
CD1	CS/G	0.5300	2.5090	12.4720	15.5110
CD3	CS/G	0.0185	-0.0152	1.3160	1.3193
CD4	CS/G	0.0150	-0.0208	1.1330	1.1272
CD5	CS/G	0.0458	0.2400	2.3800	2.6658
CD6	CS/G	0.0928	1.1120	3.6530	4.8578
CD7	CS/G	0.0440	0.2630	2.8340	3.1410
CD8	CS/G	0.2980	1.8170	9.7780	11.8930
CD9	CS/G	0.5300	2.2760	12.4280	15.2340
CD10	CS/G	0.3910	3.3140	12.3530	16.0580
CD12	CS/G	0.0888	1.7660	5.0740	6.9288
CD13	CS/G	0.0577	0.4130	3.7220	4.1927
CD14	CS/G	0.0367	0.2540	2.9170	3.2077
CD15	CS/G	0.2710	1.7610	10.0600	12.0920
CD16	CS/G	0.5570	2.6360	14.5100	17.7030
CD17	CS/G	1.2640	3.6620	20.4410	25.3670
CD19	CS/G	2.3750	4.7070	27.9250	35.0070
CD20	CS/G	0.1290	1.0990	6.6170	7.8450
CD21	CS/G	NA	NA	NA	NA
CD22	CS/G	NA	NA	NA	NA
CD23	CS/G	0.5018	2.6170	13.5340	16.6528
CD24	CS/BK	NA	NA	NA	NA
CD25	CS/G	3.4350	NA	NA	3.4350
CD27	CS/BK	NA	NA	NA	NA
CD28	CS/SL	NA	NA	NA	NA
CD29	CS/G	NA	NA	NA	NA
CD30	Q/G	1.0350	2.4630	11.7420	15.2400

APPENDIX B TABLE 15
E.O.T. ENERGY IN TRIAXIAL COMPRESSION TESTS

Test	Test Type	Energy Consol. MPa	ϵ_v Energy to E.O.T MPa	$\sigma_1 - \sigma_3$ Energy to E.O.T. MPa	Total Energy to E.O.T. MPa
CD31	Q/G	2.6870	3.7800	22.6490	29.1160
CD32	Q/G	4.0388	4.7430	36.2470	45.0288
CD33	Q/G	1.7530	3.0410	19.1640	23.9580
CD34	Q/G	0.5577	1.8580	8.5930	11.0087
TCT2	CS/G	NA	NA	NA	NA
TCT3	CS/G	NA	NA	NA	NA
TCT4	CS/G	NA	NA	NA	NA
TCT6	CS/G	NA	NA	NA	NA
TCT9	CS/G	NA	NA	NA	NA
	Undrained Tests				
CU3	CS/G	0.5020	NA	1.8820	2.3840
CU4	CS/G	0.4690	NA	1.7890	2.2580
CU6	CS/G	0.5000	NA	2.0750	2.5750
CU12	CS/T	4.2330	NA	3.1890	7.4220
CU13	CS/G	4.1740	NA	4.4580	8.6320
CU14	CS/G	1.7540	NA	2.7990	4.5530
CU15	CS/G	0.1060	NA	1.8650	1.9710
CU17	CS/G	4.8460	NA	6.0570	10.9030
CU19	CS/G	3.4080	NA	3.6140	7.0220
CU20	CS/G	2.6360	NA	2.9030	5.5390
CU21	CS/G	1.8460	NA	2.5100	4.3560
CU22	CS/G	1.6900	NA	2.6000	4.2900
CU23	CS/G	1.7780	NA	2.3450	4.1230
CU25	CS/T	NA	NA	NA	NA
CU26	CS/T	NA	NA	NA	NA
CU27	CS/T	NA	NA	NA	NA
CU32	CS/G	NA	NA	NA	NA

APPENDIX B TABLE 15
E.O.T. ENERGY IN TRIAXIAL COMPRESSION TESTS

Test	Test Type	Energy Consol. MPa	ϵ_v Energy to E.O.T MPa	$\sigma_1 - \sigma_3$ Energy to E.O.T. MPa	Total Energy to E.O.T. MPa
CU33	CS/G	NA	NA	NA	NA
CU10	CS/T	1.9090	NA	1.2590	3.1680
CU16	CS/T	4.9320	NA	0.1549	5.0869
	Undrained Tests with Different Total Stress Paths				
CUCM1	CS/G	3.3700	NA	3.6230	6.9930
CUCM3	CS/G	3.4100	NA	3.8060	7.2160
CUCM4	CS/G	1.8840	NA	2.5900	4.4740
CUCM5	CS/G	1.8080	NA	1.4250	3.2330
	Drained/Undrained Stability Tests				
CSTAB2	CS/G	0.5636	1.8280	6.9310	9.3226
CSTAB3	CS/SL	0.5382	1.3760	4.0000	5.9142
CSTAB4	CS/G	0.5289	2.3050	9.3800	12.2139
CSTAB5	CS/G	0.5807	0.8340	3.0850	4.4997
CSTAB6	CS/G	0.5389	0.4607	0.3573	1.3569
CSTAB7	CS/G	1.2100	1.2160	4.2170	6.6430
	Isotropic Compression/B-Value Tests				
ISO4	CS/G	NA	1.3190	NA	1.3190
ISO6	CS/G	NA	1.1190	NA	1.1190
ISO7	CS/G	NA	4.7840	NA	4.7840

APPENDIX B TABLE 16
E.O.T. ENERGY IN TRIAXIAL EXTENSION TESTS

Test	Test Type	Energy Consol. MPa	ϵ_v Energy to E.O.T. MPa	$\sigma_1 - \sigma_3$ Energy to E.O.T. MPa	Total Energy to E.O.T. MPa
	Successful Drained Uniform Strain Tests				
ECD36	CS/U/G	0.0157	-0.0249	0.1096	0.1004
ECD39	CS/U/G	0.1008	0.0329	0.3242	0.4579
ECD40	CS/U/G	0.2603	0.3365	0.6831	1.2799
ECD48	CS/U/G	0.2142	0.2440	0.8550	1.3132
ECD49	CS/U/G	0.4356	0.5625	0.9499	1.9480
ECD50	CS/U/G	4.5970	3.6960	4.8580	13.1510
ECD52	CS/U/G	0.1422	0.0904	0.6354	0.8680
ECD54	CS/U/G	1.1910	1.6000	2.0660	4.8570
ECD70	CS/U/G	0.6140	1.0680	1.7940	3.4760
ECD72	CS/U/G	1.0338	1.4886	1.5881	4.1105
ECD74	CS/U/G	1.2110	1.6850	2.5910	5.4870
ECD75	CS/U/G	1.1920	1.6800	2.3840	5.2560
ECD79	CS/U/G	0.0027	-0.0198	0.0608	0.0437
ECD81	CS/U/G	0.0007	-0.0101	0.0255	0.0161
ECD83	CS/U/G	0.0054	-0.0331	0.0844	0.0567
ECD84	CS/U/G	1.2530	1.5160	1.7480	4.5170
ECD85	CS/U/G	0.0454	-0.0104	0.2228	0.2579
ECD86	CS/U/G	0.9128	1.2760	1.8580	4.0468
ECD87	CS/U/G	0.6153	0.7713	0.9378	2.3244
ECD88	CS/U/G	0.1287	0.0950	0.5333	0.7570
ECD92	CS/U/G	0.5871	0.7930	1.0890	2.4691
ECD93	CS/U/G	2.0420	2.1960	2.4620	6.7000
ECD94	CS/U/G	2.5540	2.4420	2.8170	7.8130
ECD95	CS/U/G	3.3230	2.9100	3.3970	9.6300

APPENDIX B TABLE 16
E.O.T. ENERGY IN TRIAXIAL EXTENSION TESTS

Test	Test Type	Energy Consol. MPa	ϵ_v Energy to E.O.T. MPa	$\sigma_1 - \sigma_3$ Energy to E.O.T. MPa	Total Energy to E.O.T. MPa
	Drained Conventional Tests with Strain Localization				
ECD2	CS/C	0.0425	0.0060	0.1264	0.1749
ECD7	CS/C/UP	NA	NA	NA	NA
ECD8	CS/C	0.1285	0.0863	0.3404	0.5552
ECD9	CS/C	0.6059	0.9831	1.5690	3.1580
ECD10	CS/C	1.9500	2.1260	2.8780	6.9540
ECD11	CS/C	NA	NA	NA	NA
ECD12	CS/C	0.5659	0.7076	0.7805	2.0540
ECD15	CS/C/T	0.5737	0.6021	0.5184	1.6942
ECD16	CS/C	0.5604	0.8022	0.9772	2.3398
ECD17	CS/C	0.6204	0.9777	1.2670	2.8651
ECD18	CS/C/T	0.5731	0.6377	0.6251	1.8359
ECD19	CS/C/T	0.6578	0.6749	0.5626	1.8953
ECD20	CS/C/T	0.5381	0.7123	0.8387	2.0891
ECD21	CS/C	0.5507	1.0390	2.0230	3.6127
ECD25	CS/C	4.4750	2.7780	2.0600	9.3130
ECD28	CS/C	4.6610	3.4470	4.5724	12.6804
ECD29	CS/C	3.2100	2.2680	1.6760	7.1540
ECD30	CS/C	3.2170	2.8780	3.5990	9.6940
ECD31	CS/C	2.4410	2.3690	2.9190	7.7290
ECD76	CS/C	0.0059	-0.0115	0.0383	0.0327
ECD77	CS/C	0.0020	-0.0176	0.0623	0.0467
ECD78	CS/C	0.0007	-0.0112	0.0305	0.0200
	Drained Uniform Strain Tests with Strain Localization				
ECD34	CS/U/B	0.0448	-0.0244	0.1866	0.2070
ECD35	CS/U/B	NA	NA	NA	NA
ECD37	CS/U/B	0.1432	0.0757	0.3236	0.5425

APPENDIX B TABLE 16
E.O T. ENERGY IN TRIAXIAL EXTENSION TESTS

Test	Test Type	Energy Consol. MPa	ϵ_v Energy to E.O.T. MPa	$\sigma_1 - \sigma_3$ Energy to E.O.T. MPa	Total Energy to E.O.T. MPa
ECD38	CS/U/B	0.5294	0.6593	0.7613	1.9500
ECD41	CS/U/B	0.6085	0.7854	0.9716	2.3655
ECD42	CS/U/B	2.0210	1.3490	0.6902	4.0602
ECD43	CS/U/B	1.9390	2.0000	3.0040	6.9430
ECD55	CS/U/B/F	NA	NA	NA	NA
ECD58	CS/U/B/F	NA	NA	NA	NA
ECD62	CS/U/B/F	NA	NA	NA	NA
ECD63	CS/U/B/F	NA	NA	NA	NA
ECD65	CS/U/B	0.2786	0.3865	0.7537	1.4188
ECD66	CS/U/B	0.5933	0.8365	1.1428	2.5726
ECD73	CS/U/B	1.2587	1.6200	2.1860	5.0647

APPENDIX B TABLE 16
E.O.T. ENERGY IN UNDRAINED TRIAXIAL EXTENSION & OTHER TESTS

Test	Test Type	Energy Consol. MPa	Shearing Energy ϵ_v &/or $\sigma_1 - \sigma_3$ MPa	Total Energy to E.O.T. MPa
	Successful Undrained Uniform Strain Tests			
ECU8	CS/U/G	2.5260	0.9570	3.4830
ECU9	CS/U/G	0.6154	0.4739	1.0893
ECU10	CS/U/G	1.2400	0.6372	1.8772
ECU11	CS/U/G	0.2851	0.5791	0.8642
ECU12	CS/U/G	3.2800	1.1550	4.4350
	Undrained Uniform Strain Tests with Strain Localization			
ECU2	CS/U/B	NA	NA	NA
ECU3	CS/U/B	2.0370	0.4255	2.4625
ECU4	CS/U/B	3.4140	1.1317	4.5457
ECU5	CS/U/B	4.6000	1.4480	6.0480
ECU6	CS/U/B	0.2832	0.3701	0.6533
ECU7	CS/U/B	1.2485	0.5975	1.8460
ECU13	CS/U/B	4.6620	1.5270	6.1890
ECU14	CS/U/B	4.6940	1.4250	6.1190
	Successful Drained/Undrained Uniform Strain Stability Tests			
ESTAB2	CS/U/G	0.5960	0.8503	1.4463
ESTAB3	CS/U/G	0.6069	0.8299	1.4368
ESTAB4	CS/U/G	1.2800	0.9922	2.2722
ESTAB5	CS/U/G	2.0140	1.2903	3.3043

APPENDIX B TABLE 17
STRESS-DILATANCY IN DRAINED TRIAXIAL COMPRESSION TESTS

Test	Test Type	Actual ϕ' degree	$d\epsilon_v/d\epsilon_1$	Rowe's Dilatancy Corrected ϕ' degree	Bishop's Dilatancy Corrected ϕ' degree
CD1	CS/G	33.7	0.0737	35.5	34.2
CD3	CS/G	34.4	-0.0552	33.1	34.0
CD4	CS/G	34.8	-0.1283	31.9	34.0
CD5	CS/G	32.5	0.0921	34.8	33.1
CD6	CS/G	32.9	0.2122	38.5	34.4
CD7	CS/G	32.6	0.1652	36.9	33.8
CD8	CS/G	33.7	0.1171	36.7	34.5
CD9	CS/G	33.3	0.0751	35.1	33.8
CD10	CS/G	33.7	0.0929	36.0	34.4
CD12	CS/G	33.4	0.1837	38.1	34.6
CD13	CS/G	32.5	0.1828	37.2	33.8
CD14	CS/G	33.3	0.1639	37.5	34.4
CD15	CS/G	34.0	0.1298	37.3	34.9
CD16	CS/G	33.8	0.0718	35.6	34.3
CD17	CS/G	33.7	0.0269	34.3	33.9
CD19	CS/G	33.3	-0.0079	33.1	33.3
CD20	CS/G	33.1	0.1728	37.6	34.3
CD21	CS/G	33.9	0.0762	35.7	34.4
CD22	CS/G	33.6	0.0841	35.7	34.2
CD23	CS/G	34.2	0.0805	36.2	34.7
CD24	CS/BK	NA	NA	NA	NA
CD25	CS/G	33.5	-0.0086	33.3	33.4
CD27	CS/BK	NA	NA	NA	NA
CD28	CS/SL	NA	NA	NA	NA
CD29	CS/G	33.2	0.0000	33.2	33.2
CD30	Q/G	33.8	-0.0100	33.6	33.7
CD31	Q/G	33.5	-0.0990	31.3	32.8

APPENDIX B TABLE 17
STRESS-DILATANCY IN DRAINED TRIAXIAL COMPRESSION TESTS

Test	Test Type	Actual ϕ' degree	$d\epsilon_v/d\epsilon_1$	Rowe's Dilatancy Corrected ϕ' degree	Bishop's Dilatancy Corrected ϕ' degree
CD32	Q/G	33.8	-0.0292	33.1	33.6
CD33	Q/G	33.7	-0.0590	32.3	33.3
CD34	Q/G	33.3	0.0258	33.9	33.4
TCT2	CS/G	37.8	-0.4985	28.1	34.8
TCT3	CS/G	38.3	-0.4891	28.8	35.5
TCT4	CS/G	37.9	-0.5408	27.5	34.7
TCT6	CS/G	41.3	-0.7739	27.8	37.5
TCT9	CS/G	39.5	-0.4821	30.3	37.0

APPENDIX B TABLE 18
STRESS-DILATANCY IN DRAINED TRIAXIAL EXTENSION TESTS

Test	Test Type	Actual ϕ' degree	$d\epsilon_v/d\epsilon_1$ Failure	$d\epsilon_v/d\epsilon_3$ Failure	Rowe's Dilatancy Corrected ϕ' degree	Bishop's Dilatancy Corrected ϕ' degree
	Successful Drained Uniform Strain Tests					
ECD36	CS/U/G	36.6	-0.619	-0.241	30.1	20.4
ECD39	CS/U/G	35.1	-0.156	-0.074	33.3	29.4
ECD40	CS/U/G	32.3	0.220	0.124	35.0	43.8
ECD48	CS/U/G	33.1	0.101	0.053	34.4	37.6
ECD49	CS/U/G	31.9	0.302	0.177	35.8	50.0
ECD50	CS/U/G	31.5	0.325	0.192	35.7	51.6
ECD52	CS/U/G	34.2	-0.050	-0.025	33.6	32.0
ECD54	CS/U/G	31.4	0.365	0.222	36.1	55.8
ECD70	CS/U/G	31.4	0.399	0.249	36.6	60.9
ECD72	CS/U/G	31.9	0.471	0.307	38.2	87.4
ECD74	CS/U/G	31.3	0.415	0.262	36.8	63.4
ECD75	CS/U/G	32.3	0.362	0.220	36.9	57.5
ECD79	CS/U/G	40.6	-0.992	-0.332	31.3	17.2
ECD81	CS/U/G	43.8	-1.124	-0.360	33.8	17.2
ECD83	CS/U/G	39.4	-0.899	-0.310	30.7	17.7
ECD84	CS/U/G	32.0	0.395	0.240	37.0	60.6
ECD85	CS/U/G	36.3	-0.335	-0.144	32.7	26.0
ECD86	CS/U/G	32.5	0.379	0.233	37.4	60.7
ECD87	CS/U/G	31.7	0.423	0.268	37.3	66.2
ECD88	CS/U/G	33.9	-0.112	-0.054	32.6	29.8
ECD92	CS/U/G	31.9	0.368	0.225	36.7	57.8
ECD93	CS/U/G	32.0	0.456	0.294	38.1	77.2
ECD94	CS/U/G	31.0	0.366	0.223	35.8	55.3
ECD95	CS/U/G	31.7	0.318	0.189	35.8	51.4

APPENDIX B TABLE 18
STRESS-DILATANCY IN DRAINED TRIAXIAL EXTENSION TESTS

Test	Test Type	Actual ϕ' degree	$d\epsilon_v/d\epsilon_1$ Failure	$d\epsilon_v/d\epsilon_3$ Failure	Rowe's Dilatancy Corrected ϕ' degree	Bishop's Dilatancy Corrected ϕ' degree
	Drained Conventional Tests with Strain Localization					
ECD2	CS/C	31.3	-0.346	-0.148	27.3	31.4
ECD7	CS/C/UP	NA	NA	NA	NA	NA
ECD8	CS/C	30.4	0.190	0.105	32.8	30.3
ECD9	CS/C	30.7	0.388	0.240	35.8	30.6
ECD10	CS/C	31.3	0.368	0.224	36.1	31.2
ECD11	CS/C	31.0	0.286	0.166	34.7	30.9
ECD12	CS/C	29.3	0.427	0.270	35.1	29.3
ECD15	CS/C/T	NA	NA	NA	NA	NA
ECD16	CS/C	30.5	0.378	0.232	35.5	30.4
ECD17	CS/C	30.6	0.424	0.268	36.2	30.5
ECD18	CS/C/T	NA	NA	NA	NA	NA
ECD19	CS/C/T	NA	NA	NA	NA	NA
ECD20	CS/C/T	NA	NA	NA	NA	NA
ECD21	CS/C	30.4	0.411	0.257	35.9	30.4
ECD25	CS/C	27.0	0.506	0.338	34.1	27.0
ECD28	CS/C	29.0	0.326	0.194	33.3	29.0
ECD29	CS/C	26.3	0.565	0.393	34.5	26.3
ECD30	CS/C	29.2	0.302	0.177	33.1	29.1
ECD31	CS/C	28.9	0.370	0.227	33.9	28.9
ECD76	CS/C	33.2	-0.635	-0.241	26.3	NA
ECD77	CS/C	40.1	-1.091	-0.353	29.9	NA
ECD78	CS/C	39.7	-1.051	-0.345	29.7	NA

APPENDIX B TABLE 19
CRUSHING PARAMETERS IN TRIAXIAL COMPRESSION TESTS

Test	Test Type	Hardin's B_r	Marsal's B	L. & F. D_{15i}/D_{15f}	$(1-D_{10f}/D_{10i})$
	Drained Tests				
CD1	CS/G	0.341	58.850	15.873	0.956
CD3	CS/G	0.032	10.700	1.333	0.400
CD4	CS/G	0.024	9.670	1.214	0.344
CD5	CS/G	NA	NA	NA	NA
CD6	CS/G	0.151	28.780	3.831	0.844
CD7	CS/G	0.113	22.700	2.674	0.765
CD8	CS/G	0.262	43.390	8.696	0.926
CD9	CS/G	0.299	51.190	10.101	0.935
CD10	CS/G	0.342	66.430	14.430	0.953
CD12	CS/G	NA	NA	NA	NA
CD13	CS/G	0.143	26.680	3.559	0.844
CD14	CS/G	0.167	27.140	3.300	0.833
CD15	CS/G	0.282	53.400	8.850	0.923
CD16	CS/G	0.343	66.450	13.755	0.945
CD17	CS/G	0.361	71.900	15.198	0.950
CD19	CS/G	0.341	65.800	13.089	0.944
CD20	CS/G	0.248	41.510	7.576	0.914
CD21	CS/G	NA	NA	NA	NA
CD22	CS/G	NA	NA	NA	NA
CD23	CS/G	0.297	53.410	8.772	0.927
CD24	CS/BK	NA	NA	NA	NA
CD25	CS/G	NA	NA	NA	NA
CD27	CS/BK	NA	NA	NA	NA
CD28	CS/SL	NA	NA	NA	NA
CD29	CS/G	NA	NA	NA	NA
CD30	Q/G	NA	NA	NA	NA
CD31	Q/G	NA	NA	NA	NA
CD32	Q/G	NA	NA	NA	NA

APPENDIX B TABLE 19
CRUSHING PARAMETERS IN TRIAXIAL COMPRESSION TESTS

Test	Test Type	Hardin's B_r	Marsal's B	L. & F. D_{15i}/D_{15f}	$(1-D_{10f}/D_{10i})$
CD33	Q/G	NA	NA	NA	NA
CD34	Q/G	NA	NA	NA	NA
TCT2	CS/G	NA	NA	NA	NA
TCT3	CS/G	NA	NA	NA	NA
TCT4	CS/G	NA	NA	NA	NA
TCT6	CS/G	NA	NA	NA	NA
TCT9	CS/G	NA	NA	NA	NA
	Undrained Tests				
CU3	CS/G	0.097	19.800	2.222	0.671
CU4	CS/G	0.090	19.030	2.132	0.634
CU6	CS/G	0.090	20.360	2.299	0.695
CU12	CS/T	0.252	46.620	7.143	0.914
CU13	CS/G	0.271	50.160	7.937	0.921
CU14	CS/G	0.196	35.540	5.263	0.883
CU15	CS/G	0.060	14.210	1.613	0.552
CU17	CS/G	0.316	61.870	10.000	0.931
CU19	CS/G	0.292	57.060	9.901	0.936
CU20	CS/G	0.257	48.160	7.576	0.925
CU21	CS/G	NA	NA	NA	NA
CU22	CS/G	NA	NA	NA	NA
CU23	CS/G	0.199	35.610	5.128	0.883
CU25	CS/T	NA	NA	NA	NA
CU26	CS/T	NA	NA	NA	NA
CU27	CS/T	NA	NA	NA	NA
CU32	CS/G	NA	NA	NA	NA
CU33	CS/G	NA	NA	NA	NA
CU10	CS/T	0.192	34.430	4.630	0.879
CU16	CS/T	0.152	26.410	3.279	0.824
	Undrained Tests with Different Total Stress Paths				

APPENDIX B TABLE 19
CRUSHING PARAMETERS IN TRIAXIAL COMPRESSION TESTS

Test	Test Type	Hardin's B_r	Marsal's B	L. & F. D_{15i}/D_{15f}	$(1-D_{10f}/D_{10i})$
CUCM1	CS/G	NA	NA	NA	NA
CUCM3	CS/G	NA	NA	NA	NA
CUCM4	CS/G	NA	NA	NA	NA
CUCM5	CS/G	0.165	29.810	3.378	0.824
	Drained/Undrained Stability Tests				
CSTAB2	CS/G	0.281	50.640	10.000	0.939
CSTAB3	CS/SL	0.163	29.890	3.378	0.823
CSTAB4	CS/G	NA	NA	NA	1.000
CSTAB5	CS/G	0.198	34.570	5.319	0.891
CSTAB6	CS/G	0.051	14.550	1.626	0.521
CSTAB7	CS/G	0.267	50.130	8.130	0.926
	Isotropic Compression Tests				
ISO4	CS/G	NA	NA	NA	NA
ISO5	CS/G	0.028	9.860	1.370	0.354
ISO7	CS/G	0.124	25.300	3.106	0.810

APPENDIX B TABLE 20
CRUSHING PARAMETERS IN TRIAXIAL EXTENSION TESTS

Test	Test Type	Hardin's B_r	Marsal's B	L. & F. D_{15i}/D_{15f}	$(1-D_{10f}/D_{10i})$
	Successful Drained Uniform Strain Tests				
ECD36	CS/U/G	0.005	0.576	1.011	0.111
ECD39	CS/U/G	0.045	3.060	1.266	0.247
ECD40	CS/U/G	0.045	11.020	1.493	0.410
ECD48	CS/U/G	0.029	8.680	1.414	0.335
ECD49	CS/U/G	0.067	15.320	1.692	0.543
ECD50	CS/U/G	0.222	36.840	6.369	0.905
ECD52	CS/U/G	NA	NA	NA	NA
ECD54	CS/U/G	0.176	28.940	3.215	0.804
ECD70	CS/U/G	0.139	22.860	2.519	0.721
ECD72	CS/U/G	0.186	29.240	3.257	0.812
ECD74	CS/U/G	0.170	29.140	3.759	0.840
ECD75	CS/U/G	0.202	31.590	4.098	0.853
ECD79	CS/U/G	0.013	0.380	1.157	0.182
ECD81	CS/U/G	0.012	0.676	1.112	0.162
ECD83	CS/U/G	0.005	0.635	1.007	0.074
ECD84	CS/U/G	0.239	37.850	5.848	0.902
ECD85	CS/U/G	0.016	2.870	1.088	0.173
ECD86	CS/U/G	0.173	28.380	3.205	0.809
ECD87	CS/U/G	0.113	20.040	2.183	0.653
ECD88	CS/U/G	0.044	7.820	1.256	0.299
ECD92	CS/U/G	0.120	20.460	2.212	0.656
ECD93	CS/U/G	0.197	32.680	4.505	0.861
ECD94	CS/U/G	0.219	34.500	5.208	0.883
ECD95	CS/U/G	0.225	35.040	5.650	0.893
	Drained Conventional Tests with Strain Localization				
ECD2	CS/C	NA	NA	NA	NA
ECD7	CS/C/UP	NA	NA	NA	NA
ECD8	CS/C	0.023	5.020	1.387	0.296

APPENDIX B TABLE 20
CRUSHING PARAMETERS IN TRIAXIAL EXTENSION TESTS

Test	Test Type	Hardin's B_r	Marsal's B	L. & F. D_{15i}/D_{15f}	$(1-D_{10f}/D_{10i})$
ECD9	CS/C	0.135	24.990	2.193	0.760
ECD10	CS/C	0.230	41.940	6.173	0.905
ECD11	CS/C	NA	NA	NA	NA
ECD12	CS/C	0.090	19.090	2.066	0.629
ECD15	CS/C/T	NA	NA	NA	NA
ECD16	CS/C	0.128	24.320	2.681	0.749
ECD17	CS/C	0.125	22.930	2.463	0.706
ECD18	CS/C/T	0.090	17.450	1.908	0.595
ECD19	CS/C/T	0.090	17.170	1.869	0.576
ECD20	CS/C/T	0.095	19.600	2.110	0.637
ECD21	CS/C	0.131	24.290	2.597	0.716
ECD25	CS/C	0.196	32.900	5.682	0.899
ECD28	CS/C	0.247	43.480	7.576	0.922
ECD29	CS/C	0.189	33.000	5.076	0.883
ECD30	CS/C	0.250	42.980	7.752	0.925
ECD31	CS/C	0.223	37.370	6.494	0.912
ECD76	CS/C	0.025	NA	1.103	0.201
ECD77	CS/C	0.001	0.424	1.000	0.007
ECD78	CS/C	0.006	0.412	1.014	0.107
	Drained Uniform Strain Tests with Strain Localization				
ECD34	CS/U/B	0.015	1.430	1.198	0.210
ECD35	CS/U/B	NA	NA	NA	NA
ECD37	CS/U/B	0.018	4.440	1.247	0.252
ECD38	CS/U/B	0.073	17.170	1.873	0.580
ECD41	CS/U/B	0.087	19.490	2.096	0.633
ECD42	CS/U/B	0.086	19.900	2.128	0.638
ECD43	CS/U/B	0.195	33.460	5.102	0.883
ECD55	CS/U/B/F	NA	NA	NA	NA
ECD58	CS/U/B/F	NA	NA	NA	NA

APPENDIX B TABLE 20
CRUSHING PARAMETERS IN TRIAXIAL EXTENSION TESTS

Test	Test Type	Hardin's B_r	Marsal's B	L. & F. D_{15f}/D_{15f}	$(1-D_{10f}/D_{10i})$
ECD62	CS/U/B/F	NA	NA	NA	NA
ECD63	CS/U/B/F	NA	NA	NA	NA
ECD65	CS/U/B	0.076	12.480	1.575	0.469
ECD66	CS/U/B	0.121	19.880	2.165	0.648
ECD73	CS/U/B	0.196	31.380	4.016	0.849
	Successful Undrained Uniform Strain Tests				
ECU8	CS/U/G	0.137	28.960	2.985	0.783
ECU9	CS/U/G	0.049	13.290	1.577	0.483
ECU10	CS/U/G	0.093	19.970	2.132	0.640
ECU11	CS/U/G	0.022	8.860	1.325	0.329
ECU12	CS/U/G	0.166	30.210	3.663	0.835
	Undrained Uniform Strain Tests with Strain Localization				
ECU2	CS/U/B	NA	NA	NA	NA
ECU3	CS/U/B	0.121	24.610	2.681	0.742
ECU4	CS/U/B	0.156	29.420	3.546	0.832
ECU5	CS/U/B	0.181	32.410	4.425	0.857
ECU6	CS/U/B	0.005	5.760	1.144	0.237
ECU7	CS/U/B	0.057	13.350	1.595	0.490
ECU13	CS/U/B	0.187	32.950	4.673	0.864
ECU14	CS/U/B	0.199	34.330	5.025	0.877
	Successful Uniform Strain Drained/Undrained Stability Tests				
ESTAB2	CS/U/G	0.079	16.710	1.832	0.575
ESTAB3	CS/U/G	0.081	18.360	1.976	0.602
ESTAB4	CS/U/G	0.116	23.400	2.451	0.693
ESTAB5	CS/U/G	0.155	29.580	3.247	0.810

APPENDIX B TABLE 21
SOIL COMPRESSIBILITY AND B-VALUES

SOIL COMPRESSIBILITY				
σ_{cell} MPa	Soil Porosity	Virgin Soil Compr. 1/MPa	Elastic Loading Soil Compress. 1/MPa	Elastic Unloading Soil Compress. 1/MPa
0.07	0.343	4.880e-03	2.406e-03	1.601e-03
2.98	0.335	4.880e-03	2.406e-03	1.601e-03
7.98	0.324	4.330e-03	9.598e-04	7.050e-04
11.98	0.316	3.012e-03	7.018e-04	4.989e-04
17.48	0.302	3.370e-03	5.038e-04	3.687e-04
25.98	0.281	2.963e-03	3.942e-04	2.688e-04
33.98	0.264	2.412e-03	3.031e-04	2.163e-04
51.98	0.235	1.538e-03	2.210e-04	1.513e-04
60.98	0.225	1.261e-03	1.846e-04	1.283e-04
68.98	0.217	1.058e-03	1.523e-04	9.175e-05

B-Values				
Cambria Sand V_i = 707.33 cm^3		Vol. Device Stiff. = 0.0199 kg/cm^2 Membrane Stiff. = 0.0027 kg/cm^2 Compress. of Water = 4.707e-05		
σ_{cell} MPa	Porosity	Virgin Soil B-Value	Elastic Loading Soil B-Value	Elastic Unloading Soil B-Value
0.07	0.343	0.986	0.985	0.985
2.98	0.335	0.968	0.937	0.940
7.98	0.324	0.965	0.861	0.860
11.98	0.316	0.952	0.822	0.780
17.48	0.302	0.959	0.777	0.730
25.98	0.281	0.956	0.745	0.680
33.98	0.264	0.950	0.705	0.620
51.98	0.235	0.932	0.662	0.530
60.98	0.225	0.921	0.631	0.520
68.98	0.217	0.910	0.594	0.480

APPENDIX B TABLE 22
DERIVED ELASTIC PARAMETERS FROM TEST CDLU3 FOR CAMBRIA SAND

σ_{cell} MPa	Poisson's Ratio	Young's Modulus MPa
4.0	0.320	1146.7
8.0	0.331	1617.7
16.0	0.350	2084.6
32.0	0.371	2645.6
64.0	0.419	2985.1

APPENDIX B TABLE 23
SIEVE ANALYSES FOR DRAINED TRIAXIAL COMPRESSION TESTS

Test	Sieve Size in mm								
	2.00	1.40	0.85	0.60	0.425	0.25	0.18	0.106	0.075
	Percent Passing Sieve								
CD1	100.0	67.5	51.4	43.7	36.4	28.6	23.4	17.2	13.0
CD3	100.0	20.5	10.7	7.2	4.9	3.4	2.6	1.8	1.3
CD4	100.0	18.2	9.7	6.5	4.4	3.0	2.3	1.6	1.1
CD7	100.0	35.8	22.7	16.7	12.1	8.5	7.2	5.0	3.4
CD6	100.0	42.8	28.8	21.8	16.3	11.6	8.8	5.8	3.3
CD8	100.0	58.7	43.4	35.4	28.2	21.1	16.0	10.9	7.1
CD9	100.0	63.0	48.3	40.4	33.1	25.6	17.5	12.2	8.5
CD10	100.0	74.9	51.6	42.8	34.6	26.9	22.0	15.9	12.1
CD12	100.0	27.7	20.9	14.9	10.7	7.6	6.0	4.3	3.2
CD13	100.0	40.3	26.7	20.6	15.5	11.4	9.0	6.3	4.4
CD14	100.0	58.1	27.1	20.2	14.9	10.8	8.6	6.2	4.8
CD15	100.0	67.5	46.0	37.2	29.5	21.9	16.4	10.4	6.1
CD16	100.0	74.5	52.1	43.2	35.4	27.6	22.4	15.5	10.3
CD17	100.0	77.9	54.1	44.9	36.8	28.7	23.4	17.0	11.8
CD19	100.0	73.1	52.8	44.5	37.1	29.2	23.5	14.7	10.2
CD20	100.0	59.9	41.5	33.4	26.1	19.6	14.5	9.4	6.3
CD23	100.0	64.6	48.9	40.7	33.2	24.8	16.1	10.9	7.7

APPENDIX B TABLE 23
SIEVE ANALYSES FOR DRAINED TRIAXIAL COMPRESSION TESTS

Test	Sieve Size in mm								
CD28	100.0	76.1	54.9	45.9	38.2	30.7	25.5	18.8	14.5

APPENDIX B TABLE 24
SIEVE ANALYSES FOR UNDRAINED TRIAXIAL COMPRESSION TESTS

Test	Sieve Size in mm								
	2.00	1.40	0.85	0.60	0.425	0.25	0.18	0.106	0.075
	Percent Passing Sieve								
CU3	100.0	38.2	19.8	14.1	9.7	6.7	5.2	3.6	2.6
CU4	100.0	35.3	19.0	13.4	9.3	6.4	5.0	3.4	2.5
CU6	100.0	31.3	20.4	14.6	10.3	7.0	5.3	3.4	2.2
CU9	100.0	11.7	4.6	2.5	1.3	0.7	0.5	0.3	0.1
CU10	100.0	54.9	34.4	25.8	18.6	12.9	10.7	7.4	5.3
CU12	100.0	63.5	43.2	34.2	25.4	18.0	13.8	9.4	6.6
CU13	100.0	64.3	46.0	36.9	28.5	20.5	15.1	10.1	5.8
CU14	100.0	52.9	35.5	27.0	19.9	14.2	11.0	7.4	4.6
CU15	100.0	27.9	14.2	10.1	7.1	4.9	3.8	2.6	2.0
CU16	100.0	50.0	26.4	20.2	14.8	10.5	8.2	5.6	4.1
CU17	100.0	71.0	50.9	42.1	33.7	25.2	17.7	11.8	7.8
CU18	100.0	49.7	32.7	24.5	17.5	12.1	9.3	6.2	4.4
CU19	100.0	70.1	47.1	37.7	29.1	21.6	17.1	12.2	8.9
CU20	100.0	66.4	41.8	32.2	25.8	18.3	14.6	10.5	8.0
CU21	100.0	62.6	37.0	27.7	20.2	14.4	11.3	8.0	6.1
CU23	100.0	54.6	35.6	26.8	19.7	14.0	10.9	7.7	5.4

APPENDIX B TABLE 25
SIEVE ANALYSES FOR DRAINED TRIAXIAL EXTENSION TESTS

Test	Sieve Size in mm								
	2.00	1.40	0.85	0.60	0.425	0.25	0.18	0.106	0.075
	Percent Passing Sieve								
ECD2	100.0	46.8	16.6	10.4	6.5	4.2	3.1	2.1	1.5
ECD3	100.0	16.0	0.9	0.4	0.2	0.1	0.0	0.0	0.0
ECD5	100.0	23.5	7.2	4.1	1.9	1.1	0.7	0.3	0.2
ECD6	100.0	23.1	6.9	4.1	2.3	1.5	1.1	0.7	0.5
ECD7	100.0	16.3	1.0	0.5	0.2	0.1	0.1	0.0	0.0
ECD8	100.0	32.8	5.0	2.9	1.7	1.0	0.7	0.5	0.3
ECD9	100.0	50.0	25.0	17.6	12.1	8.3	6.4	4.4	3.2
ECD10	100.0	63.6	38.5	29.4	21.9	15.9	12.6	8.8	6.6
ECD12	100.0	40.1	19.1	12.6	8.2	5.4	4.1	2.7	2.0
ECD14	100.0	41.5	18.0	11.6	7.4	4.8	3.6	2.3	1.7
ECD15	100.0	18.7	0.8	0.4	0.2	0.1	0.1	0.0	0.0
ECD16	100.0	47.1	24.3	17.0	11.7	8.1	6.3	4.3	3.2
ECD17	100.0	51.4	22.9	15.7	10.6	7.2	5.5	3.8	2.8
ECD18	100.0	45.6	17.4	11.4	7.3	4.7	3.6	2.4	1.7
ECD19	100.0	47.6	17.2	10.8	6.8	4.4	3.2	2.1	1.5
ECD20	100.0	42.5	19.6	12.9	8.4	5.6	4.2	2.8	2.1
ECD21	100.0	49.4	24.3	17.1	11.9	8.2	6.3	4.3	3.1
ECD25	100.0	51.7	32.9	26.3	20.4	15.1	11.9	8.5	6.3
ECD28	100.0	64.5	39.0	31.3	24.6	18.4	14.6	10.2	7.6
ECD29	100.0	51.6	33.0	25.6	19.2	13.9	10.9	7.7	5.7
ECD30	100.0	62.9	40.2	32.3	25.1	18.8	14.9	10.6	7.8
ECD31	100.0	58.2	37.4	29.3	22.4	16.5	13.1	9.4	7.0
ECD32	100.0	22.6	7.3	4.4	2.6	1.6	1.2	0.7	0.5
ECD33	100.0	42.8	18.5	12.6	8.4	5.7	4.4	3.0	2.2
ECD34	100.0	22.2	1.4	0.8	0.4	0.2	0.2	0.1	0.1
ECD35	100.0	16.9	1.1	0.6	0.3	0.2	0.1	0.1	0.1
ECD36	100.0	15.1	0.6	0.3	0.2	0.1	0.1	0.0	0.0

APPENDIX B TABLE 25
SIEVE ANALYSES FOR DRAINED TRIAXIAL EXTENSION TESTS

Test	Sieve Size in mm								
	2.00	1.40	0.85	0.60	0.425	0.25	0.18	0.106	0.075
	Percent Passing Sieve								
ECD37	100.0	22.9	4.4	2.5	1.4	0.8	0.5	0.3	0.2
ECD38	100.0	35.3	17.2	10.9	6.8	4.3	3.1	2.5	1.8
ECD39	100.0	25.1	3.1	1.7	0.9	0.6	0.4	0.2	0.2
ECD40	100.0	29.9	11.0	6.9	4.2	2.6	1.9	1.2	0.8
ECD41	100.0	37.6	19.5	12.8	8.3	5.4	4.0	2.5	1.7
ECD42	100.0	36.5	19.9	13.0	8.5	5.5	4.0	2.6	1.8
ECD43	100.0	55.3	33.5	25.9	19.4	14.0	10.9	7.6	5.6
ECD44	100.0	38.5	15.6	9.7	6.0	3.7	2.7	1.6	1.1
ECD45	100.0	37.2	16.2	10.1	6.0	3.3	2.1	1.1	0.5
ECD46	100.0	37.2	16.2	10.1	5.9	3.3	2.1	1.1	0.5
ECD48	100.0	28.5	8.7	5.2	3.0	1.7	1.2	0.6	0.4
ECD49	100.0	36.2	15.3	9.9	6.2	3.9	2.8	1.7	1.1
ECD50	100.0	61.3	35.6	28.4	22.2	16.3	12.7	8.7	6.4
ECD51	100.0	59.6	37.3	28.6	21.4	15.6	12.4	8.6	6.4
ECD52	100.0	33.0	15.9	13.4	2.0	1.1	0.8	0.4	0.3
ECD53	100.0	57.9	26.4	18.3	12.4	8.5	6.5	4.4	3.2
ECD54	100.0	53.9	28.9	20.6	14.3	9.7	7.3	4.8	3.4
ECD55	100.0	50.7	25.3	17.3	11.3	7.2	5.2	3.1	1.9
ECD56	100.0	66.0	46.1	36.5	28.0	20.6	16.2	11.7	8.9
ECD57	100.0	40.0	20.5	13.8	8.8	5.7	4.1	2.6	1.7
ECD58	100.0	56.5	35.1	26.0	18.5	12.7	9.4	6.1	4.1
ECD59	100.0	55.8	33.2	26.3	20.1	14.5	11.2	7.5	5.4
ECD60	100.0	55.2	31.2	23.8	17.4	12.1	9.2	6.1	4.3
ECD61	100.0	30.6	10.1	6.1	3.6	2.2	1.6	1.0	0.6
ECD62	100.0	58.3	36.1	28.8	22.2	16.3	12.7	8.8	6.4
ECD63	100.0	23.3	9.5	5.6	3.0	1.5	0.9	0.4	0.2
ECD64	100.0	24.6	9.8	6.1	3.8	2.4	1.8	1.1	0.7

APPENDIX B TABLE 25
SIEVE ANALYSES FOR DRAINED TRIAXIAL EXTENSION TESTS

Test	Sieve Size in mm								
	2.00	1.40	0.85	0.60	0.425	0.25	0.18	0.106	0.075
	Percent Passing Sieve								
ECD65	100.0	34.4	12.5	7.9	5.0	3.2	2.3	1.5	1.0
ECD66	100.0	44.3	19.9	13.3	8.8	5.9	4.4	2.9	2.1
ECD69	100.0	59.4	34.1	26.7	20.4	14.7	11.3	7.6	5.4
ECD70	100.0	45.4	22.9	15.9	10.9	7.5	5.7	3.9	2.9
ECD71	100.0	45.5	22.5	15.4	10.4	7.0	5.4	3.6	2.7
ECD72	100.0	58.7	29.2	20.8	14.6	10.0	7.7	5.3	3.9
ECD73	100.0	54.9	31.4	23.2	16.7	11.3	9.1	6.2	4.6
ECD74	100.0	41.9	29.1	22.1	16.1	11.3	8.7	6.0	4.3
ECD75	100.0	57.9	31.6	23.4	16.9	12.0	9.4	6.7	4.9
ECD76	100.0	17.2	4.5	2.9	2.1	1.6	1.1	0.5	0.2
ECD77	100.0	11.4	0.4	0.1	0.1	0.0	0.0	0.0	0.0
ECD78	100.0	15.0	0.4	0.1	0.0	0.0	0.0	0.0	0.0
ECD79	100.0	20.3	0.4	0.1	0.0	0.0	0.0	0.0	0.0
ECD81	100.0	18.3	0.7	0.4	0.2	0.0	0.0	0.0	0.0
ECD82	100.0	18.3	0.4	0.2	0.1	0.1	0.1	0.0	0.0
ECD83	100.0	13.5	0.6	0.2	0.1	0.1	0.0	0.0	0.0
ECD84	100.0	61.0	36.9	28.8	21.2	15.3	12.1	8.7	6.6
ECD85	100.0	17.0	2.9	1.4	0.8	0.5	0.3	0.2	0.1
ECD86	100.0	50.9	28.4	20.3	14.3	9.9	7.7	5.3	3.9
ECD87	100.0	37.3	20.0	13.5	9.0	6.0	4.6	3.1	2.2
ECD88	100.0	20.5	7.8	5.0	3.4	2.6	2.2	1.8	1.5
ECD89	100.0	29.1	11.7	7.2	4.4	2.9	2.1	1.4	1.0
ECD90	100.0	33.8	17.4	11.3	7.3	4.8	3.6	2.4	1.8
ECD91	100.0	40.2	20.8	14.2	9.6	6.5	4.9	3.3	2.3
ECD92	100.0	41.6	20.5	13.7	9.1	6.1	4.6	3.1	2.2
ECD93	100.0	49.8	32.7	24.7	18.0	12.7	9.8	6.7	4.9
ECD94	100.0	57.0	34.5	26.6	19.7	14.1	11.0	7.5	5.6

APPENDIX B TABLE 25
SIEVE ANALYSES FOR DRAINED TRIAXIAL EXTENSION TESTS

Test	Sieve Size in mm								
	2.00	1.40	0.85	0.60	0.425	0.25	0.18	0.106	0.075
	Percent Passing Sieve								
ECD95	100.0	56.5	35.0	27.5	20.7	15.0	11.7	8.0	5.8
ECD96	100.0	50.1	22.6	15.2	9.9	6.3	4.5	2.7	1.7

APPENDIX B TABLE 26
SIEVE ANALYSES FOR UNDRAINED TRIAXIAL EXTENSION TESTS

Test	Sieve Size in mm								
	2.00	1.40	0.85	0.60	0.425	0.25	0.18	0.106	0.075
	Percent Passing Sieve								
ECU2	100.0	25.4	11.7	7.3	4.3	2.5	1.6	1.4	1.1
ECU3	100.0	43.5	24.6	17.2	11.5	7.8	6.0	4.0	2.9
ECU4	100.0	46.9	29.4	21.9	15.6	10.9	8.4	5.8	4.3
ECU5	100.0	53.1	32.4	24.6	17.9	12.5	9.6	6.4	4.7
ECU6	100.0	18.2	5.8	3.4	2.0	1.2	0.9	0.6	0.4
ECU7	100.0	34.2	13.3	8.3	5.2	3.4	2.5	1.7	1.2
ECU8	100.0	46.0	27.0	19.2	13.2	8.9	6.8	4.6	3.3
ECU9	100.0	30.2	13.3	8.1	4.9	3.1	2.3	1.5	1.0
ECU10	100.0	40.1	20.0	13.1	8.5	5.6	4.2	2.8	2.0
ECU11	100.0	22.5	8.9	5.2	3.2	2.0	1.5	1.0	0.7
ECU12	100.0	51.9	30.2	22.4	15.9	11.1	8.5	5.8	4.3
ECU13	100.0	54.2	33.0	25.3	18.6	13.0	10.0	6.8	5.0
ECU14	100.0	57.4	34.3	26.5	19.4	13.8	10.6	7.3	5.4

APPENDIX B TABLE 27
SIEVE ANALYSES FOR OTHER TESTS

Test	Sieve Size in mm								
	2.00	1.40	0.85	0.60	0.425	0.25	0.18	0.106	0.075
	Percent Passing Sieve								
CSTAB2	100.0	65.0	45.7	36.5	28.5	21.4	17.3	12.3	9.4
CSTAB3	100.0	52.8	29.9	21.7	15.3	10.6	8.2	5.5	4.0
CSTAB4	100.0	52.8	29.9	21.6	15.3	10.6	8.2	5.6	4.0
CSTAB5	100.0	53.7	34.6	26.3	19.7	14.4	11.4	8.0	6.0
CSTAB6	100.0	26.0	14.6	9.2	5.9	3.9	3.0	2.0	1.5
CSTAB7	100.0	66.1	44.1	34.6	26.5	19.5	15.3	10.6	8.1
ESTAB2	100.0	40.1	16.7	10.8	6.9	4.5	3.4	2.3	1.7
ESTAB3	100.0	38.8	18.4	11.7	7.3	4.6	3.2	2.0	1.3
ESTAB5	100.0	50.4	29.6	21.0	14.6	10.0	7.6	5.1	3.8
ESTAB4	100.0	45.4	23.4	15.7	10.3	6.9	5.2	3.5	2.6
CUCM1	100.0	46.7	24.1	16.8	11.2	7.4	5.5	3.5	2.4
CUCM3	100.0	68.4	46.9	37.2	27.1	19.6	15.1	10.5	7.9
CUCM4	100.0	24.4	12.2	7.9	5.0	3.2	2.4	1.6	1.2
CUCM5	100.0	54.9	29.8	21.5	15.2	10.5	8.1	5.5	4.1
ISO4	100.0	57.4	37.6	28.4	20.8	14.8	11.4	7.9	5.8
ISO6	100.0	23.3	9.9	6.2	3.7	2.4	1.8	1.2	0.8
ISO7	100.0	34.6	25.3	19.2	14.0	10.0	7.8	5.5	4.1

APPENDIX B TABLE 28
INITIAL GRADATION OF CAMBRIA SAND

Sieve Size in mm					
2.00	1.40	1.18	1.00	0.85	0.075
Percent Passing Sieve					
100.0	11.75	6.58	3.78	0.00	0.00

APPENDIX C

APPENDIX C TABLE 1 - DRAINED TRIAXIAL COMPRESSION TESTS

Test CD1 DRAINED TRIAXIAL COMPRESSION
σ_3' = 16.89 MPa e_i = 0.518 H/D = 2.50
Cambria sand ϕ' = 33.7 2.54 CM/HR

ϵ_1 %	ϵ_v %	$\sigma_1 - \sigma_3$ MPa	σ_1'/σ_3'	p' MPa	Time second
0.0	0.00	0.06	1.00	16.56	-0.0
0.1	0.03	1.23	1.07	16.93	17.2
0.4	0.34	4.21	1.25	17.94	103.0
0.5	0.45	4.71	1.28	18.11	131.4
0.7	0.62	5.41	1.33	18.35	172.4
1.0	0.94	6.59	1.40	18.74	247.7
2.0	1.96	9.83	1.60	19.79	505.8
3.0	2.79	12.13	1.73	20.59	737.6
4.0	3.66	14.29	1.86	21.31	995.7
5.0	4.40	16.01	1.97	21.86	1232.1
6.0	5.12	17.82	2.08	22.50	1496.2
7.0	5.78	19.33	2.17	22.98	1732.0
8.0	6.46	20.91	2.26	23.51	1991.5
9.0	7.06	22.27	2.35	23.93	2233.8
10.0	7.63	23.68	2.43	24.44	2479.4
11.0	8.21	25.11	2.52	24.92	2740.8
12.0	8.71	26.28	2.59	25.31	2977.4
13.0	9.22	27.52	2.66	25.72	3226.1
14.0	9.69	28.85	2.74	26.23	3486.9
15.0	10.06	29.44	2.78	26.36	3726.2
16.0	10.44	30.29	2.83	26.65	3972.2
17.0	10.81	31.12	2.88	26.90	4224.3
18.0	11.14	31.88	2.93	27.16	4468.5
19.0	11.46	32.79	2.98	27.46	4709.5
20.0	11.78	33.66	3.04	27.76	4976.9
21.0	12.06	34.20	3.07	27.92	5217.8
22.0	12.30	35.05	3.12	28.24	5458.9
23.0	12.56	35.84	3.16	28.51	5722.7
24.0	12.79	36.43	3.20	28.68	5967.3
25.0	13.01	36.78	3.22	28.80	6210.5
26.0	13.21	38.02	3.29	29.25	6453.7
27.0	13.40	38.25	3.31	29.29	6704.9
28.0	13.59	38.88	3.35	29.53	6966.5
29.0	13.75	39.51	3.39	29.72	7205.1
30.0	13.91	39.74	3.40	29.79	7451.1
31.0	14.05	40.18	3.43	29.91	7696.3
32.0	14.19	40.37	3.45	29.96	7949.7
33.0	14.31	40.70	3.47	30.06	8194.5
34.0	14.42	40.95	3.47	30.22	8439.5
35.0	14.53	40.96	3.48	30.21	8698.8
36.0	14.61	40.98	3.48	30.21	8941.5
36.6	14.66	41.65	3.49	30.77	FAILURE
37.0	14.69	41.00	3.48	30.22	9187.8
39.0	14.82	40.96	3.46	30.28	9686.4
40.0	14.88	40.56	3.45	30.09	9941.2

APPENDIX C TABLE 2 - DRAINED TRIAXIAL COMPRESSION TESTS

Test CD3 — DRAINED TRIAXIAL COMPRESSION
σ_3' = 2.22 MPa — e_i = 0.512 — H/D = 2.51
Cambria sand — ϕ' = 33.4 — 2.54 CM/HR

ϵ_1 %	ϵ_v %	$\sigma_1 - \sigma_3$ MPa	σ_1'/σ_3'	p' MPa	Time second
0.0	0.00	0.06	1.03	2.19	-0.0
0.1	0.03	0.34	1.16	2.29	17.6
0.3	0.14	1.26	1.58	2.60	66.3
0.5	0.27	2.18	2.00	2.91	122.6
0.7	0.35	2.80	2.29	3.11	178.1
1.0	0.42	3.27	2.50	3.27	242.8
2.0	0.52	4.22	2.93	3.59	501.2
3.0	0.52	4.72	3.15	3.77	753.6
4.0	0.45	5.05	3.29	3.89	1003.5
5.0	0.35	5.26	3.39	3.96	1266.1
6.0	0.25	5.43	3.45	4.02	1511.5
7.0	0.14	5.51	3.49	4.05	1754.0
8.0	-0.02	5.60	3.53	4.09	2021.5
9.0	-0.08	5.65	3.55	4.10	2263.9
10.0	-0.18	5.71	3.57	4.12	2514.0
11.0	-0.27	5.73	3.58	4.13	2760.4
12.0	-0.35	5.76	3.58	4.15	3009.5
12.1	-0.37	5.77	3.59	4.15	*FAILURE*
13.0	-0.43	5.73	3.58	4.14	3263.2
14.0	-0.49	5.72	3.57	4.13	3530.0
15.0	-0.54	5.70	3.56	4.13	3776.7
16.0	-0.58	5.65	3.53	4.11	4025.2
17.0	-0.62	5.56	3.53	4.05	4270.9
18.0	-0.64	5.53	3.51	4.04	4522.6
19.0	-0.65	5.46	3.49	4.01	4789.1

APPENDIX C TABLE 3 - DRAINED TRIAXIAL COMPRESSION TESTS

Test CD4 — DRAINED TRIAXIAL COMPRESSION
σ_3' = 2.11 MPa — e_1 = 0.505 — H/D = 2.50
Cambria sand — ϕ' = 34.8 — 2.54 CM/HR

ϵ_1 %	ϵ_v %	$\sigma_1 - \sigma_3$ MPa	σ_1'/σ_3'	p' MPa	Time second
0.0	0.00	0.04	1.02	2.06	0.0
0.1	0.02	0.24	1.12	2.13	17.9
0.3	0.12	1.02	1.50	2.39	69.5
0.5	0.25	2.05	2.00	2.73	131.7
0.7	0.32	2.57	2.25	2.92	174.6
1.0	0.40	3.23	2.58	3.13	257.9
2.0	0.48	4.20	3.03	3.47	501.9
3.0	0.45	4.72	3.25	3.67	749.1
4.0	0.36	5.02	3.39	3.77	991.2
5.0	0.24	5.26	3.49	3.87	1241.8
6.0	0.09	5.40	3.56	3.91	1499.9
7.0	-0.05	5.50	3.60	3.94	1749.7
8.0	-0.19	5.53	3.63	3.95	1999.3
9.0	-0.32	5.59	3.64	3.97	2243.4
9.9	-0.43	5.62	3.66	3.99	FAILURE
10.0	-0.45	5.62	3.65	3.99	2509.7
11.0	-0.56	5.61	3.65	3.98	2754.8
12.0	-0.66	5.61	3.64	3.99	3002.2
13.0	-0.76	5.53	3.63	3.95	3246.2
14.0	-0.84	5.51	3.61	3.94	3492.9
15.0	-0.91	5.46	3.59	3.93	3746.9
16.0	-0.95	5.41	3.57	3.91	3995.3
17.0	-0.98	5.37	3.54	3.90	4243.0
18.0	-1.01	5.32	3.52	3.88	4512.3
19.0	-1.02	5.24	3.49	3.85	4757.5
20.0	-1.02	5.20	3.48	3.84	5008.8
21.0	-1.00	5.15	3.46	3.81	5256.6
22.0	-0.99	5.10	3.44	3.79	5501.3

APPENDIX C TABLE 4 - DRAINED TRIAXIAL COMPRESSION TESTS

Test CD6 — DRAINED TRIAXIAL COMPRESSION
σ_3' = 5.85 MPa — e_i = 0.518 — H/D = 2.49
Cambria sand — ϕ' = 32.9 — 2.54 CM/HR

ϵ_1 %	ϵ_v %	$\sigma_1 - \sigma_3$ MPa	σ_1'/σ_3'	p' MPa	Time second
0.0	0.00	0.04	1.01	5.84	-0.0
0.1	0.05	1.01	1.17	6.17	34.0
0.3	0.15	2.19	1.37	6.59	70.0
0.5	0.29	3.41	1.58	6.98	122.0
0.7	0.40	4.15	1.71	7.22	166.0
1.0	0.60	5.12	1.88	7.55	244.8
2.0	1.12	6.82	2.17	8.10	496.1
3.0	1.59	7.81	2.34	8.42	756.5
4.0	1.97	8.55	2.46	8.71	990.9
5.0	2.37	9.11	2.56	8.88	1255.3
6.0	2.71	9.52	2.63	9.02	1493.8
7.0	3.04	9.90	2.69	9.15	1741.6
8.0	3.37	10.20	2.74	9.25	1991.2
9.0	3.69	10.43	2.79	9.30	2246.5
10.0	4.00	10.69	2.83	9.39	2492.7
11.0	4.33	10.98	2.87	9.53	2757.5
12.0	4.61	11.14	2.91	9.56	2997.0
13.0	4.92	11.36	2.94	9.63	3255.1
14.0	5.21	11.54	2.97	9.70	3494.3
15.0	5.49	11.75	3.01	9.77	3743.0
16.0	5.78	11.86	3.03	9.79	3998.2
17.0	6.07	12.01	3.06	9.82	4258.2
18.0	6.34	12.22	3.09	9.91	4502.1
19.0	6.59	12.37	3.12	9.97	4754.6
20.0	6.85	12.53	3.14	10.03	4995.7
21.0	7.12	12.69	3.17	10.08	5241.6
22.0	7.38	12.84	3.19	10.13	5490.7
23.0	7.65	12.98	3.22	10.18	5743.9
24.0	7.90	13.14	3.24	10.24	5993.3
25.0	8.15	13.22	3.26	10.25	6245.5
26.0	8.38	13.36	3.29	10.29	6491.6
27.0	8.61	13.44	3.31	10.29	6736.3
28.0	8.85	13.61	3.32	10.40	6995.0
29.0	9.07	13.69	3.34	10.42	7242.1
30.0	9.28	13.79	3.36	10.45	7486.6
31.0	9.50	13.85	3.36	10.47	7743.4
31.3	9.57	13.92	3.38	10.49	FAILURE
32.0	9.71	13.80	3.36	10.45	7992.3

APPENDIX C TABLE 5 - DRAINED TRIAXIAL COMPRESSION TESTS

0.524 H/D = 2.53
Cambria sand $\phi' = 32.6$ 2.54 CM/HR

ϵ_1 %	ϵ_v %	$\sigma_1 - \sigma_3$ MPa	σ_1'/σ_3'	p' MPa	Time second
0.0	0.00	0.05	1.01	3.97	-0.0
0.1	0.04	0.54	1.14	4.15	33.6
0.3	0.08	0.99	1.25	4.29	70.2
0.5	0.20	2.23	1.56	4.71	124.0
0.7	0.31	3.03	1.77	4.97	168.5
1.0	0.47	4.02	2.01	5.31	246.5
2.0	0.84	5.56	2.41	5.81	509.8
3.0	1.11	6.35	2.61	6.07	765.9
4.0	1.32	6.90	2.73	6.29	1008.4
5.0	1.52	7.28	2.83	6.41	1260.2
6.0	1.71	7.64	2.91	6.54	1526.5
7.0	1.87	7.81	2.97	6.57	1769.0
8.0	2.03	8.00	3.02	6.63	2017.8
9.0	2.18	8.17	3.06	6.70	2274.7
10.0	2.34	8.30	3.09	6.75	2524.4
11.0	2.49	8.40	3.12	6.77	2782.0
12.0	2.66	8.49	3.14	6.80	3040.5
13.0	2.82	8.53	3.16	6.80	3297.7
14.0	2.98	8.63	3.18	6.83	3541.9
15.0	3.14	8.69	3.19	6.85	3797.9
16.0	3.31	8.71	3.21	6.85	4042.7
17.0	3.48	8.78	3.22	6.88	4300.4
18.0	3.65	8.82	3.24	6.89	4562.1
19.0	3.82	8.94	3.25	6.96	4810.8
20.0	4.00	8.98	3.26	6.97	5069.6
21.0	4.17	9.02	3.27	6.98	5310.8
22.0	4.36	9.07	3.28	7.00	5570.2
23.0	4.54	9.12	3.29	7.02	5814.9
24.0	4.73	9.13	3.30	7.02	6072.0
25.0	4.91	9.20	3.31	7.04	6322.9
26.0	5.09	9.24	3.32	7.06	6581.2
27.0	5.27	9.24	3.33	7.05	6831.3
28.0	5.46	9.25	3.33	7.06	7088.9
29.0	5.64	9.26	3.34	7.05	7351.3
29.3	5.69	9.36	3.34	7.12	FAILURE
30.0	5.81	9.25	3.33	7.05	7590.4
31.0	5.99	9.22	3.33	7.02	7851.8

APPENDIX C TABLE 6 - DRAINED TRIAXIAL COMPRESSION TESTS

Test CD8 — DRAINED TRIAXIAL COMPRESSION
σ_3' = 11.48 MPa — e_i = 0.534 — H/D = 2.53
Cambria sand — ϕ' = 33.7 — 2.54 CM/HR

ϵ_1 %	ϵ_v %	$\sigma_1 - \sigma_3$ MPa	σ_1'/σ_3'	p' MPa	Time second
0.0	0.00	0.05	1.00	11.48	0.0
0.1	0.04	1.47	1.13	11.98	33.7
0.3	0.11	1.98	1.17	12.13	70.9
0.5	0.21	2.45	1.21	12.29	117.9
0.7	0.32	2.62	1.23	12.35	175.1
1.0	0.50	3.56	1.31	12.66	259.5
2.0	1.40	6.23	1.54	13.53	493.7
3.0	2.28	8.10	1.71	14.16	747.4
4.0	3.10	9.61	1.84	14.68	1002.8
5.0	3.84	10.90	1.95	15.11	1254.1
6.0	4.54	12.01	2.05	15.49	1508.4
7.0	5.20	13.01	2.13	15.80	1756.2
8.0	5.85	13.96	2.22	16.12	2013.0
9.0	6.44	14.79	2.29	16.38	2258.7
10.0	7.02	15.66	2.36	16.70	2511.0
11.0	7.55	16.47	2.43	16.98	2756.3
12.0	8.09	17.25	2.50	17.22	3014.5
13.0	8.59	18.01	2.57	17.47	3266.9
14.0	9.06	18.70	2.63	17.68	3513.5
15.0	9.51	19.49	2.70	17.99	3764.1
16.0	9.95	20.14	2.76	18.16	4018.0
17.0	10.37	20.86	2.82	18.43	4268.1
18.0	10.77	21.56	2.88	18.65	4528.4
19.0	11.13	22.16	2.93	18.85	4767.1
20.0	11.49	22.83	2.99	19.08	5024.9
21.0	11.84	23.39	3.04	19.26	5281.5
22.0	12.14	23.91	3.08	19.45	5516.1
23.0	12.45	24.53	3.14	19.66	5771.4
24.0	12.75	25.09	3.19	19.85	6023.1
25.0	13.03	25.54	3.22	19.99	6281.1
26.0	13.27	25.98	3.27	20.13	6522.8
27.0	13.52	26.38	3.30	20.25	6776.4
28.0	13.75	26.91	3.34	20.47	7030.1
29.0	13.97	27.29	3.38	20.58	7288.2
30.0	14.16	27.48	3.40	20.62	7529.7
31.0	14.34	27.83	3.43	20.75	7776.4
32.0	14.52	28.13	3.45	20.88	8032.3
33.0	14.69	28.35	3.47	20.95	8291.3
34.0	14.83	28.49	3.48	20.99	8534.1
35.0	14.97	28.55	3.49	20.99	8788.5
36.0	15.09	28.69	3.50	21.05	9032.7
36.3	15.13	28.70	3.50	21.05	FAILURE
37.0	15.22	28.69	3.50	21.05	9290.4
39.0	15.42	28.61	3.49	21.04	9793.9
40.0	15.52	28.49	3.47	21.01	10043.3

APPENDIX C TABLE 7 - DRAINED TRIAXIAL COMPRESSION TESTS

Test CD9 DRAINED TRIAXIAL COMPRESSION
σ_3' = 15.00 MPa e_i = 0.502 H/D = 2.52
Cambria sand ϕ' = 33.3 2.54 CM/HR

ϵ_1 %	ϵ_v %	$\sigma_1 - \sigma_3$ MPa	σ_1'/σ_3'	p' MPa	Time second
0.0	0.00	0.11	1.01	14.99	-0.0
0.1	0.04	0.99	1.07	15.28	33.2
0.3	0.10	1.52	1.10	15.47	68.0
0.5	0.26	2.76	1.18	15.87	122.7
0.7	0.52	3.71	1.25	16.20	182.3
1.0	0.82	4.55	1.30	16.48	250.8
2.0	1.80	6.99	1.47	17.28	502.3
3.0	2.66	8.87	1.59	17.92	742.1
4.0	3.52	10.66	1.71	18.51	996.8
5.0	4.30	12.26	1.82	19.04	1244.6
6.0	5.03	13.71	1.92	19.53	1489.2
7.0	5.75	15.03	2.01	19.96	1744.0
8.0	6.40	16.47	2.10	20.46	1991.0
9.0	7.01	17.57	2.18	20.80	2235.6
10.0	7.60	18.85	2.26	21.26	2487.2
11.0	8.16	20.03	2.34	21.65	2735.3
12.0	8.69	21.14	2.41	22.01	2989.1
13.0	9.18	22.24	2.49	22.37	3236.6
14.0	9.65	23.31	2.56	22.71	3483.3
15.0	10.10	24.39	2.63	23.08	3735.6
16.0	10.54	25.46	2.70	23.46	3994.9
17.0	10.94	26.45	2.77	23.78	4240.1
18.0	11.30	27.35	2.83	24.08	4485.4
19.0	11.65	28.24	2.89	24.36	4731.8
20.0	11.97	29.15	2.95	24.67	4982.2
21.0	12.27	29.95	3.01	24.92	5228.2
22.0	12.55	30.72	3.05	25.20	5482.4
23.0	12.81	31.54	3.11	25.48	5727.0
24.0	13.06	32.22	3.15	25.70	5979.7
25.0	13.29	32.86	3.20	25.91	6229.4
26.0	13.50	33.43	3.24	26.08	6478.8
27.0	13.69	34.09	3.28	26.32	6726.4
28.0	13.87	34.60	3.31	26.50	6973.2
29.0	14.03	34.97	3.34	26.61	7218.7
30.0	14.18	35.38	3.36	26.76	7469.1
31.0	14.32	35.75	3.39	26.90	7731.5
32.0	14.44	35.76	3.39	26.87	7969.4
33.0	14.54	36.09	3.42	26.97	8218.2
34.0	14.65	36.35	3.43	27.10	8484.8
34.9	14.72	36.45	3.43	27.15	FAILURE
35.0	14.73	36.13	3.42	26.96	8722.3
36.0	14.80	36.32	3.43	27.07	8969.5
37.0	14.87	36.27	3.42	27.08	9218.7
38.0	14.93	36.02	3.41	26.98	9477.3
40.0	15.02	35.82	3.39	26.95	9963.2

APPENDIX C TABLE 8 - DRAINED TRIAXIAL COMPRESSION TESTS

Test CD10 DRAINED TRIAXIAL COMPRESSION
σ_3' = 15.00 MPa e_i = 0.514 H/D = 2.54
Cambria sand ϕ' = 33.7 2.54 CM/HR

ϵ_1 %	ϵ_v %	$\sigma_1 - \sigma_3$ MPa	σ_1'/σ_3'	p' MPa	Time second
0.0	0.00	0.08	1.01	14.98	-0.00
0.1	0.04	1.04	1.07	15.32	33.56
0.3	0.12	2.08	1.14	15.65	67.40
0.5	0.32	3.43	1.23	16.10	121.11
0.7	0.57	4.48	1.30	16.45	184.50
1.0	0.82	5.32	1.36	16.73	245.13
2.0	1.73	8.06	1.54	17.67	499.71
3.0	2.58	10.14	1.68	18.33	754.84
4.0	3.33	11.96	1.80	18.96	1000.36
5.0	4.07	13.47	1.90	19.45	1258.46
6.0	4.78	14.96	2.00	19.95	1511.33
7.0	5.41	16.19	2.08	20.35	1753.94
8.0	6.08	17.47	2.17	20.78	2016.87
9.0	6.65	18.60	2.24	21.18	2258.54
10.0	7.24	19.72	2.32	21.55	2516.58
11.0	7.78	20.74	2.39	21.88	2764.79
12.0	8.29	21.82	2.46	22.24	3015.08
13.0	8.78	22.79	2.52	22.57	3266.09
14.0	9.26	23.79	2.59	22.91	3527.87
15.0	9.70	24.68	2.65	23.20	3773.55
16.0	10.13	25.65	2.71	23.52	4024.56
17.0	10.56	26.54	2.77	23.81	4283.75
18.0	10.93	27.38	2.83	24.09	4521.80
19.0	11.30	28.18	2.89	24.34	4771.82
20.0	11.66	29.08	2.94	24.68	5032.88
21.0	11.99	29.90	3.00	24.93	5283.72
22.0	12.30	30.80	3.05	25.27	5532.15
23.0	12.59	31.41	3.10	25.45	5781.08
24.0	12.89	32.27	3.15	25.76	6048.95
25.0	13.14	32.81	3.19	25.91	6292.43
26.0	13.38	33.48	3.24	26.13	6541.13
27.0	13.61	34.04	3.28	26.31	6788.85
28.0	13.82	34.65	3.32	26.52	7037.00
29.0	14.03	35.27	3.35	26.76	7308.50
30.0	14.21	35.54	3.37	26.82	7549.18
31.0	14.38	36.07	3.41	27.01	7795.58
32.0	14.54	36.39	3.43	27.09	8046.20
33.0	14.68	36.69	3.45	27.18	8301.50
34.0	14.82	37.11	3.48	27.35	8555.25
35.0	14.94	37.16	3.48	27.34	8806.59
36.0	15.05	37.31	3.49	27.41	9062.32
36.8	15.13	37.50	3.50	27.50	FAILURE
37.0	15.15	37.43	3.50	27.46	9305.09
38.0	15.24	37.43	3.49	27.49	9559.89
40.0	15.39	37.10	3.48	27.34	10058.67

APPENDIX C TABLE 9 - DRAINED TRIAXIAL COMPRESSION TESTS

Test CD12 DRAINED TRIAXIAL COMPRESSION
σ_3' = 5.85 MPa e_i = 0.515 H/D = 2.50
Cambria sand ϕ' = 33.4 2.54 CM/HR

ϵ_1 %	ϵ_v %	$\sigma_1 - \sigma_3$ MPa	σ_1'/σ_3'	p' MPa	Time second
0.0	0.00	0.04	1.01	5.81	0.0
0.1	0.02	0.47	1.08	5.94	21.5
0.3	0.13	1.83	1.32	6.40	65.3
0.5	0.26	2.96	1.51	6.81	119.5
0.7	0.39	3.83	1.66	7.10	169.8
1.0	0.58	4.80	1.83	7.40	244.9
2.0	1.17	6.71	2.15	8.05	506.3
3.0	1.61	7.68	2.32	8.38	741.3
4.0	2.06	8.48	2.47	8.61	1008.4
5.0	2.44	9.07	2.56	8.83	1249.9
6.0	2.82	9.55	2.64	9.00	1500.1
7.0	3.19	9.97	2.71	9.15	1756.0
8.0	3.53	10.29	2.77	9.24	1999.6
9.0	3.87	10.60	2.82	9.35	2247.3
10.0	4.22	10.86	2.87	9.44	2509.6
11.0	4.53	11.13	2.91	9.53	2752.1
12.0	4.84	11.31	2.95	9.57	3005.0
13.0	5.15	11.52	2.98	9.67	3259.7
14.0	5.45	11.74	3.01	9.75	3499.3
15.0	5.76	11.94	3.05	9.81	3755.0
16.0	6.04	12.11	3.08	9.86	3997.9
17.0	6.34	12.30	3.11	9.92	4252.2
18.0	6.63	12.53	3.15	10.01	4510.7
19.0	6.89	12.64	3.17	10.03	4751.3
20.0	7.17	12.80	3.21	10.06	5013.4
21.0	7.42	12.99	3.23	10.15	5253.4
22.0	7.69	13.18	3.26	10.23	5509.3
23.0	7.93	13.32	3.28	10.27	5748.8
24.0	8.20	13.51	3.31	10.36	6011.6
25.0	8.43	13.61	3.33	10.37	6251.8
26.0	8.68	13.69	3.35	10.39	6505.6
27.0	8.92	13.83	3.37	10.43	6759.6
28.0	9.15	13.91	3.39	10.46	7004.5
29.0	9.37	14.03	3.41	10.51	7252.0
30.0	9.59	13.98	3.41	10.45	7509.5
31.0	9.82	14.14	3.43	10.53	7771.3
32.0	10.01	14.20	3.43	10.56	8005.3
33.0	10.23	14.28	3.44	10.59	8268.2
34.0	10.41	14.26	3.44	10.58	8504.6
34.1	10.43	14.33	3.45	10.63	FAILURE
35.0	10.61	14.27	3.44	10.59	8764.7
36.0	10.78	14.24	3.44	10.58	9004.3
37.0	10.97	14.22	3.44	10.57	9268.9
38.0	11.14	14.20	3.44	10.56	9515.5
40.0	11.47	14.07	3.41	10.52	10014.6

APPENDIX C TABLE 10 - DRAINED TRIAXIAL COMPRESSION TESTS

Test CD13 DRAINED TRIAXIAL COMPRESSION
σ_3' = 4.50 MPa e_i = 0.520 H/D = 2.51
Cambria sand ϕ' = 32.5 2.54 CM/HR

ϵ_1 %	ϵ_v %	$\sigma_1 - \sigma_3$ MPa	σ_1'/σ_3'	p' MPa	Time second
0.0	0.00	0.09	1.02	4.49	-0.0
0.1	0.03	0.58	1.13	4.64	21.8
0.3	0.17	1.92	1.43	5.11	73.5
0.5	0.30	2.88	1.64	5.42	123.7
0.7	0.42	3.60	1.81	5.67	173.8
1.0	0.56	4.35	1.97	5.92	243.2
2.0	0.99	5.86	2.31	6.42	496.2
3.0	1.33	6.70	2.50	6.69	750.8
4.0	1.62	7.30	2.63	6.90	1006.8
5.0	1.88	7.70	2.73	7.03	1247.7
6.0	2.13	8.05	2.81	7.13	1500.9
7.0	2.38	8.38	2.87	7.28	1759.5
8.0	2.60	8.57	2.92	7.33	2003.0
9.0	2.83	8.79	2.96	7.40	2258.0
10.0	3.06	8.93	2.99	7.46	2511.3
11.0	3.28	9.05	3.02	7.50	2770.5
12.0	3.48	9.16	3.05	7.53	3011.8
13.0	3.70	9.26	3.07	7.55	3265.4
14.0	3.92	9.36	3.10	7.59	3514.7
15.0	4.13	9.44	3.13	7.59	3777.1
16.0	4.34	9.49	3.13	7.61	4019.5
17.0	4.56	9.61	3.15	7.66	4273.7
18.0	4.78	9.73	3.15	7.76	4524.4
19.0	4.99	9.73	3.18	7.71	4769.3
20.0	5.22	9.86	3.20	7.76	5028.2
21.0	5.44	9.97	3.21	7.83	5286.1
22.0	5.63	9.99	3.23	7.81	5527.6
23.0	5.85	10.03	3.24	7.82	5786.8
24.0	6.06	10.10	3.26	7.85	6036.1
25.0	6.27	10.16	3.27	7.86	6277.1
26.0	6.48	10.24	3.28	7.91	6529.7
27.0	6.69	10.21	3.29	7.87	6775.5
28.0	6.90	10.28	3.31	7.89	7037.7
29.0	7.09	10.31	3.31	7.90	7278.7
30.0	7.30	10.35	3.31	7.93	7536.0
31.0	7.50	10.37	3.32	7.93	7786.1
32.0	7.70	10.44	3.32	7.98	FAILURE
33.0	7.89	10.36	3.31	7.93	8290.6
34.0	8.08	10.33	3.31	7.92	8545.0
35.0	8.26	10.36	3.31	7.93	8788.3
36.0	8.44	10.26	3.30	7.88	9038.9
37.0	8.62	10.26	3.29	7.89	9289.9
38.0	8.80	10.24	3.29	7.89	9546.4
39.0	8.97	10.18	3.28	7.87	9798.3
40.0	9.15	10.20	3.26	7.91	10053.0

APPENDIX C TABLE 11 - DRAINED TRIAXIAL COMPRESSION TESTS

Test CD14 — DRAINED TRIAXIAL COMPRESSION
σ_3' = 3.50 MPa — e_i = 0.529 — H/D = 2.53
Cambria sand — ϕ' = 33.3 — 2.54 CM/HR

ϵ_1 %	ϵ_v %	$\sigma_1 - \sigma_3$ MPa	σ_1'/σ_3'	p' MPa	Time second
0.0	0.00	0.05	1.01	3.46	0.0
0.1	0.04	0.60	1.18	3.64	21.4
0.3	0.17	1.70	1.49	4.02	69.8
0.5	0.30	2.63	1.76	4.33	120.5
0.7	0.41	3.31	1.96	4.55	170.2
1.0	0.56	4.07	2.17	4.84	249.7
2.0	0.94	5.29	2.52	5.24	502.6
3.0	1.23	5.99	2.72	5.48	753.6
4.0	1.48	6.46	2.86	5.64	1012.7
5.0	1.70	6.82	2.96	5.76	1270.6
6.0	1.90	7.08	3.04	5.84	1530.6
7.0	2.08	7.30	3.10	5.91	1781.9
8.0	2.24	7.46	3.15	5.96	2024.1
9.0	2.41	7.63	3.19	6.02	2284.5
10.0	2.57	7.72	3.22	6.05	2527.6
11.0	2.73	7.81	3.25	6.07	2782.3
12.0	2.90	7.89	3.27	6.10	3048.8
13.0	3.07	7.99	3.29	6.16	3290.0
14.0	3.25	8.07	3.31	6.18	3555.1
15.0	3.40	8.13	3.33	6.20	3797.3
16.0	3.57	8.15	3.34	6.20	4052.5
17.0	3.74	8.22	3.36	6.22	4307.6
18.0	3.92	8.29	3.37	6.26	4567.2
19.0	4.09	8.31	3.39	6.26	4825.5
20.0	4.25	8.30	3.39	6.23	5064.6
21.0	4.42	8.37	3.40	6.27	5319.4
22.0	4.60	8.39	3.42	6.27	5578.8
23.0	4.78	8.43	3.41	6.30	5836.2
24.0	4.94	8.42	3.42	6.28	6081.2
25.0	5.12	8.46	3.43	6.29	6337.4
25.9	5.28	8.54	3.44	6.35	FAILURE
26.0	5.29	8.40	3.44	6.25	6590.1
27.0	5.48	8.48	3.43	6.32	6849.7
28.0	5.66	8.47	3.43	6.31	7106.9
29.0	5.84	8.47	3.43	6.30	7354.3
30.0	6.01	8.47	3.42	6.32	7602.6
31.0	6.19	8.48	3.43	6.32	7856.9
32.0	6.37	8.43	3.42	6.30	8118.9
33.0	6.54	8.40	3.41	6.29	8378.8
34.0	6.69	8.34	3.39	6.26	8617.5
35.0	6.86	8.32	3.39	6.26	8875.5
36.0	7.01	8.25	3.36	6.24	9126.8
37.0	7.16	8.17	3.34	6.22	9387.0

APPENDIX C TABLE 12 - DRAINED TRIAXIAL COMPRESSION TESTS

Test CD15 DRAINED TRIAXIAL COMPRESSION
σ_3' = 11.50 MPa e_i = 0.519 H/D = 2.50
Cambria sand ϕ' = 34.0 2.54 CM/HR

ϵ_1 %	ϵ_v %	$\sigma_1 - \sigma_3$ MPa	σ_1'/σ_3'	p' MPa	Time second
0.0	0.00	0.06	1.00	11.48	-0.0
0.1	0.03	0.78	1.07	11.73	23.8
0.3	0.16	2.45	1.21	12.27	71.1
0.5	0.38	3.57	1.31	12.66	124.8
0.7	0.58	4.36	1.38	12.92	175.0
1.0	0.87	5.39	1.47	13.27	253.6
2.0	1.71	7.78	1.68	14.05	493.9
3.0	2.53	9.67	1.84	14.70	749.9
4.0	3.25	11.12	1.97	15.19	991.0
5.0	3.94	12.34	2.08	15.58	1238.2
6.0	4.63	13.51	2.18	15.96	1495.5
7.0	5.23	14.50	2.26	16.31	1736.6
8.0	5.86	15.46	2.35	16.62	1996.4
9.0	6.41	16.30	2.42	16.88	2238.1
10.0	6.93	17.14	2.50	17.18	2478.3
11.0	7.44	17.95	2.56	17.46	2735.0
12.0	7.92	18.67	2.63	17.71	2978.4
13.0	8.41	19.51	2.70	17.99	3241.1
14.0	8.85	20.14	2.76	18.19	3485.9
15.0	9.28	20.85	2.82	18.43	3727.8
16.0	9.69	21.44	2.87	18.59	3974.6
17.0	10.09	22.14	2.93	18.84	4227.8
18.0	10.47	22.81	2.99	19.07	4475.8
19.0	10.82	23.37	3.04	19.25	4718.1
20.0	11.16	23.98	3.09	19.46	4971.2
21.0	11.47	24.51	3.14	19.62	5213.8
22.0	11.78	25.07	3.19	19.82	5467.2
23.0	12.07	25.55	3.23	19.96	5717.1
24.0	12.34	26.11	3.27	20.18	5959.3
25.0	12.60	26.64	3.32	20.36	6211.3
26.0	12.86	26.93	3.35	20.44	6471.4
27.0	13.09	27.33	3.38	20.57	6716.9
28.0	13.30	27.66	3.41	20.69	6959.8
29.0	13.50	28.10	3.44	20.87	7202.8
30.0	13.69	28.38	3.47	20.94	7451.7
31.0	13.87	28.52	3.49	20.95	7704.4
32.0	14.03	28.83	3.51	21.11	7948.6
33.0	14.19	28.84	3.51	21.10	8206.0
34.0	14.33	28.97	3.52	21.13	8455.8
34.4	14.37	29.21	3.54	21.24	FAILURE
35.0	14.46	29.02	3.53	21.14	8692.9
36.0	14.58	28.97	3.53	21.09	8945.7
37.0	14.69	28.83	3.52	21.05	9202.6
38.0	14.80	28.88	3.51	21.15	9451.7
40.0	14.98	28.63	3.49	21.06	9951.1

APPENDIX C TABLE 13 - DRAINED TRIAXIAL COMPRESSION TESTS

Test CD16 DRAINED TRIAXIAL COMPRESSION
σ_3' = 17.23 MPa e_i = 0.519 H/D = 2.50
Cambria sand ϕ' = 33.8 2.54 CM/HR

ϵ_1 %	ϵ_v %	$\sigma_1 - \sigma_3$ MPa	σ_1'/σ_3'	p' MPa	Time second
0.0	0.00	0.14	1.01	17.22	-0.0
0.1	0.03	1.05	1.06	17.52	22.5
0.3	0.12	2.20	1.13	17.91	64.8
0.5	0.33	3.67	1.21	18.40	119.9
0.7	0.55	4.52	1.26	18.68	171.2
1.0	0.84	5.49	1.32	19.03	241.7
2.0	1.85	8.48	1.49	20.03	497.7
3.0	2.72	10.77	1.63	20.78	739.1
4.0	3.59	12.91	1.75	21.52	997.1
5.0	4.34	14.76	1.86	22.14	1232.6
6.0	5.10	16.41	1.96	22.63	1481.8
7.0	5.79	18.08	2.05	23.24	1723.6
8.0	6.47	19.62	2.14	23.74	1972.6
9.0	7.13	21.21	2.23	24.27	2230.1
10.0	7.70	22.56	2.31	24.71	2464.6
11.0	8.27	23.99	2.39	25.24	2714.1
12.0	8.82	25.24	2.47	25.58	2969.1
13.0	9.32	26.62	2.55	26.06	3212.3
14.0	9.79	27.81	2.62	26.45	3458.5
15.0	10.25	29.24	2.70	26.96	3707.6
16.0	10.68	30.33	2.77	27.26	3951.7
17.0	11.09	31.56	2.83	27.73	4202.1
18.0	11.47	32.70	2.90	28.11	4448.8
19.0	11.83	33.73	2.96	28.44	4696.1
20.0	12.17	34.76	3.02	28.76	4955.4
21.0	12.46	35.83	3.08	29.15	5191.6
22.0	12.73	36.83	3.14	29.48	5428.2
23.0	13.02	37.63	3.19	29.73	5692.9
24.0	13.26	38.30	3.23	29.95	5932.7
25.0	13.50	39.27	3.27	30.36	6185.3
26.0	13.71	40.18	3.33	30.65	6437.3
27.0	13.90	40.54	3.36	30.71	6682.0
28.0	14.08	41.21	3.39	30.96	6930.4
29.0	14.23	41.71	3.42	31.13	7166.6
30.0	14.38	42.25	3.44	31.37	7410.8
31.0	14.51	42.34	3.46	31.30	7666.5
32.0	14.63	42.76	3.48	31.48	7916.1
33.0	14.74	42.92	3.49	31.54	8169.4
34.0	14.83	42.84	3.50	31.44	8399.9
35.0	14.91	43.23	3.51	31.64	8661.6
35.4	14.94	43.25	3.51	31.65	FAILURE
36.0	14.98	43.10	3.50	31.61	8894.6
37.0	15.05	42.67	3.48	31.46	9151.7
38.0	15.10	42.32	3.47	31.24	9395.5
40.0	15.19	41.75	3.44	31.04	9890.3

APPENDIX C TABLE 14 - DRAINED TRIAXIAL COMPRESSION TESTS

Test CD17 — DRAINED TRIAXIAL COMPRESSION
σ_3' = 26.00 MPa — e_i = 0.522 — H/D = 2.50
Cambria sand — ϕ' = 33.7 — 2.54 CM/HR

ϵ_1 %	ϵ_v %	$\sigma_1 - \sigma_3$ MPa	σ_1'/σ_3'	p' MPa	Time second
0.0	0.00	0.09	1.00	25.99	0.0
0.1	0.02	1.23	1.05	26.34	24.7
0.3	0.11	2.91	1.11	26.94	69.2
0.5	0.31	4.59	1.18	27.50	119.0
0.7	0.52	5.57	1.21	27.82	167.0
1.0	0.89	6.92	1.27	28.28	246.5
2.0	1.92	10.46	1.40	29.45	485.8
3.0	2.93	13.87	1.53	30.59	741.0
4.0	3.83	16.83	1.65	31.58	983.7
5.0	4.71	19.74	1.76	32.50	1235.4
6.0	5.44	22.30	1.86	33.41	1461.7
7.0	6.21	25.09	1.97	34.34	1711.8
8.0	6.92	27.73	2.07	35.21	1961.9
9.0	7.55	29.93	2.15	35.90	2198.5
10.0	8.16	32.61	2.26	36.85	2449.6
11.0	8.76	35.24	2.36	37.74	2698.8
12.0	9.28	37.55	2.44	38.51	2935.9
13.0	9.78	39.73	2.53	39.20	3181.1
14.0	10.24	41.90	2.61	39.95	3426.8
15.0	10.68	44.08	2.70	40.68	3676.4
16.0	11.07	46.05	2.77	41.33	3912.0
17.0	11.43	47.75	2.84	41.88	4159.0
18.0	11.76	49.69	2.91	42.52	4404.1
19.0	12.06	51.48	2.98	43.14	4648.8
20.0	12.34	53.37	3.05	43.81	4900.9
21.0	12.58	54.47	3.10	44.12	5138.8
22.0	12.81	55.95	3.16	44.60	5380.1
23.0	13.02	57.43	3.21	45.14	5638.1
24.0	13.20	58.76	3.26	45.57	5875.3
25.0	13.36	59.70	3.30	45.87	6115.0
26.0	13.51	60.70	3.34	46.16	6363.7
27.0	13.64	61.83	3.37	46.64	6607.5
28.0	13.75	62.43	3.40	46.79	6861.7
29.0	13.84	62.93	3.42	46.93	7111.4
30.0	13.92	63.02	3.43	46.94	7353.0
31.0	13.99	64.07	3.47	47.32	7604.7
32.0	14.04	64.38	3.48	47.44	7830.6
33.0	14.09	64.68	3.48	47.57	8093.4
33.5	14.11	64.74	3.49	47.58	FAILURE
34.0	14.12	64.23	3.48	47.34	8326.4
35.0	14.14	63.72	3.45	47.22	8565.3
36.0	14.16	63.80	3.46	47.19	8813.7
37.0	14.17	63.28	3.43	47.10	9063.3
38.0	14.17	63.45	3.43	47.21	9310.5
40.0	14.15	62.07	3.38	46.73	9795.5

APPENDIX C TABLE 15 - DRAINED TRIAXIAL COMPRESSION TESTS

Test CD19 DRAINED TRIAXIAL COMPRESSION
σ_3' = 40.0 MPa e_i = 0.519 H/D = 2.50
Cambria sand ϕ' = 33.3 2.54 CM/HR

ϵ_1 %	ϵ_v %	$\sigma_1 - \sigma_3$ MPa	σ_1'/σ_3'	p' MPa	Time second
0.0	0.00	0.31	1.01	40.07	0.0
0.0	0.01	1.51	1.04	40.48	11.6
0.3	0.16	5.33	1.13	41.76	69.6
0.5	0.36	7.06	1.18	42.34	121.4
0.7	0.59	8.47	1.21	42.80	174.0
1.0	0.85	9.92	1.25	43.30	233.8
2.0	1.89	15.36	1.38	45.09	486.3
3.0	2.80	20.23	1.51	46.73	724.5
4.0	3.66	24.91	1.62	48.25	964.7
5.0	4.50	29.65	1.74	49.85	1217.0
6.0	5.23	34.17	1.85	51.39	1453.9
7.0	5.95	38.70	1.97	52.90	1703.5
8.0	6.56	42.51	2.06	54.14	1933.3
9.0	7.14	46.77	2.17	55.57	2168.0
10.0	7.69	50.97	2.27	57.00	2419.7
11.0	8.17	54.54	2.36	58.15	2654.3
12.0	8.65	58.34	2.46	59.44	2911.7
13.0	9.03	62.04	2.55	60.71	3133.9
14.0	9.44	65.48	2.64	61.83	3385.4
15.0	9.81	68.84	2.72	62.96	3638.5
16.0	10.10	71.84	2.80	63.96	3861.6
17.0	10.40	74.80	2.87	64.89	4113.3
18.0	10.64	77.37	2.93	65.83	4349.4
19.0	10.88	80.32	3.01	66.75	4603.9
20.0	11.07	82.93	3.07	67.75	4831.8
21.0	11.25	85.33	3.13	68.45	5069.8
22.0	11.41	87.35	3.18	69.14	5315.9
23.0	11.54	89.63	3.24	69.94	5558.2
24.0	11.66	90.62	3.27	70.10	5798.3
25.0	11.75	92.41	3.31	70.87	6038.4
26.0	11.83	94.01	3.35	71.26	6290.6
27.0	11.89	95.23	3.37	71.84	6524.0
28.0	11.94	96.31	3.40	72.26	6777.1
29.0	11.97	96.82	3.41	72.39	7012.5
30.0	11.99	96.51	3.42	72.07	7251.7
31.0	12.00	97.48	3.43	72.48	7487.2
32.0	12.00	96.90	3.42	72.27	7741.8
32.2	12.00	97.60	3.44	72.53	FAILURE
33.0	11.99	97.18	3.42	72.48	7983.1
34.0	11.97	96.53	3.41	72.31	8218.0
35.0	11.95	95.97	3.40	71.99	8471.8
36.0	11.91	95.65	3.39	71.97	8704.8
37.0	11.88	93.39	3.34	71.09	8948.8
38.0	11.83	93.40	3.33	71.14	9203.2
39.0	11.79	92.33	3.31	70.80	9432.6

APPENDIX C TABLE 16 - DRAINED TRIAXIAL COMPRESSION TESTS

Test CD20 — DRAINED TRIAXIAL COMPRESSION
σ_3' = 8.00 MPa — e_i = 0.523 — H/D = 2.51
Cambria sand — ϕ' = 33.1 — w.81 CM/HR

ϵ_1 %	ϵ_v %	$\sigma_1 - \sigma_3$ MPa	σ_1'/σ_3'	p' MPa	Time second
0.0	0.00	0.07	1.01	8.01	0.0
0.0	0.02	0.41	1.05	8.17	13.2
0.3	0.10	1.70	1.21	8.50	45.6
0.5	0.20	2.44	1.31	8.81	83.2
0.7	0.29	3.07	1.38	9.02	114.9
1.0	0.48	4.10	1.51	9.35	165.2
2.0	1.20	6.54	1.82	10.17	325.4
3.0	1.90	8.10	2.01	10.69	498.4
4.0	2.51	9.22	2.15	11.08	660.9
5.0	3.12	10.17	2.27	11.38	838.9
6.0	3.63	10.84	2.36	11.60	997.2
7.0	4.15	11.50	2.44	11.83	1168.7
8.0	4.64	12.08	2.51	12.03	1338.8
9.0	5.08	12.58	2.57	12.20	1498.5
10.1	5.56	13.07	2.63	12.35	1677.5
11.0	5.98	13.49	2.69	12.49	1843.6
12.0	6.36	13.88	2.74	12.62	1998.9
12.9	6.76	14.27	2.78	12.78	2161.3
14.0	7.18	14.70	2.83	12.92	2343.7
15.0	7.55	15.01	2.88	13.00	2506.5
16.0	7.90	15.33	2.93	13.07	2669.9
17.0	8.24	15.70	2.97	13.22	2833.7
17.9	8.56	16.04	3.01	13.33	2996.1
19.0	8.91	16.35	3.05	13.43	3175.0
20.0	9.22	16.66	3.08	13.56	3337.3
21.0	9.52	16.94	3.12	13.65	3499.6
22.0	9.83	17.27	3.15	13.78	3676.9
23.0	10.10	17.54	3.19	13.88	3836.0
24.0	10.37	17.71	3.22	13.90	3999.8
25.0	10.65	17.97	3.25	13.99	4177.3
26.0	10.90	18.25	3.28	14.09	4342.8
27.0	11.15	18.43	3.30	14.16	4510.9
28.0	11.37	18.59	3.32	14.20	4667.7
29.0	11.60	18.78	3.34	14.28	4832.8
30.0	11.83	18.96	3.36	14.34	5015.0
31.0	12.03	19.03	3.38	14.35	5180.3
32.0	12.22	19.11	3.39	14.37	5340.4
33.0	12.40	19.19	3.40	14.40	5502.4
33.9	12.56	19.28	3.41	14.43	FAILURE
34.0	12.57	19.21	3.40	14.42	5668.1
35.0	12.74	19.22	3.40	14.40	5838.0
36.0	12.90	19.24	3.41	14.41	6002.9
37.0	13.05	19.16	3.39	14.39	6171.6
38.0	13.20	19.13	3.39	14.39	6349.6
40.0	13.45	18.89	3.36	14.30	6671.9

APPENDIX C TABLE 17 - DRAINED TRIAXIAL COMPRESSION TESTS

Test CD21 DRAINED TRIAXIAL COMPRESSION
σ_3' = 17.23 MPa e_i = 0.522 H/D = 2.50
Cambria sand ϕ' = 45.9 7.62 CM/HR

ϵ_1 %	ϵ_v %	$\sigma_1 - \sigma_3$ MPa	σ_1'/σ_3'	p' MPa	Time second
0.0	0.00	0.35	1.02	17.35	0.0
0.1	0.02	1.09	1.06	17.59	15.6
0.3	0.22	3.80	1.22	18.50	40.5
0.8	0.60	5.66	1.33	19.12	70.8
1.3	1.02	7.01	1.41	19.57	106.0
1.6	1.33	8.02	1.47	19.90	133.7
2.0	1.67	9.01	1.52	20.23	163.2
3.0	2.56	11.52	1.67	21.07	243.2
3.9	3.36	13.58	1.79	21.76	321.9
4.9	4.19	15.55	1.90	22.41	406.9
5.9	4.91	17.27	2.00	22.99	489.0
7.1	5.72	19.14	2.11	23.61	584.2
8.0	6.34	20.56	2.19	24.08	662.4
9.0	6.91	21.99	2.28	24.56	744.7
10.0	7.48	23.35	2.36	25.01	824.9
11.0	8.01	24.62	2.43	25.44	902.5
11.9	8.53	25.87	2.50	25.85	982.5
13.0	9.05	27.15	2.58	26.28	1066.9
13.9	9.49	28.36	2.65	26.68	1143.3
14.9	9.98	29.62	2.72	27.10	1230.2
15.9	10.41	30.81	2.79	27.50	1312.3
17.1	10.85	32.07	2.86	27.92	1404.6
18.0	11.20	33.11	2.92	28.27	1481.5
19.0	11.55	34.13	2.98	28.61	1563.1
20.0	11.87	35.09	3.04	28.93	1642.2
20.9	12.17	36.00	3.09	29.23	1723.8
21.9	12.46	36.90	3.14	29.53	1806.2
22.9	12.72	37.65	3.19	29.78	1885.9
24.0	12.99	38.48	3.23	30.06	1975.2
24.9	13.20	39.19	3.27	30.29	2048.6
25.9	13.42	39.97	3.32	30.55	2132.2
27.0	13.64	40.69	3.36	30.79	2221.1
27.9	13.82	41.21	3.39	30.97	2300.3
29.1	14.01	41.78	3.42	31.16	2395.0
30.1	14.16	42.29	3.45	31.33	2475.7
31.0	14.30	42.69	3.48	31.46	2555.1
32.0	14.42	42.96	3.49	31.55	2636.4
33.0	14.53	43.15	3.50	31.61	2716.6
34.0	14.63	43.28	3.51	31.66	2798.1
35.0	14.73	43.36	3.52	31.68	2880.6
35.9	14.80	43.40	3.52	31.70	FAILURE
37.0	14.88	43.21	3.51	31.63	3042.5
37.9	14.93	43.02	3.50	31.57	3123.0
39.0	14.99	42.77	3.48	31.49	3206.9
40.0	15.03	42.33	3.46	31.34	3290.5

APPENDIX C TABLE 18 - DRAINED TRIAXIAL COMPRESSION TESTS

Test CD22 — DRAINED TRIAXIAL COMPRESSION
σ_3' = 17.23 MPa — e_i = 0.522 — H/D = 2.50
Cambria sand — ϕ' = 33.6 — 0.53 CM/HR

ϵ_1 %	ϵ_v %	σ_1 MPa	σ_3 MPa	σ_1'/σ_3'	p' MPa	Time second
0.0	0.00	0.17	1.01	17.26		0.0
0.1	0.04	0.62	1.04	17.41		102.4
0.3	0.14	1.08	1.06	17.57		340.4
0.5	0.28	2.22	1.13	17.96		602.1
0.7	0.46	3.20	1.19	18.28		819.7
1.0	0.77	4.39	1.26	18.68		1187.5
2.0	1.72	7.37	1.43	19.65		2355.7
3.0	2.64	9.91	1.58	20.53		3518.4
4.0	3.54	12.13	1.70	21.25		4730.6
5.0	4.41	14.21	1.82	21.97		5981.6
6.0	5.17	15.93	1.92	22.54		7125.9
7.0	5.87	17.52	2.02	23.05		8264.1
8.0	6.57	19.08	2.11	23.57		9448.3
9.0	7.26	20.65	2.20	24.11		10605.3
10.0	7.85	21.98	2.28	24.55		11813.4
11.0	8.42	23.31	2.35	24.99		12955.3
12.0	8.99	24.66	2.43	25.44		14158.2
13.0	9.50	25.90	2.50	25.87		15292.7
14.0	9.99	27.10	2.57	26.26		16436.0
14.9	10.45	28.33	2.64	26.68		17593.1
16.0	10.92	29.59	2.72	27.10		18859.3
17.0	11.31	30.70	2.78	27.46		19978.8
18.0	11.71	31.83	2.85	27.82		21168.2
19.0	12.10	33.03	2.92	28.25		22418.8
20.0	12.42	34.00	2.97	28.57		23547.2
21.0	12.72	34.93	3.03	28.89		24673.7
22.0	13.00	35.83	3.08	29.17		25785.4
23.0	13.28	36.70	3.13	29.46		26975.3
24.0	13.55	37.56	3.18	29.76		28236.2
25.0	13.78	38.30	3.22	30.00		29358.2
25.9	13.99	39.04	3.27	30.24		30481.4
27.0	14.20	39.74	3.31	30.46		31681.9
28.0	14.39	40.43	3.35	30.69		32929.6
29.0	14.56	41.04	3.38	30.92		34061.1
30.0	14.71	41.51	3.41	31.08		35203.7
31.0	14.85	41.89	3.43	31.20		36336.6
32.0	14.99	42.25	3.45	31.33		37541.2
33.0	15.10	42.51	3.47	31.41		38671.7
34.0	15.20	42.66	3.47	31.46		39814.1
34.9	15.29	42.72	3.48	31.48		FAILURE
36.0	15.38	42.62	3.47	31.45		42216.4
37.1	15.44	42.47	3.46	31.39		43358.4
37.9	15.49	42.23	3.45	31.32		44368.4
39.0	15.54	41.91	3.43	31.21		45515.2
40.0	15.58	41.49	3.41	31.07		46644.4

APPENDIX C TABLE 19 - DRAINED TRIAXIAL COMPRESSION TESTS

Test CD23 DRAINED TRIAXIAL COMPRESSION
σ_3' = 17.23 MPa e_i = 0.524 H/D = 2.51
Cambria sand ϕ' = 34.2 7.62 CM/HR

ϵ_1 %	ϵ_v %	$\sigma_1 - \sigma_3$ MPa	σ_1'/σ_3'	p' MPa	Time second
0.0	0.00	0.10	1.01	17.23	0.0
0.1	0.01	0.52	1.03	17.42	12.9
0.5	0.19	2.66	1.15	18.42	52.1
1.0	0.53	4.89	1.29	18.73	83.4
1.4	0.92	6.28	1.37	19.11	118.8
1.8	1.26	7.25	1.42	19.58	148.6
2.2	1.60	8.35	1.49	19.97	181.9
3.0	2.31	10.24	1.60	20.61	245.0
4.1	3.31	12.70	1.74	21.41	339.7
5.1	4.07	14.53	1.85	22.02	417.4
6.0	4.80	16.19	1.94	22.58	497.9
7.0	5.48	17.71	2.03	23.11	576.0
8.0	6.17	19.23	2.12	23.60	661.1
9.0	6.80	20.67	2.20	24.08	744.5
9.9	7.35	21.95	2.28	24.52	820.6
11.1	7.99	23.44	2.36	25.01	913.7
11.9	8.48	24.54	2.43	25.37	988.0
12.9	9.00	25.81	2.50	25.79	1070.6
13.9	9.48	26.97	2.57	26.19	1150.6
14.9	9.95	28.14	2.64	26.55	1234.7
15.9	10.35	29.06	2.69	26.90	1315.9
17.0	10.76	30.07	2.75	27.22	1404.8
17.9	11.09	30.88	2.80	27.42	1482.6
19.1	11.46	31.87	2.86	27.71	1577.9
20.1	11.77	32.82	2.92	28.00	1662.1
21.1	12.07	33.76	2.97	28.33	1742.7
22.0	12.34	34.66	3.03	28.59	1822.8
23.0	12.59	35.44	3.08	28.81	1900.3
23.9	12.82	36.26	3.13	29.04	1977.3
25.0	13.07	37.09	3.18	29.29	2064.9
25.9	13.28	37.88	3.23	29.52	2144.5
27.0	13.49	38.74	3.28	29.75	2230.7
27.9	13.67	39.40	3.32	29.95	2306.8
29.1	13.88	40.22	3.37	30.17	2404.6
30.0	14.04	40.88	3.41	30.35	2483.2
31.0	14.19	41.51	3.44	30.58	2563.5
32.3	14.37	42.10	3.49	30.69	2671.5
33.0	14.45	42.41	3.50	30.80	2725.0
33.9	14.56	42.81	3.53	30.89	2802.0
34.9	14.67	42.97	3.55	30.87	2884.6
35.9	14.77	43.21	3.56	30.94	2968.9
37.0	14.86	43.40	3.57	30.97	FAILURE
37.9	14.93	43.30	3.57	30.91	3134.6
39.1	15.01	43.18	3.57	30.83	3230.8
40.0	15.06	43.09	3.56	30.80	3310.9

APPENDIX C TABLE 20 - DRAINED TRIAXIAL COMPRESSION TESTS

Test CD24 DRAINED TRIAXIAL COMPRESSION
σ_3' = 52.00 MPa e_i = 0.525 H/D = 2.51
Cambria sand ϕ' = ? 1.27 CM/HR
Test specimen buckled during shearing

ϵ_1 %	ϵ_v %	$\sigma_1 - \sigma_3$ MPa	σ_1'/σ_3'	p' MPa	Time second
0.0	0.00	0.13	1.00	52.03	0.0
0.0	0.01	0.55	1.01	52.24	13.1
0.3	0.03	1.96	1.04	52.62	73.6
0.5	0.06	3.01	1.06	53.00	126.7
0.7	0.09	3.68	1.07	53.24	163.9
1.0	0.15	5.20	1.10	53.73	234.2
2.0	0.59	15.03	1.29	57.00	485.1
3.0	1.26	21.28	1.41	59.09	715.6
4.0	1.95	26.44	1.51	60.78	968.8
5.0	2.56	30.57	1.59	62.20	1200.3
6.0	3.23	34.37	1.66	63.45	1443.8
7.0	3.78	37.43	1.72	64.45	1681.8
8.0	4.32	40.46	1.78	65.45	1926.2
9.0	4.79	43.03	1.83	66.33	2165.1
10.0	5.24	45.88	1.88	67.28	2401.2
11.0	5.68	48.45	1.93	68.15	2649.3
12.0	6.06	50.69	1.97	68.92	2888.4
13.0	6.41	53.08	2.02	69.71	3134.1
14.0	6.73	55.21	2.06	70.35	3371.7
15.0	7.04	57.80	2.11	71.25	3610.7
15.9	7.34	60.38	2.16	72.05	3838.5
17.0	7.65	63.53	2.22	73.16	4101.3
18.0	7.91	66.81	2.28	74.30	4325.1
19.0	8.18	69.73	2.34	75.27	4576.3
20.0	8.42	73.03	2.40	76.35	4817.9
21.0	8.64	76.38	2.47	77.46	5050.5
22.0	8.86	79.99	2.54	78.68	5287.3
23.1	9.08	83.62	2.61	79.95	5546.9
24.0	9.25	86.86	2.67	81.02	5768.3
25.0	9.42	90.27	2.74	82.11	6017.5
26.0	9.57	92.92	2.79	82.89	6255.0
27.0	9.72	96.97	2.86	84.41	6507.6
28.0	9.84	99.20	2.91	84.97	6736.2
29.0	9.95	102.52	2.97	86.16	6982.9
30.0	10.04	105.07	3.02	86.99	7227.8
31.0	10.12	108.19	3.08	88.14	7466.0
32.0	10.19	108.67	3.09	88.11	7711.6
33.0	10.24	110.81	3.14	88.84	7951.1
34.0	10.27	113.13	3.18	89.72	8187.9
35.0	10.30	114.66	3.20	90.35	8434.1
36.0	10.32	114.54	3.20	90.14	8672.3
37.0	10.34	115.50	3.22	90.51	8912.2
38.0	10.34	116.39	3.24	90.86	9151.0
38.9	10.35	117.54	3.26	91.18	9371.1

APPENDIX C TABLE 21 - DRAINED TRIAXIAL COMPRESSION TESTS

Test CD25 DRAINED TRIAXIAL COMPRESSION
σ_3' = 52.00 MPa e_i = 0.522 H/D = 2.50
Cambria sand ϕ' = 33.5 2.54 CM/HR

ϵ_1 %	ϵ_v %	$\sigma_1 - \sigma_3$ MPa	σ_1'/σ_3'	p' MPa	Time second
0.0	0.00	0.12	1.00	52.06	0.0
0.0	0.01	1.17	1.02	52.45	13.6
0.3	0.06	2.69	1.05	52.92	72.2
0.5	0.16	5.72	1.11	53.94	126.9
0.7	0.25	7.17	1.14	54.42	163.9
1.0	0.49	9.77	1.19	55.29	235.9
2.0	1.49	17.03	1.33	57.68	480.4
3.0	2.45	23.77	1.46	59.94	726.4
4.0	3.29	29.87	1.57	61.98	955.6
5.0	4.07	35.84	1.69	63.96	1191.3
6.0	4.77	41.65	1.80	65.93	1432.1
7.0	5.42	47.24	1.91	67.77	1667.9
8.0	6.07	52.99	2.02	69.70	1916.5
9.0	6.63	58.03	2.12	71.35	2151.0
10.0	7.14	63.30	2.22	73.14	2386.6
11.0	7.61	68.27	2.31	74.77	2626.2
12.0	8.07	73.31	2.41	76.51	2872.6
13.0	8.46	77.41	2.49	77.82	3111.4
14.0	8.82	82.06	2.58	79.42	3362.9
15.0	9.10	84.95	2.63	80.29	3581.9
16.0	9.37	89.53	2.72	81.87	3822.1
17.0	9.62	92.98	2.79	83.01	4063.1
18.0	9.86	96.83	2.86	84.30	4315.8
19.0	10.03	100.31	2.93	85.49	4538.9
20.0	10.20	103.40	3.02	85.64	4782.0
21.0	10.34	106.10	3.10	85.92	5023.7
22.0	10.46	109.52	3.14	87.73	5263.2
23.0	10.57	112.35	3.16	89.44	5496.7
24.0	10.66	115.57	3.23	90.35	5734.2
25.0	10.73	117.85	3.31	90.27	5980.6
26.0	10.79	119.67	3.31	91.79	6213.8
27.0	10.83	120.62	3.34	91.86	6459.9
28.0	10.87	123.07	3.38	92.77	6696.2
29.0	10.89	124.66	3.40	93.42	6949.8
30.0	10.90	124.63	3.41	93.26	7186.2
31.0	10.91	125.38	3.43	93.48	7426.8
32.0	10.91	127.01	3.45	94.13	7664.8
32.5	10.91	127.64	3.46	94.54	FAILURE
33.0	10.90	126.25	3.44	93.85	7902.1
34.0	10.89	126.07	3.44	93.76	8144.5
35.0	10.87	125.89	3.43	93.69	8391.0

APPENDIX C TABLE 22 - DRAINED TRIAXIAL COMPRESSION TESTS

Test CD27 DRAINED TRIAXIAL COMPRESSION
σ_3' = 60.00 MPa e_i = 0.522 H/D = 2.50
Cambria sand ϕ' = ? 2.54 CM/HR
Test specimen buckled during shearing

ϵ_1 %	ϵ_v %	$\sigma_1 - \sigma_3$ MPa	σ_1'/σ_3'	p' MPa	Time second
0.0	0.00	0.19	1.00	60.03	0.0
0.0	0.01	0.99	1.02	60.37	12.6
0.3	0.05	2.55	1.04	60.86	72.7
0.5	0.10	4.03	1.07	61.32	124.8
0.7	0.18	6.15	1.10	62.03	176.6
1.0	0.31	8.54	1.14	62.85	235.3
2.0	1.18	17.85	1.30	65.95	472.9
3.0	2.11	25.70	1.43	68.56	714.9
4.0	2.96	33.15	1.55	71.03	956.0
5.0	3.73	40.20	1.67	73.37	1195.1
6.0	4.42	47.49	1.79	75.86	1432.6
7.0	5.08	53.96	1.90	77.97	1666.2
8.0	5.70	61.05	2.02	80.36	1911.2
9.0	6.22	66.77	2.11	82.23	2147.4
10.0	6.70	73.24	2.22	84.48	2390.1
11.0	7.14	79.09	2.32	86.37	2622.6
12.0	7.40	80.83	2.35	86.99	2868.2
13.0	7.57	80.40	2.34	86.67	3105.2
14.0	7.81	83.94	2.40	87.97	3344.0
15.0	7.98	86.10	2.43	88.76	3593.9
16.0	8.13	87.68	2.46	89.25	3817.0
17.0	8.25	88.99	2.48	89.72	4055.3
18.0	8.38	91.42	2.52	90.43	4296.0
19.0	8.57	96.92	2.61	92.38	4547.5
20.0	8.73	100.35	2.68	93.33	4779.6
21.0	8.87	104.90	2.75	94.95	5015.5
22.0	9.00	107.90	2.80	95.87	5266.3
23.0	9.10	111.15	2.85	97.02	5490.8
24.0	9.19	112.80	2.88	97.50	5742.9
25.0	9.26	115.12	2.92	98.22	5972.6
26.0	9.32	118.37	2.97	99.52	6213.5
27.0	9.38	117.30	2.96	99.00	6465.4
28.0	9.43	118.77	2.98	99.53	6697.1
29.0	9.46	119.79	2.99	100.02	6927.2
30.0	9.50	118.75	2.98	99.47	7170.9
31.0	9.52	119.61	2.99	99.83	7405.8
32.0	9.54	118.29	2.97	99.35	7648.7
33.0	9.55	117.17	2.96	98.96	7883.1
34.0	9.56	115.98	2.93	98.61	8129.3
35.0	9.56	115.44	2.93	98.41	8359.9

APPENDIX C TABLE 23 - DRAINED TRIAXIAL COMPRESSION TESTS

Test CD28 DRAINED TRIAXIAL COMPRESSION
σ_3' = 60.00 MPa e_i = 0.526 H/D = 1.86
Cambria sand ϕ' = ? 2.54 CM/HR
Test specimen slipped on lubricated end during shearing.

ϵ_1 %	ϵ_v %	$\sigma_1 - \sigma_3$ MPa	σ_1'/σ_3'	p' MPa	Time second
0.0	0.00	0.08	1.00	60.04	-0.0
0.1	0.01	0.63	1.01	60.25	11.0
0.3	0.03	1.78	1.03	60.64	63.9
0.5	0.06	2.56	1.04	60.88	114.8
0.7	0.08	2.99	1.05	61.00	140.8
1.0	0.18	5.80	1.10	61.94	215.8
2.0	0.77	14.81	1.25	64.96	429.1
3.0	1.46	23.11	1.39	67.68	647.6
4.0	2.19	29.62	1.49	69.87	851.7
5.0	2.82	35.44	1.59	71.82	1063.0
6.0	3.42	40.10	1.67	73.33	1273.3
7.0	4.06	45.21	1.75	75.02	1491.8
8.0	4.67	50.52	1.84	76.85	1712.6
9.0	5.19	55.35	1.92	78.47	1917.8
10.0	5.65	59.23	1.99	79.79	2136.7
11.0	6.04	62.49	2.04	80.87	2343.6
12.0	6.42	66.34	2.10	82.17	2559.2
13.0	6.77	69.55	2.16	83.17	2765.5
14.0	7.17	74.48	2.24	84.74	2983.9
15.0	7.50	79.66	2.33	86.61	3192.6
16.0	7.77	83.43	2.39	87.93	3413.9
17.0	8.01	86.24	2.44	88.75	3619.4
18.0	8.21	89.83	2.49	90.05	3824.3
19.0	8.41	93.24	2.55	91.18	4044.3
20.0	8.58	95.53	2.59	91.86	4251.5
21.0	8.76	99.58	2.66	93.25	4476.3
22.0	8.94	104.95	2.75	95.01	4687.4
23.0	9.10	108.15	2.80	96.05	4913.1
24.0	9.21	111.00	2.85	97.00	5113.1
25.0	9.32	115.27	2.92	98.52	5325.7
26.0	9.41	117.16	2.95	99.01	5547.1
27.0	9.48	118.70	2.98	99.47	5748.4
27.9	9.55	121.30	3.02	100.39	5959.0
29.0	9.60	126.01	3.10	102.09	6182.8
29.9	9.64	127.72	3.13	102.67	6381.7
30.9	9.67	129.83	3.16	103.38	6592.9
32.0	9.69	130.96	3.18	103.67	6817.9
33.0	9.71	130.77	3.18	103.50	7030.6
34.0	9.72	133.57	3.22	104.59	7250.4
35.0	9.72	135.68	3.26	105.29	7450.3
36.0	9.72	137.10	3.28	105.73	7683.9

APPENDIX C TABLE 24 - DRAINED TRIAXIAL COMPRESSION TESTS

Test CD29 DRAINED TRIAXIAL COMPRESSION
σ_3' = 47.01 MPa e_i = 0.525 H/D = 1.87
Cambria sand ϕ' = 33.2 2.16 CM/HR

ϵ_1 %	ϵ_v %	$\sigma_1 - \sigma_3$ MPa	σ_1'/σ_3'	p' MPa	Time second
0.0	0.00	0.16	1.00	47.05	-0.0
0.1	0.01	0.74	1.02	47.31	13.0
0.3	0.06	3.38	1.07	48.10	52.7
0.5	0.17	5.39	1.11	48.79	97.0
0.7	0.24	6.26	1.13	49.07	121.8
1.0	0.45	8.49	1.18	49.85	177.0
2.0	1.42	15.02	1.32	52.01	359.9
3.0	2.31	20.30	1.43	53.73	529.0
4.0	3.13	25.80	1.55	55.60	705.5
5.0	3.92	31.04	1.66	57.35	878.7
6.0	4.66	36.06	1.77	59.01	1056.6
6.9	5.31	41.29	1.88	60.81	1227.5
8.0	5.96	45.72	1.97	62.23	1408.1
9.0	6.57	50.58	2.08	63.89	1587.1
9.9	7.02	55.19	2.17	65.46	1756.1
11.0	7.52	59.50	2.26	66.89	1940.1
11.9	7.92	62.89	2.34	67.98	2105.5
13.0	8.33	66.64	2.41	69.33	2291.9
14.0	8.68	70.11	2.49	70.45	2472.2
15.0	9.03	74.59	2.59	71.91	2652.0
16.0	9.33	77.75	2.65	72.90	2837.1
17.0	9.56	79.93	2.70	73.65	3003.4
18.0	9.79	83.51	2.77	74.93	3175.3
18.9	9.99	85.86	2.83	75.61	3349.1
20.0	10.18	88.95	2.90	76.59	3549.4
21.0	10.33	91.05	2.93	77.41	3718.3
22.0	10.46	94.31	3.00	78.49	3886.7
23.1	10.58	96.97	3.06	79.30	4078.4
24.0	10.67	97.76	3.09	79.42	4247.4
25.0	10.75	100.64	3.14	80.62	4414.1
25.9	10.82	102.18	3.18	80.98	4586.8
27.0	10.88	103.98	3.21	81.70	4778.0
27.9	10.93	105.02	3.24	81.86	4946.5
29.1	10.97	107.33	3.28	82.85	5142.9
30.0	11.00	107.32	3.29	82.58	5312.7
31.0	11.02	109.43	3.33	83.51	5483.7
32.0	11.03	110.12	3.35	83.55	5657.3
33.0	11.04	110.10	3.35	83.51	5834.8
33.9	11.04	111.06	3.37	83.88	6005.9
35.0	11.04	112.69	3.39	84.64	6191.2
36.0	11.04	112.94	3.41	84.55	6368.2
37.0	11.04	113.85	3.42	85.08	6537.8
37.2	11.04	113.89	3.42	85.10	FAILURE
37.9	11.04	113.61	3.41	85.01	6706.0
39.0	11.04	111.39	3.38	84.02	6896.7

APPENDIX C TABLE 25 - DRAINED TRIAXIAL COMPRESSION TESTS

Test CD30 DRAINED TRIAXIAL COMPRESSION
σ_3' = 17.23 MPa e_i = 0.675 H/D = 1.86
Quartz sand ϕ' = 33.8 2.54 CM/HR

ϵ_1 %	ϵ_v %	$\sigma_1 - \sigma_3$ MPa	σ_1'/σ_3'	p' MPa	Time second
0.0	0.00	0.11	1.01	17.26	0.0
0.1	0.02	0.46	1.03	17.42	12.6
0.3	0.06	1.19	1.07	17.63	52.4
0.5	0.13	1.81	1.11	17.84	84.5
0.7	0.25	2.51	1.15	18.06	129.1
1.0	0.45	3.48	1.20	18.38	184.7
2.0	1.46	5.90	1.34	19.17	355.5
3.0	2.48	8.12	1.47	19.94	532.5
4.0	3.48	10.03	1.58	20.58	709.2
5.0	4.45	11.97	1.69	21.22	894.3
6.0	5.29	13.58	1.79	21.74	1064.6
7.0	6.13	15.47	1.90	22.41	1254.5
7.9	6.83	16.90	1.98	22.86	1418.6
9.0	7.55	18.52	2.07	23.40	1600.8
10.0	8.22	19.90	2.16	23.83	1782.2
11.1	8.87	21.54	2.25	24.39	1972.7
12.0	9.39	22.78	2.32	24.80	2134.9
13.0	9.90	24.17	2.40	25.28	2318.6
14.0	10.38	25.42	2.48	25.69	2501.4
15.0	10.81	26.62	2.54	26.14	2673.8
16.0	11.21	27.74	2.61	26.45	2850.0
17.0	11.59	29.03	2.68	26.94	3030.4
18.0	11.93	30.03	2.75	27.20	3203.9
19.0	12.27	31.35	2.82	27.69	3397.9
20.0	12.53	32.36	2.88	28.01	3567.2
21.0	12.78	33.21	2.93	28.27	3743.6
22.0	13.02	34.21	2.98	28.64	3923.7
23.0	13.22	35.24	3.04	29.00	4103.6
24.1	13.41	36.24	3.10	29.33	4291.8
25.0	13.56	36.81	3.14	29.47	4453.5
26.0	13.71	37.79	3.19	29.85	4637.8
27.1	13.85	38.34	3.23	29.97	4827.4
28.0	13.96	39.28	3.28	30.33	4998.7
29.0	14.06	40.02	3.33	30.49	5183.3
30.0	14.14	40.76	3.36	30.84	5360.6
31.0	14.21	41.04	3.39	30.86	5528.3
32.0	14.27	41.73	3.42	31.16	5703.1
33.0	14.31	42.14	3.45	31.28	5888.4
34.0	14.34	42.32	3.47	31.27	6066.6
35.0	14.37	43.09	3.49	31.65	6236.1
36.0	14.37	42.95	3.49	31.53	6419.5
37.0	14.37	43.08	3.50	31.61	6602.5
37.3	14.37	43.27	3.51	31.66	FAILURE
38.0	14.36	42.81	3.49	31.48	6771.4
40.0	14.30	42.96	3.49	31.60	7136.6

APPENDIX C TABLE 26 - DRAINED TRIAXIAL COMPRESSION TESTS

Test CD31 — DRAINED TRIAXIAL COMPRESSION
σ_3' = 35.00 MPa — e_i = 0.672 — H/D = 1.86
Quartz sand — ϕ' = 33.5 — 2.54 CM/HR

ϵ_1 %	ϵ_v %	$\sigma_1 - \sigma_3$ MPa	σ_1'/σ_3'	p' MPa	Time second
0.0	0.00	0.07	1.00	35.01	0.0
0.1	0.01	0.53	1.01	35.21	12.6
0.3	0.03	1.06	1.03	35.33	44.1
0.5	0.08	2.66	1.08	35.87	95.0
0.7	0.13	3.32	1.10	36.10	122.0
1.0	0.24	4.85	1.14	36.60	176.4
2.0	0.91	10.79	1.31	38.58	346.6
3.0	1.75	15.41	1.44	40.10	526.7
4.0	2.50	18.83	1.54	41.25	689.8
5.0	3.24	22.15	1.63	42.38	862.8
6.0	3.92	24.97	1.71	43.33	1035.5
7.0	4.64	27.97	1.80	44.30	1225.6
8.0	5.22	30.18	1.86	45.00	1388.8
9.0	5.77	32.80	1.94	45.92	1557.4
10.0	6.33	35.37	2.01	46.74	1743.7
11.0	6.79	37.69	2.08	47.54	1907.3
12.1	7.29	40.71	2.16	48.58	2096.5
13.0	7.68	42.94	2.23	49.31	2263.4
14.0	8.05	45.22	2.29	50.05	2431.0
15.0	8.41	47.84	2.37	50.93	2607.4
16.0	8.74	50.57	2.44	51.86	2779.5
17.0	9.04	53.03	2.52	52.68	2955.9
18.0	9.30	55.43	2.58	53.47	3128.7
19.0	9.56	58.39	2.67	54.50	3311.3
20.0	9.76	60.18	2.72	55.03	3477.2
20.9	9.95	62.77	2.79	55.92	3641.5
21.9	10.12	65.15	2.86	56.76	3815.5
23.0	10.28	67.20	2.92	57.35	4008.3
24.1	10.41	69.45	2.98	58.15	4183.1
25.0	10.50	71.53	3.04	58.85	4342.3
26.0	10.60	73.51	3.10	59.49	4515.8
27.0	10.69	75.22	3.15	60.01	4703.6
28.1	10.75	77.57	3.21	60.91	4876.8
29.0	10.79	78.69	3.25	61.19	5034.7
30.0	10.83	80.43	3.30	61.80	5217.6
30.9	10.85	81.81	3.34	62.26	5381.7
31.9	10.86	82.72	3.37	62.55	5554.6
33.0	10.87	83.85	3.40	62.94	5732.7
34.0	10.87	85.14	3.43	63.42	5904.0
35.0	10.86	84.81	3.43	63.17	6089.0
36.0	10.85	86.22	3.46	63.77	6269.5
36.8	10.84	86.52	3.47	63.89	FAILURE
37.0	10.84	86.28	3.46	63.77	6436.3
38.0	10.82	85.86	3.45	63.60	6610.4
40.0	10.80	84.72	3.43	63.17	6956.9

APPENDIX C TABLE 27 - DRAINED TRIAXIAL COMPRESSION TESTS

Test CD32 DRAINED TRIAXIAL COMPRESSION
σ_3' = 52.00 MPa e_i = 0.672 H/D = 1.86
Quartz sand ϕ' = 33.8 2.54 CM/HR

ϵ_1 %	ϵ_v %	$\sigma_1 - \sigma_3$ MPa	σ_1'/σ_3'	p' MPa	Time second
0.0	0.00	0.09	1.00	52.03	-0.0
0.1	0.00	0.58	1.01	52.26	12.6
0.3	0.06	1.19	1.02	52.38	44.9
0.5	0.08	1.88	1.04	52.63	79.7
0.7	0.12	3.31	1.06	53.12	122.1
1.0	0.21	5.54	1.11	53.87	176.9
2.0	0.82	13.91	1.27	56.65	338.3
3.0	1.74	20.71	1.40	58.92	511.2
4.0	2.61	27.13	1.52	61.05	685.1
5.0	3.35	33.05	1.64	63.04	852.4
6.0	4.10	39.14	1.75	65.06	1025.9
7.0	4.82	45.28	1.87	67.11	1209.6
8.0	5.44	50.82	1.98	68.93	1374.0
9.0	5.97	56.19	2.08	70.74	1539.9
10.0	6.50	61.57	2.18	72.52	1716.5
11.0	6.94	66.80	2.28	74.32	1882.5
12.0	7.35	71.78	2.38	75.95	2061.8
13.0	7.72	76.41	2.47	77.44	2238.6
14.0	8.04	81.22	2.56	79.03	2413.0
15.0	8.31	85.74	2.65	80.61	2580.1
16.0	8.54	89.48	2.72	81.84	2745.9
17.0	8.74	93.26	2.79	83.11	2912.7
18.0	8.92	97.17	2.87	84.40	3088.1
19.0	9.07	100.73	2.93	85.63	3270.5
20.0	9.18	104.14	3.00	86.75	3428.3
21.0	9.28	107.03	3.06	87.69	3600.2
22.0	9.36	110.59	3.12	88.97	3776.8
23.0	9.42	112.36	3.16	89.40	3959.2
24.0	9.46	115.51	3.22	90.51	4116.5
25.0	9.49	117.53	3.26	91.18	4301.5
26.0	9.50	119.25	3.29	91.72	4462.6
27.1	9.50	122.02	3.34	92.80	4651.7
28.0	9.50	122.82	3.36	92.93	4808.2
29.0	9.49	124.61	3.40	93.55	4977.1
30.0	9.47	126.58	3.43	94.25	5154.8
31.0	9.44	127.49	3.45	94.59	5317.4
32.0	9.41	128.17	3.46	94.74	5499.3
33.0	9.37	128.30	3.47	94.71	5666.8
34.0	9.34	129.86	3.49	95.41	5835.9
34.7	9.31	130.85	3.51	95.69	FAILURE
34.9	9.30	130.18	3.50	95.43	6000.4
36.0	9.26	129.69	3.49	95.22	6183.2
37.0	9.23	129.50	3.48	95.29	6345.0
37.9	9.19	128.94	3.48	95.01	6521.8
40.0	9.12	127.62	3.45	94.66	6860.6

APPENDIX C TABLE 28 - DRAINED TRIAXIAL COMPRESSION TESTS

Test CD33 DRAINED TRIAXIAL COMPRESSION
σ_3' = 26.00 MPa e_i = 0.665 H/D = 1.84
Quartz sand ϕ' = 33.7 2.54 CM/HR

ϵ_1 %	ϵ_v %	$\sigma_1 - \sigma_3$ MPa	σ_1'/σ_3'	p' MPa	Time second
0.0	0.00	0.17	1.01	26.02	0.0
0.1	0.02	0.65	1.03	26.25	14.6
0.3	0.06	1.98	1.08	26.60	47.3
0.5	0.17	3.24	1.12	27.07	94.3
0.7	0.26	3.90	1.15	27.27	121.3
1.0	0.50	5.38	1.21	27.78	176.0
1.9	1.47	8.89	1.34	28.94	345.2
3.0	2.45	12.19	1.47	30.06	530.9
4.0	3.38	15.04	1.58	31.00	707.5
4.9	4.21	17.65	1.68	31.85	880.0
6.0	5.04	20.35	1.78	32.76	1061.0
7.0	5.78	22.86	1.88	33.55	1238.4
7.9	6.43	25.31	1.97	34.42	1412.4
9.0	7.09	27.87	2.07	35.26	1594.2
10.0	7.69	30.26	2.17	36.05	1774.1
10.9	8.22	32.53	2.25	36.82	1946.4
12.0	8.75	34.68	2.34	37.49	2133.6
13.0	9.19	36.52	2.41	38.04	2303.0
14.0	9.58	39.24	2.51	39.10	2481.1
14.9	9.96	41.26	2.59	39.74	2657.7
16.0	10.31	43.19	2.66	40.39	2844.8
17.0	10.61	45.10	2.73	41.03	3020.2
18.0	10.88	46.85	2.80	41.60	3200.1
19.0	11.11	48.56	2.87	42.18	3375.4
20.0	11.31	50.18	2.93	42.78	3548.2
21.0	11.50	51.48	2.98	43.11	3731.3
22.0	11.65	52.84	3.04	43.55	3904.7
23.0	11.78	54.60	3.10	44.18	4083.6
24.0	11.90	55.82	3.15	44.59	4264.5
25.0	11.99	57.14	3.20	45.03	4437.1
26.0	12.07	58.22	3.24	45.35	4622.9
27.0	12.13	59.10	3.27	45.69	4795.6
28.0	12.18	59.99	3.31	45.92	4979.3
29.1	12.21	61.33	3.37	46.32	5166.7
29.9	12.23	62.28	3.41	46.60	5321.8
31.0	12.24	62.72	3.43	46.66	5520.9
31.9	12.24	63.32	3.45	46.98	5679.1
33.1	12.23	64.02	3.47	47.31	5882.4
34.0	12.21	64.17	3.48	47.31	6046.4
35.0	12.17	63.77	3.47	47.07	6219.9
36.0	12.13	63.92	3.47	47.14	6406.2
37.0	12.08	63.75	3.47	47.10	6572.7
37.1	12.07	64.74	3.49	47.58	FAILURE
37.9	12.01	64.18	3.49	47.20	6746.4
39.9	11.87	62.94	3.44	46.78	7102.1

APPENDIX C TABLE 29 - DRAINED TRIAXIAL COMPRESSION TESTS

Test CD34 DRAINED TRIAXIAL COMPRESSION
σ_3' = 12.00 MPa e_i = 0.672 H/D = 1.83
Quartz sand ϕ' = 33.3 2.54 CM/HR

ϵ_1 %	ϵ_v %	$\sigma_1 - \sigma_3$ MPa	σ_1'/σ_3'	p' MPa	Time second
0.0	0.00	0.08	1.01	12.01	-0.0
0.1	0.02	0.44	1.04	12.17	13.9
0.3	0.10	1.55	1.13	12.50	45.3
0.5	0.23	2.22	1.18	12.73	81.8
0.7	0.43	2.75	1.23	12.89	125.2
1.0	0.66	3.27	1.27	13.07	174.8
2.0	1.63	5.00	1.42	13.67	355.9
3.0	2.64	6.51	1.54	14.17	537.1
4.0	3.62	7.82	1.65	14.62	720.9
5.0	4.54	9.12	1.76	15.02	900.3
6.0	5.28	10.14	1.85	15.37	1062.9
7.0	6.09	11.27	1.94	15.76	1241.3
8.0	6.84	12.31	2.03	16.10	1420.3
9.0	7.58	13.32	2.11	16.43	1605.2
10.0	8.19	14.25	2.18	16.78	1776.8
11.0	8.82	15.14	2.26	17.04	1958.3
12.0	9.41	16.03	2.34	17.34	2137.3
13.0	9.95	16.86	2.41	17.60	2315.5
14.0	10.46	17.66	2.47	17.87	2492.9
15.0	10.95	18.48	2.54	18.18	2677.0
16.0	11.36	19.22	2.60	18.40	2848.0
17.0	11.75	19.90	2.66	18.66	3027.1
18.0	12.10	20.35	2.70	18.75	3206.5
19.0	12.44	21.00	2.75	19.00	3387.8
20.0	12.75	21.66	2.80	19.22	3561.9
21.0	13.03	22.22	2.85	19.40	3738.1
22.0	13.31	22.87	2.91	19.61	3921.4
23.0	13.56	23.39	2.95	19.77	4101.7
24.0	13.81	24.11	3.01	20.03	4286.8
25.0	14.01	24.60	3.05	20.18	4458.1
26.0	14.19	25.10	3.09	20.35	4632.6
27.0	14.39	25.71	3.14	20.57	4814.7
28.0	14.55	26.19	3.18	20.73	5002.3
29.0	14.69	26.44	3.21	20.76	5171.0
30.0	14.83	27.10	3.26	21.03	5343.7
31.0	14.95	27.53	3.29	21.17	5530.1
32.0	15.06	27.99	3.33	21.35	5705.7
33.0	15.15	28.10	3.34	21.36	5886 7
33.9	15.22	28.48	3.37	21.52	6052.9
35.0	15.29	28.68	3.39	21.55	6245.7
35.9	15.35	28.86	3.41	21.60	6410.5
37.0	15.39	29.06	3.42	21.70	6605.7
37.9	15.42	29.19	3.43	21.73	FAILURE
38.0	15.43	28.90	3.41	21.61	6782.1
40.0	15.47	28.95	3.42	21.63	7129.2

APPENDIX D

APPENDIX D TABLE 1 - UNDRAINED TRIAXIAL COMPRESSION TESTS

Test CU3 UNDRAINED TRIAXIAL COMPRESSION
σ_{3i}' = 16.68 MPa e_i = 0.534 H/D = 2.52
Cambria sand ϕ' = 34.2 2.54 CM/HR

ϵ_1 %	u MPa	$\sigma_1 - \sigma_3$ MPa	σ_1'/σ_3'	p' MPa	Time second
0.0	0.57	0.05	1.00	16.66	-0.0
0.1	0.72	0.77	1.05	16.79	17.6
0.3	2.22	2.75	1.18	15.92	73.0
0.5	4.09	4.41	1.34	14.61	119.2
0.7	6.12	5.74	1.52	13.02	174.4
1.0	8.57	6.84	1.79	10.95	256.3
2.0	12.13	7.42	2.45	7.57	498.1
3.0	13.34	7.28	2.87	6.33	753.3
4.0	13.77	7.25	3.09	5.88	1002.4
5.0	13.96	7.25	3.21	5.70	1247.7
6.0	14.04	7.33	3.30	5.63	1484.8
7.0	14.10	7.36	3.36	5.58	1731.5
8.0	14.11	7.45	3.41	5.58	1991.5
9.0	14.19	7.51	3.44	5.58	2227.3
10.0	14.19	7.49	3.46	5.54	2476.4
10.9	14.24	7.54	3.49	5.54	MAX. DEV.
11.0	14.19	7.47	3.49	5.50	2732.1
12.0	14.25	7.49	3.51	5.48	2974.7
13.0	14.27	7.46	3.52	5.44	3224.1
14.0	14.32	7.43	3.54	5.40	3473.0
15.0	14.35	7.36	3.55	5.34	3726.5
16.0	14.38	7.28	3.55	5.28	3969.2
17.0	14.42	7.18	3.56	5.20	4215.8
18.0	14.47	7.08	3.57	5.12	4471.0
19.0	14.52	6.97	3.57	5.03	4721.2
19.4	14.53	6.93	3.57	5.00	FAILURE
20.0	14.58	6.85	3.57	4.95	4964.3
21.0	14.60	6.71	3.57	4.85	5212.3
22.0	14.65	6.57	3.57	4.75	5460.7
23.0	14.72	6.42	3.56	4.65	5712.4
24.0	14.79	6.29	3.56	4.55	5961.8
25.0	14.81	6.16	3.55	4.47	6212.7
26.0	14.84	6.01	3.53	4.38	6463.2
26.9	15.19	5.89	3.50	4.31	6699.0

APPENDIX D TABLE 2 - UNDRAINED TRIAXIAL COMPRESSION TESTS

Test CU4 — UNDRAINED TRIAXIAL COMPRESSION
σ_{3i}' = 16.71 MPa — e_i = 0.530 — H/D = 2.55
Can.bria sand — ϕ' = 34.7 — 2.54 CM/HR

ϵ_1 %	u MPa	$\sigma_1 - \sigma_3$ MPa	σ_1'/σ_3'	p' MPa	Time second
0.0	0.47	0.05	1.00	16.76	-0.0
0.1	0.58	0.71	1.04	16.93	17.2
0.3	1.28	1.49	1.09	16.44	66.8
0.5	3.51	4.10	1.30	15.07	126.6
0.7	5.68	5.55	1.48	13.39	181.8
1.0	7.82	6.61	1.70	11.60	246.1
2.0	12.03	7.41	2.42	7.68	497.5
3.0	13.36	7.24	2.87	6.29	758.4
4.0	13.80	7.19	3.10	5.83	1006.6
5.0	13.99	7.25	3.24	5.65	1255.8
6.0	14.08	7.33	3.32	5.60	1491.2
7.0	14.12	7.40	3.38	5.58	1744.9
8.0	14.15	7.43	3.41	5.56	1995.0
8.8	14.18	7.49	3.45	5.56	MAX. DEV.
9.0	14.18	7.48	3.45	5.54	2248.6
10.0	14.22	7.45	3.47	5.49	2490.5
11.0	14.24	7.44	3.49	5.47	2746.6
12.0	14.26	7.43	3.52	5.43	2993.5
13.0	14.33	7.38	3.53	5.38	3256.9
14.0	14.35	7.29	3.54	5.30	3503.9
15.0	14.40	7.24	3.56	5.24	3743.0
16.0	14.45	7.13	3.57	5.15	3993.3
17.0	14.50	7.03	3.58	5.08	4258.0
18.0	14.54	6.92	3.57	4.99	4490.4
19.0	14.59	6.80	3.57	4.91	4755.2
20.0	14.64	6.65	3.57	4.81	4997.1
21.0	14.71	6.55	3.58	4.72	5255.6
22.0	14.73	6.56	3.62	4.69	5501.3
22.8	14.76	6.54	3.65	4.65	FAILURE
23.0	14.71	6.39	3.61	4.58	5750.0
24.0	14.80	6.32	3.61	4.53	5991.8
25.0	14.84	6.17	3.59	4.44	6241.3

APPENDIX D TABLE 3 - UNDRAINED TRIAXIAL COMPRESSION TESTS

Test CU6 — UNDRAINED TRIAXIAL COMPRESSION
σ_{3i}' = 16.89 MPa — e_i = 0.527 — H/D = 2.53
Cambria sand — ϕ' = 34.3 — 2.54 CM/HR

ϵ_1 %	u MPa	$\sigma_1 - \sigma_3$ MPa	σ_1'/σ_3'	p' MPa	Time second
0.0	0.33	0.03	1.00	16.90	-0.0
0.1	0.64	1.00	1.06	16.98	16.5
0.3	2.83	3.82	1.26	15.68	74.5
0.5	4.53	5.20	1.41	14.43	118.2
0.7	6.53	6.42	1.60	12.82	175.3
1.0	8.7	7.35	1.87	10.93	256.6
1.6	11.15	7.79	2.28	8.67	MAX. DEV.
2.0	11.98	7.76	2.48	7.84	496.6
3.0	13.14	7.58	2.85	6.63	743.7
4.0	13.61	7.48	3.06	6.12	996.6
5.0	13.79	7.50	3.19	5.92	1247.8
6.0	13.90	7.55	3.28	5.83	1503.0
7.0	13.99	7.59	3.34	5.78	1750.1
8.0	14.04	7.58	3.37	5.73	1995.8
9.0	14.08	7.58	3.40	5.68	2247.5
10.0	14.11	7.53	3.42	5.62	2510.1
11.0	14.16	7.50	3.45	5.56	2750.1
12.0	14.19	7.45	3.46	5.51	2996.8
13.0	14.25	7.42	3.48	5.47	3263.2
14.0	14.27	7.37	3.49	5.41	3500.4
15.0	14.33	7.32	3.52	5.35	3751.1
16.0	14.37	7.22	3.53	5.27	4016.1
17.0	14.41	7.15	3.53	5.20	4255.0
18.0	14.46	7.05	3.54	5.12	4506.1
19.0	14.50	6.95	3.55	5.04	4755.4
20.0	14.56	6.87	3.56	4.97	5001.8
21.0	14.59	6.75	3.56	4.88	5258.5
22.0	14.66	6.62	3.56	4.79	5508.4
22.9	14.71	6.53	3.58	4.71	FAILURE
23.0	14.70	6.52	3.58	4.70	5763.7
24.0	14.75	6.36	3.56	4.60	6009.6
25.0	14.78	6.24	3.56	4.51	6259.7
26.0	14.84	6.13	3.56	4.44	6507.1
27.0	14.88	6.01	3.55	4.35	6757.8
28.0	14.92	5.88	3.54	4.28	7007.0
29.0	14.96	5.73	3.52	4.18	7253.4

APPENDIX D TABLE 4 - UNDRAINED TRIAXIAL COMPRESSION TESTS

Test CU12 UNDRAINED TRIAXIAL COMPRESSION
σ_{3i}' = 61.65 MPa e_i = 0.531 H/D = 2.52
Cambria sand ϕ' = 35.4 2.54 CM/HR
Shearing terminated early due to leak.

ϵ_1 %	u MPa	$\sigma_1 - \sigma_3$ MPa	σ_1'/σ_3'	p' MPa	Time second
0.0	0.41	0.13	1.00	61.70	-0.0
0.1	0.67	2.34	1.04	62.23	33.9
0.3	1.08	3.24	1.05	62.08	66.1
0.5	2.36	4.83	1.08	61.36	126.0
0.7	[illegible]	9.14	1.16	60.35	157.6
1.0	13.84	16.39	1.34	53.73	247.1
2.0	33.58	23.97	1.84	36.50	489.5
2.5	39.15	24.47	2.06	31.13	MAX. DEV.
3.0	43.16	24.18	2.27	27.04	713.6
4.0	48.23	22.73	2.64	21.45	957.2
5.0	50.86	21.25	2.90	18.27	1197.5
6.0	52.53	20.10	3.10	16.26	1452.4
7.0	53.45	19.32	3.23	15.08	1691.7
8.0	54.11	18.70	3.33	14.27	1932.0
9.1	54.62	18.30	3.42	13.67	2177.1
10.0	54.90	17.93	3.49	13.19	2416.7
11.0	55.16	17.64	3.54	12.82	2655.8
12.0	55.39	17.39	3.58	12.53	2893.0
13.0	55.55	17.18	3.62	12.29	3134.4
14.0	55.70	16.99	3.65	12.06	3373.2
15.0	55.85	16.83	3.68	11.88	3614.7
16.0	55.95	16.70	3.71	11.72	3848.0
17.0	56.08	16.59	3.74	11.59	4085.8
17.3	56.09	16.54	3.75	11.54	

APPENDIX D TABLE 5 - UNDRAINED TRIAXIAL COMPRESSION TESTS

Test CU13 — UNDRAINED TRIAXIAL COMPRESSION
σ_{3i}' = 61.65 MPa — e_i = 0.519 — H/D = 2.50
Cambria sand — ϕ' = 35.0 — 2.54 CM/HR

ϵ_1 %	u MPa	$\sigma_1 - \sigma_3$ MPa	σ_1'/σ_3'	p' MPa	Time second
0.0	0.46	0.07	1.00	61.65	-0.0
0.1	0.51	3.72	1.06	62.83	33.0
0.3	1.38	7.00	1.12	63.03	63.3
0.5	5.93	11.99	1.21	60.15	117.4
0.7	11.29	15.86	1.31	56.10	166.7
1.0	17.81	19.46	1.44	50.78	230.8
2.0	36.43	24.85	1.97	33.95	487.7
2.2	37.80	24.95	2.03	32.65	MAX. DEV.
3.0	44.58	24.20	2.38	25.58	710.2
4.0	48.99	22.49	2.72	20.60	953.7
5.0	51.21	21.00	2.93	17.88	1189.2
6.0	52.59	19.89	3.09	16.13	1443.7
7.0	53.33	19.20	3.19	15.18	1684.2
8.0	53.84	18.63	3.26	14.44	1920.8
9.0	54.28	18.29	3.33	13.94	2159.4
10.0	54.58	17.93	3.38	13.51	2400.9
11.0	54.79	17.60	3.41	13.16	2628.5
12.0	55.00	17.39	3.45	12.90	2869.0
13.0	55.17	17.20	3.48	12.67	3109.1
14.0	55.34	17.03	3.52	12.43	3348.8
15.0	55.45	16.90	3.54	12.28	3600.2
16.0	55.52	16.81	3.56	12.16	3833.1
17.0	55.66	16.72	3.60	12.01	4070.3
18.0	55.75	16.62	3.61	11.90	4306.4
19.0	55.85	16.49	3.63	11.77	4549.2
20.0	55.93	16.47	3.65	11.70	4800.9
21.0	55.99	16.25	3.66	11.53	5034.2
22.0	56.07	16.17	3.67	11.45	5266.9
23.0	56.13	16.03	3.68	11.33	5500.7
24.0	56.15	15.83	3.68	11.19	5740.5
24.7	56.24	15.75	3.69	11.11	FAILURE

APPENDIX D TABLE 6 - UNDRAINED TRIAXIAL COMPRESSION TESTS

Test CU14 — UNDRAINED TRIAXIAL COMPRESSION
σ_{3i}' = 34.01 MPa — e_i = 0.514 — H/D = 2.50
Cambria sand — ϕ' = 35.4 — 2.54 CM/HR

ϵ_1 %	u MPa	$\sigma_1 - \sigma_3$ MPa	σ_1'/σ_3'	p' MPa	Time second
0.0	0.44	0.02	1.00	34.02	0.0
0.0	0.61	0.98	1.03	34.19	13.0
0.3	2.48	4.31	1.13	33.41	72.8
0.5	5.27	6.94	1.24	31.50	119.4
0.7	9.12	9.62	1.38	28.56	174.3
1.0	13.42	11.73	1.56	24.95	240.2
1.9	22.47	13.61	2.14	16.52	MAX. DEV.
2.0	23.22	13.56	2.21	15.77	485.8
3.0	27.00	12.65	2.69	11.68	729.6
4.0	28.60	11.77	3.00	9.81	970.0
5.0	29.36	11.21	3.20	8.83	1215.7
6.0	29.80	10.83	3.33	8.26	1459.0
7.0	30.11	10.55	3.42	7.88	1706.8
8.0	30.30	10.35	3.49	7.61	1955.6
9.0	30.43	10.19	3.53	7.42	2182.7
10.0	30.56	10.05	3.57	7.26	2428.3
11.0	30.60	9.90	3.60	7.10	2667.1
12.0	30.74	9.83	3.63	7.01	2912.2
13.0	30.79	9.67	3.65	6.88	3161.2
14.0	30.87	9.57	3.67	6.78	3400.4
15.0	30.94	9.42	3.68	6.66	3658.0
16.0	31.00	9.34	3.70	6.57	3887.4
17.0	31.07	9.23	3.71	6.48	4133.7
18.0	31.12	9.09	3.72	6.37	4390.0
19.0	31.17	8.97	3.73	6.28	4617.8
20.0	31.23	8.83	3.73	6.18	4875.6
21.0	31.27	8.72	3.74	6.09	5100.9
21.7	31.33	8.67	3.75	6.04	FAILURE
22.0	31.35	8.58	3.74	5.99	5352.9
23.0	31.38	8.42	3.74	5.88	5599.4
24.0	31.43	8.29	3.74	5.79	5846.3
25.0	31.49	8.13	3.74	5.68	6091.7
26.0	31.54	8.02	3.74	5.60	6319.5
27.0	31.58	7.87	3.74	5.50	6560.1
28.0	31.63	7.65	3.71	5.37	6806.5
29.0	31.69	7.47	3.69	5.26	7066.8

APPENDIX D TABLE 7 - UNDRAINED TRIAXIAL COMPRESSION TESTS

Test CU15 — UNDRAINED TRIAXIAL COMPRESSION
σ_{3i}' = 6.45 MPa — e_i = 0.515 — H/D = 2.50
Cambria sand — ϕ' = 33.4 — 2.54 CM/HR

ϵ_1 %	u MPa	$\sigma_1 - \sigma_3$ MPa	σ_1'/σ_3'	p' MPa	Time second
0.0	0.58	0.04	1.01	6.43	0.0
0.1	0.74	0.70	1.11	6.51	22.3
0.3	1.66	2.42	1.45	6.15	66.1
0.5	2.47	3.54	1.78	5.69	121.7
0.7	3.04	4.10	2.04	5.33	172.0
1.0	3.59	4.52	2.32	4.92	255.6
2.0	4.16	5.03	2.78	4.50	499.0
3.0	4.30	5.42	3.01	4.51	749.5
4.0	4.30	5.74	3.12	4.62	992.2
5.0	4.26	6.03	3.20	4.75	1246.4
6.0	4.23	6.24	3.25	4.84	1491.8
7.0	4.20	6.41	3.29	4.93	1746.3
8.0	4.18	6.53	3.32	5.00	2001.4
9.0	4.17	6.63	3.34	5.03	2246.5
10.0	4.18	6.66	3.36	5.04	2496.9
10.2	4.18	6.70	3.37	5.06	MAX. DEV.
11.0	4.18	6.67	3.37	5.03	2743.8
12.0	4.19	6.65	3.38	5.01	2994.2
13.0	4.23	6.61	3.39	4.97	3249.2
14.0	4.28	6.58	3.40	4.93	3503.8
15.0	4.30	6.50	3.41	4.86	3751.0
16.0	4.35	6.41	3.41	4.79	4010.8
17.0	4.41	6.34	3.43	4.72	4251.8
18.0	4.45	6.22	3.43	4.63	4508.8
19.0	4.49	6.12	3.44	4.55	4750.2
20.0	4.52	5.96	3.42	4.44	5011.9
20.5	4.56	5.99	3.45	4.44	FAILURE
21.0	4.58	5.90	3.44	4.39	5249.4
22.0	4.64	5.76	3.43	4.28	5503.4
23.0	4.70	5.59	3.42	4.17	5759.8
24.0	4.74	5.49	3.43	4.09	5998.9
25.0	4.80	5.38	3.42	4.02	6246.7
26.0	4.85	5.27	3.42	3.94	6501.9
27.0	4.85	5.14	3.40	3.85	6756.3
28.0	4.88	5.03	3.39	3.78	7008.9
29.0	4.93	4.93	3.38	3.71	7249.5
30.0	4.97	4.79	3.36	3.63	7503.4
31.0	5.02	4.68	3.35	3.55	7748.0
32.0	5.05	4.56	3.33	3.48	8003.6

APPENDIX D TABLE 8 - UNDRAINED TRIAXIAL COMPRESSION TESTS

Test CU17 — UNDRAINED TRIAXIAL COMPRESSION
σ_{3i}' = 68.92 MPa — e_i = 0.519 — H/D = 2.51
Cambria sand — ϕ' = 35.6 — 2.54 CM/HR

ϵ_1 %	u MPa	$\sigma_1 - \sigma_3$ MPa	σ_1'/σ_3'	p' MPa	Time second
0.0	0.56	0.49	1.01	69.05	-0.0
0.1	0.75	1.97	1.03	69.44	14.4
0.3	3.24	7.11	1.11	68.61	64.1
0.5	8.22	12.92	1.21	65.56	115.8
0.7	13.88	17.18	1.31	61.31	167.2
1.0	20.35	21.05	1.43	56.12	228.2
2.0	37.93	27.89	1.88	40.83	469.0
2.5	44.02	28.68	2.13	35.02	MAX. DEV.
3.0	48.01	28.43	2.33	30.91	723.5
4.0	53.08	27.39	2.67	25.55	960.8
5.0	55.85	25.88	2.90	22.23	1189.0
6.0	57.79	24.62	3.11	19.88	1422.9
7.0	59.15	23.45	3.27	18.13	1676.6
8.0	59.95	22.69	3.38	17.10	1901.3
9.0	60.50	22.11	3.47	16.32	2142.6
10.0	60.96	21.66	3.54	15.75	2382.6
11.0	61.25	21.31	3.59	15.32	2618.1
12.0	61.49	21.00	3.63	14.98	2856.8
13.0	61.68	20.75	3.67	14.69	3094.4
14.0	61.87	20.57	3.70	14.48	3335.6
15.0	61.99	20.37	3.72	14.27	3565.4
16.0	62.11	20.22	3.75	14.10	3809.7
17.0	62.21	20.00	3.76	13.92	4050.1
18.0	62.14	19.92	3.72	13.97	4282.9
19.0	61.98	20.28	3.70	14.27	4525.2
20.0	61.77	20.20	3.63	14.42	4760.9
21.0	62.12	20.26	3.75	14.13	4996.3
22.0	62.27	19.93	3.77	13.84	5244.1
22.1	62.28	19.96	3.78	13.83	FAILURE
23.0	62.39	19.63	3.77	13.62	5487.5
24.0	62.50	19.35	3.76	13.45	5714.7
25.0	62.54	19.01	3.75	13.25	5956.9
26.0	62.63	18.80	3.75	13.11	6189.6
27.0	62.71	18.51	3.74	12.93	6425.0
28.0	62.72	18.32	3.74	12.80	6663.4

APPENDIX D TABLE 9 - UNDRAINED TRIAXIAL COMPRESSION TESTS

Test CU19 — UNDRAINED TRIAXIAL COMPRESSION
σ_{3i}' = 52.00 MPa — e_i = 0.529 — H/D = 2.51
Cambria sand — ϕ' = 35.6 — 2.54 CM/HR

ϵ_1 %	u MPa	$\sigma_1 - \sigma_3$ MPa	σ_1'/σ_3'	p' MPa	Time second
0.0	0.45	0.20	1.00	52.04	0.0
0.1	1.10	2.17	1.04	52.16	23.2
0.3	2.83	4.29	1.09	51.02	73.4
0.5	5.41	7.64	1.16	49.58	127.3
0.7	8.30	10.57	1.24	47.68	165.2
1.0	14.50	14.92	1.39	42.94	241.3
2.0	30.23	20.31	1.91	28.98	482.7
2.3	33.65	20.49	2.09	25.63	MAX. DEV.
3.0	38.23	19.92	2.40	20.86	717.4
4.0	42.04	18.46	2.77	16.57	965.0
5.0	43.91	17.30	3.02	14.32	1207.4
6.0	44.94	16.44	3.19	12.99	1448.4
7.0	45.60	15.82	3.31	12.12	1692.6
8.0	46.05	15.37	3.40	11.53	1937.7
9.0	46.35	15.03	3.46	11.11	2168.6
10.0	46.60	14.78	3.52	10.79	2412.6
11.0	46.78	14.46	3.56	10.48	2665.1
12.0	46.94	14.23	3.58	10.25	2891.9
13.0	47.08	14.01	3.61	10.04	3129.3
14.0	47.19	13.86	3.64	9.88	3380.8
15.0	47.29	13.73	3.66	9.74	3614.8
16.0	47.39	13.59	3.68	9.60	3859.6
17.0	47.47	13.43	3.70	9.45	4103.7
18.0	47.57	13.27	3.71	9.32	4349.8
19.0	47.63	13.17	3.73	9.21	4595.1
20.0	47.70	13.05	3.74	9.10	4827.5
21.0	47.80	12.93	3.76	9.00	5071.8
22.0	47.83	12.78	3.77	8.87	5319.4
23.0	47.87	12.61	3.77	8.76	5546.4
23.7	47.96	12.51	3.78	8.68	FAILURE
24.0	47.96	12.43	3.77	8.64	5789.8

APPENDIX D TABLE 10 - UNDRAINED TRIAXIAL COMPRESSION TESTS

Test CU20 — UNDRAINED TRIAXIAL COMPRESSION
σ_{3i}' = 43.0 MPa — e_i = 0.525 — H/D = 2.51
Cambria sand — ϕ' = 35.6 — 2.54 CM/HR

ϵ_1 %	u MPa	$\sigma_1 - \sigma_3$ MPa	σ_1'/σ_3'	p' MPa	Time second
0.0	0.46	0.11	1.00	43.01	-0.0
0.0	0.77	1.03	1.02	43.11	14.5
0.3	2.58	3.91	1.10	42.21	80.0
0.5	3.84	5.18	1.13	41.33	117.1
0.7	5.86	7.27	1.19	39.98	165.9
1.0	11.02	11.41	1.35	36.23	245.2
2.0	25.12	16.64	1.91	23.88	476.6
2.4	28.60	16.90	2.14	20.50	MAX. DEV.
3.0	32.32	16.20	2.46	16.52	728.7
4.0	35.19	15.04	2.82	13.27	966.4
5.0	36.57	14.09	3.06	11.54	1212.0
6.0	37.39	13.55	3.22	10.63	1445.1
7.0	37.84	13.11	3.34	9.98	1692.2
8.0	38.17	12.75	3.42	9.52	1933.8
9.0	38.43	12.54	3.49	9.22	2180.9
10.0	38.61	12.36	3.54	8.98	2411.4
11.0	38.77	12.14	3.58	8.75	2656.5
12.0	38.89	11.99	3.63	8.56	2909.6
13.0	39.07	11.89	3.66	8.43	3145.9
14.0	39.05	11.66	3.68	8.23	3389.6
15.0	39.18	11.55	3.71	8.11	3635.3
16.0	39.26	11.42	3.73	7.99	3865.9
17.0	39.33	11.32	3.75	7.88	4111.7
18.0	39.41	11.17	3.77	7.76	4356.1
19.0	39.48	11.02	3.78	7.64	4595.5
20.0	39.55	10.86	3.78	7.52	4842.7
21.0	39.57	10.62	3.77	7.38	5079.7
21.9	39.69	10.55	3.79	7.31	FAILURE
22.0	39.67	10.50	3.78	7.28	5326.2
23.0	39.75	10.31	3.77	7.15	5572.8

APPENDIX D TABLE 11 - UNDRAINED TRIAXIAL COMPRESSION TESTS

Test CU21 UNDRAINED TRIAXIAL COMPRESSION
σ_{3i}' = 34.01 MPa e_i = 0.52.47 H/D = 2.51
Cambria sand ϕ' = 35.8 2.54 CM/HR

ϵ_1 %	u MPa	$\sigma_1 - \sigma_3$ MPa	σ_1'/σ_3'	p' MPa	Time second
0.0	0.55	0.11	1.00	34.00	-0.0
0.1	0.93	1.03	1.03	34.03	22.7
0.3	1.64	1.90	1.06	33.51	70.6
0.5	3.20	3.85	1.12	32.61	119.4
0.7	5.06	5.62	1.19	31.35	171.4
1.0	8.23	8.17	1.31	29.01	235.3
2.0	20.67	13.31	1.96	18.25	479.6
2.4	23.91	13.48	2.26	15.15	MAX. DEV.
3.0	26.27	12.89	2.56	12.54	737.4
4.0	28.28	12.03	2.92	10.26	974.6
5.0	29.25	11.37	3.16	9.04	1227.0
6.0	29.78	11.00	3.32	8.42	1464.0
7.0	30.10	10.72	3.43	7.99	1708.8
8.0	30.33	10.51	3.51	7.69	1958.4
9.0	30.50	10.37	3.57	7.49	2196.7
10.0	30.61	10.21	3.61	7.31	2435.8
11.0	30.72	10.10	3.65	7.17	2688.2
12.0	30.81	10.00	3.69	7.05	2926.3
13.0	30.88	9.89	3.72	6.94	3174.3
14.0	30.96	9.82	3.75	6.85	3418.4
15.0	31.02	9.71	3.76	6.75	3656.8
16.0	31.08	9.61	3.78	6.66	3904.6
17.0	31.14	9.50	3.80	6.57	4151.8
18.0	31.19	9.34	3.80	6.45	4390.7
19.0	31.24	9.22	3.81	6.36	4635.5
20.0	31.33	9.09	3.82	6.26	4881.7
21.0	31.36	8.92	3.81	6.14	5122.5
21.9	31.43	8.84	3.82	6.08	FAILURE
22.0	31.41	8.74	3.81	6.03	5378.1
23.0	31.43	8.58	3.80	5.92	5618.3
24.0	31.50	8.41	3.79	5.82	5866.4
25.0	31.57	8.26	3.77	5.73	6100.1

APPENDIX D TABLE 12 - UNDRAINED TRIAXIAL COMPRESSION TESTS

Test CU22 — UNDRAINED TRIAXIAL COMPRESSION
σ_{3i}' = 34.01 MPa — e_i = 0.508 — H/D = 2.50
Cambria sand — ϕ' = 34.5 — 7.62 CM/HR

ϵ_1 %	u MPa	$\sigma_1 - \sigma_3$ MPa	σ_1'/σ_3'	p' MPa	Time second
0.0	0.16	0.08	1.00	34.01	-0.0
0.1	0.40	0.63	1.02	34.07	15.2
0.4	1.70	1.64	1.05	33.78	44.6
0.9	5.08	5.95	1.20	31.46	76.8
1.3	10.01	9.90	1.41	27.51	104.2
1.8	16.59	12.79	1.73	21.88	143.8
2.2	20.42	13.42	1.98	18.23	176.1
2.4	21.92	13.47	2.10	16.73	MAX. DEV.
2.9	24.59	13.17	2.38	13.96	235.8
3.9	27.22	12.22	2.77	10.99	318.1
5.1	28.51	11.45	3.04	9.43	414.1
6.0	29.05	11.08	3.17	8.79	490.7
7.0	29.39	10.80	3.27	8.36	568.6
7.9	29.62	10.63	3.35	8.07	645.1
8.9	29.80	10.46	3.40	7.84	724.1
9.9	29.92	10.31	3.45	7.66	805.0
11.0	30.04	10.20	3.49	7.50	890.2
12.1	30.15	10.06	3.52	7.35	983.2
13.1	30.25	9.95	3.54	7.23	1063.6
14.0	30.29	9.87	3.56	7.14	1139.3
15.0	30.36	9.75	3.57	7.04	1216.6
16.0	30.42	9.66	3.58	6.95	1297.1
17.0	30.48	9.54	3.60	6.86	1379.9
17.9	30.53	9.44	3.60	6.77	1456.8
18.5	30.55	9.37	3.61	6.72	FAILURE
18.9	30.58	9.27	3.60	6.66	1537.4
19.9	30.64	9.11	3.60	6.54	1618.2
21.0	30.71	8.98	3.60	6.45	1703.1
22.0	30.73	8.82	3.60	6.34	1782.9
22.9	30.72	8.67	3.59	6.24	1859.4
24.0	30.85	8.49	3.58	6.12	1946.2
25.0	30.91	8.29	3.56	6.01	2029.0
25.9	30.94	8.13	3.54	5.91	2103.5

APPENDIX D TABLE 13 - UNDRAINED TRIAXIAL COMPRESSION TESTS

Test CU23 — UNDRAINED TRIAXIAL COMPRESSION
σ_{3i}' = 34.01 MPa — e_i = 0.508 — H/D = 2.50
Cambria sand — ϕ' = 34.0 — 0.55 CM/HR

ϵ_1 %	u MPa	$\sigma_1 - \sigma_3$ MPa	σ_1'/σ_3'	p' MPa	Time second
0.0	0.36	0.17	1.00	34.03	0.0
0.1	1.26	1.07	1.03	33.45	136.4
0.3	2.51	2.32	1.07	32.62	347.1
0.5	4.56	4.47	1.15	31.30	618.4
0.7	7.11	6.75	1.25	29.49	882.1
1.0	11.32	9.48	1.41	26.20	1246.3
2.0	22.38	12.89	2.08	16.26	MAX. DEV.
2.9	26.71	12.26	2.60	11.73	3507.8
3.9	28.48	11.45	2.95	9.69	4605.6
5.1	29.43	10.83	3.19	8.56	5879.2
6.0	29.83	10.52	3.33	8.03	6978.9
7.0	30.10	10.32	3.42	7.70	8072.9
8.0	30.28	10.13	3.48	7.46	9163.6
9.0	30.40	9.93	3.51	7.27	10267.7
10.0	30.51	9.69	3.52	7.07	11363.5
10.9	30.63	9.40	3.52	6.87	12455.6
12.0	30.74	9.15	3.53	6.67	13640.1
12.2	30.76	9.10	3.53	6.62	FAILURE
13.0	30.85	8.85	3.52	6.46	14730.6
13.9	30.94	8.59	3.52	6.27	15818.0
15.1	31.05	8.32	3.52	6.08	17099.8
16.0	31.12	8.09	3.50	5.93	18188.4
17.0	31.18	7.89	3.48	5.80	19295.4
18.0	31.23	7.68	3.46	5.69	20387.2
19.0	31.27	7.51	3.44	5.59	21473.4
20.0	31.32	7.29	3.40	5.47	22558.7
20.9	31.34	7.19	3.38	5.41	23657.2
22.0	31.36	7.07	3.36	5.35	24831.5
22.9	31.39	6.98	3.34	5.30	25910.9
24.1	31.41	6.81	3.31	5.21	27190.3
25.0	31.46	6.57	3.27	5.08	28277.6
26.0	31.49	6.18	3.16	4.92	29365.8

APPENDIX D TABLE 14 - UNDRAINED TRIAXIAL COMPRESSION TESTS

Test CU25 UNDRAINED TRIAXIAL COMPRESSION
σ_{3i}' = 34.01 MPa e_i = 0.520 H/D = 2.50
Cambria sand ϕ' = ? 0.045 CM/HR
Test aborted during shearing

ϵ_1 %	u MPa	$\sigma_1 - \sigma_3$ MPa	σ_1'/σ_3'	p' MPa
0.0	0.00	0.00	1.00	34.02
0.1	2.09	0.75	1.02	32.16
0.3	3.98	2.19	1.07	30.76
0.5	6.74	5.09	1.19	28.97
0.7	8.59	6.27	1.25	27.51
1.0	13.39	9.73	1.47	23.86
1.2	16.55	11.15	1.64	21.18
1.5	19.63	12.11	1.84	18.42
1.8	21.98	12.49	2.04	16.20
1.9	23.18	12.56	2.16	15.02
2.0	23.62	12.54	2.21	14.57
3.3	28.00	11.60	2.93	9.88
4.7	29.30	10.72	3.28	8.29
5.1	29.53	10.53	3.35	8.00
6.3	29.93	10.19	3.50	7.48
6.8	30.09	10.11	3.58	7.30
8.0	30.29	9.91	3.66	7.02
9.2	30.45	9.78	3.75	6.82
10.0	30.53	9.69	3.78	6.72
11.2	30.61	9.61	3.82	6.59
12.1	30.67	9.59	3.87	6.53
13.2	30.75	9.53	3.92	6.43
14.1	30.81	9.48	3.96	6.36
14.5	30.84	9.47	3.99	6.33

APPENDIX D TABLE 15 - UNDRAINED TRIAXIAL COMPRESSION TESTS

Test CU26 UNDRAINED TRIAXIAL COMPRESSION
σ_{3i}' = 34.01 MPa e_i = 0.522 H/D = 2.50
Cambria sand ϕ' = 36.0 0.53 CM/HR

ϵ_1 %	u MPa	$\sigma_1 - \sigma_3$ MPa	σ_1'/σ_3'	p' MPa	Time second
0.0	0.02	0.06	1.00	34.01	0.0
0.1	0.68	0.76	1.02	33.58	118.1
0.3	2.39	2.96	1.09	32.60	373.0
0.5	4.91	5.20	1.18	30.83	643.5
0.7	7.30	7.03	1.26	29.06	893.6
1.0	11.47	9.71	1.43	25.78	1269.4
2.0	22.35	12.90	2.11	15.97	2460.5
2.1	22.62	12.91	2.13	15.69	MAX. DEV.
3.0	26.58	12.21	2.64	11.50	3559.8
4.0	28.30	11.38	2.99	9.50	4665.1
5.0	29.14	10.84	3.22	8.48	5816.6
6.0	29.59	10.45	3.36	7.90	6974.0
7.0	29.85	10.24	3.46	7.57	8037.7
8.0	30.05	10.04	3.53	7.31	9187.7
9.0	30.17	9.88	3.59	7.12	10303.3
10.0	30.29	9.78	3.63	6.97	11454.6
11.0	30.38	9.69	3.67	6.86	12516.6
12.0	30.46	9.60	3.71	6.75	13622.5
13.0	30.53	9.52	3.74	6.65	14760.7
14.0	30.60	9.46	3.77	6.56	15898.5
15.0	30.66	9.38	3.80	6.48	17035.5
16.0	30.71	9.30	3.82	6.40	18166.6
17.0	30.77	9.20	3.84	6.31	19330.2
18.0	30.82	9.11	3.85	6.23	20392.4
19.0	30.87	8.97	3.85	6.13	21493.8
20.0	30.91	8.81	3.85	6.03	22631.8
21.0	30.96	8.67	3.85	5.94	23775.6
22.0	31.03	8.50	3.84	5.83	24928.3
23.0	31.07	8.33	3.83	5.72	26064.1
24.0	31.10	8.26	3.84	5.66	27120.7
24.6	31.14	8.18	3.86	5.59	FAILURE
25.0	31.16	8.12	3.85	5.56	28255.6
26.0	31.21	7.96	3.84	5.45	29399.1
27.0	31.25	7.76	3.82	5.34	30535.0
28.0	31.30	7.60	3.80	5.24	31633.5

APPENDIX D TABLE 16 - UNDRAINED TRIAXIAL COMPRESSION TESTS

Test CU27 UNDRAINED TRIAXIAL COMPRESSION
σ_{3i}' = 34.01 MPa e_i = 0.527 H/D = 2.53
Cambria sand ϕ' = ? 0.045 CM/HR
Test aborted during shearing

ϵ_1 %	u MPa	$\sigma_1 - \sigma_3$ MPa	σ_1'/σ_3'	p' MPa	Time second
0.0	0.52	0.08	1.00	34.03	0.0
0.1	2.41	1.15	1.04	32.50	1583.3
0.3	4.10	2.51	1.08	31.27	4465.7
0.5	7.19	5.77	1.21	29.26	7834.1
0.7	10.45	8.12	1.34	26.79	10974.8
1.0	15.07	10.48	1.54	22.94	15687.5
1.2	17.80	11.58	1.69	20.59	
1.4	19.96	12.08	1.83	18.60	
1.6	21.75	12.36	1.97	16.90	
1.8	23.42	12.45	2.12	15.25	MAX. DEV.
2.0	24.42	12.39	2.23	14.24	30610.8
2.3	25.74	12.21	2.39	12.87	
2.7	27.05	11.93	2.60	11.45	
3.0	27.73	11.70	2.72	10.70	44288.2
3.5	28.57	11.21	2.88	9.70	
4.0	29.13	10.92	3.02	9.04	58224.1
5.0	29.80	10.39	3.20	8.19	71756.7
6.0	30.21	10.14	3.35	7.70	84558.8
7.0	30.47	9.90	3.44	7.36	97378.6
8.0	30.63	9.75	3.50	7.15	
9.0	30.75	9.66	3.56	6.99	
9.3	30.76	9.64	3.19	20.80	

APPENDIX D TABLE 17 - UNDRAINED TRIAXIAL COMPRESSION TESTS

Test CU32 — UNDRAINED TRIAXIAL COMPRESSION
σ_{3i}' = 34.01 MPa — e_i = 0.557 — H/D = 2.50
Cambria sand — ϕ' = 35.8 — 1.16 CM/HR

ϵ_1 %	u MPa	$\sigma_1 - \sigma_3$ MPa	σ_1'/σ_3'	p' MPa	Time second
0.0	0.53	0.55	1.02	34.17	0.0
0.1	0.83	1.06	1.03	34.02	37.6
0.3	1.71	1.64	1.05	33.37	151.2
0.5	2.97	2.78	1.09	32.49	289.5
0.7	4.48	4.35	1.14	31.50	394.2
1.0	7.25	6.82	1.25	29.54	554.3
2.0	20.12	12.75	1.89	18.64	1140.0
2.3	22.66	12.95	2.09	16.18	MAX. DEV.
3.0	25.87	12.54	2.45	12.84	1667.8
4.0	28.15	11.64	2.83	10.25	2190.6
5.0	29.17	11.04	3.06	9.04	2684.5
6.0	29.76	10.59	3.22	8.29	3213.7
7.0	30.10	10.31	3.33	7.86	3726.3
8.0	30.34	10.12	3.42	7.56	4247.1
9.0	30.51	9.98	3.49	7.34	4781.4
10.0	30.66	9.84	3.54	7.15	5312.1
11.0	30.76	9.74	3.58	7.01	5843.3
12.0	30.84	9.67	3.63	6.91	6341.5
13.0	30.92	9.60	3.66	6.80	6874.9
14.0	30.99	9.52	3.69	6.71	7408.5
15.0	31.03	9.45	3.72	6.63	7913.7
16.0	31.10	9.38	3.74	6.55	8440.5
17.0	31.16	9.28	3.75	6.46	8973.5
18.0	31.20	9.21	3.77	6.39	9504.0
19.0	31.26	9.13	3.78	6.32	9995.1
20.0	31.29	9.04	3.80	6.24	10524.3
21.0	31.34	8.90	3.80	6.15	11082.1
22.0	31.38	8.81	3.80	6.08	11584.4
23.0	31.44	8.68	3.80	5.99	12114.0
24.0	31.48	8.56	3.81	5.91	12642.6
24.6	31.50	8.53	3.82	5.87	FAILURE
25.0	31.52	8.46	3.81	5.83	13153.8
26.0	31.56	8.35	3.82	5.75	13682.3
27.0	31.59	8.24	3.81	5.68	14207.0
28.0	31.64	8.11	3.81	5.60	14740.5
29.0	31.67	7.99	3.80	5.52	15273.5

APPENDIX D TABLE 18 - UNDRAINED TRIAXIAL COMPRESSION TESTS

Test CU33 — UNDRAINED TRIAXIAL COMPRESSION
σ_{3i}' = 34.01 MPa — e_i = 0.557 — H/D = 2.50
Cambria sand — ϕ' = 36.2 — 0.259 CM/HR

ϵ_1 %	u MPa	$\sigma_1 - \sigma_3$ MPa	σ_1'/σ_3'	p' MPa	Time second
0.0	0.80	0.77	1.02	33.98	51.5
0.1	1.39	1.13	1.03	33.52	181.1
0.3	3.39	3.02	1.10	32.14	788.0
0.5	5.34	4.75	1.16	30.78	1325.6
0.7	7.19	6.31	1.23	29.44	1801.5
1.0	11.20	8.99	1.39	26.33	2620.6
2.0	22.52	12.81	2.07	16.27	5180.0
2.1	23.25	12.83	2.14	15.54	MAX. DEV.
3.0	26.92	12.24	2.61	11.68	7566.0
4.0	28.62	11.49	2.95	9.73	9796.0
5.0	29.46	11.00	3.17	8.73	12188.4
6.0	29.92	10.67	3.32	8.16	14495.0
7.0	30.23	10.42	3.42	7.77	16906.4
8.0	30.42	10.27	3.51	7.52	19174.7
9.0	30.60	10.12	3.58	7.30	21576.3
10.0	30.73	10.01	3.64	7.13	23959.4
11.0	30.83	9.91	3.68	7.00	26274.0
12.0	30.93	9.83	3.72	6.89	28654.3
13.0	30.99	9.78	3.77	6.79	31029.1
14.0	31.06	9.68	3.79	6.70	33290.3
15.0	31.11	9.60	3.81	6.62	35621.2
16.0	31.14	9.54	3.82	6.56	38007.0
17.0	31.19	9.47	3.84	6.50	40271.9
18.0	31.24	9.39	3.86	6.42	42664.1
19.0	31.28	9.30	3.86	6.35	44996.6
20.0	31.33	9.22	3.88	6.28	47394.7
21.0	31.36	9.10	3.88	6.20	49790.6
22.0	31.41	8.96	3.87	6.11	52166.8
23.0	31.45	8.86	3.88	6.03	54395.5
24.0	31.49	8.78	3.89	5.96	56756.0
25.0	31.53	8.58	3.87	5.85	59092.0
26.0	31.56	8.50	3.87	5.79	61483.3
27.0	31.60	8.40	3.87	5.72	63734.2
28.0	31.64	8.28	3.87	5.65	66080.8
28.3	31.66	8.28	3.89	5.63	FAILURE
29.0	31.67	8.17	3.87	5.58	68459.9

APPENDIX D TABLE 19 - UNDRAINED TRIAXIAL COMPRESSION TESTS

Test CUCM1 UNDRAINED TRIAXIAL COMPRESSION
σ_{3i}' = 52.00 MPa e_i = 0.525 H/D = 2.51
Cambria sand ϕ' = 35.6 2.54 CM/HR
Constant total mean normal stress maintained during shearing

ϵ_1 %	u MPa	$\sigma_1 - \sigma_3$ MPa	σ_1'/σ_3'	p' MPa	Time second
0.0	0.47	0.03	1.00	51.99	0.0
0.1	0.48	0.82	1.02	52.41	17.9
0.2	0.48	1.59	1.03	51.87	55.6
0.5	0.49	3.31	1.07	52.00	131.6
0.7	0.51	4.64	1.09	51.98	166.9
1.0	9.22	14.00	1.32	47.92	240.9
2.0	20.10	19.00	1.59	38.70	471.3
2.5	25.18	20.18	1.98	27.32	MAX. DEV.
3.0	29.53	19.99	2.23	22.95	714.9
4.0	34.92	18.53	2.64	17.47	960.4
5.0	37.73	17.20	2.93	14.63	1214.6
6.0	39.23	16.47	3.12	13.26	1436.5
7.0	40.21	15.83	3.25	12.30	1683.7
8.0	40.89	15.35	3.36	11.61	1918.7
9.0	41.31	15.01	3.44	11.14	2164.8
10.0	41.67	14.73	3.51	10.78	2415.6
11.0	41.91	14.52	3.56	10.51	2646.2
12.0	42.16	14.32	3.60	10.29	2881.0
13.0	42.31	14.11	3.63	10.07	3123.6
14.1	42.47	13.95	3.66	9.89	3382.0
15.0	42.68	13.80	3.68	9.75	3605.7
16.0	42.92	13.71	3.71	9.64	3851.5
17.0	42.97	13.58	3.73	9.50	4102.6
18.0	43.08	13.42	3.74	9.37	4332.0
19.0	43.17	13.29	3.76	9.25	4561.0
20.0	43.24	13.15	3.77	9.13	4806.1
21.0	43.40	12.91	3.77	8.96	5063.4
22.0	43.64	12.86	3.78	8.91	5296.9
23.0	43.72	12.68	3.78	8.78	5532.2
23.7	43.73	12.56	3.79	8.69	FAILURE
24.0	43.80	12.50	3.79	8.66	5767.9
25.0	43.97	12.31	3.78	8.53	6011.6

APPENDIX D TABLE 20 - UNDRAINED TRIAXIAL COMPRESSION TESTS

Test CUCM3 UNDRAINED TRIAXIAL COMPRESSION
σ_{3i}' = 52.00 MPa e_i = 0.527 H/D = 2.51
Cambria sand ϕ' = 36.0 2.54 CM/HR
Constant total mean normal stress maintained during shearing

ϵ_1 %	u MPa	$\sigma_1 - \sigma_3$ MPa	σ_1'/σ_3'	p' MPa	Time second
0.0	0.46	0.17	1.00	52.02	-0.0
0.1	1.03	1.70	1.03	52.08	24.1
0.3	1.54	3.88	1.08	50.84	62.5
0.4	2.57	5.98	1.13	49.69	106.2
0.7	4.94	9.33	1.21	47.38	160.4
1.0	9.85	13.93	1.37	42.40	239.7
2.0	24.49	19.81	1.93	27.90	488.2
2.3	26.83	20.24	2.07	25.73	MAX. DEV.
3.0	32.01	19.69	2.42	20.45	717.4
4.0	36.12	18.25	2.79	16.30	962.2
5.0	38.32	17.13	3.04	14.11	1211.5
6.0	39.60	16.46	3.21	12.94	1439.3
6.9	40.39	15.89	3.33	12.12	1673.5
8.0	40.97	15.39	3.42	11.50	1918.3
9.0	41.35	15.07	3.49	11.07	2160.7
10.0	41.83	14.84	3.55	10.76	2418.5
11.0	41.92	14.65	3.60	10.51	2639.0
12.0	42.19	14.37	3.63	10.25	2890.7
13.0	42.40	14.23	3.67	10.07	3135.0
14.0	42.51	14.05	3.70	9.88	3372.8
15.0	42.68	13.96	3.73	9.77	3611.5
16.0	42.70	13.72	3.74	9.58	3850.5
17.0	42.95	13.66	3.76	9.50	4090.1
18.0	43.08	13.52	3.79	9.36	4347.2
19.0	43.24	13.38	3.80	9.25	4570.0
20.0	43.31	13.24	3.81	9.12	4819.2
21.0	43.43	13.12	3.82	9.02	5061.4
22.0	43.55	12.97	3.83	8.90	5310.2
23.0	43.82	12.87	3.84	8.82	5532.1
24.0	43.79	12.67	3.84	8.68	5785.5
24.1	43.89	12.68	3.85	8.68	FAILURE
25.0	43.88	12.42	3.83	8.53	6026.7
26.0	43.96	12.23	3.82	8.42	6256.6

APPENDIX D TABLE 21 - UNDRAINED TRIAXIAL COMPRESSION TESTS

Test CUCM4 UNDRAINED TRIAXIAL COMPRESSION
σ_{3i}' = 34.01 MPa e_i = 0.529 H/D = 2.51
Cambria sand ϕ' = 35.7 2.54 CM/HR
Constant mean normal stress maintained during shearing

ϵ_1 %	u MPa	$\sigma_1 - \sigma_3$ MPa	σ_1'/σ_3'	p' MPa	Time second
0.0	0.54	0.09	1.00	34.01	-0.0
0.1	0.99	1.09	1.03	34.10	18.2
0.3	1.50	3.37	1.11	32.89	68.8
0.4	2.37	4.70	1.15	31.98	108.1
0.7	4.90	7.57	1.28	29.57	180.2
1.0	8.06	10.11	1.44	26.46	246.3
2.0	17.68	13.46	2.08	16.99	486.1
2.1	18.14	13.50	2.12	16.54	MAX. DEV.
3.0	22.39	12.78	2.63	12.11	737.4
4.0	24.47	11.94	2.97	10.05	979.7
5.0	25.57	11.38	3.18	9.02	1217.1
6.0	26.13	10.98	3.32	8.40	1455.5
7.0	26.51	10.67	3.42	7.97	1714.7
8.0	26.85	10.50	3.49	7.71	1957.5
9.0	27.10	10.36	3.56	7.51	2208.9
10.0	27.20	10.22	3.59	7.34	2432.6
11.0	27.28	10.08	3.63	7.19	2679.3
12.0	27.41	9.95	3.66	7.06	2922.4
13.0	27.53	9.91	3.70	6.98	3171.9
14.0	27.64	9.77	3.72	6.86	3416.7
15.0	27.82	9.68	3.73	6.77	3661.0
16.0	27.83	9.57	3.75	6.67	3903.3
17.0	27.97	9.45	3.77	6.57	4149.5
18.0	28.06	9.33	3.78	6.46	4391.7
19.0	28.18	9.21	3.79	6.37	4634.1
20.0	28.28	9.05	3.79	6.26	4876.7
21.0	28.42	8.92	3.80	6.16	5128.0
22.0	28.54	8.75	3.79	6.05	5371.8
23.0	28.54	8.61	3.80	5.95	FAILURE
24.0	28.68	8.42	3.79	5.83	5860.4
25.0	28.79	8.23	3.77	5.71	6107.8
26.0	28.94	8.04	3.75	5.60	6355.8

APPENDIX D TABLE 22 - UNDRAINED TRIAXIAL COMPRESSION TESTS

Test CUCM5 UNDRAINED TRIAXIAL COMPRESSION
σ_{3i}' = 34.01 MPa e_i = 0.522 H/D = 2.50
Cambria sand ϕ' = 36.3 0.64 CM/HR
Decreasing total mean normal stress (3 to 1) during shearing

ϵ_1 %	u MPa	$\sigma_1 - \sigma_3$ MPa	σ_1'/σ_3'	p' MPa	Time second
0.0	0.55	0.10	1.00	34.01	-0.0
0.1	0.85	0.67	1.02	33.89	26.1
0.3	1.25	1.30	1.04	32.78	224.5
0.5	1.74	3.66	1.12	31.50	342.6
0.7	2.72	5.29	1.19	29.99	478.6
1.0	4.34	8.19	1.33	27.56	637.6
2.0	13.77	13.01	2.07	16.51	1255.0
2.4	16.09	13.23	2.37	14.05	MAX. DEV.
3.0	18.20	12.86	2.66	12.05	1557.4
4.0	20.65	11.96	3.00	9.96	1877.9
5.0	21.99	11.16	3.20	8.79	2109.0
6.0	22.58	11.01	3.38	8.31	2343.6
7.0	23.24	10.60	3.47	7.82	2707.2
8.0	24.14	10.53	3.54	7.66	2935.5
9.0	23.65	10.43	3.61	7.47	3109.5
10.0	23.93	10.09	3.63	7.19	3320.2
11.0	24.10	9.98	3.68	7.05	3655.7
12.0	24.31	9.89	3.72	6.94	4000.1
13.0	24.46	9.79	3.74	6.83	4337.3
14.0	24.48	9.67	3.76	6.72	4653.7
15.0	24.71	9.60	3.78	6.65	4988.8
16.0	24.81	9.46	3.80	6.53	5328.0
17.0	24.98	9.39	3.82	6.46	5659.1
18.0	25.06	9.28	3.83	6.37	5989.9
19.0	25.19	9.19	3.85	6.29	6333.3
20.0	25.29	9.09	3.87	6.20	6668.3
21.0	25.39	8.99	3.88	6.11	6992.8
22.0	25.45	8.97	3.90	6.08	FAILURE
22.9	25.52	8.93	3.89	6.07	7401.9
23.9	26.33	8.75	3.86	5.97	7528.9
25.0	25.78	8.60	3.85	5.88	7626.9

APPENDIX E

APPENDIX E TABLE 1 - DRAINED/UNDRAINED STABILITY TESTS IN TRIAXIAL COMPRESSION

Test CSTAB2 DRAINED/UNDRAINED TRIAXIAL COMPRESSION
σ_{3i}' = 17.23 MPa e_i = 0.524 H/D = 2.51
Cambria sand ϕ' = 35.32.54 CM/HR
Test turned undrained at effective stress ratio of 2.67

ϵ_1 %	u MPa	ϵ_v %	$\sigma_1 - \sigma_3$ MPa	σ_1'/σ_3'	p' MPa	Time second
0.0	0.49	0.00	0.11	1.01	17.29	-0.0
0.1	0.49	0.03	0.86	1.05	17.50	29.1
0.3	0.50	0.11	2.01	1.12	17.91	68.6
0.5	0.50	0.25	2.87	1.17	18.19	126.3
0.7	0.50	0.42	3.65	1.21	18.46	178.4
1.0	0.50	0.69	4.63	1.27	18.79	250.5
2.0	0.52	1.64	7.39	1.43	19.70	493.9
3.0	0.50	2.59	9.84	1.57	20.54	743.4
4.0	0.50	3.45	11.83	1.69	21.18	986.4
5.0	0.51	4.29	13.78	1.80	21.83	1241.3
6.0	0.50	5.04	15.50	1.90	22.43	1485.5
7.0	0.50	5.76	17.12	1.99	22.96	1734.8
8.0	0.51	6.42	18.58	2.08	23.42	1979.7
9.0	0.52	7.06	20.05	2.16	23.91	2222.4
10.0	0.50	7.69	21.50	2.25	24.41	2480.3
11.0	0.50	8.26	22.90	2.33	24.89	2722.4
12.0	0.50	8.81	24.23	2.40	25.33	2970.8
13.0	0.51	9.33	25.55	2.48	25.76	3220.7
14.0	0.49	9.80	26.84	2.56	26.20	3467.0
15.0	0.50	10.28	28.01	2.63	26.58	3715.3
15.8	0.51	10.61	28.90	2.67	26.87	UNDRAINED
16.1	2.42	10.61	28.33	2.82	24.99	3966.9
17.1	6.67	10.61	25.43	3.08	20.73	4011.3
18.0	8.53	10.61	23.55	3.24	18.37	4045.0
18.9	9.79	10.61	22.19	3.37	16.77	4082.0
20.0	10.71	10.61	21.16	3.47	15.63	4122.3
21.1	11.33	10.61	20.41	3.54	14.84	4162.4
21.9	11.76	10.61	19.89	3.58	14.33	4195.8
23.0	12.16	10.61	19.37	3.63	13.83	4236.1
24.0	12.47	10.61	18.95	3.65	13.46	4272.9
25.0	12.76	10.61	18.54	3.68	13.10	4313.0
26.1	13.02	10.61	18.18	3.70	12.79	4353.1
26.9	13.23	10.61	17.90	3.71	12.57	4386.6
27.9	13.43	10.61	17.60	3.72	12.32	4423.3
29.0	13.64	10.61	17.27	3.73	12.08	4463.5
30.0	13.84	10.61	16.94	3.73	11.84	FAILURE
30.9	13.99	10.61	16.68	3.73	11.67	4537.1
31.9	14.15	10.61	16.37	3.72	11.47	4573.9
33.0	14.31	10.61	16.05	3.71	11.27	4614.0
34.0	14.48	10.61	15.70	3.69	11.07	4653.9
34.9	14.60	10.61	15.41	3.67	10.91	4687.4
36.0	14.76	10.61	15.07	3.65	10.72	4727.4
37.0	14.89	10.61	14.74	3.62	10.55	4764.2
38.0	15.03	10.61	14.37	3.58	10.36	4804.3

APPENDIX E TABLE 2 - DRAINED/UNDRAINED STABILITY TESTS IN TRIAXIAL COMPRESSION

Test CSTAB3 DRAINED/UNDRAINED TRIAXIAL COMPRESSION
σ_{3i}' = 17.23 MPa e_i = 0.520 H/D = 2.50
Cambria sand ϕ' = 32.8 2.54 CM/HR
Test turned undrained at effective stress ratio of 2.30
Specimen appeared to have slipped on base near failure

ϵ_1 %	u MPa	ϵ_v %	$\sigma_1 - \sigma_3$ MPa	σ_1'/σ_3'	p' MPa	Time second
0.0	0.51	0.00	0.09	1.01	17.26	0.0
0.1	0.51	0.03	0.69	1.04	17.52	27.0
0.3	0.51	0.07	1.03	1.06	17.58	70.2
0.5	0.52	0.18	2.42	1.14	18.03	117.9
0.7	0.52	0.35	3.38	1.20	18.36	172.1
1.0	0.52	0.61	4.35	1.25	18.68	243.9
2.0	0.52	1.55	7.29	1.42	19.64	490.4
3.0	0.51	2.46	9.82	1.57	20.52	734.9
4.0	0.52	3.34	11.92	1.69	21.19	985.3
5.0	0.52	4.15	13.84	1.80	21.83	1233.4
6.0	0.50	4.92	15.58	1.90	22.44	1485.7
7.0	0.51	5.63	17.22	2.00	22.98	1726.5
8.0	0.51	6.31	18.74	2.09	23.48	1975.5
9.0	0.52	6.94	20.07	2.17	23.91	2220.1
10.0	0.52	7.58	21.53	2.25	24.41	2475.9
10.7	0.52	7.99	22.44	2.30	24.72	UNDRAINED
11.3	4.87	7.99	21.05	2.59	20.29	2728.1
12.0	7.89	7.99	19.25	2.80	17.08	2754.8
13.0	10.09	7.99	17.41	3.03	14.38	2790.8
13.9	11.27	7.99	16.27	3.17	12.93	2826.9
15.0	12.05	7.99	15.38	3.25	11.95	2865.9
16.0	12.60	7.99	14.66	3.30	11.27	2902.0
17.0	13.02	7.99	14.04	3.33	10.72	2938.4
17.9	13.39	7.99	13.46	3.34	10.25	2974.6
18.9	13.70	7.99	12.98	3.34	9.87	3010.9
20.0	14.00	7.99	12.56	3.34	9.51	FAILURE
20.1	14.02	7.99	12.52	3.36	9.49	3052.8
21.0	14.30	7.99	12.06	3.35	9.15	3088.9
22.0	14.51	7.99	11.63	3.33	8.86	3124.8
22.9	14.73	7.99	11.24	3.31	8.62	3160.5
24.0	14.93	7.99	10.78	3.27	8.35	3199.4
24.9	15.09	7.99	10.44	3.23	8.16	3235.1
26.1	15.26	7.99	10.07	3.19	7.96	3276.6
27.0	15.42	7.99	9.65	3.13	7.74	3312.3
28.0	15.55	7.99	9.37	3.09	7.60	3348.3
29.0	15.68	7.99	9.04	3.05	7.43	3384.2
29.9	15.86	7.99	8.67	3.00	7.22	3420.0

APPENDIX E TABLE 3 - DRAINED/UNDRAINED STABILITY TESTS IN TRIAXIAL COMPRESSION

Test CSTAB4 DRAINED/UNDRAINED TRIAXIAL COMPRESSION
σ_{3i}' = 17.23 MPa e_i = 0.520 H/D = 2.49
Cambria sand ϕ' = 34.5 2.54 CM/HR
Test turned undrained at effective stress ratio of 3.20

ϵ_1 %	u MPa	ϵ_v %	$\sigma_1 - \sigma_3$ MPa	σ_1'/σ_3'	p' MPa	Time second
0.0	0.52	0.00	0.10	1.01	17.26	0.0
0.1	0.52	0.03	0.80	1.05	17.44	29.2
0.3	0.52	0.08	1.19	1.07	17.63	71.2
0.5	0.52	0.21	2.67	1.15	18.13	121.8
0.7	0.52	0.41	3.60	1.21	18.43	177.5
1.0	0.52	0.67	4.56	1.26	18.75	250.8
2.0	0.51	1.59	7.39	1.43	19.69	490.8
3.0	0.51	2.52	9.87	1.57	20.53	734.7
4.0	0.53	3.43	12.06	1.70	21.23	992.5
5.0	0.52	4.20	13.79	1.80	21.81	1228.0
6.0	0.51	4.97	15.61	1.91	22.44	1477.6
7.0	0.52	5.67	17.16	2.00	22.94	1721.3
8.0	0.49	6.33	18.68	2.08	23.48	1966.8
9.0	0.51	6.97	20.12	2.17	23.95	2214.5
10.0	0.51	7.59	21.53	2.25	24.41	2465.8
11.0	0.52	8.16	22.87	2.33	24.85	2711.6
12.0	0.53	8.70	24.13	2.40	25.25	2956.2
13.0	0.51	9.23	25.54	2.48	25.76	3211.0
14.0	0.51	9.71	26.69	2.55	26.12	3451.4
15.0	0.51	10.16	27.93	2.62	26.55	3697.7
16.0	0.51	10.59	29.19	2.69	26.97	3943.8
17.0	0.52	10.97	30.20	2.75	27.29	4184.2
18.0	0.53	11.35	31.47	2.83	27.71	4429.2
19.0	0.50	11.72	32.45	2.88	28.07	4679.3
20.0	0.50	12.07	33.50	2.94	28.39	4934.8
21.0	0.50	12.37	34.37	2.99	28.69	5171.7
22.0	0.50	12.66	35.49	3.06	29.08	5417.7
23.0	0.51	12.94	36.36	3.11	29.36	5669.3
24.0	0.51	13.22	37.20	3.16	29.59	5923.1
24.6	0.52	13.38	37.83	3.20	29.85	UNDRAINED
24.9	1.22	13.38	37.83	3.27	29.26	6142.9
26.0	3.65	13.38	35.86	3.41	26.85	6191.6
27.1	5.11	13.38	33.93	3.49	24.91	6231.5
28.0	5.94	13.38	32.78	3.55	23.80	6264.8
28.9	6.62	13.38	31.80	3.58	22.90	6301.6
30.0	7.18	13.38	30.92	3.61	22.15	6341.5
30.9	7.56	13.38	30.28	3.62	21.64	6375.0
31.7	7.84	13.38	29.75	3.62	21.26	FAILURE
32.0	7.92	13.38	29.58	3.62	21.14	6414.9
33.0	8.20	13.38	29.00	3.62	20.75	6451.6
34.0	8.47	13.38	28.39	3.60	20.37	6491.5
34.9	8.65	13.38	27.92	3.59	20.09	6524.9

APPENDIX E TABLE 4 - DRAINED/UNDRAINED STABILITY TESTS IN TRIAXIAL COMPRESSION

Test CSTAB5 DRAINED/UNDRAINED TRIAXIAL COMPRESSION
σ_{3i}' = 17.23 MPa e_i = 0.524 H/D = 2.51
Cambria sand ϕ' = 34.7 2.54 CM/HR
Test turned undrained at effective stress ratio of 1.87

ϵ_1 %	u MPa	ϵ_v %	$\sigma_1 - \sigma_3$ MPa	σ_1'/σ_3'	p' MPa	Time second
0.0	0.52	0.00	0.10	1.01	17.25	-0.0
0.1	0.52	0.04	0.97	1.06	17.55	29.5
0.3	0.52	0.10	1.87	1.11	17.83	69.1
0.5	0.53	0.30	3.12	1.18	18.26	126.5
0.7	0.53	0.49	3.90	1.23	18.51	179.1
1.0	0.53	0.76	4.82	1.28	18.83	250.1
2.0	0.54	1.72	7.62	1.44	19.75	494.2
3.0	0.53	2.69	10.07	1.58	20.58	749.6
4.0	0.53	3.53	12.07	1.70	21.24	991.1
5.0	0.54	4.36	13.90	1.81	21.84	1239.4
5.6	0.54	4.84	14.97	1.87	22.21	UNDRAINED
6.0	4.21	4.84	14.87	2.09	18.54	1463.0
6.9	9.98	4.84	13.38	2.58	12.92	1514.7
8.1	11.92	4.84	11.93	2.94	10.12	1559.4
9.0	12.47	4.84	11.23	3.12	9.04	1595.1
10.0	12.98	4.84	10.76	3.25	8.37	1635.8
11.0	13.29	4.84	10.43	3.34	7.93	1677.8
12.1	13.54	4.84	10.16	3.42	7.59	1722.8
12.9	13.69	4.84	9.99	3.46	7.39	1757.9
13.9	13.82	4.84	9.82	3.50	7.20	1798.6
15.0	13.94	4.84	9.66	3.54	7.03	1843.0
15.9	14.03	4.84	9.53	3.56	6.89	1882.6
16.9	14.11	4.84	9.41	3.59	6.77	1923.0
18.0	14.19	4.84	9.26	3.60	6.65	1968.0
19.1	14.26	4.84	9.12	3.62	6.52	2013.9
19.9	14.32	4.84	9.01	3.63	6.44	2049.0
20.9	14.37	4.84	8.89	3.63	6.34	2088.0
22.0	14.43	4.84	8.75	3.64	6.23	2132.4
23.0	14.49	4.84	8.61	3.64	6.13	2176.4
23.9	14.53	4.84	8.49	3.64	6.04	2212.5
25.0	14.59	4.84	8.35	3.64	5.94	2257.4
25.9	14.64	4.84	8.20	3.64	5.84	2298.0
27.0	14.70	4.84	8.04	3.64	5.73	2342.8
27.3	14.72	4.84	8.02	3.64	5.70	FAILURE
28.1	14.76	4.84	7.89	3.64	5.62	2387.9
28.9	14.80	4.84	7.76	3.63	5.53	2421.9
29.9	14.85	4.84	7.61	3.62	5.44	2461.5
31.0	14.88	4.84	7.43	3.60	5.34	2507.5
32.1	14.93	4.84	7.27	3.58	5.24	2551.2
32.9	14.97	4.84	7.14	3.57	5.16	2585.5

APPENDIX E TABLE 5 - DRAINED/UNDRAINED STABILITY TESTS IN TRIAXIAL COMPRESSION

Test CSTAB7 DRAINED/UNDRAINED TRIAXIAL COMPRESSION
σ_{3i}' = 26.00 MPa e_i = 0.522 H/D = 2.50
Cambria sand ϕ' = 35.3 2.54 CM/HR
Test turned undrained at effective stress ratio of 2.70

ϵ_1 %	u MPa	ϵ_v %	$\sigma_1 - \sigma_3$ MPa	σ_1'/σ_3'	p' MPa	Time second
0.0	0.53	0.00	0.08	1.00	26.01	-0.0
0.1	0.53	0.02	0.73	1.03	26.21	25.7
0.3	0.54	0.05	1.16	1.04	26.36	70.4
0.5	0.54	0.11	2.46	1.09	26.79	118.3
0.7	0.54	0.23	3.52	1.14	27.15	171.0
1.0	0.54	0.43	4.82	1.19	27.58	240.3
2.0	0.55	1.43	8.86	1.34	28.92	485.1
3.0	0.53	2.44	12.50	1.48	30.15	738.1
4.0	0.54	3.35	15.65	1.60	31.20	979.0
5.0	0.53	4.20	18.45	1.71	32.13	1221.0
5.6	0.53	4.68	20.13	1.77	32.70	UNDRAINED
6.0	7.19	4.68	20.14	2.04	26.06	1495.2
6.8	13.61	4.68	19.10	2.45	19.56	1564.4
7.9	17.26	4.68	17.01	2.83	14.94	1612.1
9.1	19.05	4.68	15.64	3.09	12.68	1662.9
10.0	19.88	4.68	14.87	3.24	11.59	1706.8
11.0	20.41	4.68	14.31	3.34	10.88	1751.8
12.0	20.77	4.68	13.91	3.42	10.39	1795.8
13.0	21.04	4.68	13.61	3.48	10.02	1839.8
14.0	21.25	4.68	13.35	3.53	9.72	1885.3
15.0	21.41	4.68	13.13	3.57	9.48	1929.2
16.0	21.56	4.68	12.92	3.60	9.27	1974.3
17.0	21.68	4.68	12.74	3.63	9.09	2018.9
18.0	21.78	4.68	12.56	3.65	8.92	2062.9
19.0	21.88	4.68	12.40	3.67	8.77	2107.0
19.9	21.96	4.68	12.23	3.69	8.63	2150.8
20.9	22.05	4.68	12.06	3.70	8.48	2195.1
21.9	22.14	4.68	11.91	3.72	8.35	2240.0
22.9	22.21	4.68	11.75	3.73	8.23	2285.3
23.9	22.28	4.68	11.57	3.73	8.10	FAILURE
24.9	22.34	4.68	11.39	3.73	7.98	2375.8
25.9	22.40	4.68	11.19	3.72	7.84	2421.1
26.9	22.47	4.68	11.00	3.72	7.71	2464.9
27.9	22.53	4.68	10.80	3.71	7.58	2509.8
28.9	22.60	4.68	10.58	3.70	7.45	2554.4
30.0	22.64	4.68	10.36	3.68	7.31	2602.1
31.0	22.71	4.68	10.15	3.67	7.19	2646.9
32.0	22.76	4.68	9.95	3.65	7.08	2690.8
33.0	22.81	4.68	9.73	3.63	6.95	2735.1

APPENDIX F

APPENDIX F TABLE 1 - SUCCESSFUL DRAINED UNIFORM STRAIN TRIAXIAL EXTENSION TESTS

Test ECD36 DRAINED TRIAXIAL EXTENSION
σ_1' = 2.22 MPa e_i = 0.526 H/D = 1.91
Cambria sand ϕ' = 36.8 1.02 CM/HR
Successful uniform strain test with steel plates.

ϵ_3 %	ϵ_v %	$\sigma_1 - \sigma_3$ MPa	σ_1'/σ_3'	p' MPa	Time second
0.0	0.00	0.05	1.02	2.21	-0.0
0.0	-0.01	0.34	1.18	2.13	21.0
0.1	-0.01	0.50	1.29	2.04	39.0
0.1	-0.00	0.72	1.48	1.98	68.9
0.3	0.02	1.05	1.91	1.85	149.8
0.4	0.03	1.13	2.04	1.84	184.0
0.5	0.05	1.21	2.21	1.81	235.4
0.6	0.06	1.25	2.30	1.79	275.1
0.7	0.07	1.30	2.42	1.78	325.8
0.8	0.08	1.33	2.53	1.76	377.2
1.0	0.08	1.40	2.70	1.75	480.3
1.3	0.07	1.45	2.88	1.74	611.4
1.5	0.06	1.48	2.99	1.74	715.5
1.7	0.05	1.51	3.06	1.74	802.9
2.0	0.01	1.53	3.17	1.72	945.8
2.3	-0.03	1.55	3.27	1.72	1079.2
2.5	-0.07	1.56	3.33	1.71	1181.8
2.7	-0.11	1.57	3.37	1.71	1284.4
3.0	-0.16	1.59	3.47	1.71	1413.5
3.3	-0.22	1.60	3.51	1.70	1567.9
3.5	-0.26	1.61	3.55	1.70	1652.3
3.7	-0.30	1.61	3.58	1.70	1750.6
4.0	-0.37	1.62	3.65	1.69	1895.7
4.5	-0.48	1.64	3.74	1.70	2120.9
5.0	-0.60	1.65	3.82	1.69	2358.6
5.5	-0.73	1.67	3.88	1.69	2610.4
6.0	-0.84	1.67	3.91	1.69	2835.9
6.2	-0.89	1.68	3.96	1.68	FAILURE
6.5	-0.96	1.67	3.93	1.69	3070.7
7.0	-1.08	1.67	3.85	1.70	3308.8

APPENDIX F TABLE 2 - SUCCESSFUL DRAINED UNIFORM STRAIN TRIAXIAL EXTENSION TESTS

Test ECD39 DRAINED TRIAXIAL EXTENSION
σ_1' = 6.00 MPa e_i = 0.520 H/D = 1.89
Cambria sand ϕ' = 35.1 1.02 CM/HR
Successful uniform strain test with steel plates.

ϵ_3 %	ϵ_v %	$\sigma_1 - \sigma_3$ MPa	σ_1'/σ_3'	p' MPa	Time second
0.0	0.00	0.03	1.01	5.99	0.0
0.1	-0.01	0.40	1.07	5.88	12.5
0.1	-0.00	0.71	1.13	5.77	44.8
0.1	-0.00	1.00	1.20	5.66	63.8
0.3	0.05	1.95	1.48	5.34	142.1
0.4	0.09	2.42	1.68	5.18	192.4
0.5	0.12	2.65	1.79	5.11	225.2
0.6	0.17	2.90	1.94	5.03	276.9
0.7	0.21	3.08	2.06	4.97	325.3
0.8	0.24	3.21	2.15	4.91	366.6
1.0	0.32	3.43	2.34	4.84	470.6
1.3	0.40	3.62	2.52	4.78	602.3
1.5	0.45	3.72	2.64	4.75	694.0
1.7	0.50	3.81	2.75	4.72	799.4
2.0	0.55	3.90	2.86	4.70	931.5
2.3	0.59	3.97	2.96	4.67	1077.6
2.5	0.61	4.01	3.03	4.66	1161.6
2.7	0.64	4.05	3.09	4.64	1252.9
3.0	0.66	4.11	3.18	4.63	1408.6
3.3	0.68	4.14	3.22	4.62	1539.9
3.5	0.69	4.17	3.28	4.61	1643.8
3.7	0.70	4.20	3.33	4.60	1726.9
4.0	0.71	4.22	3.37	4.60	1871.8
4.5	0.71	4.26	3.45	4.58	2104.6
5.0	0.71	4.30	3.52	4.57	2332.6
5.5	0.70	4.33	3.59	4.56	2561.3
6.0	0.69	4.36	3.63	4.56	2799.4
6.5	0.66	4.37	3.68	4.55	3028.3
6.9	0.64	4.39	3.71	4.55	FAILURE
7.0	0.63	4.39	3.69	4.56	3263.7
7.5	0.60	4.37	3.67	4.55	3494.4
8.0	0.56	4.37	3.65	4.56	3732.1

APPENDIX F TABLE 3 - SUCCESSFUL DRAINED UNIFORM STRAIN TRIAXIAL EXTENSION TESTS

Test ECD40 DRAINED TRIAXIAL EXTENSION
σ_1' = 12.00 MPa e_i = 0.521 H/D = 1.89
Cambria sand ϕ' = 33.8 1.02 CM/HR
Successful uniform strain test with steel plates.

ϵ_3 %	ϵ_v %	$\sigma_1 - \sigma_3$ MPa	σ_1'/σ_3'	p' MPa	Time second
0.0	0.00	0.03	1.00	11.97	-0.0
0.1	-0.01	0.47	1.04	11.83	13.0
0.1	-0.00	0.85	1.08	11.73	46.5
0.1	-0.01	1.34	1.13	11.52	66.8
0.3	0.04	2.98	1.33	10.98	149.6
0.4	0.09	3.69	1.45	10.75	185.9
0.5	0.16	4.36	1.57	10.52	227.5
0.6	0.26	4.99	1.71	10.32	283.3
0.7	0.33	5.31	1.79	10.22	320.7
0.8	0.42	5.66	1.90	10.08	372.2
1.0	0.58	6.15	2.06	9.92	468.4
1.3	0.79	6.60	2.23	9.77	606.6
1.5	0.91	6.82	2.33	9.69	696.5
1.7	1.02	7.02	2.42	9.62	792.2
2.0	1.18	7.22	2.52	9.56	930.5
2.3	1.32	7.38	2.61	9.50	1069.1
2.5	1.40	7.47	2.66	9.47	1159.0
2.7	1.48	7.56	2.72	9.44	1259.5
3.0	1.59	7.68	2.79	9.42	1396.3
3.3	1.70	7.77	2.85	9.39	1531.6
3.5	1.76	7.83	2.89	9.36	1623.2
3.7	1.82	7.88	2.92	9.35	1720.8
4.0	1.91	7.94	2.97	9.33	1855.1
4.5	2.05	8.05	3.04	9.30	2100.3
5.0	2.16	8.12	3.10	9.27	2320.8
5.5	2.27	8.19	3.16	9.25	2558.6
6.0	2.37	8.21	3.18	9.23	2794.8
6.5	2.46	8.27	3.23	9.22	3033.3
7.0	2.53	8.31	3.27	9.19	3258.5
7.5	2.60	8.33	3.29	9.20	3491.5
7.9	2.66	8.33	3.29	9.19	FAILURE
8.0	2.67	8.32	3.28	9.20	3725.1
8.5	2.73	8.30	3.26	9.20	3969.0
9.0	2.79	8.27	3.23	9.22	4192.2

APPENDIX F TABLE 4 - SUCCESSFUL DRAINED UNIFORM STRAIN TRIAXIAL EXTENSION TESTS

Test ECD48 DRAINED TRIAXIAL EXTENSION
σ_1' = 10.00 MPa e_i = 0.519 H/D = 1.89
Cambria sand ϕ' = 33.1 1.02 CM/HR
Successful uniform strain test with steel plates.

ϵ_3 %	ϵ_v %	$\sigma_1 - \sigma_3$ MPa	σ_1'/σ_3'	p' MPa	Time second
0.0	0.00	0.05	1.00	9.98	-0.0
0.1	-0.00	0.47	1.05	9.84	12.4
0.1	-0.00	0.69	1.07	9.79	37.2
0.1	-0.01	1.32	1.15	9.56	67.7
0.3	0.02	2.30	1.30	9.22	132.1
0.4	0.07	2.95	1.42	9.00	183.6
0.5	0.13	3.56	1.55	8.81	230.6
0.6	0.19	4.12	1.70	8.60	282.9
0.7	0.24	4.41	1.79	8.51	318.7
0.8	0.31	4.68	1.88	8.43	362.3
1.0	0.46	5.17	2.07	8.27	468.6
1.3	0.64	5.56	2.27	8.10	607.1
1.5	0.74	5.76	2.36	8.06	694.1
1.7	0.84	5.93	2.46	8.00	796.0
2.0	0.95	6.11	2.58	7.94	929.5
2.3	1.05	6.26	2.69	7.88	1065.6
2.5	1.12	6.33	2.74	7.86	1155.4
2.7	1.20	6.41	2.80	7.84	1254.2
3.0	1.28	6.50	2.87	7.81	1391.6
3.3	1.36	6.58	2.94	7.78	1526.2
3.5	1.41	6.63	2.98	7.77	1618.5
3.7	1.46	6.68	3.03	7.75	1721.2
4.0	1.52	6.73	3.07	7.73	1852.5
4.5	1.60	6.81	3.15	7.70	2079.9
5.0	1.68	6.87	3.22	7.68	2311.6
5.5	1.74	6.93	3.28	7.66	2551.7
6.0	1.79	6.97	3.32	7.65	2767.8
6.5	1.84	7.00	3.35	7.65	3008.4
7.0	1.88	7.02	3.38	7.63	3233.2
7.5	1.94	7.04	3.40	7.62	3463.3
8.0	1.98	7.04	3.40	7.62	3706.9
8.1	1.99	7.05	3.41	7.62	FAILURE
8.5	2.01	7.04	3.39	7.63	3934.4
9.0	2.04	7.02	3.37	7.64	4171.1
9.5	2.14	7.00	3.35	7.64	4397.2
10.0	2.21	6.98	3.34	7.64	4635.4
10.5	2.25	6.94	3.30	7.65	4855.9
11.0	2.30	6.90	3.25	7.67	5088.6
11.5	2.34	6.84	3.22	7.65	5326.9
12.0	2.36	6.81	3.15	7.71	5552.8
12.5	2.40	6.77	3.11	7.72	5782.6
13.0	2.43	6.70	3.05	7.74	6022.9

APPENDIX F TABLE 5 - SUCCESSFUL DRAINED UNIFORM STRAIN TRIAXIAL EXTENSION TESTS

Test ECD49 DRAINED TRIAXIAL EXTENSION
σ_1' = 14.50 MPa e_i = 0.521 H/D = 1.88
Cambria sand ϕ' = 31.9 1.02 CM/HR
Successful uniform strain test with steel plates.

ϵ_3 %	ϵ_v %	$\sigma_1 - \sigma_3$ MPa	σ_1'/σ_3'	p' MPa	Time second
0.0	0.00	0.05	1.00	14.45	-0.0
0.0	0.00	0.11	1.01	14.43	2.9
0.1	-0.00	1.59	1.12	13.94	57.8
0.2	-0.00	2.59	1.22	13.59	84.5
0.3	0.06	4.07	1.39	13.10	136.7
0.4	0.16	5.08	1.54	12.77	190.4
0.5	0.24	5.61	1.63	12.59	228.8
0.6	0.33	6.13	1.74	12.41	275.0
0.7	0.45	6.54	1.83	12.28	327.4
0.8	0.53	6.82	1.89	12.18	365.5
1.0	0.72	7.30	2.02	12.03	461.0
1.3	0.94	7.80	2.17	11.86	592.0
1.5	1.08	8.05	2.26	11.78	682.0
1.7	1.23	8.29	2.35	11.69	780.0
2.0	1.42	8.54	2.45	11.60	916.3
2.3	1.61	8.74	2.51	11.62	1053.2
2.5	1.70	8.88	2.59	11.52	1144.8
2.7	1.81	8.99	2.64	11.48	1241.1
3.0	1.94	9.13	2.71	11.42	1374.2
3.3	2.07	9.24	2.77	11.39	1506.3
3.5	2.17	9.32	2.81	11.36	1611.8
3.7	2.26	9.38	2.85	11.34	1693.4
4.0	2.37	9.46	2.89	11.32	1830.6
4.5	2.56	9.58	2.97	11.25	2077.6
5.0	2.72	9.70	3.03	11.24	2295.6
5.5	2.87	9.78	3.09	11.21	2531.4
6.0	3.00	9.85	3.14	11.18	2749.5
6.5	3.12	9.91	3.17	11.17	2976.5
7.0	3.25	9.95	3.20	11.15	3214.0
7.5	3.35	9.98	3.22	11.14	3438.7
7.9	3.43	10.01	3.24	11.13	FAILURE
8.0	3.45	10.00	3.23	11.15	3673.1
8.5	3.56	9.99	3.23	11.14	3908.9
9.0	3.65	9.98	3.23	11.14	4125.2
9.5	3.74	9.96	3.21	11.15	4368.5
10.0	3.81	9.91	3.18	11.15	4585.1
10.5	3.88	9.89	3.16	11.17	4827.7

APPENDIX F TABLE 6 - SUCCESSFUL DRAINED UNIFORM STRAIN TRIAXIAL EXTENSION TESTS

Test ECD50 DRAINED TRIAXIAL EXTENSION
σ_1' = 68.00 MPa e_i = 0.518 H/D = 1.93
Cambria sand ϕ' = 31.5 1.02 CM/HR
Successful uniform strain test with steel plates.

ϵ_3 %	ϵ_v %	$\sigma_1 - \sigma_3$ MPa	σ_1'/σ_3'	p' MPa	Time second
0.0	0.00	0.10	1.00	67.95	-0.0
0.1	0.00	0.82	1.01	67.70	12.3
0.1	0.02	1.49	1.02	67.52	45.1
0.1	0.03	2.30	1.03	67.21	62.8
0.3	0.06	6.03	1.10	65.97	138.2
0.4	0.09	7.75	1.13	65.39	172.4
0.5	0.13	9.91	1.17	64.67	213.8
0.6	0.21	12.69	1.23	63.76	269.1
0.7	0.27	14.48	1.27	63.15	302.5
0.8	0.38	17.44	1.35	62.16	355.6
1.0	0.61	22.11	1.48	60.61	439.8
1.3	1.03	27.67	1.69	58.76	581.2
1.5	1.27	30.03	1.79	57.97	663.3
1.7	1.51	32.07	1.89	57.29	754.6
2.0	1.84	34.50	2.03	56.47	888.9
2.3	2.13	36.31	2.15	55.87	1018.4
2.5	2.32	37.29	2.22	55.54	1110.8
2.7	2.51	38.29	2.29	55.21	1210.7
3.0	2.74	39.32	2.37	54.87	1338.3
3.3	2.94	40.24	2.45	54.58	1461.1
3.5	3.09	40.84	2.50	54.39	1565.6
3.7	3.21	41.22	2.54	54.23	1646.3
4.0	3.37	41.88	2.60	54.03	1772.3
4.5	3.65	42.84	2.70	53.72	2006.9
5.0	3.88	43.63	2.79	53.45	2224.4
5.5	4.09	44.23	2.86	53.25	2441.8
6.0	4.28	44.81	2.93	53.06	2668.3
6.5	4.45	45.35	3.00	52.86	2901.9
7.0	4.60	45.61	3.04	52.80	3115.1
7.5	4.74	46.04	3.10	52.64	3336.8
8.0	4.87	46.31	3.14	52.55	3567.1
8.5	4.97	46.49	3.16	52.49	3780.2
9.0	5.07	46.48	3.16	52.51	4000.8
9.5	5.16	46.52	3.17	52.49	4223.0
9.6	5.18	46.69	3.19	52.44	FAILURE
10.0	5.23	46.50	3.16	52.48	4445.1
10.5	5.30	46.25	3.13	52.57	4671.1
11.0	5.35	45.93	3.08	52.68	4905.2
11.5	5.39	45.60	3.04	52.79	5118.5
12.0	5.43	45.31	3.00	52.88	5345.1

APPENDIX F TABLE 7 - SUCCESSFUL DRAINED UNIFORM STRAIN TRIAXIAL EXTENSION TESTS

Test ECD52 DRAINED TRIAXIAL EXTENSION
σ_1' = 8.00 MPa e_i = 0.535 H/D = 1.90
Cambria sand ϕ' = 34.2 1.02 CM/HR
Successful uniform strain test with steel plates.

ϵ_3 %	ϵ_v %	$\sigma_1 - \sigma_3$ MPa	σ_1'/σ_3'	p' MPa	Time second
0.0	0.00	0.03	1.00	7.97	0.0
0.1	-0.01	0.40	1.05	7.86	11.4
0.1	-0.01	0.71	1.10	7.76	42.0
0.1	-0.01	1.18	1.17	7.60	62.8
0.3	0.02	2.65	1.50	7.09	138.5
0.4	0.08	3.22	1.68	6.90	189.4
0.5	0.13	3.60	1.82	6.78	239.2
0.6	0.17	3.79	1.91	6.71	272.4
0.7	0.23	4.02	2.02	6.63	324.2
0.8	0.28	4.17	2.10	6.58	367.2
1.0	0.38	4.45	2.26	6.49	470.4
1.3	0.49	4.68	2.43	6.41	607.0
1.5	0.56	4.82	2.53	6.36	701.0
1.7	0.62	4.93	2.62	6.32	801.8
2.0	0.69	5.05	2.73	6.28	933.3
2.3	0.76	5.14	2.82	6.25	1067.3
2.5	0.80	5.20	2.88	6.23	1163.1
2.7	0.84	5.25	2.94	6.22	1253.1
3.0	0.89	5.31	3.00	6.20	1406.1
3.3	0.93	5.37	3.07	6.18	1536.0
3.5	0.96	5.41	3.12	6.16	1639.0
3.7	0.98	5.43	3.14	6.15	1722.6
4.0	1.02	5.48	3.20	6.14	1868.4
4.5	1.06	5.54	3.28	6.12	2096.5
5.0	1.10	5.58	3.35	6.10	2333.1
5.5	1.12	5.63	3.40	6.09	2561.0
6.0	1.13	5.67	3.46	6.08	2802.4
6.5	1.15	5.71	3.51	6.08	3036.1
7.0	1.15	5.72	3.53	6.07	3265.5
7.5	1.15	5.73	3.54	6.07	3494.7
7.8	1.15	5.74	3.56	6.07	FAILURE
8.0	1.15	5.73	3.54	6.07	3727.5
8.5	1.15	5.71	3.52	6.08	3966.3
9.0	1.14	5.71	3.50	6.09	4195.1
9.5	1.14	5.68	3.46	6.10	4442.2
10.0	1.13	5.64	3.40	6.11	4675.2
10.5	1.13	5.60	3.35	6.12	4902.1
11.0	1.13	5.56	3.28	6.14	5132.0
11.5	1.13	5.51	3.23	6.15	5365.7
12.0	1.13	5.46	3.18	6.14	5601.2

APPENDIX F TABLE 8 - SUCCESSFUL DRAINED UNIFORM STRAIN TRIAXIAL EXTENSION TESTS

Test ECD54 DRAINED TRIAXIAL EXTENSION
σ_1' = 26.00 MPa e_i = 0.527 H/D = 1.90
Cambria sand ϕ' = 31.4 1.02 CM/HR
Successful uniform strain test with steel plates.

ϵ_3 %	ϵ_v %	$\sigma_1 - \sigma_3$ MPa	σ_1'/σ_3'	p' MPa	Time second
0.0	0.00	0.04	1.00	25.98	0.0
0.1	-0.00	0.59	1.02	25.81	13.4
0.1	0.01	0.95	1.04	25.74	45.3
0.1	0.01	1.56	1.06	25.47	62.6
0.3	0.04	3.21	1.14	24.92	140.9
0.4	0.07	4.14	1.19	24.58	177.7
0.5	0.13	5.18	1.25	24.26	226.0
0.6	0.21	6.20	1.31	23.91	276.3
0.7	0.27	6.88	1.36	23.69	311.7
0.8	0.38	8.06	1.45	23.28	364.9
1.0	0.62	9.97	1.62	22.67	458.6
1.3	0.97	11.70	1.82	22.08	588.6
1.5	1.24	12.61	1.94	21.78	692.8
1.7	1.44	13.14	2.02	21.60	777.0
2.0	1.74	13.81	2.13	21.39	907.5
2.3	2.03	14.38	2.24	21.18	1050.3
2.5	2.19	14.66	2.30	21.09	1136.9
2.7	2.36	14.95	2.36	20.99	1232.6
3.0	2.58	15.22	2.42	20.89	1362.6
3.3	2.82	15.53	2.49	20.80	1514.1
3.5	2.94	15.68	2.53	20.74	1595.5
3.7	3.07	15.88	2.58	20.66	1690.6
4.0	3.26	16.06	2.61	20.65	1825.8
4.5	3.54	16.34	2.69	20.54	2049.6
5.0	3.80	16.61	2.77	20.45	2281.5
5.5	4.05	16.80	2.83	20.39	2508.5
6.0	4.28	17.01	2.90	20.30	2751.4
6.5	4.48	17.16	2.95	20.25	2973.1
7.0	4.66	17.28	2.98	20.23	3195.1
7.5	4.84	17.41	3.03	20.18	3423.8
8.0	5.01	17.50	3.06	20.16	3658.7
8.5	5.17	17.59	3.09	20.13	3892.2
9.0	5.31	17.67	3.13	20.09	4119.6
9.5	5.44	17.72	3.14	20.07	4345.9
10.0	5.56	17.75	3.16	20.06	4572.3
10.3	5.62	17.78	3.17	20.05	FAILURE
10.5	5.67	17.74	3.15	20.07	4797.2
11.0	5.77	17.71	3.14	20.08	5031.0
11.5	5.88	17.66	3.12	20.09	5264.3
12.0	5.96	17.56	3.09	20.12	5480.4
12.5	6.05	17.45	3.04	20.17	5710.3
13.0	6.13	17.33	3.01	20.19	5942.4

APPENDIX F TABLE 9 - SUCCESSFUL DRAINED UNIFORM STRAIN TRIAXIAL EXTENSION TESTS

Test ECD70 DRAINED TRIAXIAL EXTENSION
σ_1' = 17.50 MPa e_i = 0.525 H/D = 1.90
Cambria sand ϕ' = 31.4 1.02 CM/HR
Successful uniform strain test with steel plates.

ϵ_3 %	ϵ_v %	$\sigma_1 - \sigma_3$ MPa	σ_1'/σ_3'	p' MPa	Time second
0.0	0.00	0.04	1.00	17.48	-0.0
0.1	-0.00	0.56	1.03	17.28	15.5
0.1	0.01	0.83	1.05	17.31	45.1
0.1	0.01	1.00	1.06	17.19	64.0
0.3	0.04	2.44	1.16	16.67	140.4
0.4	0.10	3.49	1.25	16.31	195.7
0.5	0.15	4.03	1.30	16.14	228.9
0.6	0.23	4.77	1.38	15.90	271.4
0.7	0.33	5.83	1.50	15.54	320.5
0.8	0.45	6.60	1.61	15.29	367.4
1.0	0.73	7.81	1.81	14.87	472.9
1.3	1.07	8.71	1.99	14.57	604.7
1.5	1.27	9.14	2.10	14.44	691.2
1.7	1.48	9.50	2.19	14.32	787.1
2.0	1.75	9.91	2.31	14.16	925.9
2.3	2.00	10.21	2.40	14.10	1071.4
2.5	2.14	10.36	2.45	14.04	1158.9
2.7	2.28	10.52	2.51	13.99	1255.3
3.0	2.47	10.67	2.56	13.94	1390.7
3.3	2.66	10.86	2.64	13.88	1534.2
3.5	2.77	10.95	2.67	13.85	1618.5
3.7	2.88	11.04	2.71	13.82	1712.2
4.0	3.04	11.15	2.76	13.78	1851.2
4.5	3.30	11.33	2.84	13.72	2097.3
5.0	3.52	11.47	2.91	13.66	2328.5
5.5	3.73	11.61	2.97	13.62	2559.1
6.0	3.92	11.70	3.02	13.60	2782.5
6.5	4.10	11.78	3.06	13.57	3014.1
7.0	4.27	11.86	3.11	13.54	3247.5
7.5	4.43	11.91	3.14	13.52	3481.9
8.0	4.57	11.95	3.16	13.50	3708.9
8.4	4.67	11.96	3.17	13.49	FAILURE
8.5	4.71	11.94	3.15	13.51	3953.4
9.0	4.85	11.87	3.11	13.54	4187.1
9.5	4.95	11.74	3.04	13.57	4411.3
10.0	5.04	11.55	2.94	13.64	4640.1
10.5	5.13	11.32	2.82	13.75	4869.2
11.0	5.21	11.03	2.70	13.83	5100.2
11.5	5.28	10.81	2.62	13.89	5338.2
12.0	5.35	10.57	2.52	13.98	5579.6
12.5	5.42	10.35	2.45	14.06	5809.0
13.0	5.49	10.05	2.35	14.15	6034.6
13.5	5.56	9.67	2.23	14.29	6267.7

APPENDIX F TABLE 9(cont) - SUCCESSFUL DRAINED UNIFORM STRAIN TRIAXIAL EXTENSION TESTS

ϵ_3 %	ϵ_v %	$\sigma_1 - \sigma_3$ MPa	σ_1'/σ_3'	p' MPa	Time second
14.0	5.62	9.38	2.16	14.38	6497.2
14.5	5.68	9.08	2.08	14.48	6738.0
15.0	5.74	8.83	2.02	14.56	6963.5
15.5	5.79	8.59	1.96	14.64	7195.4
16.0	5.86	8.31	1.90	14.73	7422.4
16.5	5.92	7.95	1.83	14.86	7662.1
17.0	5.98	7.57	1.76	14.98	7901.5
17.5	6.03	7.25	1.71	15.09	8124.9
18.0	6.11	6.80	1.63	15.24	8357.0

APPENDIX F TABLE 10 - SUCCESSFUL DRAINED UNIFORM STRAIN TRIAXIAL EXTENSION TESTS

Test ECD72 DRAINED TRIAXIAL EXTENSION
σ_1' = 24.0 MPa e_i = 0.528 H/D = 1.90
Cambria sand ϕ' = 31.9 1.02 CM/HR
Successful uniform strain test with steel plates.

ϵ_3 %	ϵ_v %	$\sigma_1 - \sigma_3$ MPa	σ_1'/σ_3'	p' MPa	Time second
0.0	0.00	0.03	1.00	24.05	-0.0
0.0	0.00	0.07	1.00	24.03	3.2
0.1	0.02	1.61	1.07	23.50	60.0
0.2	0.04	2.32	1.11	23.28	86.0
0.3	0.08	3.78	1.19	22.80	137.0
0.4	0.16	5.20	1.28	22.32	188.2
0.5	0.26	6.75	1.39	21.79	239.7
0.6	0.36	7.73	1.47	21.46	275.9
0.7	0.52	8.84	1.58	21.10	327.1
0.8	0.66	9.65	1.67	20.83	371.1
1.0	0.99	11.00	1.84	20.38	475.7
1.3	1.37	12.13	2.02	20.01	605.8
1.5	1.62	12.71	2.12	19.81	702.8
1.7	1.83	13.11	2.20	19.70	788.1
2.0	2.15	13.67	2.32	19.49	929.4
2.3	2.42	14.05	2.41	19.35	1067.6
2.5	2.61	14.27	2.46	19.29	1163.3
2.7	2.78	14.51	2.52	19.20	1264.8
3.0	3.01	14.76	2.59	19.11	1398.7
3.3	3.23	14.98	2.65	19.06	1541.6
3.5	3.37	15.12	2.69	19.02	1641.6
3.7	3.48	15.23	2.73	18.98	1724.9
4.0	3.68	15.42	2.79	18.91	1873.0
4.5	3.95	15.62	2.85	18.84	2096.3
5.0	4.22	15.83	2.93	18.77	2332.0
5.5	4.48	16.02	2.99	18.71	2573.9
6.0	4.70	16.15	3.05	18.66	2803.4
6.5	4.91	16.29	3.10	18.63	3031.6
7.0	5.10	16.37	3.13	18.60	3261.8
7.5	5.29	16.49	3.18	18.56	3508.1
8.0	5.45	16.53	3.20	18.54	3730.6
8.5	5.61	16.58	3.22	18.52	3964.0
8.6	5.65	16.61	3.24	18.49	FAILURE
9.0	5.75	16.59	3.23	18.50	4201.4
9.5	5.89	16.54	3.20	18.54	4434.4
10.0	6.01	16.47	3.18	18.55	4663.6
10.5	6.14	16.31	3.11	18.60	4901.5

APPENDIX F TABLE 11 - SUCCESSFUL DRAINED UNIFORM STRAIN TRIAXIAL EXTENSION TESTS

Test ECD74 DRAINED TRIAXIAL EXTENSION
σ_1' = 25.01 MPa e_i = 0.531 H/D =
Cambria sand ϕ' = 31.3 1.27 CM/HR
Successful uniform strain test with steel plates.

ϵ_3 %	ϵ_v %	$\sigma_1 - \sigma_3$ MPa	σ_1'/σ_3'	p' MPa	Time second
0.0	0.00	0.05	1.00	24.98	0.0
0.1	0.00	0.58	1.02	24.78	13.8
0.1	0.00	0.98	1.04	24.74	39.6
0.2	0.00	2.02	1.09	24.34	67.6
0.3	0.02	3.33	1.15	23.89	105.1
0.4	0.06	4.83	1.24	23.38	150.4
0.5	0.13	6.01	1.32	22.99	184.9
0.6	0.24	7.64	1.44	22.45	228.6
0.7	0.35	8.68	1.53	22.09	262.7
0.8	0.50	9.66	1.63	21.77	305.0
1.0	0.79	10.95	1.78	21.34	380.6
1.3	1.19	12.19	1.95	20.92	493.1
1.5	1.48	12.86	2.06	20.70	581.2
1.7	1.70	13.32	2.14	20.55	656.4
2.0	2.01	13.88	2.25	20.36	767.9
2.3	2.31	14.33	2.35	20.20	888.1
2.5	2.49	14.55	2.40	20.13	963.8
2.7	2.66	14.78	2.45	20.04	1042.1
3.0	2.89	15.04	2.51	19.96	1154.1
3.3	3.11	15.27	2.57	19.90	1272.7
3.5	3.25	15.43	2.61	19.85	1350.5
3.7	3.38	15.57	2.65	19.81	1430.2
4.0	3.57	15.76	2.71	19.73	1533.8
4.5	3.88	16.05	2.80	19.64	1734.6
5.0	4.13	16.28	2.86	19.59	1919.5
5.5	4.38	16.48	2.93	19.51	2115.8
6.0	4.60	16.63	2.99	19.45	2311.9
6.5	4.80	16.76	3.04	19.41	2496.0
7.0	4.99	16.88	3.08	19.36	2691.2
7.5	5.16	16.98	3.11	19.35	2880.4
8.0	5.32	17.02	3.14	19.31	3079.1
8.5	5.46	17.06	3.15	19.30	3274.6
8.7	5.52	17.07	3.16	19.29	FAILURE
9.0	5.59	17.05	3.15	19.31	3460.9
9.5	5.71	17.02	3.14	19.31	3658.0
10.0	5.81	16.96	3.11	19.33	3846.9
10.5	5.91	16.88	3.09	19.33	4043.8
11.0	5.99	16.73	3.03	19.39	4240.8
11.5	6.07	16.61	2.98	19.45	4432.7
12.0	6.13	16.48	2.93	19.52	4617.1
12.5	6.20	16.28	2.87	19.58	4815.4
13.0	6.26	16.07	2.80	19.66	4996.7
13.5	6.32	15.84	2.73	19.72	5189.5

APPENDIX F TABLE 11(cont) - SUCCESSFUL DRAINED UNIFORM STRAIN TRIAXIAL EXTENSION TESTS

ϵ_3 %	ϵ_v %	$\sigma_1 - \sigma_3$ MPa	σ_1'/σ_3'	p' MPa	Time second
14.0	6.38	15.61	2.66	19.80	5388.4
14.5	6.44	15.36	2.59	19.89	5585.7
15.0	6.50	15.12	2.53	19.96	5773.2
15.5	6.55	14.84	2.46	20.07	5974.2
16.0	6.61	14.60	2.40	20.13	6151.3
16.5	6.68	14.30	2.34	20.23	6355.4
17.0	6.74	14.05	2.28	20.32	6541.6

APPENDIX F TABLE 12 - SUCCESSFUL DRAINED UNIFORM STRAIN TRIAXIAL EXTENSION TESTS

Test ECD75 DRAINED TRIAXIAL EXTENSION
σ_1' = 26.0 MPa e_i = 0.522 H/D = 2.00
Cambria sand ϕ' = 32.3 1.27 CM/HR
Successful uniform strain test with steel plates.

ϵ_3 %	ϵ_v %	$\sigma_1 - \sigma_3$ MPa	σ_1'/σ_3'	p' MPa	Time second
0.0	0.00	0.04	1.00	25.97	-0.0
0.0	-0.00	0.60	1.02	25.80	15.0
0.1	-0.00	1.60	1.07	25.47	38.8
0.2	-0.00	2.77	1.12	25.07	65.6
0.3	0.04	4.88	1.23	24.36	114.0
0.4	0.10	6.36	1.32	23.86	148.3
0.5	0.21	8.02	1.45	23.31	190.3
0.6	0.40	9.60	1.58	22.81	243.5
0.7	0.49	10.23	1.65	22.57	270.8
0.8	0.62	10.91	1.72	22.35	305.1
1.0	0.96	12.23	1.89	21.91	397.4
1.3	1.30	13.19	2.03	21.59	501.0
1.5	1.55	13.77	2.13	21.39	580.8
1.7	1.76	14.19	2.20	21.25	657.7
2.0	2.06	14.77	2.32	21.05	772.3
2.3	2.34	15.23	2.42	20.89	893.3
2.5	2.52	15.49	2.47	20.84	976.6
2.7	2.68	15.69	2.52	20.76	1054.2
3.0	2.90	15.97	2.60	20.66	1170.0
3.3	3.10	16.20	2.65	20.59	1282.3
3.5	3.25	16.36	2.70	20.53	1374.5
3.7	3.38	16.49	2.73	20.49	1452.2
4.0	3.54	16.61	2.77	20.45	1556.8
4.5	3.82	16.91	2.86	20.35	1758.8
5.0	4.08	17.15	2.94	20.27	1962.2
5.5	4.30	17.31	3.00	20.21	2149.0
6.0	4.52	17.44	3.04	20.17	2346.1
6.5	4.71	17.57	3.08	20.15	2538.5
7.0	4.89	17.67	3.13	20.09	2732.6
7.5	5.06	17.76	3.16	20.06	2935.8
8.0	5.21	17.83	3.19	20.03	3128.1
8.5	5.34	17.91	3.22	20.00	3326.6
9.0	5.46	18.00	3.26	19.97	3517.3
9.4	5.55	18.07	3.29	19.93	FAILURE
9.5	5.57	18.07	3.29	19.94	3710.7
10.0	5.68	17.99	3.26	19.97	3916.2
10.5	5.77	17.82	3.17	20.08	4101.1
11.0	5.87	17.46	3.05	20.17	4307.5
11.5	5.95	17.07	2.91	20.30	4493.4
12.0	6.06	16.60	2.77	20.46	4692.6
12.5	6.14	16.18	2.65	20.60	4882.7
13.5	6.28	15.49	2.48	20.81	5278.3
14.5	6.41	14.78	2.32	21.07	5664.6

APPENDIX F TABLE 13 - SUCCESSFUL DRAINED UNIFORM STRAIN TRIAXIAL EXTENSION TESTS

Test ECD79 DRAINED TRIAXIAL EXTENSION
σ_1' = 0.50 MPa e_i = 0.531 H/D = 1.92
Cambria sand ϕ' = 40.8 2.54 CM/HR
Successful uniform strain test with steel plates.

ϵ_3 %	ϵ_v %	$\sigma_1 - \sigma_3$ MPa	σ_1'/σ_3'	p' MPa	
0.000	0.000	0.000	1.000	0.500	
0.092	-0.024	0.195	1.638	0.435	
0.184	-0.038	0.275	2.219	0.408	
0.276	-0.049	0.303	2.535	0.399	
0.368	-0.060	0.316	2.724	0.395	
0.460	-0.068	0.327	2.883	0.391	
0.552	-0.079	0.334	3.005	0.389	
0.645	-0.095	0.339	3.111	0.387	
0.737	-0.113	0.344	3.203	0.385	
0.921	-0.143	0.351	3.359	0.383	
1.105	-0.185	0.357	3.491	0.381	
1.289	-0.223	0.361	3.599	0.380	
1.473	-0.269	0.365	3.698	0.378	
1.750	-0.338	0.370	3.845	0.377	
2.210	-0.459	0.376	4.019	0.375	
2.762	-0.618	0.381	4.199	0.373	
3.315	-0.781	0.385	4.357	0.372	
3.867	-0.953	0.388	4.447	0.371	
4.420	-1.132	0.390	4.566	0.370	
4.972	-1.313	0.392	4.622	0.369	
5.525	-1.481	0.391	4.604	0.370	
6.077	-1.659	0.394	4.699	0.369	
6.446	-1.781	0.394	4.728	0.369	
6.998	-1.955	0.393	4.691	0.369	
7.551	-2.138	0.394	4.732	0.369	FAILURE
8.103	-2.321	0.393	4.693	0.369	
8.840	-2.555	0.392	4.611	0.369	
9.576	-2.761	0.384	4.302	0.372	
10.313	-2.952	0.379	4.145	0.374	
11.050	-3.138	0.374	3.977	0.375	
12.155	-3.387	0.368	3.787	0.377	
13.260	-3.608	0.358	3.518	0.381	
14.365	-3.765	0.347	3.260	0.384	
15.470	-3.873	0.332	2.969	0.389	
16.575	-3.963	0.261	2.095	0.413	

APPENDIX F TABLE 14 - SUCCESSFUL DRAINED UNIFORM STRAIN TRIAXIAL EXTENSION TESTS

Test ECD81 DRAINED TRIAXIAL EXTENSION
σ_1' = 0.25 MPa e_i = 0.528 H/D = 1.94
Cambria sand ϕ' = 44.0 2.54 CM/HR
Successful uniform strain test with steel plates.

ϵ_3 %	ϵ_v %	$\sigma_1 - \sigma_3$ MPa	σ_1'/σ_3'	p' MPa	
0.000	0.000	0.000	1.000	0.250	
0.036	-0.015	0.104	1.715	0.215	
0.091	-0.018	0.141	2.293	0.203	
0.182	-0.024	0.158	2.728	0.197	
0.274	-0.040	0.167	3.006	0.194	
0.365	-0.051	0.172	3.214	0.193	
0.456	-0.068	0.176	3.386	0.191	
0.638	-0.110	0.182	3.658	0.189	
0.821	-0.154	0.185	3.849	0.188	
1.094	-0.227	0.189	4.068	0.187	
1.368	-0.301	0.191	4.227	0.186	
1.641	-0.385	0.193	4.393	0.186	
2.006	-0.477	0.195	4.573	0.185	
2.553	-0.660	0.198	4.784	0.184	
3.100	-0.847	0.200	4.958	0.183	
3.648	-1.036	0.201	5.053	0.183	
4.195	-1.236	0.202	5.209	0.183	
4.742	-1.432	0.203	5.307	0.182	
5.289	-1.632	0.203	5.298	0.182	
5.836	-1.839	0.204	5.411	0.182	
6.383	-2.039	0.204	5.491	0.182	FAILURE
6.931	-2.233	0.204	5.417	0.182	
7.478	-2.444	0.204	5.426	0.182	
8.025	-2.629	0.199	4.895	0.184	
8.572	-2.814	0.196	4.633	0.185	
9.119	-2.992	0.192	4.309	0.186	
10.031	-3.357	0.182	3.679	0.189	
11.308	-3.687	0.175	3.333	0.192	
12.402	-3.940	0.165	2.928	0.195	
13.496	-4.057	0.152	2.562	0.199	

APPENDIX F TABLE 15 - SUCCESSFUL DRAINED UNIFORM STRAIN TRIAXIAL EXTENSION TESTS

Test ECD83 DRAINED TRIAXIAL EXTENSION
σ_1' = 1.00 MPa e_i = 0.533 H/D = 2.05
Cambria sand ϕ' = 39.6 2.54 CM/HR
Successful uniform strain test with steel plates.

ϵ_3 %	ϵ_v %	$\sigma_1 - \sigma_3$ MPa	σ_1'/σ_3'	p' MPa	
0.000	0.000	0.000	1.000	1.000	
0.018	0.013	0.142	1.166	0.953	
0.036	0.008	0.213	1.271	0.929	
0.055	0.003	0.292	1.412	0.903	
0.091	-0.003	0.414	1.706	0.862	
0.182	-0.003	0.565	2.301	0.812	
0.273	-0.005	0.613	2.585	0.796	
0.364	-0.010	0.637	2.751	0.788	
0.454	-0.018	0.652	2.877	0.783	
0.545	-0.029	0.653	2.880	0.782	
0.636	-0.039	0.665	2.988	0.778	
0.818	-0.070	0.676	3.085	0.775	
1.000	-0.101	0.691	3.233	0.770	
1.181	-0.135	0.701	3.350	0.766	
1.454	-0.195	0.710	3.452	0.763	
1.818	-0.278	0.721	3.584	0.760	
2.181	-0.374	0.731	3.724	0.756	
2.726	-0.525	0.741	3.854	0.753	
3.272	-0.754	0.750	3.992	0.750	
3.817	-0.908	0.757	4.114	0.748	
4.362	-1.084	0.762	4.200	0.746	
4.726	-1.188	0.766	4.273	0.745	
5.271	-1.368	0.769	4.331	0.744	
5.816	-1.545	0.771	4.376	0.743	
6.361	-1.714	0.774	4.423	0.742	
6.725	-1.823	0.774	4.429	0.742	
7.270	-2.000	0.776	4.467	0.741	
7.815	-2.169	0.777	4.475	0.741	FAILURE
8.361	-2.338	0.775	4.441	0.742	
8.906	-2.499	0.774	4.427	0.742	
9.451	-2.663	0.771	4.359	0.743	
10.542	-2.975	0.768	4.308	0.744	
11.269	-3.149	0.756	4.096	0.748	
11.996	-3.313	0.743	3.894	0.752	

APPENDIX F TABLE 16 - SUCCESSFUL DRAINED UNIFORM STRAIN TRIAXIAL EXTENSION TESTS

Test ECD84 DRAINED TRIAXIAL EXTENSION
σ_1' = 26.00 MPa e_i = 0.521 H/D = 2.03
Cambria sand ϕ' = 32.0 1.27 CM/HR
Successful uniform strain test with steel plates.

ϵ_3 %	ϵ_v %	$\sigma_1 - \sigma_3$ MPa	σ_1'/σ_3'	p' MPa	Time second
0.0	0.00	0.08	1.00	26.00	-0.0
0.1	0.00	0.56	1.02	25.83	15.2
0.1	0.00	1.16	1.05	25.62	39.9
0.2	0.00	2.10	1.09	25.32	65.2
0.3	0.02	3.85	1.17	24.73	115.5
0.4	0.06	4.96	1.24	24.35	148.1
0.5	0.13	6.42	1.33	23.88	188.9
0.6	0.27	8.34	1.47	23.23	242.6
0.7	0.35	9.08	1.54	22.99	266.5
0.8	0.54	10.32	1.66	22.57	317.8
1.0	0.81	11.59	1.80	22.14	391.4
1.3	1.21	12.88	1.98	21.71	505.2
1.5	1.45	13.49	2.08	21.51	582.3
1.7	1.67	14.00	2.17	21.34	657.4
2.0	1.99	14.62	2.28	21.13	777.0
2.3	2.29	15.14	2.40	20.95	902.5
2.5	2.47	15.41	2.45	20.88	981.3
2.7	2.63	15.60	2.50	20.83	1056.9
3.0	2.84	15.92	2.58	20.71	1169.6
3.3	3.04	16.17	2.64	20.62	1280.9
3.5	3.19	16.35	2.69	20.56	1371.6
3.7	3.32	16.51	2.74	20.51	1449.3
4.0	3.49	16.66	2.78	20.46	1554.2
4.5	3.78	16.95	2.87	20.37	1759.5
5.0	4.03	17.13	2.93	20.30	1947.8
5.5	4.27	17.30	2.98	20.26	2146.4
6.0	4.49	17.44	3.03	20.20	2347.9
6.5	4.67	17.57	3.08	20.15	2536.2
7.0	4.86	17.67	3.12	20.11	2730.8
7.5	5.03	17.78	3.16	20.08	2936.2
8.0	5.17	17.85	3.19	20.06	3118.3
8.5	5.31	17.92	3.22	20.03	3314.5
9.0	5.45	17.97	3.23	20.03	3518.2
9.2	5.49	17.98	3.25	19.99	FAILURE
9.5	5.55	17.93	3.22	20.02	3704.1
10.0	5.66	17.89	3.20	20.04	3902.7
10.5	5.75	17.82	3.17	20.09	4103.0
11.0	5.83	17.72	3.13	20.12	4298.0

APPENDIX F TABLE 17 - SUCCESSFUL DRAINED UNIFORM STRAIN TRIAXIAL EXTENSION TESTS

Test ECD85 DRAINED TRIAXIAL EXTENSION
σ_i' = 4.00 MPa e_i = 0.524 H/D = 2.03
Cambria sand ϕ' = 36.3 1.27 CM/HR
Successful uniform strain test with steel plates.

ϵ_3 %	ϵ_v %	$\sigma_1 - \sigma_3$ MPa	σ_1'/σ_3'	p' MPa	Time second
0.0	0.00	0.11	1.03	3.98	0.0
0.0	0.00	0.14	1.04	3.98	2.7
0.1	-0.01	0.57	1.16	3.84	33.2
0.2	-0.00	0.92	1.30	3.69	62.5
0.3	0.04	1.42	1.55	3.53	117.4
0.4	0.08	1.79	1.80	3.41	168.8
0.5	0.11	1.91	1.91	3.37	195.2
0.6	0.15	2.07	2.08	3.31	245.2
0.7	0.17	2.15	2.16	3.28	277.0
0.8	0.20	2.24	2.27	3.25	319.9
1.0	0.25	2.35	2.43	3.21	399.3
1.3	0.30	2.49	2.65	3.17	531.4
1.5	0.33	2.56	2.76	3.16	609.3
1.7	0.34	2.60	2.85	3.13	686.6
2.0	0.36	2.65	2.97	3.12	796.3
2.3	0.36	2.71	3.09	3.10	925.3
2.5	0.37	2.74	3.14	3.10	1002.2
2.7	0.37	2.77	3.20	3.10	1077.4
3.0	0.36	2.80	3.27	3.10	1200.1
3.3	0.34	2.82	3.33	3.09	1333.6
3.5	0.33	2.84	3.37	3.09	1409.4
3.8	0.31	2.86	3.44	3.08	1514.1
4.0	0.29	2.87	3.47	3.08	1602.8
4.5	0.24	2.91	3.55	3.08	1809.1
5.0	0.19	2.93	3.64	3.07	2005.9
5.5	0.12	2.95	3.72	3.06	2211.8
6.0	0.05	2.98	3.79	3.05	2415.0
6.5	-0.02	2.99	3.83	3.05	2621.9
7.0	-0.09	3.00	3.89	3.04	2816.1
7.3	-0.14	3.01	3.91	3.04	FAILURE
7.5	-0.16	3.00	3.89	3.03	3012.2
8.0	-0.23	2.99	3.85	3.05	3212.2

APPENDIX F TABLE 18 - SUCCESSFUL DRAINED UNIFORM STRAIN TRIAXIAL EXTENSION TESTS

Test ECD86 DRAINED TRIAXIAL EXTENSION
σ_1' = 22.00 MPa e_i = 0.513 H/D = 2.02
Cambria sand ϕ' = 32.5 1.27 CM/HR
Successful uniform strain test with steel plates.

ϵ_3 %	ϵ_v %	$\sigma_1 - \sigma_3$ MPa	σ_1'/σ_3'	p' MPa	Time second
0.0	0.00	0.06	1.00	21.99	-0.0
0.1	0.00	0.52	1.02	21.82	15.7
0.1	0.00	1.28	1.06	21.57	43.0
0.2	0.00	2.07	1.10	21.30	66.4
0.3	0.03	3.68	1.20	20.78	119.6
0.4	0.06	4.66	1.27	20.47	153.3
0.5	0.14	6.04	1.38	19.99	196.2
0.6	0.22	7.11	1.48	19.64	228.5
0.7	0.37	8.30	1.61	19.24	274.3
0.8	0.48	8.97	1.69	19.01	308.0
1.0	0.75	10.13	1.85	18.63	386.2
1.3	1.13	11.23	2.04	18.26	503.9
1.5	1.34	11.71	2.14	18.10	577.6
1.7	1.56	12.13	2.23	17.95	660.8
2.0	1.85	12.64	2.35	17.78	782.9
2.3	2.12	13.04	2.46	17.65	906.4
2.5	2.27	13.25	2.52	17.57	983.0
2.7	2.41	13.46	2.58	17.50	1058.2
3.0	2.61	13.68	2.65	17.43	1167.9
3.3	2.79	13.90	2.71	17.38	1283.9
3.5	2.92	14.03	2.76	17.33	1365.3
3.7	3.03	14.12	2.79	17.31	1438.6
4.0	3.21	14.27	2.84	17.25	1563.0
4.5	3.46	14.47	2.92	17.18	1755.0
5.0	3.71	14.63	2.98	17.13	1956.4
5.5	3.92	14.77	3.04	17.09	2142.8
6.0	4.12	14.88	3.09	17.05	2343.3
6.5	4.30	14.98	3.13	17.02	2536.6
7.0	4.47	15.10	3.19	16.97	2732.2
7.5	4.63	15.21	3.24	16.93	2929.2
8.0	4.78	15.26	3.26	16.92	3120.4
8.5	4.91	15.32	3.29	16.90	3317.9
9.0	5.04	15.33	3.30	16.90	3509.8
9.2	5.09	15.37	3.32	16.87	FAILURE
9.5	5.16	15.34	3.30	16.90	3715.5
10.0	5.26	15.32	3.30	16.88	3902.7
10.5	5.36	15.32	3.30	16.88	4094.7
11.0	5.46	15.30	3.28	16.90	4302.5
11.5	5.54	15.23	3.25	16.91	4494.6
12.0	5.61	15.12	3.20	16.95	4693.5
12.5	5.68	14.98	3.14	17.00	4878.7
13.0	5.75	14.85	3.08	17.04	5075.4

APPENDIX F TABLE 19 - SUCCESSFUL DRAINED UNIFORM STRAIN TRIAXIAL EXTENSION TESTS

Test ECD87 DRAINED TRIAXIAL EXTENSION
σ_1' = 17.50 MPa e_i = 0.521 H/D = 2.03
Cambria sand ϕ' = 31.7 1.27 CM/HR
Successful uniform strain test with steel plates.

ϵ_3 %	ϵ_v %	$\sigma_1 - \sigma_3$ MPa	σ_1'/σ_3'	p' MPa	Time second
0.0	0.00	0.07	1.00	17.49	-0.0
0.0	0.00	0.10	1.01	17.48	2.5
0.1	0.00	0.84	1.05	17.27	32.9
0.2	0.01	1.63	1.10	16.95	60.6
0.3	0.04	2.89	1.20	16.54	113.7
0.4	0.11	3.89	1.29	16.22	163.9
0.5	0.16	4.33	1.33	16.07	189.3
0.6	0.26	5.21	1.42	15.76	239.6
0.7	0.34	5.94	1.51	15.52	272.2
0.8	0.45	6.75	1.63	15.26	312.6
1.0	0.69	7.86	1.82	14.88	393.5
1.3	1.01	8.77	2.00	14.59	508.0
1.5	1.19	9.22	2.11	14.43	583.3
1.7	1.37	9.56	2.20	14.31	658.9
2.0	1.64	10.01	2.34	14.16	784.7
2.3	1.86	10.34	2.45	14.04	905.1
2.5	2.00	10.52	2.51	13.97	981.2
2.7	2.13	10.65	2.56	13.95	1060.5
3.0	2.32	10.88	2.65	13.86	1182.5
3.3	2.48	11.05	2.71	13.84	1289.3
3.5	2.59	11.15	2.75	13.80	1365.1
3.7	2.70	11.26	2.80	13.77	1455.2
4.0	2.84	11.37	2.85	13.73	1567.2
4.5	3.06	11.56	2.94	13.66	1761.9
5.0	3.27	11.72	3.02	13.61	1961.4
5.5	3.46	11.84	3.09	13.57	2159.1
6.0	3.64	11.91	3.13	13.53	2358.8
6.5	3.79	11.99	3.17	13.52	2545.2
7.0	3.94	12.00	3.18	13.50	2745.9
7.5	4.08	12.02	3.19	13.49	2940.6
7.6	4.11	12.04	3.21	13.48	FAILURE
8.0	4.21	12.03	3.20	13.49	3146.6
8.5	4.32	12.01	3.19	13.49	3336.2

APPENDIX F TABLE 20 - SUCCESSFUL DRAINED UNIFORM STRAIN TRIAXIAL EXTENSION TESTS

Test ECD88 DRAINED TRIAXIAL EXTENSION
σ_1' = 8.00 MPa e_i = 0.522 H/D = 1.95
Cambria sand ϕ' = 32.0 1.27 CM/HR
Successful uniform strain test with steel plates.

ϵ_3 %	ϵ_v %	$\sigma_1 - \sigma_3$ MPa	σ_1'/σ_3'	p' MPa	Time second
0.0	0.00	0.07	1.01	8.00	0.0
0.0	-0.00	0.47	1.06	7.87	15.1
0.1	-0.00	0.96	1.14	7.71	39.2
0.2	-0.00	1.45	1.22	7.53	65.0
0.3	0.05	2.13	1.36	7.31	116.3
0.4	0.08	2.44	1.44	7.20	149.9
0.5	0.14	2.88	1.56	7.06	192.7
0.6	0.18	3.24	1.68	6.93	227.8
0.7	0.24	3.60	1.81	6.82	269.7
0.8	0.28	3.82	1.91	6.73	303.5
1.0	0.39	4.18	2.09	6.62	378.4
1.3	0.52	4.52	2.29	6.51	495.4
1.5	0.59	4.69	2.41	6.45	571.2
1.7	0.66	4.80	2.50	6.40	647.2
2.0	0.76	4.96	2.63	6.35	775.1
2.3	0.83	5.07	2.73	6.31	877.8
2.5	0.88	5.12	2.79	6.28	957.0
2.7	0.93	5.19	2.84	6.28	1032.1
3.0	0.98	5.28	2.93	6.25	1156.2
3.3	1.02	5.35	3.02	6.21	1266.8
3.5	1.05	5.38	3.04	6.22	1337.6
3.7	1.07	5.41	3.08	6.20	1419.0
4.0	1.10	5.47	3.16	6.18	1542.3
4.5	1.15	5.52	3.23	6.16	1724.7
5.0	1.18	5.58	3.28	6.16	1928.4
5.5	1.21	5.61	3.34	6.14	2104.1
6.0	1.22	5.66	3.40	6.12	2297.2
6.5	1.23	5.68	3.43	6.12	2503.6
7.0	1.24	5.71	3.47	6.11	2687.7
7.5	1.24	5.72	3.49	6.11	2885.5
8.0	1.24	5.73	3.49	6.11	3071.4
8.4	1.23	5.74	3.52	6.11	FAILURE
8.5	1.23	5.73	3.49	6.11	3267.3
9.0	1.22	5.71	3.47	6.12	3453.2
9.5	1.21	5.69	3.43	6.14	3651.6
10.0	1.20	5.66	3.39	6.14	3836.3

APPENDIX F TABLE 21 - SUCCESSFUL DRAINED UNIFORM STRAIN TRIAXIAL EXTENSION TESTS

Test ECD92 DRAINED TRIAXIAL EXTENSION
σ_1' = 17.50 MPa e_i = 0.520 H/D = 2.05
Cambria sand ϕ' = 31.9 1.27 CM/HR
Successful uniform strain test with steel plates.

ϵ_3 %	ϵ_v %	$\sigma_1 - \sigma_3$ MPa	σ_1'/σ_3'	p' MPa	Time second
0.0	0.00	0.02	1.00	17.49	0.0
0.0	0.00	0.07	1.00	17.48	2.8
0.1	0.00	0.83	1.05	17.21	35.3
0.2	0.00	1.41	1.09	17.02	61.8
0.3	0.03	2.83	1.19	16.56	117.4
0.4	0.07	3.75	1.27	16.25	153.5
0.5	0.16	5.03	1.40	15.82	197.9
0.6	0.25	5.92	1.51	15.52	233.2
0.7	0.39	6.80	1.64	15.23	280.2
0.8	0.50	7.35	1.73	15.04	317.1
1.0	0.71	8.12	1.87	14.78	389.6
1.3	1.03	8.96	2.05	14.51	507.0
1.5	1.23	9.39	2.16	14.37	587.4
1.7	1.45	9.76	2.26	14.24	683.9
2.0	1.66	10.10	2.37	14.12	789.1
2.3	1.87	10.40	2.46	14.05	906.2
2.5	2.00	10.57	2.53	13.97	989.1
2.7	2.13	10.71	2.58	13.94	1068.7
3.0	2.32	10.90	2.65	13.89	1198.3
3.3	2.46	11.05	2.71	13.81	1305.5
3.5	2.56	11.14	2.75	13.79	1386.4
3.7	2.66	11.22	2.79	13.77	1467.3
4.0	2.80	11.33	2.84	13.72	1583.3
4.5	3.02	11.48	2.91	13.67	1785.7
5.0	3.22	11.62	2.97	13.64	1980.8
5.5	3.41	11.75	3.04	13.59	2184.8
6.0	3.57	11.83	3.08	13.56	2379.6
6.5	3.74	11.90	3.12	13.55	2591.4
7.0	3.87	11.97	3.16	13.52	2781.5
7.5	4.01	12.04	3.20	13.50	2979.2
8.0	4.13	12.08	3.23	13.47	3185.1
8.2	4.18	12.10	3.24	13.46	FAILURE
8.5	4.24	12.08	3.23	13.48	3377.3
9.0	4.34	12.03	3.20	13.49	3571.2
9.5	4.43	11.94	3.15	13.52	3781.3
10.0	4.50	11.83	3.09	13.54	3973.2

APPENDIX F TABLE 22 - SUCCESSFUL DRAINED UNIFORM STRAIN TRIAXIAL EXTENSION TESTS

Test ECD93 DRAINED TRIAXIAL EXTENSION
σ_1' = 35.00 MPa e_i = 0.518 H/D = 2.15
Cambria sand ϕ' = 32.0 1.40 CM/HR
Successful uniform strain test with steel plates.

ϵ_3 %	ϵ_v %	$\sigma_1 - \sigma_3$ MPa	σ_1'/σ_3'	p' MPa	Time second
0.0	0.00	0.09	1.00	34.99	0.0
0.1	0.00	0.62	1.02	34.80	14.9
0.1	0.01	1.73	1.05	34.39	45.9
0.2	0.02	3.00	1.09	34.01	72.5
0.3	0.05	4.66	1.15	33.45	110.5
0.4	0.10	6.51	1.23	32.83	154.0
0.5	0.16	7.55	1.28	32.49	181.2
0.6	0.24	8.92	1.34	32.03	217.1
0.7	0.38	10.81	1.45	31.39	263.8
0.8	0.47	11.85	1.51	31.05	290.6
1.0	0.80	14.41	1.70	30.19	372.2
1.3	1.25	16.64	1.91	29.45	482.3
1.5	1.56	17.74	2.03	29.07	564.8
1.7	1.78	18.38	2.10	28.92	633.2
2.0	2.10	19.33	2.23	28.58	740.8
2.3	2.39	20.02	2.34	28.34	847.7
2.5	2.59	20.39	2.39	28.23	921.9
2.7	2.79	20.78	2.46	28.08	1004.8
3.0	3.05	21.26	2.55	27.93	1118.7
3.3	3.27	21.61	2.61	27.81	1222.7
3.5	3.43	21.89	2.67	27.72	1304.7
3.7	3.55	22.07	2.70	27.65	1369.8
4.0	3.77	22.39	2.78	27.54	1494.0
4.5	4.07	22.80	2.87	27.39	1679.1
5.0	4.33	23.07	2.93	27.31	1864.6
5.5	4.57	23.37	3.01	27.21	2042.1
6.0	4.79	23.60	3.07	27.13	2225.0
6.5	5.00	23.84	3.13	27.08	2411.8
7.0	5.19	24.01	3.18	27.02	2603.6
7.5	5.36	24.11	3.21	26.98	2783.7
8.0	5.51	24.21	3.24	26.95	2969.7
8.1	5.54	24.26	3.26	26.89	FAILURE
8.5	5.66	24.20	3.24	26.94	3163.4
9.0	5.79	24.19	3.24	26.95	3338.8
9.5	5.90	24.14	3.22	26.97	3521.8
10.0	6.01	24.02	3.19	27.01	3715.9
10.5	6.11	23.86	3.14	27.07	3899.8
11.0	6.19	23.72	3.10	27.10	4091.4

APPENDIX F TABLE 23 - SUCCESSFUL DRAINED UNIFORM STRAIN TRIAXIAL EXTENSION TESTS

Test ECD94 DRAINED TRIAXIAL EXTENSION
σ_1' = 42.00 MPa e_i = 0.523 H/D = 2.14
Cambria sand ϕ' = 31.0 1.40 CM/HR
Successful uniform strain test with steel plates.

ϵ_3 %	ϵ_v %	$\sigma_1 - \sigma_3$ MPa	σ_1'/σ_3'	p' MPa	Time second
0.0	0.00	0.11	1.00	41.98	0.0
0.0	0.00	0.88	1.02	41.69	15.2
0.1	0.00	1.88	1.05	41.37	42.6
0.2	0.00	3.17	1.08	40.94	67.9
0.3	0.02	6.30	1.18	39.90	118.0
0.4	0.04	8.21	1.24	39.27	145.0
0.5	0.11	10.66	1.34	38.45	178.5
0.6	0.25	13.03	1.45	37.65	220.1
0.7	0.38	14.56	1.53	37.15	254.2
0.8	0.55	16.12	1.62	36.63	297.3
1.0	0.88	18.33	1.77	35.89	377.2
1.3	1.27	20.26	1.93	35.23	480.5
1.5	1.54	21.28	2.03	34.90	556.4
1.7	1.78	22.16	2.12	34.57	632.0
2.0	2.07	23.04	2.22	34.30	732.9
2.3	2.37	23.89	2.32	34.02	843.9
2.5	2.54	24.34	2.38	33.85	913.4
2.7	2.73	24.77	2.44	33.75	991.7
3.0	2.96	25.25	2.51	33.58	1102.3
3.3	3.19	25.65	2.57	33.45	1224.9
3.5	3.30	25.87	2.60	33.37	1285.1
3.7	3.43	26.12	2.65	33.29	1362.9
4.0	3.63	26.49	2.71	33.18	1482.7
4.5	3.90	27.00	2.80	32.97	1664.1
5.0	4.15	27.34	2.86	32.89	1851.2
5.5	4.37	27.63	2.92	32.79	2031.7
6.0	4.57	27.90	2.98	32.70	2211.0
6.5	4.75	28.13	3.03	32.62	2395.5
7.0	4.92	28.24	3.05	32.58	2585.7
7.5	5.08	28.36	3.08	32.54	2768.8
8.0	5.22	28.43	3.10	32.51	2956.1
8.5	5.33	28.46	3.10	32.51	3134.7
8.6	5.35	28.52	3.12	32.46	FAILURE
9.0	5.45	28.45	3.10	32.50	3320.6
9.5	5.54	28.35	3.08	32.54	3500.5
10.0	5.63	28.16	3.04	32.58	3695.4
10.5	5.72	27.89	2.98	32.72	3873.6
11.0	5.79	27.56	2.91	32.83	4057.1

APPENDIX F TABLE 24 - SUCCESSFUL DRAINED UNIFORM STRAIN TRIAXIAL EXTENSION TESTS

Test ECD95 DRAINED TRIAXIAL EXTENSION
σ_1' = 52.00 MPa e_i = 0.518 H/D = 2.15
Cambria sand ϕ' = 31.7 1.40 CM/HR
Successful uniform strain test with steel plates.

ϵ_3 %	ϵ_v %	$\sigma_1 - \sigma_3$ MPa	σ_1'/σ_3'	p' MPa	Time second
0.0	0.00	0.06	1.00	52.02	0.0
0.0	0.00	0.15	1.00	51.99	3.0
0.1	0.00	1.39	1.03	51.58	32.1
0.2	0.01	2.93	1.06	51.07	59.9
0.3	0.02	5.66	1.12	50.14	113.9
0.4	0.04	7.14	1.16	49.67	140.9
0.5	0.08	9.22	1.22	48.96	174.3
0.6	0.15	11.64	1.29	48.15	217.5
0.7	0.24	13.48	1.35	47.55	254.5
0.8	0.36	15.46	1.42	46.89	295.2
1.0	0.61	19.12	1.58	45.67	371.7
1.3	0.99	22.70	1.77	44.46	471.8
1.5	1.27	24.64	1.90	43.81	546.2
1.7	1.55	26.14	2.01	43.31	626.3
2.0	1.88	27.75	2.14	42.77	732.2
2.3	2.18	28.90	2.25	42.38	837.2
2.5	2.38	29.58	2.32	42.15	914.3
2.7	2.57	30.23	2.39	41.93	991.0
3.0	2.80	30.90	2.46	41.74	1090.9
3.3	3.02	31.58	2.54	41.50	1203.9
3.5	3.15	31.91	2.59	41.39	1272.6
3.7	3.29	32.25	2.63	41.29	1346.6
4.0	3.48	32.78	2.70	41.12	1460.5
4.5	3.74	33.46	2.80	40.88	1636.2
5.0	4.00	33.89	2.87	40.73	1821.4
5.5	4.22	34.33	2.94	40.59	1998.7
6.0	4.42	34.73	3.01	40.46	2181.0
6.5	4.61	35.08	3.07	40.33	2374.3
7.0	4.78	35.24	3.10	40.28	2557.9
7.5	4.92	35.43	3.14	40.21	2738.5
8.0	5.06	35.63	3.17	40.15	2919.7
8.5	5.18	35.71	3.19	40.12	3097.8
9.0	5.28	35.75	3.20	40.11	3276.7
9.1	5.30	35.79	3.21	40.09	FAILURE
9.5	5.38	35.63	3.17	40.14	3464.3
10.0	5.46	35.48	3.14	40.22	3638.0
10.5	5.53	35.26	3.10	40.26	3831.4

APPENDIX G

APPENDIX G TABLE 1 - DRAINED CONVENTIONAL TRIAXIAL EXTENSION TESTS

Test ECD2 DRAINED TRIAXIAL EXTENSION
σ_1' = 4.00 MPa e_i = 0.524 H/D = 1.88
Cambria sand ϕ' = 31.3 1.91 CM/HR
Conventional test with only membranes surrounding specimen.

ϵ_3 %	ϵ_v %	$\sigma_1 - \sigma_3$ MPa	σ_1'/σ_3'	p' MPa	Time second
0.0	0.00	-0.03	0.99	4.44	0.0
0.0	0.00	0.03	1.01	4.47	2.9
0.1	-0.01	0.55	1.16	4.64	31.3
0.2	-0.01	0.84	1.26	4.76	62.1
0.4	-0.01	1.22	1.44	4.87	89.5
0.5	-0.01	1.56	1.64	4.98	115.5
0.6	-0.01	1.78	1.82	5.05	142.8
0.7	-0.01	1.95	1.96	5.11	169.7
0.8	-0.00	2.06	2.08	5.13	195.8
0.9	0.01	2.15	2.18	5.17	220.6
1.0	0.01	2.21	2.26	5.17	245.4
1.3	0.02	2.36	2.47	5.22	319.9
1.5	0.02	2.43	2.58	5.23	373.2
1.7	0.02	2.48	2.66	5.26	423.0
2.0	0.01	2.55	2.78	5.29	503.7
2.3	-0.01	2.61	2.88	5.33	581.0
2.5	-0.02	2.63	2.93	5.35	631.4
2.7	-0.04	2.66	2.99	5.38	679.2
3.0	-0.08	2.70	3.06	5.43	756.3
3.3	-0.11	2.71	3.10	5.46	818.9
3.5	-0.14	2.72	3.13	5.50	871.3
3.7	-0.17	2.74	3.16	5.54	FAILURE
4.0	-0.21	2.72	3.13	5.57	992.3
4.5	-0.27	2.58	2.80	5.58	1115.7
5.0	-0.31	2.36	2.43	5.54	1246.8

APPENDIX G TABLE 2 - DRAINED CONVENTIONAL TRIAXIAL EXTENSION TESTS

Test ECD7 DRAINED TRIAXIAL EXTENSION
σ_1' = 8.00 MPa e_i = 0.515 H/D = 1.87
Cambria sand *0.64 CM/HR*
Conventional test, but cap uplift occurred.

ϵ_3 %	ϵ_v %	$\sigma_1 - \sigma_3$ MPa	σ_1'/σ_3'	p' MPa	Time second
0.0	0.00	0.03	1.00	7.96	0.0
0.1	-0.00	0.29	1.04	7.89	11.3
0.1	-0.00	0.45	1.06	7.86	46.1
0.2	-0.00	0.83	1.12	7.71	116.1
0.3	-0.00	2.18	1.38	7.23	220.0
0.4	0.03	2.79	1.54	7.04	297.3
0.5	0.07	3.19	1.67	6.89	370.3
0.6	0.11	3.49	1.78	6.80	444.8
0.7	0.15	3.71	1.87	6.73	518.1
0.8	0.19	3.90	1.96	6.66	592.3
1.0	0.26	4.10	2.06	6.59	739.2
1.3	0.36	3.70	1.87	6.73	952.7
1.5	0.40	3.39	1.74	6.83	1099.7
1.7	0.44	3.11	1.64	6.92	1253.8
2.0	0.51	2.39	1.43	7.16	1482.5
2.3	0.57	1.74	1.28	7.38	1692.9
2.5	0.59	1.57	1.24	7.44	1842.4
2.7	0.61	1.35	1.21	7.51	1987.4
3.0	0.63	1.21	1.18	7.56	2211.5
3.3	0.65	0.97	1.14	7.64	2428.3
3.5	0.66	0.88	1.12	7.67	2581.1
3.7	0.67	0.77	1.11	7.71	2735.9
4.0	0.68	0.62	1.09	7.75	2945.3
4.5	0.70	0.43	1.06	7.83	3313.1
5.0	0.72	0.18	1.02	7.89	3695.1
5.5	0.73	0.20	1.03	7.91	4062.3
6.0	0.74	0.19	1.02	7.90	4424.9
6.5	0.74	0.17	1.02	7.94	4792.0

APPENDIX G TABLE 3 - DRAINED CONVENTIONAL TRIAXIAL EXTENSION TESTS

Test ECD8 DRAINED TRIAXIAL EXTENSION
σ_1' = 8.00 MPa e_i = 0.532 H/D = 1.87
Cambria sand ϕ' = 30.4 0.89 CM/HR
Conventional test with only membranes surrounding specimen.

ϵ_3 %	ϵ_v %	$\sigma_1 - \sigma_3$ MPa	σ_1'/σ_3'	p' MPa	Time second
0.0	0.00	0.08	1.01	7.96	0.0
0.0	-0.02	0.75	1.10	7.75	12.6
0.1	-0.03	1.61	1.25	7.47	61.2
0.2	-0.03	2.13	1.36	7.28	86.1
0.3	-0.00	3.20	1.67	6.90	164.7
0.4	0.04	3.62	1.83	6.76	216.4
0.5	0.08	3.91	1.96	6.67	268.3
0.6	0.12	4.12	2.07	6.59	318.1
0.7	0.17	4.29	2.17	6.53	372.3
0.8	0.22	4.45	2.26	6.49	446.6
1.0	0.28	4.59	2.36	6.43	523.6
1.3	0.38	4.80	2.51	6.37	685.6
1.5	0.44	4.89	2.59	6.34	790.1
1.7	0.49	4.97	2.66	6.31	892.4
2.0	0.55	5.06	2.74	6.28	1049.4
2.3	0.62	5.12	2.80	6.26	1216.8
2.5	0.65	5.18	2.86	6.24	1318.9
2.7	0.68	5.22	2.90	6.23	1420.9
3.0	0.72	5.28	2.94	6.24	1582.0
3.3	0.76	5.32	2.99	6.22	1749.8
3.5	0.78	5.34	3.01	6.21	1849.8
3.7	0.80	5.35	3.03	6.20	1949.6
3.9	0.82	5.37	3.05	6.20	FAILURE
4.0	0.82	5.36	3.04	6.21	2104.8
4.5	0.85	5.30	2.97	6.23	2382.9
5.0	0.87	5.19	2.86	6.25	2637.8
5.5	0.89	5.04	2.71	6.31	2905.0
6.0	0.92	4.82	2.52	6.38	3173.9
6.5	0.97	4.48	2.28	6.49	3432.7
7.0	1.05	4.10	2.05	6.63	3692.7

APPENDIX G TABLE 4 - DRAINED CONVENTIONAL TRIAXIAL EXTENSION TESTS

Test ECD9 DRAINED TRIAXIAL EXTENSION
σ_1' = 17.50 MPa e_i = 0.540 H/D = 1.90
Cambria sand ϕ' = 30.7 1.02 CM/HR
Conventional test with only membranes surrounding specimen.

ϵ_3 %	ϵ_v %	$\sigma_1 - \sigma_3$ MPa	σ_1'/σ_3'	p' MPa	Time second
0.0	0.00	0.03	1.00	17.45	0.0
0.1	-0.00	0.63	1.04	17.27	13.0
0.1	-0.00	0.94	1.06	17.19	37.2
0.1	-0.00	1.94	1.12	16.80	65.5
0.3	0.07	4.46	1.34	15.99	141.5
0.4	0.17	5.60	1.47	15.60	190.6
0.5	0.30	6.43	1.58	15.32	239.1
0.6	0.43	7.08	1.68	15.10	288.3
0.7	0.56	7.56	1.76	14.94	336.5
0.8	0.65	7.86	1.82	14.87	371.3
1.0	0.89	8.48	1.94	14.65	463.6
1.3	1.21	9.14	2.10	14.45	604.9
1.5	1.40	9.45	2.18	14.32	697.5
1.7	1.60	9.73	2.26	14.23	795.5
2.0	1.84	10.02	2.34	14.14	930.0
2.3	2.08	10.31	2.44	14.04	1075.7
2.5	2.23	10.46	2.49	13.98	1173.9
2.7	2.37	10.59	2.54	13.94	1271.4
3.0	2.55	10.75	2.60	13.88	1404.7
3.3	2.73	10.88	2.65	13.84	1550.1
3.5	2.83	10.97	2.69	13.81	1638.6
3.7	2.94	11.05	2.72	13.79	1734.1
4.0	3.09	11.14	2.76	13.75	1868.4
4.5	3.32	11.29	2.83	13.70	2102.3
5.0	3.54	11.43	2.89	13.66	2345.5
5.5	3.74	11.53	2.95	13.61	2577.9
6.0	3.91	11.61	2.99	13.58	2809.2
6.5	4.08	11.68	3.02	13.56	3040.6
7.0	4.25	11.75	3.05	13.57	3287.1
7.5	4.38	11.78	3.07	13.55	3514.4
7.9	4.48	11.80	3.08	13.54	FAILURE
8.0	4.51	11.77	3.06	13.56	3744.2
8.5	4.63	11.75	3.05	13.55	3981.3
9.0	4.74	11.68	3.01	13.59	4211.7
9.5	4.84	11.60	2.97	13.61	4458.0
10.0	4.93	11.49	2.92	13.65	4689.5
10.5	5.01	11.36	2.85	13.70	4919.8
11.0	5.09	11.19	2.78	13.75	5160.9
11.5	5.17	11.00	2.69	13.82	5396.5
12.0	5.24	10.83	2.63	13.87	5627.3
12.5	5.31	10.63	2.55	13.94	5855.8
13.5	5.45	10.18	2.40	14.08	6338.7
14.5	5.58	9.67	2.25	14.18	6804.4

APPENDIX G TABLE 5 - DRAINED CONVENTIONAL TRIAXIAL EXTENSION TESTS

Test ECD10 DRAINED TRIAXIAL EXTENSION
σ_1' = 35.00 MPa e_i = 0.523 H/D = 1.90
Cambria sand ϕ' = 31.3 1.27 CM/HR
Conventional test with only membranes surrounding specimen.

ϵ_3 %	ϵ_v %	$\sigma_1 - \sigma_3$ MPa	σ_1'/σ_3'	p' MPa	Time second
0.0	0.00	0.06	1.00	34.97	-0.0
0.0	0.00	0.10	1.00	34.96	2.6
0.1	0.01	0.66	1.02	34.91	33.0
0.2	0.01	1.84	1.06	34.38	59.4
0.3	0.03	4.28	1.14	33.56	112.1
0.4	0.06	5.76	1.20	33.06	145.9
0.5	0.10	7.06	1.25	32.63	172.8
0.6	0.20	9.29	1.36	31.88	215.7
0.7	0.32	10.94	1.46	31.34	251.4
0.8	0.50	12.73	1.57	30.74	297.4
1.0	0.81	14.70	1.72	30.09	370.1
1.3	1.24	16.61	1.90	29.45	476.7
1.5	1.51	17.57	2.01	29.13	551.4
1.7	1.71	18.20	2.08	28.91	611.4
2.0	2.07	19.20	2.22	28.57	731.4
2.3	2.36	19.84	2.31	28.39	835.8
2.5	2.53	20.23	2.37	28.23	909.2
2.7	2.70	20.58	2.43	28.10	982.1
3.0	2.93	20.98	2.50	27.98	1086.5
3.3	3.15	21.38	2.57	27.87	1196.5
3.5	3.28	21.58	2.61	27.78	1268.1
3.7	3.42	21.79	2.65	27.72	1341.6
4.0	3.60	22.03	2.70	27.64	1448.9
4.5	3.89	22.44	2.79	27.51	1638.4
5.0	4.13	22.76	2.86	27.40	1813.6
5.5	4.36	23.05	2.93	27.30	1998.1
6.0	4.58	23.30	2.99	27.22	2188.7
6.5	4.78	23.52	3.05	27.15	2363.0
7.0	4.95	23.64	3.08	27.12	2539.6
7.5	5.11	23.79	3.13	27.05	2720.8
8.0	5.25	23.85	3.14	27.04	2904.3
8.5	5.38	23.85	3.14	27.03	3098.7
8.7	5.43	23.89	3.16	27.00	FAILURE
9.0	5.49	23.84	3.14	27.03	3278.3
9.5	5.59	23.73	3.11	27.08	3461.8
10.0	5.67	23.59	3.07	27.11	3646.3
10.5	5.74	23.38	3.02	27.18	3821.1
11.0	5.80	23.08	2.94	27.29	4000.5
11.5	5.86	22.69	2.85	27.41	4186.4
12.0	5.92	22.35	2.77	27.53	4363.4
12.5	5.97	21.96	2.69	27.67	4542.1
13.0	6.01	21.48	2.59	27.82	4727.0
13.5	6.06	21.03	2.51	27.97	4907.4

APPENDIX G TABLE 6 - DRAINED CONVENTIONAL TRIAXIAL EXTENSION TESTS

Test ECD11 DRAINED TRIAXIAL EXTENSION
σ_1' = 17.50 MPa e_i = 0.530 H/D = 1.91
Cambria sand ϕ' = 31.0 1.91 CM/HR
Conventional test with only membranes surrounding specimen.

ϵ_3 %	ϵ_v %	$\sigma_1 - \sigma_3$ MPa	σ_1'/σ_3'	p' MPa	Time second
0.0	0.00	0.09	1.00	17.44	0.0
0.0	-0.00	0.66	1.04	17.27	11.7
0.1	-0.01	1.65	1.10	16.90	39.7
0.2	-0.00	2.97	1.20	16.47	65.9
0.3	0.06	4.52	1.35	15.95	104.7
0.4	0.17	5.78	1.49	15.55	150.9
0.5	0.26	6.41	1.58	15.33	178.7
0.6	0.42	7.23	1.71	15.06	229.9
0.7	0.49	7.53	1.76	14.96	254.6
0.8	0.59	7.89	1.82	14.83	288.8
1.0	0.83	8.62	1.98	14.59	378.1
1.3	1.06	9.20	2.11	14.40	478.8
1.5	1.22	9.50	2.20	14.28	553.1
1.7	1.37	9.75	2.26	14.21	629.4
2.0	1.56	10.05	2.36	14.11	738.8
2.3	1.75	10.32	2.45	14.01	856.7
2.5	1.87	10.47	2.50	13.97	936.9
2.7	1.97	10.60	2.55	13.92	1012.8
3.0	2.11	10.74	2.60	13.88	1112.2
3.3	2.25	10.91	2.66	13.84	1224.7
3.5	2.34	10.99	2.69	13.82	1301.9
3.7	2.42	11.05	2.71	13.80	1372.3
4.0	2.55	11.14	2.76	13.77	1497.5
4.5	2.73	11.30	2.82	13.73	1675.3
5.0	2.89	11.42	2.88	13.68	1860.5
5.5	3.04	11.51	2.93	13.64	2050.7
6.0	3.17	11.59	2.97	13.61	2227.1
6.5	3.30	11.67	3.01	13.60	2417.8
7.0	3.42	11.76	3.06	13.56	2613.8
7.5	3.52	11.80	3.08	13.55	2792.0
8.0	3.62	11.84	3.10	13.53	2972.8
8.5	3.71	11.86	3.11	13.52	3170.1
8.8	3.76	11.87	3.12	13.51	FAILURE
9.0	3.79	11.86	3.11	13.52	3344.9
9.5	3.87	11.83	3.10	13.53	3546.8
10.0	3.94	11.77	3.06	13.55	3723.4
10.5	4.00	11.67	3.01	13.58	3903.7
11.0	4.05	11.59	2.97	13.61	4090.7
11.5	4.11	11.46	2.91	13.65	4286.2
12.0	4.15	11.32	2.84	13.70	4466.8
12.5	4.20	11.17	2.77	13.76	4646.3
13.0	4.24	11.02	2.71	13.80	4839.3
13.5	4.28	10.81	2.62	13.88	5035.2
14.0	4.32	10.63	2.55	13.94	5220.1

APPENDIX G TABLE 7 - DRAINED CONVENTIONAL TRIAXIAL EXTENSION TESTS

Test ECD12 DRAINED TRIAXIAL EXTENSION
σ_1' = 17.50 MPa e_i = 0.522 H/D = 1.88
Cambria sand ϕ' = 29.3 1.27 CM/HR
Conventional test with only membranes surrounding specimen.

ϵ_3 %	ϵ_v %	$\sigma_1 - \sigma_3$ MPa	σ_1'/σ_3'	p' MPa	Time second
0.0	0.00	0.03	1.00	17.49	0.0
0.1	0.00	0.44	1.03	17.36	11.5
0.1	0.01	0.68	1.04	17.34	35.8
0.2	0.01	1.37	1.09	17.04	60.3
0.3	0.03	2.89	1.20	16.52	108.0
0.4	0.09	4.21	1.32	16.10	144.0
0.5	0.22	5.69	1.48	15.58	194.4
0.6	0.29	6.20	1.55	15.42	218.1
0.7	0.40	6.84	1.64	15.21	254.0
0.8	0.54	7.44	1.74	15.01	298.4
1.0	0.74	8.07	1.86	14.81	361.0
1.3	1.08	8.90	2.04	14.53	480.3
1.5	1.24	9.18	2.10	14.45	541.8
1.7	1.43	9.51	2.19	14.32	622.0
2.0	1.68	9.86	2.29	14.20	736.3
2.3	1.88	10.12	2.37	14.11	841.0
2.5	2.01	10.29	2.43	14.06	914.9
2.7	2.13	10.41	2.47	14.02	987.5
3.0	2.32	10.61	2.54	13.95	1104.5
3.3	2.46	10.74	2.59	13.90	1203.2
3.5	2.57	10.83	2.63	13.87	1278.4
3.7	2.67	10.90	2.66	13.83	1352.9
4.0	2.82	11.03	2.71	13.80	1473.4
4.5	3.03	11.19	2.78	13.75	1652.1
5.0	3.23	11.32	2.83	13.73	1828.5
5.5	3.41	11.43	2.88	13.70	2014.4
6.0	3.57	11.49	2.91	13.67	2191.6
6.3	3.65	11.51	2.92	13.66	FAILURE
6.5	3.72	11.47	2.90	13.67	2391.3
7.0	3.85	11.20	2.78	13.75	2573.3
7.5	3.97	10.72	2.58	13.93	2748.5

APPENDIX G TABLE 8 - DRAINED CONVENTIONAL TRIAXIAL EXTENSION TESTS

Test ECD15 *DRAINED TRIAXIAL EXTENSION*
σ_1' = 17.50 MPa e_i = 0.526 H/D = 1.87
Cambria sand 1.27 CM/HR
Conventional test with only membranes surrounding specimen.
Test intentionally terminated prior to failure.

ϵ_3 %	ϵ_v %	$\sigma_1 - \sigma_3$ MPa	σ_1'/σ_3'	p' MPa	Time second
0.0	0.00	0.09	1.01	17.44	-0.0
0.1	0.00	0.56	1.03	17.28	11.2
0.1	0.01	1.24	1.08	17.02	39.8
0.2	0.02	2.06	1.13	16.77	68.7
0.3	0.06	3.06	1.21	16.47	101.8
0.4	0.13	4.66	1.36	15.93	146.2
0.5	0.20	5.44	1.45	15.66	171.6
0.6	0.35	6.64	1.61	15.26	222.6
0.7	0.45	7.13	1.69	15.11	252.0
0.8	0.56	7.59	1.77	14.95	284.9
1.0	0.78	8.30	1.90	14.71	353.7
1.3	1.11	9.06	2.08	14.44	467.7
1.5	1.29	9.42	2.17	14.34	537.1
1.7	1.48	9.72	2.25	14.24	614.2
2.0	1.72	10.07	2.36	14.12	727.5
2.3	1.92	10.30	2.44	14.04	825.7
2.5	2.06	10.46	2.49	14.00	901.9
2.7	2.19	10.61	2.55	13.93	978.6
3.0	2.37	10.75	2.60	13.90	1085.7
3.3	2.54	10.91	2.66	13.83	1199.1
3.5	2.63	10.99	2.69	13.82	1260.4
3.7	2.73	11.07	2.73	13.78	1336.8
4.0	2.88	11.19	2.78	13.73	1455.1
4.5	3.10	11.33	2.85	13.69	1632.4
5.0	3.30	11.41	2.89	13.66	1809.8

APPENDIX G TABLE 9 - DRAINED CONVENTIONAL TRIAXIAL EXTENSION TESTS

Test ECD16 DRAINED TRIAXIAL EXTENSION
σ_1' = 17.50 MPa e_i = 0.529 H/D = 1.87
Cambria sand ϕ' = 30.5 1.27 CM/HR
Conventional test with only membranes surrounding specimen.

ϵ_3 %	ϵ_v %	$\sigma_1 - \sigma_3$ MPa	σ_1'/σ_3'	p' MPa	Time second
0.0	0.00	0.04	1.00	17.46	-0.0
0.1	0.00	0.47	1.03	17.33	11.6
0.1	0.01	0.91	1.06	17.18	38.2
0.2	0.01	1.96	1.13	16.82	70.6
0.3	0.05	2.86	1.20	16.52	105.8
0.4	0.12	3.81	1.28	16.20	149.1
0.5	0.18	4.36	1.33	16.02	175.8
0.6	0.26	5.22	1.43	15.73	212.2
0.7	0.39	6.27	1.56	15.37	256.0
0.8	0.47	6.78	1.64	15.20	282.5
1.0	0.74	7.91	1.83	14.81	365.2
1.3	1.06	8.78	2.01	14.53	474.1
1.5	1.24	9.13	2.10	14.42	538.0
1.7	1.41	9.44	2.17	14.34	609.7
2.0	1.67	9.84	2.29	14.20	723.8
2.3	1.88	10.11	2.37	14.11	827.4
2.5	2.04	10.29	2.43	14.05	907.6
2.7	2.16	10.42	2.47	14.03	974.8
3.0	2.35	10.61	2.55	13.94	1082.1
3.3	2.51	10.78	2.61	13.89	1189.2
3.5	2.64	10.86	2.64	13.87	1269.8
3.7	2.73	10.94	2.67	13.83	1338.7
4.0	2.89	11.07	2.73	13.79	1452.5
4.5	3.11	11.21	2.79	13.74	1630.0
5.0	3.33	11.35	2.85	13.69	1817.5
5.5	3.52	11.45	2.90	13.66	1998.1
6.0	3.69	11.55	2.94	13.64	2186.3
6.5	3.84	11.61	2.98	13.60	2354.4
7.0	3.99	11.66	3.01	13.58	2538.2
7.5	4.13	11.71	3.03	13.56	2720.0
8.0	4.26	11.75	3.05	13.56	2906.8
8.4	4.36	11.75	3.06	13.58	FAILURE
8.5	4.38	11.73	3.05	13.55	3080.9
9.0	4.48	11.73	3.05	13.56	3263.2
9.5	4.59	11.66	3.02	13.55	3448.0

APPENDIX G TABLE 10 - DRAINED CONVENTIONAL TRIAXIAL EXTENSION TESTS

Test ECD17 DRAINED TRIAXIAL EXTENSION
σ_1' = 17.50 MPa e_i = 0.529 H/D = 1.87
Cambria sand ϕ' = 30.6 1.27 CM/HR
Conventional test with only membranes surrounding specimen.

ϵ_3 %	ϵ_v %	$\sigma_1 - \sigma_3$ MPa	σ_1'/σ_3'	p' MPa	Time second
0.0	0.00	0.03	1.00	17.45	0.0
0.1	0.01	0.50	1.03	17.28	12.0
0.1	0.03	1.14	1.07	17.05	41.9
0.2	0.05	1.95	1.13	16.80	68.7
0.3	0.13	3.07	1.21	16.43	115.4
0.4	0.19	3.61	1.26	16.25	142.3
0.5	0.27	4.24	1.32	16.03	177.2
0.6	0.38	5.18	1.42	15.71	223.1
0.7	0.46	5.86	1.50	15.53	252.5
0.8	0.57	6.56	1.60	15.29	287.2
1.0	0.80	7.56	1.76	14.95	355.6
1.3	1.17	8.57	1.96	14.63	469.8
1.5	1.37	8.99	2.06	14.47	538.2
1.7	1.58	9.38	2.16	14.35	618.7
2.0	1.82	9.73	2.26	14.23	717.5
2.3	2.07	10.04	2.35	14.13	827.7
2.5	2.24	10.23	2.41	14.06	906.0
2.7	2.38	10.36	2.46	14.02	977.5
3.0	2.59	10.55	2.52	13.96	1085.6
3.3	2.77	10.71	2.58	13.90	1190.9
3.5	2.90	10.81	2.62	13.86	1266.3
3.7	3.02	10.90	2.66	13.84	1341.5
4.0	3.16	11.01	2.71	13.79	1440.7
4.5	3.41	11.18	2.78	13.74	1626.2
5.0	3.63	11.33	2.85	13.69	1804.6
5.5	3.85	11.44	2.90	13.64	1998.7
6.0	4.05	11.54	2.94	13.65	2174.8
6.5	4.24	11.61	2.97	13.62	2354.9
7.0	4.42	11.68	3.02	13.58	2539.6
7.5	4.60	11.72	3.03	13.58	2716.4
8.0	4.75	11.76	3.06	13.56	2889.9
8.3	4.84	11.78	3.07	13.54	FAILURE
8.5	4.90	11.77	3.07	13.54	3076.1
9.0	5.03	11.75	3.05	13.56	3259.0
9.5	5.15	11.70	3.03	13.57	3437.6
10.0	5.25	11.64	2.99	13.60	3620.0
10.5	5.35	11.54	2.95	13.62	3813.3
11.0	5.43	11.42	2.89	13.67	3979.0
11.5	5.51	11.29	2.83	13.71	4166.8
12.0	5.58	11.14	2.76	13.76	4341.8

APPENDIX G TABLE 11 - DRAINED CONVENTIONAL TRIAXIAL EXTENSION TESTS

Test ECD18 DRAINED TRIAXIAL EXTENSION
σ_i' = 17.50 MPa e_i = 0.529 H/D = 1.87
Cambria sand 1.27 CM/HR
Conventional test with only membranes surrounding specimen.
Test intentionally terminated prior to failure.

ϵ_3 %	ϵ_v %	$\sigma_1 - \sigma_3$ MPa	σ_1'/σ_3'	p' MPa	Time second
0.0	0.00	0.07	1.00	17.45	-0.0
0.0	-0.00	0.54	1.03	17.31	11.2
0.1	-0.00	1.42	1.09	16.95	41.6
0.2	0.01	2.29	1.15	16.71	69.0
0.3	0.05	3.26	1.23	16.38	105.1
0.4	0.13	4.24	1.32	16.06	145.2
0.5	0.20	5.24	1.43	15.72	180.7
0.6	0.32	6.25	1.56	15.39	223.5
0.7	0.40	6.73	1.63	15.21	249.0
0.8	0.51	7.28	1.71	15.04	285.8
1.0	0.73	8.07	1.86	14.77	358.2
1.3	1.06	8.90	2.04	14.50	478.2
1.5	1.22	9.26	2.13	14.39	544.5
1.7	1.38	9.53	2.20	14.31	610.5
2.0	1.62	9.90	2.31	14.19	724.7
2.3	1.85	10.19	2.40	14.08	842.3
2.5	1.95	10.34	2.45	14.03	903.9
2.7	2.08	10.47	2.49	14.00	980.2
3.0	2.27	10.66	2.56	13.93	1099.8
3.3	2.42	10.79	2.61	13.88	1200.9
3.5	2.53	10.89	2.65	13.86	1277.5
3.7	2.63	10.97	2.68	13.82	1350.8
4.0	2.76	11.07	2.73	13.78	1453.0
4.5	2.97	11.22	2.79	13.74	1633.6
5.0	3.17	11.34	2.85	13.69	1814.8
5.5	3.36	11.46	2.90	13.65	2010.4
6.0	3.52	11.52	2.93	13.64	2187.2

APPENDIX G TABLE 12 - DRAINED CONVENTIONAL TRIAXIAL EXTENSION TESTS

Test ECD20 DRAINED TRIAXIAL EXTENSION
σ_1' = 17.50 MPa e_i = 0.526 H/D = 1.87
Cambria sand 1.27 CM/HR
Conventional test with only membranes surrounding specimen.
Test intentionally terminated prior to failure.

ϵ_3 %	ϵ_v %	$\sigma_1 - \sigma_3$ MPa	σ_1'/σ_3'	p' MPa	Time second
0.0	0.00	0.05	1.00	17.46	0.0
0.1	0.00	0.54	1.03	17.29	11.9
0.1	0.02	1.11	1.07	17.10	39.3
0.2	0.03	2.23	1.15	16.74	70.6
0.3	0.07	3.91	1.29	16.17	105.9
0.4	0.17	5.48	1.46	15.62	149.1
0.5	0.26	6.17	1.55	15.40	178.0
0.6	0.37	6.86	1.65	15.18	211.7
0.7	0.51	7.52	1.76	14.98	254.5
0.8	0.62	7.95	1.84	14.81	289.3
1.0	0.85	8.59	1.96	14.64	359.2
1.3	1.17	9.24	2.12	14.41	468.2
1.5	1.37	9.60	2.22	14.27	544.3
1.7	1.53	9.83	2.28	14.21	612.0
2.0	1.78	10.15	2.38	14.10	720.0
2.3	2.02	10.42	2.47	14.01	835.6
2.5	2.17	10.54	2.52	13.98	911.3
2.7	2.30	10.69	2.57	13.93	986.5
3.0	2.49	10.86	2.64	13.85	1092.3
3.3	2.65	10.98	2.69	13.82	1190.8
3.5	2.78	11.08	2.73	13.79	1272.7
3.7	2.91	11.16	2.76	13.77	1353.4
4.0	3.07	11.26	2.81	13.73	1455.9
4.5	3.32	11.41	2.88	13.66	1638.4
5.0	3.54	11.51	2.93	13.64	1819.7
5.5	3.76	11.53	2.94	13.63	2003.7

APPENDIX G TABLE 13 - DRAINED CONVENTIONAL TRIAXIAL EXTENSION TESTS

Test ECD18 DRAINED TRIAXIAL EXTENSION
σ_1' = 17.50 MPa e_i = 0.529 H/D = 1.87
Cambria sand 1.27 CM/HR
Conventional test with only membranes surrounding specimen.
Test intentionally terminated prior to failure.

ϵ_3 %	ϵ_v %	$\sigma_1 - \sigma_3$ MPa	σ_1'/σ_3'	p' MPa	Time second
0.0	0.00	0.07	1.00	17.45	-0.0
0.0	-0.00	0.56	1.03	17.29	11.6
0.1	0.00	1.25	1.08	17.04	39.6
0.2	0.01	2.09	1.14	16.78	64.6
0.3	0.06	3.71	1.27	16.24	117.0
0.4	0.11	4.55	1.35	15.96	143.6
0.5	0.19	5.51	1.46	15.64	176.8
0.6	0.30	6.42	1.58	15.35	218.4
0.7	0.40	7.02	1.67	15.13	252.4
0.8	0.52	7.54	1.76	14.97	291.7
1.0	0.75	8.29	1.90	14.71	367.0
1.3	1.02	8.98	2.06	14.49	468.8
1.5	1.21	9.37	2.16	14.35	546.3
1.7	1.39	9.67	2.24	14.24	624.2
2.0	1.61	9.98	2.33	14.13	727.6
2.3	1.80	10.23	2.41	14.05	827.8
2.5	1.94	10.40	2.47	14.00	904.6
2.7	2.06	10.53	2.52	13.96	977.0
3.0	2.22	10.70	2.58	13.92	1082.1
3.3	2.39	10.84	2.63	13.87	1194.8
3.5	2.50	10.93	2.67	13.83	1270.6
3.7	2.60	11.03	2.70	13.84	1344.0
4.0	2.72	11.10	2.74	13.77	1448.2
4.5	2.94	11.27	2.82	13.73	1629.5
5.0	3.14	11.40	2.88	13.67	1822.0
5.5	3.31	11.49	2.92	13.65	1998.2
6.0	3.47	11.57	2.96	13.62	2172.9
6.5	3.63	11.64	2.99	13.59	2354.3
7.0	3.77	11.68	3.02	13.57	2542.8
7.5	3.90	11.72	3.04	13.55	2720.5
8.0	4.03	11.73	3.04	13.56	2901.7

APPENDIX G TABLE 14 - DRAINED CONVENTIONAL TRIAXIAL EXTENSION TESTS

Test ECD21 DRAINED TRIAXIAL EXTENSION
σ_1' = 17.50 MPa e_i = 0.529 H/D = 1.87
Cambria sand ϕ' = 30.4 1.27 CM/HR
Conventional test with only membranes surrounding specimen.

ϵ_3 %	ϵ_v %	$\sigma_1 - \sigma_3$ MPa	σ_1'/σ_3'	p' MPa	Time second
0.0	0.00	0.02	1.00	17.48	-0.0
0.1	0.00	0.44	1.03	17.33	12.4
0.1	0.00	0.94	1.06	17.19	36.6
0.2	0.01	1.83	1.12	16.87	65.9
0.3	0.05	3.09	1.21	16.46	116.3
0.4	0.09	3.64	1.26	16.27	141.9
0.5	0.14	4.30	1.33	16.05	175.1
0.6	0.23	5.29	1.43	15.71	218.1
0.7	0.32	6.15	1.54	15.43	254.3
0.8	0.41	6.75	1.63	15.24	285.4
1.0	0.62	7.76	1.80	14.89	357.8
1.3	0.95	8.73	2.00	14.57	472.4
1.5	1.14	9.13	2.09	14.43	547.7
1.7	1.32	9.46	2.18	14.31	623.0
2.0	1.53	9.79	2.28	14.21	721.6
2.3	1.75	10.08	2.37	14.11	832.2
2.5	1.89	10.25	2.42	14.06	909.1
2.7	2.02	10.38	2.47	13.99	981.0
3.0	2.19	10.57	2.54	13.93	1090.3
3.3	2.38	10.69	2.58	13.88	1212.5
3.5	2.46	10.80	2.62	13.86	1272.7
3.7	2.56	10.87	2.65	13.83	1343.8
4.0	2.69	10.98	2.70	13.79	1448.9
4.5	2.91	11.14	2.76	13.74	1635.9
5.0	3.12	11.28	2.82	13.72	1818.1
5.5	3.29	11.38	2.87	13.68	1993.7
6.0	3.48	11.47	2.91	13.64	2188.8
6.5	3.64	11.55	2.94	13.66	2370.3
7.0	3.79	11.62	2.98	13.61	2549.7
7.5	3.93	11.65	3.00	13.60	2728.0
8.0	4.06	11.70	3.03	13.58	2908.8
8.5	4.19	11.74	3.04	13.57	3090.1
8.6	4.22	11.75	3.05	13.57	FAILURE
9.0	4.31	11.74	3.04	13.57	3271.0
9.5	4.42	11.70	3.02	13.58	3450.9
10.0	4.53	11.63	2.99	13.61	3630.9
10.5	4.62	11.54	2.94	13.64	3812.0
11.0	4.71	11.43	2.89	13.67	4004.7
11.5	4.79	11.29	2.82	13.72	4183.1
12.0	4.87	11.17	2.77	13.76	4357.2
12.5	4.95	11.01	2.70	13.81	4545.2
13.0	5.01	10.84	2.63	13.86	4721.6
13.5	5.09	10.65	2.55	13.95	4912.0
14.0	5.15	10.45	2.49	14.00	5092.6

APPENDIX G TABLE 14(cont) - DRAINED CONVENTIONAL TRIAXIAL EXTENSION TESTS

ϵ_3 %	ϵ_v %	$\sigma_1 - \sigma_3$ MPa	σ_1'/σ_3'	p' MPa	Time second
14.5	5.22	10.25	2.42	14.06	5267.7
15.0	5.29	10.05	2.35	14.12	5448.6
15.5	5.36	9.85	2.29	14.20	5635.4
16.0	5.42	9.64	2.23	14.26	5813.1
16.5	5.49	9.41	2.17	14.34	6004.7
17.0	5.56	9.19	2.11	14.41	6177.9
17.5	5.62	8.95	2.05	14.48	6362.7
18.0	5.70	8.71	1.99	14.57	6555.0
18.5	5.76	8.47	1.94	14.64	6727.8
19.0	5.82	8.22	1.89	14.71	6907.2
19.5	5.89	7.99	1.84	14.81	7088.1

APPENDIX G TABLE 15 - DRAINED CONVENTIONAL TRIAXIAL EXTENSION TESTS

Test ECD25 DRAINED TRIAXIAL EXTENSION
σ_1' = 68.00 MPa e_i = 0.524 H/D = 1.88
Cambria sand ϕ' = 27.0 1.27 CM/HR
Conventional test with only membranes surrounding specimen.

ϵ_3 %	ϵ_v %	$\sigma_1 - \sigma_3$ MPa	σ_1'/σ_3'	p' MPa	Time second
0.0	0.00	0.07	1.00	67.97	-0.0
0.0	0.00	0.72	1.01	67.76	11.1
0.1	0.00	2.62	1.04	67.06	42.8
0.2	0.01	4.65	1.07	66.45	70.1
0.3	0.02	7.70	1.13	65.43	105.5
0.4	0.06	11.32	1.20	64.21	144.8
0.5	0.10	13.64	1.25	63.45	168.3
0.6	0.23	18.15	1.36	61.93	219.0
0.7	0.32	19.99	1.42	61.33	246.3
0.8	0.42	21.81	1.47	60.71	274.6
1.0	0.71	25.72	1.61	59.40	353.1
1.3	1.10	29.56	1.77	58.12	460.3
1.5	1.35	31.50	1.86	57.48	536.2
1.7	1.55	32.82	1.93	57.03	597.5
2.0	1.85	34.66	2.04	56.42	701.3
2.3	2.12	36.08	2.13	55.94	805.5
2.5	2.28	36.93	2.19	55.69	877 8
2.7	2.45	37.74	2.25	55.42	955.1
3.0	2.66	38.66	2.32	55.10	1058.0
3.3	2.85	39.43	2.38	54.85	1162.2
3.5	2.99	39.92	2.42	54.69	1240.7
3.7	3.09	40.29	2.45	54.55	1299.5
4.0	3.27	40.94	2.51	54.36	1419.7
4.5	3.50	41.62	2.58	54.12	1579.9
5.0	3.73	42.26	2.64	53.90	1772.1
5.5	3.91	42.46	2.66	53.83	*FAILURE*
6.0	4.08	41.69	2.58	54.10	2115.3

APPENDIX G TABLE 16 - DRAINED CONVENTIONAL TRIAXIAL EXTENSION TESTS

Test ECD28 DRAINED TRIAXIAL EXTENSION
σ_1' = 68.00 MPa e_i = 0.524 H/D = 1.88
Cambria sand ϕ' = 29.0 1.27 CM/HR
Conventional test with only membranes surrounding specimen.

ϵ_3 %	ϵ_v %	$\sigma_1 - \sigma_3$ MPa	σ_1'/σ_3'	p' MPa	Time second
0.0	0.00	0.11	1.00	67.96	-0.0
0.0	0.00	0.88	1.01	67.71	10.6
0.1	0.00	2.12	1.03	67.24	37.6
0.2	0.01	3.67	1.06	66.77	63.9
0.3	0.02	5.89	1.09	66.02	99.1
0.4	0.05	8.35	1.14	65.20	140.0
0.5	0.08	10.52	1.18	64.48	174.7
0.6	0.14	12.94	1.24	63.68	212.7
0.7	0.20	15.33	1.29	62.88	244.9
0.8	0.32	18.26	1.37	61.91	286.8
1.0	0.53	22.12	1.48	60.62	349.1
1.3	0.94	27.31	1.67	58.88	465.9
1.5	1.14	29.15	1.75	58.27	523.5
1.7	1.37	30.95	1.84	57.67	594.0
2.0	1.72	33.43	1.97	56.84	714.3
2.3	1.96	34.87	2.05	56.34	804.8
2.5	2.14	35.88	2.12	56.02	881.9
2.7	2.30	36.62	2.17	55.78	950.7
3.0	2.52	37.71	2.25	55.39	1057.3
3.3	2.73	38.57	2.31	55.12	1167.2
3.5	2.87	39.17	2.36	54.91	1244.1
3.7	2.97	39.46	2.38	54.88	1298.2
4.0	3.14	40.21	2.45	54.59	1410.4
4.5	3.39	41.11	2.53	54.29	1583.6
5.0	3.61	41.82	2.60	54.05	1759.6
5.5	3.82	42.45	2.66	53.85	1940.1
6.0	3.99	42.96	2.72	53.66	2111.5
6.5	4.14	43.36	2.76	53.53	2287.0
7.0	4.29	43.67	2.80	53.44	2462.6
7.5	4.42	43.98	2.83	53.33	2644.2
8.0	4.54	44.21	2.86	53.26	2817.9
8.5	4.64	44.35	2.88	53.21	2998.7
8.6	4.66	44.39	2.88	53.19	FAILURE
9.0	4.73	44.35	2.88	53.22	3170.1
9.5	4.81	44.26	2.87	53.24	3348.2
10.0	4.88	43.98	2.83	53.34	3528.3
10.5	4.94	43.67	2.80	53.44	3703.8
11.0	4.99	43.17	2.74	53.59	3881.6
11.5	5.03	42.48	2.67	53.83	4064.7
12.0	5.07	41.84	2.60	54.05	4226.7

APPENDIX G TABLE 17 - DRAINED CONVENTIONAL TRIAXIAL EXTENSION TESTS

Test ECD29 DRAINED TRIAXIAL EXTENSION
σ_1' = 52.00 MPa e_i = 0.521 H/D = 1.88
Cambria sand ϕ' = 26.3 1.27 CM/HR
Conventional test with only membranes surrounding specimen.

ϵ_3 %	ϵ_v %	$\sigma_1 - \sigma_3$ MPa	σ_1'/σ_3'	p' MPa	Time second
0.0	0.00	0.06	1.00	51.96	0.0
0.1	0.00	0.70	1.01	51.76	11.5
0.1	0.01	1.21	1.02	51.66	36.7
0.2	0.00	3.06	1.06	50.94	65.5
0.3	0.01	5.29	1.11	50.22	101.5
0.4	0.05	8.26	1.19	49.22	144.9
0.5	0.10	10.51	1.25	48.48	177.6
0.6	0.20	13.49	1.35	47.48	219.5
0.7	0.28	14.96	1.40	47.00	244.4
0.8	0.40	16.83	1.48	46.37	279.1
1.0	0.68	19.80	1.62	45.36	351.1
1.3	1.10	22.71	1.78	44.41	460.9
1.5	1.34	24.15	1.87	43.92	530.3
1.7	1.60	25.40	1.96	43.50	610.0
2.0	1.91	26.67	2.05	43.07	712.0
2.3	2.20	27.69	2.14	42.75	821.7
2.5	2.34	28.24	2.19	42.56	881.7
2.7	2.51	28.78	2.24	42.39	956.0
3.0	2.72	29.38	2.30	42.19	1057.5
3.3	2.96	30.06	2.37	41.96	1178.5
3.5	3.07	30.28	2.39	41.90	1237.9
3.7	3.20	30.61	2.43	41.79	1314.5
4.0	3.36	31.00	2.48	41.66	1418.0
4.5	3.62	31.55	2.54	41.47	1594.7
5.0	3.85	31.91	2.59	41.34	1768.1
5.3	3.99	31.95	2.59	41.33	FAILURE
5.5	4.06	31.75	2.57	41.41	1947.7
6.0	4.23	30.51	2.42	41.82	2125.2

APPENDIX G TABLE 18 - DRAINED CONVENTIONAL TRIAXIAL EXTENSION TESTS

Test ECD30 DRAINED TRIAXIAL EXTENSION
σ_1' = 52.00 MPa e_i = 0.518 H/D = 1.89
Cambria sand ϕ' = 29.2 1.27 CM/HR
Conventional test with only membranes surrounding specimen.

ϵ_3 %	ϵ_v %	$\sigma_1 - \sigma_3$ MPa	σ_1'/σ_3'	p' MPa	Time second
0.0	0.00	0.10	1.00	51.96	-0.0
0.0	0.00	0.84	1.02	51.72	11.6
0.1	0.00	2.12	1.04	51.24	40.0
0.2	0.00	3.60	1.07	50.79	66.9
0.3	0.02	5.81	1.13	50.07	103.6
0.4	0.06	8.97	1.21	49.00	146.0
0.5	0.10	11.06	1.27	48.29	171.8
0.6	0.19	13.41	1.35	47.51	206.5
0.7	0.33	15.99	1.44	46.65	250.5
0.8	0.43	17.16	1.49	46.27	276.3
1.0	0.76	20.41	1.65	45.17	362.8
1.3	1.16	23.05	1.80	44.30	466.2
1.5	1.38	24.28	1.88	43.88	530.2
1.7	1.61	25.37	1.95	43.51	599.9
2.0	1.93	26.69	2.06	43.09	711.8
2.3	2.21	27.68	2.14	42.77	817.1
2.5	2.38	28.27	2.19	42.56	886.3
2.7	2.55	28.76	2.24	42.41	962.9
3.0	2.77	29.48	2.31	42.16	1067.7
3.3	2.98	30.03	2.37	41.99	1176.0
3.5	3.12	30.38	2.41	41.86	1251.7
3.7	3.22	30.67	2.44	41.77	1312.7
4.0	3.42	31.12	2.49	41.60	1434.8
4.5	3.66	31.66	2.56	41.44	1598.5
5.0	3.90	32.16	2.62	41.27	1778.5
5.5	4.12	32.58	2.68	41.13	1969.2
6.0	4.30	32.95	2.73	41.00	2143.8
6.5	4.47	33.22	2.77	40.92	2316.9
7.0	4.63	33.47	2.81	40.83	2496.5
7.5	4.76	33.66	2.84	40.77	2665.1
8.0	4.89	33.83	2.86	40.69	2849.6
8.5	5.01	33.95	2.88	40.67	3027.4
9.0	5.12	34.02	2.89	40.64	3205.5
9.2	5.16	34.04	2.90	40.63	FAILURE
9.5	5.21	34.00	2.89	40.63	3384.0
10.0	5.29	33.92	2.88	40.67	3559.2
10.5	5.36	33.76	2.85	40.77	3737.9
11.0	5.42	33.46	2.80	40.86	3914.6
11.5	5.48	33.09	2.75	40.97	4098.5

APPENDIX G TABLE 19 - DRAINED CONVENTIONAL TRIAXIAL EXTENSION TESTS

Test ECD31 DRAINED TRIAXIAL EXTENSION
σ_1' = 42.00 MPa e_i = 0.513 H/D = 1.89
Cambria sand ϕ' = 28.9 1.27 CM/HR
Conventional test with only membranes surrounding specimen.

ϵ_3 %	ϵ_v %	$\sigma_1 - \sigma_3$ MPa	σ_1'/σ_3'	p' MPa	Time second
0.0	0.00	0.16	1.00	41.94	0.0
0.1	-0.00	1.01	1.02	41.63	12.9
0.1	-0.00	2.01	1.05	41.28	41.9
0.2	-0.00	3.70	1.10	40.73	71.2
0.3	0.01	5.55	1.15	40.13	99.9
0.4	0.08	9.22	1.28	38.90	152.2
0.5	0.15	11.07	1.36	38.27	181.2
0.6	0.24	12.50	1.42	37.81	209.3
0.7	0.37	14.05	1.50	37.28	245.0
0.8	0.55	15.64	1.59	36.75	291.8
1.0	0.79	17.28	1.70	36.20	354.6
1.3	1.18	19.22	1.84	35.57	460.4
1.5	1.42	20.19	1.93	35.23	531.9
1.7	1.66	21.09	2.01	34.96	612.3
2.0	1.97	22.04	2.10	34.66	721.8
2.3	2.25	22.85	2.19	34.37	831.1
2.5	2.44	23.33	2.25	34.20	910.7
2.7	2.57	23.60	2.28	34.12	968.0
3.0	2.80	24.14	2.35	33.93	1078.5
3.3	3.00	24.54	2.41	33.79	1185.2
3.5	3.14	24.83	2.45	33.70	1262.7
3.7	3.25	25.01	2.47	33.65	1327.4
4.0	3.43	25.35	2.53	33.51	1437.5
4.5	3.70	25.78	2.59	33.38	1620.2
5.0	3.96	26.13	2.65	33.27	1808.1
5.5	4.17	26.45	2.70	33.15	1983.0
6.0	4.37	26.73	2.75	33.06	2164.2
6.5	4.55	26.94	2.79	32.99	2351.0
7.0	4.71	27.09	2.82	32.93	2516.4
7.5	4.86	27.24	2.85	32.88	2705.5
8.0	5.00	27.32	2.87	32.86	2690.3
8.4	5.08	27.35	2.87	32.84	FAILURE
8.5	5.11	27.32	2.87	32.85	3057.5
9.0	5.21	27.26	2.85	32.87	3241.7
9.5	5.31	27.17	2.83	32.93	3427.3
10.0	5.39	26.94	2.79	33.01	3614.1
10.5	5.46	26.71	2.75	33.07	3780.6
11.0	5.52	26.34	2.68	33.21	3971.5
11.5	5.58	25.99	2.62	33.33	4139.0
12.0	5.64	25.54	2.55	33.47	4325.0

APPENDIX G TABLE 20 - DRAINED CONVENTIONAL TRIAXIAL EXTENSION TESTS

Test ECD76 DRAINED TRIAXIAL EXTENSION
σ_i' = 1.00 MPa e_i = 0.530 H/D = 1.90
Cambria sand ϕ' = 33.2 2.54 CM/HR
Conventional test with only membranes surrounding specimen.

ϵ_3 %	ϵ_v %	$\sigma_1 - \sigma_3$ MPa	σ_1'/σ_3'	p' MPa	
0.000	0.000	0.000	1.000	1.000	
0.075	-0.016	0.269	1.368	0.910	
0.093	-0.020	0.315	1.459	0.895	
0.187	-0.032	0.471	1.889	0.843	
0.317	-0.038	0.546	2.201	0.818	
0.373	-0.043	0.561	2.276	0.813	
0.466	-0.050	0.582	2.392	0.806	
0.653	-0.070	0.611	2.574	0.796	
0.933	-0.133	0.637	2.752	0.788	
1.306	-0.197	0.657	2.917	0.781	
1.866	-0.316	0.676	3.089	0.775	
2.425	-0.447	0.689	3.213	0.770	
2.799	-0.542	0.695	3.279	0.768	
3.172	-0.633	0.700	3.328	0.767	
3.731	-0.786	0.705	3.395	0.765	
4.104	-0.883	0.708	3.424	0.764	FAILURE
4.291	-0.919	0.707	3.417	0.764	
4.851	-0.917	0.696	3.290	0.768	
5.224	-1.010	0.693	3.257	0.769	
5.784	-1.152	0.687	3.192	0.771	

APPENDIX G TABLE 21 - DRAINED CONVENTIONAL TRIAXIAL EXTENSION TESTS

Test ECD77 DRAINED TRIAXIAL EXTENSION
σ_1' = 0.50 MPa e_i = 0.530 H/D = 1.92
Cambria sand ϕ' = 40.1 2.54 CM/HR
Conventional test with only membranes surrounding specimen.

ϵ_3 %	ϵ_v %	$\sigma_1 - \sigma_3$ MPa	σ_1'/σ_3'	p' MPa	
0.000	0.000	0.000	1.000	0.667	
0.092	-0.042	0.221	1.792	0.593	
0.184	-0.071	0.315	2.702	0.562	
0.276	-0.091	0.347	3.271	0.551	
0.368	-0.110	0.359	3.554	0.547	
0.460	-0.128	0.365	3.716	0.545	
0.552	-0.146	0.370	3.835	0.543	
0.736	-0.194	0.374	3.958	0.542	
0.920	-0.252	0.377	4.065	0.541	
1.196	-0.338	0.380	4.180	0.540	
1.471	-0.420	0.383	4.264	0.539	
1.839	-0.541	0.386	4.387	0.538	
2.207	-0.660	0.388	4.472	0.537	
2.575	-0.784	0.389	4.510	0.537	
2.943	-0.903	0.390	4.554	0.537	
3.311	-1.029	0.391	4.587	0.536	
3.587	-1.126	0.391	4.607	0.536	
3.862	-1.219	0.391	4.605	0.536	
4.138	-1.318	0.392	4.609	0.536	FAILURE
4.506	-1.446	0.390	4.540	0.537	
4.966	-1.603	0.389	4.497	0.537	
5.426	-1.753	0.386	4.402	0.538	
6.253	-2.018	0.380	4.162	0.540	
7.173	-2.286	0.374	3.962	0.542	
8.093	-2.531	0.365	3.714	0.545	
9.012	-2.745	0.354	3.431	0.549	
9.932	-2.941	0.344	3.205	0.552	
10.852	-3.078	0.333	2.999	0.556	
12.507	-3.288	0.318	2.746	0.561	
14.346	-3.399	0.293	2.418	0.569	
16.185	-3.467	0.277	2.241	0.574	
18.392	-3.524	0.253	2.027	0.582	

APPENDIX G TABLE 22 - DRAINED CONVENTIONAL TRIAXIAL EXTENSION TESTS

Test ECD78 DRAINED TRIAXIAL EXTENSION
σ_1' = 0.25 MPa e_i = 0.530 H/D = 1.93
Cambria sand ϕ' = 39.5 2.54 CM/HR
Conventional test with only membranes surrounding specimen.

ϵ_3 %	ϵ_v %	$\sigma_1 - \sigma_3$ MPa	σ_1'/σ_3'	p' MPa
0.000	0.000	0.000	1.000	0.250
0.091	-0.017	0.082	1.486	0.223
0.182	-0.024	0.132	2.116	0.206
0.274	-0.031	0.152	2.563	0.199
0.365	-0.039	0.161	2.797	0.196
0.456	-0.052	0.165	2.958	0.195
0.638	-0.085	0.171	3.172	0.193
0.821	-0.122	0.175	3.325	0.192
1.094	-0.186	0.179	3.500	0.190
1.368	-0.258	0.181	3.626	0.190
1.641	-0.330	0.184	3.760	0.189
2.006	-0.439	0.186	3.885	0.188
2.736	-0.667	0.188	4.059	0.187
3.283	-0.844	0.189	4.115	0.187
3.830	-1.030	0.191	4.230	0.186
4.377	-1.213	0.192	4.311	0.186
5.107	-1.460	0.192	4.335	0.186
5.836	-1.725	0.193	4.398	0.186
6.566	-1.972	0.194	4.468	0.185
7.113	-2.158	0.194	4.474	0.185
7.842	-2.416	0.195	4.535	0.185
8.572	-2.661	0.192	4.330	0.186
9.301	-2.903	0.191	4.214	0.186
10.031	-3.120	0.189	4.116	0.187
10.761	-3.336	0.187	3.940	0.188
12.037	-3.679	0.182	3.700	0.189
13.131	-3.931	0.177	3.423	0.191
14.591	-4.191	0.170	3.116	0.193
16.050	-4.392	0.162	2.854	0.196
16.779	-4.475	0.160	2.769	0.197

APPENDIX H

APPENDIX H TABLE 1 - DRAINED UNIFORM STRAIN TRIAXIAL EXTENSION TESTS WITH STRAIN LOCALIZATION

Test ECD34 DRAINED TRIAXIAL EXTENSION
σ_1' = 4.00 MPa e_i = 0.518 H/D = 1.88
Cambria sand 1.02 CM/HR
Uniform strain test with plates, but strain localization occurred.

ϵ_3 %	ϵ_v %	$\sigma_1 - \sigma_3$ MPa	σ_1'/σ_3'	p' MPa	Time second
0.0	0.00	0.03	1.01	3.97	-0.0
0.0	-0.01	0.34	1.09	3.87	11.5
0.1	-0.02	0.62	1.19	3.77	43.9
0.1	-0.02	1.00	1.33	3.66	69.6
0.3	-0.00	1.70	1.74	3.41	145.1
0.4	0.01	1.86	1.88	3.35	177.2
0.5	0.03	2.05	2.08	3.27	229.9
0.6	0.05	2.16	2.20	3.24	271.7
0.7	0.07	2.27	2.33	3.22	324.0
0.8	0.08	2.35	2.45	3.19	375.6
1.0	0.10	2.44	2.59	3.15	460.1
1.3	0.12	2.57	2.83	3.12	605.2
1.5	0.12	2.62	2.93	3.10	690.6
1.7	0.12	2.67	3.04	3.09	784.6
2.0	0.11	2.73	3.17	3.08	922.9
2.3	0.10	2.79	3.31	3.06	1068.4
2.5	0.08	2.81	3.39	3.05	1167.7
2.7	0.06	2.84	3.45	3.05	1252.1
3.0	0.03	2.87	3.54	3.04	1395.4
3.3	0.00	2.88	3.60	3.03	1523.7
3.5	-0.03	2.90	3.65	3.03	1625.5
3.7	-0.05	2.92	3.69	3.03	1710.5
4.0	-0.10	2.92	3.72	3.02	1851.3
4.5	-0.18	2.94	3.77	3.02	2081.3
5.0	-0.26	2.94	3.76	3.02	2320.9
5.5	-0.35	2.93	3.71	3.03	2546.5
6.0	-0.45	2.90	3.63	3.03	2787.0
6.5	-0.54	2.84	3.44	3.06	3013.9

APPENDIX H TABLE 2 - DRAINED UNIFORM STRAIN TRIAXIAL EXTENSION TESTS WITH STRAIN LOCALIZATION

Test ECD35 DRAINED TRIAXIAL EXTENSION
σ_1' = 4.00 MPa e_i = 0.521 H/D = 1.88
Cambria sand 1.02 CM/HR
Uniform strain test with plates, but strain localization occurred.

ϵ_3 %	ϵ_v %	$\sigma_1 - \sigma_3$ MPa	σ_1'/σ_3'	p' MPa	Time second
0.0	0.00	0.04	1.01	3.97	-0.0
0.0	-0.01	0.43	1.12	3.86	20.0
0.1	-0.02	0.70	1.21	3.74	38.0
0.1	-0.02	1.00	1.33	3.65	62.0
0.3	-0.00	1.68	1.73	3.41	138.3
0.4	0.02	1.96	1.98	3.30	192.5
0.5	0.03	2.07	2.09	3.28	226.3
0.6	0.05	2.20	2.24	3.24	277.3
0.7	0.06	2.27	2.34	3.21	318.8
0.8	0.08	2.35	2.45	3.18	369.9
1.0	0.10	2.45	2.61	3.16	474.7
1.3	0.11	2.53	2.76	3.13	601.2
1.5	0.11	2.59	2.87	3.11	706.4
1.7	0.11	2.62	2.94	3.10	785.2
2.0	0.10	2.68	3.06	3.09	934.1
2.3	0.08	2.72	3.15	3.08	1066.3
2.5	0.07	2.74	3.19	3.08	1154.0
2.7	0.05	2.76	3.25	3.07	1249.7
3.0	0.02	2.79	3.33	3.06	1399.6
3.3	-0.01	2.81	3.37	3.06	1533.0
3.5	-0.04	2.83	3.43	3.05	1629.5
3.7	-0.07	2.84	3.48	3.04	1718.9
4.0	-0.11	2.86	3.52	3.04	1865.3
4.5	-0.18	2.88	3.57	3.04	2099.0
5.0	-0.26	2.89	3.61	3.04	2326.7

APPENDIX H TABLE 3 - DRAINED UNIFORM STRAIN TRIAXIAL EXTENSION TESTS WITH STRAIN LOCALIZATION

Test ECD37 DRAINED TRIAXIAL EXTENSION
σ_1' = 8.00 MPa e_i = 0.531 H/D = 1.90
Cambria sand 1.02 CM/HR
Uniform strain test with plates, but strain localization occurred.

ϵ_3 %	ϵ_v %	$\sigma_1 - \sigma_3$ MPa	σ_1'/σ_3'	p' MPa	Time second
0.0	0.00	0.06	1.01	7.97	-0.0
0.1	-0.01	0.39	1.05	7.87	11.3
0.1	-0.01	0.61	1.08	7.81	38.2
0.1	-0.01	0.92	1.13	7.67	64.0
0.3	0.00	1.97	1.33	7.32	139.0
0.4	0.03	2.71	1.51	7.08	191.9
0.5	0.08	3.22	1.6	6.90	242.2
0.6	0.11	3.49	1.78	6.82	276.4
0.7	0.15	3.73	1.88	6.73	318.4
0.8	0.21	3.97	1.99	6.67	370.7
1.0	0.30	4.28	2.15	6.57	470.3
1.3	0.40	4.56	2.33	6.46	605.3
1.5	0.47	4.70	2.43	6.41	696.7
1.7	0.53	4.82	2.52	6.37	797.0
2.0	0.60	4.95	2.63	6.33	935.4
2.3	0.66	5.05	2.73	6.29	1083.5
2.5	0.70	5.11	2.78	6.28	1166.3
2.7	0.72	5.16	2.83	6.26	1257.7
3.0	0.77	5.25	2.92	6.24	1411.5
3.3	0.80	5.30	2.98	6.21	1548.5
3.5	0.82	5.32	3.00	6.21	1629.2
3.7	0.84	5.35	3.03	6.20	1730.4
4.0	0.86	5.40	3.09	6.18	1870.5
4.5	0.89	5.45	3.16	6.16	2098.7
5.0	0.91	5.51	3.23	6.15	2347.5
5.5	0.93	5.54	3.27	6.14	2578.6
6.0	0.93	5.57	3.30	6.13	2799.9
6.5	0.94	5.54	3.27	6.14	3035.5

APPENDIX H TABLE 4 - DRAINED UNIFORM STRAIN TRIAXIAL EXTENSION TESTS WITH STRAIN LOCALIZATION

Test ECD38 DRAINED TRIAXIAL EXTENSION
σ_1' = 17.50 MPa e_i = 0.522 H/D = 1.90
Cambria sand 1.02 CM/HR
Uniform strain test with plates, but strain localization occurred.

ϵ_3 %	ϵ_v %	$\sigma_1 - \sigma_3$ MPa	σ_1'/σ_3'	p' MPa	Time second
0.0	0.00	0.03	1.00	17.46	-0.0
0.1	-0.00	0.47	1.03	17.32	12.4
0.1	0.00	0.81	1.05	17.26	40.3
0.1	0.00	1.14	1.07	17.09	62.5
0.3	0.03	2.83	1.19	16.51	138.5
0.4	0.09	3.74	1.27	16.22	189.9
0.5	0.13	4.39	1.34	16.00	223.7
0.6	0.23	5.56	1.47	15.61	277.5
0.7	0.32	6.32	1.57	15.36	319.4
0.8	0.45	7.08	1.68	15.10	372.6
1.0	0.66	7.94	1.83	14.82	463.1
1.3	0.97	8.84	2.02	14.54	610.0
1.5	1.13	9.17	2.10	14.43	691.3
1.7	1.31	9.51	2.20	14.30	792.2
2.0	1.52	9.82	2.28	14.21	922.1
2.3	1.73	10.10	2.37	14.11	1060.1
2.5	1.86	10.30	2.43	14.05	1157.9
2.7	1.97	10.41	2.47	14.02	1237.5
3.0	2.16	10.60	2.54	13.95	1393.2
3.3	2.30	10.73	2.59	13.91	1518.6
3.5	2.41	10.84	2.63	13.87	1623.6
3.7	2.50	10.92	2.66	13.84	1708.9
4.0	2.64	11.02	2.71	13.80	1856.1
4.5	2.85	11.17	2.77	13.75	2093.6
5.0	3.04	11.29	2.82	13.72	2321.9
5.5	3.21	11.40	2.87	13.69	2552.8
6.0	3.36	11.47	2.91	13.65	2782.7
6.5	3.50	11.54	2.94	13.63	3007.8
7.0	3.62	11.54	2.95	13.63	3241.9
7.5	3.74	11.47	2.91	13.66	3470.2

APPENDIX H TABLE 5 - DRAINED UNIFORM STRAIN TRIAXIAL EXTENSION TESTS WITH STRAIN LOCALIZATION

Test ECD41 DRAINED TRIAXIAL EXTENSION
σ_1' = 17.50 MPa e_i = 0.524 H/D = 1.90
Cambria sand 1.02 CM/HR
Uniform strain test with plates, but strain localization occurred.

ϵ_3 %	ϵ_v %	$\sigma_1 - \sigma_3$ MPa	σ_1'/σ_3'	p' MPa	Time second
0.0	0.00	0.08	1.00	17.47	0.0
0.1	-0.00	0.50	1.03	17.31	11.8
0.1	0.01	0.84	1.05	17.26	40.1
0.1	0.01	1.07	1.06	17.15	64.3
0.3	0.04	2.79	1.19	16.56	143.0
0.4	0.09	3.58	1.26	16.30	191.1
0.5	0.13	4.04	1.30	16.15	223.8
0.6	0.21	4.75	1.37	15.90	274.6
0.7	0.28	5.37	1.44	15.70	318.1
0.8	0.38	6.23	1.55	15.42	368.3
1.0	0.62	7.56	1.76	14.97	468.7
1.3	0.92	8.54	1.95	14.65	599.3
1.5	1.11	8.98	2.06	14.50	686.4
1.7	1.31	9.36	2.15	14.37	781.2
2.0	1.56	9.78	2.27	14.22	919.0
2.3	1.79	10.06	2.36	14.12	1052.8
2.5	1.94	10.25	2.42	14.06	1150.2
2.7	2.07	10.41	2.47	14.0	1235.1
3.0	2.27	10.65	2.56	13.93	1386.3
3.3	2.42	10.79	2.61	13.90	1512.8
3.5	2.54	10.91	2.66	13.86	1614.5
3.7	2.64	10.97	2.68	13.85	1701.3
4.0	2.79	11.10	2.73	13.80	1842.6
4.5	3.02	11.24	2.80	13.75	2073.3
5.0	3.23	11.39	2.87	13.69	2304.0
5.5	3.41	11.49	2.91	13.67	2528.7
6.0	3.59	11.59	2.96	13.64	2756.9
6.5	3.75	11.64	2.99	13.62	2985.1
7.0	3.90	11.74	3.04	13.59	3219.1
7.5	4.05	11.79	3.06	13.57	3450.3
8.0	4.18	11.81	3.08	13.54	3680.8
8.5	4.29	11.81	3.08	13.56	3912.1
9.0	4.40	11.79	3.07	13.56	4138.2

APPENDIX H TABLE 6 - DRAINED UNIFORM STRAIN TRIAXIAL EXTENSION TESTS WITH STRAIN LOCALIZATION

Test ECD42 DRAINED TRIAXIAL EXTENSION
σ_1' = 35.00 MPa e_i = 0.531 H/D = 1.90
Cambria sand 1.27 CM/HR
Uniform strain test with plates, but strain localization occurred.

ϵ_3 %	ϵ_v %	$\sigma_1 - \sigma_3$ MPa	σ_1'/σ_3'	p' MPa	Time second
0.0	0.00	0.09	1.00	34.95	0.0
0.0	0.00	0.67	1.02	34.74	11.1
0.1	0.01	1.46	1.04	34.46	39.0
0.2	0.02	2.56	1.08	34.12	65.4
0.3	0.06	4.79	1.16	33.37	116.8
0.4	0.09	5.75	1.20	33.04	140.1
0.5	0.16	6.96	1.25	32.64	172.9
0.6	0.26	8.37	1.31	32.17	213.1
0.7	0.36	9.53	1.37	31.79	247.3
0.8	0.50	11.08	1.46	31.27	289.2
1.0	0.79	13.35	1.62	30.51	365.7
1.3	1.20	15.52	1.80	29.81	471.7
1.5	1.48	16.55	1.90	29.46	549.6
1.7	1.74	17.32	1.98	29.21	624.7
2.0	2.05	18.14	2.08	28.95	726.7
2.3	2.34	18.82	2.17	28.67	831.0
2.5	2.54	19.23	2.22	28.57	905.6
2.7	2.72	19.58	2.27	28.44	979.2
3.0	2.95	19.95	2.33	28.33	1082.4
3.3	3.18	20.28	2.38	28.21	1191.0
3.5	3.33	20.47	2.41	28.14	1263.3
3.7	3.47	20.62	2.44	28.09	1338.6
4.0	3.66	20.54	2.42	28.12	1446.1

APPENDIX H TABLE 7 - DRAINED UNIFORM STRAIN TRIAXIAL EXTENSION TESTS WITH STRAIN LOCALIZATION

Test ECD43 DRAINED TRIAXIAL EXTENSION
σ_1' = 35.00 MPa e_i = 0.540 H/D = 1.90
Cambria sand 1.27 CM/HR
Uniform strain test with plates, but strain localization occurred.

ϵ_3 %	ϵ_v %	$\sigma_1 - \sigma_3$ MPa	σ_1'/σ_3'	p' MPa	Time second
0.0	0.00	0.11	1.00	34.96	-0.0
0.1	0.00	0.70	1.02	34.75	11.5
0.1	0.01	1.21	1.04	34.62	37.9
0.2	0.02	2.59	1.08	34.12	66.0
0.3	0.07	4.75	1.16	33.42	119.1
0.4	0.11	5.93	1.20	33.00	147.1
0.5	0.16	7.21	1.26	32.57	174.0
0.6	0.30	9.72	1.38	31.74	223.5
0.7	0.39	10.75	1.44	31.40	248.5
0.8	0.53	11.96	1.52	31.00	284.3
1.0	0.84	13.92	1.66	30.34	359.9
1.3	1.27	15.75	1.82	29.72	468.0
1.5	1.55	16.63	1.91	29.43	541.3
1.7	1.81	17.38	1.99	29.17	620.1
2.0	2.15	18.20	2.09	28.90	731.2
2.3	2.40	18.80	2.16	28.72	835.1
2.5	2.58	19.17	2.21	28.60	910.2
2.7	2.76	19.48	2.26	28.50	986.0
3.0	2.99	19.88	2.32	28.36	1090.2
3.3	3.20	20.19	2.36	28.27	1194.0
3.5	3.34	20.40	2.40	28.19	1267.9
3.7	3.49	20.61	2.43	28.12	1347.6
4.0	3.66	20.86	2.48	28.04	1447.2
4.5	3.95	21.22	2.54	27.92	1628.5
5.0	4.20	21.55	2.60	27.80	1805.1
5.5	4.45	21.83	2.66	27.72	1990.2
6.0	4.68	22.06	2.71	27.63	2182.5
6.5	4.86	22.21	2.74	27.58	2354.2
7.0	5.04	22.39	2.78	27.52	2534.4
7.5	5.20	22.51	2.80	27.48	2715.8
8.0	5.36	22.61	2.83	27.45	2910.6
8.5	5.51	22.65	2.84	27.43	3091.6
9.0	5.62	22.62	2.83	27.43	3267.6
9.5	5.73	22.60	2.83	27.44	3443.2
10.0	5.84	22.49	2.80	27.48	3626.3
10.5	5.93	22.34	2.77	27.53	3800.3
11.0	6.01	22.16	2.73	27.59	3984.6
11.5	6.09	21.87	2.67	27.68	4176.0
12.0	6.16	21.60	2.61	27.78	4355.1
12.5	6.24	21.31	2.56	27.90	4536.8
13.0	6.29	20.96	2.49	28.02	4709.6
13.5	6.35	20.59	2.43	28.13	4892.8
14.5	6.49	19.74	2.30	28.41	5265.4

APPENDIX H TABLE 8 - DRAINED UNIFORM STRAIN TRIAXIAL EXTENSION TESTS WITH STRAIN LOCALIZATION

Test ECD55 DRAINED TRIAXIAL EXTENSION
σ_1' = 26.00 MPa e_i = 0.518 H/D = 1.88
Cambria sand 1.02 CM/HR
Uniform strain test with plates, but soil/plate friction occurred.

ϵ_3 %	ϵ_v %	$\sigma_1 - \sigma_3$ MPa	σ_1'/σ_3'	p' MPa	Time second
0.0	0.00	0.04	1.00	25.98	-0.0
0.1	0.01	1.03	1.04	25.71	37.6
0.1	0.01	2.14	1.09	25.27	66.0
0.2	0.02	3.01	1.13	24.99	92.8
0.3	0.05	4.64	1.22	24.45	130.9
0.4	0.11	6.80	1.35	23.72	175.3
0.5	0.25	8.75	1.51	23.08	231.4
0.6	0.36	9.73	1.60	22.73	269.3
0.7	0.49	10.56	1.68	22.47	312.1
0.8	0.65	11.47	1.79	22.18	366.0
1.0	0.92	12.63	1.94	21.78	454.9
1.3	1.30	13.88	2.15	21.36	589.0
1.5	1.55	14.56	2.28	21.13	685.9
1.7	1.75	15.03	2.37	20.97	770.8
2.0	2.04	15.67	2.52	20.76	903.5
2.3	2.34	16.19	2.65	20.60	1044.2
2.5	2.51	16.47	2.73	20.50	1137.2
2.7	2.67	16.73	2.81	20.41	1225.9
3.0	2.90	17.03	2.90	20.32	1360.8
3.3	3.12	17.32	2.99	20.23	1496.7
3.5	3.27	17.53	3.08	20.13	1594.9
3.7	3.40	17.69	3.13	20.10	1683.2
4.0	3.58	17.90	3.21	20.03	1818.6
4.5	3.87	18.25	3.36	19.91	2051.8
5.0	4.13	18.49	3.47	19.82	2271.1
5.5	4.40	18.73	3.59	19.73	2509.9
6.0	4.60	18.91	3.67	19.69	2727.8
6.5	4.82	19.02	3.73	19.65	2953.1
7.0	5.01	19.19	3.82	19.58	3185.0
7.5	5.19	19.29	3.89	19.54	3422.0
8.0	5.34	19.31	3.90	19.54	3637.4

APPENDIX H TABLE 9 - DRAINED UNIFORM STRAIN TRIAXIAL EXTENSION TESTS WITH STRAIN LOCALIZATION

Test ECD58 DRAINED TRIAXIAL EXTENSION
σ_1' = 35.00 MPa e_i = 0.524 H/D = 1.87
Cambria sand 1.02 CM/HR
Uniform strain test with plates, but soil/plate friction occurred.

ϵ_3 %	ϵ_v %	$\sigma_1 - \sigma_3$ MPa	σ_1'/σ_3'	p' MPa	Time second
0.0	0.00	0.05	1.00	34.98	0.0
0.1	0.00	0.71	1.02	34.76	11.8
0.1	0.01	1.21	1.04	34.61	37.7
0.2	0.01	2.78	1.09	34.09	67.7
0.3	0.04	6.73	1.24	32.75	131.0
0.4	0.12	9.23	1.36	31.91	175.0
0.5	0.27	11.60	1.50	31.12	230.9
0.6	0.38	12.85	1.58	30.70	268.2
0.7	0.53	14.11	1.68	30.28	313.3
0.8	0.71	15.23	1.77	29.91	366.1
1.0	0.96	16.63	1.91	29.44	446.5
1.3	1.38	18.33	2.10	28.86	587.5
1.5	1.61	19.13	2.21	28.60	674.4
1.7	1.83	19.79	2.30	28.38	762.3
2.0	2.15	20.62	2.44	28.09	899.6
2.3	2.48	21.34	2.56	27.88	1046.7
2.5	2.64	21.71	2.64	27.75	1132.8
2.7	2.79	22.01	2.69	27.66	1211.2
3.0	3.02	22.48	2.80	27.48	1349.1
3.3	3.25	22.77	2.86	27.41	1485.9
3.5	3.38	23.03	2.92	27.32	1575.0
3.7	3.51	23.25	2.98	27.24	1662.9
4.0	3.70	23.52	3.05	27.14	1801.3
4.5	3.99	23.93	3.16	27.01	2032.0
5.0	4.25	24.23	3.25	26.92	2253.8
5.5	4.52	24.56	3.35	26.80	2487.1
6.0	4.73	24.83	3.44	26.72	2709.5
6.5	4.93	25.07	3.53	26.64	2927.1
7.0	5.12	25.31	3.62	26.55	3152.2
7.5	5.29	25.50	3.69	26.48	3388.4
8.0	5.44	25.67	3.76	26.42	3604.9
8.5	5.57	25.75	3.80	26.37	3829.0
9.0	5.70	25.82	3.82	26.36	4059.3
9.5	5.84	25.87	3.83	26.38	4281.8
10.0	5.95	25.89	3.84	26.36	4516.5
10.5	6.05	25.82	3.81	26.39	4741.7
11.0	6.14	25.73	3.78	26.42	4966.3
11.5	6.21	25.62	3.73	26.45	5179.4
12.0	6.28	25.52	3.69	26.48	5422.5
12.5	6.34	25.46	3.67	26.50	5639.6
13.5	6.44	25.24	3.59	26.59	6096.8
14.5	6.54	24.84	3.45	26.71	6534.8

APPENDIX H TABLE 10 - DRAINED UNIFORM STRAIN TRIAXIAL EXTENSION TESTS WITH STRAIN LOCALIZATION

Test ECD62 DRAINED TRIAXIAL EXTENSION
σ_1' = 17.50 MPa e_i = 0.516 H/D = 1.89
Cambria sand 1.02 CM/HR
Uniform strain test with plates, but soil/plate friction occurred.

ϵ_3 %	ϵ_v %	$\sigma_1 - \sigma_3$ MPa	σ_1'/σ_3'	p' MPa	Time second
0.0	0.00	0.13	1.01	17.44	-0.0
0.1	0.00	0.65	1.04	17.25	11.5
0.1	0.01	1.06	1.06	17.13	44.0
0.1	0.02	1.69	1.11	16.91	68.2
0.3	0.08	3.41	1.24	16.33	135.0
0.4	0.15	4.46	1.34	15.98	184.5
0.5	0.24	5.41	1.45	15.67	234.0
0.6	0.32	6.22	1.55	15.38	269.5
0.7	0.45	7.29	1.72	15.04	322.4
0.8	0.57	7.96	1.84	14.82	365.7
1.0	0.81	8.93	2.05	14.49	452.1
1.3	1.17	9.94	2.32	14.15	596.3
1.5	1.38	10.39	2.47	13.99	685.0
1.7	1.59	10.77	2.61	13.87	780.8
2.0	1.86	11.21	2.80	13.72	917.5
2.3	2.12	11.56	2.96	13.60	1061.9
2.5	2.28	11.78	3.08	13.52	1161.0
2.7	2.41	11.92	3.14	13.52	1244.1
3.0	2.62	12.17	3.30	13.42	1392.4
3.3	2.80	12.34	3.40	13.37	1523.3
3.5	2.91	12.45	3.47	13.33	1611.2
3.7	3.02	12.55	3.55	13.30	1707.4
4.0	3.18	12.69	3.66	13.24	1842.3
4.5	3.44	12.87	3.80	13.18	2079.4
5.0	3.66	13.01	3.91	13.14	2308.4
5.5	3.87	13.14	4.03	13.10	2540.7
6.0	4.06	13.23	4.12	13.06	2773.5
6.5	4.23	13.32	4.20	13.03	3000.4
7.0	4.38	13.36	4.24	13.03	3224.9
7.5	4.53	13.41	4.30	13.01	3457.7
8.0	4.66	13.45	4.32	13.01	3689.2
8.5	4.77	13.43	4.33	12.99	3917.3
9.0	4.87	13.41	4.30	13.00	4148.0
9.5	4.97	13.35	4.24	13.02	4379.2
10.0	5.06	13.32	4.21	13.04	4609.8
10.5	5.14	13.27	4.15	13.06	4844.4
11.0	5.22	13.26	4.15	13.05	5083.9
11.5	5.29	13.20	4.09	13.07	5313.3
12.0	5.35	13.23	4.13	13.06	5538.5
12.5	5.41	13.25	4.14	13.05	5765.3
13.5	5.55	12.97	3.88	13.15	6229.2
14.5	5.66	12.97	3.88	13.14	6690.6

APPENDIX H TABLE 11 - DRAINED UNIFORM STRAIN TRIAXIAL EXTENSION TESTS WITH STRAIN LOCALIZATION

Test ECD63 DRAINED TRIAXIAL EXTENSION
σ_1' = 12.00 MPa e_i = 0.525 H/D = 1.90
Cambria sand 1.02 CM/HR
Uniform strain test with plates, but soil/plate friction occurred.

ϵ_3 %	ϵ_v %	$\sigma_1 - \sigma_3$ MPa	σ_1'/σ_3'	p' MPa	Time second
0.0	0.00	0.03	1.00	11.98	0.0
0.0	-0.00	0.54	1.05	11.81	12.1
0.1	-0.00	1.03	1.09	11.67	43.5
0.1	-0.01	1.79	1.18	11.39	71.0
0.3	0.03	3.83	1.47	10.70	139.2
0.4	0.11	4.79	1.66	10.39	189.3
0.5	0.21	5.50	1.85	10.16	241.8
0.6	0.27	5.83	1.95	10.04	274.5
0.7	0.37	6.22	2.08	9.91	324.5
0.8	0.46	6.54	2.20	9.80	375.4
1.0	0.62	6.99	2.40	9.64	468.2
1.3	0.85	7.51	2.68	9.47	618.0
1.5	0.97	7.71	2.81	9.41	703.3
1.7	1.10	7.90	2.94	9.34	799.9
2.0	1.26	8.15	3.12	9.28	940.4
2.3	1.42	8.33	3.27	9.22	1083.3
2.5	1.52	8.45	3.39	9.18	1187.1
2.7	1.60	8.54	3.47	9.15	1272.4
3.0	1.73	8.69	3.63	9.09	1423.8
3.3	1.83	8.77	3.72	9.07	1549.6
3.5	1.90	8.86	3.81	9.06	1649.9
3.7	1.96	8.90	3.88	9.03	1740.2
4.0	2.06	9.00	4.03	8.98	1885.4
4.5	2.23	9.11	4.16	8.96	2123.2
5.0	2.35	9.21	4.32	8.92	2356.9
5.5	2.47	9.28	4.42	8.90	2601.7
6.0	2.56	9.33	4.50	8.88	2832.1
6.5	2.65	9.38	4.60	8.86	3068.1
7.0	2.73	9.41	4.63	8.86	3301.4
7.5	2.81	9.39	4.62	8.86	3543.0
8.0	2.86	9.40	4.61	8.86	3771.3
8.5	2.91	9.39	4.60	8.87	4003.6

APPENDIX H TABLE 12 - DRAINED UNIFORM STRAIN TRIAXIAL EXTENSION TESTS WITH STRAIN LOCALIZATION

Test ECD65 DRAINED TRIAXIAL EXTENSION
σ_1' = 12.00 MPa e_i = 0.525 H/D = 1.90
Cambria sand 1.02 CM/HR
Uniform strain test with plates, but strain localization occurred.

ϵ_3 %	ϵ_v %	$\sigma_1 - \sigma_3$ MPa	σ_1'/σ_3'	p' MPa	Time second
0.0	0.00	0.08	1.01	11.96	0.0
0.1	-0.00	0.25	1.02	11.85	14.2
0.1	0.00	0.58	1.05	11.85	44.4
0.1	0.00	0.92	1.08	11.67	67.6
0.3	0.03	2.29	1.24	11.22	146.7
0.4	0.07	2.78	1.30	11.05	181.5
0.5	0.13	3.32	1.38	10.87	227.8
0.6	0.20	4.01	1.50	10.64	283.5
0.7	0.25	4.49	1.60	10.48	319.5
0.8	0.34	4.97	1.71	10.33	366.4
1.0	0.52	5.74	1.92	10.06	474.0
1.3	0.74	6.32	2.12	9.87	610.9
1.5	0.86	6.55	2.21	9.79	693.1
1.7	0.98	6.77	2.30	9.70	788.1
2.0	1.18	7.05	2.43	9.64	939.7
2.3	1.33	7.25	2.53	9.57	1080.3
2.5	1.41	7.34	2.58	9.54	1166.3
2.7	1.49	7.43	2.63	9.50	1255.8
3.0	1.62	7.55	2.70	9.46	1396.0
3.3	1.74	7.65	2.76	9.44	1540.4
3.5	1.81	7.71	2.81	9.41	1631.9
3.7	1.88	7.77	2.84	9.40	1731.1
4.0	1.98	7.83	2.89	9.38	1863.5
4.5	2.13	7.95	2.98	9.33	2107.6
5.0	2.26	8.05	3.05	9.30	2331.4
5.5	2.39	8.13	3.11	9.27	2569.9
6.0	2.51	8.20	3.16	9.25	2806.9
6.5	2.61	8.27	3.22	9.24	3033.9
7.0	2.71	8.31	3.26	9.22	3268.1
7.5	2.80	8.37	3.31	9.20	3507.7
8.0	2.89	8.39	3.34	9.18	3744.8
8.5	2.97	8.43	3.37	9.18	3967.9
9.0	3.05	8.46	3.40	9.17	4203.7
9.5	3.13	8.47	3.41	9.15	4445.5
10.0	3.20	8.44	3.39	9.16	4665.8

APPENDIX H TABLE 13 - DRAINED UNIFORM STRAIN TRIAXIAL EXTENSION TESTS WITH STRAIN LOCALIZATION

Test ECD66 DRAINED TRIAXIAL EXTENSION
σ_1' = 17.50 MPa e_i = 0.511 H/D = 1.89
Cambria sand 1.02 CM/HR
Uniform strain test with plates, but strain localization occurred.

ϵ_3 %	ϵ_v %	$\sigma_1 - \sigma_3$ MPa	σ_1'/σ_3'	p' MPa	Time second
0.0	0.00	0.05	1.00	17.46	-0.0
0.1	-0.00	0.64	1.04	17.26	15.9
0.1	0.01	0.96	1.06	17.26	43.4
0.1	0.01	1.62	1.10	16.94	69.3
0.3	0.07	3.48	1.25	16.31	148.8
0.4	0.12	4.31	1.33	16.04	183.6
0.5	0.21	5.33	1.44	15.70	227.8
0.6	0.30	6.06	1.53	15.45	268.6
0.7	0.44	6.87	1.65	15.19	323.5
0.8	0.55	7.35	1.73	15.02	365.9
1.0	0.81	8.21	1.89	14.73	471.6
1.3	1.11	8.93	2.05	14.49	605.2
1.5	1.29	9.27	2.13	14.39	691.4
1.7	1.47	9.59	2.22	14.27	789.4
2.0	1.71	9.95	2.32	14.16	925.2
2.3	1.92	10.23	2.42	14.01	1061.6
2.5	2.06	10.39	2.47	14.01	1152.9
2.7	2.20	10.54	2.52	13.95	1253.1
3.0	2.38	10.72	2.59	13.90	1391.1
3.3	2.55	10.86	2.64	13.86	1525.5
3.5	2.67	10.99	2.70	13.80	1632.9
3.7	2.76	11.05	2.72	13.78	1712.1
4.0	2.90	11.17	2.78	13.73	1849.3
4.5	3.14	11.34	2.86	13.67	2086.6
5.0	3.35	11.49	2.92	13.65	2315.4
5.5	3.55	11.60	2.98	13.59	2555.1
6.0	3.73	11.70	3.03	13.58	2781.5
6.5	3.89	11.78	3.07	13.55	3015.7
7.0	4.05	11.82	3.09	13.54	3248.9
7.5	4.18	11.82	3.09	13.54	3479.5
8.0	4.30	11.72	3.04	13.57	3707.8
8.5	4.40	11.54	2.94	13.64	3948.9
9.0	4.48	11.31	2.84	13.70	4170.0
9.5	4.56	11.02	2.71	13.80	4401.4
10.0	4.65	10.69	2.58	13.91	4644.2
10.5	4.72	10.51	2.51	13.97	4866.2

APPENDIX H TABLE 14 - DRAINED UNIFORM STRAIN TRIAXIAL EXTENSION TESTS WITH STRAIN LOCALIZATION

Test ECD73 DRAINED TRIAXIAL EXTENSION
σ_1' = 26.00 MPa e_i = 0.531 H/D = 1.95
Cambria sand 1.14 CM/HR
Uniform strain test with plates, but strain localization occurred.

ϵ_3 %	ϵ_v %	$\sigma_1 - \sigma_3$ MPa	σ_1'/σ_3'	p' MPa	Time second
0.0	0.00	0.05	1.00	26.00	-0.0
0.0	0.00	0.54	1.02	25.83	14.2
0.1	0.00	1.36	1.06	25.54	41.5
0.2	0.00	2.32	1.10	25.24	67.7
0.3	0.02	4.02	1.18	24.67	117.3
0.4	0.10	5.80	1.29	24.07	168.6
0.5	0.17	7.07	1.37	23.65	203.2
0.6	0.30	8.45	1.48	23.20	246.6
0.7	0.42	9.44	1.57	22.86	283.1
0.8	0.56	10.34	1.66	22.56	324.9
1.0	0.86	11.63	1.81	22.14	409.3
1.3	1.25	12.86	1.98	21.72	528.2
1.5	1.55	13.55	2.09	21.48	627.9
1.7	1.76	13.98	2.16	21.34	705.5
2.0	2.07	14.53	2.27	21.16	829.1
2.3	2.31	14.91	2.35	21.03	937.7
2.5	2.51	15.22	2.41	20.92	1033.9
2.7	2.68	15.45	2.46	20.88	1110.9
3.0	2.91	15.73	2.53	20.77	1237.7
3.3	3.13	15.97	2.59	20.70	1364.4
3.5	3.25	16.09	2.62	20.64	1437.6
3.7	3.38	16.22	2.66	20.61	1522.5
4.0	3.56	16.39	2.70	20.55	1642.5
4.5	3.84	16.64	2.78	20.46	1848.8
5.0	4.11	16.84	2.84	20.40	2065.5
5.5	4.33	17.00	2.89	20.34	2264.1
6.0	4.55	17.14	2.93	20.29	2470.2
6.5	4.75	17.24	2.97	20.26	2672.2
7.0	4.92	17.33	3.00	20.23	2875.9
7.5	5.09	17.38	3.02	20.20	3087.0
8.0	5.24	17.42	3.03	20.21	3290.8
8.5	5.37	17.42	3.03	20.19	3496.1
9.0	5.49	17.38	3.02	20.20	3701.0
9.5	5.59	17.29	2.99	20.23	3906.1
10.0	5.69	17.19	2.95	20.26	4111.1
10.5	5.78	17.07	2.91	20.33	4323.1
11.0	5.86	16.90	2.85	20.39	4524.2
11.5	5.93	16.69	2.79	20.45	4728.9
12.0	6.00	16.47	2.73	20.51	4940.2
12.5	6.06	16.24	2.66	20.60	5143.7
13.0	6.12	15.99	2.60	20.68	5350.8
13.5	6.19	15.71	2.52	20.79	5562.3
14.0	6.24	15.44	2.46	20.87	5765.1

APPENDIX I

APPENDIX I TABLE 1 - SUCCESSFUL UNDRAINED UNIFORM STRAIN TRIAXIAL EXTENSION TESTS

Test ECU8 UNDRAINED TRIAXIAL EXTENSION
σ_{1i}' = 42.00 MPa e_i = 0.518 H/D = 2.03
Cambria sand ϕ' = 34.6 1.14 CM/HR
Successful uniform strain test with steel plates.

ϵ_3 %	u MPa	$\sigma_1 - \sigma_3$ MPa	σ_1'/σ_3'	p' MPa	Time second
0.0	0.53	0.13	1.00	41.95	0.0
0.0	0.53	0.87	1.02	41.66	15.5
0.1	0.55	1.80	1.04	41.36	40.6
0.2	0.57	2.61	1.07	41.05	66.1
0.3	0.69	4.89	1.13	40.19	119.0
0.4	1.07	6.98	1.20	39.13	173.3
0.5	1.52	8.04	1.24	38.32	206.5
0.6	2.31	9.22	1.30	37.14	246.9
0.7	3.60	10.49	1.37	35.41	299.7
0.8	4.51	11.29	1.42	34.23	334.6
1.0	7.18	13.28	1.60	30.90	432.0
1.3	10.60	15.10	1.90	26.87	562.9
1.5	12.44	15.50	2.06	24.90	639.7
1.7	14.17	15.64	2.23	23.13	722.1
1.8	14.88	15.70	2.32	22.39	MAX. DEV.
2.0	16.29	15.60	2.47	21.02	844.6
2.3	18.17	15.28	2.68	19.26	975.9
2.5	19.24	15.06	2.83	18.27	1070.4
2.7	20.01	14.83	2.93	17.57	1146.9
3.0	21.04	14.49	3.07	16.65	1268.4
3.3	21.93	14.16	3.20	15.87	1394.3
3.5	22.50	13.91	3.28	15.39	1491.9
3.7	22.88	13.75	3.34	15.05	1568.9
4.0	23.44	13.50	3.42	14.57	1693.5
4.5	24.20	13.12	3.53	13.93	1912.9
5.0	24.82	12.78	3.59	13.45	2120.3
5.5	25.26	12.50	3.63	13.08	FAILURE
6.0	25.74	12.12	3.59	12.75	2560.1
6.5	26.06	11.83	3.54	12.54	2767.7
7.0	26.27	11.59	3.49	12.38	2971.6
7.5	26.54	11.34	3.44	12.21	3197.9

APPENDIX I TABLE 2 - SUCCESSFUL UNDRAINED UNIFORM STRAIN TRIAXIAL EXTENSION TESTS

Test ECU9 UNDRAINED TRIAXIAL EXTENSION
σ_3 = 17.57 MPa e_i = 0.52? H/D = 2.04
Cambria sand ϕ' = 35.3 1.14 CM/HR
Successful uniform strain test with steel plates.

ϵ_3 %	u MPa	$\sigma_1 - \sigma_3$ MPa	σ_1'/σ_3'	p' MPa	Time second
0.0	0.54	0.09	1.01	17.53	0.0
0.1	0.50	0.67	1.04	17.33	13.5
0.1	0.58	0.99	1.06	17.21	37.1
0.1	0.59	1.89	1.12	16.86	64.1
0.3	1.07	3.65	1.27	15.79	126.1
0.4	1.69	4.68	1.40	14.84	168.7
0.5	2.46	5.59	1.56	13.73	221.1
0.6	3.28	6.06	1.69	12.77	270.5
0.7	3.76	6.27	1.78	12.24	302.3
0.8	4.41	6.52	1.91	11.50	350.7
1.0	5.51	6.70	2.14	10.34	446.2
1.2	6.44	6.75	2.38	9.40	MAX. DEV.
1.3	6.61	6.69	2.40	9.26	568.0
1.5	7.17	6.64	2.55	8.71	651.4
1.7	7.68	6.56	2.71	8.22	746.3
2.0	8.24	6.45	2.90	7.70	881.0
2.3	8.62	6.36	3.05	7.35	1007.3
2.5	8.82	6.31	3.14	7.16	1096.5
2.7	8.99	6.27	3.22	7.01	1191.4
3.0	9.17	6.23	3.32	6.84	1316.8
3.3	9.29	6.20	3.40	6.72	1446.5
3.5	9.37	6.19	3.45	6.65	1549.7
3.7	9.43	6.18	3.50	6.59	1625.6
4.0	9.50	6.18	3.56	6.53	1759.7
4.5	9.53	6.20	3.63	6.49	1976.9
5.0	9.56	6.22	3.69	6.46	2207.6
5.5	9.54	6.24	3.72	6.46	2418.0
6.0	9.53	6.26	3.72	6.48	2636.0
6.5	9.51	6.27	3.72	6.49	2853.5
6.2	9.48	6.31	3.75	6.50	FAILURE
7.0	9.49	6.28	3.69	6.52	3076.9
7.5	9.44	6.28	3.65	6.56	3304.0

APPENDIX I TABLE 3 - SUCCESSFUL UNDRAINED UNIFORM STRAIN TRIAXIAL EXTENSION TESTS

Test ECU10 UNDRAINED TRIAXIAL EXTENSION
σ_{1i}' = 26.00 MPa e_i = 0.526 H/D = 2.04
Cambria sand ϕ' = 34.2 1.14 CM/HR
Successful uniform strain test with steel plates.

ϵ_3 %	u MPa	$\sigma_1 - \sigma_3$ MPa	σ_1'/σ_3'	p' MPa	Time second
0.0	0.52	0.05	1.00	25.98	0.0
0.1	0.51	0.45	1.02	25.80	13.8
0.1	0.53	0.90	1.04	25.74	39.5
0.2	0.53	1.62	1.07	25.47	65.0
0.3	0.60	3.45	1.15	24.76	123.0
0.4	0.82	4.78	1.23	24.11	160.2
0.5	1.43	6.61	1.36	22.88	220.1
0.6	2.07	7.53	1.44	21.94	253.5
0.7	2.18	8.51	1.57	20.50	303.0
0.8	4.14	9.13	1.69	19.34	345.9
1.0	5.88	9.76	1.90	17.39	430.1
1.2	7.83	10.04	2.16	15.34	MAX. DEV.
1.3	8.35	10.03	2.24	14.81	575.1
1.5	9.34	9.97	2.38	13.86	650.9
1.7	10.24	9.86	2.54	12.97	738.3
2.0	11.38	9.59	2.73	11.94	870.2
2.3	12.15	9.40	2.89	11.23	995.3
2.5	12.58	9.28	3.00	10.83	1084.0
2.7	13.01	9.14	3.08	10.47	1178.7
3.0	13.46	8.97	3.18	10.09	1305.3
3.3	13.81	8.82	3.26	9.78	1432.6
3.5	13.98	8.76	3.32	9.61	1521.2
3.7	14.14	8.70	3.38	9.45	1615.0
4.0	14.36	8.61	3.43	9.28	1743.9
4.5	14.65	8.48	3.49	9.05	1956.3
5.0	14.84	8.37	3.53	8.89	2179.6
5.5	14.98	8.28	3.54	8.78	2394.5
5.7	15.00	8.27	3.56	8.75	FAILURE
6.0	15.04	8.23	3.54	8.72	2612.0
6.5	15.16	8.14	3.51	8.67	2841.0
7.0	15.18	8.07	3.48	8.64	3047.8
7.5	15.26	7.98	3.42	8.62	3262.3

APPENDIX I TABLE 4 - SUCCESSFUL UNDRAINED UNIFORM STRAIN TRIAXIAL EXTENSION TESTS

Test ECU11 UNDRAINED TRIAXIAL EXTENSION
σ_{1i}' = 12.00 MPa e_i = 0.526 H/D = 2.04
Cambria sand ϕ' = 34.6 1.27 CM/HR
Successful uniform strain test with steel plates.

ϵ_3 %	u MPa	$\sigma_1 - \sigma_3$ MPa	σ_1'/σ_3'	p' MPa	Time second
0.0	0.52	0.08	1.01	11.97	0.0
0.0	0.48	0.63	1.06	11.81	15.1
0.1	0.46	1.49	1.14	11.56	38.9
0.2	0.53	2.32	1.24	11.21	62.9
0.3	1.04	3.60	1.46	10.27	118.8
0.4	1.53	4.14	1.60	9.61	161.0
0.5	1.96	4.34	1.72	9.09	196.3
0.6	2.43	4.68	1.86	8.53	240.8
0.7	2.76	4.77	1.96	8.17	274.2
0.8	3.12	4.87	2.08	7.76	316.5
1.0	3.68	4.94	2.27	7.18	392.9
1.3	4.36	4.95	2.55	6.50	525.2
1.5	4.65	4.93	2.67	6.24	598.7
1.7	4.86	4.91	2.79	6.02	675.8
2.0	5.11	4.90	2.96	5.77	802.7
2.3	5.27	4.91	3.09	5.62	918.2
2.5	5.34	4.91	3.17	5.54	1006.9
2.7	5.37	4.94	3.25	5.49	1088.6
3.0	5.42	4.96	3.31	5.45	1196.2
3.3	5.43	4.99	3.38	5.42	1316.4
3.5	5.40	5.02	3.42	5.43	1394.5
3.7	5.42	5.04	3.45	5.42	1473.4
4.0	5.39	5.10	3.51	5.43	1600.4
4.5	5.30	5.19	3.57	5.49	1804.9
5.0	5.21	5.28	3.60	5.55	2004.5
5.5	5.08	5.37	3.62	5.63	2207.6
5.9	5.16	5.33	3.63	5.57	MAX. S.R.
6.0	4.98	5.44	3.61	5.71	2393.2
6.5	4.86	5.51	3.59	5.81	2599.2
7.0	4.78	5.56	3.55	5.89	2800.7
7.5	4.64	5.64	3.54	5.98	2993.4
8.0	4.56	5.68	3.49	6.07	3199.2
8.5	4.45	5.72	3.46	6.14	3401.2
9.0	4.36	5.75	3.40	6.23	3608.4
9.4	4.30	5.78	3.37	6.29	FAILURE
9.5	4.30	5.77	3.36	6.29	3794.5
10.0	4.29	5.76	3.30	6.34	3995.4
10.5	4.20	5.75	3.25	6.40	4199.7
11.0	4.16	5.73	3.19	6.43	4399.7

APPENDIX I TABLE 5 - SUCCESSFUL UNDRAINED UNIFORM STRAIN TRIAXIAL EXTENSION TESTS

Test ECU12 UNDRAINED TRIAXIAL EXTENSION
σ_{1i}' = 52.00 MPa e_i = 0.521 H/D = 2.14
Cambria sand ϕ' = 33.6 1.27 CM/HR
Successful uniform strain test with steel plates.

ϵ_3 %	u MPa	$\sigma_1 - \sigma_3$ MPa	σ_1'/σ_3'	p' MPa	Time second
0.0	0.53	0.29	1.01	51.92	-0.0
0.0	0.55	0.95	1.02	51.63	15.5
0.1	0.61	1.68	1.03	51.35	39.8
0.2	0.68	2.57	1.05	51.00	66.6
0.3	0.89	4.50	1.10	50.13	118.6
0.4	1.16	6.03	1.13	49.37	154.7
0.5	1.78	7.98	1.19	48.08	200.3
0.6	2.62	9.40	1.23	46.78	238.7
0.7	3.86	10.98	1.29	45.01	285.2
0.8	4.67	11.95	1.33	43.87	314.9
1.0	7.29	14.58	1.48	40.39	398.3
1.3	11.33	17.39	1.73	35.41	517.8
1.5	13.74	18.41	1.90	32.62	593.5
1.7	16.00	18.97	2.08	30.19	672.1
1.9	18.32	19.19	2.30	27.78	MAX. DEV.
2.0	19.13	19.02	2.32	27.08	796.7
2.3	21.34	18.88	2.54	24.87	913.1
2.5	22.71	18.58	2.65	23.62	993.2
2.7	23.89	18.30	2.77	22.53	1075.7
3.0	25.34	17.86	2.91	21.24	1192.4
3.3	26.61	17.43	3.05	20.12	1321.8
3.5	27.31	17.14	3.12	19.51	1404.1
3.7	27.74	16.98	3.18	19.11	1468.4
4.0	28.69	16.51	3.25	18.35	1600.0
4.5	29.68	16.03	3.35	17.50	1794.7
5.0	30.47	15.62	3.43	16.85	1988.6
5.5	31.20	15.13	3.44	16.29	2194.5
5.9	31.48	14.93	3.48	16.03	FAILURE
6.0	31.71	14.76	3.44	15.90	2389.6
6.5	32.19	14.36	3.40	15.57	2584.9
7.0	32.56	14.00	3.34	15.32	2788.6
7.5	32.86	13.67	3.28	15.12	2986.1

APPENDIX J

APPENDIX J TABLE 1 - UNDRAINED UNIFORM STRAIN TRIAXIAL EXTENSION TESTS WITH STRAIN LOCALIZATION

Test ECU2 UNDRAINED TRIAXIAL EXTENSION
σ_{1i}' = 17.57 MPa e_i = 0.528 H/D = 1.93
Cambria sand ϕ' = 30.6 1.02 CM/HR
Uniform strain test with plates, but strain localization occurred.

ϵ_3 %	u MPa	$\sigma_1 - \sigma_3$ MPa	σ_1'/σ_3'	p' MPa	Time second
0.0	0.53	0.08	1.00	17.53	-0.0
0.0	0.51	0.50	1.03	17.41	16.0
0.1	0.51	0.98	1.06	17.24	44.0
0.1	0.54	1.62	1.10	17.01	68.4
0.3	1.14	3.56	1.27	15.76	148.2
0.4	1.59	4.35	1.36	15.05	184.3
0.5	2.17	5.05	1.47	14.23	226.9
0.6	2.87	5.59	1.58	13.35	276.7
0.7	3.53	5.96	1.69	12.56	326.3
0.8	4.28	6.19	1.81	11.75	382.9
1.0	5.14	6.39	1.97	10.83	465.2
1.2	6.19	6.47	2.19	9.73	MAX. DEV.
1.3	6.29	6.43	2.20	9.66	603.7
1.5	6.86	6.41	2.33	9.10	696.3
1.7	7.35	6.34	2.44	8.62	798.2
2.0	7.92	6.23	2.57	8.12	937.9
2.3	8.30	6.15	2.68	7.75	1083.0
2.5	8.45	6.11	2.73	7.60	1166.7
2.7	8.63	6.07	2.79	7.44	1263.7
3.0	8.81	6.03	2.86	7.27	1405.0
3.3	8.91	6.02	2.92	7.15	1557.0
3.5	9.00	6.00	2.94	7.09	1638.4
3.7	9.04	6.00	2.97	7.05	1735.4
4.0	9.11	5.99	3.01	6.98	1874.4
4.5	9.15	5.99	3.04	6.93	2104.3
5.0	9.18	5.99	3.06	6.91	2339.8
5.5	9.17	6.00	3.06	6.92	2575.0
5.6	9.15	6.02	3.07	6.92	FAILURE
6.0	9.13	6.01	3.05	6.93	2806.1
6.5	9.14	6.01	3.03	6.96	3059.8
7.0	9.08	6.00	3.00	7.00	3292.0
7.5	9.03	6.01	2.99	7.02	3526.4
8.0	9.00	6.01	2.96	7.07	3756.9
8.5	8.99	5.98	2.92	7.10	3990.6
9.0	9.12	5.87	2.89	7.01	4217.9
9.5	9.13	5.84	2.87	7.02	4454.3
10.0	9.10	5.79	2.82	7.05	4688.9
10.5	9.12	5.72	2.77	7.05	4922.0

APPENDIX J TABLE 2 - UNDRAINED UNIFORM STRAIN TRIAXIAL EXTENSION TESTS WITH STRAIN LOCALIZATION

Test ECU3 UNDRAINED TRIAXIAL EXTENSION
σ_{1i}' = 35.00 MPa e_i = 0.518 H/D = 1.93
Cambria sand ϕ' = 33.0 1.14 CM/HR
Uniform strain test with plates, but strain localization occurred.

ϵ_3 %	u MPa	$\sigma_1 - \sigma_3$ MPa	σ_1'/σ_3'	p' MPa	Time second
0.0	0.53	0.08	1.00	34.96	0.0
0.0	0.53	0.69	1.02	34.75	14.6
0.1	0.54	1.74	1.05	34.36	42.8
0.2	0.57	2.70	1.08	34.05	65.7
0.3	0.76	4.98	1.17	33.10	119.1
0.4	1.30	7.02	1.26	31.88	168.9
0.5	1.97	8.37	1.33	30.77	201.2
0.6	3.21	9.82	1.44	29.05	243.6
0.7	4.23	10.75	1.52	27.70	276.8
0.8	5.67	11.53	1.63	26.03	321.0
1.0	8.09	12.47	1.83	23.26	406.4
1.3	10.94	12.78	2.08	20.32	525.6
1.4	11.12	12.78	2.10	20.14	MAX. DEV.
1.5	12.58	12.70	2.24	18.71	610.2
1.7	13.99	12.49	2.38	17.36	699.4
2.0	15.40	12.21	2.55	16.04	811.0
2.3	16.65	11.87	2.70	14.91	932.6
2.5	17.33	11.63	2.77	14.31	1015.2
2.7	17.93	11.44	2.86	13.77	1105.3
3.0	18.58	11.18	2.94	13.21	1216.5
3.3	19.16	10.99	3.05	12.69	1342.9
3.5	19.50	10.83	3.08	12.41	1421.9
3.7	19.79	10.71	3.13	12.17	1506.5
4.0	20.12	10.58	3.20	11.86	1627.9
4.5	20.61	10.36	3.28	11.45	1828.7
5.0	21.00	10.16	3.33	11.13	2028.6
5.5	21.39	9.93	3.36	10.83	2236.7
6.0	21.59	9.81	3.38	10.65	2436.8
6.1	21.61	9.81	3.39	10.64	FAILURE
6.5	21.82	9.62	3.36	10.49	2643.2
7.0	21.93	9.54	3.37	10.40	2838.8
7.5	22.12	9.34	3.29	10.30	3044.9

APPENDIX J TABLE 3 - UNDRAINED UNIFORM STRAIN TRIAXIAL EXTENSION TESTS WITH STRAIN LOCALIZATION

Test ECU4 UNDRAINED TRIAXIAL EXTENSION
σ_{1i}' = 52.00 MPa e_i = 0.517 H/D = 1.93
Cambria sand ϕ' = 32.0 1.14 CM/HR
Uniform strain test with plates, but strain localization occurred.

ϵ_3 %	u MPa	$\sigma_1 - \sigma_3$ MPa	σ_1'/σ_3'	p' MPa	Time second
0.0	0.54	0.10	1.00	51.95	0.0
0.1	0.51	0.90	1.02	51.67	13.6
0.1	0.58	1.56	1.03	51.46	39.2
0.2	0.59	3.28	1.07	50.84	68.2
0.3	0.87	6.27	1.14	49.56	118.9
0.4	1.74	9.47	1.23	47.62	168.0
0.5	2.74	11.53	1.30	45.90	200.4
0.6	4.75	13.96	1.41	43.11	250.4
0.7	5.80	14.89	1.47	41.76	274.9
0.8	7.95	16.42	1.58	39.09	327.1
1.0	10.96	17.83	1.75	35.61	404.6
1.3	14.80	18.61	1.97	31.52	518.7
1.5	17.41	18.75	2.15	28.86	MAX. DEV.
1.7	19.25	18.57	2.26	27.08	690.0
2.0	21.35	18.25	2.42	25.05	797.5
2.3	23.43	17.80	2.58	23.15	925.8
2.5	24.49	17.51	2.67	22.19	1006.2
2.7	25.38	17.23	2.74	21.39	1083.0
3.0	26.64	16.79	2.84	20.29	1209.5
3.3	27.58	16.42	2.93	19.46	1325.2
3.5	28.13	16.18	2.97	18.99	1402.6
3.7	28.73	15.93	3.03	18.48	1496.1
4.0	29.29	15.70	3.09	17.98	1606.0
4.5	30.27	15.22	3.17	17.17	1811.8
5.0	30.97	14.84	3.22	16.58	2009.1
5.5	31.65	14.42	3.24	16.06	2220.3
5.7	31.80	14.34	3.25	15.93	FAILURE
6.0	32.16	14.09	3.24	15.67	2416.0
6.5	32.54	13.75	3.21	15.39	2611.3
7.0	32.93	13.42	3.18	15.11	2817.1
7.5	33.20	13.15	3.13	14.93	3012.2

APPENDIX J TABLE 4 - UNDRAINED UNIFORM STRAIN TRIAXIAL EXTENSION TESTS WITH STRAIN LOCALIZATION

Test ECU5 UNDRAINED TRIAXIAL EXTENSION
σ_{1i}' = 68.00 MPa e_i = 0.530 H/D = 2.03
Cambria sand ϕ' = 31.0 1.14 CM/HR
Uniform strain test with plates, but strain localization occurred.

ϵ_3 %	u MPa	$\sigma_1 - \sigma_3$ MPa	σ_1'/σ_3'	p' MPa	Time second
0.0	0.58	0.44	1.01	67.79	-0.0
0.0	0.60	1.50	1.02	67.44	14.6
0.1	0.67	4.45	1.07	66.35	43.4
0.2	0.86	7.23	1.12	65.25	69.9
0.3	2.01	11.57	1.21	62.65	120.3
0.4	4.11	14.76	1.30	59.49	170.1
0.5	5.65	16.49	1.36	57.37	203.1
0.6	7.78	18.43	1.44	54.60	248.1
0.7	9.46	19.65	1.50	52.51	284.0
0.8	11.94	20.83	1.58	49.70	334.4
1.0	15.20	22.42	1.73	45.85	414.4
1.3	20.11	23.41	1.94	40.60	546.8
1.5	22.71	23.44	2.05	38.00	627.3
1.6	22.87	23.64	2.08	37.73	MAX. DEV.
1.7	24.93	23.42	2.16	35.77	708.1
2.0	28.04	23.06	2.32	32.78	839.8
2.3	30.58	22.55	2.46	30.45	971.4
2.5	31.82	22.24	2.54	29.27	1053.0
2.7	32.99	21.89	2.61	28.23	1133.7
3.0	34.43	21.41	2.69	26.95	1248.8
3.3	35.77	20.90	2.76	25.78	1377.4
3.5	36.57	20.57	2.81	25.10	1462.4
3.7	37.20	20.34	2.85	24.54	1543.6
4.0	38.14	19.94	2.91	23.73	1675.0
4.5	39.38	19.42	2.99	22.69	1881.5
5.0	40.34	18.95	3.05	21.86	2090.6
5.5	41.18	18.51	3.10	21.18	2296.9
5.9	41.83	18.16	3.13	20.63	FAILURE
6.0	41.92	18.07	3.12	20.56	2523.2
6.5	42.54	17.65	3.12	20.08	2728.5
7.0	43.14	17.16	3.09	19.65	2939.9
7.5	43.68	16.66	3.04	19.29	3138.7

APPENDIX J TABLE 5 - UNDRAINED UNIFORM STRAIN TRIAXIAL EXTENSION TESTS WITH STRAIN LOCALIZATION

Test ECU6 UNDRAINED TRIAXIAL EXTENSION
σ_{1i}' = 12.00 MPa e_i = 0.527 H/D = 1.93
Cambria sand ϕ' = 31.4 1.14 CM/HR
Uniform strain test with plates, but strain localization occurred.

ϵ_3 %	u MPa	$\sigma_1 - \sigma_3$ MPa	σ_1'/σ_3'	p' MPa	Time second
0.0	0.53	0.04	1.00	11.98	-0.0
0.1	0.42	0.52	1.05	11.88	13.7
0.1	0.50	0.81	1.07	11.81	38.3
0.2	0.43	1.60	1.15	11.53	65.8
0.3	0.81	2.83	1.32	10.76	120.6
0.4	1.35	3.70	1.49	9.93	173.0
0.5	1.70	4.04	1.60	9.47	205.2
0.6	2.17	4.38	1.73	8.88	249.9
0.7	2.63	4.58	1.87	8.35	298.2
0.8	2.97	4.69	1.97	7.98	337.0
1.0	3.56	4.77	2.14	7.37	414.6
1.3	4.30	4.77	2.39	6.62	547.4
1.5	4.63	4.73	2.50	6.32	624.2
1.7	4.87	4.73	2.61	6.08	706.9
2.0	5.18	4.68	2.75	5.79	839.9
2.3	5.35	4.67	2.87	5.61	968.6
2.5	5.38	4.69	2.94	5.55	1040.9
2.7	5.48	4.69	3.00	5.48	1130.5
3.0	5.55	4.69	3.05	5.41	1272.2
3.3	5.55	4.71	3.09	5.39	1386.4
3.5	5.58	4.72	3.11	5.38	1484.3
3.7	5.56	4.73	3.13	5.37	1560.5
4.0	5.56	4.75	3.15	5.37	1685.9
4.5	5.51	4.79	3.17	5.41	1893.3
4.6	5.50	4.82	3.17	5.43	FAILURE
5.0	5.47	4.80	3.14	5.45	2108.0
5.4	5.39	4.83	3.12	5.50	MAX.DEV.
5.5	5.40	4.81	3.08	5.52	2318.3
6.0	5.31	4.79	2.98	5.61	2532.3
6.5	5.23	4.72	2.86	5.69	2742.4
7.0	5.23	4.62	2.74	5.74	2952.1
7.5	5.25	4.51	2.63	5.77	3156.0
8.0	5.38	4.32	2.53	5.70	3371.5

APPENDIX J TABLE 6 - UNDRAINED UNIFORM STRAIN TRIAXIAL EXTENSION TESTS WITH STRAIN LOCALIZATION

Test ECU7 UNDRAINED TRIAXIAL EXTENSION
σ_{ii}' = 26.00 MPa e_i = 0.522 H/D = 1.92
Cambria sand ϕ' = 33.5 1.14 CM/HR
Uniform strain test with plates, but strain localization occurred.

ϵ_3 %	u MPa	$\sigma_1 - \sigma_3$ MPa	σ_1'/σ_3'	p' MPa	Time second
0.0	0.51	0.07	1.00	25.98	-0.0
0.1	0.44	0.68	1.03	25.77	14.1
0.1	0.63	1.12	1.05	25.58	40.6
0.2	0.60	1.98	1.08	25.23	65.0
0.3	1.00	3.48	1.16	24.35	115.2
0.4	1.74	4.81	1.24	23.18	166.7
0.5	2.37	5.59	1.30	22.29	201.5
0.6	3.13	6.42	1.38	21.25	241.2
0.7	4.14	7.43	1.50	19.91	293.1
0.8	4.72	7.90	1.57	19.18	320.3
1.0	6.41	9.03	1.82	17.10	405.9
1.3	8.53	9.61	2.15	14.79	528.6
1.4	9.38	9.68	2.30	13.90	MAX. DEV.
1.5	9.61	9.67	2.34	13.68	607.0
1.7	10.60	9.59	2.51	12.73	691.2
2.0	11.78	9.35	2.73	11.63	819.0
2.3	12.65	9.06	2.88	10.86	949.5
2.5	13.03	8.92	2.96	10.51	1024.2
2.7	13.38	8.79	3.03	10.20	1103.8
3.0	13.87	8.59	3.12	9.77	1233.8
3.3	14.25	8.42	3.18	9.47	1347.6
3.5	14.41	8.37	3.24	9.32	1426.6
3.7	14.59	8.29	3.28	9.17	1517.1
4.0	14.78	8.20	3.32	9.00	1634.9
4.5	15.06	8.06	3.38	8.76	1837.7
5.0	15.30	7.96	3.43	8.59	2042.7
5.5	15.43	7.86	3.44	8.46	2245.8
6.0	15.52	7.80	3.44	8.39	2452.6
6.1	15.49	7.82	3.46	8.39	FAILURE
6.5	15.61	7.71	3.42	8.33	2658.7
7.0	15.68	7.63	3.38	8.29	2866.3
7.5	15.72	7.56	3.35	8.26	3073.1

APPENDIX J TABLE 7 - UNDRAINED UNIFORM STRAIN TRIAXIAL EXTENSION TESTS WITH STRAIN LOCALIZATION

Test ECU13 UNDRAINED TRIAXIAL EXTENSION
σ_{1i}' = 68.00 MPa e_i = 0.524 H/D = 2.13
Cambria sand ϕ' = 32.5 1.27 CM/HR
Uniform strain test with plates, but strain localization occurred.

ϵ_3 %	u MPa	$\sigma_1 - \sigma_3$ MPa	σ_1'/σ_3'	p' MPa	Time second
0.0	0.51	0.08	1.00	67.99	0.0
0.0	0.51	0.82	1.01	67.73	14.1
0.1	0.52	1.85	1.03	67.36	40.9
0.2	0.53	2.93	1.05	66.99	65.3
0.3	0.63	5.36	1.09	66.10	117.4
0.4	0.85	7.95	1.13	65.01	167.3
0.5	1.07	9.56	1.17	64.27	191.4
0.6	2.13	13.39	1.25	61.93	243.8
0.7	3.24	15.55	1.31	60.09	275.1
0.8	5.06	17.98	1.40	57.47	317.0
1.0	8.68	21.30	1.55	52.74	394.9
1.3	13.84	24.09	1.79	46.64	511.5
1.5	17.43	25.03	1.96	42.75	602.5
1.7	20.01	25.34	2.09	40.05	677.0
1.8	21.58	25.43	2.18	38.46	MAX. DEV.
2.0	23.74	25.28	2.30	36.35	801.8
2.3	26.51	24.94	2.46	33.68	915.7
2.5	28.25	24.56	2.56	32.08	997.3
2.7	29.68	24.18	2.65	30.78	1074.0
3.0	31.62	23.58	2.77	29.03	1199.6
3.3	33.22	22.96	2.86	27.65	1321.0
3.5	34.08	22.61	2.91	26.90	1398.6
3.7	34.86	22.31	2.96	26.23	1475.7
4.0	35.93	21.79	3.02	25.32	1598.2
4.5	37.27	21.25	3.13	24.15	1792.1
5.0	38.51	20.64	3.21	23.12	1999.4
5.5	39.51	20.15	3.27	22.31	2205.1
6.0	40.24	19.73	3.31	21.69	2391.1
6.1	40.47	19.59	3.32	21.52	FAILURE
6.5	41.00	19.10	3.27	21.15	2594.9
7.0	41.63	18.50	3.21	20.71	2795.8
7.5	42.22	17.90	3.13	20.35	2993.4

APPENDIX J TABLE 8 - UNDRAINED UNIFORM STRAIN TRIAXIAL EXTENSION TESTS WITH STRAIN LOCALIZATION

Test ECU14 UNDRAINED TRIAXIAL EXTENSION
σ_{1i}' = 68.00 MPa e_i = 0.524 H/D = 2.13
Cambria sand ϕ' = 29.9 1.27 CM/HR
Uniform strain test with plates, but strain localization occurred.

ϵ_3 %	u MPa	$\sigma_1 - \sigma_3$ MPa	σ_1'/σ_3'	p' MPa	Time second
0.0	0.52	0.00	1.00	67.99	0.0
0.0	0.71	2.34	1.04	67.02	16.4
0.1	1.43	4.16	1.07	65.69	35.0
0.2	2.61	5.41	1.09	64.11	64.5
0.3	4.52	7.70	1.14	61.42	113.9
0.4	6.02	9.64	1.18	59.29	150.3
0.5	7.92	11.74	1.24	56.68	195.5
0.6	9.60	13.43	1.30	54.43	233.2
0.7	11.67	15.41	1.37	51.69	278.3
0.8	12.98	16.76	1.43	49.95	306.8
1.0	16.47	19.60	1.60	45.51	388.9
1.3	20.71	21.82	1.84	40.54	502.3
1.5	23.45	22.48	2.00	37.57	588.5
1.7	25.35	22.70	2.11	35.60	655.3
1.8	26.70	22.83	2.20	34.21	MAX. DEV.
2.0	28.42	22.77	2.31	32.51	780.3
2.3	30.65	22.36	2.44	30.40	895.9
2.5	31.92	22.17	2.53	29.22	969.4
2.7	33.08	21.85	2.61	28.16	1050.1
3.0	34.52	21.29	2.67	26.91	1163.7
3.3	35.72	20.80	2.73	25.86	1280.3
3.5	36.46	20.54	2.78	25.21	1358.1
3.7	37.17	20.17	2.81	24.62	1438.2
4.0	38.03	19.83	2.86	23.87	1557.2
4.5	39.31	19.16	2.91	22.82	1762.5
5.0	40.34	18.74	2.98	21.94	1956.1
5.5	41.14	18.14	2.96	21.34	2146.8
5.1	40.54	18.63	2.99	21.78	FAILURE
6.0	41.81	17.60	2.93	20.84	2332.5
6.5	42.39	17.14	2.91	20.41	2523.3
7.0	42.88	16.62	2.84	20.10	2724.6
7.5	43.36	16.19	2.80	19.78	2926.8

APPENDIX K

APPENDIX K TABLE 1 - SUCCESSFUL DRAINED/UNDRAINED UNIFORM STRAIN STABILITY TESTS IN TRIAXIAL EXTENSION

Test ESTAB2 DRAINED/UNDRAINED TRIAXIAL EXTENSION
σ_{1i}' = 17.57 MPa e_i = 0.519 H/D = 2.03
Cambria sand ϕ' = 35.7 1.27 CM/HR
Successful uniform strain test with steel plates.
Test turned undrained at effective stress ratio of 2.40

ϵ_3 %	u MPa	ϵ_v %	$\sigma_1 - \sigma_3$ MPa	σ_1'/σ_3'	p' MPa	Time second
0.0	0.51	0.00	0.07	1.00	17.56	-0.0
0.0	0.50	0.00	0.12	1.01	17.55	2.8
0.1	0.49	-0.00	0.96	1.06	17.29	43.8
0.1	0.49	-0.00	1.50	1.09	17.07	63.8
0.3	0.50	0.01	3.02	1.21	16.58	128.2
0.4	0.50	0.06	4.10	1.30	16.22	178.8
0.5	0.50	0.11	4.93	1.39	15.93	213.4
0.6	0.50	0.21	6.11	1.53	15.55	265.4
0.7	0.50	0.30	6.79	1.63	15.32	303.8
0.8	0.50	0.41	7.47	1.74	15.10	351.8
1.0	0.50	0.61	8.32	1.90	14.81	435.6
1.3	0.51	0.92	9.18	2.10	14.50	563.2
1.5	0.51	1.13	9.60	2.20	14.38	662.6
1.7	0.51	1.29	9.90	2.29	14.28	747.0
1.9	0.51	1.50	10.19	2.40	14.17	UNDRAINED
2.0	0.63	1.50	10.16	2.39	14.07	882.0
2.3	1.58	1.50	10.13	2.60	13.10	952.7
2.5	2.26	1.50	10.01	2.75	12.39	972.8
3.3	3.78	1.50	9.20	3.14	10.43	1006.0
3.7	4.39	1.50	9.03	3.26	10.02	1016.9
3.9	4.83	1.50	8.91	3.35	9.74	1025.8
4.2	5.23	1.50	8.82	3.42	9.51	1034.9
4.4	5.58	1.50	8.74	3.49	9.33	1043.8
4.7	5.92	1.50	8.67	3.55	9.17	1052.8
5.1	6.26	1.50	8.59	3.63	8.99	1065.7
5.6	6.47	1.50	8.48	3.72	8.77	1086.3
6.1	6.66	1.50	8.40	3.77	8.63	1103.4
6.6	6.77	1.50	8.34	3.80	8.54	1119.2
7.0	6.85	1.50	8.29	3.81	8.48	FAILURE
7.4	6.90	1.50	8.24	3.79	8.44	1150.1
7.9	6.94	1.50	8.19	3.76	8.42	1165.2
8.3	6.97	1.50	8.14	3.74	8.40	1180.3
8.7	7.00	1.50	8.09	3.71	8.38	1195.0
9.1	7.04	1.50	8.02	3.66	8.37	1210.1
9.5	7.07	1.50	7.95	3.60	8.36	1224.7
10.0	7.12	1.50	7.86	3.52	8.35	1239.9

APPENDIX K TABLE 2 - SUCCESSFUL DRAINED/UNDRAINED UNIFORM STRAIN STABILITY TESTS IN TRIAXIAL EXTENSION

Test ESTAB3 DRAINED/UNDRAINED TRIAXIAL EXTENSION
σ_{1i}' = 17.57 MPa e_i = 0.521 H/D = 2.03
Cambria sand ϕ' = 35.6 1.14 CM/HR
Successful uniform strain test with steel plates.
Test turned undrained at effective stress ratio of 2.90

ϵ_3 %	u MPa	ϵ_v %	$\sigma_1 - \sigma_3$ MPa	σ_1'/σ_3'	p' MPa	Time second
0.0	0.51	0.00	0.11	1.01	17.62	-0.0
0.0	0.51	0.00	0.18	1.01	17.58	4.1
0.1	0.51	0.00	0.95	1.06	17.45	30.8
0.1	0.50	0.01	1.29	1.08	17.26	59.5
0.3	0.51	0.03	2.87	1.19	16.69	133.7
0.4	0.52	0.08	3.62	1.26	16.45	175.4
0.5	0.51	0.14	4.37	1.33	16.20	220.5
0.6	0.51	0.20	5.08	1.40	15.96	260.5
0.7	0.51	0.29	6.03	1.52	15.64	305.7
0.8	0.51	0.39	6.76	1.62	15.40	346.3
1.0	0.51	0.64	7.98	1.82	15.00	442.5
1.3	0.52	0.95	8.94	2.03	14.67	566.3
1.5	0.52	1.14	9.39	2.14	14.52	652.3
1.7	0.52	1.31	9.74	2.23	14.40	736.7
2.0	0.53	1.56	10.16	2.36	14.26	867.8
2.3	0.53	1.79	10.46	2.46	14.16	1003.4
2.5	0.53	1.92	10.68	2.54	14.08	1091.0
2.7	0.53	2.05	10.81	2.58	14.03	1176.2
3.0	0.50	2.24	11.04	2.66	13.99	1305.1
3.3	0.51	2.41	11.21	2.74	13.93	1441.7
3.5	0.51	2.53	11.30	2.78	13.89	1523.4
3.7	0.51	2.65	11.39	2.81	13.87	1620.7
4.0	0.51	2.78	11.52	2.88	13.82	1744.0
4.3	0.51	2.92	11.62	2.90	13.79	UNDRAINED
4.5	0.84	2.92	11.61	3.05	13.42	1944.5
4.8	1.38	2.92	11.43	3.19	12.85	1973.1
5.5	2.44	2.92	10.86	3.42	11.73	2000.3
6.0	3.45	2.92	10.55	3.55	11.17	2018.4
6.6	4.07	2.92	10.26	3.67	10.69	2038.4
7.1	4.48	2.92	10.04	3.75	10.34	2057.0
7.4	4.74	2.92	9.88	3.78	10.14	FAILURE
7.5	4.87	2.92	9.77	3.77	10.04	2074.5
7.9	5.23	2.92	9.45	3.69	9.80	2090.0
8.4	5.58	2.92	8.98	3.49	9.59	2107.0

APPENDIX K TABLE 3 - SUCCESSFUL DRAINED/UNDRAINED UNIFORM STRAIN STABILITY TESTS IN TRIAXIAL EXTENSION

Test ESTAB4 DRAINED/UNDRAINED TRIAXIAL EXTENSION
σ_{1i}' = 26.00 MPa e_i = 0.518 H/D = 2.03
Cambria sand ϕ' = 37.7 1.14 CM/HR
Successful uniform strain test with steel plates.
Test turned undrained at effective stress ratio of 1.86

ϵ_3 %	u MPa	ϵ_v %	$\sigma_1 - \sigma_3$ MPa	σ_1'/σ_3'	p' MPa	Time second
0.0	0.51	0.00	0.06	1.00	25.99	-0.0
0.0	0.50	0.00	0.47	1.02	25.84	10.0
0.1	0.51	0.00	1.15	1.05	25.65	45.1
0.1	0.51	0.00	1.77	1.07	25.40	63.7
0.3	0.51	0.03	3.64	1.16	24.78	125.1
0.4	0.51	0.08	5.00	1.24	24.34	172.5
0.5	0.51	0.14	6.54	1.34	23.82	214.0
0.6	0.51	0.26	8.14	1.46	23.29	260.6
0.7	0.52	0.41	9.33	1.56	22.90	302.7
0.8	0.52	0.57	10.38	1.66	22.54	351.3
1.0	0.52	0.84	11.66	1.81	22.11	429.5
1.1	0.52	0.95	12.01	1.86	21.99	UNDRAINED
1.3	3.52	0.95	12.04	2.10	18.98	579.8
1.5	5.27	0.95	12.03	2.30	17.24	667.4
1.7	6.49	0.95	12.01	2.51	15.99	714.2
1.9	7.49	0.95	11.95	2.70	14.98	737.4
2.2	8.91	0.95	11.62	2.99	13.58	758.5
2.9	10.64	0.95	11.02	3.36	12.02	780.6
3.2	11.55	0.95	10.76	3.52	11.43	793.3
3.8	12.41	0.95	10.37	3.79	10.63	817.4
4.3	12.90	0.95	10.16	3.94	10.23	835.6
4.8	13.22	0.95	10.01	4.04	9.96	852.2
5.2	13.46	0.95	9.86	4.09	9.77	867.9
5.7	13.68	0.95	9.73	4.13	9.60	884.1
6.1	13.84	0.95	9.61	4.14	9.46	900.2
6.4	13.97	0.95	9.52	4.14	9.38	FAILURE
6.6	14.01	0.95	9.47	4.14	9.34	919.2
7.1	14.14	0.95	9.37	4.12	9.25	935.8
7.5	14.24	0.95	9.27	4.09	9.18	952.3
7.9	14.37	0.95	9.15	4.05	9.10	967.9
8.4	14.54	0.95	9.00	4.02	8.97	983.4
8.8	14.68	0.95	8.84	3.95	8.89	999.0
9.2	14.81	0.95	8.69	3.88	8.81	1014.6
9.6	14.98	0.95	8.50	3.80	8.71	1030.2
10.1	15.25	0.95	8.16	3.63	8.55	1045.8

APPENDIX K TABLE 4 - SUCCESSFUL DRAINED/UNDRAINED UNIFORM STRAIN STABILITY TESTS IN TRIAXIAL EXTENSION

Test ESTAB5 DRAINED/UNDRAINED TRIAXIAL EXTENSION
σ_{1i}' = 35.00 MPa e_i = 0.521 H/D = 2.03
Cambria sand ϕ' = 36.9 1.14 CM/HR
Successful uniform strain test with steel plates.
Test turned undrained at effective stress ratio of 1.86

ϵ_3 %	u MPa	ϵ_v %	$\sigma_1 - \sigma_3$ MPa	σ_1'/σ_3'	p' MPa	Time second
0.0	0.53	0.00	0.13	1.00	34.98	-0.0
0.0	0.52	0.00	0.58	1.02	34.80	9.8
0.1	0.53	0.01	1.35	1.04	34.58	45.0
0.1	0.52	0.02	2.02	1.06	34.33	62.9
0.3	0.53	0.05	4.42	1.14	33.53	129.1
0.4	0.53	0.08	5.66	1.19	33.10	165.5
0.5	0.53	0.16	7.66	1.28	32.45	218.6
0.6	0.53	0.23	8.84	1.34	32.06	251.5
0.7	0.53	0.36	10.62	1.44	31.46	301.9
0.8	0.53	0.48	11.92	1.52	31.02	340.4
1.0	0.52	0.79	14.17	1.68	30.28	424.5
1.2	0.52	1.21	16.23	1.86	29.59	UNDRAINED
1.3	0.75	1.21	16.22	1.88	29.30	563.6
1.5	3.70	1.21	16.25	2.04	26.41	754.4
1.7	6.05	1.21	16.25	2.23	24.05	967.6
2.0	8.23	1.21	16.25	2.47	21.86	1117.9
2.3	10.13	1.21	16.04	2.72	20.03	1167.8
3.2	13.14	1.21	14.81	3.24	16.47	1208.1
3.6	14.44	1.21	14.34	3.42	15.49	1222.8
3.9	15.27	1.21	14.07	3.52	14.95	1232.6
4.1	15.93	1.21	13.87	3.61	14.55	1241.5
4.4	16.54	1.21	13.68	3.69	14.20	1250.4
4.6	17.09	1.21	13.51	3.77	13.90	1259.3
5.2	17.78	1.21	13.18	3.90	13.33	1278.8
5.7	18.32	1.21	12.87	3.97	12.91	1297.8
6.2	18.74	1.21	12.60	4.00	12.59	FAILURE
6.6	19.04	1.21	12.36	3.99	12.37	1332.0
7.0	19.27	1.21	12.15	3.96	12.21	1346.6
7.4	19.48	1.21	11.96	3.92	12.07	1361.2
7.9	19.67	1.21	11.75	3.86	11.94	1376.8
8.3	19.84	1.21	11.56	3.80	11.84	1392.5
8.7	20.00	1.21	11.37	3.73	11.74	1407.0
9.1	20.15	1.21	11.19	3.67	11.65	1421.6
9.5	20.28	1.21	11.01	3.60	11.58	1436.2
9.9	20.45	1.21	10.80	3.52	11.49	1451.8

APPENDIX L

APPENDIX L TABLE 1 - ISOTROPIC COMPRESSION/B-VALUE TESTS

Test ISO4 — ISOTROPIC COMPRESSION/B-VALUE TEST
Cambria sand — e_i = 0.524 — H/D = 2.51

u MPa	σ_{cell} MPa	ϵ_v %	Time Second
0.53	0.60	0.01	6.65
0.54	0.69	0.29	34.55
0.55	0.80	0.58	62.51
0.55	0.94	0.86	90.57
0.55	1.12	1.14	118.58
0.55	1.36	1.41	146.60
0.53	1.63	1.67	174.72
0.53	1.98	1.92	202.79
0.53	2.30	2.12	239.86
0.53	2.61	2.28	270.29
0.53	3.05	2.48	303.41
0.51	3.49	2.69	350.97
0.52	3.49	2.71	410.18
0.53	3.50	2.71	460.06
0.55	3.52	2.73	506.58
0.81	3.78	2.73	541.46
1.14	4.12	2.73	577.38
1.23	4.22	2.73	609.34
1.27	4.25	2.73	650.54
1.28	4.25	2.73	696.79
1.22	4.17	2.73	744.35
0.93	3.86	2.73	781.32
0.66	3.58	2.73	817.40
0.53	3.68	2.77	873.65
0.53	4.23	2.92	908.03
0.53	4.75	3.08	937.14
0.54	5.28	3.25	971.30
0.54	5.49	3.33	1013.21
0.54	5.50	3.34	1068.47
0.61	5.55	3.37	1113.94
0.98	5.93	3.37	1147.72
1.21	6.16	3.37	1182.60
1.30	6.25	3.37	1217.59
1.33	6.25	3.37	1264.82
1.34	6.25	3.36	1315.52
1.24	6.11	3.36	1368.14
0.95	5.78	3.36	1405.21
0.82	5.64	3.36	1439.21
0.71	5.51	3.36	1475.19
0.54	6.07	3.45	1538.35
0.55	6.76	3.59	1568.45
0.55	7.41	3.75	1597.62
0.55	8.06	3.90	1628.71
0.52	8.54	4.05	1668.53
0.52	8.50	4.08	1729.22
0.55	8.51	4.12	1778.87

APPENDIX L TABLE 1(cont) - ISOTROPIC COMPRESSION/B-VALUE TESTS

u MPa	σ_{cell} MPa	ϵ_v %	Time Second
0.79	8.71	4.12	1811.61
1.12	9.04	4.12	1844.34
1.34	9.23	4.12	1883.45
1.41	9.25	4.12	1938.54
1.45	9.25	4.12	1987.20
1.48	9.25	4.12	2036.91
1.51	9.25	4.12	2086.07
1.54	9.25	4.12	2133.69
1.52	9.21	4.12	2187.79
1.24	8.87	4.12	2222.78
0.99	8.58	4.12	2256.72
0.52	8.79	4.16	2320.55
0.52	9.49	4.25	2351.64
0.52	10.19	4.39	2382.72
0.52	10.86	4.54	2412.93
0.52	11.50	4.70	2442.15
0.53	12.17	4.88	2474.23
0.53	12.46	5.04	2518.94
0.53	12.50	5.11	2574.63
0.53	12.50	5.14	2625.38
0.87	12.69	5.16	2663.28
1.25	13.01	5.16	2695.08
1.53	13.23	5.16	2730.79
1.64	13.25	5.16	2775.93
1.72	13.25	5.16	2826.08
1.77	13.25	5.16	2873.26
1.81	13.25	5.16	2920.44
1.75	13.10	5.16	2973.83
1.47	12.75	5.16	3007.89
0.53	12.37	5.19	3074.73
0.53	13.00	5.25	3103.95
0.53	13.57	5.32	3133.17
0.53	14.04	5.42	3162.39
0.53	14.44	5.53	3191.61
0.53	14.95	5.66	3223.80
0.54	15.53	5.82	3254.94
0.54	16.06	5.98	3284.16
0.54	16.58	6.14	3313.38
0.55	17.13	6.32	3344.91
0.52	17.60	6.48	3375.17
0.52	17.95	6.64	3414.11
0.52	17.97	6.74	3455.69
0.54	18.00	6.83	3508.92
1.14	18.24	6.83	3544.95
1.63	18.58	6.83	3578.01
1.95	18.77	6.83	3613.00
2.10	18.75	6.83	3661.17

APPENDIX L TABLE 1(cont) - ISOTROPIC COMPRESSION/B-VALUE TESTS

u MPa	σ_{cell} MPa	ϵ_v %	Time Second
2.22	18.75	6.83	3707.86
2.31	18.75	6.83	3755.59
2.39	18.75	6.83	3803.26
2.46	18.75	6.83	3850.99
2.50	18.72	6.83	3903.23
2.21	18.30	6.83	3941.18
2.06	18.07	6.83	3976.44
0.52	17.98	6.92	4043.07
0.52	18.91	7.00	4073.38
0.52	19.70	7.11	4102.66
0.52	20.32	7.26	4131.94
0.52	20.91	7.43	4162.25
0.52	21.45	7.61	4191.53
0.53	22.00	7.78	4220.70
0.53	22.56	7.96	4249.86
0.53	23.15	8.15	4283.91
0.54	23.39	8.29	4318.24
0.54	23.50	8.42	4366.14
0.54	23.50	8.51	4423.86
0.54	23.50	8.56	4472.14
0.54	23.50	8.59	4519.98
0.54	23.50	8.62	4567.82
0.54	23.50	8.67	4621.10
0.97	23.66	8.67	4656.25
1.38	23.94	8.67	4688.00
1.75	24.22	8.67	4718.87
1.98	24.25	8.67	4772.53
2.12	24.24	8.66	4820.21
2.24	24.25	8.66	4870.90
2.34	24.25	8.66	4917.64
2.43	24.26	8.66	4965.32
2.50	24.25	8.66	5012.06
2.27	23.86	8.66	5058.09
2.14	23.63	8.66	5091.15
0.54	23.43	8.72	5157.67
0.51	24.37	8.77	5190.35
0.52	25.34	8.85	5221.38
0.52	26.20	8.97	5250.49
0.52	26.89	9.12	5279.60
0.52	27.55	9.29	5309.70
0.52	28.25	9.48	5339.80
0.53	28.91	9.66	5368.91
0.53	29.60	9.88	5402.86
0.53	29.85	10.04	5438.23
0.53	29.99	10.17	5485.24
0.64	30.01	10.28	5539.95
1.46	30.19	10.28	5573.13

APPENDIX L TABLE 1(cont) - ISOTROPIC COMPRESSION/B-VALUE TESTS

u MPa	σ_{cell} MPa	ϵ_v %	Time Second
2.12	30.56	10.28	5606.14
2.59	30.74	10.28	5645.74
2.91	30.75	10.28	5701.38
3.12	30.72	10.28	5755.09
2.89	30.26	10.28	5790.30
2.83	30.06	10.28	5824.41

APPENDIX L TABLE 2 - ISOTROPIC COMPRESSION/B-VALUE TESTS

Test ISO6 — ISOTROPIC COMPRESSION/B-VALUE TEST
Cambria sand — e_i = 0.521 — H/D = 2.50

u MPa	σ_{cell} MPa	ϵ_v %	Time Second
0.51	0.58	0.01	6.65
0.53	0.72	0.45	45.81
0.53	0.91	0.88	85.08
0.53	1.21	1.29	124.35
0.54	1.65	1.67	163.90
0.51	2.16	1.99	208.88
0.52	2.47	2.15	249.97
0.51	2.80	2.30	290.94
0.51	3.15	2.45	335.98
0.51	3.39	2.55	376.95
0.51	3.50	2.62	500.48
0.51	3.50	2.63	681.95
0.56	3.56	2.65	808.72
0.72	3.72	2.65	853.71
1.00	4.02	2.65	902.86
1.18	4.21	2.66	975.70
1.22	4.25	2.66	1095.27
1.20	4.23	2.66	1202.81
1.23	4.27	2.66	1322.00
1.05	4.07	2.66	1385.39
0.63	3.62	2.66	1429.38
0.49	3.48	2.65	1471.78
0.51	4.06	2.78	1520.17
0.51	4.72	2.97	1563.45
0.51	5.42	3.17	1605.53
0.51	6.18	3.37	1647.33
0.52	7.05	3.58	1689.12
0.52	7.95	3.79	1730.92
0.52	8.52	3.95	1781.73
0.52	8.50	4.02	1981.00
0.52	8.50	4.04	2177.85
0.51	8.49	4.06	2367.73
0.52	8.50	4.07	2567.44
0.52	8.50	4.08	2748.42
0.52	8.50	4.08	2933.79
0.51	8.50	4.09	3113.78
0.54	8.53	4.11	3271.47
0.71	8.73	4.11	3316.24
0.88	8.92	4.11	3361.00
1.06	9.10	4.11	3405.76
1.20	9.26	4.11	3463.82
1.22	9.25	4.11	3569.55
1.24	9.26	4.11	3669.35
1.25	9.25	4.11	3771.62
1.26	9.25	4.11	3873.84
1.27	9.25	4.11	3975.07

APPENDIX L TABLE 2(cont) - ISOTROPIC COMPRESSION/B-VALUE TESTS

u MPa	σ_{cell} MPa	ϵ_v %	Time Second
1.28	9.25	4.11	4079.37
1.29	9.25	4.11	4182.63
1.22	9.16	4.11	4253.59
1.06	8.97	4.11	4297.48
0.84	8.70	4.11	4342.24
0.49	8.44	4.11	4385.31
0.50	9.07	4.15	4429.85
0.51	10.09	4.29	4473.90
0.51	10.88	4.45	4514.82
0.50	11.71	4.65	4557.66
0.50	12.42	4.86	4605.50
0.51	12.50	5.02	4773.19
0.51	12.50	5.08	4957.57
0.51	12.50	5.11	5144.93
0.50	12.50	5.14	5330.74
0.50	12.50	5.15	5512.65
0.50	12.50	5.17	5692.15
0.50	12.51	5.18	5882.52
0.50	12.49	5.19	6079.70
0.50	12.50	5.20	6269.53
0.50	12.50	5.21	6458.80
0.50	12.50	5.22	6646.15
0.50	12.50	5.23	6831.52
0.66	12.67	5.24	6885.18
0.84	12.87	5.24	6930.00
1.02	13.07	5.24	6974.77
1.19	13.26	5.24	7017.56
1.24	13.25	5.24	7134.05
1.27	13.25	5.24	7233.80
1.31	13.25	5.24	7335.08
1.33	13.25	5.24	7433.84
1.36	13.25	5.24	7543.03
1.37	13.23	5.24	7655.13
1.17	12.97	5.24	7710.17
0.81	12.52	5.24	7759.10
0.50	12.72	5.26	7806.29
0.51	13.69	5.33	7848.03
0.51	14.69	5.46	7889.94
0.50	15.45	5.63	7930.86
0.51	16.23	5.86	7973.70
0.51	16.96	6.09	8014.62
0.52	17.58	6.32	8057.62
0.49	17.78	6.55	8137.98
0.50	18.00	6.76	8330.27
0.50	18.00	6.84	8515.59
0.50	18.00	6.89	8701.90
0.50	18.00	6.92	8892.71

APPENDIX L TABLE 2(cont) - ISOTROPIC COMPRESSION/B-VALUE TESTS

u MPa	σ_{cell} MPa	ϵ_v %	Time Second
0.50	17.99	6.95	9072.65
0.50	18.00	6.97	9255.06
0.50	18.00	6.99	9441.42
0.50	18.00	7.01	9626.35
0.50	18.00	7.03	9808.26
0.50	18.00	7.04	9995.56
0.50	18.00	7.05	10175.94
0.50	18.00	7.06	10364.11
0.50	18.00	7.07	10546.52
0.50	18.00	7.08	10730.46
0.50	18.00	7.09	10913.42
0.49	17.99	7.10	11094.29
0.49	18.00	7.11	11278.62
0.50	18.01	7.12	11460.09
0.50	18.00	7.12	11645.96
0.49	17.99	7.13	11828.42
0.49	18.00	7.14	12020.28
0.49	18.00	7.14	12203.68
0.49	18.00	7.15	12387.51
0.53	18.03	7.17	12547.78
0.71	18.25	7.17	12592.71
0.89	18.46	7.17	12637.70
1.08	18.67	7.17	12682.63
1.22	18.77	7.17	12764.74
1.24	18.74	7.17	12876.95
1.30	18.76	7.17	12989.16
1.33	18.73	7.17	13107.80
1.39	18.76	7.17	13222.98
1.40	18.73	7.17	13316.91
1.16	18.40	7.17	13363.04
0.88	18.01	7.17	13411.76
0.49	18.10	7.18	13460.37
0.49	19.24	7.23	13503.27
0.49	20.45	7.32	13544.30
0.49	21.44	7.45	13585.33
0.49	22.20	7.64	13626.36
0.50	22.89	7.87	13668.21
0.50	23.62	8.10	13710.06
0.51	24.38	8.34	13750.93
0.51	25.15	8.57	13791.79
0.51	25.80	8.80	13836.50
0.49	26.34	8.98	13879.89
0.49	26.27	9.27	14036.87
0.49	25.95	9.29	14082.73
0.49	25.92	9.31	14121.95
0.49	25.83	9.32	14167.70
0.49	26.35	9.36	14212.52

APPENDIX L TABLE 2(cont) - ISOTROPIC COMPRESSION/B-VALUE TESTS

u MPa	σ_{cell} MPa	ϵ_v %	Time Second
0.50	26.82	9.41	14257.34
0.49	27.25	9.47	14303.31
0.49	26.93	9.50	14355.27
0.49	26.56	9.51	14399.16
0.49	26.10	9.52	14476.22
0.49	26.07	9.52	14522.57

APPENDIX L TABLE 3 - ISOTROPIC COMPRESSION/B-VALUE TESTS

Test ISO7 — ISOTROPIC COMPRESSION/B-VALUE TEST
Cambria sand — e_i = 0.522 — H/D = 2.50

u MPa	σ_{cell} MPa	ϵ_v %	Time Second
0.54	0.62	0.02	6.6
0.56	0.75	0.41	40.2
0.57	0.91	0.80	73.7
0.54	1.13	1.14	107.4
0.55	1.47	1.49	140.9
0.54	1.90	1.82	174.6
0.54	2.25	2.03	211.4
0.55	2.54	2.18	246.3
0.55	2.85	2.33	281.3
0.56	3.19	2.47	316.2
0.55	3.52	2.60	349.9
0.55	3.50	2.64	527.6
0.55	3.50	2.65	689.5
0.55	3.50	2.67	848.9
0.63	3.58	2.67	955.9
0.84	3.80	2.67	994.1
1.04	4.02	2.67	1032.4
1.23	4.23	2.68	1072.5
1.23	4.23	2.68	1158.6
1.24	4.25	2.68	1255.8
1.24	4.25	2.68	1352.0
1.25	4.25	2.68	1438.4
1.24	4.25	2.68	1525.3
1.24	4.25	2.69	1611.6
1.23	4.25	2.69	1697.5
1.12	4.12	2.69	1745.6
0.95	3.95	2.69	1784.0
0.74	3.72	2.69	1821.4
0.52	3.49	2.67	1860.3
0.55	3.83	2.73	1898.2
0.55	4.38	2.88	1935.0
0.56	4.92	3.04	1969.9
0.56	5.47	3.20	2004.8
0.56	6.06	3.37	2042.6
0.56	6.49	3.48	2078.5
0.54	6.98	3.60	2115.5
0.54	7.50	3.73	2150.4
0.54	8.03	3.86	2185.3
0.54	8.53	3.99	2227.2
0.54	8.50	4.06	2405.0
0.54	8.50	4.09	2560.0
0.54	8.50	4.10	2727.3
0.54	8.50	4.13	2883.6
0.54	8.50	4.14	3038.1
0.54	8.50	4.14	3194.1
0.54	8.50	4.15	3352.4

APPENDIX L TABLE 3(cont) - ISOTROPIC COMPRESSION/B-VALUE TESTS

u MPa	σ_{cell} MPa	ϵ_v %	Time Second
0.58	8.55	4.16	3468.8
0.73	8.71	4.15	3507.0
0.88	8.87	4.16	3545.3
1.04	9.03	4.16	3584.4
1.23	9.25	4.16	3622.7
1.25	9.24	4.16	3721.4
1.27	9.24	4.15	3808.7
1.30	9.25	4.15	3895.5
1.31	9.25	4.15	3981.9
1.32	9.25	4.15	4065.7
1.33	9.25	4.15	4151.7
1.35	9.26	4.15	4246.9
1.33	9.23	4.15	4347.2
1.37	9.26	4.15	4445.4
1.36	9.25	4.16	4533.3
1.36	9.23	4.16	4627.1
1.34	9.20	4.16	4704.5
1.20	9.04	4.16	4741.9
0.97	8.77	4.16	4780.7
0.73	8.48	4.16	4820.2
0.54	8.69	4.17	4861.3
0.54	9.49	4.25	4897.3
0.54	10.21	4.37	4933.3
0.54	10.80	4.51	4968.2
0.54	11.38	4.66	5004.0
0.54	11.97	4.82	5039.1
0.55	12.51	4.99	5079.3
0.55	12.50	5.15	5236.7
0.55	12.50	5.21	5391.2
0.55	12.50	5.26	5560.1
0.55	12.50	5.28	5715.5
0.55	12.50	5.30	5873.0
0.55	12.50	5.32	6036.4
0.55	12.50	5.33	6198.2
0.55	12.50	5.34	6361.1
0.54	12.50	5.35	6520.5
0.55	12.50	5.36	6675 0
0.55	12.50	5.37	6829.5
0.60	12.56	5.38	6930.8
0.76	12.72	5.38	6969.3
0.94	12.91	5.38	7008.8
1.17	13.17	5.38	7047.3
1.28	13.25	5.38	7117.7
1.30	13.23	5.38	7213.8
1.38	13.27	5.38	7314.2
1.38	13.23	5.38	7414.1
1.41	13.24	5.38	7514.4

APPENDIX L TABLE 3(cont) - ISOTROPIC COMPRESSION/B-VALUE TESTS

u MPa	σ_{cell} MPa	ϵ_v %	Time Second
1.44	13.25	5.38	7612.3
1.47	13.25	5.38	7707.2
1.49	13.25	5.38	7794.7
1.49	13.24	5.38	7883.7
1.52	13.25	5.38	7973.4
1.54	13.26	5.38	8059.3
1.54	13.24	5.38	8154.6
1.56	13.25	5.38	8242.0
1.46	13.11	5.38	8288.5
1.30	12.91	5.38	8327.1
1.09	12.65	5.38	8364.8
0.52	12.40	5.39	8402.1
0.55	12.99	5.42	8444.1
0.55	13.88	5.50	8480.0
0.55	14.63	5.60	8515.0
0.56	15.23	5.74	8549.9
0.53	15.65	5.90	8588.0
0.53	16.19	6.07	8624.9
0.53	16.68	6.24	8659.8
0.53	17.18	6.41	8694.8
0.53	17.68	6.58	8729.8
0.54	17.87	6.79	8806.6
0.54	18.00	6.98	8984.3
0.54	18.01	7.05	9141.8
0.54	18.00	7.10	9304.1
0.54	17.99	7.14	9464.5
0.54	17.99	7.17	9638.3
0.54	18.00	7.21	9803.2
0.54	18.00	7.23	9970.5
0.54	18.00	7.25	10128.4
0.54	18.00	7.26	10285.3
0.54	18.00	7.27	10441.8
0.64	18.08	7.28	10543.3
0.82	18.26	7.28	10581.8
1.03	18.46	7.28	10621.2
1.28	18.72	7.28	10660.5
1.40	18.75	7.28	10740.7
1.47	18.74	7.28	10828.6
1.54	18.74	7.28	10920.5
1.60	18.75	7.28	11006.4
1.66	18.76	7.28	11092.3
1.72	18.77	7.28	11187.6
1.74	18.75	7.28	11273.0
1.78	18.75	7.28	11359.9
1.82	18.75	7.28	11457.2
1.85	18.75	7.28	11548.1
1.86	18.73	7.28	11625.7

APPENDIX L TABLE 3(cont) - ISOTROPIC COMPRESSION/B-VALUE TESTS

u MPa	σ_{cell} MPa	ϵ_v %	Time Second
1.73	18.54	7.28	11664.2
1.52	18.26	7.28	11702.6
1.33	17.99	7.28	11742.4
0.54	18.30	7.32	11782.9
0.54	19.34	7.38	11820.1
0.54	20.23	7.46	11855.1
0.54	21.05	7.59	11892.1
0.55	21.73	7.75	11927.1
0.55	22.31	7.94	11962.2
0.56	22.88	8.14	11997.3
0.53	23.45	8.35	12037.3
0.54	24.05	8.53	12072.5
0.53	24.65	8.72	12107.5
0.54	25.26	8.90	12142.6
0.53	25.88	9.09	12177.6
0.54	26.41	9.27	12216.0
0.54	26.50	9.56	12360.5
0.54	26.51	9.69	12517.4
0.54	26.50	9.77	12676.8
0.54	26.49	9.82	12843.6
0.54	26.51	9.87	13011.5
0.54	26.51	9.92	13174.9
0.54	26.50	9.95	13344.7
0.54	26.51	9.97	13500.2
0.54	26.51	9.99	13666.5
0.54	26.51	10.01	13830.8
0.52	26.49	10.03	14001.7
0.74	26.64	10.04	14057.9
0.95	26.83	10.04	14096.4
1.16	27.00	10.04	14135.0
1.40	27.22	10.04	14174.5
1.58	27.25	10.04	14273.5
1.73	27.27	10.04	14373.3
1.82	27.23	10.04	14476.8
1.93	27.25	10.04	14577.2
2.02	27.26	10.04	14677.6
2.08	27.24	10.04	14767.1
2.15	27.25	10.04	14866.5
2.21	27.25	10.04	14966.3
2.26	27.24	10.04	15059.8
2.34	27.28	10.04	15162.1
2.37	27.26	10.04	15260.9
2.35	27.18	10.04	15323.1
2.15	26.88	10.04	15363.0
1.92	26.54	10.04	15401.7
0.54	26.34	10.07	15433.9
0.55	27.44	10.11	15479.4

APPENDIX L TABLE 3(cont) - ISOTROPIC COMPRESSION/B-VALUE TESTS

u MPa	σ_{cell} MPa	ϵ_v %	Time Second
0.55	28.63	10.17	15515.5
0.55	29.79	10.26	15551.6
0.56	30.79	10.38	15586.8
0.56	31.53	10.56	15627.0
0.53	32.17	10.73	15666.1
0.53	32.93	10.91	15702.3
0.53	33.65	11.10	15737.4
0.53	34.23	11.29	15776.5
0.53	34.25	11.50	15849.5
0.54	34.50	11.73	16021.7
0.53	34.50	11.83	16178.1
0.54	34.48	11.90	16349.9
0.54	34.50	11.95	16510.7
0.54	34.51	11.99	16667.6
0.54	34.51	12.04	16827.5
0.54	34.49	12.07	16994.3
0.54	34.50	12.09	17151.3
0.54	34.50	12.11	17309.7
0.53	34.50	12.13	17470.0
0.60	34.53	12.15	17617.8
0.84	34.71	12.15	17656.2
1.07	34.90	12.15	17694.6
1.30	35.08	12.15	17733.0
1.51	35.26	12.15	17770.5
1.68	35.25	12.15	17877.1
1.80	35.25	12.15	17964.9
1.88	35.23	12.16	18053.2
1.99	35.27	12.16	18149.0
2.12	35.27	12.16	18249.2
2.20	35.24	12.16	18346.4
2.30	35.24	12.16	18445.6
2.39	35.26	12.16	18533.0
2.47	35.26	12.16	18623.4
2.53	35.25	12.16	18716.6
2.59	35.24	12.16	18804.1
2.49	35.06	12.16	18844.2
2.31	34.77	12.16	18883.7
2.15	34.50	12.16	18923.1
0.54	34.84	12.20	18964.8
0.54	36.08	12.24	19001.8
0.54	37.26	12.30	19036.8
0.54	38.35	12.38	19077.7
0.54	38.17	12.42	19120.5
0.54	38.04	12.44	19156.9
0.54	37.93	12.46	19193.3
0.54	37.85	12.48	19229.7
0.54	37.77	12.49	19266.1

APPENDIX L TABLE 3(cont) - ISOTROPIC COMPRESSION/B-VALUE TESTS

u MPa	σ_{cell} MPa	ϵ_v %	Time Second
0.54	37.70	12.51	19302.5
0.54	37.64	12.52	19338.9
0.54	37.58	12.53	19375.3
0.54	37.54	12.54	19411.7
0.54	37.49	12.54	19448.0
0.54	37.44	12.55	19484.4
0.54	37.41	12.56	19520.8
0.54	37.37	12.57	19557.2
0.54	37.33	12.57	19593.6
0.54	37.30	12.58	19630.0
0.54	37.27	12.59	19666.4
0.54	37.24	12.59	19702.8
0.54	37.21	12.60	19739.2
0.54	37.17	12.60	19788.4
0.54	37.15	12.61	19825.5
0.54	37.12	12.61	19862.5
0.54	37.10	12.62	19899.7
0.54	37.15	12.62	19936.8
0.55	38.14	12.65	19973.7
0.54	38.08	12.66	20002.8
0.55	38.41	12.68	20037.9
0.55	39.59	12.73	20077.1
0.55	40.71	12.80	20112.2
0.55	41.72	12.89	20147.2
0.52	42.64	13.02	20188.0
0.53	43.52	13.16	20224.2
0.53	44.41	13.32	20260.5
0.53	45.30	13.49	20295.6
0.53	46.19	13.65	20330.6
0.53	47.14	13.83	20366.5
0.53	48.11	14.00	20401.6
0.54	49.19	14.18	20437.6
0.54	50.29	14.36	20474.7
0.54	51.23	14.52	20509.9
0.54	52.24	14.70	20549.0
0.55	52.54	14.94	20648.5
0.55	52.50	15.10	20811.9
0.55	52.50	15.19	20966.8
0.56	52.50	15.25	21124.7
0.52	52.50	15.30	21281.2
0.53	52.50	15.35	21434.7
0.53	52.50	15.38	21590.6
0.53	52.50	15.41	21744.1
0.53	52.50	15.43	21903.1
0.53	52.49	15.45	22068.8
0.53	52.50	15.47	22229.7
0.55	52.50	15.49	22393.1

APPENDIX L TABLE 3(cont) - ISOTROPIC COMPRESSION/B-VALUE TESTS

u MPa	σ_{cell} MPa	ϵ_v %	Time Second
0.93	52.83	15.49	22434.5
1.37	53.28	15.49	22474.9
1.71	53.25	15.49	22584.0
1.96	53.23	15.49	22683.3
2.16	53.25	15.49	22776.3
2.33	53.25	15.49	22863.3
2.47	53.25	15.49	22952.8
2.61	53.25	15.49	23040.3
2.75	53.27	15.49	23133.1
2.82	53.16	15.49	23243.8
3.00	53.25	15.49	23348.1
3.09	53.24	15.49	23436.5
3.11	53.16	15.49	23511.6
2.97	52.88	15.49	23550.5
2.81	52.59	15.49	23589.2
0.52	52.35	15.52	23624.9
0.53	53.39	15.55	23669.7
0.53	54.82	15.58	23705.8
0.53	56.19	15.63	23740.9
0.53	57.51	15.68	23776.1
0.53	58.87	15.75	23812.2
0.53	60.21	15.84	23848.3
0.53	61.40	15.95	23890.0
0.53	61.50	16.18	24070.4
0.53	61.50	16.29	24227.9
0.53	61.50	16.35	24382.4
0.53	61.50	16.40	24539.8
0.53	61.50	16.45	24698.2
0.53	61.49	16.50	24855.1
0.53	61.50	16.53	25011.5
0.53	61.50	16.55	25166.9
0.53	61.50	16.57	25326.3
0.53	61.51	16.59	25484.6
0.53	61.50	16.61	25640.0
0.53	61.50	16.63	25795.9
0.61	61.53	16.64	25919.4
0.95	61.82	16.64	25958.8
1.29	62.12	16.64	25997.2
1.65	62.25	16.64	26077.4
1.92	62.25	16.64	26169.1
2.15	62.25	16.64	26261.4
2.33	62.25	16.64	26347.3
2.50	62.25	16.64	26433.7
2.65	62.25	16.64	26520.0
2.78	62.25	16.64	26605.9
2.91	62.25	16.64	26691.8
3.03	62.25	16.64	26775.6

APPENDIX L TABLE 3(cont) - ISOTROPIC COMPRESSION/B-VALUE TESTS

u MPa	σ_{cell} MPa	ϵ_v %	Time Second
3.13	62.24	16.64	26857.5
3.02	61.99	16.64	26898.6
2.83	61.61	16.64	26937.2
0.53	61.36	16.67	26970.1
0.53	62.72	16.69	27015.7
0.53	64.18	16.73	27051.7
0.53	65.59	16.76	27086.8
0.53	66.95	16.81	27121.8
0.53	68.27	16.87	27156.9
0.54	69.59	16.94	27198.3
0.54	69.50	17.10	27386.5
0.54	69.51	17.17	27540.8
0.54	69.50	17.25	27714.1
0.54	69.50	17.29	27870.0
0.54	69.50	17.33	28026.9
0.54	69.50	17.35	28183.3
0.54	69.50	17.38	28341.7
0.54	69.50	17.40	28497.0
0.54	69.50	17.42	28654.5
0.54	69.51	17.44	28812.8
0.54	69.50	17.46	28968.2
0.87	69.72	17.47	29023.6
1.23	70.02	17.47	29062.0
1.53	70.26	17.47	29097.2
1.93	70.26	17.47	29206.7
2.19	70.24	17.47	29294.6
2.41	70.24	17.47	29380.4
2.63	70.25	17.47	29471.3
2.81	70.23	17.47	29568.0
3.03	70.28	17.47	29665.7
3.16	70.25	17.47	29757.1
3.30	70.23	17.47	29847.9
3.45	70.26	17.47	29945.1
3.59	70.25	17.47	30045.3
3.68	70.25	17.47	30124.6
3.54	69.93	17.47	30166.7
3.37	69.58	17.47	30205.3
0.54	69.34	17.50	30240.2
0.51	67.81	17.49	30287.3
0.51	66.31	17.47	30320.8
0.51	64.82	17.46	30354.3
0.50	63.42	17.44	30388.8
0.50	62.12	17.42	30422.3
0.50	60.84	17.41	30455.9
0.50	59.56	17.39	30489.4
0.50	58.28	17.37	30522.9
0.50	57.01	17.36	30556.4

APPENDIX L TABLE 3(cont) - ISOTROPIC COMPRESSION/B-VALUE TESTS

u MPa	σ_{cell} MPa	ϵ_v %	Time Second
0.50	55.74	17.34	30589.9
0.50	54.48	17.32	30623.4
0.50	53.24	17.30	30656.9
0.50	51.99	17.28	30690.4
0.50	50.69	17.26	30724.9
0.50	49.29	17.24	30758.4
0.50	47.90	17.22	30791.9
0.50	46.51	17.19	30825.4
0.50	45.15	17.17	30859.0
0.50	43.68	17.15	30893.4
0.50	42.25	17.12	30927.0
0.50	40.71	17.09	30961.4
0.50	39.22	17.06	30994.9
0.50	37.74	17.03	31028.4
0.50	36.28	17.00	31062.0
0.50	34.81	16.97	31095.5
0.50	33.36	16.94	31129.0
0.50	31.92	16.91	31162.5
0.50	30.41	16.87	31197.0
0.50	28.93	16.84	31230.5
0.50	27.45	16.80	31264.0
0.50	25.89	16.76	31298.5
0.50	24.38	16.72	31332.0
0.50	22.89	16.67	31365.5
0.50	21.33	16.62	31400.0
0.50	19.79	16.57	31433.5
0.50	18.28	16.52	31467.0
0.50	16.79	16.46	31500.5
0.49	15.32	16.40	31534.0
0.49	13.87	16.34	31567.7
0.49	12.45	16.27	31601.3
0.49	11.07	16.20	31634.9
0.49	9.73	16.12	31668.6
0.49	8.42	16.03	31702.2
0.49	7.19	15.94	31737.8
0.49	6.09	15.85	31771.4
0.49	5.07	15.74	31807.0
0.49	4.18	15.63	31841.6
0.48	3.41	15.52	31875.3
0.48	2.73	15.39	31909.9
0.47	2.17	15.26	31944.5
0.50	1.71	15.10	31979.3
0.50	1.35	14.93	32013.9
0.50	1.08	14.72	32048.5
0.50	0.90	14.48	32084.3
0.50	0.78	14.25	32118.9
0.50	0.71	13.99	32153.5

APPENDIX L TABLE 3(cont) - ISOTROPIC COMPRESSION/B-VALUE TESTS

u MPa	σ_{cell} MPa	ϵ_v %	Time Second
0.50	0.66	13.71	32188.9
0.49	0.63	13.46	32222.4
0.47	0.54	12.90	32257.8
0.50	0.53	11.85	32299.9
0.50	0.53	11.81	32336.3

APPENDIX M

APPENDIX M TABLE 1 - ONE DIMENSIONAL COMPRESSION TESTS

Test 1DCAM1 ONE-DIMENSIONAL COMPRESSION TEST
Cambria sand W = 156.0 gm V = 89.77 cm^3
e_i = 0.548 H/D = 2.07

ϵ_a %	σ_a Mpa	e	Ko Total	Ko Incre.
0.00	0.00	0.548		
0.00	0.00	0.548		
0.00	0.09	0.548		
0.06	0.54	0.547		
0.21	1.38	0.545		
0.37	2.35	0.542		
0.56	3.61	0.539		
0.85	5.52	0.535		
1.15	7.34	0.530		
1.35	8.60	0.527	0.46	0.41
1.66	10.43	0.522		
2.29	14.05	0.512		
2.93	17.57	0.503		
3.47	20.26	0.494		
3.69	21.40	0.491	0.43	0.39
4.14	23.70	0.484		
4.69	26.56	0.475		
5.36	29.98	0.465		
5.81	32.24	0.458		
6.15	34.03	0.453	0.41	0.37
8.79	47.55	0.412	0.40	0.36
11.32	63.30	0.373	0.39	0.38
13.78	83.49	0.335	0.39	0.36
16.14	110.47	0.298	0.38	0.37
18.29	146.01	0.265	0.38	0.38
19.92	183.43	0.240	0.38	0.39
21.42	233.63	0.216	0.38	0.38
22.82	298.00	0.195	0.38	0.39
23.75	350.23	0.180	0.38	0.37
24.45	401.30	0.169	0.38	0.38
25.03	449.67	0.161	0.38	0.39
25.47	493.55	0.154	0.38	0.38
25.90	540.40	0.147	0.38	0.36
26.31	590.39	0.141	0.38	0.39
26.64	631.39	0.136	0.38	0.37
26.93	673.19	0.131	0.38	0.39
27.20	714.72	0.127	0.38	0.38
27.46	757.14	0.123	0.38	0.39
27.69	793.21	0.119	0.38	0.39
27.88	825.57	0.116	0.38	0.28
27.91	787.24	0.116	0.38	0.29
27.90	743.55	0.116	0.39	0.28
27.88	696.56	0.116	0.40	0.32
27.86	654.43	0.117	0.40	0.29
27.82	568.08	0.117	0.42	0.29

APPENDIX M TABLE 1(cont) - ONE DIMENSIONAL COMPRESSION TESTS

ϵ_a %	σ_a Mpa	e	Ko Total	Ko Incre.
27.78	484.19	0.118	0.44	0.30
27.73	402.60	0.119	0.47	0.29
27.64	290.56	0.120	0.54	0.30
27.55	181.00	0.122	0.69	0.33
27.43	87.45	0.123	1.08	0.46
27.12	30.24	0.128	2.27	0.89

APPENDIX M TABLE 2 - ONE DIMENSIONAL COMPRESSION TESTS

Test 1DCAM2 ONE-DIMENSIONAL COMPRESSION TEST
Cambria sand W = 156.0 gm V = 99.62 cm^3
e_i = 0.713 H/D = 2.29

ϵ_a %	σ_a Mpa	e	Ko Total	Ko Incre.
0.00	0.00	0.713	NO READINGS	
0.00	0.10	0.713		
0.09	0.45	0.711		
0.29	1.02	0.708		
0.61	2.10	0.702		
0.98	3.33	0.696		
1.47	4.86	0.688		
1.85	5.92	0.681		
1.98	6.27	0.679		
2.10	6.61	0.677		
2.60	8.00	0.668		
3.64	10.49	0.650		
4.68	12.93	0.633		
5.58	15.10	0.617		
7.03	18.40	0.592		
7.55	19.75	0.584		
8.07	21.01	0.575		
8.98	23.52	0.559		
9.88	25.93	0.544		
10.27	27.12	0.537		
13.20	36.86	0.487		
16.01	49.17	0.439		
18.82	64.73	0.390		
21.56	88.75	0.343		
23.61	114.17	0.308		
25.52	148.32	0.276		
27.12	186.61	0.248		
28.36	231.16	0.227		
28.97	257.44	0.217		
29.44	278.97	0.209		
30.64	351.97	0.188		
30.93	372.26	0.183		
31.48	418.20	0.174		
31.89	454.71	0.167		
32.26	494.60	0.160		
32.61	536.31	0.154		
32.87	567.02	0.150		
33.12	601.24	0.145		
33.37	637.01	0.141		
33.60	674.05	0.137		
33.82	707.57	0.134		
33.98	734.52	0.131		
34.15	763.60	0.128		
34.31	793.38	0.125		
34.46	823.46	0.122		

APPENDIX M TABLE 2(cont) - ONE DIMENSIONAL COMPRESSION TESTS

ϵ_a %	σ_a Mpa	e	Ko Total	Ko Incre.
34.61	850.36	0.120	NO READINGS	
34.63	813.26	0.120		
34.62	754.41	0.120		
34.60	688.56	0.120		
34.57	618.26	0.121		
34.54	555.16	0.121		
34.52	488.05	0.122		
34.49	422.32	0.122		
34.46	364.93	0.123		
34.41	303.85	0.123		
34.37	250.27	0.124		
34.28	142.06	0.126		
34.21	98.19	0.127		
34.07	59.62	0.129		
33.98	32.16	0.131		
33.73	11.12	0.135		

APPENDIX M TABLE 3 - ONE DIMENSIONAL COMPRESSION TESTS

Test 1DCAM3 ONE-DIMENSIONAL COMPRESSION TEST
Cambria sand W = 150.0 gm V = 91.50 cm^3
e_i = 0.641 H/D = 2.11

ϵ_a %	σ_a Mpa	e	Ko Total	Ko Incre.
0.00	0.00	0.641		
0.00	0.04	0.641		
0.08	0.65	0.640		
0.09	0.74	0.640		
0.20	1.20	0.638		
0.62	2.48	0.631		
1.10	4.22	0.623	0.45	0.44
1.27	4.83	0.620		
1.76	6.59	0.612		
2.09	7.81	0.607		
2.26	8.35	0.604		
2.75	9.99	0.596		
2.92	10.46	0.593	0.44	0.38
4.11	14.41	0.574		
4.80	16.51	0.562	0.42	0.36
5.83	19.58	0.545		
6.70	22.17	0.531	0.40	0.39
6.88	22.80	0.528		
8.62	28.34	0.500	0.40	0.47
10.37	34.16	0.471	0.41	0.45
12.27	41.75	0.440	0.42	0.36
14.15	50.65	0.409	0.41	0.43
16.01	61.77	0.378	0.41	0.37
17.84	75.68	0.348	0.40	0.41
19.62	93.83	0.319	0.41	0.34
21.00	111.46	0.296	0.39	0.43
22.17	130.56	0.277	0.40	0.39
23.12	149.47	0.262	0.40	0.41
24.04	171.18	0.246	0.40	0.39
24.70	189.29	0.236	0.40	0.41
25.30	207.97	0.226	0.40	0.38
25.77	224.82	0.218	0.40	0.41
26.25	243.09	0.210	0.40	0.38
26.71	262.60	0.203	0.40	0.41
27.17	283.39	0.195	0.40	0.38
27.61	305.64	0.188	0.40	0.43
27.95	324.44	0.182	0.40	0.40
28.57	363.03	0.172	0.40	0.45
28.87	383.41	0.167	0.40	0.31
29.16	404.89	0.163	0.40	0.41
29.41	425.05	0.158	0.40	0.41
29.62	442.69	0.155	0.40	0.36
29.83	460.78	0.152	0.40	0.43
30.03	479.35	0.148	0.40	0.40
30.23	498.27	0.145	0.40	0.41
30.41	517.83	0.142	0.40	0.43

APPENDIX M TABLE 3(cont) - ONE DIMENSIONAL COMPRESSICN TESTS

ϵ_a %	σ_a Mpa	e	Ko Total	Ko Incre.
30.59	536.12	0.139	0.40	0.45
30.77	556.82	0.136	0.40	0.37
30.96	577.80	0.133	0.40	0.41
31.15	599.20	0.130	0.40	0.41
31.33	621.09	0.127	0.40	0.42
31.50	643.42	0.124	0.40	0.41
31.67	666.15	0.121	0.40	0.44
31.85	689.31	0.118	0.40	0.40
32.01	712.89	0.116	0.40	0.38
32.17	736.93	0.113	0.40	0.41
32.31	756.64	0.111	0.40	0.42
32.43	775.11	0.109	0.40	0.48
32.54	791.95	0.107	0.40	0.38
32.66	810.63	0.105	0.40	0.30
32.71	819.12	0.104	0.40	0.27
32.74	808.26	0.104	0.40	0.23
32.72	751.77	0.104	0.42	0.28
32.68	694.59	0.105	0.43	0.25
32.65	633.74	0.105	0.45	0.26
32.60	574.66	0.106	0.46	0.27
32.56	521.28	0.107	0.48	0.25
32.51	464.74	0.108	0.51	0.24
32.46	410.25	0.108	0.55	0.25
32.40	363.04	0.109	0.59	0.27
32.31	315.01	0.111	0.64	0.28
32.20	270.22	0.113	0.69	0.34
32.08	230.95	0.115	0.75	0.35
31.96	181.23	0.117	0.87	0.36
31.81	138.24	0.119	1.02	0.44
31.65	92.76	0.122	1.31	0.55
31.43	53.77	0.125	1.86	0.66
31.19	23.40	0.129	3.42	1.05
30.81	5.12	0.135	11.86	2.59

APPENDIX M TABLE 4 - ONE DIMENSIONAL COMPRESSION TESTS

Test 1DQ1 ONE-DIMENSIONAL COMPRESSION TEST
Quartz sand W = 138.0 gm V = 86.87 cm^3
e_i = 0.679 H/D = 2.01

ϵ_a %	σ_a Mpa	e	Ko Total	Ko Incre.
0.00	0.00	0.679		
	0.15	0.679		
	0.24	0.678		
0.27	0.80	0.675	0.76	0.52
	1.01	0.674		
	2.15	0.668		
1.04	3.17	0.662	0.58	0.43
2.13	5.99	0.644	0.51	0.50
3.13	8.44	0.628	0.51	0.50
4.25	10.88	0.609	0.51	0.45
7.40	17.69	0.557	0.49	0.47
10.65	25.71	0.504	0.48	0.30
13.88	36.52	0.451	0.43	0.44
16.00	46.83	0.416	0.43	0.38
18.10	60.58	0.382	0.42	0.49
20.15	79.42	0.349	0.44	0.32
23.11	123.83	0.301	0.39	0.37
24.95	167.03	0.273	0.39	0.37
26.67	226.41	0.247	0.38	0.37
28.07	291.09	0.226	0.38	0.38
29.48	379.73	0.205	0.38	0.38
30.53	462.84	0.190	0.38	0.37
31.32	535.63	0.179	0.38	0.37
32.02	607.74	0.170	0.38	0.34
32.71	685.23	0.160	0.37	0.39
33.20	745.57	0.154	0.37	0.34
33.72	809.25	0.147	0.37	0.30
33.74	798.08	0.147	0.37	0.27
33.68	770.04	0.147	0.38	0.32
33.61	735.59	0.147	0.38	0.27
33.42	657.64	0.148	0.39	0.31
33.10	530.83	0.149	0.41	0.29
32.73	397.18	0.151	0.45	0.30
32.36	280.26	0.153	0.51	0.35
31.98	179.16	0.155	0.61	0.35
31.27	59.06	0.160	1.12	0.62
30.05	4.42	0.175	7.38	2.03

APPENDIX M TABLE 5 - ONE DIMENSIONAL COMPRESSION TESTS

Test 1DQ2 — ONE-DIMENSIONAL COMPRESSION TEST
Quartz sand — W = 134.0 gm — V = 96.43 cm^3
e_i = 0.901 — H/D = 2.22

ϵ_a %	σ_a Mpa	e	Ko Total	Ko Incre.
0.00	0.00	0.901		
0.17	0.14	0.898		
	0.41	0.895		
0.51	0.60	0.892		
1.71	1.07	0.882		
2.73	1.74	0.869	0.87	0.60
3.75	3.28	0.850	0.74	0.22
6.46	8.81	0.778	0.42	0.35
10.03	14.03	0.711	0.39	0.29
13.76	20.48	0.640	0.36	0.39
17.51	29.31	0.568	0.37	0.40
21.19	41.52	0.498	0.38	0.38
24.85	60.73	0.429	0.38	0.35
27.69	85.29	0.375	0.37	0.39
29.85	115.39	0.334	0.37	0.36
31.60	152.67	0.300	0.37	0.39
32.89	191.66	0.276	0.38	0.36
33.91	232.08	0.256	0.37	0.39
34.77	275.45	0.240	0.38	0.34
35.53	322.54	0.226	0.37	0.40
36.09	364.00	0.215	0.37	0.39
36.62	409.85	0.205	0.38	0.37
37.09	457.19	0.196	0.37	0.37
37.56	510.35	0.187	0.37	0.34
37.92	554.46	0.180	0.37	0.39
38.24	598.87	0.174	0.37	0.35
38.55	645.09	0.168	0.37	0.40
38.83	690.79	0.163	0.37	0.35
39.10	740.35	0.158	0.37	0.37
39.33	786.68	0.153	0.37	0.36
39.51	824.34	0.150	0.37	0.35
39.59	841.70	0.149	0.37	-1.44
39.62	845.27	0.148	0.36	0.25
39.63	806.49	0.148	0.37	0.31
39.62	771.96	0.148	0.37	0.33
39.62	745.55	0.148	0.37	0.30
39.60	683.84	0.148	0.38	0.31
39.57	627.59	0.149	0.39	0.26
39.54	567.60	0.149	0.40	0.33
39.51	514.11	0.150	0.41	0.29
39.48	456.91	0.151	0.42	0.31
39.45	403.92	0.151	0.43	0.27
39.39	337.23	0.152	0.47	0.32
39.32	278.92	0.154	0.50	0.31
39.24	222.72	0.155	0.54	0.30
39.17	165.76	0.157	0.63	0.33

APPENDIX M TABLE 5(cont) - ONE DIMENSIONAL COMPRESSION TESTS

ϵ_a %	σ_a Mpa	e	Ko Total	Ko Incre.
39.06	111.67	0.159	0.77	0.34
38.89	60.32	0.162	1.13	0.54
38.61	29.65	0.167	1.75	0.56
38.26	10.28	0.174	4.00	1.06
37.79	1.99	0.183	16.23	2.53

APPENDIX M TABLE 6 - ONE DIMENSIONAL COMPRESSION TESTS

Test 1DQ3 — ONE-DIMENSIONAL COMPRESSION TEST
Quartz sand — W = 130.0 gm — V = 84.56 cm^3
e_i = 0.724 — H/D = 1.95

ϵ_a %	σ_a Mpa	e	Ko Total	Ko Incre.
0.00	0.00	0.724		
0.00	0.01	0.724		
0.10	0.56	0.722		
0.18	0.85	0.721		
0.22	1.02	0.720		
0.67	2.71	0.712		
1.19	4.31	0.703	0.57	0.41
1.89	6.09	0.691		
2.63	7.72	0.678		
3.19	8.86	0.669	0.49	0.41
4.32	10.93	0.649		
5.26	12.67	0.633	0.46	0.43
7.34	16.36	0.597	0.45	0.40
11.70	25.40	0.522	0.43	0.34
13.76	31.23	0.486	0.42	0.28
15.83	38.31	0.451	0.39	0.39
17.88	47.72	0.415	0.39	0.40
19.90	60.17	0.381	0.39	0.39
21.87	77.43	0.347	0.39	0.44
23.60	98.63	0.317	0.40	0.38
25.07	123.17	0.292	0.40	0.40
26.40	153.18	0.269	0.40	0.37
27.26	176.93	0.254	0.39	0.41
27.94	200.24	0.242	0.40	0.37
28.58	226.47	0.231	0.39	0.37
29.21	255.68	0.220	0.39	0.37
29.75	282.88	0.211	0.39	0.37
30.20	308.12	0.203	0.39	0.43
30.58	333.10	0.197	0.39	0.38
30.95	357.92	0.190	0.39	0.33
31.25	380.15	0.185	0.39	0.42
31.54	403.72	0.180	0.39	0.35
31.77	421.95	0.176	0.39	0.34
31.97	441.53	0.173	0.38	0.40
32.18	460.32	0.169	0.38	0.37
32.38	480.57	0.166	0.38	0.34
32.57	502.22	0.162	0.38	0.40
32.76	522.97	0.159	0.38	0.40
32.93	543.45	0.156	0.38	0.37
33.11	565.76	0.153	0.38	0.39
33.28	583.25	0.150	0.38	0.39
33.40	600.49	0.148	0.38	0.39
33.55	616.00	0.145	0.38	0.32
33.67	634.80	0.143	0.38	0.40
33.81	651.80	0.141	0.38	0.32
33.92	670.93	0.139	0.38	0.39

APPENDIX M TABLE 6(cont) - ONE DIMENSIONAL COMPRESSION TESTS

ϵ_a %	σ_a Mpa	e	Ko Total	Ko Incre.
34.05	688.64	0.137	0.38	0.35
34.17	708.26	0.135	0.38	0.36
34.28	727.48	0.133	0.38	0.43
34.39	745.12	0.131	0.38	0.32
34.50	764.16	0.129	0.38	0.42
34.62	783.34	0.127	0.38	0.37
34.73	803.80	0.125	0.38	0.41
34.82	819.81	0.124	0.38	0.22
34.89	791.23	0.122	0.39	0.29
34.87	729.67	0.123	0.39	0.25
34.83	664.43	0.123	0.41	0.28
34.79	606.25	0.124	0.42	0.25
34.75	543.97	0.125	0.44	0.20
34.69	484.39	0.126	0.47	0.24
34.63	431.53	0.127	0.50	0.22
34.55	377.82	0.128	0.54	0.29
34.44	332.13	0.130	0.57	0.30
34.30	285.40	0.133	0.61	0.33
34.16	243.86	0.135	0.66	0.34
34.02	201.35	0.137	0.73	0.46
33.88	164.11	0.140	0.79	0.37
33.71	126.67	0.143	0.91	0.46
33.55	93.48	0.145	1.08	0.59
33.36	67.82	0.149	1.26	0.61
33.10	41.30	0.153	1.67	0.88
32.83	21.63	0.158	2.40	1.12
32.39	6.87	0.165	5.14	1.75
31.78	0.92	0.176	26.97	3.53

APPENDIX M TABLE 7 - ONE DIMENSIONAL COMPRESSION TESTS

Test 1DSAC3 ONE-DIMENSIONAL COMPRESSION TEST
Sacramento River sand W = 156.0 gm V = 89.77 cm^3
e_i = 0.728 H/D = 2.07

ϵ_a %	σ_a Mpa	e	Ko Total	Ko Incre.
0.00	0.00	0.728		
0.11	0.14	0.726		
1.20	0.60	0.707		
1.34	0.66	0.705		
2.04	1.16	0.693		
2.27	1.34	0.689		
2.52	1.60	0.684	0.57	0.294
2.92	2.06	0.678		
3.86	3.44	0.661		
4.78	5.24	0.645		
5.44	6.79	0.634	0.36	0.206
6.23	8.97	0.620		
6.89	11.01	0.609		
7.67	13.73	0.595		
8.19	15.70	0.587	0.27	0.228
8.84	18.40	0.575		
9.62	21.90	0.562		
10.51	26.32	0.546		
11.02	29.14	0.538	0.25	0.346
13.79	47.83	0.490	0.29	0.304
15.99	68.17	0.452	0.29	0.352
17.84	91.94	0.420	0.31	0.424
19.30	117.24	0.395	0.33	0.283
20.57	143.37	0.373	0.32	0.435
21.60	167.58	0.355	0.34	0.383
22.63	194.53	0.337	0.35	0.392
23.38	217.61	0.324	0.35	0.388
24.13	243.55	0.311	0.35	0.390
24.85	272.74	0.299	0.36	0.385
25.42	298.20	0.289	0.36	0.394
25.92	323.88	0.280	0.36	0.362
26.41	351.08	0.272	0.36	0.407
26.88	380.07	0.264	0.37	0.378
27.34	410.56	0.256	0.37	0.369
27.79	442.76	0.248	0.37	0.385
28.16	471.09	0.241	0.37	0.388
28.48	497.49	0.236	0.37	0.371
28.79	525.13	0.231	0.37	0.392
29.09	553.83	0.225	0.37	0.360
29.39	583.35	0.220	0.37	0.386
29.67	612.59	0.215	0.37	0.380
29.95	644.12	0.210	0.37	0.356
30.19	670.40	0.206	0.37	0.367
30.39	694.91	0.203	0.37	0.412
30.58	719.94	0.200	0.37	0.355
30.77	745.36	0.196	0.37	0.499

APPENDIX M TABLE 7(cont) - ONE DIMENSIONAL COMPRESSION TESTS

ϵ_a %	σ_a Mpa	e	Ko Total	Ko Incre.
30.94	769.93	0.193	0.38	0.259
31.12	796.00	0.190	0.37	0.386
31.25	817.63	0.188	0.37	2.217
31.28	815.58	0.188	0.37	0.322
31.28	772.94	0.187	0.37	0.260
31.28	721.40	0.187	0.38	0.309
31.27	671.72	0.188	0.38	0.298
31.26	626.74	0.188	0.39	0.294
31.24	578.97	0.188	0.40	0.301
31.23	535.47	0.188	0.40	0.295
31.22	488.95	0.189	0.42	0.288
31.21	443.55	0.189	0.43	0.350
31.19	397.75	0.189	0.44	0.299
31.16	344.17	0.190	0.46	0.330
31.12	296.67	0.190	0.48	0.310
31.07	247.17	0.191	0.51	0.309
31.04	199.58	0.192	0.56	0.360
30.98	156.02	0.193	0.62	0.316
30.91	105.37	0.194	0.76	0.417
30.81	66.24	0.196	0.97	0.401
30.58	28.77	0.200	1.71	0.447
30.20	8.24	0.206	4.85	1.002

APPENDIX N

APPENDIX N TABLE 1 - DRAINED TRIAXIAL COMPRESSION LOADING/UNLOADING TEST

Test CDLU3 DRAINED TRIAXIAL COMPRESSION TEST
LOAD/UNLOAD AT FIVE DIFFERENT CONFINING PRESSURES
σ_{cell} = 4.0, 8.0 16.0, 32.0 and 64.0 MPa
e_i = 0.519 H/D = 1.89
Cambria Sand NO LUBRICATED ENDS

LOAD/UNLOAD CYCLE AT σ_{cell} = 4.0 MPa

$\sigma_1 - \sigma_3$ MPa	ϵ_1 %	ϵ_v %	
0.09	0.06	0.00	START 1ST LOADING
0.30	0.12	0.02	
0.64	0.18	0.04	
0.83	0.21	0.05	
1.06	0.26	0.07	
1.30	0.31	0.10	
1.51	0.35	0.12	
1.78	0.40	0.15	
1.98	0.43	0.17	
2.21	0.48	0.19	
2.43	0.52	0.22	
2.64	0.57	0.25	
2.82	0.60	0.27	
2.97	0.64	0.29	
3.13	0.68	0.32	
3.28	0.72	0.34	
3.41	0.76	0.36	
3.53	0.79	0.38	
3.66	0.83	0.41	
3.76	0.83	0.43	
3.88	0.87	0.45	
3.98	0.90	0.47	
4.10	0.94	0.49	
4.19	0.99	0.52	
4.29	1.02	0.54	
4.40	1.07	0.56	
4.50	1.11	0.59	
4.58	1.15	0.61	
4.66	1.19	0.63	
4.74	1.22	0.65	
4.84	1.27	0.67	
4.92	1.32	0.70	
4.99	1.36	0.72	
5.05	1.40	0.74	
5.11	1.43	0.75	
5.16	1.47	0.77	
5.23	1.51	0.79	
5.30	1.56	0.81	
5.36	1.59	0.83	
5.42	1.63	0.85	
5.47	1.67	0.87	
5.53	1.71	0.88	

APPENDIX N TABLE 1(cont) - DRAINED TRIAXIAL COMPRESSION LOADING/UNLOADING TEST

LOAD/UNLOAD CYCLE AT σ_{cell} = 4.0 MPa

$\sigma_1 - \sigma_3$ MPa	ϵ_1 %	ϵ_v %	
5.58	1.74	0.90	
5.63	1.78	0.92	
5.68	1.82	0.93	
5.71	1.85	0.95	
5.76	1.89	0.96	
5.81	1.93	0.98	
5.85	1.96	1.00	
5.88	2.00	1.01	
5.92	2.04	1.03	
5.98	2.08	1.04	
6.01	2.11	1.06	
6.06	2.15	1.07	
6.10	2.19	1.09	
6.13	2.23	1.10	
6.17	2.26	1.12	
6.21	2.30	1.13	
6.25	2.34	1.15	
6.29	2.38	1.16	
6.32	2.42	1.18	
6.36	2.45	1.19	
6.38	2.49	1.20	
6.42	2.53	1.22	
6.46	2.57	1.23	
6.49	2.60	1.25	
6.34	2.64	1.26	START 1ST UNLOADING
5.99	2.61	1.25	
5.06	2.56	1.25	
4.53	2.52	1.25	
4.01	2.52	1.24	
3.32	2.46	1.22	
2.82	2.41	1.22	
2.31	2.37	1.21	
1.90	2.33	1.20	
1.56	2.29	1.20	
1.22	2.26	1.19	
0.91	2.22	1.19	
0.63	2.18	1.19	
0.37	2.15	1.19	
0.15	2.12	1.19	
0.00	2.08	1.19	
0.00	0.00	1.19	
0.00	0.00	1.19	
0.00	0.00	1.19	
0.00	0.00	1.19	
0.00	0.00	1.19	
0.00	0.00	1.19	
0.00	0.00	1.19	

APPENDIX N TABLE 1(cont) - DRAINED TRIAXIAL COMPRESSION LOADING/UNLOADING TEST

LOAD/UNLOAD CYCLE AT σ_{cell} 4.0 MPa

σ_1 -σ_3 MPa	ϵ_1 %	ϵ_v %	
0.00	0.00	1.19	
0.00	0.00	1.19	
0.00	0.00	1.19	
0.00	0.00	1.19	
0.00	0.00	1.19	
0.00	0.00	1.19	
0.00	0.00	1.19	
0.00	0.00	1.19	
0.00	0.00	1.19	
0.00	0.00	1.19	
0.00	0.00	1.19	
0.00	0.00	1.19	
0.00	0.00	1.19	
0.00	0.00	1.19	
0.00	0.00	1.19	
0.00	0.00	1.19	
0.00	0.00	1.19	
0.00	0.00	1.19	
0.00	0.00	1.19	
0.00	0.00	1.19	
0.00	0.00	1.19	
0.00	0.00	1.19	
0.00	0.00	1.19	
0.00	0.00	1.19	
0.00	0.00	1.19	
0.00	0.00	1.19	
0.00	0.00	1.22	
0.00	0.00	1.23	
0.00	0.00	1.23	
0.00	0.00	1.21	
0.00	0.00	1.19	
0.00	0.00	1.19	
0.00	0.00	1.20	
0.00	0.00	1.20	
0.00	0.00	1.20	
0.00	0.00	1.20	
0.00	0.00	1.20	
0.00	0.00	1.20	
0.00	0.00	1.20	
0.00	0.00	1.20	
0.00	0.00	1.20	
0.00	0.00	1.20	
0.00	0.00	1.20	
0.00	0.00	1.20	
0.07	2.04	1.20	START RELOADING
0.07	2.08	1.20	

APPENDIX N TABLE 1(cont) - DRAINED TRIAXIAL COMPRESSION LOADING/UNLOADING TEST

LOAD/UNLOAD CYCLE AT σ_{cell} = 4.0 MPa

$\sigma_1 - \sigma_3$ MPa	ϵ_1 %	ϵ_v %	
0.42	2.14	1.20	
1.10	2.18	1.23	
1.59	2.25	1.26	
2.25	2.30	1.27	
2.81	2.34	1.28	
3.24	2.39	1.30	
3.84	2.42	1.32	
4.33	2.47	1.33	
4.87	2.51	1.35	
5.24	2.55	1.36	
5.54	2.58	1.37	
5.82	2.62	1.39	
6.06	2.65	1.40	
6.24	2.69	1.41	
6.38	2.72	1.42	
6.49	2.76	1.43	
6.58	2.80	1.44	
6.64	2.84	1.45	
6.71	2.87	1.46	
6.76	2.92	1.47	
6.82	2.96	1.48	
6.86	3.00	1.49	
6.85	3.05	1.50	
6.91	3.09	1.52	
6.94	3.13	1.53	
6.96	3.16	1.54	
6.98	3.20	1.55	
7.01	3.24	1.56	
7.03	3.28	1.57	
7.05	3.31	1.58	
7.07	3.35	1.59	
7.08	3.38	1.60	
7.11	3.42	1.62	
7.13	3.46	1.63	
7.15	3.50	1.64	
7.18	3.55	1.65	
7.18	3.57	1.66	START 2ND UNLOADING
7.00	3.52	1.67	
6.62	3.48	1.66	
5.83	3.43	1.66	
5.19	3.40	1.66	
4.64	3.35	1.64	
3.99	3.30	1.64	
3.34	3.26	1.63	
2.86	3.23	1.62	
2.47	3.19	1.61	
2.09	3.14	1.61	

APPENDIX N TABLE 1(cont) - DRAINED TRIAXIAL COMPRESSION LOADING/UNLOADING TEST

LOAD/UNLOAD CYCLE AT σ_{cell} = 4.0 MPa

$\sigma_1 - \sigma_3$ MPa	ϵ_1 %	ϵ_v %
1.64	3.11	1.60
1.34	3.06	1.60
0.98	3.02	1.60
0.64	2.98	1.60
0.36	2.94	1.60
0.18	2.90	1.60

APPENDIX N TABLE 1(cont) - DRAINED TRIAXIAL COMPRESSION LOADING/UNLOADING TEST

Test CDLU3 DRAINED TRIAXIAL COMPRESSION TEST
LOAD/UNLOAD AT FIVE DIFFERENT CONFINING PRESSURES
σ_{cell} = 4.0, 8.0 16.0, 32.0 and 64.0 MPa
e_i = 0.519 H/D = 1.89
NO LUBRICATED ENDS

LOAD/UNLOAD CYCLE AT σ_{cell} = 8.0 MPa

$\sigma_1 - \sigma_3$ MPa	ϵ_1 %	ϵ_v %	
0.15	2.96	0.00	START 1ST LOADING
0.98	3.03	0.02	
1.49	3.06	0.04	
2.35	3.13	0.07	
2.89	3.16	0.09	
3.45	3.20	0.11	
4.12	3.25	0.13	
4.63	3.29	0.15	
5.08	3.33	0.17	
5.62	3.38	0.20	
6.05	3.42	0.22	
6.39	3.46	0.25	
6.76	3.50	0.28	
7.04	3.55	0.31	
7.30	3.59	0.34	
7.51	3.64	0.37	
7.71	3.69	0.41	
7.84	3.73	0.44	
7.96	3.76	0.47	
8.05	3.80	0.50	
8.15	3.84	0.52	
8.23	3.87	0.55	
8.32	3.91	0.58	
8.39	3.95	0.61	
8.46	3.99	0.64	
8.51	4.02	0.67	
8.59	4.07	0.70	
8.64	4.11	0.73	
8.68	4.15	0.76	
8.77	4.20	0.80	
8.80	4.24	0.83	
8.84	4.28	0.86	
8.91	4.33	0.90	
8.95	4.38	0.93	
9.00	4.42	0.96	
9.05	4.46	0.99	
9.09	4.49	1.02	
9.12	4.53	1.05	
9.18	4.57	1.08	
9.20	4.62	1.11	
9.28	4.67	1.15	
9.32	4.71	1.17	

APPENDIX N TABLE 1(cont) - DRAINED TRIAXIAL COMPRESSION LOADING/UNLOADING TEST

LOAD/UNLOAD CYCLE AT σ_{cell} = 8.0 MPa

$\sigma_1 - \sigma_3$ MPa	ϵ_1 %	ϵ_v %	
9.33	4.75	1.20	
9.41	4.81	1.24	
9.43	4.84	1.26	
9.47	4.89	1.30	
9.53	4.94	1.33	
9.55	4.98	1.36	
9.62	5.03	1.39	
9.63	5.07	1.42	
9.70	5.13	1.46	
9.74	5.16	1.48	
9.77	5.21	1.51	
9.82	5.25	1.54	
9.54	5.29	1.57	START 1ST UNLOADING
9.21	5.25	1.57	
8.34	5.22	1.57	
7.31	5.17	1.57	
6.44	5.12	1.56	
5.69	5.08	1.55	
4.92	5.03	1.54	
4.35	5.00	1.54	
3.80	4.97	1.53	
3.27	4.94	1.53	
2.77	4.91	1.53	
2.23	4.87	1.52	
1.78	4.83	1.52	
1.23	4.79	1.52	
0.73	4.74	1.52	
0.26	4.70	1.51	
0.00	4.66	1.51	
0.00	0.00	1.52	
0.00	0.00	1.52	
0.00	0.00	1.52	
0.00	0.00	1.52	
0.00	0.00	1.52	
0.00	0.00	1.52	
0.00	0.00	1.52	
0.00	0.00	1.52	
0.00	0.00	1.53	
0.00	0.00	1.53	
0.00	0.00	1.53	
0.00	0.00	1.53	
0.00	0.00	1.53	
0.00	0.00	1.53	
0.00	0.00	1.53	
0.00	0.00	1.53	
0.00	0.00	1.53	

APPENDIX N TABLE 1(cont) - DRAINED TRIAXIAL COMPRESSION LOADING/UNLOADING TEST

LOAD/UNLOAD CYCLE AT σ_{cell} = 8.0 MPa

$\sigma_1 - \sigma_3$ MPa	ϵ_1 %	ϵ_v %	
0.00	0.00	1.53	
0.00	0.00	1.53	
0.00	0.00	1.53	
0.00	0.00	1.53	
0.00	0.00	1.53	
0.00	0.00	1.53	
0.00	0.00	1.53	
0.00	0.00	1.53	
0.00	0.00	1.53	
0.00	0.00	1.53	
0.00	0.00	1.53	
0.00	0.00	1.53	
0.00	0.00	1.53	
0.00	0.00	1.53	
0.00	0.00	1.53	
0.00	0.00	1.55	
0.00	0.00	1.57	
0.00	0.00	1.56	
0.00	0.00	1.55	
0.00	0.00	1.54	
0.00	0.00	1.53	
0.00	0.00	1.54	
0.00	0.00	1.54	
0.00	0.00	1.54	
0.00	0.00	1.54	
0.00	0.00	1.54	
0.00	0.00	1.54	
0.00	0.00	1.54	
0.00	0.00	1.54	
0.00	0.00	1.54	
0.00	0.00	1.54	
0.00	0.00	1.54	
0.00	0.00	1.54	
0.00	0.00	1.54	
0.00	0.00	1.54	
-0.02	4.71	1.54	
0.18	4.73	1.54	START 2ND LOADING
0.87	4.78	1.55	
1.44	4.82	1.57	
2.32	4.87	1.59	
2.96	4.91	1.60	
3.54	4.94	1.61	
4.38	4.99	1.63	
5.03	5.04	1.64	
5.59	5.07	1.66	
6.37	5.13	1.67	
6.89	5.16	1.69	
7.38	5.20	1.70	

APPENDIX N TABLE 1(cont) - DRAINED TRIAXIAL COMPRESSION LOADING/UNLOADING TEST

LOAD/UNLOAD CYCLE AT σ_{cell} = 8.0 MPa

$\sigma_1 - \sigma_3$ MPa	ϵ_1 %	ϵ_v %	
7.82	5.24	1.71	
8.24	5.27	1.73	
8.60	5.31	1.74	
8.93	5.34	1.75	
9.21	5.38	1.77	
9.46	5.42	1.79	
9.66	5.45	1.80	
9.82	5.49	1.82	
9.94	5.53	1.84	
10.05	5.56	1.86	
10.14	5.60	1.88	
10.21	5.63	1.90	
10.28	5.67	1.92	
10.35	5.71	1.94	
10.39	5.75	1.96	
10.43	5.78	1.98	
10.47	5.82	2.00	
10.51	5.86	2.02	
10.54	5.89	2.04	
10.58	5.93	2.06	
10.61	5.97	2.08	
10.64	6.00	2.10	
10.68	6.04	2.12	
10.71	6.08	2.15	
10.73	6.11	2.17	
10.77	6.15	2.19	
10.78	6.19	2.21	
10.83	6.22	2.23	
10.84	6.26	2.25	
10.87	6.30	2.27	
10.90	6.33	2.30	
10.53	6.36	2.32	START 2ND UNLOADING
10.21	6.32	2.32	
8.95	6.27	2.32	
8.11	6.24	2.31	
7.24	6.19	2.30	
6.47	6.15	2.30	
5.65	6.10	2.29	
4.96	6.06	2.28	
4.37	6.02	2.28	
3.85	5.99	2.27	
3.34	5.96	2.27	
2.80	5.93	2.27	
2.34	5.89	2.26	
1.83	5.85	2.26	
1.31	5.81	2.25	
0.84	5.77	2.25	

APPENDIX N TABLE 1(cont) - DRAINED TRIAXIAL COMPRESSION LOADING/UNLOADING TEST

LOAD/UNLOAD CYCLE AT σ_{cell} = 8.0 MPa

$\sigma_1 - \sigma_3$ MPa	ϵ_1 %	ϵ_v %
0.45	5.73	2.25
0.10	5.70	2.25
-0.08	5.66	2.25

APPENDIX N TABLE 1(cont) - DRAINED TRIAXIAL COMPRESSION LOADING/UNLOADING TEST

Test CDLU3 DRAINED TRIAXIAL COMPRESSION TEST
LOAD/UNLOAD AT FIVE DIFFERENT CONFINING PRESSURES
σ_{cell} = 4.0, 8.0 16.0, 32.0 and 64.0 MPa
e_i = 0.519 H/D = 1.89
NO LUBRICATED ENDS

LOAD/UNLOAD CYCLE AT σ_{cell} = 16.0 MPa

$\sigma_1 - \sigma_3$ MPa	ϵ_1 %	ϵ_v %	
0.09	5.72	0.00	START 1ST LOADING
0.71	5.76	0.01	
1.88	5.82	0.04	
2.80	5.87	0.07	
3.45	5.91	0.08	
4.20	5.96	0.11	
4.99	6.01	0.14	
5.76	6.07	0.17	
6.23	6.10	0.19	
6.68	6.14	0.22	
7.12	6.17	0.24	
7.57	6.22	0.27	
7.93	6.25	0.30	
8.28	6.29	0.33	
8.57	6.33	0.36	
8.89	6.37	0.40	
9.21	6.42	0.45	
9.43	6.46	0.48	
9.70	6.51	0.53	
9.90	6.56	0.58	
10.06	6.60	0.62	
10.27	6.66	0.67	
10.37	6.70	0.71	
10.48	6.74	0.75	
10.64	6.79	0.80	
10.73	6.84	0.85	
10.84	6.87	0.89	
10.98	6.93	0.94	
11.06	6.97	0.99	
11.15	7.01	1.03	
11.27	7.06	1.08	
11.33	7.10	1.12	
11.42	7.15	1.16	
11.54	7.20	1.21	
11.60	7.24	1.25	
11.90	7.28	1.29	
11.80	7.33	1.34	
11.86	7.38	1.39	
11.98	7.43	1.44	
12.04	7.47	1.47	
12.12	7.52	1.52	
12.21	7.56	1.56	

APPENDIX N TABLE 1(cont) - DRAINED TRIAXIAL COMPRESSION LOADING/UNLOADING TEST

LOAD/UNLOAD CYCLE AT σ_{cell} = 16.0 MPa

$\sigma_1 - \sigma_3$ MPa	ϵ_1 %	ϵ_v %	
12.28	7.60	1.60	
12.37	7.65	1.64	
12.44	7.70	1.69	
12.52	7.74	1.72	
12.62	7.78	1.77	
12.70	7.83	1.81	
12.79	7.87	1.85	
12.86	7.92	1.89	
12.95	7.96	1.93	
13.01	8.00	1.97	
13.09	8.04	2.00	
13.16	8.08	2.04	
13.23	8.12	2.08	
13.30	8.16	2.11	
13.39	8.21	2.15	
13.46	8.26	2.20	
13.57	8.31	2.24	
13.63	8.36	2.28	
13.69	8.40	2.32	
13.83	8.45	2.37	*START 1ST UNLOADING*
13.87	8.49	2.40	
13.36	8.53	2.45	
13.54	8.51	2.46	
11.93	8.46	2.46	
10.26	8.41	2.45	
9.22	8.36	2.45	
8.03	8.31	2.44	
7.06	8.26	2.44	
6.22	8.22	2.43	
5.18	8.17	2.43	
4.24	8.13	2.42	
3.52	8.09	2.42	
2.82	8.05	2.42	
2.17	8.01	2.42	
1.54	7.98	2.42	
0.90	7.94	2.42	
0.37	7.90	2.42	
0.00	0.00	2.42	
0.00	0.00	2.42	
0.00	0.00	2.43	
0.00	0.00	2.43	
0.00	0.00	2.43	
0.00	0.00	2.43	
0.00	0.00	2.43	
0.00	0.00	2.43	
0.00	0.00	2.43	
0.00	0.00	2.44	

APPENDIX N TABLE 1(cont) - DRAINED TRIAXIAL COMPRESSION LOADING/UNLOADING TEST

LOAD/UNLOAD CYCLE AT σ_{cell} = 16.0 MPa

$\sigma_1 - \sigma_3$ MPa	ϵ_1 %	ϵ_v %	
0.00	0.00	2.44	
0.00	0.00	2.44	
0.00	0.00	2.44	
0.00	0.00	2.44	
0.00	0.00	2.44	
0.00	0.00	2.44	
0.00	0.00	2.44	
0.00	0.00	2.44	
0.00	0.00	2.44	
0.00	0.00	2.44	
0.00	0.00	2.44	
0.00	0.00	2.44	
0.00	0.00	2.44	
0.00	0.00	2.44	
0.00	0.00	2.44	
0.00	0.00	2.44	
0.00	0.00	2.45	
0.00	0.00	2.45	
0.00	0.00	2.45	
0.00	0.00	2.45	
0.00	0.00	2.45	
0.00	0.00	2.45	
0.00	0.00	2.45	
0.00	0.00	2.45	
0.00	0.00	2.45	
0.00	0.00	2.45	
0.00	0.00	2.46	
0.00	0.00	2.46	
0.00	0.00	2.45	
0.00	0.00	2.45	
0.00	0.00	2.45	
0.00	0.00	2.45	
0.00	0.00	2.45	
0.00	0.00	2.45	
0.00	0.00	2.45	
0.00	0.00	2.45	
0.00	0.00	2.45	
0.00	0.00	2.45	
0.00	0.00	2.45	
0.00	0.00	2.45	
0.00	0.00	2.45	
0.00	0.00	2.45	
0.00	0.00	2.45	
0.00	0.00	2.45	
0.13	7.92	2.46	START 2ND LOADING

APPENDIX N TABLE 1(cont) - DRAINED TRIAXIAL COMPRESSION LOADING/UNLOADING TEST

LOAD/UNLOAD CYCLE AT σ_{cell} = 16.0 MPa

$\sigma_1 - \sigma_3$ MPa	ϵ_1 %	ϵ_v %	
1.65	7.99	2.48	
2.76	8.05	2.49	
3.59	8.09	2.51	
4.77	8.14	2.52	
5.66	8.19	2.54	
6.45	8.23	2.55	
7.49	8.28	2.57	
8.35	8.32	2.58	
9.10	8.36	2.59	
10.00	8.41	2.61	
10.77	8.46	2.63	
11.58	8.51	2.65	
12.18	8.56	2.67	
12.66	8.60	2.69	
13.08	8.64	2.71	
13.46	8.69	2.74	
13.75	8.73	2.76	
13.98	8.77	2.79	
14.19	8.81	2.82	
14.35	8.85	2.84	
14.50	8.89	2.87	
14.62	8.93	2.90	
14.74	8.96	2.93	
14.84	9.00	2.95	
14.93	9.04	2.98	
15.02	9.08	3.01	
15.09	9.12	3.04	
15.17	9.16	3.07	
15.28	9.21	3.11	
15.35	9.26	3.15	
15.45	9.30	3.18	
15.53	9.35	3.22	
15.59	9.39	3.25	
15.66	9.43	3.28	
15.71	9.47	3.29	
15.80	9.51	3.32	
15.85	9.55	3.35	
15.92	9.59	3.38	
15.98	9.63	3.41	
15.50	9.63	3.43	
14.66	9.59	3.44	START 2ND UNLOADING
13.08	9.54	3.44	
11.70	9.49	3.43	
10.61	9.44	3.43	
9.54	9.40	3.42	
8.65	9.36	3.42	
7.83	9.32	3.42	

APPENDIX N TABLE 1(cont) - DRAINED TRIAXIAL COMPRESSION LOADING/UNLOADING TEST

LOAD/UNLOAD CYCLE AT σ_{cell} = 16.0 MPa

$\sigma_1 - \sigma_3$ MPa	ϵ_1 %	ϵ_v %
6.78	9.28	3.41
5.78	9.23	3.41
4.91	9.18	3.40
4.20	9.15	3.40
3.29	9.10	3.39
2.51	9.06	3.39
1.75	9.01	3.39
1.17	8.98	3.39
0.51	8.94	3.39
0.00	8.90	3.39

APPENDIX N TABLE 1(cont) - DRAINED TRIAXIAL COMPRESSION LOADING/UNLOADING TEST

Test CDLU3 DRAINED TRIAXIAL COMPRESSION TEST
LOAD/UNLOAD AT FIVE DIFFERENT CONFINING PRESSURES
σ_{cell} = 4.0, 8.0 16.0, 32.0 and 64.0 MPa
e_i = 0.519 H/D = 1.89
NO LUBRICATED ENDS

LOAD/UNLOAD CYCLE AT σ_{cell} = 32.0 MPa

$\sigma_1 - \sigma_3$ MPa	ϵ_1 %	ϵ_v %	
-0.02	8.96	0.00	START 1ST LOADING
0.09	8.98	0.01	
0.46	9.02	0.01	
1.48	9.08	0.03	
2.56	9.12	0.05	
3.35	9.16	0.07	
4.41	9.22	0.10	
5.32	9.27	0.13	
6.06	9.31	0.15	
6.67	9.35	0.18	
7.54	9.41	0.22	
8.15	9.46	0.25	
8.65	9.49	0.28	
9.27	9.55	0.32	
9.81	9.59	0.36	
10.32	9.64	0.41	
10.75	9.69	0.45	
11.11	9.73	0.49	
11.51	9.78	0.53	
11.82	9.82	0.58	
12.10	9.87	0.62	
12.44	9.92	0.67	
12.74	9.97	0.72	
13.04	10.02	0.77	
13.33	10.07	0.82	
13.56	10.11	0.87	
13.72	10.15	0.91	
13.91	10.19	0.95	
14.08	10.23	0.99	
14.25	10.26	1.02	
14.52	10.33	1.09	
14.80	10.38	1.15	
15.02	10.43	1.21	
15.20	10.48	1.26	
15.42	10.53	1.31	
15.60	10.58	1.36	
15.77	10.62	1.40	
15.96	10.67	1.45	
16.09	10.70	1.49	
16.27	10.75	1.53	
16.43	10.79	1.58	
16.65	10.84	1.63	

APPENDIX N TABLE 1(cont) - DRAINED TRIAXIAL COMPRESSION LOADING/UNLOADING TEST

LOAD/UNLOAD CYCLE AT σ_{cell} = 32.0 MPa

$\sigma_1 - \sigma_3$ MPa	ϵ_1 %	ϵ_v %	
16.82	10.89	1.68	
16.96	10.93	1.72	
17.18	10.98	1.77	
17.34	11.03	1.82	
17.50	11.07	1.86	
17.71	11.12	1.91	
17.86	11.17	1.96	
18.01	11.21	1.98	
18.19	11.26	2.02	
18.36	11.32	2.07	
18.57	11.37	2.12	
18.72	11.41	2.16	
18.89	11.46	2.21	
19.11	11.51	2.26	
19.26	11.56	2.31	
19.41	11.60	2.34	
18.74	11.64	2.40	START 1ST UNLOADING
19.00	11.61	2.41	
17.69	11.56	2.42	
15.73	11.51	2.42	
14.48	11.48	2.42	
12.87	11.42	2.42	
11.77	11.38	2.41	
10.68	11.34	2.41	
9.61	11.30	2.41	
8.61	11.26	2.40	
7.65	11.23	2.40	
6.64	11.19	2.40	
5.62	11.14	2.40	
4.45	11.10	2.40	
3.40	11.05	2.40	
2.34	11.01	2.40	
1.54	10.97	2.40	
0.59	10.93	2.40	
-0.17	10.88	2.40	
0.00	0.00	2.41	
0.00	0.00	2.41	
0.00	0.00	2.42	
0.00	0.00	2.42	
0.00	0.00	2.42	
0.00	0.00	2.42	
0.00	0.00	2.43	
0.00	0.00	2.43	
0.00	0.00	2.43	
0.00	0.00	2.43	
0.00	0.00	2.43	
0.00	0.00	2.43	

APPENDIX N TABLE 1(cont) - DRAINED TRIAXIAL COMPRESSION LOADING/UNLOADING TEST

LOAD/UNLOAD CYCLE AT σ_{cell} = 32.0 MPa

$\sigma_1 - \sigma_3$ MPa	ϵ_1 %	ϵ_v %	
0.00	0.00	2.44	
0.00	0.00	2.44	
0.00	0.00	2.44	
0.00	0.00	2.44	
0.00	0.00	2.44	
0.00	0.00	2.44	
0.00	0.00	2.44	
0.00	0.00	2.44	
0.00	0.00	2.44	
0.00	0.00	2.44	
0.00	0.00	2.44	
0.00	0.00	2.44	
0.00	0.00	2.44	
0.00	0.00	2.45	
0.00	0.00	2.45	
0.00	0.00	2.45	
0.00	0.00	2.45	
0.00	0.00	2.45	
0.00	0.00	2.45	
0.00	0.00	2.45	
0.00	0.00	2.45	
0.00	0.00	2.45	
0.00	0.00	2.46	
0.00	0.00	2.46	
0.00	0.00	2.45	
0.00	0.00	2.45	
0.00	0.00	2.45	
0.00	0.00	2.45	
0.00	0.00	2.45	
0.00	0.00	2.46	
0.00	0.00	2.46	
0.00	0.00	2.46	
0.00	0.00	2.46	
0.00	0.00	2.46	
0.00	0.00	2.46	
0.00	0.00	2.46	
0.00	0.00	2.46	
0.00	0.00	2.46	
0.00	0.00	2.46	
0.00	0.00	2.46	
0.00	0.00	2.46	
0.00	0.00	2.46	
0.00	0.00	2.46	
0.00	0.00	2.46	
0.16	10.94	2.46	START 2ND LOADING
1.26	10.98	2.47	
2.38	11.03	2.48	

APPENDIX N TABLE 1(cont) - DRAINED TRIAXIAL COMPRESSION LOADING/UNLOADING TEST

LOAD/UNLOAD CYCLE AT σ_{cell} = 32.0 MPa

$\sigma_1 - \sigma_3$ MPa	ϵ_1 %	ϵ_v %	
3.38	11.06	2.49	
4.56	11.11	2.50	
6.17	11.17	2.52	
7.36	11.21	2.53	
8.85	11.27	2.55	
9.77	11.31	2.56	
11.14	11.36	2.57	
12.19	11.40	2.59	
13.22	11.45	2.60	
14.33	11.50	2.62	
15.26	11.54	2.63	
16.31	11.60	2.66	
17.01	11.64	2.67	
17.73	11.68	2.70	
18.38	11.73	2.72	
19.01	11.78	2.75	
19.50	11.83	2.78	
19.88	11.87	2.80	
20.26	11.92	2.83	
20.59	11.96	2.87	
20.90	12.01	2.90	
21.16	12.05	2.94	
21.42	12.10	2.97	
21.66	12.15	3.01	
21.85	12.20	3.05	
22.07	12.24	3.09	
22.25	12.29	3.12	
22.44	12.33	3.16	
22.63	12.38	3.20	
22.79	12.42	3.23	
22.95	12.47	3.27	
23.09	12.51	3.30	
23.27	12.55	3.34	
23.40	12.59	3.37	
23.55	12.63	3.41	
23.67	12.67	3.44	
23.81	12.71	3.47	
23.95	12.75	3.50	
24.13	12.81	3.55	
24.26	12.85	3.58	
24.42	12.89	3.62	
24.56	12.93	3.65	
24.69	12.97	3.68	
24.82	13.01	3.72	
24.00	13.01	3.75	START 2ND UNLOADING
24.29	12.98	3.76	
21.82	12.92	3.76	

APPENDIX N TABLE 1(cont) - DRAINED TRIAXIAL COMPRESSION LOADING/UNLOADING TEST

LOAD/UNLOAD CYCLE AT σ_{cell} = 32.0 MPa

$\sigma_1 - \sigma_3$ MPa	ϵ_1 %	ϵ_v %
20.39	12.88	3.76
18.85	12.83	3.76
17.23	12.78	3.75
15.87	12.73	3.75
14.72	12.69	3.74
13.59	12.65	3.74
12.54	12.61	3.74
11.50	12.58	3.73
10.49	12.54	3.73
9.49	12.50	3.73
8.50	12.46	3.72
7.55	12.43	3.72
6.55	12.39	3.72
5.58	12.35	3.72
4.69	12.31	3.72
3.81	12.28	3.71
2.96	12.24	3.71
2.08	12.20	3.71
1.24	12.16	3.71
0.43	12.13	3.71
-0.11	12.08	3.71

APPENDIX N TABLE 1(cont) - DRAINED TRIAXIAL COMPRESSION LOADING/UNLOADING TEST

Test CDLU3 DRAINED TRIAXIAL COMPRESSION TEST
LOAD/UNLOAD AT FIVE DIFFERENT CONFINING PRESSURES
σ_{cell} = 4.0, 8.0 16.0, 32.0 and 64.0 MPa
e_i = 0.519 H/D = 1.89
NO LUBRICATED ENDS

LOAD/UNLOAD CYCLE AT σ_{cell} = 64.0 MPa

$\sigma_1 - \sigma_3$ MPa	ϵ_1 %	ϵ_v %
-0.17	12.14	0.00
-0.14	12.20	0.01
-0.10	12.25	0.01
0.08	12.31	0.01
0.23	12.33	0.01
0.95	12.37	0.02
2.20	12.43	0.04
3.48	12.48	0.05
4.79	12.53	0.07
6.01	12.59	0.09
6.91	12.63	0.11
8.06	12.68	0.14
9.00	12.73	0.16
10.10	12.78	0.19
10.78	12.82	0.21
11.64	12.87	0.24
12.31	12.91	0.26
13.38	12.97	0.30
14.16	13.02	0.33
15.12	13.09	0.38
15.87	13.14	0.41
16.61	13.19	0.45
17.13	13.24	0.49
17.78	13.29	0.53
18.44	13.34	0.57
19.02	13.39	0.61
19.52	13.44	0.64
20.15	13.49	0.69
20.64	13.55	0.73
21.09	13.59	0.77
21.63	13.64	0.82
22.11	13.70	0.86
22.47	13.74	0.90
22.99	13.79	0.95
23.38	13.84	0.99
23.76	13.88	1.03
24.25	13.94	1.08
24.66	13.99	1.12
25.12	14.05	1.17
25.54	14.10	1.22
25.85	14.14	1.25
26.32	14.20	1.30

APPENDIX N TABLE 1(cont) - DRAINED TRIAXIAL COMPRESSION LOADING/UNLOADING TEST

LOAD/UNLOAD CYCLE AT σ_{cell} = 64.0 MPa

$\sigma_1 - \sigma_3$ MPa	ϵ_1 %	ϵ_v %
26.68	14.25	1.35
26.99	14.29	1.38
27.43	14.34	1.43
27.79	14.39	1.48
28.13	14.44	1.52
28.56	14.50	1.57
28.94	14.55	1.61
29.38	14.61	1.66
29.81	14.67	1.71
30.13	14.71	1.75
30.57	14.77	1.80
30.91	14.82	1.85
31.20	14.86	1.88
31.61	14.92	1.93
31.94	14.97	1.97
32.24	15.01	2.00
32.64	15.07	2.05
32.90	15.10	2.08
33.29	15.16	2.13
33.62	15.21	2.17
33.92	15.25	2.20
34.32	15.31	2.25
34.58	15.35	2.28
34.92	15.40	2.32
35.32	15.45	2.37
35.64	15.50	2.41
34.51	15.51	2.44
35.00	15.48	2.46
34.77	15.44	2.46
33.10	15.39	2.47
30.95	15.34	2.47
29.10	15.29	2.47
27.27	15.24	2.47
25.72	15.20	2.47
24.42	15.15	2.47
23.05	15.11	2.46
21.70	15.06	2.46
20.43	15.02	2.46
19.18	14.98	2.46
17.86	14.94	2.46
16.57	14.89	2.45
15.28	14.85	2.45
14.02	14.81	2.45
12.74	14.76	2.45
11.52	14.72	2.45
10.28	14.68	2.45
9.08	14.63	2.45

APPENDIX N TABLE 1(cont) - DRAINED TRIAXIAL COMPRESSION LOADING/UNLOADING TEST

LOAD/UNLOAD CYCLE AT σ_{cell} = 64.0 MPa

$\sigma_1 - \sigma_3$ MPa	ϵ_1 %	ϵ_v %
7.87	14.59	2.45
6.70	14.55	2.45
5.53	14.51	2.45
4.39	14.46	2.45
3.26	14.42	2.45
2.17	14.38	2.45
1.16	14.34	2.45
0.16	14.29	2.45
0.00	14.24	2.45
0.00	0.00	2.45
0.00	0.00	2.46
0.00	0.00	2.46
0.00	0.00	2.46
0.00	0.00	2.47
0.00	0.00	2.47
0.00	0.00	2.47
0.00	0.00	2.47
0.00	0.00	2.47
0.00	0.00	2.47
0.00	0.00	2.47
0.00	0.00	2.48
0.00	0.00	2.48
0.00	0.00	2.48
0.00	0.00	2.48
0.00	0.00	2.48
0.00	0.00	2.48
0.00	0.00	2.48
0.00	0.00	2.48
0.00	0.00	2.48
0.00	0.00	2.48
0.00	0.00	2.48
0.00	0.00	2.48
0.00	0.00	2.48
0.00	0.00	2.49
0.00	0.00	2.49
0.00	0.00	2.49
0.00	0.00	2.49
0.00	0.00	2.49
0.00	0.00	2.49
0.00	0.00	2.49
0.00	0.00	2.49
0.00	0.00	2.49
0.00	0.00	2.49
0.00	0.00	2.49
0.00	0.00	2.49
0.00	0.00	2.49

APPENDIX N TABLE 1(cont) - DRAINED TRIAXIAL COMPRESSION LOADING/UNLOADING TEST

LOAD/UNLOAD CYCLE AT σ_{cell} = 64.0 MPa

$\sigma_1 - \sigma_3$ MPa	ϵ_1 %	ϵ_v %
0.00	0.00	2.49
0.00	0.00	2.49
0.00	0.00	2.49
0.00	0.00	2.50
0.00	0.00	2.50
0.00	0.00	2.50
0.00	0.00	2.50
0.00	0.00	2.50
0.00	0.00	2.50
0.00	0.00	2.50
0.00	0.00	2.50
0.00	0.00	2.50
0.00	0.00	2.50
0.00	0.00	2.50
0.00	0.00	2.50
-0.15	14.30	2.50
0.18	14.32	2.50
1.75	14.38	2.51
2.93	14.42	2.52
4.26	14.47	2.52
6.17	14.53	2.53
8.30	14.60	2.55
10.25	14.67	2.56
11.44	14.71	2.57
12.95	14.76	2.58
14.77	14.82	2.59
16.24	14.87	2.60
17.64	14.92	2.61
19.14	14.97	2.62
20.32	15.01	2.63
21.93	15.07	2.64
23.29	15.12	2.65
25.11	15.19	2.67
26.22	15.23	2.68
27.60	15.29	2.69
28.96	15.34	2.71
29.94	15.38	2.72
31.10	15.44	2.74
32.29	15.49	2.76
33.41	15.55	2.78
34.19	15.60	2.80
35.11	15.65	2.82
35.86	15.70	2.85
36.68	15.76	2.88
37.30	15.81	2.90
37.80	15.85	2.92
38.35	15.90	2.95

APPENDIX N TABLE 1(cont) - DRAINED TRIAXIAL COMPRESSION LOADING/UNLOADING TEST

LOAD/UNLOAD CYCLE AT σ_{cell} = 64.0 MPa

$\sigma_1 - \sigma_3$ MPa	ϵ_1 %	ϵ_v %
38.87	15.95	2.98
39.36	15.99	3.01
39.76	16.03	3.04
40.16	16.08	3.06
40.72	16.14	3.10
41.07	16.18	3.13
41.53	16.24	3.17
41.92	16.29	3.20
42.36	16.34	3.24
42.71	16.39	3.27
43.03	16.44	3.30
43.36	16.48	3.33
43.70	16.53	3.37
44.05	16.58	3.40
44.40	16.63	3.43
44.71	16.67	3.46
45.00	16.71	3.49
45.28	16.75	3.52
45.56	16.80	3.55
45.83	16.84	3.58
46.12	16.88	3.60
45.21	16.90	3.64
44.00	16.87	3.65
45.23	16.82	3.66
42.90	16.76	3.66
41.11	16.72	3.66
39.05	16.66	3.66
36.72	16.60	3.66
35.00	16.55	3.66
33.57	16.50	3.66
31.90	16.45	3.65
30.29	16.40	3.65
28.87	16.35	3.65
27.35	16.30	3.64
25.75	16.25	3.64
24.16	16.20	3.64
22.60	16.15	3.64
21.34	16.11	3.63
19.66	16.05	3.63
18.14	16.00	3.63
16.71	15.96	3.62
15.24	15.90	3.62
13.98	15.86	3.62
12.66	15.82	3.62
11.23	15.77	3.61
9.69	15.71	3.61
8.31	15.66	3.61

APPENDIX N TABLE 1(cont) - DRAINED TRIAXIAL COMPRESSION LOADING/UNLOADING TEST

LOAD/UNLOAD CYCLE AT σ_{cyl} = 64.0 MPa

$\sigma_1 - \sigma_3$ MPa	ϵ_1 %	ϵ_v %
6.60	15.60	3.61
5.46	15.56	3.60
4.16	15.51	3.60
2.68	15.45	3.60
1.44	15.40	3.60
0.40	15.36	3.60
-0.28	15.30	3.60